Proceedings of the 12th Symposium on Small Satellites for Earth Observation

Rainer Sandau
Klaus Brieß
Eberhard Gill
Editors

International Academy of Astronautics
IAA Book Series
Conference and Symposium Proceedings

Proceedings of the 12th Symposium on Small Satellites for Earth Observation

IAA Book Series-Volume 2 Number 11

Conference and Symposium Proceedings

Cover illustrations:
Various small satellites for Earth observation: TET-1, BIROS, Technosat, BEESAT-4 (from left to right). Composition by Jens Großhans (TU Berlin)

Proceedings of the 12th Symposium on Small Satellites for Earth Observation

Editors

Rainer Sandau
International Academy of Astronautics
Berlin
Germany

Klaus Brieß
Technische Universität Berlin
Berlin
Germany

Eberhard Gill
Delft University of Technology
Delft
The Netherlands

IAA Book Series-Volume 2 Number 11

Conference and Symposium Proceedings

The International Academy of Astronautics (IAA), an independent nongovernmental organization recognized by the United Nations, was founded in 1960. The purposes of the IAA are to foster the development of astronautics for peaceful purposes, to recognize individuals who have distinguished themselves in areas related to astronautics, and to provide a program through which the membership can contribute to international endeavors and cooperation in the advancement of aerospace activities.

International Academy of Astronautics
6 rue Galilée, Po Box 1268-16,
75766 Paris Cedex 16, France
www.iaaweb.org

ISBN/EAN IAA : 978-2-917761-70-0

Other IAA Publications

Available at https://shop.iaaweb.org
IAA Book Series

Volume 1 Small Satellites

Number 1 - Novel Ideas for Nanosatellite Constellation Missions

Number 2 - Small Satellite Missions for Earth Observation - New Mission Concepts and Technological Challenges

Number 3 - Innovative Ideas for Micro/Nano-satellite Missions

Number 4 - Small Satellites for Earth Observation - Missions & Technologies, Operational Responsive Space, Commercial Constellations

Number 5 - Inventive Ideas for Micro/Nano-Satellites - The MIC3 Report

Number 6 - Technology for Small Satellite Research - Payloads and Subsystem Technologies Small Satellite Applications, Missions, and In-Orbit Experiences

Number 7 - Innovative Ideas on Micro/Nano Satellite Missions and Systems Report on - Deorbit Device Competition(DDC) - Mission Idea Contest4(MIC4)

Number 8 - Small Satellites for Earth Observation - Missions & Technologies

Volume 2 Conference Proceedings

Number 1 - Proceedings of the 1st IAA Conference on University Satellite Mission and Cubesat Workshop

Number 2 - Proceedings of the 2nd IAA Conference on University Satellite Mission and Cubesat Workshop

Number 3 - Proceedings of the 1st IAA Latin American CubeSat Workshop

Number 4 - Proceedings of the 3rd IAA Conference on University Satellite Mission and Cubesat Workshop

Number 5 - Proceedings of the 2nd IAA Latin American CubeSat Workshop

Number 6 - Proceedings of the 1st IAA North East Asia Symposium on Small Satellites

Number 7 - Proceedings of the IAA Symposium on Space International Cooperation in Promoting Economic and Social Development of Developing Countries

Number 8 - Proceedings of the 7th CSA / IAA Conference on Advanced Space Technology Space Technology Innovation

Number 9 - Proceedings of the 1st IAA Latin American Symposium on Small Satellites

Number 10 - Proceedings of the 5th Mission Idea Contest (MIC5), the 6th Mission Idea Contest (MIC6), and the 2nd Debris Mitigation Competition (DMC2)

Number 11 - Proceedings of the 12th Symposium on Small Satellites for Earth Observation

Number 12- Proceedings of the 2nd IAA Latin American Symposium on Small Satellites

Volume 3 Disaster Management

Number 1 - Natural Disaster and Spatial Information System

Volume 4 History of Space

Number 1 - History of Chinese Astronautics

Number 2 - History of Russian Cosmonautics

PREFACE

The 12th IAA Symposium on Small Satellites for Earth Observation was initiated by the International Academy of Astronautics (IAA) and is hosted by the German Aerospace Center (DLR) and Technische Universität Berlin (TU Berlin).

This volume contains the proceedings of the contributions to the technical sessions, the poster session, and a special student paper session. The papers cover a wide range of different areas like small satellite mission programs, objectives for small satellite missions, mature (off-the-shelf) systems, advanced technology approaches, low-cost management aspects, and results of small satellite missions and lessons learned. They reflect the growing interest in the use of small satellites for dedicated missions applied to Earth observation, from scientific Earth observation missions to technology demonstration missions. It will become obvious that this type of mission can be conducted relatively quickly and inexpensively and provide increased opportunity for access to space. The spacecraft bus and the instruments can be based either on optimized off-the-shelf systems, with little or no requirements for new technology, or on new high technology systems.

We would like to thank the members of the Scientific Program Committee and of the Program Committee for their active support in organizing the Symposium and selecting the papers. Special thanks go to the Program Coordinator, Martin von der Ohe, without whose efforts the publication of these proceedings would not have been possible.

Rainer Sandau
Klaus Brieß
Eberhard Gill

Scientific program committee

J.-N. Bricout (CNES, France)
J.-M. Contant (IAA, France)
C. Elachi (NASA/JPL, USA)
L. Gratton (Colomb Institute, Argentina)
S. Hardhienata (LAPAN, Indonesia)
M. Hetscher (DLR, Germany)
P. Lier (CNES, France)
Y.-A. Liou (CSRSR, Taiwan, China)
L. Maresi (ESA/ESTEC)
S. Mostert (SCS Space, South Africa)
S. Nakasuka (Univ. of Tokyo, Japan)
R. Navalgund (ISRO, India)
S. Neeck (NASA/HQ, USA)
F. Ongaro (ESA/ESTEC)
M. Ovchinnikov (KIAM, Russia)
P. Patterson (USU/SDL, USA)
L. Paxton (JHU/APL, USA)
H. Reile (DLR, Germany)
M. Sandaar (MSPRS, Mongolia)
Sir Martin Sweeting (SSTL, UK)
C. F. Varotto (CONAE, Argentina)
Y. Zhu (CAST, Beijing, China)

Program committee

L. Alkalai (NASA/JPL, USA)
J. Esper (NASA/GSFC, USA)
W. Halle (DLR, Germany)
H. Kuiper (TU Delft, The Netherlands)
R. Laufer (Baylor University, USA)
H. Müller (DLR, Germany)
M. von der Ohe (TU Berlin, Germany)
S. Roemer (Antwerp Space, Belgium)
A. Rogers (Maxar, USA)
T. Segert (BST, Germany)
A. da Silva Curiel (SSTL, UK)

Student paper evaluation committee

L. Alkalai (NASA/JPL, USA)
K. Brieß (TU Berlin, Germany)
J. Esper (NASA/GSFC, USA)
R. Laufer (Baylor University, USA)
K.-S. Low (NUS, Singapore)
M. Ovchinnikov (KIAM, Russia)
R. Sandau (IAA, France/ Germany)
W.H. Steyn (Stellenbosch, South Africa)
J. Torley (University of Colorado, USA)
C. Underwood (Surrey Space Centre, UK)

Symposium Report for 2019 IAA Symposium on Small Satellites for Earth Observation

Conference Date:	6-10 May 2019
Location:	Berlin Brandenburgische Akademie der Wissenschaften (BBAW); Berlin, Germany
Date Submitted:	9th May 2019
Prepared By:	Aaron Q. Rogers (Maxar), Chief Rapporteur

With Session Chair Inputs Provided By:

M. Barschke, TU Berlin, DE
I. Belokonov, SSAU, RUS
K. Brieß, TU Berlin, DE
A. Court, TNO, NL
A. da Silva Curiel, SSTL, UK
N. Frischauf, SpaceTec Partners, DE
E. Gill, TU Delft, NL
L. Gratton, Colomb Inst., ARG
W. Halle, DLR, DE
M. Hetscher, DLR, DE
R. Kawashima, UNISEC, JP
S. Kennedy, OAI, USA
S. Klinkner, IRS Stuttgart, DE
O. Koudelka, TU Graz, AUT
H. Kuiper, TU Delft, NL
R. Laufer, Baylor, USA
S. Mostert, SCS, ZAF
J.-N. Bricout, CNES, FR
S. Neeck, NASA/HQ, USA
M. Ovchinnikov, KIAM, RUS
P. Patterson, USU/SDL, USA
L. Paxton, JHU/APL, USA
S. Roemer, Antwerp Space, BEL
A. Rogers, Maxar, USA
M. Saandar, MSPRS, MON
R. Sandau, IAA, FR
GP Sandhoo, NRL, USA
W.H. Steyn, SUN, ZAF
T. Terzibaschian, DLR, DE
F. Teston, ESA, NL
C. Underwood, SSC, UK
Z. Yoon, TU Berlin, DE
A. Zuccaro Marchi, ESA, NL

Esteemed Members of the Academy and Colleagues,

With the successful conclusion of the 12th International Academy of Astronautics Symposium on Small Satellites for Earth Observation, held the 6-10th of May 2019, as the Chief Rapporteur I am pleased to provide the following summary report. Gathering again at the Berlin Brandenburg Academy of Sciences, we enjoyed not only great hospitality and accommodation, but another successful gathering of 270 representatives from across the industry, government, and academic institutions of 37 countries. The symposium was opened by an illuminating keynote address, followed by not only a rich technical program with more than 60 paper presentations across 15 sessions, a special panel discussion, two poster sessions comprised of more than 40 summaries, but also an exhibition with a wide array of system and subsystem offerings needed for developing small satellite missions, launch accommodation, ground services, and information processing. A highly competitive student conference again highlighted exciting new contributors to the space community, featuring six finalists from three continents. Awards were given for both best papers and posters, as determined by committee and participant voting. Finally, not to be missed were also the many enjoyable social opportunities and local excursions made possible by the symposium and supporting organizations, including a hosted “floating” reception as part of a delightful riverboat tour of Berlin.

The symposium was convened and warmly welcomed to Berlin by several distinguished guests, beginning with Bernd Lietzau, representing the State of Berlin Senate, who noted the fitting location of the symposium in a city with a long history and diverse community of traditional and NewSpace companies. On behalf of the conference Chairmen and Secretary General of the IAA, Rainer Sandau noted that when the symposium first started, small satellites were regarded as toys, but much has changed since, and they are now considered invaluable tools. Moreover, the forum has served as means for invaluable exchange between established, global experts in the field and upcoming ones. The Executive Board Chair of the German Space Agency, Prof. Dr. Pascale Ehrenfreund, emphasized the broad use of small satellites for making impactful scientific contributions and the importance of seeking ways to collaborate. From her executive perspective, she highlighted DLR contributions to space research across their 47 globally distributed research facilities, and noted the increasing significance—and opportunity—for the space mission developer community to leverage artificial intelligence, New Space capabilities, services of pending mega constellations, and cutting-edge remote sensing techniques like hyperspectral imagery.

The symposium was then honored to receive the Department Head for Systems at ESA/ESTEC, Mr. Frederic Teston, for his keynote address titled, “Small(er) Satellites at ESA.” In his remarks he touched upon highlights of a rich history of ESA science missions beginning with its first small satellite in 1968 (ESRO-1), with now routine use of the mission class, best exemplified with its PROBA technology program. Remarkably, since PROBA-1 launched 20 years ago, the average mass of ESA satellites has dramatically decreased with more satellites being launched in even smaller form-factors. These have targeted scientific applications (e.g., Smart-1, Lisa Pathfinder, and CHEOPS), as well as driven the capabilities and industries of member states. Today, small satellites can be relied upon to provide critical science and observation data, such as with PROBA-2 for space weather monitoring.

ESA employs a disciplined process for “Discovery, Preparation, and Development” to capture and mature disruptive ideas, concepts for future missions, and enabling technologies. Typically, beginning with foundational elements, technology readiness level mapping and enabler roadmaps are considered (e.g., propulsion, star trackers, reflectarray flat antenna, vision based navigation, and hyperspectral imagers) which might first be validated using cubesat missions spanning 2U-12U. In conjunction, this progressively matriculating framework commonly utilizes studies, leading to broad competitions to identify compelling missions, which are then matured into flight programs. It is notable, that in addition to pursuing a broad portfolio of core science and exploration initiatives, ESA has recently expanded its focus to also address Space Safety, including increasingly topical considerations pertaining to space weather, space protection, debris remediation, and automated collision avoidance.

With an eye to the future, ESA has undertaken a strategic exercise entitled Space19+ to define and direct Europe’s “next generation” ambitions in space. As part of this exercise, a roadmap is being developed that now formally includes constellation missions, close proximity operations missions, and beyond LEO missions (e.g., M-ARGO 12U cubesat). Pursuant to these goals, the PROBA-3 mission will demonstrate formation flying small satellites to overcome the physical limitations of single platform. Additionally, ESA is seeking the means by which small satellites can further enhance the ecosystem of science/application/service capabilities. In this regard, ESA is enabling industrial partners to “Fast Fly Forward,” through a host of new SmallSat challenges, such as the Sentinel Small Sat (S^3) in Copernicus Master Challenge and Scout Missions. In doing so, Mr. Teston believes, they will help strengthen the competiveness of European smallsat operations, while also contributing to the shared equities of the global community.

In the technical sessions that followed, a diverse array of papers were presented spanning missions, instruments, lessons learned, programmatics, new spacecraft platforms, and enabling subsystem designs. These talks—along with a special roundtable panel—were all of high quality and

relevance, received by a full auditorium with many good question-and-answer exchanges. Moreover, the collective body of topics addressed also had strong linkages to many of the remarks shared by the Chairmen's welcome and in the keynote address. When considered in their full context, four important, topical points were made that served to frame the current state of the community from both a capabilities and enabler's perspective, as well new expanded scopes of attention and expectations for increased access to the myriad uses of space supported by small satellites:

1. Small satellites are executing important missions that are directly contributing to the global understanding of our world and beyond.

Setting an important baseline, we expanded our present understanding of current ESA program highlights, with an overview of the portfolio led by NASA, many of which are discriminately using small satellites to provide broad, critical contributions to Earth science and to improve our understanding of climate, weather, and other natural events. In related capacities, we also learned of other demonstration programs seeking to make critical contributions to our global understanding of climate change, such as Green House Gas Sat (SFL), PRETTY (TU Graz), RAVAN (APL), and SHACS (SSC). Underpinning these and other programs are a number of international collaborations, such as the 10-satellite CloudCT constellation for coordinated photogrammetric cloud observation to create 3D imaging solutions for climate prediction. Fundamental to all of these programs and others that were presented, was a mature design baseline of small satellites that have progressively moved the technology risk away from the platform themselves, to instead rightly place the "new endeavor" on the payload. Among many offerors reporting continued development progress in this regard, was Technical University Berlin who've now built 16 satellites for Earth observation, communication, and technology demonstration. By implicit consensus, it is clear that small satellites will continue to be utilized for missions requiring distributed measurements to drive temporal and spatial knowledge, while supporting affordable and responsive programmatics.

2. Continued investments are being made in mission-enabling technologies and integrated capabilities.

We enjoyed a strong host of talks pertaining to enhanced and innovative subsystems, such as optical downlinks, as well as ground networks to support expected scaling of future small satellite constellation missions. With the latter in mind, there were several updates on successfully demonstrated capabilities for executing formation flight, including the coordinated operation of BIROS and BEESAT-4, as well as the S-Net mission. Additionally, we addressed the greater integration and efficacy of autonomous fault detection isolation and recovery (FDIR) techniques that are being explored in programs like Eu: CROPIS, as well as onboard target validation and dynamic re-tasking based upon imposing external factors, like cloud obscuration on the Diwata-2 mission. With a similar focus on seeking ways to further reduce operational latencies and risk from human-in-loop of the fault recovery process, the SONATE technology demonstration mission will seek to flight qualify two highly autonomous processing payloads for on-orbit scheduling and diagnostic / fault management algorithms. The application and merits of applying modular open-system architecture (MOSA) approaches to the satellite design and development lifecycle were also discussed.

Beyond the capabilities of individual sensor systems, the forum converged to agreement that integrated applications are not only a matter of data nor earth observation, but combining satellite systems with other sensor systems, across both commercial and government institutions. In this respect, ESA is developing broad, cross-domain business collaborations for applications spanning communications, navigation, earth observation, and others. To evaluate how disparate, yet

complementary systems may be effectively integrated, we were introduced to the concept of an Observing System Simulation Experiment (OSSE) that can integrate a heterogeneous system of data sources, to provide a more informed basis for decision making on courses of action and where additional measurements using small satellites might be smartly added to improve assimilative models for forward-looking projections.

3. The world is expanding the obligations and scope of space operations.

With greater cognizance and concern for the preservation of our space environment, there is now global attention and emphasis on becoming better stewards of the domain, through space debris mitigation, management, and remediation. The keynote provided several remarks on ESA's Space Safety initiative, where the specific anthropogenic hazards have also been broadly considered by the United Nations Committee on the Peaceful Uses of Outer Space (COPOUS) resulting in 21 non-binding guidelines. The COPOUS working group noted several distinctions between the design and operation of small satellites relative to larger ones, most notably their reduced ability for ground-based tracking and means for safe end of life disposal. Regarding the latter, to provide subject matter based guidance to developers of small satellites, the IAA has created a "Handbook for Post-Mission Disposal of Satellites Less Than 100 kg." Among the viable courses of action and engineering options to satisfy post-mission disposal requirements, dra g augmentation was again effectively flight validated by the recently completed InflateSail mission. In all, the forum discussion was focused on the pragmatic, considerate methods by which future missions should be executed with concern for responsibly preserving our collective access-to and use-of the space environment.

4. There is an evolving outlook on the roles & responsibilities for driving future capabilities in Earth observation.

As we look to the future, it is worth contemplating who holds the mantle of responsibility for making the investments of both treasure and talent to advance our collective understanding of the world. A special roundtable panel directly discussed this topic as it pertains to space-based earth observation, convening informed representatives from both business and government sectors. It was foremost noted that Earth observation (EO) is driven by having satellites and, in this regard, Governments are currently the largest consumer of EO data and remain essential to all businesses working with EO products across the raw data (pixels) to knowledge/analytics value chain. While Governments do own and operate their own earth observation systems, there are many existing commercial providers (e.g., Planet, Digital Globe, and Airbus). In all cases, EO is driven by the capabilities of information technology, with cloud services and emerging machine learning tools coming online to transform imagery into actionable products. Among other remote sensing techniques that are being actively pursued, is synthetic aperture radar (SAR). With several demonstrations underway globally, programs such as the Japanese Strix-α X-band SAR among others, are seeking to leverage initial Government investments to then deploy large commercially operated constellations within the next five years.

While the use of space is not globally ubiquitous, during the symposium we were witness to a number of new paper and poster contributions from previously under- or non-represented nations, such as Algeria and Bangladesh. We received a timely update on African space policy and strategy, with emphasis on 17 Sustainable Development Goals that could be furthered through space capabilities. Whereas there are now multiple African nations with active national space programs and several with supporting initiatives, like other emerging actors, we must collectively seek a sustainable ecosystem that can address the equities and stakeholders of Africa, including an eventual sovereign capability to develop necessary space capabilities.

In conclusion, the symposium was another success, providing a great opportunity for technical exchange, broad community engagement, and communication across a diverse international representation. More importantly, it brought forward both new ideas and the opportunity to discuss perspectives on developing important earth observation missions using small satellites. As we have now reflected upon the accomplishments and lessons learned, I would like to again invoke an appropriate question and challenge from my predecessor Chief Rapporteur, Dr. Eberhard Gill, who asked “Quo vadis? Where are we going?” To conclude this symposium, I believe we have again provided an exciting roadmap for future endeavors and I look forward to seeing where we are upon our return to Berlin two years hence.

CONTENTS

Session 1: Programmatics

Session 2: Missions

Session 3: Sensor Systems

Session 4: Constellations/ Formations

Session 5: Integrated Applications

Session 6: Student Conference

Session 7: AOCS

Session 8: Lessons Learned

Session 9: On-Board Processing

Session 10: New Platforms

Session 12: Communications

Session 13: Ground Segment

Session 14: Special Aspects

Small Satellites for NASA Earth Science

Steven P. Neeck (M2)

NASA Headquarters, Science Mission Directorate
Washington, DC 20546, USA
Phone: +1 202-358-0832, Mail: steven.neeck@nasa.gov

Abstract: NASA's Earth Science Division (ESD) seeks to develop a scientific understanding of Earth and its response to natural and human-induced changes. Earth is a system comprised of diverse components interacting in complex ways. Understanding Earth's atmosphere, surface and interior, oceans and surface water, ice and snow, and life as a single connected system is necessary in order to improve our predictions of climate, weather, and natural hazards. The ESD's Flight Program consists of a coordinated series of satellite and airborne systems providing long and short-term, global and regional observations. In addition, the Flight Program provides infrastructure for operating these missions, processing their scientific data, and distributing them on a free and open basis to researchers, operational users, and the public. The Flight Program currently has 25 operating Earth observing space missions and instruments. There are 18 more missions and instruments planned for launch over the next five years. These comprise missions recommended by the National Academies 2017 Earth Science Decadal Survey, missions and selected instruments to ensure availability of key climate data sets, operational missions to sustain the land imaging provided by the Landsat system, and small-sized competitively selected orbital and instrument missions of opportunity belonging to the Earth Venture (EV) program. The Earth Science Decadal Survey, released in early 2018, recommended four new Flight Program elements in addition to the above activities that comprise the Program of Record (POR). Small satellites (~500 kg or less) are essential components of these activities. Presently, there is an increasing use of micro and nanosatellites (or CubeSats) in constellations to support NASA ESD's scientific objectives. These include the Cyclone Global Navigation Satellite System (CYGNSS) for observing tropical cyclone intensification and evolution, the Timed-Resolved Observations of Precipitation structure and storm Intensity with a Constellation of Smallsats (TROPICS) mission, and the Polar Radiant Energy in the Far InfraRed Experiment (PREFIRE) CubeSat mission. ESD small satellite initiatives like the Small Satellite Constellation Data Buy and Venture Class Launch Services (VCLS) are also underway. The Earth Science Technology Office's (ESTO) In-Space Validation of Earth Science Technologies (InVEST) and the Venture Technology program elements have launched seven 3U and 6U CubeSat missions to validate advanced instruments and related technologies. An equivalent number of InVEST and other technology demonstration CubeSats are being prepared for launch in the next year. An overview of plans and current status including topics related to small satellite enabling activities will be presented.

1. NASA'S EARTH SCIENCE DIVISION

The study of the Earth from space is a key element of the National Aeronautics and Space Act of 1958 and the National Aeronautics and Space Administration's (NASA) Strategic Plan. The National Aeronautics and Space Act of 1958 (as amended), which established NASA, states the objective of "The expansion of human knowledge of the Earth and of phenomena in the atmosphere and space." Strategic Goal 1 in NASA's Strategic Plan is to "Expand human knowledge through new scientific discoveries" and its Strategic Objective 1.1 is to "Understand the Sun, Earth, Solar System, and Universe" with a core context of "Safeguarding and improving life on Earth." NASA's Earth Science Division (ESD) advances scientific understanding of the Earth in service to the United States and the world. This involves the pursuit of answers to fundamental science questions about the Earth system on all time scales to the benefit of humanity. Accordingly, NASA developed, in concert with the scientific research community, the following hierarchy of key science questions:

- How is the global Earth system changing?
- What causes these changes in the Earth system?
- How will the Earth system change in the future?
- How can Earth system science provide societal benefit?

These science questions are associated with six scientific focus areas. These focus areas guide the ESD's selection of investigations and other programmatic decisions:

Climate variability and change	Atmospheric composition
Carbon cycle and ecosystems	Water and energy cycle
Weather	Earth surface and interior

NASA has key responsibilities in meeting United States (U.S.) civilian needs for Earth observations from space (excepting terrestrial and space weather). In this context, NASA responds through the interagency Satellite Needs Working Group (SNWG) to needs for sustained measurements from multiple Federal agencies. Through its partnerships with agencies that maintain forecast and decision support systems, such as the National Oceanic and Atmospheric Administration (NOAA) and the U. S. Geological Survey (USGS), NASA improves capabilities to predict weather, climate, natural hazards, and to manage resources. NASA's Earth science activities are an essential part of national and international efforts to use Earth observations and scientific understanding in service to society. NASA maintains an expansive network of partnerships with foreign space agencies and international organizations to conduct scientific research and field campaigns, data sharing agreements, and joint development of satellite missions. NASA Earth science receives external guidance on its research, applications, and observational activities. In January 2018, the National Academies released the second Decadal Survey for Earth Science. It supersedes the 2007 Decadal Survey and endorses the current program of record (POR), as well as making recommendations for a number of future activities. NASA also receives input from the Earth Science Advisory Committee (ESAC) to ensure that proposed programs maximize scientific productivity within the general framework established by the National Academies [1,2,3].

2. EARTH SCIENCE FLIGHT PROGRAM

The ESD is organized around four programmatic areas: flight, research, applied sciences, and technology. The Flight Program is responsible for collecting and disseminating space and airborne observations. It provides management of all ESD spaceflight missions from advanced concept studies through flight hardware development to on-orbit operations. These activities are managed within the Earth Systematic Missions (ESM) and Earth System Science Pathfinder (ESSP) Programs. The ESM Program includes a broad range of multidisciplinary science missions aimed at understanding the Earth system. The ESM Program implements legacy missions, including the Earth Observing System (EOS) and other missions that predate and include those recommended by the 2007 Decadal Survey. In addition, the program implements sustainable land imaging missions, and climate continuity missions. The ESSP Program implements low to moderate cost missions through

competitive selections to accommodate new and emerging scientific and applications priorities. It includes Earth Venture (EV) program elements consisting of low-cost Principal Investigator (PI) led suborbital and orbital missions, instruments for participation on spaceflight missions of opportunity, and CubeSats. The ESSP Program also includes operating missions that were competitively selected including the Orbiting Carbon Observatory-2 (OCO-2) small satellite and other legacy missions. These activities represent the POR, as noted above, endorsed by the 2017 Decadal Survey. The Decadal Survey has also recommended four new Flight Program elements: Designated, Earth Explorer, Incubation, and Earth Venture Continuity (EVC). The ESD is actively planning for these new elements and has initiated four major Designated studies, planning for the first EVC solicitation, and planning for the first Earth Explorer and Incubation solicitations [4,5].

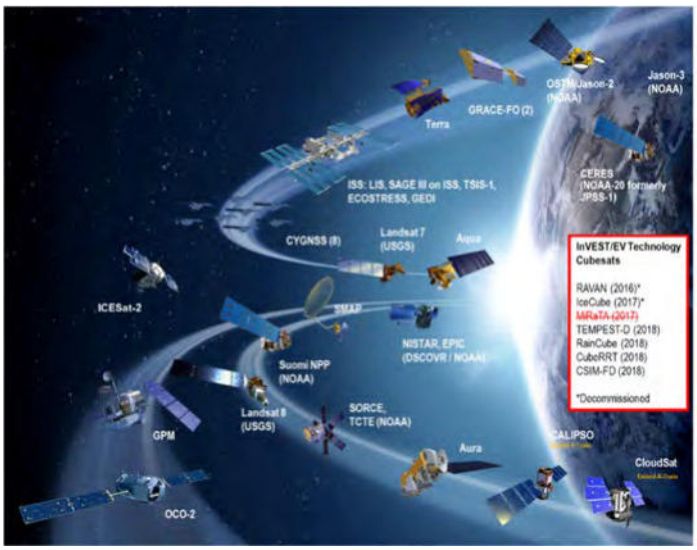

Figure 1. Currently Operating NASA Earth Science Missions

Figure 1 illustrates the 25 ESD missions and instruments that are currently operating. An additional 16 missions and instruments are planned for launch by 2024 and are pictured in Figure 2. Eight passive optical and LIDAR instruments are operating or scheduled to fly on the International Space Station (ISS). The Tropospheric Emissions: Monitoring of Pollution (TEMPO), Geostationary Carbon Cycle Observatory (GeoCARB), and Multi-angle Imager for Aerosols (MAIA) instruments will be hosted on GEO and LEO commercial satellites. The fifth Earth Venture Instruments for Flights of Opportunity (EVI) selection is planned to fly by 2024. Of these 41 missions, 14 fall into the small satellite (~500 kg or less) category. Numerous minisatellite (~500-100 kg) missions in operations or in development include the Solar Radiation and Climate Experiment (SORCE), Cloud-Aerosol Lidar and Infrared Pathfinder Satellite Observations (CALIPSO), Jason-2/Ocean Surface Topography Mission (OSTM), Orbiting Carbon Observatory-1 (OCO-2), Deep Space Climate Observatory (DSCOVR), Jason-3, Gravity Recovery and Climate Experiment Follow-On (GRACE FO), and MAIA hosted on Orbital Testbed-2 (OTB-2). These also include NASA's first and second Earth science CubeSat constellation missions, Timed-Resolved Observations of Precipitation structure and storm Intensity with a Constellation of Smallsats (TROPICS) and Polar Radiant Energy in the Far InfraRed Experiment (PREFIRE) [6,7]. Numerous CubeSats are also being used for technology validation and measurement demonstration.

Figure 2. Planned NASA Earth Science Research Missions (2019-2024)

3. SMALL SATELLITES SUPPORTING NASA EARTH SCIENCE

In implementing the Decadal Survey, POR, and EV satellite missions, the ESD is leveraging the increasing capabilities of small satellites and their constellations. The eight satellite (18 kg each) CYGNSS constellation mission completed its baseline mission of tropical storms and hurricane surface wind measurements and is in extended operations. The EVI program element includes the TROPICS mission with six 3U CubeSats (8 kg each) to address critical science questions related to Tropical Cyclone (TC) intensification and evolution. The EVI PREFIRE mission uses a pair of 6U CubeSats (14 kg each) to measure the first full spectral measurements of far infrared radiation over the Arctic. The Decadal Survey Designated Observable studies underway are considering small satellite architecture options. To leverage increasing commercial small satellite constellation capabilities, the ESD awarded three contracts under the Small Satellite Constellation Data Buy initiative. Improved access to space for small satellites has been demonstrated through a recent Rocket Labs Electron rocket launch funded through the joint ESD-NASA Launch Services Program (LSP) Venture Class Launch Services (VCLS) initiative [8,9].

The Earth Science Technology Office (ESTO) In-Space Validation of Earth Science Technologies (InVEST) program provides in-space, orbital technology validation and risk reduction for components and systems. Eight CubeSats are in operation or development in this program. The Flight Program has also funded two innovative, technologically advance measurement demonstration CubeSat missions through the EV Technology program [10]. Additional details and status on these programs are provide below.

4. CYCLONE GLOBAL NAVIGATION SATELLITE SYSTEM (CYGNSS)

The CYclone Global Navigation Satellite System (CYGNSS) CYGNSS mission, led by the University of Michigan, is a small spaceflight investigation that is part of the Earth Venture Mission (EVM) program. CYGNSS makes measurements of ocean surface winds throughout the life cycle of tropical storms and hurricanes to improve forecasting. It uses a dense sampling constellation of eight 18 kg microsatellites. The CYGNSS data

will enable scientists to probe key air-sea interaction processes that take place near the center of the storms and play large roles in the genesis and intensification of hurricanes. CYGNSS's microsatellites receive direct and reflected signals from Global Positioning System (GPS) satellites. The direct signals pinpoint CYGNSS observatory positions while the reflected signals respond to ocean surface roughness from which wind speed is retrieved. CYGNSS was launched on a Pegasus XL small class launch vehicle in 2016 into a 35 degree inclination 526 km altitude orbit. The project has successfully completed its two year baseline mission and is in extended operations approved through September 2020. The CYGNSS flight segment hardware performance has proved to be stable and reliable. The ground segment operations and data flow have been highly automated. Data assimilation into TC numerical forecasts are underway. Numerous other science applications of ocean wind observations have been demonstrated. Continued improvements in Level 1 calibration and Level 2 retrieval algorithms as well as development of new ocean and land science products are planned during the extended operations period [5]. The CYGNSS constellation is pictured in Figure 3. An example of improvement in hurricane storm structure prediction is pictured in Figure 4 [11].

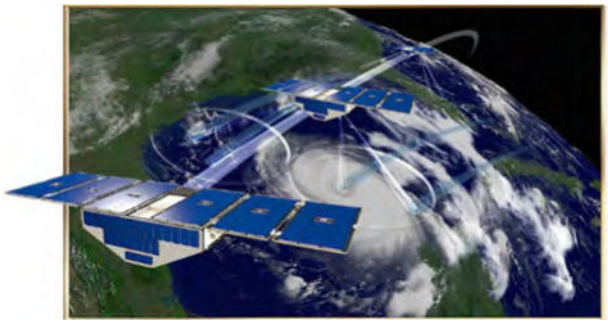

Figure 3. CYGNSS Microsatellite Constellation

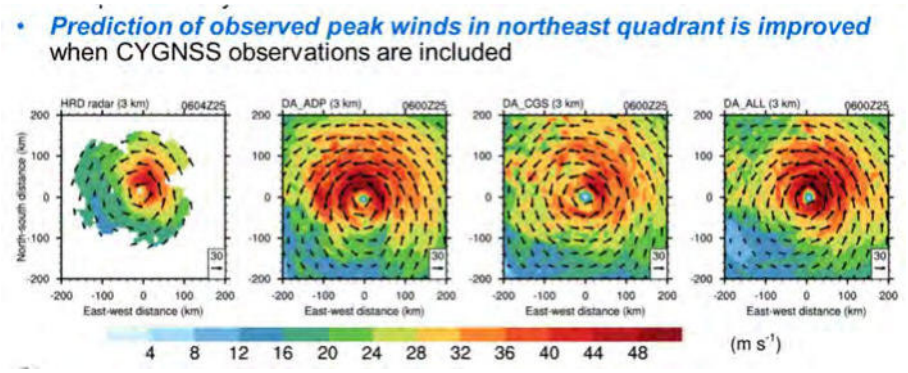

Figure 4. Harvey Storm Structure Predictions (courtesy of Zhaoxia Pu, U-Utah)

5. TIMED-RESOLVED OBSERVATIONS OF PRECIPITATION STRUCTURE AND STORM INTENSITY WITH A CONSTELLATION OF SMALLSATS (TROPICS)

The Timed-Resolved Observations of Precipitation structure and storm Intensity with a Constellation of Smallsats (TROPICS) mission was selected in 2016 from the EVI-3 solicitation. It is the first CubeSat science mission for ESD. Led by the Massachusetts Institute of Technology/Lincoln Laboratory (MIT/LL), TROPICS consists of six 3U CubeSats (8 kg each) flying in three separate orbital planes at an altitude of 550 km and an inclination of 30 degrees. The science goals of the mission are to increase understanding of critical processes driving significant and rapid changes in TC storm structure/intensity; provide high-revisit microwave observations of precipitation, temperature, and humidity in the tropics and subtropics; complement the Global Precipitation Measurement (GPM), CYGNSS, and Geostationary Operational Environmental Satellite-R/S (GOES-R/S) missions with high refresh, near-all-weather measurements of precipitation and thermodynamic structure. Each CubeSat carries a compact cross-track scanning microwave radiometer that provides simultaneous soundings of precipitation structure near 90 GHz, of O_2 (118 GHz) and H_2O vapor (183 GHz) absorption lines, and of ice structure near 206 GHz. The CubeSat buses are provided by Blue Canyon Technologies. The project is currently in Implementation (Phase C) in the midst of its Assembly, Integration, and Test (AIT) program. Access to space will be provided by the ESSP Program in the 2021/2022 timeframe following delivery of the CubeSats later in 2019. Figures 5 and 6 provide overviews of the CubeSat and radiometer payload [12].

Figure 5. CubeSat Overview

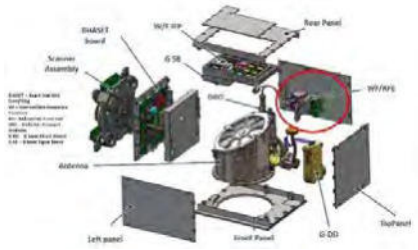

Figure 6. Radiometer Payload

6. POLAR RADIANT ENERGY IN THE FAR INFRARED EXPERIMENT (PREFIRE)

The Polar Radiant Energy in the Far InfraRed Experiment (PREFIRE) mission was selected in 2017 from the EVI-4 solicitation. Led by the University of Wisconsin, PREFIRE consists of two 6U CubeSats (14 kg each) flying in two separate near polar orbits at 470-650 km altitude. The mission science objective is to provide the first full spectral measurements of Far InfraRed (FIR) radiation (4 mm – 54 μm), revealing the full spectrum of Arctic radiant energy. This will fill a major gap in knowledge of the Arctic energy budget and the role of FIR radiation in Arctic warming, sea ice loss, ice sheet melt, and sea level rise. Each CubeSat carries a Thermal Infrared Spectrometer (TIRS). These grating imaging spectrometers are of a Schwarschild/Offner optical form and use a thermopile focal plane. The Jet Propulsion Laboratory (JPL) provides the TIRS instruments and Space

Dynamics Laboratory (SDL) provides the CubeSat buses. The project is currently in Formulation (Phase B) having completed its System Requirements Review/Mission Definition Review (MDR). Access to space will be provided by the ESSP Program in the 2022/2023 timeframe following delivery of the CubeSats in 2021. Figures 7 and 8 provide overviews of the CubeSat concept and its details.

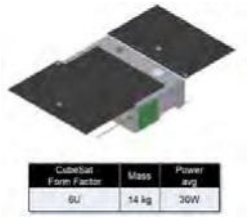

Figure 7. CubeSat Concept

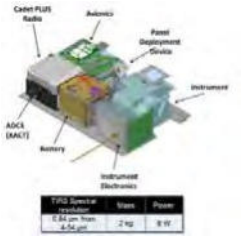

Figure 8. CubeSat Detail

7. ESTO INVEST AND EARTH VENTURE TECHNOLOGY CUBESATS

The ESTO InVEST program provides space flight validation of technology and risk reduction for NASA Earth science instruments, instrument subsystems, onboard processing, or other technologies at TRL 5. The space platforms are 3U or 6U CubeSats and access to space is provide through the Human Exploration and Operations Mission Directorate (HEOMD) CubeSat Launch Initiative (CSLI). Validation typically last for one year. Thirteen CubeSats have been selected since 2012 through three competitive solicitations. To date, five have been launched with two remaining in operation (two completed their missions and one failed on-orbit following launch). Six are in development and planned for launch by 2021. The ESD Flight Program also funds EV Technology CubeSats to provide demonstrations of innovative measurement technologies in direct support of programmatic objectives. Two are currently operating on-orbit. Figure 9 shows the most recent CubeSats from the InVEST-17 selections and the recently launched CSIM-FD EV Technology CubeSat.

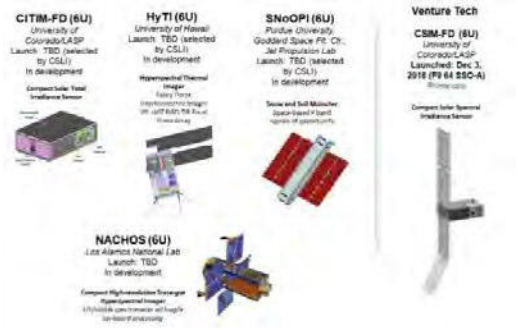

Figure 9. InVEST-17 and EV Technology CubeSats

8. EARTH OBSERVATIONS FROM PRIVATE SECTOR SMALL SATELLITE CONSTELLATIONS PILOT

The ESD has initiated a pilot to determine the feasibility of using commercial small satellite constellation data. This consists of a purchase of existing data products related to Essential Climate Variables (ECVs) from private sector-funded small-satellite constellations (three satellite minimum constellation, full longitude coverage) for evaluation by

NASA researchers to determine their value to NASA Earth science research and applications. In 2018, ESD purchased data from three companies: Planet, DigitalGlobe, and Spire. ESD-funded researchers are currently assessing these data products during a one year evaluation period. Based on the outcome of this assessment, purchased data may augment or replace some NASA-collected data in the future.

9. VENTURE CLASS LAUNCH SERVICES (VCLS)

The ESD has partnered with the NASA Launch Services Program (LSP) through the Venture Class Launch Services (VCLS) program to stimulate development of small, lower cost, reliable, and dedicated launch vehicles to improve access to space for small satellite (CubeSat, microsatellite, and nanosatellite) missions. In 2015, VCLS awarded firm fixed-price contracts to Rocket Lab USA ($6.9M) and Virgin Orbit ($4.7M) to provide demonstration launches of a 60 kg payload minimum to a 500 km Sun synchronous or equivalent orbit. On December 16, 2018, Rocket Lab successfully launched its Electron rocket with a payload of 10 NASA-sponsored CubeSats from its New Zealand launch site. Virgin Orbit is planning its VCLS launch using its LauncherOne rocket later in 2019. Assuming continued success, ESD anticipates using VCLS launch systems for selected future small satellite missions.

10. CONCLUSION

Small satellites, now more than ever, are critical contributors to NASA's Earth science measurements supporting its Earth system science research and applications objectives. The EV program is using small satellite constellations for lower cost, new science enabling missions like the CYGNSS microsatellite constellation, now in extended operations. The TROPICS and PREFIRE CubeSat constellations now in development will demonstrate unique new science capabilities. NASA Earth science is using numerous CubeSats for instrument technology space validation as well as for measurement demonstrations of innovative and enabling techniques. ESD also has programs for small satellite launcher demonstrations and commercial small satellite constellation data evaluation.

11. REFERENCES

[1] National Aeronautics and Space Act of 1958, Pub.L.No.85-568, 72 Stat. 426-438 (Jul. 29, 1958) As Amended, NASA, Washington (2008)
[2] 2014 Science Plan for NASA's Science Mission Directorate, NASA, Washington (2014)
[3] 2018 Strategic Plan, NASA, Washington (2018)
[4] Thriving on Our Changing Planet: A Decadal Strategy for Earth Observation from Space, National Academies Press, Washington (2018)
[5] https://science.nasa.gov/earth-science/decadal-surveys
[6] https://tropics.ll.mit.edu/CMS/tropics/
[7] https://news.wisc.edu/uw-madison-to-aid-nasas-push-to-measure-arctics-radiant-energy/
[8] https://science.nasa.gov/nasa-evaluates-commercial-small-sat-earth-data-science
[9] https://www.nasa.gov/feature/small-satellites-to-get-their-own-ride-to-space
[10] http://esto.gsfc.nasa.gov/
[11] Z. Cui, Z. Pu, V. Tallapragada, R. Atlas, C. Ruf, A Preliminary Impact Study of CYGNSS Ocean Surface Wind Speeds on Numerical Simulations of Hurricanes. Geophysical Research Letters (published online 13 March 2019)
[12] W.J. Blackwell, S. Braun, B. Zavodsky, C. Velden, T. Greenwald, D. Herndon, R. Bennartz, M. DeMaria, G. Chirokova, R. Atlas, J. Dunion, F. Marks, R. Rogers, H. Christophersen, B. Annane, Overview of the NASA TROPICS CubeSat constellation mission, SPIE Proceedings, 10769 (2018)

Advancing Space Technology in Africa - The transition from national programs to sustainable Space Programs

Sias Mostert[1]
[1]SCS Aerospace Group,
email: sias@scs-space.com

Abstract
A global consensus on acceptable standards across a large number of domains have been achieved with the adoption of the Sustainable Development Goals (SDGs). The SDGs being of a global nature begs the question how can space programs in Africa can contribute. The number of countries in Africa that are active in space technology have lagged the global average. Establishing critical infrastructure in Africa is important as the geography of the continent is so large that it calls for new approaches to addressing the needs for standard of living that are largely lagging for the largest part of the population in Africa. Can space technology play a role in crossing the divide?

To date individual countries have embarked on space programs in collaboration with international partners. A pan-African program called the African Resource Management constellation have also been undertaking. However, there are few reports on successful results, other than program announcements, advances in human capital development and launch announcements. There are also limited reports on the commercial success of national telecommunication satellites.

Offers by international vendors adds further uncertainty and opportunity to national science and technology development trajectories. Reflecting on the presentations at the Unispace+50 conference, answers vary from building an own capacity (SCS) [1], to using available data (Planet) [2], to just benefiting from the results (Greensense) [3]. In analyzing the economic development trajectory of a country [4 WEF] it is not an either this approach or that approach, but the parallel implementation of an investment in the innovation economy, the efficiency economy and the factor economy at the same time.

The approach discussed in this paper reviews progress in Africa from a space ecosystem perspective. All the elements constitute an integrated approach at the level of a country that benefits from an holistic roll-out strategy in a global market context. The formation of a Global African Critical Space Infrastructure combines the priorities of the needs of a continent such as Africa, with a global market potential for similar services that are prioritized around the resource constrained context of Africa. Such infrastructure can be built up from a number of multi-mission constellations.

The paper will begin with looking at a measure of success by which to measure progress and achievement. from an Africa Space Policy and Strategy perspective. The core functions that are required from the system are then listed. Global trends and African wide initiatives are then reviewed. Finally the advances in small satellite technology is integrated into the implementation based on the impact of key technology trends impacting on nano- and micro-satellites provide some clues on how space technology from Africa can contribute.

1. INTRODUCTION

The science and technology (S&T) innovation systems in African countries have in many cases yet to form a critical mass where high value jobs are retained in Africa. Satellite technology programmes have long been promoted as a vehicle to achieve the outcomes of sustainable development within a S&T context. . Countries in Africa that have pursued such programs over the past decades include South Africa, Algeria, Nigeria, Kenya, Egypt and Morocco. Countries that have joined the space race through nano-satellite projects are Ghana, Nigeria. Countries that invested in large commercial systems include Angola. The question is what framework should be used for a sustainable space science and technology program?

Mapping the African Space Strategy User Requirements in relation to the Sustainable Development Goals provides a guide to investment in African Space Infrastructure. The relationship can be seen in Figure 1 with the African Space Strategy User Requirements.

African Space Strategy User Needs	Sustainable Development Goals with number		Remote Sensing	Navigation and Positioning	Satellite Communication	Space Science & Astronomy
Disasters	13	Climate Action	√	√	√	√
Health	3	Good health and well-being	√	√	√	
Energy	7	Affordable and clean energy	√	√	√	√
Climate	13	Climate Action	√	√		√
Water	6	Clean water and sanitation	√	√		
Weather	13	Climate Action	√	√	√	√
Ecosystems	14,	Life below water, Life on land	√	√		
Agriculture	2	Zero hunger	√	√	√	
Biodiversity	14,	Life below water, Life on land	√	√		
Peace, Safety and Security	16	Peace, justice and strong institutions	√	√	√	√
Human Migration and Settlements	11	Sustainable Cities and Communities	√	√	√	
Education and Human Resources	4	Quality Education	√	√	√	√
Communications		Cross cutting	√	√	√	√
Trade and Industry	9	Industry, innovation and infrastructure	√	√	√	
Transport	12	Responsible consumption and production	√	√	√	
Infrastructure	9	Industry, innovation and infrastructure	√	√	√	
		Not Covered				
	1	No poverty		√	√	
	5	Gender equality				
	8	Decent work and economic growth		√	√	
	10	Reduced inequalities		√	√	
	17	Partnerships for the Goals		√	√	

Figure 1 African Space Strategy User Needs mapped to Sustainable Development Goals in relation to required Critical Space Infrastructure

It is also insightful to see the SDGs written in text as opposed to the appealing graphic symbols that are often used. The underlying meaning is sobering to say the least. The next section reviews a number of initiatives and programs that are currently undertaken in Africa.

Core elements of a holistic space eco-system

With the African Space Policy and Strategy in place, the following elements together make up a complete space eco-system:
Human Capital Development, Ground Infrastructure, Satellite Technology, Space Programs, Exploration, Industry development, Market development, Services as consumed by users. The following section reviews the first six elements of a holistic space eco-system.

2. PROGRAMS AND INITIATIVES THAT IMPACT THE AFRICAN SPACE ECOSYSTEM

Human Capital Development

Human capital development has been the foundation of the space program and initiatives in South Africa, Algeria, Morocco, Nigeria, Kenya and Egypt. At an African Union level this has been recognized and a pan-African University has been established with five satellite campuses in the topics as indicated in Figure 2.

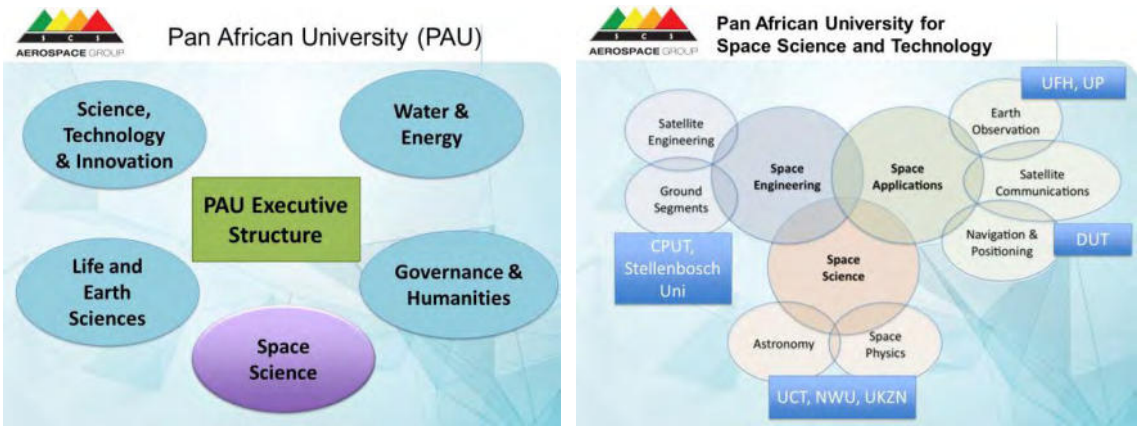

Figure 2 Pan-African University and Space Science and Technology distributed Campus

The Space Science and Technology campus of the Pan African University, has been allocated to South Africa. The campus has been defined as a distributed campus that combines the best of all the universities in South Africa that relate to topcs in the space domain. See Figure 2 for the allocation of campuses. The Pan-African University in Space Science and Technology (PAUST) is expected to start operating in January 2020.

Ground Infrastructure

The Square Kilometer Array (SKA) project in South Africa requires remote stations in a number of African countries. The radio astronomy instruments detect radio signals from the universe in different frequencies. Radio astronomy instruments are placed in the 'quietist' parts of the Earth. The locations are also good places for ground stations for receiving satellite data. However, being remote makes infrastructure management costly. A co-location synergy has been developed in conjunction with the African Very Long Baseline Interferometry project in collaboration with the SKA. One of the co-location site investment options is a satellite ground station at each location. See the map in Figure 3 for the participating countries.

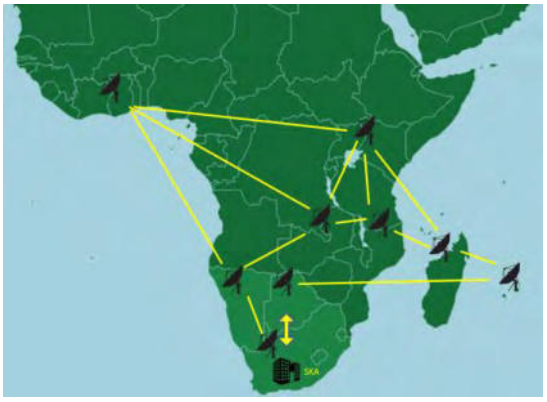

Figure 3 Candidate ground infrastructure locations in Africa

Satellite Technology

Space technology benefit from a number of trends that increase the cost/benefit ratio of nano- and micro-satellites. The useful trends are:

1. Miniturisation of sensors, processors, memory
2. Standardization of launch interfaces, in particular for nano-satellites
3. 'Unlimited' processing power – subject to available power on-board the satellite
4. 'Unlimited' memory as opposed to a still bandwidth limited data transmission capacity.

The technology trends are ultimately leading to the establishment of new business models.

The begging question for a country with an emerging space program is then, can the advances in technology be used to address the economic activities in the efficiency and factor economies? Or in the context of SDGs, can one expect to close the gap on addressing a number of gaps in access to a standard of living standards, aptly described by the Sustainable Development Goals. The following section reviews some of the satellite programs and initiatives in Africa.

Satellite Programs and Initiatives

In South Africa the legacy of the South African space technology started with GreenSat, that was never launched, but the GreenSat programme spawned a range of satellites and capabilities that has grown till this day. Sunsat (64kg, 12m GSD, 1999) was the pioneering satellite that demonstrated COTS components for earth observation missions. The next satellite Sumbandilasat was another technology demonstrator with updated performance of 6m GSD within a 81 kg satellite (2009). Since then four nano-satellites have seen the light from South African entities with the latest imagers providing a 6m GSD capability within a 6 kg satellite (2019). The recent nSight-1 mission demonstrated 30m GSD in 2.5 kg launched from the ISS orbit.

In the micro-satellite class the technology advances have lead to operation performance of better than 1m GSD in a 100kg class satellite for optical systems and 1m GSD SAR in a 250kg class satellite.

Space Exploration and Lunar Missions

SCS have two instruments in beyond lunar orbits. The NCLE mission, in collaboration with Radboudt University in the Netherlands is a data processer contribution to a long wave radio-astronomy instrument hosted on the Change-4 Data Relay satellite in support of the China lunar lander project.

A planned mission is the African to the Moon mission that is an ambitious mission to deploy a distributed radio telescope on the far side of the moon with 54 antennas, one for each African country.

Industrial Development

The impact of space programs in Africa are only going to be sustainable if a market is created and if the industrial eco-system is established. A recent Ph.D. study at Cape Town University [3] shows the industrial eco-system required in support of Human Suborbital Space Transportation Industry. The industry value flow diagram clearly indicates the full supply chain required to support a space port in Africa.

Figure 4 Industry Value Flow diagram for the Human Suborbital Space Transportation Industry

4. CONCLUSION

There are many of the eco-system building blocks available and actively being developed in Africa. The challenge is to ensure critical mass of capability and capacity in each building block and a long term investment in the mission building blocks. In 2019, African only contributes 3% to the global GDP, but has 16% of the global population. Space has a growth future in Africa.

References

[1] Denner, Francois, 2018, Unispace+50- Industry Forum -SCS, Planet, GreenSense
[2] World Economic Forum, Country Report 2018.
[3] Davidian, Kenneth John, Accumulation Model Processes of Human Suborbital Space Transportation Industry, phd, UCT

Programmatic Aspects of the Small Satellites of the Technische Universität Berlin

Klaus Brieß
Technische Universität Berlin
Marchstr. 12, 10587 Berlin, Germany
Phone: +49 30 314 21339, Mail: Klaus.briess@tu-berlin.de

Abstract: The Technische Unversität Berlin has already launched and operated 16 small satellites for Earth observation, communication or technology demonstration. After the 7 satellites of the TUBSAT family the CubeSats BEESAT 1 to 4 are launched and operated and supplemented by nanosatellites for technology demonstration like TECHNOSAT or for communication objectives like the SNET satellite formation. All technology demonstration missions and also the communication mission SNET stands in close connection with Earth observation missions because they prepare and demonstrate new technologies for future small satellite Earth observation missions. The paper gives an overview to the status of these activities and to the future applications of the new demonstrated technologies in Earth observation small satellite missions.

1. INTRODUCTION

The System Earth is changing continuously its characteristic parameters especially due to anthropogenic impacts. It is important to know these impacts and the effects on the atmosphere, lithosphere and hydrosphere in a global and local scale. Large satellite missions deliver remote sensing data of the system Earth for short- and for long-term investigations. Climate changes, melting of polar caps and other global changes are already discovered and observed by means of conventional satellites series. But small satellites can deliver supplementary information to these topics [1]. Small satellite missions can be built and in a larger number, they can be operated simultaneously what gives a higher area and time coverage of target areas [2] and they can have a higher mission frequency. They can use the advanced technologies even if they do not have space heritage up to now and they can be operated more flexible in comparison to conventional satellites. But they have some drawbacks: up to now they cannot use instruments with large apertures; they have to be designed for a very limited life time in space (one to four years maximum) and the platform performance parameters are limited to a certain values. To improve the last to points the TU Berlin is carry out technology research and space technology demonstration together with partners from industry and research. And the space activities of the TU Berlin are not only directed to demonstrate new technologies in space but also on the improvement of all elements of a small satellite mission like:

- small satellite platform,
- launch service for small satellites,
- use of small satellite ground station networks,
- cost-effective management and quality assurance procedures.

2. SMALL SATELLITE PROGRAMMATICS

TU Berlin drives the research and development of small satellite platforms in different classes forward. For practical reasons the spacecraft can be subdivided in different classes (see Tab.1).

Tab. 1 Satellite classes of TU Berlin

Satellite class	Satellite mass
Microsatellites	ca. 20 kg to ca. 120 kg
Nanosatellite bus TUBiX20	10 kg to 20 kg
Nanosatellite bus TUBiX10	4.0 kg to 10 kg
CubeSats of the BEESAT family	1.0 kg to 4.0 kg
Picosatellites of the BEESAT family	0.1 kg to 1 kg

The microsatellite program of TU Berlin [3] and the so called TUBSAT family were founded by Professor Udo Renner. Under his guidance 7 satellites are built and operated successfully mostly dedicated to Earth observation.

The TUBiX20 nanosatellite bus [4] is operating in space successfully since 14.07.2017 in the frame of the TechnoSat mission. It demonstrates in orbit new technologies for German universities and for a DLR institute. It is a three axis stabilized satellite with new technologies for attitude control and demonstrating also Earth remote sensing by a color camera. The next mission with the TUBiX20 bus is called TUBIN (TU Berlin Infrared satellite) dedicated to fire remote sensing from space by means of a 20 kg nanosatellite. The launch is planned for 2019.

The TUBiX10 bus is a nanosatellite with a total mass of 10 kg. The bus is developed for the S-Net mission [5], see fig.1. The S-Net mission is launched on 1. February 2018 from Vostochny and is fully operational. The mission has successfully demonstrated a multi-hub inter-satellite communication in S-band with four nodes. The four nodes enable six independent communication links. Now the mission is in the extension phase to demonstrate a distributed system for on-board processing of data products.

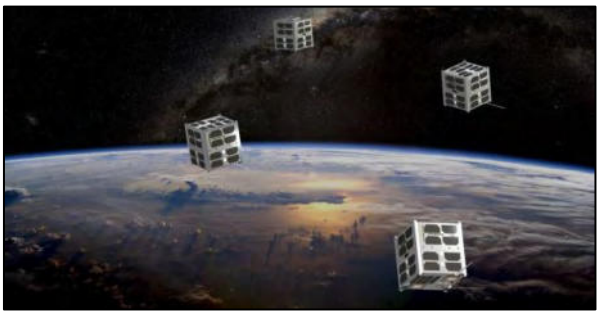

Fig. 1: The nanosatellite formation of the S-Net mission operates in space since 1.February 2018

The CubeSats and the Picosatellites of TU Berlin are called “BEESAT” what means “Berlin Educational and Experimental Satellite”. The hands-on education of students and the in-orbit verification of new technologies are in the focus of the BEESAT missions. Up to now BEESAT-1, -2, -3 and -4 are designed, built and operated successfully in space (see fig. 2).

Fig. 2: Image taken by BEESAT-2 on the 22nd of Dec. 2015 at 15:26 UTC showing a cyclone south of Iceland

BEESAT-5 to 8 are picosatellites with a total mass of 250 g each (Fig. 3). All four together fits in a 1U CubeSat deployer. They are scheduled to launch in 2019. They demonstrate a communication network in orbit in the UHF band and other picosatellite technologies.

Fig. 3: Picosatellites BEESAT-5 to -8 of TU Berlin with a precise onboard orbit determination module and inter satellite link

The BEESAT-9 is another CubeSat what will be launched in 2019 with technology experiments for precise in orbit determination of the satellite position. Additionally two 2U CubeSats are in preparation for a launch in 2021. They shall demonstrate a formation flight by active orbit control and should demonstrate a stereoscopic view on Earth to deliver data to generate a local 3D terrain model of distinctive target areas.

The activities of TU Berlin to launch small satellites are directed more and more to a partnership with the local spin-off company of TU Berlin the ECM launch service. They offer interesting launch opportunities for our small satellite missions and give all necessary support in the fields of deployment or separation technology, export of satellites and custom clarification.

3. PROGRAMMATIC ASPECTS IN THE GROUND SEGMENT

The ground segment for the small satellites missions of TU Berlin consists of the primary ground station with antennas for the VHF/UHF-band, for the S-band and in the near future also fort the K-band and the Mission Control Center in Berlin and a secondary ground station in Svalbard in the VHF/UHF band. Additionally cooperation with the Colomb Institute in Argentina includes the mutual ground station support and offer the option of ground station operations for TU Berlin satellites via ground stations in Argentina. Beside this TU Berlin became part of the SatNOGS project what is a platform of a open satellite ground-station network [6]. Some operational experiments with TU Berlin satellites and SatNOGS ground stations and the SatNOGS network are done successfully. The telemetry frames of TU Berlin satellites are received and decoded anywhere in the world and transmitted to TU Berlin.

4. SUMMARY

The small satellite programmatic of TU Berlin covers the space segment, the ground segment, the launch segment and the program segment. In the space segment different satellite classes with advanced technologies are under research and development. Some main points of in orbit verification are the inter-satellite communication, the precise onboard orbit determination, precise pointing positioning, formation flight of satellites, remote sensing of the Earth in visible and infrared wavelength range and onboard data processing. The use of the local provider ECM launch services brings several advantages for the procedure of satellite delivery and launch preparation. The programmatic in the ground segment covers the inclusion of several partner ground stations and the experimental use of the worldwide ground station network SatNOGS. The program segment is characterized by a mission preparation and implementation according to the ECSS guidelines in combination with a tailored quality management system dedicated to university small satellite missions. Up to now all 16 already launched satellites of TU Berlin have operated successfully or are still in operation.

5. REFERENCES

[1] Sandau, R., Briess, K., The Role of Small Satellite Missions in Global Change Studies. In: E. Chuvieco et al. (eds.): Advances in Earth Observation of Global Change. Springer B.V. (2010)

[2] Sandau, R., Briess, K., D'Errico, M., Small satellites for global coverage: Potential and limits. ISPRS Journal of Photogrammetry and Remote Sensing, Vol. 65, Issue 6, Nov. 2010, Pages 492-504

[3] Barschke, M., Brieß, K., Renner, U., Twenty-Five Years of Satellite Development at Technische Universität Berlin. Proc. Small Satellites Systems and Services Symposium (4S), Valetta, Malta (2016)

[4] Barschke, M., Baumann, F., Ballheimer, W., Großekatthöfer, K., Nitzschke C., Brieß, K., TUBiX20 - The novel Nanosatellite Bus of TU Berlin. 9th IAA Symposium on Small Satellites for Earth Observation, 93-96. (2013)

[5] Yoon, Z., Frese, W., Bukmaier, A., Briess, K., Mission Design of a S-Band Network of Cooperative Nanosatellites. International Workshop on Spacecraft Constellation and Formation Flight, (2013)

[6] SatNOGS website. https://satnogs.org/. retrieved 20.01.2019

Technologies for Small Optical Systems leading to Disruptive Innovations for Remote Sensing

Alessandro Zuccaro Marchi[1], Luca Maresi[1]

[1]ESA / ESTEC
Address: Keplerlaan 1, Noordwijk, The Netherlands
Phone: +31 71 5658254, Mails: alessandro.zuccaro.marchi@esa.int, luca.maresi@esa.int

Abstract
The worldwide growing interest in small payloads and platforms requires the use of compact solutions that are also easy to align and test. The recent progress of design and manufacturing technologies makes possible to build miniaturized optical systems that still allow retrieving valuable end-products.
The European Space Agency is leading several R&D activities in the field of compact multispectral and hyperspectral payloads. These activities encompass technology developments of novel optical designs, focusing on evolution of materials and processes, new detectors, engineering of EEE components and dedicated data processing to achieve innovative and cost-effective solutions.
By combining these developments, a portfolio of innovative multispectral and hyperspectral instruments has been developed, spanning from high spatial resolution to large swath width, targeting applications from cubesat to minisatellites.
Furthermore, powerful data processors and large data storage components open the doors to new types of operations, such as on board generation of level 2 data, and within a foreseeable future, artificial intelligence tasks. This new type of operation allows overcoming the bottlenecks of nano/cubesats, i.e. the limited downlink capability. Exploiting the flexibility and interoperability conceived in these systems, a large number of applications can be targeted.
The combination of novel performing compact optical instruments and availability of on-board data processing opens therefore new ways of using the space asset, providing the user with turnkey solutions and fast response to their specific needs.
The paper provides an overview of the latest technology developments, the status of the instruments manufactured so far, their performance and their expected applications. First flight results of the HyperScout, a hyperspectral instrument flying on a 6U cubesat, are presented.

1. INTRODUCTION

The trend in Earth observation towards smaller platforms and miniaturized instrumentation, as well as a demand for higher spatial and spectral resolution, is nowadays possible thank to the increased technological maturity in fields like CMOS detectors, hyperspectral filters, electronics miniaturization and optical quality. It is now possible to obtain valuable hyperspectral data in several areas like climate changing, water quality, land cover and land use with a small system. Even if the quality of the data acquired with such systems are inherently different from the data acquired by large ones, the low-cost operations open the way to new potential markets and data exploitations.

The European Space Agency (ESA) leads the development of several compact hyperspectral instruments. The activities running now under ESA contracts cover a wide range of technologies and specifications: compact hyperspectral payloads with large swath width (HyperScout), with high spatial resolution (STREEGO), combined instrumentation (HyperSTREEGO), hyperspectral imagers with high spectral resolution (CHIEM) and compact free-form grating spectrometers (CHIMA). Some activities are focused on the development of components; others in the development and test of protoflight hardware. HyperScout, a 1U Cubesat payload, is a hyperspectral instrument developed not only to

prove the technological challenges to build such a performing compact payload, but also to perform on-board real time L0-L2 data processing.

Obtaining end data product directly on board greatly reduces the data volume, thus overcoming the major cubesat limitation, i.e. the downlink capability. The flexibility built in the on-board processing allows continuously tuning the end data product to satisfy the needs of multiple users, even over the same area of interest.

2. HYPERSCOUT: ONBOARD PROCESSING OF HYPERSPECTRAL IMAGING DATA ON A NANOSATELLITE

HyperScout is a hyperspectral nanosatellite payload operating in the VNIR spectral range with very low mass and volume, fitting 1.2 cubesat unit. It features a large field of view (31° across track x 16° along track) and a spectral resolution of about 12 nm (Figure 1). Taking advantage of technology developments such as CMOS detectors, hyperspectral filtering, electronics miniaturisation and state of art microprocessors, it is shaped around a Three Mirror Anastigmatic (TMA) telescope with a Linear Variable Filter (LVF). One of its key features is the possibility to implement an onboard artificial intelligence, enabling a large variety of land and vegetation operational applications, for which cost efficiency and timeliness are of foremost importance.

Figure 1. HyperScout, the flight model.

The hyperspectral data of HyperScout is more than 1TeraByte per orbit, too large for downlink data rate of a typical cubesat platform, i.e. around 1 Mbit/s. To overcome this constraint, HyperScout employs an on-board payload data processing chain that extracts relevant high-level information, reducing the hyperspectral data into high-level data products to be sent down to Earth within the downlink capacity of the nanosatellite, and during the same orbit as the data was acquired. More in detail, HyperScout features an optimized L0 to L2A processing chain resulting in a hyperspectral data cube, after which application - specific processing is performed. These processing capabilities encompass Normalized Difference Vegetation Index (NDVI) and Normalized Difference Water Index (NDWI) calculations, and detection of anomalies such as flooding, forest fire, volcanic eruption, landslides within minutes from their occurrence.

This system is extremely flexible and re-configurable in orbit: different users may employ the same sensor for different real time applications. The instrument, together with a distributed network of ground stations, can easily enable early warnings in a cost efficient manner. Furthermore, in a constellation scenario the revisit time can be greatly increased.

Since February 2nd 2018, HyperScout Proto-Flight Model (PFM) is being flying as a payload on board of the Danish 6-units Gomx-4B cubesat, to prove hardware and processing functionalities. The instrument was developed in the frame of a GSTP (General Support Technology Programme) IOD (In-Orbit Demonstration) activity. This PFM has been tailored to fit in the Gomx-4B platform by reducing the across track field of view to 23°. With a pixel pitch of 5.5 µm, it now achieves a swath of 220 km and about 70 m ground sampling distance (GSD) from 500 km altitude.

"First light", at the beginning of commissioning phase, was acquired in summer 2018: a single frame over Cuba with a footprint of about 200 x 150 km^2, proving that the full chain is operational (Figure 1). After completion of the commissioning phase, HyperScout ran nominal IOD operations, ended in December 2018. Together with spectral, radiometric and geometrical vicarious targets, about 14 ROIs (Regions Of Interest) were acquired and analyzed, forming some hyperspectral data cubes. One software experiment was also conducted. Some examples are shown in the images here below.

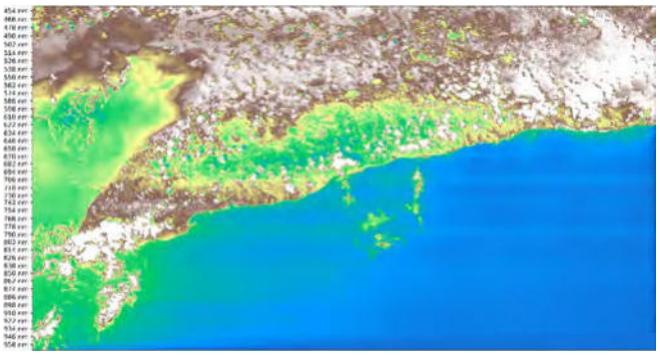

Figure 2. "First light" over Cuba.

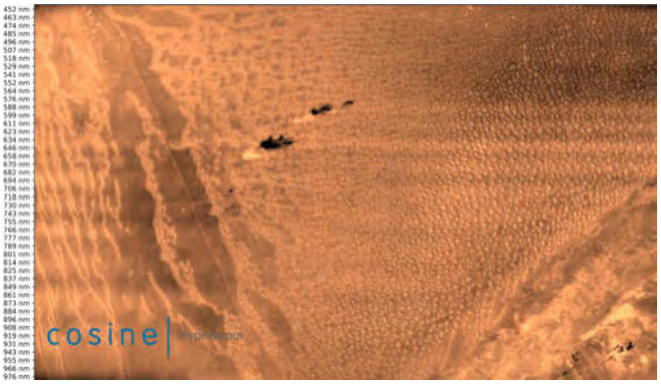

Figure 3. Algeria, Nov 2018. Collection of subsequent frames for geometrical processing.

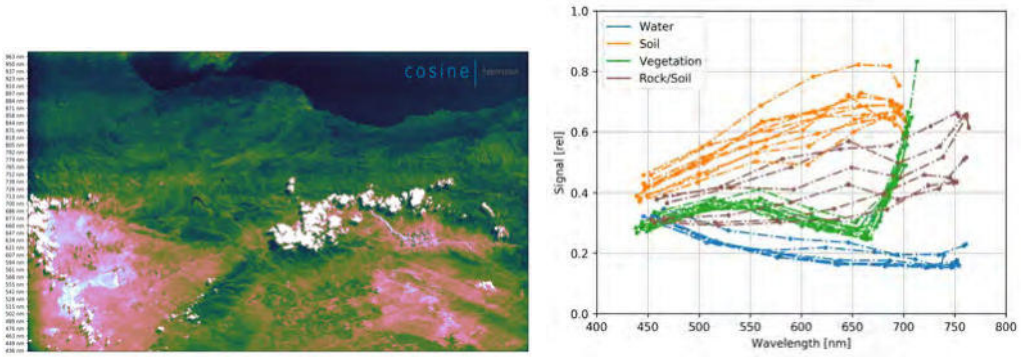

Figure 4. California, Aug 2018. Multispectral data frame, spectral and radiometric response (left). Agricultural application: typical profiles over a few land users (right).

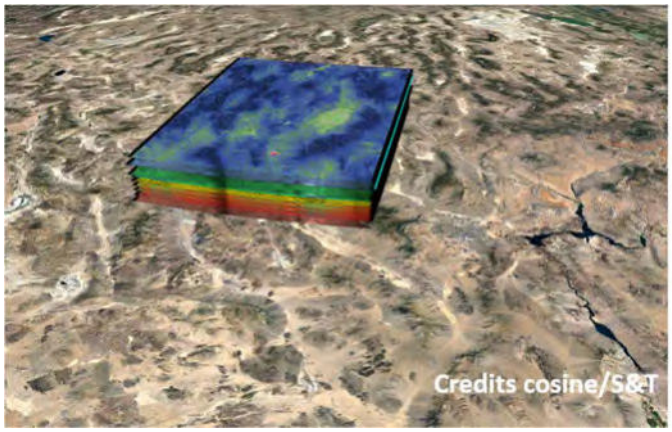

Figure 5. Nov 2018, on-orbit L2 level data production.

Within the GSTP programme, HyperScout is being developed by a consortium led by cosine Research B.V. (NL), including VITO NV (BE), S[&]T AS (NO) and TU Delft (NL).

3. HYPERSTREEGO: REACTIVE PAYLOAD

Thanks to its on-board image processing capability, HyperScout can be used as a viewfinder in the VIS-NIR for a high spatial resolution instrument, dubbed STREEGO. STREEGO is a multispectral/panchromatic (upgradable to hyperspectral) TMA instrument for small platforms developed by Medialario (I) under a GSTP contract, working the wavelength range from 450 nm to 900 nm, with GSD in the meter range and a field of view of 1.08° x 0.81°.

HyperSTREEGO concept couples the two instruments by placing a quad configuration of HyperScouts (renamed “Panorama”) in a pointing direction of 45° in front of STREEGO, which will be pointing Nadir. The idea is to use the HyperScouts to identify the cloud-free pixels and to detect real time anomalies, and then to point STREEGO on these anomalies within a minute, for higher resolution observations.

4. CHIEM: A NEW COMPACT HYPERSPECTRAL IMAGER

An Engineering Model of a new compact hyperspectral imager called CHIEM ("Compact Hyperspectral Instrument Engineering Model") has been developed under a GSTP activity. The baseline instrument design is for a satellite mission operating at 600 km, offering a swath of 100 km and a GSD of 24.4 m.

The core of this activity is the direct deposition of the LVF, made by thin film Fabry-Perot interference filters, onto the CMV 12000 detector array at wafer level, thus eliminating alignment issues of a classical LVF filter and allowing more flexible geometric filter designs. Furthermore, the direct deposition enables more pixel-precise spectral response control and the application of one spectral band over several pixels. The spectral range is from 470 nm to 900 nm, with a narrow spectral resolution (FWHM) between 5 and 10 nm. The LVF was directly deposited on front side illuminated sensors, but the deposition process was tested also on the back side illuminated ones, being a new development and higher risk but providing higher optical efficiency. The instrument development also includes the optical design of a TMA front telescope with FoV about 9.5° x 7.2° and the readout electronics (ROE), providing all required sensor interfaces (power, control, data) enabling its full performance operation.

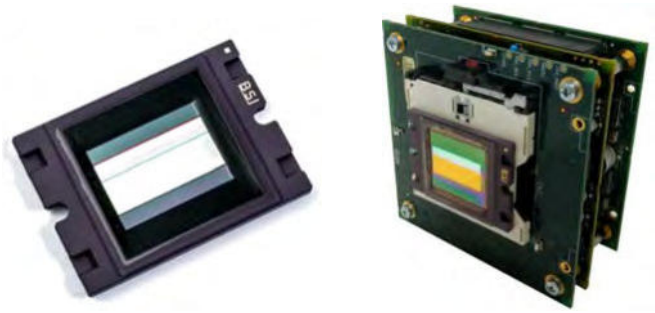

Figure 6. CHIEM hyperspectral chip (left) and ROE (right).

The GSTP follow-ups are focusing first on the improvement and characterization of the ROE and then on the production of a proto-flight version with modified characteristics (500 km altitude, 80 km swath, 20 m GSD), suitable for a 12U cubesat IOD. This PFM, named CSIMBA ("Compact Smartspectral Imager for Monitoring Bio-agricultural Areas"), will develop a smart spectral solution, consisting in on-board processing of images collected with high frame rates and digital TDI. This activity will serve as a precursor in view of a high-resolution hyperspectral satellite constellation (10-15) with a 2-3 days revisit time.

Within the GSTP programme, the CHIEM continuation activities are being developed by a Belgian consortium led by VITO, with AMOS, IMEC, ASL and DELTATEC.

5. FREE-FORM DIFFRACTION GRATING FOR HYPERSPECTRAL IMAGER

Free-form gratings (FFG) are a very promising solution to achieve compact and cost effective hyperspectral spectrometers with unprecedented SNR and spectral resolution, opening new opportunities to remote sensing from small satellites.

ESA is investigating the possibility to overcome the major limitation of such development, i.e. the availability of manufacturing techniques to realize free-form gratings, with the goal to improve the performance of grating-based hyperspectral spectrometers for various space remote sensing applications. Besides, such instruments are quite light and compact, thus simplifying the overall constraints related to a space mission.

In the frame of ESA's Technological Research Programme (TRP), two activities were kicked-off with AMOS (BE). The first one addressed the technological feasibility of a modified Offner spectrometer design, where all the optical elements, including the convex freeform grating, are built with Single Point Diamond Turning (SPDT). The target application was hyperspectral data collection of land observations, for which a spectral resolution < 2.5 nm was desired in the spectral range of 450 to 900 nm. With a diameter of 35 mm, a radius of curvature of 80 mm and a groove density of 104 lp/mm, the convex freeform grating, designed without any rotational symmetry, was manufactured by diamond machining on Nickel-plated Aluminum substrate and successfully characterized.

The goal of the second TRP activity is to build a more challenging compact spectrometer configuration with a new free-form grating with no rotational symmetry. The aim is to prove the potentialities of such a configuration for atmospheric chemistry observations in small satellites, which require high signal to noise ratio and very high spectral resolution. As for the previous study, the performance is achieved by means of the use of non-rotational symmetric substrate in a 3-mirror spectrometer (Offner-type) design.

The core of the activity is the design of the spectrometer and the manufacturing of a free-form grating with around 1000 lp/mm providing 0.5 nm / pixel spectral resolution, working in the 600-800 nm waveband. The need of such a high spatial frequency of the grooves prevents from using the SPDT manufacturing technique: the approach followed is free-form holographic replication. The spectrometer is designed to achieve high SNR (>1000), high image quality (MTF >0.5 at Nyquist), with overall low image (smile and keystone) distortion, and fitting an envelope of about 350 x 250 mm^2. The long (60 mm) slit is demagnified with 3:1.

At the time of writing, the activity was recently concluded with the manufacturing and characterization of the breadboard. Excellent imaging (MTF >50 at Nyquist), SNR (>1000) and focal plane distortion performance have been achieved, using the manufactured blazed diffraction grating with high groove count and good roughness control (~2 nm RMS) on a mild freeform substrate.

Figure 7. The Breadboard with the Freeform Grating.

The TRP activity named “Free-form diffraction Gratings and Mirrors - breadboarding” has been developed by AMOS (BE), in collaboration with Horiba Jobin-Yvon (F).

Acknowledgements

The authors are thankful to the following colleagues for their contribution on the development of the various payloads: Micael Miranda for the support to the FreeForm Grating activity and Helene Strese for CHIEM continuation activities, both from ESA TEC-MMO section; the teams of HyperScout, led by Marco Esposito from cosine; for CHIEM, led by Bavo Delauré from VITO; for the Freeform Grating, led by Vincent Moreau from AMOS.

On-Orbit Greenhouse Gas Emissions Monitoring with the GHGSat Constellation

Laura M. Bradbury[1], Michael Ligori[1], Robert Spina[1], Robert E. Zee[1], and Stephane Germain[2]

[1]Space Flight Laboratory, University of Toronto Institute for Aerospace Studies
4925 Dufferin Street, Toronto, ON, Canada, M3H 5T6
Phone: +1 416 667 7448, Mail: lbradbury@utias-sfl.net

[2]GHGSat Inc.
3981 St-Laurent, Suite 500, Montréal, QC, Canada, H2W 1Y5

Abstract: Industrial operators are increasingly motivated by regulatory imperatives to quantify their greenhouse gas (GHG) and air quality gas (AQG) emissions with the intent of ultimately reducing them. In June 2016, GHGSat-D (Claire) was launched, becoming the first high-resolution microsatellite designed to measure greenhouse gas emissions from point sources. The satellite bus was provided by the Space Flight Laboratory (SFL) under contract to GHGSat Inc. Claire measures carbon dioxide (CO_2) and methane (CH_4) emissions with a field of view of approximately 12 × 12 km and a spatial resolution of less than 50 m. To extend the service capability and as a precursor to a full constellation, GHGSat-C1 and GHGSat-C2 are the next two microsatellites under development. Bus platform modifications such as enhanced electromagnetic compatibility and hardware redundancy will result in increased performance and reliability. Enhancements to the payload include reduced stray light effects, onboard calibration capability, and additional radiation mitigation. Furthermore, the inclusion of an optical downlink will result in greater data downlink capacity. These upgrades are entirely accomplished with the same volume and power constraints as Claire. The development of GHGSat-C1 and GHGSat-C2 is currently underway and the first of the two is scheduled for launch mid-2019.

1. INTRODUCTION

The increase of atmospheric concentration of greenhouse gases (GHG), such as carbon dioxide (CO_2) and methane (CH_4), is one of the factors contributing to Earth's changing climate. Atmospheric methane has been measured from space since 2003 [1]. Utilizing novel satellite technology, GHGSat Inc. of Montréal, Canada intends to become the global leader of remote sensing of GHG, AQG, and other trace gas emissions from any source in the world. The GHGSat-D microsatellite (Claire) was a technology demonstration and proof-of-concept. It launched on June 22, 2016 at 03:56 UTC into a 512 km, 09:30 LTDN sun synchronous orbit. It is the world's first satellite designed to measure GHG emissions from point sources, such as oil and gas facilities, coal mines, landfills, and power plants. Claire has successfully collected greenhouse gas measurements from over 3000 sites around the world, and one such measurement of methane emissions from a hydroelectric dam in Africa was released publicly in early 2017 (Figure 1). The GHGSat microsatellites have a different observing strategy than other satellites on orbit with the capability of detecting carbon dioxide and methane. Whereas previous satellites have had spatial resolution on the order of kilometres, the spatial resolution of the GHGSat microsatellites is less than 50 m.

GHGSat's idea started with the implementation of carbon cap-and-trade programs in various Canadian provinces and US states [2]. Several provinces in Canada have carbon pricing systems in place; British Columbia has had a carbon tax in place since 2008, and Quebec and Ontario adopted a cap-and-trade system in 2013 and 2017, respectively.

Therefore companies are increasingly needing to answer to governmental environmental regulation regimes. The data observed by GHGSat-D is allowing organizations to manage their financial risk by allowing them to understand their emissions, which will ultimately allow for control and reduction. GHGSat-C1 and GHGSat-C2, the next two microsatellites in the GHGSat constellation, will further increase the data collection of GHG emissions around the world.

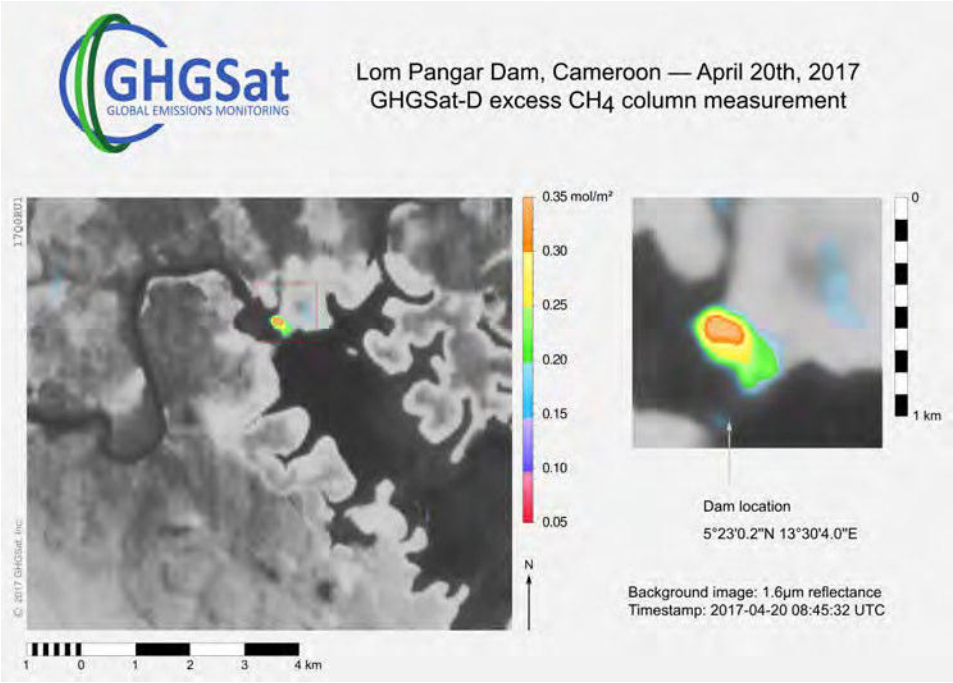

Figure 1. Methane emissions from the Lom Pangar Dam in Cameroon.

2. SATELLITE OVERVIEW

GHGSat-C1 and GHGSat-C2 are based on the Next Generation Earth Monitoring and Observation (NEMO) microsatellite platform designed by the Space Flight Laboratory (SFL) at the University of Toronto Institute for Aerospace Studies (UTIAS). The 422 × 200 × 267 mm platform is built around a robust dual-tray concept, which houses avionics in a convenient layout that facilitates rapid integration and testing. The trays are enclosed with structural panels that provide a mounting area for attitude sensors, solar cells, antennas, and any other necessary components. It supports a main payload mass of 6 kg with an overall satellite mass of 15.4 kg. The power architecture is based on SFL's Modular Power System (MPS), which generates up to 28 W of power from body-mounted, high-efficiency, triple-junction solar arrays, and uses a 12 V Lithium-ion battery for energy storage. The command and data handling architecture is based on two onboard computers, which are cross-connected to a UHF receiver, an S-band transmitter, and all other spacecraft hardware. The attitude determination and control subsystem relies on six sun sensors, a three-axis magnetometer, a rate sensor, and a star tracker for attitude determination. Attitude control is achieved through three vacuum-core magnetorquers and four reaction wheels.

3. PAYLOADS

The GHGSat-C1 and GHGSat-C2 satellites each have a single main payload onboard intended for GHG measurements. It is a Fabry-Perot imaging spectrometer operating in the short-wave infrared (SWIR) wavelengths between 1600-1700 nm, and with a spectral resolution on the order of 0.1 nm. The optical design of the instrument includes three lens groups, in addition to the Fabry-Perot interferometer, as well as beam folding mirrors required to fit the telescope within a microsatellite bus. The payload avionics include a Q7 processor provided by Xiphos Systems Corporation. GHGSat-D flew the first iteration of this payload, shown to the left in Figure 2. It has been operating successfully on-orbit for nearly three years, which has allowed GHGSat to assess the quality of the retrieved data to identify areas for improvement. These modifications have been made to the GHGSat-C1 payload (Figure 2) with the intent of improving retrievals for the planned constellation.

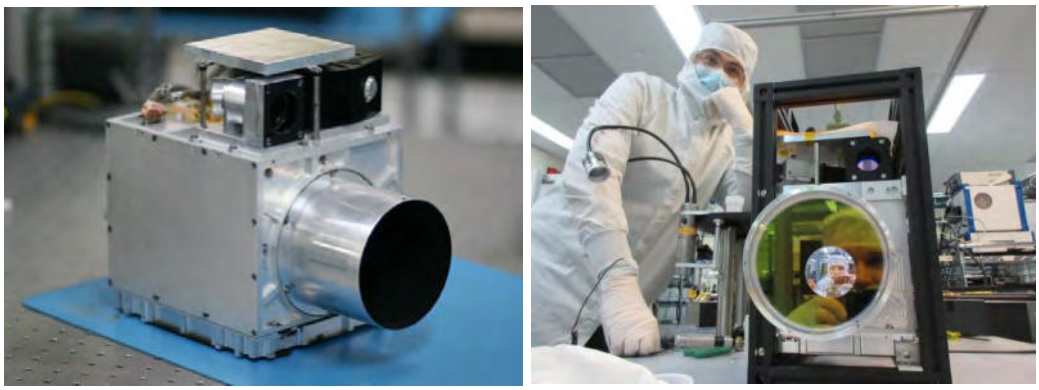

Figure 2. GHGSat-D fully integrated payload (left) and GHGSat-C1 payload (right).

3.1 Main Payload Upgrades

Several changes were made to the payload for GHGSat-C1 and GHGSat-C2 to improve upon the performance. These include upgrades to further mitigate stray light, ghosting, and radiation effects. Stray light is extra light observed by the payload which is not intended to be observed. During nominal satellite operations, it was determined that up to 5% stray light was encountered on GHGSat-D with much of that being from off-axis incoming light. To improve upon this, several elements of the optical system were redesigned. Ghosting was another effect observed on GHGSat-D, which is rotated, reflected, zoomed, or translated copies of the intended image. To reduce the effects of ghosting, anti-reflective coatings were either updated or newly applied to various surfaces in the optical system. The GHGSat-D payload restricted the incident spectral passband to a wavelength region between 1600-1700 nm, which was selected for the presence of spectral features of methane and carbon dioxide, as well as relatively little interference from other atmospheric species. However, attempting to capture both methane and carbon dioxide lines proved to be inefficient. Therefore, the passband was narrowed in order to focus on methane. Lastly, on GHGSat-D radiation in the space environment affected the detector. To help increase the lifetime of the detector, radiation shielding was introduced around the IR camera for GHGSat-C1 and GHGSat-C2.

GHGSat-D also had a cloud and aerosol camera secondary payload, which ultimately did not contribute significantly to the mission. Therefore it was replaced with a visible

light auxiliary camera, providing higher resolution imagery to improve image alignment and georeferencing.

3.2 Darkstar Optical Downlink

GHGSat-D, along with GHGSat-C1 and GHGSat-C2, have a custom-designed S-band transmitter from commercial-off-the-shelf components. The data rate and modulation can be scaled automatically during an Earth station pass from 32 kbps to 2048 kbps and the antenna system is an omnidirectional pair of patch antennas bonded to opposing satellite faces. Earth stations located at SFL in Toronto, Canada and Inuvik, Canada make contact with GHGSat-D on most orbits and monthly data volumes in excess of 7 GB are readily achieved.

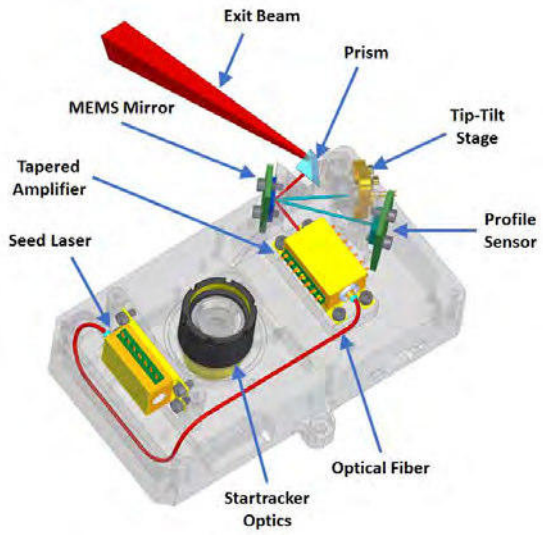

Figure 3. Darkstar internal layout [3].

In addition to the S-band transmitter, GHGSat-C1 and GHGSat-C2 are including an experimental optical downlink, "Darkstar", which is intended to achieve downlink rates of up to 1 Gbps. Designed by Sinclair Interplanetary, GHGSat-C1 will be the first satellite to fly this payload and once commissioned, will contribute significantly to the data downlink capacity. The wavelength of the laser is 785 nm, in the near-IR range. The optical downlink is built on the reverse side of the optical bench of an expanded Sinclair Interplanetary ST-16RT2 star tracker. Its mass is approximately 400 g and its outer dimensions are 100 × 68 × 68 mm. An inside view of the Darkstar is shown in Figure 3.

Darkstar interfaces with a Q8 processor designed by Xiphos Systems Corporation. The Q8 processor is a new design and is included on GHGSat-C1 and GHGSat-C2 to gain flight heritage. The Q8 interfaces with the payload avionics via an Ethernet connection for high speed data transfer. Payload data stored onboard the Q7 processor can be quickly transferred to the Q8 for downlink by Darkstar. The primary means of downlinking payload data will still initially be via the S-band transmitter, but tests and characterization of the optical downlink system will be done with the large volume of data generated by the main payload.

4. SATELLITE PLATFORM OVERVIEW

4.1 NEMO Platform

The Next Generation Earth Monitoring and Observation (NEMO) platform is SFL's first bus designed for microsatellite missions. This standard bus consists of two trays and six panels as seen in Figure 4. It supports a main payload mass of maximum 6 kg with an overall spacecraft mass ranging from 10-20 kg depending on secondary payloads and optional SFL avionics required to meet current and future missions.

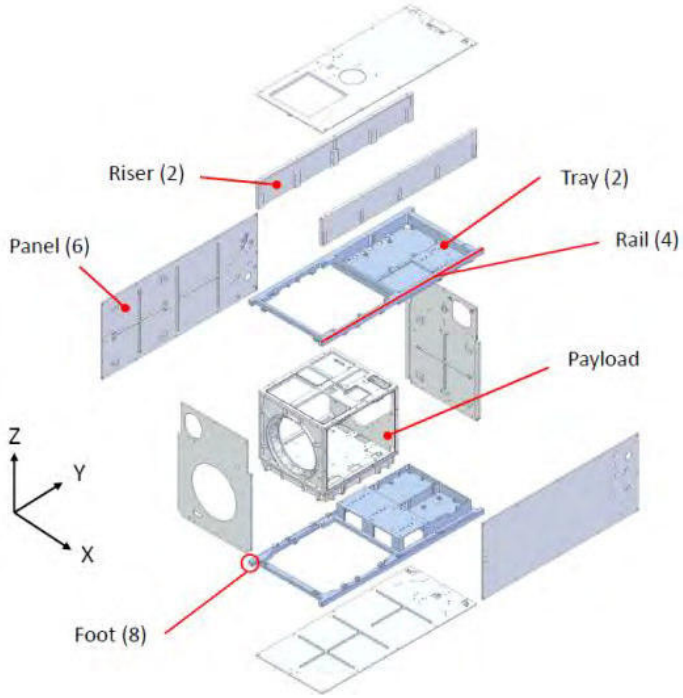

Figure 4. GHGSat-D structure exploded view.

The nominal volume is 20 × 30 × 40 cm with a peak power between 50-100 W. Higher power is achieved through optional pre-deployed solar wings. The bus design supports a main payload of volume 8000 cm^3 with a payload power of up to 45 W and 40% duty cycle.

The NEMO platform supports various attitude control system (ACS) sensors and actuators including sun sensors, magnetometer, rate sensor, magnetorquers, and reaction wheels. This allows for 2σ pointing accuracy with approximately 2° in sunlight and 5° in eclipse. When missions demands are higher, a star tracker can be used which increases ACS stability to about 10-60 arc seconds. Orbital position and velocity measurements are sampled by a GPS receiver and antenna.

The platform for GHGSat-C1 and GHGSat-C2 uses an UHF uplink and S-band downlink. A UHF receiver is used to provide the uplink channel at a fixed data rate of 4 kbps. The downlink is controlled by an S-band transmitter where the data rate can be scaled on-the-fly from 32 kbps to 2048 kbps with either BPSK or QPSK modulation and 0.5 rate convolutional encoding. If required by the mission, the NEMO platform can be further enhanced to use an S-band uplink.

Depending on deployed appendages, the NEMO platform is compatible with two SFL separation systems, which are the XPOD Duo and XPOD Delta. These separation systems are compatible with virtually any launch vehicle.

4.2 Improvements for GHGSat-C1/C2

The mechanical design of GHGSat-C1 and GHGSat-C2 has been constrained to match the design of GHGSat-D as closely as possible. Changes were made due to upgrades in SFL hardware, updates to the primary payload, addition of new payloads, and to mitigate electromagnetic interference (EMI). The satellite exterior solid model is shown in Figure 5.

Figure 5. GHGSat-C1/C2 exterior solid model.

4.2.1 SFL Hardware Upgrades

Several updates to the S-band transmitter have been implemented across all NEMO-class satellites to enhance performance. Coaxial cables with improved shielding were added. These cables offer reduced insertion loss and, along with the higher power S-band transmitter that has been baselined, will increase the transmit gain allowing for increases in data transfer using just S-band communication. These improvements have been proven during on-orbit testing of other SFL satellites.

A fourth reaction wheel has been added for redundancy, shown in Figure 6. It uses a skew orientation where it has control authority in all three of the principal spacecraft axes and thus can act as a backup. Although it is nominally a cold spare for redundancy, it can also be turned on to assist with avoiding zero-crossings during imaging since pointing accuracy is significantly affected at low wheel speeds. In a three reaction wheel configuration, the desired control torque and the individual wheel actuation is mapped one-to-one. With a fourth wheel, the control torque can be distributed to the wheels in a number of ways. This is useful as the torque can be distributed in order to drive the wheel speeds to a desired value and avoid zero-crossings.

Figure 6. Configuration of the four reaction wheels.

A permanent magnet has also been included to ensure positive power margin in Safehold operations. The payload face has no solar cells and therefore if it becomes locked in an attitude that faces the Sun the satellite would be power negative until the attitude is changed. The magnet was sized to impart a permanent dipole to the satellite which interacts with Earth's magnetic field inducing a torque that prevents it from getting stuck in the sun-stare attitude. Figure 7 shows the average Safehold power generation of the satellite over a number of orbits for different Y-axis dipole values, as compared to the power needed for Safehold operations. A dipole of 0.125 Am^2 was selected as it forces the satellite out of inertial lock in less than two orbits and has minimal impact on pointing performance.

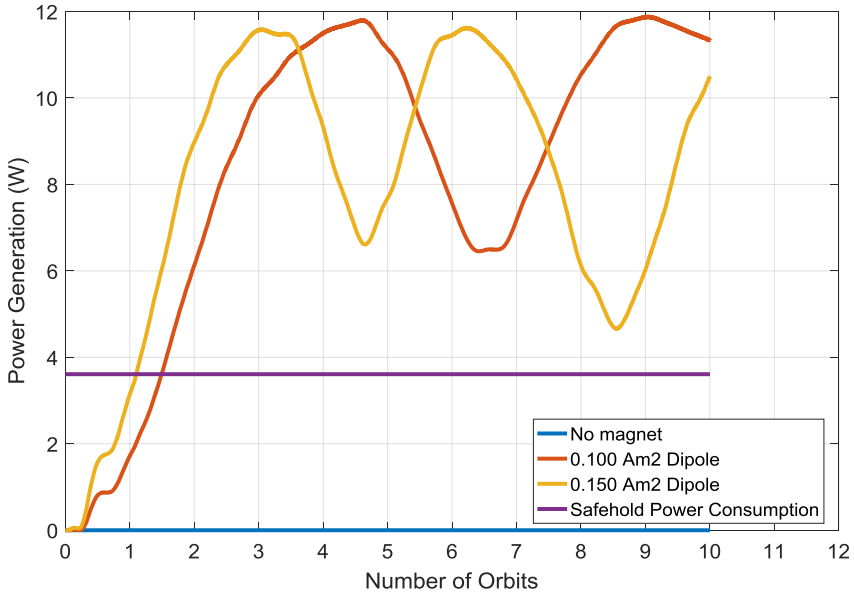

Figure 7. Average satellite power generation for various dipoles along the Y-axis in a payload face sun stare attitude.

4.2.2 Addition of New Payloads

The addition of Darkstar has resulted in several changes to the GHGSat-C1 and GHGSat-C2 satellites. A new bracket needed to be designed to simultaneously ensure that the laser downlink had adequate line-of-sight to its ground station while maintaining a sufficient star tracker viewing angle to prevent impingement from the Sun or Earth in nominal operations. A much larger cutout in the panel was required to accommodate this and a split panel design was implemented to facilitate both reducing the EMI sensitivity and ease of assembly as seen in Figure 8. By installing each part of the panel around Darkstar the actual size of the panel cutout was minimized, reducing the effect of EMI on the satellite avionics.

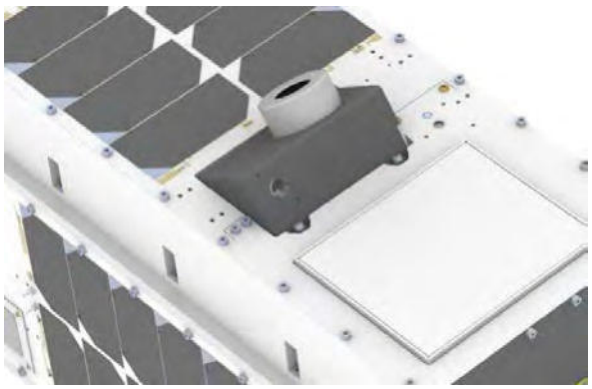

Figure 8. Split panel design to accommodate Darkstar.

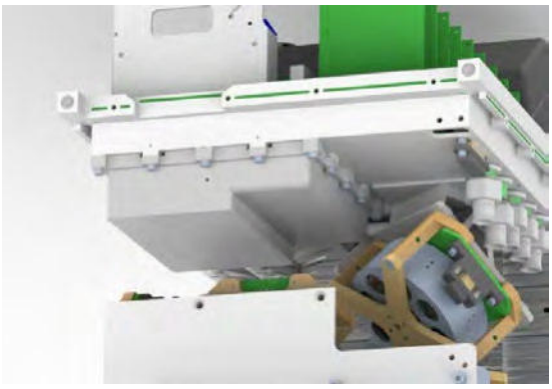

Figure 9. Q8 processor enclosure.

Due to frequency conflicts between the Q8 high-speed data transfer connection and other spacecraft components it was necessary to contain the board within an enclosure and shield the associated cabling to prevent undesired interferences. The addition of this payload posed some challenges because of extremely tight clearances especially with moving components such as the reaction wheels. The enclosure placement within the bus can be seen in Figure 9.

4.2.3 EMI Sensitivity Reduction

To further improve uplink sensitivity of the bus EMI gaskets were added to the primary satellite panels. Adjustments to the panel-to-panel and panel-to-tray interfaces were required to ensure there was sufficient material present for the gasket cutouts. Additionally, EMI gaskets were added to the UHF enclosure, as shown in Figure 10.

Figure 10. EMI gaskets for UHF receiver (shown in red) and the panel-tray (shown in green.)

5. CURRENT STATUS & FUTURE CONSTELLATION PLANS

The second and third GHGSat microsatellites will assure continuity of observations and expand GHGSat's customer capacity. GHGSat-C1 is currently assembled (Figure 11) and is proceeding with system-level and environmental testing. It is scheduled to launch in September 2019 into a 515 km 10:30 LTDN sun synchronous orbit. More satellites will enable more frequent tracking of sites. GHGSat-C1 and GHGSat-C2 are the first two satellites in a planned constellation of 10 GHG monitoring satellites.

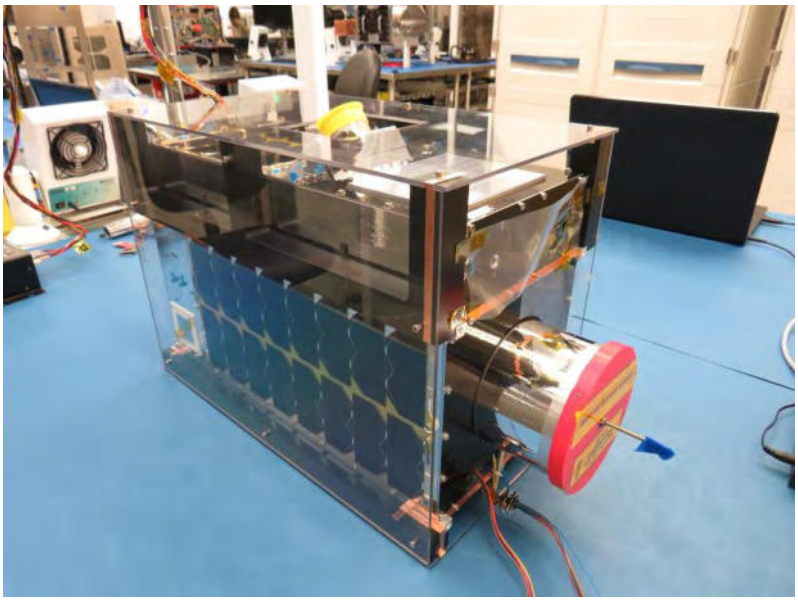

Figure 11. Fully assembled GHGSat-C1 satellite in the SFL cleanroom.

6. CONCLUSION

GHGSat-C1 and GHGSat-C2 will assure continuity of observations and will expand GHGSat's customer capacity. More satellites will enable more frequent tracking of sites. GHGSat-C1 and GHGSat-C2 are the first two microsatellites in a planned constellation of GHG monitoring satellites. The improvements made to both the payload and satellite bus will improve the retrievals and in turn, allow for better tracking of industrial GHG emissions.

7. REFERENCES

[1] D. J. Jacob, A. J. Turner, J. D. Maasakkers, J. Sheng, K. Sun, X. Liu, K. Chance, I. Aben, J. McKeever, and C. Frankenberg, "Satellite observations of atmospheric methane and their value for quantifying methane emissions," *Atmospheric Chemistry and Physics*, vol. 16, pp. 14371-14396, 2016.

[2] S. Germain, B. Durak, J. McKeever, V. Latendresse, C. Grant, and J. J. Sloan, "Global Monitoring of Greenhouse Gas Emissions," in Proc. 30th Annual AIAA/USU Conference on Small Satellites, 2016.

[3] D. Sinclair and K. Riesing, "The Rainbow Connection – Why Now is the Time for Smallsat Optical Downlinks," in Proc. 31st Annual AIAA/USU Conference on Small Satellites, 2017.

PRETTY- A Passive Reflectometry and Dosimetry Mission Using a 3U CubeSat

Otto Koudelka, M3[1], M.Wenger[1], A.Hörmer[1], R.Zeif[1],
H.Fragner[2], A.Dielacher[2], M.Moritsch[2]
P.Beck[3], C. Tscherne[3], M.Wind[3]
R.Walker[4] , M.Martin-Neira[4], Franco Perez-Lissi[4]

[1]Graz University of Technology, Institute of Communication Networks and Satellite Communications
Inffeldgasse 12, 8010 Graz, Austria
Phone: +43 316 873-7440, Mail: koudelka@tugraz.at

[2]RUAG Space GmbH
Stachegasse 16, 1120 Vienna, Austria
Phone: +43 1 801995526, heinrich.fragner@ruag.com

[3]Seibersdorf Labor GmbH
2444 Seibersdorf, Austria
Phone: +43 50 550 4305, peter.beck@seibersdorf-laboratories.at

[4]European Space Agency, ESTEC
Keplerlaan 1, NL2200Ag Noordwijk, The Netheralnds
Phone: +31 71 5656565, Mail: roger.walker@esa.int, manuel.martin-neira@esa.int, franco.perez-lissi@esa.int

Abstract: The PRETTY (Passive REflectomeTry and DosimeTrY) nanosatellite mission has the objective to demonstrate and validate passive reflectometry in space. PRETTY includes a demonstrator payload for passive reflectometry focusing on very low elevation angles, whereby the direct and reflected signal from a GNSS satellite will be received via the same antenna. Furthermore, a novel dosimeter payload for measuring the space radiation environment during the PRETTY space mission will be on board. The hardware platform is composed of a software-defined radio front-end and a powerful system-on-chip processor with a large FPGA providing sufficient resources for the implementation of the correlating receiver. The altimeter will be used to survey i.e. the height of sea waves and may thus contribute to climate research using a small and low-cost nanosatellite. PRETTY will be a 3U CubeSat with deployable solar arrays to provide up to 24 W effective power. A novel ADCS system with horizon detectors and four reaction wheels is expected to provide a pointing accuracy of 1 deg. which was found to be required to satisfy the scientific requirements. The paper describes the system architecture, provides details of the passive reflectometer and the dosimeter payloads as well as operations of the spacecraft from a low-cost tracking station.

1. INTRODUCTION

The exploitation of signals stemming from global navigation systems has been proposed and implemented within numerous studies. The fact that such missions do not rely on high power amplifiers, nor on high-gain antennas with large geometrical dimensions, make them ideally suitable for small satellite missions. Applications where a continuous high coverage is needed, i.e. disaster warning, demand a high number of satellites in orbit, which in turn requires small and low-cost satellites. The PRETTY (Passive REflectomeTry and DosimeTrY) nanosatellite mission shall demonstrate and validate interferometric passive reflectometry in space. It was proposed to ESA in the framework of the Austrian CubeSat competition. A Phase A/B contract was completed by a consortium composed of RUAG Space Austria as Prime Contractor and Graz University of Technology and Seibersdorf Laboratories as subcontractors. PRETTY includes a de-

monstrator payload for passive reflectometry focusing on very low elevation angles, whereby the direct and reflected signal from a GNSS satellite will be received via the same antenna. The correlation of both signals will be done by a specific FPGA-based hardware implementation. The demonstration of a passive reflectometer without the use of local code replicas implicitly shows that also signals of unknown data modulation can be exploited for such a purpose. RUAG and TU Graz proved the feasibility of the passive reflectometry approach in the framework of the Austrian Aeronautics and Space Applications Program. Furthermore, Seibersdorf Laboratories designed a novel dosimeter payload for measuring the space radiation environment during the PRETTY space mission. The dosimeter system will assess total ionizing dose (TID) by the use of radiation integrating sensors, as well as LET (linear energy transfer) spectral information, which is related to single-event effects (SEE) in electronic components. PRETTY will determine the total mission dose as well as dose rates in regions with naturally elevated radiation levels, such as the polar regions and the South Atlantic Anomaly (SAA).

The hardware platform is composed of a software-defined radio front-end and a powerful system-on-chip processor with a large FPGA providing sufficient resources for the implementation of the correlating receiver. This platform was developed by TU Graz and will be flown first on the ESA nanosatellite mission OPS-SAT. An improved variant with a flat-panel GNSS antenna tailored for the altimetry mission is currently under development.

The concept of passive reflectometry is to compare direct incident signals from such spacecraft with the same signals reflected from earth or ocean surface. Typically, GNSS spacecraft have an orbit of about 20.000 km while a passive reflectometry instrument would be placed in Low-Earth Orbit (LEO), typically below 600 km.
Study and early demonstrator results show that there can be substantial information extracted from the correlation of the direct and indirect microwave beam. Surface conditions like wave structure on oceans as well as atmospheric conditions can be deduced by the scientists.

Within several previous ESA projects the development of such a passive reflectometry instrument was fostered by performing studies and conducting airborne demonstration campaigns. In particular an application-specific hardware processing core was developed under supervision of ESA in the framework of the PARIS correlator project [1]. In the GEROS ISS Phase A study the necessary considerations to integrate the digital processing platform within the complete instrument on board of the ISS were done [2]. Nevertheless, there are certain aspects which are different with respect to an instrument flying on-board the ISS to an instrument flying on a Cubesat. In particular the antenna performance and processing power will be less on a Cubesat than the ISS GEROS instrument, but on the other hand the visibility of observations will not be compromised by the ISS structure.The altimeter will be used to survey i.e. sea ice height and the height of sea waves and may thus contribute to climate research using a small and low-cost nanosatellite.

In the course of the Phase B study of the PRETTY project, the concept of the dosimeter payload was substantially extended. The novel dosimeter payload will use two different integrating sensor technologies for total ionizing dose (TID) assessment: A RADFET, a discrete p-channel MOSFET optimized for radiation sensitivity and an FGDOS, a float-

ing gate dosimeter. Both sensors will be installed on board the PRETTY satellite in an unshielded and a shielded configuration. A comparison of shielded and un-shielded devices is used to discriminate dose contribution from electrons against the contribution from protons (=non-electrons). The RADFET will be used to measure the accumulated dose over the full mission. A maximum total dose of 1 kGy (100 krad) is taken into account. The FGDOS will be used to measure doses in regions with elevated radiation levels. Due to its low minimal detectable dose of 200 µGy (20 mrad), measurements in 1 - 10 min intervals will be possible. Short measurement intervals correlate with high spatial resolution. Thus, the measurements can provide a dose rate map of the orbit as function of time and space. Another improvement of the dosimeter is the implementation of a LET spectrometer allowing an energy-dependent spectral analysis of the space radiation environment. The derived linear energy transfer spectrum allows the assessment of single event effects (SEE), caused by single energetic particles that lead to a broad spectrum of soft to fatal errors in electronic devices. During Phase B the concepts of using a single PIN diode was investigated and compared to a design using a telescope. The angular dependency of the LET by a single particle due to geometry of the p-n barrier has been investigated by simulations using Monte Carlo codes. From the simulation results we concluded that a single PIN diode has significant advantages vis-à-vis a telescope design.

2. ARCHITECTURE

The satellite bus consists of two GomSpace Nanomind on-board computers, a NanoCom UHF transceiver as backup telemetry, an S-band transceiver as the primary telemetry which will be able to provide a downlink data rate of up to 2 Mbit/s. The EPS (electric power subsystem) supports solar cells, mounted on two double-folded solar arrays and solar cells mounted on the satellite body. The effective maximum available power is 24 W. Redundant Li-Ion batteries with battery charge and discharge regulators provide power in eclipse phases and when the payload draws more power than the solar cells deliver. The first Nanomind computer acts as the OBC (on-board computer), while the second Nanomind is responsible for attitude determination and control (ADCS). Sun sensors on all six panels of the satellite, a three-axis magnetometer, a gyro and a new horizon detector comprise the sensor system. The actuators consist of three magnetorquers and four momentum wheels provided by Astrofein.

The payload section houses two experiments, the altimeter and the dosimeter. The altimeter has two parts: two Satellite Experiment Payload Processors (SEPP) in cold redundancy and a software-defined radio (SDR) front-end. The SEPP is based on an ALTERA Cyclone-V system-on-module with two ARM-9 processors and a large field-programmable array (FPGA). The SDR covers the L1 GNSS frequency with a bandwidth of 20 MHz. The front-end which includes a low-noise amplifier is connected to an antenna with 8 patches providing a gain of about 16 dB. This hardware was developed by TU Graz. The firmware for the correlation receiver is a development by RUAG Space Austria. Fig.1 depicts the 3D drawing of PRETTY.

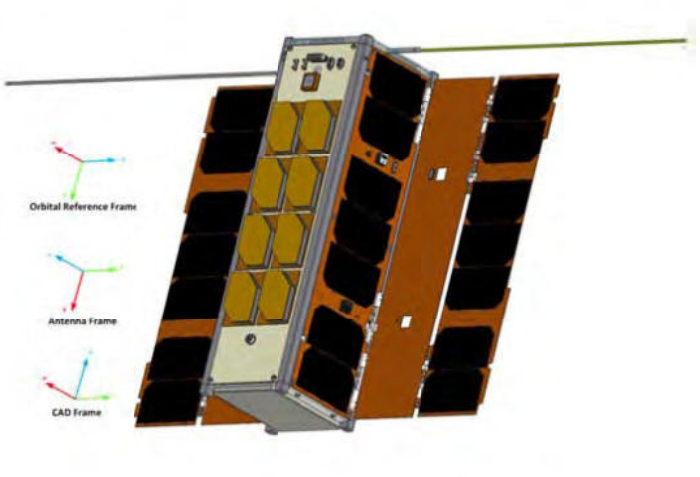

Fig.1: PRETTY Spacecraft and Reference Frame

3. EXPERIMENTATION

The current implementation of the reflection point algorithm shows that on-board calculation of the reflection points without the need for on-ground processing is feasible.
Considering the Orbital Reference Frame (Fig.1), where the velocity direction is in the x-axis and z directs toward nadir, we determine the position of the reflection points. Most of the reflection points are within +/-45 degree (i.e. rising and settling satellites). The longest reflection point tracks can be found at around 90 degree (i.e. perpendicular to the flight direction) A trade-off between numbers of measurements, battery DoD and data volume has to be made. Each measurement has a duration of about 20 ms, hence 50 measurements per second, with a data packet size of 64 kbit leading to a data volume of 400 kbyte per second. Since the ground station is only visible for about 30 min per day, this amount of data cannot be stored nor downloaded in time. Also the thermal design of the payload does not allow continuous operation. Therefore the payload needs to be operated with a duty-cycle of around 30%. The nominal operation time is during eclipse in order to reduce disturbances due to ionospheric charging.
The dosimeter payload will feature a customizable integration time for the dose-integrating radiation sensors RADFET and FGDOS, as well as for the LET spectrometer, selectable from ground between 1 and 10 minutes. The operation of the dosimeter payload during flight is autonomous. The dosimeter payload stores data in a flash memory and sends data upon request by the satellite experimental processing platform (SEPP) which is then downlinked to the ground station. The estimated data size for the dosimeter payload is 1 MB per day.

4. REFERENCES

[1] Martin-Neira, M., “A Passive Reflectometry and Interferometry System (PARIS): Application to ocean altimetry”. ESA Journal, vol. 17, pp. 331–355, Dec. 1993.

[2] Wickert, J. et al., “GEROS-ISS: GNSS Reflectometry, Radio Occultation, and Scatterometry Onboard the International Space Station”, IEEE Journal of Selected Topics in Applied Earth Observations and Remote Sensing, Vol.9, No. 10, pp. 4552-4581, Oct. 2016. doi: 10.1109/JSTARS.2016.2614428

Measuring Earth's Energy Budget from a CubeSat

William H. Swartz[1], Steven R. Lorentz[2], Philip M. Huang[1]

[1]Johns Hopkins University Applied Physics Laboratory
11100 Johns Hopkins Road, Laurel, Maryland 20723, USA
Phone: +1 240 228 8462, Mail: bill.swartz@jhuapl.edu

[2]L-1 Standards and Technology
10364 Battleview Parkway, Manassas, Virginia 20109, USA
Phone: +1 571 428 2227, Mail: lorentz@l-1.biz

Abstract: Measuring Earth's energy budget from space is an essential ingredient for understanding and predicting climate. Observational requirements to achieve climate accuracy and continuity with existing datasets drive cost and define measurement approaches. The Radiometer Assessment using Vertically Aligned Nanotubes (RAVAN) 3U CubeSat mission is a pathfinder that demonstrates technologies for the measurement of Earth's radiation budget. RAVAN collected data in orbit for over 20 months, successfully demonstrating the use of vertically aligned carbon nanotubes (VACNTs) as absorbers in broadband radiometers for measuring Earth's outgoing radiation and the total solar irradiance and a pair of gallium phase-change black body cells that are used as a stable reference to monitor the degradation of RAVAN's radiometer sensors. Four radiometers (two VACNT, two cavity) show excellent long-term stability over the course of the mission and a high correlation between the VACNT and cavity radiometer technologies. Short-term variability is a challenge to climate accuracy that remains, consistent with insufficient thermal knowledge and control on a CubeSat. This paper includes details of the in-space validation and efforts to evaluate the applicability of the RAVAN CubeSat as a whole to measurement of Earth's energy budget, such as short- and long-term stability and comparison with independent spaceborne measurements.

1. INTRODUCTION

Future climate change is driven by changes in Earth's global energy budget resulting from a very small yet important imbalance between the incoming solar energy reaching the Earth and the outgoing solar-reflected and thermally emitted energy [1, 2, 3]. Current research suggests that the imbalance is about +1 out of 340 W/m^2 on an annual global mean basis (meaning that the outgoing energy is less than the incoming solar energy by about 0.3%), due to the net effect of anthropogenic emissions of greenhouse gases and aerosols [4]. The absolute accuracy of our current best satellite-based estimates of the radiation imbalance is several W/m^2, limited by both absolute calibration and sampling of Earth's outgoing radiation [5]—not good enough to resolve the imbalance. The needed climate accuracy is on the order of tenths of a W/m^2 (or about 0.1% of the roughly 340 W/m^2 outgoing radiation signal). As a next-generation Earth radiation budget (ERB) concept, *Wiscombe and Chiu* proposed a space-based constellation of sensors that would be able to overcome the sampling limitations and provide global, diurnal measurements [6]. *Gristey et al.* showed how a notional ERB constellation of wide field-of-view (WFOV) broadband radiometers could recover both spatial and temporal information [7].

The Radiometer Assessment using Vertically Aligned Nanotubes (RAVAN) CubeSat project is a technology demonstration to prove two technologies that could enable an ERB constellation and/or play a role in the next generation of ERB measurement technologies: radiometers with vertically aligned carbon nanotube (VACNT) absorbers and gallium black body phase-transition calibration sources [8–11]. Carbon nanotubes are an allotrope of carbon that, at a microscopic level, are essentially long, hollow graphene

cylinders. These nanostructures have a number of unusual properties that make them ideal for certain applications. VACNT "forests" are some of the lowest-reflectivity ("blackest") materials known and have an extremely flat spectral response over a wide wavelength range. The second key technology is the gallium calibration source. Two gallium fixed-point black bodies serve as on-orbit infrared sources that, when coupled with deep space looks, provide an additional means to determine the radiometer gains. We use the gallium solid–liquid phase transition (29.76°C) as a stable, repeatable reference for the black body emission to track the long-term degradation of the radiometers.

2. CUBESAT PAYLOAD

The basic design concept is to treat Earth outgoing radiation as a simple irradiance measurement, employing thermal detectors with a black and spectrally flat absorber and precision aperture. For RAVAN this resulted in a set of four broadband radiometers with both VACNTs (primary pair) and traditional black-painted cavities (secondary pair) as radiometer absorbers. The primary advantages of VACNTs are their better inherent blackness, better sensitivity for a given time constant, and compactness. Each radiometer pair includes a total (Total) channel whose spectral band is set by the absorber and is sensitive to nearly all Earth outgoing radiation, from the ultraviolet to the far infrared, and a shortwave (SW) channel whose band is limited by a sapphire dome, nominally sensing reflected solar radiation. The radiometers are actively temperature controlled and thermally isolated from the spacecraft. Two reusable doors each contain a gallium reference source and open wide enough to clear the 135° fields of view of the radiometers and close to protect the radiometers when they are not being used, having a locking feature for storage and launch. Custom radiation-tolerant electronics control the payload, collect data, and communicate with the spacecraft. The RAVAN payload flies on a 3U CubeSat built by Blue Canyon Technologies (Boulder, Colorado, USA).

3. IN-SPACE VALIDATION

Launched in November 2016, the RAVAN payload collected data for 20 months (the spacecraft is still operating as of this writing, with the payload powered off). The largest obstacle to operations was local UHF ground interference at 450 MHz, which made continuous operations as designed impossible. Fortunately, this did not limit the primary technology demonstration.

Calibration of the RAVAN radiometers was achieved on orbit with periodic observations of dark space (for offsets) and the Sun (for absolute scale). Prerequisites for well-behaved ERB measurements are stable or smoothly varying offsets and gains. The long-term behavior was excellent, with the VACNT Total and SW channels changing smoothly by less than 0.4% and 0.5% over the course of the project, respectively. The heater gains were stable for both channels at less than a few tenths of a percent. Measurements of the total solar irradiance (solar views) were stable and also varied by only a few tenths of a percent. A similar assessment of stability can be found from the gallium black body calibrations. Over the course of the entire project, the cavity radiometer signal slowly changed by less than 2.5%, as shown in Figure 1. Based on the presumption that the gallium black body transitions occurred at an invariant temperature of the melting point of pure gallium and that the black body emissivity remained constant, changes in the infrared measurements from one phase transition to the next is taken to be the variability

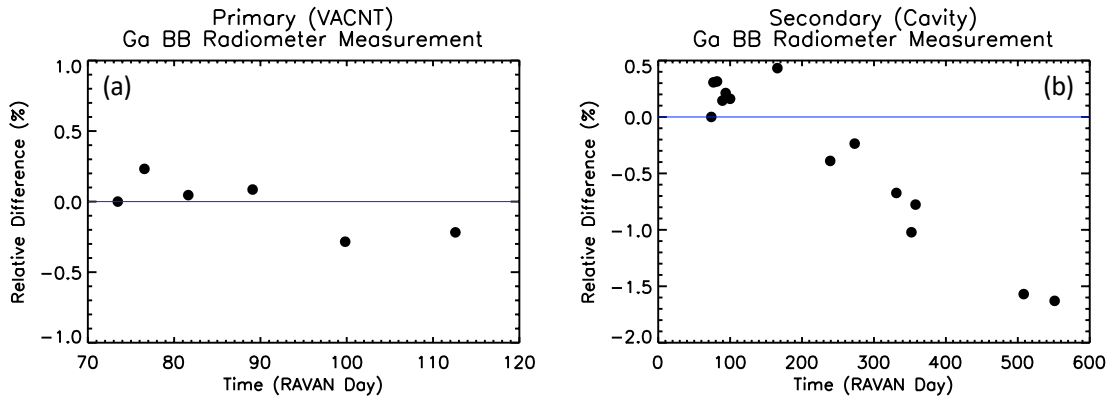

Figure 1. Relative changes in (a) VACNT and (b) cavity radiometer Total channel response to gallium black body melts as a function of days since RAVAN launch (11 November 2016) [11, adapted from Figure 14]. Note that the black body associated with the primary (VACNT) radiometer failed in March 2017.

of the radiometer itself. The black body associated with the primary (VACNT) radiometer failed in March 2017, but the other black body continued to operate throughout the entire mission. The observed change in signal, if from the radiometer, could have resulted from changes in the radiometer offsets. Although RAVAN had excellent long-term stability, its shorter-term variability, however, may be a challenge for measurements at the level ultimately required for "climate accuracy" (~0.1%).

Inter-calibration of the VACNT- and cavity-based radiometers viewing the Earth shown in Figure 2 have overall good correlation between the new and "old" technologies, with r^2 values exceeding 0.99 for the Total and SW channels. Linear fits of the comparisons indicate that on average, the VACNT Total channel was about 3% higher than the cavity Total; the VACNT SW channel was about 6% higher than the cavity SW. These biases are larger than the 0.1% goal.

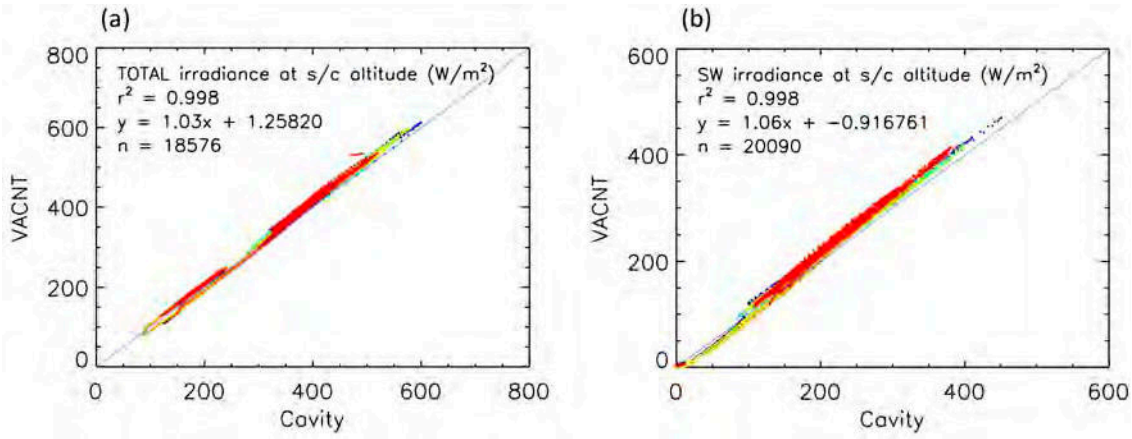

Figure 2. Radiometer intercomparison for the (a) Total and (b) SW channels [11, adapted from Figure 18]. Linear fits forced through the origin are indicated. Data between RAVAN days 200 and 400 are shown, focusing on the period of greatest calibration stability. The data points are color-coded by time, with earlier times more blue and later times more red.

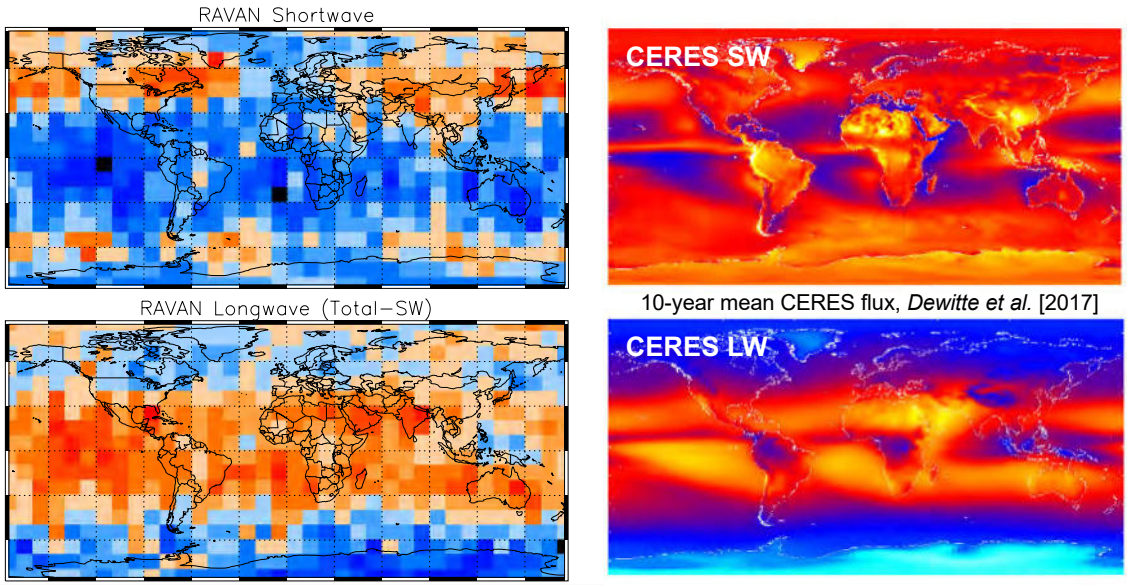

Figure 3. Earth outgoing flux measurements from space. (Left) RAVAN Earth outgoing flux measurements (at spacecraft altitude) for the SW and longwave (Total–SW), binned into a 10° × 10° latitude–longitude geographic grid for the entire mission. (Right) Analogous SW and longwave top-of-the-atmosphere flux (at 20 km) from a 10-year mean of CERES Energy Balanced And Filled (EBAF) data [12, adapted from Figures 4 and 5].

RAVAN was designed to measure Earth outgoing radiation continuously, apart from calibration maneuvers, and our original plan was to compare global monthly mean values of outgoing radiation with that derived from the Clouds and the Earth's Radiant Energy System (CERES) instruments. However, due to downlink constraints and other limitations, the RAVAN dataset is episodic, and simple quantitative monthly mean comparisons are not possible. As a preliminary attempt at CERES comparison—more qualitative in nature—we binned the entire RAVAN nadir irradiance dataset into a 10° × 10° latitude–longitude geographic grid, irrespective of month. The results are shown in Figure 3. The RAVAN data are not continuous, so there is temporal aliasing, but despite this limitation there is qualitative agreement between RAVAN and CERES, showing similar latitudinal and even longitudinal patterns.

4. CONCLUSIONS

The RAVAN project successfully demonstrated the use of vertically aligned carbon nanotubes as broadband radiometer absorbers and gallium phase-change black body cells on a 3U CubeSat, launched November 2016. RAVAN made periodic observations of the Earth outgoing irradiance, the Sun, and deep space, with its four radiometers: Total and shortwave channels based on VACNT and cavity absorber technologies. In addition, RAVAN also employed observations of its internal gallium black bodies to monitor long-term radiometer drift. Apart from the failure of one of the gallium black bodies after four months, the payload worked well and proved to be radiation-tolerant; technical difficulties associated with the CubeSat bus could be resolved straightforwardly in a future mission.

Beyond the technology demonstration, RAVAN represents a benchmark for making Earth radiation budget measurements from a CubeSat. RAVAN had excellent long-term

stability; shorter-term variability may be a challenge for measurements at the level required for climate accuracy, on the order of tenths of a W/m^2 (or about 0.1% of the roughly 340 W/m^2 Earth outgoing radiation signal). The short-term variability is not unlike the results from the Earth Radiation Budget Experiment (ERBE) nonscanner, which was ultimately limited by insufficient thermal knowledge and control [13].

Broadband observations from a RAVAN-like platform or its underlying technologies may be a part of the solution to the sustainable ERB challenge. For example, RAVAN technologies enable a constellation mission (either small satellite or hosted payload). The results from RAVAN, while not at the level required for climate measurements, are an important step for the development of science-grade ERB instruments on small satellite platforms.

5. ACKNOWLEDGMENTS

RAVAN was funded by NASA's Earth Science Technology Office, through its In-Space Validation of Earth Science Technologies (InVEST) program, via NASA grant NNX13AM53G, with subsequent analysis through the Rapid Response and Novel Research in Earth Science program, NASA grant 80NSSC18K1523.

6. REFERENCES

[1] K. E. Trenberth and J. T. Fasullo, Tracking Earth's energy, Science, 328, 316–317, doi: 10.1126/science.1187272 (2010)

[2] J. Hansen, et al., Earth's energy imbalance and implications, Atmospheric Chemistry and Physics, 11, 13,421–13,449, doi:10.5194/acp-11-13421-2011 (2011)

[3] K. von Schuckmann, M. D. Palmer, K. E. Trenberth, A. Cazenave, D. Chambers, N. Champollion, J. Hansen, S. A. Josey, N. Loeb, P.-P. Mathieu, B. Meyssignac, and M. Wild, An imperative to monitor Earth's energy imbalance, Nature Clim. Change, 6, 138–144, doi:10.1038/NCLIMATE2876 (2016)

[4] K. E. Trenberth, J. T. Fasullo, and J. Kiehl, Earth's global energy budget, Bull. Amer. Meteorol. Soc., 311–324 (2009)

[5] N. G. Loeb, B. A. Wielicki, T. Wong, and P. A. Parker, Impact of data gaps on satellite broadband radiation records, J. Geophys. Res., 114, D11109, doi:10.1029/2008JD011183 (2009)

[6] W. Wiscombe and C. Chiu, The next step in Earth radiation budget measurements, in Radiation Processes in the Atmosphere and Ocean (IRS2012), AIP Conf. Proc. 1531, 648–651 (2013)

[7] J. J. Gristey, J. C. Chiu, R. J. Gurney, S.-C. Han, and C. J. Morcrette, Determination of global Earth outgoing radiation at high temporal resolution using a theoretical constellation of satellites, J. Geophys. Res., 122, 1114–1131 (2017)

[8] W. H. Swartz, L. P. Dyrud, S. R. Lorentz, D. L. Wu, W. J. Wiscombe, S. J. Papadakis, P. M. Huang, E. L. Reynolds, A. Smith, and D. M. Deglau, The RAVAN CubeSat mission: Advancing technologies for climate observation, Geoscience and Remote Sensing Symposium (IGARSS), 2015 IEEE International, 5300–5303, doi:10.1109/IGARSS.2015.7327031 (2015)

[9] W. H. Swartz, S. R. Lorentz, P. M. Huang, A. W. Smith, J. Carvo, D. M. Deglau, E. L. Reynolds, S. J. Papadakis, and D. L. Wu, The RAVAN CubeSat mission: A pathfinder for a new measurement of Earth's energy budget, Proc. 11th IAA Symposium on Small Satellites for Earth Observation, Berlin, Germany, April 24–28 (2017)

[10] W. H. Swartz, P. M. Huang, E. L. Reynolds, S. R. Lorentz, A. W. Smith, J. Briscoe, J. Carvo, and D. L. Wu, RAVAN CubeSat results: Technologies and science demonstrated on orbit, Proc. 31th Annual AIAA/USU Conference on Small Satellites, SSC17-X-07 (2017)

[11] W. H. Swartz, S. R. Lorentz, S. J. Papadakis, P. M. Huang, A. W. Smith, D. M. Deglau, Y. Yu, S. M. Reilly, N. M. Reilly, and D. E. Anderson, RAVAN: CubeSat demonstration for multi-point Earth radiation budget measurements, Remote Sens., 11, 796, doi:10.3390/rs11070796 (2019)

[12] S. Dewitte and N. Clerbaux, Measurement of the Earth radiation budget at the top of the atmosphere—A review, Remote Sensing, 9, 1143–1155, doi:10.3390/rs9111143 (2017)

[13] T. Wong, G. L. Smith, S. Kato, N. G. Loeb, G. Kopp, and A. K. Shrestha, On the lessons learned from the operations of the ERBE nonscanner instrument in space and the production of the nonscanner TOA radiation budget data set, IEEE Trans. Geosci. Remote Sens., 56, 5936–5947 (2018)

CHAFF: CubeSat Hyperspectral Application For Farming

Callum Middleton[1], Craig Underwood[1]
Emma Woolliams[2], Chris Bridges[1] and Nigel Fox[2]

[1]Surrey Space Centre,
University of Surrey, Guildford, Surrey, GU2 7XH, UK
Mail: c.j.middleton@surrey.ac.uk; c.underwood@surrey.ac.uk; c.p.bridges@surrey.ac.uk

[2]National Physical Laboratory,
Hampton Road, Teddington, Middlesex, TW11 0LW, UK
Mail: emma.woolliams@npl.co.uk; nigel.fox@npl.co.uk

Abstract: Presented here is CHAFF (CubeSat Hyperspectral Application For Farming), a design concept for a CubeSat-based Hyperspectral Imager (CHSI) intended to supply high quality hyperspectral image data cubes to the agricultural community. CHAFF has been designed holistically as a system, considering all design and operational characteristics of a CHSI instrument and platform together: including the restricted payload mass and volume associated with CubeSats, the platform pointing stability/accuracy limitations, and the restricted downlink data budget. To this end, CHAFF will employ optically aided geometric co-registration methods, which will allow on-board construction of the hyperspectral data cube. This allows the use of powerful lossless data compression schemes to mitigate the downlink data budget limitations. In addition, a calibration methodology using a tuneable laser source at NPL, will be employed pre-flight to achieve rapid and accurate spectral and radiometric calibration, essential for the production of science-grade data sets from the proposed CubeSat constellations. A benchtop prototype has been constructed and a promising spectral resolution of 3nm at around 625nm has been achieved. In addition the auxiliary imager for the optically-aided geometric co-registration has been demonstrated.

1. INTRODUCTION

A hyperspectral image is a digital image in which each pixel has spectral information from that section of the scene recorded in many narrow, contiguous bands; the image is contained within a 3D "data cube", with two spatial dimensions and a spectral dimension [1].

1.1 Agriculture

Multispectral imaging has already seen great success in the field of agriculture, via crop monitoring using, for example, the Normalised Difference Vegetation Index (NDVI) to obtain a general overview of crop health or weed identification [2, 3]. However, hyperspectral imaging, due to its increased number of spectral bands, can allow for far more sophisticated crop analysis, such as disease identification and the detection of early stage drought stress [3]. Generally, such applications require spectral resolutions of less than 5nm [3]. Hyperspectral imagers are also more versatile; for example, the NDVI can be tailored to suit specific crops by changing the bands used [4].

Satellite constellations have been highlighted as a possible means by which the high temporal resolution observations required in the agricultural sector can be achieved [5], and a fleet of CubeSats are a cost-effective means by which this may be accomplished. While CubeSat-based spectral and hyperspectral imagers are now a reality [6, 7], the desired spectral resolution for precision agriculture remains a technological challenge.

1.2 Design and System Requirements

The core aim of the project is to produce a design of a CubeSat-based Hyperspectral Imager (CHSI) capable of achieving the following design parameters.

Parameter	Value	Notes
Payload Size	<3U	Integration onto 6U CubeSat.
Spatial Resolution	<40m from 500km	Across-track GSD.
Spectral Resolution	<5nm	Vegetation Red-edge sampling.
Spectral Range	~ 460-800nm	VNIR most suitable for application.
Swath	20-30km from 500km	Increase likelihood of imaging target.
Cost	~<£10,000	Commensurate with most CubeSat budgets.

Table (1): CHAFF Design Parameters

In addition, the instrument must be able to deal with the operational limitations of the CubeSat platform, specifically the limited pointing accuracy and stability and the constrained downlink. The aim with the latter is to retain as much information from the data cube as possible without the need to downlink raw data (e.g. [7]). Finally, to ensure data fidelity and scientific utility, the CHSI will employ rapid and accurate calibration techniques, traceable to the standards of a National Metrology Institute (NMI).

2. BENCH-TOP PROTOTYPE

2.1 Holistic Design

It was decided that a pushbroom, transmission grating based system, folded in a similar fashion to [4], was the most suitable to meet the design requirements. However, due to the physical pointing instability inherent to small satellites, this leads to a problem with regards to co-registering the slit images to form the data cube.

In response to this, an optically aided co-registration method is proposed, based on the SMARTSCAN technique, which uses auxiliary images taken in conjunction with the pushbroom 1D images [8]. By employing Fourier Transform techniques on the auxiliary images, the image shift vector between each frame was determined, recorded, and used to co-register the images on the ground [8]. A beam-splitter placed behind the fore-optic (as proposed in [8]) could be used to sample some of the light before it reaches the slit of the spectrograph, thereby producing such an auxiliary image.

Instead of using opto-electronic components to calculate the image shift vectors [8], the use of Graphics Processing Units (GPUs) aboard the satellite are proposed; recent research has highlighted GPUs as a means of processing images on-board small satellites, specifically in the context of image compression [9]. The data cube can then be constructed aboard the satellite.

Building the data cube aboard the satellite allows for the use of high performance, lossless compression techniques, such as CCSDS-123, which exploit spatial, spectral and statistical redundancy in the data cube to achieve average compression ratios of 3.24 [9]. In this way, the entire data cube could be downlinked for analysis on the ground.

2.2 Bench-Top Prototype

CHAFF (CubeSat Hyperspectral Application For Farming) has been constructed as a bench-top prototype, shown below.

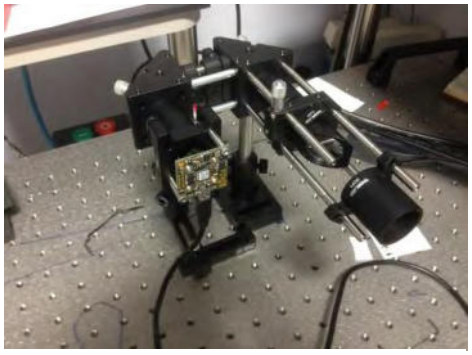

Figure (1): CHAFF bench-top prototype with the CMOS sensor on the spectral arm.

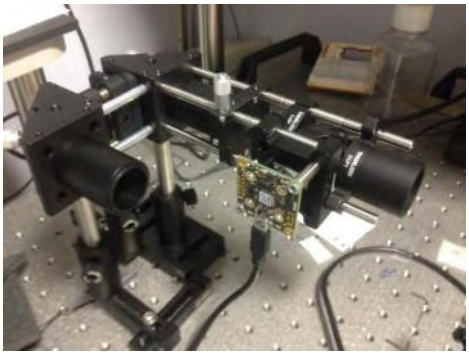

Figure (2): CHAFF bench-top prototype with the CMOS sensor in the auxiliary image position.

The approximate dimensions of the prototype are 205 x 135 x 50mm, thus making it a payload compatible with a 6U CubeSat. For the actual instrument, two CMOS sensors would be required; however, only one was available for use, and so the CMOS sensor was transferred to the auxiliary image position for capturing the auxiliary images Approximate cost of the commercial off-the-shelf (COTS) optical components was £3000.

3. EXPERIMENTAL PROCEEDURE

3.1 Spectral Calibration

CHAFF was set up with the following parameters during the experiments.

Parameter	Value
Slit Size	10µm
F-Number	F/4.23
Sensor	ON Semi MT9P031 CMOS Sensor
Pixel Depth	8 bit
Sensing Area	5.6 x 4.2 mm
Resolution	1280 x 960 (2x bin)
Pixel Pitch	2.2µm (~4.4µm with 2x pixel bin)
Exposure Time	15ms
Gain	3.5
Gamma	1

Table (2): CHAFF Experimental Parameters

CHAFF was first spectrally calibrated using a monochrometer set to 1nm precision, fed by a Xenon Arc Lamp. Images were captured with the monochrometer set to different wavelengths, and the peak locations on the CMOS sensor of each signal were defined as the centre of these wavelength bands. These points were then plotted on a graph and a linear fit applied to calculate the calibration equation (Figure (6)). Note that the calibration was calculated for the centre field of the spectral image, i.e. when the pixel index, $p_x = 639$ (out of 1280).

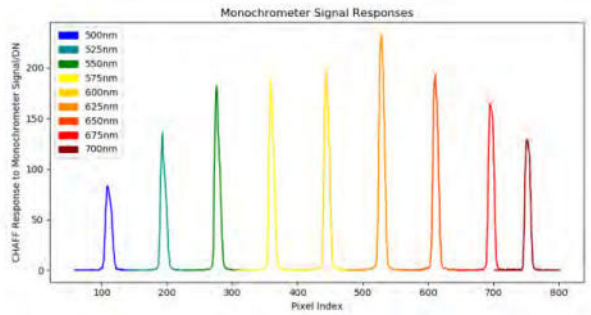

Figure (3): CHAFF Responses to the Monochrometer Signal

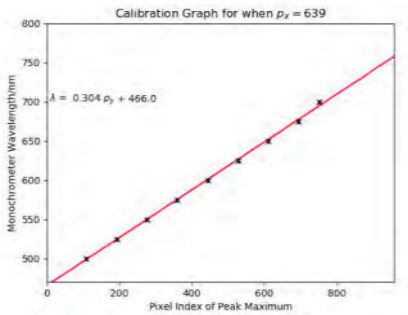

Figure (4): CHAFF Calibration

As can be seen in Figure (4), CHAFF exhibits extremely linear spectral characteristics. The slightly off result at 700nm is thought to be caused by spurious output from the monochrometer, which was performing at the limit of its operation at this wavelength. The approximate spectral range is 466-758nm, which is adequate for the measurement of the red-edge – i.e. the sharp reflectance transition from red to near-infrared associated with chlorophyll in vegetation [3]. The intended flight sensor will extend this range to 460-800nm.

3.2 Sodium Lamp Tests and Instrument Response Function

In order to test the spectral resolution, CHAFF was subjected to a Sodium Lamp, which has a very narrow spectral feature in the form of the Sodium D lines. The spectrum was calibrated using the fitted line from Figure (6); no radiometric calibration has been performed, hence the y axis is in digital numbers from the sensor (Figure (9)).

An average response to the spectral line was taken by sampling the response at locations across the field of view. A Gaussian function was then fitted to the response and the full-width half-maximum (FWHM) was calculated from the peak normalized fit (Figure (7)). The line was discovered to be ~10 pixels wide; with a dispersion per pixel of 0.304nm/pixel (see Figure (4)), this yields an approximate native spectral resolution of 3nm. This spectral resolution was confirmed by measuring the bandpass, by scanning the monochrometer across the centre pixel channel at 625nm (Figure (6)).

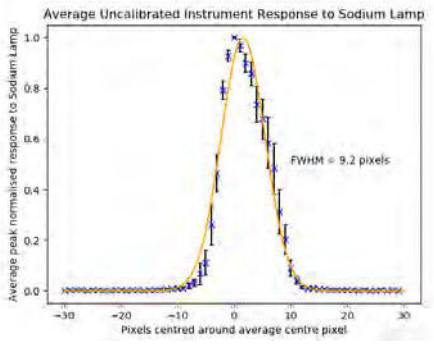

Figure (5): Measurement of the Sodium D line Width in Pixels, Using a Fitted Gaussian Function.

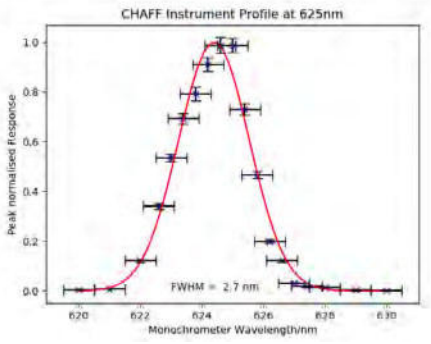

Figure (6): Measurement of the Instrument Profile Function Around 625nm.

The Sodium D lines are clearly seen in Figure (7), and their calculated location is accurate to within CHAFF's spectral resolution [10].

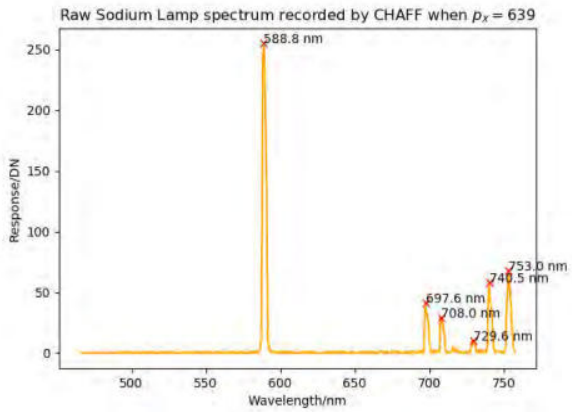

Figure (7): Sodium Lamp Spectrum with Calculated Peaks.

There appears to be a slight offset between the intended measured wavelength in Figure (6) (625nm) and the measured peak (~624nm), but this is within measurement uncertainty (±1.5nm). Another possible cause is asymmetry due to coma.

The spectral calibration from Figure (4) was calculated at the centre of the spatial field of view of the sensor. This allows for the use of the Sodium D line as a means to assess the *smile* property of CHAFF, i.e. the slight curvature of the spectral lines common to dispersive spectrometers [1]. The pixel index position of the Sodium D line was therefore calculated both in the centre of the field of view, and at the edge. This revealed a pixel shift of 6 pixels in the location of the Sodium D lines at the edge of the field of view, resulting in a shift of 1.8nm; this is a significant proportion of the spectral resolution (3nm), hence the smile must be well characterized for the flight model.

3.3 Compact Fluorescent Lamp Tests and Pixel Binning

CHAFF then recorded a spectrum from a commercial Compact Fluorescent Lamp (CFL); key peaks were then identified in the spectrum.

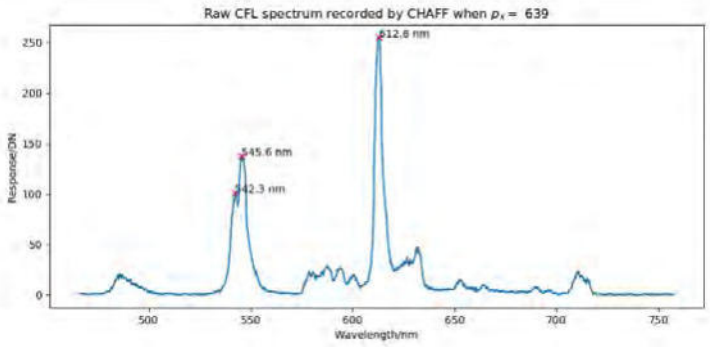

Figure (8): CFL Spectrum Recorded by CHAFF

CHAFF has been able to identify the major peaks, which are accurate to within its spectral resolution [9]. For example, the green mercury line (~546nm [10]) is clearly visible, as is a spectral feature around 3nm away at 542.3nm due to one of the elements used in the phosphors. This also confirms the spectral resolution.

The Gaussian fits in Figures (5) and (6) are reasonable, but not exact. This is thought to be caused by the asymmetry in the spectral channel, which is a product of the coma ab-

erration CHAFF suffers from. Instead of using single pixel channels (Figure (8)), pixel binning (or summing over pixels in a given range) can be used to absorb the effects of the coma and achieve a much more symmetrical instrument profile (see Figures (9) and (10)). However, this is at the cost of reducing the spectral resolution.

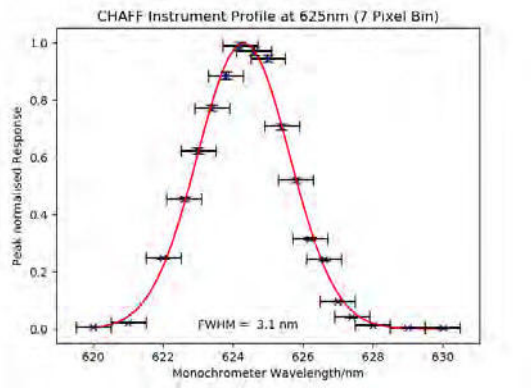

Figure (9): CHAFF Instrument Profile with a 7 Pixel Bin Size.

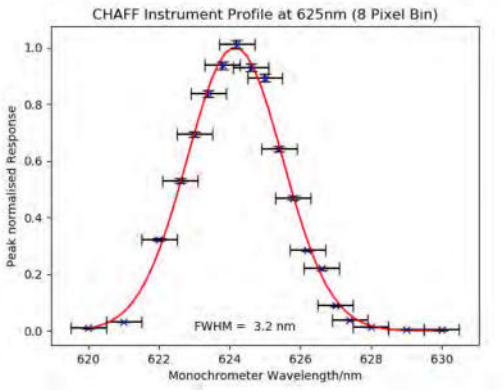

Figure (10): CHAFF Instrument Profile with an 8 Pixel Bin Size.

This drop in spectral resolution can be seen in the following CFL spectra. In Figure (11), at 7 pixel binning, the 542.3nm spectral feature from Figure (8) is barely resolved, whereas it is completely obscured at 8 binned pixels (Figure (12)). There is therefore a trade-off to be explored here.

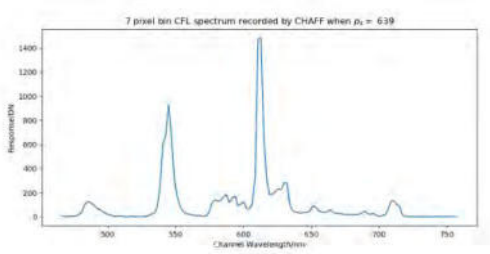

Figure (11): CFL Spectrum at 7 Pixel Bin Size.

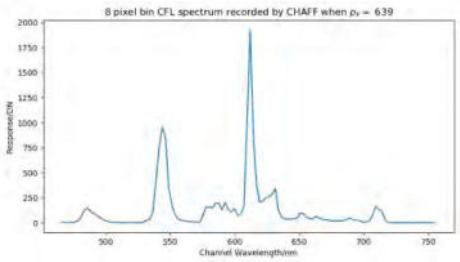

Figure (12): CFL Spectrum at 8 Pixel Bin Size.

3.4 Auxiliary Images

In order to assess the spatial optical quality of both the spectral arm and the auxiliary image, the CFL was used to illuminate a 1951 USAF test chart placed approximately 1.75m from CHAFF, and a spectral image was captured. The CMOS sensor was then transferred to the auxiliary image position (see Figure (2)) to capture the auxiliary image.

The spatial channels of the spectral imager arm have been confirmed to function, as the 1 line/mm section of the test chart is visible towards the right of Figure (13) (see insert). The auxiliary imager has also been shown to function (Figure (14)). The limit of resolution in the auxiliary image is Group 1, Element 2 on the USAF test chart; this yields a calculated spatial resolution, using the equation from [11], of ~2.24 lines/mm at 1.75m.

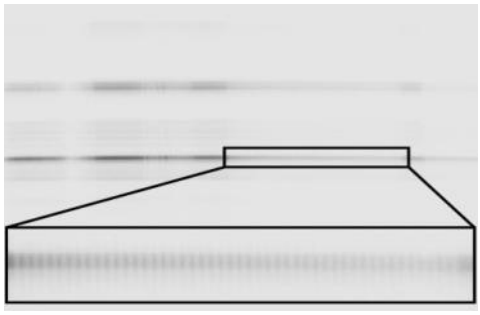

Figure (13): CFL (negative) Spectral Image Recorded from an Illuminated 1951 USAF Test Chart.

Figure (14): Auxiliary Image Associated with Figure (13).

There is, however, a noticeable offset between the spectral and auxiliary images. This can be remedied with careful alignment and characterisation. A larger problem is the apparent ghosting in the auxiliary image, which is thought to be caused by dual reflections off of the front and back surface of the beam-splitter; anti-reflection coated plate beam-splitters will therefore be investigated. There may also be a diffraction effect due to the reflective coating pattern of the polka-dot beam-splitter used.

4. CALIBRATION AND VALIDATION

The calibration of a hyperspectral imager is usually a time consuming and meticulous process, due to the large number of spectral bands. For rapid calibration pre-flight, the use of a tuneable laser system at the United Kingdom's National Physical Laboratory (NPL) is proposed (e.g. [12]); this will allow the spectral and radiometric calibration to be accomplished with the same source, as well as stray light characterization.

This will also allow for the instrumental calibration to be traceable to the standards of a National Metrology Institute (NMI), which will increase the fidelity of the data collected by the instrument. Traceability will be maintained in-flight using vicarious calibration techniques, utilizing NMI traceable sites such as those operated by RadCalNet [13].

5. CONCLUSION AND FUTURE WORK

To conclude, CHAFF has reached the bench-top prototype stage and is showing promising spectral resolution and range of 3nm (at 625nm) and 466-758nm respectively. A holistic system design has been proposed, including an optically aided geometric co-registration method, and the required auxiliary imager has been shown to function.

Future work includes improvements to the optical quality of the auxiliary image by investigating anti-reflection coated beam-splitters. The geometric co-registration method will then be developed and tested, in preparation for its utilization on a GPU. The optical quality of the measured spectrum will also be improved, through investigation of the source of the coma and ways to mitigate its effects, possibly through binning (summing) pixels in the spectral direction, or further refinement of the optical design. Once bench-top testing is complete, a portable prototype will be constructed and taken to NPL for calibration. Investigation into the spectral, radiometric and stray light characteristics of CHAFF will be undertaken, and best calibration practices for a constellation of such an instrument will be developed. After this, field trials can commence of the portable prototype, either using a ground based vehicle, or possibly a small unmanned aerial vehicle, which shares similar platform limitations with CubeSats.

6. ACKNOWLEDGEMENTS

This PhD research is sponsored by the UK Engineering and Physical Sciences Research Council (EPSRC) through an iCASE award with NPL as the industrial partner.

7. REFERENCES

[1] D. Manolakis, R. Lockwood & T. Cooley (2016), Hyperspectral Imaging Remote Sensing: Physics, Sensors and Algorithms. Cambridge University Press, Cambridge.

[2] B. Brisco, R.J. Brown, T. Hirose, H. McNairn & K. Staenz (1998), Precision Agriculture and the Role of Remote Sensing: A Review, Canadian Journal of Remote Sensing, 24:3, 315-327, DOI: 10.1080/07038992.1998.10855254

[3] A. Lowe, N. Harrison & A.P. French (2017), Hyperspectral image analysis techniques for the detection and classification of the early onset of plant disease and stress, Plant Methods, 13:80, DOI: 10.1186/s13007-017-0233-z

[4] S. Satori, Y. Takeuchi, T. Itoh & S. Satori (2015), Hokkaido Satellite Project: Development of Hyperspectral Camera for Agricultural Remote Sensing and Spin-off Business Creation, in International Symposium on Space Technology and Science, ISTS-2015-f-09

[5] P. Schweizer, L. L. Zhang, M. Heumesser, L. A. C. Velasco & A. Narayanamoorthi (2017), Roadmap to small satellite solutions for agricultural challenges, in 11th International Symposium of the IAA (Small Satellite for Earth Observation Conference), pp. 159 – 162

[6] eoPortal Directory (2019), Aalto-1: The Finnish Nanosatellite, Available at: https://directory.eoportal.org/web/eoportal/satellite-missions/a/aalto-1 (Accessed 11/01/2019)

[7] M. Esposito, S.S. Conticello, N. Vercruyssen, C.N. van Dijk, P. Foglia Manzillo, C.J. Koeleman, B. Delauré, I. Benhadj, J. Blommaert, S. Livens, A. Jochemsen, M. Soukup, M. Menenti, B. Gorte, E. Hosseini Aria (2018), Demonstration in space of a smart hyperspectral imager for nanosatellites, in 32nd Annual AIAA/USU Conference on Small Satellites, SSC18-I-07, Available at: https://digitalcommons.usu.edu/cgi/viewcontent.cgi?article=4069&context=smallsat (Accessed 11/01/2019)

[8] K. Janschek, V. Tchernykh & S. Dyblenko (2006), SMARTSCAN – smart pushbroom imaging system for shaky space platforms, in 20th Annual AIAA/USU Conference on Small Satellites, SSC06-VI-3

[9] R.L. Davidson & C.P. Bridges (2016), Adaptive Multispectral GPU Accelerated Architecture for Earth Observation Satellites, in "2016 IEEE International Conference on Imaging Systems and Techniques (IST)", pp. 117 – 122

[10] C. D. Elvidge, D. M. Keith, B. T. Tuttle, & K. E. Baugh (2010). Spectral identification of lighting type and character. Sensors, 10(4), 3961-3988. doi:http://dx.doi.org/10.3390/s100403961

[11] Edmund Optics (2019), 1951 USAF Resolution Calculator. Available at: https://www.edmundoptics.com/resources/tech-tools/1951-usaf-resolution/ (Accessed 08/04/2019)

[12] National Physical Laboratory (2019), Using lasers to radiometrically calibrate and spectrally characterize satellites. Available at: https://www.npl.co.uk/our-work/projects/radiometrically-calibrate-satellites (Accessed 05/04/2019)

[13] Radiation Calibration Network Portal (2019), Welcome to the Radiation Calibration Network Portal, Available at: https://www.radcalnet.org/#!/ (Accessed 23/01/2019)

Design and test of a COTS based imaging system for stereoscopic meteor observations

Jona Petri[1], Alexander Schmidt, Julia Zink, Sabine Klinkner

[1]Institute of Space Systems
Pfaffenwaldring. 29, 70569 Stuttgart, Germany
Phone: +49 711 685 63094, Mail: petri@irs.uni-stuttgart.de

Abstract: The Technische Universität Berlin and the University of Stuttgart are planning a joint mission for the observation of meteors and dust particles using a formation of two 30 kg satellites in low earth orbit. The satellite bus of the two spacecrafts is developed by the Technische Universität Berlin while the University of Stuttgart designs payload and payload data downlink system. The payload includes a miniature dust sensor and a camera for meteor observations. The mission consists of two identical satellites flying in formation to allow for stereoscopic meteor observation and thus the calculation of the meteor's trajectory. The paper describes the camera selection for meteor observations. Therefore, a simulation script based on Python has been developed, which calculates the limiting magnitude to which a meteor can be observed. The chosen GenieNano M1920 of Teledyne Technologies is a commercial-off-the-shelf camera, which limits cost and development effort. For the required space qualification, a thermal-vacuum test is conducted and the camera is tested during an outside test campaign and in the laboratory.
Finally, another simulation script was developed, to calculate the number of meteors observed using different orbits, combinations of satellite orientation and phase, camera lenses, as well as different limiting magnitudes determined with the first simulation.

1. INTRODUCTION

The Technische Universität Berlin and the University of Stuttgart are planning a mission to observe meteors and dust particles using two 30 kg satellites in low earth orbit. The two scientific objectives are to measure and characterize dust in the low earth orbit and calculate the trajectory of meteors hence their orbit and point of origin. Toward this end, the IRS (Institute of space systems) has developed two payloads: a small dust sensor and a meteor observation camera. This mission will also serve to demonstrate new green water based propulsion system, developed by IRS in cooperation with Airbus, along with an X-band transmitter and the usage of COTS (Commercial of the Shelf) parts in the camera system for meteor detection. The pre-study of this mission is completed (see [1]). In this paper we describe the current development status of the meteor observation camera. We derive the camera requirements using a simulation and outline the camera testing with respect to scientific performance and space qualification. These results are used as inputs for another simulation to determine the ideal satellite orbit and orientation to optimize the observation strategy and scientific output.

The scientific objective of the meteor observation camera is to determine meteor trajectories using stereoscopic observations. The resulting trajectory can be propagated back to an orbit to gain information about the meteor's parent body. Although this principle is already used with ground based observation systems, such as the CILBO system on Tenerife [2], a space-based system can aid these kind of ground based observations, by providing a weather independent view of meteors, in which light curves are not absorbed by the atmosphere. Depending system's field of view, a larger area could also be covered, thus yielding more meteor observations [3].

2. DERIVATION OF CAMERA REQUIREMENTS

Before choosing a camera, the requirements are among others derived via a Python simulation. The first goal here is to derive design drivers for the meteor observation system. Thus, the simulation incorporates camera and lens parameters, such as pixel size, quantum efficiency and focal length, when calculating the signal generated by a meteor. The meteor properties (speed, angle and distance) influence the generated signal and can be set by the user. Finally, the signal-to-noise ratio (SNR) is calculated for different magnitudes. The SNR as a function of magnitude indicates the limiting magnitude of the camera system After identifying the main design drivers, the simulation is used to evaluate various camera and lens options and choose the most suitable camera.

2.1 Simulation Approach

The signal generated by a meteor μ_e is calculated by using the formula from the EMVA1288 standard [4], which gives the number of electrons generated from a given irradiance (E) during an exposure time (I) taking into account the pixel size (F_{px}) and the quantum efficiency (η) (see Equation 1). Furthermore, the wavelength (λ), Planck constant (h) and speed of light (c) are needed.

$$\mu_e = \frac{F_{px}[m^2] * E[\mathrm{W/m^2}] * I[\mathrm{s}] * \eta[-] * \lambda[\mathrm{m}]}{h[\mathrm{Js}] * c[\mathrm{m/s}]}$$

Equation 1

All parameters in this equation are either physical constants or known camera parameters, only the irradiance must be calculated. Therefore, the formula from [5] is used, which derives the irradiance E (W/m^2) from the (spectral) radiance L_λ ($\mathrm{W/(m^2 * nm * sr)}$). The irradiance depends on the wavelength range ($\Delta\lambda$), the angle between camera boresight and nadir (x), the lens f-number ($f_\#$) as well as the transmission of the whole system (T):

$$E = \frac{\pi * T[-] * \Delta\lambda[nm] * L_\lambda * \cos(x[rad])^4}{4 * f_\#^2[-]}$$

Equation 2

The spectral radiance of a meteor L_λ is difficult to obtain, in this simulation we use data from [6]. This book gives the spectral irradiance in the three Johnson Filter bands B, V and R, which are used as L_λ in Equation 2. The full-width-half-maximum (FWHM) of each filter is used as $\Delta\lambda$. Putting the calculated irradiance in Equation 1 gives the signal in each filter band, the total signal is the sum of all three signals. The quantum efficiency in Equation 1 depends on the wavelength. The efficiency belonging to the wavelength at which the transmission of a filter reaches its maximum is used for the whole filter bandwidth range. The resulting signal gives the amount of electrons generated by a meteor with magnitude zero. The signal can be scaled to different magnitudes by dividing the magnitude zero signal with $10^{0.4*m}$, with m being the desired magnitude.

Different noise sources are taken into account, this includes the shot noise (poisson distribution of the signal, depends on signal strength/number of photons), dark noise (depends on temperature and exposure time), read out noise as well as background noise (from city lights, lightning). The background noise is difficult to calculate, in the simulation we use data from [7], who determined the artificial light pollution using satellite data and calculate the artificial sky brightness. We assume this sky brightness is the noise reaching the camera in orbit in the visual Johnson filter band (V band).

Finally, the simulation takes into account that a moving meteor causes the signal to spread over several pixels reducing the signal strength. The magnitude reduction is derived using an equation taken from [8]. This equation takes into account the FOV (Field of view), meteor speed, distance, angle between meteor trajectory and boresight, integration time as well as the FWHM (Full-Width Half-Maximum) of a star. The last value must be assumed or taken from real sky images. Furthermore, depending on the distance between meteor and camera, the apparent magnitude is reduced. The above mentioned radiance values are valid for a meteor as seen from a distance of 100 km. The magnitude loss due to distance is easily calculated by $\Delta m = 2.5 * \log_{10}((d_1/d_2)^2)$, where d_2 is the distance between meteor and satellite and d_1 is set to 100 km.

Assumptions and Limitations

Despite giving good results and being used to compare cameras, the simulation is limited and some assumptions have been made. As already mentioned, the irradiance is calculated from the meteor spectral irradiance in the three Johnson Filters U, B and V. While the calculations are valid, the calculated irradiance does not represent the actual meteor brightness. This is due to the fact, that the meteor does not have the same spectral irradiance over the whole filter bandwidth. Also, using the FWHM instead of the whole filter wavelength bandwidth means not taking into account all irradiance. On the other hand, the filter curves are overlapping which could result in overestimating the irradiance. Using the actual filter transmission curve and integrating the spectral irradiance over the according filter wavelength would result in a more accurate irradiance. But this would be more complex. Overall, the conversion of the apparent magnitude to the corresponding irradiance shall be understood as a “rule-of-thumb”, that allows us to approximate actual expectations.
Another problem could be the accuracy of parameters used: The quantum efficiency for example needs to be known for the according Johnson filters. We estimated them using the spectral response or a quantum efficiency diagram. Furthermore, the quantum efficiency is assumed to be constant over the filter bandwidth.

Even more complicated is the estimation of the correct FWHM of a star to calculate the magnitude loss due to the meteor movement. This is because the FWHM depends not only on the sensor, but on the used lens as well. While the FWHM can be measured, this requires the real camera and lens. For a simulation, before deciding which camera to use, an assumption has to be made.
Another inaccuracy is the noise value: Additionally to the noise generated by the sensor (shot and dark noise), the background noise is taken into account as another noise source. This noise value is a worst case value when the satellite is passing over a city. A drawback of this approach is, that the noise is only given in the V filter band. Noise in other wavelength bands are not considered. Furthermore, this value describes the sky brightness as

seen from the ground, for a satellite this value could be different. This is not a concern for comparing cameras, but for getting an accurate prediction for the final instrument.
Finally, the magnitude is calculated for a meteor with the given speed and angle, it is assumed the meteor passes over the sensor horizontally. Furthermore, the limiting magnitude is only calculated for a meteor passing the center of the lens. A meteor at the edge of the FOV suffers from two additionally magnitude losses which are not taken into account. First, meteors that appear at the edge of the FOV have a larger distance to the camera, compared to centered appearing ones, when the camera is looking in nadir direction. Second, the larger deviation to the optical axis results in vignetting [9] and reduction of lens colleting area. The latter magnitude loss is calculated, but not further taken into account.

2.2 Simulation Results and Verification

The simulation gives the limiting magnitude for a meteor as seen from orbit and ground as well as for a stars. This is done by calculating the magnitude for the SNR value of 5 for each curve (see Figure 1). It is assumed, that a meteor needs to have a SNR of 5 to be detected.

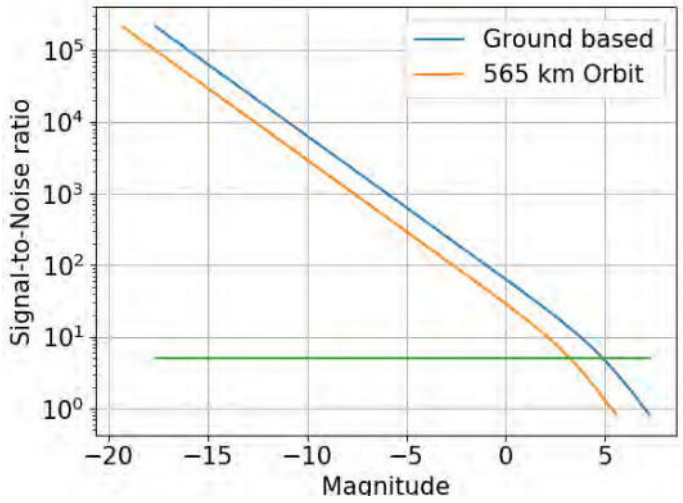

Figure 1 Signal-to-Noise ratio for an example camera (Genie Nano M1920). Note: The intersection between the green line (showing SNR=5) and blue/orange lines indicates the magnitude/brightness to which meteors can be observed, depending on whether the meteor is observed from ground or orbit.

Using those diagrams, the effect of different camera and lens parameters on the limiting magnitude is evaluated (see Table 1). After simulating different cameras and lens, a suitable combination was selected. The chosen lens series (Schneider-Kreuznach Cinegon ruggedized) has already been used on satellites and is not further tested against environmental conditions in space. The camera (Dalsa-Teledyne GenieNano M1920) is further tested as described in the following paragraphs.

Table 1 Design driver and influence on meteor observation. (+) and (-) indicate advantages and disadvantages, respectively

Parameter	Change	Effect
FOV	Smaller	Smaller area (-), smaller travel distance (+). Smaller aperture area (-)
Int Time	Larger	Increased dark noise (-), increased background noise (-)
Pixel size	Larger	Longer dwell time (+), more sky noise, larger limiting magnitude (+)
Binning	Larger	Smaller image size (+), Longer dwell time (+), larger limiting magnitude (+), lower resolution (-)
Orbit height	Higher	smaller travel distance (+), higher distance to meteor (-), smaller limiting magnitude (-), larger area covered (+)
Resolution	Smaller	Smaller travel distance (+)
Framerate	Smaller	less data (+), worse velocity determination (-)

Before conducting environmental tests, the simulation needs to be verified, which is done by determining the limiting magnitude in real sky tests and comparing the results to the simulation. Please note that a different lens (Kowa LM6JC) was used for the ground based tests in contrast to the intended lens to be used on the satellite to limit costs. The camera was tested on the roof of the IRS during a meteor shower as well as inside the planetarium in Stuttgart. The limiting magnitude was determined by comparing the image to a map of stars and determine the magnitude of the faintest visible star. While this method is widely used, it is not accurate in this case. This is due to the fact that the stars were manually compared and the camera orientation varied during testing. The simulations have been conducted with the same settings used in the real sky test respectively in the planetarium.

Table 2 Limiting stellar magnitude from measurements and simulation

Image Source	Limiting stellar magnitude	Binning	Exposure Time (ms)
IRS roof	5.26	1	810
Simulation	6.70	1	810
IRS roof	4	1	250
Simulation	5.32	1	250
Planetarium	6.54	2	166
Simulation	5.09	2	166
Simulation no noise	6.94	2	166

As can be seen in Table 2 the simulation values are close to the measured values, although the simulation predicts higher magnitude values for the real sky tests. This is due to the fact, that the simulation takes only sky noise in the V-Band into account, during the image campaign on the roof the light pollution was quite high. This resulted in a lower limiting magnitude. For the planetarium tests, the calculated magnitude is lower than the measured one. This can also be explained with the noise levels present. In the planetarium was no light pollution present, but the simulation takes it into account. Without the simulated noise, the values of measurement and simulation are quite close.

All in all the simulation results are close to the real sky values. The remaining offset is easily explained with the limitations and assumptions made in the simulation, the different noise levels during the measurements as well as the uncertainties in determining the limiting magnitude from the images. This means the simulation can be used to further evaluate different camera and lens options as well as to determine design drivers in the camera system development. Furthermore, the calculated limiting magnitude can be used in another simulations, to determine the number of meteors, which can be observed.

3. CAMERA SYSTEM DESIGN, QUALIFICATION AND TESTING

Table 3 Genie Nano M1920 and Kowa LM6JC data

Parameter	Value
Resolution	1936x1216 px^2
Pixel Size	5.86x5.86 μm^2
Bit Depth	8/12-bit
Frame Rate	0.06-38.8 fps
Exposure Time	34.23 µs to 16 s
Sensor Type	CMOS (Sony IMX249)
Sensor Size	1/1.2”
Power Dissipation	3.8 to 4.9 W
Interface	Gigabit Ethernet
Temperature (Op/Non-Op)	-20-60°C/-40-80°C
Focal Length	6 mm
Minimal F#	1.4
Mount Type	C-Mount

The chosen camera (Genie Nano M1920) is a commercial of the shelf (COTS) camera, to limit the costs and demonstrate the feasibility of using COTS parts in space. This implies modification of the camera as well as testing is required, to operate the camera in space. This includes the mainly the radiation issue, the vacuum and thermal behavior. The camera and lens data can be found in Table 3, please note that a different lens (Kowa LM6JC) was used for the ground based tests in contrast to the intended lens to be used on the satellite to limit costs.

3.1 Housing Development

We performed a radiation analyses using orbit data from Phase A to characterize the radiation environment and evaluate different wall thicknesses for the housing. According to the simulations performed with SPENVIS a TID of 1200 rad is expected in the worst case with a 3 mm housing thickness. Even this value is quite low, a housing for the camera was developed. The housing shields from radiation and is also responsible to conduct the heat from camera to the satellite. The housing was developed by using thermal simulations, to ensure a proper heat conduction.

3.2 Thermal-Vacuum Test

A thermal vacuum test has been conducted, with several objectives: Make sure the camera is able to operate in vacuum, to determine the thermal behavior and to measure the dark current at different temperatures. The last point is part of the planned camera characterization according to the EMVA1288 standard [4]. Prior to this test, holes were drilled into the camera to allow a venting.

The camera was successfully tested in the TV-chamber of the Institute of Space Systems. Therefore, we tested the camera at different temperatures in the range defined by the

manufacturer. Starting at room temperatures, the temperature was set to -20°C and increased in 10°C or 20°C steps until the camera housing reached the critical temperature of 60°C. At each temperature step a functional test was performed, which included taking dark frames at different exposure times. These images were later used to determine the temperature influence on the dark current. The camera housing temperatures were logged during the whole test, allow comparing the results with thermal simulations made before.

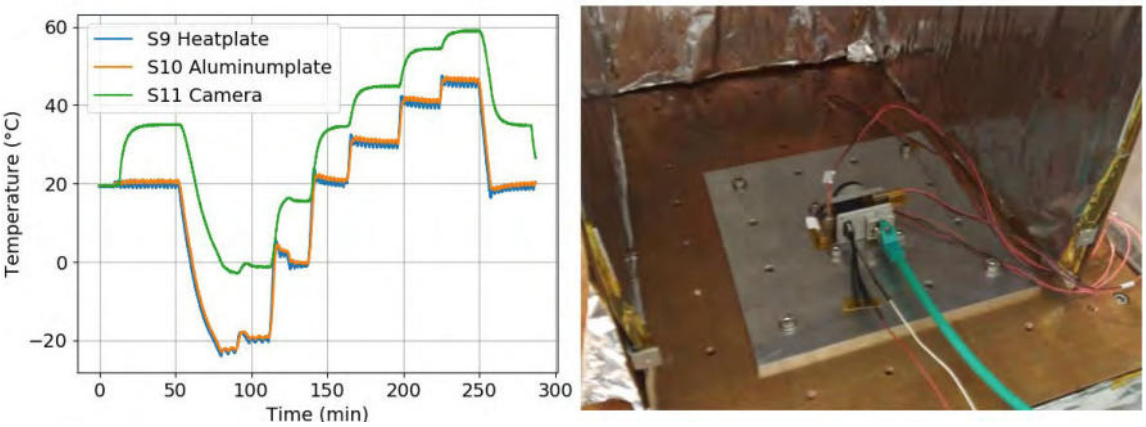

Figure 2 Left: Temperature of camera housing (S11) at different temperatures set at the aluminum base plate (S10) and heating plate (S9). The camera temperature rises, when turned on, the offset between plate and camera is roughly 10 to 15 K. Right: TV-Test setup.

All in all the camera worked well in vacuum. The camera produced quite a lot of heat, the offset between mounting plate (S10) and camera housing is between 10 and 15 K, with a higher offset at lower temperatures. The temperatures during the test are shown in Figure 2. During another TV test the camera was tested inside the developed housing, which worked as expected. The doubling temperature of the dark current is about 1.76°C.

4. SATELLITE ORIENTATION AND DISTANCE ANALYSIS

After choosing the camera and lens series using a simulation and testing the camera, it is also necessary to simulate the satellite formation, to get the most suitable satellite distance and orientation, orbit as well as the ideal FOV of the lens. This is done by simulating the numbers of meteors which can be observed with the given parameters. The parameters include the FOV, orbit height and limiting magnitude derived from the first simulation. The SWARMS simulation, developed by Alexis Bouquet et al. (see [3]) is adapted to simulate the number of meteors observable per time unit and to evaluate different lens options. The modifications include among others the implementation of a second satellite and calculation of the overlapping FOV areas. For the simulation we used the limiting magnitude of the Genie Nano M1920, set the upper and lower orbit simulated to 300 and 565 km and choose three different lens from the Schneider-Kreuznach Cinegon ruggedized series with different FOVs. The distance between the satellites as well as their orientation were calculated in a way that the overlapping area is maximized. In addition, we investigated the observation time by calculating the time span were both satellite are in eclipse using an ASTOS simulation.

We found with the help of the simulation, that different FOVs are suitable depending on the scientific objective. With a smaller FOV less meteors are observed, but the angular resolution is greater allowing a more accurate trajectory determination. For this mission

a FOV of approximately 48°x31° is chosen, depending on orbit height and meteor flux model used, a meteor rate of 0.06 up to 7.5 meteors per hour is expected. The area covered depends on the orbit and tilt of the satellite, for a 565 km orbit and zero tilt angle an area of 100.000 km^2 is covered. This can be increased to 400.000 km^2 at a tilt angle of 40°. The area covered from two satellites depends additionally on the distance between them. A detailed description of the results is behind the scope of this paper and will be published in future paper.

5. CONCLUSION AND FURTHER WORK

All in all we obtained requirements and design drivers for a meteor observation camera using a simulation. We also verified the simulation results using real sky and planetarium tests. The chosen camera could be qualified with a TV test and the developed housing worked as expected to spread the heat. However, more tests, like shaker tests, are needed to qualify the camera completely. Further developments include the characterization of the camera using the EMVA1288 standard as well as a radiometric and geometric calibration. The complete instruments consist of the camera, the lens as well as a payload computer. Further developments include the design of the computer as well as the software. The software is not only responsible for the camera control, but is also needed to detect meteors to reduce the number of images downlinked to the ground. As a future concept the whole system should be modular, to adapt the meteor observation system to different mission. This includes an easy replacement of the camera, lens or payload computer to adapt the system different scientific objectives and satellite platforms.

Literature

[1] F. Hufgard, M. Lengowski, M. F. Barschke, N.-E. Harmansa, S. Klinkner und K. Brieß, „PRELIMINARY STUDY OF AN ACADEMIC MICRO-SATELLITE FORMATION MISSION FOR METEOROID TRAJECTORIES DETERMINATION AND DUST MASS FLOW MEASUREMENT," in *Proceedings $s Symposium*, Sorrento, 2018.

[2] D. Koschny, F. Bettonvil, J. Licandro, C. v. d. Luijt, J. Mc Auliffe, H. Smit, H. ,. W. F. Svedhem, O. Witasse und J. Zender, „A double-station meteor camera set-up in the Canary Islands – CILBO," *Geoscientific Instrumentation, Methods and Data Systems,* Bd. 2, Nr. 2, pp. 339-348, 2013.

[3] A. Bouquet, D. Baratoux, J. Vaubaillon, M. Gritsevich, D. Mimoun, O. Mousis und S. Bouley, „Simulation of the capabilities of an orbiter for monitoring the entry of interplanetary matter into the terrestrial atmosphere," *Planetary and Space Science ,* Nr. 103, pp. 238-249, 2014.

[4] European Machine Vision Association, *EMVA1288,* 2016.

[5] J. George, Building earth observation cameras, CRC Press, 2015.

[6] P. Jenniskens, Meteor Showers and their Parent Comets, New York: Cambridge University Press, 2008.

[7] P. Cinzano, F. Falchi und C. D. Elvidge, „The first world atlas of the artificial night sky brightness," *Monthly Notices of the Royal Astronomical Society,* Bd. 328, pp. 689--707, 2001.

[8] A. Kingery und R. Blaauw, „Determination of the meteor limiting magnitude," *Planetary and Space Science,* Bd. 143, pp. 67-70, 2017.

[9] T. Albin, D. Koschny, S. Molau, R. Srama und B. Poppe, „Analysis of the technical biases of meteor video cameras used in the CILBO system. Geoscientific Instrumentation, Methods and Data Systems," *Geoscientific Instrumentation, Methods and Data Systems,* 2017.

Maximizing CubeSat Payload Volume in Milli-gravity to Improve CubeSat Earth Observation from Space

Maharshi Bhattacharya, José M. Díez, Brennan T. Lutkewitte, Hugh MacLellan, Sebastían Ospina, Nicholas P. Smith
Technical Advisors: Dr.-Ing Sebastian Grau, Dipl.-Ing. Martin Buscher, Jens Groβhans, M.Sc.

Department of Aeronautics and Astronautics, Marchstraße 12, 10587 Berlin, Germany
Technische Universität Berlin,
Berlin, Germany

maharshi.bhattacharya@campus.tu-berlin.de
jose.diez@campus.tu-berlin.de
lutkewitte@campus.tu-berlin.de
h.maclellan@campus.tu-berlin.de
sebastian.ospina@campus.tu-berlin.de
nicholas.smith@campus.tu-berlin.de

Abstract: TU Berlin Pico- and nano-satellite EXperiment 7 (TUPEX-7) is a student mission to develop and demonstrate miniaturized space technologies for a 1U CubeSat bus through deployment of a Free-Falling Unit (FFU) in the milli-gravity environment. The FFU is being developed such that its design can be utilized for a future TU Berlin CubeSat with potential for Earth observation. The miniaturized technologies include Highly-Integrated Side Panels (HISPs), incorporating a complete Attitude Determination and Control (ADCS) subsystem, and a Software-Defined Radio (SDR). The high payload-to-volume ratio, successful communication by the SDR, and successful maneuvers performed by the HISPs would demonstrate a CubeSat bus that is optimized for a substantial Earth observation payload; in the bigger picture, a successful mission will greatly contribute to new and expanded possibilities of small satellites.

1. INTRODUCTION

The ever-increasing growth in the development, use, and capability of small satellites is both a driver and a result of the miniaturization of space technologies. Such advancement has allowed for pico-, nano-, and CubeSats to conduct meaningful science and technology development through their payloads. However, the payloads are often constrained by the volume required for the various subsystems necessary for base-level operation. Therefore, there currently exists a unique opportunity to further reduce the required volume for satellite subsystems, to allow for greater payloads, and to push the boundaries of what small satellites can achieve.

TUPEX-7 is a student-led project, taking part in the German-Swedish student program Rocket/Balloon Experiments for University Students (REXUS/BEXUS), in which technology to enable on-board payload expansion of CubeSats will be developed, integrated, and tested. It is anticipated that the successful implementation of these technologies will enable establishment of a CubeSat bus well-suited for Earth observation missions.

Specifically, the experimental technology consists of Highly-Integrated Side Panels (HISPs) and a Software-Defined Radio (SDR). The HISPs will incorporate several subsystems to minimize the overall space required. Principally, they will include pico Fluid Dynamic Actuators (pFDAs), an attitude actuation technology being developed at TU Berlin. The mission will demonstrate the volume efficiency of pFDAs and investigate their effectiveness in performing routine satellite maneuvers through attitude data collection and analysis.

The SDR, having frequency and modulation adjustable by software, allows for flexible communication between ground and satellite and will reduce the volume required for communication on varied channels. As a parachute is required for FFU recovery, a flexible monopole antenna will be developed and integrated with its cords to send and receive signals. The potential of the SDR system will be evaluated through its transmission and reception of data to and from ground.

The FFU will be launched on a REXUS launch vehicle and deployed in the milli-gravity environment, demonstrating the technologies' potential for application in small satellites. The inclusion of a parachute, comprising a substantial volume of the FFU, will inherently demonstrate the expanded payload capacity. Additionally, the FFU will include a custom camera platform with a degree of flexibility for the optics, further allowing for potential Earth exploration from space.

This paper describes the student mission and experiment, as well as its implications for future small satellite technology.

2. SCIENTIFIC/TECHNICAL BACKGROUND

In recent years there has been a rapid increase in the number of nano- and microsatellite launches. The majority of such satellites are in the 3-6kg weight category and have a 3U form factor [1]. As a result of the standardized and miniaturized form factor, the cost of developing and operating space systems has decreased, enabling the "New Space" industry. As a result of this trend, there is a growing demand for volume efficient and highly-integrated small satellite components [2, p. 3-37].

The miniaturization of satellite components is an ongoing area of research at TU Berlin. In this context, miniaturized reaction wheels and cameras have been developed [3] and implemented on Berlin Experimental and Educational Satellite (BEESAT) missions since 2009 [4]. On the latest BEESAT mission, BEESAT-4, three of these reaction wheels are used for attitude control. The attitude determination and control system (ADCS) takes up approximately one quarter of the overall volume of BEESAT-4 [5].

Advancing the state of the art in the field of ADCS, a novel type of attitude control actuator known as pico Fluid Dynamic Actuator (pFDA) has been developed at TU Berlin. Their principle of operation is the same as that of reaction wheels, namely the use of exchange of angular momentum. pFDAs consist of a closed channel filled with a liquid metal and a driver unit composed of a controller, PCB and an electromagnetic pump that accelerates the fluid within the channel, thereby creating an angular momentum which results in the overall system moving in the opposite direction due to conservation of angular momentum [6]. A key advantage of this type of actuator is that the fluid channel can be shaped in a variety of ways depending on the mission requirements; for example, an L-shaped channel affords redundancy by producing an angular momentum vector that is not constrained to a single plane in the body-fixed frame of the satellite, while planar pFDAs allow designers to optimize for volume efficiency [7]. L-shaped pFDAs are being tested on the TUPEX-6 mission [8], and TUPEX-7 will test planar actuators.

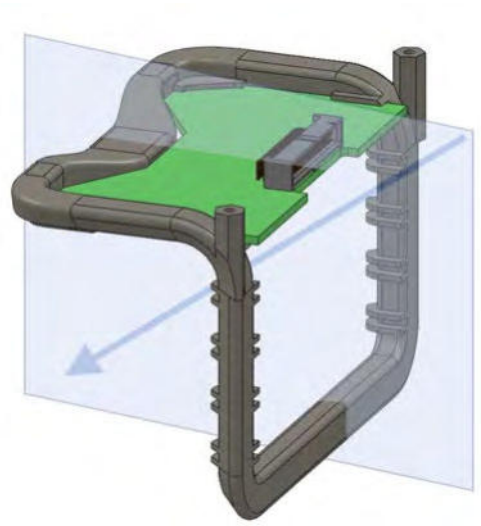

Fig. 1: L-shaped pFDA with angular momentum vector [8]

Furthermore, the research of TUPEX-7 project advisor Dr.- Ing Sebastian Grau has yielded design guidelines for HISPs incorporating components comprising the ADCS, the communications subsystem (COMMS), the electrical power subsystem (EPS), and the structures and mechanisms subsystem (SMS) [9 , Ch. 6.2]. A “fully loaded” HISP can contain solar cells, a radio antenna, sun sensor, gyroscope, magnetometer, pFDA, and magnetorquer, as well as a local microcontroller which processes attitude control commands from the satellite bus and fuses the sensor measurements to output attitude determination data [9, 105–108]. By coalescing these subsystems, an unprecedented payload-to-volume ratio of up to 60% can be achieved [9, 117–118]. Traditional 1U CubeSat buses have less than 25% payload-to-volume ratio [10]. TUPEX-7 seeks to achieve a maximized volume for the greatest flexibility and potential of future payloads.

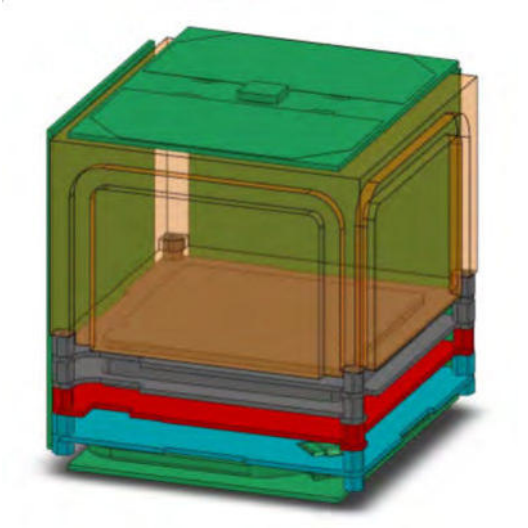

Fig. 2: Sketch of a 1U CubeSat using HISPs [9]

Additionally, there is growing interest in the use of SDR on spacecraft due to their inherent flexibility [2, D-9]. In SDRs, the TX and RX frequencies can be adjusted in software, as well as the modulation techniques. On traditional communications subsystems, a dedicated hardware transceiver module is required for each frequency band [11, p. 4]. By exploiting the flexibility of SDRs, it is possible to further miniaturize the communications system. However, low-cost SDRs have very weak output power [12] (meaning that power amplifiers are needed for communication over non-trivial distances) and they can produce undesired artifacts in the RF spectrum if proper filters are not implemented in the RF front-end. Developing a low cost SDR transceiver design using as many commercial off-the-shelf (COTS) components as possible will advance the state of the art in picosatellite communication systems. In order to ensure a reliable communications link with the ground station while demostrating the SDR capabilities, a flexible monopole antenna will be integrated into the cords of the parachute.

Noting the importance of capturing mission images for scientific, educational, and outreach purposes, a camera system will be integrated into the FFU. Its design, selected hardware components, and allotted space will allow for flexibility in future designs, permitting a range of optical parameters for a variety of imaging possibilities.

3. MISSION STATEMENT

The TUPEX-7 mission aims to demonstrate that HISPs can be used to develop a picosatellite bus with a very favorable payload-to-volume ratio by utilizing each of the components in operational scenarios applicable to satellites, including angular rate determination, de-tumbling, slew maneuvers, and duplex communication.

The performance of these components will be recorded throughout the mission, both by an FFU and by equipment on the ground, and later analyzed to compare the expected performance with the flight data.

4. EXPERIMENT OBJECTIVES

TABLE I: TUPEX-7 mission objectives

ID	Objective	%	
MO1	Development of low-cost HISPs.	15	
MO2	Development of a low-cost SDR transceiver.	15	
MO3	Pass qualification campaign.	10	
MO4	Launch of TUPEX-7 hardware.	10	
MO5	Demonstration of the capabilities of HISPs in an operational environment.	15	
MO5.1	Demonstration of three-axis ADCS.		5
MO5.2	Characterization of actuators and sensors in a space-like environment.		5
MO5.3	Independent verification of ADCS using an imager.		5
MO6	Demonstration of duplex communication using an SDR transceiver.	15	
MO7	Recovery of FFU data storage.	20	

5. EXPERIMENT CONCEPT

In order to fulfill the mission objectives, an FFU will be ejected from the rocket and it will then perform a preprogrammed sequence of experiments. Immediately after ejection, the FFU will determine its angular rate and commence a maneuver to reduce

its angular momentum using the magnetorquers incorporated in the HISPs. Afterwards, it will perform one or more slew angle maneuvers using the pFDAs, magnetorquers, or a combination of both. Between each maneuver there will be a period of stillness, during which one or more images will be acquired for the purpose of verifying the accuracy of the ADCS independently.

After the ADCS experiment, the parachute will deploy according to a time-based triggering system, and then the communications experiment will begin. During this phase, the FFU will transmit a fixed data payload that is known by the FFU and Ground Station (GS) ahead of time (henceforth referred to as the "known payload") to the GS, and the GS will do the same in the reverse direction. This exchange of information will allow an assessment of bit error rate of the communications system. Additionally, the FFU will transmit housekeeping data and a fraction of the payload data acquired during the milli-gravity phase of the experiment to the GS in order to demonstrate that the SDR transceiver can be used in an operational scenario.

Finally, when the FFU is close to the ground, the GPS recovery system will be enabled, which will transmit the location of the FFU to the GlobalStar simplex network. The location will be received by the TUPEX-7 team, which will subsequently direct the recovery personnel to the landing area.

Performance data will be measured throughout both experiments and stored in nonvolatile memory within the FFU and GS, which will be retrieved and analyzed after a successful recovery campaign.

5.1 Experiment System Overview

The overall TUPEX-7 system is separated into three segments, each with independent functions.

- **Rocket-Borne Equipment (RBE)**: Consists of a mechanism to support the FFU during the ascent of the rocket and eject it from the Experiment Module at a pre-determined altitude, as well as an RBE Electronics (RBEE) PCB which acts as the interface between the REXUS Service Module (RXSM) and the FFU. Its functions are to sample the rocket signals, act as a communications bridge between the FFU and RXSM, and to provide the necessary voltages for charging the FFU's batteries. All of the components of the RBE stay within the experiment module for the duration of the mission, except for the outer hatch.
- **Free-Falling Unit**: Contains all of the subsystems needed to perform the experiments.
- **Ground Staton**: Consists of a computer system connected to the REXUS network to perform pre-flight checks and receive housekeeping telemetry from the FFU before ejection, and a mobile radio ground station that will track and communicate with the FFU during its descent.

5.2 Experiment Phases

The experiment is divided into five main phases, shown in Fig. 3.

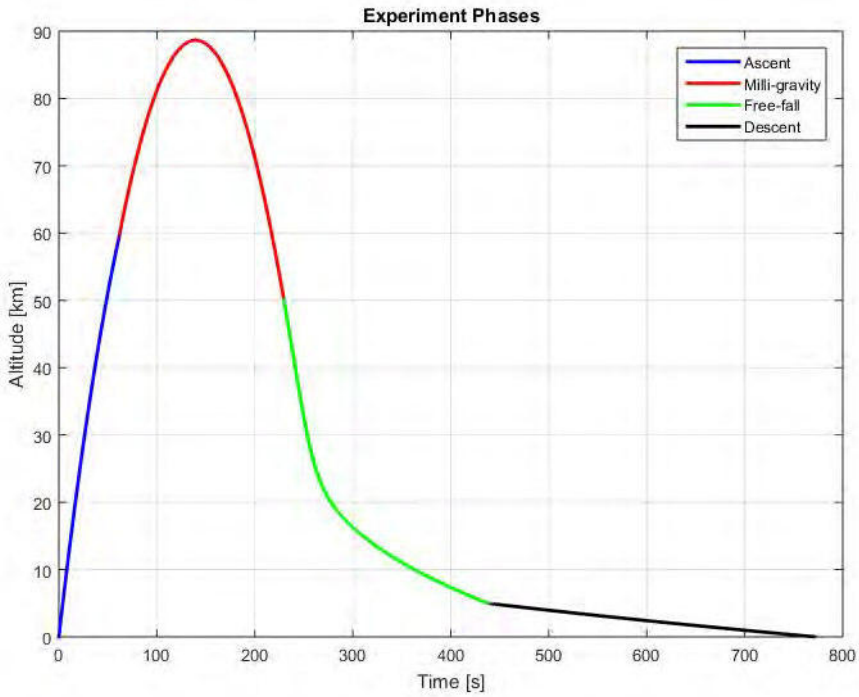

Fig. 3: Project Phases of the flight

- **Ascent**: Time period from launch start until yo-yo despin of the rocket, at which point the RBE will eject the FFU when given the signal at approximately 55 km.
- **Mill-gravity**: Time period from the ejection of the FFU until it reaches 50 km on the way down. At the beginning of this phase, the FFU will actuate the pFDAs located in the relevant axes to de-tumble and reach rotational equilibrium. Then, the FFU executes the ADCS experiment by performing a sequence of maneuvers involving three-axis actuation, whilst taking pictures.
- **Free-fall**: Time period after leaving the milli-gravity area until parachute deployment at 5 km of altitude. During this phase the FFU does not execute any experiment.
- **Descent**: Time period from parachute deployment to landing of the FFU. During this phase the known payload, the experiment data and telemetry are transmitted to and received from the GS, which is the sequence of the communications experiment using the SDR. Also, the coordinates of the FFU will be sent through the STINGR module so it can be retrieved once it lands.

6. ANTICIPATED RESULTS

TUPEX-7 is a mission focused on miniaturization of existing technology and enabling of novel technologies to increase available payload volume on a CubeSat bus. To that end, the incorporation of a (near) complete set of satellite subsystems within a 1U CubeSat form factor along with the inclusion of the parachute recovery compartment, which in itself occupies about 50% of the 1U CubeSat volume, accomplishes this primary goal. That said, it is critical that each newly developed subsystem functions as expected and as required, or the primary goal cannot be considered accomplished. This criticality is reflected in the mission objectives. Therefore, the requirements and antici-

pated performance of the HISPs and SDR experiments are detailed below.

6.1 HISPs Requirements and Expected Results

The team anticipates that through the HISPs a full three-axis ADCS system will be integrated which is capable of:

- attitude determination to minimum accuracy of 1 degree
- pointing accuracy of 5 degrees over a period of 10 seconds
- actuation of a 60-degree slew maneuver within 30 seconds

Attitude determination is done by fusion of the light sensor, gyroscope, and magnetometer measurements during the flight. Attitude control is performed by the pFDAs and magnetic coils (used for desaturation of the pFDAs' angular momentum). Independent verification of the attitude determination and control is performed by comparisons of images taken by the on-board camera pre- and post- free-fall maneuvers.

The performance data will be stored on SD cards during flight and recovered for analytical comparison to simulated performance post-flight.

6.2 SDR Requirements and Expected Results

The SDR will integrate duplex communication capabilities in multiple frequencies. At a minimum, the team expects the communication on-board the FFU to:

- Communicate in the UHF band with ground station during parachute descent
- Transmit and receive data at a minimum of 1 kbps
- Decode data sent from the ground station
- Measure received signal strength from both the FFU at the ground station and from the ground station at the FFU

Bit error rates, signal strengths, and data rates will also be stored on SD cards during flight and analyzed against existing CubeSat standard technologies for performance comparison.

7. NEXT STEPS

The development of the TUPEX-7 bus entails concurrent design, manufacture, and verification of the subsystems and their components. The team is iteratively designing the subsystems in parallel according to the system requirements. This parallel development will continue with the manufacture and test of individual components, working up through each component to the subsystem and system levels. This process will begin with design and test on breakout boards, integration boards, and structural models, and then progress into a proto-flight model and finally, the flight model.

Throughout the development, the team is drawing upon the Department's expertise through both their current and past satellite missions. Furthermore, the team has the opportunity to learn from the experience of TUPEX-6, an experiment to be launched with the preceding REXUS mission, building upon previous designs where applicable (for example, the RBE and the parachute compartment). Additionally, certain components and hardware employed on TUPEX-6 will be evaluated and re-used if possible.

TUPEX-7 will begin its final flight model acceptance tests in January 2020 and launch aboard the REXUS 28 launch vehicle in March 2020.

8. CONCLUSION

With TUPEX-7's FFU designed and developed as a virtually complete CubeSat short of just a few components, the milligravity experiment will take place in the ideal environment to test and potentially raise the Technology Readiness Level of various components and subsystems for use in space. Effective duplex communication with the SDR and flexible monopole antenna will support the future volume-saving application of SDRs in small satellites. Successful function of highly integrated side panels with pFDAs and a complete attitude determination and control system will establish a robust and adaptable CubeSat design. Though only for a short duration in milli-gravity, the camera platform will demonstrate true Earth observation, designed to offer design flexibility for various Earth imaging goals. TUPEX-7's operation and use of its suite of miniaturized technologies in the milli-gravity environment will demonstrate a vast improvement in volume-to-payload ratio and ultimately enhance the potential for Earth observation by CubeSats and other small satellites.

8. REFERENCES

[1] B. Doncaster, C. Williams, and J. Shulman, "Nano/microsatellite market forecast," SpaceWorks Enterprises, Inc, Tech. Rep., 2017.

[2] B. Lal, E. de la Rosa Blanco, J. R. Behrens, B. A. Corbin, E. K. Green, A. J. Picard, and A. Balakrishnan, "Global trends in small satellites," Science & Technology Policy Institute, Tech. Rep. P-8638, 2017.

[3] H. Kayal and K. Brieß, "Pico and Nano Satellite Technologies at the Technical University of Berlin (IAC-05-B5.6.B.03)," in 56th International Astronautical Congress (IAC), Fukuoka (Japan), 10 2005.

[4] H. Kayal, F. Baumann, and K. Brieß, "BeeSat – A pico satellite of TU Berlin for the in-orbit verification of miniaturised wheels (IAC- 08-B4.4.B10)," in 59th International Astronautical Congress (IAC), Glasgow (Scottland), 10 2008.

[5] K. Brieß, F. Baumann, and S. Trowitzsch, "Present and future picosatellite missions at TU Berlin," in 8th IAA Symposium Small Satellites for Earth Observation, Berlin, Germany, April 4-8 2011.

[6] S. Grau, D. Noack, and K. Brieß, "An angular momentum ring storage device prototype for cubesats based on a liquid metal actuator," in 66th International Astronautical Congress (IAC), Jerusalem, Israel.

[7] S. Grau, L. Kobow, and J. F. Furstenau, "Investigation of redundancy strategies in fluid-dynamic attitude control," in 69th International Astronautical Congress (2018), 2018.

[8] D. A. Sullivan, J. F. Fürstenau, S. Grau, and K. Brieß, "Development of an ejectable cubesat onboard a sounding rocket," in 2nd Symposium on Space Educational Activities, Budapest, Hungary, 2018.

[9] S. Grau, "Contributions to the advance of the integration density of cubesats," unpublished, 2018.

[10] Clyde Space, https://www.clyde.space/what-we-do/platforms.

[11] R. Wilke, "S-band, uhf and vhf communication system for cubesats including ground station software," 06 2015.

[12] Lime Microsystems, "LimeSDR Mini Specifications," https://www.crowdsupply.com/lime-micro/limesdr-mini.

SHACS: Spatial Heterodyne Atmospheric Carbon-Dioxide Spectrometer

Ikpaya Ikpaya[1], Craig Underwood[1]

[1]Surrey Space Centre, University of Surrey,
Guildford, Surrey, GU2 7XH, UK
Phone: +44 1483 686755, Mail: ikpaya.ikpaya@surrey.ac.uk, c.underwood@surrey.ac.uk

Abstract: Climate change is of increasing concern and efforts to mitigate its effects are targeted on reducing fossil CO_2 emissions. Satellite observations play a key role in the understanding and management of the problem. Whilst detecting CO_2 optically is relatively straight-forward, and has been achieved with small satellites, accurate quantitative mapping of CO_2 requires very high precision (<1%) measurements of gas concentration. This is usually achieved through identifying CO_2 by its spectral absorption bands at 1.56-1.62μm and 1.92-2.06μm wavelength by using high resolution spectrometers (e.g. 0.27cm^{-1} resolution at a signal-to-noise ratio (SNR) of >300:1). This normally requires high performance, large and complex instruments whose high cost, mass, volume, and power requirements preclude their use on small satellites. This paper presents the developmental stage of a single channel (1.6 μm) compact precision Spatial Heterodyne Atmospheric Carbon-Dioxide Spectrometer (SHACS), which utilises the Spatial Heterodyne Spectrometer (SHS) technique to form a robust, compact, no-moving-part Fourier Transform Spectrometer (FTS). This instrument achieves a high spectral resolution of 0.25cm^{-1} at a high SNR of >700:1 and can fit into a micro-satellite platform. With this performance, high quality measurements of atmospheric CO_2 concentration with measurement precision of <4 ppm can be achieved.

1. INTRODUCTION

The application of Fourier Transform Spectrometers (FTS) for remote sensing of the atmosphere has proven to offer high accuracy measurements owing to its very high spectral resolution. However, conventional FTS instruments, based on a Michelson Interferometer (MI) with moving mirrors, are usually characterized by high complexities and cost – particularly when used in a spaceflight context, where the mechanisms have to actuate in hard vacuum. At the Surrey Space Centre (SSC), we have applied, instead, the technique of the Spatial Heterodyne Spectrometer (SHS). This is similar in operating principle to a conventional FTS, in that it is also based on a MI, however, it differs in that the moving mirrors are replaced by fixed reflection diffraction gratings. In our context, this then forms a Spatial Heterodyne Atmospheric Carbon-dioxide Spectrometer (SHACS): an atmospheric CO_2 monitoring instrument. As with a conventional FTS, the SHS offers a high light throughput, due to its relatively large aperture, and a high spectral resolution. However unlike the conventional FTS, the SHS incorporates no-moving parts. This then removes much of the complexity and cost of the traditional FTS design, whilst also reducing the mass, volume and power requirements of the instrument – making it eminently suitable for small satellites.

We built and tested a single-channel bench-top prototype of this instrument and tested it under laboratory conditions using an artificial light source, under a 2013 PhD research programme sponsored by the National Space Research and Development Agency (NASRDA) of Nigeria. In this paper, we present the progress made in the design and build phase of the SHACS instrument and the results of the measurements taken from laboratory samples of CO_2 with known concentration as well as that of measurements taken in open air using natural sunlight as the illuminating source. For this current work, we acknowledge the support of the Commonwealth Rutherford Fellowship.

1.1 Atmospheric Carbon-dioxide (CO_2) Monitoring

The observation and measurement of radiation emitted from, or absorbed by, atoms and molecules provides information about their identity, structure and physical environment [1]. Monitoring atmospheric CO_2 from space therefore entails being able to identify its spectral signature, through the measurement of its absorption of sunlight, either reflected from the Earth's surface (nadir viewing instruments), or transmitted through the atmosphere (limb viewing instruments). For this application, we are focusing on monitoring atmospheric CO_2 around the tropics. Studies such as [2, 3] have shown that it has been difficult to determine the extent of atmospheric CO_2 fluxes in the tropics especially in regions around the equatorial zone due to the sparseness of *in situ* terrestrial CO_2 measurement networks. Therefore, knowledge of these regional fluxes and processes can be vastly improved through additional space-based observations – provided these are able to supply precise, accurate and reliable CO_2 measurement data.

The Short-Wave Infrared (SWIR) CO_2 absorption bands near 1.6µm (1.56µm to 1.62µm – weak CO_2) and 2.0µm (1.92µm to 2.06µm – strong CO_2) provide information on the near-surface concentrations. However, the spectral region near 1.6µm is well suited for retrieving column CO_2 because the solar flux at this wavelength region is higher than at longer wavelength regions [4]. The spectral regions around 1.6µm and 2.0µm wavelengths are also capable of monitoring water vapor (H_2O), which is also an important greenhouse gas. Monitoring the strong and weak bands simultaneously allows the interfering effect of water to be reduced. However, for these measurements to be useful, it also requires the oxygen (O_2) A-band at 0.76µm to be measured in order to correct for air mass and identify cloud effects [3, 5, 6]. The O_2 A-band is used to characterize scattering by clouds/aerosols at spectral regions around 1.6µm while the spectral region around 2.0µm is used in conjunction with the O_2 A-band to constrain the wavelength dependence of atmospheric scattering [2].

Using the PcModWin software – a graphical user interface environment based on MODTRAN5® from ONTAR [7] – the atmospheric CO_2 and H_2O spectral transmissions were created from the Mid-Latitude Summer model atmosphere, which is a standard atmospheric model with an input CO_2 mixing ratio of 400ppm, under clear sky conditions with background aerosols devoid of clouds.

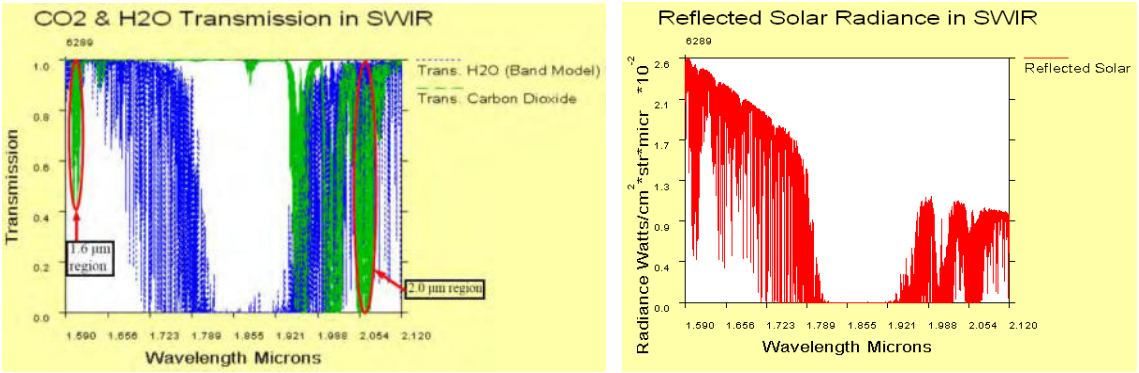

(a) (b)

Figure 1: (a) Spectral transmission model of CO_2 and H_2O between 1.59 µm and 2.12 µm (b) Reflected solar radiance within same ROI

The viewing angle was set at nadir with a Solar Zenith Angle (SZA) of 42.5º while a surface albedo of 0.3 was used. Equally, the source brightness, which is referred to as

the input radiance, was simulated using similar conditions to obtain the reflected spectral radiance using the same conditions of a nadir viewing geometry from a Low Earth Orbit (LEO) of about 700km. The spectral radiance Region of Interest (ROI) covered the 1.6µm (6250cm^{-1}) and 2.0µm (5000cm^{-1}) wavelength regions. The spectral transmission of CO_2 and H_2O is shown in Figure 1(a) while the reflected solar radiance is presented in Figure 1(b).

2. SHACS INSTRUMENT

The Spatial Heterodyne Atmospheric Carbon-Dioxide Spectrometer (SHACS) previously called the Compact Spatial Heterodyne Short-Wave Infrared (COMSSWIR) spectrometer, is a high resolution CO_2 monitoring instrument that utilises the SHS technique. In its novel implementation, it uses low groove density standard gratings in a configuration similar to the Echelle-mode SHS [8] and applies a cross tilt, α, as shown in Figure 2(a) to one of the gratings. By introducing the tilt, ambiguities resulting from superimposed spectral components are resolved and the Fizeau fringes recorded on the detector are no longer perpendicular to the *x*-axis, but rather, the tilt introduces a spatial modulation perpendicular to the modulation produced by the grating dispersion. This results in Fizeau fringes perpendicular to the *y*-axis, thereby creating a two-dimensional (2-D) interferogram, which is recorded on the detector. Full details of this implementation and equations can be found in [9, 10].

The final flight model SHACS instrument would make use of two optical benches (identified as Channel-1 and Channel-2) as shown in Figure 2(b), each tuned to one of the key CO_2 absorption bands (strong and weak). The first channel covers the 1599nm to 1605nm spectral band, while the second channel covers the 2045nm to 2064nm spectral band. Both benches share a common receiver three-mirror-reflector (TMR) telescope, which splits the incoming signal with the aid of a dichroic beam-splitter for the two channels.

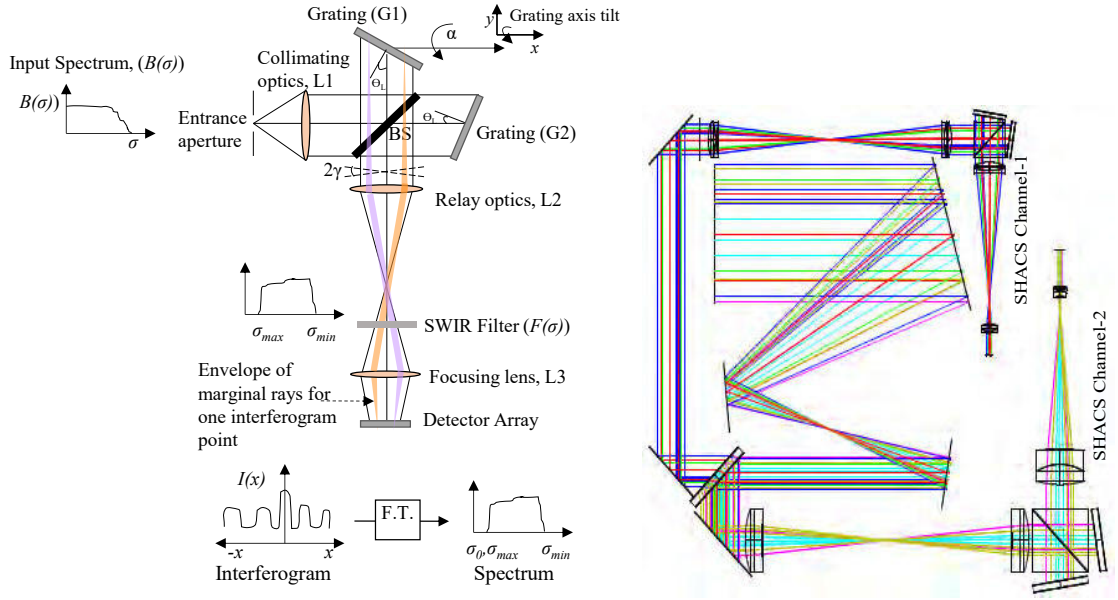

Figure 2: (a) Schematic representation of the SHS as used in SHACS Instrument (b) Optical model of SHACS Instrument showing two channels

2.1 SHACS Set-Up

Selecting appropriate commercial-off-the-shelf (COTS) optical and opto-mechanical components for the SHACS instrument, to minimize costs, has been a challenge especially as we need to operate in the SWIR. Efforts to prove the feasibility of the SHACS concept were targeted at developing a COTS-based bench-top prototype demonstrator, focusing on the 1.6μm band.

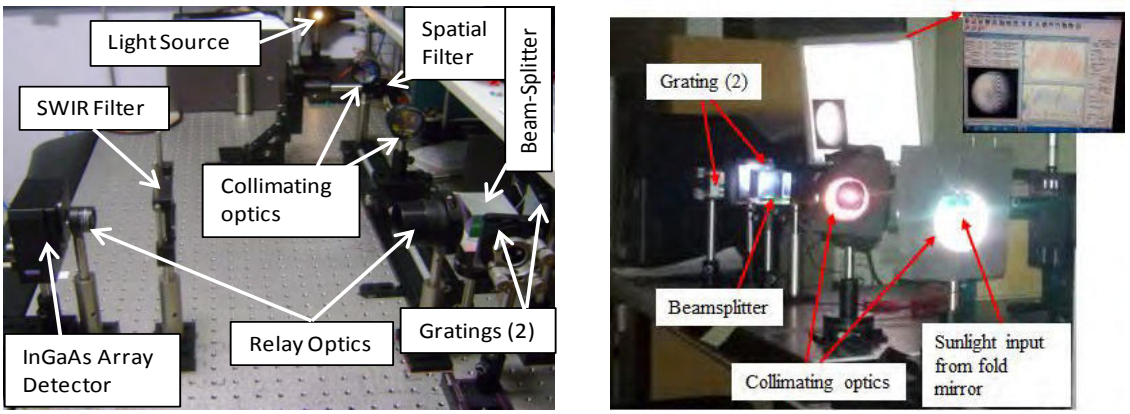

(a) (b)

Figure 3: SHACS Instrument Set-up (a) Using Halogen lamp (b) using natural Sunlight

At the first stage of this demonstration, the set-up was carried out using a Quartz Halogen Lamp as the input light source as shown in Figure 3(a) where known concentrations of CO_2 were introduced into the laboratory. It was necessary to arrange the set-up this way to test the proof-of-concept demonstrator. During measurements, the laboratory is kept dark by using anodized material with an absorbing surface finish to minimize the amount of stray light reaching the instrument focal plane.

The next stage of this experiment was to set-up the prototype demonstrator in a laboratory facility within the SSC where natural sunlight could be channeled into it with the aid of a fold mirror as shown in Figure 3(b). As expected, the result obtained shows good retrieval of CO_2 transmission spectrum within the bandwidth of interest. The bandwidth ROI was selected to avoid the effect of the water vapour absorption lines having an adverse effect in the form of contamination of the spectrum. The calibration of the instrument has been performed following the method described in [9, 10].

3. SHACS SIGNAL-TO-NOISE RATIO (SNR) ANALYSIS

3.1 Source Brightness and Signal-to-Noise Ratio (SNR)

To quantify the Signal-to-Noise Ratio (SNR), the intensity of the signal must be determined by adequately analyzing the source brightness. The SNR is the end performance metric that determines the ability to collect spectra. It is a function of the source's brightness, the instrument's entrance aperture, the optical throughput, integration time and detector performance. All these are key factors to consider for accurate quantification of the SNR [9]. Considering the 1.6μm ($6250cm^{-1}$) channel and selecting a wavelength range of 1591.60nm to 1609.53nm, the reflected solar radiance and the background radiance were modelled using the PcModWin software. This model was used to compute the SNRs, assuming the signal was falling on a photon noise limited detector.

Following the analysis given in [11], the signal falling on a photon noise limited detector over an integration time, *t*, can be represented as;

$$I(x) = \frac{1}{hc} \int_{\sigma_0}^{\sigma} B_1(\sigma)\sigma \cos\,[2\pi(4(\sigma - \sigma_0)x\tan\theta_L)]d\sigma, \quad (1)$$

where h is the Planck's constant (6.626×10^{-34} J.s), c is the speed of light (2.998×10^{8} m/s), and B_1 is the detector spectral radiant exitance which is given as [11] ;

$$B_1(\sigma) = \frac{1}{2}\left[A\Omega_0\left(L_s(\sigma) + L_{bg}(\sigma) + \frac{\Omega_{sys}}{\pi}M_{op}(\sigma)\right)\right]\tau.q_e, \quad (2)$$

where L_s is the signal radiance as shown in Figure 1(b) (W/(cm^2.sr.cm^{-1})) over a bandwidth $\Delta\sigma$, L_{bg} is the background radiance (W/(cm^2.sr.cm^{-1})), A is the area of the entrance aperture, q_e is the detector quantum efficiency, τ, is optical transmission efficiency which includes the filter transmission, lenses and grating efficiencies, Ω_0 is the solid angle subtended at the entrance aperture and Ω_{sys} is the system solid angle given as [11];

$$\Omega_0 = \Omega_{sys} = \frac{\pi D^2}{4f^2}, \quad (3)$$

where D is the diameter of entrance aperture and f is the focal length.

The aperture solid angle given in Eq. (3) is equivalent to the system solid angle as there is no obstruction in the system. A detailed expression of Eqs. (1) and (2) is given in Ref. [11]. The product of the area of entrance aperture, A, and the solid angle, Ω_0, gives the system throughput, Θ.

Using Hamamatsu's C11512-01 Multi-channel detector with its inbuilt G11097-0707S InGaAs area image sensor of 128 x 128 pixels operating in the SWIR, the given spectral response (photosensitivity) range from 0.95µm to 1.7µm was converted to quantum efficiency and incorporated into the Eq. (2) to estimate the SNR. Although 50.8mm optics are used in the bench-top prototype demonstration, the clear aperture in which the actual signal passes through is usually estimated as having a diameter of about 42.8mm. This is because, as the signal travels through the system, the factor that leads to the estimation of the solid angle and the throughput of the signal is the illuminated part of the grating, which can be estimated as two-thirds of the 50.8mm optics. The integration time set to capture the interferograms from a position sensitive SWIR detector is limited to 10s for the prototype testing. The noise is estimated as the square root of the signal. The theoretical SNR given in Figure 4(a) shows a SNR of 734:1 at 1.6µm. This is above the required SNR of >300:1 [5] and therefore meets the scientific requirement.

3.1.1 The Halogen Lamp Case

The sensitivity of the signal was initially calculated and analysed while carrying out the experiment under laboratory conditions using the Quartz Halogen lamp as the input source. The method used involved the computation of the Quartz Thompson Halogen lamp radiance, the modelling of the background radiance as discussed in [11], an integration time of 10s, the detector parameters and the calibration values of the measured interferogram and instrument parameters. The calculated SNR across the wavelength ROI is given in Figure 4(b) with the SNR at 1.6µm being 564:1.

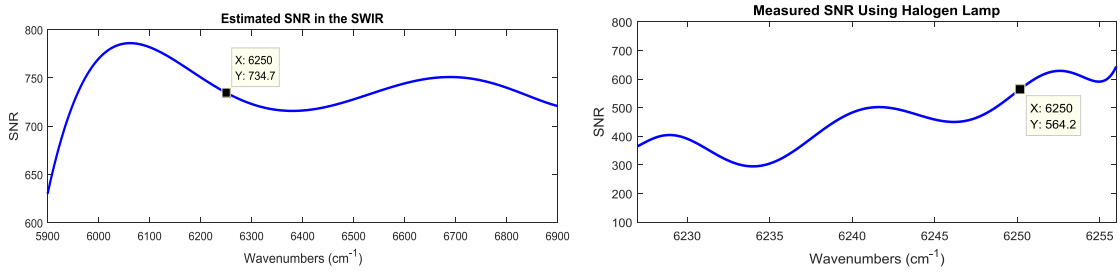

(a) (b)

Figure 4: (a) Simulated SNR across the SWIR (b) Measured SNR using Quartz Halogen Lamp

3.1.2 The Sunlight Case

The set-up for the sunlight measurement was such that sunlight entering the laboratory was horizontally reflected off a fold mirror positioned outside the laboratory in order to allow the input light reach the entrance optics of the instrument (Figure 3(b)). This method yielded a higher SNR ratio. Using the reflected solar radiance model and the calibration values derived from the measured interferogram of SHACS single channel sunlight measurements whose illuminated grating diameter is 34mm corresponding to the actual entrance aperture diameter which forms about two-thirds (2/3) of the optic's clear aperture diameter, the calculated SNR at 1600nm is 990:1 as shown in Figure 5 based on a narrow bandwidth of about 6nm, spectral resolution of 0.25cm^{-1} @ Full Width at Half Maximum (FWHM) and integration time of 10s.

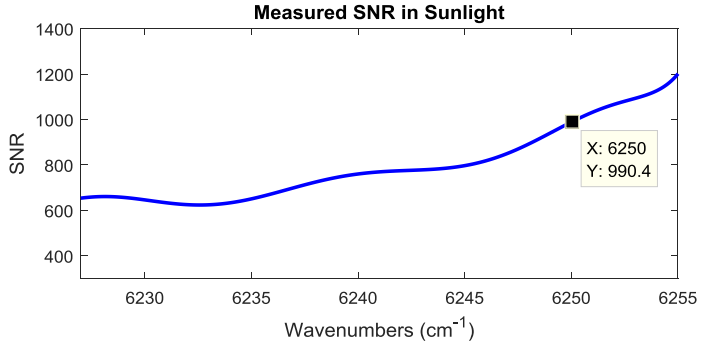

Figure 5: Measured SNR using natural sunlight as the input light source

Clearly, the optical throughput advantage of an FTS instrument which is also an advantage of the SHS, is seen to have a positive effect on the measured SNR.

4. RETRIEVAL PROCESS

The retrievals of the measured CO_2 spectrum and concentration of measured CO_2 by the SHACS prototype instrument is achieved using inverse Fourier Transforms and an Inverse Model, as discussed in [9, 10]. This is primarily based on the work of Rodgers [12]. The data processing algorithm for the retrieval process involved masking the interferogram to eliminate inherent defective pixels in the detector, to yield an increase in the SNR and improve quality of recovered transmission spectrum. Full details of the practical implementation of this work is explained in [9].

To obtain the optimal solution, $\hat{x}$, an iterative Gauss-Newton scheme is adopted [12];

$$x_{i+1} = \mathbf{x}_a + \mathbf{S}_a\mathbf{K}_i^T(\mathbf{K}_i\mathbf{S}_a\mathbf{K}_i^T + \mathbf{S}_\epsilon)^{-1}[\mathbf{y} - \mathbf{F}(\mathbf{x}_i) + \mathbf{K}_i(\mathbf{x}_i - \mathbf{x}_a)], \quad (4)$$

where $\mathbf{x}_a$ is the *a priori* value of the state, $\mathbf{S}_a$ is the *a priori* covariance matrix, $\mathbf{S}_\epsilon$ is the covariance matrix of the measurement representing the measurement error $\boldsymbol{\epsilon}$ and ^{T} represents the matrix transpose, while $\mathbf{K}$, is a weighting function also referred to as the Jacobian matrix or matrix of derivatives. The measurement vector, $\mathbf{y}$ is related to the state vector $\mathbf{x}$ and the forward model at $\mathbf{x}$, $\mathbf{F}(\mathbf{x})$,which is used in the retrieval with approximations of the true physics of the measurement, can be expressed as: $\mathbf{y} = \mathbf{F}(\mathbf{x}) + \boldsymbol{\epsilon}$ [13]. The state vector, $\mathbf{x}_i$ is updated for each iteration, $\mathbf{F}(\mathbf{x}_i)$ is the forward model at $\mathbf{x}_i$ and $\mathbf{K}_i = \frac{\partial \mathbf{F}(\mathbf{x}_i)}{\partial x_i}$ is the corresponding Jacobian matrix. For simplicity, an *a priori* state, $\mathbf{x}_a$ which is obtained using a portable CO_2 gas sensor measures the local CO_2 concentrations while SHACS measurement is in progress. This *a priori* state is used to represent the first-guess state vector $\mathbf{x}_i$ [14]. Equally, the Jacobian matrix together with the covariance matrices are calculated at each iteration.

4.1 Results

Although the automation of retrieval process for the set-up is in progress, the recorded interferogram as given in Figure 6(a), obtained from sunlight measurements of atmospheric CO_2, was processed by performing an inverse Fourier transform on the modulated part of the interferogram to recover the CO_2 transmission spectrum as shown in Figure 6(b). Following the iterative process documented in [9], the retrieved concentration of the measured CO_2 from a set of samples is 439.29ppm and the calculated bias of 0.21 ppm was achieved, where the *a priori* independently measured value is 439.5ppm (Figure 6(c)). The bias (error of retrieval) is taken from the percentage of the difference between the inverted concentrations and the true value (which was measured using a CO_2 gas sensor). A standard deviation of the retrieved state gives a measurement precision of 0.469ppm.

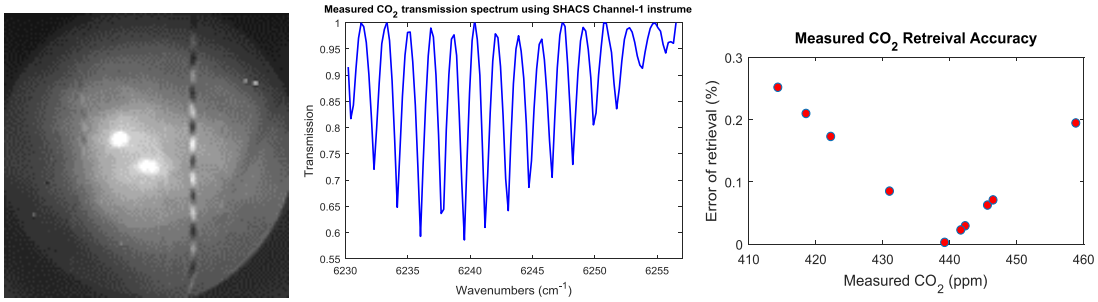

(a) (b) (c)

Figure 6: (a) Recorded Interferogram from sunlight measurement (b) Measured CO_2 transmission spectrum (c) Retrieval accuracy showing iteration to point of convergence

5. CONCLUSION

The SHACS instrument offers a unique capability for a microsatellite constellation from a LEO orbit deployed for the monitoring of atmospheric CO_2 along the tropics. We have presented the progress made in the development of a prototype demonstration of a single channel of the instrument using a COTS InGaAs detector of 128 x 128 pixels. This compact robust instrument that incorporates no-moving parts, meets the scientific requirement by achieving a spectral resolution of 0.249cm^{-1} at FWHM and a SNR of >700:1 with a resolving power of 25,082. As expected, the measured SNR in the sunlight case is >900:1. The qualitative results (CO_2 spectrum) and quantitative results

(concentration of measured CO_2) yields a measurement precision of <1%, thereby making it suitable for spaceborne deployment.

6. REFERENCES

[1] S. P. Davis, M. C. Abrams and J. W. Brault, Fourier transform spectrometry, San Diego, California, USA: Academic Press, 2001.

[2] Z. Kuang, J. Margolis, G. Toon, D. Crisp and Y. Yung, "Spaceborne measurements of atmospheric CO2 by high-resolution NIR spectrometry of reflected sunlight: An introductory study," *Geophysical Research Letters,* vol. 29, no. 15, pp. 11-1-11-4, 2002.

[3] D. M. O'Brien, R. M. Mitchell, S. A. English and G. A. Da Costa, "Airborne Measurements of Air Mass from O2 A-Band Absorption Spectra," *Journal of Atmospheric and Oceanic Technology,* vol. 15, no. 6, pp. 1272-1286, 1998.

[4] J. Mao and S. R. Kawa, "Sensitivity Studies for Space-Based Measurement of Atmospheric Total Column Carbon Dioxide by Reflected Sunlight," *Applied Optics,* vol. 43, no. 4, pp. 914-927, 2004.

[5] A. Kuze, H. Suto, M. Nakajima and T. Hamazaki, "Thermal and near infrared sensor for carbon observation Fourier-transform spectrometer on the Greenhouse Gases Observing Satellite for greenhouse gases monitoring," *Appl. Opt.,* vol. 48, no. 35, pp. 6716-6733, 2009.

[6] D. Crisp, R. M. Atlas, F. M. Breon, L. R. Brown, J. P. Burrows, P. Ciais and et al., "The Orbiting Carbon Observatory (OCO) mission," *Advances in Space Research,* vol. 34, no. 4, pp. 700-709, 2004.

[7] Ontar Corporation, *PcModWin Manual,* North Andover, MA, USA: Ontar Corporation, 2009.

[8] J. E. Lawler, Z. E. Labby, J. M. Harlander and F. L. Roesler, "Broadband, high-resolution spatial heterodyne spectrometer," *Appl. Opt.,* vol. 47, no. 34, pp. 6371-6384, 2008.

[9] I. O. Ikpaya, "Compact Spatial Heterodyne SWIR Spectrometer for Atmospheric CO2 Monitoring," PhD Thesis, Surrey Space Centre, University of Surrey, Guildford, 2013.

[10] I. Ikpaya and C. I. Underwood, "Design Analysis of Compact Short-Wave Infrared Spatial Heterodyne Fourier Transform Spectrometer for an Atmospheric CO2 Monitoring Micro-Satellite Constellation," in *9th IAA Symposium on Small Satellites for Earth Observation, International Academy of Astronautics (IAA)*, Berlin, Germany, 2013.

[11] B. J. Cooke, T. S. Lomheim, B. E. Laubscher, J. L. Rienstra, W. B. Clodius, S. C. Bender and et al., "Modeling the MTI electro-optic system sensitivity and resolution," *IEEE Transactions on Geoscience and Remote Sensing,* vol. 43, no. 9, pp. 1950-1963, 2005.

[12] C. D. Rodgers, Inverse Methods for Atmospheric Sounding: Theory and Practice, vol. 2, F. W. Taylor, Ed., New Jersey: World Scientific Publishing Co. Pte. Ltd, USA, 2000, p. 238.

[13] K. W. Bowman, "Application of Inverse Methods to Atmospheric Remote Sensing," 28 07 2016. [Online]. Available: https://www.asp.ucar.edu/sites/default/files/2_Bowman_07_28_2016.pdf. [Accessed 01 04 2018].

[14] C. W. O'Dell, B. Connor, H. Bösch, D. O'Brien, C. Frankenberg, R. Castano and et al., "The ACOS CO2 retrieval algorithm – Part 1: Description and validation against synthetic observations," *Atmos. Meas. Tech.,* vol. 5, no. 1, pp. 99-121, 2012.

High Performance EO Payloads for Smallsats

Roland Geyl[1], Daniel Farina[1], Jean-Philippe Girault[2]

[1]Safran Reosc
Avenue de la Tour Maury, 91280 Saint Pierre du Perray, France
Phone: +33 (0)1 69 89 76 51, Mail: roland.geyl@safrangroup.com

[2]Safran Electronics & Defense
18/20 quai du Point du Jour, Boulogne-Billancourt, France
Phone: +33 (0)1 55 60 38 00, Mail: jean-philippe.girault@safrangroup.com

ABSTRACT

Safran, EU leader in high performance space optics and in defense optronics is introducing two optical payloads for microsatellites offering high performances and unique extremely low Size, Weight and Power (SWaP) factor.

The first one delivers 1.5-m high resolution over 11x8 km² from 500 km orbit

The second one delivers 10-m medium resolution over 60x40 km² from durable 600 km orbit with high sensitivity for imagery and objects detection under twilight conditions.

Both instruments are fitted with 6600 x 4400 pixels 35 mm Full Frame sensor and designed with advanced innovative optics to offer extremely low SWaP factor with total volume less than 8 liters, mass around 6-8 kg only with low power need making them ideal solutions for 15-50 kg microsatellites or be a compact companion paylaod.

1. INTRODUCTION

The New Space spirit and emergence of constellations with short revisit time is calling for EO payloads with optimal performances within smallest volume and weight. Thanks to its expertise and long heritage in high performance space optics and optronic systems for defence Safran is now offering to the space community EO payloads with ultimate low SWaP factor for 18–27 U cubesats or 15-100 kg class of microsatellites. Such compact payload has now gained a first customer and is expecting to become a standard thanks to its modular design and multiplicity of potential applications.

2. TARGET NICHE FOR SMALLSAT EO PAYLOADS

We aim to offer to the community optics and EO payloads enabling the maximum of potential applications for smallsats.

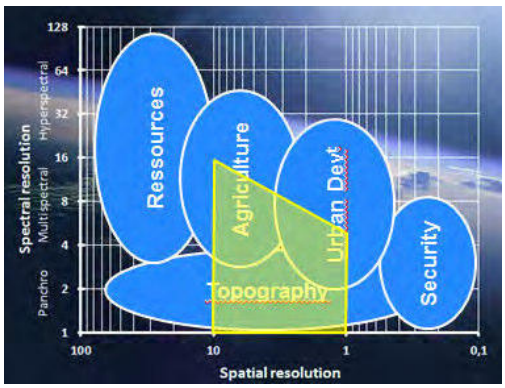

Sentinel 2 is delivering imagery down to 10-m GSD and below 1-m the business will remain driven by the ‘conventional’ prime contractors.

It therefore remains the niche between 1 and 10-m GSD where some opportunities may be found, especially with differentiating products of low size, weight and power well adapted for cubesats and nanosatellites.

3. THE SEEING 1.5-M PAYLOAD

Our concept of **S**mall sat**E**llite instrument for **E**arth imag**ING** with 1.5-m resolution (SEEING 1.5-m) is presented on the figure below. This system is designed to take snapshots of a 10 x 7 km² area, with 1.5-m resolution in panchro or with few spectral bands.

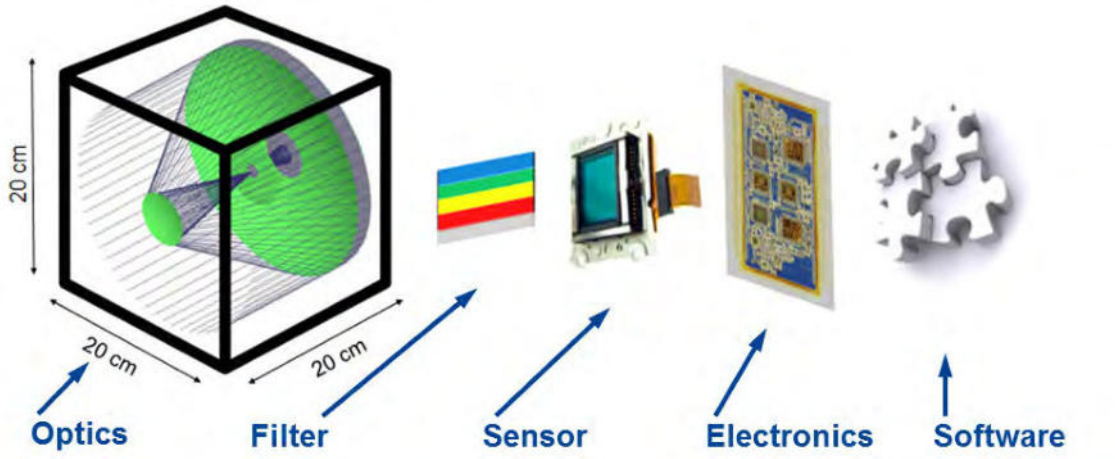

3.1 The optics

The detailed design of the optics is kept confidential at this time. It is a 190 mm aperture, 1800 mm focal length telescope system delivering diffraction limited image over 24x36 mm image format corresponding to 1.14° x 0.76° field of view, or 11 x 8 km² from 500 km orbit. The optics is a pure mirror telescope system, thus covering broadband spectral domain and fitted within a nearly cubic very small volume thus enabling unique compactness and low weight for a space camera in this range of high level performances.

The optics nominal MTF is better than 35% at 91 lp/mm corresponding to 5.5 µm pixel size and 1.5-m GSD from 500 km orbit. The distortion is very low, below 0,05%.

The optical design includes efficient baffling thanks to a field stop around an intermediate image. Such pure mirror design is therefore offering many decisive advantages:

- Wide spectral domain and total absence of chromatic aberration
- No glass sensitive to temperature and space radiations
- Simple broadband and durable reflective coatings
- Inherent efficient baffling and stray-light reduction
- Adaptation to high performance mono-material opto-mechanical concept

3.2 The filter and its technology

A 2D structured filter can be placed just in front of the detector for spectral band selection. The required number of spectral bands is distributed through the Along Track dimension of the FoV. Each spectral band is therefore captured over an 11 km x 8/N km² area, with N the number of spectral bands.

Acquiring and combining these images taken every 8/N km along the orbit of the satellite will therefore allow the rebuild the image of the entire 11 km wide trace on the earth with the desired N spectral bands. N can be tuned for each specific mission from 1 to 8.

Since two decades Safran Reosc is offering stripe filters for push broom optical instruments made of several tiny stripes of high efficiency bandpass coating deposited close to each other on a substrate placed in front of the linear detector. Typical transmission curves are shown on figure at right.

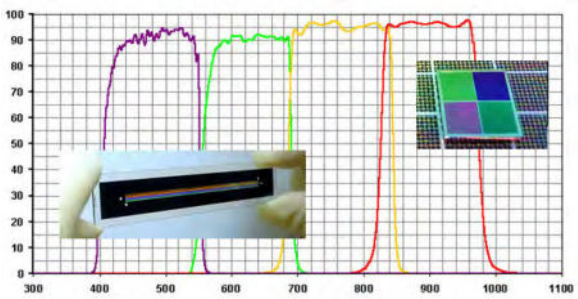

More recently, the technology of depositing spectral filters directly on the detector has emerged. This consists in depositing simple Fabry Perot based spectral filters onto the detector surface and 2D structuring them properly. We conducted similar developments on the subject from visible up to thermal IR spectral domain.

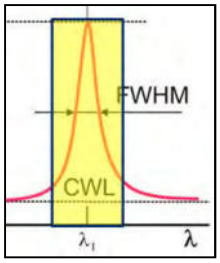

However, let's point out that our Multi Layer Dielectric (MLD) coatings technology offers much better throughput than the simple Fabry Perot as shown on the figure at left. Considering a total spectral bandwidth of about twice the FWHM bandwidth of the Fabry Perot filter one can realize that the total integrated throughput of the MLD is quite double. This is a major advantage which benefits to the EO payload solid SNR performance.

3.3 The 2D sensor

A strategic choice has been made to select an ambitious 2D sensor format of 35 mm Full Frame, i.e. 24x36 mm². This will allow using sensors from several vendors and to benefit from evolution of the sensor technologies driven by the strong technology push provided by the photographic market without redesigning our optomechanics. The choice between CCD and CMOS technology also remains open per the specific intended mission.

We have conducted detailed evaluation of the SNR offered by the instrument with MODTRAN software. On typical vegetation or urban ground scenes, we evaluate the SNR to 140 in Panchro, 100 in 4 bands MS and about 80 in 8 bands MS.

3.4 The electronics

The electronics will be adapted to the detector. This activity is one of Safran Electronics & Defense's core skills. There are also some reputed image sensor specialists serving the market with innovative approaches. Modular electronic concept is thus being developed to drive the 2D sensor and acquire the data.

3.5 The software

Safran Electronics & Defense extensive catalog of image processing modules can be implemented for on-board image pre-processing and data volume reduction before transmission to the ground. We offer full flexibility to rapidly develop this section of the payload per the targeted mission of the instrument.

Typical image processing functions are: automatic cloud or water regions removal from the images, contrast enhancement and de-noising, detection of specific targets like ships on the sea, or specified infra-structures, etc.

Furthermore, super-resolution algorithm allows targeting 1-m GSD.

- Page 77 -

3.6 The structure: SWaP factor and thermal engineering

Our concept is fitted within an 8 liters volume onaly, 10 times smaller than other instruments with similar performances.

Thanks to this, the mass of the optics alone is kept below 5 kg. Adding the sensor and its electronics, the thermal protections and interface mounting flexures biods, the total mass of the instrument is evaluated to 6 kg only, i.e. 3 times lower than alternate offers.

Our today preliminary evaluation of the electrical power needed to operate the sensor, its electronics, the various heaters, etc… is established to around 30 W.

Thermal effects management onboard microsatellites or cubesats are known to be a key issue because, due to the smaller size of the satellite, the instrument and its optics become more exposed to thermal perturbations. This subject has been very seriously taken into account in our design in several ways:

_First, we propose to place the satellite on a sun-synchronous orbit that will allow the progressive installation of a stable thermal configuration within the satellite: Sun on one side, deep space on the other and the earth surface in front.

_Second, all state-of-the-art passive MLI thermal insulation dispositions will be implemented to reduce the thermal load coming from the sun side and the thermal sink on the opposite side.

_Adequate management of the heat generated at detector and its electronic level will also contribute to reduce the thermal perturbation on the opto-mechanics. This will be done in the usual way of thermal straps used to passively evacuate heat generated by the detector and heaters to be used in the case of temperature coming below the safe operation range.

_The optomechanical engineering itself is inherenty thermally stable because the optics is based on a mono-material telescope system. Any change in temperature generates a global dilatation of the system, thus keeping the sensor in focus and the image quality through the field unchanged.

_Sensitivity to thermal gradients, probably the most challenging point, is also kept very low thanks to the use of ceramic material, nearly 10 times more efficient than aluminum under this aspect.

Today, we are evaluating the operational temperature range to stay within 15-25°C.

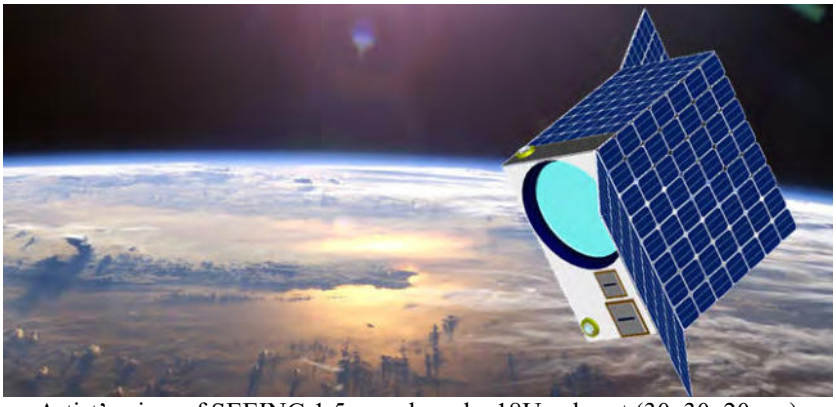

Artist’s view of SEEING 1.5-m onboard a 18U cubesat (30x30x20 cm)

4. THE SEEING 10-M PAYLOAD

We have also matured the concept of SEEING 10-m, another EO payload dedicated to other applications from space with cubesats and nanosatellites.

SEEING 10-m payload is designed to take snapshots of 60x40 km² areas from the long life 600 km orbit with 10-m GSD in panchro or several spectral bands. Its differentiation is a high F/# enabling to take pictures with solid SNR under low light conditions.

The architecture of the paylaod is very similar to the on of SEEING 1.5-m: an optics, a filter, a 35 mm Full Frame sensor, electronics plus on-board data processing in option.

The optics is a 130 mm aperture, 6.3°x4.3° FoV and 330 mm focal length system with diffraction limited performance over 475 to 900 nm spectral domain.

The system shows very low distortion of less than 1.5 µm, i.e. below 0,001%. The design MTF is better than 55% for the 91 lp/mm corresponding to 5.5 µm pixel size and 10-m GSD from 600 km orbit. The high relative aperture of F/2.5 offer unique capabilities of imagery in low light conditions like twilight and close to the poles.

The design is pushed to a very high level performance level in order to be still able to offer sufficient MTF level with 50 Mpx sensors that may appear soon on the market. This will enable 7-m GSD imagery over the same 60x40 km² from 600 km orbit. Another option is to run super-resolution algorithm for quite the same net result.

Again, the volume of the optics alone is kept as compact as possible and remains within less than 160x160x150 mm3. The whole payload can then easily fit within an 8U or 12U cubesat. An entrance baffle limits the stray light through the system.

With performances directly comparable or even better than the one of the SPOT-1 satellite developed more than 30 years ago our today SEEING 10-m payload can be qualified as '*SPOT-1 in a shoebox*'.

4.1 Again ultra low SWaP design principle

Thanks to its extremely compact design the mass of the optics itself is kept below 6 Kg. Including the sensor and its electronics, the thermal protections and interface mounting flexures, the total mass of the instrument is evaluated to less than 7 kg.

Our preliminary evaluation of the electrical power needed to operate the sensor, its electronics and the temperature control system is established at around 30 W.

5. CONCLUSION

Safran is developping the SEEING EO payload offering exceptional low SWAP factor with 10 times smaller volume and 3 times lower weight than other instrument offering similar performances. SEEING 1.5-m is delivering high performance imagery with 1.5-m GSD from 500 km durable orbit. Super resolution processing shall allow to reach sub-meter GSD. We are also convinced that such exceptional payload will find other applications in the domain of science, debris detection or Space Situation Awareness, pseudo-satellite or UAV and defense and become a standard in space optics.

On the other hand SEEING 10-m is designed for modest 10-m GSD but over 60x40 km² wide FOV and is differentiating with low F/# for imagery under twilight conditions.

Multispectral Time Delay Integration image sensor for high resolution earth observation

Pierre Boulenc[1], Steven Thijs[1], Jonas Bentell[1], Vasyl Motsnyi[1], Pilar Gonzalez[1], Klaas Tack[1], Celso Cavaco[1], Maarten Rosmeulen[1], Stefano Guerrieri[1], Piet De Moor[1]

[1]imec
Kapeldreef 75, 3001 Leuven, Belgium
Phone: +32 16 28 15 44, Mail: pierre.boulenc@imec.be

Abstract: High resolution earth observation from small satellites requires fast and sensitive line-scan imagers with a small pixel pitch operating at low power consumption and ideally featuring spectral sensitivity. Imec's CCD-in-CMOS technology allowed to develop a 7-band TDI image sensor with 256 TDI rows each, using 4096 columns at a pitch of 5.4 micron. Both CCD row drivers and fast 12-bit analog-to-digital converters (ADCs) at each column are integrated. A quantum efficiency close to 100% is obtained thanks to backside illumination. As the 7 CCD TDI bands are operated separately, they can be used to sense in 7 different wavelength bands. In order to achieve this, we are developing the integration of band-pass filters directly on top of the image sensor. Chosen approach is to use glass-based broadband (100 nm) filters glued together and finally integrated directly on top of the CCD bands on the line-scan imager. A filter assembly with 6 bandpass filters and one panchromatic channel is currently under development.

1. INTRODUCTION

Time Delay Integration (TDI) imagers have been proven to be the best imaging solution for low orbit earth observation. In this study, we propose to use a TDI imager using a specifically developed technology [1-3] which combines the benefits of a classical CCD TDI with the advantages of the System-On-a-Chip (SoC) integration of CMOS. In order to achieve multi-spectral imaging, an existing 7-band CCD-in-CMOS TDI device is employed to demonstrate the integration of dedicated multi-spectral filters (panchromatic + 6 multi-spectral). Section 2 presents the technology used to manufacture the TDI imager. Section 3 focuses on the SoC architecture needed to allow multi-spectral TDI imaging together with pixel and circuit performance. Finally, Section 4 demonstrates a color filter integration on a manufactured imager.

2. TECHNOLOGY DEVELOPMENT

Imec's CCD-in-CMOS platform was realized by adding a few process modules to a standard 0.13 µm CMOS process flow containing dual gate oxide standard nMOS and pMOS transistors (1.2 and 3.3V).

Dedicated well and junction implants for the CCD elements and readout transistors have been developed to ensure CMOS compatible operating voltages (*Figure 1*).

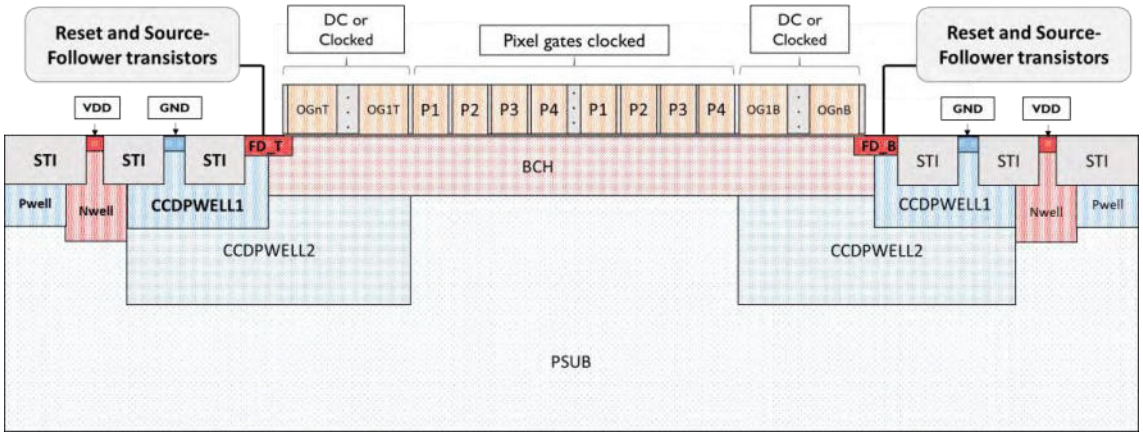

Figure 1: Cross-section schematic of a CCD column; charges can be transported towards the top (resp. bottom) of each column and readout at FD_T (resp. FD_B) depending on motion of scene with respect to the sensor

Row drivers with slew rate control ensure fast and proper clocking of the CCD gates between -1.5 V and +3.3 V while keeping Charge Transfer Inefficiency (CTI) per line as low as 10^{-5} between a 20 kHz and 1 MHz line rate (*Figure 2*).

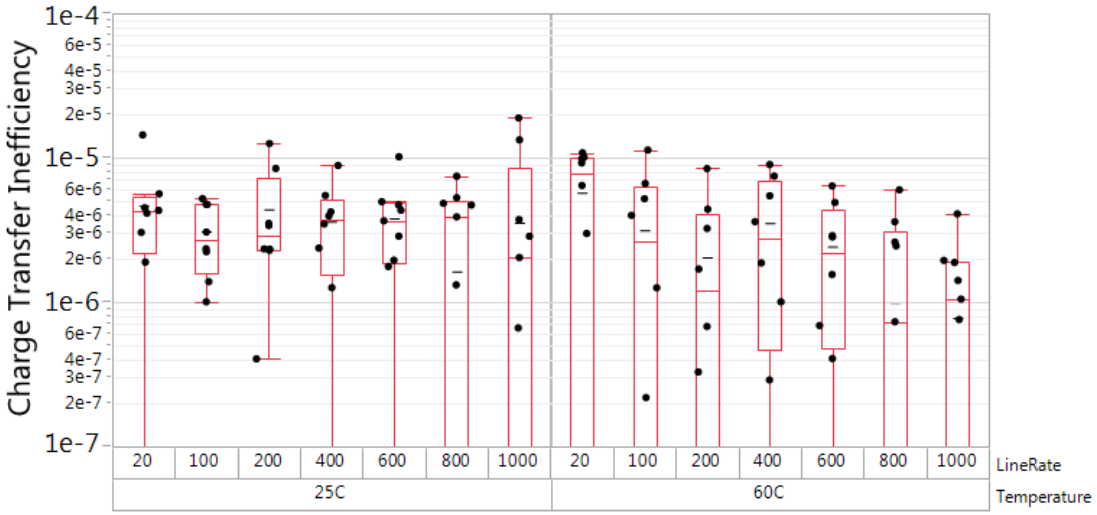

Figure 2: Charge Transfer Inefficiency per line at various line rates (in kHz) and temperatures (ºC) for signals up till linear Full-Well-Capacity measured on a CCD-in-CMOS test vehicle with 5 µm pitch pixels

3. MULTI-BAND SYSTEM ON CHIP

Using mentioned technology, we have designed and fabricated a multi-band TDI sensor [3]. The sensor consists of 7 CCD bands, with 256 rows and 4096 columns each. The pixel size is 5.4 µm to accommodate the column ADCs within the minimum design rules of the employed CMOS technology.

3.1 System on Chip architecture

The sensor's architecture is depicted in *Figure 3*. Each band uses individual on-chip sequencers and CCD drivers for the four-phase CCD pixels. As such, the CCD bands

operate continuously and time interleaved. The 7 bands can be individually switched on/off and can be reconfigured in terms of active number of TDI rows or direction of charge transport individually. Such features allow to center the dynamic range to the relative specific spectral intensity of the scene and the transmission losses of filters.

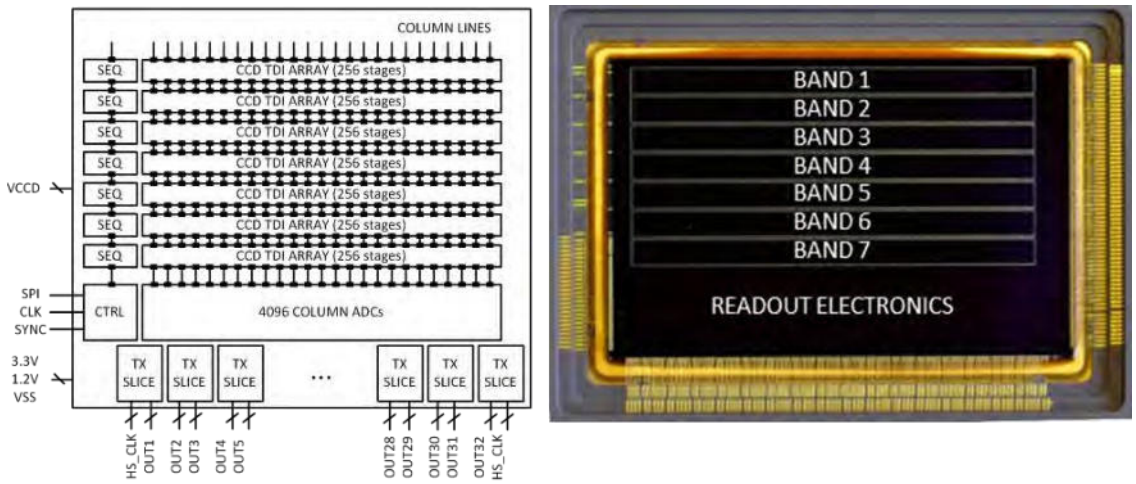

Figure 3: 7-band CCD-in-CMOS TDI schematic diagram (left) and photograph of a Back-Side-Illuminated sample (right)

3.2 Measurement results

Dedicated processing has been employed to allow Back-Side-Illumination (BSI) and ensure optimal light sensitivity in the visible range (*Figure 4*).

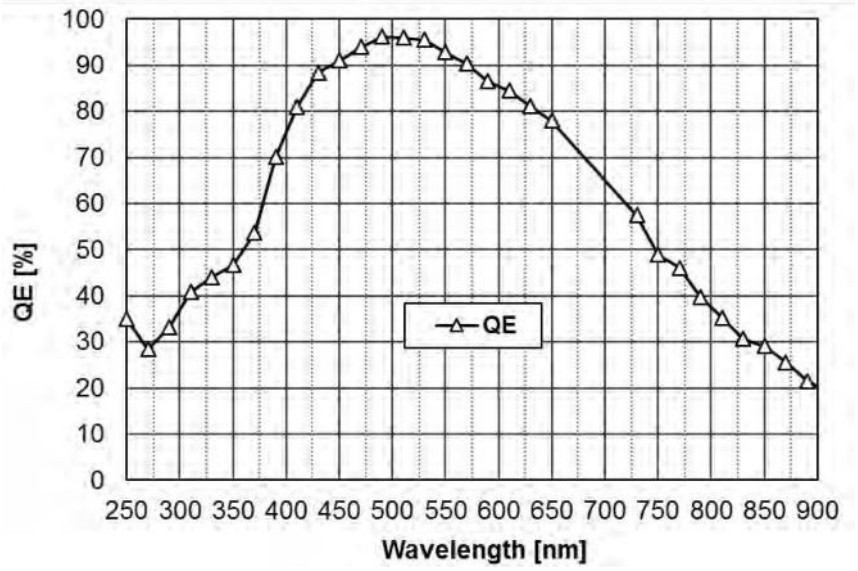

Figure 4: Quantum Efficiency vs. wavelength for a BSI sample; peak is 96% at 490nm

3.3 Multispectral filter integration

We chose to directly integrate on the TDI sensor a 7-band assembled filter stack consisting of 7 different glass substrates (*Figure 5*). Black epoxy is used to glue the filters to-

gether and cover the chip outside CCD arrays in order to limit parasitic light. Color filters are placed at the bottom and an anti-reflection coating at the top. Compared to the integration on the package lid, distance between the filter and the pixels is minimized.

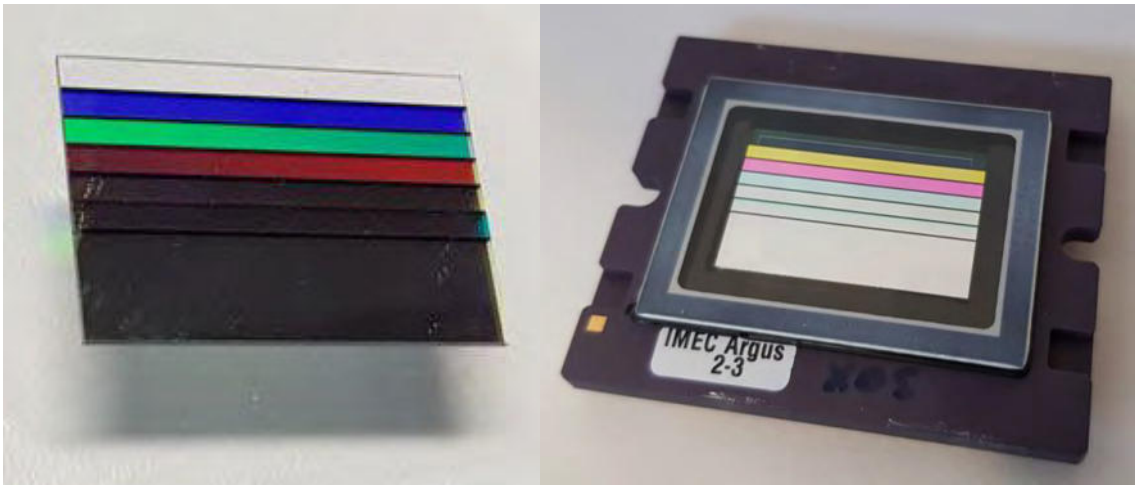

Figure 5: 7-band assembled glass filters before (left) and after (right) direct integration onto the multi-band CCD-in-CMOS TDI imager

4. CONCLUSIONS

In this paper we have presented how Imec's CCD-in-CMOS technology enables the fabrication of a high performance multispectral TDI imager. Measurements on pixels have shown proper operation up-till 1 MHz. Thanks to compatibility with standard CMOS process, complex digital sequencers, high speed serial links and high-resolution column level ADCs allow simultaneous multi-band imaging. Finally, the direct integration of multi-band glass color filters turns the sensor into a very compact and power efficient multi-spectral imager that can be customized to meet small satellite specifications.

5. ACKNOWLEDGEMENTS

This project has received funding from the Electronic Component Systems for European Leadership Joint Undertaking under grant agreement No 662222. This Joint Undertaking receives support from the European Union's Horizon 2020 research and innovation program and Belgium, Netherlands, Greece, France. The filter integration is part of the ESA AO/1- 9315/18/NL/AR contract MICROM-HIDE: Technologies For Microsatellites Multispectral High Definition Imager.

6. REFERENCES

[1] P. De Moor et al., "Enhanced time delay integration imaging using embedded CCD in CMOS technology", International Electron Devices Meeting (2014)
[2] P. Boulenc et al., "High Speed Backside Illuminated TDI CCD-in-CMOS Sensor", International Image Sensor Workshop (2017)
[3] D. San Segundo Bello et al., "A 7-band CCD-in-CMOS Multispectral TDI Imager", International Image Sensor Workshop (2017)
[4] N. Tack et al. "A compact, high-speed, and low-cost hyperspectral imager", Proc. SPIE 8266, Silicon Photonics VII 8266(0), 8266Q (2012)

DESIS – DLR Earth Sensing Imaging Spectrometer

David Krutz[1], Ilse Sebastian[1], Ingo Walter[1], Burghardt Günther[1], Holger Venus[1], Michael Neidhardt[1], Ralf Reulke[2], Bernd Zender[1], Rupert Müller[3], Simone Arloth[1], Matthias Lieder[1], Ute Grote[1], Andreas Wojtkowiak[1], Friedrich Schrandt[1]

[1]Deutsches Zentrum für Luft- und Raumfahrt e.V.
Institute of Optical Sensor Systems, Rutherfordstraße 2, 12489 Berlin, Germany
Mail: david.krutz@dlr.de

[2]Humboldt Universität zu Berlin
Institute for Computer Science, Rudower Chaussee 25, 12489 Berlin

[3] Deutsches Zentrum für Luft- und Raumfahrt e.V.
Remote Sensing Technology Institute, Oberpfaffenhofen, 82234 Weßling, Germany

Abstract: Space-based hyperspectral instruments are used in many applications requiring identification of materials or helping to monitor the environment. Although there are lots of useful applications, the amount of space born data is limited. The DLR Earth Sensing Imaging Spectrometer (DESIS) is a new space-based hyperspectral instrument developed by DLR and operated under collaboration between the German Aerospace Center (DLR) and Teledyne Brown Engineering (TBE). The primary goal of DESIS is to measure and analyze quantitative diagnostic parameters describing key processes on the Earth surface. This goal can be reached with the instrument parameters of 235 spectral bands from 400 nm to 1000 nm and a GSD of 30 m. DESIS was installed on the International Space Station on the MUSES platform in August 2018 and is providing hyperspectral Earth Observation in the wavelength range from visible to near-infrared with high resolution and near global coverage. This contribution presents the design of the compact instrument. With its interface constraints it would be also suitable for small satellite platforms.

1. INTRODUCTION

With hyperspectral instrument hundreds of spectral bands can be measured. With these bands spectral properties like reflectance or emission of Earth surface can be reconstruct. The spectral signatures can be used for the identification of material or the measurement of concentrations. Hyperspectral remote sensing data are applicable for monitoring of the vegetation, forestry and agriculture[1], coastal and inland water [2], mining, geology[3] and soils[4]. Since the 2000s space-based hyperspectral sensing instruments have been launched. The first instrument was Hyperion[5], launched in 2000. The classical space-based instruments are operating for medium size satellites like EnMAP[6] or PRISMA[7], or are operating from the International Space Station (ISS) like HICO [10]. With the integration of the Multi-User System for Earth Sensing (MUSES) on the ISS, a new platform for earth observation was established. The first instrument on MUSES is the DLR Earth Sensing Imaging Spectrometer (DESIS). DESIS is opening up new special fields of application. The off-nadir capability of DESIS with ±15° along track during a datatake enables investigations of the BRDF (Bi-Directional Reflectance Distribution Function) of objects on Earth and thus provides additional target-specific information. The variable recording times due to the non-sun-synchronous orbit of the ISS allow investigations of solar-induced chlorophyll fluorescence and photosynthesis[8].

2. DESIS

The DESIS instrument parameter are shown in Table 1. DESIS was launched in June 2018 with SpaceX-15. After the robotic integration of the DESIS instrument to the MUSES platform in August 2018, a commissioning and validation phase was performed. In early 2019 the operational phase has been started. From specification to delivery the instrument was developed in a time of just three and a half years.

Parameter	Value
$F_{\#}$	2.8
focal length	320 mm
field of view	4.1°
instantaneous field of view	0.004°
ground sampling distance	30.0 m
spatial pixels	1024
swath	30 km
spectral range	400 nm - 1000 nm
spectral channels	235
spectral sampling distance	2.55 nm
spectral binning modes	1, 2, 3, 4
signal-to-noise ratio (albedo 0.3, 45°SZA, 232 Hz @ 550 nm)	195 (no binning) 386 (binning 4)
radiometric linearity	>95% (10%-90% full well capacity)
radiometric resolution	12 bit + 1 bit gain
modular transfer function value at Nyquist	>20%
full width at half maximum	<3 nm
pixel size	24 μm x 24 μm
maximum frame rate	232 Hz in Rolling Shutter Mode
polarization	<5%
along track pointing capability	±15°
pointing accuracy	<0.004°
mass	88 kg
ISS orbit	400 km

Table 1: DESIS parameters

3. DESIS DESIGN

An overview of the DESIS design is shown in Figure 1. The DESIS telescope is a Three-Mirror-Anastigmat (TMA) which focus the radiation from Earth on a slit (see Figure 2). The spectrometer design is inspired by an Offner design type, but equipped with specific free-form mirror as described in [9]. The grating is manufactured by mechanical diamond ruling. It is a convex grating with a binary groove form. Optimized on 1st order it suppresses any higher order to less than 2%. To further reduce higher spectral orders an order sorting filter in front of the detector is additionally used. The measured wavefront degradation of the full optics system with rms=84 nm @ 632.8 nm on axis resulting in full optical system performance of about λ/8 on-axis. The detector is a backside thinned CMOS sensor with 24µm pixel from Fairchild Imaging (BAE Systems Imaging Solutions). It is spectral sensitivity ranges from 400 nm to 1000 nm. From the existing 256×1024 pixel only 235 spectral lines are used by the instrument. The function of the pointing unit (POI) is to change the line of sight of the instrument. The pointing mirror will be controlled by a stepper motor. Two modes of operation are supported: Earth observation mode and forward motion compensation mode. In the Earth observa-

tion mode the nominal image strip acquisition will be performed. The Line of Sight is programmable between ±15◦ with a repeatability accuracy of 0:003◦ (34 of pixel). The forward motion compensation mode will be used for improving the SNR by increasing the integration time. Dedicated positions of the mirror will be detected by magnetic sensors. These position sensors will also be used for auto-calibration of the stepper motor (homing) and for in-flight calibration by Calibration Unit (CAL) view. The calibration unit will be used for the in-flight spectral and radiometric calibration of the DESIS instrument. The Calibration Unit consists of two identical LED bank arrays. Each bank has 9 different types of LED /colors. In front of each LED Integrated Micro Optical Systems (IMOS) lens are used to narrow the light cone to ±16◦. The LED banks are temperature stabilized. The instrument view on Calibration Unit will be used also for dark signal and PRNU cross-calibration in-flight likewise. In this case the Calibration Unit leave switched off. This will be the reference for the later spectral in-flight calibration.

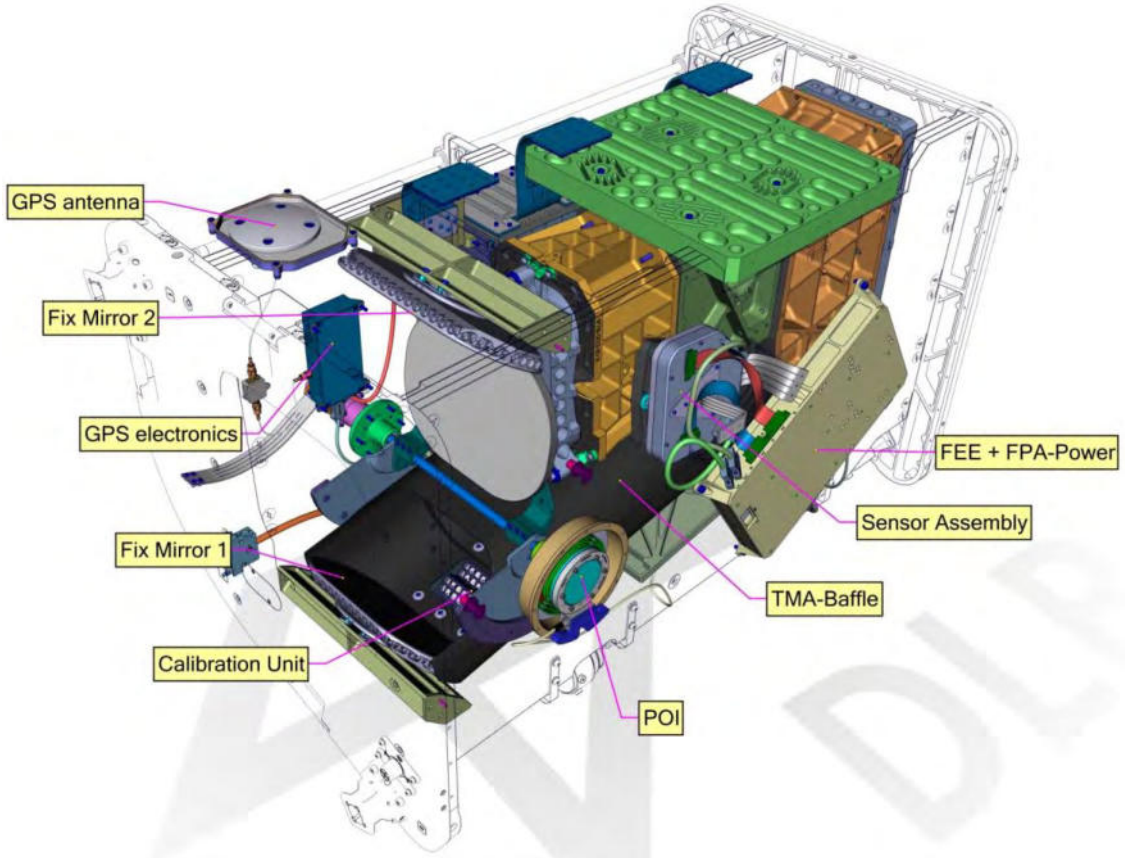

Figure 1: DESIS instrument

4. SUMMARY AND OUTLOOK

The DESIS instrument is a hyperspectral instrument for the visible to near-infrared range onboard of the ISS. It has 235 spectral bands from 400 nm to 1000 nm with 30 m GSD. With an instrument mass of 35kg (without container) and ca. 400mm x 400 mm x 500 mm the instrument is suitable for small satellites. The operating onboard of the ISS shows the high performance which is possible with the instrument design.

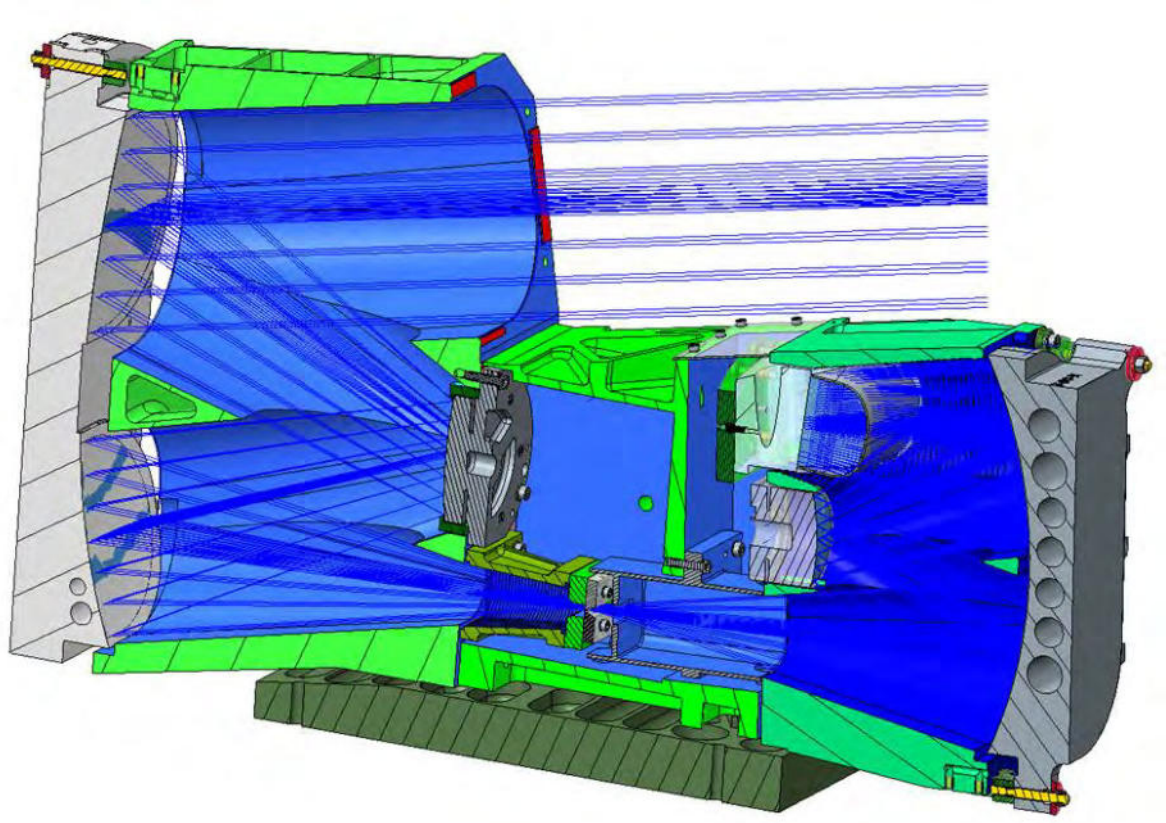

Figure 2: Cut-view of the DESIS opto-mechanical system. The TMA is on the left, the Offner on the right side [TBD].

5. REFERENCES

[1] Hill, J.et al. Imaging Spectroscopy of Forest Ecosystems: Perspectives for the Use of Space-borne Hyperspectral Earth Observation Systems. *Surveys in Geophysics* 2019

[2] Giardino, C. et al., Imaging Spectrometry of Inland and Coastal Waters: State of the Art, Achievements and Perspectives. *Surveys in Geophysics* 2018

[3] Mielke, C. et al. EnGeoMAP 2.0 - Automated Hyperspectral Mineral Identification for the German EnMAP Space Mission. *Remote Sensing* 2016, *8*, 127

[4] Steinberg, A. et al. Prediction of Common Surface Soil Properties Based on Vis-NIR Airborne and Simulated EnMAP Imaging Spectroscopy Data: Prediction Accuracy and Influence of Spatial Resolution. *Remote Sensing* 2016, *8*, 613

[5] Pearlman, J.S. et al. Hyperion, a space-based imaging spectrometer. *IEEE Transactions on Geoscience and Remote Sensing* 2003, *41*, 1160–1173

[6] Guanter, L. et al. The EnMAP Spaceborne Imaging Spectroscopy Mission for Earth Observation. *Remote Sensing* 2015, *7*, 8830–8857

[7] Pignatti, S. et al. The PRISMA hyperspectral mission: Science activities and opportunities for agriculture and land monitoring. *2013 IEEE International Geoscience and Remote Sensing Symposium - IGARSS* 2013, pp. 4558–4561

[8] Nichol, C. et al. Diurnal and Seasonal Solar Induced Chlorophyll Fluorescence and Photosynthesis in a Boreal Scots Pine Canopy. *Remote Sensing* **2019**, *11*, 273.

[9] Peschel, T.; Damm, C.; Beier, M.; Gebhardt, A.; Risse, S.; Walter, I.; Sebastian, I.; Krutz, D. Design of an imaging spectrometer for earth observation using freeform mirrors. *Proc.SPIE* **2017**, *10562*.

[10] Keith, D. et al. Remote sensing of selected water-quality indicators with the hyperspectral imager for the coastal ocean (HICO) sensor. *International Journal of Remote Sensing* **2014**, *35*, 2927–2962

iSIM 170 QM and qualification test campaign

Rafael Guzmán Llorente[1,2], Eider Ocerin Martínez[1], Aitor Conde Rodríguez[1]
[1]SATLANTIS MICROSATS SL
Edificio Sede, Parque Científico Campus UPV BIZKAIA, 48940 Leioa, Bizkaia, Spain
Phone: +34 944 344 780, Mail: ocerin@satlantis.com

[2]Department of Astronomy
Bryant Space Science Center, University of Florida, Gainesville, FL 32611, USA
Phone: +1 352 283 4845, Mail: guzman@satlantis.com

Abstract: iSIM, the integrated Standard Imager for Microsatellites, is a compact and high-resolution imager for Earth Observation applications developed by SATLANTIS. iSIM 170 has a mass of less than 15kg, an effective aperture of 150mm, a focal length of 1500mm, providing a GSD/GRD of 1.8m/2.5m in its panchromatic version from a height of 500km. The electronics combine COTS components with SATLANTIS' proprietary technology. In order to demonstrate its readiness for its first orbital flight, currently scheduled for Q1 2020, a QM version was manufactured in Spain during Q3 and Q4 2018. This QM performed functional, thermal-vacuum cycling, vibration tests during Q4 2018 while radiation tests have been performed during Q1 2019. On this paper a discussion on the qualification campaign is presented.

1. INTRODUCTION

iSIM, the integrated Standard Imager for Microsatellites, is a compact and high-resolution imager for Earth Observation applications developed by SATLANTIS. The technology behind iSIM combines four key components: (1) a binocular diffraction-limited telescope based on a Maksutov-Cassegrain design, (2) a high precision, robust and light alloy structure with carbon fibre rods, (3) a set of innovative CMOS matrix detectors, and (4) a high-performance and reconfigurable on-board computer for payload control and image processing. Thanks to iSIM's design characteristics, iSIM payloads will be able to record data continuously without the need to stabilize the satellite, and therefore the imager is especially suited for the monitorization of linear structures on the Earth's surface such as coastlines, pipelines and borders.

iSIM 170, SATLANTIS' first payload, has a mass below 15kg, an effective aperture of 150mm, a focal length of 1500mm, and two CMOS sensors of 12.5 Mpixels. The payload is developed to provide images in 1 spectral band (Panchromatic), with a GSD/GRD of 1.8m/2.5m at 450nm-1micron and a swath of 7.5km from a 500km orbit.

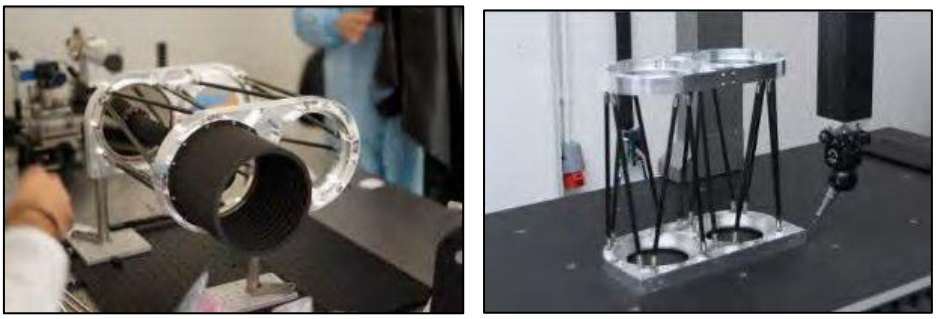

Figure 1. iSIM 170 QM manufactured and ready for the test campaign

The structure is composed of two plates (rear and front) connected by 14 struts and connected to the satellite surface by 3 blades in an isostatic configuration. The plates hold the optical elements with the use of flexures, the detectors, and have 3 pairs of baffles to reduce stray light. This structure combines materials with low density, high strength and appropriate thermal expansion coefficients in a design that ensures thermal stability. Moreover, all mechanical structure elements are coated to reduce stray light and protect the system from radiation.

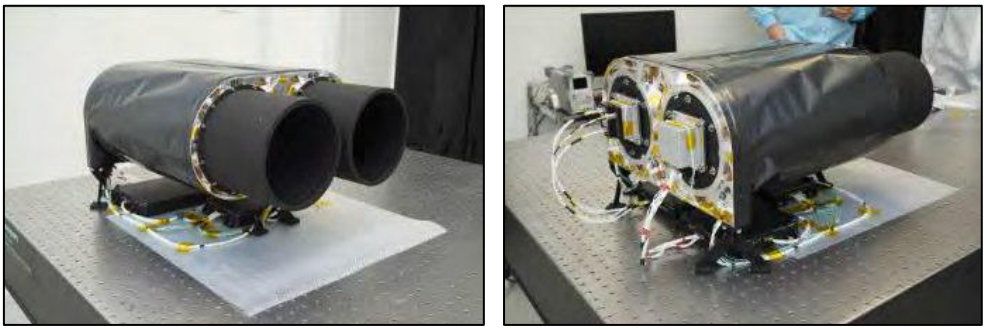

Figure 2. iSIM 170 QM manufactured and ready for the test campaign

For the ECS, SATLANTIS is developing a powerful subsystem suitable for the iSIM payload, the ECS Hybrid Solution, i.e. a combination of COTS components with SATLANTIS' proprietary technology. The main components of the QM of the iSIM ECS are (1) COTS camera: covers the functionalities of a photodetector, i.e. image acquisition, and image generation, (2) SmartCIA: covers the functionalities of a processing unit and a communication interface adapter; (3) The Monitoring and Testing Platform: contains the iSIM ECS Management App and Monitoring and Validation Tool (M&VTool) and forms part of the Payload EGSE.

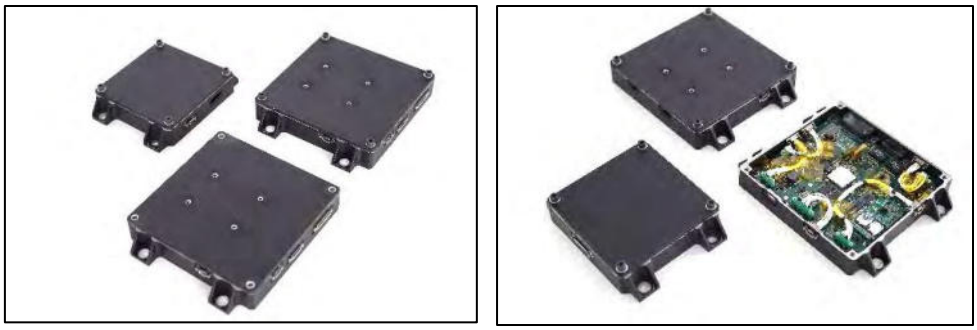

Figure 3. ECS boxes

The results of the qualification test campaign include functional, thermal-vacuum cycling, vibration, and radiation tests.

2. TEST FACILITIES

The tests facilities selected are: (1) Thermal vacuum at ALTER TECHNOLOGY TÜV NORD S.A.U in Tres Cantos (Madrid), (2) Vibration at VIRLAB S.A. in Asteasu (Basque Country), and (3) Radiation at the facilities of CAN-ALTER RADLAB located in Sevilla (Andalucía), all of them in Spain.

The thermal vacuum chamber used was 700 x 700 x 700mm^3, capable of reaching pressure levels below 10^{-7} mbar and temperatures between -180ºC and 200ºC. It has an optical window that was used to monitor the quality of the image during the tests. Image quality was evaluated measuring the PSF (Point Spread Function) in 9 different areas of the image sensor. The PSF was generated using a laser and a collimator directly facing the iSIM camera.

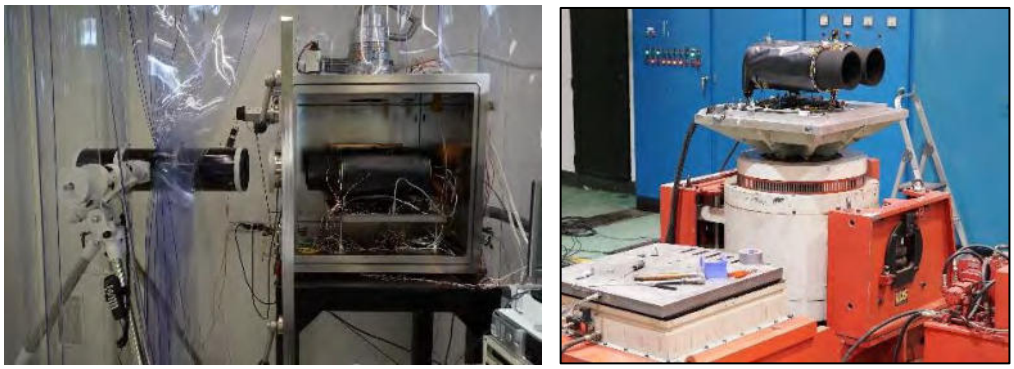

Figure 4. TVAC and Vibration testing of iSIM170

The vibration tests were performed using an Electrodynamic Shaker that can provide up to 26686 N of force, frequencies from DC to 3200Hz, maximum acceleration of 60 g's RMS and a maximum displacement of 19mm. The vibration tests were performed with the iSIM 170 switched off and only pre and post measurements were performed to evaluate any picture degradation.

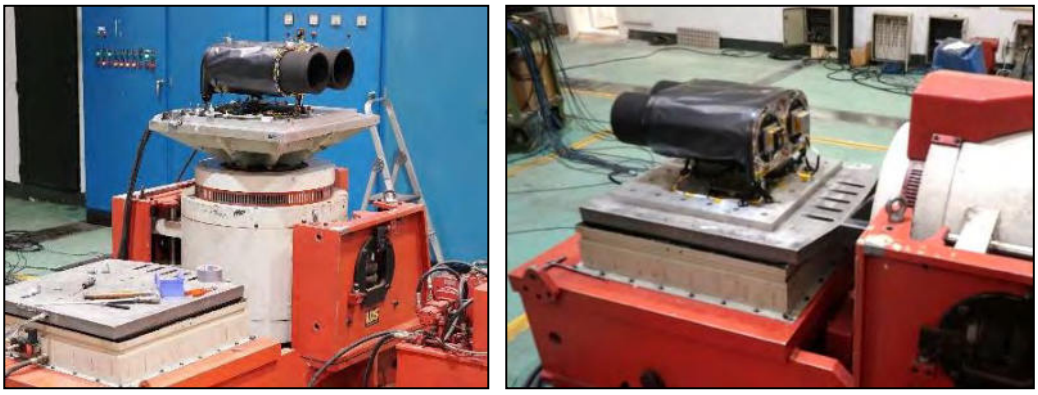

Figure 5. Vibration testing of iSIM170 on Z and Y axis

The radiation tests have been performed by ALTER in the RADLAB laboratory from the CNA (Centro Nacional de Aceleradores). The facilities provide a Gamma radiation using Co66 source with nominal activity 444 TBq (12 kCi) with range of dose from 0.26 to 360Gy/h. The facilities provide two different dose rates: 220 rad/h and 30 rad/h depending on user needs.

Figure 6.Radiation testing of iSIM electronics

3. TEST PLAN

A functional test was performed before and after each test. A functional test involves switching on the electronics, run a self-test and taking pictures to evaluate the quality of the PSF.

3.1 Thermal Vacuum

The Thermal Vacuum testing was performed for 5 days. Functional tests were performed at every thermal cycle and before and after performing the tests. A total of 4 cycles were performed with temperatures reaching from -30ºC to 60ºC. Optical tests were performed with every functional test.

3.2 Vibration

A functional test and PSF measurements were done before and after vibration campaign. The vibration testing was performed on 3 different axes: x, y and z. Each test performed was preceded and followed by a Resonance search (from 5 to 2000Hz with 0.25g and 2octaves per minute) and an optical inspection in order to evaluate success of the test. The vibration tests were 2: (1) Quasi Static Sine Burst (frequency of 25 Hz with an amplitude of 5 g in x and y and 12 g on z for 7 cycles), and (2) Random Noise (from 20 to 2000 Hz with global accelerations of 8.29 g rms for 120 s).

3.3 Radiation

A radiation test campaign was conducted on the electronics. The testing lasted for 5 days with a total dose of 25krad at a dose rate of 220 rad/h without using any protection metal shields. In orbit the electronics will be shielded at least with 3mm thickness, reducing significantly the total dose, but it will depend on the final mission orbit and duration of the mission. During this test the electronics have been continuously switched-on, performing functional tests and being continuously monitored externally, logging any events and anomalies and power cycling the electronics in case of any anomalies.

4. TEST RESULTS

During TVAC testing the Electronic boxes reached temperatures from -35ºC to 70ºC and the opto-mechanics reached temperatures from -10ºC to 60ºC. PSF measurements were performed on both, while the camera was inside and outside of its designed working temperature. The optical quality was unaffected by the vacuum environment while the opto-mechanics was in its designed working temperature range. Image quality degraded when outside its temperature range however, as expected, the image quality was restored when the working temperature ranges were reached again.

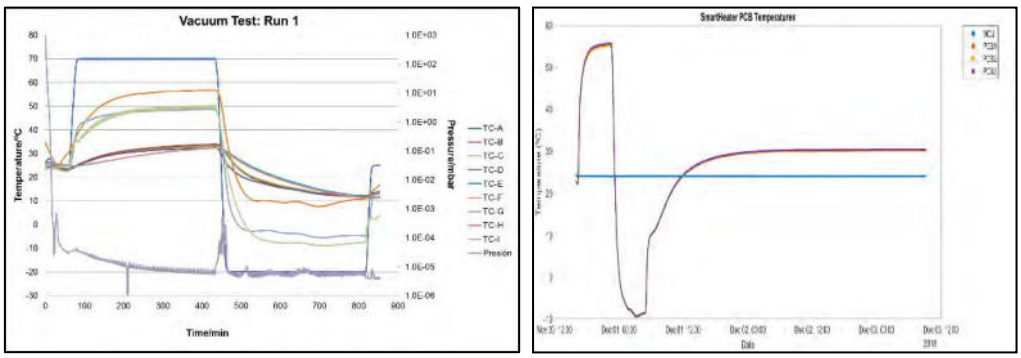

Figure 8. On the left the first thermal cycle, on the right the electronics reached temperatures in one thermal cycle

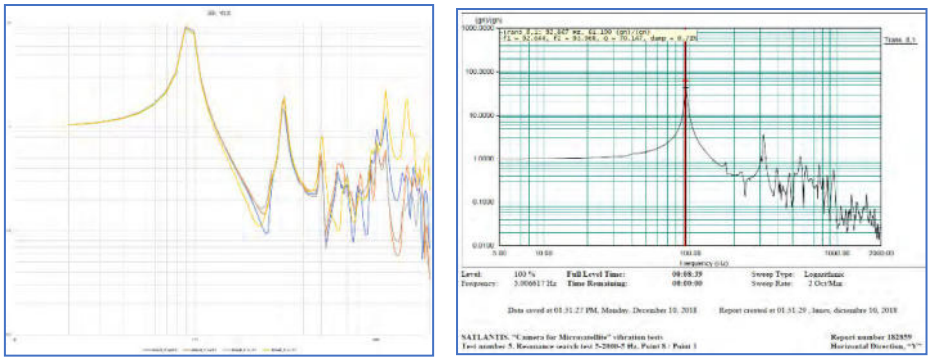

Figure 9. On the left the predicted FEM and on the right the measured during vibration testing

During vibration tests, the Resonance Search tests showed expected values and did not change from before the vibration tests and after, showing that the structural integrity was maintained. Image quality was not degraded after the vibration campaign.

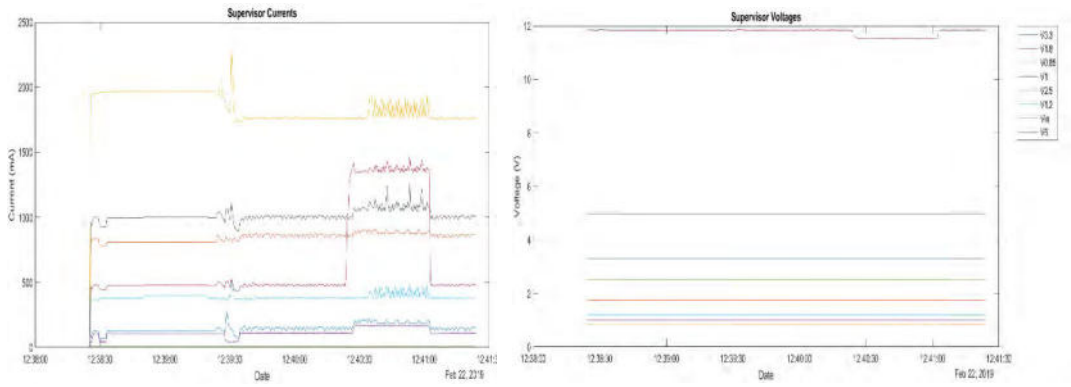

Figure 10. Currents and Voltages were monitored on every power rail of the electronics during radiation testing in order to detect latch-ups. On the figure a reboot and picture acquisition are shown

During radiation testing, the electronics suffered of 3 latch-ups that were correctly detected by the supervisor and the electronics were power-cycled safely. A total of three reboots were needed during the 5 day testing.

All the functional tests and PSF measurements were performed successfully during the qualification campaign.

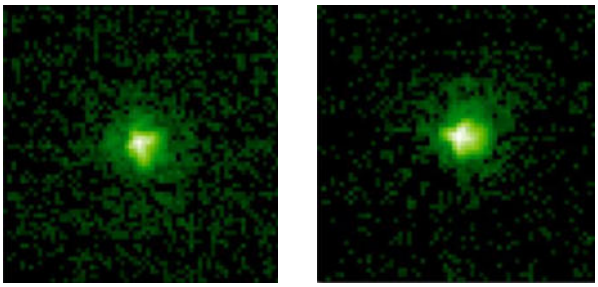

Figure 11. On the left the PSF before the test campaign and on the right the after the test campaign

5. REFERENCES

[1] Guzmán, R., Ocerin, E., Larburu, M., "The Integrated Standard Imager for Microsatellites: Novel electronics control system and post-processing results", *4S Symposium*, Sorrento (2018).
[2] Larburu, M., Conde, A., Cordovilla, R., Dasí-Espuig, M., "Sistema de electrónica y control de cámara integrada estándar para microsatélites. Filosofía COTS", *VI Congreso Nacional de I+D en Defensa y Seguridad,* Valladolid (2018).
[3] European Cooperation for Space Standardization. ECSS-E-ST-10-03C, Space Engineering, Testing, 1 June 2012. Noordwijk, the Netherlands.

TDI CMOS Image Sensor for Earth Observation

Philip Brown, Charles Woffinden & Paul Jerram

Teledyne e2v, 106 Waterhouse Lane, Chelmsford, Essex, CM1 2QU, UK

Phone: +44 1245 493493, Mail: philip.brown@Teledyne.com

Abstract: Teledyne is one of the world's leaders in the provision of CCD and CMOS sensors for space applications. This paper presents results obtained with the latest charge domain TDI CMOS technology operating at very high data rates and with highly integrated readout circuitry. This is intended to provide performance, which would not be achievable with CCDs. A new device intended for very high-resolution Earth observation is also discussed.

1. INTRODUCTION

There are a number of different types of scanning imaging systems that are used for Earth Observation (EO) and planetary observation applications. For systems requiring the highest resolution, multiple lines are added together using Time Delay Integration (TDI) operation to improve the signal to noise ratio to a point where good quality images can be obtained. The preferred means to achieve TDI operation is to move the signal in electrons down the image sensor at a rate that corresponds to the motion of the satellite over the Earth, referred to as charge domain TDI (qTDI). This behaviour is inherent to CCD operation. The drive for increased resolution requires higher line rates - over 30 kHz, and pixel sizes significantly below 7µm as well as more complex sensors with higher numbers of multispectral lines. In order to achieve these requirements the use of a CMOS sensor with on-chip digitisation becomes essential.

2. PROTOTYPE EVALUATION

A prototype qTDI CMOS device, has been developed to test pixel structures of 5 and 10 µm pitch as well as to demonstrate high line rates (300lines/s). The image area is composed of a TDI-CCD structure of 4096 columns with 256 or 64 TDI stages depending on the pixel pitch.

A 12-bit ADC within each column converts the data within 0.9ns to enable the high line rate. The digitized output is then sent to a gigabit transmitter (GTX) composed of a serializer working in double data rate mode (DDR) at 3.6GHz and a CML (3.6Gb/s) data driver. A high-speed CML output driver has been selected to minimize the number of output ports to simplify the interface to the data-capturing device. Input signals such as clock, integration control and SPI interface use LVDS format.

3. PROTOTYPE DEVICE RESULTS

3.1 Results summary

Table 1 summarizes the target and obtained results. These demonstrate good performance and readiness for use in space applications.

Feature	**Unit**	**Target**	**Measured**
Pixel pitch	µm	5 & 10	5 & 10
Vertical resolution	Pixels	256	256
1D stitchable		Yes	Yes
Bi-directionality		Required	Demonstrated
Stage selection		64/128/192/256	64/128/192/256
CTE / gate		> 0.99998	> 0.99999
FWC - 5 µm pixel	electrons	> 20 K (Non-AB)	> 30 k (AB)
Noise Floor	electrons	< 15	12
Anti-Blooming (AB)	×Sat	> 100	***TBC***
Max line rate	kHz	> 300	>270 confirmed *(Read-out chain limited)*
Dark Current @ 25°C	nA/cm^2	< 10	3.7
Non-linearity	%	< 2	< 2
Peak QE (FSI)	%	≥ 40	> 45 @ 650 nm
ADC	bit	12	12
Data streaming - Format - Interface		 8b/10b encoded 8 ports 3.6 Gbps	 8b/10b encoded 8 ports 3.6 Gbps

Table 1: Prototype summary results.

A more detailed summary of the results can be found in [1]. The dark current has a temperature doubling factor of 9.5°C. Measurement has demonstrated a pixel conversion gain of 35µV/e^-; this is designed to optimise the noise floor versus full well and hence the dynamic range.

3.3 Radiation

The radiation immunity is a key aspect of validation of a new sensor. For a qTDI detector, the specific aspects of interest are how the CCD structure behaves with Gamma and Proton exposure – specifically the impact on dark signal and CTE.

The Single Event Effect (SEE) results from heritage Teledyne e2v CMOS devices using similar peripheral structures have been presented elsewhere [2], and are considered acceptable for the application.

The dark current results [3] show a good behaviour with acceptable results for a flight mission:

	Pre-radiation	Post Gamma 30krad	Post proton - $5x10^{10}$ p/cm^2
Without AB	3-4nA/cm^2	< x2	<x3
With AB	3-4nA/cm^2	~x2.5	<x4

Table 2 Dark current summary after radiation exposure for anti-bloomed (AB) and non-anti-bloomed variants.

The results below show a very small CTE degradation of both the AB and non-AB versions of the prototype device with gamma and proton up to doses that would be expected in typical space based applications.

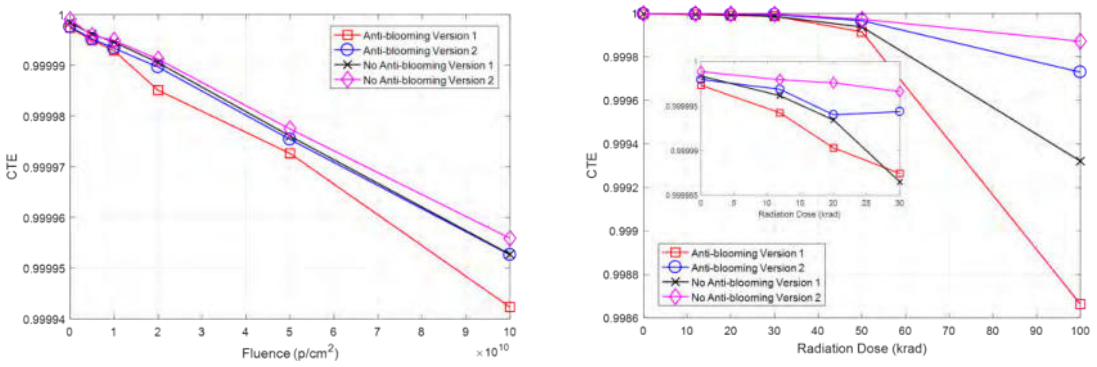

Figure 10 CTE versus proton fluence (left) and gamma dose (Right).

4. NEXT ACTIVITIES

The technology used for the prototype is now being used to make a qTDI CMOS image sensor intended for earth observation, called the CIS125 in a program funded by the UK Space Agency (CEOI). The architecture, composed of 4 panchromatic (PAN) bands and 6 multi-spectral (MS) bands is shown Figure 11. Each PAN and MS are composed of sub-TDI bands (A&B) that enhance the full well by adding digital summation to the charge domain performance.

Pixel count		Pixel size (µm)		Max. Line rate (kHz)	
PAN	MS	PAN	MS	PAN	MS
16k	8k	5	10	14	7

Table 4 CIS125 Configuration for CEOI program.

The high speed ADC per column allows a line rate of up to 14kHz if all of the sensor lines and sub-TDI bands are read.

The number of TDI stages per band are user selectable between 1 and 64 for the PAN and 1 and 32 for the MS.

This sensor will be made with a 0.18µm Imaging CMOS process using high resistivity epitaxial silicon. The device is back-illuminated to improve fill factor and it will be thinned (using Teledyne e2v process) to optimise QE versus MTF. An anti-reflection coating will be deposited to enhance QE as well as black coating between channels to avoid straight light effects.

CIS125 is designed as a modular platform to allow adaptability to a wide range of configurations with lower risk than a new development.

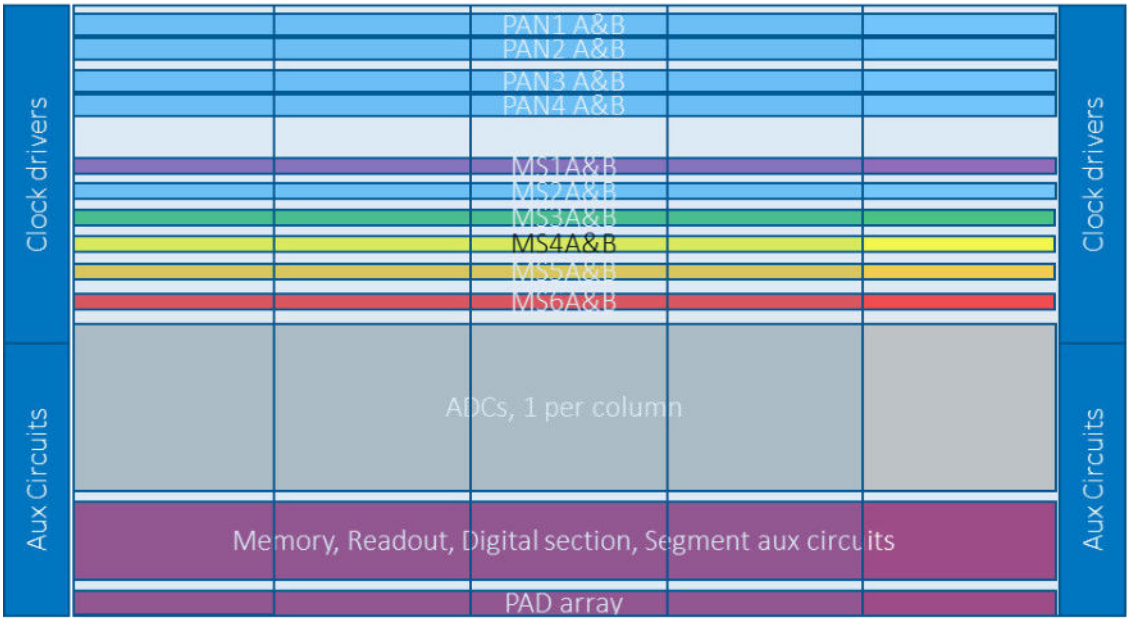

Figure 11 Sensor Architecture

It is expected that the device will be available from 2020 for space applications.

5. REFERENCES

[1] Hyun Jung, Lee et al., "Charge-Coupled CMOS TDI Imager," Image Sensors Workshop (2017)

[2] Pratlong, J. et al., "TDI-CMOS Image Sensor for Earth Observation", ICSO Conference (October 2018)

[3] Owen Cherry et al., "Radiation Tolerance of a Charge Domain TDI CMOS Imager," CNES workshop (November 2017).

Constellation of Small SAR Satellites with Deployable Planar Antenna for Commercial Use

Toshihiro Obata, Shinichi Nakasuka[1], Hirobumi Saito, Koji Tanaka, Makoto Mita[2], Seiko Shirasaka, Keiichi Hirako[3]

[1]The University of Tokyo
RM110 Engineering Bldg. No.7 7-3-1 Hongo, Bunkyo-ku, Tokyo JAPAN
Phone: +81-3-5841-8679, Mail: toshi.obata.space@gmail.com

[2] Japan Aerospace Exploration Agency
3-1-1 Yoshinodai, Chuo-ku, Sagamihara, Kanagawa 252-5210, JAPAN
Phone: + 81-50-3362-2657, Mail: saito.hirobumi@jaxa.jp

[3] Keio University
Yokohama, Kanagawa 223-8526 Japan
Phone: +81-45-564-2581, Mail: shirasaka@sdm.keio.ac.jp

Abstract: Expectations for SAR (Synthetic Aperture Radar) satellites that can observe a target area through clouds and during nighttime are emerging, especially in Asia where high cloud cover rate prevent from the satellite monitoring with optical sensors. We are now developing a small SAR satellite based on technologies of ImPACT (Impulsing PAradigm Change through disruptive Technologies) program. This program aims to develop a responsive earth observation system with the small SAR satellite, originally target for disaster monitoring. We will build a constellation of the small SAR satellites to realize short term revisits, shorter than one day to take advantage of SAR sensor that can acquire data regardless of weather and time in a day. We expect the constellation expands needs of the SAR data to business and private decision making, and develop a market for commercial use. We have almost completed the development of mission FM components of the first demo satellite. The bus system is under EM testing and FM procurements. We will launch the first demo satellite in Q1 of 2020. We are already preparing to build the second satellite and will make six satellite constellation until 2021. Our final goal is to build a constellation of 25 satellites.

1. INTRODUCTION

Expectations for SAR (Synthetic Aperture Radar) satellite that can observe a target area through clouds and during nighttime are emerging, especially in Asia where high cloud cover rate prevent from the satellite monitoring with optical sensors. However, because the SAR data is expensive and the number of SAR satellites is limited, main users of the SAR data are governments and agencies. So, the SAR data market is still limited. In recent years, the development of small SAR satellites aimed at commercial use in the private sector has been active. Moreover, they are trying to improve revisit time and increasing the amount of SAR data by building a constellation of them. Therefore, offering a low cost, high frequency, and a large amount of SAR data is getting more feasible, especially for users who have not use the SAR data.

We are now developing the small SAR satellite in collaboration of ImPACT (Impulsing PAradigm Change through disruptive Technologies) program. The ImPACT is a Japanese government's high-risk and high-impact research and development program that aims to bring industry and society revolutionary changes by innovative science and technology such as cyber, chemistry, material and robotics with big funding. 16 pro-

grams have been selected and our responsive observation satellite program is one of them.

In the ImPACT program, development of the mission system was carried out. The items developed within the ImPACT program are a SAR Antenna, a Power Amp, a SAR Electronics, a Data Recorder, a Data Transmitter and so on [1][2].

We also developed technologies for the bus system in the ImPACT program, related to the EPS (Electrical Power Subsystem), which are unique ones to the SAR mission. We have developed a Power Control & Destruction Unit and a Battery to realize 700 W class power generation and 1.6kW peak power consumption in a 100kg class satellite, which has usually 100 W class power generation and power consumption.

A whole satellite development began in April 2018, as we have successfully gained private funding to procure and develop the rest of satellite components and procure its launcher.

2. KEY FUNCTIONS OF OUR SMALL SAR SATELLITE

One of the key functions is a deployable planar SAR antenna. Unlike the conventional active phased array antenna or the parabola antenna, it can be compactly stored in a simple configuration. Thin film solar cells are mounted on the back side of the antenna to generate high power that is necessary for small SAR satellites. Fig.1 shows the on-orbit configuration and the launch configuration of our satellite.

When we build the satellite constellation for commercial use, satellite mass reduction is important to reduce launch cost and to maximize the number of satellites in a single launcher. We have to realize unique key functions for the SAR satellites in a 100kg class small satellite. Those required functions are usual for SAR satellites that weigh 300kg to 1 ton, however, it is a challenge to realize them in the 140kg small satellite.

Since the satellite consumes peak power of 1.6 kW during SAR observation, it has a battery with large capacity and capable outputting large current. In order to charge the large battery in a short period of time to enable frequent observation, it has solar cells with 700 W power generation. We mount the solar cells on the back side of the large SAR Antenna.

A block diagram is shown in Fig. 2. The development speed and fewer risks to achieve it is important for commercial use, so we selected our heritage components from Hodoyoshi satellites[3] as much as we can.

For attitude control, there are two Star Trackers (STT), four Reaction Wheels (RW) and a Gyro (FOG). The reason for having two STTs is that attitude determination accuracy is necessary for SAR observation. The reason why four RWs are needed is that angular velocity is required to change the attitude before, after and during the observation. Because the antenna for SAR observation is large, the inertial moment of the satellite is larger than that of a normal small satellite, and the angular momentum of RW needs to be large.

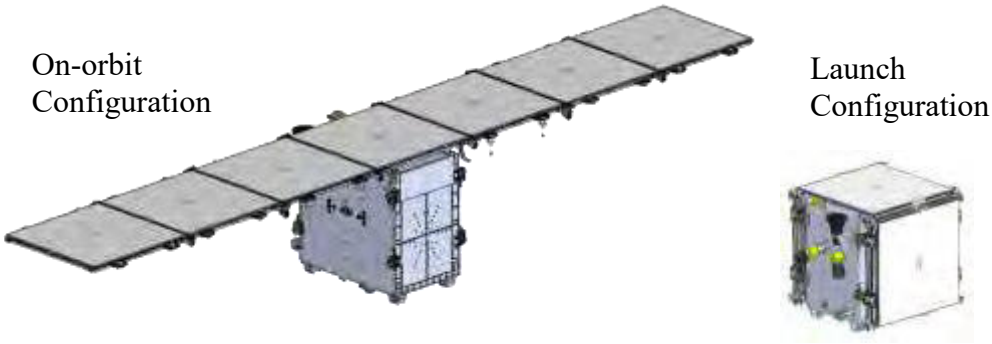

Fig. 1 Satellite Configurations

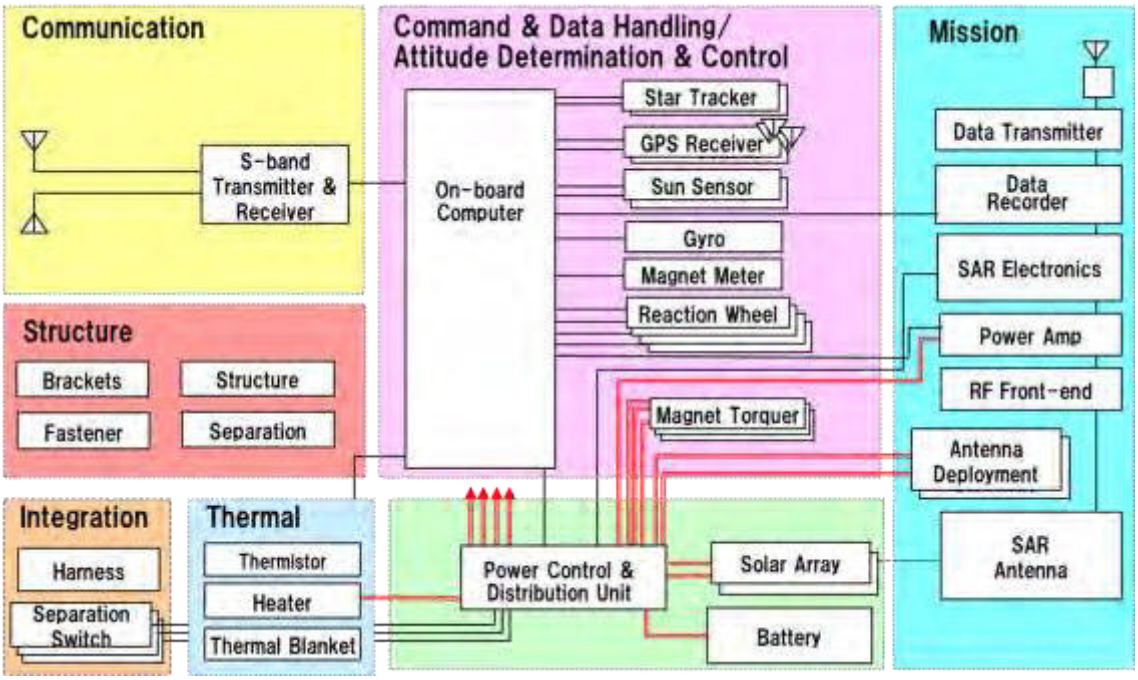

Fig. 2 Block Diagram

An orbit determination accuracy is also important for observation. Therefore, two different GPS Receivers (GPSR) are also mounted. One is a device that has been used in the past project and is capable of highly accurate orbit determination, and one is an affordable device. We will use them on the same satellite and determine which one is adequate for the future GPSR by comparing the accuracy of the two.

The accuracy of estimated satellite time is also important. If the observation timing is only 10ms off, it will result in a positioning error of about 80 m. The satellite has a new function to estimate the time accurately and synchronize it with the time of the SAR Electronics based on the time obtained from GPSR.

Autonomous operation is important for achieving complicated observation operations with the constellation of multiple satellites. It is also important to realize the mission while coping with off-nominal conditions. In order to realize these, we developed autonomous operation functions using state transition models and successfully demonstrated on-orbit using CubeSat in February 2018. [4]

3. DEVELOPMENT STATUS

Fig. 3 shows the test configurations we have conducted until April 2019. We have almost completed the development of mission components FM (SAR antenna, SAR Electronics, Power Amp, Data Transmitter and Data Reorder) for the first demo satellite during the ImPACT program. The bus system is under EM phase testing and FM procurements. After an interface verification of the mission system and the bus system, we will conduct assembly, integration, and test of satellite FM.

One of the biggest issues in verifying the system functions is the power interfaces associated with the high power required by the SAR. We confirmed them between the Power Control & Distribution Unit and other SAR mission specific components like the Power Amp, SAR Electronics, the Data Transmitter and the Data Recorder at an early stage.

The other issue is the dissipated heat during the observation operation. A thermal vacuum test was conducted to verify the thermal mathematical model of the satellite structure. In March, we conducted the FlatSat, the electrical interface tests where all the components were on the table and connected via harnesses to confirm electrical interfaces, power interfaces, and operation procedures. In April, we conducted through electrical tests with all the components mounted on the satellite structure and confirmed that issues in the design and the manufacturing. We also conducted those test under temperature conditions to confirm all the functions and the interfaces work correctly under high temperature and low-temperature conditions.

After those tests, we will make some modifications to fix issues founded during the tests. The first integration for the Initial Electrical Test for Flight Model will start in May.

We use the ISAS (Institute of Space and Astronautical Science) facility for the first demonstration satellite development and the testing under the collaboration agreement with JAXA.

We are also developing autonomous operation functions that enable robust operations against anomalous events and easy operations. Current satellite operations highly depend on the operation procedures that are prepared beforehand and vulnerable against unexpected status changes like components ON/OFF, battery state of charge, free memory of data recorder, attitude, and temperatures. To maximize the efficiency of the operations, operators have to understand behaviors of the satellite and predict its status at the timing of designing the operation procedures. Only limited experienced operators can achieve this. We designed our autonomous operation functions to have a model of the behavior of the satellite and understand the latest satellite status, so as to cope with those issues related to the current operations.

We expected operations of the small SAR constellation require huge efforts. We will apply the autonomous operation function to the small SAR satellites and achieve more robust and easier operations. We have already demonstrated our autonomous operation functions with the 3U CubeSat, TRICOM-1R, in February 2018.

We will develop the first demonstration satellite until the end of 2019 and will launch it in Q1 2020 (Fig.4).

(a) Power Interface Test

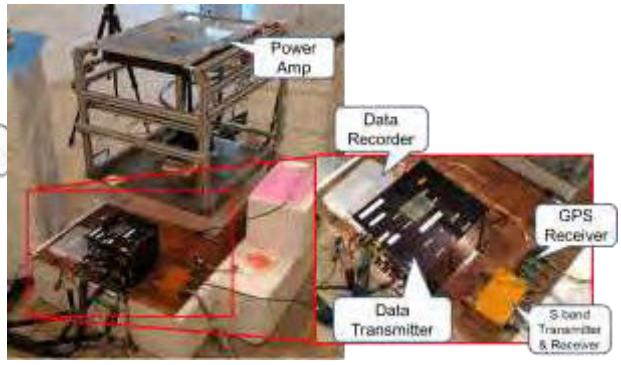

(b) Electrical & Magnetic Interference Test


(c) Antenna Vibration Test

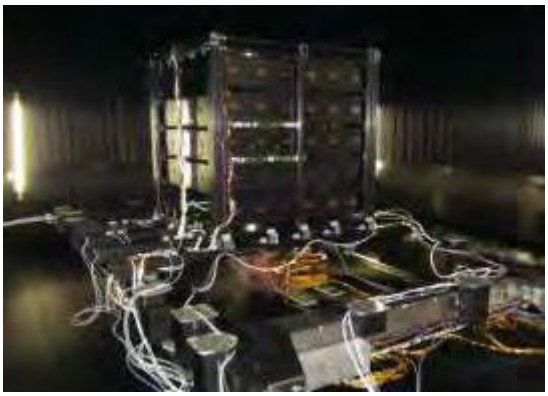
(d) Thermal Vacuum Test

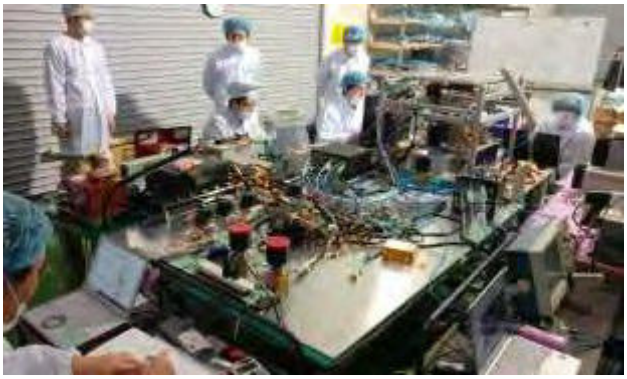
(c) Electrical Interface Test


(d) Thermal Cycle Test

Fig. 3 Development Test Configurations

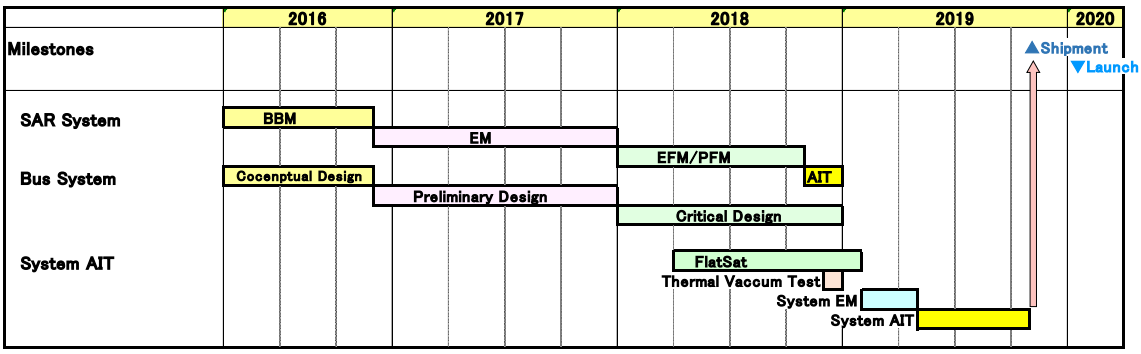

Fig. 4 Development Schedule

4. SUMMARY

We are developing the small SAR satellite and will deploy a lot of them on orbit to enable frequent and persistent observations. We expect the constellation expands needs of the SAR data to business and its data is used to solve social problems symbolized by SDGs (Sustainable Development Goals).

We will launch the first demo satellite at Q1 of 2020. We are already preparing to build the second satellite and will make six satellite constellation until 2021. The first two satellites are demonstration satellite and the third satellite will be designed and developed as a mass-production model. Our final goal is to build a constellation of 25 satellites that enable daily or shorter revisits at some specific targets especially in Japan and Asian area.

5. REFERENCES

[1] K. Hirako, S. Shirasaka, T. Obata, S. Nakasuka, T. Tohara, N. Nakamura, “Preliminary System Design of Micro Satellite for Compact SAR Mission”, 4S Symposium Sorrento, Italy, (2018)

[2] H. Saito, P. R. Akbar, K. Tanaka, M. Mita, B. Pyne, T. Kaneko, T. Obata, S. Nakasuka, J. Hirokawa, S. Shirasaka, H. Watanabe, K. Hirako, K. Ijichi, “Engineering-Model Results of X-band Synthetic Aperture Radar for Small Satellite and Its Application to Constellation Mission”, 32nd Annual Small Satellite Conference, USA, (2018)

[3] S. Yoshimoto, S. Nakasuka, Y. Tsuruda, Y. Aoyanagi, T. Tanaka, H. Sahara, T. Ohira, Y. Araki, I. Mase, M. Ito, V. KAINOV, A. Karandaev, O. Silkin, “ Cluster Launch of Hodoyoshi-3 and -4 Satellites from Yasny by Dnepr Launch Vehicle” Trans. JSASS Aerospace Tech. Japan, Vol. 14, No. ists30, pp. Pf_35-Pf_43, (2016)

[4] T. Obata, S. Nakasuka, Y. Aoyanagi, T. Matsumoto, S. Shirasaka, “On-Orbit Demonstrations of Robust Autonomous Operations on CubeSat”, 32nd Annual AIAA/USU Conference on Small Satellites, USA, (2018)

Novel Nanosatellite Cluster Deployment Strategy by Precise Orbit Insertion – Design, Verification and Flight Results

Zizung Yoon[1], Walter Frese[1], Klaus Briess[1], Siegfried Voigt[2]

[1] Department of Aeronautics and Astronautics, Technische Universität Berlin
Marchstr. 12, 10587 Berlin, Germany
Phone: +49 30 314 24438, Mail: zizung.yoon@tu-berlin.de

[2]German Space Administration (DLR Raumfahrtmanagement)
Koenigswinterer Str. 522-524, 53227 Bonn, Germany
Phone: +49 228 447-312, Mail: siegfried.voigt@dlr.de

Abstract: This article describes a novel strategy to optimize the deployment condition for small satellite formation or clusters. It presents an approach how distance boundary conditions can be kept even without propulsion system, solely relying on the initial conditions. A proper trade-off between reducing collision risk during deployment and at the same time minimizing the relative drift among the satellites has been investigated.
The strategy has been implemented in the distributed nanosatellite mission S-NET, where four nanosatellites were deployed into orbit solely relying on initial conditions for passive cluster keeping. As a design trade-off, propulsion system was omitted, instead was the design optimized for precise orbit insertion. Thus, the article includes the mechanical design specification of a satellite bus (TUBiX10) and deployer (SNL) as well specific launch vehicle requirements for multi-satellite piggy back deployment. The satellite bus (TUBiX10) and deployer (SNL) are designed to minimize mechanical friction during deployment phase and thus deliver an extremely precise ejection velocity vector and minimum spinning rate.

1. INTRODUCTION

Keeping of small satellite formation or clusters requires control of relative distance, which is normally performed by propulsion or differential drag control. The initial relative distance drift among the satellites is mainly determined by the deployer ejection velocity vector and upper stage performance such as pointing direction and accuracy. Especially for Cubesats and nanosatellite missions, they mostly rely on the deployment condition defined by the ejection container and upper stage with few space for optimization. Furthermore, to minimize collision risk, mostly they are deployed in along-track direction, which is counterproductive for cluster keeping. Minimizing the initial drift by precise orbit insertion not only reduces the delta V required for distance control but could even result in omitting costly propulsion systems.

1. CLUSTER DEPLOYMENT OF NANOSATELLITES

1.1 Considerations for piggy-back swarm deployment

In general, the orbit insertion condition of share-ride missions are not as flexible as the primary payloads and are constrained by the upper stage configuration and ejection mechanism. Hence, for optimal deployment of multiple spacecrafts, the following constraints must be considered:

- All piggy-back satellites of a launch are normally deployed in a single orbit (e.g. Dove Satellites). Re-ignition capability of upper stage may allow for several orbits.

- The attitude determination and control accuracy of upper stage must be considered when defining the ejection direction. Typical values of attitude determination accuracy are few degrees in orbit.
- Cubesats and nanosatellites are mostly separated from upper stage by a dispenser / container using a spring mechanism. Compared to the classical pyro actuator, spring mechanism is beneficial in controlling the relative ejection velocity and direction.
- For precise deployment, even the mechanical tolerance of the dispenser mounted on the upper stage must be considered.

Primarily the initial deployment condition is set to minimize collision risk with the upper stage or other spacecrafts of the deployment sequence. Depending on mission requirements, the secondary requirement would be to minimize the relative drift of satellites (e.g. distributed nanosatellites of mission S-NET) or maximize to achieve broad distribution in short time (e.g. 3U Dove constellation by Planet Inc.).

1.2 Existing deployment strategies for swarms

For swarm deployment, the first couple of orbits right after the orbit injection are the most critical in terms of collision risk. Even if satellites are equipped with propulsion, especially for secondary payloads, a fixed waiting time for initial activation (e.g. 30 minutes for 6U Cubesats [2] in order to protect the main payload prohibits active orbit control within that critical phase.

Dove satellites, a reference in this sector, have been deployed in different ways. For example, 8 Flock 2E and Flock 2E' satellites were deployed from the ISS in May 2016. They were deployed in groups of two over four deployment windows by a spring deployer supplied by NanoRacks. The system was attached to the Multi-Purpose Experiment Platform of the Japanese Experiment Module. This is grappled and set in deployment position and orientation by the Japanese Remote Manipulator System [3].

2. NOVEL STRATEGY: PRECISE ORBIT INSERTION FOR EXTREMELY LOW DRIFT

2.1 Perturbation consideration

The orbital perturbations implemented and applied for obtaining the results of this publication are J2 (EAGF) and atmospheric drag (USSA76), which are the ones that affect the orbits of LEO satellites.

2.2 Deployment direction

According to Clohessy-Wiltshire equation for relative motion, an along-track impulse produces a change in the shape and size of the orbit (a and i), and also in the orientation in-plane (ω and ν), but does not modify the plane. The random variation from the ideal deployment velocity vector $\mathbf{v_D}$ is derived from the sum of following uncertainties:

- e_{dis}: variation of ejection velocity vector due to the ejection mechanism (generally spring or linear actuator) and mechanical tolerance of dispenser itself
- e_{mech}: tolerance of the mechanical alignment between dispenser and upper stage

- e_{us}: error in attitude control of upper stage

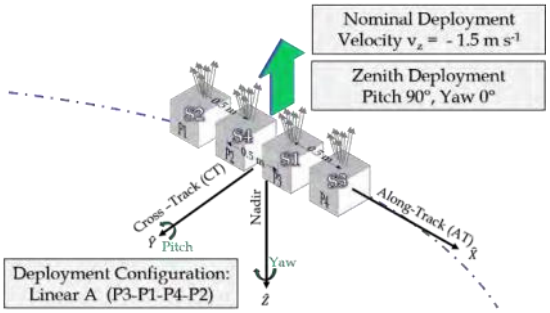

Figure 1: Schematic of the upper stage's attitude for deployment towards zenith direction.

2.3 Trade-off between collision and drift

Especially for formation flight missions without propulsion, where the satellites should minimize their relative distance drift passively, the initial ejection parameters must find a proper trade-off between collision probability and relative drift. Figure 2 shows the collision probability and relative drift for $v_D = 1.5\frac{m}{s} \pm 3\%(1\sigma)$.

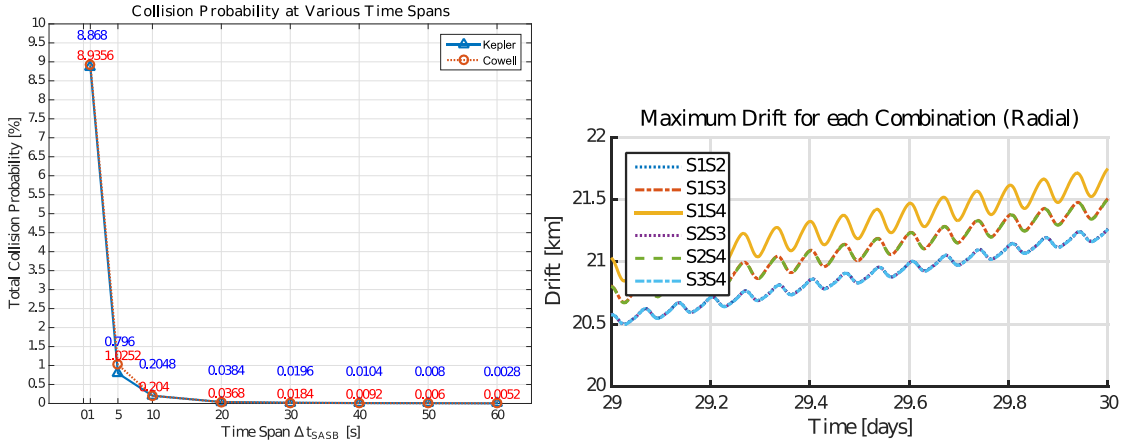

Figure 2: collision probability over time span between separation (left), simulated relative drift between satellites at a time span of 10 s (right)

3. IMPLEMENTATION FOR MISSION S-NET

The mission goal of S-NET is to demonstrate intersatellite communication with distributed nanosatellites. The mission consists of four satellites, to test multi-hop communication with different protocols and routing algorithm.

To reduce system complexity of the space segment, a propulsion system was omitted, and therefore the relative formation will be controlled by the initial separation parameters. The goal is to keep the satellites within a range of 400 km to enable a stable ISL for at least four months. A summary of mission parameters is provided in Table 1.

Table 1: Mission parameters of S-NET

Parameter	Value
No. of satellites	4
Orbit height	580 km SSO
Launch date	2018-02-01
Design life time	1 year
Mass, Volume	8.8 kg, 240 x 240 x 240 mm^3 per SC
Communication	UHF (satellite bus), S-Band (payload)
Attitude Control	Three axis with MEMS sensor arrays, 3 × reaction wheels, 3 × magnetorquers
Payload	SLink TRX for ISL, UL DL Laser reflector for high precision position measurement

Table 2: Deployment parameters for mission S-NET

Element	Value
Semi-Major Axis	6971±8 km
Eccentricity	0.0001± 0.0016
Inclination	97.75±0.12
Argument of Perigee	205.02±150
Right Ascension of Ascending Node	226.25°
True Anomaly	120°
Magnitude of $\mathbf{v_D}$	$1.5m/s \pm 3\%(1\sigma)$
Direction of $\mathbf{v_D}$	$zenith \pm 2°(1\sigma)$
Time span between separation	10 s

4. FLIGHT RESULTS

4.1 Long Term Drift

The relative drift among the satellites was measured in orbit using the signal run time of the S-band radio during ISL sessions. The measurement was correlated with TLE data and laser ranging data to increase the accuracy and is illustrated in Figure 3. Interestingly, the max. value of measured distance occurs between satellite S4 and S2 and coincides with the simulation result for zenith deployment. Overall, it implies that the deployment strategy worked out and underlying assumptions were right.

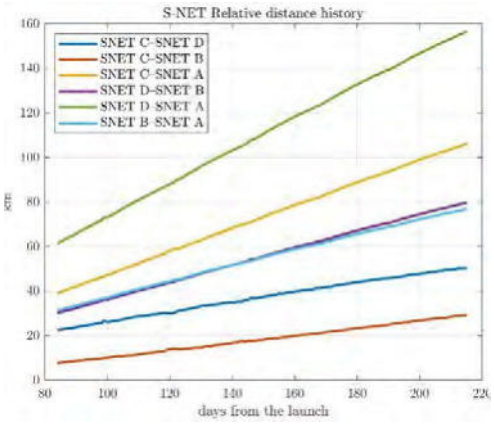

Figure 3: Flight results of relative drift development of S-NET satellites

4.2 Validation of Orbit Insertion Condition

From long term drift, the initial orbit insertion conditions could be reconstructed as illustrated in Figure 4. The deployment vectors are illustrated in the LVLH frame, where x-axis is toward zenith direction, z-axis along the orbit normal vector and y-axis towards the along-track (flight) direction.

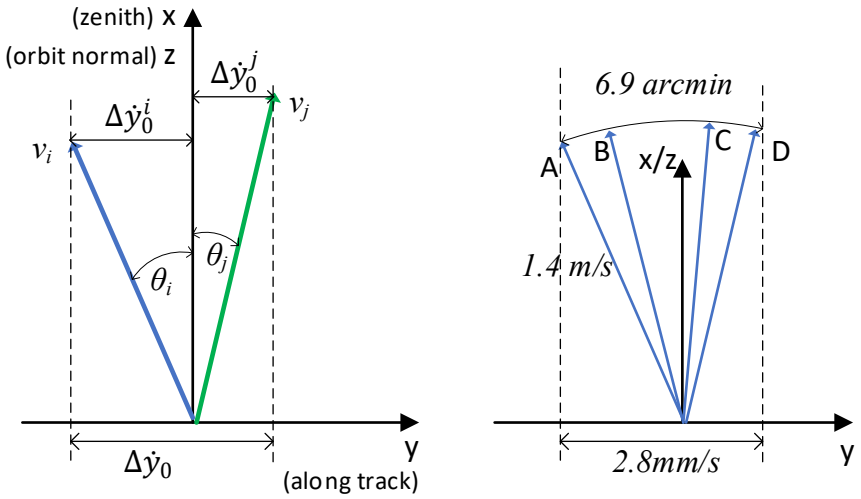

Figure 4: Reconstructing the initial conditions from long-term drift analysis

$\Delta\dot{y}_0$ is the difference of initial velocity in along track direction of two satellites and can be obtained from the Clohessy-Wiltshire (CW) equation for relative motion.

$$x(t) = \left(\frac{\dot{x}_0}{n}\right)\sin n\,t - \left(3x_0 + \frac{2\dot{y}_0}{n}\right)\cos n\,t + 4x_0 + \frac{2\dot{y}_0}{n}$$

$$y(t) = \left(\frac{2\dot{x}_0}{n}\right)\cos n\,t + \left(6x_0 + \frac{4\dot{y}_0}{n}\right)\sin t - (6nx_0 + 3\dot{y}_0)t - \frac{2\dot{x}_0}{n} + y_0$$

$$z(t) = \left(\frac{\dot{z}_0}{n}\right)\sin n\,t + z_0\cos n\,t$$

If the periodic terms are cancelled out for long term analysis, we obtain for the relation between along-track position y and initial velocity's along-track component $\dot{y}_0$ simply

$$y(t) = -3t\dot{y}_0$$

and thus

$$\dot{y}_0 = \frac{y(t)}{-3t}$$

From this relation, we can obtain the relative along-track component of initial velocity between two satellites $\Delta\dot{y}_0$ following equation. The corresponding flight result values are given in **Fehler! Verweisquelle konnte nicht gefunden werden.**.

$$\Delta\dot{y}_0 = \frac{\Delta y(t)}{-3t}$$

Once assuming the relative distance among the S-NET satellites Δd as Δy since the satellites are moving on the same orbital plane (inclination and semi major axis and $\Delta d \ll r_{Earth}$), the geometric relation illustrated in Figure 4 allows to get the relative initial angle in along track direction between two satellites $\Delta\theta_0 = \theta_i + \theta_j$ from

$$\Delta\dot{y}_0^i = v_i \sin\theta_i$$

$$\Delta\dot{y}_0^j = v_j \sin\theta_j$$

where i and j are the satellite indices. Since $\Delta\dot{y}_0$ is obtained from long-term analysis,

$$\Delta\dot{y}_0 = \Delta\dot{y}_0^i + \Delta\dot{y}_0^j = |v_i| \sin\theta_i + |v_j| \sin\theta_j$$

when assuming the same initial deployment velocity for each satellite $v_i = v_j = v_0$ then

$$\Delta\dot{y}_0 = |v_0|(\sin\theta_i + \sin\theta_j)$$

Finally, the relative initial angle in along track direction between two satellites $\Delta\theta_0$ is given by

$$\Delta\theta_0 = \theta_i + \theta_j = \frac{\Delta\dot{y}_0}{|v_D|}$$

Satellite A and D have the largest relative distance $\Delta d = 146.7km$ after 200 days since launch, and the reconstructed overall $\Delta\dot{y}_0$ is only 2.8 mm/s at insertion time. The respective $\Delta\theta_0 = 6.9arcmin$ for $v_D = 1.4m/s$ is the sum of all error sources from container, upper stage pointing and mechanical tolerance and fulfills totally the specified separation requirements.

4.3 Drag Control Support

The time t_{ND} to reduce the relative drift to zero by differential drag is relevant for mission operation and can be obtained by following linear equation

$$\ddot{y}_{drag} \cdot t_{ND} + \Delta\dot{y}_0 = 0$$

where

$$\Delta\dot{y}_0 = |v_D| \cdot \Delta\theta_0$$

Thus we get

$$t_{ND} = -\frac{|v_D|}{\ddot{y}_{drag}} \cdot \Delta\theta_0$$

with

$$\ddot{y}_{drag} = \frac{3}{2}\rho v_{rel}^2 \left(\frac{1}{BC_L} - \frac{1}{BC_H}\right)$$

This allows to examine the relation between initial condition $\Delta\theta_0$, drag acceleration and t_{ND}. $\ddot{y}_{drag}$ apparently depends on the satellite form factor, orbit altitude and atmospheric density.

Figure 5: Drag control result

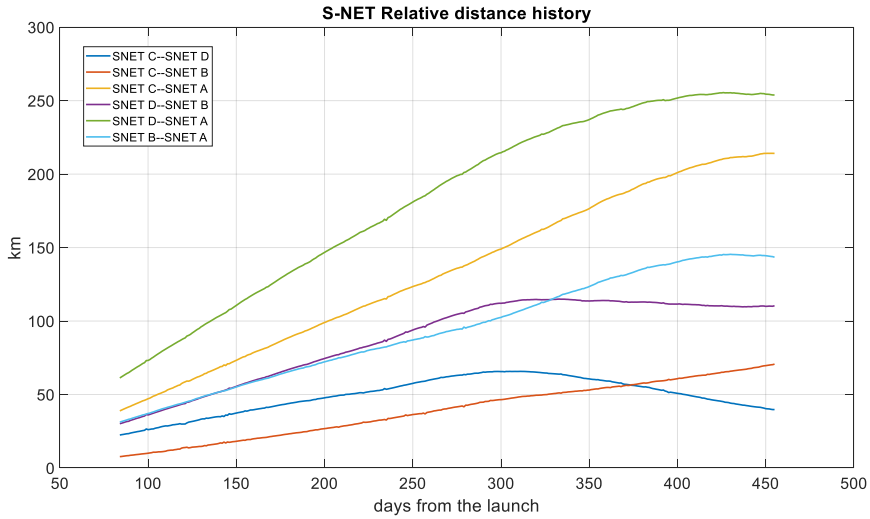

5. CONCLUSION

A novel cluster deployment strategy to minimize relative drift by relying on precise initial conditions of orbit insertion has been described.

The orbit injection requirements are derived from the trade-off analysis between collision probability and drift. For the collision and drift analysis, orbital perturbations must be considered.

The design considerations to implement a precise deployment vector have been described. This includes a precise interface between satellite and launch container and a stiff mechanical mount on the upper stage.

The analysis of S-NET flight data validated the precision of the described methodology and requirements. It saved the usage of a rather complex / expensive propulsion system.

This strategy can be applied for clusters / swarms / formation when

- satellites are ejected into same orbital plane
- relative distance drift should be minimized
- upper stage is flexible w.r.t to ejection direction
- upper stage can provide solid attitude stability

5. REFERENCES

[1] Yoon, Z., Frese W., Bukmaier, A., Briess K., System design of an s-band network of distributed nanosatellites, CEAS Space Journal 6 (1). doi:10.1007/s12567-013-0058-1.

[2] Frese, W., Yoon, Z., Briess, K., and Voigt, S.,Communication network in LEO: In-orbit verification of intersatellite link by nanosatellite cluster S-NET. International Astronautical Congress 2018, Bremen (2018)

Symbols

y	along-track position
$\dot{y}_0$	initial velocity's along-track component
Δd	relative distance among two satellites
Δy	difference of along-track position between two satellites
$\Delta \dot{y}_0$	initial velocity's along-track component between two satellites
$\ddot{y}_{drag}$	acceleration induced by differential drag
v_i	deployment velocity of satellite i
v_D	ideal deployment velocity vector
$\Delta \theta_0$	relative initial angle in along track direction between two satellites
t_{ND}	time to bring relative drift to zero

New Techniques in Spacecraft Modeling and Simulation Environments to Support Next Generation Satellite Constellations

Stanley O. Kennedy Jr.[1], Alexander Dunn[1]

[1]Oakman Aerospace, Inc.
9092 S. Ridgeline Blvd
Littleton, CO, USA 80129
Phone: +1 303-904-6060

Abstract: The next generation of satellite constellations promise to bring innovative, life changing technologies to the world. These constellations will need economical, yet reliable spacecraft platforms to maximize operational capability. Small satellite attributes such as agility and functionality can enable these constellations for critical operational purposes. However, current accepted risk of small satellites will not meet the threshold for these constellations. This creates an industry challenge of maintaining the low-cost small satellite attributes while increasing mission assurance to meet the threshold of next generation constellations.

A Modular Open System Architecture (MOSA) approach was used to develop a modeling and simulation (M&S) environment with the objective of reducing lifecycle costs while increasing mission assurance. This approach achieves the objectives in the following ways:

1) New, streamlined data ingestion for Commercial-off-the-Shelf (COTS) component targeting
2) High fidelity Design Reference Missions (DRMs)
3) International collaboration in M&S environments

The three applications outlined have shown a significant increase in mission assurance and substantial reduction of lifecycle costs and schedules in small satellite missions. The tool transcends international borders, a necessary feature to support the next generation small satellite constellations.

1. INTRODUCTION AND PROBLEM IDENTIFICATION

Today's aerospace industry is engineering exciting concepts such as "Space Dial Tone," Internet of Things (IOT), reliable global access to internet, on-demand Earth observation, and remote sensing. These concepts are driving the development of next generation satellite constellations. These constellations will require precise, efficient processes and techniques to achieve the required spacecraft output volume within cost and time effective thresholds.

Building spacecraft is inherently challenging due to the complexity of the systems. Minimizing mission risk and designing high mission assurance satellites has been the anchor metrics for traditional operational spacecraft. These systems are expensive and require long development cycles, but are necessary for critical operations requiring high reliability. Small satellite (smallsat, any satellite less than 500 kg) platforms emerged as a viable option for missions needing to more quickly demonstrate capabilities on-orbit. The smallsat industry has expanded quickly in recent years, mostly due to the success of science and technology (S&T) and pathfinder missions. Establishing common standards such as the CubeSat standard has helped facilitate Commercial-off-the-Shelf (COTS) components integration and enable ride share opportunities. These efficiencies help to reduce cost and lower the barrier to entry, allowing non-traditional customers to test new capabilities. Smallsat platforms achieved shorter development timelines and reduced costs at the expense of mission reliability and mission assurance.

Market utilization trends show the industry's recognition of smallsats as viable options for constellations [1]. Smallsat projected applications (Figure 1) is shifting from S&T missions to functional, operational multi-satellite missions. The large increases in the communication applications indicates this projection. Earth Observation/Remote Sensing (EO/RS) and communication applications (common objectives for constellations) are projected to make up well more than half of nano/microsat applications in the near future.

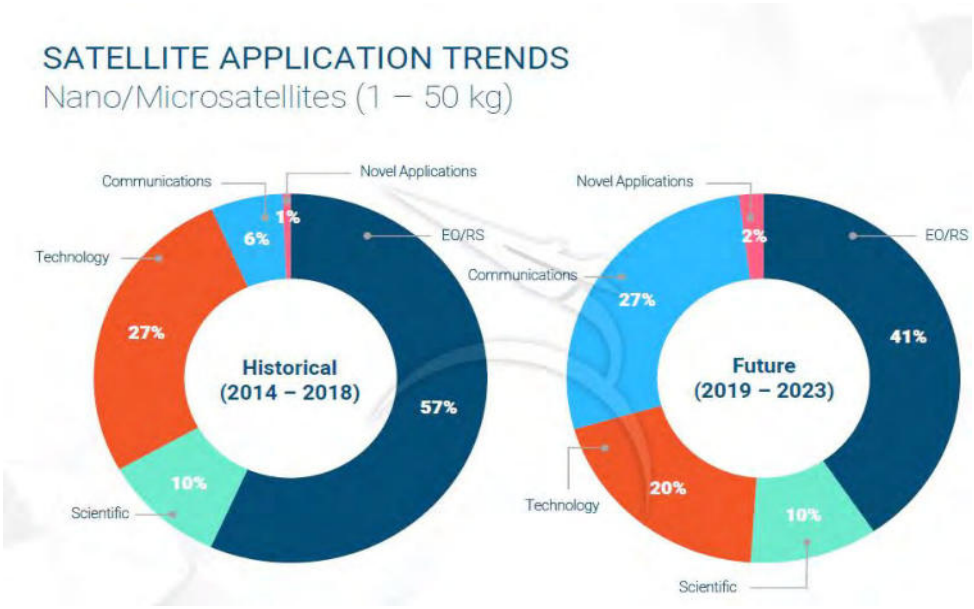

Figure 1 Nano/Microsat Applications [1]

There have been many public announcements of companies aiming to launch constellations of smallsats. Some current examples include SpaceX Starlink, BlackSky, Planet, Spire, and OneWeb. These constellations will seek the shorter development timelines smallsats can offer but will require higher mission reliability. A shorter, streamlined design and production method will enable these constellations to reach on-orbit operation capacity quickly, update/replace rate of on-orbit satellites relatively frequently, and inject technology advancement into the spacecraft without delaying or disturbing the production process. An effective system which optimizes the *mission reliability vs. cost/schedule* design trade would be extremely valuable for these constellations. The authors here recognized the need for a "New Space" technique to optimize this trade study for satellite design.

1.1 OPTIMIZING RELIABILTY VS. COST AND SCHEDULE

Traditional spacecraft design carries too high of cost and schedule burdens to meet the demands of the next generation constellations. Smallsat platforms can meet the cost demands, but sacrifice reliability and mission assurance. A typical lifecycle (Figure 2) for a smallsat revolves around a 2-year timeline [2]. The phases of the lifecycle are mostly co-dependent with little overlap/parallel development between phases. A good example is spacecraft system design must be mostly complete before emulated models are created and before hardware is procured. This linear approach is an inhibitor and is magnified within design teams consisting of multiple entities. De-coupling the depend-

encies between the lifecycle phases is an important aspect when optimizing new techniques to enable constellations.

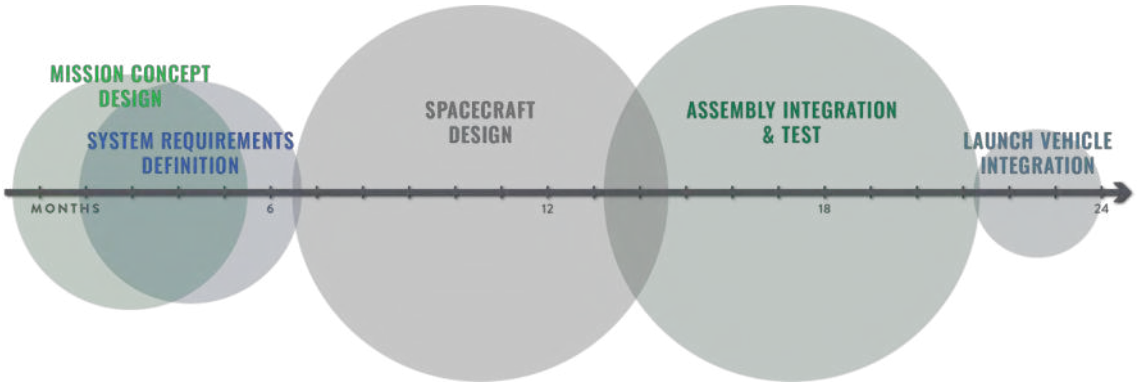

Figure 2 Smallsat Design Lifecycle [2]

The objectives of new techniques were to identify and implement a design process which de-couples the dependencies between lifecycle phases and enables parallel development within the lifecycle. A new modeling and simulation (M&S) tool enabled by Modular Open System Architectures (MOSA) in an effort to achieve the observed objectives was investigated and applied. The MOSA M&S technique has shown to 1) reduce the magnitude of both the spacecraft design and Assembly, Integration, and Test (AIT) phases, and 2) de-couple the dependencies between spacecraft design before AIT for parallel development. This approach resulted in reduced cost and schedule for satellite design, interoperability among sub-systems for more effective update rates, and achieved a higher mission assurance.

2. MODULAR OPEN SYSTEM ARCHITECTURES (MOSA)

MOSA is a design approach for highly complex systems. MOSA has been successfully implemented in a number of other technical industries: automobiles, mobile phones/app markets, Linux, USB, etc. The benefits these technical industries have been able to capitalize on are very well known and documented. Their success has driven some sectors within the aerospace community to attempt to implement MOSA. Government was an initial force advocating for MOSA and standardized spacecraft design, having recognized the need to modernize and control costs of space systems. The past decade has shown numerous and continued government (U.S. and international) initiatives to foster MOSA, demonstrating an established desire for MOSA adoption. Previous U.S. government studies have shown utilizing MOSA reduces total lifecycle costs by as much as 27% while maintaining reliability. Notably, the U.S. Department of Defense (DoD) has issued directives for a modular open system approach to be utilized within DoD programs. The goals of the DoD in these MOSA directives were to 1) enhance competition, 2) facilitate technology refresh, 3) incorporate innovation, 4) enable cost savings, and 5) improve interoperability [3].

Small satellites are a great example of a highly complex system which will benefit from a MOSA design approach. When implemented correctly, the complex system is devolved into independent modules (sub-systems) that maintain a cohesive integration application into the complete system design. A MOSA design enables the rapid reconfiguration of the modules in a system design without drastically altering the perfor-

mance or operability of the system. Re-configurability plays an important role in reducing the spacecraft design phase by enabling design trade studies while minimizing re-engineering work.

Unfortunately, the widespread adoption and implementation of MOSA has been slow. Globally, it can be observed the lack of MOSA implantation is mostly due to the inability for a common, open standard to emerge as the dominating standard in the industry. There are many open standards available and used in current space systems. There are also many "open standards" developed by traditional space system providers that are, in-fact, closed or restricted for select use. Establishing a single open-system standard throughout the global industry is a very difficult problem to solve for many reasons; performance characteristics of standards, security vulnerabilities, politics, to name a few. Examples of industry collaborative bodies seeking to establish common open standards include International Standards Organization (ISO), Consultative Committee for Space Data Systems (CCSDS), European Cooperation for Space Standardization (ECSS), American Institute of Aeronautics and Astronautics (AIAA), and others.

Globally, many novel, new technologies which improve the design, development, test, and operations of the spacecraft are constantly being developed by disparate entities. The next generation of constellations would benefit from integration of these disparate entities into a cohesive collaborative environment. Collaboration and integration between these different engineering teams has identified significant challenges. As a result, the maximum technical potential has been hindered. In the absence of a single common global standard, the smallsat community must turn to new technologies, tools, and strategies to implement truly MOSA approaches within satellite designs.

2.1 Implementing MOSA into a M&S tool

A MOSA enabled M&S environment can be leveraged to create a dynamic platform for satellite design. Functionally, the tool must efficiently ingest an adequate number of different common and/or open standards worldwide (instead of relying on a single standard) and harmonize each into a cohesive design. This is achieved by utilizing a *bridge* application to interface communications between applications and components with differing message application programming interfaces (APIs). As a result, the MOSA M&S environment supports a number of different MOSA messaging frameworks with different levels of attributes, functionality, and restrictions placed. The MOSA framework also enables other messaging protocols and services to be developed via the API definition for implementation. The key feature of the bridge application within the M&S testbed is the message transfers over disparate protocols, alleviating the need for a single standard adopted across an engineering team. This is what creates the independent modules and ensures the rapid reconfiguration within the environment. These are key aspects for the M&S environment to be truly MOSA and has shown to increase reliability through iterative development and testing. The MOSA M&S technique reduced mission lifecycle cost and schedule while achieving higher mission assurance through the following applications.

2.1.1 Targeting Commercial-off-the-Shelf (COTS) components

MOSA modules can target Commercial-off-the-Shelf (COTS) satellite components to be integrated into the simulation and modeled in a relevant environment. These modules

are interoperable and enable engineers to more efficiently conduct design trades, Monte Carlo simulations, or optimization design analyses much earlier in the satellite design lifecycle. Since the M&S environment is MOSA based and consists of independent modules, the communications between each module do not rely on a single, conforming protocol, but rather translates between any number of disparate protocols. This enables COTS component emulators to be efficiently created and utilized within the M&S environment.

A significant advantage occurs when design engineers develop their initial CONOPS scoping while targeting COTS components in parallel within the design. This is the first step in de-coupling the design lifecycle by enabling system design at the component level early in the CONOPS definition phase. MOSA makes this design process fluid and interchangeable within both design circles. The modules are also much more realistic models of the components being evaluated for implementation into the spacecraft design. As the CONOPS changes and requirements are defined, interchanging component modules will identify optimal and sub-optimal designs.

COTS component databases provided the design engineers with an ample amount of data from which to create these modules. SmallSat Parts On Orbit Now (SPOON), a NASA managed COTS component database, is intended to be a one-stop-shop for small satellite component models. The database includes a variety of small satellite components and entries which compose many of the common spacecraft subsystems. Similarly, *satsearch* is an independent, up-to-date, parametric search engine for space products and suppliers. The company is part of the incubative program at European Space Agency (ESA) Business Incubation Center in Noordwijk. These satellite component databases are valuable data sets for satellite design engineers. MOSA M&S environments enable these databases to feed individual component modules within the design environment for rapid reconfiguration and interoperability. Integrating components from multiple vendors for design trades disrupts the vertical integration side effect of single-vendor dependency. Multiple, disparate components cohesively integrated in a stable design increases competition (which inherently drives supply chain costs and delivery schedules down), facilitates improved designs integration, and ensures the interoperability of the sub-systems within the satellite design.

Within large constellation design and operation, MOSA M&S environments enable the rapid design and reconfiguration for replacing on-orbit nodes. The production lines needed to feed these constellations will rely on COTS components to meet the projected volume of spacecraft and support pre-planned, block upgrades. Constellation providers are able to select from multiple vendors without necessarily requiring a large surge in production capability from a single vendor to meet demand. The technique can also reduce the largely static block upgrade process by converting the upgrade cycles into continuous, “on-the-assembly-line” upgrades. Continuous constellation upgrades will smooth constellation operations and maintain forward-backward compatibility between the on-orbit nodes. The technology refresh enabled by the MOSA M&S environment serves to increase reliability and enable cost savings.

2.1.2 High Fidelity Design Reference Mission Models

Targeting COTS hardware in the modeling and simulation efforts significantly increases the fidelity of the system models. Using these COTS targeted sub-system models in the mission CONOPS design phase similarly translates to much higher fidelity Design Ref-

erence Missions (DRMs). Engineering COTS hardware models for use in DRMs is not a trivial task. It takes significant engineering effort to create high fidelity models. Traditionally, this engineering time is custom with limited reusability. This means detailed emulator models of hardware are usually developed after the spacecraft is designed.

MOSA provides the structure to automate this process. Significant efforts on this front are documented in [4]. Digitalization of the supply chain has shown to increase reliability in other technical industries. [4] discusses the technical efforts to create "structured, machine-readable, human-readable" Electronic Data Sheets (EDS). The EDS contain the necessary data inputs required by the M&S tool for component module definition. The MOSA approach enables these modules to be tailored to ingest non-traditional data inputs for COTS components which are typically deferred until later in the critical AIT phase. Communication protocols, mechanical models including moments of inertia (MOI) and products of inertia (POI), fault detection protocols, mechanical/electrical/software interface control descriptions (ICDs) are examples of improved fidelity that can be inserted into the M&S environment via MOSA EDS.

Higher fidelity DRMs will propagate mission assurance throughout the entire satellite lifecycle. The propagation streamlines the AIT phase of the design, significantly reducing the cost and schedule magnitudes of traditional design processes. MOSA ensures the disparate components operate in a compatible system. The usual burdens in AIT (inconsistent hardware/software/electrical interface control descriptions, data communication protocols, time-sequencing, etc.) are either eliminated or significantly reduced.

Eliminating the dependency of strictly defined mission/CONOPS before spacecraft design, and similarly, the dependency of spacecraft critical design before the procurement of hardware and initial AIT is known as Built in Test and Emulation (BITE). BITE is the practice of iteratively and continuously testing the system internally throughout the program lifecycle against a common, defined baseline. Higher fidelity MOSA modules inherently include the test and verification parameters within the models. It is a critical function of MOSA enabled M&S designs and identifying anomalies or change effects in the spacecraft design phase. Identifying the potential risks early plays an important role in the streamlined AIT.

Streamlining AIT via BITE and, more acutely, MOSA enabled M&S design environments, provides a number of value-add attributes to the overall mission. Cost/schedule savings are evident in the reduction of the magnitude of the design and AIT phases. It enables more design overlap between the spacecraft design and AIT phases. The modules developed are also reusable with minimal engineering work to reconfigure the modules. The approach provides design teams with the API knowledge to develop their own custom implementations and incorporate unique, innovative concepts into the design. Higher fidelity DRMs, streamlined AIT, and BITE within the satellite design phases are all critical for smallsats to be an operational solution for constellations.

2.1.3 International Collaboration in M&S environments

Multiple, globally distributed engineering and research teams could significantly increase a constellation's capability set if an enabling, collaborative design environment exists. MOSA M&S environments provide a cohesive design environment and more effectively enable technical improvements. Much like MOSA allows disparate sub-

systems to integrate into a common system, MOSA enables disparate design teams to collaborate within the same Integrated Design Environment (IDE, Figure 3).

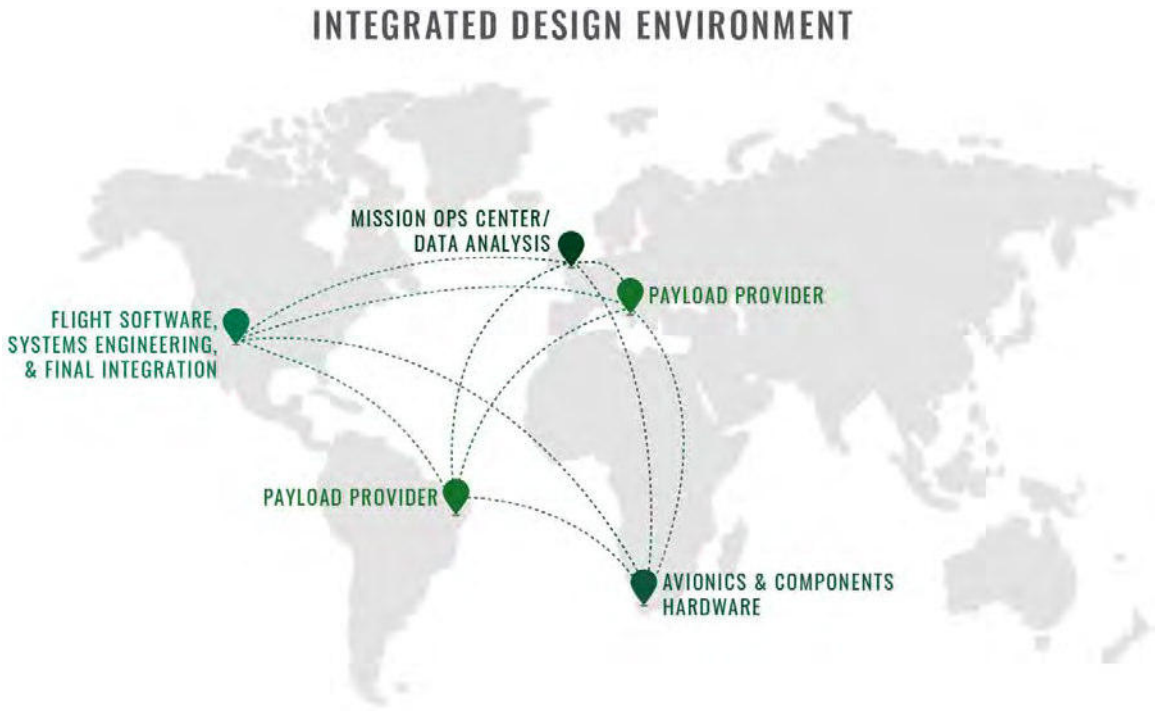

Figure 3 Globally Distributed Integration Design Environment

IDEs expand the technical potential for a constellation provider through international collaboration capabilities. These constructs are necessary to realize lower cost, reduced timelines, and collaborative missions of interest. The M&S framework enables disparate team members to collaborate within the same M&S environment through structured MOSA concepts. Virtual nodes of the M&S tool can be distributed globally. The MOSA bridges within the environment enable multiple, disparate team members to interface with the M&S environments to run BITE of COTS hardware and software solutions. The virtual M&S nodes allow for engineering teams to collaboratively design and execute sub-clusters within a constellation based on the local engineering team's area of expertise. Heterogeneous constellation design, enabled by distributed IDE nodes, will inject enormous capability into the next generation of constellations. This early integration and higher-level verification significantly increases mission reliability. MOSA M&S environments bring this capability to the global team.

3. CONCLUSIONS

A MOSA M&S environment is a "New Space" solution which drives down cost and schedule (Figure 4) and increases mission reliability in smallsats. The approach enables engineers to target COTS components and software within their design. These disparate sub-systems can seamlessly integrate to execute the next generation of satellite constellations. It also drives the industry to develop and improve EDS for COTS components. MOSA M&S with EDS ingestion significantly reduces the engineering effort to develop highly detailed emulated models of spacecraft sub-systems. DRMs utilizing these advanced models enable BITE within a satellite design. BITE propagates mission assurance throughout the shortened lifecycle, resulting in a final risk level more acceptable

by constellations. Not only does this shorten the development lifecycle, it allows for more frequent replacement of on-orbit nodes and continuous upgrades of satellites being deployed for a constellation. The capabilities and achievements of future constellations will also expand with the increase in technical diversity through disparate design teams now empowered to collaborate in the market.

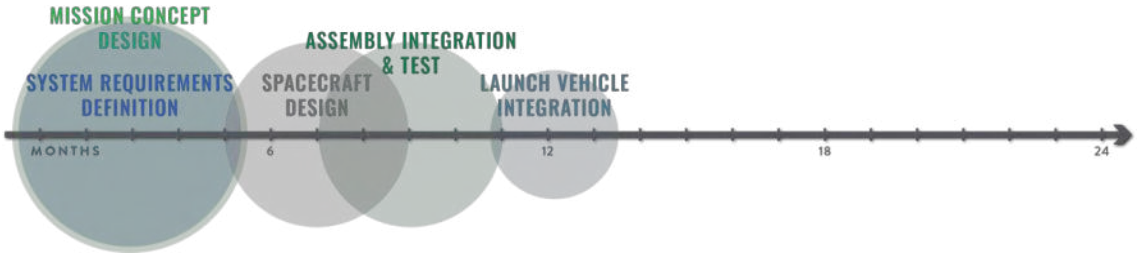

Figure 4 Results of MOSA M&S Environment on Smallsat Lifecycle

4. REFERENCES

[1] S. DelPozzo, C. Williams, B. Doncaster, Nano/Microsatellite Market Forecast, 9th Edition (2019) Figures and illustrations, L. Carapaica, D. Gerber

[2] A. Dunn, S. Kennedy Jr., "Reducing Small Satellite Development Timelines through Market Analytics and Systems Engineering", Spanish Small Satellites International Forum, Malaga, Spain, 2019.

[3] DoD Systems Engineering: Initiatives, Modular Open System Approach https://www.acq.osd.mil/se/initiatives/init_mosa.html (Accessed April 2019)

[4] K. Kumar, A. Dunn, S. Kennedy Jr., A. Vaccarella, N. Nagendra, Improving AIT through integration of supply chain data into early-phase concept design. Simulation and EGSE for Space Programmes (sesp2019), The Netherlands (2019)

Feasibility Analysis of Low Earth Orbit Nanosatellite Formations with Limited Delta-V Budget

Debdeep Roychowdhury[1], Yeerang Lim[2], Sascha Weiß[3]

[1] Technische Universität Berlin
Marchstr. 12, 10587 Berlin, Germany
Phone: +49 30 314-22345, Mail: roychowdhury@tu-berlin.de

[2] Technische Universität Berlin
Marchstr. 12, 10587 Berlin, Germany
Phone: +49 30 314-22345, Mail: yeerang.lim@tu-berlin.de

[3] Technische Universität Berlin
Marchstr. 12, 10587 Berlin, Germany
Phone: +49 30 314 75872, Mail: sascha.weiss@tu-berlin.de

Abstract: NanoFF, Nanosatellites in Formation Flight is a new CubeSat mission initiated and led by the Chair of Space Technology at the Technische Universität Berlin in cooperation with the German Aerospace Center. The mission aims to demonstrate formation flight capabilities using two 2U CubeSats equipped with state-of-art electrothermal propulsion systems. A key mission objective is to establish a helix formation for a certain period, thereby ensuring passive safety due to different eccentricities, argument of perigees and ascending nodes. Also, formations in a projected circular orbit and an along track orbit will be established. For a successful mission, it is necessary to guarantee a safe deployment, avoid any risk of collision without drifting too far from each other during commissioning and ensure sufficient delta-v for formation flying. This paper investigates the collision avoidance measures and delta-v requirements of the NanoFF mission before the actual process of formation-flying can start, that is - after deployment from the upper stage, during commissioning and during the recovery of the satellites to bring them close enough for formation-flying. Preliminary results show that the necessary safety and delta-v requirements are feasible with the proposed separation and recovery strategies.

1. INTRODUCTION

This paper presents a formation-flying concept involving two 2U CubeSats which will be launched in 2021 into a 550 km Sun Synchronous Orbit (SSO). With a combined delta-v of 30 m/s, the two NanoFF CubeSats will establish a helix formation for a certain period as the primary formation-flying objective. As secondary objectives, formations in a Projected Circular Orbit (PCO) and an Along Track Orbit (ATO) will be set up. The formation flying concept will be based on the relative eccentricity/inclination vector separation method which was first developed for the geostationary satellites [1] and later modified for formation flying [2]. This mission will adopt a simple, safe and robust approach to satisfy the educational purpose and collect first-hand experience while minimizing efforts and risks. The relevant formation-flying concepts used in previously successful formation-flying missions such as CanX-4 and CanX-5 [3], TerraSAR-X/TanDEM-X [4] and Prisma [5] will also be utilized for the NanoFF mission.

As of 30 April 2019, preliminary mission simulations have been carried out to estimate delta-v requirements in preparation for performing formation flight maneuvers. These are - collision analysis after deployment from the Upper Stage (US), drift analysis during commissioning and recovery analysis for reducing the relative distance after commissioning. The worst-case consideration assumes a maximum timeframe of 2

months for the commissioning of the satellite. One of the requirements is to complete the recovery with a maximum allowable delta-v usage of 3 m/s. The research in this paper heavily relies on relative orbital elements (ROEs), which are defined as:

$$\delta\alpha = \begin{bmatrix} \delta a \\ \delta\lambda \\ \delta e_x \\ \delta e_y \\ \delta i_x \\ \delta i_y \end{bmatrix} = \begin{bmatrix} (a_2 - a_1)/a_1 \\ u_2 - u_1 + (\Omega_2 - \Omega_1)\cos i_1 \\ e_2 \cos\omega_2 - e_1 \cos\omega_1 \\ e_2 \sin\omega_2 - e_1 \sin\omega_1 \\ i_2 - i_1 \\ (\Omega_2 - \Omega_1)/\sin i_1 \end{bmatrix} \quad (1)$$

where subscript 1 denotes the terms of the chaser satellite/NanoFF-1 and subscript 2 denotes the target satellite/NanoFF-2. The terms a, e, i, ω, Ω and M denote the classical Keplerian elements and $u = M + \omega$, i.e., argument of latitude.

2. SEPARATION STRATEGY

The separation strategy is based on the method introduced in [3] for the AVANTI mission: the separation delta-v components in the Radial-Transverse-Normal (RTN) frame centered on the chaser satellite depends on the performance uncertainty of the deployment mechanism and the intended final relative radial and normal distances. This, along with a drift reduction maneuver 1.5 revolutions after separation guarantees a passive safety through parallel/anti-parallel relative eccentricity/inclination vector separation [2].

In case of NanoFF, the situation is more complicated as the separation strategy involves three spacecrafts – target, chaser and the US, as compared to AVANTI where two spacecrafts were involved – Biros and Beesat-4. Although the tangential component of the separation delta-v ensures collision safety after separation, the relative distance can increase to large distances in the commissioning period (up to 3000 km over a 2-month period), unless controlled by differential drag maneuvers.

Thus, the ejection of the two CubeSats from the same US is extremely challenging, regarding the objective to safely keep them close enough to each other to enable formation flying after commissioning. The important parameters are – deployment direction from US (radial, cross-track and tangential components), deployment interval of the two CubeSats (e.g., 10 and 20 seconds) and the location in orbit of the US (mean argument of latitude, u) during the deployments. The last parameter is important to understand if the cross-track motion (of the target satellite with respect to the chaser satellite) is built by Δi (inclination difference between the CubeSats) or $\Delta\Omega$ (right ascension of ascending node difference between the CubeSats), which has consequences in terms of safety (phasing of relative eccentricity and inclination vectors) and delta-v cost for formation keeping [2]. It is a good choice to keep $\Delta i = 0$ to minimize the effects from J2 on the relative motion [2]. This provides a passive stability to the formation.

One option is to perform the deployments from the US near the poles ($u = \pm \pi/2$) with different cross track components of the deployment vectors, which will induce a small offset in the right ascension of their ascending nodes, but the inclination of both CubeSats will be identical to the US, therefore satisfying the condition $\Delta i = 0$. This approach,

including the analysis of the relative dynamics right after separation, has been investigated in detail through simulations in MATLAB and GMAT.

2.1 Collision Analysis

As of 30 April 2019, our potential launch service provider has confirmed it is possible to specify an arbitrary launch direction. Keeping this in mind, Monte-Carlo simulations were performed with simultaneous radial, cross-track and tangential components for both the deployments with a separation interval of 10 seconds. The deployments were checked at every mean argument of latitude of the US orbit (at which the chaser is launched) at an interval of 0.05°. Considering the large simulation times involved, the number of deployment vectors for each satellite was limited to 100 vectors (i.e., 10000 vector combinations). The same set of 100 deployment vectors per satellite were checked throughout the US orbit. The simulation duration was limited to 2 orbital periods after launch. The considered performance error was 10% in magnitude and 2° in direction.

As mentioned before, the AVANTI mission involved only one deployment, whereas for the NanoFF mission, two deployments will take place. At a 550 km altitude, the distance between two 10-second-interval deployment locations amounts to almost 76 km. In order to determine the absolute individual separation delta-v components using [3], the distance between deployments were ignored for simplicity and the relative individual separation delta-v components were considered.

In this paper, the origin of the RTN frame is located at the center of mass of the chaser satellite. When the target satellite leads the chaser satellite in flight direction (as planned for the NanoFF mission), the relative radial and tangential separation delta-v values should be negative for collision safety [3]. Consequently, the relative normal component of the separation delta-v should be positive in this case for establishing anti-parallel relative eccentricity/inclination configuration [3].

For example, considering a deployment error of 10% at a 550 km altitude, the required final minimum magnitudes of $a\delta e$ and $a\delta i$ for collision safety come out to be 548 m and 337 m respectively. For $a\delta i$, a minimum value of 200 m has been considered along with a margin of 137 m [3]. The magnitudes of $a\delta e$ and $a\delta i$ define the size of the final relative orbit in the radial and normal directions respectively. Consequently, the required (relative) separation delta-v comes out to be $[v_x \;\; -0.15 \;\; 0.3694]^T$ m/s in the RTN frame, where the magnitude of v_x depends on the total available delta-v magnitudes of the two individual deployments. As mentioned before, in this case the polarity of the v_x is negative. Figure 1 shows the collision probability with respect to the mean argument of latitude of the US (at which the launch of the chaser satellite/NanoFF-1 takes place).

The individual components of the separation delta-v values only provide temporary safety due to ejection uncertainty and does not provide a bounded passively safe orbit with parallel/anti-parallel ***e/i*** vector separation. A drift reduction maneuver is necessary to achieve a stable and safe bounded relative orbit. Using a relative tangential separation velocity of 0.15 m/s can cause large drifts of more than 4000 km over a 2-month commissioning period. Therefore, the drift reduction maneuver will be divided into several smaller maneuvers, which has been addressed in Section 3.

In order to reduce the drift during the commissioning period, the final minimum magnitude of $a\delta e$ is reduced to 348 m and the final minimum magnitude of $a\delta i$ is changed to 387 m, which make the required relative separation delta-v $[v_x \ -0.095 \ 0.4235]^T$ m/s in the RTN frame. The maximum drift gets reduced to less than 3600 km. The effect of this modified relative separation delta-v on the collision safety has been shown in Figure 2. The effects of relative tangential separation delta-v values of 0.15 m/s and 0.095 m/s on the drift is discussed in Section 2.2.

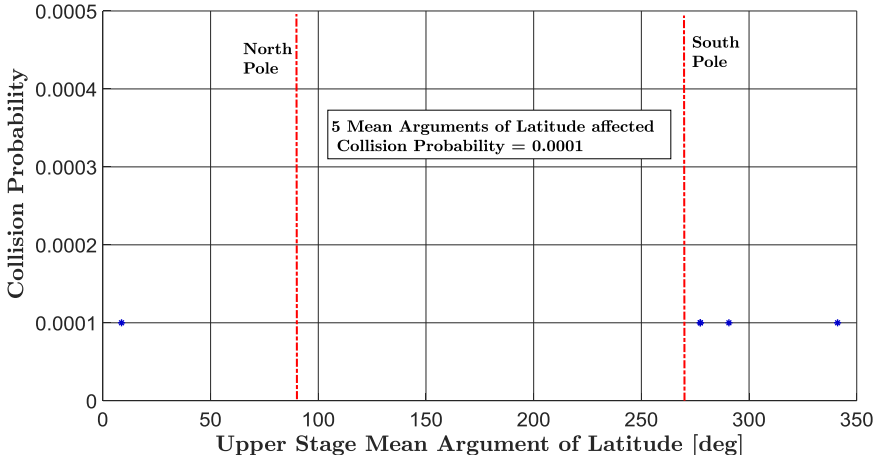

Figure 1 Collision probability for an intended relative tangential separation Δv = 0.15 m/s over US mean u at which chaser/NanoFF-1 is launched

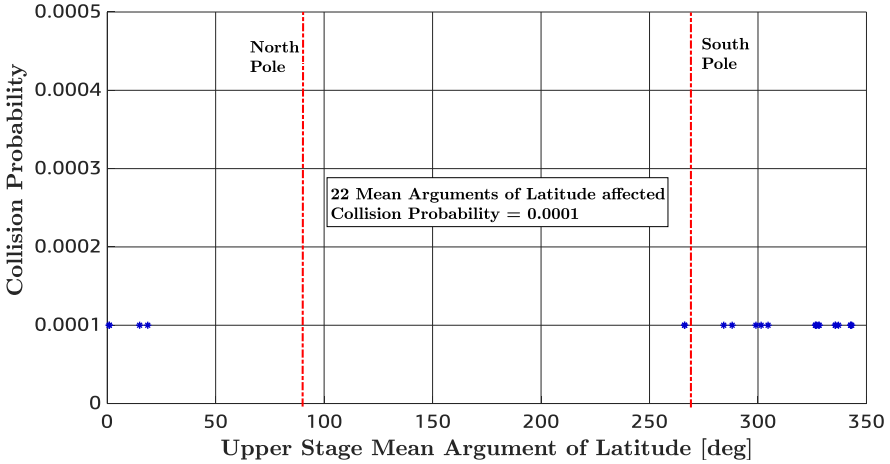

Figure 2 Collision probability for an intended relative tangential separation Δv = 0.095 m/s over US mean u at which chaser/NanoFF-1 is launched

Simulation results show that when the relative tangential separation velocity is 0.15 m/s (Figure 1), a total of 5 mean arguments of latitude (out of 7200 locations equally distributed on the US orbit) are affected by 1 collision each (out of 10000 vector combinations), giving a collision probability of 0.0001 at these locations. At other locations, the collision probability is 0. The mean arguments of latitude of 90° and 270° (near north and south poles) are particularly important for the NanoFF mission as the satellites will be launched from the US at one of those mean arguments of latitude values.

When the relative tangential separation velocity is 0.095 m/s (Figure 2), a total of 22 mean arguments of latitude are affected by 1 collision each. Although this decreases the percentage of safe US mean arguments of latitude from 99.93% to 99.69%, this does not

increase the collision risk in a significant way. In general, a higher relative tangential separation velocity reduces collision risk at the cost of increased drift during the commissioning period.

2.2 Drift Analysis

The magnitude of the relative tangential component of the separation delta-v directly affects the relative distance during the commissioning period (unless controlled by differential drag). The following examples show how performance and direction errors in deployments affect the final relative distances during the commissioning period.

In the first case, an *intended* relative tangential separation delta-v of 0.15 m/s produces a relative distance of more than 4300 km over 2 months. In this case, a combination of errors in magnitude and direction for both the deployments increases the *actual* relative tangential separation delta-v to 0.27 m/s. If insignificant errors in magnitude and direction are considered for both the deployments (e.g., 0.16 m/s actual relative tangential separation delta-v), the relative distance after two months is limited to 2500 km.

Considering the second case of intended relative tangential separation delta-v of 0.095 m/s, the relative distance produced can reach close to 3400 km if the actual relative tangential separation delta-v reaches 0.22 m/s due to deployment errors. However, in case of insignificant error in magnitude and direction (e.g., 0.098 m/s actual relative tangential separation delta-v), this distance is limited to 1500 km.

Figure 3 summarizes the relationship between relative tangential separation velocity and the relative distance after a 2-month commissioning period. This includes data from both intended separation delta-v values of $[v_x \ \text{-}0.15 \ 0.3694]^T$ m/s and $[v_x \ \text{-}0.095 \ 0.4235]^T$ m/s.

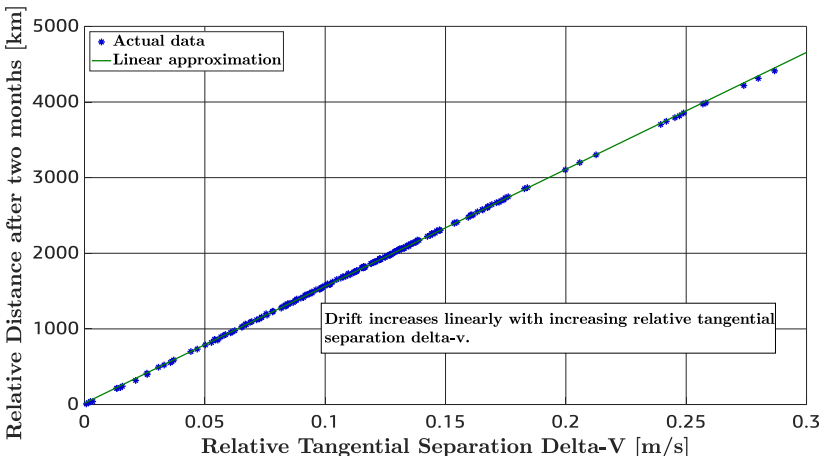

Figure 3 Dependency of drift on relative tangential separation velocity

Simulation results (from Figure 3) show that that dependency of the drift during the commissioning period on the relative tangential separation velocity is approximately linear. This can be used to predict the drift between the NanoFF satellites during the commissioning period by checking the actual separation delta-v magnitude and direction for both the satellites.

3. RECOVERY ANALYSIS

The recovery maneuver will be split into several steps, so that the maneuver execution errors of each burn can be checked before concluding the reconfiguration. This is especially important during the later stages of the recovery maneuver, to avoid collisions with high kinetic energy. The recovery analysis aims to establish a bounded passively safe orbit having parallel/anti-parallel relative eccentricity/inclination vector separation [6]. The analytical impulsive reconfiguration approach presented in [6] has been modified for the NanoFF mission to consider the significantly larger relative distances involved. This has been shown in this paper with an example.

A relative tangential separation velocity of 0.16 m/s and a separation near the north pole ($u = +\pi/2$) cause the ROE set to take the following values after a commissioning period of 2 months:

$$a_1\delta\alpha_{initial} = [-323.60 \quad 2579064.72 \quad 265.66 \quad 177.38 \quad -4.5990 \quad 1344.0267]\ \text{m} \qquad (2)$$

In order to establish a bounded passively safe orbit after the recovery maneuver, the following ROE set is desired:

$$a_1\delta\alpha_{desired} = [0 \quad 1000 \quad 0 \quad -300 \quad 0 \quad 300]\ \text{m} \qquad (3)$$

As the difference in relative longitude ($a_1\delta\lambda$) is more than 2 million meters, 4 *minimum delta-v* maneuvers groups are used to bring $a_1\delta\lambda$ to 10000 m, followed by 4 maneuver groups in the *maximum observability* mode. As defined in [6], a *minimum delta-v mode* involves going directly from the initial ROE to the final desired ROE in order to minimize delta-v usage. In *maximum observability mode*, multiple intermediate ROEs are selected as waypoints in order to maximize supervision over the reconfiguration problem at the cost of higher delta-v consumption. Using a single *minimum delta-v* maneuver group for the entire recovery does not lead to the desired results due to the large distances involved in the NanoFF mission. Also, when $a_1\delta\lambda$ gets reduced to 10000 m, the delta-v mode is changed from *minimum delta-v* to *maximum observability* to increase supervision for collision safety. Additionally, passive safety is maintained during the *maximum observability mode* through anti-parallel eccentricity/inclination vector separation. The intermediate and final ROEs during the *minimum delta-v* mode are listed in Table 1. The delta-v values required to attain them are 0.56 m/s, 0.20 m/s, 0.06 m/s and 0.01 m/s respectively.

ROEs	$a_1\delta a$ [m]	$a_1\delta\lambda$ [m]	$a_1\delta e_x$ [m]	$a_1\delta e_y$ [m]	$a_1\delta i_x$ [m]	$a_1\delta i_y$ [m]	Orbits req.
$a_1\delta\alpha_{roe2}$	17.04	84893.35	-81.09	-453.32	-3.46	371.81	773
$a_1\delta\alpha_{roe3}$	0.44	20080.14	36.53	-361.55	-0.84	275.87	58
$a_1\delta\alpha_{roe4}$	0.08	12007.99	10.77	-299.41	-0.10	296.99	28
$a_1\delta\alpha_{roe5}$	0.03	9988.90	-0.23	-301.27	-0.03	299.22	24

Table 1 Intermediate and final ROEs during the *minimum delta-v* recovery period

The ROEs $a_1\delta\alpha_{desired}$ and $a_1\delta\alpha_{roe5}$ are already similar except the value of $a_1\delta\lambda$. During the *maximum observability* mode, the changes in relative eccentricity and inclination vectors are insignificant. $a_1\delta\lambda$ is reduced in steps, as shown in Table 2. The evolution of ROEs during the *maximum observability mode* is listed in Table 2.

ROEs	$a_1\delta a$ [m]	$a_1\delta\lambda$ [m]	$a_1\delta e_x$ [m]	$a_1\delta e_y$ [m]	$a_1\delta i_x$ [m]	$a_1\delta i_y$ [m]	Orbits req.
$a_1\delta\alpha_{roe6}$	28.67	9943.80	-36.74	-301.62	-0.07	299.38	50
$a_1\delta\alpha_{roe7}$	38.20	7283.18	-23.90	-296.04	-0.02	298.59	10
$a_1\delta\alpha_{roe8}$	28.65	3699.17	-11.90	-293.84	-0.02	298.43	10
$a_1\delta\alpha_{final}$	0.06	1007.23	-0.61	-301.62	-0.01	298.98	10

Table 2 Intermediate and final ROEs during the *maximum observability* recovery period

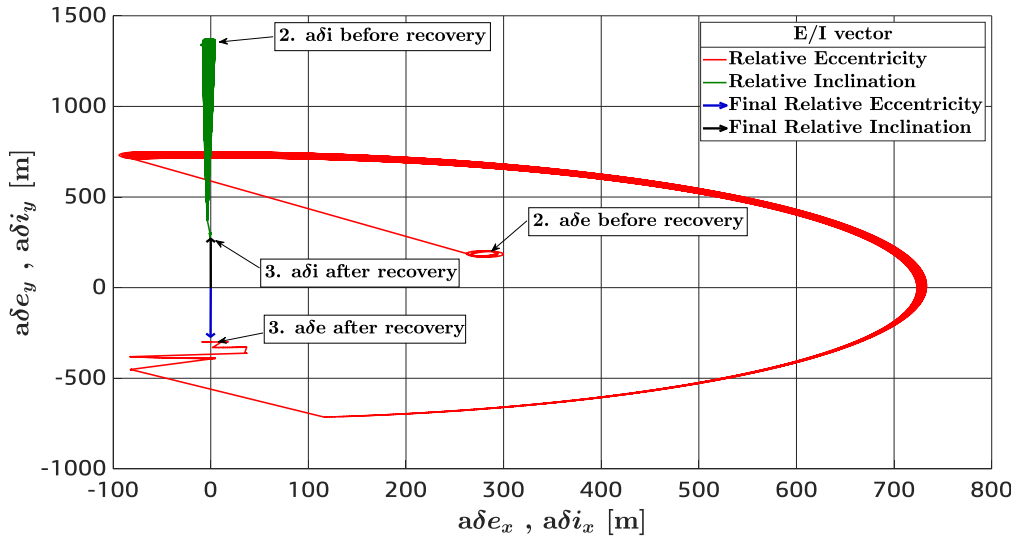

Figure 4 Relative ***e/i*** vector during recovery

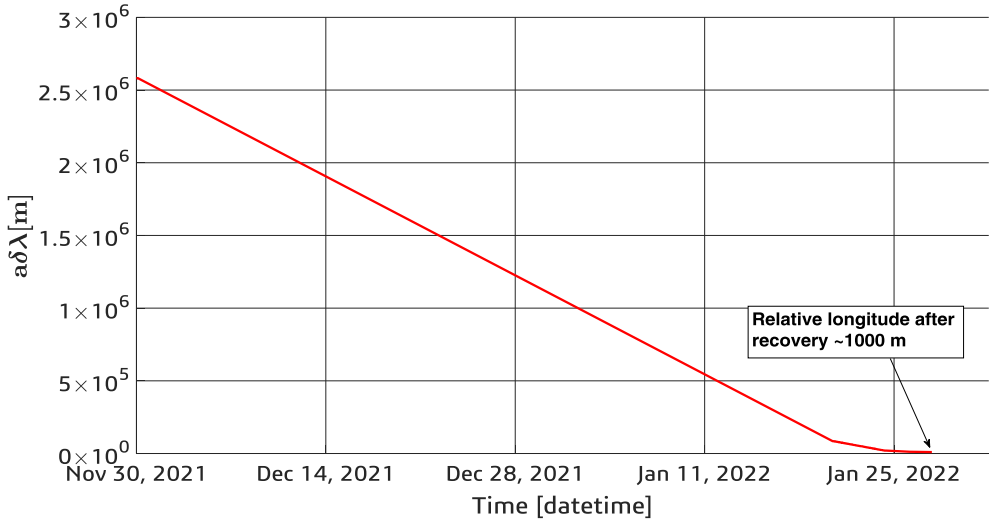

Figure 5 Relative longitude during recovery

As presented in Table 2, the final ROE after the recovery period, $a_1\delta\alpha_{final}$ is similar to the desired ROE, $a_1\delta\alpha_{desired}$. $a_1\delta\alpha_{final}$ can be further improved by applying small maneuvers. The entire recovery takes 963 orbits with a delta-v consumption of 0.904 m/s. Figure 5 shows the relative ***e/i*** vector during recovery. At the end of the recovery period, the desired anti-parallel relative ***e***/***i*** vector configuration is achieved, which leads to the formation of a bounded passively safe relative orbit. Figure 5 shows the relative longitude during recovery, which achieves a value of approximately 1000 m after the recovery period.

4. CONCLUSION

The NanoFF mission will demonstrate passively safe formation flying approaches by using the relative eccentricity/inclination vector separation method along with a robust and simple relative navigation system. Safety analysis of the formation, starting from deployment at a fixed argument of latitude at predetermined separation delta-v values until the end of the mission shall be conducted in terms of relative orbital elements. Natural perturbed relative dynamics will be exploited to lower delta-v usage during the mission. This will allow the possibility of performing more experiments and extending the mission lifetime. The results from the collision analysis show that overall, the collision risk is very low when sufficient relative tangential separation velocity is maintained, at the cost of high drifts after the commissioning period. The recovery analysis shows that using natural perturbed relative dynamics and minimum delta-v, the relative distance can be brought to the desired value with a delta-v usage of less than 3 m/s.

5. REFERENCES

[1] M. C. Eckstein, C. K. Rajasingh and P. Blumer, Colocation strategy and collision avoidance for the geostationary satellites at 19 degrees west. International Symposium on Space Flight Dynamics, Vol. 6 (1989, November).

[2] S. D'Amico and O. Montenbruck, Proximity operations of formation-flying spacecraft using an eccentricity/inclination vector separation. Journal of Guidance, Control, and Dynamics, Vol 29, No. 3 (2006).

[3] M. Wermuth, G. Gaias and S. D'Amico, Safe Picosatellite Release from a Small Satellite Carrier, Journal of Spacecraft and Rockets, Vol. 52, No. 5 (2015).

[4] R. Kahle, B. Schlepp, F. Meissner, M. Kirschner and R. Kiehling, TerraSAR-X/TanDEM-X formation acquisition–analysis and flight results. 21st AAS/AIAA Space Flight Mechanics meeting (2011).

[5] E. Gill, O. Montenbruck and S. D'Amico, Autonomous formation flying for the PRISMA mission. Journal of Spacecraft and Rockets, Vol. 44, No. 3 (2007).

[6] G. Gaias, S. D'Amico and J. S. Ardaens, Generalized Multi-Impulsive Maneuvers for Optimum Spacecraft Rendezvous in Near-Circular Orbit. International Journal of Space Science and Engineering, Vol. 3, No. 1 (2015).

CubeSat Formation Flying using Low Power Inter-Satellite Communication in Earth Observation Missions

Roland Haber[1], Iurii Motroniuk[1], Klaus Schilling[1]

[1]Zentrum fuer Telematik e.V.
Magdalene-Schoch-Strasse 5, 97074 Wuerzburg, Germany
Phone: +49 (931) 615 633 - 39, Mail: roland.haber@telematik-zentrum.de

Abstract: One of the next steps in tapping the vast potential of CubeSats is the extensive utilization of constellations and formations. These multi-satellite systems can be used to carry out a broad spectrum of tasks, such as earth observation, climate prediction, and disaster monitoring at very low costs in comparison to traditional constellations consisting of larger satellites. In order to have multiple CubeSats operate in unison, reliable inter-satellite communications must be established. While larger satellites can afford to house big antennas with tremendous transmission powers, CubeSats have to find solutions that fit their limited mass, volume, and power budgets. Therefore, in our formation flying missions in Wuerzburg, we are working with CubeSat modems and antennas in the UHF and S-band spectrum to enable inter-satellite connections as well as high speed downlinks. Our CubeSats use electric propulsion for formation forming and upkeep as well as reaction wheels for pointing toward their observation targets. In order to establish communication crosslinks, the omnidirectional UHF is used for initial position and attitude exchange as well as data transmissions between the satellites. Next, the high bandwidth directional S-band system will be used by precisely pointing the satellites towards our ground station in Wuerzburg.

1. INTRODUCTION

Earth observation using multi-satellite systems requires robust communications between the satellites for coordination. This coordination can then be applied to simultaneous target tracking and photogrammetric Earth observation. In TOM (Telematics Earth Observation Mission) these efforts are being realized using a formation of three CubeSats [1]. In addition to the omni-directional UHF communication these satellites will be equipped with directional S-Band systems for high bandwidth communications. This will allow high speed data downlink of images taken by the cameras. With the help of elaborate antenna placements, each of the satellites of the formation will have omnidirectional reception and transmission as well as the option for high speed directional communication to the ground. This work will outline the design and development process of the inter-satellite links as well as the elaborate testing procedures involving our 3-axis dynamic bench test facility.

2. FORMATION FLYING

Efforts toward cooperating small satellite systems have been ongoing in Wuerzburg for many years [2]. Currently, there are three formation flying missions in development. Each formation is based on a similar premise, relying on previously developed enabling technologies. These technologies include precise orbit and attitude determination as well as precise orbit and attitude control [3]. The satellite bus is based on the UNISEC Europe standard [4], which has been proven to provide a robust framework for housing the satellite subsystems. For the act of establishing and holding a formation, data has to

be exchanged between the satellites. Therefore, the satellites are equipped with crosslink transceivers, that enable inter-satellite communication in the UHF spectrum. Besides being based a common satellite platform, each mission has its individual requirements and subsystems depending on the mission objectives. Formations in general also do not require individual control of each satellite from ground, but are rather capable of autonomously operating in orbit [5]. Using electric propulsion for formation forming and upkeep as well as reaction wheels for pointing toward their observation targets, these CubeSats are capable of operating homogeneously, rather than as individual satellites. Especially when considering large scale formations, traditional satellites would be prohibitively expensive. Hence, a large formation must rely on small satellites, which become increasingly more powerful, reliable, and easier to produce in large quantities. With that approach, multi-satellite systems consisting of hundreds of small satellites can be realized efficiently and cost-effectively, enabling new opportunities for Earth observation, climate monitoring, and globally spanning communication networks.

2.1 NetSat

The formation flying mission NetSat is a technology demonstration mission that consists of four cooperating CubeSats. Using electric propulsion and UHF inter-satellite links, various formation topologies will be demonstrated during this mission. These satellites will be launched in 2019 and are the first nanosatellite formation from Wuerzburg. It is planned to demonstrate each technology that will enable future formation flying mission and thereby paving the way towards more application driven missions. While NetSat will not carry cameras for Earth observation, it will still test formation topologies and especially target pointing capabilities that make simultaneous Earth observations with multiple satellites possible [6]. These 3U satellites will also test electric propulsion systems, which enable precise orbit control for demonstrating various formation topologies within the available power budget.

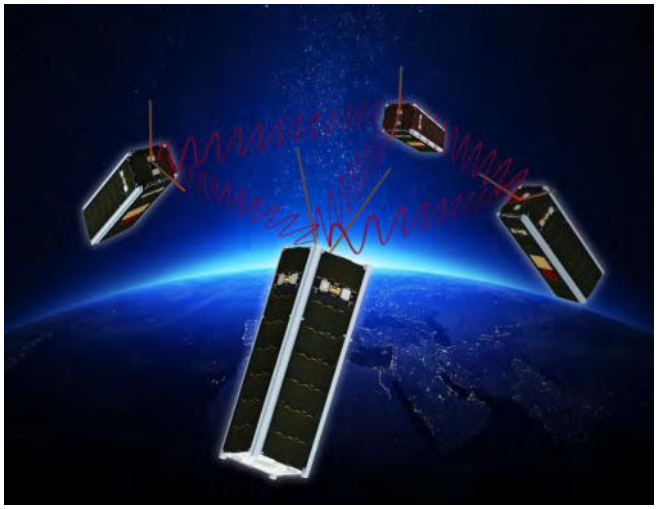

Figure 1: NetSat formation demonstrating precision orbit and attitude control and inter-satellite communication.

2.2 TOM

The TOM (Telematics Earth Observation) mission will be a formation of three CubeSats that will use photogrammetric Earth observation for disaster monitoring. Especially the measurement of volcanic ash clouds is the focus of this mission.

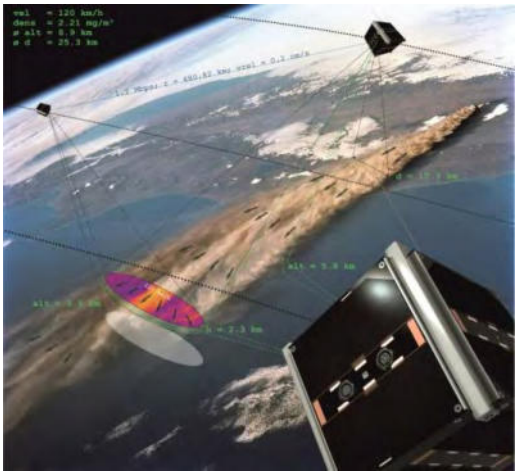

Figure 2: TOM formation during volcanic ash cloud observations.

These satellites will build upon the NetSat mission by also carrying cameras for Earth observation. The previously demonstrated technologies will be applied to this particular use case in order to take 3D images of volcanic ash clouds [7]. Additionally, S-Band transmitters are planned for high bandwidth data downlinks of the pictures taken by the satellites. The TOM formation will also make use of omnidirectional UHF antennas and transceivers for reliable inter-satellite communications [8].

2.2 CloudCT

CloudCT is an upcoming mission for 2019 that will consist of ten CubeSats. These Satellites will be used for climate prediction, especially cloud monitoring. CloudCT will take the developed technologies to the next level and use state-of-the-art subsystems for creating such a large constellation of satellites. The requirements for developing and operating such a large multi satellite system are very high and the necessary sensors for this mission have to be accurately integrated into the satellite bus. With a planned launch for 2022, these satellites will be a great contribution to climate monitoring and weather predictions. For the downlinking of the captured images and data, X-band transmitters are being integrated with miniature patch antennas on the panels. Inter-Satellite communication will be included with a range of 100km per satellite pair. Thus, the entire formation will span over 1000km. One of the outcomes of this project is an impact on future innovative satellite formation missions, both for Earth observation and for new architectures in future global communication networks [9].

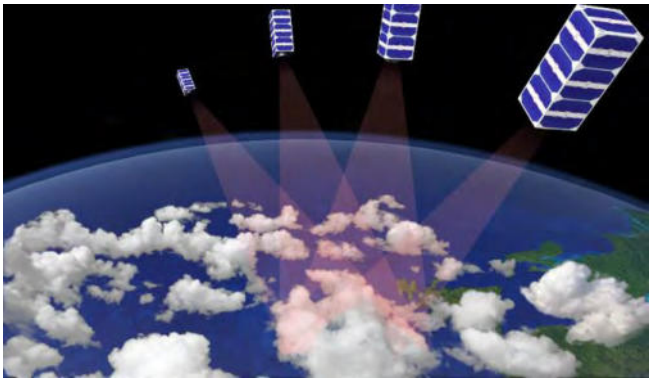

Figure 3: CloudCT formation performing cloud monitoring experiments.

3. INTER SATELLITE COMMUNICATION

ISL (inter-satellite links) are essential to formation flying missions. Autonomous formations in particular require a reliable data exchange between the satellites. Therefore, the previously mentioned multi satellite systems rely on robust UHF transceivers that have proven to be reliable for low bandwidth data exchange. Using omnidirectional antennas, each satellite can be in contact with all the others in the formation at all times. This availability is especially important when it comes to precise pointing maneuvers or proximity operations. By utilizing autonomous target detection and operations, it is important to also be able to rely on the continuous position and attitude data exchange of the satellites [10]. The previously mentioned missions will be using low power UHF transceivers in a redundant configuration as well as omnidirectional λ/4 dipole antennas. Each of the two transceivers has dedicated signal lines on the UNISEC bus that connect directly to the OBC (On-Board Computer). While only one transceiver will be active at any given time, switching between the two modems can be done manually or automatically in case of a communication problem. Additionally, the same modems will be used for UHF data links to the ground station in Wuerzburg as well as for commanding. Depending on the baseline of the formation, the frequency of attitude and orbit data exchange varies [12]. While proximity CubeSat formations have to be in contact on a second or millisecond basis, formations that have several kilometres distances may increase ISL intervals to several minutes or longer, only conducting more frequent contacts during time sensitive operations and experiments.

3.1 CubeSat UHF Communication

UHF communication has been used on CubeSat missions for years [11]. The relatively small antennas can be easily stowed on the satellites and deployed in orbit. While not providing very high data throughput, due to the limited bandwidth available in the 70cm spectrum, they are still a viable option for simple and reliable data transfers.

3.2 Omnidirectional ISL Antennas

For the purpose of having readily available crosslinks during the whole orbit and regardless of the current satellite attitudes, omnidirectional antennas are essential. For low data rates, UHF dipoles are ideal. Due to the comparatively high power demand of transmissions, the transceivers will be chiefly operated in a standby mode so that signals

from the other satellites of the formation can be received at all times. For higher data rates, other frequency bands have to be considered. For that purpose, higher bands, such as S-band or X-band, offer a wider spectrum for inter-satellite data links. These frequencies also denote a different antenna geometry, usually patch antennas. These patch antennas will not have an omnidirectional radiation pattern, but rather a pointed signal that has a higher gain in the center beam. Consequently, the satellite has to be pointed at its communication target prior to the initialization of the radio link. On a different approach, if enough space is available, multiple antennas might be used to circumvent this pointing requirement and thereby creating a quasi-omnidirectional antenna setup.

4. HIGH SPEED DATA DOWNLINK

Earth observation missions usually also require the image data to be sent to ground. Therefore, TOM will also carry the OSIRIS optical communication system for high-speed data downlink. Future combinations of optical communication, quantum encryption, and small satellite formations will thereafter facilitate revolutionary applications in the small satellite and space science sectors. Besides optical links, higher frequency radio bands will also be prevalent in upcoming missions. These bands have the advantage of more bandwidth being available for use in comparison to more crowded frequencies in the lower spectra. However, the attenuation due to FSPL (free space path loss) is subjected to a quadratic growth with respect to the employed frequency.

$$\mathrm{FSPL} = \left(\frac{4\pi d}{\lambda}\right)^2 \tag{1}$$

As Eq. (1) shows, the FSPL is also a quadratic function of the distance between the satellite and its target. Therefore, in formation flying missions, especially when using low transmission powers, the distance between the satellites should be minimized in order to satisfy the link budget [13].

5. CONCLUSION AND OUTLOOK

A common factor, independent of the formation baseline, is the need for reliable crosslinks. The operational advantage of using omnidirectional antennae outweighs the increased gain of directional patch antennae in most cases. While patch antennae usually offer higher data rates and a better link margin, the satellites can only establish crosslinks by precisely pointing toward another. This pointing operation might be based on pre-determined time slots or can be coordinated using additional omnidirectional crosslinks. After preliminary communication and attitude exchange over dipoles, the high gain patch antennae can then be used for image or experiment data transmissions once the pointing has been realized. These combined paths, as well as combinations of ISL and uplink/downlink using the same transceivers will be advantageous is optimizing the performance of future CubeSat Earth observation missions.

6. ACKNOWLEDGEMENTS

NetSat is funded by the ERC Advanced Grant (320377). TOM is funded by the Bavarian Ministry of Economic Affairs and Media, Energy and Technology. Project partners in TOM are University of Wuerzburg, TU Munich, DLR-IKN, and ZfT. CloudCT is funded by the ERC Synergy Grant. Projects partners in CloudCT are Technion - Israel Institute of Technology, Weizmann Institute of Science, and ZfT.

6. REFERENCES

[1] K. Zaksek and T. Tzschichholz, Telematics Earth Observation Mission, 11th IAA Symposium on Small Satellites for Earth Observation (2017)

[2] P. Bangert and A. Kramer, UWE-4: Integration State of the First Electrically Propelled 1U CubeSat, 31st Annual AIAA/USU Conference on Small Satellites (2017)

[3] F. Reichel and P. Bangert, The Attitude Determination and Control System of the Picosatellite UWE-3, 19th IFAC Symposium on Automatic Control in Aerospace (2013)

[4] S. Busch and P. Bangert, UWE-3, In-Orbit Performance and Lessons Learned of a Modular and Flexible Satellite Bus for Future Pico-Satellite Formations, Acta Astronautica Vol. 117. 2015, pp.73-89 (2015)

[5] K. Schilling, Perspectives for Miniaturized, Distributed, Networked Systems for Space Exploration, Robotics and Autonomous Systems Vol. 90, p. 118–124 (2017)

[6] A. Kramer and P. Azari, Orbit control on the Pico-Satellite UWE 4 using a NanoFEEP propulsion system and a directive adaptive guidance algorithm, 35th International Electric Propulsion Conference (2017)

[7] K. Schilling and T. Tzschichholz, TOM: A Formation for Photogrammetric Earth Observation by Three Cubesats, 4th IAA Conference on University Satellite Missions and CubeSat Workshop (2017)

[8] K. Zakšek and R. Haber, Telematics Earth Observation Mission, IAA Symposium on Small Satellites for Earth Observation (2017)

[9] K. Schilling and Y. Schechner, CloudCT – Computed Tomography of Clouds by a Small Satellite Formation, 12th IAA Symposium on Small Satellites for Earth Observation (2019)

[10] R. Haber and S. Busch, X-Band Kommunikation fuer Autonome CubeSat Formationen, DGLR-Netzpublikation (2017)

[11] NASA Small Spacecraft Technology State of the Art, Ames Research Center (2015)

[12] O. Kondrateva and H. Doebler, Throughput-optimal joint routing and scheduling for low-earth-orbit satellite networks, Wireless On-demand Network Systems and Services (WONS), pp: 59-66 (2018)

[13] R. Sun and D. Maessen, “Enabling Inter-Satellite Communication and Ranging for Small Satellites”. Small Satellite Systems and Services Symposium (4S), 2017, Funchal, Portugal

Single Nanosatellite Launcher SNL – high precision launch container for nanosatellite networks

Thomas Hellwig[1], Roy Bretfeld[1], Antje Deckert[1], Sebastian Scheiding[1]

[1]Astro- und Feinwerktechnik Adlershof GmbH
Albert-Einstein-Straße 12 12, 12489 Berlin, Germany
Phone: +49 30 63 92-1000, Mail: info@astrofein.com

Abstract: For the intersatellite communication mission S-NET, TU Berlin was looking for customized launch containers allowing for deployment of four separately accommodated nanosatellites (each weighing 8.72 kg and having a size of 240 x 240 x 240 mm³). "The high deployment precision was essential for the mission success" [1], in order to ensure an adequate mission duration by slow separation of the four spacecrafts due to natural drift. Astro- und Feinwerktechnik Adlershof GmbH (Astrofein) had 1U Cubesat deployer successfully launched at the time the request came along. With its heritage of building Cubesat deployers since the early 2010s and being a long-term partner of the TU Berlin, Astrofein was given the privilege designing the S-NET launch container – called "Single Nanosatellite Launcher" (SNL). The design approach of Astrofein's nanosatellite and Cubesat deployers with special emphasize on the high demands of the S-NET mission will be described in the following. Furthermore, the verification and qualification test campaign of the SNL will be presented.

1. INTRODUCTION

The SNL was designed and built on the basis of the 1U deployer knowledge. The same release mechanism principle has been utilised that has shown to be very reliable and at the same time being a low cost and low power variant compared to other deployer release mechanisms. For S-NET, the satellite velocity deviation for the four satellites was required to be ± 4.5 cm/s. With help of the design of Astrofein's SNL's, a devition of ± 2 cm/s has been achieved. The S-NET mission was successfully launched onboard of a Soyuz rocket on 01/02/2018.

2. SNL DESIGN AND FUNCTIONAL PRINCIPLE

The SNL is a custom-made deployer for nanosatellites. Hence, it differs in shape and function from a typical deployer for Cubesat Nanosatellites of sizes 12U or 16U. The main differences put also an extra challenge into the development as non-standard mechanisms were used. The SNL comprises of the following main components: A Chassis frame that gives the deployer its shape and size and encloses together with the lid of the deployer the S-NET satellite. Those two parts separate, together with side covers, the satellite from other payload, especially the prime. This separation is a protection mechanism preventing debris in either direction to interfere in case of an incident during launch. This lid/frame combination is now fitted with some precise mechanisms and precision engineering in order to allow the deployer to open and eject the satellite at the exact time with the right speed required. The satellite itself has pins at 8 points (4 at the top and 4 at the bottom) that sit inside half-spheres of the deployer locating and retaining the satellites in order to avoid any distortion and safe travel during launch. In order to open the deployer, we used an electromechanical release mechanism that is used amongst all our other Astrofein deployers, but was altered in shape in order fit to the SNL deployer. This electromechanical release mechanism uses two principles: on the one hand, a magnet field holds an anchor plate that itself is pulled by a spring. Both are in equilibrium via a mechanism until we activate our device, releasing the hooks that

hold down the spring-loaded lid, which then in turn opens. The satellite at this point is still retained by yet another mechanism that gives only way after the lid has opened fully. This retaining mechanism allows a lid collision-free release of the satellite. After the satellite is released a plate is pushing it out the deployer using a strong, large spring that is well characterized together with all other friction contributing parts of the motion., in order to achieve the required deployment velocity accuracy.

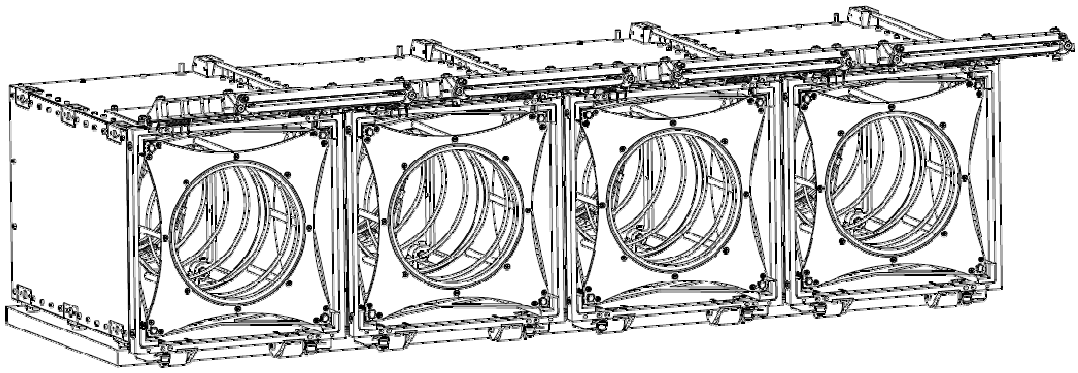

Figure 1 All four FM SNL deployer next to each other

3. QUALIFICATION TEST CAMPAIGN

3.1 Deployment Velocity Measurement

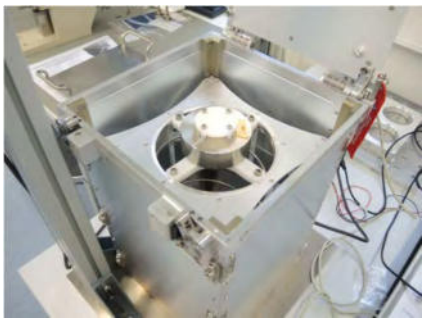

Figure 2 Test set-up for deployment velocity measurement (SNL qualification model shown)

A major challenge for designing the SNL was the required deployment velocity accuracy of ± 4.5 cm/s. Therefore, the deployment velocity has been measured for all flight models of the SNL using a laser triangulation measurement of the motion of the ejection carriage, refer toFigure 2. For the measurements, a dummy mass with damping elements has been used to avoid damage collision of the carrier with the limit stop of the containers.

During the test, no gravity compensation has been applied, therefore the measurement results can only be used to verify the deviation of the deployment velocity for the flight models. The results are listed in Table 1. The maximum occurring deviation was ± 1.625 cm/s, which meets the requirement very well.

Max. Deviation (cm/s)		Flight Model No.				
		1	2	3	4	5
Flight Model No.	1	-	-1.625	-1.400	-0.150	-0.475
	2	1.625	-	0.225	1.475	1.150
	3	1.400	-0.225	-	1.250	0.925
	4	0.150	-1.475	-1.250	-	-0.325
	5	0.475	-1.150	-0.925	0.325	-

Table 1 Maximum deviation of the deployment velocity between the different flight models (incl. one spare model)

3.2 Magnetic Field Determination

Since the satellite deployment is triggered by magnets, the magnetic field of the actuator had to analysed carefully, in order to properly size the deployment mechanism. Therefore, the magnetic field has been simulated using FEMM (Finite Elements Method Magnetics), refer to Figure 3. On the basis of these results and knowing the threshold of the used reed switch (1.7 mT), the switching distance between magnet and surface of the magnet holder could be determined to be 20.6 mm.

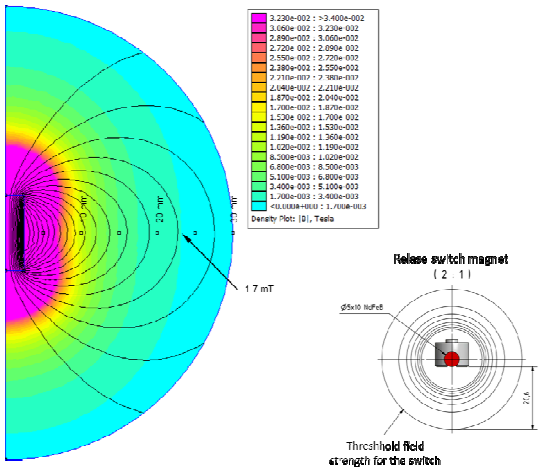

Figure 3 Magnetic field of the deployment switch magnets

3.3 Environmental Loads and Requirements

The environmental (vibration, shock, thermal-vacuum, and thermal) test campaign of the SNL has been carried out at Astrofein's in-house test facilities. The environmental conditions (e.g: 1000g shocks, 13.25 Grms Random) to be covered by the qualification tests were according to TU Berlin's specification and covered a range of launch vehicles (eg.: PSLV, Soyuz, LM2D) and mounting configurations (vertical and horizontal) in order to give most flexibility to launch vehicle choice to the TU Berlin.

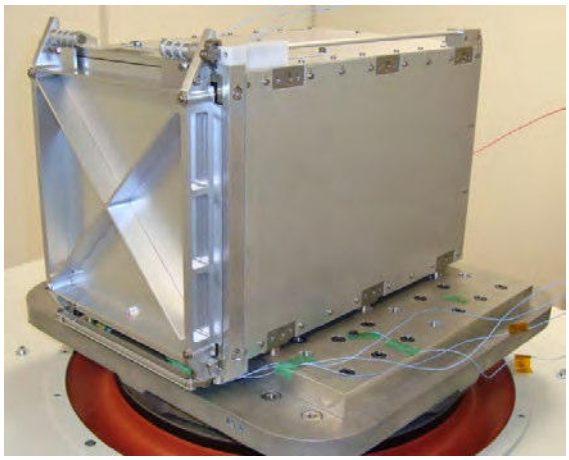

Figure 4 SNL QM on shaker during qualification

4. S-NET MISSION RESULTS

Launch of the four S-Net satellites was from Vostochny Cosmodrome on 01/02/2018. After a few hours all satellites communication with all satellites was established and later health checks showed no issues with the satellites meaning that objective one was met: Save transport of satellites and release into orbit. A few weeks we received the

second good news. The maximum distance between the satellites was far lower than expected at this stage of the mission. The achieved speed deviation between the satellites was estimated to be ± 2.0 cm/s which is much better than the required: ± 4.5 cm/s. Hence, mission target two was accomplished, too.

Figure 5 SNL containing S-Net satellites on Soyuz-2.1a at the Vostochny Space Center [2]

5. THE CUBESAT DEPLOYER FAMILY

The knowledge gathered during the SNL project further helped developing our other 2U, 3U and 12U Cubesat deployer systems which by now helped putting Cubesats multiple times into orbit. The latest "member" of the product family is the 6U system that was qualified in November 2018 for launch in early 2019.

Figure 6 Cubesat deployer family of Astrofein

6. REFERENCES

[1] German Aerospace Centre, S-NET: Neues Netzwerk aus Nanosatelliten. Press Report, https://www.dlr.de/dlr/presse/desktopdefault.aspx/tabid-10172/213_read-25914/ (February 1st, 2018)
[2] Snapshot from video edited by "Go To Space", footage courtesy: "Roscosmos", Youtube: https://www.youtube.com/watch?v=dxwvv_EZQnc/ (January 26th, 2018)

Integrated Applications: an overview from Space to Earth

Andrew Court

TNO

Stieltjesweg 1, 2628 CK, Delft, The Netherlands

Phone: +31 888668110. Email: andy.court@tno.nl

Abstract: Integrated applications has become an accepted methodology for systems in which data is combined from many sources to provide information for institutional and commercial services. One of the key areas which started such processes is in astronomy and the need to combine and derive the physics from images and spectra from diverse astrophysical sources. Today integrated applications are much more associated with combining remotes sensing data, where the sources are on the ground, in earth orbit and more recently in aircraft, UAV's and HAPS platforms. This paper will examine each of these areas and explain how the new paradigms of space and society need the power of integrated applications to provide the data for decisions for policies and commercial benefit.

1. Introduction

It is a simple statement that through the combination of multiple streams of data, information can be gained which exceeds the sum of the individual parts. In the same way it can be simply stated that integrated applications have become a methodology to bring together diverse systems to act together and provide more information or a system less susceptible to impairment if one or more parts fail.

The path to what is now considered the field of Integrated Applications has been driven by the increasing range of data being acquired here on earth, in the skies and beyond. Acquiring, collating and storing and organizing these datasets so that they can be used for daily purposes to give societal information or longer-term analysis for scientific purposes has become a major challenge.

Astronomy has led the way in creating the need for methods to store large diverse datasets for later analysis and where data must be calibrated and sorted into information sets allowing spectral and imaging properties to be correlated across many different measurement platforms.

Earth sensor systems have been widely distributed to provide ground networks monitoring a great range of measurements from local atmospheric pollution, ocean state and ground movements. Whilst these are normally static measurement points the positioning is often strategic and creates a local matrix of information to be interpreted and used by local authorities.

Space based remote sensing satellites have been in orbit now for more than 50 years allowing global measurements which can be used to determine weather forecasts as well as longer term analysis of worldwide phenomena and are now treated as mainstream knowledge for use by society. The sheer quantity and range of data generated by these

systems now and in the future is a key driver for the creation of sophisticated integrated applications for transmission, storage, distribution and analysis of the information now available.

The space between ground and space is also available for remote sensing of the earth on scales and resolutions not achievable by satellite systems, but these are necessarily limited by geography and politics as to the range and places at which measurements can be obtained.

Each of these application areas will be considered in more detail and an overall conclusion of the need for integrated applications will be explained.

2. Astronomy as the start of integrated data applications

In the field of astronomy scientists seek to understand the physics of objects based on the received signals (electromagnetic and more recently gravitational). The range of available instruments are usually limited by the spectral range over which measurements are made with the extension from radio, visible light wavelengths to uv, x-ray and gamma-ray and beyond only becoming available in recent decades. In earlier times to understand all the processes of an astrophysical object required considerable extrapolation and theories, and as time has gone ion astrophysics is a field which first started to generate massive quantities of data for analysis[1]. As ground and space instruments have increased in number and range the integration of information has allowed the understanding of objects and phenomena to be better understood. Generally astronomical projects revolve around one type of measurement system at a time, for example in space XMM-Newton, Chandra, IUE, HST, ISO, Herschel-Planck have all over time provided sections of spectra which must all be correlated together to achieve a common calibration over decades of measurements[2]. These same measurements must also be connected across other wavelengths using ground based astronomical systems such as radio telescopes[3].

3. Earth Remote Sensing from ground networks

The observation of the atmosphere for future weather prediction has of coursed been carried out since time immemorial (red sky at night etc.). In modern time scientists can turn to the use of sophisticated networks of instruments in a range of locations to provide a global set of data points to assist in understanding weather and climate change. International organizations also cooperate to create such networks. A prime example of this is the Network for the Detection of Atmospheric Composition Change[4] which not only link worldwide sites for atmospheric analysis, but also provides direct access to the public to download data. NDACC is one of many national and international networks established for continuous coverage of atmospheric data, and to provide correlating data to satellite instruments for vicarious validation of the data from those instruments.

In general data collection and distribution is maintained at a country level and provides a record dating back decades for use in assessing trends in the evolution of climate phenomena.

4. Space remote sensing

Satellites can obtain images and spectra for use in analyzing the atmosphere, oceans, land and cryosphere. Since the early 1960's satellites have been launched with cameras and other sensors to image and record the earth. From simple images in visible and infrared wavelengths this has expanded to cover the electromagnetic spectrum from UV through to microwave and radio wavelengths. Satellites operate in low earth or geostationary orbits providing a range of coverage and spatial information from cm's to km's. Until recently all such missions were institutional in nature, sponsored by or through government agencies to provide civil or scientific data. In recent years the cost and access to space for commercial missions has become possible leading to the establishment of companies such as Planet and DigitalGlobe, which provide detailed images of the earth using in-orbit satellites, with the objective of creating a commercial market for the resale of images. More recently GHGSat have launched small satellites for measurement of methane and carbon dioxide as a commercial product.

Institutional programs such as the European Copernicus series of satellites for which the space segment is implemented by the European Space Agency (ESA)[5], have been established to provide a wide range of data products for global monitoring of the environment with an objective to provide free data to all users who register to receive it. The range of instruments available cover surface morphology (by SAR), land and ocean imaging and atmospheric chemistry. This is soon to be extended to also include specific mission for ocean topography, greenhouse gas measurements and arctic ice monitoring. Copernicus combines space data with ground sensor systems (e.g. from NDACC) to provide services such as spatial and urban planning, forest, water and agriculture management to ensure food security, nature conservation and ecosystem monitoring.

The petabytes of data generated by Copernicus and other similar initiatives must be stored and made easily available to users. As the trend is now that much of this data will be used for business, commercial, applications around the world the access to such databases requires the sophisticated coordination of computer and software systems for distribution, quality control and calibration of the data to ensure that it is correct for use. Programs such as the ESA ARTES program have been established to help to provide the tools need for this to happen. The advent of small satellite instruments will vastly increase the range of measurements available for not only for commercial applications, but also to provide complimentary measurements to complete data gaps not possible to be covered by the larger institutional missions.

5. Systems Near Space to Earth.

Whilst ground and space-based systems have increased in scope and complexity over recent decades there has been a newcomer to the field in the form of UAV's and HAPS platforms which can carry camera payloads for imaging and more recently spectrometers for ground and atmospheric measurements[6,7]. Whilst balloons are also capable of providing information through the atmosphere (e.g. sondes for temperature, pressure etc.) UAV and HAPS carry out measurements at specific altitudes and under a

much greater degree of control. Such systems have commonly been used to provide validation data for satellite instruments as well as carrying out specific measurements for monitoring especially local environments (e.g. lakes, precision agricultural)[8,9].

6. Summary

Integrated applications cover a range of definitions, from simply combining datasets in an ordered way to ensure harmonisation across wavelengths to coordinating distribution of validated data for use in not only in commercial applications but also as key knowledge to inform and assist policy makers in achieving societal goals. The growing amount of data requires constant improvements to data channels and processing systems as well as offering possibilities for the discovery of phenomena through combining diverse and different datasets.

7. REFERENCES

1. Brunner, R. J., Djorgovski, S. G., Prince, T. A., & Szalay, A. S. (2002). Massive datasets in astronomy. ArXiv Preprint ArXiv:Astro-Ph/0106481, 931–979.

2. Pauluhn, A., Huber, M. C. E., Smith, P. L., & Colina, L. (2016). Spectroradiometry with space telescopes. The Astronomy and Astrophysics Review, 24(1), 3.

3, Coe, M. J., Bowring, S. R., Court, A. J., Hall, C. J., & Stephen, J. B. (1983). Confirmation of periodic radio outbursts from LSI + 61° 303 ≡ GT 0236 + 61. Monthly Notices of the Royal Astronomical Society, 203(3), 791–794.

4. http://www.ndaccdemo.org/

5. *"ESA, Copernicus, Overview". ESA. 28 October 2014.*,

6. Eastwood, M. L., Sarture, C. M., Chrien, T. G., Green, R. O., & Porter, W. M. (1991). Current instrument status of the airborne visible/infrared imaging spectrometer (AVIRIS). In San Diego, '91, San Diego, CA (Vol. 1540, pp. 164–176).

7. Court, A., Siegl, M., Leemhuis, A., Valk, N. van der, Levelt, P., Veefkind, P., & Bézy, J.-L. (2018). Compact hyperspectral instrument for NO2 remote sensing. In Sensors, Systems, and Next-Generation Satellites XXII.

8. Babey, S. K., & Anger, C. D. (1993). Compact airborne spectrographic imager (CASI): a progress review. In Optical Engineering and Photonics in Aerospace Sensing (Vol. 1937, pp. 152–163).

9. Yang, C., Everitt, J. H., Du, Q., Luo, B., & Chanussot, J. (2013). Using High-Resolution Airborne and Satellite Imagery to Assess Crop Growth and Yield Variability for Precision Agriculture. Proceedings of the IEEE, 101(3), 582–592.

Overview of ESA Business Applications

R. Mugellesi[1], F. Feliciani[2], A. Schoenenberg[3]

[1]Affiliation
ECSAT, Fermi Avenue, Harwell, United Kingdom
Phone: +44 1235 444 320, Mail: roberta.mugellesi.dow@esa.int

[2]Affiliation
ESTEC, Nordwijk, The Netherlands
Phone: +31 71 565 4109 , Mail: francesco.feliciani@esa.int

[3]Affiliation
ESTEC, Nordwijk, The Netherlands
Phone: +31 71 565 5900 , Mail: andreas.schoenenberg@esa.int

Abstract: In the frame of the ARTES (Advanced Research in TElecommunication Systems) programme of the European Space Agency, a specific element is dedicated to develop and validate downstream applications and services based on the use of space based technologies. With more than 400 activities placed so far, this part of the programme, called Business Applications, has the final objective to facilitate the creation of novel business opportunities leading to sustainable use of space technologies for the everyday life, and indirectly help the uptake of the space domain as a whole. The purpose of this paper is to provide an overview of the Business Applications programme objectives and initiatives.

1 INTRUDUCTION

ESA Business Applications programme was introduced more than 10 years age as Integrated Applications Promotion (IAP) programme aiming to pursue an holistic approach to space applications, enabling cross-cutting functionalities among the relevant space capabilities. In doing so it builds upon the rich competences developed within ESA, to address the utilisation of space capabilities for enhancing daily life and to create value along the entire satellite applications value chain.

The programme has developed a range of new applications by utilising and integrating different space assets (e.g. Satellite Communication, Satellite Navigations, Satellite Earth Observations) , resulting in new or improved services for the citizens of Europe on a regional, European and even global scale. Intrinsic to these new applications are the added value of space as a facilitating capability and the long-term sustainability of the resulting services. The programme does not push any particular technology but instead explores and responds to users' needs, addressing a variety of thematic areas, such as:

- Aviation
- Health
- Infrastructure & Smart Cities
- Media, Culture and Sport
- Transport & Logistics
- Safety & Security
- Energy

- Education & Training
- Food & Agriculture
- Finance, Investment & Insurance
- Tourism
- Environment, wildlife and natural resources
- Maritime and Aquatic

Specific focus is given to the involvement of user and the service demonstration in a pre-operational environment, where pilot user validate the added value brought in their business context. A successful activity does not require only the identification of promising opportunities but also the development of complete business cases, combining technical aspects with commercial, financial, legal and regulatory considerations.

Within the Business Applications programme ESA offer's:

- Financial support (Co-funding)
- Technical and business guidance
- Access to network of partners
- Credibility of the ESA brand

to activities that utilize space technologies at large and combine existing space and terrestrial assets, in order to provide users with the best solution available to meet their particular needs.

2 PROGRAMME OBJECTIVES

The focus of the Business Applications programme is the application of space capabilities into a non-space business context with focus on promoting the utilization of space technology or space-derived data in a multiplicity of economic market sectors identifying opportunities for utilization of space capabilities to the benefits of suppliers, users and the wider eco-systems.

The programme objectives and requirements are:

- Promotion of space applications to a wider range of users;
- Development of new operational and economically sustainable services which respond to identified users' needs;
- Utilisation of at least one space asset (e.g. Satellite Communications, Satellite Earth Observation, Satellite Navigation and Human Spaceflight technologies), leading to a better exploitation of the existing space capabilities and know-how;
- Activity cost are co-fund by ESA and industry and/or users ;
- User involvement in the development activities is a pre-requisite.

The programme does not push any particular technology but instead explores and responds to users' needs. The user-driven approach of the programme ensures that the

user needs are satisfied by providing solutions that are technically, economically viable and cost effective.

Figure 1 shows the important aspects that needs to be considered for promising application / service proposals.

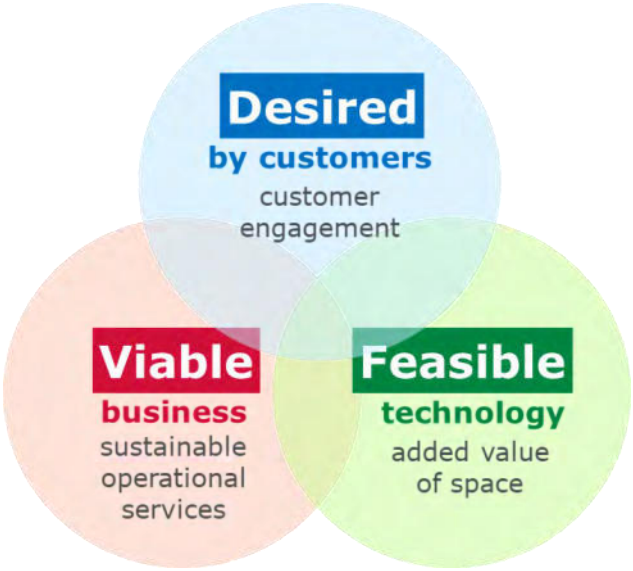

Figure 1: Pre-requisites for promising services

3 PROGRAMME IMPLEMENTATION

Activities proposed within the Business Applications (BA) programme are either implemented as feasibility study or demonstrations project. Feasibility studies provide the preparatory framework to identify, analyse and define new potentially sustainable applications and services. The study is required to provide definitions of the technical solutions that can be envisaged, and an assessment of the investment and of the running costs providing a first evaluation of the sustainability of an operational system. The study is also required to identify technological adaptations and gaps in current systems which need to be filled for the service to be operational and sustainable. The applications and/or services have to be customer/user driven, benefit from the integrated use of at least one space asset, and aim to evolve the targeted applications and services to marketability and operational roll-out, potentially through an BA demonstration project after successful completion of the feasibility study.

Kick-start studies are a subcategory of feasibility studies to be initiated by industry / institutions following thematic calls for ideas or opportunities initiated by the Agency. Kick-start activities aim at exploring the viability of new service / application concepts while fostering innovation and reaching out to new players. This instrument has been successfully targeted at new entrants to the Space Economy and provides an accessible starting point for smaller companies to work with ESA. Following an analysis on the awarded contracts for kick-start studies it emerged that more 80% were conducted by SMEs.

Demonstration projects are dedicated to the implementation and demonstration of pre-operational services, they have to be customer/user driven (including user involvement and contribution) and benefit from the integrated use of at least one space asset, with clear potential to become sustainable in the post project phase. Demonstration projects can be initiated following a successful feasibility study or as a spontaneous proposal by users or industry. The engagement of prospective customers (either public or private) in the activity is considered essential to mitigate the commercial risk and ensure that customers' feedback is adequately considered in the consolidation of the service offer and preparation for the commercialization phase.

Proposals for a feasibility study or a demonstration projects can be provided based on the permanent "OPEN CALL FOR PROPOSAL FOR IAP- ESA BUSINESS APPLICATIONS"[1], which explains the bidding process as well as the tender condition and contract conditions.

Before engaging in more detailed elaboration of a potential outline or full proposal, an Activity Pitch Questionnaire allows the Tenderer in a reduced, standardised pitch form to present his initial idea to ESA, and it allows ESA to quickly take an informed decision on the next steps pointing the Tenderer to the most appropriate activity stream and providing support on the further implementation steps.

Depending on the envisaged space based service (subject) the proposing team should have know-how, skills and experience in:

- SatCom, SatNav, SatEO, Human Space Flight, Space Weather
- Earth Observation value adding services, GIS & mapping services
- In-situ sensors & data collection
- Terrestrial technologies & services
- Data fusion & modelling
- Subject specific expertise
- Commercial expertise
- Service provisioning in the subject area

The Agency admits for evaluation proposals from a bidding team composed of a company and/or organisation - be it as Prime or Subcontractor - residing in any of those States that subscribed to Business Applications, which are to date: Austria, Belgium, Czech Republic, Denmark, Finland, France, Germany, Greece, Ireland, Italy, Luxembourg, the Netherlands, Norway, Poland, Portugal, Romania, Sweden, Switzerland and the United Kingdom.

Information on all ongoing and concluded activities is available on Business Applications portal[2] and can be search by thematic area and space assets utilized for the service offer, see also figure 2.

[1] https://emits.sso.esa.int/emits/owa/emits.mainl
[2] https://business.esa.int/projects

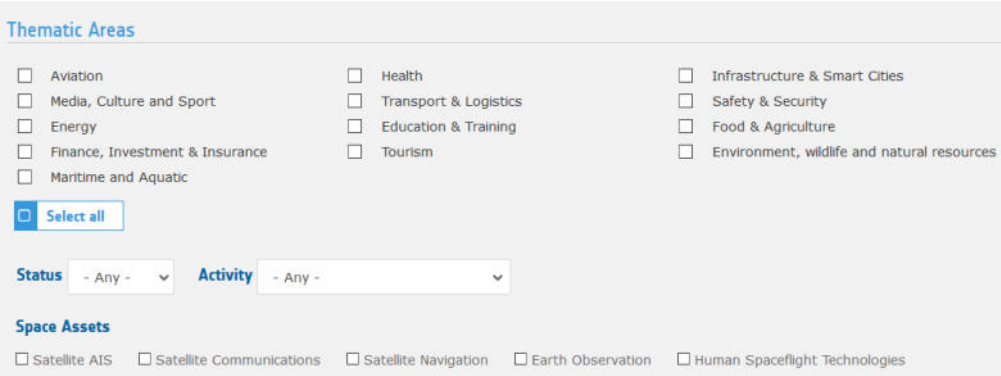

Figure 2: Business Applications portal overview based on thematic areas and space assests

4 BUSINESS ACQUISITION

To understand the impact generated by the activities supported by the Business Applications programme an analyses of the Socio-Economic Impact and Return on Investment (SEI & ROI) is conducted regularly taken into account the indicators shown in table 1.

Capital Generated	Indicator
Financial & Human Capital	Revenue
	Jobs
	Exports
	Investment Leverage
	Addressable Market
Innovation & Intellectual Capital	Market & Product Innovation
	R&D Uplift
Network & Societal Capital	Extent of Value Chain
	Value Creation
	Societal Benefits

Table 1: Types of capital generated from investment and associated socio-economic indicators

Current evidence suggests that the strongest SEI & ROI has been generated by projects that reached a sufficient maturity and critical mass to overcome barriers to market entry, that the involvement of private investors is an indicator of future success, and that commercially motivated projects generate stronger commercial returns than those serving institutional needs.

Figure 3 shows the investment leverage of the ESA funding, for every 1€ invested by ESA 1.7€ of investment is generated through industry and private investors.

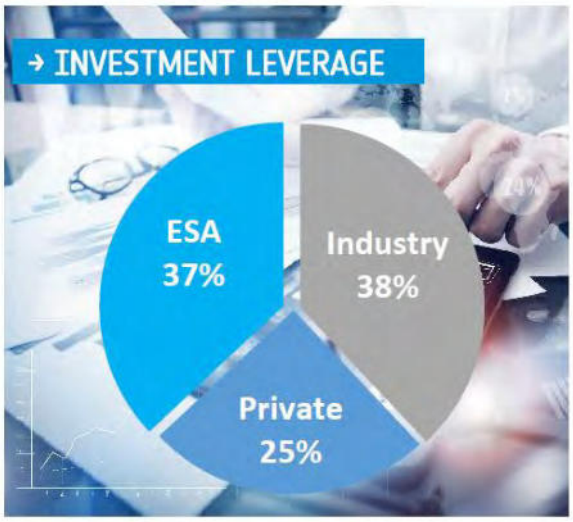

Figure 3 – Investment leverage

Figure 4 shows that a significant part of the revenue are derived from the export market

Figure 4: about 50% of the revenues are obtained from export of the services

5 PARTNERSHIPS

ESA Business Applications has established many successful partnerships over the years with institutional organizations like EMSA and Frontex or industry association as well non-profit organisation. These partnership were concluded to federate user needs addressing specific user communities (e.g. maritime) and support pre-operational demonstrations towards operational services.

Partnerships have been also set up with organizations outside of the members states as the Tata Group and the Indian Energy Storage Alliance.

The partnership with the UK investor and business support community, including Seraphim Space Fund, Newable, KX / First Derivatives and Founders Factory has generate referrals of a rising number of promising companies offering also additional finance and resources for the companies with ESA contracts. Further formal and informal partnerships are continuously explored, extending the approach on partnership benefitting the entire programme participating Member States and favouring the ones with global commercial reach.

6 REFERENCES

[RD1] ARTES Declaration, ESA/C(2017)65
[RD2] Integrated Application Promotion Specific Implementing Rules, ESA/C/CCV/Rules 4, rev.3

- Page 148 -

Small Satellites and Integrated Applications

Larry J. Paxton (M1)[1]

[1]Johns Hopkins University Applied Physics Laboratory
11100 Johns Hopkins Rd, Laurel MD 20723
Phone: +001 2402286871, Mail: larry.paxton@jhuapl.edu

Abstract: Small satellites can play a vital role in providing missing pieces of information to decision makers. Data by themselves are rarely actionable. Even when we think we have a piece of actionable information, we are applying, whether we realize it or not, rules, decision making criteria as we interpret the data. For reproducible, transferable and defensible decision support, data must be coupled with analysis tools and, ideally, a method of simulating the impact on systems of interest. The result must enable effective decision-making. There are many "small" environmental problems that affect the lives of millions that are not addressed adequately by the monitoring and research satellites currently on orbit. Small satellites can provide the missing piece of data, or more observations with a higher revisit rate, to drive predictive models that enable NGOs and governments to take timely and effective action. The goal is to create a cost-effective 'integrated application' that transforms the users command of the decision-making process from intuition to a formalism that captures the lessons learned and removes individual biases from the process.

1. INTRODUCTION

Small satellites have shown a remarkable growth in both the number of satellites flown and capabilities. Small satellites can broaden their market and impact by shifting toward an "integrated application" approach wherein the satellite and its sensors are seen as the means to collect and/or distribute data to create actionable/decisionable information. The process of defining a system that can produce decisionable information is summarized in Figure 1.

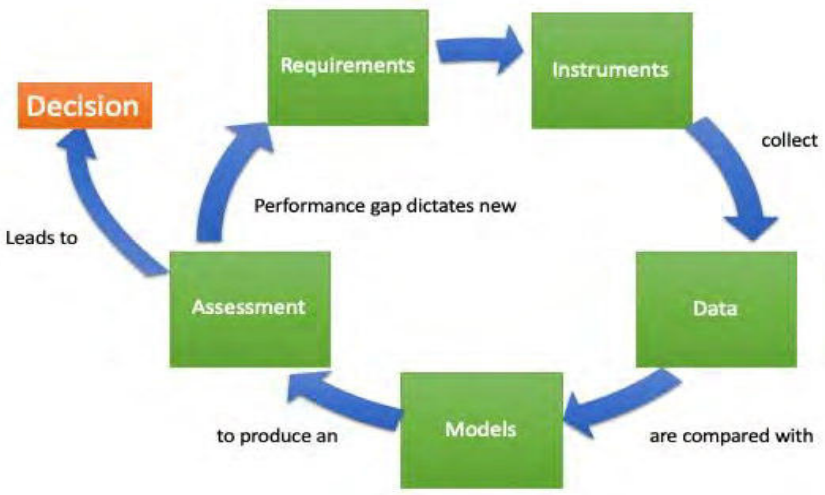

Figure 1. Summary of the integrated application environment. The goal of the creation of a small satellite element of the integrated application is achieve a cost-effective solution that enables a decision or provides other value to the sponsor. The virtuous circle can be read beginning at any point. Models are any mathematical or prescriptive

formulation that are used to produce an assessment (e.g. "Is it going to rain tomorrow?"). The assessment leads to a decision. Performance gaps, when identified, may warrant a change in requirements that leads to a new sensor (e.g. if the weather prediction is bad). The ability to produce a new satellite, place it in operation and demonstrate its utility is the key to ensuring value to the sponsor.

Table 1. Key Ideas

- Constellation: a collection of identical satellites e.g. Iridium, OneWeb, Intelsat, etc directed toward a common goal
- Heterogeneous Constellation: a collection of satellites of different sizes, sensors, orbits directed toward a common goal e.g. NASA's "A Train"
- Virtual Constellation: a collection of satellites, operating independently with differing goals - this can include suborbital or groundbased instruments or data sources
- OSSE – Observing System Simulation Experiment – a tool for simulating the collection of data, as a function of time, in order to reproduce the functioning of the (virtual) constellation
- Assimilative Model: the means to incorporate data into a first principles, basic physics, prediction of the state of the system to predict the present global state of the system and its future trajectory
- Virtual Observatory: a 'tool' that enables the user to connect to data sources, either on demand or routinely, to acquire data from many sources to addresses a query posed by a user
- Machine Learning: any of a variety of algorithms and statistical methods that enable a task to be performed without explicit knowledge of the underlying system.

Table 1 summarizes the major key ideas in this approach that we use to develop integrated applications. We connect the users' needs to the minimum irreducible set of measurements that must be provided in order to address a problem. The only way that one can insure the most cost-effective solution is to include in the assessment all the other sources of information (and the relative stability and accuracy of that information).

Thirty years ago, there were few sources of spacebased data and they were largely either focused on one key market or a scientific mission. There were few if any constellations outside of the geosynchronous weather satellites. Those were, arguably, homogeneous constellations. Data access was restricted and cumbersome. As our knowledge of the coupled Earth system grew, the need for more and different measurements was recognized. This was addressed by the use of heterogenous resources to address particular problems. Spacebased heterogenous constellations such as the NASA A Train came into use but were and are relatively rare – these heterogeneous solutions are often difficult to fund as a solution for a problem. In practice, one need only assemble the right information sources. A virtual constellation is one that a particular user thinks of as providing a source of data to address their issues. A virtual constellation is an ad hoc construct and may span many organizations and types of information. OSSEs (discussed below) provide a powerful tool for demonstrating the value of an addition to a virtual or homogenous constellation. To demonstrate value, we use an assimilative model to show in a quantitative manner that incorporating a new data source into the current predictions improves their

accuracy and value. Virtual observatories or 'VxO' provide a seamless way to connect users with data sources. The VxO enables data to be routinely incorporated into decision making.

2. OPPORTUNITIES FOR INTEGRATED APPLICATIONS

Global climate disruption is changing our world in ways that we have not yet fully come to terms with. We have hardly begun to see the impacts because, at this time, our system is sufficiently resilient as to be able to adjust to changes. For example, global climate determines the assurance of continued agricultural productivity and water availability throughout the world. Changes in water availability from the impact of floods and rainfall pattern alteration on agricultural productivity[1], to the opening of the Arctic Ocean to navigation during Northern Hemisphere Summer[2] will challenge foreign policy stances throughout the world.

In the last decade we have seen and enormous increase in the availability of launch vehicles, satellites buses and opportunities. The UNCOPUOS program tracks satellite launches [3]. In 2018 they recorded 382 objects launched into space. Of that, the greatest number were small satellites. Launches such, as those carried out by SpaceX on 4 December 2018 in which the Falcon 9 deployed 64 small spacecraft from 34 organizations representing 17 countries[4], are now relatively common. This ready availability of reliable launch vehicles and the excess capacity to orbit opens the market to entities that may not have considered a presence in space.

Many of these small satellites are a technology demonstration or created largely for heuristic purposes; their cost may be sufficiently low that the process is more valuable than the product (data or satellite). Recently there has been growing interest in the use of small satellites in low Earth orbit (LEO) to accomplish the tasks traditionally relegated to much larger satellites in LEO such as the creation of large synthetic apertures[5]. This hews to the traditional view that the small satellite industry need only produce a platform that can acquire the required data. However, the small satellite, by virtue of its low-cost may enable an advance in our understanding by providing more measurements. An example of this is the recent announcement that the Environmental Defense Fund, a non-governmental organization (NGO) plans to independently fund, fly and operate its own small satellite to track methane emissions[6]. Methane is known to be an important 'greenhouse gas' i.e. a trace gas that is very efficient at trapping long wavelength infrared radiation.

The Earth environment is dynamic. This means that there are a wide range of spatial and temporal scales. In the biosphere there are yearly, seasonal, tidal (monthly) and diurnal scales evident. Weather changes the optical and radar signatures of elements on the biosphere on even shorter time scales. Data reflecting the state of the environment may be collected by objects (e.g. mobile phones, home assistants, agricultural irrigation systems, etc) in the internet-of-things (IoT) on the ground, dedicated groundbased sensors, sensors on UAS, or spacebased sensors. The mixing of spatial and temporal signatures is handled by approximations.

For decision-making and academic research, we are often concerned with our ability to predict the current state of the system on a global basis and/or our ability to predict its future state. By 'state of the system' we note that each use case will have a different emphasis and region of interest in terms of spatial and temporal extent. The prediction of

the state of a system that is represented by a first principles model (represented as *G*) is limited by our ability to specify the initial conditions and the drivers for the physical system (represented by D). Note that the response of the system depends on the current state of the system and the past history of the drivers acting upon that system.

$$S(r,t)=G[S_0(r_0,t_0);\ D(t,t_0)]$$

Incorporating as many constraints of different kinds on the system and evaluating as many environmental parameters as possible, helps us understand the gaps in our understanding. Understanding the gaps in our knowledge leads to the specification of the elements of the system that need to be improved.

An Observing System Simulation Experiment (OSSE) provides the tools for assessing the value of the additional component in the solution space. An OSSE is, just as the name suggests, a simulation of what an observing system would actually observe. The OSSE takes into account the orbital dynamics, sensor design and capabilities of the system under study. The OSSE uses a physical model as the truth. The physical model uses all available data to initialize the model's calculation of the current state and project it forward in time for the test period. This is often referred to as the 'nature' or 'true' run. A data assimilation technique is used to construct the expected state of the system based the available observations. The assimilation run or 'trial' and the nature runs are compared. The degree by which the postulated system component (in our case that would be additional small satellite components) improves the forecast is assessed. The OSSE enables one to demonstrate the value of a proposed, additional, component of the system without having to fly a space-segment mission. For example, OSSEs were used to evaluate the value of a LEO polar orbiting component to weather forecasts.[7]

Small satellites can be used to produce those data that constitutes the irreducible minimum that must be provided in order to support a decision. This missing element is determined based on the gaps that exist in current capabilities. That gap was uncovered through the comparison of models (predictions) of physical processes and observations wherein the model (predictions) failed to produce the required actionable information. Small satellites can be an affordable path to address the knowledge gaps, for particular users.

Figure 2 shows the decision loops that enable and drive new mission designs. Data can arrive in real time to inform the current state of the system (via the assimilative models) and it can arrive after the fact and aid in pruning the number of possible paths the projected state of the system can take. Model output can, if properly handled, inform decisions. Machine learning techniques, coupled with traditional analytics and visualization tools that enable the incorporation of input from skilled forecasters, enables us to answer current questions and formulate the next level of queries needed to advance our state of knowledge. New investigations can be formulated to either constrain our knowledge of the system or of the drivers and feedback mechanisms that describe the boundary conditions on the models we use to make predictions.

In an increasingly cost-conscious environment, in which the public has become accustomed to the precondition that services or abstract knowledge will be provided by existing assets, it becomes difficult to either enhance the environmental data services or to market replacements. Government agencies are constrained to deliver services within a specified budget. In the United States the major civil space agencies, NASA and NOAA produce

particular services and avoid competition with commercial companies. The Office of Space Commerce[8] (OSC) handles space commerce activities for the US Department of Commerce (DoC) of which NOAA is an element. One element of the OSC strategic plan is to reduce extreme weather impacts; these impacts are expected to increase as a direct consequence of global climate disruption.[9] The cost of climate change, and the failure to adapt to it, is enormous[10]. The National Climate Assessment[11] summarizes the range of impacts for a country that currently has an extremely well-developed infrastructure. The consequences for the spread of disease (human, livestock and plants)[12] and changes in agricultural productivity and water security will have profound effects on failed nation states and ones that are in marginal stability conditions.

The pace of climate change, and the severe and multi-faceted nature of its impacts, suggests that governments and the public at large may not respond quickly to the need for new observations of the coupled Earth system and its impact on humans nor be able to provide accurate decisionable (e.g. forecast) information in a timely fashion. Non-governmental agencies (NGO) are free from many of the legislative restraints placed on government entities. NGOs may have the charter as well as the means to take an end-to-end view of a focused environmental problem. Consider that the Gates Foundation spends over $2B/yr on a variety of programs closely linked to climate change driven issues including malaria and infectious diseases. World Wildlife Fund generates over $220M in revenue each year to address environmental issues. Often, they (and other NGOs) need information that either doesn't exist or are difficult to obtain due to the physical or political constraints on the system.

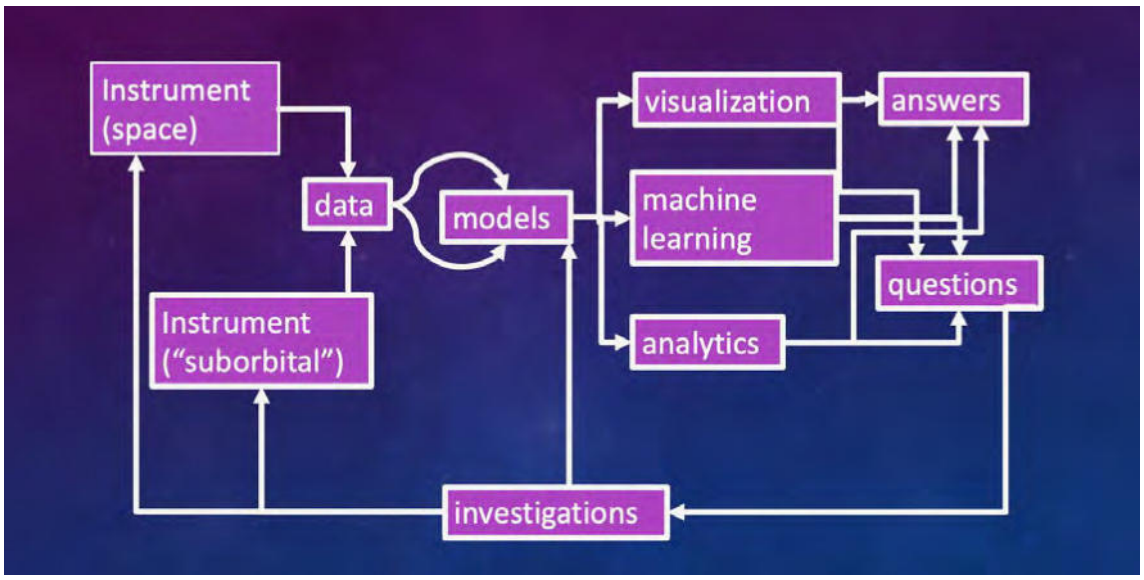

Figure 2. Small satellites enable us to provide the key observations that fill in the gaps in our knowledge.

3. SMALL SATELLITES AND FOCUSED DATA SETS

As one example of the utility of a particular data collect, we consider the forecasting of disease outbreaks. Many diseases, such as cholera, are related to particular environmental conditions. Cholera develops in water where *Vibrio cholerae* attach to zooplankton. The close association of zooplankton and *V. cholerae* can be exploited to provide warnings of

where there is likely to be a cholera outbreak[13] . This remote sensing dataset must be augmented with other information (*Vibrio* has no optical signature of its own) including sea surface temperatures and rainfall as well as knowledge of the waste water treatment facilities status. An integrated application can be built from existing capabilities but when the NASA Aqua satellite fails this capability will disappear.

While applicable datasets may be available, they are not likely to be optimized for the particular purpose of interest to a particular user. To create a tailored, successful integrated application, the performance of the new application has better performance and at a lower cost. Small satellite payloads featuring a narrow field of view, hyperspectral imager with an on-board cloud detection algorithm for autonomous scheduling would be able to provide data sets that would not otherwise be collected.

The very nature of small, low-cost satellites provides an additional advantage; one can afford to place them in different orbits as part of an observing cluster. A small number of satellites in a set of low inclination orbits may be sufficient to ensure that the Nyquist sampling of the growth phase of a threat (e.g. flooding, algal bloom, etc.) is met whereas large polar-orbiting sensors (such as Landsat) rarely see a particular hectare more than a few times during the growing season due to the prevalence of cloud cover. Timely warning, and forecasting, is necessary to effectively combat a time-dependent threat such as cholera.

As another example, APL's HAVOC[14] project examined the augmentation of commercial synthetic aperture radar data with small satellite and UAS imagery as well as AIS information to track ships in the Arctic and in maritime protected areas. These same design ideas can be applied to a wide range of problems. For example, illegal unreported and unregulated (IUU) fishing is a global problem that is likely to increase as North Atlantic fish stocks move into the Arctic and global fisheries collapse due to unstainable yields. A key area of contention will be the part of the Arctic Ocean that is not 'territorial waters' of any country. On a global basis, hyperspectral imagery optimized for ocean color data collections as well as detection of dark ships provides the means for NGOs and governments to monitor activities over their horizon. This will become more of an issue as the pelagic fish stocks feel greater pressure.

4. EMERGING TRENDS

In the early years of the development of small satellites, there was no economy of scale. New ventures, such as spacebased internet (e.g. SpaceX's plans for a 4,425 satellite constellation for $10B[15]), are liable to bring about that automation that makes it possible to produce reliable launch vehicles and satellites at a very low cost. In the US, research satellites still cost more than $3M/kg. Even cubesats routinely cost around $1M/kg. Each spacecraft is still built and tested by hand. Clearly Starlink and OneWeb cannot afford costs at that level.

If they can solve these problems there will be three major classes of benefits for the growth of integrated applications:

1) Low cost presence in space either on dedicated satellites via rideshares or with instruments provided as hosted payloads. Note that ready access to space means

that the design life can now be made shorter enabling continual updates in technology.

2) Ready availability of data extraction links to/from remote locations for timely data collection. The IoT will achieve global dimensions and sensor ubiquity can be achieved. Data collection and sensor operation/configuration can be more effectively managed. Currently, valuable information is not available in realtime due to the lack of connectivity.
3) AI presence on board the spacecraft to optimize data collection and transfer as well as monitoring the spacecraft and instrument performance. The use of AI for spacecraft health, safety and operations, much as a car's Controller Area Network (CAN) continually monitors your car for anomalies or developing issues, will significantly reduce the operating costs of small satellites. These smart spacecraft will be the equivalent of self-driving cars, capable of making decisions that optimize data return such as seeking cloud-free scenes. This will be an enabling development in terms of the economies of scale for large constellations of satellites.

5. REFERENCES

[1] https://www.climatehubs.oce.usda.gov/agriculture-changing-climate; https://19january2017snapshot.epa.gov/climate-impacts/climate-impacts-agriculture-and-food-supply_.html
[2] https://oceanservice.noaa.gov/economy/arctic/
[3] http://www.unoosa.org/oosa/en/spaceobjectregister/index.html retrieved 21 January 2019
[4] https://www.industryweek.com/technology-and-iiot/spacex-launches-64-small-satellites-earth-orbit retrieved 22 January 2019.
[]5 D'Errico, M., Distributed Space Missions for Earth System Monitoring, Space Technology Library vol. 31, Springer Science+Business Media, New York, https://doi.org/10.1007/978-1-4614-4541-8, (2013).
[6] https://www.edf.org/climate/how-methanesat-is-different
[7]https://www.wmo.int/pages/prog/www/OSY/Meetings/IPET-OSDE1/documents/IPET-OSDE1-Doc-8.1-OSEs.pdf; https://sites.nationalacademies.org/cs/groups/ssbsite/documents/webpage/ssb_178352.pdf
[8] https://www.space.commerce.gov/about/mission/ retrieved 21 January 2019
[9] Rosenzweig, Cynthia, Ana Iglesias, X. B. Yang, Paul R. Epstein, and Eric Chivian. "Climate change and extreme weather events; implications for food production, plant diseases, and pests." *Global change and human health* 2, no. 2 (2001): 90-104.
Easterling, David R., J. L. Evans, P. Ya Groisman, Thomas R. Karl, Kenneth E. Kunkel, and P. Ambenje. "Observed variability and trends in extreme climate events: a brief review." *Bulletin of the American Meteorological Society* 81, no. 3 (2000): 417-426.
Stott, Peter. "How climate change affects extreme weather events." *Science* 352, no. 6293 (2016): 1517-1518.
[10] https://www.scientificamerican.com/article/heres-how-much-climate-change-could-cost-the-u-s/ (accessed 19 January 2019)
[11] https://nca2018.globalchange.gov (accessed 18 January 2019)
[12]Wu, X., Lu, Y., Zhou, S., Chen, L., & Xu, B. (2016). Impact of climate change on human infectious diseases: Empirical evidence and human adaptation. *Environment international*, *86*, 14-23.
[13] https://www.nasa.gov/press-release/nasa-investment-in-cholera-forecasts-helps-save-lives-in-yemen (accessed 17 January 2019)
[14] Paxton, LJ, and C.H. Hibbitts, HAVOC – High Altitude Vehicle Observations Constellation: An Innovative Approach to Guarding Frontiers, Small Satellites for Earth Observation, April 24-28, 2017, IAA -B11-1501, 2017
[15] https://www.pcmag.com/article/362695/why-satellite-internet-is-the-new-space-race

An architecture for efficient processing and visualization of data from a space mission: MarconISSta case study

José Manuel Díez[1], Fynn Boyer[2], Alexander Maximilian Bauer[3], Tim Malte Gräfje[4], Martin Buscher[5]
TU Berlin, Department of Aeronautics and Astronautics
Marchstr. 12, 10587 Berlin, Germany
[1]jose.diez@campus.tu-berlin.de, [2]f.boyer@campus.tu-berlin.de, [3]alexanderbauer@win.tu-berlin.de
[4]tim.graefje@gmx.de, [5]martin.buscher@tu-berlin.de

Abstract: Data acquisition, storage, processing, and visualization are key aspects of a space mission which may be overlooked when most of the effort is focused on solving the technical challenges associated with the payload. This paper describes the system for managing and visualizing data that was developed for the MarconISSta mission, an RF spectrum analyzer installed on the International Space Station. The key drivers for this architecture are to maximize the experimental flexibility, minimize the manual interventions required by astronauts, to provide efficient data storage and retrieval, and to support multiple types of visualizations. The techniques and optimizations used to implement the User Interface and visualization algorithms are explained, along with lessons learned during the initial phases of utilization. The first results from this project are presented, along with an outline of future work.

1. INTRODUCTION

Since 2013, the number of launches of nano- and microsatellites has grown very rapidly, and the growth is predicted to continue in coming years [1]. This creates pressure on the existing frequency allocations for telemetry and telecommand channels, due to an increased risk of interference which creates a need for more coordination between satellite operators and better spectrum monitoring capabilities. The International Telecommunication Union has identified this as one of the challenges it faces in the 21st century [2].

The MarconISSta experiment seeks to investigate and quantify the utilization of VHF, UHF, L band and S band frequencies from as well as to identify potential sources of interference using antennas provided by the Amateur Radio on the International Space Station (ARISS) program and a Software-Defined Radio (SDR). A number of aspects of the MarconISSta mission were designed by students, including hardware design, manufacture and testing [3]. The experiment generates a relatively large amount of data, on the order of 800 MB per week, which needs to be processed and made accessible to multiple users in an efficient manner. In this paper, we present the data processing architecture that was developed for this purpose by a group of students from different backgrounds (Computer Science, Space Engineering, among others) in their free time without any compensation.

2. OPERATIONAL CONCEPT

The space segment is composed of the UHF/VHF, S- and L-band antennas installed on the ISS, together with RF components that were sent as part of the MarconISSta mission. An RF coupler is used to allow ARISS equipment and the MarconISSta hardware to utilize the antennas without requiring intervention from the crew. A LimeSDR is used to receive the RF signals, and it is connected via USB to an AstroPi (a modified Raspberry Pi Single-Board Computer).

At the start of each period, a configuration file is uploaded to the AstroPi. This file contains the schedule for when to acquire data and on which frequencies, and any other configuration parameters for the spectrum analyzer software.

An experiment control script running on the AstroPi checks if new configuration files are available, and when one is found, it waits until the specified time to start the RF software. Every day, a program is run on the ground whose purpose is to store the current set of TLEs for the ISS on the database.

At the end of each period, the operations team at BioTESC connects to the AstroPi using the Joint Station LAN and downloads the data that was collected. It is then sent to the MarconISSta team, where each file is run through a program which processes the data files and stores them on the database.

3. DATABASE DESIGN, INSERTION AND RETRIEVAL PROCESSES

3.1 Data model

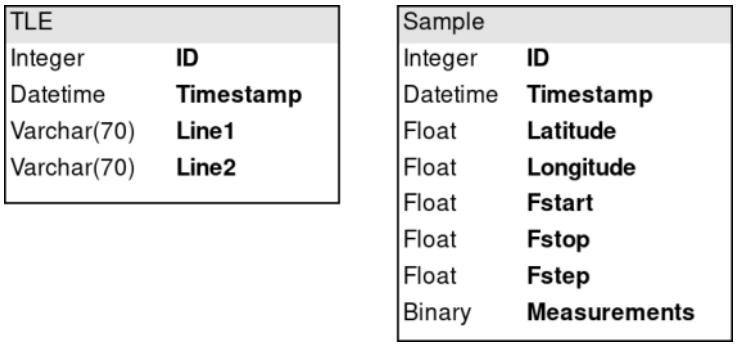

***Figure 1**: Main tables in the MarconISSta database*

The database is implemented as a collection of tables on a MySQL server. This allows multiple users to access the data simultaneously.

3.2 Data insertion

The data insertion process converts the space-inefficient text-based CSV files containing of the measurement values to a binary string. Then, the position of the ISS is calculated by retrieving the TLE set whose timestamp is closest to the measurement timestamp and using a SGP4 propagator. Finally, the sample is added to the database.

3.3 Data retrieval

The criteria for retrieving data are: time of sample acquisition, location of the ISS at the time of measurement, and frequency. These criteria are given as ranges, e.g. “measurements between 8:00 PM and 9:00 PM”, or “measurements between 433MHz and 436MHz”.

As can be seen from the data layout presented in section 4.1, filtering by time is trivial: this can be achieved with a "timestamp greater than" and a "timestamp less than" condition. Similarly, if the location criteria is a rectangle, then a pair of "greater than" and "less than" conditions for both latitude and longitude are sufficient.

However, filtering by frequency presents a problem: there can be samples which contain measurements in frequencies that fall within the requested range, but whose start and stop frequency range [f_{start}, f_{stop}] is not be entirely contained within the bounds provided by the user, namely [f_{lower}, f_{upper}]. In fact, there are four cases for matching samples:

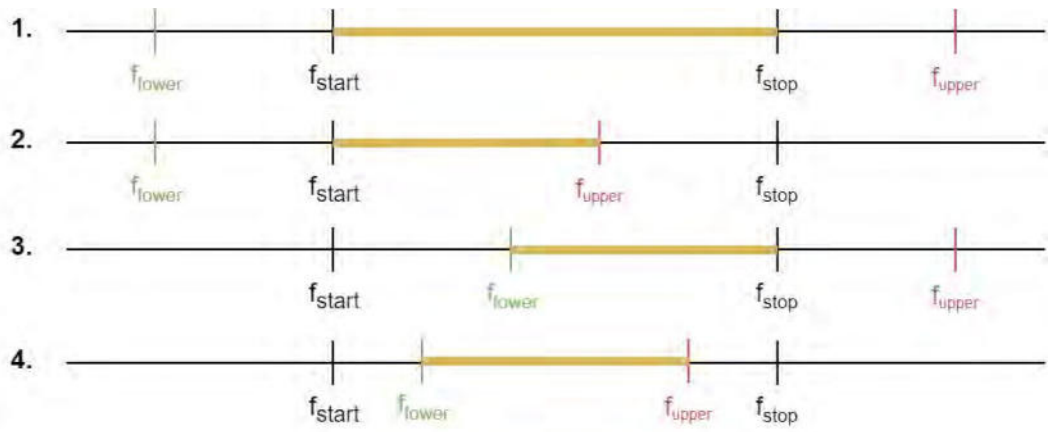

***Figure 2**: Visualization of the cases of sample filtering by frequency range. The section highlighted in yellow are the matching measurements in each case.*

1. **When f_{start} is greater than or equal to f_{lower} and f_{stop} is less than or equal to f_{upper}**. This is the trivial case; all measurements in this sample are part of the requested range.

2. **When f_{start} is greater than or equal to f_{lower} and less than f_{upper}**. In this case, measurements between f_{upper} and f_{stop} are outside the desired range and are discarded in post-processing.

3. **When f_{stop} is greater than f_{lower} and less than or equal to f_{upper}**. In this case, measurements between f_{start} and f_{lower} are discarded.

4. **When f_{start} is less than or equal to f_{lower} and f_{stop} is greater than or equal to f_{upper}**. In this case, measurements between f_{start} and f_{lower}, and between f_{upper} and f_{stop} are discarded.

While at first glance it may seem inefficient to request data that is known to be outside the bounds specified by the user, the alternative is to store each measurement as an entry on a separate table. And indeed, the first version of the data model was implemented in this way, but it was quickly found that the level of indirection imposed by this scheme introduced an unacceptable performance penalty.

4. VISUALIZATION TOOLS

4.1 Graphical User Interface

When developing the GUI, the objective was to give the user a tool to access and display the data in a fast, intuitive and easy-to-use fashion. Elements to allow flexible queries and an error control have been implemented as well. It was created using PyQt5, a popular framework for GUI development.

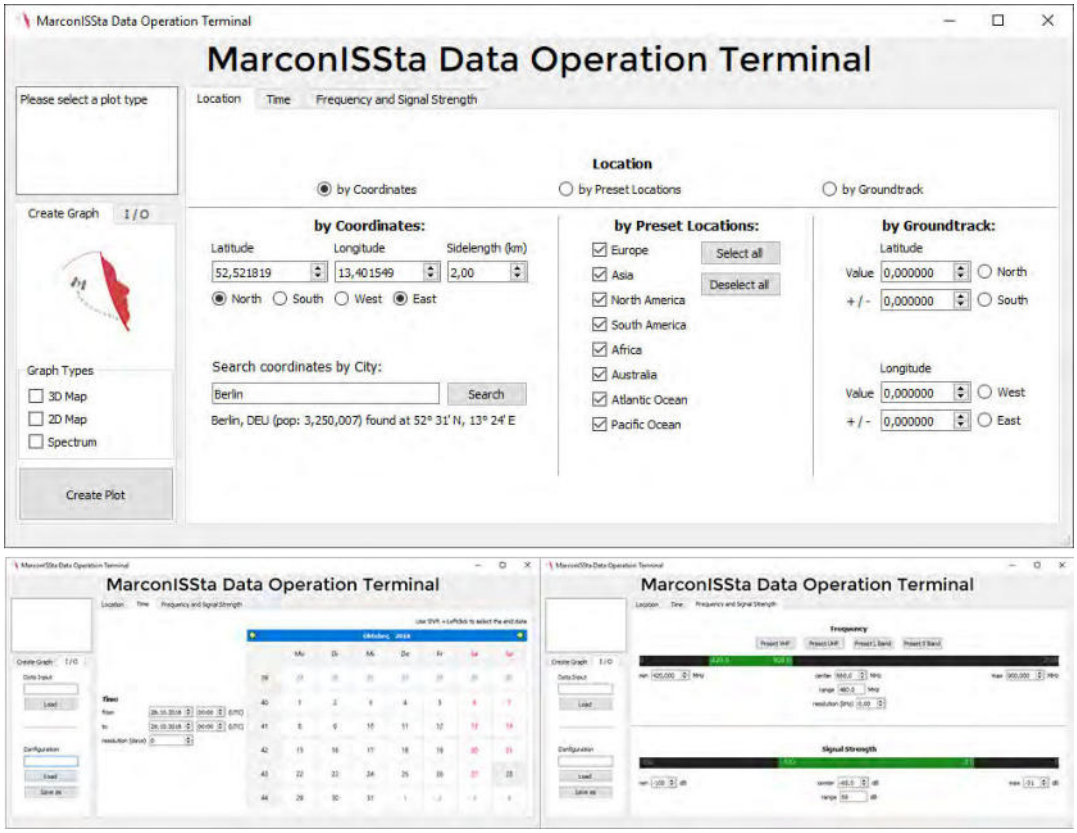

Figure 3: *Elements of the GUI*

The GUI is split into 3 logically separated parts of the query: the location, the time period and the measurement data (frequency and signal strength). This is done for clarity but specially to decrease the size of the window to be able to display it even on small screens. To give the user a lot of flexibility when formulating the query there are different ways to access the same data (e.g. the user can define the position by coordinates, preset locations or by the ground track of the ISS).

To save the user of time-consuming tasks, tools have been implemented to speed up the workflow. For example: the date range is selected using a calendar widget. Clicking a date sets the start date, holding shift while clicking selects the end date. Presets for commonly used frequency bands can be selected with a single button click. Furthermore, it is possible to save and load individual queries as XML-files. The GUI also detects missing or wrong query specifications and notifies the user which part of the query must be improved to create an executable, meaningful query.

4.2 Waterfall plot

This plot shows the RSSI as a function of time and frequency. A map shows the position of the ISS at the time indicated by the position of the mouse in the plot area.

The waterfall plot uses matplotlib as its plotting library, which is widely used for publication-quality visualizations. One challenge with this visualization is that the frequency and time resolution is potentially different over the whole dataset, depending on the recording parameters uploaded each week.

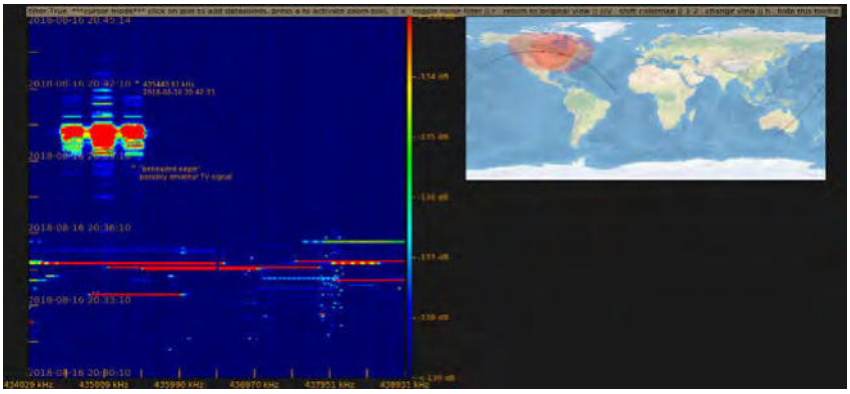

Figure 4: *Waterfall plot with ISS ground track map and cursor*

4.3 Heatmap

The purpose of the heatmap plot is generate a visualization of the pattern of utilization of the different frequency bands in a geographic context. To achieve this, the projected surface of the Earth is divided into rectangles. The width and height of each rectangle is determined by two parameters: the latitude and longitude resolution[1]. Then, all measurements within each area segment are averaged, and finally they are plotted as a color mesh using *matplotlib* over a contour map provided by *Cartopy*.

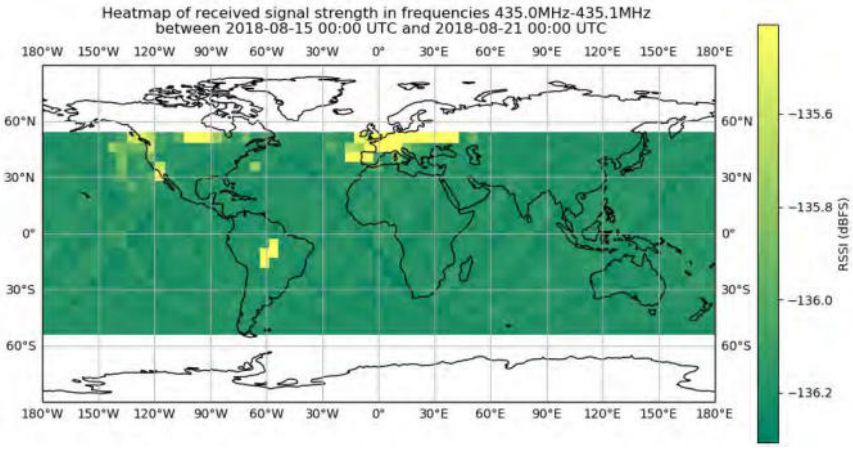

Figure 5: *An example heatmap plot for frequencies between 435MHz and 435.1MHz*

[1]Currently, these parameters are set to 5º per division. However, in the future this may be adjusted dynamically.

5. PUBLIC DATABASE QUERY WEBSITE

The data visualization tools presented in section 4 were used by the MarconISSta team to explore the downlinked dataset during and after operation of the experiment on board the ISS. However, the large amount of information contained in this database and the limited resources of the team means that only some of the interesting features have been identified.

Therefore, the team started to work on a solution to allow interested individuals to query the MarconISSta database. Early on it was decided to avoid releasing data from the experiment in raw form, because it contains several artifacts (radio emissions from the ISS itself, systematic signals from the experiment hardware, and others) that can lead to incorrect conclusions if they are not considered. However, the team does not discard the option of publishing a processed data set in the future.

Instead, the team found that creating a website to allow users to generate graphs like those in figures 3 and 4 (subject to certain limits) would be a good first step. This section describes the software architecture of the website that was made for this purpose.

4.1 Front end

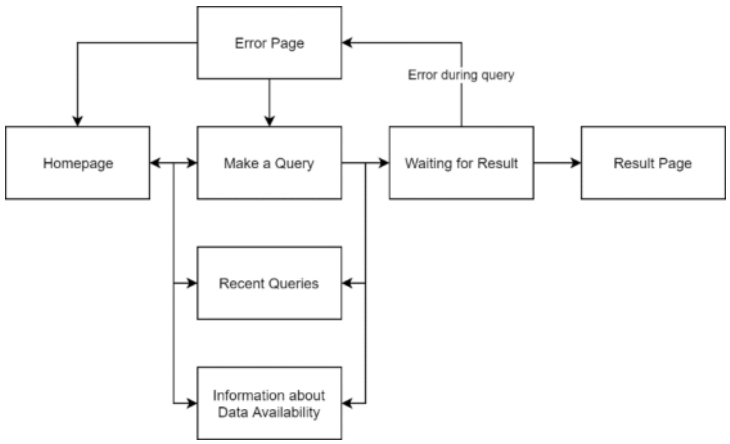

Figure 6: Flow between the different pages of the Web UI

The frontend provides the interface that users use to request queries and browse recent queries and information about the data. It was designed in a responsive manner, to enable a variety of user devices (desktop computer, tablets, mobile phones) to use the website.

Since requests can take up to a few minutes to process, and can fail before or during processing, a “waiting” and “result” page were necessary. The allowable movement between pages can be seen in figure 4.

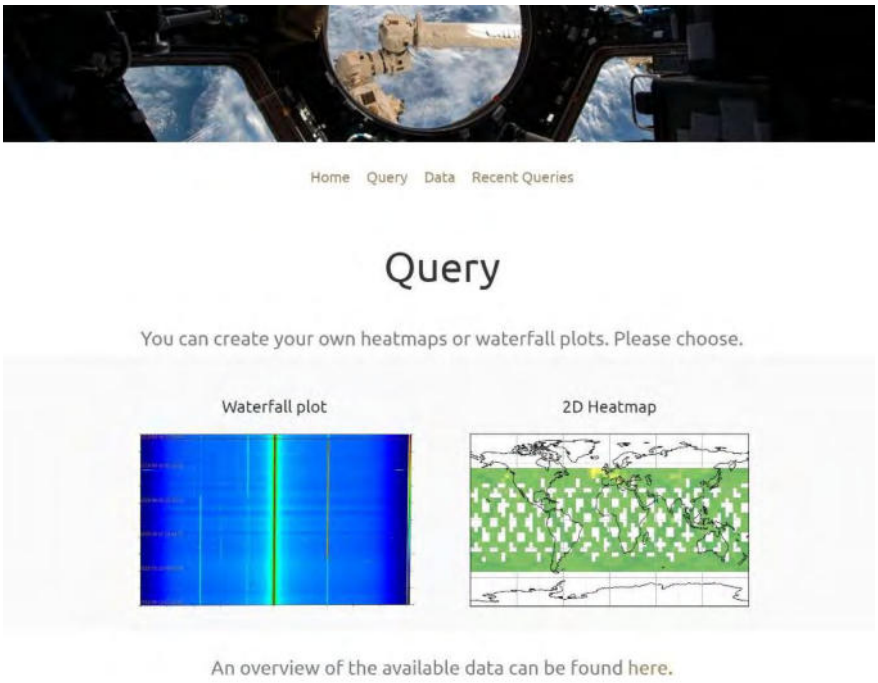

***Figure 7**: Screenshot of the "make a query" page in the web UI*

4.2 Back end

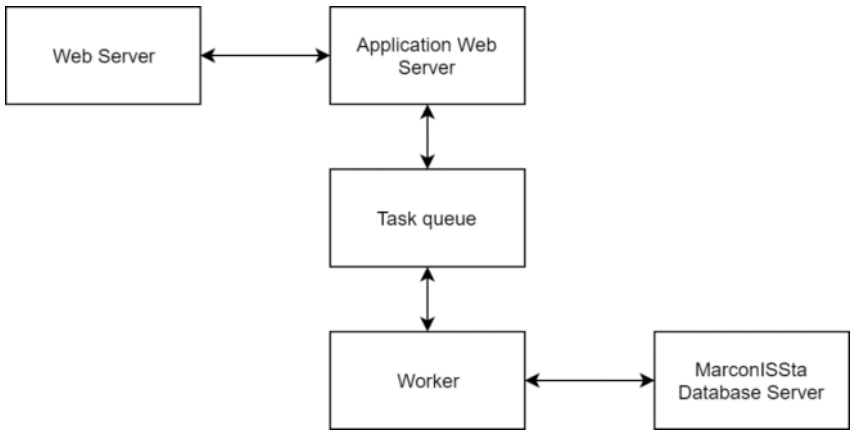

***Figure 8**: Overview of the components of the web UI and their connections*

The first blocks in the figure 4 represent the web servers that users interact. The first web server is responsible for terminating the SSL (Secure Socket Layer) connection and forwarding requests as a reverse proxy to the application server. Nginx is used for this purpose. The requests then reach a Docker container with restricted permissions for security reasons.

In order to support multiple simultaneous queries, a task queue (using the NoSQL Redis server software) is used. Using a Python package known as Celery, tasks are inserted into the queue where they can be performed by one or more worker processes.

It is important to note that the MarconISSta Database is only connected to the worker, and this is a read-only connection. This serves two purposes:

1. To prevent alteration of the database by malicious attacks.
2. To separate the responsibilities such that there is only one part of the code that accesses the database. This simplifies the task of auditing database access.

5. FUTURE WORK

Currently, there is no way to collaboratively annotate the signals found on the waterfall plot. In the future, a marker system will be implemented which will allow users to place comments at a chosen (time, frequency) coordinate, and these comments will be stored in the database and displayed to others.

Some of the samples contain data that should not be included in the visualizations (e.g. due to noise sources coming from the ISS itself). Therefore, a masking system will be added to the system to enable the user to exclude a range of samples, and this exclusion will also be stored in the database.

In addition, the team realizes the potential of using the Web UI / worker framework to enable a controlled distribution of data from scientific missions. In the future, it is envisaged to reduce some of the limits on computation time and add more control over the resulting graphs. Interactive features such as the ability to zoom in to heatmap plots, and scrolling the waterfall plots are being discussed.

Furthermore, the team is looking forward to collaborating with other Earth observation missions, such as SALSAT [4], to provide data analysis and visualization tools.

REFERENCES

[1] Doncaster, B., Williams, C., Shulman, J., (SpaceWorks) 2017 Nano/Microsatellite Maket Forecast.
[2] Matas, A., The ITU – Challenges in the 21st Century Related to Small Satellites. ITU Symposium (2016).
[3] Skrypnyk, I., Bhat-Hire, J., Design and AIV of Ongoing ISS Based Student Project for Analysis of RF Spectrum Utilization. 32nd Annual AIAA-USU Conference on Small Satellites (2018)
[4] Buscher, Martin; Großhans, Jens; Balke, Alexander; Lohse, Alexander; Maaß, Alexander; Brieß, Klaus (2018). RF Spectrum Analysis Missions at TU Berlin. Proceedings the Small Satellites & Services Symposium 2018 - 4S 2018

Moon CubeSat Hazard Assessment (MOOCHA) – An International Earth-Moon Small Satellite Constellation

Alexandros Binios[1a,b], Janis Dalbins[2c], Sean Haslam[d], Rusnė Ivaškevičiūtė[e], Ayush Jain[c], Maarit Kinnari[a], Joosep Kivastik[c], Fiona Leverone[f], Juuso Mikkola[a], Ervin Oro[c], Laura Ruusmann[c], Janis Sate[g], Hector-Andreas Stavrakakis[3h], Nandinbaatar Tsog[i], Karin Pai[c], Jaan Praks[a], René Laufer[j,k]

[a]Aalto University, Espoo, Finland; [b]University of Helsinki, Helsinki, Finland; [c]University of Tartu, Tartu, Estonia; [d]Metropolia University of Applied Sciences, Helsinki, Finland; [e]Vilnius University, Vilnius, Lithuania; [f]Delft University of Technology (TU Delft), Delft, The Netherlands; [g]University of Latvia, Riga, Latvia; [h]National Technical University of Athens, Athens, Greece; [i]Mälardalen University, Västerås, Sweden; [j]Baylor University, Waco, Texas, USA; [k]University of Cape Town, Rondebosch, South Africa

Abstract: Recent developments in space exploration have reinstated the Moon as a primary target for near future space missions. The principal reasons include the Moon being the closest testbed and analogue for planetary space missions and the prospect of a scientific lunar base within the next decade. Space missions have vastly improved our understanding on hazards of human spaceflights but not fully regarding the threats affecting a prospective lunar base. Micrometeorite hazard has been partially addressed as an issue which can potentially impact both astronauts health and safety and create issues for a lunar base, such as degradation or permanent damage of equipment and facilities. Current understanding is based partly on dust and micrometeoroid flux measurements and impact flash observations. However, observations with improved spatial and temporal resolution are imperative for advancing existing hazard models. In this paper, we propose a mission concept of a constellation of nanosatellites – similar to the QB50 project – that can both observe larger parts of cislunar and translunar space and provide higher temporal resolution. Nanosatellite missions are a cost-effective solution providing data for significant improvement of our current understanding. Additionally, such a distributed constellation mission will offer countless opportunities for academia, students and young scientists worldwide.

1. INTRODUCTION

The Nordic-European Astrobiology Campus Summer School 2018 themed "Microsatellites in Planetary and Atmospheric Research" took place from August 6–11, 2018 in Tartu, Estonia, co-organized by the Stockholm University Astrobiology Centre, the University of Tartu, the European Astrobiology Campus and the Nordic Network of Astrobiology and supported by European Union's European Regional Development Fund and Estonia. 35 participants and over a dozen lecturers from all over the world worked for a week on micro- and nanosatellite concepts for lunar and planetary exploration. As proposed by two of the summer school lecturers and co-authors, we considered the possibility of a QB50-like [1] constellation to perform scientific investigations of the Moon and its near vicinity. After rapid concept development, the team proposed Moon CubeSat Hazard Assessment mission, MOOCHA, presented in this paper. The mission aims to address the hazards of the Moon environment in a novel approach and make a hazard assessment for future Moon missions and facilities. We hope to achieve an international support for a platform which makes space, especially

[1] corresponding author: alexandros.binios@gmail.com
[2] corresponding author: janis.dalbins@estcube.eu
[3] corresponding author: hecstavrakakis@gmail.com

Moon missions, achievable for everyone who is interested in joining the MOOCHA project.

2. MISSION OBJECTIVES

The prime objective of the MOOCHA mission is to perform lunar hazard assessment with regards to permanent human presence on the Moon and cislunar space. Permanent presence will require manned missions, lunar bases, and equipment placed on the Moon all of which are susceptible to various hazards. Micrometeorite flux and impacts are identify as a main and constant hazard, as they pose one of the most damaging hazard risk both for the equipment, bases and for the future lunar personnel and even travellers. and astronauts. The hazard assessment of the micrometeorites will be primarily achieved by the monitoring of impact flashes caused by them bombarding the Moon's surface. At the same time, MOOCHA mission can provide a real-time monitoring system that can be the basis for a future lunar system or orbiting station . Furthermore, an additional desire of the mission is to create an environment for national and international collaborations for young scientists on various small satellite and lunar topics.

The primary mission objective will be achieved by utilizing on-board instruments to observe the flux of micrometeorites in the lunar environment over an entire solar cycle as solar radiation pressures fluctuate altering the intensity of meteorid objects. Over the duration of a complete solar cycle, the solar radiation pressure varies which affect the environment of the Moon and the general of likelihood of micrometeorite impacts on the lunar surface.[2] This requires and justifies the need to have systematic observations for a minimum of one full solar cycle. While similar Earth-based observations have been conducted for many years, for the indirect measurement of NEO objects by meteorid streams utilizing the Moon surface several limitations exist. Earth's atmospheric interference in conjunction with weather limitations and Sun luminosity on the Moon surface does not allow monitoring of the entire lunar surface area at all times.[3,4,5] As an example the NELIOTA project has only 95 hours of lunar observation for 824 days of the project run up to this point.[5] Flashes occurring in polar regions as well as on the far side of the Moon are hidden from the Earth's field of view greatly limiting the number of observed impact flashes. Regarding the lunar cycle between 10-42% of the Moon surface can be monitored for impact flashes during the different phases of the lunar cycle from Earth observation stations. For these measurements, investigations from Moon orbiting missions will be of the highest value due to a significant increase in detection of even the smallest events and regular coverage of the complete lunar surface compared to Earth-based observations.

The secondary mission objective is to acquire more information about the lunar environment and subsurface. More specifically, accurate data related to the chemical composition of the surface,how water present is dispersed in the regolith and analytic measurements of Moon's magnetic fields in order to support the lunar base placement selection process. In this way a more analytical assessment can be made as per an ideal location for a base combining both resources potentials as well as hazard risks. At the same time the satellite constellation can provide a platform for more real time monitor and information system, that could be a useful tool for a future lunar base or surface activities. Additionally, the whole mission provides valuable opportunity to extend the small satellite and lunar research network and to train new scientists and engineers. This

will be achieved by providing opportunities for students and early career scientists to participate in lunar exploration by the construction of their own satellite or by providing services for the mission. This can be achieved either by designing a satellite in conjunction with this project basic requirements, and then either building it by themselves or by collaboration with experts in the industry Other opportunities include collaborations between industry and academia as each satellite will need to incorporate at least some similar components due to the mission requirements. The activity shall create a lunar science and space engineering hub – especially for young professionals and scientists – connecting people from all around the globe and providing the basis for larger future space mission projects such as a Mars mission.

3. MISSION CONCEPT

The mission aims to conduct scientific measurements and observations over at least one full solar cycle of 11 years. This shall be achieved by operating a large number of small spacecraft, creating a satellite constellation, with a minimum spacecraft expected lifetime of 2 years. The mission idea naturally enables the usage of ridesharing using a single launch per multitude of MOOCHA mission satellites to lunar orbits.The orbital parameters, period of observations and number of satellites will be determined by the available and feasible piggyback ride opportunities of microsatellite and nanosatellite launch providers. To achieve the mission objectives it is suggested to add fleets of satellites to the overall constellation of at least 8 microsatellites or nanosatellites per launch. This will ensure that at least 3 observations per impact flash will be made to get the most accurate data of the impact flashes and their locations. A new batch of satellites is launched before the end-of-life of the previous batch to ensure continuous mission operation.The common factor of the satellites in the mission is to use the same payload package for monitoring the impact flashes, that will also be the basic requirement to enter the project. Apart from the standardized payload the satellites will be able to add other non-common secondary payloads to their satellites as well as, other components such as the type of on board computer, power supply and navigation.

The proposed MOOCHA mission will consist of a large number of microsatellites and nanosatellites which will be designed, built, and operated independently by various academic and partner institutions. These include commercial companies, and research and space agencies who wish to contribute to the overall mission and its objectives. The common factor of the satellites in the mission is to use the similar or comparable payload packages for monitoring the impact flashes, and to be able to add other non-common secondary payloads to their satellites as well. The mission idea naturally enables the usage of ridesharing using a single launch per multitude of MOOCHA mission satellites to lunar orbits. The mission aims to conduct scientific measurements and observations over at least one full solar cycle of 11 years. This shall be achieved by operating a large number of small spacecraft with an expected lifetime for at least 2 years at a time and overlap in its missions to cover the overall time frame. The orbital parameters, period of observations and number of satellites will be determined by the available and feasible piggyback ride opportunities of microsatellite and nanosatellite launch providers. To achieve the objectives it is suggested to add batches of satellites to the overall constellation of at least 8 microsatellites or nanosatellites per launch. This will ensure that at least 3 observations per impact flash are made to get the most accurate data of the impact flashes and their locations.

4. TECHNICAL REQUIREMENTS

The technical requirements of the MOOCHA mission satellites are defined by the needs of the mission objectives. Instruments and the satellite bus shall be able to observe impact flashes of meteoroids on the lunar surface and to survive the lunar orbit environment.[6]. Additional technical requirements are introduced based on the level of modification and deviation of the primary mission goals, such as by using a different than suggested power system, and secondary or tertiary payloads. One example of requirements derived from the lunar environmental conditions is that satellites with their components shall survive a Total Ionizing Dose (TID) of a minimum 200 krad, which is to be expected in the lunar vibinity [7]. Such requirement is difficult to implement on small satellites, especially on CubeSats, due to mass and volume limitations, but not impossible. This additionally provides the opportunity for new innovations in the material science field. In order for better monitoring and utilizing the best luminosity angles for better impact flash detection orbital changes that will require propulsion systems will be required. Combining the low mass and volume one possible technology that could be utilized for propulsion, is the Electric Solar Wind Sail, or E-Sail, which provides thrust by using the dynamic pressure of the solar wind's ions [8]. A required communication downlink shall be greater than 1 bps for beacon and housekeeping data, and at least 500 bps for science date, to ensure successful data retrieval. New technologies can also make possible the use of an either independent or with secondary payload satellite that will function as communications centre. This apart from helping achieve possible higher data rates and it will allow for communication irrespective with the ground station locations and the satellite’s orbit in the Moon at all times.

5. ORBITS

The selection and design of the constellation orbits for the mission have to overcome various challenging obstacles. The initial obstacles are found in the scope, the aim and the duration design of the mission idea creating various challenges in the management of various satellites. However, the most serious challenges are found in the environment in which the mission profile will be developing. It has been known for many years that lunar surface is more anomorphogenic than the Earth’s.

These characteristics of the Moon environment create some criteria than will be favored more or less in the orbis design for an ideal orbit. The anomorphogenic nature of the lunar surface has created large-scale gravitational anomalies making low lunar orbits unstable and resulting in a lunar crash, constitute the first criteria. The second criteria is connected with the high level of high energy radiation and susceptibility to space weather phenomena malfunctioning electronic in satellites. A final criteria that is not closely related with science is added. Primarily, focusing on the PFS 1 and PFS 2 and the reduction of space debris, a useful consideration about the orbit design shall be made in order to minimize or if possible eradicate possible space debris utilizing the Moon’s gravity. Special attention therefore is needed when selecting the lunar orbits. In that regard, only three orbit design methods are favored and can be selected for the mission as they require minimal changes in their orbital parameters through their predicted lifetime. These design methods utilize the lunar frozen orbits and Earth- Moon free-return trajectories. Each orbit method has it benefits and drawbacks. The so called frozen lunar orbits have been found to be at inclinations of 27 °, 50 °, 76 ° and 86 °.

This allows covering the covering the most essential blind spots from Earth-based observations. However, due to the gravitational anomalies at low lunar orbit at altitudes of 100 km deviation from this inclination can cause even rapid altitude decrease in a short period of time that will eventually without corrections result in a crash. This deviation might be used in order to cover the third criteria and reduce space debris especially in the aforementioned inclinations. The free-return trajectories need to be taken in account the gravitational anomalies of the lunar surface. In contrast, however, with the frozen orbits they require different approach angle but do not require a precise inclination of half orbit. Such orbit can possible allow for even very close low lunar orbit flybys collecting even more accurate data. Due to the orbit parameters the satellites will be experiencing lower amounts of radiation due to been cover by the van Allen belts for a significant time of the orbit. In addition, due to having a passage close to data transfer can more easily be achieved as well as without the need and assistance of an intermediate data relay satellite from the lunar orbit.

In addition, it is vital with spacecraft, especially small-scale nanosatellites with low available system masses, to plan and choose the orbits wisely since orbital maintenance maneuvers require a Delta-V velocity increment of between 80 and 150 m/s/year, for an lunar orbit inclination of 55°, a rarely available thrust capability in small nanosatellites[7]. The orbits shall also have low propulsion consumption if any at all for their expected life design.With it E-Sail technologies, or other electric propulsion systems, a satellite may enter into orbital inclinations outside of the frozen orbits and gather data from lower altitudes, using the thrust provided to make course corrections. Furthermore, such maneuverability will allow the satellites to become “Moon wanderers” by entering various lunar orbits to gather data, even returning to Earth’s vicinity for data transmission, and targeting a new lunar orbit, simplifying the communication between satellites and ground stations

6. PAYLOADS

The mission payload is divided into two main categories. The first category consist of the mission payloads that include all the necessary equipment in order to monitor, process and transmit the impact flash data. The first category also includes the required associate payloads such as the power supply, telemetry transmitters and propulsion in order to accomplish the mission objectives.

The second category includes all other payloads that will be utilized for small satellites apart from the camera payload. This will create small satellites that will not provide data for the impact flashes but still be critical system either for other hazard monitoring such as radiation or communications hub..The mission idea is also a welcoming project for such payloads. In addition, usually, most space vehicles are manufactured and equipped in order to accomplish multiple goals, within the design parameters maximizing the mass and volume capabilities in parallel with the main mission objective. Therefore, probably many satellites will include both type of payloads.

As per the first category in order to meet the objective of the mission, a high resolution camera capable of impact flash detection (Table 1, initial requirements) is proposed as the payload.

Table 1. Payload requirements

Parameter	Value
Flash magnitude	> +10
FWC	> 80 ke
QE	> 90 %
Resolution	> 1000 px × 1000 px
Pixels	> 10 μm
Focal length	> 7 cm
Field of View	20–120 degrees
Mass	< 2 kg
Power (continuous)	< 4 W
Monochrome	VIS

The camera shall be supported by on-board imaging software capable of the initial process on the image, such as analyzing the taken images of the assumed flashes, and ultimately determining flashes – similar to LUMIO [9]. The second category includes, all the payloads that are secondary to the functions of the mission critical payload. The secondary payload, if any, is free to the discretion of the manufacturer and as such can include either additional scientific or process equipment or experimental equipment such as an E-sail propulsion system.

However, the second payload category must try not to indefer with the payload of the first category in order not to hinder the performance of it. Therefore, in a case for example where a additional secondary payloads are included the power system of it must either be independent or if it is expanded in it lowest performance and setting be able to power the mission critical payload.

Small satellites have not been utilized apart from the Insight's MARCO cubesats by NASA and the HERA mission concept cubesats out side of Low Earth Orbit. [10, 11]. In that sense the mission is proving also design flexibility and therefore allowing the development of various design proposal for satellites. Furthermore, experimental components are specifically encouraged due to the nature and environment of the Moon and Lunar Orbit. This especially more the case in the area of small and nano satellites, where apart from scientific and technological goals that can be achieved, an additional goals of education and learning are introduced by the involvement of young scientists and student to the manufacturing team In example the mission could be used for radiation testing of components and even radio astronomical observations, when beyond the far-side of the Moon, protected from the Earth's radio interference.

As it was discussed, for extended maneuverability E-Sail propulsion technology is suggested. However, the use of only or mainly such systems for propulsion can create problems with orbital maneuvers as it is still an experimental technology, even though it would allow large-scale proof-of-concept testing and control the satellite's orbit. Therefore, alternate such as water propulsion taking into account also are the small size of the satellites

7. LAUNCH OPPORTUNITIES

The mission is partially inspired by the successful LEO-nanosatellite constellation QB50 mission, and it will also mostly depend on piggyback ride launches and CubeSat launch providers who provide Lunar Transfer Orbit (LTO) launches. Since a constellation mission requires a multi-year development time the individual launches shall be scheduled after the year 2020. Currently, there are various launches to the Moon planned for the next decade. A list of possible launches offering rideshares is given in Table 2 [12,13,14].

Table 2. Possible launches for piggyback rides.

Mission	Launch	Launch Vehicle
Peregrine	2020	Atlas V
Luna 25	May 2021	Soyuz-2.1b / Fregat-M
SLIM	2021	H-IIA 202
DESTINY+	2022	Epsilon
Chang'e 6	2020s	Long March 5
SELENE-2	2020s	H3
Orion EM-2	June 2022	SLS Block 1
DearMoon	2023	BFR
Orion EM-3	2024	SLS Block 1B

8. CONCLUSIONS

The MOOCHA mission is a feasible, and highly beneficial concept to support future human exploration missions to the Moon as well as providing excellent opportunities for academic and commercial organizations all around the world to participate in lunar science and exploration. Recent developments regarding miniaturized satellites, such as CubeSats, and rideshare satellite launches make the MOOCHA mission concept very viable. The mission offers a broad platform for research, exploration, and technology demonstration through international collaborations and valuable return on scientific questions regarding the Moon still open to be answered. Finally, successful small lunar satellite missions pave the way to miniaturized spacecraft missions to other celestial bodies in our Solar System, and beyond.

Further refining of the MOOCHA mission concept with respect to orbital mechanics, satellite bus design and subsystems, payload instrumentation, ground and launch segment and other mission elements will be performed during the follow-up two-week workshop in July/August 2019 at the University of Tartu, Estonia. The increase in workshop duration from one to two weeks will be dedicated in particular to increase the level of detail of the mission concepts proposed during the 2018 workshop due to iterations and further analyses of the mission design and the mission elements.

9. ACKNOWLEDGMENTS

The authors wish to thank the organizers, lecturers and hosts of the Nordic-European Astrobiology Campus Summer School 2018 in Tartu, Estonia, co-organized by the Stockholm University Astrobiology Centre, the University of Tartu, the European Astrobiology Campus and the Nordic Network of Astrobiology and supported by European Union's European Regional Development Fund and Estonia. The authors would also like to acknowledge the various institutional support for participants and lecturers to be able to attend the summer school and to express their gratitude to the staff of the Tartu Observatory for their generous hospitality and assistance.

10. REFERENCES

1. D. Masutti, A. Denis, R. Wicks, J. Thoemel, D. Kataria, A. Smith, J. Muylaert. (2018). The QB50 Mission for the Investigation of the Mid-Lower Thermosphere: Preliminary Results and Lessons Learned. 15th Annual International Planetary Probe Workshop (IPPW) 2018, June 11-15, 2018, University of Colorado Boulder, Colorado, USA.
2. Yano, Hajime. (2012). Micrometeoroid Flux in the Earth-Venus Region Measured by the IKAROS-ALADDIN. 39th COSPAR Scientific Assembly
3. Madiedo, José M. & Ortiz, J & Morales, Nicolas & Santos-Sanz, Pablo. (2019). Multiwavelength observations of a bright impact flash during the 2019 January total lunar eclipse. Monthly Notices of the Royal Astronomical Society. 486. 3380. 10.1093/mnras/stz932.
4. Bonanos, Alceste & Liakos, Alexios & Xilouris, Manolis & Boumis, P & Bellas-Velidis, Ioannis & Marousis, A & Dapergolas, Anastasios & Fytsilis, Anastasios & Noutsopoulos, Andreas & Charmandaris, Vassilis & Tsiganis, Kleomenis & Tsinganos, Kanaris & Els, Sebastian & Koschny, Detlef & Lock, Tim & Navarro, Vicente. (2016). NELIOTA: ESA's new NEO lunar impact monitoring project with the 1.2m telescope at the National Observatory of Athens. 991122. 10.1117/12.2232453.
5. https://neliota.astro.noa.gr/
6. A. M. Cipriano, D. A. Dei Tos, F. Topputo. (2018). Orbit Design for LUMIO: The Lunar Meteoroid Impacts Observer. Frontiers in Astronomy and Space Sciences. 5. 10.3389/fspas.2018.00029.
7. O. Zeile, M. Lachenmann, E. Baumstark, A. Mohr, D. Bock, R. Laufer, N. Sneeuw, H. Röser. Analyses of orbital lifetime and observation conditions of small lunar satellites. Acta Astronautica 66(3-4):516-527, February 2010. DOI: 10.1016/j.actaastro. 2009.07.008.
8. P. Janhunen. Electric Sail for Producing Spacecraft Propulsion. Patent (WO2007099201) PCT/FI2007/000056. September 7, 2007.
9. F. Topputo et al.(2017). LUMIO: Lunar Meteoroid Impacts Observer.
10. https://www.jpl.nasa.gov/cubesat/missions/marco.php
11. https://www.esa.int/Our_Activities/Space_Safety/Hera/Hera_s_APEX_CubeSat_will_reveal_the_stuff_that_asteroids_are_made_of
12. *S.* Pietrobon. (11 July 2018). "Russian Launch Manifest". Retrieved 29 October 2018.
13. H. Toyota, K. Nishiyama, Y. Kawakatsu (15 August 2017). "DESTINY+: Deep Space Exploration Technology Demonstrator and Explorer to Asteroid 3200 Phaethon" (PDF). Low-Cost Planetary Missions Conference. Retrieved 29 October 2018
14. *ISIS Launches https://www.isispace.nl/launch-services/#upcoming-launches*

A LOW-COST, PORTABLE, EASY-ASSEMBLY AND EXPANDABLE SDR GROUND STATION

Barbara Ojur[1], Peter Martinez[2]

[1]Student, Engineering and Built Environment, SpaceLab, University of Cape Town, Rondebosch 7700, South Africa, E-Mail: ojrbar001@myuct.ac.za

[2]Professor, Engineering and Built Environment, SpaceLab, University of Cape Town, Rondebosch 7700, South Africa, E-Mail: peter.martinez@uct.ac.za

Abstract: Small satellites are nowadays being launched by a multitude of private and public organizations around the world. They are innately less costly and less complex to assemble than their larger counterparts. With the inception of more small satellites being launched there is an increased influx of data available from them, however such information is not being utilized efficiently, possibly due to high expenses associated with developing a traditionally hardware-based ground station. With the introduction of Software Defined Radios (SDRs), many of the operations formally done using hardware can now be implemented in software at a reduced cost - something of great interest for institutions especially in emerging and developing countries. A low-cost, portable, easy-assembly and expandable SDR ground station was developed at the University of Cape Town's SpaceLab in 2018 to participate in the movement towards developing SDR ground stations to communicate with small satellites. In an initial step the SDR ground station has allowed users to listen to, view and analyze distinctive small satellite signals and frequency patterns as well as receive and decode data packets from LEO small satellites operating in the 70 cm (UHF) band. It is the intention of this SDR ground station to enable and encourage data usage, national and international collaboration and education outreach in different sectors to promote space activities and its potential to everyone, especially on the African continent.

1. INTRODUCTION

Small satellites are nowadays being launched by a multitude of private and public organizations around the world. They are innately less costly than their large counterparts. This attribute, and additional ones, such as their lower complexity of assembly nature and the convenience of using widely available commercially off-the-shelf components to build them has largely enhanced their popularity. Now that getting into space has become more accessible there is an influx of data available from small satellites, however the information is not always fully being utilized efficiently on and for Earth. One evident reason is due to traditional ground stations being largely hardware dependent, and therefore quite expensive to setup. However, with the introduction of Software Defined Radios (SDRs) many of the operations formally done using hardware can now be implemented in software. Using a SDR can substantially reduce the cost of a traditionally hardware-based ground station. A number of universities and other organizations have or are developing SDR ground stations to communicate with satellites in various orbits. The ability to transmit and especially receive signals is important because it can encourage data usage, national and international collaboration and education outreach.

The receiving SDR ground station, presented in this paper, was developed at the SpaceLab of the University of Cape Town in 2018. The ground station attempts to enable participation in the movement towards small satellite communication using SDR technology by developing a low cost, portable, easy to assemble and expandable ground station to listen to, view and analyze small satellites data transmissions, frequency patterns as well as receive and decode packets and downlinked data.

2. MISSION OBJECTIVE, REQUIREMENTS AND CONSTRAINTS

Table 2.1 presents the qualitative objectives set out before the development of the SDR ground station. Table 2.2 presents qualitative functional and operational requirements. The functional requirements refer to the systems capability and the operational requirements refer to aspects that should be prevalent when the system is in use. Table 2.3 presents the constraints in which the SDR ground station had to be developed in.

Type	Objective
Primary	Design, develop and build a low cost, portable and expandable SDR ground station to establish communication (to listen, view, receive and decode) with LEO small satellites.
Secondary	Enable and encourage small satellite data usage.
	Education outreach (internally within SpaceLab)
	Data sharing
	National and international cooperation
Hidden	Participate and contribute to national/international projects
	Support future SpaceLab missions
	Highlight SpaceLab's capabilities

Table 2.1 Qualitative Mission Objectives

Functional	Operational
A user shall be able to select one satellite to track from a catalogue of satellites.	The SDR ground station shall be able to track a satellite intermittently for a maximum of 5 minutes.
	Satellites operating in the 70 cm band (UHF, 430-440MHz).
	Tracked satellites shall be located in LEO
	Tracking accuracy shall be within ±7% of the tracked satellite.
The SDR ground station shall be able to establish contact (receive signal/packets) with at least one small satellite at	The user shall be able to store downlinked data in at least

a time.	one database.
The SDR ground station shall be able to at least decode one type of the data (sound, packets) it receives.	The decoding shall be completed within one hour.
The SDR ground station shall be able to enable a user to zone in and investigate one frequency within the 70cm band at any given moment.	The user shall be able to change and monitor a different frequency, at any given time, during the 5 minute operation time.
The antenna system when static/off shall have a maximum height (vertical length) of 2.5m and width (horizontal length) of 2m	If elements of the SDR ground station have moving parts, the moving parts should + only be able to extend vertically to a height of 3 m and horizontally 2 m.

Table 2.2 Mission Functional and Operational Requirements

Constraint	Explanation
Cost	The total cost of the SDR ground station shall be below R2000.
Schedule	The SDR ground station shall be operational within one year (365 days).
Regulations	The SDR ground station shall not be able to uplink a single signal.
Environment	The ground station equipment shall be able to work between 10-26°C.
Interfaces	All control interfaces of the SDR ground station shall be able to be operated by one computer.
Portability/ Weight	The system shall have a mass of less than 50 kilograms.
Automation	Tracking shall be automated.
Power	The SDR ground station only house equipment that are rated 230 V / 50 Hz or lower.

Table 2.3 Mission Constraints

3. SDR GROUND STATION DEESIGN

Figure 3.1depicts the design of the SDR ground station. Parts were first sourced locally in South Africa and then internationally. The whole development process took place in South Africa at the University of Cape Town's SpaceLab. The SDR ground station can track small satellites, operating in the 70 cm (UHF) band and it is equipped with an azimuth and elevation rotator from Yaesu. In the azimuth plane it has 450 degree of freedom and in the elevation plane it has 180 degree of freedom. The rotator is controlled automatically via an Arduino board. A user can select a satellite from a satellite tracking application, installed on a computer, to direct the rotators to point the antenna towards a small satellite when it is in line of sight. Currently one small satellite can be tracked at a

time and the system can only run for a 5-minute period before resting for 15-minutes to not overwork the rotator.

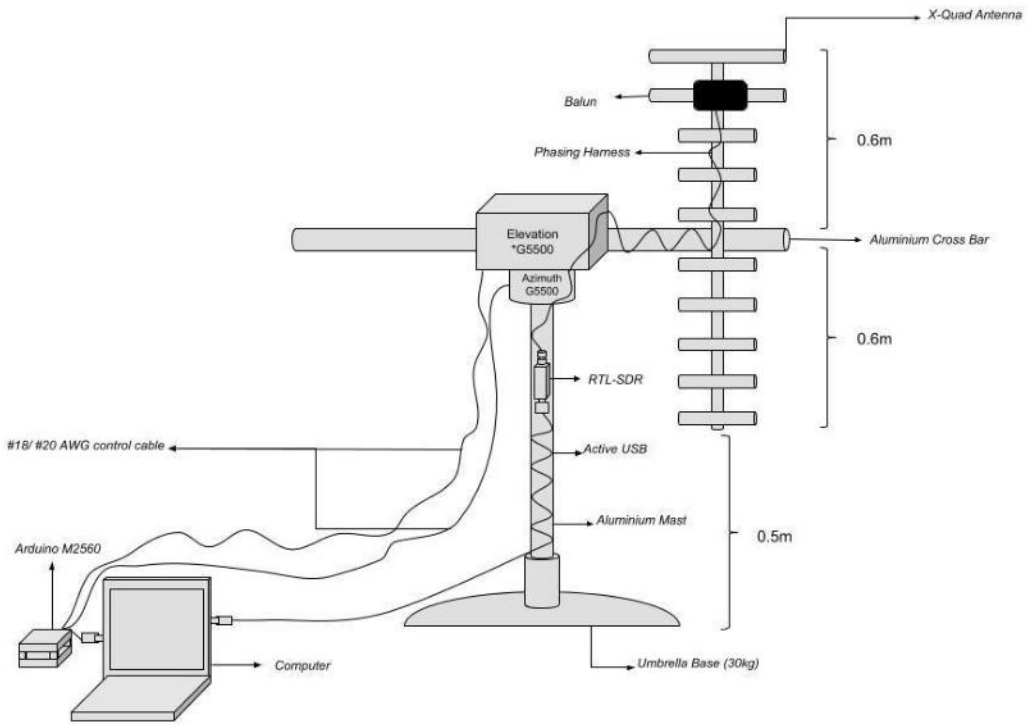

Figure 3.1 The SDR ground station developed at the University of Cape Town's SpaceLab.

4. RESULTS

The SDR ground station has allowed users to:

- Listen to and view distinctive small satellite transmissions
- Visualize distinctive small satellite frequency transmissions
- Receive data packets

5. CONCLUSIONS AND RECCOMMENDATIONS

The SDR ground station, the first of its kind at the SpaceLab, has introduced new capabilities that will enable future research at the SpaceLab. Its inception provides opportunities for collaboration with other institutions (in example with Sapienza University in Italy and other partners). Further development of this low-cost, portable, easy assembly and expandable SDR ground station design will help to promote space data utilization in the Western Cape Region, South Africa and hopefully other parts of the African continent.

Observing the Impact of Air Pollution in Dhaka City using APOSat

Masrur Khan[1], Monirul Islam Pavel[2], Mustafa Jamil[3]and Md. Tausif Rahman[4]

(1)Department of Electrical and Electronic Engineering, BRAC University, 66 Mohakhali, Dhaka, Bangladesh, Phone: +8801534991918, Email: masrur.khan@g.bracu.ac.bd; masrur.khan.annan@gmail.com

(2)Department of Computer Science and Engineering, BRAC University, 66 Mohakhali, Dhaka, Bangladesh, Phone: +8801708080102, Email: monirul.islam.pavel@g.bracu.ac.bd; mipavel07@gmail.com

(3)Department of Electrical and Electronic Engineering, BRAC University, 66 Mohakhali, Dhaka, Bangladesh, Phone: +8801872792208, Email: mstfjamil@gmail.com

(4)Department of Electrical and Electronic Engineering, BRAC University, 66 Mohakhali, Dhaka, Bangladesh, Phone: +8801986226821, Email: md.tausif.rahman@g.bracu.ac.bd; trarnab031@gmail.com

1. ABSTRACT:

Global air pollution is on the rise, with Carbon Dioxide having already crossed a significant threshold of 400 ppm (parts per million) in 2016 and Dhaka has been one of the worst affected cities. Bangladesh is a densely populated country with Dhaka being the center for gaining a standard livelihood. Keeping the air quality in check is an extremely difficult task, let alone improving the conditions. In order to deal with this challenge, this paper proposes on a microsatellite, the Air Pollution Observatory Satellite or APOSat to be built and deployed for scientific observations, analyzing air quality while orbiting over Bangladesh. Experimental results include a hardware prototype and a software simulation, both of which are compared to get an overview of data readings and accuracy under certain conditions. The software simulation also helps in determining the appropriate launch site and the prototype helps in determining the type of sensors suitable for the microsatellite.

2. INTRODUCTION:

According to the Air Quality Index set by The United States Environmental Protection Agency in March 2018, Dhaka scored 443 which falls under the category 'very unhealthy'. The Bangladesh capital has been ranked the second most polluted city in the world. However, this is nothing new for the 14 million people who live there. This issue has prevailed for many years and in a densely populated city, it was always going to get worse. Air pollution is one of the top ten causes of death in the country, so in order to monitor the air quality, a proposal has been made to create the APOSat for scientific observation.

3. LITERATURE REVIEW:

GOSat (Greenhouse gases Observing Satellite) [1,2] was the mission of JAXA and manufactured by Mitsubishi Electric to observe the greenhouse gases like methane (CH_4), carbon dioxide (CO_2) and ozone (O_3) using TANSO-FTS (Thermal And Near-infrared Sensor for carbon Observation - Fourier Transform Spectrometer), SWIR-FTS (Shortwave Infrared-Fourier Transform Spectrometer), TIR-FTS (Thermal Infrared- Fourier Transform Spectrometer) and TANSO-CAI (Thermal And Near-infrared Sensor for carbon Observation

- Cloud and Aerosol Imager). The orbital altitude of GOSat is 666 km with inclination of 98°. E. A. Kort et al [3] presented a model of space-based carbon dioxide observation for megacities like Los Angeles and Mumbai using GOSat. The authors showed the potential of earth observing satellite which uses CO_2 dry air mole fraction where they showed 3.2 ± 1.5 ppm increment in Los Angeles and 2.4 ± 1.2 ppm in Mumbai which indicates 22% enhanced emission.

4. MISSION OBJECTIVE:

Some of the major sources of air pollution in Dhaka include smoke from brick fields, tanneries, textiles and emission from vehicles running on diesel. The pollutant elements are mainly Carbon Dioxide (CO_2), Carbon Monoxide (CO), Sulphur Dioxide (SO_2) and Nitrogen oxides. Gathering satellite data regarding air quality from foreign sources is beyond expensive from a research point of view. The main objective of the APOSat is to monitor the air quality in Dhaka on a daily basis and allow necessary measures to be taken to improve air quality with respect to the obtained data without needing to reach foreign sources.

5. MISSION OPERATIONS:

The APOSat is planned to be launched from Launch Complex 1, a rocket launching site located in Mahia Peninsula, New Zealand. Orbital inclinations [4] from here can be up to 39°. The reason to choose this site is justified in article 6.1. There will be two ground stations set in Dhaka, one at the main city and the other in Savar Upazilla, which is 24 km away to the northwest of Dhaka city. Gathering data of air pollutants in Savar will give a deeper insight since the majority of brick fields are located there. The APOSat will range at an altitude between 400 to 500 km during orbit, convenient for most small satellites.

6. EXPERIMENTS:

Before determining the necessary equipment of the actual microsatellite, a hardware prototype and a software simulation experiment were performed. The outcome of these two experiments were useful in choosing the orbit and the equipment.

6.1 Orbit Simulation:

To determine the expected inclination angle, a code on orbit simulation was tested in MATLAB software, considering a general small satellite. This code had four major parameters to be set; position vector, velocity direction vector, velocity magnitude and number of revolutions. After performing several test runs while adjusting the values of these parameters for different types of orbits and considering 15 revolutions for each test; the inclination angle of 28.81° (orbital inclination from Mahia can be up to 39° as stated earlier) gave the best result in the simulation, with the microsatellite orbiting over Bangladesh four times a day from an altitude of about 400 km, thus falling under the category of Low Earth Orbit or LEO. For an orbital height of 400 km, the estimated orbital speed and orbital period [5] were calculated to be 7.67 km/s and 1.54 hours respectively. The proposed inclination has been selected because of the convenience for observing the central region of Bangladesh where Dhaka is located. The simulation results are shown in Figures 1 & 2.

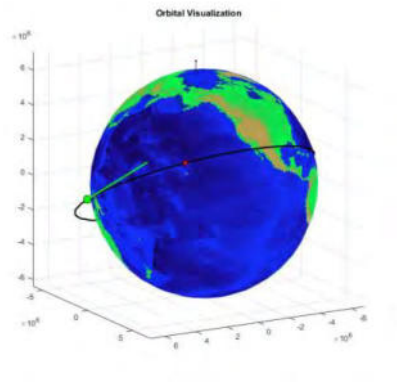

Fig. 1: Orbit Visualization in 3D

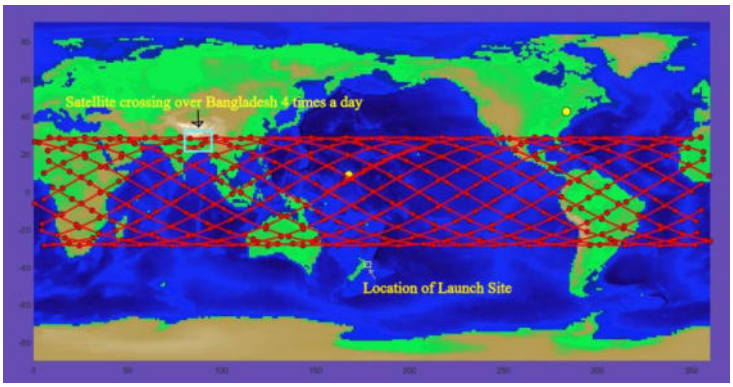

Fig. 2: Orbit pathway after 15 revolutions

6.2 Gas Sensor Prototype:

A prototype equipment (Figure 3) was built to take readings [6] from the environment. It consisted of a temperature & humidity sensor, a module for data communication and two gas sensors reading CO_2 and CO in ppm connected to an Arduino Nano microcontroller board.

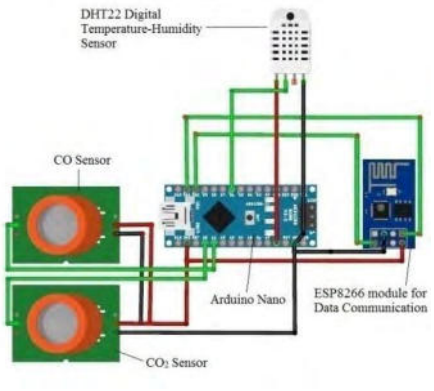

Fig. 3: Circuit schematic of Prototype

The following data was collected from the location named Mohammadpur in Dhaka during October 7-8, 2018, considering time in 24-hour format:

Table 1: Data reading of Prototype between October 7-8, 2018

(Month/Date/Year) Time	Temperature (°C)	Humidity (%)	CO_2 (ppm)	CO (ppm)
10/7/2018 13:11:54	30.5	76	394.31	1
10/7/2018 13:12:54	30.6	75.3	394.31	1
10/7/2018 13:13:54	30.5	75.3	394.31	1
10/8/2018 14:23:51	31.6	73.7	449.4	1
10/8/2018 14:24:51	31.5	74.5	449.4	1
10/8/2018 14:25:51	31.5	74.6	452.28	1
10/8/2018 14:26:51	31.5	76	449.4	1
10/8/2018 14:27:51	31.3	75.2	452.28	1
10/8/2018 14:28:51	31.5	75.8	449.4	1
10/8/2018 14:29:51	31.4	74.8	449.4	1

The above data shows that from October 8th, 2018, CO_2 breaches the 400 ppm barrier and just regularly stays around 450 ppm, which is an alarming increase in today's atmosphere. Considering the type of intense monitoring required from the 400 km altitude, sophisticated sensors, cameras and modules need to be equipped in the APOSat as payload.

7. MICROSATELLITE PAYLOAD:

Due to a number of small payloads [7], a 3 Unit (3U) structured CubeSat will be feasible for the shape of APOSat. It is a rectangular box that has a 3 unit storage space for 3 cube satellites. The high quality camera will accommodate one unit of it and the rest of the modules including gas sensors for measuring data on gaseous substances will be accommodated in the remaining two units. For the attitude control, ADCS-6 (Attitude Determination and Control System-6) attitude controller shield will be used. It also includes a GPS (Global Positioning System) module and a reaction wheel. For efficient power control, P-60 subsystem power module will be used, as the loads chosen will be operated in different voltages. The subsystem has three configurable output voltages per module of 3.3V, 5V, 8V, 12V, 18V and 24V. For effective communication, an S-Band ('S' for Short) radio transceiver will be used as the satellite will have the frequency within the S-Band [8] which is 2.20 to 2.29 GHz. An S-Band patch will also be connected for high speed communication. The patch will have flexible power interface from 8V to 18V. There will be an On-Board Computer (OBC) at one of the units of the satellite which will be the core controller of the satellite. The chosen model for this figure is NanoCom SR2000 (SR meaning S-Band Radio) which is compatible in a 3U structure. For power backups and supply, NanoPower MSP will be used where MSP means Modular Solar Panel. These solar cells are made of GaAs (Gallium Arsenide) and gives 28.5% cell efficiency. The cells will charge up 50 W-hr batteries via an approximately 0.48 m^2 solar radiation. For taking high quality photos Chameleon Imager camera will be used which has 9.6 meter spatial resolution giving high quality photos and high pixel rates in every image. The mass of APOSat is estimated to be around 5.20 kg. The following figures show the structural design and payload distribution of the satellite:

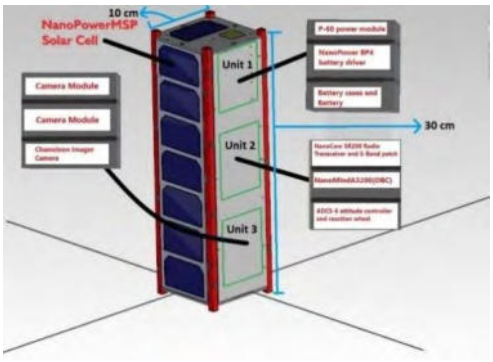

Fig.4: APOSat payload distribution

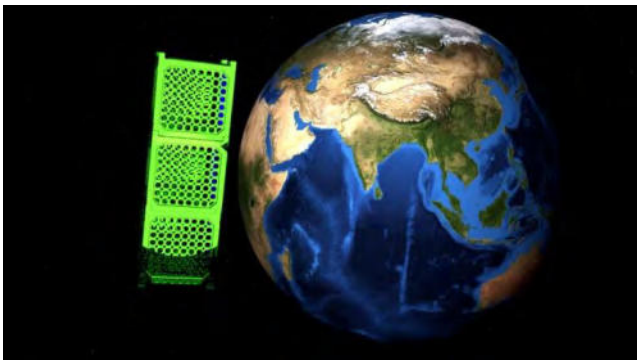

Fig.5: Illustration of APOSat orbiting Earth

8. CONCLUSION:

The average reading of CO_2 from Table 1 data is 433.449 ppm; which is an 8.36% increase from the 400 ppm threshold. That rate will increase more in the coming years and will raise the challenges to improve air quality. The APOSat is one such approach to monitor the air and allow necessary measures to purify from pollutants. For a densely populated city like Dhaka, this will take a long time, but the effectiveness of the APOSat's response to provide air quality data may cut some delay time.

9. FUTURE WORKS:

For further improvement of this APOSat, two developed methods will be taken; one is for reusable temporary drop test; another technique is to integrate the proposed methodology with on-board image processing, combining with Zigbee based communication system. These two methods are planned to be tested with a view to measuring the green house effect in the ozone layer and fetch image data for forecasting weather and natural hazard in Bangladesh.

10. REFERENCES:

[1] GOSAT (Greenhouse gases Observing Satellite) / Ibuki - Satellite Missions - eoPortal Directory. Available online at : https://eoportal.org/web/eoportal/satellite-missions/content/-/article/gosat#footback1 (accessed May 2019)

[2] T. Yokota, Y. Yoshida, N. Eguchi, Y. Ota, T. Tanaka, H. Watanabe and S. Maksyutov, "Global concentrations of CO2 and CH4 retrieved from GOSAT: First preliminary results". Sola, 5, 160-163. (2009)

[3] E. A. Kort, C. Frankenberg, C. E. Miller, and T. Oda, "Space-based observations of megacity carbon dioxide", Geophysical Research Letters, 39, 17. (2012)

[4] G. Quaglione, and M.Giovannoni, "Orbital Inclination Effects on Communications Satellite System Design", IEEE Transactions on Aerospace and Electronic Systems, 19, 3, 447-453. (1983)

[5] Earth Orbit Calculator, http://www.calctool.org/CALC/phys/astronomy/earth_orbit (accessed May 2018)

[6] M. B. Marinov, I. Topalov, E. Gieva, G. Nikolov, "Air quality monitoring in urban environments", 39th International Spring Seminar on Electronics Technology (ISSE),443-448. (2016)

[7] GOMSPACE Payloads, https://gomspace.com/shop/subsystems/default.aspx (accessed May 2019)

[8] L. H. Abderrahmane, M. Benyettou, and M. N. Sweeting, "An S Band Antenna System Used for Communication on Earth Observation Microsatellite", IEEE Aerospace Conference. (2006)

Attitude and orbital dynamics fine coupling for high area-to-mass ratio satellites

Cristiano Contini[1], Camilla Colombo[2]

[1]Department of Aerospace Science and Technology, Politecnico di Milano
Via Giuseppe La Masa 34, 20156
Milano, Italy
Phone: +39 339 67 99 049, Mail: cristiano.contini@mail.polimi.it

[2]Department of Aerospace Science and Technology, Politecnico di Milano
Via Giuseppe La Masa 34, 20156
Milano, Italy
Phone: +39 02 2399 8352, Mail: camilla.colombo@polimi.it

Abstract: ZodiArt iSEE mission is characterised by a set of MicroSat flying in formation and constituting an artificial constellation in the sky, easily recognisable from ground. People can interact with the system using a mobile app to prove the fulfilment of the Global Sustainable Development Goals, [1], obtaining from the constellation a picture of the surroundings, when the formation will pass above the user. In this paper the ZodiArt Attitude, Determination and Control Subsystem simulator is presented, characterised by orbital and attitude dynamics coupling and a complete disturbances model including: Earth zonal harmonics, Moon & Sun third body perturbations, Solar Radiation Pressure, drag and lift. The simulator is capable to provide innovative results about precise relative satellite positioning in a formation flying on Low Earth Orbit. With reference to the ZodiArt iSEE mission, compact plots, here called "Orbital long-track envelopes", will be presented, graphically showing the differential gain/loss in altitude and relative long-track shift obtained performing differential drag, depending on the manoeuvre epoch, angle of attack and true anomaly. Thanks to the tool implemented, these plots can be generalized to every kind of small satellites and orbit.

Symposium topics: Small satellite mission programs, high area-to-mass ratio satellites, attitude, determination and control subsystem, orbit perturbations.

1 INTRODUCTION

The Global Sustainable Development Goals [1] are 17 objectives addressing global challenges such as poverty, inequality, climate, environmental degradation, peace and justice, and they are the focus of the ZodiArt iSEE project, whose mission is characterised by a set of MicroSat flying in formation and constituting an artificial constellation in the sky, easily recognisable from ground. This is possible thanks to high reflective balloons embarked on the top of platforms. The orbit was identified after a trade-off analysis presented in [2], providing good visibility from the most important cities of the world during twilight. The selected orbital elements are reported in Figure 1:

$a(km)$	$e(-)$	$i(°)$	$\Omega(°)$	$\omega(°)$	$\theta(°)$
7266,5	0.001	99	285	0	0

Figure 1: Orbit Keplerian parameters

The constellation will generally point the Nadir direction, performing Earth observation. Each ZodiArt platform is characterised by a 1×1×1 m bus with a global weight of 122 kg (including a 20 % margin) and a 10 m diameter balloon weighting 4.4 kg. Once the

balloon is inflated, the distance between the solar and atmospheric wind centre of pressure and the centre of mass increases to uncommon values for this class of small satellites, inducing great torques on the platforms, even if the altitude is 888 km, where at least drag effects would have been neglected for common spacecrafts. The great challenge for the Attitude, Determination and Control Subsystem (ADCS), equipped with 3 reaction wheels and 3 magnetic torquers, is to maintain a 1° pointing accuracy during Nadir pointing, counteracting the environmental disturbances without saturating the reaction wheels before half a period. After having performed the preliminary simulations assuming the attitude was decoupled from the orbital dynamics, granting the pointing budget requested, the platform coupled dynamics has been analysed, considering the effects of Earth zonal harmonics, Moon & Sun third body perturbations, Solar Radiation Pressure, atmospheric drag and lift, with the aim of building an "Orbital long-track envelope", useful to plan attitude manoeuvres and capable to perform fine relative positioning in the context of formation flying.

2 ORBITAL-ATTITUDE MODEL AND RESULTS

With respect to a reference configuration, the platform configuration with the maximum area exposed to the atmospheric and solar wind lowers the orbit semi-major axis, due to the resulting increase of drag and solar radiation pressure, while the one exposing the minimum area lowers it. According to elementary orbital dynamics, if two bodies are orbiting with different altitudes around the same attractor, they will experience a long-track drift, proportional to the difference in altitude. In particular the body characterised by the higher orbit will shift in the backward direction with respect to the other body and viceversa. Performing differential drag/lift means that the satellite will be exposed to the relative atmospheric wind, in order to achieve a desired long-track position and a certain altitude with respect to another orbiting body, which, in this case, is another satellite of the constellation. Nevertheless, the same concept can be applied to the solar radiation pressure. An attitude-orbit propagator model was developed to this scope, including the effects of atmospheric drag, lift, solar radiation pressure, Moon & Sun third body perturbations and the zonal effects of the Earth gravity field, which integrates the Euler equations and the attitude quaternion, governing the spacecraft angular velocities and attitude dynamics, coupled with the Gauss planetary equations, providing the osculating orbital elements.

2.1 Differential drag/lift

Usually in literature the most exploited perturbation to control a spacecraft is the atmospheric drag only, as reported for instance in [3]. Instead, in this work both lift and drag have been considered and their effects have been evaluated performing many simulations, varying: the initial epoch, spanning from the 6th of December 2018 to the 21th of November 2019, with a time interval of 15 days, and the cross exposed area, spanning from 0° to 90° the bus inclination with respect to the velocity vector, since the balloon exposed surface is always the same. This has been performed with respect to a reference configuration attitude, inclined of 45°, integrating over one orbital period. The results are collected in Figure 2, that represents the "Orbital long-track envelope", showing the differential height and shift achieved performing a differential drag/lift manoeuvre, under the effect of all the previously mentioned perturbances, at different epochs, in function of the platform angle of attack and given the initial true anomaly.

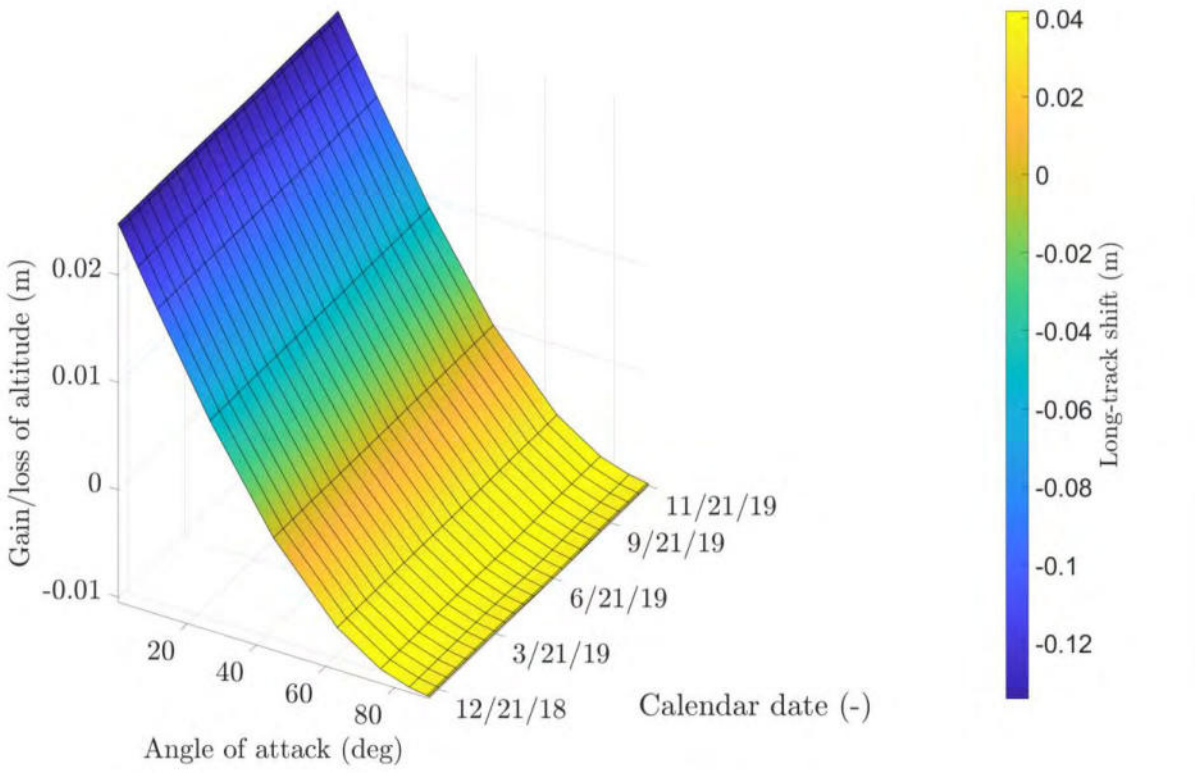

Figure 2: Orbital envelope due to drag effect only.

Figure 2 also evidences, as expected, that differential drag/lift is independent on the Sun position with respect to the orbit and, as a consequence, to initial epoch. Moreover, the gain in altitude and the consequent backward shift are higher with respect to the altitude loss and advancing shift. This is due to the fact that, in the first case, the dynamics is evolving in the same direction of drag, while in the second case it is counteracted by the atmospheric wind. The increase/decrease in altitude after one period is quite small compared to the one achievable at lower orbits with solar sails, but it can still be exploited, especially if the differential drag manoeuvre lasts longer.

2.2 Solar Radiation Pressure effect

The solar radiation pressure effect is strictly related to the Sun position with respect to the orbital plane, resulting in a high dependence on the initial epoch and true anomaly. The very same set of simulations have been performed also considering the solar radiation pressure effect only, resulting in a more complex dynamics due to the fact that the exposed surface orientation is not optimised to point the Sun, but it is oriented towards the relative atmospheric wind. Close to the spring and autumn equinoxes the effects of the solar radiation pressure are the lowest, since the Sun is almost orthogonal to the orbital plane, acting mostly on the cross-track orbital evolution rather than the long-track one. However, the most interesting effect is that the gain/loss in altitude and shift are related to the true anomaly initial condition, since it drives the illumination initial condition: in fact, if the platform starts the manoeuvre at the end of the eclipse period, it will fully exploit the solar wind acceleration, lowering its orbit the most. This happens at $\theta = 90°$ during summer solstice and at $\theta = 270°$ close to winter solstice, as shown in Figure

3 and Figure 4. During the summer solstice, ZodiArt platform begins its manoeuvre in eclipse, with declination almost null, meaning that, after less than a quarter of orbit, it will start to experience solar radiation pressure, accelerating while covering the illuminated part of orbit, and finally continuing to slightly move in the direction of perturbation once entered in eclipse, due to the inertia acquired. During the winter solstice, on the contrary, the spacecraft is characterised by almost null declination but it is in Sunlight, meaning that the perturbative acceleration will affect the spacecraft for slightly more than a quarter of orbit, then it will enter in eclipse and finally it will experience again the solar wind pressure. This means that, in the second case, the platform can not continuously accelerate in the illuminated half of orbit, resulting in a reduced gain/loss of altitude.

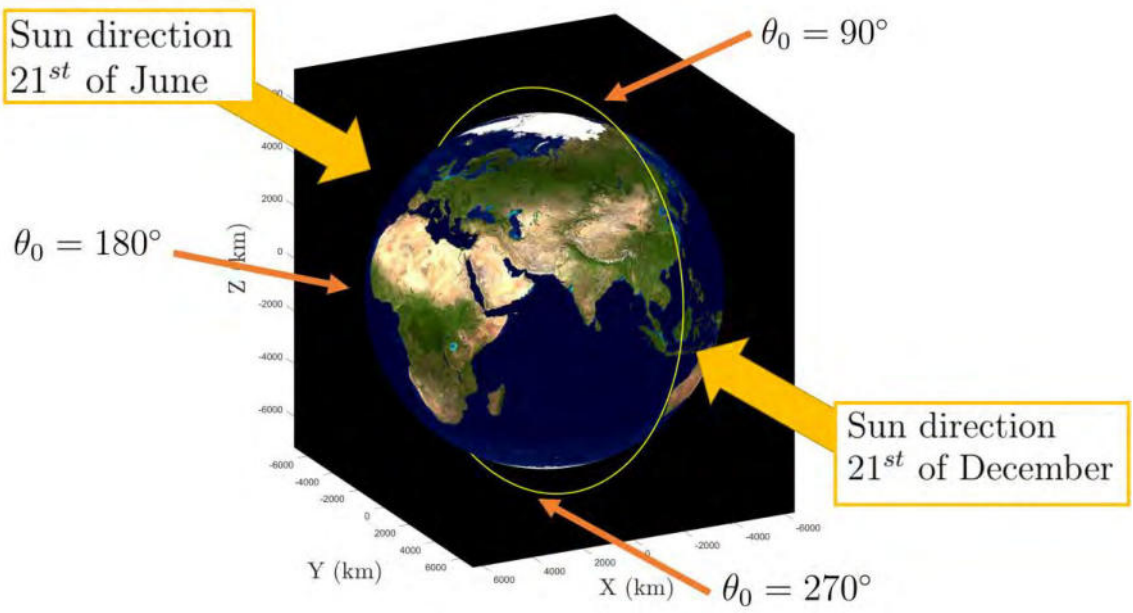

Figure 3: Orbit and platform Sun exposition depending on initial θ true anomaly and date.

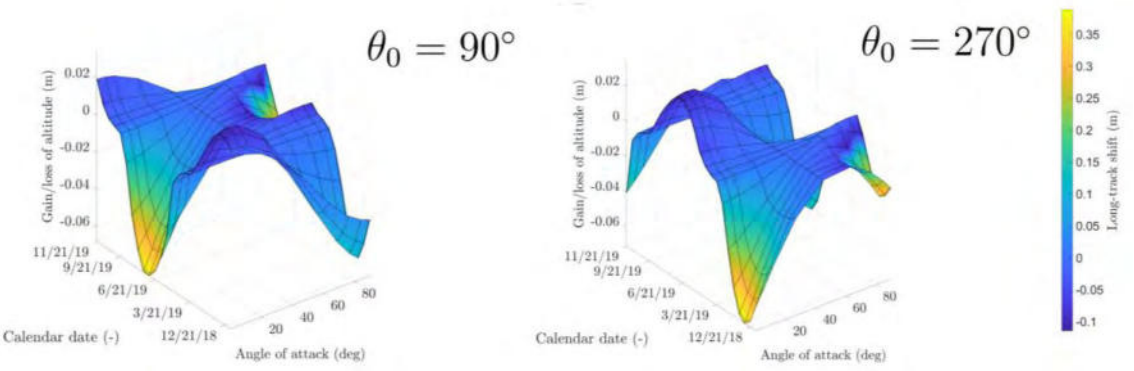

Figure 4: Orbital long-track envelope related to solar radiation pressure effect only.

In particular:

- At $\theta_0 = 90°$, the 21st of June 2019, the platform starts the manoeuvre just at the end of the eclipse, maximizing the acceleration due to SRP and, as a result, the deepest peak is reached.
- At $\theta_0 = 180°$, the spacecraft does not exploit completely the acceleration due to solar radiation pressure.
- At $\theta_0 = 270°$, the dynamics is the opposite to the $\theta_0 = 90°$ case, since the spacecraft can exploit the overall perturbative acceleration only during the winter solstice.

2.3 Differential drag, lift and SRP

In Figure 5 the SRP and drag/lift differential cumulative effects are represented and it is possible to appreciate that in correspondence of equinoxes the gain and loss in altitude are the same achievable with differential drag only, while in the remaining periods of the year SRP is the driving perturbation. In the case of different initial true anomalies, the same trend evidenced with the solar wind long-track envelopes is obtained.

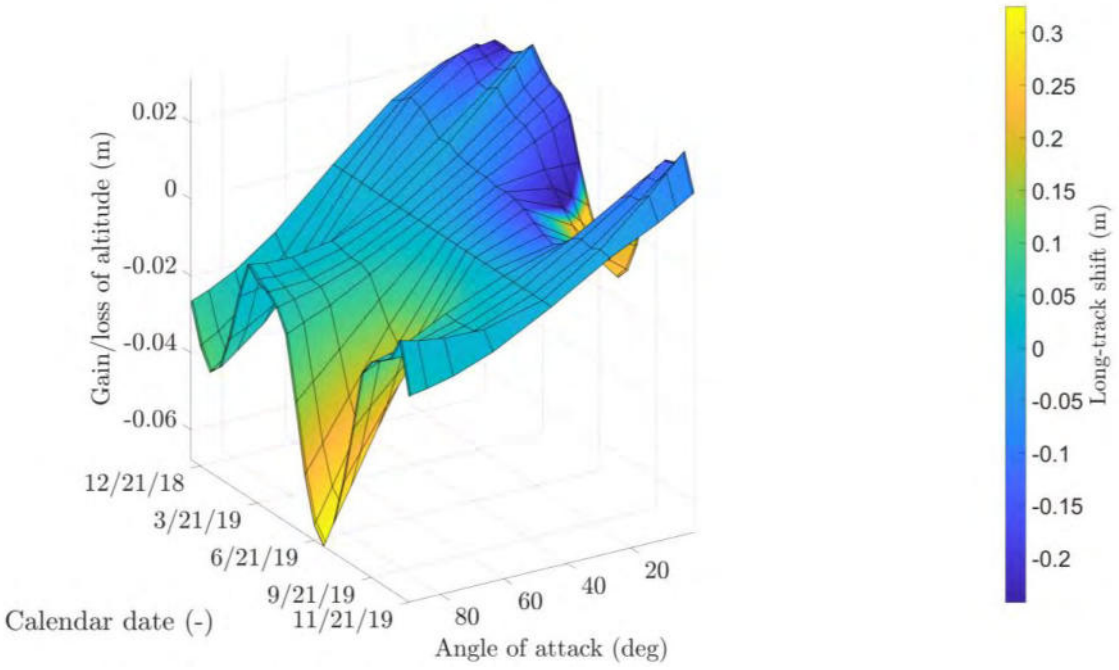

Figure 5: Orbital long-track envelope related to solar radiation pressure and lift/drag at $\theta = 0°$.

3 LONG-TERM DIFFERENTIAL DRAG

It has been demonstrated that, during equinoxes, differential drag can be exploited, independently from solar wind, to control the spacecraft. However, the differential height and shift acquired are quite small compared to the ones achievable at lower orbits and equipped with solar sails. For this reason, long-term differential drag/lift manoeuvres can be inspected to increase the effects of these perturbation.

In order to test one of these manoeuvres, a reference scenario was selected: three simulations, with the same initial condition but the initial orientation with respect to the velocity vector ($\boldsymbol{q}_0$), were performed over 10 periods with initial epoch at the spring equinox. In particular:

- The reference configuration: tilted of 45° with respect to the velocity vector.
- The advancing configuration: characterised by the maximum exposed surface, which will lower the altitude and shift in the same direction of velocity vector.
- The receding configuration: characterised by the minimum surface exposed, which will rise the altitude and shift in the opposite direction of velocity vector.

Together with solar radiation pressure and drag/lift, also Earth oblateness and Moon/Sun third body perturbation were considered. During the manoeuvre, all the three spacecrafts experience saturation of the wheels, resulting in loss of pointing accuracy when the reaction wheels (RWs) cannot provide the desired torque anymore. The dynamics is shown in Figure 6, where the plots in the first line represent the reaction wheels angular momenta, while the ones on the second raw, the pointing error.

In order to help the reader to visualise the scenario, an animation performed with STK by AGI was created, animating the results obtained in Matlab™. In Figure 7 a frame is shown, representing the three platform configurations position after 10 orbits, while in Figures 8 and 9, the resulting shifts are reported. If supported by the pdf reader used, it is possible to animate the frame by clicking on the image.

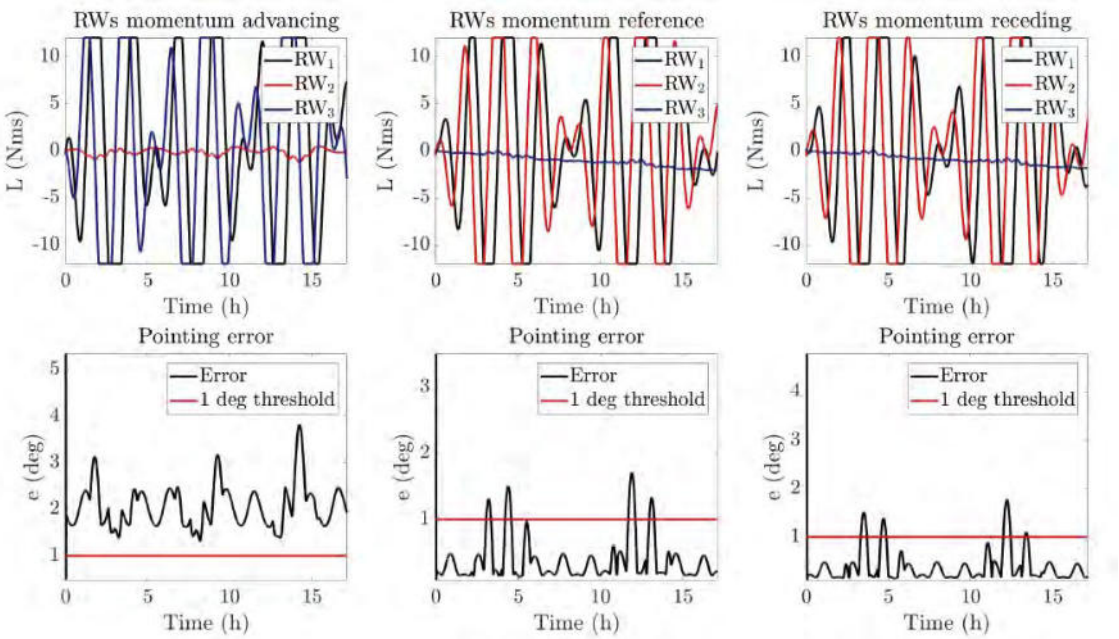

Figure 6: Saturation during 10 periods performing differential drag and pointing error (*e*).

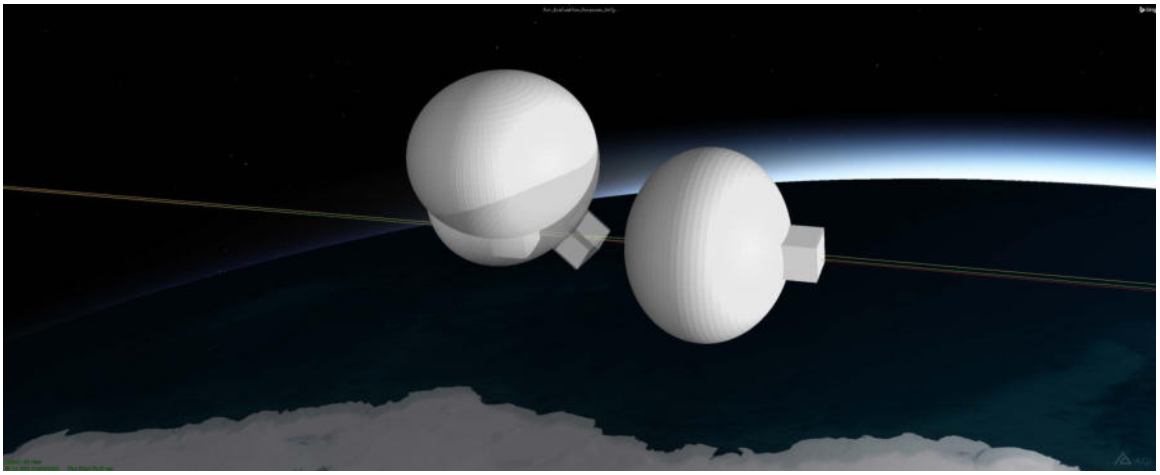

Figure 7: STK by AGI animation over 10 orbits. The transparent platform is the reference configuration tilted of 45° in the direction of the velocity vector.
If supported by the pdf reader used, it is possible to animate it by clicking on the image.

Moreover, the same trend evidenced in Figure 2 is evidenced also in this case: the platform rising its orbit acquires more height in altitude with respect to the one lost by the platform lowering its orbit, because, in the first case, the dynamic evolution is in the same direction of drag action, while, in the second case, it is partially counteracted by drag and lift. In conclusion, performing a manoeuvre lasting 10 periods it is possible to achieve a gain in altitude of 0.29 m, with a correspondent backward shift of -12.6 m, and a loss in altitude of -0.12 m, with a frontward shift of 3.9 m, with respect of the orbital motion.

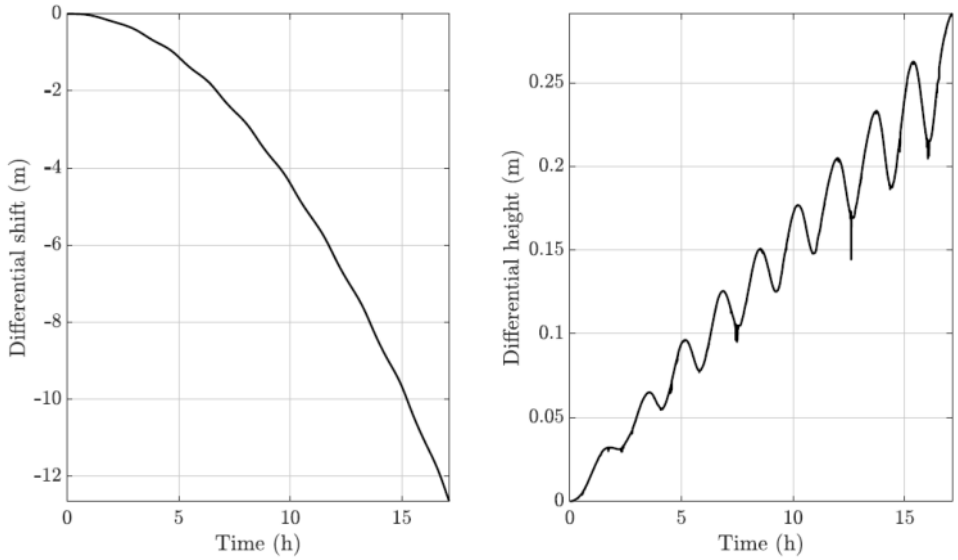

Figure 8: Receding configuration gain altitude and shift in 10 periods.

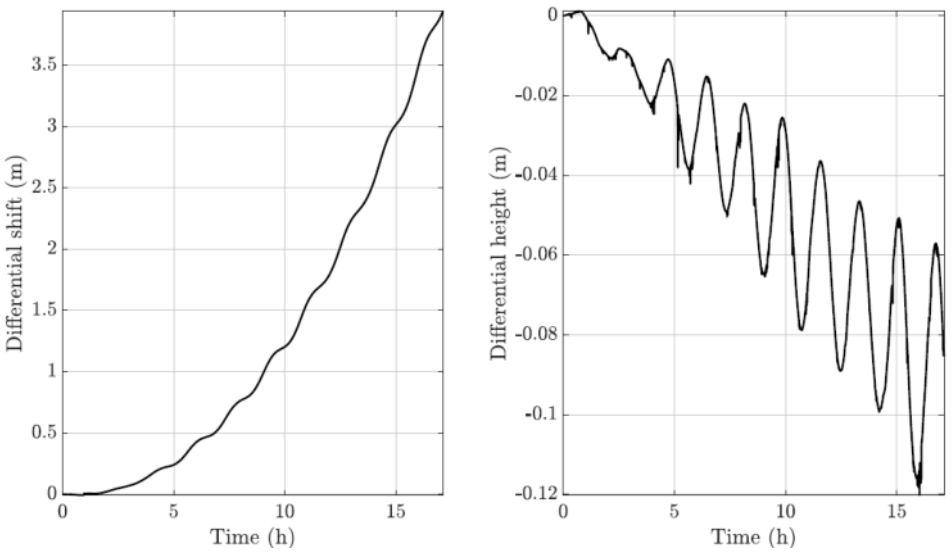

Figure 9: Advancing configuration gain altitude and shift in 10 periods.

4 CONCLUSIONS

The developed simulator is capable of providing "Orbital long-track envelopes" for any kind of small satellite, under the effects of all the major environmental disturbances, such as the Earth zonal harmonics, the Moon and Sun third body perturbations, solar radiation pressure, atmospheric drag and lift and considering the fine coupling between attitude and orbital dynamics. Performing differential drag during solstices maximises the loss in altitude with correspondent forward shift and accepting a pointing error of some degrees, it is possible to perform long-term differential drag/lift manoeuvres, increasing the platform shifts in altitude and in long-track distance. For the mission analysed the best times of the year to perform differential drag are the equinoxes, while differential solar radiation pressure is advisable to be exploited during solstices. These results become fundamental when considering small satellites flying in formation, as for ZodiArt iSEE mission. Future developments of this work could be the improvement of the simulator including the sensors bias estimation performed by the Kalman filter and an orbital estimator or the implementation on a dedicated machine to interface also the hardware to the software.

5 REFERENCES

[1] About the Sustainable Development Goals. Sept. 2018, url: https://www.un.org/ sustainabledevelopment/.
[2] Roccioletti M. P., "Mission Analysis and concept design for a reflective balloon mission", Department of Aerospace Science and Technology, MSc Thesis, Politecnico di Milano, 2018, Supervisor: C.Colombo.
[3] Gurfil P. "Long-Term Cluster Flight of Multiple Satellites Using Differential Drag", Journal of Guidance Control and Dynamics, Nov. 2013, Vol. 36, No.6, pp.1731-1740, doi:10.2514/1.61496.

ACKNOWLEDGEMENTS: The research leading to these results has received funding from the European Research Council (ERC) under the European Union's Horizon 2020 research and innovation programme as part of project COMPASS (Grant agreement No 679086). The animations produced with STK by AGI have been possible only thanks to Fabrizio Gemma, GMSPAZIO Marketing Manager, who allowed me to have part of the software's Pro licence.

PCB design and layout for future TUPEX missions optimized for manufacture and verification

Brian Treacy

Technische Universität Berlin
Marchstr. 12, 10587 Berlin, Germany
Phone: +49 1749 767273, Mail: brian.treacyhotmail.com

Abstract: The TUPEX (Technical University of Berlin Pico EXperiment) student project is a re-occurring opportunity for students within the Technische Universität Berlin to design and build a CubeSat like system which can perform space related experiments. This system, similar to a CubeSat, is called Free-Falling Unit (FFU) due to it not reaching an orbital velocity. The FFU is launched on board of a sounding rocket to approximately 80km altitude where it experiences about two minutes of micro gravity to conduct experiments. The system then free falls back to the ground where a recovery of the FFU can be attempted.

As per TUPEX-6, future TUPEX missions, will comprise of sub-systems such as on-board computer (OBC), electrical power system (EPS), attitude determination and control (ADCS) and printed circuit board (PCB) payloads. An improved baseline PCB, which has a standardized layout for common components, will aid in the manufacturing and verification of each sub-system. This new baseline PCB layout is driven by common requirements for all PCB mounted sub-systems which are expected in future missions. Future TUPEX projects will benefit from spending less time to develop, manufacture and verify TUPEX PCBs.

1. INTRODUCTION

The TUPEX-6 mission was a participant of the German-Swedish student program REXUS/BEXUS where student teams from across Europe can carry out scientific and technological experiments [1]. TUPEX-6 FFU was launched on board of the RX26 sounding rocket from Esrange, Sweden, in mid-March 2019 as shown in Figure 1. In all TUPEX missions, experiments are situated within their module, where multiple modules stack upon each other to make the rocket body. After launch, the FFU is ejected from its experiment module using the deployer. Once away from the experiment module, it is in free space, free falling in a micro-gravity environment.

Figure 1 Launch of RX26 and the TUPEX-6 experiment [1]

Once in the micro gravity environment, payloads are operated, and experimental data recorded. Later in the free fall, the parachute is deployed, and the tracking device enabled. It is expected that future TUPEX mission will conduct a similar mission timeline and demonstrate similar versions of the payload used on TUPEX-6 with different geometries and additional PCB mounted payloads. The TUPEX-6 FFU mission objective was to demonstrate the operation of attitude control actuators while in the milli-gravity environment.

1.1 FFU Bus

The TUPEX-6 system architecture allows for up to five PCBs, that can be fitted within the frame crated by its attitude control actuators. Additional PCBs can be positioned both above and below this frame as required. Due to the high quantity of possible PCBs variations within a TUPEX bus, it is necessary to have a new baseline PCB layout from which any sub-system can be built upon to reduce the development, manufacturing and verification time.

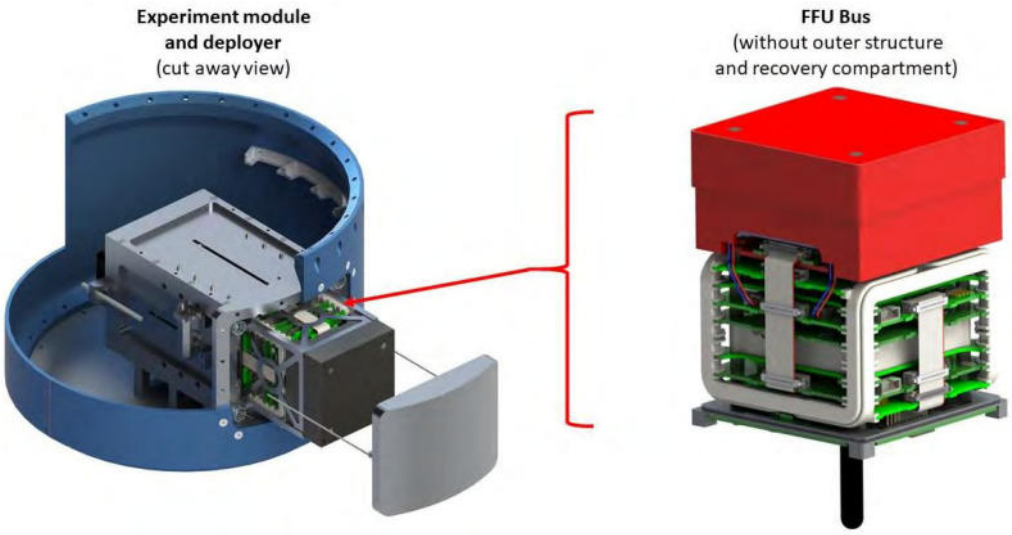

Figure 2 Section view of ejecting FFU and TUPEX-6 electrical bus/payload [2]

The FFU contains a bus which supports a recovery sub-system and a payload. The recovery sub-system contains a commercial off-the-shelf tracking device, parachute and parachute deployment mechanism. The payload comprises of four of attitude control actuators.

The purpose of these actuators is to allow for a precise attitude control for picosatellites [3]. The purpose of these actuators is to be an alternative attitude control system solution to what is currently available for CubeSat, like reaction wheels. Figure 2 shows an image of the FFU ejecting from the deployer, which is mounted within the experiment module, and an image of the TUPEX-6 electrical bus with integrated payload. Prior to launch the TUPEX-6 FFU was fully functional. The FFU was successfully deployed and other elements of the mission performed nominally. However, the TUPEX-6 mission failed to achieve its objectives due to an unknown failure at lift-off of the FFU.

2. DISCUSSION

Issues experienced with TUPEX-6 PCBs can be grouped into three groups: development, manufacturing and verification.

Development: due to multiple subsystems being developed in parallel, PCB layouts for each subsystem such as EPS, OBC and communications are unique to each PCB, with no standardization for common functions between PCBs (e.g. micro controller peripherals and controller area network (CAN) transceivers).

Manufacturing: for assembly, a significant amount of time was lost due to rework on each of the boards. This rework included: fixing component placement, troubleshooting electrical components which have become damaged due to additional heat while reworking and solder bridges across feet of surface mounted packages. Each subsystem used different types of footprints for the same parts. Global settings for traces, pours solder mask and solder pads were not consistent between designs.

Verification: when verifying the functionality of each PCB mounted sub-system, other inefficiencies were found. Test points which were circular solid pad footprints on the PCBs would wear out due to repeated use with probes. Box headers housings on each PCB would become damaged due to repeated connecting and disconnecting of to EGSE. In addition, individual pin-out tables for connectors on each side of the board were chosen which made each board susceptible to being incorrectly connected to EGSE. Finally, when testing sub-systems together, the assembly in some cases would need to be disassembled in order to flash each PCB.

These issues increased time and effort required to make a final working board suitable for integration and testing with other boards, delaying the progress of the project. Other consequences were cost, material and time waste incurred through having to replace components and re-ordering of new PCBs. These differences increased the complexity and time spent on development, manufacture and verification. From these lessons learnt, several design requirements have been derived for an improved new PBC baseline design.

2.1 BASELINE PCB REQUIREMENTS

The baseline PCB layout will be required to meet the following set of requirements which have been found to be applicable to all sub-systems mounted PCBs. Not all new requirements that resulted in design improvements have been included for the sake of brevity.

1. The PCB shall be programmable over UART and JTAG.

2. Common components between sub-systems should form part of the baseline PCB.

3. All footprints for passive parts should be hand solderable and of the same size when possible.

4. Tests points for all power and data lines should have the same location and footprint between board.

5. All PCB micro controllers should be programmable through one common interface, when assembled.

2.2 Baseline PCB layout

The layout for the new baseline PCB can be seen in Figure 4. It shows the positioning of all common components between expected sub-systems. The purple region highlights the micro controller, two CAN transceivers (one for redundancy) and their supporting passive components. The area required for an SD card connector was also included if future missions decide to make this a common component for each board.

To support verification and testing of each sub system, the new baseline board has one power LED (red) and two debugging LEDs (green and blue) found in the yellow regions. Each power line and data line have their own test points, see red regions. The board can be programmed via UART connector seen in grey and JTAG pogo pads seen on the underside of the board in blue. Using the test points, JTAG and UART pads an EGSE PCB with pogo pins could program, debug and test the functionality of each subsystem.

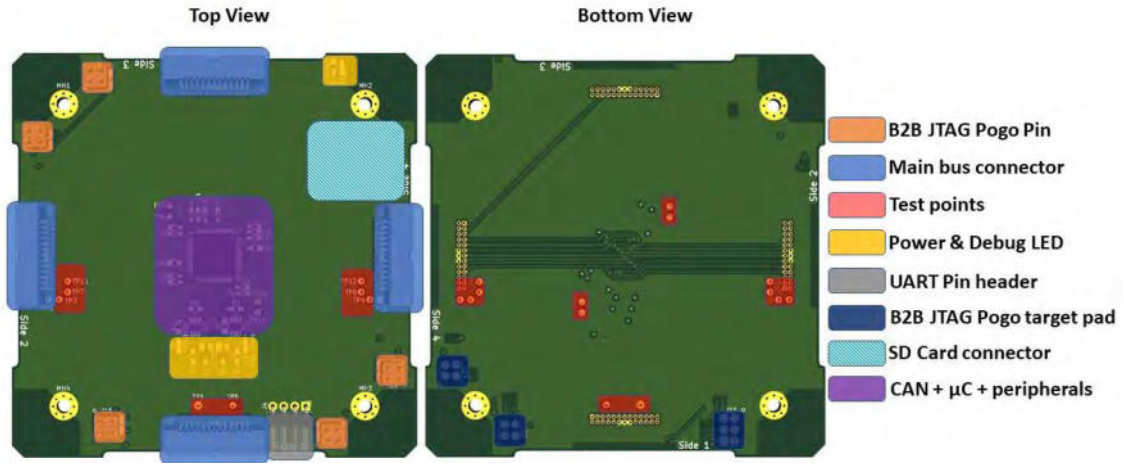

Figure 3 Baseline PCB component positions

All common passive components (e.g. LEDs, resistor, inductors and capacitors) have an imperial 0603 footprint. Footprints for other packages such as SOT-23, SOIC8 and LQFP have been assigned with hand solderable footprints. Experience from TUPEX-6 showed that hand solderable footprints (excl passives components) were simpler to rework when required.

Pogo Pin connectors

Pogo pin connectors are used on this baseline PCB to daisy chain all micro controllers through their JTAG programming interface. Populating the positions shown in Figure 4 with pogo pins will connect each TDI and TDO pin appropriately to the micro controller above. Using the 26-position connector to daisy chain between micro controllers is pos-

sible but is an inefficient use of connector pins. The total number of connector pins dedicated to daisy chaining would be equal to the number of micro controllers plus one. The selected pogo pin connector has a mid-stroke height of 4.9mm which is suitable for the current between board height of 4.8mm.

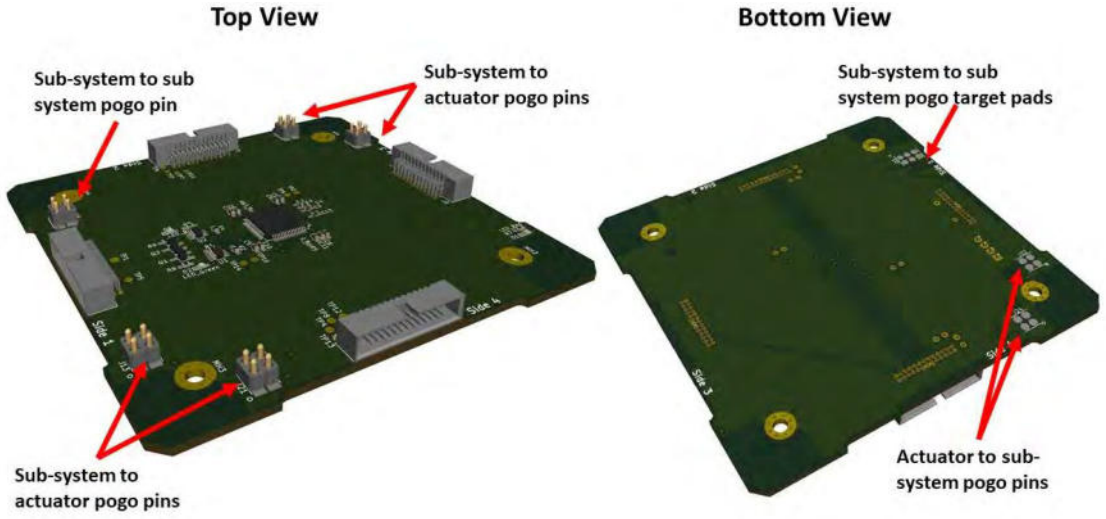

Figure 4 Baseline PCB pogo pins and target pads

It was considered to use this pogo pin connector for data and power lines, to remove the need for a ribbon cable on all four sides of the FFU bus. This option was found not be feasible due to the high number of lines and the minimum pitch of supplied pogo pins being 100 mil. The footprint of such pogo pin connector is not practical and does not compete with the 50 mil spacing of the 26 position connector.

Power and Data line bus

Each side of the PCB can be connected to the ribbon cable power and data line bus via a 26-position connector. The pin-out for each side is identical and allows flexibility for each subsystem. The power and data line bus carries the following shown in **Error! Not a valid bookmark self-reference.**;

Table 1 Power and Data line bus

Power lines	12V	5V	3V3	GND	$V_{battery}$	V_{charge}
Data lines	PPS	WDT	CAN High (x2)	CAN Low (x2)	CAN Select (x2)	

Repeated connecting of the female ribbon cable connector can damage the male connectors box housing on the board. The housing lifts and rotates about its solder joint to the board when the required amount of pressure is applied to insert the female connector. The effect applies unwanted strain on the solder joint which would break due to fatigue.

To mitigate against this, a small amount of glue should be applied near the edge of the mating area between the PCB and the connector housing. On the new baseline PCB, the

glue mating area is masked, exposing the FR-4 material. Figure 5 shows the prepared glue mating area.

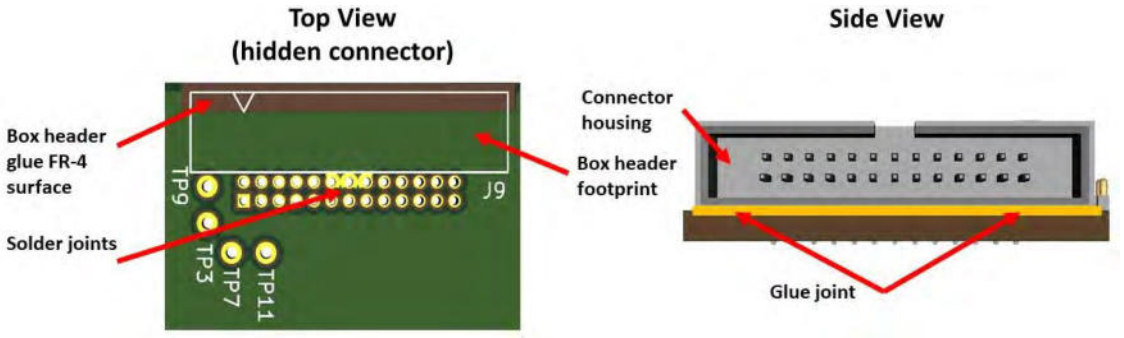

Figure 5 Connector (26 position) glued mating area

4. CONCULSIONS

The new baseline board design has shown that it is feasible to meet these requirements whilst maintaining the existing FFU architecture and using off-the self-components. Future work on enhancing the baseline board design should focus on improving the board to cable connector. It should be taken under consideration to remove the board to cable connectors on the side of each PCB with ultra-low-profile board to board connectors. These connectors supplied by SAMTEC could eliminate the need for a cable harness along each side of the FFU and potentially the need for the pogo pin interface. This option was not included in this proposed new baseline PCB due to time constrains.

Future TUPEX missions should use a standardised PCB similar to the one proposed in this paper to reduce the workload required to make their system flight-ready and increase the likelihood of mission success. Lessons learnt from the previous TUPEX-6 missions have been captured in a new set of requirements that are applicable to future missions, and future missions should expand on these requirements as appropriate.

5. AKOWLEDGEMENTS

Gratitude is given to the TUPEX-6 team for their support and participation in the project, in particular to the electrical and software teams whom spent many hours aiding the creation of the TUPEX-6 PCBs. Special thanks are shared with project advisors: Sebastian Grau, Martin Buscher, Jens Großhans and other members of the TU Berlin's Chair of Space Technology who provided technical assistance to student team members over the entire project duration. Finally, special gratitude is shared with all the entities of the REXUS/BEXUS: DLR, SNSA, ESA, ZARM, MORABA and Eurolaunch for providing the project the opportunity to be launched on RX26.

6. REFERENCES

[1] REXUS/BEXUS, RX26 Launch Photo, (Mar 2019)
[2] Blogs.tu-berlin.de, (2019), TUPEX-6, [online] Available at: https://blogs.tu-berlin.de/space_tupex6/ [Accessed 4 May 2019].
[3] S.Grau, An angular momentum ring storage device prototype for CubeSats based on a liquid metal actuator. IAC-15-C1.6.8

Semi-Passive Three Axis Attitude Stabilization for Earth Observation Satellites using the Drag Maneuvering Device

Sanny Omar[1], Camilo Riano Rios[1], Riccardo Bevilacqua[1]

[1]University of Florida
939 Sweetwater Dr., Gainesville, Florida, United States
Phone: +1-352-846-1477, Mail: sanny.omar@gmail.com

Abstract: The rise of small satellites has led to many missions with simple attitude and orbit control requirements. For example, a small Earth imaging satellite may require keeping one face nadir pointing within 10 degrees while maintaining a slot in a low Earth orbit within ± 100 km. However, legacy attitude and orbit control techniques including reactions wheels and thrusters can easily cost hundreds of thousands of dollars and provide more control capability than is needed for such a mission.

This paper introduces the Drag Maneuvering Device (DMD) that could replace such systems on many missions and consists of four retractable tape spring booms deployed in a dart configuration. The DMD can actively modulate the drag area of the host satellite for orbital maneuvering and post-mission disposal while providing passive 3-axis attitude stability using aerodynamic and gravity gradient torques. Magnetorquers integrated into the DMD damp attitude oscillations and help ensure the satellite stabilizes with the correct face nadir pointing. An overview of the DMD design is provided in this paper and the results of the attitude and orbit simulations used to characterize the DMD performance and devise a control and operations methodology are detailed.

1. INTRODUCTION

Attitude and orbit control have been important considerations since the early days of space exploration [1]. Traditionally, attitude control has been performed using reaction wheels, control moment gyros, and thrusters, and orbit control has been performed using thrusters [2], [3]. These legacy attitude and orbit control systems have been complicated and expensive, but highly accurate and rapidly responding, making them well suited to large, high-budget satellite missions. Alternative attitude and orbit control methodologies using environmental forces and torques have been proposed [4] and have become particularly valuable in recent years with the introduction of small satellites such as CubeSats [5] that lack the volume, power, or budget for the legacy systems. Aerodynamic drag force is a naturally occurring effect that is dependent on the satellite's orientation, geometry, and orbital regime [4]. Aerodynamic drag has been utilized for orbital maneuvering, and methods for using aerodynamic torques for attitude control have been investigated in prior literature [6]. Gravity gradient torques are dependent on the spacecraft moments of inertia and can be harnessed for attitude stabilization through the use of a gravity gradient boom [3], [7]. In low Earth orbits, electromagnets (called magnetorquers) embedded in the satellite can interact with the Earth's magnetic field to impart torques on the satellite. Magnetorquers have commonly been used for detumble and for reaction wheel de-saturation [8]. These effects have been investigated for attitude control in prior literature, but prior solutions either do not provide 3-axis attitude control or require actuators like thrusters or wheels to provide complete control that is robust and reliable. Methods that do investigate 3-axis attitude control would require costly sensors to provide 3-axis attitude determinations. Techniques that use aerodynamic torques for ram-alignment [6], gravity gradient torques for zenith alignment [7], or magnetic torques for magnetic field alignment [9] all leave one axis of rotation unconstrained. To date, there is no device or control

solution to the authors' knowledge that facilitates aerodynamically based orbital maneuvering while enabling 3-axis attitude stabilization without the need for attitude determination.

This paper introduces the Drag Maneuvering Device (DMD) which provides such an attitude and orbit control solution. The theory, operations, and control methodology behind the DMD are discussed and a 6DOF high fidelity attitude and orbit model is introduced to validate the semi-passive 3-axis attitude stabilization of the DMD.

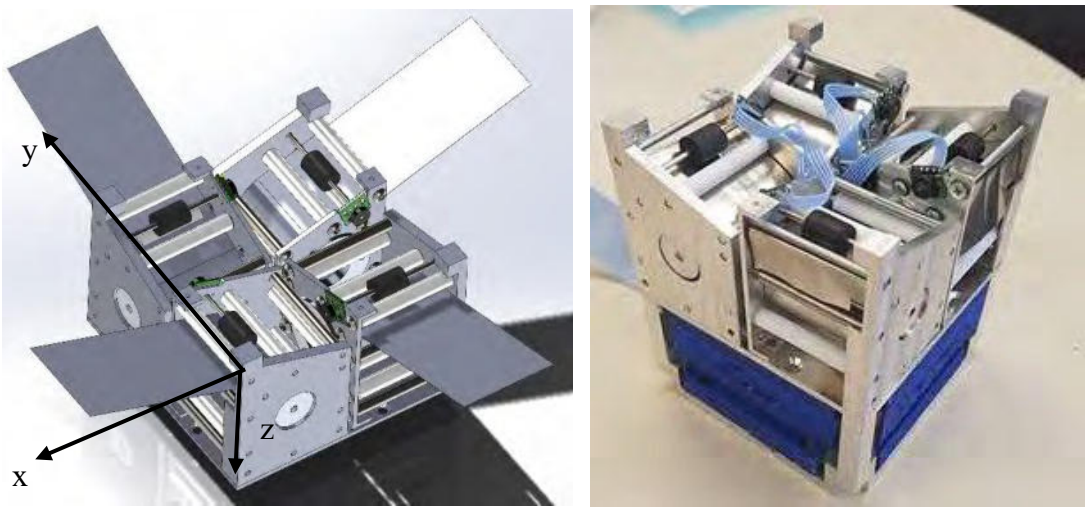

Figure 1. Drag Maneuvering Device (DMD) CAD model and Prototype

2. DRAG MANEUVERING DEVICE DESIGN

The Drag Maneuvering Device (DMD), formerly called the Drag DeOrbit Device (D3) [10], consists of four tape spring booms, each 3.7 m long and 4 cm wide, inclined at a 20 degree angle relative to the face of the satellite to which the DMD is attached as shown in Figure 1. The booms are deployed in this shuttlecock configuration to provide passive aerodynamic attitude stability. Additionally, one pair of opposing booms can be partially retracted while the other pair is fully deployed to create a clear minimum moment of inertia axis along the direction of the deployed booms. Gravity gradient torques

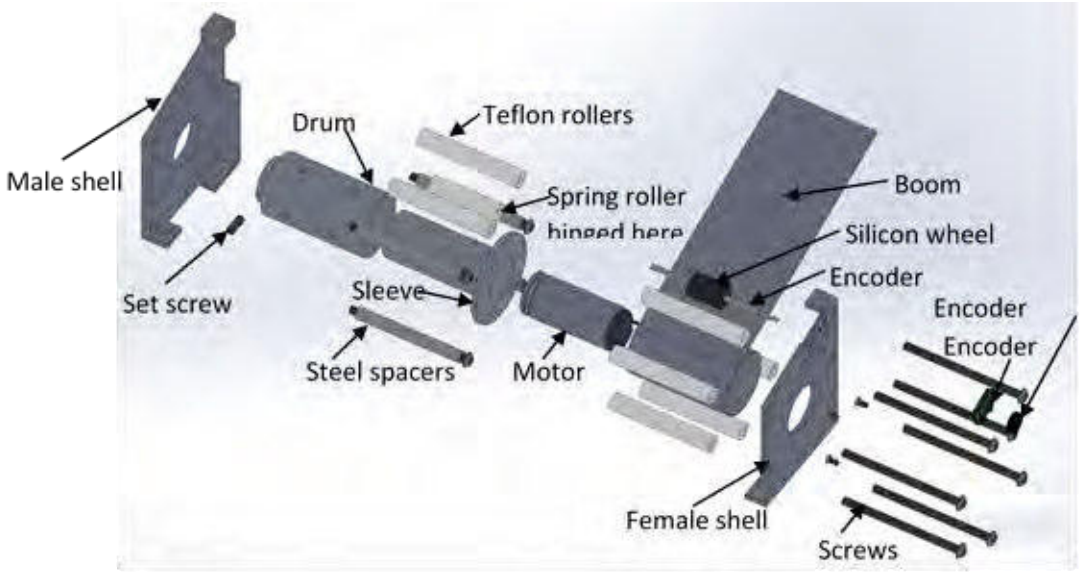

Figure 2. DMD Deployer Expanded View

will then work to passively align this axis with the nadir or zenith vector. Running the B-Dot de-tumble law [7] using magnetorquers embedded in the DMD serves to damp initial satellite rotation rates and the attitude oscillations that will persist after boom deployment. The combination of aerodynamic, gravity gradient, and magnetic torques generated by the DMD provide 3-axis attitude stabilization and ensure that a single face of the satellite is pointing toward Earth with negligible power usage after the initial detumble and stabilization. As a bonus, the DMD booms can be collectively deployed or retracted to vary the cumulative aerodynamic drag experienced by the satellite which can be utilized for orbital maneuvering, constellation phasing, collision avoidance, and controlled re-entry [11]. Each DMD deployer (Figure 2) contains a brushed DC motor (Faulhaber 1516-006SR with 262:1 spur gearbox) that drives a drum to which the boom is connected. As the motor rotates, the boom deploys and drives a rotary encoder that precisely measures the amount of boom deployment.

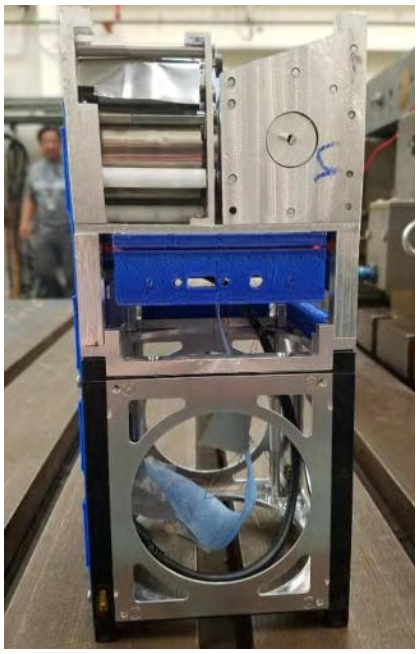

Figure 3. Prototype of DMD with CubeSat Structure

The DMD attaches to a host CubeSat via a structural interface adapter that also contains the magnetorquers wrapped around 3D printed Ultem brackets, increasing its size by 1U and increases the drag area by up to .5 m^2. DMD mass is approximately 1.3 kg. Figure 3 shows a DMD prototype attached to a 1U CubeSat structure to make a 2U CubeSat form factor.

3. ATTITUDE AND ORBIT SIMULATION FRAMEWORK

To simulate the attitude and orbital dynamics of the satellite, a 6 degree of freedom numerical attitude and orbit propagator was created. The satellite state vector was $\boldsymbol{x} = [\boldsymbol{r^T} \quad \boldsymbol{v^T} \quad \boldsymbol{q^T} \quad \boldsymbol{\omega^T}]^T$ where $\boldsymbol{r}$ is the satellite position vector in the ECI (Earth Centered Inertial) frame, $\boldsymbol{v}$ is the ECI velocity vector, $\boldsymbol{\omega}$ is the angular velocity of the satellite body frame with respect to the ECI frame, and $\boldsymbol{q}$ is the quaternion defining the rotation from the ECI frame to the satellite body frame. $\boldsymbol{q}$ is defined as [12]

$$\boldsymbol{q} = \begin{bmatrix} \hat{\boldsymbol{e}} \sin(\theta/2) \\ \cos(\theta/2) \end{bmatrix} = [q_1 \quad q_2 \quad q_3 \quad q_4]^T \tag{1}$$

Such that a rotation of the ECI frame by angle θ about axis $\hat{\boldsymbol{e}}$ would align it with the spacecraft body frame. At each time step the state derivative is computed and numerically integrated using the RK78 numerical integration method [13].

$$\dot{\boldsymbol{x}} = [\boldsymbol{v^T} \quad \dot{\boldsymbol{v}}^{\boldsymbol{T}} \quad \dot{\boldsymbol{q}}^{\boldsymbol{T}} \quad \dot{\boldsymbol{\omega}}^{\boldsymbol{T}}]^T \tag{2}$$

Where [12]

$$\dot{\boldsymbol{q}} = \frac{1}{2}\begin{bmatrix} q_4 & -q_3 & q_2 & q_1 \\ q_3 & q_4 & -q_1 & q_2 \\ -q_2 & q_1 & q_4 & q_3 \\ -q_1 & -q_2 & -q_3 & q_4 \end{bmatrix}\begin{bmatrix} \omega_x \\ \omega_y \\ \omega_z \\ 0 \end{bmatrix} \tag{3}$$

$$\dot{\boldsymbol{\omega}} = \boldsymbol{I^{-1}}\left(\boldsymbol{T_{net}} - \boldsymbol{\omega} \times (\boldsymbol{I\omega})\right) \tag{4}$$

$$\dot{\boldsymbol{v}} = \frac{\boldsymbol{F_{net}}}{m} \tag{5}$$

Where $\boldsymbol{I}$ is the satellite moment of inertia about the center of mass, $\boldsymbol{T_{net}}$ is the net torque, $\boldsymbol{F_{net}}$ is the net force, and m is the satellite mass. The effects of Earth's non-uniform gravitational field on the orbit are modeled using the EMG2008 gravitational model with spherical harmonics through degree and order ten [14]. The gravitational force including the most significant perturbation (J_2) can be computed by [15]

$$\boldsymbol{F_g} = -\frac{\mu_e}{r^3}\boldsymbol{r} + \left(\frac{3J_2\mu_e R_e^2}{2r^5}\begin{bmatrix} r_x(5r_z^2/r^2 - 1) \\ r_y(5r_z^2/r^2 - 1) \\ r_z(5r_z^2/r^2 - 3) \end{bmatrix}\right) \tag{6}$$

Where R_e is the equatorial radius of the Earth, μ_e is earth's gravitational parameter, and J_2 is a constant related to the oblateness of the Earth. To compute the aerodynamic drag force and torque acting on the spacecraft, the satellite is discretized into a collection of rectangular panels. The aerodynamic force acting at the centroid of each panel is calculated by

$$\boldsymbol{F_p} = -\frac{1}{2}C_d A \rho v_\perp \boldsymbol{v}_\perp \tag{7}$$

Where C_d is the drag coefficient, ρ is ambient density, A is the surface area of the panel, and $\boldsymbol{v}_\perp$ is the projection of the velocity vector relative to the atmosphere ($\boldsymbol{v}_\infty$) along the panel normal vector $\hat{\boldsymbol{n}}_{\boldsymbol{p}}$. If $\boldsymbol{v}_\infty$ and $\hat{\boldsymbol{n}}_{\boldsymbol{p}}$ are more than 90 degrees apart, the panel does not experience any drag force and $\boldsymbol{v}_\perp$ is set to zero. $\boldsymbol{v}_\infty$ and $\boldsymbol{v}_\perp$ are computed by

$$\boldsymbol{v}_\infty = \boldsymbol{v} - \boldsymbol{\omega_e} \times \boldsymbol{r} \tag{8}$$

$$\boldsymbol{v}_\perp = \max(\boldsymbol{v}_\infty \cdot \hat{\boldsymbol{n}}_{\boldsymbol{p}}, 0) \tag{9}$$

Where $\boldsymbol{\omega_e}$ is the rotation rate of the Earth. If $\boldsymbol{r_p}$ is the vector from the satellite center of mass to the panel centroid, the aerodynamic torque resulting from the panel is

$$\boldsymbol{\tau_p} = \boldsymbol{r_p} \times \boldsymbol{F_p} \tag{10}$$

The aerodynamic forces and torques generated by each panel are summed to get the net aerodynamic force and torque. The spacecraft's attitude, position, and moment of inertia tensor are utilized to compute the gravity gradient torques with Eq. 3.155 in [2].

$$\boldsymbol{\tau_{gg}} = \frac{3\mu_e}{r^3}\hat{\boldsymbol{n}} \times (\boldsymbol{J}\hat{\boldsymbol{n}}) \tag{11}$$

Where r is the distance from the center of the Earth to the satellite center of mass, $\hat{\boldsymbol{n}}$ is the nadir vector expressed in the spacecraft body frame, and $\boldsymbol{J}$ is the satellite moment of inertia tensor about the center of mass. Finally, the magnetic torques acting on the satellite are given by [2]

$$\boldsymbol{\tau_{mag}} = \boldsymbol{\mu} \times \boldsymbol{B} \tag{12}$$

Where $\boldsymbol{\mu}$ is the spacecraft magnetic moment vector and $\boldsymbol{B}$ is the Earth's magnetic field vector.

4. CONTROL METHODOLOGY

The satellite will begin in a tumbling state after deployment into space with the DMD booms retracted. At this point, the BDot de-tumble controller will be activated and the magnetorquers will be used to set the spacecraft magnetic moment to [16]

$$\boldsymbol{\mu_{bdot}} = -K\dot{\hat{\boldsymbol{B}}} = -K\left(\hat{\boldsymbol{B}} \times \boldsymbol{\omega}\right) \approx -K\frac{\hat{\boldsymbol{B}}_2 - \hat{\boldsymbol{B}}_1}{\Delta t} \tag{13}$$

Where K is a user defined, positive gain and $\dot{\hat{\boldsymbol{B}}}$ is the rate of change of the unit Earth magnetic field vector in the spacecraft body frame as measured by a magnetometer. As shown in Figure 4, this ensures that the direction of the resulting magnetic torque vector given by Eq. (12) will be as close as possible to $-\boldsymbol{\omega}$ and thus will reduce spacecraft angular velocity to the extent possible. This can be proven more formally as follows.

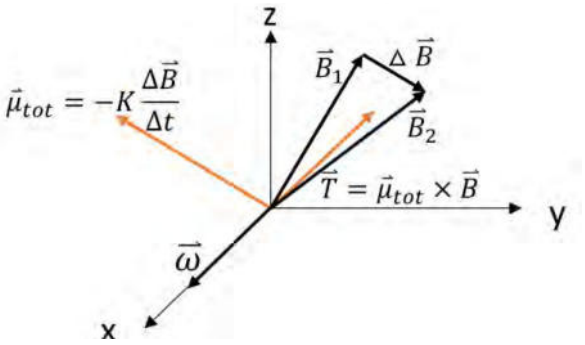

Figure 4. BDot Detumble Controller

Substituting Eq. (13) into Eq. (12) gives the magnetic torque vector from the BDot law

$$\boldsymbol{\tau_{bdot}} = -K\left(\hat{\boldsymbol{B}} \times \boldsymbol{\omega}\right) \times \boldsymbol{B} \tag{14}$$

The triple vector product rule states that for any three vectors $\boldsymbol{A}, \boldsymbol{B}$, and $\boldsymbol{C}$ [17]

$$(\boldsymbol{A} \times \boldsymbol{B}) \times \boldsymbol{C} = -\boldsymbol{A}(\boldsymbol{B} \cdot \boldsymbol{C}) + \boldsymbol{B}(\boldsymbol{A} \cdot \boldsymbol{C}) \tag{15}$$

Applying this to Eq. (14) yields

$$\boldsymbol{\tau_{bdot}} = K\hat{\boldsymbol{B}}\left(\omega B\cos(\theta)\right) - K\boldsymbol{\omega}B \tag{16}$$

Where θ is the angle between $\boldsymbol{\omega}$ and $\boldsymbol{B}$. Taking the dot product of Eq. (16) and $\hat{\boldsymbol{\omega}}$ gives the component of $\boldsymbol{\tau_{bdot}}$ along the $\boldsymbol{\omega}$ direction. If this component is negative, then $\boldsymbol{\omega}$ will be reduced in magnitude.

$$\begin{aligned} \boldsymbol{\tau_{bdot}} \cdot \boldsymbol{\omega} &= K\cos(\theta)\left(\omega B\cos(\theta)\right) - K\omega B \\ &= -KB\omega(1 - \cos^2(\theta)) \leq 0 \end{aligned} \tag{17}$$

Eq. (17) will be less than zero in all cases except for when θ equals zero. This occurs when the magnetic field is aligned with angular velocity vector and will result in zero magnetic torque (no reduction in angular velocity). However, because the direction of the magnetic field vector changes along the orbit, a condition with $\theta = 0$ will not persist for any significant time. This ensures that the BDot law will be able to reliably reduce the angular velocity of the satellite.

In addition to $\boldsymbol{\mu_{bdot}}$, a fixed magnetic moment vector along the desired zenith-pointing satellite axis (in this case the x-axis in Figure 1), will be superimposed on $\boldsymbol{\mu_{bdot}}$ after de-tumble and partial boom deployment. This fixed magnetic moment will work to align the x-axis with the Earth's magnetic field. At the point in the orbit when the magnetic field (and hence the satellite x-axis) is most-zenith pointing (as determined in advance through orbit propagation), the two DMD booms along the x-axis will be fully deployed and the two booms along the y-axis will be partially deployed. This creates a minimum moment of inertia about the x-axis which gravity gradient torques will naturally align with the zenith vector. Aerodynamic torques will simultaneously align the DMD z-axis (Figure 1) with the velocity vector, resulting in passive 3-axis attitude stabilization. All booms can be simultaneously deployed or retracted to facilitate orbital maneuvering while maintaining this attitude stability.

5. SIMULATIONS RESULTS

Figure 5 displays the attitude in the Local-Vertical-Local-Horizontal (LVLH) [3] frame of a 2U, DMD-equipped CubeSat initially deployed from the International Space Station (circular orbit with inclination of 52 degrees and semi major axis of 6778 *km*). Note that the LVLH x-axis is aligned with the zenith vector and the z-axis is aligned with the orbit angular momentum vector. In the first 10,000 seconds of the simulation, only the B-Dot

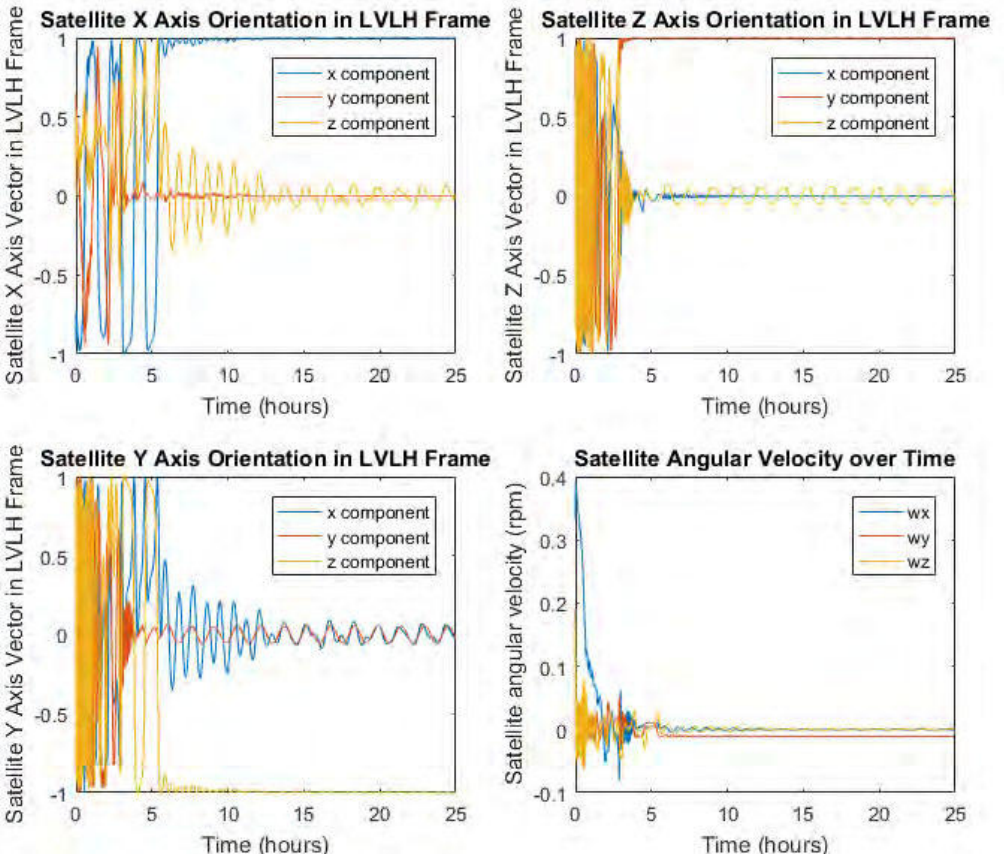

Figure 5. Satellite Orientation in LVLH Frame for 400 km Circular ISS Orbit

controller is run (retracted booms) with a BDot gain of -5 to de-tumble the satellite. Between t=10,000 and t=20,000 seconds, all booms are deployed to 1 m and a fixed magnetic moment of .015 $A*m^2$ along the satellite body frame x-axis is superimposed on the B-Dot magnetic moment. The $+y$ and $-y$ booms are then deployed to 1.85 m and the $+x$ and $-x$ booms are deployed to 3.7 m at the point in the next orbit when the magnetic field is most zenith pointing (t=20,800 s). After this, the fixed magnetic moment is removed and only the B-Dot controller continues running to damp attitude oscillations. Note that the attitude oscillations are never completely removed due to the movement of the zenith and velocity vectors in inertial space over the course of each orbit. The satellite eventually stabilizes with the z-axis aligned with the velocity vector and the x-axis aligned with the zenith vector with a steady state pointing error of less than five degrees. Figure 6 shows the error angle between the actual and desired orientation over time.

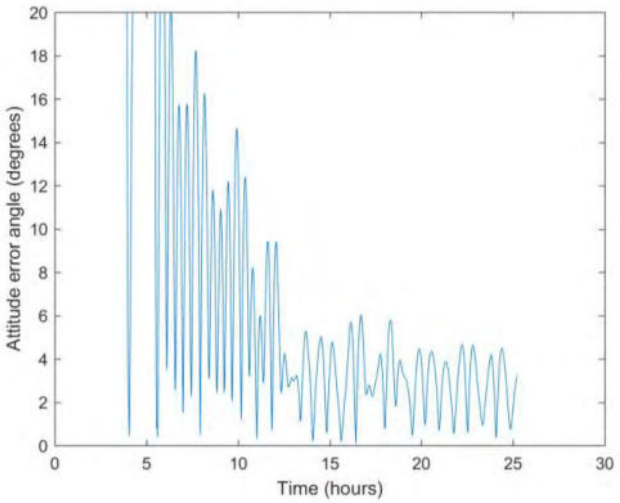

Figure 6. Angle Between Actual and Desired Attitude over Time

6. CONCLUSIONS

The drag maneuvering device is a unique actuator capable of providing simultaneous orbital maneuvering capabilities and semi-passive attitude stabilization. By independently actuating four tape-spring booms, the DMD can leverage naturally occurring aerodynamic and gravity gradient torques for attitude stability. Embedded magnetorquers are actuated based on magnetometer measurements to damp attitude oscillations and to ensure gravity gradient stabilization in the proper orientation. A control methodology for the DMD is developed in this paper and numerical attitude and orbit simulations verify the capabilities of the DMD. For many Low Earth Orbit satellite missions, particularly for Earth observation, the DMD could be used to entirely replace conventional attitude control and propulsion systems. For example, the DMD could maintain a camera or antenna pointed at the Earth while modulating aerodynamic drag to maintain an orbit slot.

7. REFERENCES

[1] R. E. Roberson, "Two Decades of Spacecraft Attitude Control," *Journal of Guidance, Control, and Dynamics*, vol. 2, no. 1, pp. 3–8, 1979.

[2] F. L. Markley and J. L. Crassidis, *Fundamentals of Spacecraft Attitude Determination and Control*. New York: Springer-Verlag, 2014.

[3] H. Curtis, *Orbital Mechanics for Engineering Students*, 2nd ed. Burlington, MA: Elsevier, 2009.

[4] S. K. Shrivastava and V. J. Modi, "Satellite attitude dynamics and control in the presence of environmental torques - A brief survey," *Journal of Guidance, Control, and Dynamics*, vol. 6, no. 6, pp. 461–471, Nov. 1983.

[5] H. Heidt, J. Puig-Suari, A. Moore, S. Nakasuka, and R. Twiggs, "CubeSat: A New Generation of Picosatellite for Education and Industry Low-Cost Space Experimentation," in *Proceedings of the 14th Annual AIAA/USU Conference on Small Satellites*, Logan, UT, 2000.

[6] M. Pastorelli, R. Bevilacqua, and S. Pastorelli, "Differential-Drag-based Roto-Translational Control for Propellant-less Spacecraft," *Acta Astronautica*, vol. 114, pp. 6–21, Sep. 2015.

[7] C. Arduini and P. Baiocco, "Active Magnetic Damping Attitude Control for Gravity Gradient Stabilized Spacecraft," *Journal of Guidance, Control, and Dynamics*, vol. 20, no. 1, pp. 117–122, 1997.

[8] E. Silani and M. Lovera, "Magnetic spacecraft attitude control: a survey and some new results," *Control Engineering Practice*, vol. 13, no. 3, pp. 357–371, Mar. 2005.

[9] R. R. Kumar, D. D. Mazanek, and M. L. Heck, "Simulation and Shuttle Hitchhiker validation of passive satellite aerostabilization," *Journal of Spacecraft and Rockets*, vol. 32, no. 5, pp. 806–811, Sep. 1995.

[10] D. Guglielmo *et al.*, "Drag Deorbit Device: A New Standard Reentry Actuator for CubeSats," *AIAA Journal of Spacecraft and Rockets*, vol. 56, no. 1, pp. 129–145, 2019.

[11] S. Omar and R. Bevilacqua, "Guidance, Navigation, and Control Solutions for Spacecraft Re-Entry Point Targeting using Aerodynamic Drag," *Acta Astronautica*, 2018.

[12] B. Wie, *Space Vehicle Dynamics and Control, Second Edition*. Reston ,VA: American Institute of Aeronautics and Astronautics, 2008.

[13] O. Montenbruck and E. Gill, *Satellite Orbits*, 1st ed. Springer Berlin Heidelberg, 2005.

[14] N. K. Pavlis, S. A. Holmes, S. C. Kenyon, and J. K. Factor, "An Earth Gravitation Model to Degree 2160: EGM2008," presented at the 2008 General Assembly of European Geosciences Union, Vienna, Austria, 03-Apr-2008.

[15] R. R. Bate, D. D. Mueller, and J. E. White, *Fundamentals of astrodynamics*. New York: Dover Publications, 1971.

[16] A. C. Stickler and K. t. Alfriend, "Elementary Magnetic Attitude Control System," *Journal of Spacecraft and Rockets*, vol. 13, no. 5, pp. 282–287, May 1976.

[17] G. Arfken, "Triple Scalar Product, Triple Vector Product," in *Mathematical Methods for Physicists*, 3rd ed., Orlando, FL: Academic Press, 1985, pp. 26–33.

The ALSAT-2B Gyrostellar Estimator: 2 years In-Orbit Performance

Haider BENZENIAR

Centre de développement des satellites
POS 50, Ilot T12, 31200 Bir El Djir, Oran, Algeria
Phone: +213 6 61 20 91 46, Mail: hbenzeniar@cds.asal.dz

Abstract : In this paper we present the in-orbit results of the gyrostellar estimator during the nominal mode of ALSAT-2B, a microsatellite for earth observation that was launched on 26th September 2016 placed into a 670 km sun synchronous orbit.
ALSAT-2B delivers a high-resolution products consisting of a 2.5m resolution for the panchromatic band, and a 10m resolution for the four multispectral bands, with a 17.5km swath for both modes. The attitude determination during the nominal mode is carried out by three gyroscopes and a star tracker.
The gyrostellar estimator is based on Kalman filtering; it is first initialized during the coarse pointing mode before transition to the nominal mode reason for which the estimator has enough time to converge in order to be ready for the different nominal mode pointing. The performance of this estimator in terms of pointing error and rate error shall be presented and discussed.

1. INTRODUCTION

An accurate attitude information is often essential for space applications. Several attitude sensors have been developed with star trackers (SST) being the most accurate ones for three-dimensional orientation measurements [1]. In order to further improve the attitude accuracy, multi-sensor data fusion is the common approach. Sensor fusion generally refers to the process of combining measurements from several different sensors in order to obtain a better result than considering each sensor separately [2]. The idea is to fuse sensors with complementary measure properties to combine their desired and cancel out their unwanted characteristics. The data fusion is usually done in an estimation filter, so commonly this method is referred to as inertial stellar or gyro stellar estimation. The association of the sensors gyro/star tracker is very complementary and natural. Gyro propagation allows to smooth-out star tracker noise and to continue ensuring accurate attitude determination when no star tracker (SST) updating is possible. Conversely, the star stracker allows compensating for long term gyro natural drift and gyro-scale factor errors during maneuvers [3]. E.g. while a star tracker provides low frequency long-term stable attitude measurements, the attitude computed from the high-frequency gyro measurements is only short-term stable. The motivation to fuse star tracker and gyro is to generate a long-term stable attitude estimate at gyro measurement frequency of attenuated noise compared to the star tracker measurement and, hence, to optimally bridge periods where no star tracker measurement is available. In addition to the improved attitude information, the estimator provides an estimate of the gyro angular rate bias. Figure 1 shows a comparison of the inertial attitude (gyro measurement), the optical attitude (SST measurement) and the estimated attitude from the fused (gyro plus SST) data [4]..

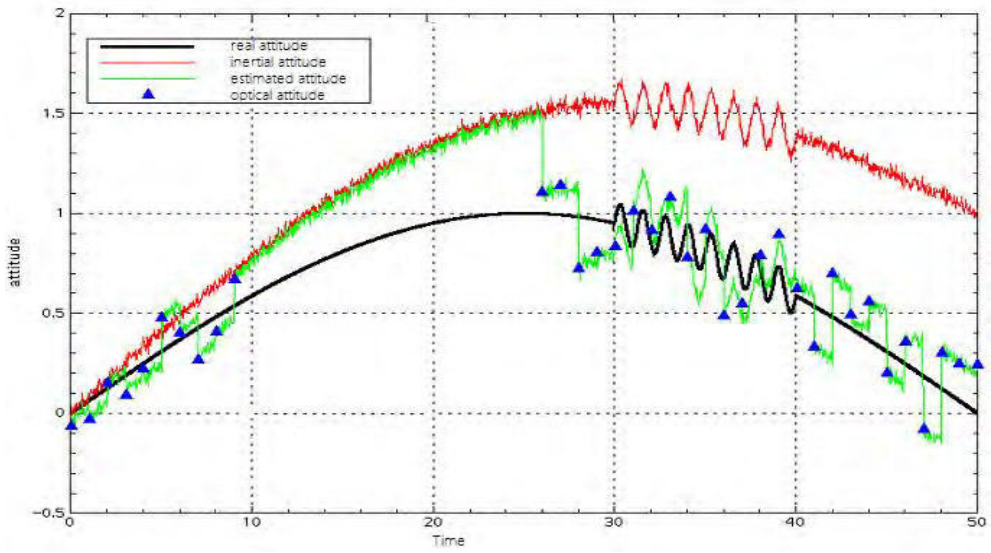

Figure 1. Gyro-stellar fusion.

2. SATEL LITE OVERV IEW

The ALSAT-2B satellite is in orbit since 26th September 2016. It accompanies the ALSAT-2A satellite to form a constellation of two satellites. The main tasks are cartography, management of agriculture, forestry, water, crop protection, management of natural disasters and land planning. The attitude determination and control subsystem is composed of three sun sensors used during the initial attitude acquisition, one magnetometer used during the first phase and also during the coarse pointing mode, three gyroscopes and one star tracker initialized during the coarse pointing mode and used for the nominal mode. As actuators, there is three magnetorquers used for detumbling at the beginning, after that they will be used for wheel unloading. Four reaction wheels mounted in pyramidal configuration aimed to increase the angular momentum and finally a propulsion subsystem with four thrusters for orbit control. The ALSAT-2 characteristics are illustrated in table 1, with the satellite in a deployable configuration shown in figure 2

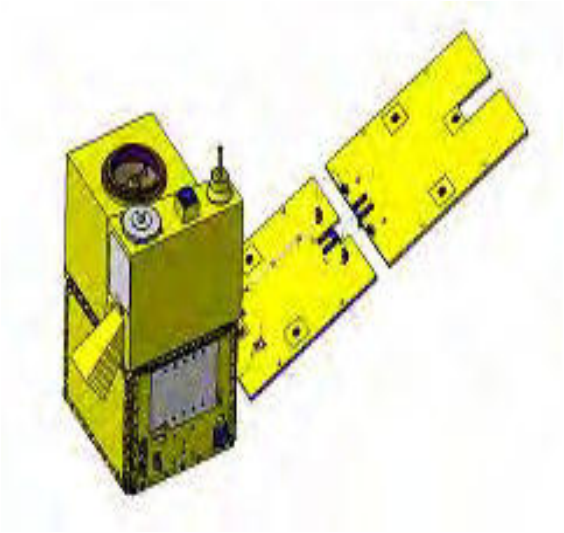

Figure 2. ALSTA-2B in depoyable configuration.

Spacecraft structure	aluminum bus structure, size: 60cm x 60 cmx 100 cm
spacecraft mass	116 kg
AOCS(Attitude & Orbit Control Subsystem)	Magnetic autonoumous acquisition Gyro-stellar attitude determination Autonomous GPS position determination 3-axis attitude control 4 reaction wheels (0.12 Nms) 1 hydrazine tank, 4.7 kg capacity (~65m/s); 4 thristers 1 N configuration
EPS (Electric Power Subsystem)	Power generated by oe depoloyable solar array (GaAs; 180W EOL) 1 Li-ion battery 15 Ah BOL; PCDU (Power & Control DistributionnUnit)
On-board data handling	On-board computer (T805, 1 Gbit DRAMEDAC, 8 Mbit Flash EEPROM) 2 S-band transceivers for communication (CCSDS, 20 kbit/s TC, 25-384 kbits TM)
Payload data manage-ment	X-band downlink: 60 Mbit/s Storage memory: 64 to 79 Gbit BOL - no compres-sion
Performance	Spacecraft launch mass: 116 kg Spacecraft agility: ±30° roll in 90s Localizationperformance: 300 m CE90 (Circular error of 90%)

Table 1. Overview of ALSAT-2 parameters. [5]

3. GYROSTELLAR ATTITUDE ESTIMATOR DESIGN

The satellite ALSAT-2 design is based on the MYRIAD platform of CNES [6]. The attitude estimation of this platform was based only upon star tracker (SST) measurements. However, due to some problems that have been seen in-flight like SST dazzling by moon several orbits a month, too many stars in the filed of view of the SST. Therefore, they call for the gyro stellar estimation. The estimation process can be split into three phases (see figure 3):

- Prediction of the state vector: From the estimated quaternion at the previous time step and the gyro measurement, a predicted quaternion is calculated. The predicted drift is equal to the estimated drift at the previous time step.
- Innovation calculation: The angular difference between SST measured quaternion and estimated quaternion is calculated at the SST measurement date, in SST axes reference.
- Correction: The predicted attitude quaternion is corrected by the innovation, previously multiplied by the estimator gain.

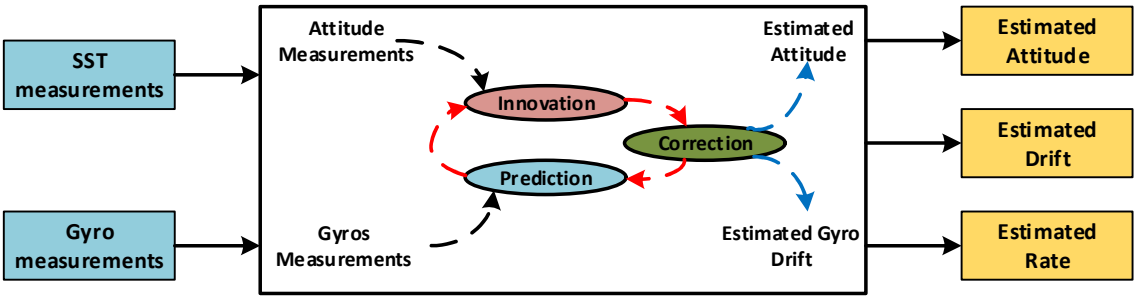

Figure 3. ALSTA-2B Gyrostellar estimator block diagram.

3.1 Prediction

The prediction is based upon the following kinematics equation:

$$\dot{Q} = \frac{1}{2} Q \otimes \Omega \tag{1}$$

here $\Omega = \begin{bmatrix} 0 \\ \underline{\omega} \end{bmatrix}$

$\underline{\omega}$ is the angular velocity rate wrt the inertial frame, expressed in the satellite frame.

$\otimes$ is the multiplication of quaternion.

The equation is discritised using Wilcox method.

$$\begin{cases} \hat{Q}_{N/N-1} = \hat{Q}_{N-1/N-1} \otimes \delta Q_N \\ \hat{d}_{N/N-1} = \hat{d}_{N-1/N-1} \end{cases} \tag{2}$$

$\hat{Q}_{N/N}$ is the estimated attitude quaternion wrt the inertial measurement frame at T_N.

$\hat{Q}_{N/N-1}$ is the predicted attitude quaternion wrt the inertial measurement frame at T_N.

$\hat{d}_{N/N-1}$ is the predicted gyro drift at T_N is the estimated gyro drift at T_{N-1} because there is not any gyro drift evolution model available.

3.2 Innovation computation

The predicted quaternion defines the rotation between the inertial frame and the satellite frame, expressed in the SST measurement frame:

$$\hat{Q}_{R_i 2 R_{SST}} = \hat{Q}_{Ri2R_{SAT}} \otimes Q_{R_{SAT}2R_{SST}} \tag{3}$$

The obtained innovation through a multiplication by the SST measurement:

$$\begin{pmatrix} 0 \\ \Delta\theta_{INNOV} \end{pmatrix} = \begin{pmatrix} 0 \\ \Delta\theta_{INNOV,x} \\ \Delta\theta_{INNOV,y} \\ \Delta\theta_{INNOV,z} \end{pmatrix} = 2\overline{\hat{Q}}_{R_i 2 R_{SST}} \otimes Q^{MES,SST}_{R_i 2 R_{SST}} \tag{4}$$

Where $Q^{MES,SST}_{R_i 2 R_{SST}}$ is the SST measurement, expressing the rotation between the inertial frame and the SST measurement frame.

$\Delta\theta_{INNOV,x}, \Delta\theta_{INNOV,Y}, \Delta\theta_{INNOV,z}$ are the Euler angles of the rotation between the predicted attitude of the satellite and the measured attitude of the satellite, expressed in SST reference .

3.3 Correct ion

The correction vector X_{COR} to be applied to the predicted state vector is:

$$\underline{X}_{COR} = \begin{pmatrix} \theta^{SST}_{COR} \\ d_{COR} \end{pmatrix} = \begin{pmatrix} \theta^{SST}_{X,COR} \\ \theta^{SST}_{Y,COR} \\ \theta^{SST}_{Z,COR} \\ d_{X,COR} \\ d_{Y,COR} \\ d_{Z,COR} \end{pmatrix} = \underline{\underline{K}}_{KALMAN} \Delta\theta_{INNOV} \tag{5}$$

$\theta^{SST}_{X,COR}, \theta^{SST}_{Y,COR}, \theta^{SST}_{Z,COR}$ are the attitude corrections expressed in the SST measurement frame.

$d_{X,COR}, d_{Y,COR}, d_{Z,COR}$ are the drift corrections.

The correction gain $\underline{\underline{K}}_{KALMAN}$ is a constant matrix. Its dimension is [7,3].

The correction Euler angles are then transferred from the SST measurement frame to the satellite reference frame:

$$\theta^{SAT}_{COR} = Q_{SAT2SST} \theta^{SST}_{COR} \overline{Q}_{SAT2SST} \tag{6}$$

Then the estimated attitude at date T_N is:

$$\hat{Q}_{N/N} = \hat{Q}_{N/N-1} \otimes Q_{COR,N} \tag{7}$$

And the estimated drift is:

$$\hat{d}_{N/N} = \hat{d}_{N/N-1} + d_{COR,N} \tag{8}$$

4. IN ORBIT PERFORMANCE

During the nominal mode, ALSAT-2B will be pointed either toward sun (heliocentric pointing) or toward earth (geocentric pointing). The heliocentric pointing is within the daylight and the geocentric pointing appears during eclipse phase or when the satellite is in imaging or downloading modes. The different satellite pointing modes are illustrated in figure 4. These different transitions allow the satellite to keep the equipments safe (e.g. star tracker dazzling, payload sun exposure), also for the solar array power generation, since the satellite solar arrays point the sun in the day phase, with ~ 0.025 deg/sec rotation about its minus X-axis, and for thermal balancing too. Now for the imaging mode and with the agility as a key feature, ALSAT-2B carries out the maneuvers to reach 30 deg either being along track or cross track [7].

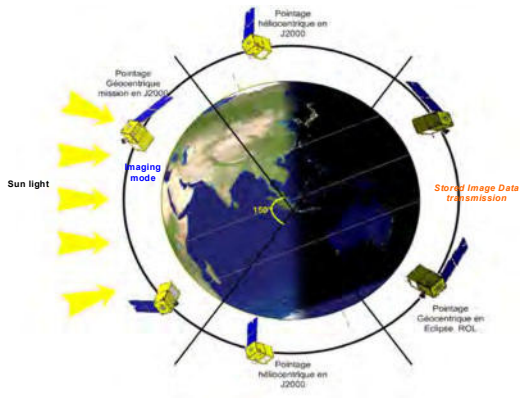

Figure 4. ALSAT-2 Operation modes with different pointing.

The assessment has been done throughout two years in orbit for the attitude estimator in terms of performance. It should be noticed here that along these two years, the obtained results fulfill the requirements and all of them fall under the specifications. The performance presented in the table 2 below does not consider the pointing error from maneuvers.

Table 2. Pointing and estimation accuracy

Require ments	Xsat	Ysat	Zsat
Pointing accuracy require ments brea k down (µra d)	500	500	500
In-orbit 1σ pointing accura cy (µra d)	<167	<167	<167
Estimation error require ments brea k down (µra d)	150	150	150
In-orbit 1σ Esti mation erro r (µra d)	<70	<70	<70

Now, regarding the gyro stellar estimator performance we tried to select the main observed performance. So, In figures 5 and 6, we present the observed SST unavailability periods through these last two years, we can notice that the SST availability is about 98% of the time when there is a mission plan uploaded and when there is no mission plan the SST availability falls down to 66%. For the estimated drift, we can say that it is stable along this period.

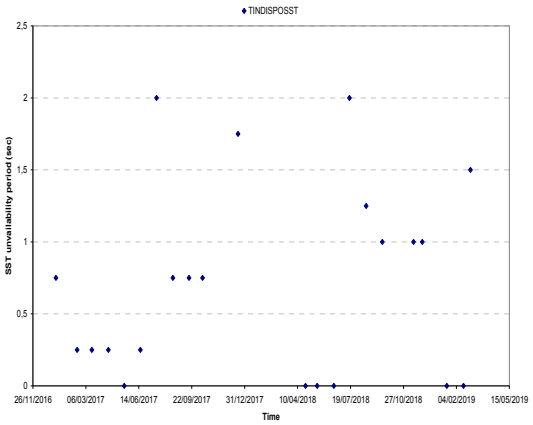

Figure 5. SST unavailibility period (sec) during two years in orbit.

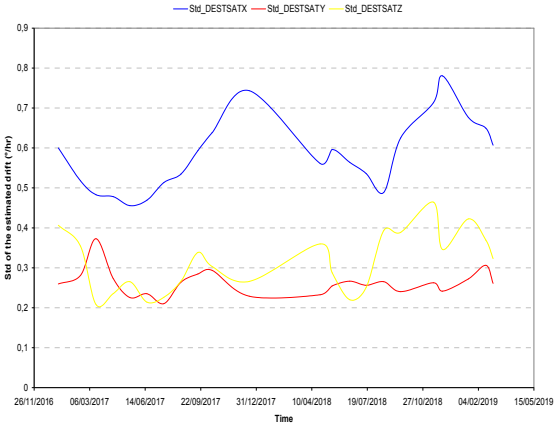

Figure 6. Standard deviation of the gyros estimated drift during two years in orbit.

Two cases of the nominal mode are presented below. First, we took the case where there is no mission plan uploaded and the satellite is in a complete sun pointing mode, the satellite attitude will be in helio-sinusoidal evolution as shown in figure 7 and 8 for the estimated quaternion and the angular rate. The star tracker in this case will be directly blinded by the earth for some periods reaching 20 minutes of unavailability measurements. The SST innovations and the estimated gyro drifts are illustrated in figures 9 and 10 where it can be seen clearly the effect of the earth blinding gaps on the SST innovations, a peak value occurs each time at the end of the earth blinding, no gyro drift calculation are done on this moment and the estimator will propagate the attitude.

12th Ja nuary 2019, no mission plan uploa ded

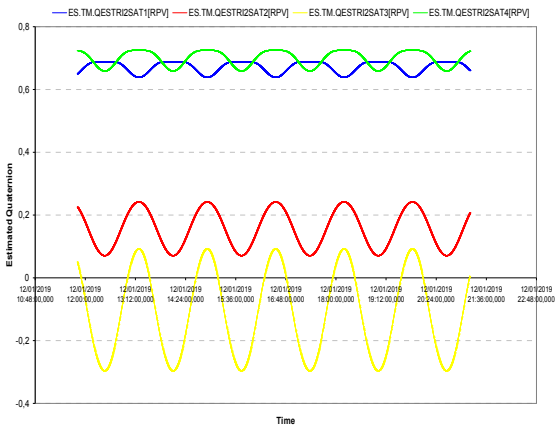

Figure 7. Estimated quaternion (12 hours observation).

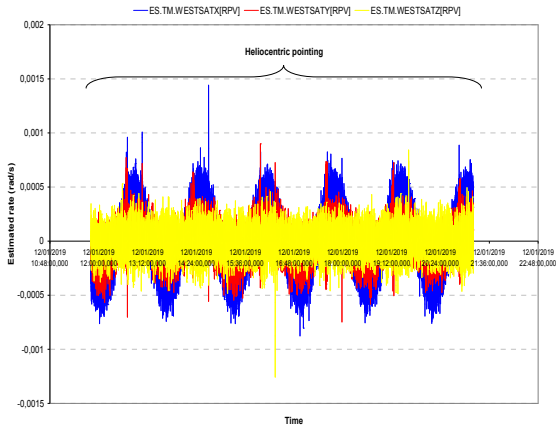

Figure 8. Estimated angular rate (12 hours observation).

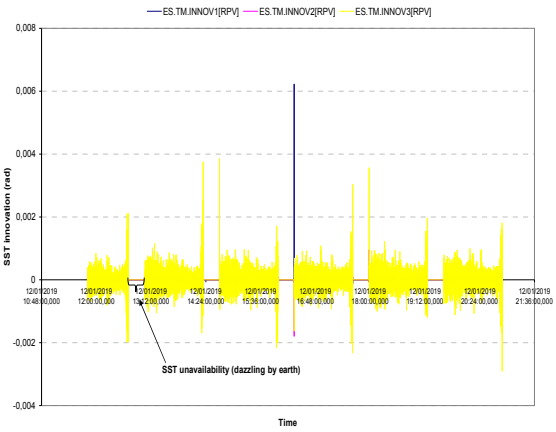

Figure 9. SST innovation (12 hours observation).

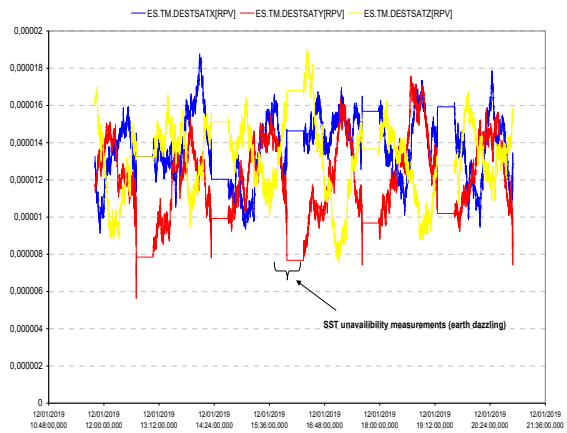

Figure 10. Estimated gyro drift (12 hours observation).

In the case where there is a mission plan uploaded containing the different maneuvers of imaging, day/night and night/day transitions; The SST will not be dazzled any more, just in the case of the moon presence, but this case happens monthly for short durations and not in imaging mode. The gyro stellar main performances as the estimated quaternion, the angular rate, the SST innovation and the estimated gyro drift are illustrated in figures 11, 12, 13 and 14 respectively. According to these observed results where there are different maneuvers and transitions from day to night and back that are well represented by the angular rates (see figure 12), we can say that the gyro stellar performances are acceptable with respect to the requirements, due to a better robustness of the SST tracking loss and a better on-board autonomy. In addition, there is a monitoring of this estimator, it concerns the gyro only estimation, if the SST is not available for a long time and the SST innovation by outing a threshold value on the level of the innovations. So, if one of these monitoring parameters is out of range a transition to survival mode is commanded.

02nd march 2019, with mission plan uploaded

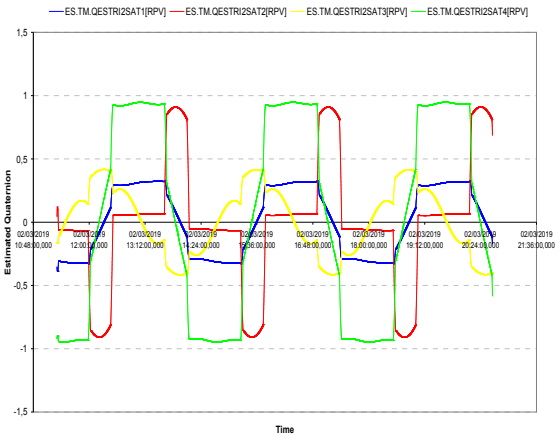

Figure 11. Estimated quaternion (12 hours observation).

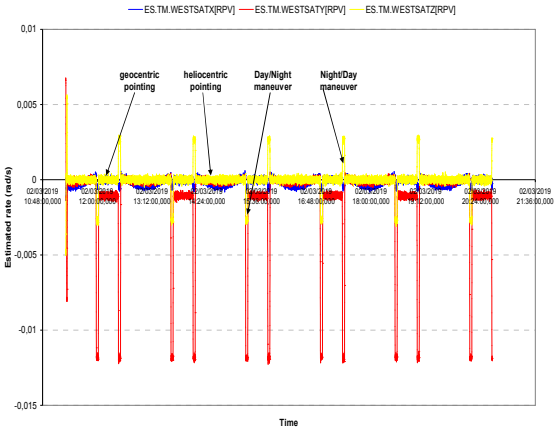

Figure 12. Estimated angular rate (12 hours observation).

Figure 13. SST innovation (12 hours observation).

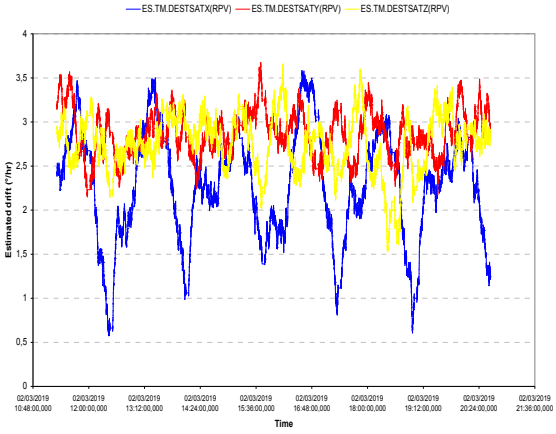

Figure 14. Estimated gyro drift (12 hours observation).

5. CONCLUSION

In this paper, we presented the observed performances of the gyro stellar estimator during the first two years in orbit of ALSAT-2B satellite, this new approach was used for the first time on ALSAT-2 satellites and until now, a nominal behavior still observed. The estimator has proved its performance and robustness along all this period, and continue providing correct measurements. Nevertheless, regarding the availability of continuous measurement, we notice some constraints for the star tracker especially when it is dazzled by the earth for long periods, but with the technological advances the robustness against earth bling will be increased. The same thing concerning the gyro drift that will be reduced.

6. REFERENCES

[1] S. Winkler, G. Wiedermann, W. Gockel, Gyro-stellar attitude estimation considering measurement noise correlation and time-variant relative sensor misalignment, International Astronautical Congress, Astrodynamics Symposium, Germany (2008).

[2] N. Duy Tan, T. Quang Vinh, and B. Trong Tuyen, A New Approach for Small Satellite Gyroscope and Star Tracker Fusion, Indian Journal of Science and Technology, Vol 9(17), DOI: 10.17485/ijst/2016/v9i17/93163, May 2016.

[3] M. Ghezal, B. polle, C. Rabejac, J. Montel, Gyro stellar attitude determination, Proceedings of the 6th International ESA Conference on Guidance, Navigation and Control Systems, Loutraki, Greece, 17-20 October 2005 (ESA SP-606, January 2006).

[4] C.C .Liebe, K. Gromov, D. M. Meller "Toward a Stellar Gyroscope for Spacecraft Attitude Determination", Journal Of Guidance,Control, And Dynamics, Vol. 27, No. 1, January–February 2004.

[5] https://directory.eoportal.org/web/eoportal/satellite-missions/a/aisat

[6] G. Limouzin, H. Lambert, "The EADS Astrium AstroSat Product Line - A New Generation of High Resolution Small and Micro Satellites Embarking Innovative Technologies," Proceedings of the Asian Space Conference 2007, Nanyang Technological University (NTU), Singapore, March 21-23, 2007.

[7] H. Benzeniar, M. A. Meghabber, "Reaction Wheels on a Pyramid Configuration 6 years In-orbit Results from AlSat-2A Remote Sensing Satellite," Proceedings of the 11th IAA Symposium on Small Satellites for Earth Observation, Berlin, Germany, April 24-28, 2017, paper: IAA-B11-1403.

Approach for estimation of nanosatellite's motion concerning of mass centre by trajectory measurements

Igor Belokonov[1], Ivan Timbai[2], Petr Nikolaev[3],

[1]Samara National Research University
34, Moskovskoye shosse, 443086, Samara, Russia
Phone: +8 846 267 4444, Mail: ibelokonov@mail.ru

[2]Samara National Research University
34, Moskovskoye shosse, 443086, Samara, Russia
Phone: +8 846 267 4444, Mail: timbai@mail.ru

[3]Samara National Research University
34, Moskovskoye shosse, 443086, Samara, Russia
Phone: +8 846 267 4444, Mail: pnikolayev@gmail.com

Abstract: The restore of the SamSat-218D nanosatellite movement by trajectory measurements is analyzed. Experimentally were confirmed features of the behavior of nanosatellites in low orbits, due to both the influence of the atmosphere and their inherent mass-inertial characteristics: the lifetime of nanosatellites is less, and the angular acceleration generated by the aerodynamic moment is much higher than that of satellites with large sizes and masses. The change in the ballistic coefficient in time is estimated from known trajectory measurements and information on the average density of the atmosphere at the points of trajectory measurements. The ballistic coefficient of the SamSat-218D nanosatellite, having the shape of a rectangular parallelepiped, depends on the spatial angle of attack and the angle of proper rotation. The ratio of the maximum value of the ballistic coefficient to the minimum value is 4.75. This made it possible to evaluate the nature of the possible motion relative to the center of mass of the nanosatellite by the nature of the change in the ballistic coefficient. The most probable motion relative to the center of mass of the SamSat-218D nanosatellite is the transitional mode of motion between different equilibrium positions, due to commensurate aerodynamic and gravitational moments and insignificant angular velocities.

1. INTRODUCTION

Since 2014, nanosatellites have been developed at the Samara University. The SamSat-218D nanosatellite [1] of the CubeSat 3U format is the first nanosatellite developed by students and scientists of Samara University. On April 28, 2016, it became a participant of the first launch campaign from the Vostochny cosmodrome, and simultaneously with two other satellites (MVL-300 and Aist-2D) was launched into orbit with an inclination of 97.3 ° and an average height of 486 km using the Soyuz 2.1a launch vehicle. SamSat-218D was designed to improve number of technological and educational tasks. First of all, it was intended for testing the orientation control algorithms of nanosatellites. However, since launching into orbit, it was not possible to establish communication with nanosatellite.

Some features of the motion of nanosatellites in low orbits are described in [2].

1) The value of the ballistic coefficient of a nanosatellite is more than that of a satellite with large dimensions and mass (with the same bulk density), which leads to a decrease in its lifetime in orbit. It makes possible, given the small planned duration of the active work of the nanosatellite (usually from six months to a year), to use low orbits effectively and to avoid clogging of near-Earth space.

2) The angular acceleration of a nanosatellite due to the aerodynamic moment is much more than that of a satellite with large dimensions and mass (for the same values of the relative static stability margin and bulk density). This expands the range of heights at which the aerodynamic moment acting on the nanosatellite is significant and can be used to passively stabilize along the velocity vector of the center of mass.

3) The value of the ballistic coefficient of a nanosatellite substantially depends on its orientation. The following formula expresses the relationship between the ballistic coefficient of a CubeSat nanosatellite and its orientation [3]

$$\sigma(\alpha,\varphi) = c_0 \tilde{S}(\alpha,\varphi) S / m,$$

where α – angle of attack; φ – angle of proper rotation; c_0 – the drag coefficient, which can take values from 2 to 3 depending on the physical properties of the gas and the surface of the nanosatellite (for design studies is assumed to be 2.2); S – characteristic area; m – nanosatellite mass; $\tilde{S}(\alpha,\varphi)$ – the projection area of a CubeSat nanosatellite on a plane perpendicular to the velocity vector, divided to the characteristic area:

$$\tilde{S}(\alpha,\varphi) = (|\cos\alpha| + k_s \sin\alpha(|\sin\varphi| + \cos|\varphi|)) / S,$$

where k_s – the ratio of the area of one of the side surfaces to the characteristic area.

To analyze the angular motion of a nanosatellite, for the case when the angular velocity of its own rotation is close to uniform, the expression for the ballistic coefficient can be averaged by the angle of proper rotation

$$\sigma(\alpha) = c_0(|\cos\alpha| + \frac{4k_s}{\pi}\sin\alpha) S / m.$$

Figure 1 shows a graph of the dependence of the SamSat-218D nanosatellite ballistic coefficient on the angle of attack for different values of the anglφe of proper rotation. The ratio of the maximum ballistic coefficient to the minimum is 4.75. This fact makes it possible to extract information on the orientation and dynamics of the movement of a nanosatellite from information on the value of a ballistic coefficient.

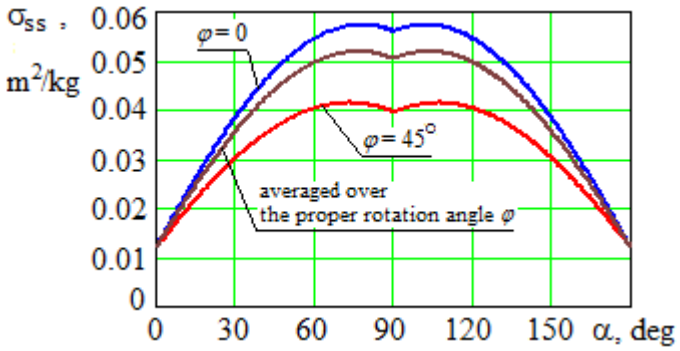

Fig.1. Dependence of the SamSat-218D nanosatellite ballistic coefficient on the angle of attack α and proper rotation angle φ

2. FORMULATION OF THE PROBLEM

Let's look at the trajectory measurements of the SamSat-218D nanosatellite. Figure 2 shows the changes in the height of its orbit. The information is based on the processing of data from the NORAD TLE files [4].

It should be noted that the considered time interval of the satellite (from April 28, 2016 till November 24, 2018) corresponds to a decrease of solar activity, which leads to a decrease in the density of the upper atmosphere and the height reduction rate.

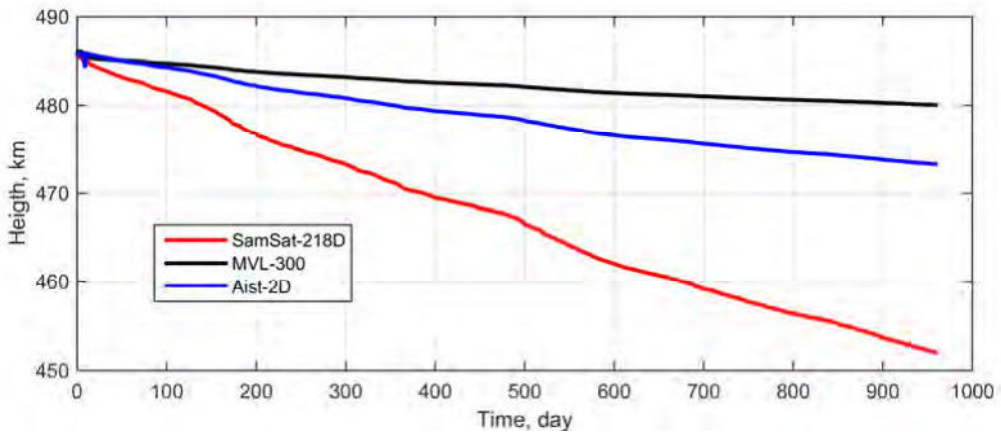

Fig.2. Changing the height of the orbits of the SamSat-218D, small satellites MVL-300 and Aist-2D

Using the information on the SamSat-218D nanosatellite height changing (trajectory measurements), as well as data on its design parameters (mass, inertia moments, aerodynamic characteristics) and the results of theoretical studies of the CubeSat3U nanosatellite movement dynamics [3] possible to solve two important tasks:

1) to study the changes in the ballistic coefficient of the SamSat-218D nanosatellite;

2) to identify the most probable mode of movement of the SamSat-218D nanosatellite relative to the center of mass, which was implemented after separation from the booster "Volga".

3. THE METHOD OF ESTIMATING THE BALLISTIC COEFFICIENT

Satellite orbit perturbations caused by the action of aerodynamic acceleration Φ, for a circular orbit, are described by the well-known formula [5]:

$$\dot{r} = 2r\sqrt{\frac{r}{\mu}}\Phi \ , \qquad (1)$$

where r – current radius vector; μ – Earth gravitational parameter; $\Phi = -\sigma q$ – disturbing aerodynamic acceleration; $q = \rho V^2 / 2$ – velocity head; ρ – atmosphere density; $V = \sqrt{\mu / r}$ – flight speed.

Using this formula, as well as the TLE files for SamSat-218D and Aist-2D satellites, the following method is proposed for calculating the average daily ballistic coefficient for the SamSat-218D nanosatellite:

1) calculation of the radius-vectors from the data of TLE files for SamSat-218D and Aist-2D satellites

$$r = \sqrt[3]{\mu / n^2},$$

where n – mean motion;

2) smoothing and re-discretization of the radius-vector data table of both satellites, by a cubic smoothing spline with a one-day sampling step and a smoothing parameter $p = 0.95$ (the selected value of the smoothing parameter provides an acceptable interpolation with the removal of high-frequency noise);

3) calculation of the derivative of the radius vector for SamSat-218D and Aist-2D by the method of numerical differentiation;

4) determination of the average daily density of the atmosphere (Figure 3a) via known deceleration of the Aist-2D satellite, for which the magnitude of the ballistic coefficient is known and equals $\bar{\sigma}_{const} = 0.0227 \ \ m^2 / kg$ (Aist-2D maintains its orientation in the orbital coordinate system)

$$\bar{\rho}_a = -\dot{r}_a / \bar{\sigma}_{const} \sqrt{\mu r_a},$$

where r_a – radius vector of Aist-2D satellite; $\dot{r}_a$ – derivative of the radius vector of Aist-2D satellite;

5) calculation of the average daily atmospheric density for the SamSat-218D satellite using the correlation formula for the upper atmosphere layers from GOST 25645.101-83 [6] (Figure 3a)

$$\bar{\rho}_{ss} = \bar{\rho}_a \times \exp\left(a_2 \left[\sqrt{r_a - a_3} - \sqrt{r_{ss} - a_3}\right]\right),$$

where coefficients $a_2 = 0.71604 \ \ km^{-1/2}$ and $a_3 = 6461.34 \ \ km$ are taken for altitude range $180 \ \ km \le h < 600 \ \ km$ and solar activity index $F_{10.7} \approx 75 \times 10^{-22} \ \ W / \left(m^2 \times Hz\right)$;

6) calculation of the daily averaged ballistic coefficient $\bar{\sigma}_{ss}$ for SamSat-218D:

$$\bar{\sigma}_{ss} = -\dot{r}_{ss} / \bar{\rho}_{ss} \sqrt{\mu r_{ss}}.$$

r_{ss} –radius vector of SamSat-218D satellite; $\dot{r}_{ss}$ –radius vector derivative for SamSat-218D satellite.

Figure 3b presents the results of estimating the averaged ballistic coefficient for the SamSat-218D nanosatellite.

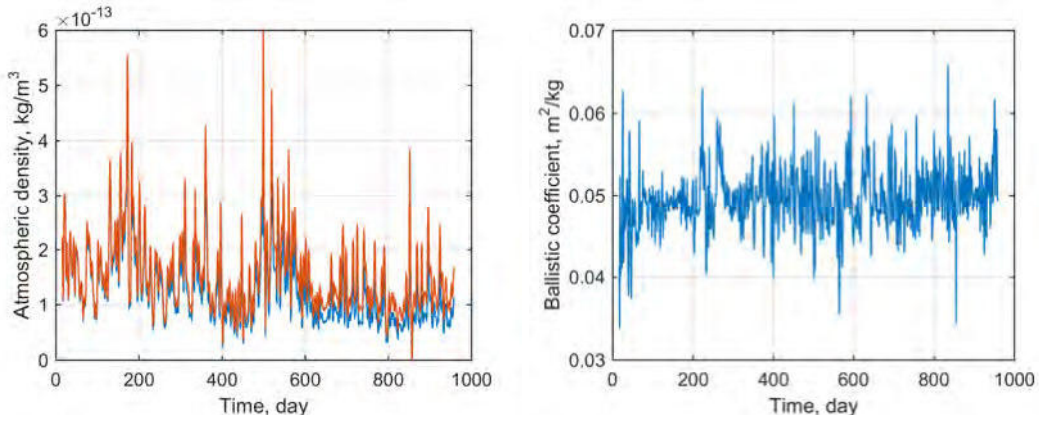

(a) (b)

Fig.3. (a) Changes in atmospheric density over time for the Aist-2D satellites (blue), SamSat-218D (red); (b) changes in averaged per day ballistic coefficient of SamSat-218D nanosatellite

Figure 4 shows a fragment of the graph of the change of the ballistic coefficient averaged per day for the time period from 16 to 100 days. It should be taken into account that variations in the averaged ballistic coefficient are caused by both errors of trajectory measurements and the nature of the angular motion of the nanosatellite.

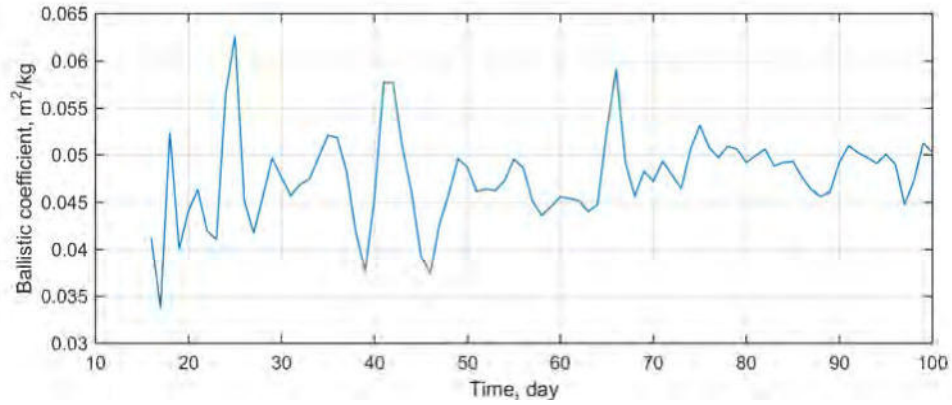

Fig.4. The change of averaged per day ballistic coefficient (from 16 to 100 days)

4. MOTION ANALYSIS

For qualitative analysis of the motion relative to the center of mass of the SamSat-218D nanosatellite, an approximate model of angular motion in the plane of a circular orbit with respect to the trajectory coordinate system is used. The model describes the change in the angle of attack under the action of the gravitational moment and the aero-dynamic recovery moment [3]:

$$\ddot{\alpha} - a(H)\sin\alpha - c(H)\sin 2\alpha = 0\,, \qquad (2)$$

where $a(H) = a_0 Slq(H)/J_n$ – coefficient characterized the aerodynamic recovery moment; a_0 – the coefficient for approximation by sinusoidal dependence of the coefficient of the aerodynamic recovery moment; l – the characteristic length of the nanosatellite; H – flight altitude; $c(H) = 3(J_n - J_x)(\omega(H))^2/(2J_n)$ – the coefficient characte-

rized the action of the gravitational moment; $\omega(H) = \sqrt{\mu/(R_3 + H)^3}$ – the angular velocity concerning the nanosatellite mass center; R_3 – Earth radius.

The change in the height of a circular orbit due to atmospheric drag occurs very slowly, and when considering the angular motion of a nanosatellite on one or several turns, it can be accepted $H = const$. In this case, for system (2) the energy integral is

$$\dot{\alpha}^2 / 2 + a\cos\alpha + c\cos^2\alpha = E_0 \qquad (3)$$

where $E_0 = a\cos\alpha_0 + c\cos^2\alpha_0 + \dot{\alpha}_0^2 / 2$ – determined by initial conditions.

The nature of the movement of the nanosatellite is determined by the ratio of a, c and E_0. In the case of $a < 0, c > 0$, there are two kinds of phase portraits.

1) $|a| \geq 2c$ (gravitational moment less than aerodynamic one). The phase portrait is similar to the oscillatory system of the pendulum type. In this case, the nanosatellite has two equilibrium positions for the angle of attack – stable with $\alpha = 0 + 2n\pi$ $(n = 0 \pm 1, \pm 2, ...)$ and unstable with $\alpha = \pi + 2n\pi$ $(n = 0 \pm 1, \pm 2, ...)$. The rotational motion mode of the nanosatellite corresponds to the condition: $E_0 > -a + c$, oscillatory motion mode relative to stable equilibrium $\alpha = 0 + 2n\pi$ $(n = 0 \pm 1, \pm 2, ...)$ corresponds to the condition: $E_0 < -a + c$. The areas of possible motions are separated by a separatrix.

2) $c > 0.5|a|$ (gravitational moment greater then aerodynamic one). With this ratio, there are four areas of motion of the nanosatellite: a rotational region and three oscillatory regions (a schematic view of the phase portrait is shown in Figure 5). The nanosatellite has four equilibrium positions for the angle of attack: $\alpha_* = \pm\arccos(-0.5a/c) + 2n\pi$ $(n = 0 \pm 1, \pm 2, ...)$, $\alpha = 0 + 2n\pi$ $(n = 0 \pm 1, \pm 2, ...)$, $\alpha = \pi + 2n\pi$ $(n = 0 \pm 1, \pm 2, ...)$. The rotational motion mode of the nanosatellite corresponds to the condition: $E_0 > -a + c$ – phase trajectory 1, oscillatory motion mode relative to the equilibrium position $\alpha = 0 + 2n\pi$ $(n = 0 \pm 1, \pm 2, ...)$ corresponds to the condition: $-a + c < E_0 > a + c$ – phase trajectory 2, oscillatory motion mode relative to the equilibrium position α_* corresponds to the condition: $E_0 < a + c$ – phase trajectory 3. The areas of possible motions modes are separated by separatrixes (phase trajectories 4 and 5).

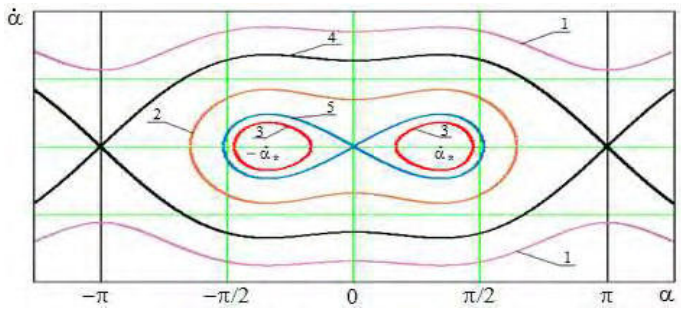

Fig.5. Possible phase portraits

Due to the uncertainty of the initial angular velocities obtained by the SamSat-218D nanosatellite after separation, multiple motion simulations were carried out in a wide range of initial angular velocities, using data on changes in the atmospheric density (Figure 3a), for ensuring compliance with the found trajectory measurements of variations in the average ballistic coefficient (Figure 3b).

Figure 6 shows the change in the ratio of the maximum values of the aerodynamic and gravitational moments for the time period from days 16 to 100, which caused by the cyclical nature of changes in the density of the atmosphere by solar activity.

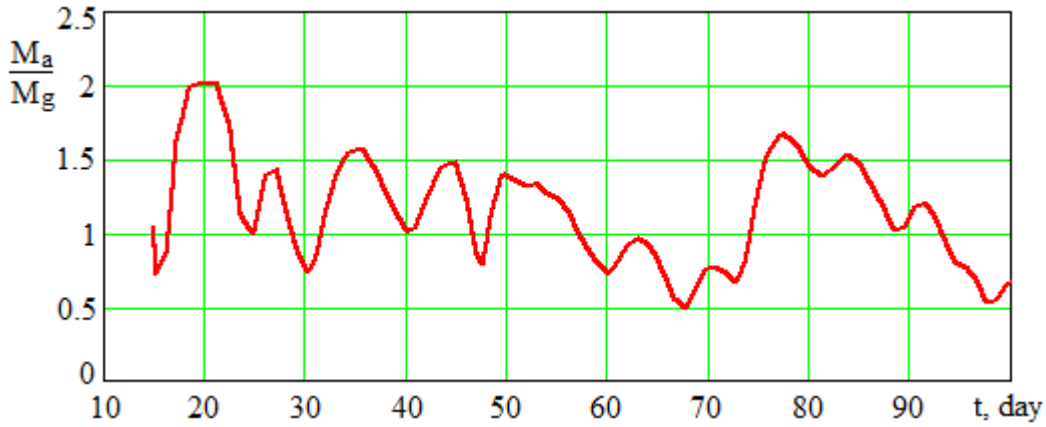

Fig.6. The change in the ratio of the maximum values of the aerodynamic and gravitational moments for the time period from 16 to 100 days

From the obtained results, it follows that the most likely movement relative to the SamSat-218D nanosatellite mass center is the transitional mode of movement between different equilibrium positions in the angle of attack. This mode of motion relative to the center of mass corresponds to the change in the angle of attack shown in Figure 7a and the change in the averaged ballistic coefficient over a specified period of time, shown in Figure 7b.

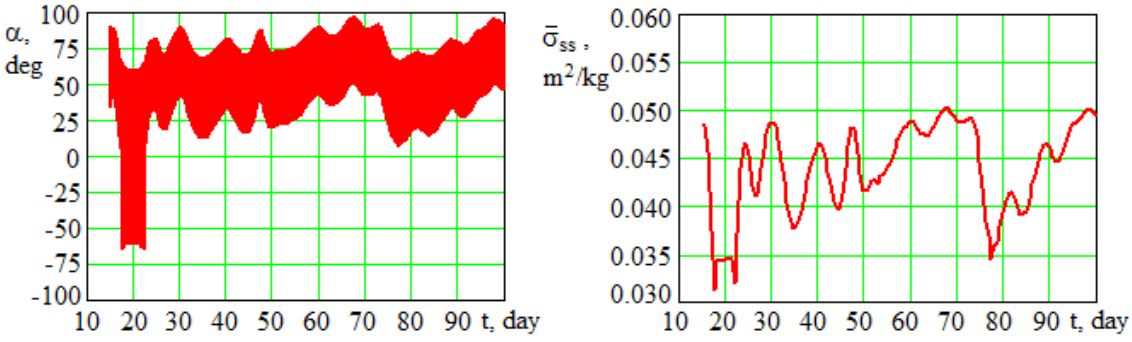

(a) (b)

Fig.7. (a) Change of angle of attack from 16 to 100 days;
(b) the change in the average ballistic coefficient from 16 to 100 days

At the beginning for a short time, the nanosatellite oscillates about the equilibrium positions of the attack angle α_* (about 65 degrees). Then, with an increase of the atmosphere density, the aerodynamic moment increases, and the nanosatellite motion transforms into oscillations with respect to the zero value of the angle of attack. Further, as

the density of the atmosphere decreases, the aerodynamic moment decreases and the nanosatellite motion transforms into oscillations with respect to the changing equilibrium position α_* (in the range of 35-75 degrees). Such a complex nature of change of motion mode is manifested only at the observed comparable values of the aerodynamic and gravitational moments.

The lack of definiteness of the conclusion about the mode of motion is due to the observed practical immutability of the density of the atmosphere during the entire time period of motion of the nanosatellite, in view of the decrease in solar activity.

In the future, it is planned to continue monitoring the braking of the SamSat-218D nanosatellite in order to increase the reliability of conclusions about the variable dynamics of movement and fairness of the developed methodology for designing an aerodynamically stabilized nanosatellites.

5. CONCLUSIONS

The proposed approach to analyzing the angular motion of a nanosatellite using trajectory measurements, tested in the framework of the SamSat-218D "passive" experiment, allows the developers of nanosatellites performing an uncontrollable motion relative to the center of mass to make conclusions about the causes of the observed motion. If a nanosatellite after its launch was to change its configuration (for example, to open solar panels or pushrods), then the use of this approach allows concluding that the operation was successful or unsuccessful.

This work was supported by the Russian Science Foundation, project no. 17-79-20215.

6. REFERENCES

[1] A. Kirillin, I. Belokonov, I. Timbai, A. Kramlikh, M. Melnik, E. Ustiugov, A. Egorov, and S. Shafran, SSAU nanosatellite project for the navigation and control technologies demonstration. J. Procedia Engineering. 104, 97-106 (2015)

[2] I. V. Belokonov, I. A. Timbai and P. N. Nikolaev, Analysis and Synthesis of Motion of Aerodynamically Stabilized Nanosatellites of the CubeSat Design. J. Gyroscopy and Navigation. 9 (4), 287-300 (2018)

[3] I. V. Belokonov, A. V. Kramlikh and I. A. Timbai, Low-orbital transformable nanosatellite: Research of the dynamics and possibilities of navigational and communication problems solving for passive aerodynamic stabilization. J. Advances in the Astronautical Sciences. 153, 383–397 (2015)

[4] Project Space Track. Available online at: https://www.space-track.org (accessed January 2019)

[5] M. S. Konstantinov, E. F. Kamenov, B. P. Perelygin, V. K. Bezverbyy, Space flight mechanics, p. 408. Mashinostroenie Publ., Moscow (1989)

[6] GOST 25645.101-83. Earth upper atmosphere. Density model for project ballistic computations of artificial earth satellites, p. 168. Standard Publ., Moscow (1984)

FDIR Handling in Eu:CROPIS

Olaf Maibaum (1), Ansgar Heidecker (2), Fabian Greif (2), Markus Schlotterer (2), Andreas Gerndt (1)

(1) German Aerospace Center (DLR), Simulation and Software Technology
Lilienthalplatz 7, 38108 Braunschweig, Germany
Phone: +49 531 295 2974, Mail: Olaf.Maibaum@dlr.de

(2) German Aerospace Center (DLR), Institute of Space Systems
Robert Hooke Str. 7, 28359 Bremen, Germany
Phone: +49 421 24420 1166, Mail: Ansgar.Heidecker@dlr.de

Abstract: Fault detection, isolation, and recovery (FDIR) mechanisms in on-board software are essential to guarantee the survival of the satellite in case of a hardware malfunction. E.g., outage of essential attitude control system (ACS) actuators or sensors can lead to mission loss. The on-board software has to handle such situation autonomously by switching to cold redundant devices or by isolation of information from hot redundant devices. The FDIR implementation for the ACS of the spin stabilized small satellite Eu:CROPIS (Euglena Combined Regenerative Organic food Production In Space) is shown in this paper.

1. INTRODUCTION

This paper shows the implemented software architecture and methods for FDIR handling in the Eu:CROPIS (Euglena Combined Regenerative Organic food Production In Space) ACS. It starts with a short introduction of the Eu:CROPIS mission and of the implemented ACS. Sections 3 and 4 show the underlying execution platform and the used services from the Package Utilization Standard (PUS) [5]. The software architecture and FDIR handling is presented in section 5. The paper closes with the conclusion and outlook on future work.

2. EU:CROPIS

The mission Eu:CROPIS is the demonstration of the feasibility of restartable and sustainable life support systems on a pure biological basis. Such systems enable the production of food and atmosphere from waste like urine and phosphate [1]. Furthermore, the system should be reliable enough for long duration missions. The biological experiments require different levels of gravity. The target gravities of Eu:CROPIS are 0.16 g (Moon) and 0.38 g (Mars) respectively in the biological experiment compartments. This is achieved by a spin stabilized satellite which can change its rotation speed and thereby the centrifugal force (gravity) in the biological experiment compartments during mission time. Experiment compartments are placed at a reference radius of 0.35 m measured from the designed spin axis. The launch of the mission was at 03.12.2018 as part of Spaceflight's SSO-A rideshare mission launched from Vandenberg Air Force Base with a Falcon 9 launch vehicle.

The used satellite bus is based on the DLR compact satellite bus program, which is a research and development platform using a component-oriented design. The bus for the Eu:CROPIS mission is a spin stabilized platform with a cylindrical body. Diameter of the body is 1000 mm and height is 1100 mm [1]. The bus has two sections: one with the separated payload compartments at the upper deck, and one with the bus section. Figure

1 shows both sections. The mass of the satellite is around 230 kg. The orbit is sun synchronous at 580 km altitude.

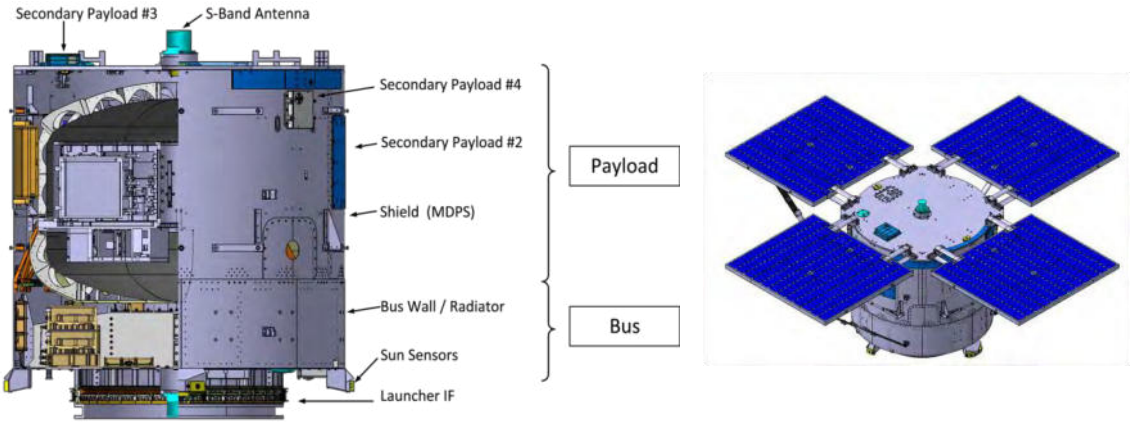

Figure 1 Eu:CROPIS Satellite Bus

2.1 ACS

The main requirement to be fulfilled by the ACS is to generate gravity in the biological compartments and orient the z-axis into sun direction to ensure power generation by the solar panels. The satellite bus is spinning around the z-axis between 5 to 31 rpm. To keep sun orientation of the solar panels, the spin axis has to be reoriented by ~1 deg/day.

As actuators, the ACS uses three magnetic torquers to control the rotation and spin axis. As sensors it uses two magnetometers, ten sun sensors and four angular rate gyroscopes. Sensor data is filtered by an Unscented Kalman Filter (UKF) which is designed for spin stabilized satellites. Table 1 shows the key figures of the ACS hardware components. For a detailed description of the used UKF and the ACS, see [3] and [4].

Amount	Hardware	Key figure
3	Magnetic Torquer	30 Am^2
2	Magnetic Field Sensor (MFS)	noise < 1000 nT (3σ)
10	Sun Sensor	noise < 0.3 deg (3σ)
4	Angular Rate Gyroscope	RW 0.08 deg/√h, Bias 9 deg/h (3σ)
2	GPS Receiver	DLR-Phoenix

Table 1 Attitude control system hardware devices

3. TASKING FRAMEWORK

The communication and processing is realized by the Tasking Framework inside the Eu:CROPIS ACS. The Tasking Framework is a reactive asynchronous execution platform with support for multicore processors and extensions for distributed on-board systems. For the Eu:CROPIS ACS, a non-distributed single core configuration is used. The mean for communication in the Tasking Framework are channels, which will specialized to different types of data buffers by overwriting the basic channel class. E.g., data

buffers are single buffers, double buffers, or FIFO queues. For application code, a channel can be specialized with own implementations, like interfaces to devices. Beside different types of data buffers as channel, the Tasking Framework provides events as specialization of a channel. An event is connected to the system clock and provides means to start task executions in a periodic or relative manner.

For computations in a system, tasks have to be implemented by overriding the execute method of the basic task class. An instance of a task implementation is connected to at least one input. Inputs control the execution of a task implementation and interface to incoming channels of a task. The number of expected data items, which have to be pushed on the associated channel to start the execution of a task, have to be configured for the input. For example, figure 1 shows a task connected to two incoming channels, one event and one outgoing channel with computation results of the task. The input of channel 1 is configured to start the task execution with one data item, whereas the input of channel 2 expects two data items on the channel. The input of the event is configured as optional input with the final attribute. In this example, the task execution is initiated by one data item pushed to channel 1 and two data items pushed to channel 2, or if one event is fired independently of the status of different inputs. Thus, the event in this example acts as time out mechanism for the task execution, e.g. when a device is faulty and did not respond with a data message. Further computation steps can be connected as tasks to the outgoing channel 3, which are triggered for execution when the task pushes data on channel 3.

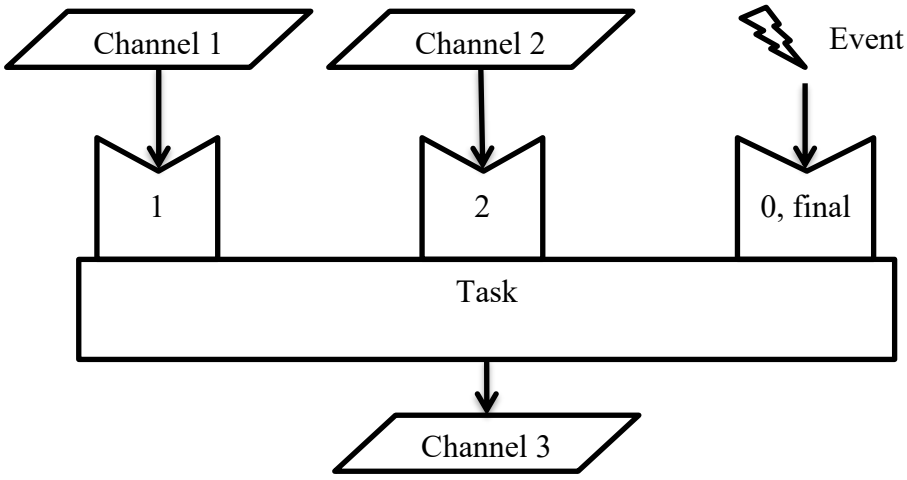

Figure 2 Task Configuration Example

4. PUS SERVICES

The implemented services in the Eu:CROPIS command and data handling system (CDH) following the Package Utilization Standard (PUS) [5]. Each application of a subsystem has to register service handler at the CDH system to provide the service implementation of the subsystem. The CDH system can call the subsystem specific implementation of a service request by the application and service identification of a PUS data package.

4.1 Device Command Distribution Service

To access parameters of the ACS, the “Distribute Register Load” Command from the “Device Command Distribution Service” (PUS service 2, subservice 2) is used in lack of the Parameter Management Service. By default, this service was foreseen to configure hardware systems but can also be used to configure software systems. The service provides means to load a parameter with specific data from the load command and, as extensions of the PUS service, a parameter dump request, and the possibility to safe parameter settings as boot configuration to a context memory.

The updated PUS [6] published in 2016 introduces the parameter management service as implemented in Eu:CROPIS. Following the updated PUS, the functionality is available by the PUS service 20. In case of software reuse of the Eu:CROPIS implementation, the service will be assigned to service 20 in following missions.

4.2 Diagnostic Reporting Service

Beside regular “Housekeeping Parameter Reports” (PUS service 3, subservice 25), the PUS Diagnostic Reporting Service provides also “Diagnostic Parameter Reports” (PUS service 3, subservice 26). For Eu:CROPIS, all ACS channels are addressable by the service “Define New Diagnostic Parameter Report” (PUS service 3, subservice 2). This allows a deep inspection of the current software state during the operational phase, which can be adapted by ground control commanding.

The generation of diagnostic parameter reports is controlled by different generation modes. The Eu:CROPIS ACS implementation provides two modes: “Periodic Diagnostic Parameter Report Generation Mode” (PUS service 3, subservice 18), and “Filtered Diagnostic Parameter Report Generation Mode” (PUS service 3, subservice 20). Instead of using only percentage parameter values and absolute delta values threshold types, the Eu:CROPIS ACS extends the standard definition of the filtered diagnostic parameter report generation by threshold types equal, bigger than, and lesser than.

The updated PUS removes filter functionalities for diagnostic reports. In case of software reuse in upcoming missions, the filter functionality will not be removed because the functionality is needed by the FDIR reporting functionality implemented in the Eu:CROPIS ACS.

4.3 Event Reporting Service

To announce outstanding events in a system, PUS defines the Event Reporting Service with different severities (PUS service 5, subservices 1, 2, 3, 4). For this purpose, the Eu:CROPIS ACS uses the implementation of the CDH subsystem. The satellite bus internal interface is a topic provided by the outpost-core library. [7]

4.4 Function Management Service

The PUS Function Management Service (PUS service 8, subservice 1) provides the mean to initiate special functionalities in the software, e.g. reset error counter values or change control modes. Each special functionality is addressed by an enumeration followed by the functionality specific parameters.

5. FAILURE HANDLING

5.1 Software Architecture

The whole software architecture of the Eu:CROPIS ACS is based on the Tasking Framework. The software architecture concepts for the implementation of hardware interfaces and the UKF are described in [4].

The FDIR handling in the Eu:CROPIS ACS has several logical layers. In the first two logical layers, which are software interfaces to actuator and sensor hardware as well as to the UKF, failures are detected and isolated. The mechanism is described in the next section. All detected failures are reported on the error channel for a further error handling and the collection of diagnostic data to analyze error cases by the satellite support team. Both tasks are activated by pushing error identifications to the error channel.

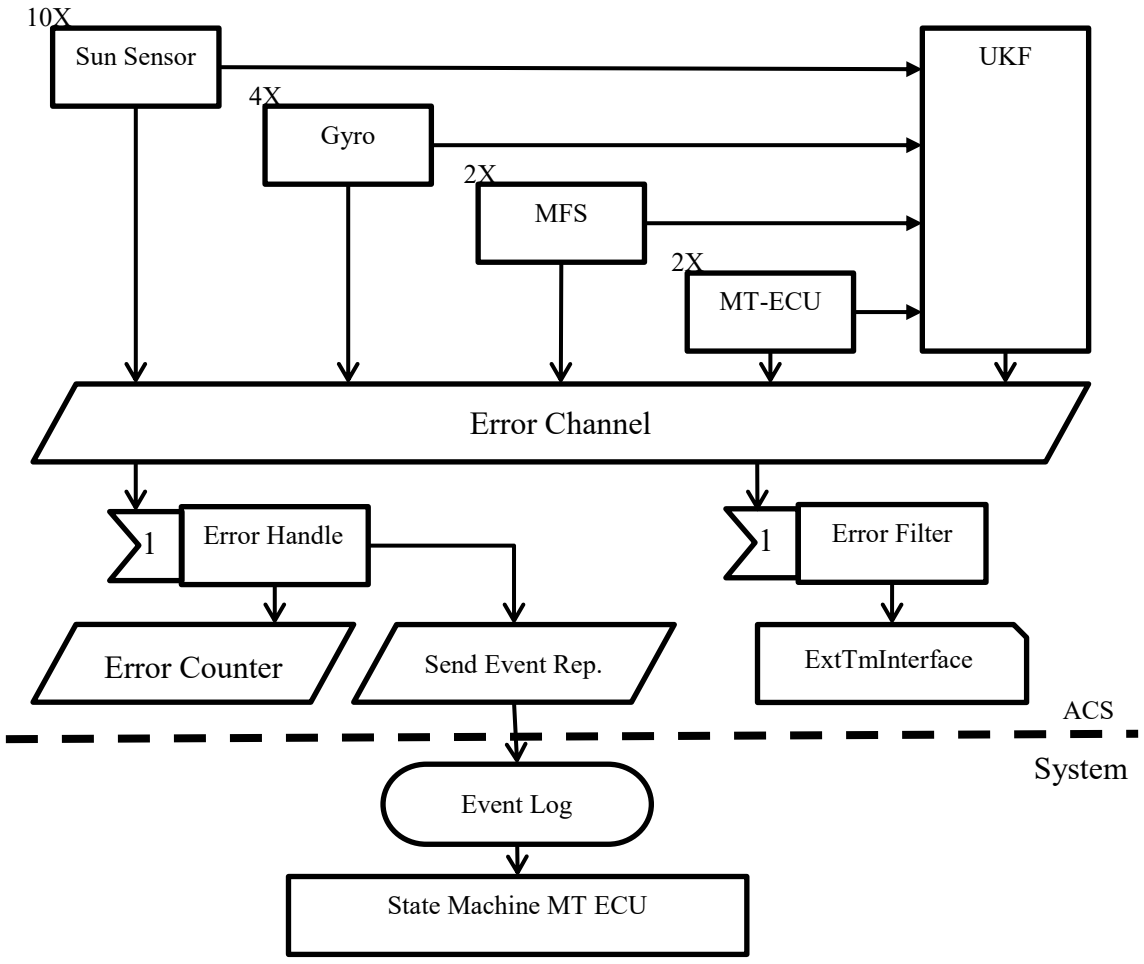

Figure 3 FDIR Software Architecture in the Eu:CROPIS ACS

The error filter sends diagnostic data by serializing data from a set of channels related to the error identification as diagnostic parameter reports. E.g., in case of a failure of the magnetic torquer, all channels related to the sender and receiver tasks of the magnetic torquer software interface are packed to a diagnostic report. The mean of error filtering is realized by the filter functionality of the “Filtered Diagnostic Parameter Report Gen-

eration Mode". The used diagnostic reports are predefined with its filter in the ACS and cannot be altered during operation, except by a software update.

The extended telemetry interface can block the sending of diagnostic reports to limit the number of diagnostic reports in case of a permanent failure. The amount of diagnostic reports is controlled by a parameter, modifiable by the Distribute Register Load Command, and the counter of sent reports is reset as standard operation during contact by one function call of the function management service.

Error handling by the error handle task has two steps. The first step is increasing the error counter of the error counter channel. The second step is to evaluate the criticality of failures. For this step, different critical failure cases are identified for each error counter, e.g. a device reports an electrical error or the communication with the device is permanently disturbed. In case of a critical failure case, an event report is sent to the event channel, which also pushes a message to the event log topic to initiate a recovery operation by the FDIR state machine on system level.

Figure 3 shows all related software components, tasks, and channels responsible for FDIR handling in the Eu:CROPIS ACS.

5.2 Detection and Isolation

Failure detection is executed by the software interfaces to the sensor and actuator hardware and, in a second step, in the UKF. In all failure cases, the fault detection is reported by an error identification on the error channel.

At first step, the communication with the sensor and actuator hardware is checked in the corresponding software interfaces. These checks are: check on successful sending of messages to the hardware; successful receiving of messages from the hardware; and format of received messages is valid. The validity check depends on the message format and encloses checksum checks and consistency of message type and message length. Further checks are performed on the message data by checking the status information reported by the device and the validity information and consistency of data. E.g., validity information are albedo state information from sun sensors or range exceed information from gyroscopes.

Depending on the failure and validity state, detected by all checks on interface level, data is not sent to the UKF or it is marked as inaccurate data to isolate them from further processing. If possible for a faulty hardware device, a failure handling is initiated by the software interface to bring the faulty hardware device back into an operational state, e.g. by sending a command sequence for the failure case advised by the manufacturer. Single failures are not handled. Consistent failures over a specified number of control cycles are reported in the error channel to initiate recovery actions, depending on the redundancy level of the faulty hardware device.

The second step in failure detection is performed by the UKF. First, it checks sensor data on validity, e.g. measured sun angle data during eclipse is invalid. For all valid sensor data, the Mahalanobis distance is computed to detect inconsistent state information from a sensor device. Implausible data will be isolated from the computation of the high accurate attitude state information which is sent to the controller task.

5.3 Recovery

Error identifications reported on the error channel are read by the error counter task. For each error identification exists an error counter in the error counter channel and an entry in the critical failure report list, which is filled in case of critical failures. By default, the error counter task reads all error identifications from the error channel and increases the corresponding error counter. When an error counter reaches a limit, the error counter task checks the list of critical failure reports and if one is defined for the error identification, the critical failure report is published on the event log to inform the system level and to report the event by the PUS event reporting service. The error counter limit can be changed by the "Distribute Register Load Command" service.

Reported critical failure events are managed by the system state machine and can initiate a power reset of hardware devices or a switch to cold redundant hardware devices. Figure 4 shows the state machine for recovery actions of the MT-ECU (magnetic torquer electronic control unit).

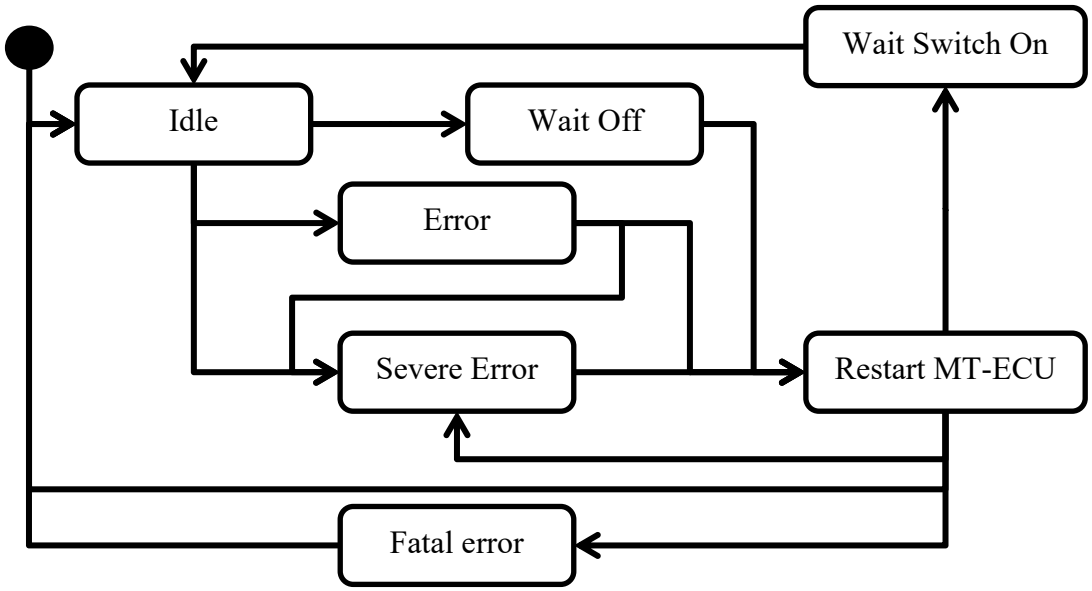

Figure 4 State Machine for Recovery Actions of Magnetic Torquer

The state machine starts in state *idle* and waits on three conditions: the cold redundant device is switched on by ground control command or an electrical or software error is received as critical error report on the event log. In the first case, the state machine goes into state *wait off* to wait until the active MT-ECU is powered off. For an electrical error, the state changes to the *severe error state*. For the software error, reported by the MT-ECU, the state changes to *error*. The state *error* switches off the active MT-ECU and commands a restart of the inactive MT-ECU, until the maximum number of allowed restarts without ground interaction on an MT-ECU is not reached. If the maximum number of restarts is reached, the state changes to *severe error*. In state *severe error,* the active MT-ECU is marked as broken and a switch over to the cold redundant MT-ECU is initiated.

The state *restart MT-ECU* switches on the MT-ECU, which is marked as active. If a failure is detected, go to state *severe error* so long the cold redundant MT-ECU is not marked as broken. Otherwise go to the state *fatal error* to wait on ground interaction. The remaining state *wait* changes to the state *idle* when the selected active module is powered on.

6. CONCLUSIONS AND OUTLOOK

The paper showed the architecture and means for the FDIR handling of the Eu:CROPIS ACS. First checks for failure detection on communication status and data from the actuators are applied at interface level. At the UKF, the Mahalanobi distance is used to isolate implausible data. Each detected fault is reported to two tasks in the ACS, one to send diagnostic data, and the other to count the detected faults and to initiate the recovery actions. On system level, a state machine is used to manage the power states of devices. First experiences in the LEOP and commissioning of the Eu:CROPIS mission show that the implemented FDIR mechanism works as expected. The analyses for the reasoning of increasing FDIR counters on the flight model in space is supported by the diagnostic reporting service itself and the reporting actions triggered by FDIR events, because we get an insight of all internal ACS data with up to an 10 Hz resolution by the diagnostic reporting service. All applied services for FDIR handling can be reused as configured in future missions.

7. REFERENCES

[1] S. Kottmeyer, C.F. Hobbie, F. Orlowski-Feldhusen, F. Nohka, T. Delovski, G. Morfill. The Eu:CROPIS Assembly, Integration and Verification Campaigns: Building the first DLR Compact Satellite. IAC 2018, Bremen (2018).

[2] F. Dannemann, F. Greif, Software Platform of the DLR Compact Satellite Series. In: Proceedings of the 4S Symposium, Mallorca, Spain (2014).

[3] A. Heidecker, T. Kato, O. Maibaum, M. Hölzel, Attitude Control System of the Eu:CROPIS Mission. IAC 2014, Toronto, Canada (2014).

[4] O. Maibaum, A. Heidecker. Software Evolution from TET-1 to Eu:CROPIS. In: Digest of the 10th International Symposium of the International Academy of Astronautics. pp. 195-198. Wissenschaft und Technik Verlag, Berlin (2015)

[5] ECSS-E-70-41A: Ground Systems and Operations – Telemetry and Telecommand Packet Utilization, 30 January 2003.

[6] ECSS-E-ST-70-41C: Telemetry and Telecommand Packet Utilization, 15. April 2016.

[7] https://github.com/DLR-RY/outpost-core: Outpost Core. Link checked at 13. December 2018.

To boldly go where no Sunsensor has gone before. part 2

Johan Leijtens, Johan Uittenhout, Dick Broekmans, Stefan Schmidt, Frank Bulk
Lens Research & Development
‘s-Gravendijckseweg 41b 2201CZ (The Netherlands)
Email: jls@lens-rnd.com Tel: +31 (71) 2020 123

Abstract: During the AIA small satellite symposium in 2017 Lens R&D presented the progress on environmental tests performed on the BiSon74-ET-RH extended temperature Sunsensor. Now Lens R&D is taking this type of product a step further in frame of an ESA GSTP program which is to lead to two different types of fully ESA qualified Sunsensors. Being small enough to fit on almost any satellite and fully optimised for volume production through the use of a dedicated pick and place machine dubbed the *MAMA* tool (Mechanical Automated Membrane Aligner), the BiSon64-ET and BiSon64-ET-B Sunsensors are expected to become Sunsensors that can be universally applied.
The last process optimisation that could be profitably performed was the membrane alignment which is now fully automated by using the MAMA tool. This not only leads to a higher non-calibrated accuracy but also to a higher repeatability in production and consequently yield.
Furthermore, lengthy discussion with ESA on quality control and associated costs have led to a qualification program which is tailored to volume production and a combination of the ESA-ECSS-Q-ST-10-03 equipment qualification and ESA-ECSS-E-60-05 quality control for hybrid circuits specifications.
The presentation will focus on the design and development of the MAMA tool, the qualification process and qualification status of the development of the BiSon64-ET and BiSon64-ET-B Sunsensors and the associated pigtail cables. The pigtails are an addition to the program to ensure availability of pigtails able to match the sun sensors extended temperature and radiation hardness without any issues. These pigtails will be flown along with 20 sensors on the ESA Proba-3 mission.

INTRODUCTION

Lens R&D has developed, built and tested *Sunsensors* (in frame of an ESA Artes 5.2 contract) that exhibit an unprecedented operating temperature range. A combination of ceramic injection moulding and careful material engineering has led to sensors that have shown to be able to operate over a temperature range spanning -125°C to +125°C.

The titanium housing, 2mm sapphire window (and diodes that have been tested up to 1.1Mrad and 10^{16} 1MeV electrons) of the Bison74-ET-RH (figure 1) provided 3mm Aluminium equivalent circumferential radiation shielding. This, together with the extended temperature range, leads to sensors that are capable of surviving even the most demanding environments.

Figure 1: BiSon74-ET-RH

The test program (reported on in part 1 of this paper) showed a good survivability of the sensor, except for some issues with the epoxy glues. Consequently, new glues had to be found matching the extended temperature range. Another issue encountered was the fact that the laser cutting process of the thick membrane presented some issues with respect to laser damage on the coating. Together with the fact that a smaller FOV was better for most applications, this has led to a redesign of the Bison74-ET-RH to the BiSon64-ET. Thus, sensor has a thinner membrane, but in the meantime, it was realized that the tested 10^{16} 1MeV electron withstanding capability would allow to operate the sensors for hundreds of years in any selected orbit, even without the thick membrane.

EXTENDED TEMPERATURE SUNSENSOR DEVELOPMENTS

Further development and full qualification of the Bison64-ET was initiated in frame of an ESA GSTP program. There still was one critical issue to be solved, the extreme demand on accuracies for the membranes, mainly in relation to the laser cutting process of the sapphire wafers. A solution was found in a change to the sensors assembly strategy had to be revised: to change the high accuracies on dimensions of the (opto-mechanical) components to a more accurate monitoring and control system during assembly. This finally led to the development of the Mechanical Automated Membrane Aligner tool (MAMA tool in short).

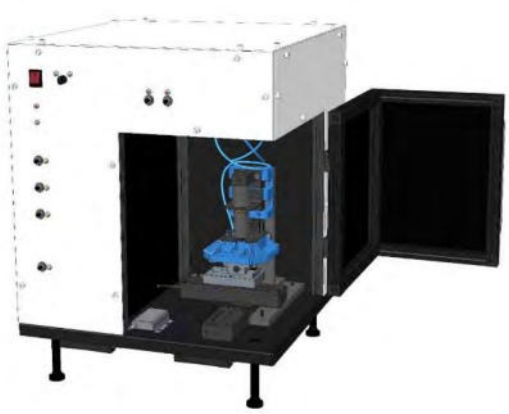

Figure 2: MAMA tool

This production tool will be used to actively align the membrane with respect to the sensor and basically consists of a X/Y/Z translation stage setup with a vacuum gripping system and a Sun-simulator.

The membrane and semi-finished Sunsensor are both placed on a special holder which can be translated in the X and Y direction and kept in place by means of vacuum. The Sunsensor is then connected to the readout electronic and after placing the membrane in the nominal pick-up position, the door is closed.

When the door is closed, the Z stage comes down and picks up the membrane. As a second step the membrane is lifted up and the sensor is positioned under the membrane at the nominal position. When nominally positioned, the membrane is lowered to the appropriate height above the sensor and the solar simulator is activated. The final positioning of the X,Y stage is then controlled in such a way that the membrane is positioned exactly centred above the photodiodes quadrant. When properly positioned, the

Z-stage lowers the membrane to its mounting surface on the sensor and the already applied UV curable glue is cured by switching on the integrated UV light sources. After the UV-curing process the membrane cannot shift with respect to the diodes anymore and the sensor assembly process can be completed by thermally post curing the glue.

In this way, the product can not only be produced with very high repeatability, but also the Zenith error will be significantly reduced, thus increasing the non-calibrated accuracy.

Figure 3: BiSon64-ET and BiSon64-ET-B

All extended temperature Sunsensors (BiSon64-ET and the baffled version BiSon64-ET-B) will be assembled using this tool and assembly approach. While the ICD specifications, except for a slight increase in mass and dimensions of the baffle, have not changed, these products are drop-in replacements for the Bison64 sensors, however with a much wider temperature range.

The sensors will be qualified using a full ESA ESCC-E-10-03C test flow but it has been agreed upon with ESA that after the full qualification, the acceptance testing of FM units will be done through LAT2 lot acceptance testing according to ESCC-Q-60-05 (hybrid circuit qualification), to avoid costly and time-consuming acceptance tests.

TEST PROGRAM

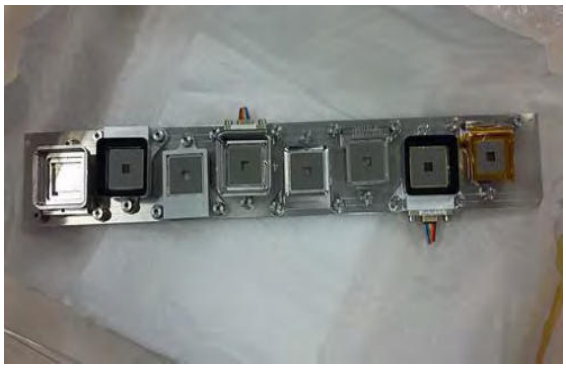

Figure 4: thermal cycling glue samples

In the meantime, several precursor tests on the selected glues have been performed, showing that the sensors with the updated glue selection are capable of surviving not only the severe temperature shock test performed by heating the parts up to +125°C and then dipping them in liquid nitrogen, but also 36.000 thermal cycles between -90°C and +95°C (which is equivalent to 7 years in LEO orbit). The maximum rate of change during the thermal cycling test—has been >15°C/min, which means the sensors are proven to be very resilient to temperature change

The thermal cycling test was performed at ESTEC by putting the samples in the same thermal cycling tests as the solar panels for the LuxSpace ESAIL mission.

The qualification program currently running is largely in line with ECSS-E-ST-10-03 and shown in Figure 5.

An additional 10 thermal cycles test was added before vibration testing to mimic the loads provided by the on-ground thermal balance testing. This reduces the risk for the

total test program, as it ensures that any failures in the bonds will be found early in the test program, avoiding costly retests to the largest extend possible.

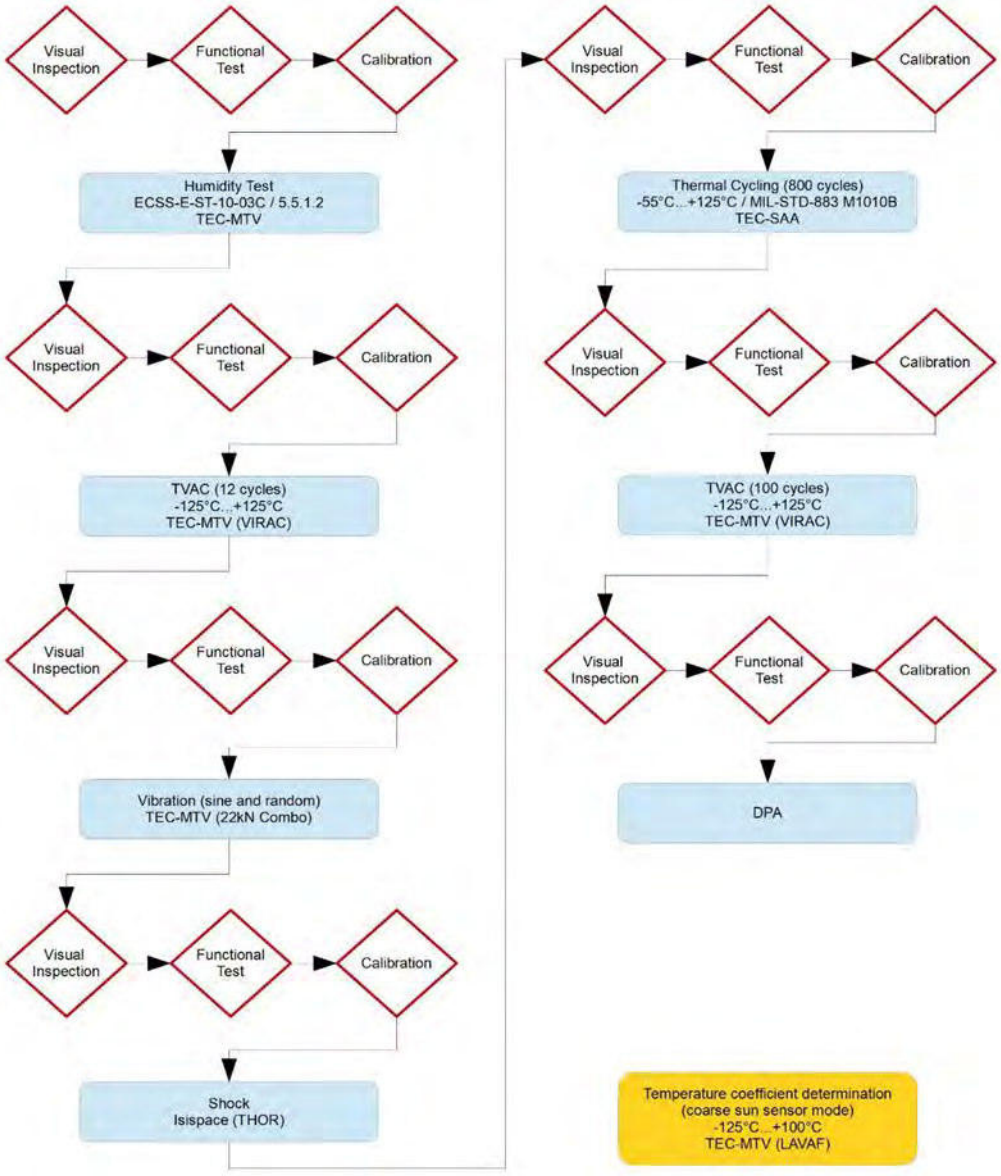

Figure 5: Bison64-ET Test Sequence

CONCLUSIONS

The earlier completed Artes 5.2 program in combination with the glue testing has shown that it is possible to produce *Sunsensors* that can withstand the large temperature excursions associated with direct solar panel mounting or interplanetary missions. The high radiation tolerance (240Mrad tested at diode level) and provided 1mm aluminium equivalent shielding will allow to use these sensors in high radiation environments. This combination qualifies the sensors for just about any mission conceivable. Flight standard sensors have been produced and are currently being put through a full qualification program. Upon completion of this qualification these sensors will have proven to be able to:

"boldly go where no Sunsensor has gone before."

Debunking Sunsensor specifications

Johan Leijtens, Stefan Schmidt, Lens Research and Development

‘s-Gravendijckseweg 41b 2201CZ (The Netherlands)

Email: jls@lens-rnd.com Tel: +31 (71) 2020 123

Abstract: Sunsensors are core components for most Launch and Early Orbit (LEOP) and Safe modes of operation for satellites. As such, these components are to be considered critical safety components. The core requirements for such sensors are related to reliability as well as pointing accuracy.

Based on comparison of many datasheets, evaluation of several technological implementations and measurements performed on several real implementations, both Lens R&D and ESA have concluded that datasheets ambiguity exists in terminology between different datasheets, and performance specifications are not uniformly used. Currently, no ECSS or other standard terminology exists yet to provide a definition of Sun sensor performance specifications.

Following the confusion on how to specify a Sunsensor properly it is advised to write a dedicated standardisation document detailing how to specify a Sunsensor in such a way that the performance values given are relevant, easily verifiable and defined properly so different sensors of different manufacturers can be readily compared.

This paper describes the application of *Sunsensors* and several issues that need to be considered in order to be able to derive an independent specification.

1. SUNSENSOR APPLICATIONS

A Sunsensor is an attitude sensor that can measure the attitude of a satellite with respect to the Sun. Although almost all satellites employ Sunsensors, their application is generally restricted to use during the LEOP and safe mode operations phases. This is mainly due to two reasons:

1) A Sunsensor cannot determine the rotation around the Sun-axis and consequently requires an additional attitude sensor to determine the full attitude of a spacecraft.
2) The accuracy of a Sunsensor is generally limited due to inaccuracies caused by albedo signals.

The reason why Sunsensors are still used, despite these drawbacks is the fact that the are generally very simple and therefore can be very robust. In addition to this, the Sun provides a very high signal to noise ratio signal that can be used to measure the attitude even at very high spin-rates. This allows to recover satellites that have gone into a high spin-rate mode due to an anomaly during orbit injection or due to a subsystem failure where star tracker-based systems lose the ability to provide a reliable solution. In general, this recovery means pointing the solar panels to the Sun so as to ensure a positive power balance during the anomaly recovery.

Only in very rare occasions a Sunsensor is used as the prime attitude sensor. In these cases, the attitude knowledge is generally driven by the sensor providing information about the third axis (most often an Earth-sensor or magnetic field sensor). This type of solution is only viable when an attitude error in the order of a few degrees is acceptable.

The last common application of Sunsensors is that of anomaly detector used to prevent the Sunlight from entering the aperture of sensitive instruments in case of an attitude failure. This again is a safe mode type of operation but generally used to shutter the aperture or in rare cases to directly activate the propulsion system so as to avoid satellite destruction (like in the case of the BepiColombo and Solo missions).

2. SUNSENSOR ACCURACY

According to the authors of this article, there is only one true definition of accuracy, and that is the difference between the true Sun aspect angle and the measured angle. Both of these angles shall be taken with respect to the mounting surface of the sensors or in case of availability to an optical reference plane provided (like a corner cube).

For an analogue fine Sunsensor, there are various effects that will lead to a deviation from the nominal value, like X/Y or Z diode-to-membrane displacements, component tilts and internal reflections. Many of these will also show some temperature dependence or aging due to thermal cycling and cosmic radiation effects. The specified accuracy of the sensors will have to take all of these effects into account. The errors caused by these effects can be in majority mitigated by adding offset and gain compensations in the formula used to calculate the actual pointing angle, but residual effects will cause a profile that can only be corrected by means of local interpolation and using error tables generated during calibration.

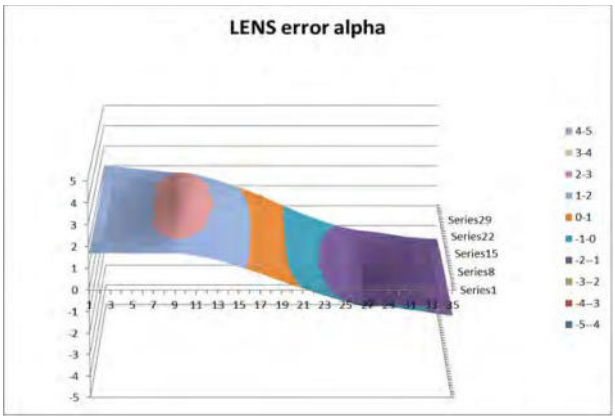

•Non calibrated

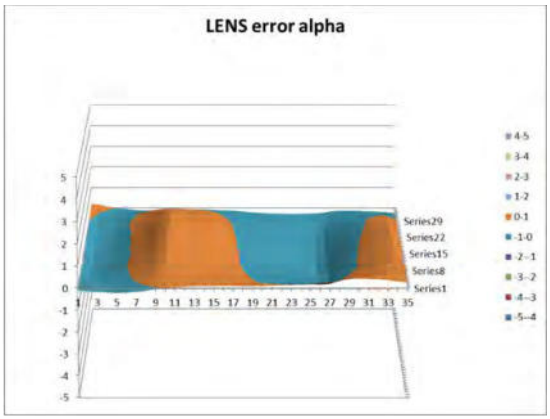

compensated

Above graphs show the error in degrees (Z axis) versus the error on the α angle (or X axis angle) measured over the two-dimensional field of view of a typical BiSon64 sensor (X/Y axis). As these measurements are BOL at 20°C, temperature and aging effects will have to be accounted for in the error budget while specifying overall accuracies. This means that either a correction value shall be provided, or multiple calibration tables. Providing calibration tables for aging or radiation effects however is not considered to be feasible because of the non-deterministic nature of the change. Therefore a budget allocation can only be made by an educated guess. The specified accuracy for the sensor however should be end of life and over temperature and aging

3. CALIBRATION ISSUES

There are several known serious issues related to the calibration of analogue Sunsensors especially when the source is an arc discharge lamp:

- Source flicker
- Bundle homogeneity
- Straylight
- Mechanical accuracy

Source flicker is a serious issue observed in arc discharge lamps causing the need for simultaneous samplers and averaging many measurements before a stable measurement is obtained. In general arc discharge lamps are driven by DC currents to avoid excessive electrode erosion but plasma oscillations, thermal runaway and localized electrode erosion cause significant intensity variations. Next to this many sources are poorly regulated, causing arc flickers at double the mains frequency. Therefore, it is in general necessary to take all samples at the same moment in time to minimize the effect of to the high variability of the momentary intensity (simultaneous sampling). In addition to this, it is generally needed to average thousands of samples taken before a measurement stability is achieved which is high enough to be confidently used as a measurement value.

As the arc of an arc discharge lamp is never at the same spot for a longer period of time, heating up the lamp for several hours does increase average output stability, but it does not increase the bundle homogeneity. This leads to errors in the calibration that will vary over time and will lead to non-repeatable measurements.

As an analogue Sunsensor merely determines the barry-centre of the impinging light, any straylight or calibration setup internal reflection will influence the outcome of the calibration. In order to have an accurate calibration, it is not sufficient to have a highly repeatable calibration, because reflections (causing straylight) can be very repeatable over time but still influence the accuracy to a much larger extend than the re-calibration repeatability would lead to believe.

Despite the fact that accurate rotation stages can be bought one has to be very careful during selection of the stages for a calibration setup. As for the Sunsensors themselves, it is easy to confuse resolution with accuracy and often the real performance of a rotation stage determined by the backlash in the driving system rather than the resolution. In order to demonstrate an accuracy of 0.5° for a Sunsensor it is good practice to limit the mechanical budget to less than $1/10^{th}$ of this. For high accuracy Sunsensors this leads to very stringent requirements on the mechanical setup which can only be obtained within a limited temperature range. For high levels of accuracy, settling of residual stresses and other relaxation effects can prove to be of influence and regular mechanical re-calibration is required.

Given the difficulty to perform a repeatable calibration, and the need to have a repeatable calibration before it can be accurate, it is obvious that people focus on producing stable calibration values first. From the quoted specifications however, it seems as often calibration repeatability is confused with accuracy when quoting sensor performance.

A lot of these uncertainties could be mitigated by asking the suppliers to specify a number of core properties independently (like accuracy, resolution, re-mounting accuracy, EOL and BOL accuracy) so as to be able to discriminate between accuracy and repeatability and see the aging effects taken into account

4. RESOLUTION AND NOISE

For Analogue Sunsensors, (unless very small diodes are used or the sensitivity is spectrally limited) resolution and noise are seldom an issue. This is because the generated signals in general are relatively high in magnitude. A current of 1.6mA is equivalent to 10^{16} electrons per second which means the shotnoise limit is in the order of $1/10^{8}$ and consequently both noise and resolution are negligibly small.

Given the high signal to noise ratio, the resolution of the sensor is in general limited by the resolution of the readout electronics. An Adcole Maryland high accuracy fine Sunsensor (https://www.adcolemai.com/high-accuracy-fine-sun-sensors) needs 100.000 bits to cover the 100° FOV at a resolution of 0.001°/bit or 17 bits. The quoted accuracy of 0.01° would require a 13 to 14 bit accuracy and despite the fact that there are electronic components that could reach this type of performance, and the noise generated by the sensor would allow for such performance, it is highly unlikely that a calibration can be performed where the straylight levels are below $1/10000^{th}$ of the primary beam intensity. If the straylight rejection of the calibration setup is not low enough the accuracy of calibration will not be high enough. At Lens R&D we have re-calibrated the same sensor ten times and every measurement taken in a 37x37 matrix over the 2-Dimensional field of view was within 0.0006° (which shows a very high degree of repeatability) yet we only specify a 0.5° accuracy.

SYSTEM REQUIREMENTS

As power production of the solar panels is ruled by the cosine law, in general a 3° to 5° accuracy is acceptable (cos(95°)= 0.996). The main reason for this is the fact that the sensors are inputting their data into an attitude control subsystem with a low bandwidth. As a consequence, any false inputs will lead to an error injection that can have an effect on the satellite attitude long after the wrong measurement has been taken. Bearing this in mind, one should be very careful in sensor placement to avoid albedo signals from providing a massive input disturbance. Even though it is generally preferred to have an as wide as possible field of view, it should be noted that Earth Albedo input significantly increases with the field of view. Consequently, a sensor with a baffle is generally preferred over a sensor without baffle and a sensor with a smaller field of view could eventually lead to a faster attitude acquisition due to the lower input disturbance.

Last but not least it should be realized that the sensor is used in closed loop. Generally, the gain factor is taken into account during loop design but the gain margin of the loop depends on the scale factor of the sensor. Therefore, the profile should be as smooth as possible and in no case the profile is allowed to become flat or reverse as this would lead to limit cycling or loop instability. In a similar way, too low a resolution on the Sunsensor data could lead to limit cycling (although a significant amount of filtering can be used to increase the actual resolution) and adding resolution to the output can be advantageous as long as the resolution is not such that the dynamic and integral non linearities become larger than 1 bit.

5. CONCLUSIONS

Without a proper definition of properties like accuracy, repeatability, resolution and long-term drift, it is very difficult to compare Sunsensor performances. Next to this, care should be taken that relevant properties are taken into account and not properties that are in actual fact more related to the properties of the test setup than to the properties of the actual sensor (like repeatability of calibration).

Cognitive Navigation

Adam Yingling[1], Evan Ward[2], Trey Morris[3], Gurpartap Sandhoo[4]

[1]Naval Research Laboratory
4555 Overlook Ave. Washington D.C., USA
Phone: +01 202 253 0370, Mail: adam.yingling@nrl.navy.mil

[2]Naval Research Laboratory
4555 Overlook Ave. Washington D.C., USA
Phone: +01 202 279 4365, Mail: evan.ward@nrl.navy.mil

[3]Naval Research Laboratory
4555 Overlook Ave. Washington D.C., USA
Phone: +01 202 279 5119, Mail: Trey.Morris@nrl.navy.mil

[4]Naval Research Laboratory
4555 Overlook Ave. Washington D.C., USA
Phone: +01 202 404 2701, Mail: gp.sandhoo@nrl.navy.mil

Abstract: Cognitive navigation proposes an image processing architecture utilizing machine learning, precision in-situ metrology [1], and on-board processing to provide precise Earth-Centered Earth-Fixed (ECEF) navigation solutions for Earth-observation platforms in space. Similar to XNAV [2] [3] [4], the spacecraft navigation solution is derived independent of all external systems; including the Global Positioning System (GPS). Unlike XNAV, however, cognitive navigation enables solutions that are more precise and minimize the need for additional size, weight, or power (SWaP) on the spacecraft. The same navigation processes also quantify observatory misalignments and enable autonomous spacecraft calibrations. The Naval Research Laboratory (NRL) has demonstrated the ability of similar neural networks to recognize objects on the Earth using flight-like electronics and is developing a cognitive navigation testbed to mature this technology for ground demonstrations. The testbed will consist of flight-representative hardware and software, hereafter referred to as a "spacecraft" that can point and image a simulated Earth-scene in the lab. The "spacecraft" will then use the information from the scene, along with the spacecraft's state and time, to determine its position relative to the Earth. The "cognitive" aspect of this process comes from the system's ability to discern knowledge and understanding through its senses and experiences. Meaning, in order to maintain long-term autonomy, the system must learn and update its experiences. The system develops experience as it gathers information over time, which is stored in the form of databases, mathematical models, and convolutional neural network (CNN) weightings. This allows objects to be recognized and geospatially understood. The goal of a cognitive system is to enable it to self-identify changes on the Earth, update its own knowledge, and share that knowledge with other systems. The cognitive navigation testbed will mature these concepts through long-duration tests in a controlled laboratory environment; in doing so, the testbed will assess and quantify system-level performance and sensitivities to variations. Cognitive navigation is a new approach to flying Earth-observation satellites that, once successful, will enable complete spacecraft autonomy, vastly improving data collection, simplifying operations and lowering overall lifetime costs.

1. THE MOTIVATION FOR COGNITIVE NAVIGATION

Artificial Intelligence is an enabling technology that can be applied to increasingly complex problems. Autonomous navigation has been around for long time, and the role of informatics in controlled flight has been discussed for over 50 years [5]. Inertial [6] and "autonomous navigation" paved the way for aerodynamic flight, cruise missiles, lunar flight, and interplanetary spacecraft. As the rate of change of technology maturation has increased and navigation is no longer a unique aerospace application, the advances that have been made in terrestrial navigation can be implemented into space systems. It is being used to create advanced adaptive automation and analytical tools. The navigation of robotic systems in natural, unstructured terrain has been a subject of extensive research [7]. Additional research has been done for automobile navigation focused on landmark-based navigation, which is a natural navigation concept for humans. A number of algorithms have been implemented in spacecraft for mission tasking, where onboard decision-making detects science events and respond autonomously to capture short -lived science events [8]. The Naval Research Laboratory (NRL) team is leveraging a number of these technologies to develop cognitive navigation for space systems, the ability for a navigation system to provide information about the states of a space vehicle without the need for a priori infrastructure such as Global Positioning Satellites (GPS), beacons, or an external map. The end goal is to have systems that can self-navigate and self-task, based on the knowledge they have gained through the learning process.

2. DEFINING COGNATIVE NAVIGATION

Landmark navigation uses recognizable terrestrial features to determine the course of a vehicle. Under visual flight rules (VFR), pilots use this form of navigation, along with their own cognitive abilities, to determine their current position and predict their future position. This navigational method, termed "dead reckoning" [9], draws from what the pilot already knows to determine what the pilot does not know. Figure 1 highlights the components used for dead reckoning.

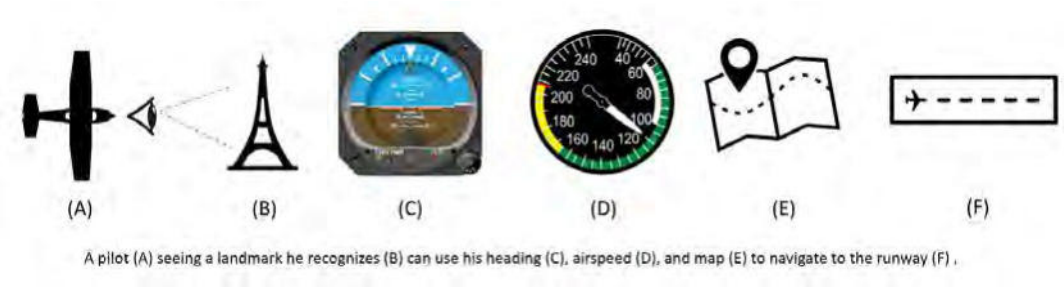

Figure 1: Dead Reckoning Components

The dead reckoning technique differs from other navigation techniques in that it minimizes the aviator's dependence on external infrastructure. In fact, during the early years of flight, navigational aids such as Automatic Direction Finder (ADF), VHF Omnidirectional range (VOR), or Global Navigation Satellite System (GNSS) did not exist. While these systems improve navigational accuracy, a pilot must always be able to fall back on the fundamental navigational skill of dead reckoning in the event that these enhancements

become unavailable. Dead reckoning is a simple and efficient approach to flight that even holds true for space flight.

The Apollo program depended on landmark navigation for calibration and back-up navigation [10]. Figure 2 shows the schematic for a space sextant. It allowed Apollo astronauts to measure the angle between a landmark on the Earth or moon and a star to determine their orbital position.

In order for a machine to fly independent of external infrastructure, thereby achieving full-autonomy, it must not only follow a similar process to the one depicted in Figure 1, but it must also be able to update its knowledge-base of objects (B and F) and maps (E) over time to fly reliably .

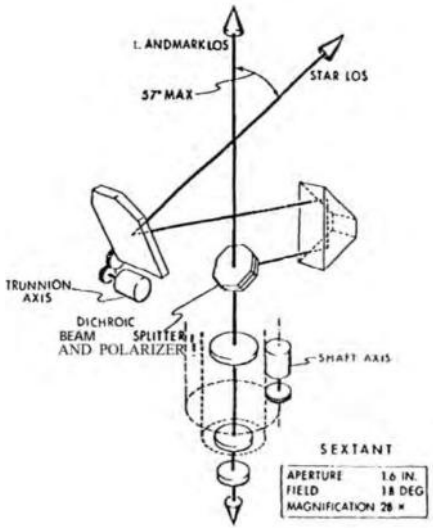

Figure 2 (above): Apollo Space Sextant; Credit [10]

As will be discussed, NRL has demonstrated the recognition process depicted in B of Figure 1 using convolutional neural networks (CNNs). While this process is rather intuitive for an aviator, the reliability of CNNs to identify objects remains low in the face of variable conditions such as lighting, atmosphere, and scene clutter. This is similar to the human visual system in that it too is subject to false positives, misidentifications, and faulty interpretations. Subconsciously, however, humans use additional context to aid in visual interpretation. Figure 3 shows three common examples of object misidentification (optical illusions).

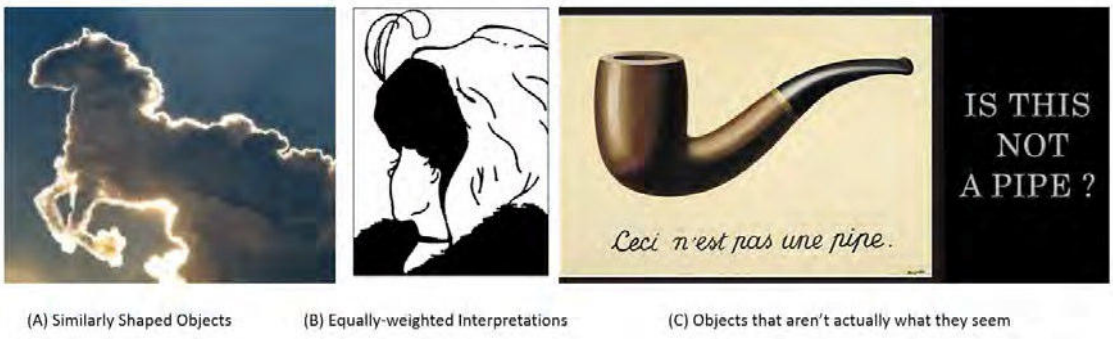

Figure 3: Common Visual Cortex Misinterpretations, credit [11] [12]

Figure 3 (A) shows what most of us would immediately identify as looking like a horse, while being intellectually aware that it is actually a cloud. Figure 3 (B) shows a drawing that can be interpreted as either an old woman with a large nose looking to the left, or a young lady wearing a necklace looking away from the camera. Obviously, Figure 3 (C) is not actually a pipe. It is a picture of a pipe. As we are all astutely aware, all of the figures in this paper only depict objects, and are not the objects themselves.

Similarly, an additional level of reasoning is required to prevent a machine from allowing sources of noise to alter its interpretation of an image. The Oxford dictionary defines "cognition" as the mental process of acquiring knowledge and understanding through

thought, experiences, and senses [13]. By analogy then, one approach to improving reliability is to supplement the "thought process" from which the machine makes a decision with contextual reasoning.

Particularly for aviators, an understanding of the context in which the data was collected and interpreting it with the aid of past-experiences is required to help them make better decisions. It is with this perspective in mind that this paper will discuss the development and testing of a machine-learning architecture, termed cognitive navigation, which autonomous Earth-observing platforms can utilize to navigate in low Earth orbit (LEO) efficiently, reliably, and fully autonomously.

3. AUTONOMOUS ORBIT DETERMINATION (AOD)

Determining the position of a satellite with respect to the surface of the Earth is essential for any remote sensing mission as this information is used to geolocate the payload's observations. For autonomous orbit determination (AOD) to be useful and effective for LEO remote sensing missions it must have three key qualities. First, AOD must determine the location of a satellite with respect to Earth's surface that is in the Earth fixed frame. Determining the satellite's position in the inertial frame is often a step towards determining the Earth fixed ephemeris, but accurate inertial orbit determination alone is not sufficient to accomplish the mission. Second, the AOD process must produce a precise and accurate solution. The desired accuracy depends on the specifics of the mission, but the goal is around 10 meters post-processed root-sum-square (RSS) since that level is commonly achieved with a GPS receiver. Third, the AOD process must be fully autonomous, that is it cannot depend on the correct operation of any systems external to the satellite including other satellites, ground stations, and operators. Using current technology, any two of these three key qualities are achievable, as the following section describes.

Currently most satellites rely on the GPS to determine their position on-board. Satellite GPS receivers provide accurate position fixes in the Earth fixed frame, but the GPS requires extensive infrastructure with its satellite constellation and globally distributed ground network, as well as human in the loop command and control, so the GPS is not an autonomous navigation technology. The same applies for other global navigation systems such as DORIS, GLONASS, Beidou, or Galileo.

Many celestial navigation methods have been proposed that use stars, natural satellites, or other measurement types not linked to Earth's surface to perform OD in the inertial frame. These methods use knowledge of the satellite's attitude in the inertial frame, provided by a star tracker, as well as directions to two or more "close" objects to generate a position fix. Some of the easiest to implement methods use a Sun sensor and a Earth sensor, as described in [6], or a Sun sensor and a magnetometer as presented by [14] [15] [16]. Stellar refraction at Earth's limb can be used a more precise Earth sensor, achieving inertial accuracies in the tens of meters as demonstrated by [17] [18]. Using moons and planets in various forms has been described by many authors including [19]. In [20] Battin describes several methods for measuring the direction to another body and includes measuring the apparent angular size of the body to provide a coarse range measurement. Of historical note, Battin recounts how Jim Lovell, with the aid of a space sextant, see Figure 2, used these types of celestial measurements to navigate Apollo 8 to the Moon and back.

Other artificial satellites in stable well-known orbits may be used in place of natural satellites and typically provide better precision because of their greater angular motion, as described in [21] [22] [23].

While these celestial navigation methods can be quite accurate and relatively autonomous, they require additional information to provide the satellite's location in the Earth fixed frame. The Earth Orientation Parameters (EOP) needed for the inertial to fixed transformation come from an external source, which means the system is no longer autonomous. Ignoring EOP updates leads to errors that start around a couple hundred meters at Earth's surface and grow over time, as shown in Figure 4.

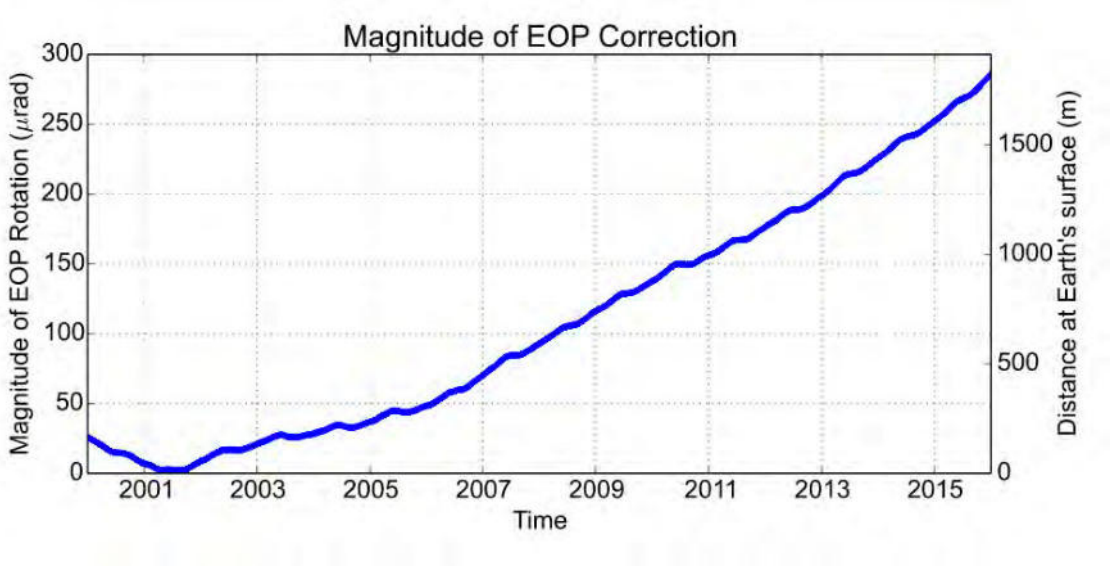

Figure 4: Earth Orientation Parameter (EOP) Error

Figure 4 shows the error due to ignoring EOP based on historical data. In contrast to celestial navigation, landmark navigation directly measures features on Earth's surface and therefore provides information on the satellite's position in the Earth fixed frame.

In 1981 Markley proposed an imaging satellite in [24] that performed AOD using only landmarks to solve the "survivability-vulnerability problem". He estimated that the proposed AOD method could achieve better than 2 km geolocation accuracy. In [25] Markley proposed augmenting the system by adding inter-satellite measurements to improve the geolocation accuracy below 100 meters. In both cases, the system simulations were only tested over 6 hours, leaving unanswered questions about the long-term behavior of such an AOD system. In [26] [27] Li et al. analyze a proposed AOD system that uses only images of Earth landmarks and estimate it has an RMS accuracy of 72 m.

Starting with the Near Earth Asteroid Rendezvous mission to Eros, landmark OD has proven effective for determining the location of the satellite with respect to the asteroid's surface. Improvements were made in the ground processing by using automated feature extraction and orbit determination, as described in [28] [29]. Researchers seeking to use LIDAR for autonomous asteroid landing describe their proposed system in [30], which achieves meter level accuracy, though it is much closer to the asteroid than typical LEO

applications of AOD. Though significant progress has been made in AOD there has still not been a demonstration of accurate AOD in LEO.

4. MACHINE LEARNING ARCHITECTURE

Much work has been accomplished in applying artificial intelligence to image processing applications [31] . NRL successfully applied Google's Inception Net [32] for object detection using space-compatible electronics [33]. Although speed and robustness will require further development for use in a fielded system, implementation onto a small LEO observation platform appears feasible. Figure 5 shows the envisioned machine learning architecture required to enable cognitive navigation.

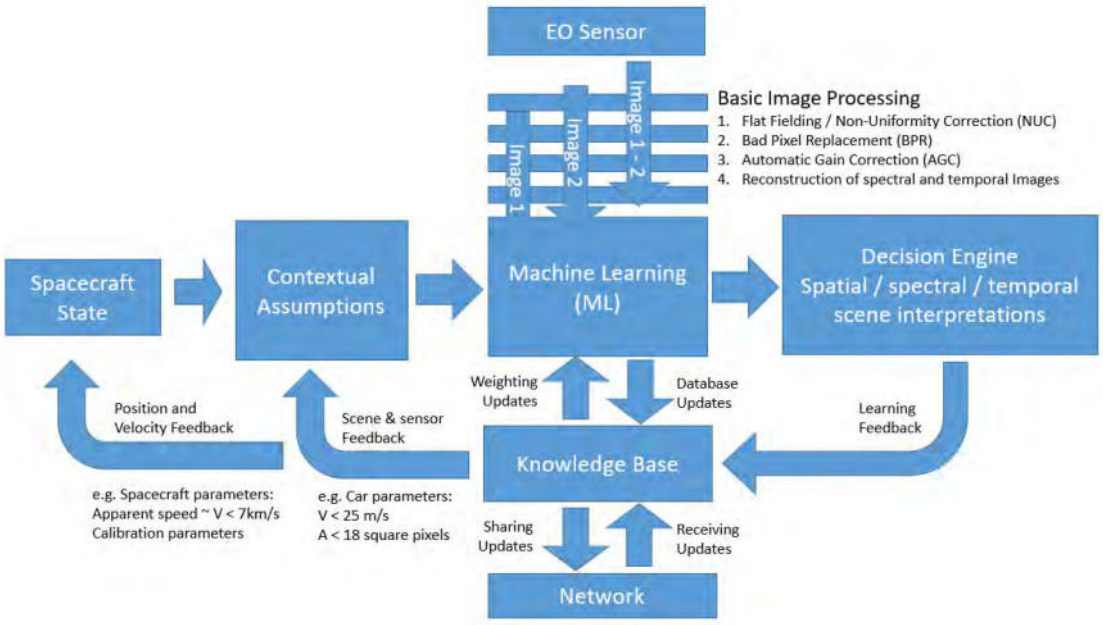

Figure 5: Cognitive Navigation Architecture.

At the top of Figure 5 is the electro-optical (EO) sensor streaming image frames. The system must process these frames in near real-time and apply the following basic image-processing techniques:

1) Flat fielding or non-uniformity corrections (NUC),
2) Bad Pixel replacement (BPR),
3) Automatic-gain correction (AGC) and,
4) Spectral image reconstruction for pixel-masked focal planes.

After these initial processes, the machine learning (ML) block depicted in the center of Figure 5 mines the images for information that is useful for satellite navigation and observatory calibration [34]. The algorithm(s) used in this block would include automated learning techniques similar to those described by [35].

The Decision Engine block interprets multiple results together to infer a higher-confidence answer. For example, assuming a red, blue, green (RGB) sensor, a high digital number in the blue frame would reinforce the assumption that the observatory imaged the ocean. Additionally, the decision engine would also check for and identify spatial aliasing that may occur due to limitations of the EO sensor, potentially vetoing results from the ML block. After interpretation, the Decision Engine updates the Knowledge Base.

The Knowledge Base seeds the spacecraft operations with expectations and assumptions. In this block, the system retains a memory consisting of mathematical models and neural network weightings that are both time and geometry-dependent. This would allow the system to expect variations more readily. For example, the system will be able to predict the variability of the shadows cast by a tall building and identify landmarks more reliably. The system would also retain a worldwide database of object locations for calibrating its alignments and orbital parameters over time.

Although the prime directive of the Decision Engine is to enable fully autonomous navigate by locating itself in space, it will also be also need to compare objects in the scene with objects in the knowledge base to keep its database current. As annotated in Figure 5, the system can both share and update its knowledge base with an external network, as connectivity allows.

The Contextual Assumptions block in Figure 5 offers real-time assumptions to the ML block. These assumptions are informed by the models in the Knowledge Base and real-time spacecraft position, velocity, and attitude. Contextual parameters include information about how the image was collected, like integration time and the scene distance, to improve interpretations. For example, for a given image, the apparent speed for a vehicle traveling 25m/s might be 70 pixels/s across the focal plane.

While the contextual assumptions can be thought of as Bayesian Priors, we do not need to specifically mathematically assign them such a rigorous definition at this time. These additional parameters are to better bound and focus the ML model and protect it from the case of being very certain but very wrong (e.g. identify the edge of a runway from London in the middle of an image of the Pacific Ocean). The output of the ML block should be a mathematically-rigorous true probability and confidence interval of the identity of pixel group X as being the geolocation of some known pixels when compared with the Knowledge Base. While current in vogue Deep Networks do not output such a mathematically founded score, it is imperative for the navigation algorithm to have such bounds. As a result, a great deal of path-finding work will be done on the mathematical foundations of ML.

Consequently, the architecture depicted in Figure 5 will make mathematically-bounded decisions of next processing steps that are human-explainable and will do so using the laws of orbital dynamics and information theory but adjustable to account for un-modeled affects, such as variable drag. This continuously updating and decision-making architecture is therefore believed to be robust to problems with low amounts of training data and will be essential for highly variable datasets where geometries, lighting conditions, and the objects in the scene itself are constantly changing with time.

5. FLIGHT SIMULATIONS FOR TESTS AND TRAINING

NRL is developing a generalized Earth-Observation testbed that is adaptable to various spacecraft hardware and software configurations. This is necessary in order to mature the cognitive navigation concept described in the previous sections. Figure 6 shows the testbed layout.

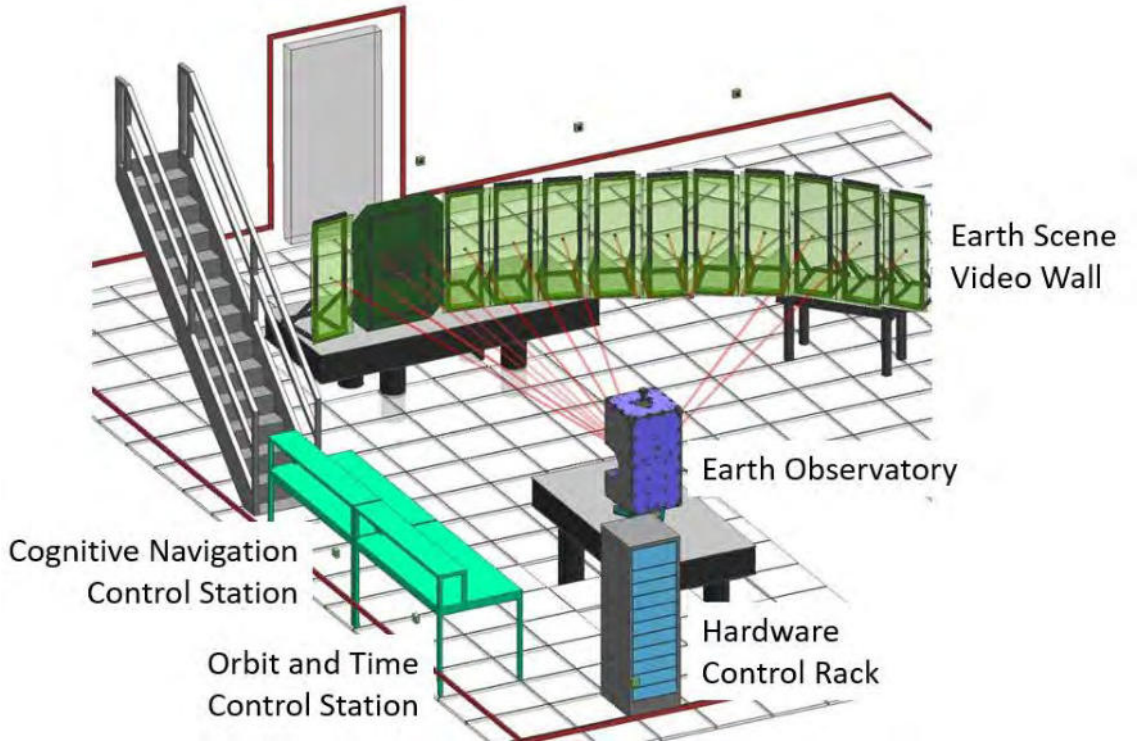

Figure 6: LEO Flight Simulator (LFS) Testbed

As depicted in Figure 6, the testbed is able to steer the observatory's line of sight (LOS) across the Earth-scene to simulate spacecraft bus attitude. The Earth Observatory consists of flight-representative hardware and software, hereafter referred to as a "spacecraft" that can point and image a simulated Earth-scene in the lab. The spacecraft will then use the information from the scene, along with the spacecraft's state and time, to determine its position relative to the Earth.

A high-resolution video wall, annotated in Figure 6, will display a photo-realistic Earth video for the spacecraft to image. Clouds, shadows, and atmospheric affects will be included in the rendered animation in order ensure the navigation solutions are robust under various operational conditions.

The testbed has two methods for maintaining alignment with the Earth Scene. First, the video wall can use the spacecraft's state information to adjust the rendered scene. Second, the testbed can use the beam steering mirror in front of the observatory's aperture to align the scene with the spacecraft's attitude. The testbed can also use the latter option to induce observatory misalignments that the system must detect and correct.

Initially, the testbed will provide time to the spacecraft to use as a part of its navigational solution. However, after the spacecraft has determined its position, it will then be possible to determine time precisely [36]. Long duration testing will be necessary to allow time to drift and determine if the system is able to detect and compensate.

Long duration testing is also required to update the knowledge base at time scales similar to those on Earth. Object models, particularly those the system uses to determine its position, need these updates in order for the system to remain properly calibrated.

The hardware control rack holds both the components for controlling the spacecraft's LOS and the system processing hardware required to execute cognitive navigation. The control rack is the interface between the spacecraft, the cognitive navigation control station, and the orbit and time control station.

The goal of the flight simulator is to provide a flexible test environment for developing the cognitive navigation concept. It will provide a high-resolution Earth scene to the spacecraft based on the orbit it simulates. This setup will enable long-duration flights for machine learning that is highly reconfigurable, predictable, and repeatable and is ideal for technology maturation and demonstrations.

6.0 CONCLUDING REMARKS

The cognitive navigation framework presented in this paper identifies how the Earth observation community can utilize machine learning to enable full spacecraft autonomy. The framework is generic and meant to encourage collaboration. While machine learning has enabled a significant degree of autonomous object recognition, there are still many challenges we need to overcome. The flight simulator testbed presented in this paper is currently under development and will be the proving grounds for realizing the cognitive navigation concept. Cognitive navigation is a new approach to flying Earth-observation satellites that, once successful, will enable complete spacecraft autonomy, vastly simplifying operations and lowering overall lifetime costs.

REFERENCES

[1] J. Kitching, "NIST on a Chip: Realizing SI units with microfabricated alkali vapour cells," in *8th Symposium on Frequency Standards and Metrology for the Journal of Physics: Conference Series 723 (2016) 012056*, Postdam, Germany, 2015.

[2] National Aeronautics and Space Administration (NASA), "NASA Team First to Demonstrate X-ray Navigation in Space," 11 January 2018. [Online]. Available:

https://www.nasa.gov/feature/goddard/2018/nasa-team-first-to-demonstrate-x-ray-navigation-in-space. [Accessed 10 April 2019].

[3] National Aeronautics and Space Administration (NASA), "Game Changing Development NICER/SEXTANT: The latest Incarnation of Celestrial-Based Navigation," March 2017. [Online]. Available: https://gameon.nasa.gov/gcd/files/2017/04/SEXTANT_FS_170414.pdf. [Accessed 10 April 2019].

[4] J. Mitchel, "X-ray Pulsar Navigation (XNAV) for Deep-Space Autonomous Applications," 16 February 2017. [Online]. Available: https://www.nasa.gov/sites/default/files/atoms/files/session_3_-_2_x-ray_pulsar_navigation_for_deep-space_autonomous_applications_jason_mitchell_0.pdf. [Accessed 10 April 2019].

[5] C. Draper, "The role of informetics in modern flight systems," *Journal of Spacecraft and Rockets,* vol. 3, no. 6, pp. 769-779, 1966.

[6] C. Draper, "Origins of inertial navigation," *Journal of Guidance, Control, and Dynamics,* vol. 4, no. 5, pp. 449-463, 1981.

[7] IEEE, "Learning for Autonomous Navigation, Advances in Machine Learning for Rough Terrain Mobility," *IEEE Robotics & Automation Magazine,* June 2010.

[8] S. Chien, "Autonomous Science on the EO-1 Mission," in *Proceedings of International Symposium on Artificial Intelligence Robotics and Automation in Space (i-SAIRAS)*, Nara, Japan, 2003.

[9] B. L. McNaughton, "“Dead Reckoning,” Landmark Learning, and the Sense of Direction: A Neurophysiological and Computational Hypothesis," *Journal of Cognitive Neuroscience,* vol. 3, no. 2, pp. 190-202, 1991.

[10] P. M. Kachmar, "Space Navigation Applications," Wiley Online Library, 1995.

[11] W. E. Hill, Artist, *Gestalt switch.* [Art]. 1962.

[12] R. Magritte, Artist, *The Treachery of Images.* [Art]. Los Angeles County Museum of Art, 1929.

[13] Oxford University, "Oxford English Dictionary," Oxford University Press, Oxford, 2019.

[14] J. a. H. R. a. B.-I. I. Deutschmann, "An innovative method for low cost, autonomous navigation for low Earth orbit satellites," in *American Institute of Aeronautics and Astronautics (AIAA) /American Astronautical Society (AAS) Astrodynamics Specialist Conference and Exhibit*, 1998.

[15] M. L. Psiaki, "Autonomous low-earth-orbit determination from magnetometer and sun sensor data," *Journal of Guidance, Control, and Dynamics,* vol. 22, no. 2, pp. 296-304, 1999.

[16] X. a. M. X. a. P. C. a. Q. W. a. F. J. Ning, "Analysis of Filtering Methods for Satellite Autonomous Orbit Determination Using Celestial and Geomagnetic Measurement," *Mathematical Problems in Engineering 2012 (2012), pp. 1,* p. 1, 2012.

[17] R. a. W. R. a. G. E. Gounley, "Autonomous satellite navigation by stellar refraction," *Journal of Guidance, Control, and Dynamics,* vol. 7, no. 2, p. 129, 1984.

[18] X. a. F. J. Ning, "An autonomous celestial navigation method for LEO satellite based on unscented Kalman filter and information fusion," *Aerospace Science and Technology,* vol. 11, no. 2-3, p. 222, 2007.

[19] A. a. L. D. a. F. D. a. G. C. Long, "Autono-mous navigation of high-Earth satellites using celestial objects and Doppler measure-ments," *Astrodynamics Specialist Conference,* 2000.

[20] R. H. Battin, "An Introduction to the Mathematics and Methods of Astrodynamics," *Revised Edition (AIAA Education) (American Institute of Aeronautics & Astronautics (AIAA),* 1999.

[21] M. L. Psiaki, "Autonomous orbit determination for two spacecraft from relative position measurements," *Journal of Guidance, Control, and Dynamics,* vol. 22, no. 2, pp. 305-312, 1999.

[22] J. R. a. C. J. L. a. J. J. L. Yim, "Autonomous orbit navigation of two spacecraft system using relative line of sight vector measurements," *Amerian Astronautical Society (AAS) Space Flight Mechanics Meeting,* 2004.

[23] K. a. B. G. Hill, "Autonomous Interplanetary Orbit Determination Us-ing Satellite-to-Satellite Tracking," *Journal of Guidance, Control, and Dynamics,* vol. 30, no. 3, p. 679, 2007.

[24] F. L. Markley, "Autonomous satellite navigation using landmarks," in *AAS/AIAA Astrodynamics Conference*, North Lake Tahoe, NV, 1981.

[25] F. L. Markley, "Autonomous Navigation Using Landmark and Intersatellite Data," in *AIAA/AAS Astrodynamcis Conference*, 1984.

[26] M. a. X. B. a. Z. L. Li, "Orbit determination for remote-sensing satel-lites using only optical imagery," *International Journal of Remote Sensing,* vol. 38, no. 5, pp. 1350-1364, 2017.

[27] M. a. X. B. Li, "Autonomous orbit and attitude determination for Earth satel-lites using images of regular-shaped ground objects," *Aerospace Science and Technology,* vol. 80, p. 192, 2018.

[28] Y. a. M. J. K. Cheng, "Autonomous landmark based spacecraft navigation system," in *AAS/AIAA Astrodynamics Specialist Conference*, Ponce, Puerto Rico, 2003.

[29] Y. a. J. A. E. a. M. L. H. a. O. C. F. Cheng, "Optical landmark detection for spacecraft navigation," in *2003*, Ponce, Puerto Rico, AAS/AIAA Astrodynamics Specialist Conference.

[30] H. a. X. S. Ma, "Only feature point line-of-sight relative navigation in asteroid exploration descent stage," *Aerospace Science and Technology,* vol. 39, p. 628, 2014.

[31] B. S. A. Z. E. O. Chapelle, Semi-Supervised Learning, London, UK: MIT Press, 2006.

[32] Google, "GitHub," Google, 26 October 2015. [Online]. Available: https://github.com/google/inception. [Accessed 10 April 2019].

[33] XIINX, "Zynq-7000," Xilinx, [Online]. Available: https://www.xilinx.com/products/silicon-devices/soc/zynq-7000.html. [Accessed 10 April 2019].

[34] B. M. Swinyard, "In-flight calibration of the Herschel-SPIRE instrument," Astronomy and Astrophysics (A&A), 518, L4, 2010.

[35] K. Xu, "Show, Attend and Tell: Neural Image Caption," in *Proceedings of the 32nd International Conference on Machine Learning*, Lille, France, 2015.

[36] K. Aksnes, "Navigation, world mapping and astronomy with Galileo's moons," in *International Astronomical Union*, 2010.

Magnetic Attitude Control of a Spinning Spacecraft Flight Results and Lessons Learned from DLR's Compact Satellite Eu:CROPIS

Ansgar Heidecker[1], Markus Schlotterer[2], Olaf Maibaum[3], Elisabeth Panzenboeck[4], Sebastian Löw[5], Markus Markgraf[6]

[1] German Aerospace Center (DLR), Institute of Space Systems
Robert-Hooke Str. 7, 28359 Bremen, Germany
Phone: +49 421 24420 1166, Mail: Ansgar.Heidecker@dlr.de

[2] German Aerospace Center (DLR), Institute of Space Systems
Robert-Hooke Str. 7, 28359 Bremen, Germany
Phone: +49 421 24420 1118, Mail: Markus.Schlotterer@dlr.de

[3] German Aerospace Center (DLR), Simulation and Software Technology,
Lilienthalplatz 7, 38108 Braunschweig, Germany
Phone: +49 531 295 2974, Mail: Olaf.Maibaum@dlr.de

[4] German Aerospace Center (DLR), Space Operations and Astronaut Training,
Münchener Str. 20, 82234 Weßling, Germany
Phone: + +49 8153 28 2725, Mail: Elisabeth.Panzenboeck@dlr.de

[5] German Aerospace Center (DLR), Space Operations and Astronaut Training,
Münchener Str. 20, 82234 Weßling, Germany
Phone: + 49 8153 28 3007, Mail: Sebastian.Loew@dlr.de

[6] German Aerospace Center (DLR), Space Operations and Astronaut Training,
Münchener Str. 20, 82234 Weßling, Germany
Phone: + 49 8153 28 3513, Mail: Markus.Markgraf@dlr.de

Abstract: The German Aerospace Center (DLR) launched on 3rd December 2018 the Euglena Combined Regenerative Organic food Production In Space (Eu:CROPIS) mission. Eu:CROPIS is a mission of DLR's compact satellite class with the objective to test several biological experiments at different levels of artificial gravity. The Eu:CROPIS mission carries experiments and payloads from University of Erlangen, NASA AMES and two DLR Institutes.

A dedicated magnetic attitude control system (ACS), which utilizes a spin stabilized concept, is part of the satellite to achieve this objective. The ACS is designed to handle the technical challenges imposed by the biological payload e.g. the inclusion of water tanks onto the satellite system. Especially during launch and early operational phase (LEOP) the ACS showed its effectiveness to even counteract unexpected anomalies. After that the ACS continued with nominal operation and performed the initial acquisition as expected.

1. INTRODUCTION

Eu:CROPIS is the latest mission within German Aerospace Center's (DLR) compact satellite program. Its major scientific goals are to test and characterize a sustainable life support system within harsh space environment at different levels of gravity. Beside the scientific goals DLR wants to establish key engineering capabilities in house to fully develop and lead a compact satellite program.

There are four payloads accommodated on board

- Eu:CROPIS - Euglena Combined Regenerative Organic food Production In Space [1] - Friedrich-Alexander-University of Erlangen-Nürnberg and DLR Cologne
- PowerCell – NASA Ames Research Center [2]
- RAMIS – RAdiation Measurment In Space – DLR Cologne
- SCORE – SCalable On-boaRd computing – an Experiment - DLR Bremen

The Eu:CROPIS satellite consists of a cylindrical central body with four deployable solar panels. The central body has a diameter of about 1 m and each solar panel can be deployed by roughly 1 m as well. The final satellite system has a mass of 226.62 kg [3] in orbit and a nominal power consumption of about 200 W [4]. Inside the satellite two greenhouse compartments are installed which operate at two different levels of gravity (Moon 0.16 g, Mars 0.38 g).

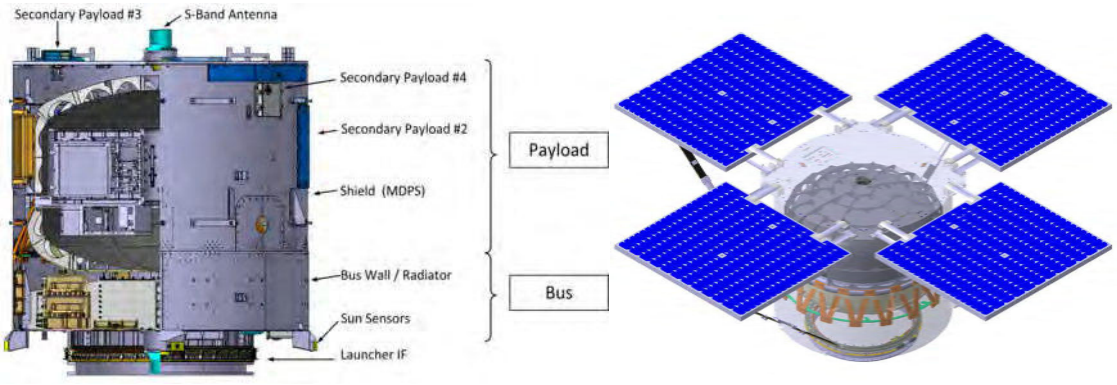

Figure 1 Eu:CROPIS satellite

The satellite is designed as a purely spin stabilized system to provide these different levels of gravity. The spin stabilization generates a centrifugal force which mimics the gravity at a predefined reference radius of 0.35 m. The greenhouses are installed in such a way that the cylindrical wall serves as the “bottom” for the biology.

2. ATTITUDE CONTROL SYSTEM

The spin stabilization is achieved purely by a magnetic attitude control system. There are three orthogonally arranged magnetic torquers on board. Each of them can provide an absolute magnetic dipole moment of 30Am². Beside the magnetic torquers two magnetometers, ten sun sensors, four angular rate gyroscopes and two GPS receivers are used as redundant sensors. An overview of all AOCS hardware components can be seen in Figure 2.

While the sensor and actuator selection follows a rather classical approach the challenging aspects during development are clearly the interface between the biological payload and the ACS. During the mission plants will grow and consume water which changes the Center of Mass (CoM) as well as the Moment of Inertia (MoI). In addition there are about eight liter [1] of liquids on board which could induce sloshing phenomena. Especially several pumps which transport liquids will induce a disturbance torque as well as a disturbing magnetic field.

Another challenging aspect for the ACS is the solar panel deployment. During deployment the satellite changes its MoI rapidly, which has to be taken into account. Therefore the solar panel deployment is not executed autonomously, but requires some supervised interaction by the operations team on ground.

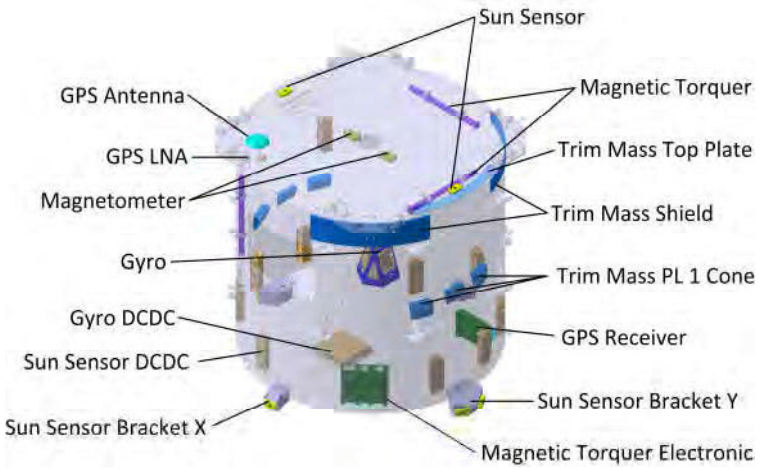

Figure 2 AOCS hardware accommodation within Eu:CROPIS

All of these aspects are addressed during design and development. They lead to a magnetic attitude control system design which enforces many requirements onto the satellite system design.

3. LAUNCH AND EARLY OPERATIONAL PHASE

Eu:CROPIS was launched at 03-Dec-2018 18:34 UTC with the SSO-A (Sun Synchronous Orbit-A) rideshare mission on a SpaceX Falcon 9 rocket. The German Space Operations Center (GSOC) of DLR was used as supervising ground control. During LEOP the ACS was monitored by six people in total, working in two shifts for a period of one week.

Eu:CROPIS was separated from the launching rocket shortly before 19:08 UTC. At this time the on board computer was being booted and the satellite started its operation. The first valid ACS measurements became available one minute later. From there on the ACS operated completely autonomously until a save attitude had been reached.

The first anomaly occurred during separation. The initial angular rate which was induced by separating the spacecraft from the launch system was significantly larger than expected. The first recorded angular rate on board of Eu:CROPIS was $\omega_{b,i}^{b} = [0.745 \quad -9.970 \quad 0.401]$ deg/s. This angular rate exceeded the designed initial angular rate (approx. 2 deg/s). Unfortunately this large angular rate was not recognized until a couple of days later. The reason therefor was that the offline housekeeping data processed inside the monitoring and control system is tagged by the on board GPS time. Due to the fact that the GPS receiver requires some time to provide a time fix, the initial separation phase had a time stamp around 6th December 1980, which is the starting period of the GPS epoch. At first contact, when the real time housekeeping could be directly seen by the operators, the angular rate was already decreased so far that no further action was required.

A classical Bdot controller was used for detumbling. It decreased the spin rate only, see [4] for further details. After the Bdot controller was automatically initiated it took approximately three hours to lower the angular rate magnitude below a threshold of 0.5 deg/s. Reaching this threshold the ACS switched to its spin-up mode.

The spin-up mode regulates the angular rate around the z-axis to a target value. The z-axis is designed to be the major moment of inertia axis. The target angular rate was set to 1 rpm providing a sufficient angular impulse against external disturbances. Eu:CROPIS managed to reach 1 rpm after approximately 2 hours. Eu:CROPIS was then being operated as a spin stabilized spacecraft and its spin-and-point mode was activated.

In spin-and-point mode the spin axis was aligned orthogonally to the satellite Sun vector. This maneuver took approx. 1.5 hours. Afterwards the initial autonomous acquisition phase was completed successfully from ACS point of view.

4. TRANSITION TO NOMINAL OPERATIONS

The moments of inertia were then recalibrated, and the satellite was aligned with its spin axis at a 60 deg angle to the Sun in preparation for solar panel deployment. The solar panel deployment took place at 05-Dec-2018 08:59 UTC. During the process the angular rate experienced an expected drop from 1 rpm down to 0.8 rpm. After deployment the spin rate was restored to 1 rpm, and the satellite's spin axis oriented towards the sun. Deployment, spin up and final orientation took approx. 4.5 hours.

The last step was to spin up the satellite to 5 rpm, which took about 16 h. By reaching 5 rpm the ACS was commanded into its spin-in mode, which is its nominal operational mode.

5. SUMMARY

The present paper gave an overview of the magnetic attitude control system of the Eu:CROPIS satellite. It elaborates on some challenges met during the design process and describes the launch and early operational phase form an attitude control system point of view.

6. REFERENCES

[1] J. Hauslage, S. M. Strauch, O. Eßmann, F. W. M. Haag, P. Richter, J. Krüger, J. Stoltze, I. Becker, A. Nasir, G. Bornemann, H. Müller, T. Delovski, T. Berger, A. Rutczynska, K. Marsalek und M. Lebert, „Eu:CROPIS – Euglena gracilis: Combined Regenerative Organic-food Production in Space - A Space Experiment Testing Biological Life Support Systems Under Lunar And Martian Gravity," *Microgravity Science and Technology,* Bd. 30, pp. 933-942, 9 2018.

[2] S. Richey und L. Rothschild, „Power Cell," 2015. [Online]. Available: https://www.nasa.gov/sites/default/files/atoms/files/powercell_fact_sheet_aug2015_0.pdf.

[3] S. Kottmeier, C. Hobbie, F. Orlowski-Feldhusen, F. Nohka, T. Delovski und G. Morfill, „The Eu:CROPIS Assembly, Integration and Verification Campaigns: Building the first DLR Compact Satellite," in *69th International Astronautical Congress*, Bremen, 2018.

[4] J. F. Pedersen, „Power System for the Eu:CROPIS Satellite,“ in *European Space Power Conference*, Greece, 2016.

[5] A. Heidecker, T. Kato, O. Maibaum und M. Hölzel, „Attitude Control System of the Eu:CROPIS Mission,“ in *65th International Astronautical Congress*, 2014.

Lessons Learned from Integrating the Dual-band Optical Transient Camera to Microsatellite RISESAT

Hannah Tomio[1], Morokot Sakal[1], Shinya Fujita[1], Toshinori Kuwahara[1], Alfred Bing-Chih Chen[2], Ted Wei-Tai Liu[2], Mike Chih-Chen Tsai[2]

[1]Tohoku University
Aoba 6-6-11, Aramaki Aza, Sendai 980-8579, Japan
Phone: +81 22 795 6991, Mail: htomio@dc.tohoku.ac.jp

[2] Institute of Space and Plasma Sciences, National Cheng Kung University
No. 1 University Road, Tainan City, 70101 Taiwan
Phone: +886-6-2757575 ext. 65915, Mail: alfred@isaps.ncku.edu.tw

Abstract: In January 2019, the Rapid International Scientific Experiment Satellite (RISESAT) was launched, marking the culmination of a project that spanned almost 10 years. Developed by the Space Robotics Laboratory (SRL) of Tohoku University, RISESAT was intended to demonstrate the rapid, cost-effective development and integration of a microsatellite bus system with numerous scientific payloads. To simplify the payload instrument-to-satellite bus interface, the Space Plug and Play Avionics (SPA) standards were referenced. This paper discusses the lessons learned during the payload-to-satellite integration using one payload in particular, the Dual-band Optical Transient Camera (DOTCam) developed by National Cheng Kung University (NCKU), to illustrate these points.

1. INTRODUCTION

In 2010, the Space Robotics Laboratory (SRL) of Tohoku University began the development of the Rapid International Scientific Experiment Satellite (RISESAT). Originally known as Hodoyoshi-2, the RISESAT project has its roots in the "Reasonably Reliable" (or *hodoyoshi*, in Japanese) micro- and nanosatellite systems concept, a Japanese FIRST (Funding Program for World-Leading Innovative R&D on Science and Technology) project under the direction of Professor Shinichi Nakasuka at the University of Tokyo [1]. The microsatellite, which is 50 by 50 by 50 cm in the stowed/launch configuration and has a mass of roughly 59 kg, was intended to demonstrate a cost-effective and reliable microsatellite bus system for scientific missions by hosting as payloads several different experimental scientific instruments from organizations around the world.

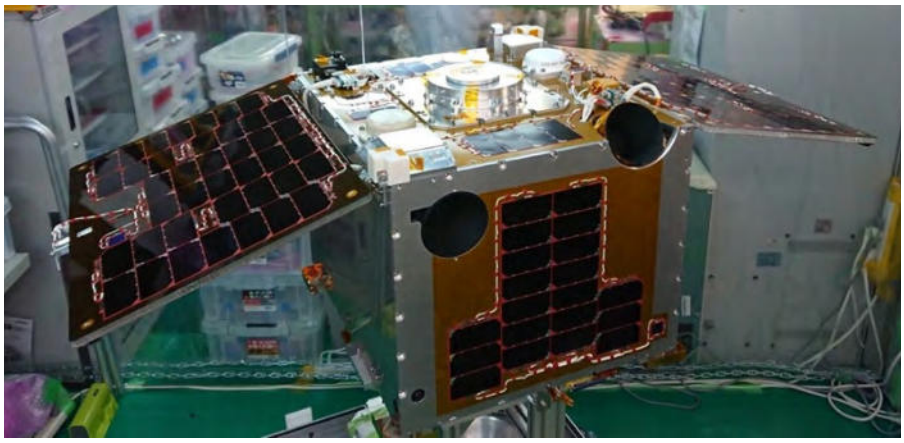

Figure 1. Flight model of RISESAT showing side solar panels deployed

At the time of inception, RISESAT had an expected launch date in 2013, and was slated to be the third 50-kg-class microsatellite developed by Tohoku University, following SPRITE-SAT [2] (renamed RISING-1 after launch in 2009) and RISING-2 [3] (later launched in 2014). Unfortunately, this launch opportunity was not realized. Another came only in 2016, when RISESAT was selected to be part of the "Innovative Satellite Technology Demonstration Program" run by the Japan Aerospace Exploration Agency (JAXA). By the time of RISESAT's launch in January 2019, it had long been preceded into space by other SRL microsatellites and CubeSats. The project had spanned almost a decade, and more than 30 SRL doctoral students, master's students, undergraduates, and interns had contributed to it – not to mention all of those involved with the development of the various payloads. In those 9 years, numerous technical and programmatic challenges were overcome, and many lessons were learned. This paper aims to elucidate a few of these experiences regarding the payload-to-satellite integration. To contextualize these points, this paper will focus on one payload in particular: the Dual-band Optical Transient Camera (DOTCam), developed by the Institute of Space and Plasma Sciences (ISAPS) at National Cheng Kung University (NCKU).

2. SPECIFICATIONS

The design of the RISESAT bus system is shown in Figure 2. While based on the SRL heritage designs of SPRITE-SAT (RISING-1) and RISING-2, the system was greatly adapted to fit the needs of the RISESAT mission. The main objective was the design of a reliable, low-cost microsatellite bus system that could still provide the necessary performance capability to support the requirements of the payloads [4].

In total, RISESAT hosts six payloads, the details of which are summarized in Table 1. A majority of these payloads are cameras that can generate large quantities of image data、which then needs to be stored and downlinked to ground. Several payloads also require precise pointing during their experiments – particularly the optical communications system, VSOTA. While all payloads were developed with the power limitations of a smaller satellite in mind, they nonetheless require a safe, robust power supply. These considerations, among others, drove the system design and necessitated the inclusion of components such as a mass memory unit (solid state recorder), high data rate X-band transmitter (XTX), fine attitude control system, and a fault tolerant power control unit (PCU) [5]. All of the payloads interface with the bus via a dedicated science handling unit (SHU), which is responsible for powering and providing data handling for the payloads.

Table 1. RISESAT payloads

Payload Name	Developer	Description
Very Small Optical TrAnsmitter (VSOTA)	National Institute for Information and Communications Technology (NICT), Japan	Lightweight laser signal transmitter for optical communications
High-Precision Telescope (HPT)	Hokkaido University, Japan, and National Central University, Taiwan	High spatial resolution multispectral imager
Ocean Observation Camera (OOC)	Hokkaido University, Tohoku University, Japan National Taiwan Ocean University, Taiwan	Multispectral wide field of view camera for ocean observation
Dual-band Optical Transient Camera (DOTCam)	Institute of Space and Plasma Sciences (ISPS), National Cheng Kung University (NCKU), Taiwan	Dual-band camera for imaging optical phenomena
Space Radiation Micro-Tracker (TIMEPIX)	Institute of Experimental and Applied Physics (IEAP), Czech Technical University,	Particle detector for space environment radiation characterization
Micro Monitoring Camera (MMC)	Tokyo University of Science, Japan	Small form-factor satellite monitoring camera

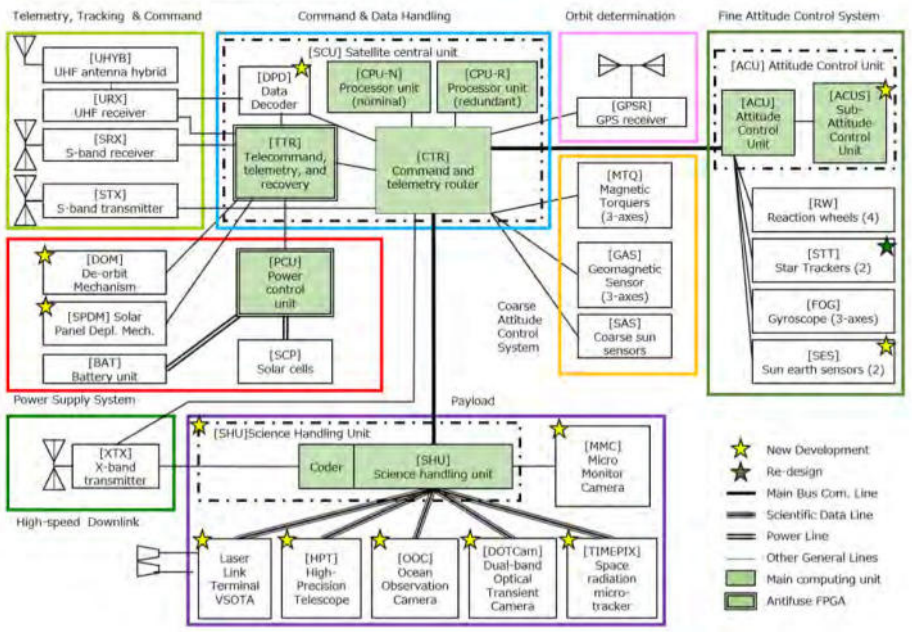

Figure 2. RISESAT system architecture

2.1 RISESAT Science Handling Unit (SHU)

In order to achieve the aforementioned goal of a reliable, low-cost satellite architecture, concepts of modularity, reusability, and versatility were explored for the interface between the payloads and the SHU. With this in mind, and to further facilitate development and integration, the payload instrument-to-satellite bus system interface was centered around the usage of commercial off-the-shelf (COTS) components designed to comply with the Space Plug-and-Play Avionics (SPA) standards (now referred to as the Modular Open Network ARCHitecture, or MONARCH). The ethos of the SPA concept revolves around modularity of components, which would allow for the rapid assembly of spacecraft. Ideally, SPA-compliant components would feature standardized interfaces and be self-describing through the use of electronic datasheets. These datasheets could then be exchanged to help form self-organizing networks, allowing satellite components to automatically connect to each other. Thus, the time required for integration could be drastically reduced. The SPA standardized interfaces were developed on top of existing standards, including USB 1.1, SpaceWire, and I2C. These are referred to as SPA-U, SPA-S, and SPA-1, respectively. The concept of Appliqué Sensor Interface Modules (ASIMs) was also introduced as a supporting technology. ASIMs are intended to convert non-SPA components such as legacy devices with flight heritage into “native” SPA modules [6].

The SHU was designed with the objective of using SPA-compliant components, which were sourced from the Sweden-based ÅAC Microtec’s Rapid Integration Architecture (RIA) product line. The components used include an ÅAC Microtec RIA OBC lite, which serves as the main computer and manages the SPA network, an RIA mass memory unit (solid state recorder), in which the data from the various payload experiments can be stored, and a Main Power Distribution Unit (MPDU) and two Distributed Power Control Units (DPCUs), the three of which together manage the power distribution within the SHU and to each of the payloads. The connections between the various components were intended to make use of both the SPA-U (USB-based) standard and the SPA-1 (I2C-based) standard. This architecture is shown in Figure 3.

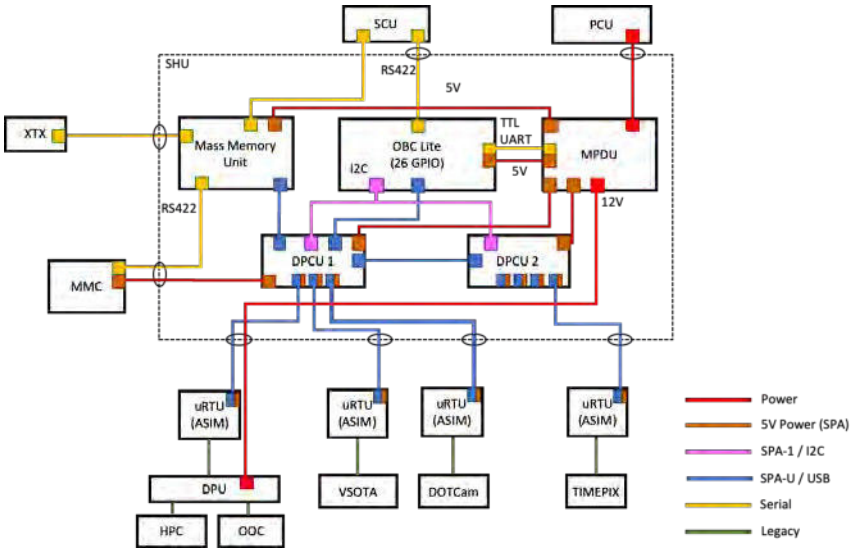

Figure 3. RISESAT science handling unit architecture

Accordingly, it was necessary for each payload instrument to comply with the SPA-U interface in order to connect to the SHU. However, many of the payloads had legacy physical and electrical interfaces inherited from previous, sometimes flight heritage models. In order to adapt them to the plug-and-play interface, each payload was outfitted with an ÅAC Microtec RIA µRTU, or "micro Remote Terminal Unit." This small board, featuring an FPGA-based soft processor with numerous peripheral devices, serves as the ASIM for the payload. It is responsible for processing commands from the SHU and decoding them into the payload instrument-specific command frames and for receiving telemetry and mission data from the payload, which is then formatted into standardized data frames to be sent to back to the SHU. This design was intended to dramatically reduce the effort required to integrate the various payload instruments and provide reliable connections between the payloads and the SHU. As an additional advantage, the bus system of RISESAT could then accommodate different payload instruments in the future without major design changes. The payload instruments themselves would have the potential to be easily integrated to another SPA-compatible satellite bus system as well. Finally, the standardization of the connector interface could simplify the wire harnessing and the structural design [7].

2.2 DOTCAM

The DOTCam payload, shown in Figure 4, is a compact camera instrument. It is designed to detect occurrences and capture images of optical phenomena such as transient luminous events (TLEs), lightning, airglow, and meteors in Earth's upper atmosphere. Weighing around 710 g, DOTCam consists of two CCDs (each equipped with specially-designed filter), an FPGA providing the processing capability, and two SRAM memory modules for data storage. The custom filters allow for the determination of the emission lifetime of specific molecules and atoms from the images taken by the DOTCam instrument. The FPGA provides the functionality to detect the occurrences of light phenomena, process, compress, and packetize the image data using lossless compression technology, and handle telemetry and commands. DOTCam has multiple modes of operation. In the most basic mode, the camera instrument simply takes a picture upon command. It can also capture images continuously at a specified rate. Alternately, images can be captured based on a trigger - when a brightness above that of a certain threshold is detected.

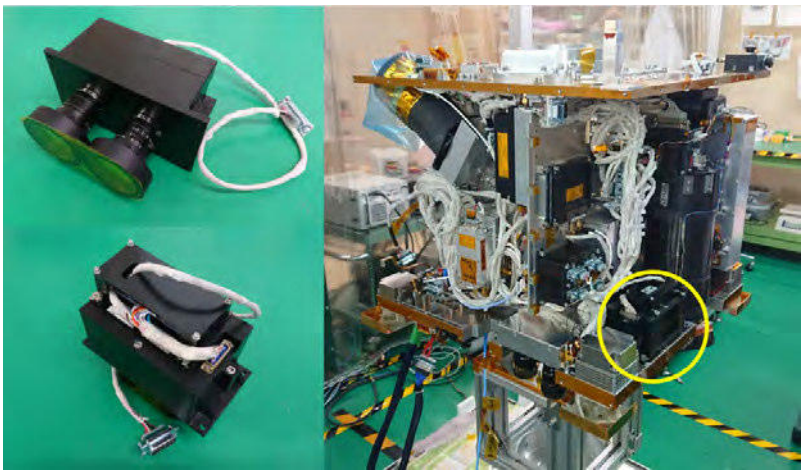

Figure 4. Flight model of DOTCam and its position in the RISESAT structure

The command and mission data interfaces are legacy and thus DOTCam was equipped with a µRTU to adapt to the requisite plug-and-play standard and interface with the SHU. In addition to handling the commands, telemetry, and science data, the µRTU also monitors the status of DOTCam, providing a level of error detection and recovery, and stores up to 36 images in a buffer until they can be successfully transferred to the mass memory unit. The µRTU receives commands from the SHU, decodes them into the DOTCam-specific command frames, and sends them to the DOTCam payload over SPI. These commands can be categorized into those that set certain parameters and those that request some status from the payload. The requested status data is likewise returned from the payload over SPI. This mechanism is used to further monitor the DOTCam payload and this monitoring data is sent to the SHU as housekeeping data.

The µRTU must also receive image data from the payload and format this data into standardized data frames to be sent back to the SHU. The image data captured by DOTCam is transferred to the SHU over a separate eight-channel parallel data transmission interface. Transmission of the image data is initiated by a custom handshaking mechanism between DOTCam and the µRTU. An illustration of this data flow is shown in Figure 5.

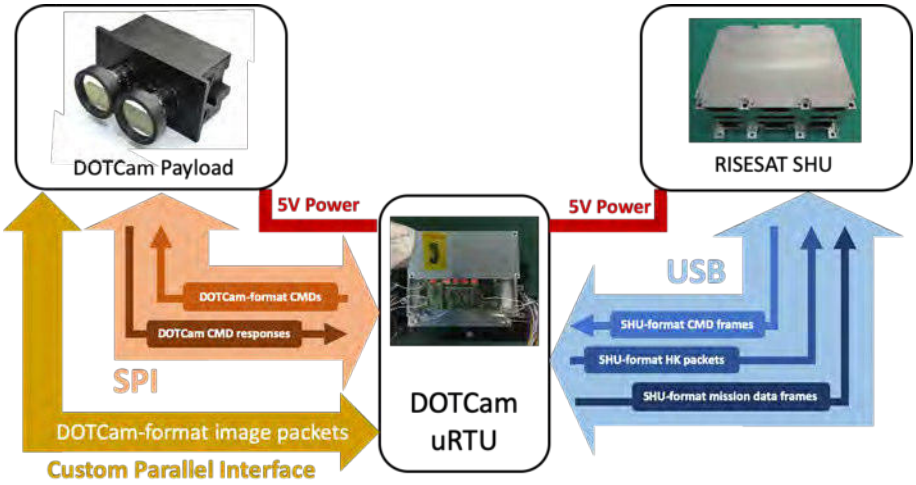

Figure 5. DOTCam to SHU data flow

3. TECHNICAL LESSONS LEARNED

The original intent in using the ÅAC Microtec components was to leverage SPA standards to make the science mission subsystem of RISESAT modular, enabling the bus system to be versatile and reusable and facilitating the integration of the payload instruments, while avoiding the International Traffic in Arms Regulations (ITAR) restrictions on SPA technology. ÅAC Microtec in particular offered ITAR-free SPA-compliant components. However, the usage of the key software applications, including the satellite data model (SDM) and the SPA services model (SSM) that replaced it, were ultimately restricted. For some time, the SPA-related software and hardware languished in a regulatory limbo, putting the usage of this technology into question for the RISESAT project. Another key factor in the decision to use ÅAC Microtec SPA-based components was the potential to use the virtual system integration (VSI) technology, which would have facilitated integration and test between the payloads and the SHU remotely [8]. Unfortunately, due to similar restrictions, the development of RISESAT proceeded without using VSI.

Ultimately, "true" SPA interfaces were abandoned in favor of simplified "SPA-inspired" plug-and-play interfaces. The SPA-U interface between the payloads and the SHU became a more standard USB bus, while the SPA-1 interface was maintained. The self-describing functionality was replaced by simply hard-programming payload identifiers in the SHU. Even with this adaptation, a certain level of reconfigurability was achieved and proved highly valuable. While assembling the flight model of RISESAT, a hardware issue arose that necessitated the rearrangement of DOTCam's connector to the SHU. Due to the standardized connectors and plug-and-play interface, swapping these ports was trivial. Thus, though the SPA standards could not be utilized as initially intended, plug-and-play functionality was very valuable, especially for the integration of DOTCam.

One lesson learned was that the development of the DOTCam-to-µRTU (or payload-to-ASIM) interface was not to be underestimated. While the physical integration between the two components was simple, since the µRTU had a small form factor and it and its housing could easily be mounted on the payload instrument, the electrical integration and the software development were more demanding. Despite the µRTU being designed to accommodate many possible use cases, DOTCam's parallel data interface necessitated the design of a custom IP core to successfully receive the mission data. DOTCam's SPI also required hardware-level changes to the µRTU SPI IP core. The ability to modify hardware was critical to the payload integration efforts. The development of the µRTU software application also took considerable time, hindered by inadequately detailed documentation. While interface control documents (ICDs) were created and distributed, the level of detail required to make the document truly valuable was underestimated. For example, the DOTCam data interfaces implemented in the FPGA hardware had to be continuously adjusted due to discrepancies and misunderstandings in the timing diagrams. Furthermore, a lack of specificity regarding the power requirements of DOTCam led to an issue with inrush current that resulted in late stage hardware modifications.

4. PROGRAMMATIC LESSONS LEARNED

The technical challenges encountered were exacerbated in part by various programmatic difficulties. The work of integrating the DOTCam payload to the RISESAT bus was completed by Tohoku University's SRL, with support from NCKU's ISAPS and ÅAC

Microtec. These groups represented three different countries, varying levels of experience (from undergraduate students to professors and professional engineers), and numerous different specialties, including aerospace and systems engineering, astrophysics and space sciences, and electrical and software engineering. Understandably, each group had different bases of knowledge, familiarity with different standards and procedures, and different cultural contexts that introduced occasional misunderstandings. Within the SRL team, majority of the payload-to-bus development and integration was conducted by master's students, as one goal of spacecraft development in a university setting is to provide an educational opportunity for hands-on development. Therefore, as with any project driven by students, it was hindered by periodically changing team members (as students graduated), differing levels of experience and engagement, and busy academic schedules.

The distribution of work, particularly regarding the development of the software application of the µRTU, was a particular hinderance. SRL was responsible for this development, which required a thorough understanding of the operation and interfaces of the DOTCam payload. This development would have been more efficient had it been carried out by the DOTCam payload engineers. However, because of schedule constraints, the development of the SHU software application was occurring in parallel and thus, detailed specifications regarding command and data formats and satellite operational procedure could not be provided to the payload teams. Had these specifications been determined and provided to DOTCam engineers, the time for integration could have been minimized. Documentation became a particular point of concern during the latter stages of the development of RISESAT. The project was essentially on hold for a prolonged period after the original launch opportunity could not be realized. During this period, there was a loss of momentum and expertise, as students graduated and engineers moved on to other opportunities. In the meantime, the SPA standards themselves changed and evolved and the component supplier ÅAC Microtec switched its focus to a new product line. Thus, when work began in earnest again, significant time was devoted to relearning and recovery. In hindsight, much of this could have been avoided by extensive documentation.

Figure 6. Flight model of RISESAT on launch vehicle © JAXA

5. OPERATIONS

RISESAT was launched on January 18th, 2019, on the Epsilon-4 launch vehicle (see Figure 6) from the JAXA Uchinoura Space Center. Communications were successfully established with the primary ground station at Tohoku University on the same day. At the time of writing, check-out of the satellite bus system is still on-going, including

calibration operations for various sensors and verification of the attitude determination and control system performance. DOTCam and the other payloads have been confirmed to be working by powering on, checking the payload housekeeping data, and taking some initial observations – with DOTCam, images of Los Angeles and Taiwan. After check-out of the satellite bus system is completed, the mission experiments of the payloads will begin.

6. CONCLUSION

This paper presented an overview of RISESAT, its payload DOTCam, and the lessons learned during their integration. These lessons covered both technical aspects, such as the usage of the SPA standard, and programmatic aspects, such as the distribution of work. In summary, the usage of a plug-and-play interface between the SHU and the payloads was beneficial, though SRL was unable to fully make use of the SPA standards as was originally intended, and the necessity for specific, detailed documentation from the outset of development was a crucial lesson learned. The RISESAT project can ultimately be viewed as a significant success. Not only are nominal operations ongoing, but the experience gained is a highly valuable asset as SRL continues to design and develop micro- and nanosatellites.

7. ACKNOWLEDGEMENTS

The authors would like to acknowledge the assistance of ÅAC Microtec AB and the support of the Innovative Satellite Technology Demonstration Program of JAXA.

8. REFERENCES

[1] Nakasuka, S., “New Paradigm of Space Development and Utilization Opened by Micro/Nano-satellites with Reasonably Reliable Systems ‘Hodoyoshi’ Concept,” The University of Tokyo, 16 January 2014, https://www.u-tokyo.ac.jp/adm/first/en/smry-nakasuka_e.html (accessed 27 January 2019)

[2] Takahashi, Y., Yoshida, K., Sakamoto, Y., Sakanoi, T., “SPRITE-SAT: A university small satellite for observation of high-altitude luminous events,” In: Sandau, R., Roeser, HP., Velanzuela, A., (eds) [Small Satellite Missions for Earth Observation], Springer, Berlin, Heidelberg, 197-206 (2010)

[3] Sakamoto, Y., Sugimura, N., Fukuda, K., Kuwahara, T., Yoshida, K., Kurihara, J., Fukuhara, T., Takahashi, Y., “Development and Flight Results of Microsatellite Bus System for RISING-2,” Trans. Japan Society for Aeronautical and Space Science, Aerospace Technology Japan 14(ists30), 89-96 (2016).

[4] Kuwahara, T., Yoshida, K., Sakamoto, Y., Tomioka, Y., Fukuda, K., “Satellite System Integration based on Space Plug and Play Avionics.” Proc. IEEE/SICE International Symposium on Space Integration, 896-901 (2011)

[5] Yoshida, K., Sakamoto, Y., Tomioka, Y., Fukuda, K., Fukuyama, M., Shibuya, Y., “International Scientific Micro-satellite RISESAT based on Space Plug and Play Avionics,” Proc. AIAA/USU Conference on Small Satellites SSC12-I-1, (2012)

[6] Lyke, J., Young, Q., Christensen, J., Anderson, D., “Lessons Learned: Our Decade in Plug-and-play for Spacecraft,” Proc. AIAA/USU Conference on Small Satellites SSC14-V-1, (2014)

[7] Kuwahara, T., Tomioka, Y., Fukuda, K., Yoshida, K., Baeckstroem, J., Bruhn, F., “Impacts of Space Plug-And-Play Technology on Micro and Nano-Satellites,” IFAC Proceedings 46(19), 289-294 (2013)

[8] Kuwahara, T., Tomioka, Y., Fukuda, K., Sugimura, N., Sakamoto, Y., Yoshida, K., Takahashi, Y., Kurihara, J., “Space Plug and Play Compatible Earth Observation Payload Instruments,” In: Sandau, R., Roeser, HP., Velanzuela, A., (eds) [Small Satellites for Earth Observation 1(4)], IAA Book Series, 107-114 (2014)

TechnoSat - Results from the first 18 months of operations

Merlin F. Barschke[1], Julian Bartholomäus[1], Juan Maria Haces Crespo[1], Karsten Gordon[2], Clément Jonglez[1], Philip von Keiser[1], Danilo Költzsch[1], Julius Leglise[1], Marc Lehmann[1], Christian Meumann[1], Steffen Reinert[1], Sven Rotter[1], Mario Starke[1], Philipp Werner[1], Lars Zander[1]

[1] Technische Universität Berlin, Institute of Aeronautics and Astronautics,
Marchstr. 12, 10587 Berlin, Germany
Phone: +49 30 314-28743, merlin.barschke@tu-berlin.de

[2] Spacegramming,
Bergerweg 4, 83707 Bad Wiessee, Germany
karsten.gordon@spacegramming.de

Abstract: TechnoSat is the first mission that is based on the highly modular TUBiX20 platform of Technische Universität Berlin. It is a 20 kg spacecraft, carrying seven in-orbit technology demonstration payloads and was launched into a 600 km SSO on the 14th of July, 2017. The payloads include components such as an S-band transmitter and a reaction wheel system comprising four wheels that are included as regular platform elements in follow-up missions such as TUBIN, an Earth observation satellite that will demonstrate wildfire detection using microbolometer technology. In the first 18 months of TechnoSat's orbit operations, the satellite was tested comprehensively, and the platform's capabilities were investigated, demonstrated and continuously improved by means of several software updates.
In this paper, we present current orbit results that showcase the capabilities of the TUBiX20 platform. Furthermore, we demonstrate how the modular hard- and software architecture supports extensive reconfiguration and enhancement on orbit and how it can be exploited to assess the platform performance.

1. INTRODUCTION

The continuous advancement of miniaturised electrical components originating from industries such as communications or automotive has enabled increasingly complex missions with ever smaller satellites. Furthermore, such components reduce the hardware expanses while the comparatively small mass of the spacecraft limits the launch costs. As a result, new components like sensors, actuators or transceivers for small spacecraft are developed at a fast pace resulting in a growing need for in-orbit verification and performance evaluation of such components [1]. The TechnoSat mission of Technische Universität Berlin meets these needs by carrying seven technology demonstration payloads for in-orbit verification. After its launch into a 600 km SSO on the 14th of July 2017, TechnoSat conducts regular experiments with all payloads successfully and the data are handed over to the experiment providers [2]. The platform could demonstrate key performance parameters regarding three axis stabilisation and payload data downlink that will be further exploited in the follow-up mission TUBIN [3]. Although the design lifetime of one year is exceeded, TechnoSat still conducts experiments on a daily basis and provides valuable practical experience which directly contribute to the development of TUBIN [4].

This paper presents orbit results from the first 18 months of operations within the TechnoSat mission through the example of two subsystems. Focussing on the electrical power system (EPS) and the attitude determination and control system (ADCS), the paper demonstrates the performance of the basic TUBiX20 configuration used for TechnoSat and gives an outlook for the performance upgrades introduced with TUBIN.

2. THE TECHNOSAT MISSION

TechnoSat is a 20 kg in-orbit demonstration mission with the primary mission objective to operate seven technology payloads in orbit and evaluate their performance. Amongst others, these payloads include fourteen commercial retroreflectors for laser ranging [5], an S-band transmitter [6], and a reaction wheel system comprised of four wheels [2], which will all be part of the TUBiX20 platform configuration for TUBIN. Another payload is a CMOS camera, whose pictures are used for the performance evaluation of the attitude determination and control system described in the next section.

As the first spacecraft of the TUBiX20 platform series of Technische Universität Berlin, the mission also verifies the overall platform design and the performance of its basic configuration.

3. TECHNOSAT FLIGHT RESULTS

After launch and commissioning of TechnoSat in 2017, experiments have been conducted continuously to evaluate the performance of payloads and platform. Furthermore, updating the flight software allowed to integrate payloads like the S-band transmitter and the reaction wheels into the platform to extend its functionality.

The S-band transmitter is now routinely used to downlink pictures and telemetry data. In this manner, several hundreds of pictures can be downlinked in one pass of the satellite instead of only one that could be downloaded via UHF in the same time. This enables the extensive use of the camera for the evaluation of the absolute attitude determination and control performance of the spacecraft (cf. section 3.2). Furthermore, experiments can be conducted at a much faster pace and more data can be recorded due to the extended telemetry downlink capacity.

The described improvements were achieved by means of several software updates to establish the following capabilities. The onboard computer node needed to be updated to be able to provide larger amounts of historical telemetry data to the payload data handling (PDH) via the centralised data bus for S-band downlink. The PDH required an extension of its storage capacity. While only five pictures could be stored at the beginning of the mission, this was soon extended to more than one thousand, which is sufficient to record an entire coherent orbit in nadir-pointing. Furthermore, the PDH required the functionality to redirect the telemetry data received from the OBC to the S-band transmitter.

Initially, it was planned to only test the wheels individually using a test application implemented on the PDH. However, this application was extended and migrated to the ADCS node to enable three-axis attitude control. Consequently, the reaction wheels are now routinely used to perform nadir, inertial and target pointing, which significantly improves downlink quality and enables a wide variety of new experiments.

These reconfigurations that were partly implemented after the satellite was already launched to orbit greatly benefitted from the modular hard- and software of the TUBiX20 platform, which is realised as a distributed network of computing nodes which communicate via a middleware. These nodes decouple the individual subsystems and devices from each other and therefore allow to modify processing tasks without interference with other

parts of the software. Within the different layers of the software architecture, unified interfaces allow to directly integrate new functionality such as additional control algorithms.

Table 1 gives an overview of some parameters of the operations that were conducted within the first 18 months of the mission.

Table 1: TechnoSat operations as of January 14th, 2019

Orbits	8,187
Passes with active operations	2,409
Pictures taken	17,000
Telemetry data downloaded	0.2 GiB
Payload data downloaded	1.3 GiB
Software updates (of single nodes)	16

In the following, selected results from evaluating the electrical power system (EPS) and the attitude determination and control system (ADCS) are presented.

3.1 Power Generation and Storage

In the course of the ongoing operations of the TechnoSat spacecraft, several experiments were conducted pursuing the verification of the electrical power system (EPS). Among those were several experiments aiming at comparing maximum solar power generation capabilities in orbit with the values predicted in the satellite's design phase. Results from one such experiment that was conducted in December 2018 are presented in the following.

TechnoSat was designed with rather conservative power generation and storage margins, to ensure fast recharging and a low depth of discharge for the batteries during eclipse. As a result, the power generation potential of the solar panels is rarely utilized during nominal operations. In order to evaluate the performance of power generation and storage, an experiment was conducted that minimized the power income at increased power consumption for one orbit while performing Sun-pointing for maximum power income during the next Sun period. Minimizing the solar power income was realized by continuously pointing the face of the satellite towards the Sun that accommodates the separation system and is therefore not equipped with solar cells. Maximum power income was achieved by pointing one face of the octagonally shaped spacecraft towards the Sun, exposing two solar panels directly and additional four panels with a 45 degrees angle to the Sun.

The top plot of Figure 1 depicts currents and voltages of one of the two hot redundantly implemented solar paths throughout the experiment. One can see that the current in the first Sun period is comparatively small and can be attributed to Earth's albedo. It is noteworthy that the Earth's albedo may, under specific circumstances, be sufficient for a positive power budget and, thus, to charge the satellite's batteries. To a certain extent, the variations of the power income due to albedo can be attributed to the position of the Earth relative to the spacecraft which changed during the Sun period due to the orbit's geometry. However, also the reflectivity of Earth's surface as seen from the satellite seems to

have a significant influence. Analysing the spacecraft's ground track for the time in question shows that the first rise of solar power income (at around 06:00 UTC) matches the satellite's pass over Antarctica and is probably enhanced by the relatively high reflectivity of ice, snow and clouds. The second and third rise of solar power generation can most likely be attributed to clouded areas over the Indian Ocean (at around 06:27 UTC) and Iran (at around 06:42 UTC).

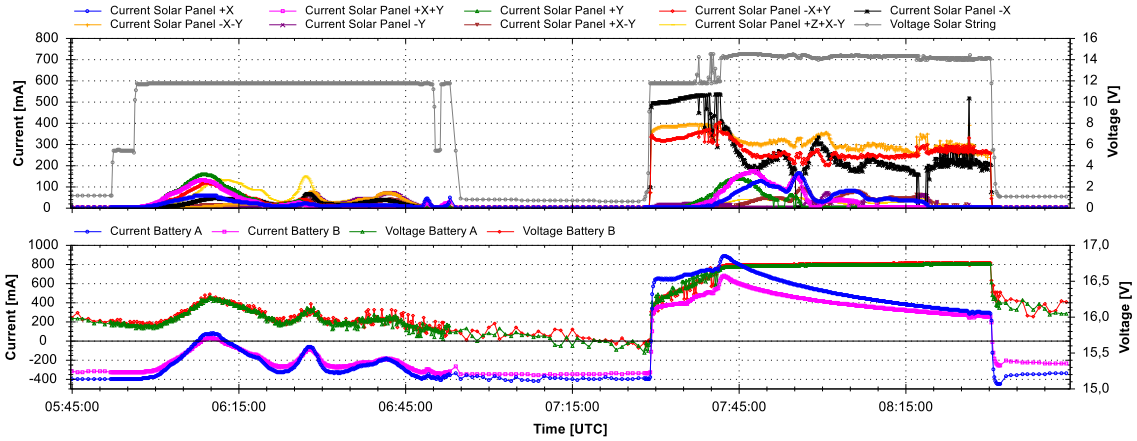

Figure 1: Telemetry gathered during an experiment to confirm the performance of the electrical power system of the TechnoSat spacecraft performed in December 2018. The upper plot shows the currents of the solar panels in one of the two solar panel strings, as well as the voltage of this string. The lower plot shows currents and voltages of the batteries.

At the beginning of the second Sun phase at around 7:29 UTC, one can see that the power income was greatly improved by the Sun-pointing. However, even with one orbit of highly minimized power income, the full power generation potential is only used for the smaller fraction of the Sun period. Supported by the Earth's albedo the maximum power generated by the solar panels adds up to well over 35 Watt, which aligns with the design assessments. Here, it needs to be noted that Figure 1 only depicts voltage and currents for one of the two solar paths to improve the transparency of the presentation.

3.2. Pointing Performance Analysis using Image Registration

For the experiment described in this section, the attitude determination relied on Sun sensors and magnetometers using the QUEST algorithm whose solution was then filtered using rate measurements from a set of fibre optic rate sensors. Attitude control was performed by the reaction wheels and the magnetorquers using a state-space controller.

TechnoSat is used to gather performance figures to ensure that the ADCS requirements of future missions that use the same sensor configuration are met within a certain confidence interval for different conditions and different modes such as nadir-pointing, inertial pointing and target pointing. Furthermore, this experiment can also be carried out on future missions to validate the ADCS performance.

Per ECSS-E-ST-60-10C [7], the (absolute) performance error, i.e. the difference between the target (desired) output of the system and the actual achieved output, and the knowledge error, i.e. difference between the known (estimated) output of the system and the actual achieved output, were used as performance indicators. In addition to these two metrics, the controller error was also analysed. It is derived from the error quaternion used

in the attitude controller on board the satellite and is retrieved from the satellite's telemetry.

To measure the ADCS performance, TechnoSat's camera can be used to take pictures of recognizable features like coastlines or islands. The position of the feature in the picture is then compared to its theoretical position based on reference data, such as Sentinel-2 pictures of the Earth's surface. This method is used operationally by Planet [8] to produce "product-driven" metrics, i.e. computed while the satellite is performing its primary mission, Earth imaging, and based on the products produced by the mission. The TechnoSat camera has a sensor with 640 by 480 pixels and a field-of-view of 4.5 by 3.4 degrees (half-angle), respectively. The low resolution results in light-weight pictures, so that a high number of pictures can be downloaded in a single ground station pass. Due to the narrow field-of-view, the accuracy is nevertheless sufficient for the given purpose.

Figure 2 shows an application of this method in nadir-pointing mode. First, the raw pictures are georeferenced based on onboard attitude and position knowledge, i.e. projected onto a latitude/longitude grid on the WGS84 reference ellipsoid. Given the ground resolution of 160 m per pixel, it was deemed unnecessary to use digital elevation models. Second, ground control points (GCPs) are manually selected in the picture and compared to reference pictures from Sentinel-2 satellites. This step, called image registration, provides both the actual geographical coordinates of the picture and the knowledge error. Third, the picture coordinates based on the commanded attitude (ideal case) are computed and compared to the actual picture coordinates which gives the absolute performance error. This step involves computing the theoretical attitude that the satellite would have if all of the following parameters were perfect: onboard clock, orbit knowledge, attitude knowledge, attitude control.

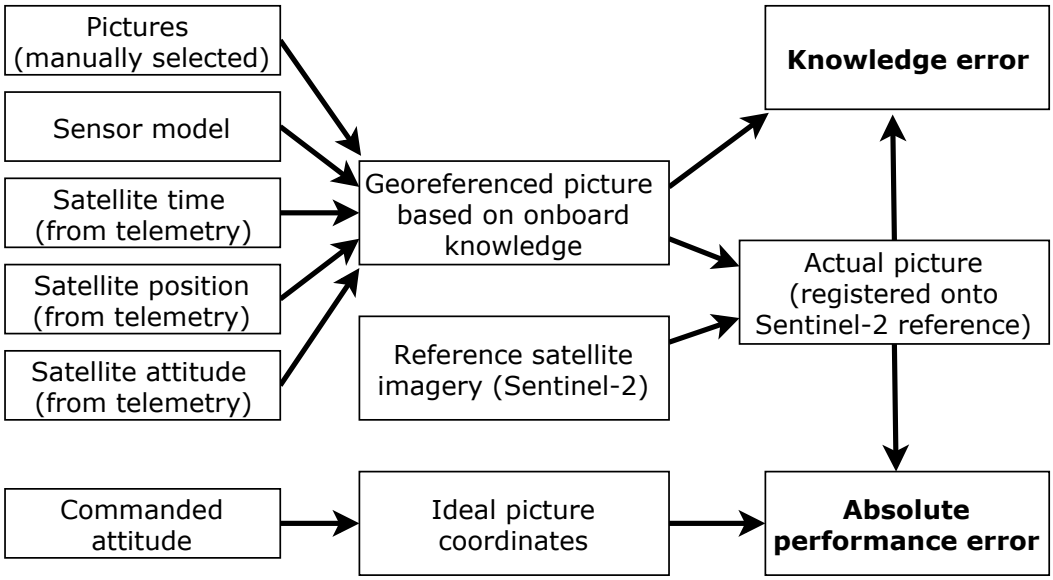

Figure 2: Pointing performance analysis in nadir mode using image registration

In Figure 3 the registration of the picture based on onboard knowledge onto the Sentinel-2 reference is shown. The coordinates of the compared GCPs and the original picture are then deformed using the thin plate spline interpolation technique to fit the Sentinel-2 reference as close as possible. These deformation vectors indicate the knowledge error.

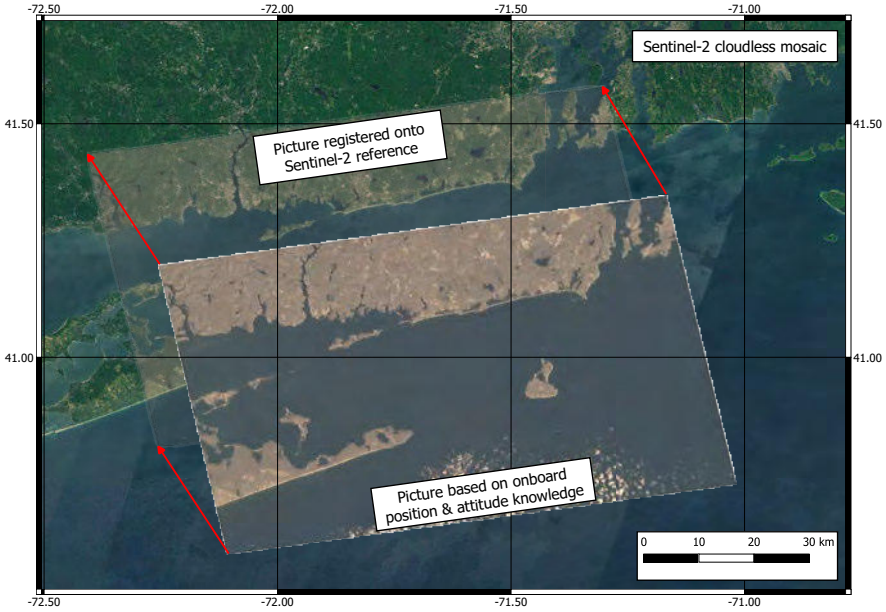

Figure 3: Registration of a TechnoSat picture onto Sentinel-2 reference

Figure 4 illustrates the difference between the picture centres for the same picture as in Figure 3. Here, the green arrow corresponds to the displacement shown in Figure 3, only for the picture centre. Furthermore, the figure includes a fourth point called “onboard nadir target”. It is based on the target on board the satellite. The difference between the onboard knowledge (yellow dot) and onboard nadir target (purple dot) is directly related to the error of the attitude controller, which is retrieved from the satellite’s telemetry.

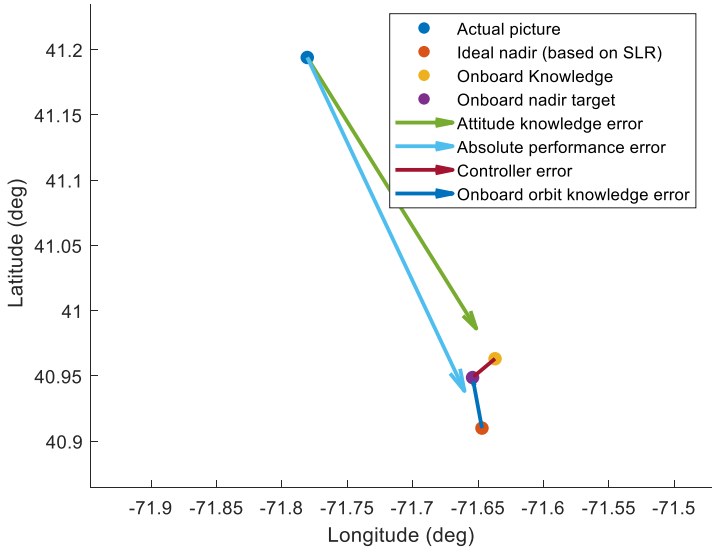

Figure 4: Picture centre, actual vs ideal nadir vs onboard knowledge

Figure 5 shows the dispersion of the three types of errors for the 14 pictures analysed during two measurement campaigns. Here, the axes show the resulting errors on the geographical coordinates of the pictures. It can be seen that the controller error is much smaller than the two other errors. Furthermore, the picture centre position based on the onboard knowledge is always very close to the one based on the commanded attitude (ideal nadir). This indicates that the satellite was pointing correctly towards the com-

manded target considering the onboard knowledge so that the actual picture centre indicates the knowledge error. Therefore, the attitude determination is the biggest source of error whereas the controller seems to follow the commanded attitude based on the onboard knowledge well.

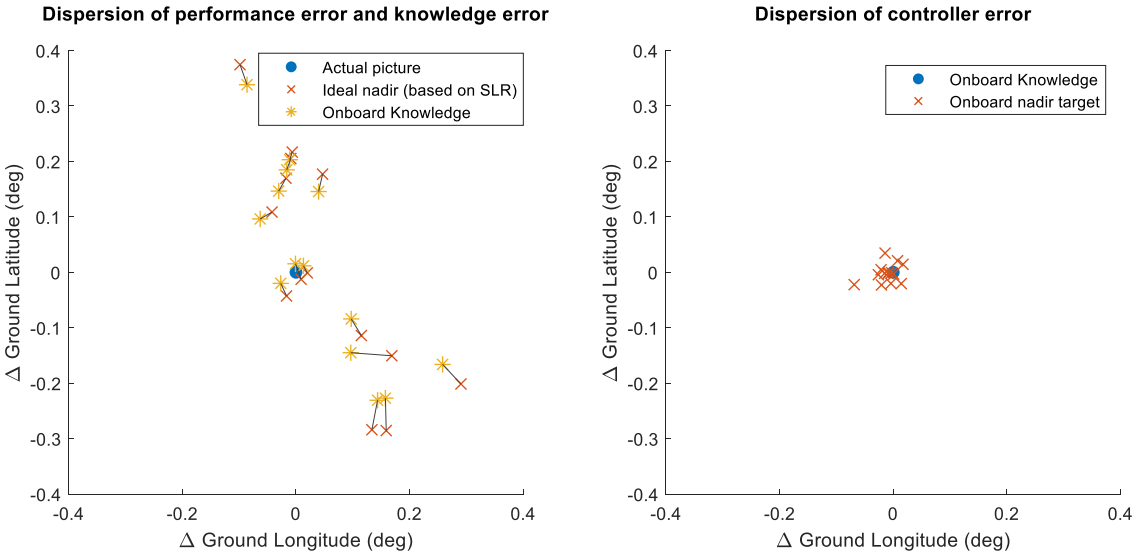

Figure 5: Dispersion of errors on the 14 pictures of the experiment

The errors in attitude knowledge can mainly be attributed to the limited performance of the used set of sensors. However, it is planned to improve the attitude knowledge performance for TechnoSat by improving the calibration and filtering of the given sensors. Another source of error is the time uncertainty due to drifting of the onboard clock and the resolution of the pictures' timestamp. It can be seen in Figure 5 that the errors are mostly spread over a line in the North-North-West direction which roughly corresponds to the flight direction. Therefore, methods to reduce the satellite's time drift are currently investigated and the resolution of the pictures' timestamp is planned to be increased.

Table 2 shows some statistics based on the 14 pictures. The last column shows the Mean + 2σ value, which corresponds to 95% probability in the case of a normal distribution. For instance, the knowledge error has a 95% probability to be below 3.7 degres. However, one must be careful about interpreting the results using the normal distribution because of the low number of samples (14).

Table 2: Summary of pointing accuracy metrics

Metric	Mean	Standard deviation σ	Mean + 2σ (95%)
Performance error	2.0°	1.2°	4.3°
Knowledge error	1.7°	1.0°	3.7°

The method presented in this paper was the first attempt at measuring absolute performance metrics of TechnoSat's ADCS. The number of measurement points is limited by the effort of manually finding recognizable features in the pictures to register them on Sentinel-2 pictures and is limited to terrestrial areas with a low cloud coverage during the orbit's Sun period.

Although there is room for improvement of the ADCS performance of TechnoSat, the results are promising and largely exceed the original pointing performance requirements. Hence, future experiments will aim at improving the attitude determination accuracy of TechnoSat and refine the applied methods for example by using the Moon as a target. Future missions such as TUBIN that carry a more sophisticated sensor suite will also benefit from this where the same methodology can be used for example to confirm the relative alignment of different payload cameras and the star trackers, respectively.

4. CONCLUSION AND FUTURE WORKS

TechnoSat is a 20 kg technology demonstration mission of Technische Universität Berlin launched in July 2017. In the first 18 months of operations, payloads and platform were tested continuously and several performance upgrades were implemented via software updates. This paper presents some of the results gathered within experiments that were conducted with the power and the attitude determination and control system. After fulfilling all mission requirements within nominal mission duration of one year, TechnoSat is still fully functional and is now operated within an extended mission were experiments are focussed on the preparation of the follow-up mission TUBIN. Furthermore, TechnoSat is used in lectures of Technische Universität Berlin for hands-on training in satellite operations.

ACKNOWLEDGEMENTS

The TechnoSat mission is funded by the Federal Ministry for Economic Affairs and Energy (BMWi) through the German Aerospace Center (DLR) on the basis of a decision of the German Bundestag (Grant No. 50 RM 1219).

REFERENCES

[1] G. Binet, G. Novelli, D. Escorial, C. Martinez, C. Arza, M. Bolchi and M. Massimiani, “Shaping a European IOD service”, presented at the Small Satellites Systems and Services Symposium, Valletta, Malta, 2016.

[2] M.F. Barschke, P. Werner, K. Gordon, M. Lehmann, W. Frese, D. Noack, L. Grunwaldt, G. Kirchner, P. Wang and B. Schlepp, “Initial results from the TechnoSat in-orbit demonstration mission”, presented at the 32st AIAA/USU Conference on Small Satellites, Logan, USA, 2018.

[3] M.F. Barschke, K. Gordon, P. von Keiser, M. Lehmann, M. Starke, P. Werner, “Initial orbit results from the TUBiX20 platform”, presented at the 69th International Astronautical Congress, Bremen, Germany, 2018.

[4] K. Gordon, M. F. Barschke, and P. Werner, "Upgrading TUBiX20 – bringing TechnoSat flight experience into the TUBIN mission", presented at the Small Satellites Systems and Services Symposium, Sorrento, Italy, 2018.

[5] L. Grunwaldt, R. Neubert, M. F. Barschke, “Optical tests of a large number of small COTS cubes” presented at the 20th International Workshop on Laser Ranging, Potsdam, Germany, 2016.

[6] R. Alavi, K. Briess, H. Podolski, J. Riesselmann, A. Weiland, and W. Frese, “In Space Verification of the Pico-Satellite S-Band Transmitter "HISPICO" on a Sounding Rocket”, presented at the 60th International Astronautical Congress, Daejeon, South Korea, 2009.

[7] ESA-ESTEC Requirements & Standards Division, Control Performance Standard ECSS-E-ST-60-10C. ECSS, 2008.

[8] L. Leung, V. Beukelaers, S. Chesi, H. Yoon, D. Walker and J. Egbert, “ADCS at Scale: Calibrating and Monitoring the Dove Constellation”, presented at the 32st AIAA/USU Conference on Small Satellites, Logan, USA, 2018.

InflateSail De-Orbit Flight Demonstration – Observed Re-Entry Attitude and Orbit Dynamics

Craig Underwood[1], Andrew Viquerat[2], Herman Steyn[3], Ben Taylor[1], Richard Duke[1], Brian Stewart[1], Chris Bridges[1], Davide Masutti[4], Amandine Denis[4]

[1]Surrey Space Centre, University of Surrey,
Guildford, Surrey, GU2 7XH, UK
Phone: +44 1483 689809, Mail: c.underwood@surrey.ac.uk, b.taylor@surrey.ac.uk,
r.duke@surrey.ac.uk, b.stewart@surrey.ac.uk, c.p.bridges@surrey.ac.uk

[2]Dept. for Mechanical Sciences, University of Surrey,
Guildford, Surrey, GU2 7XH, UK
Phone: +44 1483 686267, Mail: a.viquerat@surrey.ac.uk

[3]Dept. of Electrical & Electronic Engineering, Stellenbosch University,
Stellenbosch, South Africa
Mail: whsteyn@sun.ac.za

[4]Von Karman Institute for Fluid Dynamics, Waterloosesteenweg 72
B-1640 Sint-Genesius-Rode, Belgium
Mail: masutti@vki.ac.be, amandine.denis@vki.ac.be

Abstract: The InflateSail (QB50-UK06) CubeSat, designed and built at the Surrey Space Centre (SSC) for the Von Karman Institute (VKI), Belgium, was a technology demonstrator built under the European Commission's QB50 programme. The 3.2 kilogram 3U CubeSat was equipped with a 1 metre long inflatable mast and a $10m^2$ deployable drag sail and was one of 31 satellites that were launched simultaneously on the PSLV (polar satellite launch vehicle) C-38 from Sriharikota, India on 23rd June 2017 into a 505km, 97.44° Sun-synchronous orbit. Shortly after insertion into orbit, InflateSail automatically activated its drag-sail payload, and, as planned, began to lose altitude, causing it to re-enter the atmosphere just 72 days later – successfully demonstrating for the first time the de-orbiting of a spacecraft using European inflatable and drag-sail technologies. This paper discusses the dynamics we observed during the descent, including the sensitivity of the craft to atmospheric density changes. The InflateSail project was funded by two European Commission Framework Program Seven (FP7) projects: DEPLOYTECH and QB50. QB50 was a programme, led by VKI, for launching a network of 50 CubeSats built mainly by university teams all over the world to perform first-class science in the largely unexplored lower thermosphere.

1. INTRODUCTION

In recent years, increasing attention has been given to the problem of space debris and its mitigation. It has been observed that a major source of new space debris is due to the break-up and fragmentation of spacecraft that remain in orbit after the end of their operational mission. As a result, regulations have been drawn-up which require the removal of spacecraft at the end of operation – known as Post-Mission-Disposal (PMD) – to ensure that the spacecraft do not become a new source of space debris. For low-Earth orbit (LEO) missions, the residual atmosphere encountered in orbit offers a potentially simple and relatively low cost method of PMD through the use of deployable drag augmentation devices. The InflateSail (QB50-UK06) CubeSat, designed and built at the Surrey Space Centre (SSC) for the Von Karman Institute (VKI), Belgium, was designed to demonstrate this technique by means of a 3.2 kg 3U CubeSat carrying a $10m^2$ deployable drag-sail mounted on the end of a 1m long inflatable mast.

By deploying the drag sail from the end of the mast (i.e. such that it is separated from the spacecraft body), the centre of mass and the centre of aerodynamic pressure of the spacecraft are separated, thereby, in principle, conveying a degree of passive stability (the weathervane effect), which in turn should maximize the structure's drag by ensuring that the sail is presented normal to the free-stream air flow (see Fig. 1). The mast also ensures that the drag sail is kept clear of any host spacecraft structures which might interfere with sail deployment.

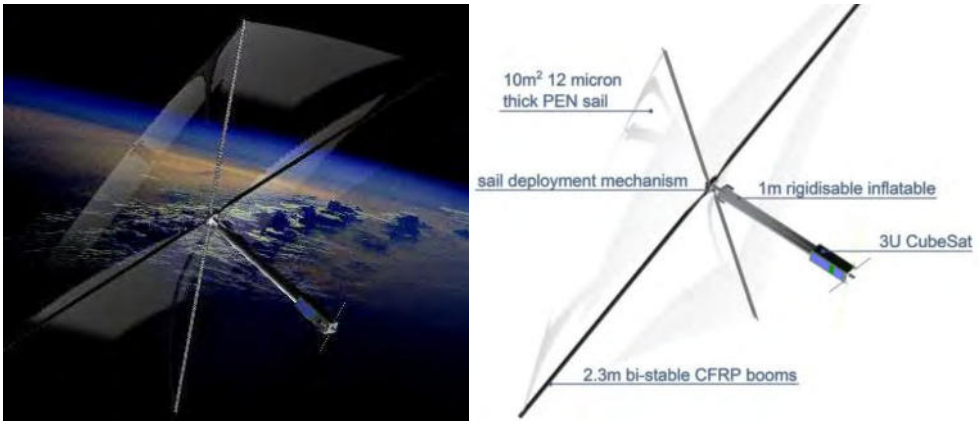

Fig. 1. (left) Artist's Rendition of InflateSail in Orbit with the PMD Mast/Sail Payload Deployed and (right) Labelled Parts of the PMD Payload

2. INFLATESAIL SPACECRAFT AND PMD PAYLOAD

InflateSail's PMD payload was developed through the European Commission (EC) Framework Program Seven (FP7) project: DEPLOYTECH [1], and comprised a 1m long inflatable, rigidisable, aluminium-polymer laminate mast [2] terminated in a deployable $10m^2$ four-quadrant transparent polymer drag-sail supported by four Bistable Rigid Composite (BRC) carbon-fibre reinforced polymer (CFRP) booms [3]. When stowed, the payload occupied approximately 2U of a standard 3U CubeSat structure. The remaining 1U volume contained the spacecraft's core avionics stack comprising a Commercial-Off-The-Shelf (COTS) Electric Power System (EPS), a specially developed Attitude Determination and Control System (ADCS) that also doubled as the On Board Computer (OBC), a COTS VHF/UHF Transceiver (TRXVU) and a bespoke Valve/Payload Controller Board (VCB) (see Fig. 2).

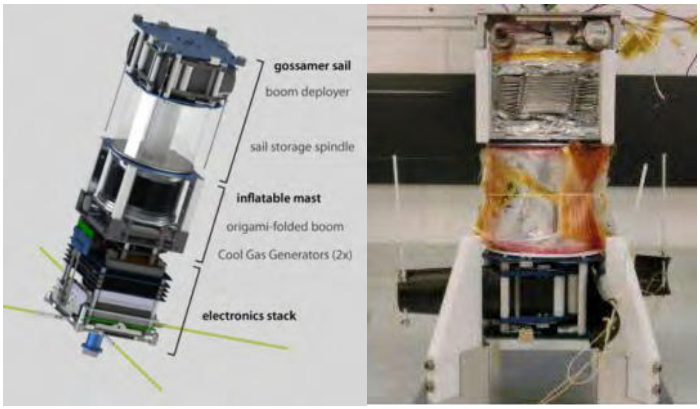

Fig. 2. (left) CAD Rendition of the Internal Systems of InflateSail and (right) the PMD Payload (upside down) Ready for Integration into the Spacecraft

The inflatable cylindrical mast consisted of a tough aluminium-BoPET (biaxially-oriented polyethylene terephthalate) polymer three-ply laminate, stored in the spacecraft by using an origami folding technique. The fold pattern used has five faces around the circumference of the cylinder, and has a repeating unit height of 60mm. The fold pattern leaves an internal space 35mm in diameter when folded, providing storage space for an internal normally open solenoid valve. When fully folded and compressed, the cylinder including its end fittings is 63mm in length (see Fig. 3).

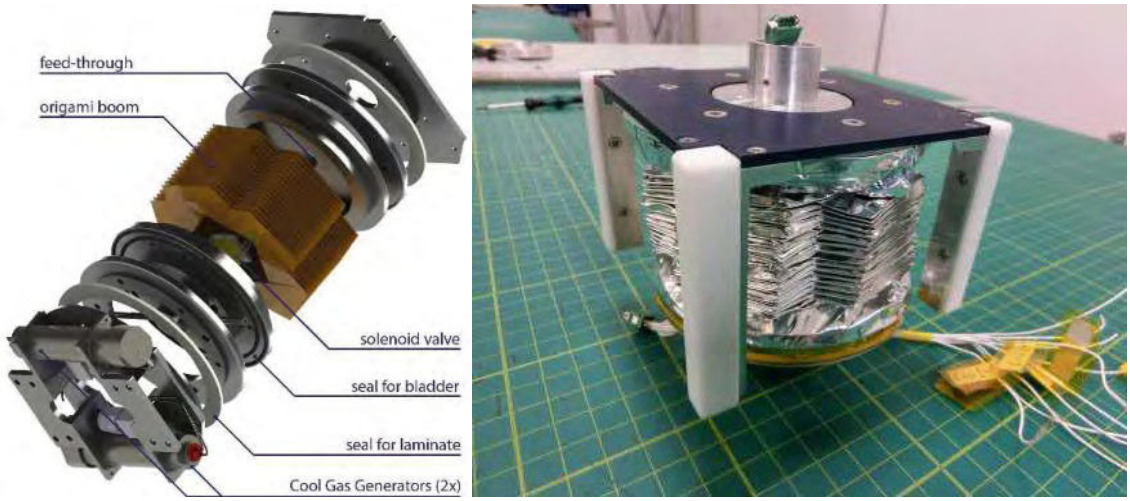

Fig. 3. (left) Inflatable Mast System Layout; (right) The Inflatable Mast in its Stowed Configuration

The two outer aluminium plies were each 13µm thick, and the central BoPET ply was also 13µm thick. The total laminate thickness, including adhesive, was 45µm. A 12µm thick BoPET bladder was used inside the cylinder to improve air-tightness against the vacuum of space. The 1m long, 90mm diameter cylinder was inflated by a Cool Gas Generator (CGG) developed by TNO and CGG Safety & Systems BV (now HDES Service & Engineering), to a pressure of approximately 50 kPa, which was found to be sufficient to cause permanent stretching deformation in the metal plies of the laminate (see Fig. 4). After inflation, the inflation gas was immediately vented in a symmetric pattern (to prevent applying a torque to the spacecraft). The resulting unpressurised rigidized cylinder has been shown to withstand compressive loads up to 50N, and bending moments up to 2Nm [4]. Thus, the inflatable structure does not depend upon long term gas-tightness for its rigidity.

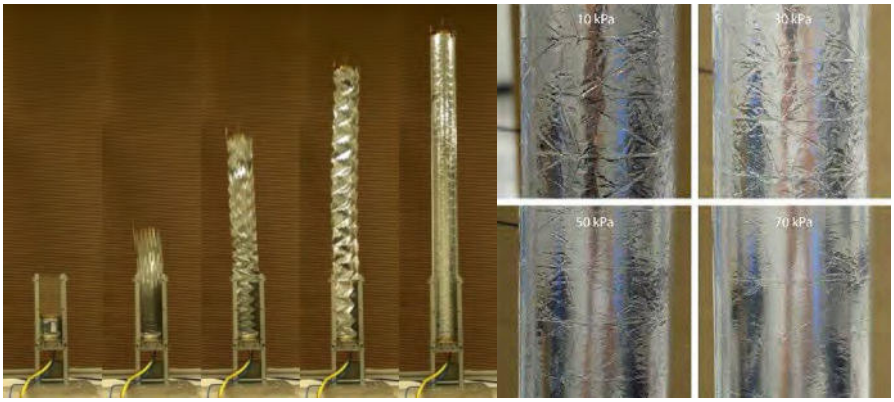

Fig. 4. (left) The Inflatable Cylindrical Mast Deployment Sequence; (right) Residual Creases after Depressurisation from Different Inflation Pressures (10–70 kPa)

The gossamer drag sail and its deployment mechanisms were developed by SSC. The sail structure consists of four separate quadrants, making up a total area of $10m^2$. The quadrants are 'Z'-folded, then wrapped around a free spinning central hub. The sail membrane is 12µm thick polyethylene naphthalate (PEN), which is naturally transparent. For the InflateSail mission, the membrane was deliberately left un-metallised so as to minimise perturbations from solar radiation pressure as the team wanted to observe the effects of atmospheric drag alone for comparison with the science results from the other QB50 spacecraft deployed alongside InflateSail. The sail support structure comprised four custom made carbon-fibre reinforced polymer (CFRP) bistable booms, which were co-coiled just above the wrapped sail membrane. These booms, developed by a UK company: RolaTube Technology (www.rolatube.com), have the property that they are mechanically stable both in coiled and deployed modes. The CFRP booms are driven in and out using a precisely controlled brushless DC motor. The fully deployed sail structure is shown in Fig. 5.

Fig. 5. InflateSail Inflatable Mast and Drag Sail Deployment Test

3. INFLATESAIL LAUNCH AND RESULTS

The InflateSail CubeSat mission was developed and executed as part of the EC FP7 project QB50 [5]. The spacecraft underwent final assembly integration and testing (AIT), full environmental testing (EVT) and full system end-to-end testing with the SSC ground-station between November 2016 and April 2017. It was delivered to ISIS (Innovative Solutions in Space) in the Netherlands on 10th April 2017 and integrated into its QuadPack launch Pod on 12th April 2017 (see Fig. 6).

Fig. 6. (left) InflateSail Team with InflateSail Ready for Delivery; (centre, right) InflateSail Being Integrated into the ISIS QuadPack

InflateSail was launched on Friday 23rd June 2017 at 3.59 am UTC into a 505km altitude, 97.44° inclination SSO. It was one of 31 satellites that were launched simultaneously on the PSLV (polar satellite launch vehicle) C-38 from Sriharikota, India. The first data were received at 09:35am BST (08:35 UTC) on InflateSail's very first pass over Surrey. A quick analysis of the real-time telemetry data from the first passes showed the spacecraft to be in good health and the spacecraft rotation rates looked to be very modest ~0.5 revolutions per minute i.e. ~3°/s (see Fig. 7).

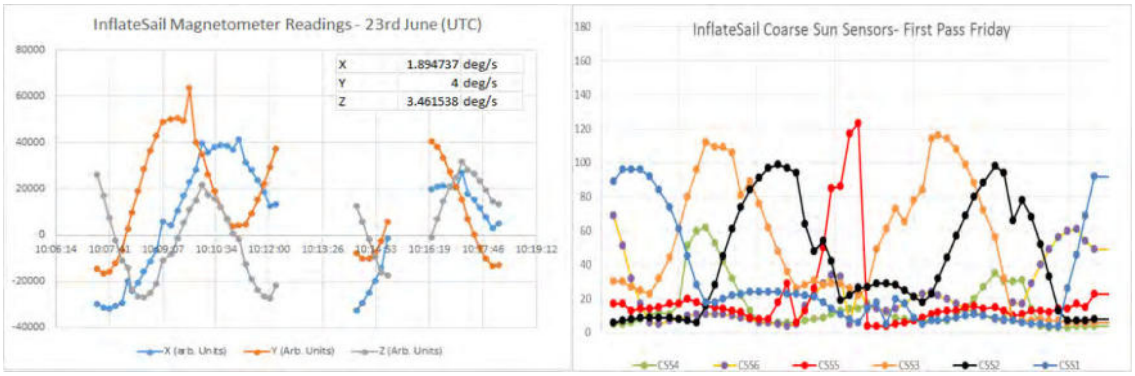

Fig. 7. (left) Initial Magnetometer Data (2nd Pass); (right) Coarse Sun Sensor Data (1st Pass: 08:34 to 08:43 UTC Friday 23rd June 2017) – Arbitrary Units

These initial results showed that InflateSail was in a relatively slow but rather complex rotation primarily about the X- (i.e. the mast) axis. Further, we noted that the B* drag value for "Object F" (later confirmed to be InflateSail) was very much higher than all the other CubeSats deployed from the launch. Both these pieces of evidence seemed to indicate that the InflateSail PMD payload might have already deployed.

We had built in some fail-safes into the spacecraft's operating software, such that the mission would be completed autonomously in the event of prolonged loss of ground communications. Detailed analysis of the system telemetry showed that this fail-safe mode had indeed been activated due to an unexpected on-board computer (OBC) reset occurring with a particular set of system recovery timings. We saw that the PMD payload had deployed automatically around 50-60 minutes after ejection from the launch pod and around three hours before the first pass over Surrey.

3.1 InflateSail Attitude Dynamics

InflateSail's attitude data was derived from the ADCS unit designed and developed by the Electronic Systems Laboratory (ESL) at Stellenbosch University and SSC at the University of Surrey specifically for the QB50 project. Table 1 gives the specifications of the unit. Fifteen ADCS units were officially supplied to the QB50 project, and it is now available commercially from Stellenbosch's spin-out company, CubeSpace.

Table 1. ADCS Unit Specifications

Sensors and Actuators	Type	Range/ Field-of-View	Error (RMS)
Magnetometer	3-Axis Magneto-resistive	±60 μT	< 40 nT
Sun Sensor	2-Axis CMOS Imager	Hemi-sphere	< 0.2°
Nadir Sensor	2-Axis CMOS Imager	Hemi-sphere	< 0.2°
Course Sun Sensor	6 Photo-diodes	Full Sphere	< 10°
Rate Sensor	MEMS Gyro	±85°/s	< 0.05°/s
Pitch Momentum Wheel	Brushless DC Motor	±1.7 mNms	< 0.001mNms
Magnetorquers	Ferro-Magnetic Rods and Air Coil	±0.2Am^2	<0.0005Am^2

The full QB50 ADCS unit (Fig. 8) comprises:

- CubeSense
- CubeControl
- CubeComputer

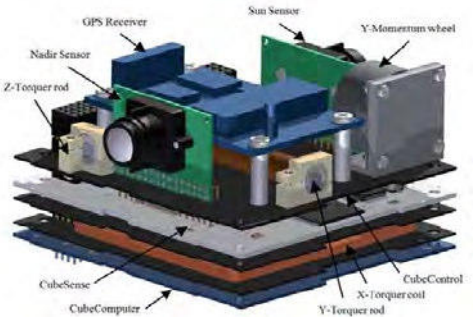

Fig. 8. QB50 ADCS Unit (Cubespace)

These include:

- CMOS Camera Digital Sun Sensor (fine Sun Sensor)
- CMOS Camera Digital Earth Sensor
- 6 Photodiode-based Course Sun Sensors (CSS)
- Micro-Electro-Mechanical-System (MEMS) Gyro
- 3-Axis Magnetoresistive Magnetometer
- 3-Axis Magnetorquer (2 Rods + 1 Air Coil)
- Pitch-Axis Small Momentum Wheel (MW)
- Optional GPS Receiver (Novatel OEM615)
- Extended Kalman Filter (EKF) Control software + SGP4 Orbit Propagator

For InflateSail, the GPS Receiver and the Pitch-Axis Momentum Wheel were not flown to save space and also due to the attitude being controlled "passively" via the weathervane effect once the PMD payload had deployed. Fig. 9 shows InflateSail's axis system. The mast and sail deploy from the +X facet and the X-Axis is the mast axis, normal to the sail. Table 2 gives the course sun sensor allocation.

Table 2. Coarse Sun Sensor Layout

Sensor	Axis
CSS1	-Y
CSS2	+Y
CSS3	-Z
CSS4	-X (Mast Axis – Dipole Antennas Side
CSS5	+X (Mast Axis – Deployed ADR Mast/Sail Side
CSS6	+Z

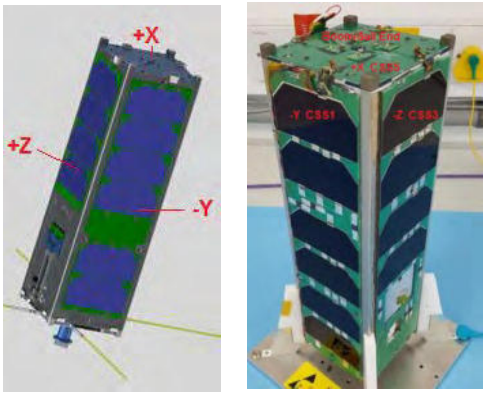

Fig. 9. InflateSail's Axes and CSS Locations

The ADCS unit provides its own independent estimate of the body rates by on-board analysis of the ADCS data. Fig.10 shows these estimates over the mission lifetime.

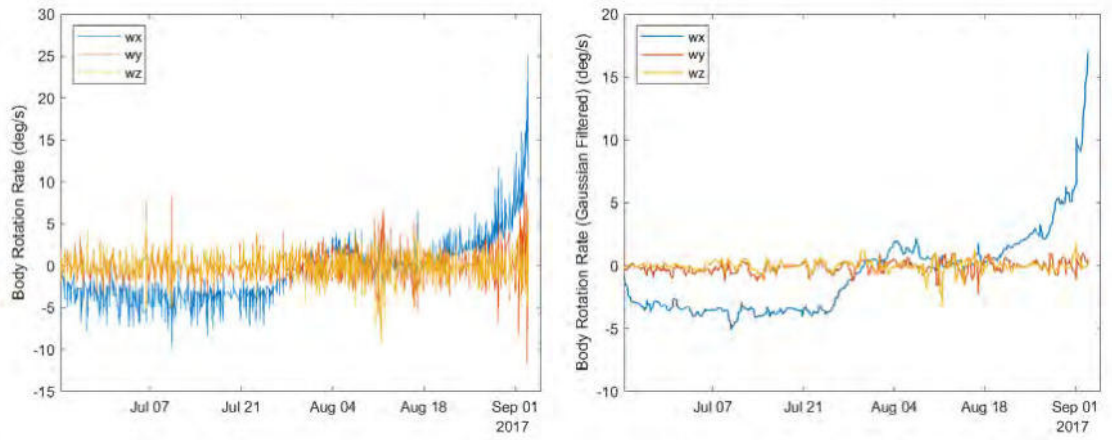

Fig. 10. ADCS Internal Body Rate Estimator Data: (top) Raw; (bottom) Smoothed

The body rate rotations for the Y-Axis (orange) and Z-Axis (yellow) are very small indeed – close to zero degrees per second. The X-Axis body rate (blue) is seen to increase initially to around -4°/s and stay there until the last week in July, when a steady decrease in X-rate occurs, approaching near zero for most of August. The early X-axis spin increases appear to show a transfer of angular momentum to the maximum moment of inertia axis – i.e. the X-axis. We suspect that this happens because of the flexible nature of the mast/sail structure, allowing such behaviour to occur. In mid-to-late August the body motion becomes complex – but everything happens at a slow rate. Beyond ~20th August, the X-rate gradually increases (positively) until re-entry occurs. We last record it at being around +20°/s. It should be noted that the body-rate estimator error bars are quite large for such slow rates ~ ±2°/s for the raw values and ~ ±0.5°/s for the smoothed values.

We interpret these body dynamics as being due to the increasing effect of atmospheric density as the satellite falls. A distinct change in body dynamics – possibly due to increasing Weathervane stability – seems to occur around the end of July, when the spacecraft has dropped to ~470km altitude. The body rates essentially go to zero.

From late August, when the satellite dropped below 450km, the increasingly positive X-Axis body rate seems to indicate a "wind-milling" effect – that is the satellite is spinning increasingly rapidly about the mast, normal to the sail, with the sail quadrants acting like the sails of a windmill. The phenomenon continues at increasing rate until contact was lost at ~250km altitude.

3.2 InflateSail Orbit Dynamics

During the first few days of monitoring, it became clear that Inflatesail was behaving very differently to the other CubeSats released from the PSLV C-38 launch. It was observed to be dropping rapidly and accelerating ahead of the others.

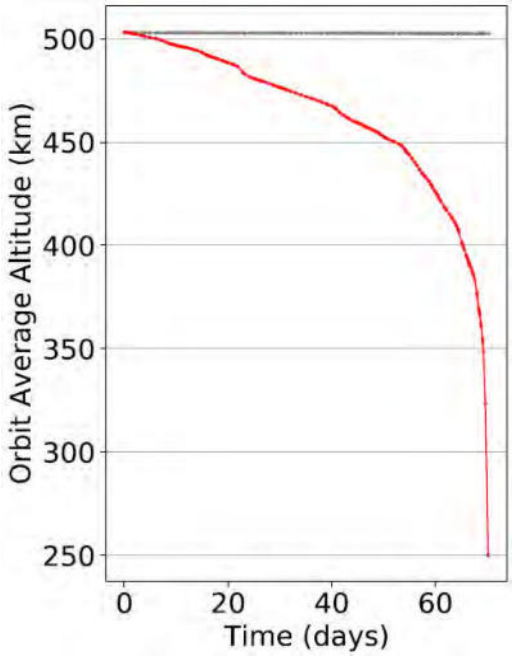

Fig. 11. InflateSail Orbit Average Altitude (red) Compared to the URSA-MAIOR 3U CubeSat Deployed at the Same Time (grey)

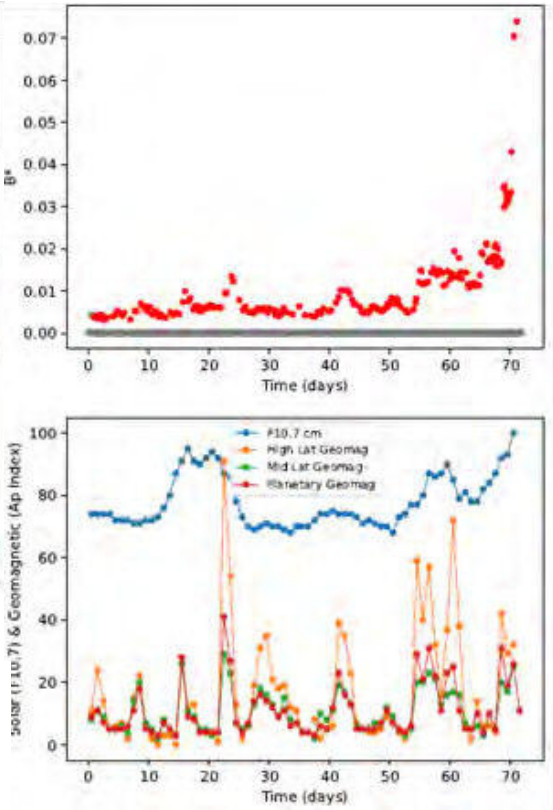

Fig. 12. (top) B* Drag Term (InflateSail = red) (bottom) NOAA Space Weather Indices

Figure 11 shows the drop in perigee altitude (as determined from the two-line element (TLE) sets provided by the North American Aerospace Defense Command – NORAD). The rapid descent of InflateSail (red) compared to the URSA-MAIOR 3U CubeSat (grey), prior to its deployment of its own drag sail, is clear. The step changes in descent rate are related to space weather phenomena – particularly noticeable for mission day ~23 (15th July) following an M2 class solar flare on 14th July 2017.

Figure 12 shows the B* drag term for the PSLV C-38 satellites. The drag is much greater for InflateSail (red) than for the others (grey). The variation in B* correlates very well with the National Oceanic and Atmospheric Administration's (NOAA's) geomagnetic indices – i.e. the effects of space weather show up very clearly on the orbital behavior.

4. CONCLUSIONS

The InflateSail mast/sail PMD system proved itself to be very effective, and InflateSail dropped from 505km to re-entry (250km) in just less than 72 days. InflateSail came down over South America at 01:27 UTC (±6 minutes) on 3rd September 2017. The last radio contact appears to have been with the SSC ground-station at 21:17 UTC on 2nd September 2017. During the descent, InflateSail's attitude and orbit dynamics changes gave insight into the effects of the atmosphere on drag sails at different altitudes and under different space weather conditions. Once below 400km, the rate of descent becomes very rapid and the sail quadrants spin like the sails of a windmill.

Acknowledgements

The authors acknowledge the help and support of many people who have made this mission possible, in particular our fellow team members in the DEPLOYTECH and QB50 FP7 projects, not least our colleagues at the Von Karman Institute (VKI), who managed and led the highly ambitious QB50 project. The authors particularly acknowledge the support of the European Commission and the FP7 programme in funding these projects: DEPLOYTECH (project reference 284474) and QB50 (project reference 284427).

5. REFERENCES

[1] DEPLOYTECH: European Commission FP7-SPACE Project ID: 284474 "Large Deployable Technologies for Space", [Online], Available: http://cordis.europa.eu/project/rcn/101853_en.html [Accessed: 15-Sep-2018]

[2] A. Viquerat, M. Schenk, B. Sanders, V. Lappas, "Inflatable Rigidisable Mast for End-of-Life Deorbiting System", European Conference on Spacecraft Structures, Materials and Environmental Testing, April 1-4, Braunschweig, Germany, 2014.

[3] J. Fernandez, A. Viquerat, V. Lappas, A. Daton-Lovett, "Bistable Over the Whole Length (BOWL) CFRP Booms for Solar Sails", 3rd International Symposium on Solar Sailing. 11-13th June, Glasgow, Scotland, 2013.

[4] A. Viquerat, M. Schenk, V.J. Lappas, B. Sanders, "Functional and Qualification Testing of the InflateSail Technology Demonstrator", 2nd AIAA Spacecraft Structures Conference, 5–9 January 2015, Kissimmee, FL, 2015.

[5] QB50: European Commission FP7-SPACE Project ID 284427 "An international network of 50 CubeSats for multi-point, in-situ measurements in the lower thermosphere and re-entry research", [Online], Available: http://cordis.europa.eu/project/rcn/102061_en.html [Accessed: 15-Sep-2018]

In-Orbit Differential Drag Control Experiment on Nanosatellite Cluster: Analysis and Flight Results

Yeerang Lim[1], Zizung Yoon[2], Walter Frese[3]

[1]Chair of Space Technology, Institute of Aeronautics and Astronautics, Technische Universität Berlin
Marchstr. 12, 10587 Berlin, Germany
Phone: +49 30 314 22345, Mail: yeerang.lim@tu-berlin.de

[2]Chair of Space Technology, Institute of Aeronautics and Astronautics, Technische Universität Berlin
Marchstr. 12, 10587 Berlin, Germany
Phone: +49 30 314 24438, Mail: zizung.yoon@tu-berlin.de

[3]Chair of Space Technology, Institute of Aeronautics and Astronautics, Technische Universität Berlin
Marchstr. 12, 10587 Berlin, Germany
Phone: +49 30 314 25611, Mail: walter.frese@ilr.tu-berlin.de

Abstract: S-NET is a satellite formation with four nanosatellites developed by Technische Universität Berlin, to demonstrate S-band communication between the satellites. All the relative distances shall be maintained less than 400km to conduct intersatellite communication experiment. Since the satellites were launched in February 2018, steady linear drifts exist between each satellite in along-track direction which could be anticipated from the linear relative equations. These drifts are caused by differences in mean motion, or in semimajor axis in other words. Differential drag control is selected to prevent further drifts and hold relative distances as constants. The foremost satellite is set as a reference with the minimum area, and the following satellites will increase cross-section. Mean motion of the satellite with larger drag area will be accelerated by decreasing the orbital energy, therefore it will chase the reference. Required time span to retain drag area difference is calculated based on in orbit trajectory and atmospheric environments. In-orbit experiment started from August 2018. This paper presents the expected differential drag effect based on the theory and compare it with experiment results.

1. INTRODUCTION

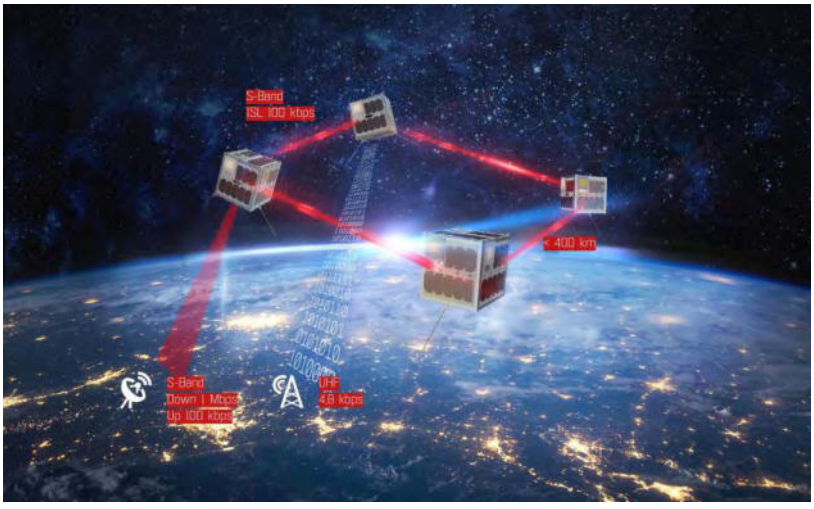

Figure 1 S-NET satellites cluster

S-NET is a nanosatellite project of Chair of Space Technology, Technische Universität Berlin, to investigate and demonstrate the methodological, theoretical and technical

foundations for reliable, modern intersatellite communication in distributed satellite systems [1]. Following table shows the mission overview and satellites' specification.

Table 1 Overview of S-NET mission

Parameter	Value
Orbit height	580 km SSO
Launch date	2018/02/01
Platform	TUBiX-10
Mass	8.8 kg per S/C
Volume	25 x 25 x 25 cm^3
TTC	UHF, RF power: 5W
Power	battery: Li-Ion 5Ah, Solar cells: GaAs 30%
Attitude determination	< 1deg with MEMS array of sun sensor, gyro, magnetometer
Attitude control	< 5deg (3-axis) with 3 reaction wheels, 3 coils

The cluster consists four identical nanosatellites and each satellite has a radio transceiver for inter-satellite communication SLink in cooperation with IQ wireless GmBH. SLink supports 100 kbps for inter-satellite link and 1 Mbps for downlink. The satellites were launched in 1st February and still generate in-orbit experiment data.

Despite the inter-satellite experiment requirement that the relative distance should not exceed 400 km, steady linear drifts exist between each satellite in along-track direction. Relative distance history between the satellites were as Figure 2. The plots are from Two Line Elements analysis.

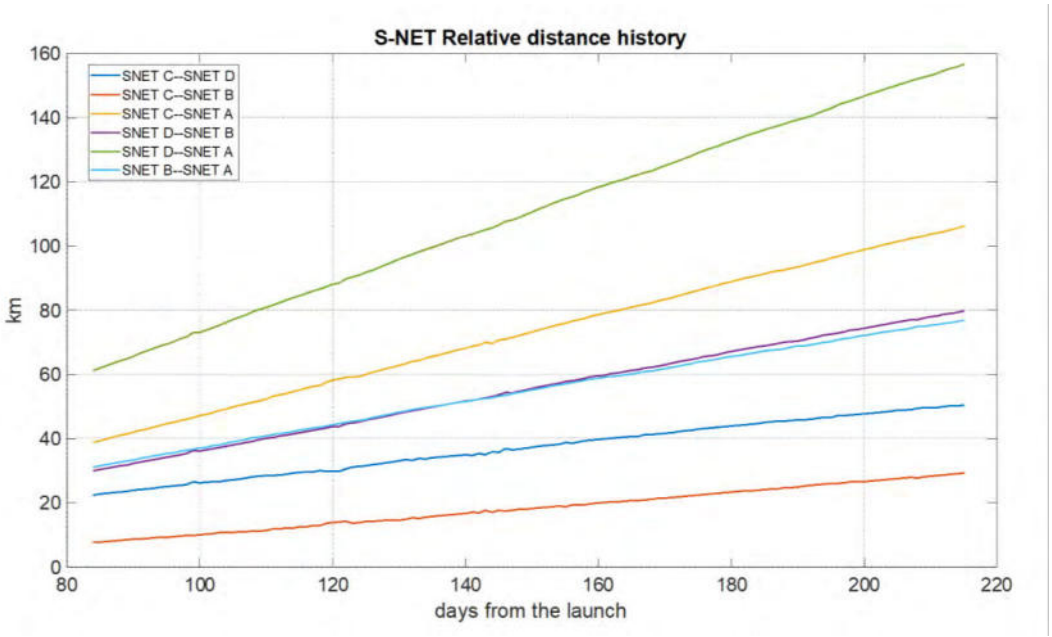

Figure 2 Relative distance between S-NET satellites, May-Aug 2018

2. DIFFERENTIAL DRAG CONTROL

These drifts were caused by semimajor axis difference. Four semimajor axes are not perfectly identical, and so mean motions of each satellite differ. Since S-NET does not carry any orbit control actuator and also the satellites are in the LEO with dense atmosphere, differential drag control is the possible option to stop the drift and bring back the satellites together. Differential drag control algorithm is addressed in detail from Dove of Planet Inc. [2][3]. Although preventing drift could be achieved as well as placing the satellites on the required position, only the first part is considered for S-NET.

Essential idea of the differential drag control is to change the following satellite's cross-sectional area A_H (as high drag mode) larger than the leading one's cross-sectional area A_L (as low drag mode). It will cause higher drag for the follower and faster semimajor axis decrease indeed. To derive differential drag effect, reference mean dynamics pressure q_{ref} should be calculated first.

$$q_{ref,k} = \frac{1}{2}\overline{\rho v_{rel}^{\ 2}} \tag{1}$$

ΔV during the discretized time period can be calculated using the observed ballistic coefficient $BC = m/C_d A$ in low and high drag modes, BC_L and BC_H.

$$\Delta V = q_{ref,k}\left(\frac{1}{BC_H} - \frac{1}{BC_L}\right)\Delta t \tag{2}$$

Eventually relative velocity in tangential direction will be affected from the drag difference as below.

$$\dot{y} \approx -3\dot{y}_0 = -3\Delta V = 3q_{ref,k}\left(\frac{1}{BC_L} - \frac{1}{BC_H}\right)\Delta t \tag{3}$$

Equation (3) could be rewritten in acceleration form.

$$\ddot{y} \approx 3q_{ref,k}\left(\frac{1}{BC_L} - \frac{1}{BC_H}\right) \tag{4}$$

For S-NET, atmospheric density is set roughly as $\rho = 2.5\times10^{-14}\,\mathrm{kg/m^3}$ from MSISE90 atmospheric model with constant flux. The density is lower than average because of minimum solar activity. q_{ref} can be calculated from ρ and current altitude 575km,

$$q_{ref} = \frac{1}{2}\times(2.5\times10^{-14})\times(7.1\ \mathrm{km/sec})^2 = 6.3\times10^{-7}\,\mathrm{kg/m/sec^2} \tag{5}$$

where the relative reference velocity with respect to the Earth atmosphere is as below.

$$v_{rel} = \sqrt{\mu / a_{ref}} - \omega_{Earth} \times a_{ref} = 7.1\text{km/sec} \tag{6}$$

Then the acceleration $\ddot{y}$ due to drag difference can be calculated with the common drag coefficient $C_d = 2.2$. The attitude of the following satellite is assumed to be tilted as $45\,\text{deg}$ to maximize the cross-sectional area, and the leading satellite is assumed to tumble continuously.

$$\begin{aligned} \ddot{y} &\approx 3 \times (6.3 \times 10^{-7}\,\text{kg/m/sec}^2) \times \left(\frac{2.2 \times (0.25\text{m})^2}{8.8\text{kg}}\right) \times \left(\frac{\sqrt{2}+1}{2} - \sqrt{2}\right) \\ &= -6.1 \times 10^{-9}\,\text{m/sec}^2 = -45.7\ \text{m/day}^2 \end{aligned} \tag{7}$$

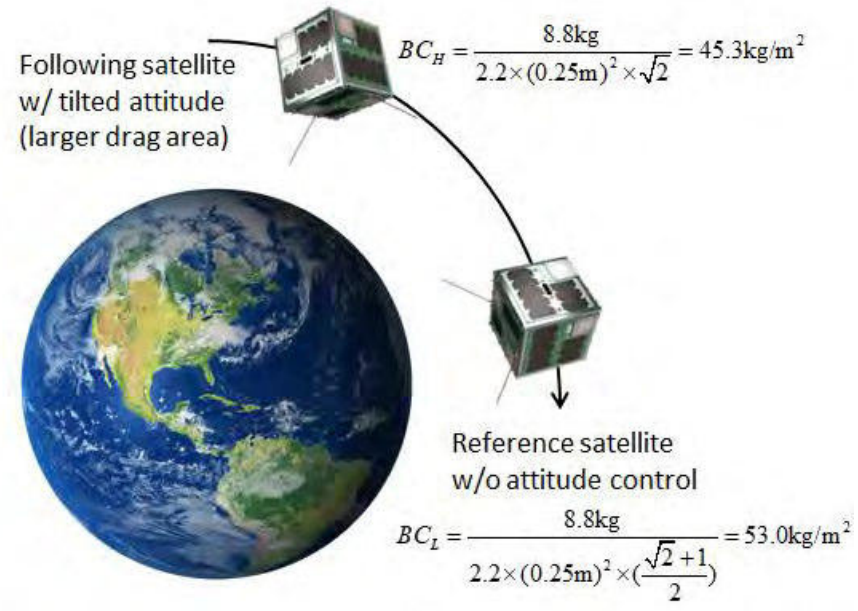

Figure 3 Differential drag control strategy and ballistic coefficients

Since relative along-track velocity $\dot{y}$ is already given from the trajectory, required experiment duration Δt could be easily calculated as $(\dot{y}/-\ddot{y})$. Table 2 shows the required Δt to compensate relative velocities between each satellite and SNET-A.

Table 2

	SNET-B	SNET-C	SNET-D
Δt estimated (day)	7.3	8.9	15.7

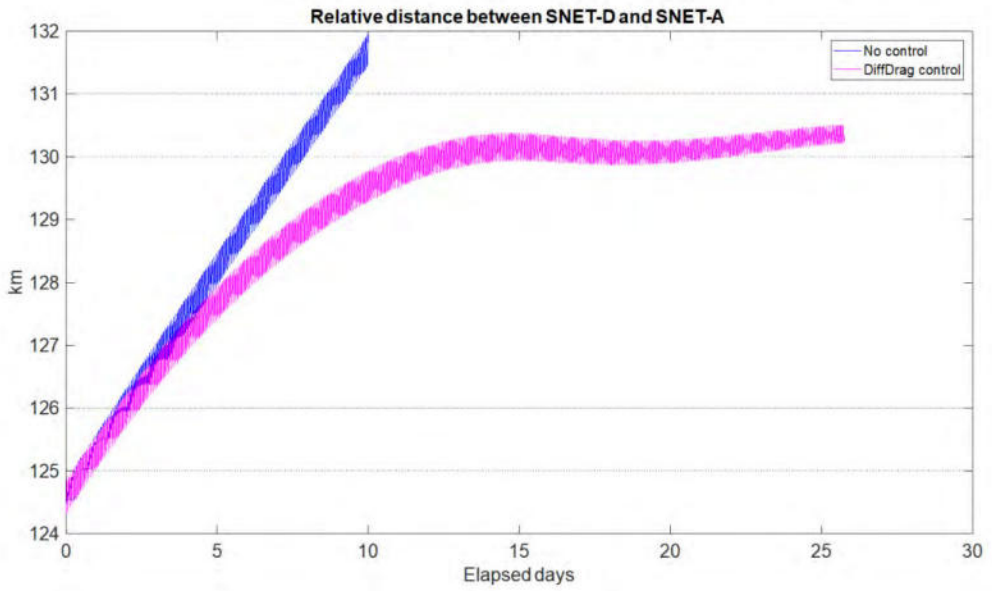

Figure 4 Simulated relative distance w/ and w/o differential drag, between SNET-D and SNET-A

Figure 4 is the estimated relative distance between SNET-D and SNET-A, with and without differential drag control. The orbits are propagated from GMAT, with 50x50 EGM96 gravitational model and MSISE90 atmospheric model with constant flux. Differential drag control is maintained during Δt as the Table 2, and the result shows that relative distance could be maintained as constant with the control.

3. IN-ORBIT EXPERIMENT

The calculation is verified with the in-orbit experiment, which started at 17th August. Figure 5 shows the actual relative distance history from September 2018. SNET-D is the slowest satellite and it is following SNET-A and SNET-C which are randomly tumbling. Same as Figure 2, the plots are from Two Line Elements analysis.

The acceleration is -0.0038km/day^2 between SNET-D and SNET-C and -0.0030km/day^2 between SNET-D and SNET-A from the plot fitting. Average acceleration is about $-3.4\ \text{m/day}^2$. Since the accumulated drag control is performed for 247.8 hours during 151 days, the expected acceleration in Equation (7) should be averaged as below.

$$\ddot{y} \approx -45.7\ \text{m/day}^2 \times (247.8/24) \div 151 = -3.1\ \text{m/day}^2 \tag{8}$$

The scaled acceleration is consistent with the in-orbit result with less than 10% error. This error could be cased by variable atmospheric density, irregular tumbling and attitude control error.

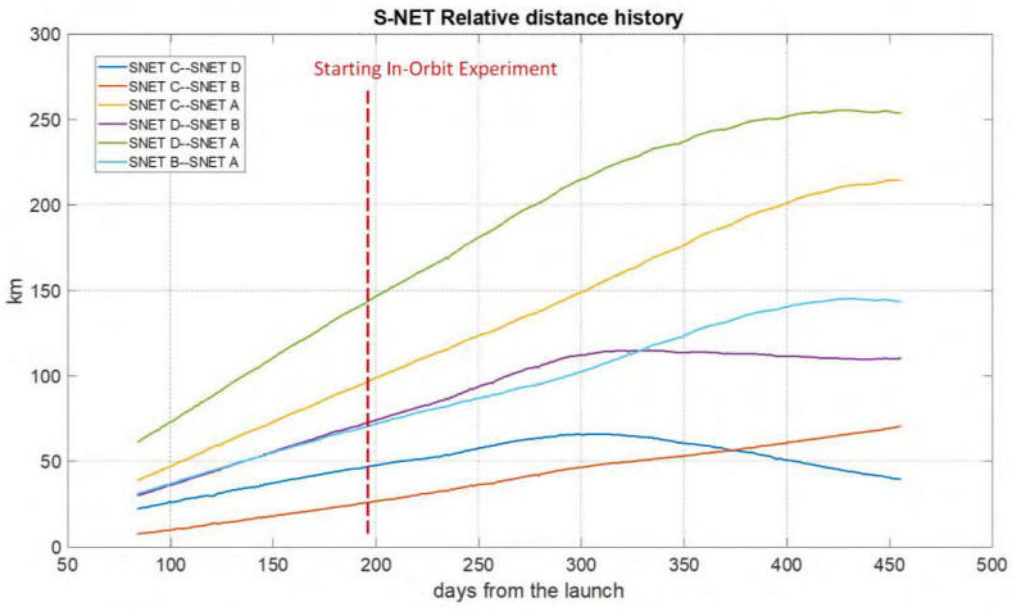

Figure 5 Relative distance between S-NET satellites, Sep 2018-Apr 2019

4. CONCLUSION

Flight results from in-orbit differential drag control experiment is presented in the paper. The purpose of the experiment is to prevent drifts between four S-NET satellites, by controlling the cross-sectional area of the satellites and inducing relative acceleration from drag difference. Relative velocities are successfully reduced, and some pairs of S-NET satellites maintain constant relative distances. This result shows that differential drag control is useful to LEO satellites, and still feasible even with cubic-shaped satellites. Control log shall be organized in the near future and accumulated control durations shall be compared to the estimation.

5. REFERENCES

[1] Frese, W., Yoon, Z., Brieß, K., and Voigt, S., Communication network in LEO: In-orbit verification of intersatellite link by nanosatellite cluster S-NET. International Astronautical Congress 2018, Bremen (2018)

[2] Foster, C., et. al, Differential Drag Control Scheme for Large Constellation of Planet Satellites and On- Orbit Results, 9th International Workshop on Satellite Constellations and Formation Flying, Boulder, Colorado, USA (2017)

[3] Foster, C., Hallam, H., and Mason, J., Orbit Determination and Differential-Drag Control of Planet Labs CubeSat Constellations, AIAA Astrodynamics Specialist Conference, Vale, Colorado, USA (2015)

About Ecoinformatics tools and GIMS-technology in the water quality monitoring

Dao Van Tuyet[1], Ngo Hoang Huy[2], Vladimir F. Krapivin[3], Ferdenant A. Mkrtchyan[3], Vladimir V. Klimov[3], Vladimir Yu. Soldatov[3]

[1] Vietnam National Space Center,
Vietnam Academy of Science and Technology
Hoang Quoc Viet 18, 129823 Hanoi, Vietnam
Phone: +84 24 379 17675, Mail: dvtuyet@vnsc.org.vn

[2] Electric Power University
Hoang Quoc Viet 235, 129823 Hanoi, Vietnam
Phone: +84 24 2218 5607, Mail: huynh@epu.edu.vn

[3] Kotelnikov Institute of Radioengineering and Electronics,
Russian Academy of Sciences, Moscow, Russian Federation.
Vvedensky 1, 141190 Fryazino, Moscow Russia
Phone: +7 49 6565 2400, Mail: vkrapivin_36@mail.ru, ferd47@mal.ru

Abstract: Results of the investigations are stated in connection with the assessment of capabilities to use the sensors of optical and microwave ranges for the diagnostics of hydrophysical and hydrochemical systems having various spatial scales. Structure of multi-functional information-modeling system (MFIMS) MFIMS consists the sensors of optical and microwave ranges and it realizes functions for the diagnostics and adaptive identification of the liquids. The system is based on the base formation of spectral standards for the liquid solutions delivered by means of multi-channel spectrophotometer or spectroellipsometer and used for adaptive recognition of spectral images. Education process and following recognition are realized in accordance with the certain series of the methods, algorithms and procedures for accumulation, analysis, sorting and processing observation data. Assembly of all tools forms the information-modeling system oriented on the operative diagnostics of the state of the water objects when multi-channel information is delivered by the on-site and remote sensors and high-performance information technologies are used for the solution of the tasks related to the classification and identification of the water objects. A solution of operative multi-pronged task of the water quality control and state of hydrochemical systems when their spatial heterogeneity is taken into consideration and series of physical, chemical and biological factors exist to be as influencing on them is realized by means of the collection of computer algorithms and models that are the hydrochemical monitoring system. This collection gives a possibility to parameterize typical water balance on restricted territory that reflects an interaction between hydrological cycle components. Under this, the system has adaptation function to the real hydrophysical object or process. The MFIMS can used under the water media or other liquids quality control under the expedition conditions when chemical laboratory no exist.
Keywords: spectroellipsometer, spectral image, cluster analysis, identification, liquid solution, algorithm, model, recfognition

1. INTRODUCTION

Numerous problems of the environmental monitoring are solved by means of the ecoinformatics technologies [1-15]. Global information systems (GIS) are the most developed elements of natural monitoring. GIS-technology has severe success and brings perceptible economic effects. GIS-technology is positioned in the interface of computer cartography, databases and remote-sensing. The GIS elements are computer net, database, data transmission net and a system for the reflection of real situation by means of computer display. Numerous GIS show that GIS-technology guarantees convenient tool for the masses use to control the monitoring object and is efficient mechanism for the integration of multi-factor information. However, GIS-technology has serious re-

strictions when complex environmental task are solved and when synthesis of dynamic image of the environment is needed on the database that is episodic at the time and fragmentary in the space. Basic GIS imperfection consists in that it does not orient on multi-plane prognosis of the monitoring object evolution. In particular, the microwave remote-sensing systems that are widely used to equip the flying laboratories and the natural-resources satellites supply the data sets that are geographically distributed. Reconstruction of the information obtained is possible only by employing methods of spatial-temporal interpolation for the development of which several techniques and algorithms of simulation modeling have been used in the past [2,7]. For example, the spatial modeling has been widely used for the interpretation of the data obtained by environmental instruments, which monitor the lithosphere, cryosphere, hydrosphere, vegetation interfaces and urban environments. For the accomplishment of the complex task of the environmental diagnostics, it is necessary to built up a system that incorporates such functions, as well as data collection (by means of remote sensing and in-situ methods), their analysis and processing. A system of this type is capable to conduct systematic observations and assessments of the environmental state, to predetermine forecasting diagnostics of changes of the environmental elements (due to anthropogenic impacts) and to analyze the evolution of environmental processes, taking into account the anthropogenic scenarios. One of the system functions is to provide warnings about undesirable changes in the environment. Attainment of such functions for environmental monitoring is feasible with the use of simulation methods allowing the development of a model for the investigation of the natural subsystem.

2. NEW ECOINFORMATICS TOOL

Important step in the GIS-technology development was made in the papers [1-15] where new technology of the GIMS synthesis was proposed. This technology eliminates many GIS imperfections and gives a possibility to synthesize the monitoring systems having prognosis function. Generally, principal GIMS-technology conception is represented in Figure 1. Remote determination of highly possible of number of parameters for the model of controlled geo-ecosystem is key element of the GIMS-technology. Just, that sort of combination of empirical and theoretical functions of the GIMS-technology allows the operative assessment of current and prediction changes in the environment.

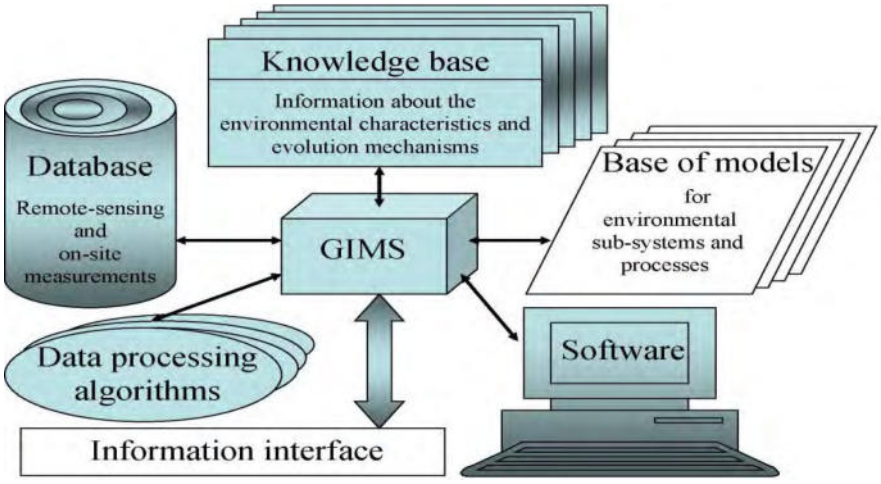

Figure 1. Conceptual diagram showing the definition of the GIMS-technology architecture.

The hierarchical structure of environmental monitoring systems optimizes the use of financial resources with high quality of final results. This is the basic argument for the creation of geoinformation monitoring systems using the technology of hierarchical synthesis.

The GIMC-technology is based on a joint use of the following structural constituents:
- remotely sensed microwave and optical data;
- *in situ* measurements;
- GIS and other available data banks information; and
- mathematical modeling of spatial-temporal variations in physical and chemical parameters of the environment.

The GIMS structure includes series of blocks that solve specific tasks.

3. THE GIMS-TECHNOLOGY PLATFORMS FOR MICROWAVE MONITORING

Series of mobile remote-sensing platforms for microwave monitoring of the environmental systems have been synthesized during last years [3-7]. These platforms realize the GIMS functions for the solution of specific tasks of nature monitoring including man-made environmental systems such as related to the melioration, hydrology, oceanology, ecology, and epidemiology [3,7,11,13]. For instance, application of the non-contact technology allows the obtaining the operative data about the soil moisture, to assess a possibility of dangerous hydrological situations and to realize the monitoring of the state of hydro-technical structures in the regions where hydrological risk is higher. In particular, the GIMS-technology can give a reliable control of the zones where water-logging of roads and railways, and the leakage across the dams are possible [4].

Practical realization of the GIMS-technology is possible with the use of mobile platform equipped by the remote-sensing sensors. Such platforms were produced and tested in different times and regions [3-6]:
- Flying laboratory IL-18 (Figure 2).
- Airborne SAR complex IMARC (Intelligent Multi-frequency Airborne polarimetric Radar Complex) equipped by the radiometric complex of ranges: X(3.9 cm), L(23 cm), P(68 cm) и VHF(2.54 m) [3,7].
- Miramap sensor aircraft-laboratory TwinCommander equipped by digital photo camera (visible 0.4-0.7 micron), lidar scanner (SW infrared 1064 nm), passive microwave scanner (2, 5, and 21 cm), and thermal camera (LW infrared 7.5-13 micron) [3-7].
- A manned “Rover” mobile type platform (Figure 3) at a height of 2 m, which provides data at a ground resolution of 1.4 m and is equipped by radiometers of ranges: 6 cm, 18 cm, and 21 cm [2, 5,10].

In the all cases, the use of these platforms to assess regional geo-ecosystem state proposes *a-priory* data presence and realization of synchronous *in-situ* measurements. The GIMS-technology reconstructs spatial distribution of the geo-ecosystem characteristics basing on the data that are episodic in the time and fragmentary in the space. The GIMS-technology overcomes situations of unremovable information uncertainty using evolution modeling methods [6,9,10]. Use of optical sensors and spectroellipsometry technology gives a possibility to calculate the water quality indicators assessing the

concentrations of chemicals in the water and distribution and parameters of the pollutant spots of the water surface [8,10,13-15].

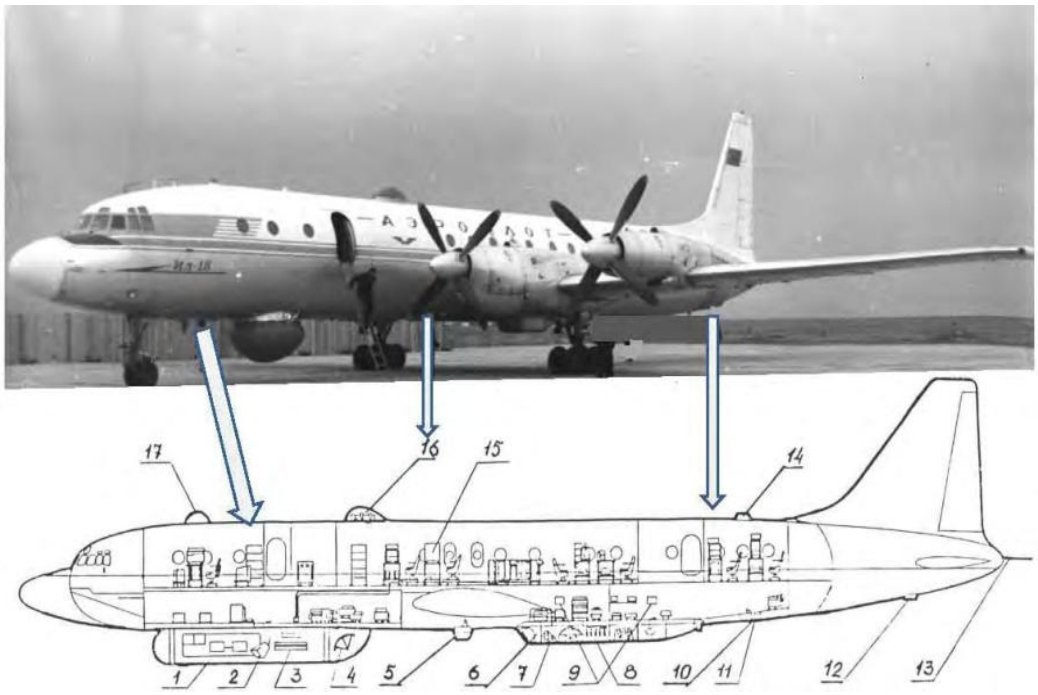

Figure 2. Scheme of positioning the antenna systems and photo-hatches on-board of flying laboratory IL-18. Notation: *Antennas*: 1,3 – radiolocators with synthetic aperture, wavelengts – 2.0 and 10.0 cm; 2,6-trace polarimeters, wavelength – 0.8 and 2.25 cm; 4 – six-channel scanning polarimeter, wavelength – 0.8, 1.35, 2.25, 10, 20 and 27 cm; 7,9 – precision altimeter and interferometer of side looking, wavelength – 2.2 cm; 13 – sub-surface sonding station of decimetric range; *Photo-hatches*:5,10,12 – large-format and frame TV, aero-camera; 11, 14 – radiometers of mm range; 16 – trace radiometers, wavelength – 0.8, 1.35, and 2.25 cm; 15 – gravimetric and inertial devices; 17 – astro-hatch.

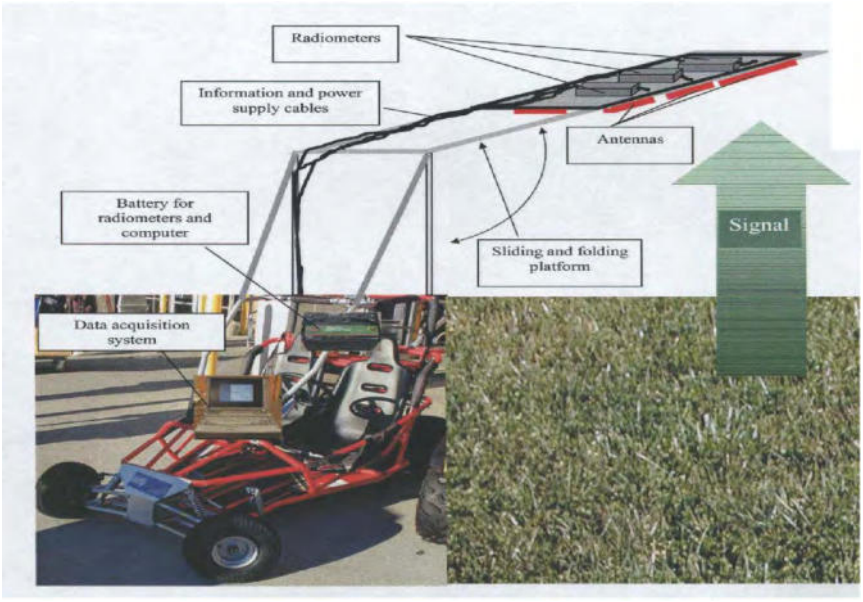

Figure 3. Subsystems and microwave radiometers on the rover's mobile platform [7].

4. GIMS - TECHNOLOGY FOR THE DIAGNOSTIC OF LIQUID SOLUTIONS

During last time, optical devices are intensively used for the investigation of characteristics of liquid and solid mediums. It allows the operative diagnostic practically in real time mode. Spectroellipsometry is the peak of polarization optics. The creation of multichannel polarization optical instrumentation and use of spectroellipsometric technology are very important for the real-time ecological monitoring of the aquatic environment. Spectroellipsometric devices give us high precision of measurements. Spectroellipsometric and their multichannel measurements in an aquatic environment provide the basis for the application of modern algorithms for the recognition and identification of pollutants. Present multi-channel spectrophotometers and spectroellipsometers deliver spectral images of controlled objects with high speed and precision. Use different algorithms and models for the processing spectral images allows the adaptive identifier synthesize that has principal difference from traditional approaches to the liquid solution control.

Combined application of instrumental tools and software for operative monitoring of the water medium on the Earth developed insufficiently on account of complexity of complex monitoring system synthesize. Tasks of the adaptation of algorithms and models to the specific monitoring system are complexity and sometimes contradictory [1,7,8,9,11], proposed new universal technology for solution these tasks. This technology based on the precision compact polarimeters and the education algorithms for recognition of spectral images. Under this, a solution effectiveness of multi-parametrical tasks is mainly determined by the sensitivity and precision of sensors, their universality, and by using wide spectral bands.

Spectral measurements of the water medium deliver information for the using the proper algorithms and models of identification and recognition of pollutants. This is the first time the combined use of real-time spectroellipsometry measurements and data processing methods have been realized as different versions of an Adaptive Identifier (AI) (Figure 4). Use of an acromatic compensator on the basis of Fresnel rhomb made of fused quartz that enhances the precision of measurements.

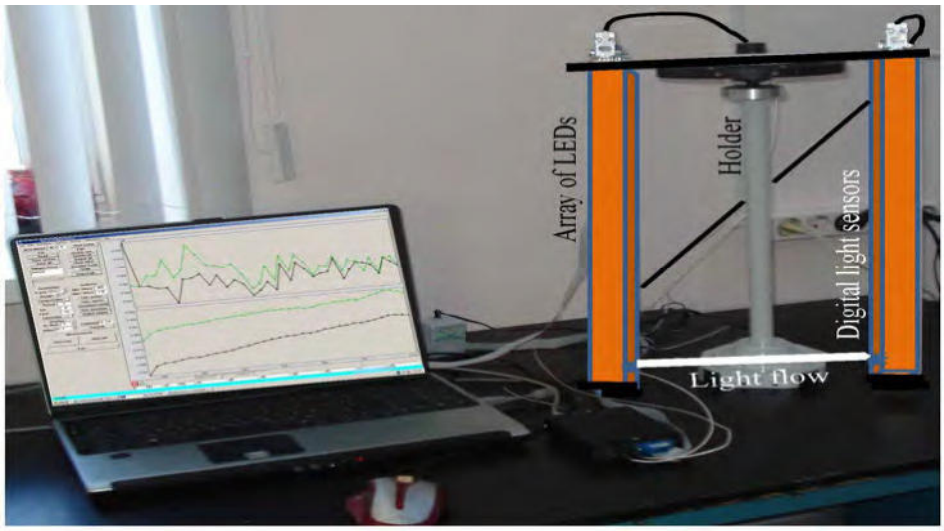

Figure 4. Adaptive Identifier. LEDs is light-emitting diodes.

Spectroellipsometric measurements deliver spectrums that are considered as spectral images of water solutions. Space of spectral images is formed during the learning procedure realized in laboratory conditions when spectral images and chemical analysis are performed at the same time. An identification of spectral image for unknown water solution is realized by means of comparison his vector – identifier with elements of the EDB. Depending from used optical device spectral image of water solution can be represented by one or two vec-tor-identifiers. Final identification is realized by means of search in the EDB of vector – identifiers which are minimal distance from considered vector-identifier Q={X1,…, Xn} of given water solution. In common case, usually the following methods are used:

- *Cluster analysis.* In this case two types of clusters are formed for $Cos\Delta$ and $Tan\Psi$ where Δ and Ψ are ellipsometric angles corresponding to complex amplitude reflection coefficients for two different polarizations.
- *Algorithm of discrepancy between spectra.* It is assessed average distance between the ordinates for both spectra and spectrum of studied case and decision is made taking into account minimal value of this distance.
- A*lgorithm of discrepancy between etalon vectors.* In this case, decision is made taking into consideration of minimal δ.
- *Inverse task solution.* This algorithm is based on linear dependence of optical spectrum on the concentration of chemical elements in water solution. In this case, subdefinite system of linear algebraic equations is solved.

The MFIMS was used in different laboratory and in-situ conditions. Table 1 gives experimental results which give possibility to compare above mention algorithms. Dependence of risk assessment as function of solution concentration is represented in Figure 5. We see that risk to have high error is growth with increase of chemical element concentration. It is caused that discrepancy between spectra is decreased with increase of chemicals concentration. In this case it is necessary to extend the database of spectral etalons.

Table 1. A precision of the MFAIMS. Comparatively assessment of algorithms for recognition of spectral images of water solutions.

Object for study	Identification algorithm and its error (%)			
	Cluster analysis	Discrepancy between spectra	Discrepancy between vector-etalons with the use equation (1)	Inverse task solution
$CuSO_4$	15	12	8	7
NaCl	17	11	7	5
$NaHCO_3$	16	10	5	5
NH_4OH	21	13	9	6
$ZnSO_4$	22	12	8	6
Potassium iodite	13	10	6	4
Na+Cu+Zn+Mn+glucose	18	9	9	8
Furaciline	23	11	5	5
Bifidbacterium	14	10	4	4

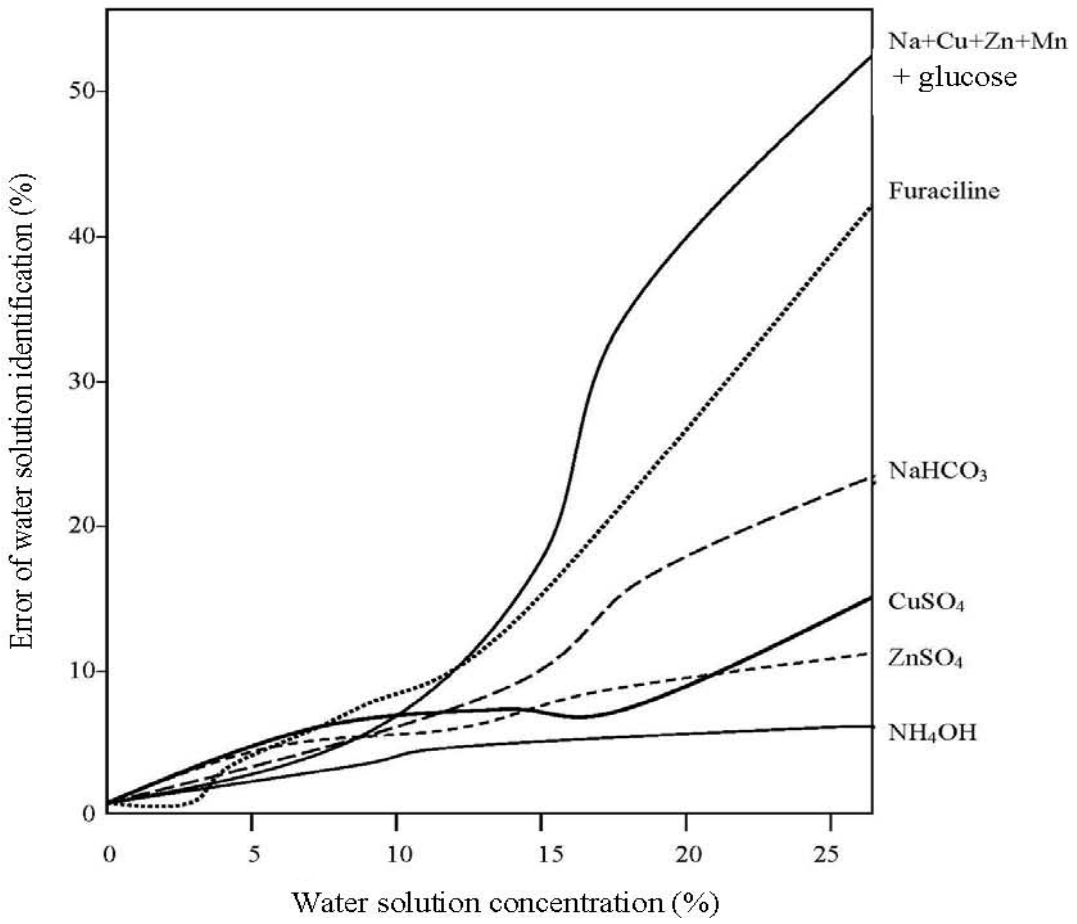

Figure 5. Dependence of spectral image identification on the solution concentration.

5. CONCLUSION

The questions discussed in this paper are some of part of numerous global ecodynamics problems a solution of which is barest necessity of today under rational management of natural systems. Basic defect of elaborated and used geo-ecological monitoring technologies consists in the efforts to do the integrating reasoning for the environmental system state on the base of study of separate systems. Therefore, many monitoring systems are not enough effective and non-informative. Set of the GIMS-technology authors focusing on this their attention [4-6] note it's the more universal character under the use of data and knowledge and a possibility to provide the most economical acquisition of new knowledge and data. This is achieved by means of adaptive package of technical and algorithmic tools harmonized by information content.

Thus, the GIMS provides remote sensing, on-ground (*on-site*) samplings, using GIS-information and mathematical modeling of physics-chemical processes in selected areas. GIMS-technology can effectively be applied for solving many agricultural, hydrological, environmental and many other Earth related problems.

6. ACKNOWLEDGEMENTS

"The reported study was partially supported by RFBR, research project No.19-07-00443-a".

7. REFERENCES

[1] V.F.Krapivin , C. Nitu , and F.A. Mkrtchyan . Algorithms for the solution of spectroellipsometry inverse task. The Scientific Bulletin of Electrical Engineering Faculty, V. 2, No.26, 3-8 (2014)

[2] V.F. Krapivin and A.M. Shutko . Information technologies for remote monitoring of the environment. Springer/Praxis, Chichester U.K.(2012)

[3] V.F. Krapivin and C.A. Varotsos . Biogeochemical cycles in globalization and sustainable development. Chichester, U.K.: Springer/PRAXIS. (2008)

[4]V.F. Krapivin , C.A. Varotsos and V.Yu. Soldatov . Mission to Mars. Reliable method for liquid solutions diagnostics. Frontiers in Environmental Science: Environmental Informatics. Sci., 2014, Vol.2, No.21, 1-8 (2014)

[5] V.F. Krapivin , C.A. Varotsos and V.Yu. Soldatov New Ecoinformatics Tools in Environmental Science:Applications and Decision-making. Springer, London, U.K.(2015)

[6] F.A. Mkrtchyan , V.F. Krapivin , V.V. Klimov and V.I., Kovalev. Hardware-software system of the water environment monitoring with use of microwave radiometry and spectroellipsometry means. Proceedings of the 28th International Symposium on Okhotsk Sea & Sea Ice. 17-21 February 2013. The Okhotsk Sea & Cold Ocean Research Association, Mombetsu, Hokkaido, Japan. 2013. 104-109 (2013)

[7] F.A. Mkrtchyan and V.F. Krapivin . An adaptive monitoring system for identify of the spots of pollutants on the water surface. // World Environment, 3(5), 165-169 (2013)

[8] F.A. Mkrtchyan, V.F. Krapivin. GIMS-Technology for the Environmental Diagnostics. Proceedings Joint International Conference on Theory, Data Handling and Modeling on GeoSpatial Information Science, Hong Kong, 26-28 May,2010/ Book(PDF-60Mo). International Archives of Photogrammetry Remote Sensing and Spatial Information Science. Volume XXXVIII – Part 2, pp. 789-795 (2010)

[9] V.F. Krapivin and F.A. Mkrtchyan. Expert System for the Operative Environmental Diagnostics. Proceedings 12th AGILE International Conference on Geographic Information Science, 2-5 June 2009, Hanover, Germany, 345-151 (2009)

[10] F.A. Mkrtchyan , V.F. Krapivin and A.M. Shutko. Microwave Monitoring of the Soil Moisture// Summaries SPIE International conference “Optics + Photonics”(SPIE-2013). San Diego , August 26-29, California, USA (2013)

[11] F.A. Mkrtchyan and V.F. Krapivin. GIMS-Technology for the Environmental Diagnostics. Proceedings Joint International Conference on Theory, Data Handling and Modeling on GeoSpatial Information Science, Hong Kong, 26-28 May,2010/ Book(PDF-60Mo). International Archives of Photogrammetry Remote Sensing and Spatial Information Science. Volume XXXVIII – Part 2, 789-795(2010)

[12] V.F. Krapivin and F.A. Mkrtchyan. Expert System for the Operative Environmental Diagnostics. Proceedings 12th AGILE International Conference on Geographic Information Science 2009, 2-5 June 2009, Hanover, Germany, 345-151, (2009)

[13] F. A. Mkrtchyan and S. M. Shapovalov. Some aspects of remote monitoring systems of marine ecosystems// Russian Journal Of Earth Sciences, 18, 4, 1-10, (2018)

[14] F.A. Mkrtchyan and C.A. Varotsos. A New Monitoring System for the Surface Marine Anomalies// Water Air Soil Pollut., 229, 8(273), 1-10, (2018)

[15] F. A. Mkrtchyan. On the Effectiveness of remote monitoring systems. Proceedings SPIE Optical Engineering + Application 2018, Volume 10764, Earth Observing Systems XXIII, 1076415, San Diego, California, USA (2018)

Using Docker in Process Level Isolation for Heterogeneous Computing on GPU Accelerated On-Board Data Processing Systems

Nandinbaatar Tsog[1], Mikael Sjödin[1], Fredrik Bruhn[1,2]

[1]Mälardalen University
Box 883, 721 23, Västerås, Sweden
Mail: {nandinbaatar.tsog, mikael.sjodin, fredrik.bruhn}@mdh.se

[2] Unibap AB (publ)
Svartbäcksgatan 5, 753 20 Uppsala, Sweden
Mail: f@unibap.com

Abstract: The technological advancements make the intelligent on-board data processing possible on a small scale of satellites and deep-space exploration spacecraft such as CubeSats. However, the operation of satellites may fall into critical conditions when the on-board data processing interferes strongly to the basic operation functionalities of satellites. In order to avoid these issues, there exist techniques such as isolation, partitioning, and virtualization. In this paper, we present an experimental study of isolation of on-board payload data processing from the basic operations of satellites using Docker. Docker is a leading technology in process level isolation as well as continuous integration and continuous deployment (CI/CD) method. This study continues with the prior study on heterogeneous computing method, which improves the schedulability of the entire system up to 90%. Based on this heterogeneous computing method, the comparison study has been conducted between the non-isolated and isolated environments.

1. INTRODUCTION

The role of intelligent on-board data processing for in-situ information value extraction is significant in space systems such as earth and atmospheric observation satellites, CubeSat constellations, and deep-space exploration spacecraft. For example, the next generation earth and atmospheric observation satellites require the sensors with high sensitivity and resolution, while, the sensors generate more data than the cross-links or downlink can handle. However, the operation of satellites may fall into critical conditions when many on-board operations and processes, including the basic operation functionalities of satellites, interfere with each other strongly. Thus, in this paper, we present an experimental study of isolation of on-board payload data processing from the basic operation functionalities of satellites in a common platform using Docker[1].

In this study, we consider heterogeneous computing for on-board data processing which is explored by using radiation tolerant on-board processing platforms[2][3]. These platforms take advantage of both commercial off-the-shelf products (COTS) and a new computer architecture, Heterogeneous System Architecture (HSA)[4], which reduces the data transfer bottle-neck by enabling coherent virtual shared memory between different processing units (e.g. CPU, GPU FPGA). Moreover, HSA simplifies the programming process of the heterogeneous computing software. The platforms inherit the advantages of the platform which is commercialized by Unibap AB and selected by NASA for high-performance on-board processing for the "HyTI" thermal hyperspectral mission[5].

Space systems require to satisfy different types of limitations such as SWaP (size, weight, and power) and radiation hardness. As being as real-time systems, timing constraints are

required as well. Further, space systems require to adopt continuous integration and continuous development/deployment (CI/CD) and automated testing in order to improve their development process and quality of the products. Thus, in this paper, we consider using Docker for isolation as well as CI/CD.

Contribution: This study continues prior work[6][3] of a heterogeneous computing method, which improves the schedulability of the entire system up to 90%. This heterogeneous computing method is well known in high performance computing[7] and supercomputers. However, to the best of our knowledge, there is a lack of prior research studies of this method on real-time embedded systems. Therefore, in this paper, we conduct an experimental study of this method in Docker isolated environments.

Organization: The rest of this paper is organized as follows. Section 2 and 3 introduce related work and necessary background information. Section 4 presents our system model and system architecture. Section 5 introduces case study and experiments and reports experimental evaluation. Lastly, Section 6 concludes this paper.

2. RELATED WORK

FPGA accelerated onboard computer is one of the main representers of heterogeneous processors used in satellites, as FPGAs are strong against in the radiation-hardened environments. For example, FPGAs are considered for on-board processing in an advanced imaging system[8] and real-time cloud detection[9] since FPGAs are good for image and video processing. On the other hand, adopting GPUs in the context of space was not appreciated, since the concern of GPUs about the radiation-hardened environments was unacceptable. Recently, adopting GPU onto the on-board computer is increasing[10, 2, 3]. Furthermore, Kosmidis et al.[11] presents benchmarking results of GPU accelerated platforms for on-board data processing.

In this paper, we focus on systems using both CPU and GPU in the context of space. As we see in the survey[12], the study of CPU-GPU systems as heterogeneous processors and heterogeneous computing is very active. Especially, the impact of GPU in supercomputers is significant as the most of supercomputers adopt GPU. However, greedy use of specific processing unit may worsen the entire system and not all the applications are suitable for parallelism[7]. Therefore, there are methods using the nature of OpenCL[13, 7] that makes heterogeneous computing easier. Because, in OpenCL, it is possible to prepare the different kernels of the same execution part on the different devices. In this paper, we perform experiments with tasks which can be executed whether on CPU or GPU.

Although there are fewer studies on GPU in real-time systems compared to high-performance computing, there exist several works which tackle with real-time properties of GPU accelerated systems. Shinpei et al. presented TimeGraph[14] and RGEM[15] along with zero-copy I/O processing for low-latency GPU computing[16]. In addition, the works[17, 18] consider worst-case timing scenarios in GPU accelerated real-time systems. Most of these works consider solving the limitation of early existing GPU hardware and device drivers such as a zero-copy technique for accelerator memories and splitting tasks into smaller chunks in order to perform preemption. However, these limitations will be solved by the latest new technologies such as unified memory, zero-copy and preemption technologies in CUDA[19] and Heterogeneous System Architecture (HSA)[4, 3].

3. BACKGROUND

3.1 Real-time system

A real-time system is a system that responds to external events within a finite and required time. In other words, both accuracy and timeliness of the response of the system are a crucial factor for the system. Thus, in real-time systems, we focus on worst-case scenarios rather than best- and average-case scenarios, while high performance computing focuses on them. Real-time systems can be divided into a hard, firm and soft real-time systems according to their timing constraints. Hard real-time systems must pass entire timing constraints. Any small deadline miss can result in failure which leads to a fatality and/or big cost damage. For example, an airbag system in cars is a hard real-time system, and any deadline miss can end up a loss of human life. On the other hand, soft real-time system can accept one or more deadline misses although it affects to its quality of service. Systems such as music player and car window opening control system are soft real-time systems since any deadline misses of these systems would not end up with catastrophic results. A firm real-time system is between hard and soft real-time systems. In satellites, a system including basic functionalities can be considered as hard real-time system, while payloads can be considered as soft real-time systems.

3.2 Docker

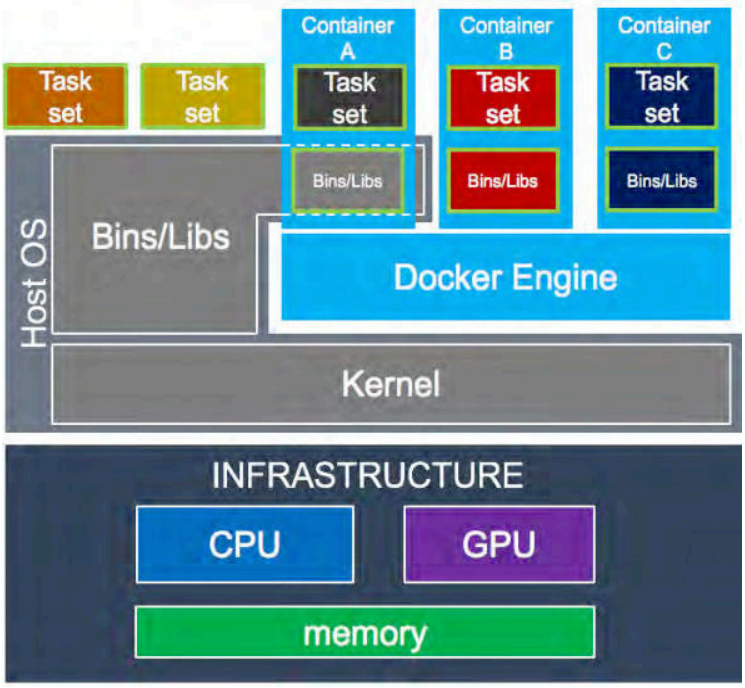

Figure 1. System architecture

To achieve the independent conduct of both on-board data processing and basic operations of satellites as real-time systems, we use Docker [1] for the process level isolation. Docker is a container and runs on top of the kernel of the host operating system (OS). In this paper, we consider Linux as the host OS. Docker uses the basic Linux features, namespaces and cgroups, in order to bring isolation for systems[1] (see Figure 1). Contrary to virtual machines, Docker containers share the same host OS and it starts running as an application in the host OS while virtual machines should first boot entire OS

installed in the virtual machines. This feature enables to keep the entire system smaller and to perform the quick startup of isolated containers.

Furthermore, containers may include different Linux distributions as long as their kernels match with the kernel included in the host OS. Hence, it is possible that the containers can use libraries and binaries of the host (*container A* in Figure 1) or other distributions (*containers B and C* in Figure 1). By using namespaces feature, a container runs under a different root from the root of the host OS, i.e., it helps to isolate container tasks from tasks running on the host OS. On the other hand, cgroups[20] helps to limit the resource usage of containers as it works as constant bandwidth server. In addition to limiting CPU and memory usages, a container can restrict system calls, e.g. terminating network access for security reason and so on. A container does not need to consume the resources when it is idle while virtual machine still consumes the resources for its OS.

4. SYSTEM MODEL AND ARCHITECTURE

4.1 System model

We consider a system *S* (Eq. 1), that deals with a task set Γ, that consists of *n* tasks, i.e., $\Gamma = \{\tau_n\}$. Each task should be assigned to one of a benchmarking environment set *E* (Eq. 2). The benchmarking environment set *E* consists of a host environment, E^{Host} or E_0, and *m* pieces of container environments, $E_m^{Container}$ or $\{E_1, .., E_m\}$.

$$S =< \Gamma, E > \quad (1)$$

$$E = E^{Host} \cup \left\{E_m^{Container}\right\} = \{E_0, \dots, E_m\} \quad (2)$$

We further define that each benchmarking environment should be able to manage *k* pieces of CPU cores, $\{P_k^{CPU}\}$, and memory limit, M_i.

$$E_i =< \{P_k^{CPU}\}, M_i >, i = \{0, \dots, m\} \quad (3)$$

4.2 System architecture

The system architecture is shown in Figure 1. This system employs a HSA compliant accelerated processing unit (APU) maintained in a system-on-chip (SoC). The APU (A10-8700P) adopts Radeon™ R6 GPU, which consists of 6 compute units, and 2 CPUs (each CPU has 2 cores). 2 cores of each CPU share one 128KB L1 cache and all four cores share 1MB L2 cache. Total processing capability of the system reaches up to 614 GFLOPS. There is no memory copy between memories of CPU and GPU since the APU is HSA compliant and they share 8GB DDR3 memory. Above this platform, Ubuntu 16.04 distribution is running as a host operating system (OS) including Linux kernel 4.15 and ROCm 1.9 driver. ROCm is an open source driver for heterogeneous computing. On top of the host OS, we run Docker 1.13.1.

5. EVALUATION

5.1 Case study

Two type of applications, basic operation functionalities of satellite and workload, are conducted to represent on-board data processing platforms of satellites. We deal with machine learning and computer vision applications as a workload on different containers in order to study interference between host-and-container and container-and-container. A simple matrix calculation along with the basic processes of the host OS are considered as the basic operation functionalities of satellites.

As shown in Figure 1, there are 3 types of containers; the container A uses binaries/libraries of the host OS and the containers B and C are based on different binaries/libraries. The allocations of the applications to the containers are shown as follows; matrix multiplication, TensorFlow[21] and Harris Corner Detector are on the container A, B and C, respectively.

TensorFlow is an open source machine learning library created by Google. In this paper, we use TensorFlow 1.12 together with ROCm 1.9 driver. Harris Corner Detector is a computer vision algorithm, which is provided by open-source computer vision library OpenCV[22]. All the containers are able to perform the applications on both CPU and GPU.

5.2 Experiments

The following 3 experiments are considered to identify the process level isolation by Docker. Due to space limitations, we only give simple explanations of the experiments.

- ***Experiment A***. The aim of this experiment is to understand the basic mechanism of the Docker container and the interference factors to the host environment.
- ***Experiment B***. In this experiment, we deal with the interference between host-and-container applications. The comparison study of the execution time of the different applications on host and container environments is performed.
- ***Experiment C.*** The interference between different container environment is the key in this experiment.

5.3 Results

Due to the space limitation, we only present interesting results. In Table 1, we see the results of Experiments A and B. The mean and measurement based worst case response time (WCRT) of computing only AlexNet and Harris Edge Detector are {7.875s; 8.036s} and {1.649s; 1.87s}, respectively. Furthermore, the WCRTs of executing both AlexNet and Harris Edge Detector together in host environment are 8.104s and 1.897s. These results are similar to the WCRTs of executing AlexNet in host environment and Harris Edge Detector in Docker. This means that we do not confirm any interferences from Docker to the systems.

Execution time [s] (measured)	**AlexNet with TensorFlow**	**Harris Edge Detector**

	Mean	WCRT	Mean	WCRT
Stand Alone	7.875	8.036	1.649	1.87
Together in Host Environment	7.906	8.104	1.821	1.897
AlexNet in Host & Harris in Docker	7.929	8.113	1.837	1.893

Table 1. Summary of experimental results

A part of the results from experiment C is shown in Table 2. Table 2 expresses the execution times of AlexNet algorithm on different environments with different data set. The mean values of AlexNet running both in host environment (12.348s) and Docker containers (12.349s) are shorter than the mean value of AlexNet running stand-alone (12.355s), although their WCRTs (12.374s and 12.371s) is longer than the WCRT of stand-alone (12.366s). This explains that we confirm no interferences from Docker container to the systems. Moreover, we do not confirm any interference to the CPU-GPU communication.

Execution time [s] (measured)	**AlexNet with TensorFlow**	
	Mean	WCRT
Stand Alone	12.355	12.366
Together in host environments	12.348	12.374
Together with payloads using Docker	12.349	12.371

Table 2. CPU-GPU communication

Finally, although it is obvious, we can state that starting up systems on Docker is much faster compared to booting the system including its host OS. This strongly supports adopting Docker in CI/CD required systems.

6. CONCLUSION

Through the experiments, we confirm that Docker helps to perform CI/CD without decreasing the computing potential. The results show that the tasks allocated in the different environments with the independent resources (CPU cores and memory) would not interfere with each other. Moreover, Docker would not worsen the computation potential when the tasks, which allocated on the different containers, share the resources. Finally, we see that our heterogeneous computing method fits with Docker for the process level isolation.

7. ACKNOWLEDGMENTS

The work presented in this paper was partially supported by the Swedish Knowledge Foundation via the research profile DPAC. The authors would like to express our sincere gratitude to Dr. Harris Gasparakis, an AMD GPGPU, Computer Vision and Machine Learning technical expert and project manager, for his great knowledge in computer vision, machine learning and HSA related areas. We would also like to express our sincere

gratitude to Dr. Moris Behnam for his great knowledge in real-time embedded systems.

8. REFERENCES

[1] Dirk Merkel, "Docker: lightweight Linux containers for consistent development and deployment", Linux Journal, Volume 2014 Issue 239, March 2014

[2] Fredrik Bruhn et al., "Introducing radiation tolerant heterogeneous computers for small satellites", 2015 IEEE Aerospace Conference, Big Sky, USA, 2015

[3] Nandinbaatar Tsog et al., "Intelligent Data Processing using In-Orbit Advanced Algorithms on Heterogeneous System Architecture", 2018 IEEE Aerospace Conference, Big Sky, USA, 2018

[4] HSA Foundation, "HSA Foundation - ARM, AMD, Imagination, MediaTek, Qualcomm, Samsung, TI". Available online at: http://www.hsafoundation.com (accessed 6 November 2018)

[5] Robert Wright, Thomas George et al., "Hyperspectral Thermal Imager (HyTI)", University of Hawaii and Saraniasat Inc. Available online at: https://esto.nasa.gov/files/solicitations/INVEST_17/ROSES2017_InVEST_A49_awards.html#george (accessed 3 August and 6 November 2018)

[6] Nandinbaatar Tsog et al., "Using Heterogeneous Computing on GPU Accelerated Systems to Advance On-Board Data Processing", The European Workshop on On-Board Data Processing 2019 (OBDP2019), ESTEC, Amsterdam, Netherlands, 2019

[7] Yuan Wen et al., "Smart multi-task scheduling for OpenCL programs on CPU/GPU heterogeneous platforms", 21st International Conference on High Performance Computing (HiPC), IEEE, Dona Paula, India, 2014

[8] Charles D. Norton et al., "An evaluation of the Xilinx Virtex-4 FPGA for on-board processing in an advanced imaging system", 2009 IEEE Aerospace Conference, Big Sky, USA, 2009

[9] John Williams et al., "FPGA-based cloud detection for real-time onboard remote sensing", 2002 IEEE International Conference on Field-Programmable Technology, Hong Kong, China, 2002

[10] R.L. Davidson and Christopher P. Bridges, "Adaptive multispectral GPU accelerated architecture for Earth Observation satellites", 2016 IEEE International Conference on Imaging Systems and Techniques (IST), Chania, Greece, 2016

[11] Leonidas Kosmidis et al., "Embedded GPU benchmarking for High-Performance On-board Data Processing", The European Workshop on On-Board Data Processing 2019 (OBDP2019), ESTEC, Amsterdam, Netherlands, 2019

[12] S Mittal and J.S. Vetter, "A Survey of CPU-GPU Heterogeneous Computing Techniques", ACM Computing Surveys (CSUR), Volume 47, 2015

[13] P Czarnul and P Rosciszewski, "Optimization of Execution Time under Power Consumption Constraints in a Heterogeneous Parallel System with GPUs and CPUs", Distributed Computing and Networking , ICDCN 2014, Coimbatore, India, 2014

[14] Shinpei Kato et al., "TimeGraph: GPU Scheduling for Real-time Multi-tasking Environments", USENIX Conference on USENIX Annual Technical Conference (USENIXATC), Portland, USA, 2011

[15] Shinpei Kato et al., "RGEM: A Responsive GPGPU Execution Model for Runtime Engines", 32nd IEEE Real-Time Systems Symposium (RTSS), Vienna, Austria, 2011

[16] Shinpei Kato et al., “Zero-copy I/O processing for low-latency GPU computing”, ACM/IEEE International Conference on Cyber-Physical Systems (ICCPS), Philadelphia, USA, 2013

[17] Glenn Elliott and Jim Anderson, “Globally Scheduled Real-time Multiprocessor Systems with GPUs”, Real-Time Systems, Volume 48, 2012

[18] Hyoseung Kim et al., “A server-based approach for predictable GPU access control”, 23rd IEEE International Conference on Embedded and Real-Time Computing Systems and Applications (RTCSA), Hsinchu, Taiwan, 2017

[19] Mark Harris, “Unified Memory for CUDA Beginners”, Available online at: https://devblogs.nvidia.com/unified-memory-cuda-beginners/ (accessed Oct 16, 2018)

[20] Rami Rosen, “Resource management: Linux kernel Namespaces and cgroups”, Available online at: https://sites.cs.ucsb.edu/~rich/class/old.cs290/papers/lxc-namespace.pdf (accessed 5 May 2019)

[21] TensorFlow. Available online at: https://www.tensorflow.org/ (accessed 31 Jan 2019)

[22] OpenCV. Available online at: https://opencv.org/ (accessed 31 Jan 2019)

3U satellite bus SONATE for technology demonstration of autonomous payloads

Oleksii Balagurin[1], Tom Baumann[2], Tobias Greiner[3], Hakan Kayal[4], Andreas Maurer[5], Thomas Rapp[6], Tobias Schwarz[7]

Affiliation
University of Würzburg, Computer Science VIII, Space Technology
Emil-Fischer-Str. 32, 97074 Würzburg, Germany
[1]Phone: +49-931-31-88637, Mail: balagurin@informatik.uni-wuerzburg.de
[2]Phone: +49-931-31-85289, Mail: tom.baumann@uni-wuerzburg.de
[3]Phone: +49-931-31-89582, Mail: tobias.greiner@uni-wuerzburg.de
[4]Phone: +49-931-31-86649, Mail: hakan.kayal@uni-wuerzburg.de
[5]Phone: +49-931-31-83241, Mail: andreas.maurer@uni-wuerzburg.de
[6]Phone: +49-931-31-85285, Mail: thomas.rapp@uni-wuerzburg.de
[7]Phone: +49-931-31-82010, Mail: tobias.schwarz@uni-wuerzburg.de

Abstract: SONATE is a technology demonstration mission specially designed for two particular highly autonomous payloads. These two payloads can plan and act independently of the ground segment. In order to support this autonomous operation a satellite bus with particular features was created. The main focus of this paper concentrates on the OBDH and the power generation and distribution subsystem, because the OBDH interacts strongly with the payload's autonomous functionalities. In addition, large amounts of observation image data will be handled by the OBDH. Since the required scheduling and diagnostic algorithms are very computationally intensive, the processing electronics of the payloads consume electric power in the range of several watts. The whole satellite system was manufactured and qualified. This paper will conclude with the results of the qualification tests.

1. INTRODUCTION

One of the most important but personnel-intensive parts of a satellite mission are the mission operations. Mission planning and scheduling, preparation of procedure sequences, creation of telecommand lists, telemetry monitoring and analysis are only a fraction of the daily tasks of the ground staff. Although this work is supported by various software tools, it is very time-consuming and requires a lot of human supervision and interaction. In order to facilitate the work of ground personnel, certain tasks of the mission operator could be performed autonomously on board of the satellite. For example, the certain aspects of mission planning and analysis tasks can be performed in orbit on the satellite. Exactly these tasks are carried out by two new autonomous payloads, ASAP and ADIA, which were developed at the University of Würzburg, Department of Computer Science 8.

The primary objectives of the SONATE mission is the on-orbit verification of the key elements of the ASAP and ADIA autonomous payloads. SONATE also contains several secondary payloads. They are described in the course of this paper.

2. PAYLOADS

The starting point for the development of the satellite bus are the requirements from the two primary payloads ASAP and ADIA.

2.1 ASAP-Light

ASAP is an autonomous sensor and planning system, which can detect unpredictable light-phenomena in the optical spectrum and autonomously plans further observation experiments [1]. Initially, the ASAP system was designed for a 27U satellite and includes two independent cameras: one with a wide field of view 42° x 42° (WFOV) and another with a narrow 4° x 4°. The image processing electronics is the same for both cameras and is based on an FPGA. Due to space limitations of a 3U mission, only the smaller camera system with the WFOV can be verified on board of SONATE. This reduced system, called ASAP-Light, allows video recording with resolutions up to 4 Mpixel and frame rates up to 30 fps. Each video frame will be analyzed by predefined image processing algorithms to extract interesting events or light phenomena.
Another special feature of ASAP-Light is a planning software, which can autonomously change mission progress depending on available resources. The planning software can schedule next actions and create new command lists for the satellite.

2.2 ADIA-Light

ADIA is a self-check and diagnostic system to determine the root cause of a just occurring failure on-board of the satellite and to predict possible future failures [2]. ADIA uses model-based procedures and algorithmic graph theory in order to find anomalies in the satellite.
ADIA runs on own hardware based on Sitara microprocessor by TI. It receives all telemetry frames from the OBDH in order to analyze the current state of the satellite and detect trends. Those telemetry frames are compared with a simulated satellite model to detect deviations. Mainly due to power consumption restrictions, only key features of ADIA, called ADIA-L will be verified onboard SONATE.

2.3 Secondary payloads

SONATE includes several secondary payloads. Two of them belong to the ADCS components. Three reaction wheels and two star sensors OP1 [3] were added to the satellite system as an experiment. An additional payload is SSTV. With this amateur radio service, it is possible to send the reduced images from ASAP-Light or from star sensors directly to radio amateurs on ground via redundant VHF transmitters and antennas.

3. SATELLITE BUS

The satellite bus of SONATE is a robust, full redundant and single-failure-tolerant system designed not only to meet all hardware requirements for the payloads, but also to respond adequately to their autonomous behavior.

3.1 OBDH

A special OBDH software and hardware was developed, which ensures safe handling of the autonomous experiments without jeopardizing the success of the mission [4]. Each of four identical OBDH-PCBs gets one of four possible roles: OBC or PDH as a master or slave. The role assignment can be adjusted dynamically.

Parallel to typical tasks such as time management and orbit propagation, telemetry collection and resource monitoring, OBC manages three telecommand lists. One of these lists is autonomously created by ASAP and can be activated during its experiment time. PDH handles all payload telemetry of SONATE including images and video sequences of ASAP-Light and prepares the collected data for sending them to the ground.

The OBDH hardware is based on a Cortex-M4 microprocessor from ST Microelectronics. For data management, 8 MByte volatile and 256 MByte non-volatile memory are available on each board.

Figure. 1. OBDH board

3.2 Communication Subsystem

The common satellite operations run via UHF band in half duplex mode with bitrates up to 9.6 kbit/s. For this purpose two redundant UHF transceivers und two antennas are integrated into the satellite bus. For transmission of payload data S-band will be used. Two transmitters und two patch antennas on opposite sides of the satellite provide a space-to-ground link with up to 1,6 Mbit/s. Complementary to the space segment, two ground stations, for UHF and S-Band, were established.

3.3 Power Subsystem

The SONATE Satellite has two full redundant 5V power busses. Each power bus gets electric energy from twelve body mounted solar cells via MPPT regulators. Four Li-Ion batteries with a total capacity of 48 Wh are used to store the energy for each power bus. The used switching boost converters can provide peak power of up to 20W and continuous power of 8W. This power is required for parallel operation of the S-Band transmitter and the ASAP-Light system in video capture mode.

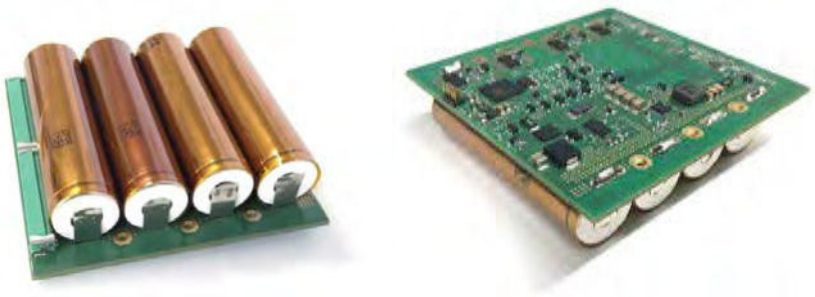

Figure. 2. Power Subsystem

3.4 ADCS

The ADCS subsystem has a classical structure for Cubesats. Initially, six sun sensors and three-axis magnetometers are used for attitude determination. Rotational rate of the satellite is measured by three-axis MEMS gyros. As actuators magnetorquers are used. Two air coils are integrated in the PCBs of the solar arrays and one rood coil is placed inside of the satellite body to serve the axis with small surface areas. The ADCS has its own control microprocessor with peripheral electronics. All mentioned ADCS components were redundantly implemented into the satellite system.
There are three reaction wheels and two star trackers on board of SONATE. First, as technology demonstration and after successful validation, they may be coupled into the control loop to achieve full three axis stabilization.

3.5 Structure and Mechanisms

As mentioned before, SONATE is a standard 3U satellite. The function of the mechanical structure is to ensure integrity of the satellite during the whole mission and to accommodate all payload and bus components. Most of the electronic boards of the satellite bus are arranged in a card-backplane system. Altogether there are eleven plug-in cards. Only a part of the payload components is connected by cable.
In the front part of the satellite there are four rolled up antennas. The lengths of the VHF and UHV antennas are 50cm and 17,5cm respectively. After unfolding they will be orthogonal to each other.

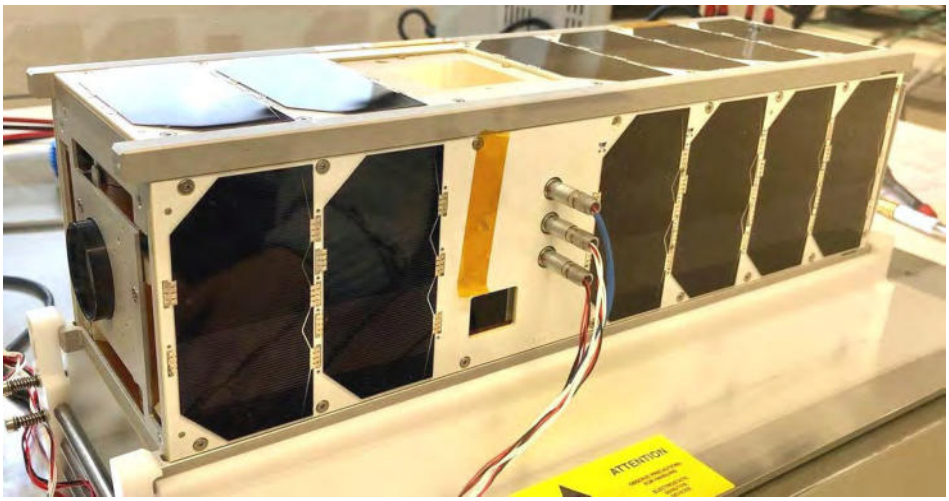

Figure. 4. SONATE Satellite EQM

4. QUALIFICATION PROGRAM

At the end of 2018 the SONATE Satellite has been subjected to a qualification program. This program includes mechanical testing and thermal-vacuum testing as well as radiation testing. The specification for mechanical tests were provided by the launch provider. These are essentially based on the requirements of the Soyuz launch vehicle. Four mechanical tests have been carried out: quasi static acceleration, sinus vibration, random vibration and shock.

All mentioned above tests were successfully carried out without significant damage to the test object.

5. SUMMERY AND OUTLOOK

After almost three years of work, the development of the space and ground segment has been successfully completed. The satellite was successfully qualified. Currently, the FM model of the satellite is being assembled. First in-orbit results will be available after the satellite launch currently planned for June 2019.

6. REFERENCES

[1] H. Wojtkowiak, O. Balagurin, G. Fellinger, W. Fischer, B. Garcia, H. Kayal, ASAP autonomous onboard mission planning, 65th AIC 2014, Toronto, Canada, IAC-14-B6.2.2
[2] G. Fellinger, K. Djebko, E. Jäger, H. Kayal, F. Puppe, ADIA++: An autonomous onboard diagnostic system for nanosatellites, AIAA Space 2016, Long Beach, California, 2491072
[3] T. Greiner, O. Balagurin, H. Kayal, T. Schwarz, Optimization tool for mission specific design of star sensors, Proceedings, 4S Symposium, Sorrento, Italy
[4] T. Rapp, O. Balagurin, T. Baumann, H. Kayal, A. Krainovic, T. Schwarz, H. Wojtkowiak, Preparing SONATE for autonomous control through ASAP, 69th IAC 2018, Bremen, Germany, IAC-18.B4.3.13
[5] H. Kayal, O. Balagurin, K. Djebko, G. Fellinger, T. Greiner, F. Puppe, A. Schneider, T. Schwarz, H. Wojtkowiak, SONATE - a nanosatellite for autonomy, 68th IAC 2017, Adelaide, Australia, IAC-17.B4.3.13

Realtime Dynamic Target Pointing using Onboard Image Processing of Cloud Cover for Earth Observation Microsatellites

Julie Ann Banatao[1], John Leur Labrador[1], Yuji Sakamoto[1], Kazuya Yoshida[1]

[1]Tohoku University
Sendai, Miyagi, Japan
Phone: +81 22 795 6991, Mail: julie@astro.mech.tohoku.ac.jp

Abstract: A system for real time onboard image processing and attitude determination is proposed in this paper. It is used to capture target areas with minimal cloud cover. In this system, off-nadir target pointing is first used to capture an image with a bigger field of view. This initial image is analyzed onboard the microsatellites to identify areas with minimal cloud cover. Algorithm for cloud cover determination uses setting of optimal RGB components threshold. This is tested using actual photos taken by microsatellites Diwata-1 and Diwata-2. From the results of image processing, a new target is selected. The microsatellite attitude is dynamically adjusted using reaction wheel configuration. The length of time for attitude adjustment is verified through attitude of actual satellite.

1. INTRODUCTION

Diwata-1, the first Philippine microsatellite, is an earth observation microsatellite developed to monitor environmental and natural resources. It was released from the International Space Station on May 2016 and has taken more than 30,000 images in its 2.5 years of operation. During its mission, some of the captured images have significant cloud coverage, hindering any useful remote sensing over the target area. To address this issue, a system for real time onboard image processing and attitude determination for target pointing is proposed in this paper.

Onboard realtime image processing is discussed in [1] and [2]. However, these can not automatically adjust when target area for capturing images is cloudy. Automatic cloud cover assessment is discussed in [3], however, it only applies to satellites having additional band other than visible for cloud cover computation. We propose a system using only RGB bands in determination of cloud cover in image.

2. TARGET CAPTURE AND ONBOARD PROCESSING

2.1 Camera Payloads

Table 2-1. Diwata-1 and Diwata-2 Camera Payloads and Field of Views

Camera Payload	Diwata-1 Microsatellite FOV (@400 km Altitude)	Ground Sample Distance (GSD)
Medium Field Camera (MFC)	121.9 x 91.4 km	185 m
Multi-Spectral Imager (SMI)	52 x 39 km	80 m
High Precision Telescope (HPT)	1.9 x 1.4 km	3 m

In the case of Diwata-1, there are three camera payloads (HPT, SMI, and WFC) for scientific earth observation and Middle Field Camera (MFC) payload for aiding in attitude control calibration and geo-locating images taken by the other payloads.

2.2 Target Pointing Maneuver

In this proposed system, off-nadir target pointing is first used to capture an image with a 121.9 km by 91.4 km area via MFC. Initial target is set from a list of areas where the microsatellite is going to pass. If initial image has no usable area to capture (e.g. all cloudy), a new image will be captured by MFC along the path of the microsatellite. However, if there is an area with minimal or no cloud cover, new target will be determined from the existing MFC image.

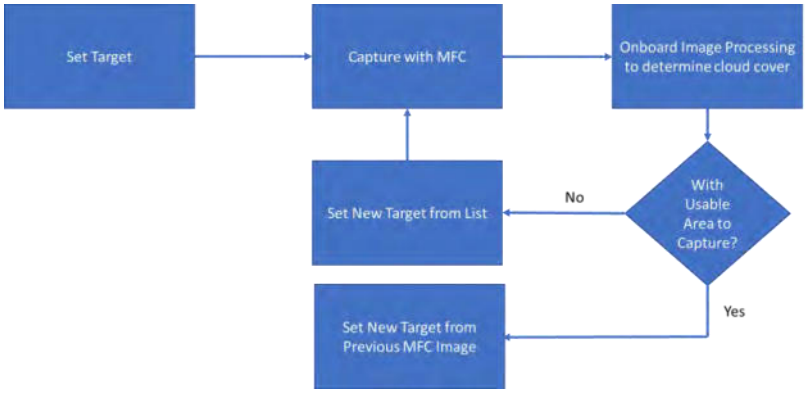

Figure 2-1. Algorithm for MFC Capture and Image Processing

2.3 Image Processing

The image captured by MFC is processed onboard the microsatellite for cloud cover identification. From [4], a fast image processing using only RGB bands of Diwata-1 images are explored for cloud cover determination. A similar approach, based on [5] is implemented in this paper as it is very important to have a very fast image processing time.

Classification of cloud cover algorithm is based on how clouds are identified visually by the naked eye. Clouds generally appear white; thus, the algorithm sets an optimal threshold of RGB values for proper classification of clouds.

After clouds are properly identified, a new target area with the least amount of cloud cover is identified. The size of the new target area depends on the scientific camera payload used in the second target capture. For SMI, desired target area size is 52 km by 39 km, while for HPT, desired size is 1.9 km by 1.4 km. The offset from the original target is calculated, and the coordinates of the new target is determined

3. ATTITUDE CONTROL

After selected target area is processed from the MFC image, satellite attitude is dynamically adjusted using reaction wheel configuration. This attitude maneuver aligns

scientific camera payload to the newly selected target. The length of time for attitude adjustment is verified through actual satellite and an attitude simulator discussed in [6], which is connected to the Engineering Model version of actual satellite.

For the attitude maneuver to work, the attitude determination and control system of the satellite should be very accurate. As the MFC image covers and area of 121.9 km by 91.4 km, the deviation of actual versus expected target should not be greater than the scope of the image.

4. RESULTS AND DISCUSSION

For the proposed real-time dynamic target pointing system to work, two processes are very important to be achieved:

1. Accurate and fast image processing for cloud cover determination
2. Accurate attitude control maneuver to adjust for new target

4.1 Image Processing

The onboard image processing is done with the goal of capturing images of target with the least amount of clouds. This target should be captured at highest possible elevation such that minimal geometric correction is necessary during scientific data extraction. To achieve this, the onboard image processing for cloud cover processing should be done before the maximum elevation of microsatellite over the intended target. There should also be enough time between initial capture of image via MFC and maximum elevation for the onboard image processing and attitude maneuver to finish.

Table 4-1. Elevation Angle During Initial Capture vs Time Before MEL of 90 Degrees for Diwata-1

Elevation Angle During MFC Capture (degrees)	**Approximate Time Before 90^{o} Elevation (seconds)**
10	175
20	121
30	80
40	58
50	43
60	35
70	22

Table-4-1 shows the elevation angle during capture of image using MFC, and the approximate time before the satellite is directly over the target, which is the timing that we want to capture image using HPT or SMI to minimize geometric distortion in image.

Experiment was conducted using actual Diwata-1 microsatellite to capture images of target with varying elevation angles to check optimal angle where cloud processing is accurate and still have enough time for image processing and attitude maneuver.

Elevation Angle	Diwata-1 MFC Sample Image	Processed Image for Cloud Cover
10	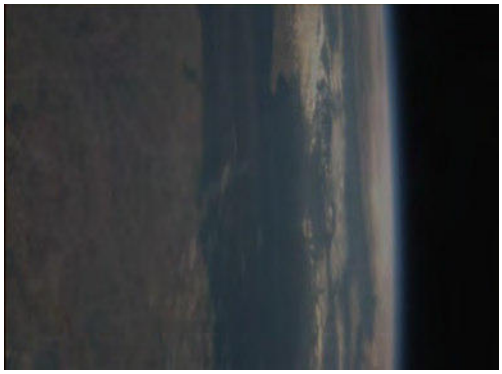	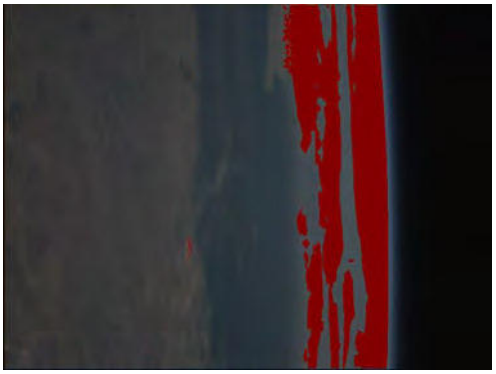
20	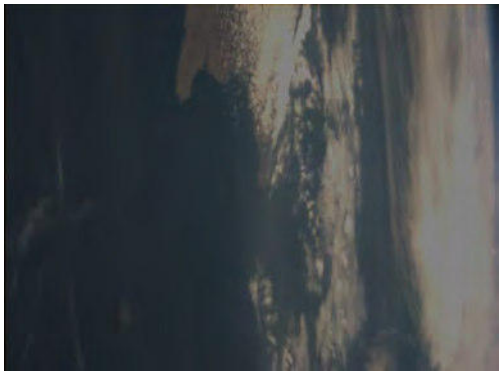	
29	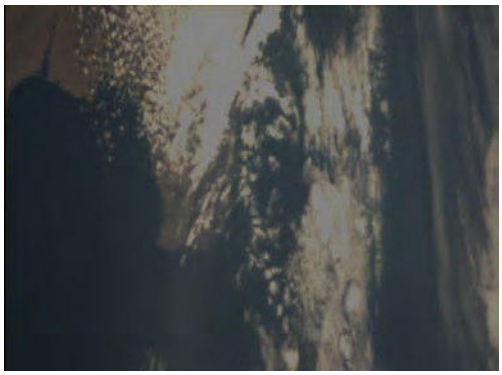	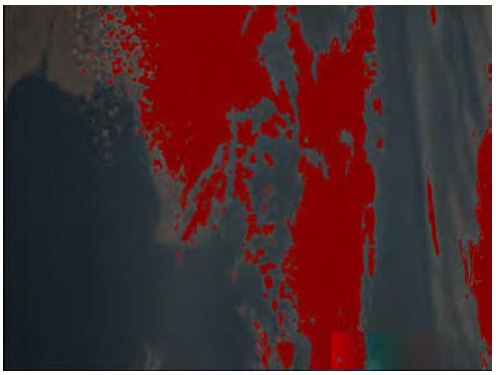
39		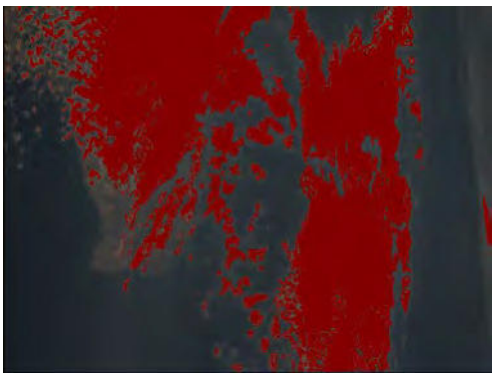

Figure 4-2. Raw Image and Post Processed MFC Image with Different Angle of Elevation During Capture

50		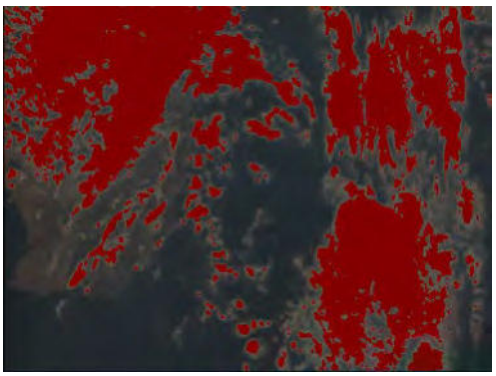
59		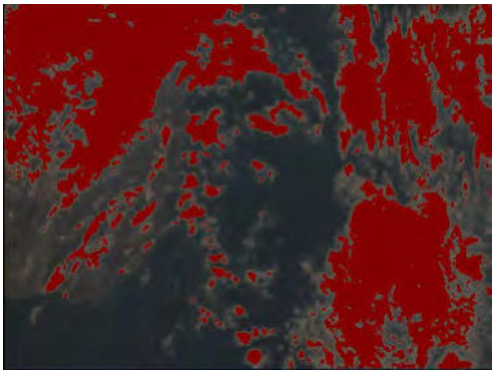
68	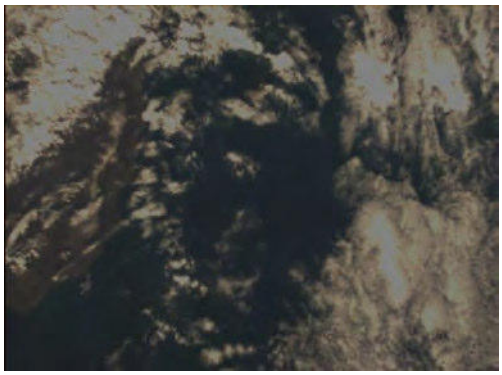	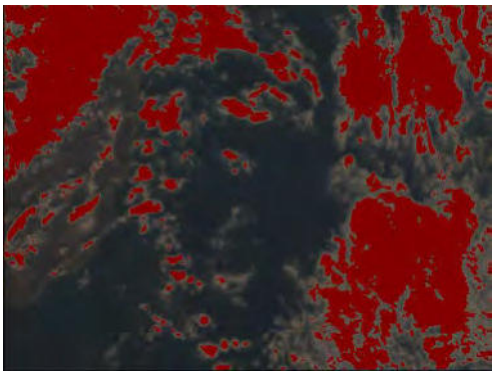

Figure 4-2. Raw and Processed MFC Images with Different Angle of Elevation During Capture (cont)

Figure 4-2 shows the raw images captured by MFC with the corresponding processed image for cloud cover. Clouds are marked as red. Images with elevation angle 10º and 20º have too much geometric distortion and it is difficult to pinpoint coordinates where there is cloud cover. Images with elevation 29º and 39º have some amount of geometric distortion. Images with elevation 50º and up has almost the same amount of geometric distortion. From these test images, 50º and up elevation angle is desired for initial capture.

For comparison of geometric distortion, Figure 4-3 shows a geometrically corrected image. Geometric correction was done via affine projection discussed in [7].

Using the algorithm for cloud cover determination using RGB composite thresholds, cloud cover from MFC image can be properly determined. A sample image and a processed image is shown in Figure 4-1. Pixels determined to be cloud pixels are

marked as red. However, the algorithm fails to classify very thin wisps of cloud as cloud cover.

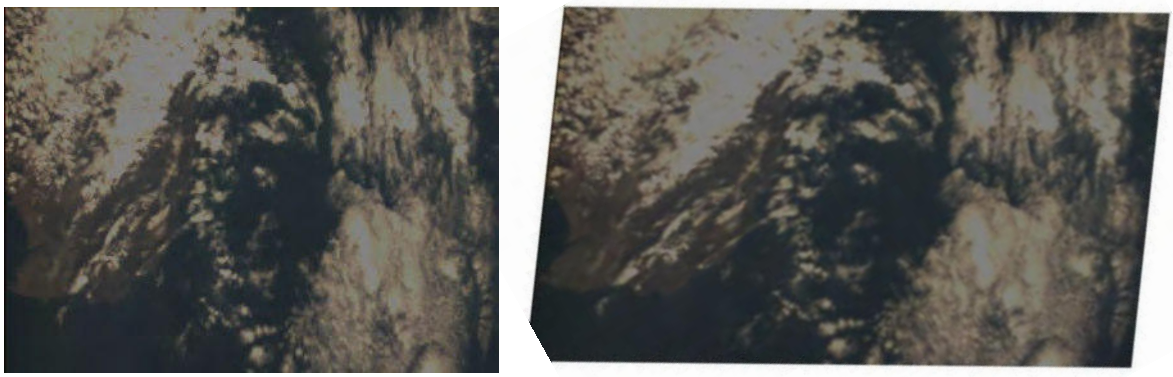

Figure 4-3. Raw vs Geometrically Corrected Image with 50^{o} elevation

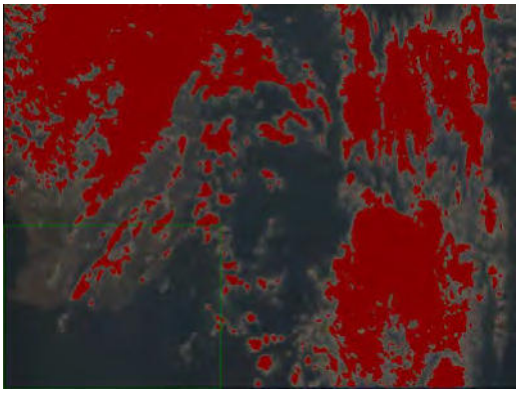

Figure 4-4. New Target Determination from MFC Image for SMI Camera Payload

After cloud cover is computed, a new target area for SMI payload is determined. SMI FOV is 52 x 39 km, thus, an area of this size within the MFC image that has the least cloud cover is computed. This area is marked in green rectangle in Figure 4-4 for the 50^{o} elevation sample image.

To calculate the coordinates of the new target, the distance of the center of the MFC image and the distance of the center of the SMI image are computed.

4.2 Attitude Control

Attitude maneuver was tested using target pointing maneuver of actual satellite. Target is normalized and set to latitude and longitude coordinates of [0, 0]. The actual location where satellite is pointed is recorded in Attitude Control Unit log files. The time for attitude to settle to minimum error is analyzed and checked if it can satisfy requirements of onboard processing system proposed.

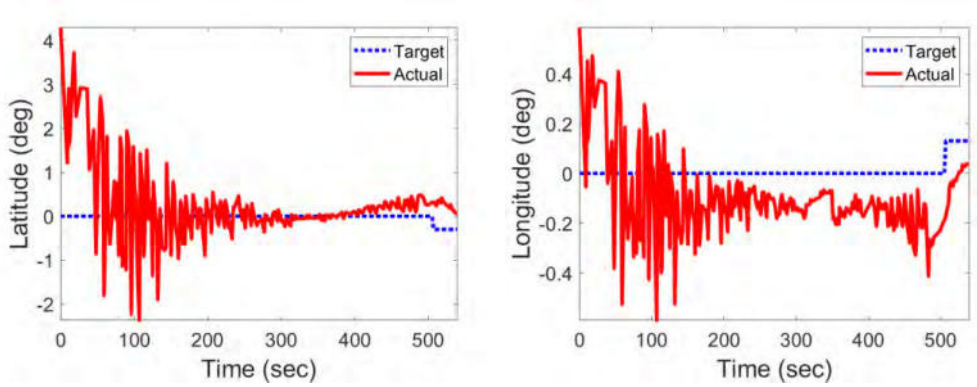

Figure 4-3. Target vs Actual Target Latitude and Longitude

Figure 4-3 shows sample attitude maneuver in microsatellite using reaction wheels for attitude control. At time 0 seconds, the satellite is in free tumbling mode and target coordinates [0, 0] is set. From time 0 to 500 seconds, reaction wheels are controlled such that satellite is pointing at target. It can be seen that it takes approximately 300 seconds to go from free tumbling mode to the minimum error in pointing. At time 500 seconds, a new target with a distance of 20 km is set. The latitude and longitude 30 seconds after the new target is set, is also shown.

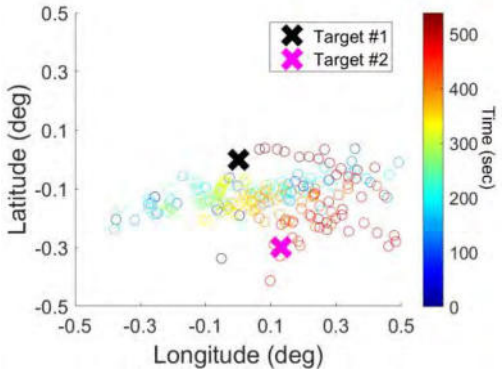

Figure 4-4. Coordinates of Actual Satellite Target

Figure 4-4 shows the actual coordinates where the satellite is pointed during the attitude maneuver while Figure 4-5 shows the distance from set target to the actual location where satellite is pointed based on the attitude data logs. When a new target is set at t = 500 seconds, distance between expected and actual target is 84 km. This is decreased to 44 km after 30 seconds.

For the adjustment of attitude control, a maximum of 45 km from the expected target is acceptable as long there is minimal cloud cover all throughout the initial MFC image. This ensures SMI image intersects with initial MFC image. However, for instances where MFC image has significant cloud cover, more accuracy is needed to ensure SMI image will intersect with computed area with low cloud cover. The shown attitude maneuver in actual satellite meets the clear MFC image requirement, but does not meet the cloudy MFC image requirement this during the first 30 seconds. It is therefore recommended to capture image earlier than 50^{o} elevation to have more time for the attitude maneuver during cloudy scenarios.

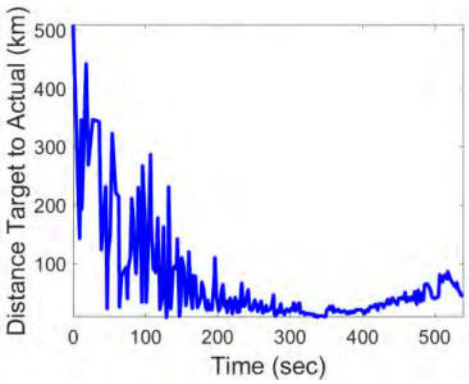

Figure 4-5. Distance Between Set Target and Actual Target

5. CONCLUSION

For low-earth orbit microsatellites, time for downloading images in a certain ground station is limited as the satellite only passes over the ground station few times per day, each pass only lasting a few minutes each. As earth observation microsatellites bottleneck is more likely how fast images can be downloaded, it is very important that the images downloaded contain useful scientific data, and not just all clouds. This method for real-time image processing and dynamic target pointing is proven to be feasible as a solution for this issue provided the attitude determination and control system of the satellite can adjust in an accurate and timely manner.

6. REFERENCES

[1] Qi B, Shi H, Zhuang Y, Chen H, Chen L. On-Board, Real-Time Preprocessing System for Optical Remote-Sensing Imagery. Sensors (Basel). 2018;18(5):1328. Published 2018 Apr 25. doi:10.3390/s18051328

[2] Yuhaniz S., Vladimirova T., Sweeting M. (2005) Embedded Intelligent Imaging On-Board Small Satellites. In: Srikanthan T., Xue J., Chang CH. (eds) Advances in Computer Systems Architecture. ACSAC 2005. Lecture Notes in Computer Science, vol 3740. Springer, Berlin, Heidelberg

[3] El-Araby E., El-Ghazawi T., Le Moigne J., Irish R. Reconfigurable processing for satellite on-board automatic cloud cover assessment. J. Real-Time Image Process. 2009;4:245–259. doi: 10.1007/s11554-008-0107-8.

[4] Ramos, M. K., Jiao, B. J., Aranas, R. K., Magallon, B. J., Amado, J., Tupas, M. E., et al: Automated Calculation of Cloud Cover from RGB Composite of Landsat 8 and Diwata-1 Satellite Imagery, 37th Asian Conference on Remote Sensing, Colombo, Sri Lanka, 2016

[5] Otsu, N., (1979). A Threshold Selection Method from Gray-level Histograms. IEEE Transactions on Systems, Man and Cybernetics, Vol. SMC-9, pp. 62 – 66.

[6] J.L. Labrador, Design and Implementation of an Attitude Determination Module with Real-Time Sensor Calibration for Small-Satellite Systems Including Performance Verification using DIWATA-1 Flight Data, Proceedings of the 31st International Symposium on Space Technology and Science 2017 Proceedings, Matsuyama, Japan, 2017.

[7] Corke, P.: Robotics, Vision and Control Fundamental Algorithms in Matlab, Springer International Publishing, 2017, pp. 252–268.

Multi-Mission Software Development for Small Spacecraft

Karsten Gordon[1], Mario Starke[2], Philip von Keiser[2], Merlin F. Barschke[2]

[1]Spacegramming
Bergerweg 4, 83707 Ringsee, Germany
Phone: +49 8022 9151874, Mail: karsten.gordon@spacegramming.com

[2]Technische Universität Berlin, Institute of Aeronautics and Astronautics
Marchstr. 12, 10587 Berlin, Germany
Phone: +49 30 314-28743, merlin.barschke@tu-berlin.de

Abstract: Throughout the last decades, spacecraft flight software has been undergoing a radical evolution. While very limited in the beginning, the processing tasks gradually shifted from on-ground to on-orbit, resulting in complex applications based on sophisticated architectures. Consequently, software development is nowadays performed by specialized teams using modern design techniques and process models. To allow its efficient and cost-saving development, reuse is a key quality criterion for flight software. This is usually addressed by establishing product lines which base on a flexible platform offering variation points for customization in regard to diverging mission goals. In this paper, we review the architecture and development process as different aspects of a software product line, giving insights into techniques applied and challenges faced with the development of the TUBiX20 spacecraft series.

1. INTRODUCTION

In recent years, the importance of software in the development of spacecraft raised significantly. Sharp et al. [1] describe the following three phases of software development for spacecraft. Firstly, in the early days of spaceflight, control logic was mostly executed on-ground and on-board processing was limited to command decoding and telemetry encoding. In the second phase, the advances in on-board computer technology enabled autonomous management of attitude, power and thermal control subsystems by the year 2000. As of the date of publication of [1] in 2010, the third phase was entered when high performance microprocessors had “enabled sophisticated software architectures and designs”. Almost a decade later, a fourth phase can be added: further miniaturization and performance upgrades of microcontrollers mainly driven by advances in automotive and consumer electronics today have paved the way for a complex application software on a spacecraft as part of a constellation of sometimes several hundred satellites.

As a result of the increased complexity of flight software throughout its evolution, the requirements regarding software development techniques and also process models increased significantly, making software one of the most resource-intensive elements of a space project. One key aspect for efficient and cost-saving software development is reuse; due to the growing proportion in regard to a project’s overall workload, it is simply not profitable to reinvent the wheel every time, considering that ever more challenging and ambitious missions are to be realized in shorter time.

As an approach to proactively plan reuse, the methodology of *software product line engineering* emerged in the late nineteen nineties in the software engineering community. In this paper, we summarize the main ideas behind this concept and emphasize different advantages but also challenges of applying this approach for space projects. Thereafter, we discuss a layered software architecture as a basis for a customizable plat-

form, drawing comparisons between four different examples from different space institutions and universities. Finally, the software development process is reviewed and the advantages of *continuous integration* are pointed out in the context of a product line which is shared between different projects or institutions. All research has been carried out during the development of Technische Universität Berlin's TUBiX20 small satellite platform [2] which is therefore briefly introduced in the following.

TUBiX20 is a modular small satellite platform which is currently the baseline for three ongoing missions, namely TechnoSat [3], TUBIN [4] and QUEEN [5]. TechnoSat is currently operated within an extended mission, and TUBIN is in production phase, while QUEEN is in the definition phase. Still fully operational after almost two years in orbit, TechnoSat has successfully reached all mission objectives [6] and the platform could "demonstrate key performance parameters regarding three axis stabilization and payload data downlink" [7], and is now used as on-orbit test platform for the TUBIN mission [8] and university courses. Figure 1 shows a rendering of the TechnoSat spacecraft.

Figure 1: Rendering of the TechnoSat Spacecraft [8]

2. SOFTWARE PRODUCT LINES

According to Pohl et al. [10], software product line engineering is a paradigm to develop software applications using platforms and (mass) customization. An analogy to clarify this definition is the automotive sector, where soon after the invention of the production line in the early nineteen hundreds, companies designed their cars to build on common parts with certain variation points for customization and hence established a platform to be reused in different models to respond the individual customer demands. An example for a software product line is an office software suite which offers different applications for text processing, spreadsheets and presentations built on the same platform to implement common features like menus, file handling or text formatting.

The approach has also been applied in the space sector. Initiated due to the limited success in reducing cost and complexity shown by early reuse efforts within NASA missions, a team of senior engineers performed "a structured heritage analysis across a decade of missions" [9]. Based on the outcome of this independently-funded research, the NASA Core Flight System (cFS) was developed, which is "currently running on three operational spacecrafts and is being used on multiple spacecraft and instrument devel-

opment efforts" [9]. In the following, the benefits of establishing a product line for spacecraft flight software will be discussed in more detail.

Firstly, the space flight software faces several challenges as pointed out by Sharp et al. [1]: the fact that a spacecraft is only remotely accessible and is exposed to an extremely harsh environment results in the need for extremely high availability and reliability. Hence, the software performs autonomously for most of the time and has to deal with unpredictable hardware anomalies. Consequently, relying on a platform of well-tested and well-documented software components reduces risk, development and verification effort.

Secondly, a spacecraft comprised of its subsystems covers various engineering domains like attitude control, communications, data handling, thermal control; and nearly all of these fields nowadays involve software. In order to master the complexity of the systems engineering, a structured platform-based design approach helps to transfer knowledge and experience from one mission or project to another.

Thirdly, the aforementioned partitioning into the different subsystems offer a variability [11] as a basis for customization: (nearly) all satellites must control their attitude, communicate with ground stations, and process commands. However, the suite of sensors and actuators used, the data volume and communication channels and the degree of autonomy vary largely from one mission to another, so there is a common functionality with a large degree of variability within each subsystem.

Fourthly, all satellite projects undergo the same (relatively short) development and production cycle, and yet the work performed and the state of the design in each phase differ strongly from the previous ones. A company or institution which builds several different spacecrafts at the same time faces the challenge to simultaneously manage projects which are in the design phase and projects which are already in the operations phase. To create synergies between these projects, a carefully planned configuration management is required.

In the following sections, different aspects of a software product line are reviewed in the context of small satellites, sharing concepts and experience gained during the development of the TUBiX20 satellites of Technische Universität Berlin. Special emphasis is placed on pointing out the dependencies and synergies between these aspects.

3. SOFTWARE ARCHITECTURE

Software architectures for projects which target reuse need to define a general structure which then allows customization regarding individual product requirements. Taking a look at the automotive industry again, the automotive open system architecture (AUTOSAR) [12] is an established open standard for a software architecture, allowing the collaboration between different partners worldwide [13]. Regarding space technology, some examples from different agencies and universities targeting reuse are the aforementioned Core Flight System [13] (NASA), the Compact Satellite Series [14] (German Aerospace Center - DLR), the Flying Laptop [15] (University of Stuttgart), and finally the TUBiX20 series [16] (Technische Universität Berlin). All of these examples use separate layers as shown in Figure 2 to abstract from the underlying

implementation and technology and hence allow for diverse variation points on different levels.

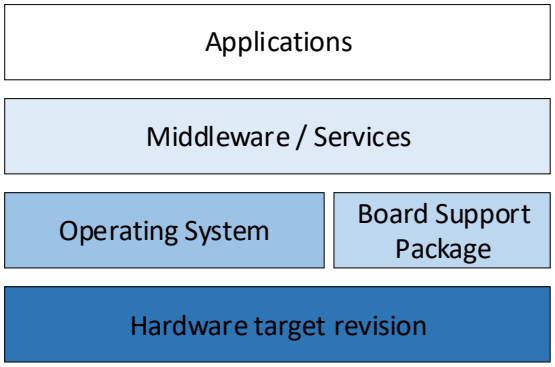

Figure 2: Software Platform Layers

Directly interacting with the microprocessor hardware, the lowest software level is comprised of the operating system (OS) and all code which is required to access the specific target hardware (such as drivers). The latter is referred to as board support package (DLR, Technische Universität Berlin) or platform support package (NASA). To support various microprocessors and peripheral devices, a hardware abstraction layer (DLR) or platform abstraction layer (NASA) provides access to this hardware-specific code via unified interfaces, hence offering variation points for the product line to use different hardware or operating systems with the same high-level software. To host the flight software applications which then perform the user tasks for a subsystem or service, a separate layer provides all required executive services for inter-process communication (University of Stuttgart) – also referred to as middleware (DLR, Technische Universität Berlin) – logging or scheduling activities. NASA calls this layer of the software architecture core Flight Executive (cFE). Since not all services provided in this layer are required in every mission, they are generally organized in a library and the list of services for an individual mission is compiled into the target software by the configuration and build management. Finally, the top layer contains the software applications. Once again, there are mission-specific parts and mission-independent parts. For example, the attitude determination and control application's inner composition depends on the sensors, actuators and control algorithms used and is hence mission-specific. But even for such an application, the internal structure can offer variation points based on abstract or unified interfaces and hence limit mission-specific adaptations, as shown for the TUBiX20 platform in [17]. On the other hand, some applications like managing certain payloads is completely mission-specific.

Hence to establish a software product line, key criteria are to minimize the mission-specific parts of the software architecture and offer all required variation points to allow for customization as required. Moreover, the abstraction from implementation details is important to introduce continuous performance upgrades into the platform in order to keep a platform competitive [18]. Due to the separate layers, it is also possible to incorporate only individual layers into another software project, e.g. the operating system, communication protocol implementations, or a library with common math functions. Hence, even if a specific satellite's design is too individual to be fully compatible with the complete platform architecture, it can still benefit from individual layers.

However, there are certain challenges which need to be mastered to make a product line accepted and successful. In most cases, there is already an existing architecture of some kind which has to be transformed in order to be compatible with the product line approach. Hence, some design rules which are required for the platform architecture might not have been in place when the original code base was written and are therefore likely violated. Shaping a more organically grown architecture into a well-structured platform comes with careful planning and often rework and therefore additional effort. Once the platform architecture is established, it must be avoided to change the interfaces, since these alterations entail adaptions for all projects using the platform, sometimes even without being noticed. Finally, if a complete product line or parts of it are shared, either publicly as open source or among different teams within a company or institution, it should come with a comprehensive documentation and a proof of its correctness, for example via built-in unit tests.

4. SOFTWARE DEVELOPMENT PROCESS

A well-structured development process allows different project teams to contribute to a complex software architecture while their individual missions might be in a different phase of the spacecraft life cycle and is therefore another prerequisite to establish a software product line. However, in order to create a solid code base steadily improved and promoted, the rigid and lengthy classic V-model [19] approach does not seem promising, since here the integration times of newly developed functionality is simply too long. As an alternative, agile development methods which have long been used in the information technology sector might be applied. In 2015, Technische Universität Berlin shared practical experience in using continuous integration within the development of the TechnoSat software [20]. In this section, the key aspects of this development process are reviewed and evaluated in regard to the goal of managing a software product line.

Continuous integration is based on the idea that newly developed features are frequently integrated into the main project to convert the integration process from a time-consuming and very complex task into a series of small steps, each applied very closely after the implementation of a new feature [21]. This is essential for large code projects where different teams work on several features in parallel for two reasons. Firstly, this means that frequent but small improvements or corrections of the software product line become visible immediately and allow for direct incorporation into ongoing missions. Secondly, the return of contributions into the platform is encouraged since their integration is less complex and time-consuming. Hence the flow of new features from one mission into the platform and from there to another mission is accelerated and occurs more frequently.

The process usually includes automated building, testing and deploying of the software. In this manner, it is ensured that the software is already well tested within the development cycle, which leads to more robust results and moreover reduces time-consuming debugging [20]. In terms of a product line, this is especially important since errors in the code might affect several missions at the same time which might be even in different phases of their life cycle. The closer a mission gets to its launch date, the less risk of introducing errors can be tolerated. Hence updates of the platform code – even if they fix a known issue – may only be integrated if it is certain that they do not entail any

new errors. In order to maximize the time a mission can benefit from platform updates, the platform's reliability and verification coverage must be maximized.

The foundation of a successful collaboration between different teams is the organized change management of the software. In other words, a version control system is required, which allows for automated storing (committing), logging and merging and is hence mandatory for all further steps [20]. The distributed version control system Git is widely used within the information technology sector and has brought new features especially useful for continuous integration which are discussed in detail through the example of TechnoSat in [20]. However, successful code management requires not only the technology but also a workflow which allows for a controllable, traceable, and verifiable introduction of new features into the code base (for further clarification, these three terms will be picked up again later). To this end, a code project can be organized through different branches. This means that in order to develop a new feature, the code from the main line is duplicated by a developer, then modified and later merged back into the mainline once the new feature is considered mature. Usually, the merge is not performed by the developers themselves but by the maintainer of the repository and only after predefined testing and a successful review to assure high code quality. A complete introduction of the branch organization established for the TUBiX20 platform of Technische Universität Berlin is given in [20].

When a software product line is used by different project teams, the platform code and the mission-specific code may even be maintained in different version control repositories, if only the platform is public but the mission-specific code is kept locally within a project. This entails the additional task of integrating one repository into another in order to receive updates. For TUBiX20, the Git subtree merge technique has been established successfully. In combination with the branch organization mentioned before, this brings further benefits. Firstly, upgrading to a new revision of the platform code becomes controllable which is not the case for a mainline-only approach without branching where all platform changes are automatically transferred. Secondly, integrating the platform repository – as opposed to e. g. downloading a single archive file of a new release – retains all its individual commits which makes changes more comprehensible and traceable. Thirdly, members of the community can propose upgrades via branches which, in combination with the aforementioned code reviews, makes the developed code verifiable.

Finally, using build servers does not only automate (and hence accelerate) software unit testing, it also assures that the deliverables of the software can be created reproducibly. This refers to executables and also documentation generated from the code. Consequently, the different missions are assured that they work not only with identical and identifiable source code files, but also with executables created by the exact same toolchain version, and finally an up-to-date documentation.

Just like with the definition of a platform architecture, there are some challenges when introducing a development process that targets a product line. The process should support all required techniques and tools to exploit the benefits of a version control strategy and a build server, but it should still offer some flexibility to adapt to each project team's or institution's habits and constraints. The new infrastructure and workflow must

be simple and fit for daily use and entail only minimum overhead to be accepted as improvements.

5. SUMMARY AND CONCLUSION

With the technological advances of microelectronics, high-performing and yet small and power-efficient components have become available. This in turn initiated the evolution of flight software from rudimentary telecommand decoding and telemetry encoding to intelligent agents performing all high-level tasks mostly autonomously. As the complexity of on-board tasks is increasing significantly, well-structured and sophisticated software design is needed.

Due to shorter development times and yet increasing requirements, software reuse is a key quality criterion for software development. Successful reuse, however, requires well-structured planning and design. A promising paradigm which has been used for a long time in the automotive sector is to establish product lines. A product line bases on a flexible platform offering variation points on the one hand, and (mass) customization to adapt to diverging requirements on the other hand.

A software architecture for a product line must abstract from mission-specific hardware and functionality and offer all required variation points to allow for customization. Moreover, these variation points are important to introduce continuous performance upgrades into the platform in order to keep a platform competitive. The development process needs to incorporate a version control system with a systematic branching strategy and use automated build servers to increase productivity and create executables and documentation updates reproducibly and frequently. As a result, the further development of the platform becomes controllable, traceable, and verifiable.

ACKNOWLEDGEMENTS

The development of the TUBiX20 platform is funded by the Federal Ministry for Economic Affairs and Energy (BMWi) through the German Aerospace Center (DLR) on the basis of a decision of the German Bundestag within the TechnoSat, the TUBIN and the QUEEN mission (Grant No. 50RM1219, 50RM1102, 50WM1754 and 50RU1801).

REFERENCES

[1] D. C. Sharp et al., “Challenges and Solutions for Embedded and Networked Aerospace Software Systems,” in Proceedings of the IEEE, vol. 98, no. 4, pp. 621-634, April 2010.

[2] M.F. Barschke and K. Gordon, “A Generic System Architecture for a Single Failure Tolerant Nanosatellite Platform,” presented at the 65th International Astronautical Congress, Toronto, Canada, 2014.

[3] M.F. Barschke, K. Gordon, M. Lehmann, and K. Brieß, “The TechnoSat Mission for On-Orbit Technology Demonstration,” presented at the German Aerospace Congress, Braunschweig, Germany, 2016.

[4] M.F. Barschke, J. Bartholomäus, K. Gordon, M. Lehmann, and K. Brieß, “The TUBIN nanosatellite mission for wildfire detection in thermal infrared,” CEAS Space Journal, p. 1–12, 2016.

[5] M.F. Barschke, A. Dinkelaker, J. Bartholomäus, P. Werner, H. Christopher, and M. Krutzik, “Optical quantum technology in space using small satellites,” presented at the 68th International Astronautical Congress, Adelaide, Australia, 2017.

[6] M.F. Barschke, P. Werner, K. Gordon, M. Lehmann, W. Frese, D. Noack, L. Grunwaldt, G. Kirchner, P. Wang, and B. Schlepp, “Initial Results from the TechnoSat in-Orbit Demonstration Mission,” in Proceedings of the 32nd AIAA/USU Conference on Small Satellites, Logan, USA, 2018.

[7] M.F. Barschke, K. Gordon, P. von Keiser, M. Lehmann, M. Starke, and P. Werner, “Initial orbit results from the TUBiX20 platform,” presented at the 69th International Astronautical Congress, Bremen, Germany, 2018.

[8] K. Gordon, M.F. Barschke, and P. Werner, “Upgrading TUBIX20 – Bringing TechnoSat Flight Experience into the TUBIN Mission,” Proceedings of the Small Satellites Systems and Services Symposium, Sorrento, Italy, 2018.

[9] D. McCormas, J. Wilmot, and A. Cudmore, “The Core Flight System (cFS) Community: Providing Low Cost Solutions for Small Spacecraft,” presented at the 30th Annual AIAA/USU Conference on Small Satellites, Logan, USA, 2016.

[10] K. Pohl, G. Böckle, F van der Linden, “Software product line engineering: foundations, principles and techniques,” Springer, 2005.

[11] J. S. Fant, H. Gomaa, and R. G. Pettit, “Software product line engineering of space flight software,” Proceedings of the 2012 Third International Workshop on Product LinE Approaches in Software Engineering (PLEASE), Zurich, Switzerland, 2012, pp. 41-44.

[12] AUTOSAR GbR. [Online]. Available: https://www.autosar.org/

[13] D. McComas, “NASA/GSFC’s Flight Software Core Flight System,” presented at the Flight Software Workshop, San Antonio, USA, 2012.

[14] F. Dannemann and F. Greif, “Software Platform of the DLR Compact Satellite Series,” Proceedings of the Small Satellites Systems and Services Symposium, Mallorca, Spain, 2014.

[15] S. Gaisser, U. Mohr, B. Baetz, K. Klemich, J. Keim, J. Eickhoff, and S. Klinkner, “In-Flight Experience with an Object-Oriented Flight Software,” Proceedings of the Small Satellites Systems and Services Symposium, Sorrento, Italy, 2018.

[16] M.F. Barschke, K. Großekatthöfer and S. Montenegro, “Implementation of a nanosatellite on-board software based on building-blocks,” Proceedings of the Small Satellites Systems and Services Symposium, Majorca, Spain, 2014.

[17] K. Gordon, “A flexible Attitude Control System for three-axis stabilized Nanosatellites,” PhD thesis, Technische Universität Berlin, 2017.

[18] M.F. Barschke, K. Gordon, and S. Junk, “Modular Architecture and time-efficient Development of a flexible Nanosatellite Platform,” Proceedings of the 11th IAA Symposium on Small Satellites for Earth Observation, Berlin, Germany, 289–292, 2017.

[19] K. Forsberg and H. Mooz, “The Relationship of System Engineering to the Project Cycle,” Proceedings of the First Annual Symposium of National Council on System Engineering, 57–65 1991.

[20] K. Gordon, A. Graf, and M.F. Barschke, “Practical Experience in using Continuous Integration within the Development of Nanosatellite Software,” presented at the 10th IAA Symposium on Small Satellites for Earth Observation, Berlin, Germany, 2015.

[21] P. Duvall, S. Matyas and A. Glover, “Continuous Integration – Improving Software Quality and Reducing Risk,” 1st edn., Addison-Wesley Professional, 2007.

cPCI Serial Space Compliant Mass Memory Board with Integrated Data Processing Capabilities

Spacecraft concepts and sub-systems

Harald Michalik[1,2], Gang Zhou[1], Rainer Preuss[1]
Christian Dierker[1], Ole Bischoff[1], Elias Hashem[1]

[1] DSI Aerospace Technology
Otto-Lilienthal-Str. 1, 28199 Bremen, Germany
Phone: +49 421 596969 0, Mail: info@dsi-as.de

[2]IDA TU Braunschweig
Hans-Sommer-Str. 66, 38106 Braunschweig, Germany
Phone: +49 531 391-5286, Mail: sekretariat@ida.ing.tu-bs.de

Abstract: With the new Compact PCI Serial Space Standard, a new design framework is available for implementation of modern modular computer architecture in space applications. It enables, like in industrial applications, to establish a wide spectrum of functional modules from which a specific on-board computer architecture can be configured. In this paper, we focus on the Compact PCI Space Serial compliant design of on-board mass memory modules for different type of applications. We provide a standard compliant solution, which can be adapted to mission specific need by means of a modular approach.

1. INTRODUCTION

Future earth observation and scientific space exploration missions require high-performance on-board processing capabilities and a high degree of flexibility. While the resolution of detectors and thus, the amount of generated data is continually increasing the downlink bandwidth remains limited. Consequently, the demands for on-board data storage in terms of capacity and data rates are growing rapidly.

Due to the availability of high-end space grade FPGAs, which on one hand support state of the art high performance interface standards over high speed serial links (HSSL) and on the other hand high bandwidth parallel I/O [1], it is feasible to create new concepts for space compliant mass memory modules.

Selected modern commercial semiconductor memory devices have been proven by radiation testing to be acceptable for space applications use for the majority of mission profiles by the inclusion of device type specific radiation effects mitigation measures in the memory controllers [2], [3].

Classically, space-borne solid-state mass memories using these modern devices are designed in one of two ways. First, as a stand-alone payload data handling unit (PDHU) allocated to the payload functions of a spacecraft, e.g. in high-end earth observation payloads with high storage capacity demands. Alternatively, they are designed as an integral component of the on-board computer system (OBC) on the spacecraft platform, e.g. in space exploration applications with medium demands in terms of storage capacity and data transfer rates.

For both cases multiple solutions from various vendors of space-borne mass memories exist, which follow typically proprietary approaches for the mechanical and thermal design but adapt to the typical interfaces as used for space on-board data handling such as SpaceWire, MIL-STD-1553B or specific high rate point to point interfaces.

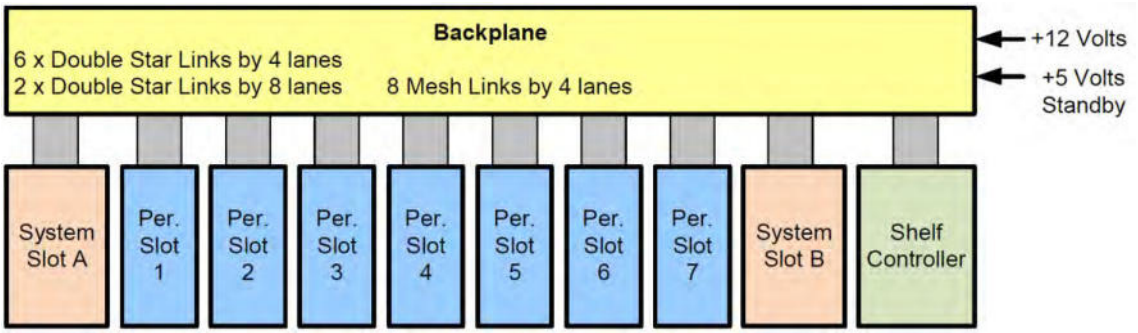

Figure 1: cPCI Serial Space Architecture *[4]*

For industrial ruggedized computer systems, modular concepts based on the CompactPCI standard are well established and have high market penetration for reliable systems. CompactPCI is based on the IEEE 1101 mechanical standards for 3U and/or 6U Eurocards and include conductive cooling solutions.

In modern computers the parallel PCI bus has been replaced meanwhile by high speed serial point to point connections, e.g. PCI Express (PCIe), but also using the traditional network technology Ethernet, e.g. as an interface for multiprocessing. For this concept customized backplanes are needed to connect the serial buses, which were standardized by PICMG (PCI Industrial Computer Manufacturers Group) into CPCI-S.0 CompactPCI Serial already in 2011 [5]. The architecture of CompactPCI Serial comprises a system slot with a star interconnect to up to eight peripheral slots, combined with a full mesh for Ethernet.

In general, the CompactPCI Serial allows for implementation of very compact ruggedized modular computers, which is of course attractive for the space application. The OBC-SA activity funded by the German space agency is based on this standard [6] but there is a need for some adaptions of the base standard to support typical space computer architectures.

In 2017 PCIMG ratified the CompactPCI Serial Space extension CPCI-S.1 [4], which removes some unnecessary features (e.g. USB, SATA). The routing of PCI Express and Ethernet links on the backplane is maintained but can be used for other serial standards as well (e.g. SpaceFibre, TTEthernet). cPCI Serial Space supports a second system slot (redundancy) with a dual star architecture. Figure 1 shows an example slot architecture. Two redundant CAN busses are available as board management busses.

We use this standard to define a new concept for mass memory modules designed to fit into a 3U compact housing and to cover both approaches for mass memories, i.e. a) an OBC-integrated mass memory module and b) a classical PDHU.

2. DSI DESIGN APPROACHES TO MASS MEMORY MODULES

2.1 OBC-MM Approach

In the ESA Study OBC Mass Memory (Contract No. 4000112970/14/NL/LF) a team of RUAG Space AB, DSI and SCISYS investigated a novel architecture for a Single Level Cell (SLC) NAND Flash based Mass Memory as an integrated module for OBCs [7]. The target applications were space exploration missions like JUICE, PLATO, Athena, SMILE etc. but also small EO missions.

Due to the typical space exploration application profile, medium storage capacities (some Tbit) and medium data rates (some 100 Mbit/s) were targeted but with a focus on high data integrity requirements. Multiple SpaceWire links (16) were implemented as payload instrument interfaces, including dedicated downlink interfaces. The OBC performs the command and control functions, including the file system via additional SpaceWire interfaces.

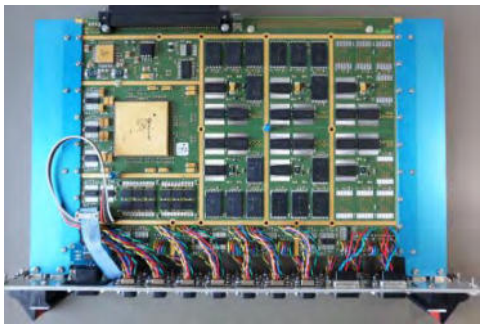

Figure 2: OBC-MM Board with Microsemi RTG4 FPGA and up to 6 NAND Flash Partitions

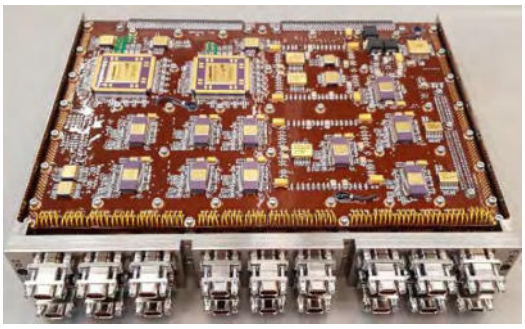

Figure 3: JUICE OBC SSMM (EQM): Dual Board Module with dual SpW Router, Microsemi RTAX FPGAs and 6 Nand Flash Partition

Figure 2 shows the OBC-MM Board, which carries as a single PCB solution of up to 6 NAND Flash memory partitions. For the implementation of the Memory Controller, a Microsemi RTG4 device was used. The memory partitions comprise 8 NAND Flash devices of up to 128 GiBit capacity. Each partition is operated with a high performance (8,6) 2 Symbol Correcting RS-Code EDAC plus inner BCH Code within the Flash pages, resulting in very high data integrity.

As an outcome of this study, DSI implements this design approach in a mission specific adaptation for the SSMM of the JUICE OBC (Figure 3). The JUICE SSSM comprises a SpaceWire routing function with two 18-port SpaceWire routers, a mass memory controller function implemented in two Microsemi RTAX2000SL FPGAs and 6 NAND Flash memory partitions with in total 6×8 NAND Flash stacks (3D-Plus 3DFN64G08VS8305 64 Gbit stacks). The SSMM module assembly contains two printed circuit boards (PCBs) with an Interface Board (IFB) as baseboard and a Mass Memory Board (MMB) as daughterboard. It provides a Begin of Life (BOL) capacity of 1.5Tbit per module, a volume of 261 × 205 × 36 mm^3, a mass of 1.8 kg with a power consumption of <13 W.

2.2 Compact PDHU Approach

DSI is currently performing a study on the design of a NAND Flash based Compact PDHU under ESA contract 4000118583/16/NL/AF. The goal here is, to use modern high capacity Flash devices and space grade FPGAs to integrate typical payload data handling and storage into a very compact self-standing unit, which provides storage capacities of some Tbit and which is capable to handle data rates of some Gbit/s within a small housing.

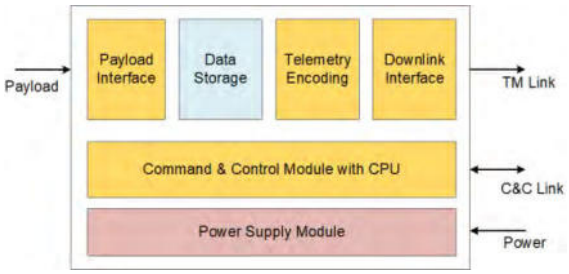

Figure 4: Compact PDHU Functions: Colours indicate allocation on three PCBs

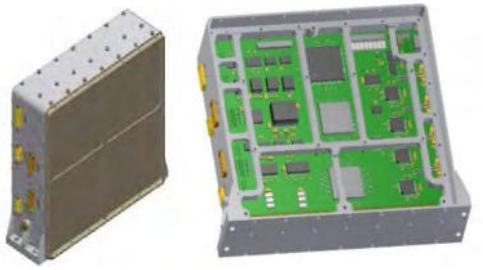

Figure 5: BioMass Compact PDHU (one half) comprising 3 PCBs

Figure 4 shows the general basic functions of such a PDHU. In addition to the data input, data storage, and data output functions it contains a CPU for command and control functionality connected to the platform OBC by a standard command & control bus (e.g. MIL-STD-1553B). It also comprises its own power supply module. As a first outcome of this study, DSI is currently implementing the PDHU for the Biomass spacecraft on this design basis.

Figure 5 shows a sketch of the Biomass approach with a slim PDHU housing comprising three PCB modules: I/O Interfaces & Processing (yellow), Mass Memory Devices (blue) and Power Supply (red). The colours of the blocks in Figure 4 indicate the allocation of functions contained in each of the three PCBs.

The Biomass PDHU consists of two PDHU slices (prime + redundant) with a volume of 260 × 133 × 224 mm³ and a mass of 6.4 kg. It accommodates 1 Tbit BOL capacity per PDHU half and communicates with an aggregate data rate of approximately 1 Gbit/s over serial links (WizardLink) with the payload instrument and by parallel LVDS with the downlink transmitter. The power consumption is <15 W max.

These implementations show that powerful mass memory modules are possible in compact designs for typical mission scenarios with medium storage capacity and data rate demands.

However, in both cases the design flexibility to scale the mass memory modules for a wider range of applications and to support both OBC-MM and PDHU types of mass memory is limited. The use of a standard modular computer architecture with modern high-speed serial interfaces such as Compact PCI Serial Space opens up the opportunity to design a mass memory module architecture with significantly more scalability.

3. CPCI SERIAL SPACE COMPLIANT MODULE DESIGN

The basic idea for the cPCI Serial Space based module is to combine elements from the two proven design approaches discussed in section 2, and allocate it on a 3U peripheral module baseboard plus a mission specific mezzanine board plugged onto the baseboard. The baseboard serves the standard backplane interfaces, i.e. 2x PCIe x4 lanes for the double star connection and e.g. SpaceFibre for the mesh connection (see e.g. [8] for SpaceFibre interface core) and a CAN bus for command and control I/F.

To be able to serve the high-speed serial links, a state of the art high performance FPGA is needed. Because the memory control function within a mass memory typically does not need in-flight adaptability, we prefer to use the Microsemi RTG4 FPGA as space grade solution. The RTG4 provides the necessary IOs supported partially by internal hard coded functions. The RTG4 also allows for mission specific adaptations of the memory control function due to its use of Flash to provide re-configurability.

In addition, the baseboard comprises local power conversion from the 12V backplane delivered power lines. Some of the high-speed serial links (8) of the FPGA are routed to the front panel in order to allow access via front panel high-speed serial links.

The FPGA provides various user I/Os (3.3V, 2.5V, DDR), the majority of which are routed to board-to-board connectors to be used by the mezzanine board.

To buffer incoming and outgoing data packets within the memory controller, DDR SDRAM is attached to the FPGA on the baseboard via the FPGA internal DDR controller.

As mentioned, the mezzanine board integrates application specific adaptations of the design:

3.1 OBC-MM-like Mass memory Module Design

For an OBC-MM-like mass memory module, the mezzanine board contains NAND Flash devices grouped in a single or multiple partitions. In addition, the mezzanine board integrates application specific interfaces, such as WizardLink devices providing high-speed serial link via the front panel. The OBC can access the flash memory via the PCIe interface of the memory controller.

For an OBC-MM-like module, the mezzanine board contains up to 2 partitions with 12 NAND Flash devices, leaving out the optional CPU memory. Using internally stacked 4-die 128 GiBit NAND Flash devices, a net BOL capacity of 2 Tbit can be provided using a (12,8) 2-Symbol RS error correction. The typical partition bus frequency achievable with asynchronous mode driven NAND Flash devices is 25 MHz, this results in a memory bus net bandwidth of 2×1.5Gbit/s max., because each partition is driven separately from the RTG4 Memory controller.

Partition power switches provide protection against persistent SEFIs for each partition, enabling SEFI Handling.

3.2 PDHU-like Mass memory Module Design

For a PDHU-like mass memory module, a CPU for an internal command & control function including a file system requires implementation. The processor itself will be represented by a soft-core implementation within the FPGA (e.g. RISC-V CPU), which is sufficient in performance. The mezzanine board contains the CPU memories (SDRAM/SRAM/NOR Flash) as well.

A PDHU-like module design will include a Soft-Core CPU in the FPGA (e.g. the Microsemi Mi-V RV32IM RISC-V based 32 bit processor), which occupies around 10-15 % of the logic resources only. The mezzanine board will then be equipped with additional CPU memory, which can be SRAM or SDRAM plus NOR Flash for program memory. Again, the system can safely achieve a 25 MHz processor clock frequency sufficient for PDHU control tasks.

The mezzanine contains a single memory partition of 20 devices with a wide memory bus (128 Bit net). The BOL net user capacity using internally stacked 4 die NAND Flash devices will be 2Tbit. With a 25 MHz clock frequency, a maximum aggregate data rate of 3 Gbit/s can be achieved over the memory bus. The partition comprises a power switch for SEFI protection and a (20,16) 2-Symbol RS error correction.

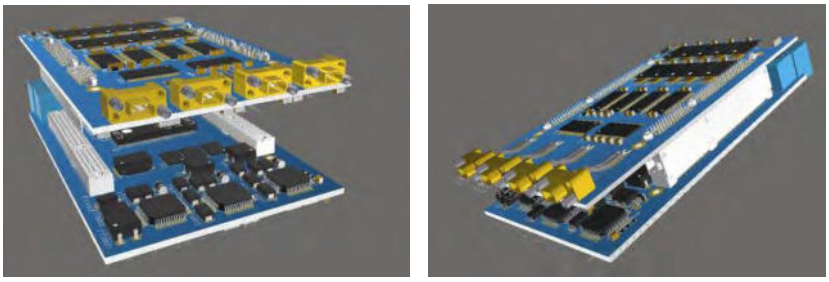

Figure 6: cPCI NAND Flash Module PCB Sketch (2-slot solution)

In principle, the cPCI Serial Space backplane provides external high-speed I/O capabilities. Because payload instrument electronics are a separate unit not integrated into cPCI Serial Space, the module provides external interfacing via the front panel. This could be HSSL (baseboard) or SerDes (e.g. WizardLink) or LVDS (e.g. SpaceWire) via the mezzanine board.

4. MECHANICAL IMPLEMENTATION CONSIDERATIONS

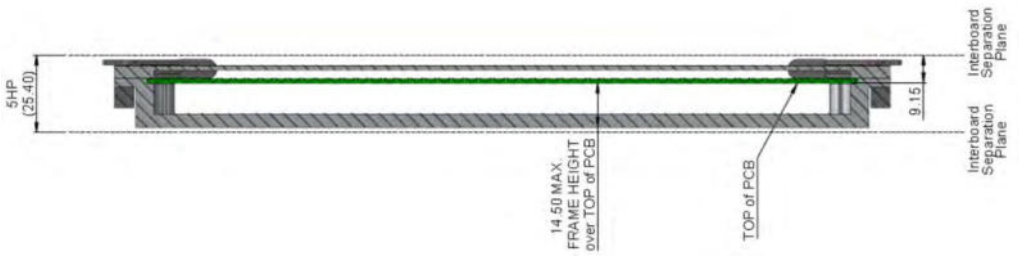

Figure 7: Conductive Cooled Assembly of cPCI Serial Space [6]

As already outlined, the design concept with a fixed baseboard design and an adaptable mezzanine board allows the implementation of various design variants for specific

applications. The cPCI Serial Space standard defines a module pitch of 25.4 mm and provides a mechanical design outline for a conductive cooled assembly (CCA) in 3U format (Figure 7). The total usable height of the frame over the top of the baseboard is 14.5 mm including frame thickness. This is critical for adaptation of a mezzanine board, which needs to be equipped with parts on both sides.

Especially for institutional space missions where the application of class 1 parts such as stacks from 3D plus are mandatory to implement the memory partitions, this will clearly not be compliant with the above-mentioned mechanical outline.

For an industrial space application, for which industrial space grade parts are applicable, there will be design variants of the module possible with slim mezzanine, which fit into the CPCI Serial Space Standard CCA frame.

The mechanical/thermal design of our module is still in progress and needs consolidation with other cPCI Serial Space Standard module suppliers.

In general, we assume, that our module occupies 2 slots within a cPCI Serial Space rack. Another possibility for a single slot solution would be to migrate the design to 6U format, but this is contradictory to our understanding of compactness and design flexibility.

5. POTENTIAL DESIGN VARIANTS

The module design concept with a fixed baseboard design and an adaptable mezzanine board is extendible to implement other design variants:

- Use of NAND Flash devices in synchronous access mode: SLC Synchronous Flash is operable with 50 MHz at the memory bus. This would double the aggregate access rate to 5-6 Gbit/s.
- Synchronous devices are also available as internally stacked devices in BGA package with 8 dies of 32 Gbit each giving a total capacity of 256 Gbit per device. This would double the capacity per partition.
- Use of DDR2 or DDR3 memory devices instead of Flash devices. Due to the fact, that the RTG4 provides DDR capable I/O, it will be possible to equip the mezzanine with volatile memory devices, which provide lower capacity but operate at a higher speed [9].
- Implementation of dedicated HW supported processing functions: The logic resources of the FPGA are not fully used (<35 % used) for the implementation of the memory controller and the CPU. As such additional HW supported processing functions are possible within the FPGA, for example a CFDP protocol handler for higher downlink data rates or even a data compression before/after data storage.

6. CONCLUSION

The cPCI Space Serial Standard opens up the implementation of storage and processing modules for implementing a modern modular computer architecture also for space application on a standardized basis. We have investigated if and how we can migrate

our standard mass memory modules approaches for OBC integrated Mass Memory type and self-standing PDHU type to the new cPCI Space Serial Standard.

Our approach uses advanced space grade FPGAs providing various HSSL links, an internal hard coded DDR controller, a large logic fabric, and a huge amount of user I/O on a fixed baseboard and adapts the storage function in a mission specific way on a mezzanine board. This implementation provides the maximum flexibility while supporting high performance connectivity via the cPCI Serial Space backplane standard.

Design challenges still require clarification, especially in the area of mechanical/ thermal design. The expectation is that there will be validated solutions also from other vendors soon.

7. REFERENCES

[1] Microsemi, "PB0051 Product Brief RTG4 FPGAs," [Online]. Available: https://www.microsemi.com/document-portal/doc_download/134430-pb0051-rtg4-fpgas-product-brief. [Accessed 29 01 2019].

[2] K. Grürmann, D. Walter, M. Herrmann and F. Gliem, "Studies of Radiation SEE Effects in NAND-Flash and DDR Types of memories," in *ESA R&D Final Presentation Days*, ESTEC / ESA, 2011.

[3] "Heavy Ion sensitivity of 16/32-Gbit NAND-Flash and 4-Gbit DDR3 SDRAM," in *IEEE NSREC Data Workshop, W-9*, Tucson, AZ, USA, 2012.

[4] PICMG, "Compact PCI Serial Space Specification, CPCI-S.1 R1.0," 2017.

[5] PICMG, "CompactPCI Serial Specification, CPCI-S.0 R2.0," 2015.

[6] A. Schüttauf, "On Board Computer System Architecture - Avionics Technology Trends," in *ESA/ADCSS Days*, Noordwijk, 2015.

[7] P. Sandin, D. Walter and G. Johnson, "OBC Mass Memories," in *Final Presentation*, ESTEC, 2016.

[8] S. Parkes, C. McClements, D. McLaren, B. Youssef, M. S. Ali, A. Gonzalez Villafranca and A. Ferrer Florit, "SpaceWire and SpaceFibre on the Microsemi RTG4 FPGA," in *IEEE Aerospace Conference*, Big Sky, MT, USA , 2016.

[9] L. Jia, T. Fichna, H. Michalik, M. Staehle, S. Parkes and J. Ilstad, "FPGA-based Advanced Mass Memory Controller Architecture for future Spacecraft Mass Memory," in *DASIA*, Oxford, UK, 2018.

SALSAT: Distributed software architecture for a Spectrum AnaLysis SATellite with modular payload capabilities

Philipp Wüstenberg[1], Jens Großhans, Alexander Balke, Huu Quan Vu, Michael Pust and Klaus Brieß

[1]Marchstr. 12-14, 10587 Berlin, Germany
Phone: +49 30 314 21336, Mail: philipp.wuestenberg@tu-berlin.de

Abstract: Radio frequency spectrum for satellite operation is a scarce resource. Along with the increasing number of launched and upcoming satellites [1], the potential of harmful interference rises and some satellite operators already experienced severe interference's with their communications systems. [2] A reliable and detailed analysis can only be done with an on-orbit spectrum analyzer system [3]. The SALSAT (Spectrum AnaLysis SATellite) mission aims to be the first nanosatellite mission to perform spectrum analysis in orbit by utilizing the SALSAT specific spectrum analyzer payload based on SDR technology. [4] The mission objective is to analyze the frequency spectrum in the VHF, UHF and S band range in the Low Earth Orbit. [5] To fulfill the mission objectives in a comparatively short development time it has been decided to utilize an existing flight spare satellite of the successfully launched S-Net mission of the Technische Universität (TU) Berlin. The current software architecture is highly specialized for the S-Net mission and its payload for an inter-satellite link communication experiment. [6] The existing hardware and software will be enhanced within the SALSAT project to match the needs of various future missions including multiple new payloads. Consequently, SALSAT will be based on the TUBiX10 satellite bus from a hard- and software perspective. It reuses the software developed in the S-Net project which is based on the space-qualified RODOS operating system. Modularization is the key philosophy to include multiple payloads and enable future use of the satellite bus. The objective is to develop a system capable of supporting multiple payloads and their needs. The payload specific adaptions to the bus software must be kept to a minimum. Therefore, software functions will be distributed throughout the payloads and the payload data handling system. Furthermore, a standardized communication between the payloads and bus subsystems will ensure a safety-oriented operation. All payloads must follow this general communication architecture. Optionally preprocessing (e.g. FFT) will be performed directly on the payloads to enable a streamlined, distributed processing and communication architecture. Resulting from this design the integration of new payloads to the satellite bus will be done in a plug and play manner. This paper will describe the SALSAT satellite and its software, focusing on the changes required to establish a modular and flexible bus architecture. Particularly, adaptions to the bus and payload data handling system are described exemplified for the SALSAT specific spectrum analyzer payload.

1. INTRODUCTION

The SALSAT project aims to launch a satellite analyzing the frequency spectrum using a Software Defined Radio (SDR) from Low Earth Orbit (LEO). [4] The S band Network for Co-operating Satellites (S-Net) project [6] build a fully functional flight spare satellite. This satellite is being reused within the SALSAT project. This approach enables a short development cycle for the integration of the new SALSAT specific payloads. Since the whole system shall be launched in 2020 software frameworks from the chair of space technology of the TU Berlin were analyzed and will be combined and used on SALSAT. This paper will describe the chosen approach on the software development within the SALSAT project, its boundary conditions and the challenges the project faces during the software development phase.

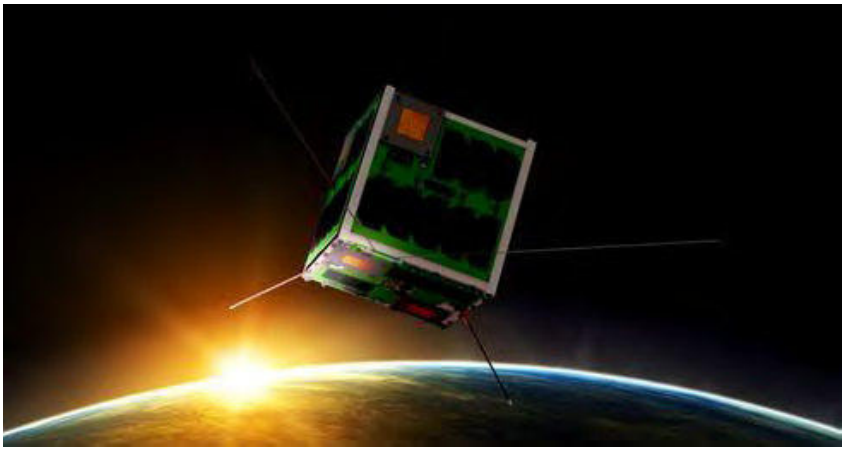

Figure 1.1: Artistic view of the SALSAT satellite

1.1 OVERVIEW OF THE SALSAT MISSION

The number of satellites launched into LEO significantly increased in the past. [1] The continuous growth poses new challenges in the field of satellite communications.[2] The number of satellite systems increases - resulting in a increasing limitation of available frequency spectrum. [5] Consequently, the potential for harmful interference in the existing bands grows. [2] As a satellite can be disturbed by signals that cannot be measured on the ground it is not sufficient to solely rely on terrestrial measurements of interference and noise levels. [3] Consequently, the primary payload of SALSAT is a satellite payload for spectrum analysis. The payload called SALSA was developed and qualified within a research project at the Technische Universität Berlin. [5] It features a spectrum analyzer based on commercially available SDR technology. [5] If the SALSA payload is activated it collects spectrum data within the amateur radio bands in the VHF and UHF frequency range as well as within the S band. The gathered spectral data will be utilized to detect and locate RF interference and to determine the global usage of the investigated bands. Additionally, the SALSAT mission features multiple secondary payloads for technology demonstration, such as a miniaturized Linux-based image processing and camera unit, a novel Fluid Dynamic Actuator (FDA) for three-axis attitude control, a miniaturized full duplex S band transceiver and laser retro-reflectors for precise orbit determination. [4]

1.2 SYSTEM OVERVIEW OF THE SALSAT MISSION

This chapter shall give a brief overview of the SALSAT system and preliminary design. SALSAT is based on the TUBiX10 bus architecture, developed at the chair of space technology of the TU Berlin. The satellite bus has been space-qualified during the S-Net mission. [6] The specification of the TUBiX10 platform has been developed during the S-Net mission of the TU Berlin. The S-Net mission successfully deployed a cluster of four nanosatellites with basic dimensions of 240 x 240 x 240 mm. [6] The TUBiX10 platform is optimized for 10 kg class satellites. [7] As previously explained the SALSAT mission will reuse the flight spare satellite. Consequently, the design of SALSAT aims to minimize changes to the existing S-Net flight spare base on the TUBiX10 platform. The mission will feature a proto flight model philosophy.

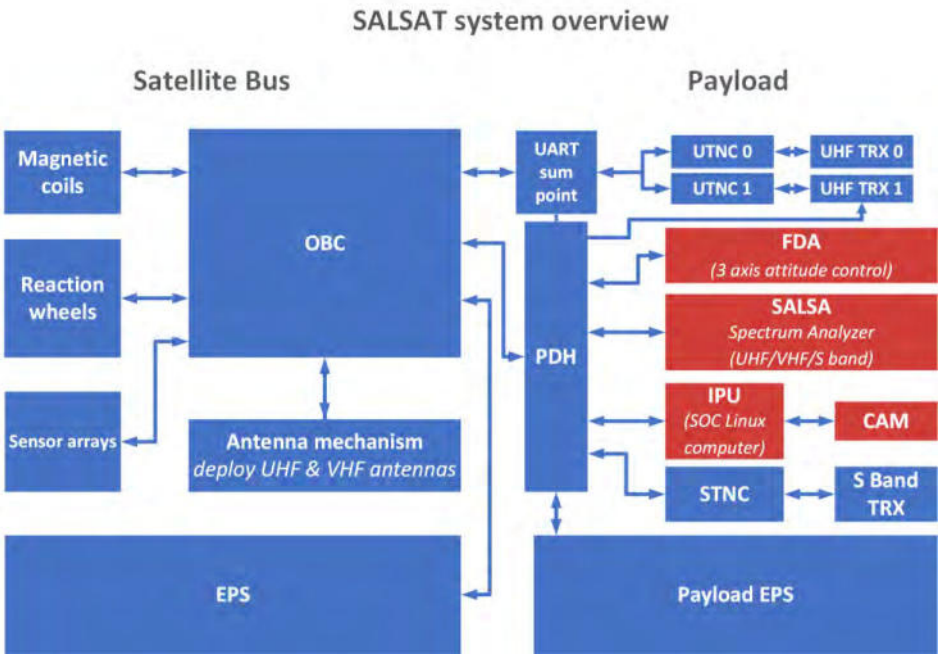

Figure 1.1: SALSAT System Overview

1.3 PAYLOADS

The primary payload of SALSAT is the spectrum analyzer SALSA. As stated above The Spectrum Analysis of LEO Satellite Allocations (SALSA) spectrum analyzer board consists of SDR technology and was developed at the TU Berlin. The receiver design is based on a modified version of the open source project LimeSDR [8] to fulfill the needs of a satellite mission. The SALSA spectrum analyzer features a novel, highly modular design approach based on commercially available components and is designed to be completely re-configurable (e.g. center frequency, bandwidth) during the mission [4] The primary goal for SALSAT is to analyze the radio frequency transmission in the VHF, UHF and S band. Since the TUBiX10 bus features UHF monopole and S band patch antennas it is required to add an additional VHF monopole antenna to fulfill the mission objectives and measure the spectrum in the desired frequency ranges. Additionally, one of the existing UHF antennas will be shared between the bus and payload and is connected to the SALSA payload via a RF switch. [4]
As previously stated SALSAT features two secondary payloads: A camera in the visual spectrum and the Fluid Dynamic Actuator (FDA) experiment. The camera is equipped with an optic for earth observation and has a direct payload data link to the ground station. The link is realized via an image processing unit, which runs a Linux based operating system and a full duplex S band transceiver. The transceiver is a custom modified version of the S-Link transceiver from IQ wireless. The commercially available camera is qualified under hazardous conditions such as shock, vibration and temperature limits that are comparable to launch and space environmental conditions. [4]
The FDA is a novel attitude control actuator for small satellites. It is based on magneto-hydrodynamics [4] The design does not include any mechanical moving parts which enables the actuator to provide strong shock and high wear resistance. [9] The FDA concept offers a high torque and low jitter in comparison to reaction wheels. [4] The novel concept of the FDA has been developed within research projects at TU Berlin.[9]

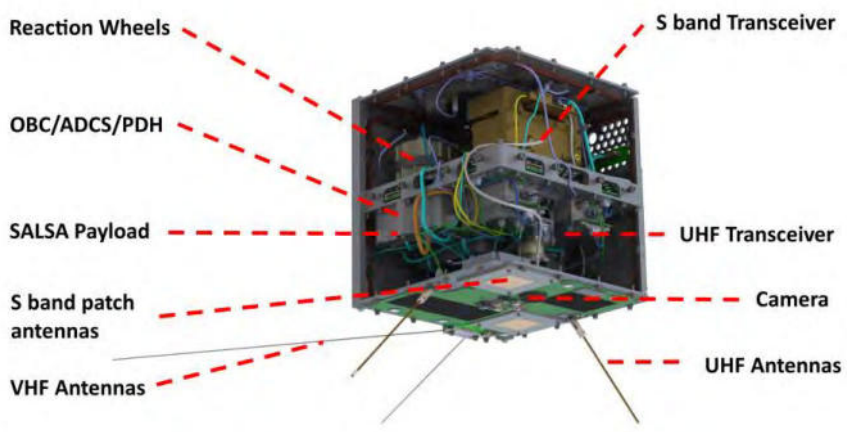

Figure 1.2: SALSAT Subsystem location

1.4 HARDWARE BUS ARCHITECTURE

The OBC of the existing TUBiX10 platform is the main processing unit for Attitude Determination and Control System as well as controls and monitors the electrical power system [EPS]. Due to the planned payloads in the space segment a new board is designed to connect all payload interfaces with the existing bus. Main parts of this board are a redundant payload data handling [PDH] and the payload electrical power supply [PLEPS]. The PLEPS supports an unregulated voltage bus and 3.3V power converters for on-board power supply and the payloads. Every power path of the PLEPS can be controlled via load switches and monitored via power sensors by the PDH. The cold redundant parts of the PDH are switched by the OBC. Supporting SPI, UART, I2C and several GPIOS to the payload, the PDH realizes the data transfer between payloads and the TUBiX10 bus. It also measures voltage levels and current flows as well as controls the PLEPS. As the main node for the payloads it communicates with the FDA, the IPU, SALSA and directly uses a downlink via S-Link. It gathers and stores data to flash memory that can be accessed via ground station.

2. SALSAT SATELLITE SOFTWARE

As described in chapter 1.2 the satellite is a reused flight model of a previous project. While big parts of the satellite are being reused the according software shall be reused as well, while relevant changes are being done. The table 2.1 below describes the underlying software framework from which each software components will be derived. The table shows that most components will be equipped with software which was flight qualified during the S-Net mission.

Heritage: / Subsystem:	TUBiX10 (RODOS)	Bare Metal	TUBiX20	ROS
OBC	X			
UHF-TNC		X		
S-BAND-TNC		X		
PDH	X			
SALSA	X	X		
IPU				X (Linux)
FDA		X		
Drivers	X		X	

Table 2.1: Framework Overview

The major design principals for the SALSAT project are reusage and modularization. While the reusage is depicted in table 2.1 is to be further described. The figure 2.1 below shows the simplified setup of the SALSAT bus architecture. As visible multiple systems are based on RODOS and on the TUBiX10 software. While these modules handle different tasks major parts of the software must fulfill the exact same functions, as for example the FDIR and Housekeeping. Therefore, the TUBiX10 software will be modularized as well to avoid unnecessary overhead by implementing the same functions multiple times.

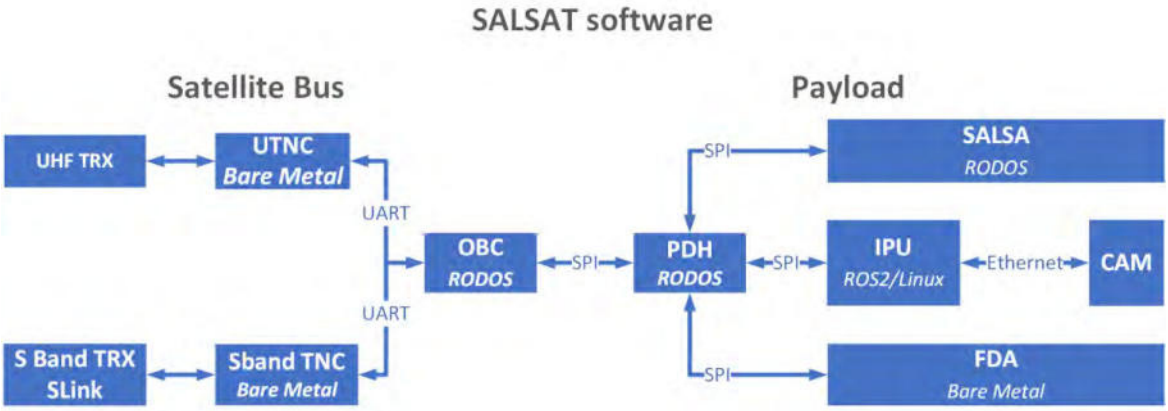

Figure 2.1: SALSAT Software System Overview

2.1 RODOS

RODOS will be the middleware for most components on SALSAT. It was originally developed by the DLR [10] and is ongoing developed and supported by the Chair of Computer Science of the Universität Würzburg. It is a real-time minimalistic and object-oriented software framework and functions as operating system and middleware. It runs on multiple different architectures and was used by the TU Berlin for multiple missions since 2004.

2.2 TUBiX10 Software

As shown in table 2.1 the satellite software is mainly derived from the software of the SNET satellite buses which is based on the RODOS middleware described previously. The TUBiX10 bus software was developed in the S-NET project at the chair of Space Technology from the TU Berlin. **T**he TUBiX10 Software will be run on the OBC, the PDH and the Payload SALSA. The software is implemented with a high focus on reliability but takes some compromises in that regard. It is therefore running on a dedicated schedule in 0.5 seconds cycle. If an application exceeds its time slot actions to solve the reason for that are being started which makes this software perfectly suited for a critical system such as the OBC. But as the real-time capability is only given within a process it is unsuitable for payload software. Therefore, the SALSAT project takes the fundamentals of this software framework and derives a real-time capable solution from it for usage on the PDH and the SALSA payload. The re-usage and adaption of the SNET framework allows the SALSAT satellite to have a low development time as a lot of reliable software is reused while also assuring a high reliability as the software which is used has already been flown on missions very successfully.

2.3 SALSA micro controller and FPGA software

The functionality of the primary payload SALSA is given by a CycloneIV FPGA interfacing with a STM32 micro controller. The spectral information received by an LMS7002M transceiver chip are collected by the FPGA via a digital parallel IQ interface, pre-handled and processed by an on board Fast-Fourier-Transformation concluding in the transfer to the SALSA MCU. The received spectral data is getting saved on two 1 Gbit payload memory units providing the capability of multiple spectral recordings over a number of orbits. While the FPGA gateware has been written during the development of SALSA, the micro controller firmware is derived from the SNET OBC software. Since the SALSA MCU and PDH software share similar functionalities the development of the SALSA MCU is done parallel to the PDH.
Software threads on the MCU simplify the transfer of incoming data to the corresponding hardware module on board. By creating a thread subscribed to the LMS7002M transceiver topic e.g. it will see all data published by the "LINK" on that specific topic. This method provides an easy way of commanding the FPGA and the LMS7002M, asking for new spectral data or reconfiguring the transceiver. Furthermore, the MCU software is capable of initializing the FPGA and rewriting the stored on board gateware into the on board flash memories for future changes and extension of the FPGA's functionalities

2.4 Drivers and Bare Metal Solutions and the use of Linux and ROS

Similarly to the TUBiX10 software framework, the TUBiX20 Bus Software was developed in the TUBIN and TechnoSat project also at the chair of space technology. From the TUBiX20 software framework a common driver basis for the whole chair was developed. The SALSAT projects supports this effort and will continuously develop drivers accordingly.
As shown in table 2.1 three software components are being developed with no underlying framework (bare metal). These three components are the two TNCs and the FDA software. All three components are highly time critical and therefore need special treatment.
Additionally, the software from the IPU is based on ROS and run on a Linux SoC computer. It is developed within a master thesis and lectures at the chair of space technology.

3. SOFTWARE PRODUCT ASSURANCE

Within terrestrial software engineering software product assurance is widely spread. Within the automotive industry for example test driven development and software in the loop are common methods to assure high software standards before the software is tested on the system. Within space industries NASA and ESA provide standards to be followed. The ESA provides the ECSS. From these standards the European governmental agencies derive standards funded projects from a certain size have to fulfill. Since the software relevant parts of the ECSS is highly based on manual reviews and documentation performed by humans this procedure is often unsuitable for small projects. Due to this a modern product assurance approach shall be used during SALSAT software development. The first step in a project reusing major parts of software components is to adapt the V-model development process. The scheme of the adapted V-model is shown

in figure 3.1. It requires the dedicated review of the design and implementation of every reused software component. This procedure shall assure that the reused software fits the software standards and design of the SALSAT mission. If necessary adaption and changes are made to the software. Afterwards it enters the standard development cycle similarly to newly developed software.

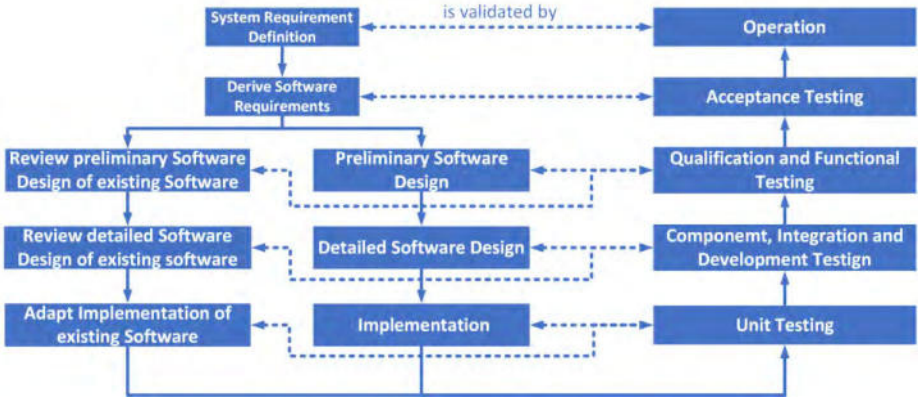

Figure 3.1: SALSAT V-model for software development

The main tests run during the development as depicted in figure 3.1 are unit, functional (summarizing component, integration and development tests) and system tests. Each is dedicated to a specific integration level and together the tests assure are fully functional software system. While the high-level tests are run on the satellite hardware a simulation environment for satellite software shall be developed parallel to the SALSAT project. Further information will be published on the IAC 2019.

Unit testing is a widely spread tool among software development to assure the correct behavior of single units and used correctly also assuring valid interworking between units. To utilize the advantages of unit testing to its maximum a build server is being set up. Within the SALSAT project unit tests shall be applied during the development of new Software on the PDH, SALSA, the IPU and on the Ground System. Applying this method for already developed software from previous projects is unfeasible as it requires the developing engineer to put in the extra effort during the unit review. All already implemented unit tests shall be added to the test routines on the build server. Reused software without unit tests are already flight proven but tests shall still be performed on functional level.

Functional tests describe component, integration and development tests. They shall be continuously applied to all implemented software parts. During functional tests functions are seen as black boxes. This makes it applicable for already implemented software such as the reused software without implemented unit tests. These functional tests focus on bigger software parts and are therefore run directly on the hardware or development boards. If possible, functional tests can be automated as well utilizing the a flatsat model to reduce the needed manpower. Finally, system tests shall be done continuously during the development as soon as two subsystems are used together. These system tests are performed by running predefined commando lists and checking the results directly on the hardware. System Tests are also being performed before, during and/or after hardware qualification tests to verify the impact to the components according to the tests.

4. CONCLUSION

The SALSAT project is an ambitious project with a highly needed main payload and multiple secondary payload run on a tight schedule. The satellite software development process needed to be changed from the usual software development process run at the chair of space technology at the TU Berlin with more time and manpower to a slim and efficient process. Within this document the combination of reusing, adapting and newly implemented software was described. This strategy allows the SALSAT project a rapid launch also from a software focused perspective. While the need of a rapid software development arose, the described strategy assures the upkeep of high software standards. Therefore, the software product assurance strategy matches the needs of the project and the available manpower accordingly by relying heavily on automated tests while limiting manual tests during low level software development to a minimum where needed. Parallel system tests are run manually using the same software tools as later during operation to verify the combined use from an early project stage.

5. ACKNOWLEDGMENT

The SALSAT mission is funded by the Federal Ministry for Economic Affairs and Energy (BMWi) through the German Space Administration on the basis of a decision of the German Bundestag under grant no. 50 YB 1805. The development of the FDA is funded by the Federal Ministry of Education and Research (BMBF) through the Deutsche Forschungsgemeinschaft (German Research Foundation) under DFG Grant No. BR 3539/5-1. The SALSAT project team would like to express its gratitude to the German Space Administration for the continuous support and positive cooperation.

6. REFERENCES

[1] Anders Kose Nervold, Joshua Berk, J. S. D. W., “A Pathway to Small Satellite Market Growth”, Advances in Aerospace Science and Technology, 1, 14-20 , June 2016.
[2] Buscher, M., Balke, A., and Brie_, K., “Spectrum requirements for small satellite TT&C and regulatory status of small satellites”, 11th IAA Symposium on Small Satellites for Earth Observation, 04 2017.
[3] Buscher, M., Großhans, J., Balke, A., Lohse, A., Maaß, A., and Brieß, K., “RF Spectrum Analysis Missions at TU Berlin”, Proceedings the Small Satellites & Services Symposium 2018 - 4S 2018, Sorrento, Italy, 05 2018.
[4] Großhans, J., Vu, H. Q., Balke, A., Lohse, A., Maaß, A., Noack, D., Buscher, M., Brieß, K., and Voigt, S., „SALSAT - An innovative nanosatellite for spectrum analysis based on SDR technology”, 69th International Astronautical Congress (IAC), 10 2018.
[5] Großhans, J., Buscher, M., Vu, H. Q., Balke, A., Lohse, A., and Maaß, A., “SALSA - A novel Spectrum Analyzer board for LEO Satellite Allocations based on SDR technology”, American Institute of Aeronautics and Astronautics, AIAA SPACE Forum 2018, 09 2018.
[6] Yoon, Z., Frese, W., Bukmaier, A., and Brieß, K., “System Design of an S-Band Network of Distributed Nanosatellites”, CEAS Space Journal, Vol. 6, No. 1, March 2013.
[7] Barschke, Merlin F.; Yoon, Z. and Brieß, K.,“TUBiX - The TU Berlin Innovative Next Generation Nanosatellite Bus”, 64th International Astronautical Congress, Beijing, China, September 2013.
[8] Microsystems, L., “LimeSDR”, 2018, https://myriadrf.org/projects/limesdr/, last access at 08/16/2018.
[9] Noack, D., Barschke, M. F., Werner, P., and Brieß, K., “FDA in Space - First in-Orbit Results of a Fluiddynamic Attitude Control System,” Proceedings of the ESA 4S Symposium, 06 2018.
[10] Klaus Hallmann, Wilfried Ley, K. W. e., „Handbuch der Raumfahrttechnik: Grundlagen, Nutzung, Raumfahrtsysteme, Produktsicherung, Projektmanagement“, HANSER, 4th ed., 2011, ISBN: 978-3446424067.

Test of the autonomous diagnostic system ADIA-Light aboard the nanosatellite mission SONATE

Gerhard Fellinger[1], Timo Burger[2], Kirill Djebko[3], Eric Jäger[4], Hakan Kayal[5], Frank Puppe[6]

Professorship of Space Technology, Computer Science VIII, University of Würzburg
Emil-Fischer-Str. 32, 97074 Würzburg, Germany

[1]Phone: +49 931 31-85144, Mail: gerhard.fellinger@uni-wuerzburg.de
[2]Phone: +49 931 31-95102, Mail: timo.burger@stud-mail.uni-wuerzburg.de
[3]Phone: +49 931 31-86405, Mail: kirill.djebko@uni-wuerzburg.de
[4]Phone: +49 931 31-95102, Mail: eric.jaeger@stud-mail.uni-wuerzburg.de
[5]Phone: +49 931 31-86649, Mail: hakan.kayal@uni-wuerzburg.de
[6]Phone: +49 931 31-86730, Mail: frank.puppe@uni-wuerzburg.de

Abstract: An autonomous diagnostic system called ADIA-Light is currently under development and prepared for operation aboard the 3U nanosatellite mission SONATE (also built at the Professorship of Space Technology, University of Würzburg). Running on dedicated hardware, the model-based diagnostic software consists of a symptom detector which regularly compares measured housekeeping values with their pre-calculated, simulated equivalents and marks pronounced deviations as anomalous, and the diagnostic core itself which uses this information to compute diagnostic metadata. Operators on the ground receive this metadata via extended housekeepings, enabling them to react much faster and in a targeted manner to disturbances than usual. After passing various on-orbit functionality tests in the context of a predefined experiment scenario, ADIA-Light is intended to be activated regularly for testing and validation throughout the satellite's lifetime. First results are expected after the launch of SONATE in the summer of 2019.

1. INTRODUCTION

Traditional on-orbit error handling involves engineers on the ground first noticing that something out of the ordinary is happening at all based on telemetry data received from the spacecraft (aided by limit breach warnings), then tracing the visible symptoms back to the actual cause, usually a faulty component. Depending on how many subsystems are involved, this procedure might require multiple specialists who might not always be available together right away, possibly delaying a necessary intervention at the peril of the mission. An autonomous diagnostic on-board system capable of computing viable error diagnoses is therefore desirable in order to shorten reaction times.

As one of two main payloads of the 3U SONATE nanosatellite mission [1], ADIA-Light is the adaptation of the desktop PC-based diagnostic software ADIA++ [2] for on-orbit deployment.[1]

2. SONATE NANOSATELLITE MISSION

SONATE is a 3U nanosatellite built at the Professorship of Space Technology, Computer Science VIII, University of Würzburg, as a platform for the testing and on-orbit validation of

[1] ADIA-Light, ASAP-Light/ATUS, and SONATE are funded by the Space Agency of the German Aerospace Center (DLR) with federal funds of the German Federal Ministry of Economic Affairs and Energy (BMWi) under FKZs 50RM1723 (ADIA-Light), 50RM1521 (ASAP-Light/ATUS), and 50RM1606 (SONATE).

various novel, autonomous payloads. SONATE's external dimensions measure 100 x 100 x 340 mm³, and it weighs in at 4.2 kg. Apart from ADIA-Light, it also carries ASAP-Light, an autonomous image sensor for the recognition of various objects and phenomena of interest in Low Earth Orbit such as sprites, elves, space debris, etc. as its main payloads. Other components designed and built at the Professorship of Space Technology which will be tested on-orbit are an SSTV camera, two miniature star sensors, sun sensors, three reaction wheels, as well as a set of magnetic coils (featuring either air or ferrite cores) for attitude control. SONATE's planned lifetime in LEO is up to one year. The launch is currently planned for the summer of 2019 from Russia's new Vostochny Cosmodrome, Amur Oblast, aboard a Soyuz carrier rocket.

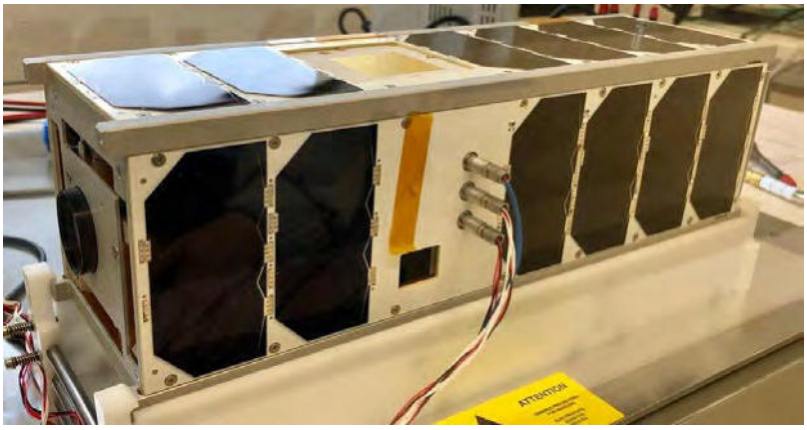

Figure 1. SONATE inside integration lab.

2. THE DIAGNOSTIC SYSTEM

The diagnostic software is model-based and utilizes quantitative models to infer diagnoses. Physical components of SONATE's subsystems such as a battery or a reaction wheel are represented by a set of inputs, a set of outputs and a quantitative description for each output. Each numerical output value is computed as a function of the respective component's various inputs, thereby forming an actual quantitative model of all analyzable components. Components identified as conspicuous by virtue of their output serve as the basis of a backwards-directed search across this graph structure for the possible root cause (i.e. a single or a set of multiple components originally responsible for the anomaly).

2.1 HARDWARE

ADIA-Light uses its own dedicated hardware to run on which consists of two cold-redundantly operated off-the-shelf BeagleCore BCM1.STR industrial computing modules featuring a Texas Instruments AM335x Cortex-A8 Sitara CPU running at 1.0 GHz, 512 MB of DDR3 RAM, as well as 4 GB of eMMC flash memory. The module has a UART interface at its disposal for data exchange with the onboard computer (transfer of housekeeping frames and telecommands) and is powered by SONATE's 5V bus consuming around 1.5W of energy during active diagnostic operation.

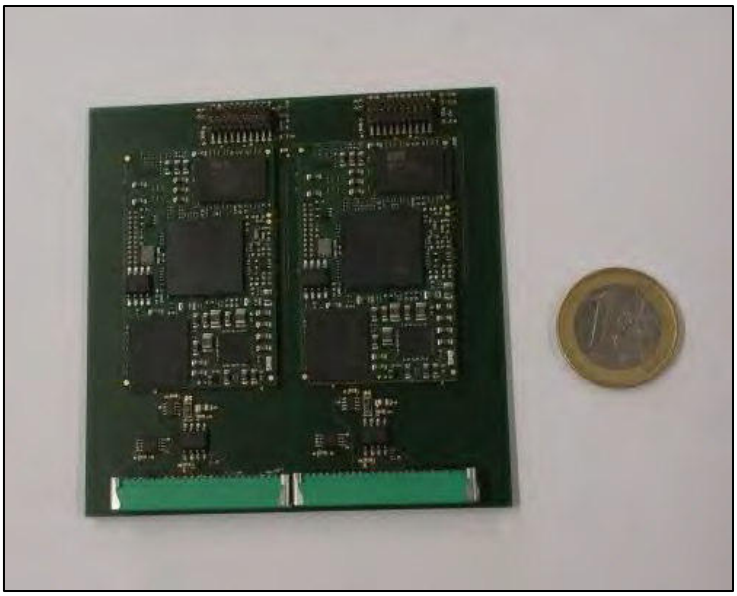

Figure 2. ADIA-Light onboard hardware module consisting of two BeagleCore BCM1.STR modules (AM335x CPU).

2.2 SOFTWARE

ADIA-Light's diagnostic engine itself is embedded into a dedicated, TI-RTOS-based support service software architecture handling communication with SONATE's onboard computer via a RODOS-derived, publisher-subscriber-based gateway for the exchange of messages and data packages, reception and processing of telecommands and regular housekeeping frames, watchdog tasks, saving and retrieval of data to and from the eMMC flash memory, and

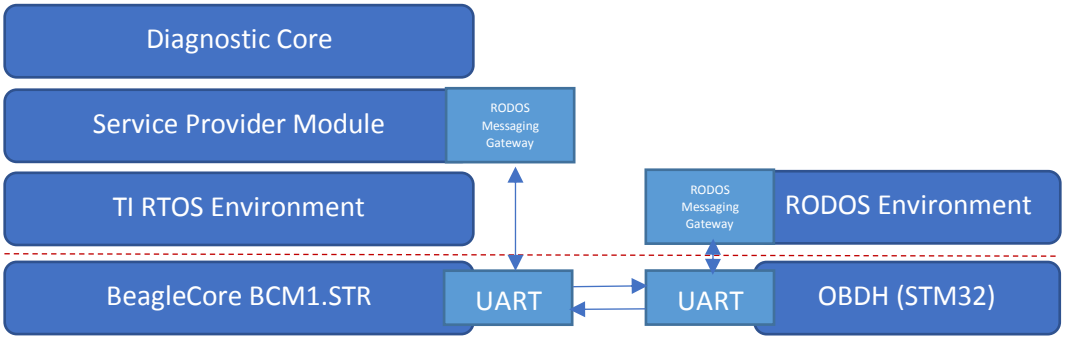

Figure 3. Outline of ADIA-Light's architecture with OBDH integration.

managing the system's operational state transitions. Receiving housekeeping frames at regular 60-second intervals, it analyzes each frame in the two-step process outlined below.

2.2.1 Symptom detection

As soon as a new housekeeping frame is received from the OBC, ADIA-Light first tries to detect any anomalies hidden therein by pre-calculating each of the values for which a simulatable quantitative model has been defined. The simulated frame obtained in this manner

is then compared to the values of the actual housekeepings as measured by the various onboard sensors. Should there be a discrepancy – within predefined margins of error – between measured and expected values, the symptom detector module marks the respective component (e.g. a reaction wheel showing an abnormal input current-torque relationship) as conspicuous and relays that information together with the IDs of the output ports involved as well as the values produced by them to the actual core diagnostic engine. The same happens if measured and simulated values are in accordance with each other but exceed a predefined upper or lower critical limit.

2.2.2 Diagnostic core

Producing a viable diagnosis is synonymous with producing a list of components whose simultaneous failure would explain all of the observed symptoms. In order to accomplish this, each symptom's so-called *conflict set* is first computed, i.e. the set of all components on which the faulty output as determined in the symptom detection step depends (this includes the symptomatic component itself). In the next step, *hitting sets* are computed from all of the available conflict sets. A hitting set itself is another set of components such that at least one component from each of the preceding conflict sets is contained (treating the AND-conjunction of all conflict sets as a Boolean formula, a hitting set is a solution to the Boolean satisfiability problem on that conjunction). Each hitting set represents one diagnosis. Diagnoses are then sorted by their likelihood (enabled by providing a priori failure probabilities for each component) and stored as a collection of extended housekeeping frames containing all relevant explanatory metadata ready to be requested by the operator on the ground.

2.2.3 SONATE simulation model

As selected components of SONATE have become available and been tested in the lab, their output has become meaningfully measurable and thus quantifiable for the purpose of formulating a diagnostic model as outlined above. Specifically, SONATE's batteries and boost converters of the power supply buses have been chosen for monitoring by ADIA-Light as far as the power subsystem is concerned. The battery models receive the battery voltage and load current values from the previous simulation iteration as well as the load current from the current iteration and compute the expected battery voltage for the current iteration. The boost converters receive as input the total load of all consumers connected to the bus as well as the batteries' output voltage and compute the expected bus voltage and battery load.

Additionally, various aspects of ADCS such as SONATE's reaction wheels as well as the magnetic coils were modeled. The reaction wheels receive the commanded RPM and the measured RPM as inputs and compute the reaction wheels power consumption. The magnetic coils receive the commanded PWM signal and compute their power consumption.

Extension of this model by monitoring and analysis of gyro measurements as well as the body-mounted solar panels is currently under active consideration.

3. QUALIFICATION REGIME

ADIA-Light's flight hardware has been both qualified in the context of radiation and thermal-vacuum tests. In the case of the former, an engineering & qualification model (EQM) of the hardware has been irradiated with 10 krad over the course of approximately four hours during a Total Ionization Dosage (TID) trial in September 2018 at the Helmholtz Zentrum Berlin's

Cobalt-60 source while continuously performing read/write operations on the eMMC memory module's 150 MB segment chosen for usage during on-orbit operations. No erroneous readouts have been recorded while power consumptions levels remained steady over the course of the entire run. Thus, voltage regulators, switches, and the eMMC memory chip were deemed sufficiently robust for operations in a typical LEO environment.

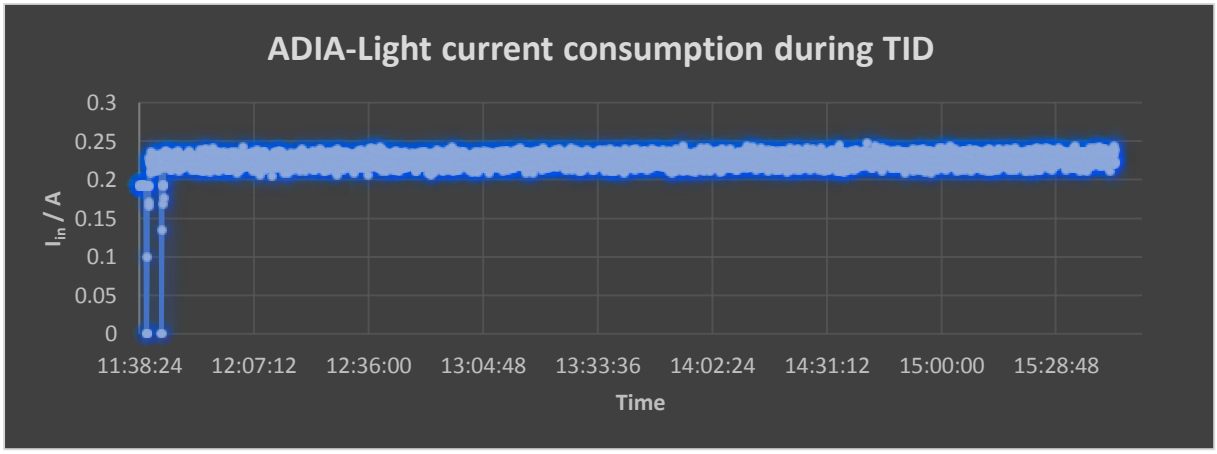

Figure 4. Power consumption during TID qualification run. No unexpected reboots or increases in demand have been observed.

Thermal-vacuum trials took place in November 2018 at our own in-house test facility where (in accordance with thermal simulations conducted within the scope of SONATE's design beforehand) temperatures as low as -20°C and as high as +55°C were measured on the outside of the AM335x Cortex-A8's processor die cap. Vacuum conditions throughout the test run were at least as low as 10^{-3} mbar, and very likely as low as the intended 10^{-5} mbar (which due to a partially defect vacuum sensor was not verifiable). The ADIA-Light EQM was continuously operating during the entire time and did not display any signs of anomalously high power consumption, memory errors, or other errative behavior such as spontaneous resets.

Due to a lack of moving parts or other complex structural elements as part of the hardware platform, ADIA-Light's mechanical & vibrational tests will be considered successfully performed after the end of SONATE's qualification regime of which the ADIA-Light hardware module as one of two main payloads will naturally be a part.

4. OPERATIONS

After launch and the completion of SONATE's LEOP procedures, basic functionality tests regarding power-up, boot-up and communciations with the onboard computer will be performed first. Afterwards, the diagnostic engine itself is evaluated on-orbit for the first time. In order to verify the proper functioning of the diagnostic engine, it will tentatively be fed regular housekeeping frames both with the diagnostic model's default parametrization enforced and altered (operator changing internal steering parameter values by telecommand) symptom detector model in order to provoke the detection of an anomaly which can then be compared to the expected diagnostic result. Default behavior by SONATE's subsystems as recorded in the lab may deviate from default in-orbit behavior, thus necessary recalibrations and adaptions can be tried out in a timely fashion without having to immediately resort to fully-fledged on-orbit software updates.

After successful completion of the test segment of the experimental scenario, regular operational cycles of ADIA-Light are intended to be conducted, in accordance with duty-cycle considerations concerning SONATE'S other instruments (chiefly the other main payload ASAP-Light). The diagnostic system's performance will be evaluated with regards to on-orbit reliability of both hardware and software, as well as quality of the results generated by the diagnostic core. Should no actual anomaly occur in any of the components monitored during this time, operators can again induce artificial errors by altering internal steering parameters via telecommand. The diagnostic metadata itself then received on the ground consists of several different types of extended housekeeping frames providing information such as components marked as anomalous, what type of discrepancy between expected and observed measurements occurred, and other data desirable for the operator.

5. SUMMARY AND OUTLOOK

ADIA-Light, an autonomous diagnostic system to be tested aboard the nanosatellite SONATE has been described First results from ADIA-Light's on-orbit trials are currently expected for the summer of 2019, shortly after the launch of SONATE.

6. REFERENCES

[1] Rapp, T., et al. *Preparing SONATE for Autonomous Control Through ASAP.* Proceedings of the 69th International Astronautical Congress (IAC), Bremen (2018).

[2] Fellinger, G., et al. *ADIA++: An Autonomous Onboard Diagnostic System for Nanosatellites.* Proceedings of the Space 2016 Conference, Long Beach (2016).

[3] Wojtkowiak, H., et al. *Autonomous Mission Operation Onboard Nano-Satellite SONATE.* Proceedings of the 68th International Astronautical Congress (IAC), Adelaide (2017).

Development of on-demand compact SAR for small satellite

Hirobumi Saito[1], Kei-ichi Hirako[2], Seiko Shirasaka[3], Toshihiro Obata[4], Shin-ichi Nakasuka[5], and Jiro Hirokawa[6]

[1]Japan Aerospace Exploration Agency, Institute of Space and Astronautical Science,
3-1-1, Yoshinodai, Chuo, Sagamihara , Kanagawa , 252-0305 Japan,
Phone: +81 50 3362 2657, Mail* koubun@isas.jaxa.jp

[2]Keio Uniersity
4-1-1, Hiyoshi, Kohoku-ku, Yokohama, 223-8526 Japan,
Phone: +81 45 564 2581, Mail: keiichi.hirako@sdm.keio.ac.jp

[3]Keio Uniersity
4-1-1, Hiyoshi, Kohoku-ku, Yokohama, 223-8526 Japan,
Phone: +81 45 564 2581, Mail: shirasaka@sdm.keio.ac.jp

[4]the University of Tokyo
7-3-1, Hongo, Bunkyo-ku, Tokyo, 113-8656 Japan,
Phone: +81 3 5841 8679, Mail: obata@space.t.u-tokyo.ac.jp

[5]the University of Tokyo
7-3-1, Hongo, Bunkyo-ku, Tokyo, 113-8656 Japan,
Phone: +81 3 5841 6590, Mail: nakasuka@space.t.u-tokyo.ac.jp

[6]Tokyo Institite of Technology,
2-12-1-S3-19 O-okayama, Meguro-ku, Tokyo, 152-8522 Japan
Phone: +81 3-5734-2567, Mail: jiro@antenna.ee.titech.ac.jp

Abstract: This paper presents the proto-flight model test results of X band synthetic aperture radar for small satellites with 130kg mass. The specifications of SAR performance are single polarization SAR with 3m ground resolution for strip map mode. Optional 1 m ground resolution can be achieved with sliding spot light mode under condition of limited value of NESZ. The paper describes the unique antenna system, the RF power amplifier, high speed data storage/transmission system, and the ground SAR response test results.

1. INTRODUCTION

Synthetic Aperture Radar (SAR) is a well-known remote sensing technique that is effective in day and night for any weather condition. Conventionally, however, SAR observation requires large or medium size satellites with hundreds kilo-grams or more. Medium SAR satellites such as SAR-Lupe[1] (Germany, total mass 770kg, 2006), TecSAR[2] (Israel, 300kg, 2008), and NovaSAR-S[3] (United Kingdom, 400kg) have been launched. These large or medium satellites cost hundreds million US dollars including launching cost. Recently small satellites with 100kg or less are being applied to SAR observation aiming at SAR satellite constellation. In 2018 January, ICEYE-1 (Finland, 70kg) was launched and demonstrated 10m ground resolution SAR observation in X band [4]

In this paper, we describe a synthetic aperture radar sensor compatible with 100kg class satellites. When this small SAR satellite is injected to typical earth observation orbit with 500-600km altitude, its ground resolution is expected to be 3m that is useful for earth observation and monitoring. Optional 1 m ground resolution can be achieved with sliding spot light mode under condition of limited value of NESZ. The main specification of SAR observation is shown in Table 1.

Table 1 SAR Observation Specification

	SAR Mode	
	Strip Map	Sliding Spot Light
Altitude	618km	618km
Resolution	3m	1m
Center Frequency	9.65GHz	
Swath	10 km	10 km
Chirp Band Width	75MHz	300MHz
Polarization	V/V	
Antenna Size	4.9 m×0.7 m	
Ant Efficiency	50%	
TX Peak Power	1000 W	
TX Duty	25%	
System Loss	0.6 dB	
System Noise Figure	2.6 dB	
Off Nadir Angle	15～45 deg	
Pulse Repitition Frequency	3000 ～ 7000 (TBD) Hz	
NESZ (beam center)	-20dB	-16dB
Ambiguity (beam center)	>15dB	

2. SYSTEM AND ANTENNA

A satellite has 130kg mass and the size is 0.7m x 0.8m x 0.9m on a rocket. A size of the deployed antenna is 4.9m x 0.7m. Fig.1 shows the configuration of SAR antenna. The waveguide is embedded at the center of the rear surface in order to feed RF to the antenna panel through coupling slots. The antenna panel consists of a dielectric honeycomb core and metal skins, which work as a parallel plate guide for RF. The front surface with two dimensional arrays of radiation slots works as an antenna radiator for ver-

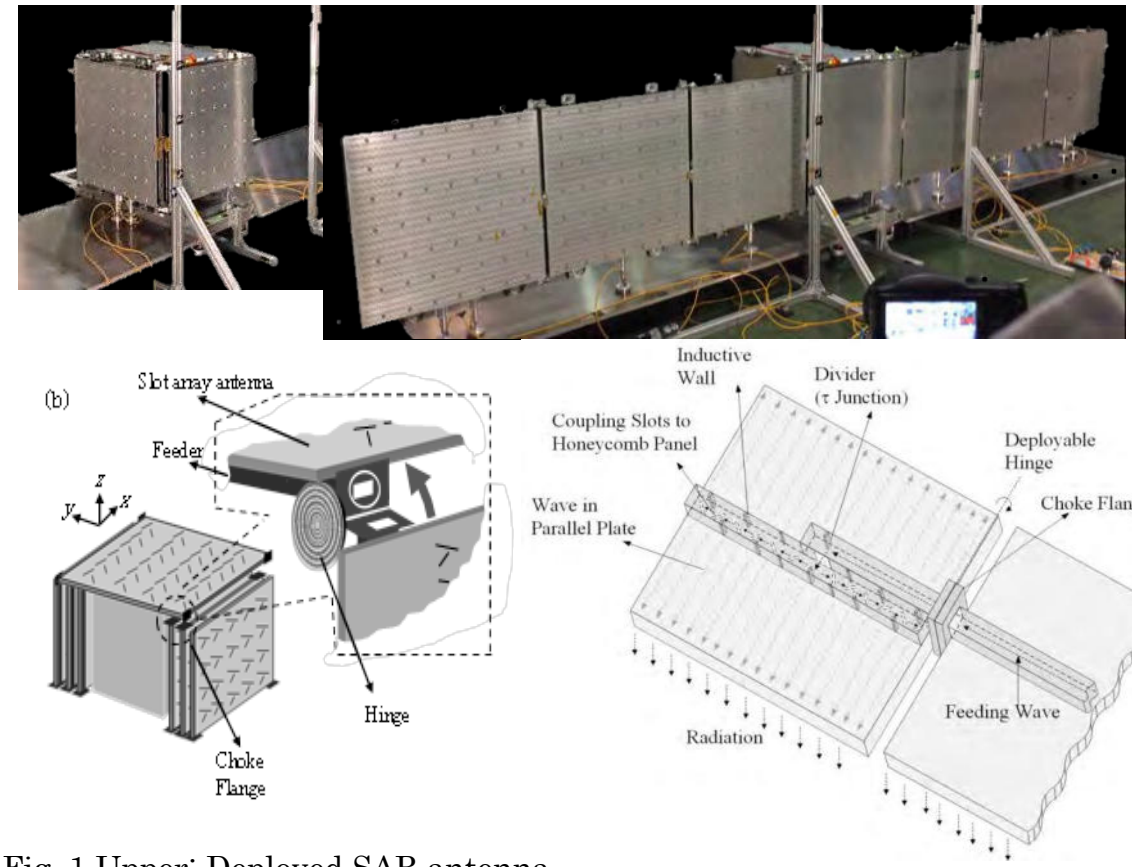

Fig. 1 Upper: Deployed SAR antenna
Lower Left: Non-contact waveguide feeding with choke flange
Lower Right: Honeycomb antenna panel with slot array and embedded waveguide

tical polarization SAR mode. In order to achieve 1m ground resolution, the antenna bandwidth should be about 300MHz. This antenna is a traveling wave array antenna. Therefore, length of an array branch should be less than about 30cm. We have developed a proto-flight model of full antenna configuration with 7 antenna panels (size of 4.9m x0.7m). Also near field RF measurement of the full antenna configuration has been performed at A-Metlab Facility, Kyoto University. The peak directivities at the center frequency 9.65GHz are 36.7dBi for one-panel, 42.4dBi for four-panels and 44.5dBi for 7-panel full configuration, respectively. These values are almost proportional to number of the panels, indicating that effective in-phase excitation of antenna panels is achieved and antenna arraying can works as designed. The aperture efficiency of 7-panel full configuration is about 69.9%.
In order to make antenna instrumentation simpler, TX and RX instruments are in the satellite body. Therefore RF should be fed from the satellite body to each panel with equal electric length. We apply choke flanges of waveguides in order to realize RF feeding with non-contacting waveguide flanges. Choke flanges have been widely used to avoid the degradation of current conduction through waveguide flanges due to manufacturing imperfections or oxidization of the flange surfaces. RF loss can be minimized by the choke connection even though there is a physical gap between two waveguide flanges.

3. ON-BOARD SAR INSTRUMENTS

The RF peak power is selected to 1000 W that is realized by GaN solid state amplifiers, instead of vacuum tube TWTAs. A chirped transmitting signal is amplified in a six GaN HEMT 200W amplifier modules to be combined in a waveguide resonator.

A SAR-Electronics Unit (S-ELU) handles transmitting signal generation, receiving signal processing (frequency conversion and analog-to-digital conversion) for SAR sensor. The S-ELU for small satellites is developed based on an airborne SAR instrument. The chirp bandwidth is 300MHz for 1m ground resolution. The received signal is converted to digital signal of 8bit x 720M sample/sec. Data compression rate is about 50%. Receiving duty cycle is about 50% to acquire reasonable signal-to-noise ratio. After time stretching process, the average data rate is 1.5Gbit/sec. In the SAR observation mode, this 1.5Gbit/sec SAR data is transferred to Mission Data Recorder (MDR) through serial RapidIO (sRIO) interface.

Mission Data Recorder MDR consists of commercial 16 NAND flash memory devices and the total memory capacity is 768Gbyte. Total dose tolerance of NAND devices is confirmed by Co60 irradiation test. Single event upset errors are corrected by standard error correction code for commercial NAND devices. A commercial Xilinx UltraScale FPGA (Field Programmable Gate Array) device is utilized for high speed data flow and standard powerful error correction code. Special cares are paid to thermal heat path and thermal stress of BGA (Ball Brid Array) packaging. In down link communication mode, stored data is transferred to high data rate X band transmitter (XTX). XTX has dual polarization (RHCP/LHCP) channels to increase its down link capability. Stored data is switched to the 2 channels and they are transferred to XTX through Xilinx Aurora data interface. The data rate between MDR and XTX is 2Gbit/sec per one channel and total data rate is 4Gbit/sec. Figure 2 shows photographs of on-board instruments as described in this section.

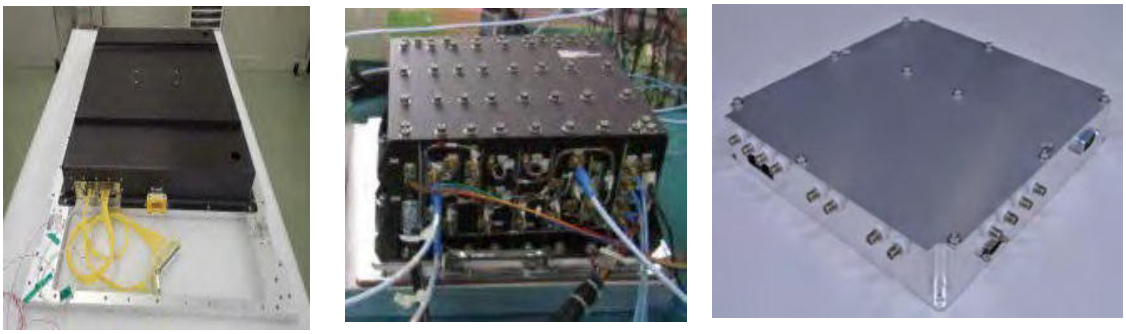

Fig.2 Left : 1kW Xband Power Amplifier installed on satellite body.
Center: SAR Electronics Unit converted from air plane application
Right : 768Gbyte, 2Gbps Mission Data Recorder with NAND memory

4. SAR IMAGING TEST WITH POINT SOURCE SIMULATOR

We have performed ground test of SAR observation with a dedicated target signal simulator. Proto-flight model of SAR-Electronics Unit (S-ELU) sends exciter signal with chirp modulation to RF Front-End (RFE) and High Power Amplifier (HPA). A dedicated target signal generator (TSG) generates echo signals from a single point target under assumption of stop and go model. The echo signals are input to S-ELU. Then S-ELU performs frequency down-conversion, conversion of analog signal to digital signal sent and then send it to the data recorder. The conventional SAR imaging processing gives us the range- azimuthal SAR image of point target as shown in Fig.3. We have confirmed 0.81m azimuthal resolution and 0.86m ground resolution at off-nadir angle 30deg with sliding spot light mode.

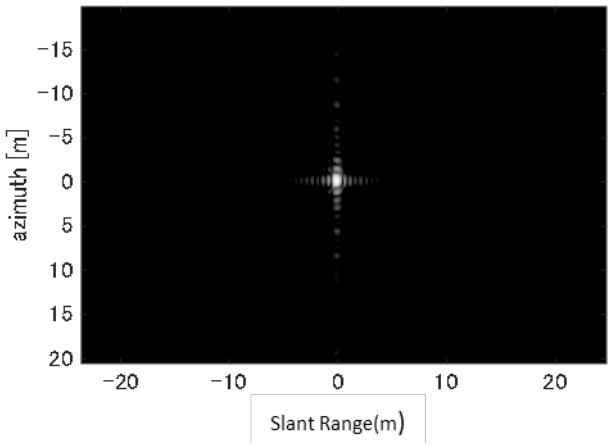

Fig.3 SAR response image of single point source with sliding spot light mode. 2D plot of slant range and azimuthal direction. Azimuthal resolution is 0.81m and slant range resolution is 0.47m (ground range resolution 0.86m at off-nadir angle 30deg).

5. SAR data down link system and its Demonstration

The observed data is transmitted to ground station through high-speed X band link. Table 2 summarizes our downlink communication technology for small satellites. We have already demonstrated high speed downlink of 64 APSK, 100Msps with Hodoyoshi 4 satellite in 2014 [5,6]. Based on this technology, we are developing dual polarization channel X band link with total 2-3Gbit/sec capability [7,8]. Figure 4 is photographs of flight model of high speed X band Transmitter (XTX), Medium Gain antenna (MGA) and 10m ground station.

Table 2. JAXA/ISAS High Speed Downlink for Small Satellite

Satellite	Down Link Speed	Symbol Rate	Modulation	rolloff factor α	Bandwidth in X band	RF Output	Tx Ant.	Rx Ant. (Dia / Tsys)
Hodoyoshi-4 (2015)[5,6]	540Mbps x 1ch	100Msps	SCCC/ 64APSK	0.5	120MHz	2W	Patch 13.5dBi	3.8m/120K
Rapis-1 (2019)[7,8]	1,270Mbps x 2ch	300Msps	DVB-S2X/ 64APSK	0.05	315MHz	1W	Corrugated Horn 17.5dBi	10m/55K

Fig.4 Left : High Speed X band Transmitte.
Center : Medium Gain Antenna (MGA).
Right : 10m Ground Station Antenna

Allocated radio frequency for earth observation is 8025-8400MHz (375MHz bandwidth). However, next band 8400-8450MHz is deep space down link band that should be protected against possible interfence. We select 64APSK modulation with 300Msymbol/sec to observe the protection regulation. We apply DVB-S2X standard to this high speed down link.

Digital processing of the transmitting signal including DVB-S2X standard formatting, I-Q mapping, route Nyquist filtering is performed by a commercial Xilinx UltraScale FPGA. A commercial, high-performance digital-to-analog converter is applied to generate 1.2 GHz IF signal. Special cares are also paid to thermal heat path and thermal stress of BGA (Ball Brid Array) packaging. This IF signal is frequency up-converted to X band and is amplified up to 1W at RF section. Nonlinearity, especially third-order inter-modulation of the final power amplifier is critical issue of the RF section. Figure 5 is demodulated constellation pattern of 64APSK (coding rate 11/15), DVBS-2X, 1.3Gbps/channel. Error vector magnitude is about -27dB rms.

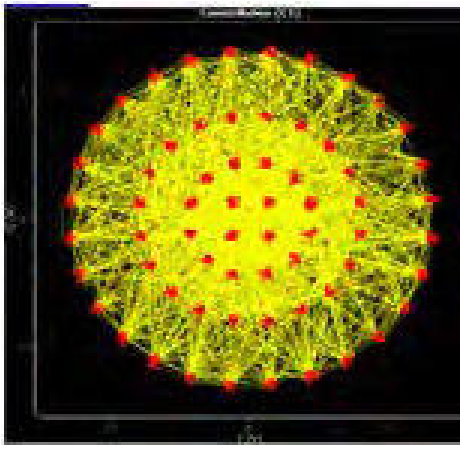

Fig.5 Demodulated constellation of 64APSK, DVB-S2X format, 1.45Gbps/ch.

In order to secure the dual polarization

channel link, Cross Polarization Discrimination (XPD) factor is important for communication link system to avoid interference between dual channels. Dominant factors are XPD of atmosphere propagation and XPD of onboard and ground antenna. We have developed the corrugated horn antenna and the septum polarizer for this purpose. The antenna gain is 17dBi and XPD is higher than 33dB.

A ground receiving antenna with 10m diameter is being developed. Existing 10m antenna for Ku band at JAXA, Usuda is converted to X band receiving antenna. The antenna gain, system noise temperature, and XPD is 56.5dBi, 55K (zenith), and >35dB, respectively.

Received RF signals at the ground station are frequency down converted and are stored at a dual channel, high speed, and large volume data recorder. Since there is no real-time demodulator of 300Msps, 64APSK modulation at present in the market, non-real time software demodulation system is being developed as a part of our project.

This high speed down link system has been demonstrated by the Mini-satellite, RAPIS-1 of "Innovative Satellite Technology Demonstration Program" in Japan and was launched in 2019, January 19th. We have received simultaneously the signal of 64APSK 11/15 (data rate 1, 270Mbps) in the RHCP channel and the signal of 16APSK 26/45 (data rate 675Mbps) in the LHCP channel. The data are stored in the dual channel data recorder. As a preliminary result, dual channel signals are successfully demodulated. The total data rate is 1,945Mbps in X band for earth observation band. We will continue receiving experiments of dual channel 64 APSK down link aiming at total 2,540Mbps speed in 2019.

6. CONCLUSION

We describe the proto-flight model test results of compact SAR. The first demonstration flight for this SAR system will be in beginning 2020 as collaboration with a private company Synspective[9] .

7. REFERENCES

[1] H. M. Braun, P. E. Knobloch, "SAR on Small Satellites- Shown on the SAR-Lupe Example" , Proceedings of the International Radar Symposium 2007 (IRS 2007), Cologne, Germany, Sept. 5-7, 2007.

[2] U. Naftaly and R. Levy - Nathansohn, "Overview of the TECSAR satellite hardware and mosaic mode," IEEE Geoscience and Remote Sensing Letters, vol.5, no. 3, pp.423–426, 2008.

[3] Philip Davies, Phil Whittaker, Rachel Bird, Luis Gomes, Ben Stern, Prof Sir Martin Sweeting, Martin Cohen, David Hall, "NovaSAR-S Bringing Radar Capability to the Disaster Monitoring Constellation" 4S Symposium, Slovenia, June 2012.

[4] https://space.skyrocket.de/doc_sdat/iceye-x1.htm

[5] H. Saito, T Fukami, H. Watanabe, T. Mizuno, A. Tomiki, and N. Iwakiri, "World Fastest Communication from a 50 kg Class Satellite − Micro Satellite Hodoyoshi-4 Succeeds in 348 Mbit Per Seconds − ." IEICE Communications Society GLOBAL NEWSLETTER Vol. 39, No.2, 2015

[6] H. Saito, T Fukami, H. Watanabe, T. Mizuno, A. Tomiki, and N. Iwakiri, “High bit-rate communication in X band for small earth observation satellites - Result of 505 Mbps demonstration and plan for 2 Gbps link -,” AIAA/Utah State University Small Satellite Conference, Utah SSC16-VII-5, Utah. Logan, USA, Aug.2016

[7] T. Kaneko, et. Al., “2Gbps Downlink System of 100kg Class Satellite for Compact Synthetic Aperture Radar Mission”, Small Satellites Systems and Services – The 4S Symposium 2018, paper 48, Sorrento, Italy. 28 May – 1 June.

[8] T. Kaneko, M. MitaA. Tomiki, and H.i Saito. #Dual circularly polarization X band 2Gbps downlink communication system,” AIAA/Utah State University Small Satellite Conference, Utah SSC18-XII-1, Utah. Logan, USA, Aug.2018.

[9] https://synspective.com/

Synthetic Aperture Radar on a nanosatellite - is it possible?

Alex da Silva Curiel[1], Phil Whittaker[1], Rachel Bird[1], Andrew Haslehurst[1], Pejman Nejadi[1], Victoria Irwin[1], Andrew Cawthorne[1], Craig Underwood[2], Martin Sweeting [1,2]

[1]Surrey Satellite Techology Ltd.
Tycho House, Surrey Research Park, Guildford, GU2 7YE, United Kingdom
Phone: +44 7824 804912, Mail: a.curiel@sstl.co.uk

[2]Surrey Space Centre
University of Surrey, Guildford, Surrey, GU2 7XE, United Kingdom

Abstract: The implementation of a viable Synthetic Aperture Radar (SAR) mission using small satellites faces significant technological and financial challenges, and this paper evaluates how small such a spacecraft could be made whilst still fulfilling a useful mission. SAR offers a range of complementary capabilities alongside other Earth Observation systems with various unique features, but developing such spacecraft has traditionally been expensive and technologically challenging. It is only in the most recent years that small satellite SAR missions have been implemented and operated, and this paper examines the state of the art and the challenges. Furthermore the opportunities of how small SAR satellites can help realise new Earth Observation capabilities not available on existing traditional SAR satellites are described using examples of missions under development or reference design missions.

1. INTRODUCTION

Space borne radar systems provide an attractive means to observe the Earth from space at times where optical systems cannot be used efficiently, for instance at night time or in areas with poor lighting such as over the poles, or in areas with extensive cloud or haze. Space borne radar can also be used in some cases to penetrate foliage, soil or water which has been exploited for instance in archaeology [1]. Furthermore, radar can also provide some information about the properties of the illuminated target that can sometimes not be established through other means, due to the reflection, absorption and scattering characteristics of the target which change with wavelength and polarization.

The figure below shows that most optical and SAR satellites observe the Earth at some very narrowly defined time slots during the day. SAR is not limited to any specific time and therefore has the as yet unexploited opportunity for higher temporal resolution.

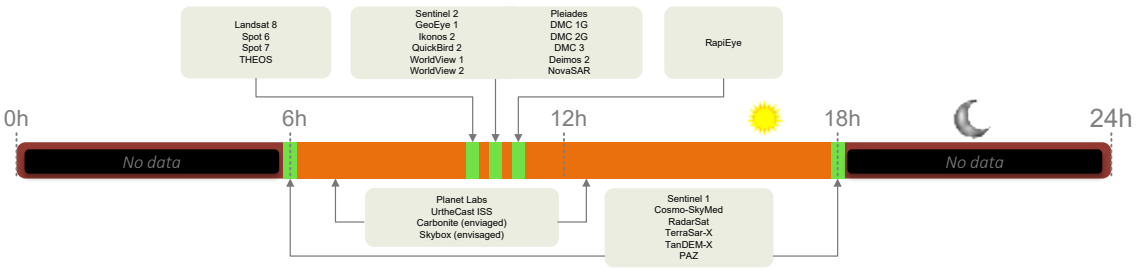

Figure 1. The majority of EO satellites sample at just a few distinct times of day.

Traditionally such space borne radar systems have required relatively large satellites. There are several reasons for this. Firstly, as an active Earth Observation system, the amount of Radio Frequency transmission power is high in the kiloWatt range leading to

designs where that power is provided direct from solar panels. Secondly, spacecraft system design tends to drive solutions towards large area antennas. Furthermore up until quite recently only major government agencies have developed such spacecraft. Their scientific or national needs have driven these missions to serve multiple applications, and as the expensive missions must serve all of the user community they include high levels of performance or features. Radar spacecraft system designs tend to lead ro solutions in 6am-6pm sun-synchronous orbits where the power generation and thermal design are most easily dealt with. As there are not many other spacecraft that benefit from such an orbit, the only limitation to the size of the SAR spacecraft becomes the size of the launch vehicle.

The table below shows that traditional SAR spacecraft have been "large" satellites with masses of around 800-4000kg. Two 300kg spacecraft have been the only small SAR spacecraft built by IAI to fit within the Shavit 300kg launch capability. In the past year however there have been a number of smaller SAR spacecraft launched, and most new systems are proposed as part of a constellation.

Table 1. A selection of historical SAR missions and their mass

SAR mission	Year	Mass (kg)	Band
ERS-1/2	1991-1995	2384	C
RadarSat-1	1995	2200	C
SARLupe	2006-	770	X
ALOS-1	2006	4000	L
TerraSAR-X	2007	1230	X
RadarSAT-2	2007	2200	C
Cosmo-Skymed	2007-	1700	X
TecSAR	2008	300	X
Tandem-X	2010	1340	X
HJ-1c	2012	890	S
RISAT-1	2012	300	X
KompSat-5	2013	1400	X
Sentinel-1a/b	2014/16	2300	C
ALOS-2	2014	2120	L
IceEye-1	2018	80	X
NovaSAR-1	2018	450	S
Capella	2018	40	X
RainCube	2018	12	Ka
Paz	2018	1350	X

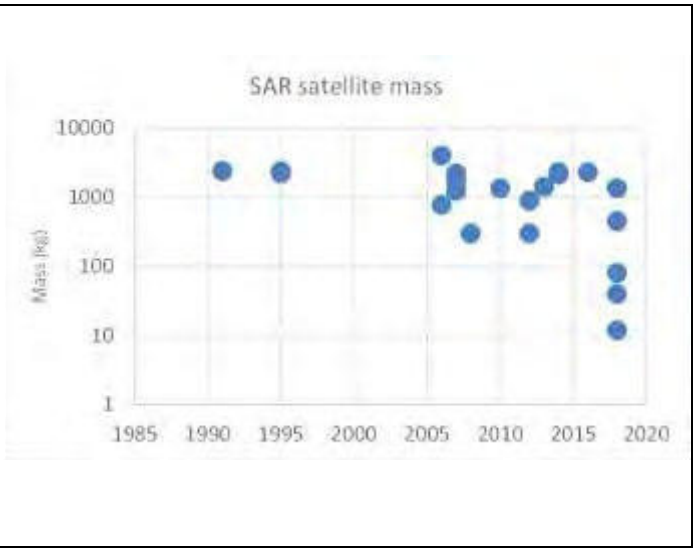

In a previous paper the authors considered how small a useful high resolution satellite could be made, given there are a combination of technological challenges to overcome, as well as some real physical limitations [2]. Similarly, this paper considers the same question for a small synthetic aperture radar satellite. There is real relevance to this question, in that some applications require high temporal resolution in the first instance, before considering any of the other desirable characteristics. An example of that is the IceEye-1 mission which was principally aimed at addressing ice thickness monitoring. This application requires both high temporal resolution and a good geographic spread of measurements, over and above quality of imagery and without needing high area coverage.

1.2 Smallsat SAR reference design

In order to establish a useful reference point for satellite size comparisons, a low cost SAR mission is defined to support disaster monitoring. It is to provide support to disaster monitoring with 1m radar imaging, with a minimum capability to image for 1 minute per orbit in a single polarization, and it must be able to return that data within the same orbit. Furthermore, as this relates to a small spacecraft, it must be able to be used as part of a constellation to provide high temporal resolution imaging capability with global reach.

The available bandwidth in these bands relates to achievable resolution, with 85Mhz, 200MHz, 120Mhz, 600Mhz bandwidth being allocated to SAR operation in L, C, S and X-band respectively, the only frequency band that can be used to achieve 1m resolution is to utilize the SAR frequency allocations at X-band. Based on the design methodology described in [3], the rough RF power requirements can be calculated for this small X-band SAR spacecraft utilising a 3m deployable dish antenna. This illustrates that a viable design is possible using 900W RF power.

Table 2. Concept design for small SAR spacecraft payload

Resolution	1	m
Frequency	9.65	GHz
Orbit altitude	500	Km
Slant angle	25	deg
RF Power	900	W
Duty Cycle	25	%
System Noise Temp	600	K
Noise Figure	4.8	dB
LNA Losses	3	dB
Antenna area	7	m2
Antenna efficiency	40	%
Bandwidth	360	MHz
σ^0_{NE}(dB)	-18	dB

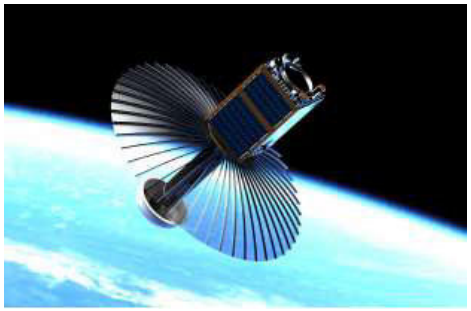

$$\sigma_{NE}{}^{\circ}\delta_r = (8\pi R^3 k T_o v_{sl})(NFL_s)\frac{\lambda}{P_{TX-ave}A^2\eta^2}$$

2. KEY TRADES IN SMALL SATELLITE SAR

2.1 Business / Application trades

The market for SAR data is projected to be worth USD1.6b in revenues by 2027, with 2018 figures being just over half of that. Typical pricing for SAR data varies from around USD85-150/km^2 today, falling to around one third of that over the coming decade [4]. Using these figures, the current worldwide annual data sales can be estimated to be 8 million km^2. The value of SAR spacecraft and commercial data capacity far outstrips the market. Furthermore, some data is made available for free from the Sentinel-1 spacecraft, although the satellite is not available for casual tasking requests.

As such, any new SAR systems must differentiate their services from those currently available in order to generate value. Given the broad capabilities and scientific quality available from current SAR missions, it is likely that such new systems will need to use quite small spacecraft initially, in order to develop a suitable base of users.

Return-On-Investment from such spacecraft, whether in money or data terms, depends strongly on the amount of *useful* data and derived value that can be generated during the mission lifetime. Furthermore, many design choices are based on the specific application that is served.

Traditional SAR missions developed by governmental agencies tend to be designed to meet highly derived and rigid performance parameters. Systems designed to support a service and a business case may see a more iterative, rather than cascaded flow down, type of requirements development. Systems designed for surveillance type applications (e.g. security and environmental monitoring) will typically be driven by resolution and revisit where object detection and feature extraction, often relating to human activity, is required. Where classification of distributed targets is required (e.g. agricultural and environmental assessment) sensitivity and radiometric aspects are more important.

2.2 Payload Trades

One of the key choices for any SAR mission is the band of operation. All of the microwave bands commonly used for spaceborne SAR will produce imagery that can be interpreted by the human eye like optical pictures. Early applications development used whatever data was available and all of the bands can serve most applications to some extent. However, where level 2 data products are derived from level 1 imagery by automated means there are differences between bands which may be important considerations for systems designed for specific applications. Shorter wavelength allocations support higher bandwidth radar pulses and better resolution images. Longer wavelength allocations have the fortuitous property that backscatter coefficient of vegetation varies more significantly with type of vegetation or growth stage. However, as can be seen by equation 2.8.8. of Curlander [5], to maintain a SNR for longer

wavelengths the aperture of antenna must be increased to mitigate loss of antenna gain and reduced backscatter coefficient.

X-band systems, where greater bandwidth is available is generally used in mapping, surveillance and security applications. Longer wavelengths in C, S and L band progressively penetrate vegetation, ice, water and soil better, but at coarser resolution. These are generally well suited to Maritime, Forestry, and Agriculture applications. It has been shown [3] that operation at shorter wavelengths are better for achieving the same resolution and quality of image on smaller spacecraft.

The trades between resolution, receiver bandwidth and look-angle also are complex. Considering that low look-angles are desirable in disaster monitoring and most other applications, bandwidth above 300MHz as required for achieving 1m resolution is only available at X-band. The graph below shows that for look-angles compatible with typical applications, relatively high receiver bandwidth is required in order to achieve 1m resolution. With such high receiver bandwidth, signals must be digitized at high speed, implying relatively high power drain during data recorder capture and record operation.

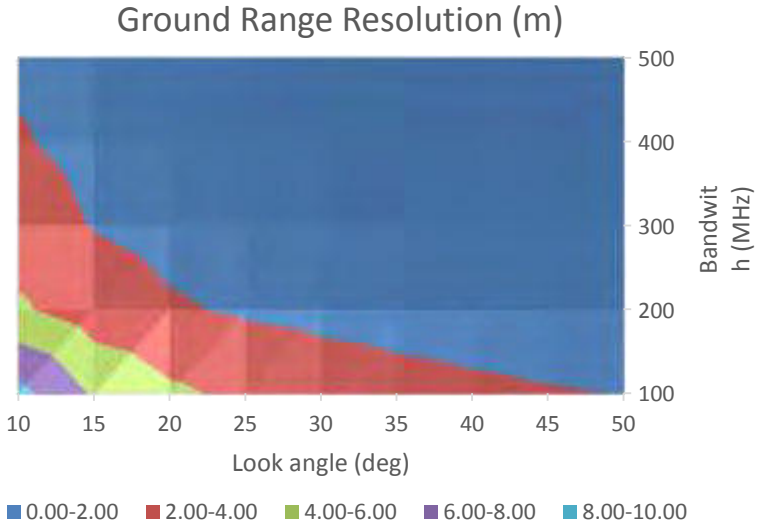

Figure 2. Range resolution achieved at different look angles alongside bandwidth requirements

Ground and airborne SAR systems can operate in Continuous Wave (CW) mode with continuous signal transmission and reception. But as the return signal power reduces with the fourth power of distance from the target, at some range such CW mode of operations becomes impractical as the receiver can no longer be isolated from the transmitted signal. As such spaceborne SAR missions tend to operate in pulsed mode.

The tension between swath and resolution is common to all designs. It is interesting to note the similarity, in terms of resolution/swath combinations, between operating modes of different systems. Whereas flexibility in parameters affecting sensitivity offer performance scalability, inherent constraints on geometry and pulse frequency constrain the swath/resolution trade space unless high NRE solutions like digital beamforming or multi-static sensors are considered.

There are numerous trades on a SAR payload that require careful selection of frequency band, pulse power, pulse repetition frequency, average transmit power, polarisations and modes covered, swath, range and azimuth resolution, and quality of data. It is beyond the scope of this paper to fully discuss these trades, but some of these parameters have a direct effect on the spacecraft design and its size. Those include:-

- Choice of radar antenna type. dish, phased array, reflector array, slotted wave-guide, etc,
- Choice of power amplifier, TWT, SSPA.
- Choice of principal mode of operation – StripSAR vs Spotlight
- Choice in support of different polarisations.

The choice of antenna is complex, and a dish antennas or a planar antennas have both been used on missions. Dish antennas are relatively simple and cost effective, and tend to have a single transmit/receive feed. This drives to the need for a single power amplifier and receiver. One of the disadvantages of dish antennas is that they can limit the swath width, and in practice elliptical dish antennas could provide wider swath at the cost of complexity. Planar antennas can also be combined with a single transmitter/receiver and can be configured to provide both wide swath and good resolution in Stripmap mode. If implemented as a phased array these can utilise distributed transmit/receive modules and thus provide potential for electronic beam steering and various modes of operation. As such these are much more complex and lead to a much heavier antenna assembly and spacecraft. Indeed [6] shows that the specific antenna weight is one of the key factor in miniaturizing a SAR spacecraft, favouring deployable dish and reflector antennas.

The key enabler for any small launch volume solution is a deployable antenna technology. Stowed reflectors tend to take a cylindrical stowed form whereas the Oxford Space Systems wrapped rib solution used by SSTL's CarbSAR satellite fits into a more launcher friendly cuboid volume. Mesh material surfaces offer the lowest mass which is not only important for launch but also has a significant impact on the design and power requirements of the attitude control subsystem. Suitable spaceborne mesh reflector antenna solutions tend to be circular. The gain, and hence aperture, requirements for a workable system mean that a circular aperture antenna will restrict the swath that can be illuminated. A planar antenna can be implemented in a more modular form suiting a rectangular aperture and a more optimised swath. At the cost of additional mass a planar antenna also suits a distributed RF feed which can support beam steering and mode flexibility. Diving this with a distributed HPA architecture has additional benefits in thermal management and redundancy. However, for a minimal platform designed for constellation solutions the inherent low duty cycle per platform and constellation redundancy open another axis in the system design trade space.

For SAR, the achievable range resolution is independent of the spacecraft height, and unambiguous imaging can only be achieved by sideways imaging away from Nadir. Range resolution depends on the achievable bandwidth of the receiver (as determined by the transmit pulse width). For sub-metre resolution the RF bandwidths required imply significant NRE on the design of both digital and RF payload electronics. With spaceborne imaging geometry an antenna aperture of several square metres is required

as a minimum. Given the simplistic relationship that best stripmap resolution is half the antenna length, then for an antenna with sufficient aperture, resolution of the order of 2m or better usually requires spotlight mode operation. Spotlight mode operation is not only more complex and more costly to implement but inherently suits applications targeted at smaller areas rather than wide regional coverage.

By considering the equation in Table 2 it is also apparent that image quality scales with the size of the spacecraft (i.e. not unexpectedly with antenna size and transmit power). Like optical imaging, multiple looks can be used to improve image quality, or to examine the scene with different polarisations. Support for multiple polarisations can be important in a number of applications beyond plain imaging and surveillance, however support for multiple polarisations can drive the need for doubling up on some of the SAR payload hardware. As such it is possible to make SAR spacecraft smaller if just supporting single polarization imagery.

In summary, the SAR payload cannot be considered in isolation from the spacecraft bus for a small spacecraft, as reducing its size and mass drive up the spacecraft power demands and bus size and mass. Higher frequency bands are advantageous for making smaller SAR spacecraft regardless of the resolution, and operating in a simple single polarisation mode is also important. Accepting lower data quality is another area that permits the spacecraft to be made smaller.

2.3 Satellite bus trades

Several characteristics of a SAR payload affect spacecraft sizing. Principally these are the required physical size and mass of the SAR antenna and associated processor, the amount of power required and the associated thermal constraints, and the matter of on-board data storage and data return. Some of these drivers mean that it is unlikely that a "standard satellite bus" can be used without modification to accommodate a SAR payload. SAR has particular characteristics which require special attention to the design of the bus power system and data handling system. The SAR payload is also likely to dominate the spacecraft shape and physical size which will require careful attention to be paid to the attitude control system. Some highly desirable SAR applications such as interferometric SAR further drive the guidance, navigation and control system.

As an active means of remote sensing, SAR requires significant power in the majority of mission implementations. In a traditional SAR mission with a single spacecraft, or a constellation of spacecraft within the same plane, that power can be taken directly from solar arrays as the spacecraft is always in sunlight a favourable 6am-6pm sun-synchronous orbit. This also provides the opportunity for continuous radiation of excess heat to deep space. However when considering constellation missions capable of imaging at different times of day, it must be assumed that the spacecraft will have to cope with eclipse and varying sun-beta angle when considering multi-plane constellations. Even if eclipse operation were to be avoided, storing power becomes desirable to reduce the size of the satellite and solar panels.

Power generation and storage are always strong drivers on any spacecraft physical size. Furthermore, as power conversion to Radio Frequency (RF) power is quite inefficient even with modern technology, a significant amount of heat is generated during SAR payload operation. As spacecraft become smaller, it becomes more difficult to thermally

manage a SAR payload. A normal bus power system is unlikely to be able to handle the pulsed power nature of a SAR spacecraft, and it necessary to introduce a power handling unit to interface the SAR payload to a typical spacecraft power system.

As the SAR return signal power reduces with the fourth power of distance from the target, one obvious way to reduce spacecraft power and hence size would be to fly in a lower orbit. Ultimately this requirement must be balanced by the amount of propellant required to maintain the spacecraft in the desired orbit during its design lifetime. Conventional propulsion systems are bulky and expensive, whereas electrical propulsion systems have much less heritage and would require significant power in order to provide adequate thrust. For this reason most SAR spacecraft are designed for operation at altitudes between 500 and 700km.

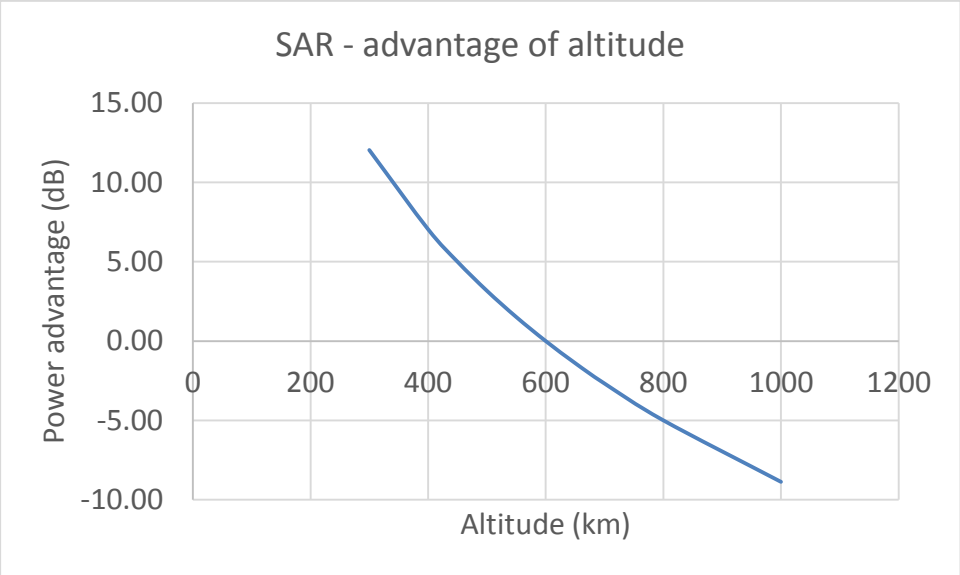

Figure 3. Power advantage over altitude (relative)

Thermal management of the spacecraft is another important consideration. Power amplifiers such as TWT's or GaN solid-state power amplifiers have system efficiencies of ~25% once incorporated into a full payload. Assuming 900W RF power being transmitted with a 25% duty-cycle that means 675W of heat being generated during payload operation. In addition data capture and the remainder of the payload are likely to generate further heat and so it is necessary to get rid of 800W during operation. Given a simple panel radiator of 30x30cm with an emissivity of 0.92, it is only possible to radiate approximately 100W of heat into deep space [7]. As such the radiator and SAR assembly will heat up 7x faster than heat can be dissipated to bring the temperature back down, which means 7 minutes of cool-down for every minute of operation. Depending on how close the payload is operating to the thermal limits, which depends on specific design and sun-beta angle at the time operation, it may be necessary to use heavy thermal heatsinking in order to maintain manageable temperatures. E.g. a 3.5kg Aluminium heatsink would increase in temperature by 0.1deg/s [8]. For smaller spacecraft clearly the mass of a heatsink and fitting an efficient 30x30cm panel may ultimately become a limit in how small a SAR spacecraft can be built given a desired imaging time for each orbit.

The tables below consider an energy budget for a simplistic scenario to help illustrate the challenges posed for a small satellite power system. It considers scenarios with SAR and downlink operation during either sunlight or during eclipse. The table assumes a modest satellite bus power drain which would have to cover all housekeeping operations and spacecraft attitude control. The downlink power needs to cover downlinking and associated data recorder (which in practice may need to be permanently powered). The SAR power needs to take account both of the imaging as well as the associated data capture.

Table 3. Energy in – per orbit

Solar Array Power	120	W
Eclipse period	30	Min
Sunlight period	70	Min
Energy generated	**140**	**Wh per orbit**
SAR power drain	1.0	kW
SAR duty cycle	1	min/orbit
Satellite bus drain	60	W
Downlink drain	120	W
Downlink duty cycle	10	min/orbit

Table 4 – Energy out – per orbit

	Sunlight operation		Eclipse operation		
	Sunlight	Eclipse	Sunlight	Eclipse	
Bus	70	30	70	30	Wh
SAR	17	0	0	17	Wh
Downlink	20	0	0	20	Wh
Battery use	67*	30	-	67	Wh
Energy out	**137**				**Wh per orbit**

* For 1 minute of SAR and 10 minutes of downlinking, as in each case power drain temporarily exceeds power generation.

The scenario illustrated in the tables below roughly balances the power-in/power out for operating the SAR payload and downlink for 1 minute per orbit. It is clear that should the duty cycle be increased, initially it will start driving up the size of the solar panel area and mass, and the battery capacity and mass. Also as the operational duty cycle goes up, the power drain of the bus becomes less significant and the payload becomes the design driver. In addition the tables show the need for careful battery design, with potentially multiple charge/discharge cycles for each SAR imaging, downlinking or eclipse event. Assuming a typical 25% DOD for the battery, a 280Wh Battery would be required (~2kg, 1 litre volume).

It is also worth examining the solar array area and mass required for this scenario. To generate 140Wh per orbit, 120W of solar array power is a minimum requirement (2 off 35x60cm wings weighing 1kg). In practice larger arrays will be required to cope with varying beta angles experienced in constellations that can image at different times of day. Inefficient “fixed” orientation arrays may need to be three times bigger.

In order to determine the effect of data volume on the spacecraft size, data generation must be examined. If we assume I/Q sampling to just 8 bits per sample across a 5km swath width, instrument data rates reach around 560Mbps, generating 4Gbytes over 1 minute of operation. To downlink this in the same orbit, an 80Mbps X-band downlink would be required as illustrated in the data budget below. Reception in two polarisations would double the data rates generated and would require doubling of the downlink data

rate. The only impact on spacecraft size would be in the inclusion of the extra receive chain. Typical downlink data rates of hundreds of Mbps need a medium gain steerable antenna, accommodation of which on a small platform can be problematic.

Table 5 Data budget

Data Generation		**Data Downlinking**	
Ground velocity (500km)	7071 m/s	Downlink rate	80Mbps
8 bits (I+Q) 1m over 5km swath	70.71 Msamples/m	Protocol Efficiency	80%
Data rate	546Mbps		
Payload duty cycle	1 min	Pass time	10 min
Data generated	4.1 GBytes	Data received	4.7 GBytes

In practical systems lifetime and reliability are also key factors. Adding simple bus redundancy can dramatically increase achievable lifetime for relatively little cost. Such trades become important in applications where return on investment is more important than simply minimising capital expenditure.

In summary, the satellite bus can be made smaller by limiting the spacecraft operational duty cycle, which limits the demand on solar panel area, battery capacity, and payload data recorder and downlink chain hardware.

3. WORKED EXAMPLES

Various small SAR spacecraft designs have been published in recent years including a at the previous IAA conference on small satellites for EO [3, 9]. Also recently RainCube [10] has demonstrated a 12kg radar satellite focused on precipitation measurement.

NovaSAR, and CarbSAR are two examples of how application trades affect a SAR spacecraft design.

3.1 NovaSAR

At the time of the NovaSAR project was started, it was the smallest SAR satellite planned to be economically sustainable in addressing commercial services [11]. In order to address a range of applications, the spacecraft was designed to operate in an unconventional SSO 10:30 orbit, utilise S-band, includes an AIS receiver, and implements a number of modes including quad-polar capability. Although it can be used as a standalone spacecraft, it is designed with operation in constellations in mind. The applications considered having commercial value minimized include (1) Ship detection and tracking (2) Oil spill monitoring, (3) Forestry management, (4) Resource monitoring, (5) Border monitoring, (6) Disaster management, (7) Land use and agriculture mapping, (8) Rice monitoring and (9) Soil moisture.

Key factors in making NovaSAR possible have been to leverage the latest high-efficiency semiconductors to reduce the needed on-board power, the choice of S-band as the transmission band, and the approach to defining modes of operation to serve a range of applications. Coupled with this, NovaSAR-1 was the first to include AIS within the radar spacecraft design, and employs a novel funding model allowing geographically disparate users to each act as owner-operator sharing the mission costs

NovaSAR- was launched in September 2018 after a minimum number of users had been secured, and first sample images have been published. It is being taken into full operation during 2019 with a small number of users sharing the full satellite capacity. The performance figures and modes are tabulated below.

Table 6.

Parameter	Value
Imaging frequency band	3.1-3.3 GHz
SAR Antenna	Microstrip patch phased array (3x1 m)
No. of phase centres	18
Peak RF power	1.8 kW
Polarisations	HH, HV, VH, VV
Imaging polarisation	Single, dual, tri or quad-polar
AIS Antenna	2 orthogonal mounted monopole antennas per receiver
Design life for operations	7 years
Design Mass	<440 kg
Optimum orbit	580 km SSO (LTAN 10:30)
Propulsion system	Xenon
Payload data memory	2xHSDR (32 GBytes) + 2xFMMU (512 Gbytes)
Downlink rate	500 Mbps
TT&C frequency band	S-band (2025-2110 MHz, 2200-2290 MHz)
Downlink frequency band	X-band (8.025-8.4 GHz)

Table 7.

Mode	Ground range resolution	Incidence angles	Swath width (across track)	Sensitivity (NESZ)	Azimuth ambiguity ratio (DTAR)	Range ambiguity ratio (DTAR)	No. of looks
0 Calibration	N/A	N/A	N/A	N/A	N/A	N/A	N/A
1a ScanSAR	20m	15.8-25.38°	100 km	<-18.5 dB	<-17 dB	<-17 dB	4
1b ScanSAR	20m	25-29.4°	50 km	<-20 dB	<-17.5 dB	<-16.5 dB	4
2 Maritime	6m range 13.7m azimuth	34.5-57.3°	400 km	<-11.4dB	N/A	<-18 dB	1
3a Stripmap	6m	16-25.38°	20 km	<-19.5 dB	<-20 dB	<-18 dB	3
3b Stripmap	6m	21.83-31.2°	13-20 km	<-18.5 dB	<-17 dB	<-16.5 dB	3
3c Stripmap	10m	13.4-27.4º	20km	<-19 dB	<-15dB	<-15dB	5
4a ScanSAR Wide	30m	14-27.39°	140 km	<-19 dB	<-17 dB	<-15.5 dB	4
4b ScanSAR Wide	30m	27.35-32.01°	55 km	<-19.5 dB	<-17.5 dB	<-15.5 dB	4

NovaSAR was designed to a budget which did not include development of a deployable antenna technology. It was not designed solely for constellations so a single satellite is designed to provide sufficient utility to justify the required investment. Although not as small as some small satellite SAR concepts that have followed, careful trading of imaging performance against other system parameters resulted in a relatively small aperture payload antenna. This enabled an innovative spacecraft design with the payload antenna integrated into the structure. The small dimensions of the antenna also helped to mitigate concerns like thermos-elastic stability.

Figure 4. NovaSAR in antenna test chamber at Airbus

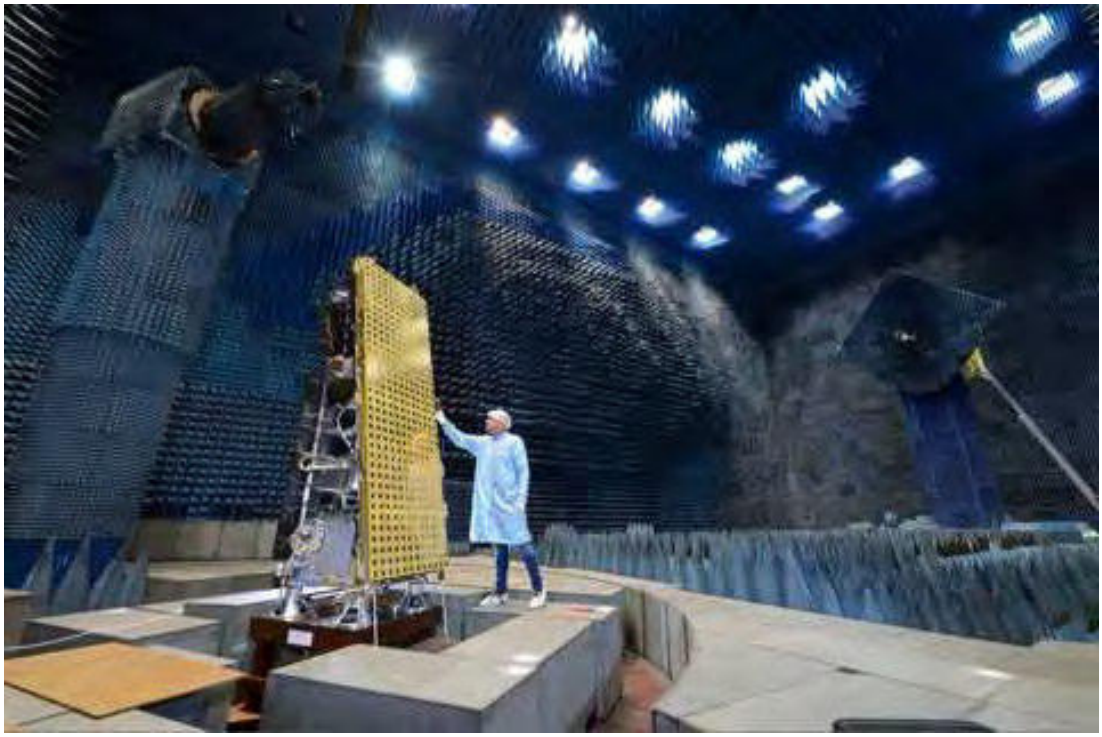

Figure 5abc. NovaSAR multi-polar images Mississippi Delta and gulf of Mexico (left), Suez Canal and red Sea (Right), and Cape of Good Hope (bottom)

3.2 CarbSAR

CarbSAR is an SSTL concept for an ultra-low cost SAR satellite intended for operation in SAR or mixed Earth Observation constellations, providing very high across relatively small scenes. CarbSAR utilises the platform heritage of the Carbonite optical satellite series and combines it with an innovative deployable X-band SAR antenna and payload. Although capable of stripmap operation its primary utility is anticipated to come from sub-metre resolution repeat visit applications.

Table 8. CarbSAR specifications

Parameter	**Specification**
GSD	0.5m
Swath	4km
Spectral bands	X-Band (9.6GHz)
Throughput	180GByte per day 45 spotlight mode images per day
Parameter	**Specification**
Reference orbit	525km SSO with 10:30 LTAN
Mission lifetime	5 Years
Launch mass	140kg
Data storage	120GByte
Downlink	500Mbps

4 CONCLUSIONS

As SAR systems become more popular with commercial companies supporting data analytics applications, there is significant room for a variety of systems that utilize small SAR spacecraft in order to address some specific markets. These system require low-cost SAR systems with payload characteristics matched to the specific market, rather than the general purpose SAR spacecraft launched under some national and space agency projects. Such small SAR spacecraft may need to be deployed into multi-plane constellations in order to observe targets at different times of the day.

It has been shown that the design of small SAR spacecraft is highly complex, and also challenging based on payload requirements and how those drive the spacecraft design. Although the physical limitations do not preclude the potential for microsatellite class (10-100kg) SAR spacecraft, the real questions is why you would develop those. Doubling the orbital duty cycle of a SAR spacecraft cycle does not double the size and cost of the overall spacecraft, and as such the only rationale for reducing the size of the spacecraft would be if working to a fixed budget, or in implementing a multi-satellite constellation.

The SAR payload itself drives spacecraft cost and size, and use of higher frequency bands, low mass density antennas, and limiting operational duty cycle are necessary. There are design compromises between bus solar array size and payload antenna size which limit spacecraft miniaturisation. Thermal design can also ultimately limit what is possible on smaller spacecraft if operational duty cycle is not restricted. It may also be necessary to limit either the image quality or the achievable resolution. As a result a good understanding of how the data will be used is required by the mission designer.

Using an “off-the-shelf” bus to host a radar spacecraft is generally problematic, and most standard bus designs would require some modification to account for the specific power and attitude control imposed by a SAR payload. Furthermore, doubling the orbital duty cycle does not double the size and cost of the overall spacecraft, and as such the only rationale for reducing the size of the spacecraft would be if working to a fixed budget, or in implementing a multi-satellite constellation.

NovaSAR, and its follow-on SAR concept CarbSAR address two particular variants of small SAR spacecraft addressing very specific applications, and have been presented as examples of how small SAR missions can help address specific markets and end-users.

5. REFERENCES

[1] Douglas C Comer, Michael J. Harrower, Mapping archaeological landscapes from space, DOI 10.1007/978-1-4614-6074-9 (accessed May 2019 https://books.google.co.uk/books?id=yWJDAAAAQBAJ&printsec=frontcover#v=onepage&q&f=false)

[2] da Silva Curiel et al, What can we expect from very high resolution small satellites, IAA Symposium on small satellites for Earth Observation, Berlin, May 2017.

[3] Saito et al, compact X-band SAR with deployable plane antenna – project of a100kg-class satellite, Small Satellite Systems and Services (4S) Symposium, Valletta, Malta, 2016.

[4] Satellite-Based Earth Observation (EO, Northern Sky Research, 10th Edition October 2018)

[5] Curlander and McDonough, Synthetic Aperture Radar Systems and Signal Processing, published by Wiley, 1991

[6] A.Freeman, Design Principles for Smallsat SARs, AIAA/USU Conference on small satellites, Logan UT August 2018

[7 [https://space.geometrian.com/calcs/radiators.php (accessed May 2019)

[8] [http://hyperphysics.phy-astr.gsu.edu/hbase/thermo/spht.html#c2 (accessed May 2019)

[9] N.Ahmed et al, An extended Chirp Mode Pulsed SAR Concept for low-cost Microsatelite SAR, IAA-B9-1301, Symposium on small satellite for Earth Observation, Berlin May 2013.

[10] https://directory.eoportal.org/web/eoportal/satellite-missions/r/raincube (accessed May 2019)

[11] Whittaker et al, Changing the Paradigm – technologies and cost trades in establishing the NovaSAR constellation. IAC-12-B1.2.10, International Astronautical Congress 2012, Naples.

STRATOS - A payload for 3U CubeSats that collects thousands of neutral atmospheric soundings per day

O. Nogués-Correig[1] , L. Tan[2], T. Yuasa[2] , R. Marshall[1], J. Ringer[2], A. Warzyński[1], V. Irisov[3] , V. Nguyen[3], T. Duly[3], S. Esterhuizen[4], P. Jales[1], D. Masters[3], D. Ector[3], J. Spark[1], J. Cappaert[1] , P. Platzer[4]

[1]Spire Global UK Ltd.
Unit 5A, Sky Park 5, 45 Finnieston Street, Glasgow, G3 8JU
Phone: +44-141-343-8260 ext 345 Mail: oleguer.nogues-correig@spire.com

[2]Spire Global Singapore PTE Ltd.
19 China Street #02-01, Far East Square Singapore 049561

[3]Spire Global Inc.
1050 Walnut Street, Suite 402, Boulder, CO 80302 USA

[4]Spire Global Luxembourg S.a.r.l.
33 rue Sainte Zithe, 2763 Luxembourg

Abstract: About 3% of the gross world product fluctuation is associated to weather variability. Improved weather forecast skill can greatly contribute to reduce its impact to the economy, and hence to create wealth and welfare. Atmospheric soundings derived from radio-occultation (RO) data greatly contribute to improved numerical weather predictions. Studies show that a daily volume of ~100k RO soundings/day would halve the error of global weather forecasts. To help reduce the impact of weather to the world economy, Spire Global is deploying a growing constellation of nanosatellites —more than 70 as of today— each of which carries the STRATOS GNSS receiver payload that collects RO data meeting the standards required by the meteorological community. As of today the Spire constellation has the capacity to collect ~5000 soundings/day, a figure the company plans to increase by at least 3 times as much by 2020. Spire launches tens of nanosatellites per year at a moderate cost. This will make the production of 100k soundings/day feasible and have a major impact on weather prediction.

1. THE IMPACT OF WEATHER TO GLOBAL ECONOMY

It is a fact that weather variability impacts the world economy. Since economy drives humans' life quality and well-being, two central questions arise:

1.1 What Fraction of World Gross Product is Disrupted by Weather Variability?

An accurate lower bound is derived considering all extreme weather events during the period 1980-2017: US $100 bn losses and 45,000 deaths per year [1].

[2] estimates an upper bound breaking the U.S. gross domestic product (GDP) for year 2000 down into industry sectors. The author subjectively identifies which sectors have either operations, demand or price sensitive to weather, concluding that ~⅓ of the private industry activities have some degree of weather and climate risk.

[3] presents a comprehensive empirical analysis of the sensitivity of the U.S. economy as a whole to weather variability, using statistical methods based on accepted economic theory. They estimate the variation in U.S. economic activity associated with weather variability to be ~3.4% of GDP.

Based on the latter, we consider ~3% as a reasonable estimate of global GDP variation directly associated to weather, totalling ~US $2.5 trillion for year 2018 [4]. At the same time, during the period 2012-2018 the world's gross product growth was ~3.5% [5]. If we could totally eliminate, at zero cost, that 3% variability due to weather, we could almost double world GDP growth. That is an ideal case.

1.2 What Actions Can We Take to Minimize Weather Impact to Global GDP?

[3] states that some portion of that 3% of global GDP variation due to weather could be mitigated by investments in production methods (e.g., insulation in the roof of a factory, better drainage systems along transportation routes, more weather resistant crops, etc.) and some portion may be mitigated by improved forecasts [6].

[3] also warn that there is nothing in their analysis to indicate how much of the GDP variability due to weather could be mitigated by investments in infrastructure, technology, or forecasting or, given that they do not know how much those actions may cost, whether the benefits would be more or less than the costs.

The latter question remains mostly unaddressed. The only well quantified fact is that extreme weather events produce globally US $100 bn losses and 45,000 deaths per year [1]. Those could be greatly minimized by improving numerical weather prediction (NWP), e.g., by improving accuracy by a few degrees or in providing one-day earlier warnings [7].

Spire's vision is to improve the skill of weather forecasts by increasing the amount and quality of weather data injected into NWP models. We believe that the benefits go far beyond mitigating the effects of extreme weather events. Weather forecasts also contribute to making better short-, mid-, and long-term decisions across many industry sectors [2] and the public, and hence are likely to foster large net gains in GDP.

2. GNSS-RO ATMOSPHERIC SOUNDINGS IMPROVE FORECASTS

2.1 The GNSS-RO Atmospheric Sounding Technique

Atmospheric radio occultation (RO) relies on the detection of a change in a radio signal as it passes through a planet's atmosphere and occults behind it. When electromagnetic radiation passes through the atmosphere, it is refracted or bent [8]. The magnitude of the refraction (bending angle α in Figure 1 below) depends on the gradient of the atmosphere refractivity $n(r)$ normal to the path, which in turn depends on the chemical composition of the air, its pressure and temperature [9]. Hence, the former can be related to temperature and water vapor content along a vertical profile normal to the radio signal path. The bending effect is most pronounced when the radiation traverses a long atmospheric limb path. At radio frequencies, the amount of bending α cannot be measured directly. Instead, the bending can be calculated using the Doppler shift of the signal given the geometry of the emitter and receiver.

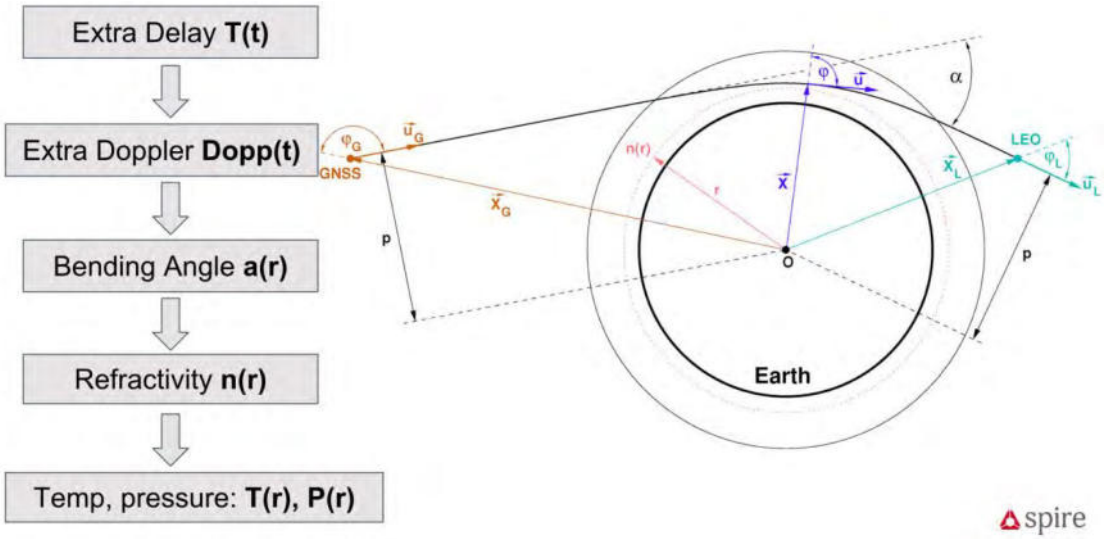

Figure 1 - Planetary atmospheric sounding basic mechanism. Right hand side: GNSS radio occultation geometry defined by its key parameters. Left hand side: inversion process of the data collected during an occultation, going from calibrated observable data (extra propagation delay of bent ray with respect to free space straight line propagation) to final vertical profile of dry temperature and pressure. On Earth, humidity is usually present below 10-12 km height. In this range, a-priori values of temperature are obtained from weather forecast models, eg, GFS [10], and that is injected on the inversion of refractivity $n(r)$ to obtain humidity estimates.

Global Navigation Satellite System Radio Occultation (GNSS-RO) refers to a radio occultation that involves a radionavigation signal transmitted by a GNSS satellite that is received by another satellite in low Earth orbit (LEO). As of January 2019 there are ~115 active GNSS satellites transmitting radionavigation signals, offering immense opportunity to collect RO atmospheric soundings from LEO (see subsection 3.1 below).

2.2 GNSS-RO Data Injects Rich Information to NWP Models

On April 2006 the COSMIC radio occultation mission was launched, consisting of six microsatellites in LEO orbits at 512 km height and 72° inclination. The satellites provided between 2,500 and 3,000 daily RO atmospheric soundings during the nominal mission timeline. So far, COSMIC has been the largest absolute contributor to the global volume of collected RO data [11]. The mission represented a revolution in atmospheric sounding from space, as it was able to prove that RO soundings provide precise, accurate, self-calibrating, all-weather global observations useful for weather, climate, and space weather research and forecasts [12].

Table 1 - Main performance characteristics of RO-derived atmospheric sounding data

Accuracy	Stability	Observing Conditions	Coverage	Vertical Resolution	Lean Sensor
< 0.05K	long-term	all-weather	global, surface to 50 km height	~100 m (at surface)	compact, low power

Subsequent analysis [13] demonstrated that GNSS-RO data produces the fifth largest impact in the weather forecast error reduction (10%) despite only representing ~3% of

the observations assimilated by NWP systems. This impact ratio is unprecedented. The GNSS-RO measurements complement the information provided by satellite-measured radiances from instruments such as AMSU, IASI, AIRS, etc. [14] because RO data have better vertical resolution and can be assimilated without bias correction.

Currently, the RO data volume publicly available for ingestion into NWP models is ~3k soundings/day (2006-2019 average [11]), though it is diminishing as COSMIC-I, the main contributor to that figure, is reaching its end of life. Given such high impact of RO data, the natural question is how much better the forecast error reduction impact would be if a larger RO observations data volume was available. [15] shows that scaling the GNSS-RO data observations up has a very positive impact. For example, they show that for a 12h forecast at 100 hPa height, scaling the current ~3k observations/day to 128k, would reduce the global average forecast error from 0.6 K to 0.3 K. If available, that RO data volume would effectively halve the weather forecast error of current NWP systems. Spire Global has today one of the largest RO data sets available on the market, and the goal to collect soon +10k soundings/day.

3. SCALING UP DAILY VOLUMES OF GNSS-RO SOUNDINGS

3.1 Maximum Possible GNSS-RO Data Harvest per LEO Satellite

As of January 2019 there are 115 active GNSS satellites transmitting radionavigation signals: GPS: 31, GLONASS: 24, Galileo: 22, QZSS: 4, Beidou: 35 [16]. Using real orbit data in computer simulations to predict positions of all GNSS satellites and one LEO satellite -averaging through mid inclination, polar, and sun-synchronous LEO orbits at 400-700 km height- we determined that on average a LEO satellite observes 17.5 RO events (vertical atmospheric soundings) per GNSS satellite and per day. Hence, as of today, the maximum possible daily GNSS-RO atmospheric sounding data harvest potential for a LEO satellite is:

(**Eq. 1**) (115 GNSS sats) x (17.5 RO events /GNSS sat /LEO sat /day) = **2000 RO events /LEO sat /day**

The aforementioned simulations show that the geolocations of these vertical atmospheric soundings is almost randomly distributed across the globe.

3.2 Spire Nanosats Constellation - A Cost-Effective Way to Scale Up RO Data

As of January 2019 Spire's space segment is made of a wholly owned and developed constellation of 72 operational 3U-cubesats [17] placed in LEO orbit [18], plus a global ground station network to download the data. The constellation keeps growing at a rate of 30-50 additional 3U-cubesats launched per year, which Spire produces in its own fully integrated satellite manufacturing, assembly, and test facilities in Glasgow, UK [19]. The satellites are produced in batches of 4 to 10 units, with a manufacturing pace per batch of around 8 satellites/month. Once produced, the batch of nanosatellites is quickly integrated to a rocket and launched to space usually within less than two months.

The company uses most launch opportunities to LEO orbits at 400-700 km height, in orbital planes ranging from mid inclination to polar and sun-synchronous, the latter

being the most common. On each new launch the company integrates a batch of up to 10 satellites on the rocket, usually as secondary payloads. This installation is done through specialized operators that offer quick access to space, e.g. [20].

This new way of proceeding is radically different to how the legacy space industry has operated since its inception and almost up to current date (Table 2). The new philosophy can also afford a quicker replacement of satellites, every two years, and makes design ruggedization less of a concern because missions are made of a network of many tens of satellites, for which failures on a few units do not put the mission goals at risk.

Table 2 - Comparison of legacy versus new space mission design approaches

Approach	Mission Cost	Design Cycle	Value on	Satellite Reconfiguration
Legacy / New	US $1 bn / $ 0.1 bn	15 yr / 5 yr	HW / Data	No / Yes

Spire has embraced this new way to operate space missions. This is what makes practical and cost-effective to multiply by almost two orders of magnitude the current GNSS-RO data harvest, from 3k events/day to 100k. To disseminate this data, Spire has launched strategic partnerships, including for example internationally recognized public institutions that are leaders in the fields of Earth science and meteorology such as NASA [21] and NOAA [22].

4. SPIRE GNSS-RO DATA COLLECTION CHAIN

The first element of the chain is the **STRATOS GNSS-RO payload** installed in a Spire LEMUR2 [23] 3U-cubesat on LEO orbit (Figure 2). The payload is made of the **STRATOS GNSS Receiver** and three antennas. The receiver simultaneously collects many dual frequency signals from the visible GNSS satellites, propagated through line-of-sight paths, using the precise orbit determination **(POD**) antenna, which has an isotropic hemispherical radiation pattern and is installed on the top of the satellite, pointing to Zenith. The receiver uses these signals for real-time (RT) positioning and to determine, on post-processing, the LEMUR2 precise trajectory with pos/vel accuracies of cm and sub-mm/s, respectively. The receiver also collects the signal from those GNSS satellites that are seen occulting behind the Earth. For this purpose it uses two high-gain radio-occultation (RO) antennas, called forward (**FRO**) and backward (**BRO**) arrays installed at the front and back of the LEMUR2 satellite, whose patterns point to the Earth horizon, aligned with the velocity and anti velocity directions. The occulted signals propagate through a refracted path that crosses the atmosphere at low grazing angles. The GNSS signals from all three antennas are separately collected and I&Q downconverted to baseband and digitized with a radio-frequency (RF) front-end that has three antenna inputs.

The digital signal processing (DSP) back-end picks up those digitized streams, tracks the observed GNSS signals on them, and creates **Raw Observation Data Files**, where it records at adequate sampling rates the observed apparent propagation delays of all tracked GNSS satellites, at two frequency bands. The reason each satellite signal is recorded at two frequencies is to remove the ionospheric delay from the observations.

The raw data is split into the following streams: (a) **Precise Orbit Determination (POD) Data**: apparent group and phase propagation delays of the line-of-sight visible GNSS satellites, close-loop tracked and sampled at 1 Hz; (b) **Radio Occultation (RO) Data**: apparent phase propagation delays of an occulted GNSS satellite, open-loop tracked [24] and sampled at 50 Hz; and (c) **Reference Satellite (RST) Data**: apparent phase propagation delays of only one line-of-sight visible GNSS satellite, sampled at 50 Hz. The latter is used on ground post-processing for ultra-precise calibration of the STRATOS receiver clock during an occultation event. During an RO observation the LEMUR2 attitude determination and control system (ADACS) logs at 1Hz **Spacecraft Attitude Data** with respect to the orbital reference frame.

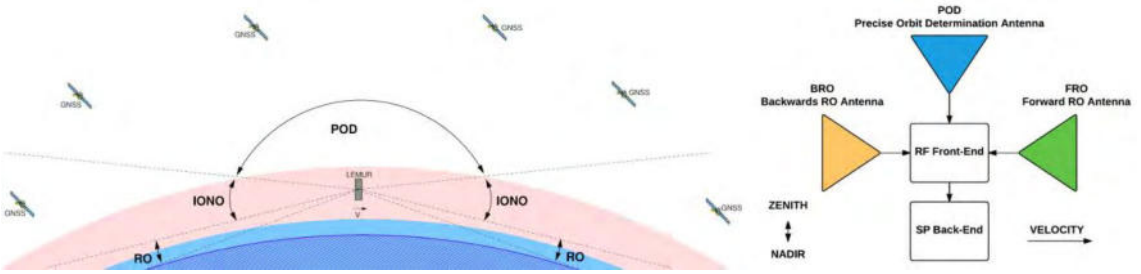

Figure 2 - STRATOS RO payload operating scenario (left) and top-level block diagram (right).

Immediately downstream there is a **Space to Ground Interface**, composed of the Spire ground stations network, plus an automated operational intelligence distributed between the LEMUR2 satellites' side and the data back-end on ground. The latter controls the automatic operation and download of the Raw Observation Data files from each STRATOS payload on orbit, to the **Spire Processing Center** on ground, where the **RO data analysis, calibration and quality check** occurs. To kick off said analysis, the automation requires all STRATOS payload aforementioned data downloaded, plus the precise orbits of the GNSS satellites tracked during the observations. These are retrieved automatically from an external provider, for example IGS [25]. At high level, this on-ground process involves: (1) compute precise orbit of the LEMUR2 center of mass (position, velocity and receiver clock error); (2) calibrate apparent propagation delay of occulted signal; (3) compute the bending angle α of the occulted signal versus height and geographical coordinates; (4) compute refractivity profile versus height with the bending angle as input; and (5) compute Pressure, Temperature and Humidity profiles versus height with the refractivity as input. The whole process is convoluted.

5. STRATOS GNSS-RO PAYLOAD PERFORMANCE

As of today (see Table 3 below) the payload is capable of observing, simultaneously, all RO events of either GPS (L2C), QZSS and GLONASS, or GPS (L2C), QZSS and GALILEO. The current combination of payload power consumption and the energy available in the present version of LEMUR2 satellite, allows for a daily RO harvest of about 500 events/satellite, leading for example to an overall daily harvest of +12,000 RO events if 25 LEMUR's are used. By 2020 the planned improved payload plus LEMUR2 performance will allow for an overall RO harvest that is multiplied 3 times (rightmost column of Table 3 below). This is consistent and aligned with the Spire goal to provide tens of thousands of profiles/day.

Table 3 - Present and planned STRATOS GNSS-RO receiver performance

FEATURE	Present - 2019 / Q1	Planned - 2020 / Q1
Observational Capability	GPS L1CA+L2C (19 sats) QZSS L1CA+L2C (4 sats) GLO L1+L2CA (24 sats) GAL E1 + E5bQ (22 sats) (*)	GPS L1CA+L2C + L2P (31 sats) QZSS L1CA+L2C (4 sats) GLO L1+L2CA (24 sats) GAL E1 + E5bQ (22 sats) BEI 2 and 3 (35 sats)
Collected Daily RO Soundings	~500 soundings/day	~1500 soundings/day
Daily Downloaded Volume (**)	~ 35 MBytes	~ 115 MBytes
Power Consumption	3.7 W	2.8 W
Mechanical	90 x 90 x 14 mm, 190 g	90 x 90 x 14 mm, 190 g
(*) GLONASS and GALILEO cannot be observed simultaneously, either one or the other. (**) equal to the daily soundings, times the average raw data volume per sounding (after compression)		

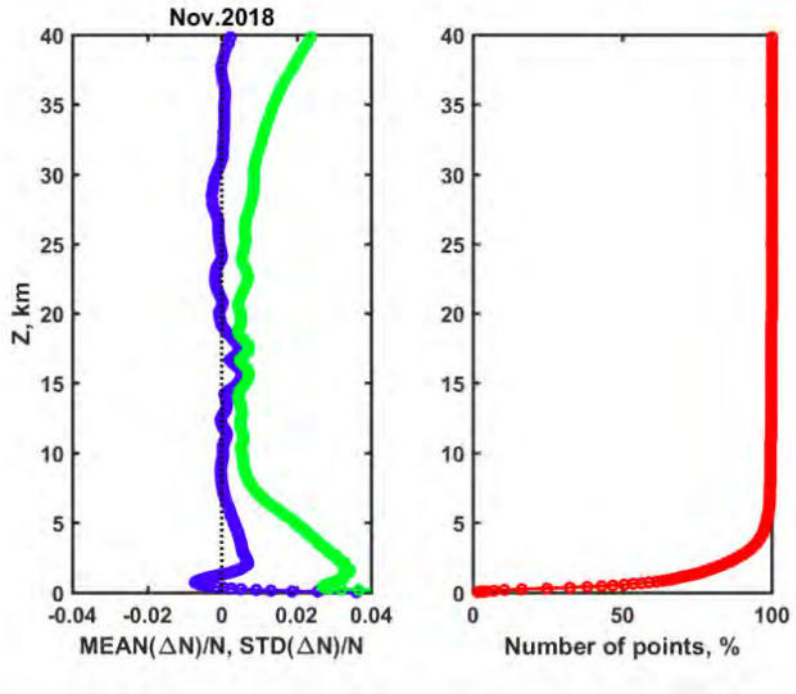

Figure 3 - Left: statistical comparison [26] of the normalized refractivity difference between Spire RO-derived atmospheric soundings, and those retrieved from the Global Forecast System [10]. The vertical axis represents the height at which the sounding is measuring refractivity. Right: percentage of soundings that penetrate down to a given height above mean sea level.

Careful statistical analysis of Spire RO data (Figure 3 above) shows that it conforms to quality standards accepted by the meteorological community [26]. About 70% of soundings reach below 1 km above mean sea level, which is better penetration than the average COSMIC-I performance. This improvement we believe is mostly attributable to refinements on the RO calibration and inversion software at the Spire ground processing center. Given that the average global land elevation above mean sea level is ~800 m [27], it is reasonable to think that Spire's RO atmospheric sounding data is close to the best possible penetration performance.

6. REFERENCES

[1] NatCatSERVICE - Data source for information on natural catastrophes worldwide. Available online at: https://natcatservice.munichre.com (accessed January 2019)
[2] J.A. Dutton, Opportunities and Priorities in a New Era for Weather and Climate Services, BAMS, 1303-1311 (September 2002)
[3] J.K. Lazo et. al., Economic Sensitivity to Weather Variability, BAMS, 709-230 (June 2011)
[4] Statista: GDP from 2010 to 2022. Available online at: https://bit.ly/2xRzOOc (accessed January 2019)
[5] Wikipedia: World GDP. Available online at: https://bit.ly/2e3XHwD (accessed January 2019)
[6] R.E. Morss and K.A. Miller, A Systematic Economic Approach to Evaluating Public Investment in Observations for Weather Forecasting, AMS Monthly Weather Review (February 2005)
[7] M. Matsueda and T. Nakazawa, Early warning products for severe weather events derived from operational medium-range ensemble forecasts, Meteorol. Appl. 22: 213–222 (2015)
[8] Wikipedia: Radio Occultation. Available online at: https://bit.ly/2RJgsbL (accessed January 2019)
[9] J.M. Rüeger, Refractive Index Formulae for Radio Waves, FIG XXII International Congress Washington, D.C. USA (April 19-26 2002)
[10] Wikipedia: Global Forecast System. Available online at: https://bit.ly/2S8Cjc5
[11] Global counter of all aggregated RO data ever produced by publicly funded institutions. Available online at: https://www.cosmic.ucar.edu/ (accessed January 2019)
[12] R.A. Anthes et. al., The COSMIC/FORMOSAT-3 Mission: Early Results, BAMS, 313-333 (March 2008)
[13] C. Cardinali and S. Healy, Impact of GPS radio occultation measurements in the ECMWF system using adjoint-based diagnostics, Q. J. R. Meteorol. Soc. 140: 2315–2320 (2014)
[14] WMO Observing Systems Capability: Instruments. Available online at: https://bit.ly/2Uud95f
[15] F. Harnisch et. al., Scaling of GNSS Radio Occultation Impact with Observation Number Using an Ensemble of Data Assimilations, Monthly Weather Review, vol 141, num 12, 4395-4413 (2013)
[16] Lists of active GNSS sats. Available online at: https://bit.ly/1TuKSDu (GPS), https://bit.ly/2Tj55DX (GLO), https://bit.ly/2SfVxMW (GAL), https://bit.ly/2BbPZZZ (BEI), https://bit.ly/2COzWRT (QZSS)
[17] California Polytechnic State University (CalPoly), CubeSat101 - Basic Concepts and Processes for First-Time CubeSat Developers, CubeSat Systems Engineering Lab (October 2017)
[18] Spire Constellation Orbits: https://www.celestrak.com/NORAD/elements/spire.txt
[19] A Peek Inside Spire's Satellite Engineering. Available online: https://youtu.be/GlNYsRsVLIk (accessed January 2019)
[20] Rocket Labs: https://www.rocketlabusa.com/, NanoRacks: http://nanoracks.com/
[21] D. Mohney, Planet and Spire score NASA commercial Earth science pilot data contracts, Space It Bridge (October 2018). Available online at: https://bit.ly/2FWv00o (accessed January 2019)
[22] Spire Works with NOAA again as part of their Commercial Weather Data Pilot Program. Available online at: https://bit.ly/2MIcRVJ (accessed January 2019)
[23] Gunter Space - LEMUR2 nanosat. Available online: https://bit.ly/2sTBhCm (accessed January 2019)
[24] O. Ao et. al., Rising and Setting GPS Occultations by Use of Open-Loop Tracking, Journal of Geophysical Research, vol 114, (February 2009)
[25] International GNSS System Products. Available online at: http://www.igs.org/products/data (accessed January 2019).
[26] V. Irisov et. al., Recent radio occultation profile results obtained from Spire's CubeSat GNSS-RO constellation, AGU Fall Meeting 2018.
[27] Quora: average land elevation AMSL. Available online: https://bit.ly/2RYpFwU (accessed Jan 2019)

Design of the first Ukrainian PlantSat nanosatellite

Vasyl Brykov[1,2], Boris Rassamakin[3], Natalia Zaimenko[4]
[1]M.G. Kholodny Institute of Botany, National Academy of Sciences of Ukraine
Tereschenkivska str. 2, 01004 Kyiv, Ukraine
Phone:+380442344041, Mail: brykov_vo@nas.gov.ua
[2]RUDN University,
Miklukho-Maklaya str.6, 117198, Moscow, Russian Federation
[3]National Technical University of Ukraine "Igor Sikorsky Kyiv Polytechnic Institute", Ukraine
Prosp. Peremohy 37, Kyiv, Ukraine
Phone:+380442048098, Mail: bmrass@gmail.com
[4]M.M. Gryshko National Botanical Garden, National Academy of Sciences of Ukraine, Kyiv, Ukraine
Timiriasevska str. 1, 01014 Kyiv, Ukraine
Phone:+380442854105, Mail: nbg@nbg.kiev.ua

Abstract: The primary scientific purpose of the PlantSat mission is to investigate the influence of microgravity on plant growth and development, its respiration and photosynthetic activity. To simplify a problem of plant growth support, we propose to develop the miniature closed ecological system (microcosm) using of which requires only corresponding temperature and light regimes. PlantSat will be equipped with sensors of temperature, light, carbon dioxide and oxygen concentration as well as an optical system to detect the plant growth and telemetry. It is planned to test the growth and physiological state of certain plant species selected for space planting in BLSS in monoculture (one crop) or polyculture (multiple crops).

1. INTRODUCTION

It is generally accepted that plants are the necessary part of Bioregenerative Life-Support Systems (BLSS) for astronauts' in the future long-term flights in deep space, visiting Mars, building Moon bases, as the sources of oxygen, food, recycled water. A lot of space experiments, which have been performed on board the orbital stations Salyut, MIR and ISS, clearly showed that plants can grow and develop in microgravity, i.e. plants adapted to the action of this factor, if they were in the more or less optimal conditions for plant growing, namely temperature, humidity, CO^2, light intensity and directivity, in the space green-houses [1, 2]. Significant changes in gene expression, protein synthesis, cell proliferation and ultrastructure in plant responses to real and simulated microgravity have been reported [2]. To date, such plants as *Arabidopsis thaliana* and *Brassica rapa* passed the full cycle of ontogenesis [3, 4, 5], from seed to seed, in space flight. Two generations of *Triticum aestivum* and four generations of *Pisum sativum* have been obtained on orbit [6, 7].

The creation of plant greenhouse BLSS using current technologies used on the ISS and results of previous experiments are not possible. At the same time the maintenance of cultivation chambers of complex design requires constant control. One of the predictable problems is that the use of a large area greenhouse can provide necessary amount of food and oxygen will require the full involvement of the crew to the process of plant celtivation [8, 9]. In addition, almost all plants that were grown on board were annuals with a short life cycle (up to 6 months), and unfortunately the duration of many experiments did not exceed 30 days. The results of previous experiments are not enough to predict the behavior of plants in long space flights. So, further investigations of plant responses and adaptation to microgravity are necessary for the further human space ex-

ploration. Unfortunately, the opportunities for the realizing of experiments with plants on board the ISS are very limited.

2. CLOSED MAN-MADE ECOLOGICAL SYSTEM – A PERSPECTIVE MODEL FOR BIOLOGICAL EXPERIMENTS ON NANOSATELITES

It is known that plants are capable to be in a closed hermetic habitat isolated from the external atmosphere for a sufficient long time (fig. 1a). Isolation of living organisms from the atmosphere is called microcosm or closed man-made ecological system (CMES), and it is a unique tool for research of fundamental processes and interrelations in the global ecosystem [10]. Potentially, the CMES can be used to create life-support systems for space exploration and support life outside the Earth's biosphere [10, 11]. Biosphere 2 project [12] and several other closed systems such as the Bios-3 facility in Krasnoyarsk, Russia [13], Closed Ecological Experimental Facility in Japan [14] are well known. The ability of an orchid *Phalaenopsis pulcherrima* to grow in CMES in 3 dm^2 over 13 years was demonstrated in the M.M. Gryshko National Botanical Garden of the National Academy of Sciences of Ukraine (fig. 1, b). In order to maintain the viability of plants in CMES, it is only necessary to provide temperature and light conditions and any more manipulations are not required, so they are suitable to use in biological experiments on nanosatellites.

Fig. 1. CMES with higher plants that developed in isolated habitats for 1 (a) and 13 (b) years. CMES were created in the M.M. Gryshko National Botanical Garden, Kyiv, Ukraine

Now CubeSats nanosateliites, as the world-wide standard for small satellites, are used for a widely range of scientific and technological experiments, that can be miniaturized, namely Earth observation, environmental sensing and fundamental biological research to testing new space flight systems. Experiments with yeast and E. coli have been performed, the first (PharmaSat1, NASA) – in 2009, the second (EcAmSat, NASA) – in 2017. For example, PharmaSat1 contained a controlled environment micro-laboratory packed with sensors, life-support and optical systems that could detect the growth, density and health of yeast cells and transmit that data for an analysis on Earth.

The primary scientific purpose of the PlantSat mission is to investigate the influence of microgravity on plant growth and development, its respiration and photosynthetic activity and plant-microbial interactions. To simplify a problem of plant growth support, we propose to develop the miniature CMES (microcosm) using of which requires only corresponding temperature and light regimes. PlantSat will be equipped with sensors of temperature, light, carbon dioxide and oxygen concentration as well as an optical system to detect the plant growth and telemetry. It is planned to test the growth and physiological state of certain plant species selected for space planting in BLSS in monoculture (one crop) or polyculture (multiple crops).

A proposed objective is the first attempt to adapt CMES technology for a space experiment with plants using nanosatellites. In future, nanosatellites may become a powerful tool for implementing plant biology programs in space. CMES proposed by us for space biology is a simple miniature artificial biosphere capable of self-regulation. Knowledge gained from the study of plant behavior in CMES in spaceflight conditions will contribute to the emergence of new technology in space biology, namely the creation of a self-regulating extraterrestrial ecosystem that can exist for a long time without human intervention

3. REFERENCES

[1] S.A. Wolff, L.H.Coelho and M. Zabrodina, E. Brinckmann, A.-I. Kittang, Plant mineral nutrition, gas exchange and photosynthesis in space: A review. Adv. Space Res. 51,465–475 (2013)

[2] E.L. Kordyum, Plant cell gravisensitivity and adaptation to microgravity. Plant Biol.16(s1),79–90 (2014)

[3] A.J. Merkys, R.S. Laurinavičius, D.V. Švegždiene, Plant growth, development and embryogenesis during Salyut-7 flight. Adv. Space Res. 4, 55–63 (1984)

[4] B.M. Link, S.J. Durst, W Zhou, B. Stankovic, Seed-to-seed growth of *Arabidopsis thaliana* on the International Space Station. Adv. Space Res. 31,2237–2243 (2003)

[5] M.E. Musgrave, A. Kuang, Y.Xiao, S.C. Stout, G.E. Bingham, L.G. Briarty, M.A. Levinskikh, V.N. Sychev, I.G. Podolski, Gravity independence of seed-to-seed cycling in *Brassica rapa*. Planta, 210,400–406 (2000)

[6] M.A. Levinskikh , V.N. Sychev , T.A. Derendiaeva, O.B. Signalova , F.B. Salisbury, W.F. Campbell, D. Babenheim, F.B. Salisbury, W.F. Campbell, The influence of space flight factors on the growth and development of super dwarf wheat cultivated in greenhouse Svet. Aerospace Environ. Med.33,37–41 (1999)

[7] V.N. Sychev, M.A. Levinskikh, S.A. Gostimsky, G.E. Bingham, I.G. Podolsky, Spaceflight effects on consecutive generations of peas grown onboard the Russian segment of the International Space Station Acta Astronaut.60,426–432 (2007)

[8] A.G. Heyenga The utilization of passive water and nutrient support systems in space flight plant cultivation and research. 6-th Eur. Symp. Space Environ. Contr. *Syst.*867–871. (1997)

[9] V.O. Brykov, Bioenergetics of plant cells in microgravity.Space Science and Technology, 21,84–93 (2015) (in Ukrainian.)

[10] J.I. Gitelson and G.M. Lisovsky, Man-made Closed Ecological Systems. CRC Press, London-New York, 416 p. (2003)

[11] M. Nelson, J. Allen, A. Ailing, W.F. Dempster, S. Silverstone, Earth applications of closed ecological systems: Relevance to the development of sustainability in our global biosphere. Adv. Space Res.31,1649–1655. (2003)

[12] M. Nelson, T. Burgess, A. Alling, N. Alvarez-Romo, W. Dempster, R. Walford, J. Allen, Using a closed ecological system to study Earth's biosphere: initial results from Biosphere 2. BioScience.43,225–236. (1993)

[13] F.B. Salisbury, J.I. Gitelson, G.M. Lisovsky, Bios-3: Siberian experiments in bioregenerative life support. Bioscience.47,575–585. (1997)

[14] K. Nitta, The CEEF closed ecosystem as a laboratory for determining the dynamics of radioactive isotopes. Adv. Space Res.27,1505–1512. (2001)

A modular platform architecture to enable system level scalability

Merlin F. Barschke

Technische Universität Berlin, Institute of Aeronautics and Astronautics,
Marchstr. 12, 10587 Berlin, Germany
Phone: +49 30 314-28743, merlin.barschke@tu-berlin.de

Abstract: In recent years small satellites continuously enhanced their performance leading to a large variety of missions with varying complexity and diverse applications. In order to decrease the development costs for an individual satellite, reuse of hard- and software between different missions is often implemented by the use of platform concepts. This paper discusses a platform to cover variants from 10 to 50 kg. To this end different terms and definitions of product platforms are discussed. Furthermore, the scope for the platform's use case is examined by analysing the range of performance to be covered by the different subsystems. Finally, it is examined how the TUBiX20 architecture of Technische Universität Berlin can be utilised to implement the required scaling capability.

1. INTRODUCTION

The recent progress in small satellite technology for missions below 50 kg can mainly be attributed to two parallel trends. Firstly, the CubeSat standard introduced by Stanford University and California Polytechnic State University greatly simplified the launcher interface, resulting in a growing number of universities, research institutions and small companies around the world developing their own satellite missions. At the same time, the advances in electrical components originally designed for terrestrial use continuously increased the performance of such spacecraft.

When designing satellites, there are generally two basic architecture approaches that can be followed. Firstly, one can strive towards the highest level of integration to maximise the performance of the spacecraft for a static configuration. Secondly, one can target a more flexible design that can be tailored for varying use-cases.

The first option is especially suitable for small form factors such as single unit CubeSats. Due to their small size, already minor increases in mass and volume capacity for the payload can significantly extend the payload options [3]. Here, a certain, relatively static spacecraft configuration may already cover the needs of a wide range of payloads that are applicable for such spacecraft, while the potential for cost or mass savings by omitting specific components is limited due to the high level of integration. However, as the satellite is designed for one specific application only, there is limited potential for reuse if the overall design shall be applied to a mission with altered requirements.

The larger the size of a spacecraft is the more complex payloads can be supported, which in turn may lead to more diverging requirements that are very specific an individual payload. Therefore, tailoring the spacecraft's performance towards this payload may result in significant savings regarding cost, mass and volume, if the design effort for this task can be limited. In this context, flexibility can be achieved by introducing scalability and modularity to allow for adapting the spacecraft according to the needs of different missions following a platform approach. Here, the initial effort required to design specific spacecraft is higher and a certain overhead in mass and volume needs to be accepted when being compared to the integrated approach [1]. However, as a broader range of hard- and

software elements, concepts and processes can be reused in subsequent missions, a platform approach is potentially more time- and cost-efficient when several subsequent missions with varying requirements are considered [2].

This paper presents a satellite platform family that covers the range between 10 and 50 kg. To this end, different platform definitions are summarised as a basis for the further analysis and scope and aspired mass range of the platform are discussed. Furthermore, the paper gives an overview of possible performance variants that may be required for each subsystem. Finally, it is outlined how the TUBIX20 architecture [4] can be used to implement the examined flexible satellite platform.

2. DEFINITIONS

The definition of the term *platform* widely diverges in literature [5]. Within this paper, the following definitions are used. A *product platform* is referred to as a set of modules that can be combined to form different *variants*, i.e. specific implementations, forming a *satellite family.* Whenever the term platform is not used to refer to the product platform, but rather to distinguish the part of the spacecraft that does not belong to the payload, the term *satellite platform* is used in this paper.

According to [5], one can distinguish between scalable, modular, and generational platforms. A scalable platform offers a number of variants with the same functionality while it allows to adjust certain parameters according to the need of a specific application. The variants of a modular platform provide different functionality which is achieved by adding and removing platform modules. For a generational platform, the variants can be distinguished by the introduction of updated modules.

The platform architecture presented in this paper aims at combining all three types of platform architecture. While the electrical power that can be provided to the payload may be scaled to the needs of an individual mission, modules like a propulsion system may be considered only if required. Furthermore, the platform shall support frequent technology updates of selected modules with minimal interference with the remainder of the platform.

3. SCOPE OF APPLICATION

The required level of scalability for a certain satellite platform strongly depends on the variety of missions it shall be applied to. While a platform design that is targeting Earth observation missions may mainly require to adopt to different instrument, storage and downlink options, a platform that aims at a wider scope of payloads may need a significantly higher number of variation points. The platform presented in this paper aims at a broad range of missions including science, Earth observation, and technology demonstration, which entails the need for a higher level of flexibility.

For spacecraft basing on the presented satellite platform family, a high level of operational robustness is aspired which has significant impact on the overall architecture. While the following requirements may not apply to each and every mission that bases on the platform, they may still affect the overall architecture:

1. The platform needs to support the implementation of single failure tolerance, which means that no single failure shall result in the loss of the mission, however, reduced performance may be accepted.

2. A spacecraft based on the platform shall be able to survive extended periods of time without performing active attitude control.
3. Communication with the ground station shall be possible regardless of the attitude.
4. Extended periods of time without any contact to the ground shall be possible without endangering the mission.

4. PLATFORM SCALING AND CONFIGURATION

The target mass range of 10 kg to 50 kg is completely covered by the CubeSat form factors from 6 to 27U [6-8]. While 6 and 12U CubeSats are widely used already, 16 and 27U designs are not yet equally popular. Although, the platform design presented in this paper shall not necessarily be restricted to the CubeSat form factor, the considered ranges of mass and volume are kept CubeSat compatible and the subdivision in units is used for simplicity.

Table 1 lists the four CubeSat form factors that are covered by the given mass range. Furthermore, the table includes an estimated range of the payload mass that may be supported by the individual form factors. This estimate is based on systems that are available on the market providing payload mass fractions between 25 and 60 percent [9-13].

Table 1: Overview of CubeSat form factors in the range of 10 to 50 kg with payload mass range [9-13]

Form factor	Maximum mass	Payload mass range*
6U CubeSat	12 kg	3 to 7 kg
12U CubeSat	24 kg	6 to 14 kg
16U CubeSat	32 kg	8 to 19 kg
27U CubeSat	54 kg	14 to 32 kg

* extrapolated from existing systems and relative to the maximum mass

In the following, each subsystem of the platform is analysed regarding its potential for scaling.

4.1 Structure and Mechanisms

The main scaling capability that is required of the structure originates from the different size variants that are to be covered by the platform, e.g. 12 or 27U. This also has direct impact on the surface available for solar cells. If body-mounted cells will not be sufficient for power generation deployable panels may be required (cf. Section 4.3). Furthermore, release mechanisms for antennae may be needed (e.g. UHF antennae, cf. Section 4.6) that can potentially be used across all size variants.

4.2 Thermal Control System

In the given mass range, the thermal control system is usually implemented passively, i.e. the temperatures within the spacecraft are adjusted by varying the optical properties of the spacecraft's outer surfaces and the thermal conductance of the interfaces between its elements. Active temperature stabilisation is mainly required for specific payloads with high requirements in the thermal domain [14]. Here, one can benefit from the similar

composition of the individual variants of a platform which simplifies the reuse of concepts, materials and simulation models.

4.3 Electrical Power System

The electrical power system can mainly be scaled regarding two performance parameters; the power generation capacity, i.e. the size of the solar panels, and the power storage capacity, i.e. the size of the battery.

To estimate a reasonable range of the power generation capacity for the platform, the potential of each size variant needs to be analysed separately. To this end, four configurations of each size variant are considered, body-mounted solar cells and the same body mounted cells complemented by one, two, four, and six unfoldable solar panels. For all calculations, triple junction solar cells with a size of 40 x 80 mm^3 are assumed [15] while the assessment of the maximum number of cells on each side is based on parallel strings of seven cells each. Figure 1 gives an overview over the maximum power that could be generated by the different configurations of the various platform sizes. For these calculations, an average cell temperature of 75°C, an attitude pointing error of 5 degrees, and a power point tracking efficiency of 0.95 are assumed [16].

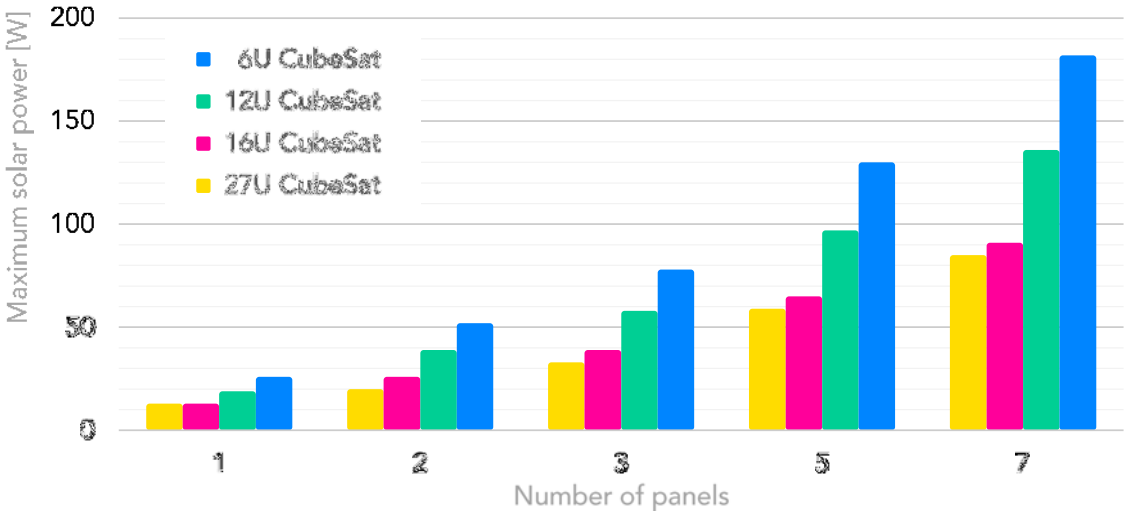

Figure 1: Maximum solar output power for different satellite size variants and solar panel options

The battery capacity required for a certain mission strongly depends on the consumption profile of the mission. However, based on the following assumptions, an order of magnitude of the battery size required for the different power generation options can be obtained:

1. The power demand of the spacecraft is constant
2. The maximum depth of discharge is 30%
3. No losses are considered
4. The orbit is assumed to provide one hour of sunlight and half an hour eclipse

Based on these assumptions, the range of battery capacities required by the different satellite size variants range from 14 Wh for body-mounted cells on a 6U design to 202 Wh when unfolding 6 panels on a 27U spacecraft.

4.4 Attitude and Orbit Determination and Control System

The attitude determination accuracy that can be achieved for a certain spacecraft mainly depends on the available sensors. In the following, possible scaling levels for the attitude determination sensor suite are listed. Here, only the sensors that contribute to the attitude determination when the highest possible accuracy is obtained are listed:

1. Accuracy on degree level can be provided by MEMS gyroscopes, Sun sensors and MEMS magnetometers [14, 17]
2. For arc minute accuracy star trackers can be integrated [18, 19]
3. If attitude knowledge in the range of several arc seconds is required, advanced star trackers need to be installed [20]

In terms of attitude pointing, most configurations will rely on a system build by reaction wheels for attitude manoeuvring and magnetorquers to desaturate these wheels. For missions that only require rate damping while no significant pointing is aspired, magnetorquers may be sufficient as actuators. Furthermore, it is possible to implement other actuator types, such as fluid-dynamic actuators [21, 22] that can deliver highest torque and also require magnetorquers for rate damping.

To obtain precise orbit determination, a GNSS receiver can be implemented. If orbit determination is only required for post processing on the ground, laser ranging retroreflectors [23, 24] can be used as an alternative or complementary to the GNSS receiver. Laser ranging comes with the advantage that highly precise orbit parameters are still available after the satellite's mission is concluded.

The addition of a propulsion system may significantly impact several subsystems of the platform variant in question. Here, the impact may vary considerably depending on the technology that is applied.

4.5 Communications System

The communication system provides the TM/TC link and payload data downlink. For the given platform family, the following options are considered:

1. A UHF transceiver system provides reliable radio link that is nearly independent of the satellite's attitude and permanent readiness to receive can be achieved with comparatively low power demand [25].
2. An additional S-band or X-band downlink channel provides higher data rates in the range from several Mbps up to more than 100 Mbps, respectively [26, 27].
3. Adding an S band uplink allows to perform commanding via S band, which significantly enhances the performance.

Furthermore, advanced technologies, such as optical downlink systems [28] may be considered for specific variants of the platform.

4.6 On-Board Computer

Within a traditional spacecraft architecture, reconfiguration towards changing mission requirements has a major impact on the interfaces, software and potentially even on the

required processing power of the on-board computer. However, the modular platform architecture described in section 5 effectively decouples the on-board computer from such variations which strongly limits the need for scalability for this subsystem.

4.7 Payload Data Handling

The payload data handling mainly needs to be scaled in terms of interfaces provided to the payloads, processing power and data storage.

4.8 Software

The increasing importance of software in the space domain results in substantial potential of reuse. A detailed discussion of software product lines for satellite applications can be found in [29].

5. PLATFORM ARCHITECTURE

Different architecture topologies have been reviewed regarding their suitability for small satellite platforms. One approach that was found well adapted to the needs of such platforms is based on a central power and data bus interconnecting a variable number of computational nodes used to interface to devices such as sensors or actuators [30]. The flight proven TUBiX20 platform architecture [4] follows this approach by implementing an adjustable number of computational nodes accommodated in a central avionics unit. In order to exploit the synergy effects within the system, all nodes build on the same basic set of hard- and software elements.

Figure 2 shows an exemplary system overview of a satellite that builds on the TUBiX20 platform architecture, highlighting the potential of tailoring the setup to the needs of a specific mission, by adding or removing nodes and the interfacing components.

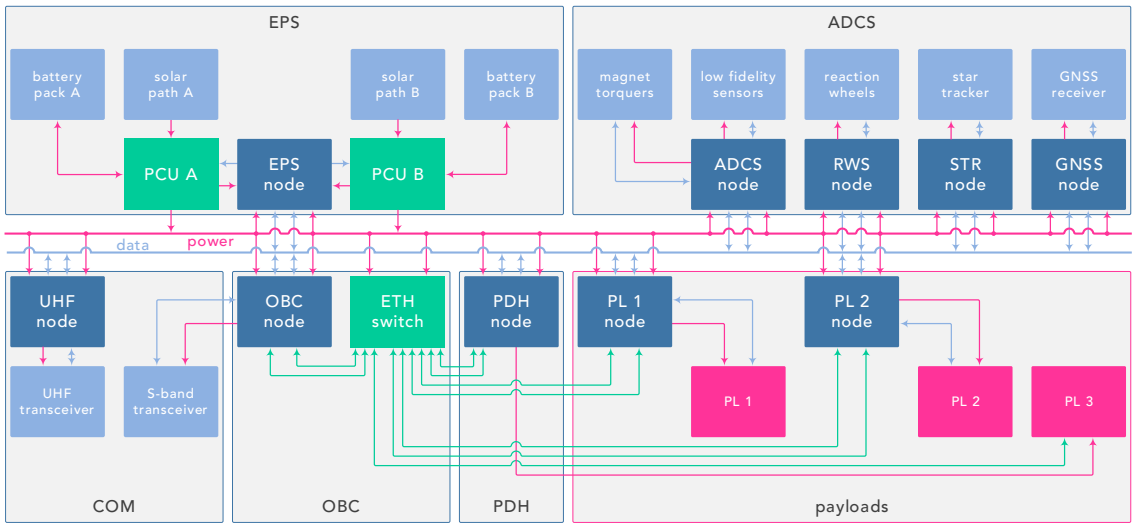

Figure 2: Exemplary system overview for a spacecraft that implements the TUBiX20 systems architecture

The level of reuse achievable for the platform is greatly increased by using the same form factor for the nodes across all size variants. Furthermore, there is a number of components like sensors, batteries, or radio transceivers that generally do not depend on the selected

platform size variant but solely on the required performance. Due to the modular architecture of the platform, such components can be implemented across all size variants without requiring modifications to the rest of the hard- and software of the spacecraft.

6. CONCLUSIONS

The introduction of the CubeSat standard as well as the continuous advancement of electronic components originating from the automotive and consumer industry have mainly driven the recent advancement of small satellites with a launch mass below 50 kg. In order to further reduce the development costs of such spacecraft, reuse between different missions is usually aspired. This can be obtained by implementing platform concepts aiming at common part maximisation between the implemented variants.

The platform presented in this paper targets a mass range of 10 kg to 50 kg. When considering missions within this mass range, one can observe considerable variation in the requirements imposed on the different subsystems. This paper analyses suitable scaling ranges of subsystem performance parameters to be covered by such a platform. Furthermore, it examines how the TUBiX20 platform architecture of Technische Universität Berlin enables reuse between different variants of the presented satellite platform family.

ACKNOWLEDGEMENTS

The development of the TUBiX20 platform is funded by the Federal Ministry for Economic Affairs and Energy (BMWi) through the German Aerospace Center (DLR) on the basis of a decision of the German Bundestag within the TechnoSat, the TUBIN and the QUEEN mission (Grant No. 50RM1102, 50RM1219, 50WM1754 and 50RU1801).

REFERENCES

[1] J. Kingston. 'Modular architecture and product platform concepts applied to multipurpose small spacecraft,' presented at the 19th Annual AIAA/USU Conference on Small Satellites, Logan, USA, 2005.

[2] E. Falkenhayn, 'Multimission modular spacecraft', presented at the AIAA Space Programs and Technologies Conference, Houston, USA, 1988.

[3] Sebastian Grau, Christian Tschoban, Klaus-Dieter Lang, Klaus Brieß, 'Highly integrated communications, power management, and attitude determination and control side panel for CubeSats', presented at the 68th International Astronautical Congress, Adelaide, Australia, 2017.

[4] M.F. Barschke and K. Gordon, 'A generic systems architecture for a single failure tolerant nanosatellite platform', presented at the 65th International Astronautical Congress, Toronto, Canada, 2014.

[5] J. R. Jiao, T. W. Simpson and Z. Siddique, 'Product family design and platform-based product development: A state-of-the-art review', *Journal of Intelligent Manufacturing*. vol. 18, pp. 5-29, 2007.

[6] CubeSat Design Specification rev. 13, The CubeSat Program, California Polytechnic State University, San Luis Obispo, USA, 2015.

[7] 6U CubeSat Design Specification rev. 1.0, The CubeSat Program, California Polytechnic State University, San Luis Obispo, USA, 2018.

[8] R. Hevner and W. Holemans, 'Payload Specification for 6U, 12U and 27U', Planetary Systems Cooperation, Silver Spring, USA, 2012.

[9] Innovative Solutions In Space B.V., 'ISIS 6U CubeSat', Available online: https://www.isispace.nl/wp-content/uploads/2018/07/ISIS-6U-CubeSat-Brochure.pdf [February 28, 2019]

[10] GomSpace, '6U Platform', Available online: https://gomspace.com/6u-platform.aspx [February 28, 2019]

[11] Berlin Space Technologies GmbH, 'LEOS-30', Available online: https://www.berlin-space-tech.com/portfolio/leos-30/ [February 28, 2019]

[12] N.M.K. Lemke, S. Tailhades, P. Bohlin, F. Sjöberg, S. Holsten, H.A. Moser and G. Mantovani, 'OHB Small Satellites', presented at the 69th International Astronautical Congress, Bremen, Germany, 2018.

[13] F.M. Pranajaya and R.E. Zee, 'The NEMO bus: A third generation high-performance nanosatellite for Earth monitoring and observation', presented at the 24th AIAA/USU Conference on Small Satellites, Logan, USA, 2010.

[14] D. Selvaa and D. Krejci, 'A survey and assessment of the capabilities of CubeSats for Earth observation', *Acta Astronautica*, vol. 74, pp. 50-68, 2012.

[15] AZURSPACE Solar Power GmbH, '30% Triple Junction GaAs Solar Cell', Heilbronn, Germany, 2016.

[16] O.Shekoofa and E. Kosari, 'Comparing the topologies of satellite electrical power subsystem based on system level specifications', in *Proceedings of the 6th International Conference on Recent Advances in Space Technologies (RAST)*, 2013, pp. 671-675.

[17] J.C. Springmann and J.W.Cutler, 'Flight results of a low-cost attitude determination system', *Acta Astronautica*, vol. 99, pp. 201-214, 2014.

[18] T. Segert, S. Engelen, M. Buhl and B. Monna, 'Development of the Pico Star Tracker ST-200 – Design Challenges and Road Ahead', presented at the 25th AIAA/USU Conference on Small Satellites, Logan, USA, 2011.

[19] A.O. Erlank, W.H. Steyn, 'Arcminute attitude estimation for CubeSats with a novel nano star tracker', IFAC Proceedings Volumes, vol. 47, iss. 3, 2014, pp. 9679-9684.

[20] C.M. Pong, 'On-Orbit Performance & Operation of the Attitude & Pointing Control Subsystems on ASTERIA', presented at the 32th AIAA/USU Conference on Small Satellites, Logan, USA, 2018.

[21] D. Noack, J. Ludwig, P. Werner, M.F. Barschke and K. Brieß, 'FDA-A6 – A fluid-dynamic attitude control system for TechnoSat', presented at the Nano-Satellite Symposium, Matsuyama-Ehime, Japan, 2017.

[22] D. Noack, M.F. Barschke, P. Werner and K. Brieß, 'FDA in space – first in-orbit results of a fluid dynamic attitude control system', presented at the Small Satellites Systems and Services Symposium, Sorrento, Italy, 2018.

[23] G. Kirchner, L. Grunwaldt, R. Neubert, F. Koidl, M.F. Barschke, Z. Yoon and H. Fiedler, 'Laser ranging to nano-satellites in LEO orbits: plans, issues, simulations', presented at the 18th International Workshop on Laser Ranging, Fujiyoshida, Japan, 2013.

[24] M.F. Barschke, P. Werner, K. Gordon, M. Lehmann, W. Frese, D. Noack, L. Grunwaldt, G. Kirchner, P. Wang and B. Schlepp, 'Initial results from the TechnoSat in-orbit demonstration mission', presented at the 32st AIAA/USU Conference on Small Satellites, Logan, USA, 2018.

[25] F. Baumann and K. Brieß, 'A Quad-channel UHF Transceiver for TUBiX20', presented at the 10th IAA Symposium on Small Satellites for Earth Observation, Berlin, Germany, 2015.

[26] R. Alavi, K. Briess, H. Podolski, J. Riesselmann, A. Weiland, and W. Frese, 'In Space Verification of the Pico-Satellite S-Band Transmitter "HISPICO" on a Sounding Rocket', presented at the 60th International Astronautical Congress, Daejeon, South Korea, 2009.

[27] D. Noack, K. Jäckel, M. Reibe, F. Hartmann, S. Pirwitz and K. Brieß, 'XLINK - A 0.3 U Sized X-Band Transceiver for NanoSats', presented at the 68th International Astronautical Congress, Adelaide, Australia, 2017.

[28] C. Schmidt and C. Fuchs, 'The OSIRIS Program - First results and Outlook', in *Proceedings of the International Conference on Space Optical Systems and Applications (ICSOS)*, 2017, pp.19-22.

[29] K. Gordon, M. Starke, P. von Keiser and M. F. Barschke, 'Multi-mission software development for small spacecraft', presented at the 12th IAA Symposium on Small Satellites for Earth Observation, 2019.

[30] T. Pitter and M. D'Errico, Multi-purpose modular plug and play architecture for space systems: Design, integration and testing, *Acta Astronautica*, vol. 69, iss. 7-8, pp. 629-643, 2011.

TIM: An International Formation for Earth Observation with CubeSats

Alexander Kleinschrodt[1], Iurii Motroniuk[2*], Anna Aumann[2], Ilham Mammadov[2], Maros Hladky[1], Mohd Bilal[1], Andreas Freimann[1], Liu Minshi[3], Jiang Lianxiang[3], Francois Malan[4], Hendrik Burger[5], Giovanni Beltrame[5], Klaus Schilling[2]

[1]University of Würzburg, Lehrstuhl für Informatik VII (Robotik und Telematik), Würzburg, Germany,
Mail: schi@informatik.uni-wuerzburg.de

[2]Zentrum für Telematik e. V., Würzburg, Germany,
Mail: iurii.motroniuk@telematik-zentrum.de

[3]Shandong Institute of Space Electronic Technology, Shandong, China,
Mail: liums49@163.com

[4]Space Advisory Company, Somerset West, South Africa,
Mail: francois@spaceadvisory.com

[5]SCS Space, Somerset West, South Africa,
Mail: hendrik@scs-space.com

[5]Polytechnique Montreal, Montreal, Canada,
Mail: giovanni.beltrame@polymtl.ca

* Corresponding author

Abstract: The Telematics International Mission (TIM) project is an international effort to create a formation of cooperating nanosatellites for joint Earth observation. For this ambitious project eight partner institutions from five continents are joining forces to present cutting edge solutions to problems such as monitoring the height of volcanic ash clouds, identification of sea vessels, monitoring thermal anomalies and many more. This contribution gives an overview of the TIM concept and introduces the different partners and their contributions. The satellite design will be based on the UNISEC standard. It is especially optimized for rapid integration and testing and provides flexibility and compatibility of components and subsystems between all partners. The current state of development is outlined, challenges for the individual as well as the joint missions are identified, and solutions are presented. Particularly, the mission's orbit control system necessary for enabling appropriate pointing accuracy will be outlined, introducing the newly developed miniature reaction wheels with a specific high rotation speed. An additional goal is the demonstration of a novel method for improving satellite attitude control by visual servoing, which calculates features of camera images on-board.

1. INTRODUCTION

Nanosatellites with a mass of up to 10 kg are being developed as a relatively affordable alternative to expensive and bulky Earth Observation satellites. Despite their low cost, these nanosatellites are becoming ever more capable. Small satellites exhibit increasing capabilities with respect to lifetime, robustness as well as attitude and orbit control performance. This enables them to address challenging scientific missions. The TIM formation aims to extend the capabilities of small satellite missions by combining several individual missions from different partner institutions to maximize synergies. Each partner contributes a number of satellites as well as the ground infrastructure to the common formation mission. The resources of the

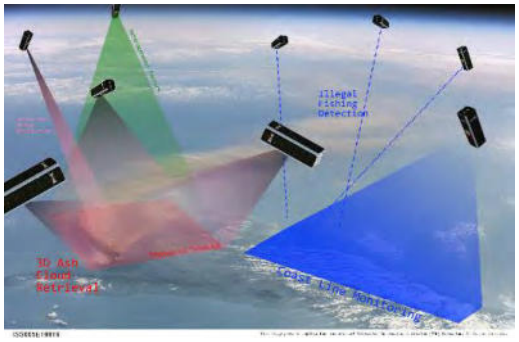

Figure 1 Overview of the different submissions of TIM - (1) monitoring of the height of ash clouds (2) the identification of sea vessels or (3) the monitoring of thermal anomalies

participating partners are used as optimally as possible by defining common objectives. Deploying such a formation offers better coverage and shorter revisit times giving the possibility to better monitor dynamic events. The overall concept is visualized in Figure 1. This paper is organized as follows. After this introduction, the mission concept is outlined. An overview of the TIM mission and its main objectives as well as the role and involvement of all partners is given. Section three outlines the mission design and gives a brief overview of the satellite platform and its subsystems. The paper concludes with a summary and outlook.

2. MISSION CONCEPT AND DESIGN

The Telematic International Mission (TIM) focuses primarily on Earth observation using a nanosatellite formation. A formation is defined in this context as a system of distributed satellites that maintain a desired relative configuration by closing the control loop in space by means of intersatellite communication [1]. This collective use of several satellites enables them to perform as a single, large, virtual his collective use of several satellites enables them to perform as a single, large, virtual instrument. The TIM formation consequently enables observation of target areas on the Earth's surface from different viewing angles, and thereby, presents solutions to cutting edge problems such as the identification of sea vessels, monitoring thermal anomalies or 3D earth observation. The latter is particularly interesting for measuring the height of ash clouds to determine their motion. Given the dynamic nature of ash clouds, which can move at 100 km/h or more, the use of a formation brings advantages as it reduces parallax errors when compared to asynchronous measurements from the same satellite of the same scene. Authors of [2] previously proposed the use of nanosatellite formations for determining Cloud Top Height (CTH) as well as cloud ascent velocity using photogrammetry. The proposed approach is shown to provide results with a resolution comparable to LIDAR [2]. Retrieving such 3D information can also be applied to monitor city expansion and illegal building processes. The satellite platform developed in the missions will be based on a 3U-Cubesat design that extends the modular design that was already successfully demonstrated on UWE-3 [3], allowing for quick and flexible integration. This concept has been elaborated into an electrical interface standard and is promoted by UNISEC Europe [4] , and will be supported in TIM-satellites in order to provide compatibility of components and subsystems between the partners. The standard is optimized for rapid integration and testing, thus reducing development time frame. Furthermore, to avoid wires complicating integration, a backplane concept is introduced for subsystem interconnection.

2.1. Mission Requirements

To allow the integration of individual missions into TIM, a common satellite platform is required such that it provides sensors capable of encompassing a large set of Earth observation applications. An optical and near-infrared payload camera combined with a high pointing accuracy are essential to achieving the desired integration and observation scenarios. Furthermore, the joint observation of target areas requires high precision autonomous

formation control strategy as well as an effective inter-satellite communication. At the same time, all TIM satellites must share the same orbit and share common operational infrastructure with minimal ground control. The keys for a successful combination of missions will be autonomy and self-organization (within the constraints of the satellites' orbits) so that TIM can be a technology demonstrator for a general-purpose Earth Observation formation, as well as accomplishing important missions for all the project partners.

2.2. TIM Partners and Missions

Figure 2 Map of international partner institutions

As already mentioned above, TIM is an international collaborative project consisting of five partner states. Each partner state contributes with different technologies and resources to achieve the mission goals. Furthermore, each partner state also carries out individual missions and experiments described as follows. Partners from Germany and China each contribute to the mission with a formation of three nanosatellites, while Brazil, South Africa and Canada will contribute with single satellite missions [5] . The individual contributions are outlined in the following sections. Figure 2 presents a map of the involved partner institutions.

2.2.1. Bavaria, Federal Republic of Germany

Germany contributes to TIM with the Telematics Earth Observation Mission (TOM) [6]. The mission is developed at the Zentrum für Telematik (ZfT) in cooperation with the Julius-Maximilians-Universität Würzburg (JMUW) and the Technische Universität München (TUM). TOM follows on the prior developments of the NetSat [7] and the UWE [3] satellite family developed previously at JMUW. In TOM three nanosatellites carrying cameras in the visible range track and perform simultaneous measurements from different perspectives of the same target on the surface of the Earth. These observations form the basis to apply photogrammetric approaches for sensor data fusion to generate three-dimensional images of the target area [2]. TOM will present one of the first formations in space where self-organizing principles will be applied in orbit in order to perform measurements by coordinated satellites. The main task of TOM will be the CTH measurements as suggested in [2] for a formation of three 3-U CubeSats.

2.2.2. Québec, Canada

The Québec team has expertise in autonomous systems, software verification, and distributed control. Québec will contribute to the overall software (on-board and ground segment) so that the entire set of TIM satellites can be controlled as a single, possibly heterogeneous, formation. With inter-satellite communication capability and a set of target applications, it is planned to develop on-board software that is modular and can be safely updated from the ground. Applications will be able to be defined both with a bottom-up approach (specifying the processing and communication of a single satellite) or top-down (specifying what the formation needs to achieve) [6]. Overall, the Québec team will provide to the TIM members with the software infrastructure and high-level communication protocols to instruct the satellites and collect the information generated by the different applications [8].

2.2.3. Shandong, People's Republic of China

The main goal of the Chinese mission is urban expansion monitoring. The mission concept includes a 3D contour reconstruction aimed at a specific target in China for testing 3D imaging reconstruction performance and its accuracy. China contributes three 3U-satellites to the TIM project. The satellites will be produced by Shandong Institute of Space Electronic Technology (SIAET), which is a subordinate institute of China Academy of Space Technology (CAST) with long term experience in satellite engineering, especially series production and standardization of components. The products are covering all the applications of nanosatellites, such as an integrated information management, measure and control, transceiver, satellite controlling system, energy control, etc.

2.2.4. Western Cape, Republic of South Africa

The main contribution from Western Cape to the international TIM partnership is to manufacture the developed Gecko imager payload to all partners. This payload comes with valuable operational space heritage [9] [10] and is available in several configurations to suit different mission needs. The contribution of this imager will be to enable stereoscopic Earth Observation under a cooperative formation flying. For this specific mission, the camera will be configured as either Bayer-pattern RGB matrix frame imager, or as line-scan imager with 4 spectral bands representing Red, Green, Blue and Near-Infra Red (NIR). The SCS group is able to support mission partners with knowledge on payload integration and CubeSat design, obtained during the course of the nSight-1 mission [10].

3. MISSION DESIGN

3.1. Optical Payload

TIM satellites will each be equipped with a primary imaging payload that can capture visible and near infra-red light. For this purpose, the Gecko imager has been identified as a suitable candidate [11]. The flexibly configurable common control unit and data storage supports a family of related CMOS matrix imaging sensors that operate in the visible and near-infrared regions. Multispectral capability is provided by custom filters manufactured to mission specifications, while hyperspectral imaging is provided by specialized detectors. The Gecko imager can be built up either as a 2D array snapshot imager, or as push broom line-scan imager. In snapshot mode, the imager will be used to acquire images up to 5 frames per second. The integrated payload control unit features integrated on-board mass storage for real-time image capture as well as optional lossy or lossless image compression. Full images or image thumbnails may be downloaded at a user-defined data rate that suits the satellite's downlink capabilities – typically limited by the available space and power budget associated with a CubeSat mission.

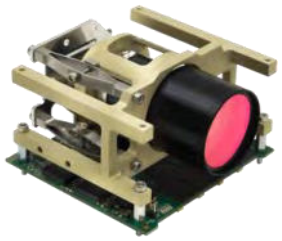

Figure 3 SCS's Gecko Imager

3.2. Coordinated Attitude Control

The accuracy of 3D reconstruction based on stereo image pairs is dependent on the viewing angles for stereoscopic measurements. Wide stereo angles provide better geometric accuracy while making point matching between images more difficult due to large differences of the two points of view. Also, narrow angles are better suited for observation scenarios with severe occlusions [12]. A stereo angle of about 10° is appropriate for photogrammetric measurements, resulting in inter-satellite distances of about 100 km [13]. Appropriate formation orbits allowing optimal inter-satellite distances will enable imaging of the target from different view angles in addition to keeping image resolution between satellites comparable. Synchronized Stereoscopic Earth Observation requires several satellites to point the camera payload towards the same position on ground, which imposes stringent accuracy demands on the attitude control subsystem. The pointing accuracy requirements are derived from the camera properties. The camera field of view determines the absolute pointing accuracy, the ground sampling distance decides the allowed relative pointing accuracy or jitter. Furthermore, the overlapping area of images must be as large as possible to achieve best triangulation results. Hereby, 80% overlap of images is a common practice. For the desired target to be part of the image, the total pointing error must be less than 25% of the payload field of view or better. An accuracy of 10% increases the overlapping area between the satellites. (SMAD) A field of view of 10° as planned in TOM therefore results in a required pointing accuracy of 1°. The attitude is determined using a Kalman filter approach based on fine sun sensors and magnetometers. The pointing accuracy will be achieved with the aid of newly developed miniature reaction wheels with a specific high rotation speed. Additionally, visual servoing experiments will increase the overlapping area imaged by all satellites by exploiting relative attitude determination. Figure 4 depicts a concept of Coordinated Attitude Control. The observation is started from ground by sending a time-tagged command. As soon as observation is possible, a coarse control loop is running, which relies on the estimated attitude and gyro measurements. As soon, as the control is stable, a fine control takes over relying on visual servoing measurements. The visual servoing algorithm computes the angular velocities necessary to track features, which are fed into the fine control loop. The found features are distributed between the satellites to find a common set of tracked features and increase the overlapping area. A more detailed description of this approach is described below. [14]

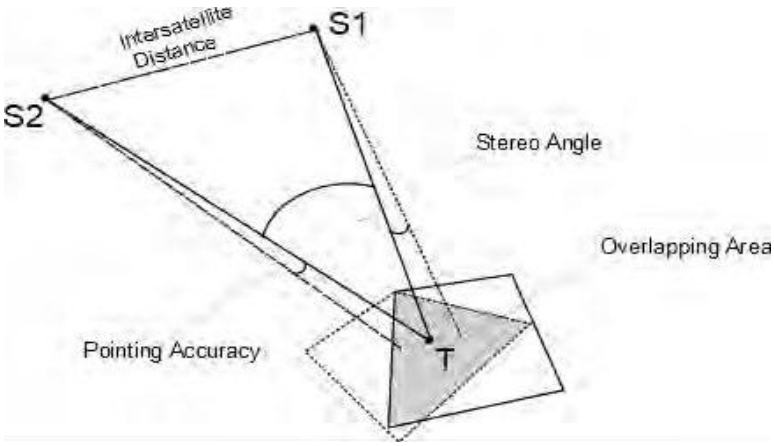

Figure 4 Concept of Coordinated Attitude Control

3.3. Visual Servoing

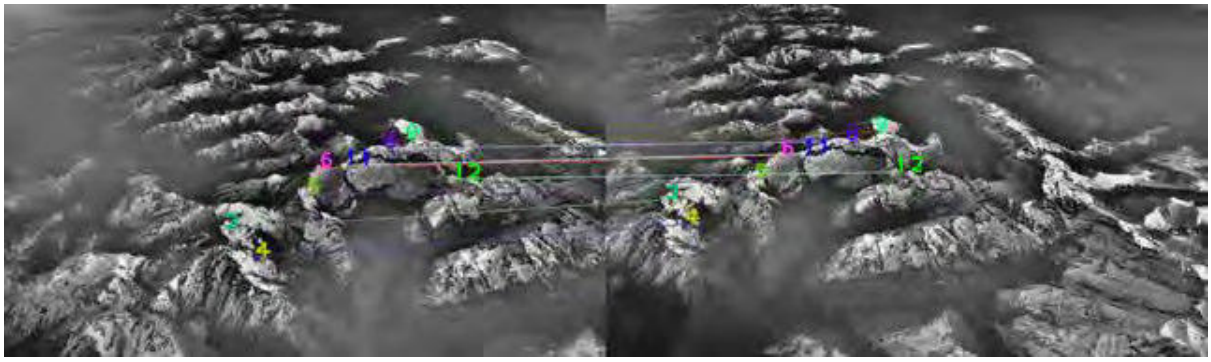

Figure 5 Example of the feature matching

Visual servoing is a complex field encompassing image processing and robotics. For this project, the satellites analyze the observed imaged area, process the input, share the data and provide the input for attitude control to keep the maximal possible overlap of the imaged areas. The method consists of feature extraction, description and distributed matching. All satellites extract distinctive features from the image, track them in the subsequent image stream and describe those in a unique way for matching. The leading satellite, e.g. S2 shares the unique descriptors of the features from its imaged area with the others. The other satellite, e.g. S1 equally track and describes its own features. Upon receiving the descriptors set from S2 satellite, S1 satellite matches them with its own. The outcome of the descriptors matching results in a set of features that are known to belong to both S2 and S1 imaged areas, therefore the attitude of S1 satellite can be adjusted based on the relative coordinates of the matched features to maximize the overlap. Throughout the processing i.e. description, sharing and matching of features, the leading satellite S2 is constantly tracking its detected features and adjusting its attitude accordingly to keep the content of the imaged area constant. Figure 5 presents an example of two different pictures in which features are detected and matched accordingly.

3.4. Formation Control

One of the crucial aspects of formation control for nanosatellite missions is the extremely limited propulsion capabilities. Hence, any formation design must utilize the orbital dynamics to its advantage. Several formation designs have been proposed over the years, however from the point of view of Earth observation, two formation types, namely, projected circular orbit (PCO) and in-track formation are of particular interest. The PCO has a circular projection onto the horizontal plane of the relative coordinate system (LVLH of the chief satellite), and hence a fixed distance between the satellites in this plane. The in-track configuration allows each satellite in the formation to have the same ground track making it an attractive formation for Earth observation. The TOM satellites are used for evaluation of these two formations from the point of view of propulsion requirements. As, previously mentioned, the photogrammetric requirements lead to the desired distance between satellites to be about 100 km, thereby leading to a large formation. In such a scenario, the traditional linear models for relative motion will not be sufficient for control design and nonlinear control techniques will be employed.

3.5. Propulsion

The propulsion subsystem is a crucial element in identifying formation acquisition and maintenance efforts. TIM satellites must be able to provide similar orbit maneuverability, and thus each satellite's propulsion subsystem must provide similar Δv and have the maximum thrust acceleration in the same range. To distribute formation control efforts fairly between different satellites, each satellite would be able to deliver enough Δv to acquire and maintain the TIM formation as if the other satellites are passive in coordination. A propulsion system based on the FEEP technology with a maximum thrust of a few hundreds of µN is considered.

3.6. Communication

The satellites will be equipped with radio systems for high speed data downlink in the S-Band, and UHF radios for telemetry downlink and low speed data transmissions. Both systems will work in the amateur radio frequencies. While up- and downlinking signals is a well-known technology, intersatellite communication between several CubeSats is a relatively new and challenging technology. Cooperating satellites of the mission must exchange data such as position data for formation keeping and image features for distributed attitude control. For downloading captured images, the TOM satellites will mainly use an S-Band transmitter. An additional optical ground-station will be used to demonstrate high speed data downlink. The distribution of partner ground stations across the globe facilitates the development of the ground station network comprised of at least five UHF stations and three S-Band stations. The ground station network is based on the OSI layer model as shown in Figure 7. While all the different ground stations have different hardware and software architectures and capabilities, the network provides an interface for common operation. This is performed through a request and response procedure over MQTT. An operator that requires to contact a given satellite through another ground station sends a request providing the details of the satellite to be communicated with. Once the receiving ground station approves the request, the overpass timings are generated by a master scheduler as described in [15]. The data collected is then stored in a stream-based database system which allows the requesting station to perform necessary analysis.

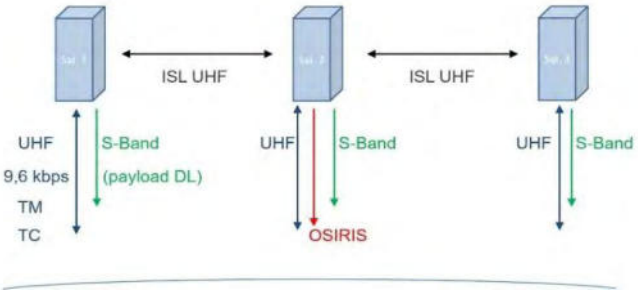

Figure 7 TIM / TOM Communication Network

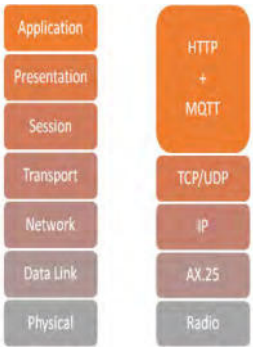

Figure 6 Groundstation Network OSI-layer model

4. SUMMARY & OUTLOOK

The Telematics International Mission is an ambitious project in terms of technology development as well as international coordination. Its success sets a precursor to future nanosatellite formation-based Earth Observation efforts. Consequently, several technologies like large formation control, coordinated attitude control, visual servoing, inter-satellite communication, and ground station networking will be realized. A successful TIM also augurs well for standardization of nanosatellite platform for Earth observation.

5. ACKNOWLEDGMENT

The authors thank all the collaborators for their contributions within the “Telematics earth Observation Mission – TOM”, supported by the Bavarian Ministry of Economics and the RLS for the cooperation in TIM.

6. REFERENCES

[1] K. Schilling, "Networked distributed pico-satellite systems for earth observation," 2011.

[2] K. Zaksek, M. R. James, M. Hort, T. Nogueira and K. Schilling, "Using picosatellites for 4-D imaging of volcanic clouds: Proof of concept using ISS photography of the 2009 Sarychev Peak eruption," in *Remote Sensing of Environment*, 2018, pp. 519-530.

[3] K. Schilling and S. Busch, "UWE-3: A modular system design for the next generation of very," in *Small Satellites Systems and Services - The 4S Symposium*, Portoroz (Slovenia), 2012.

[4] "UNISEC EUROPE," [Online]. Available: http://unisec-europe.eu/standards/bus.

[5] A. Kleinschrodt, A. Freimann, M. Schmidt and K. Schilling, "Lessons learned from in orbit operations of the uwe-3 pico-satellite," in *66th International Astronautical Congress*, Jerusalem, Israel, 2015.

[6] C. Pinciroli, A. Lee-Brown and G. Beltrame, "A tuple space for data sharing in robot swarms," in *EAI International Conference on Bio-inspired Information and Communications Technologies (BICT 2015)*, ACM Digital Library pp. 287–294, 2015.

[7] K. Schilling, P. Bangert, S. Busch, S. Dombrovski, A. Freimann, A. Kramer, T. Nogueira, D. Ris, J. Scharnagl and T. Tzschichholz, "Netsat: A four pico/nano-satellite mission for demonstration of autonomous formation flying," in *66th International Astronautical Congress*, Jerusalem, Israel, 2015.

[8] G. Beltrame, E. Merlo, J. Panerati and C. Pinciroli, "Engineering safety in swarm robotics," in *st International Workshop on Robotics Software Engineering, ser. RoSE ’18*, Gothenburg, Sweden, 2018.

[9] D. Malan, K. Wiid, D. Stanton, L. Visagie and H. Burger, "Images from nSight – 2U Earth Observation and Atmospheric Science CubeSat – Earth Observation and Science in 2U," in *68th International Astronautical Conference*, Adelaide, Australia, 2018.

[10] F. Malan, K. Wiid, L. Visagie, H. Burger and W. Steyn, "The Development of nSight-1 – Earth Observation and Science in 2U," in *AIAA/USU Conference on Small Satellites 31 (SSC17-X-10)*, Logan UT, USA, 2017.

[11] "Gecko Imager," [Online]. Available: http://scs-space.com/payloads/gecko-imager.

[12] M. Bernard and et al, "3D Capabilities of PLEIADES Satellite," International Archives of the Photogrammetry, Remote Sensing and Spatial Sciences, Vol. XXXIX-B3, 2012.

[13] T. Nogueira and et. al, "Photogrammetric Ash Cloud Observations by Small Satellite Formations," in *Metrology for Aerospace (MetroAeroSpace), 2016 IEEE*.

[14] K. Schilling, A. Aumann, I. Motroniuk, I. Mammadov, D. Garbe, O. Ruf, V. Dombrovski, M. Hladky and A. Nüchter, "TOM - A PICO-SATELLITE FORMATION FOR 3D EARTH OBSERVATION," in *The 4S Symposium*, 2018.

[15] A. Kleinschrodt, T. Nogueira, N. Reed and K. Schilling, "Mission Planning for the TIM Nanosatellite Remote Sensing Constellation," in *69th International Astronautical Congress (IAC), Bremen, Germany*, 2018.

Phase A Study for the Earth Observation and Technology Demonstration CubeSat SOURCE

Robin Schweigert[2], Annika Stier[2], Michael Lengowski[1], Daniel Galla[2], Sabine Klinkner[1]

[1]Institute of Space Systems
Pfaffenwaldring 29, 70569 Stuttgart, Germany
Phone: +49 71168569607, Mail: lengowski@irs.uni-stuttgart.de

[2]Small Satellite Student Society of the University of Stuttgart (KSat e.V.)
Pfaffenwaldring 29, 70569 Stuttgart, Germany
Mail: kontakt@source.ksat-stuttgart.de

Abstract: The small research satellite SOURCE (Stuttgart Operated University Research Cubesat for Evaluation and Education) is developed by students at the University of Stuttgart in cooperation with the Institute for Space Systems and the Small Satellite Student Society (KSat e.V.). The scientific objectives of its mission are heat flux-, pressure- and oxygen measurements in very low orbits. Since CubeSat missions with short life cycles on small budgets have become popular, SOURCE features a second group of payloads, provided by the German Aerospace Center (DLR), the Fraunhofer IPA, and industrial partners, which evaluate the usability of low cost commercial off-the-shelf technologies for space applications. A phase A study on the satellite resulted in a 3U+ CubeSat design. SOURCE is conceived for a maximum of two years in a sun-synchronous or ISS orbit and scheduled for a launch in 2020. This paper outlines the results of the phase A study by means of the satellite's subsystems.

1. INTRODUCTION

SOURCE is a CubeSat project conducted by the Institute of Space Systems (IRS), the Small Satellite Student Society KSat e.V. and students attending the associated lecture at the University of Stuttgart. Its main mission objective besides technology demonstration, earth atmospheric measurements, and optical earth observation is to function as practical education object and to provide an educational platform for university students. The development of the bus system is therefore organized and conducted by undergraduate master and bachelor students under qualified supervision by IRS staff. The project execution is oriented on the European Cooperation for Space Standardization (ECSS) standard. The completion of the 3U+ CubeSat is scheduled for 2020.

2. PAYLOADS

The main component of the technology demonstration comprises three payloads of the IRAS (Integrated Research platform for Affordable Satellites) project and its associates DLR, Fraunhofer IPA, IRS, Airbus DS, and AZUR SPACE Solar Power GmbH / SpaceTech GmbH. The goal of IRAS is to create a platform for cost-efficient satellite development. The payloads developed in the course of IRAS and demonstrated with SOURCE include a functional 3D printed sandwich structure [1] enclosing an automotive IMU. In addition, smart heaters as well as next-generation solar cells embedded in custom designed panels are implemented on SOURCE. The sandwich structure is de-

veloped at the DLR Stuttgart and will be completely produced using additive manufacturing processes. A first prototype for this structure is already described by Hümbert et al. [1]. The sandwich structure implemented on the SOURCE satellite will be an advancement to this structure. The integrity of the sandwich structure will be monitored through a health monitoring system throughout the whole mission phase.

The included IMUs will be qualified in orbit and negative effects of the space environment and radiation on their behavior and accuracy will be investigated. For this purpose, there will be a shielding directly printed into half the sandwich structure, protecting one of the two IMUs. Two radiation sensors, one placed underneath the shielding, one underneath the unshielded part of the sandwich structure will measure the different total ionizing dose and will complement the validation data of both IMUs.

In addition to those payloads, thin film solar cells by DLR Bremen will be characterized with in-situ measurements of the IV characteristic and temperatures. Lastly, a not yet space qualified commercial-of-the-shelf camera, namely the Genie Nano M1920, will be qualified in orbit. In addition to the environmental qualification, this camera will contain software for star and horizon tracking, which will also be tested during the mission. The system shall be used as a small and affordable star tracker on further missions at the IRS. Also for a future mission, the camera shall collect in-orbit images of meteors and other objects reentering Earth's atmosphere.

The scientific payload of SOURCE will conduct heat flux, pressure, and luminosity measurements during orbits lower than 200 km in order to enhance the accuracy of the IRS numerical re-entry simulation tool PICLas [2]. Flux-(Phi)-Probe-Experiment (FIPEX) [3] sensors for molecular and atomic oxygen measurements complement the atmospheric analysis for simulation correlation.

3. MISSION PLANNING

As possible orbits either an International Space Station (ISS) orbit or a 400 km to 500 km sun-synchronous orbit (SSO) are considered, matching the desired mission duration of about 1 to 2 years. The first phase of the mission will be dedicated to operating the technology demonstrators and the camera. This includes taking pictures of different spots of the Earth, trying to capture meteors in meteor observation mode and continuously monitoring the health of all technology demonstrators. In addition to this, regular measurements with FIPEX sensors are planned to gather calibration data on higher altitudes. This phase will continue until the last orbits when heat and plasmatic effects of the residual atmosphere begin to become dominant which is currently estimated at around 200km. Here, all payloads except for the atmospheric sensors will be deactivated. These sensors will start measuring at high rates to capture the lower atmosphere. Since this phase is currently estimated to only last 13 hours until re-entry, an overpass of the satellite over the ground station located in Stuttgart can no longer be guaranteed. Therefore, it is planned to use the worldwide ground station network of the IRS and to enable an inter-satellite link in order to receive data independently of the satellite's location. This ensures the longest possible transmission of all atmospheric measurement results until communication loss and demise.

4. BUS SYSTEM

An aim of the SOURCE project is to develop a bus system which is as flexible as possible for upcoming missions. This means that additional interfaces, memory, and computing capacity are included wherever the opportunity exists. In addition, all hardware should be low-cost, so the bus can be reproduced with minimal financial effort.

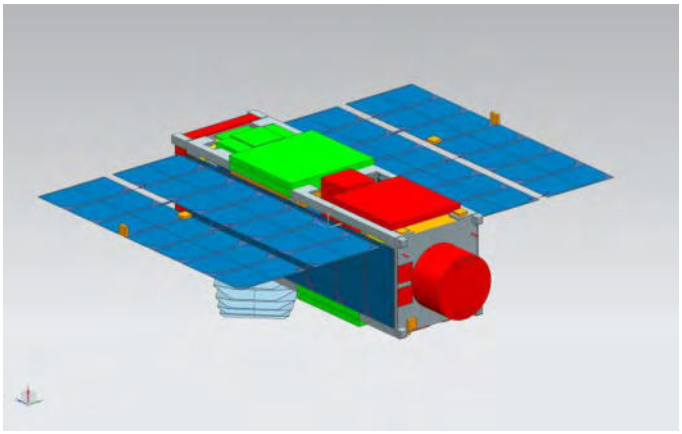

Figure 1: CAD of the in-orbit configuration of SOURCE

4.1 Structure and Mechanism

As a result of the Phase A study, the satellite is compliant with the 3U+ standard (10cm x 10cm x 34.05 cm) and shall have a mass of not more than 5 kg. It features double-deployable solar panels with double-sided solar cell tiling. This ensures power generation in all attitudes. The panels will unfold by means of a tension rod and are retained by two fusible security cords at launch. These cords will be melted after launch through redundant melting resistors. The same cords are used to secure the deployable camera baffle protecting the camera from scattered light. The baffle consists of a black Kapton foil with a protective coating of SiO2 and is folded into a self-deploying cone which cannot be retracted once unfurled. On the end of the satellite opposing the direction of the ejection, the space inside the dispenser spring of the Poly Picosatellite Orbital Deployer (P-POD) is used to accommodate a tuna can holding the FIPEX sensors with the correlating electronic box.

Inside the satellite, all boards are fixed to the aluminum primary structure, which provides sliding surfaces for the P-POD. About one unit of the satellite will contain PC104 compatible boards. These boards are slid on four threaded rods and fixed in place with nuts. The other two thirds inside the satellite will contain boards not implementing the PC104 standard. This is necessary due to some circuit boards needing more space than provided by the PC104 standard. Those boards are stacked on top of each other and screwed in place through different holding mechanisms connected to the main structure. A dedicated maintenance port for software updates and debugging will be located on one of the satellite's sides.

4.2 OnBoard Data Handling

The onboard and data handling unit on SOURCE will consist of two main processors and one processor dedicated to the payload camera. The two main processors will be two ISIS iOBCs. They will run in cold redundancy. All connections to and from the OBCs are routed through a daughter board, which is able to switch them between the OBCs. These switches can either be operated by the OBC itself or by the Power Control and Distribution Unit (PCDU). The switching through the PCDU can also be triggered via high priority commands (HPC). The OBC will evaluate and execute all commands sent by the ground station. It is able to switch on and off all component groups through the switches located on the PCDU. In addition to this, it will read all sensors located in the interior of SOURCE and all payload excluding the camera which is connected to the second processor, the payload onboard computer (PLOC). This computer will capture all images and run the preprocessing. Both the star and horizon tracking algorithms will also run on the PLOC. It will be connected to the OBC through a USB connection. Due to power restrictions, the PLOC will only be running when the camera is needed.

On the software side, SOURCE builds on the flight software framework of the Flying Laptop (FLP). This framework provides an abstraction of the hardware and is capable of handling Packet Utilization Standard (PUS) packages. It runs on FreeRTOS. Upon this, SOURCE will implement its mission specific functions and sensors in an object-oriented manner.

4.3 Power

A continuous power generation on the satellite is guaranteed by multiple solar cells in combination with the PCDU and a set of batteries.

The main solar cells are located on expandable panels. In addition to those cells, SOURCE carries solar cells all over the structure, where ever no other system needs a surface place. All solar cells are separated into a total of ten independent power input strings ensuring operability even in the case of a malfunction of a single string. For simplicity, those ten strings are combined in pairs, resulting in five input clusters connected to the PCDU.

The PCDU will be developed during the SOURCE project. On the input side, it will feature separated inputs for the different solar cell clusters. Each input features a maximum power point tracker (MPPT) including a charger circuit for the battery. After the MPPTs all strings are combined to a single power bus. The battery is connected to this bus through a switch. This battery pack contains eight cells, distributed over two cell strings. Therefore, operability of the battery pack even in case of a failure of one string is ensured. Currently, two different battery packs are considered, the GomSpace BPX and the Pumpin BM2. Both battery packs are available as ISS compliant versions so a launch from the ISS would be possible. The final decision on one battery pack will be done by a trade-off during phase B. On the output side, the PCDU provides different powerlines for different components, including a 3.3V, 5V, 12V, and an unregulated line. Each voltage regulator can be separated from the PCDU via a latch-up protected switch up front. After each voltage regulator, each component group is connected through its own power line. These lines are once again separable through latch-up protected switches. In addition to these switches, each component group has a dedicated

fuse protecting both the components and the PCDU. The controlling of all switches will be done through redundant microprocessors located on the PCDU board. These processors will also monitor all component groups for their power consumption. As an additional safety feature, the PCDU will implement a watchdog for the OBC, which can restart it if no communication is possible.

The PCDU is directly connected to the communication system for receiving HPCs. These commands bypass the OBDH, so basic operations can be issued even when the OBC is not available. This includes switching between the redundant OBCs and restarting them.

First power simulations implementing the operational concept are planned for phase B. This shall ensure that the system is capable of generating and storing enough power for sufficient payload operations.

4.4 Communication

The Communication system separates into two different transceivers, a primary and a secondary communication link.

The primary communication module communicates in the commercial S-band. It will consist of a Syrlinks EWC31 transceiver board connected to a second board featuring an FPGA implementing all necessary CCSDS protocols. This board will then be connected to the OBC via an RS232 link.

Two passive patch antennas will be developed by the SOURCE team at the University of Stuttgart. They shall be hemispherical antennas for omnidirectional communication. First simulations are planned through phase B.

The use of several CCSDS standards in the communication with ground stations ensures compatibility with a broad network of ground stations from different providers. The main ground station in use will be the one at the IRS at the University of Stuttgart currently used for the Flying Laptop satellite [5].

The operational phase of SOURCE will continue until the satellite is destroyed during re-entry. Especially the last orbits are of great interest to the scientific payload flying on SOURCE. Therefore, SOURCE must carry a secondary, position independent communication system. For this purpose, different possibilities are investigated, including Iridium and Globalstar. The final decision on a system is planned for the end of phase B.

As redundancy on the satellite, SOURCE will be able to receive command and send basic telemetry data via the inter-satellite communication. So, in case of a failure of the main S-band communication system and a specified time without communication, the satellite will automatically switch over to the inter-satellite communication. On the ground segment side, cooperations with ground stations all over the world will be established. Beside their use during LEOP and during the last orbits, those ground stations can be used in case of a failure of the main station in Stuttgart.

4.5 Attitude Control

For determination of the current position, two GPS receivers are used featuring a specialized firmware provided by the manufacturer for satellite development to overcome the restrictions of civilian systems regarding flying altitude and speed. Combined with magnetometers the position is then used to determine an attitude relative to the Earth's magnetic field. For this purpose, the World Magnetic Model will be used. In addition, redundant photodiodes on all sides of the satellite are used to determine a sun vector and gyroscopes are used to determine current rotation rates. Those values are then fused to a final attitude.

Due to volume and power limitations of the satellite, no propulsion systems or reaction wheels are implemented for attitude controlling. The only actuators are three magnetic torquers. With these, the satellite will be able to perform inertial pointing currently planned with an accuracy of at least 20°. Nadir pointing will be implemented for testing purposes, a target pointing however is not needed for the planned payloads and will therefore not be implemented.

During different modes of the ACS, different sensors are used for attitude determination. After launch and ejection from the deployer, the satellite shall reduce its spinning rates through a detumble mode. In this mode, only the magnetometers are used for attitude determination. When the satellite reaches a decreased spinning rate, the system will transit into safe mode. In this mode, in addition to the magnetometer, the sun sensors are used, and the ACS orients the satellite's main solar panels towards the sun and keeps this orientation. During nominal operation either the idle or the inertial pointing mode is active. Both modes use all available sensors for attitude determination, which includes the magnetometer, GPS, sun sensors, and gyros. In the idle mode, the satellite, like in the save mode, tries to orient itself towards the Sun, but this time also reduce spinning rates around the sun vector. This mode is used, whenever no payload or communication requires a specific attitude. During inertial pointing, the ACS orients the satellite towards a given attitude and keeps this orientation. The exact modes of ACS for communication and payload operations will be determined during phase B.

4.6 Thermal

SOURCE is a cold biased system, meaning it only carries heating elements and no active cooling elements. The operational modes are adapted to not overheat the system.

For thermal sensing, over 30 temperature sensors are distributed over the whole body of the satellite system. Those sensors are connected to resistance-to-digital converters (RTDs) which are processed by the OBC. The OBC then regulates the heating elements, which are attached to critical components yet to be determined. A first thermal simulation led to the result that the star tracking camera needs additional heaters for modes in which it is not active in the desired 500 km SSO as well as in an ISS orbit

5. SIMULATION

To guarantee a flawless operational phase, the SOURCE project includes a simulator for the whole satellite. Besides full simulations of all components, the simulator will also support software-in-the-loop (SITL) and hardware-in-the-loop (HITL) simulations. This

is realized through a variety of external connectors to the simulation hardware, where each sensor can be attached to. Prior to operations, the satellite controlling room in Stuttgart can be configured to communicate with the simulator like it would with the actual satellite. This will be used for training purposes of the ground personnel. During operations, the simulator will be used as a testing platform for software updates.

6. ORGANIZATION

The SOURCE project is mainly executed by students at the University of Stuttgart. SOURCE follows a hierarchical management structure, starting at the project lead, consisting of two students responsible for all management activities. They are supported by employees at the IRS. On the next lower management level, there are two student system engineers. They are responsible for the inter-system compatibility and assist the project lead in technical decisions. The rest of the team is separated into seven different working groups including payload, communication, onboard data handling (OBHD), power, attitude controlling (ACS), structure and thermal, as well as simulation. Each team has a group leader and is supervised by a dedicated employee at the IRS.

The necessary workforce is acquired though members of KSat e.V. and an appended lecture. This lecture teaches the basics of satellite development and is used as a team meeting discussing the current state for each subsystem and current problems. In addition, SOURCE is regularly presented in specialized lectures and courses throughout different courses of study to acquire specialized students for different regions.

Within the project, different web-services are used for communication and data handling, all hosted on own servers at the university. Most communication within the team is done via a Mattermost server, complemented by e-mails. All data is stored on a Nextcloud server with regular backups, to ensure data integrity. Software code and the documentation, written in LaTex, is synchronized and versioned via a GitLab instance. Time and work package tracking is done through OpenProject.

Since SOURCE follows a standard space project phase structure reviews are planned after each phase, include a PRR, a PDR, a CDR, an FRR, and an ORR. For those events, external experts are invited to the university, examining the project and providing the team with recommendations and improvements. In this way the phase A completed with the PRR.

7. FURTHER WORK

Phase A was successfully finished with the PRR Review conducted by experts from both industry and research. During the next phases, the design of SOURCE must be finalized. This also includes the redundancy concept, the testing, and integration and a schedule for a launch and the operational phase.

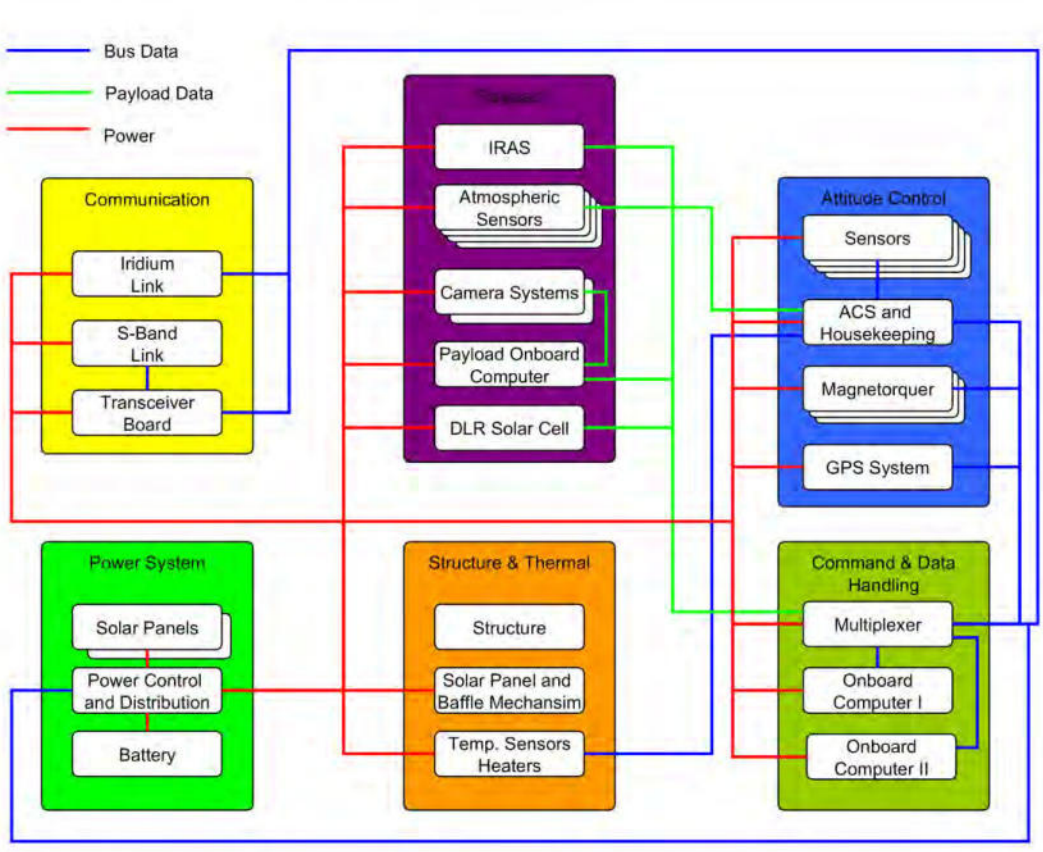

Figure 2: Block schematics of the SOURCE satellite.

8. REFERENCES

[1] S. Hümbert, L. Gleixner, E. Arce, P. Springer, M. Lengowski, I. Sakraker Özmen, MATERIAL CHARACTERIZATION OF ADDITIVELY MANUFACTURED PA12 AND DESIGN OF MULTI-FUNCTIONAL SATELLITE STRUCTURES, ECSSMET, May 28 – June 01, Noordwijk, Netherlands, 2018

[2] Fasoulas, S., Loehle, S., Steinbeck, A., & Eberhart, M., Atomic Oxygen Sensor Systems Aiming In-Flight Measurements on a Sounding Rocket, Publication Proceedings of the 20th Symposium on European Rocket and Balloon Programmes and Related Research, held in Hyére, France in October, 2011. ESA SP-700

[3] Reschke, W.; Binder, T.; Kleinert, J.; Mirza, A.; Nizenkov, P.; Pfeiffer, M.; Fasoulas, S.; Copplestone, S.; Ortwein, P.; Munz, C. D., Recent developments of DSMC within the reactive plasma flow solver PICLas, AIP Conference Proceedings, Volume 1786, Issue 1, id.130003

[4] G. Grillmayer et al., Flying Laptop--Micro-Satellite of the University of Stuttgart for Earth Observation and Technology Demonstration, 55th International Astronautical Congress, Paper IAC-04-IAA, vol. 4, p. 08. 2004.

[5] J. Keim, K. Klemich, N. Bucher, J. Burgdorf, S. Klinkner, J. Eickhoff, "Operational Experience of the Transition from Initial to Nominal Operations of the University Small Satellite "Flying Laptop"," Proceedings of the 69th IAC (International Astronautical Congress) Bremen, Germany, 1-5 October 2018, paper: IAC-18,B4,3,2

Stuttgart University's reliable, high-performance small satellite platform on its first mission "Flying Laptop"

Sabine Klinkner[1], Steffen Gaisser[1], Jonas Keim[1], Kai-Sören Klemich[1], Michael Lengowski[1], Ulrich Mohr[1]

[1]Institute of Space Systems, University of Stuttgart,
Pfaffenwaldring 29, 70569 Stuttgart
Phone: +49 711 685 62677, Mail: klinkner@irs.uni-stuttgart.de

Abstract: In the recent years, the Institute of Space Systems of the University of Stuttgart developed the small satellite "Flying Laptop". This mission is built upon a reliable, high performance small satellite platform that has been developed at the University of Stuttgart in close cooperation with space industry and research institutes. The Flying Laptop was launched in July 2017 and carries out Earth observation tasks and verifies new technologies in orbit since then. The satellite has a mass of 110 kg and is thus the largest satellite system launched by a German university. The chosen development approach for the Flying Laptop satellite led to a one-failure tolerant system, applying radiation hard components. The qualification procedures for the satellite system are based on European space standards and the satellite design and verification followed the approach of space industry. Also for the satellites operations, the university applies the same tools as used by professional managed satellite control centres. This paper gives an insight on the realisation of a satellite of such a significant mass and complexity. It will specifically focus on the robust satellite bus providing the resources for the operation of demanding state of the art payloads.

1 INTRODUCTION

The small satellite "Flying Laptop" is operated entirely by a student team using the university's ground station and mission control infrastructure. The satellite's payload includes a receiver for ship tracking, a multispectral camera system and a wide-angle camera. Two payload downlink systems are integrated, a conventional downlink system in the ham-radio S-Band with 10 Mbit/s data rate and the optical communication system OSIRISv1, provided by the German Aerospace Centre (DLR), transmitting at a data rate of up to 200 Mbit/s. Despite the increased level of complexity due to the chosen approach, the project is embedded in the university environment and fully serves educational purposes: The satellite was mainly realized by PhD-students with the support of undergraduate students and some guidance of industrial experts. The project offers perfect boundary conditions to provide hands on experience at the university and due to the professional approach a perfect preparation for a later employment in industry. Furthermore, the project is used as a valuable example within lectures providing an insight on topics of all fields of space engineering such as system design, system qualification and verification as well as operation activities.

2 MISSION STATUS

This chapter presents collected telemetry data from the satellite bus to emphasize the satellites bus reliability and performance. All listed statistics are based on data since the beginning of the mission until end of March 2019. The satellite is approaching its two-year design lifetime, however still all bus components are performing exceptionally without any sign of degradation. Due to its single point of failure tolerant design all bus components are available in a hot or cold redundant configuration. The redundant radiation hardened on-board computer (OBC) includes Error Detection and Correction (EDAC) mechanisms to correct radiation induced single event upsets.

2.1 Reliability - Satellite Platform Availability

The satellite platform availability is the percentage of time that the system is ready to conduct payload operations requiring all high-level components, this system mode is called idle mode. It can be understood as a measure of the reliability of the system and its associated operations. Time periods in which the satellite is in safe mode reduce the availability, as only basic attitude control components are active. The satellite can be in planned safe modes, for example for testing purposes. Unexpected safe modes can be triggered by reboots or core switches of the OBC or the Power Control and Distribution Unit (PCDU). Furthermore, malfunctions of individual components can trigger a Fault-Detection, Fault-Isolation and Recovery (FDIR) fall-back reaction resulting in a safe mode. To determine the availability all occurred anomalies during operations and the duration of the troubleshooting were collected.

Table 2.1 Occurred OBC Reboots

Plan.	Reboot occurred	System back to Idle	Cause
yes	2017-07-14 09:05:52		Initial boot after separation
yes	2017-11-28 09:52:06		Check out procedure redundant OBC
yes	2017-12-13 09:09:21		1. OBSW update, switch to nominal OBC
no	2018-01-12 09:16:50	2018-01-15 09:37:08	OBSW bug (TC schedule overflow)
yes	2018-02-20 09:06:28		2. OBSW update
yes	2018-07-12 09:36:57		3. OBSW update
no	2018-09-14 21:23:37	2018-09-18 09:26:26	PCDU switched operating processor
yes	2018-09-18 09:23:33		4. OBSW update
no	2018-11-23 03:17:36	2018-11-24 08:54:52	PCDU switched operating processor

As shown in Table 2.1 three unplanned reboots occurred during the mission so far, one was triggered by an on-board software (OBSW) bug, which could be fixed with the 2. OBSW update 39 days later. The other two reboots were both triggered by a switchover of the operating processor of the PCDU. After a reboot, the satellite stays in its safe mode until commanded to one of its higher modes. After most planned reboots the satellite system was commanded back to idle mode during the same pass. If unexpected reboots occurred, the satellite was left in safe mode until the error investigation was completed.

Table 2.2 shows all so far occurred safe mode fall-backs. Only one fall-back was caused by an OBSW bug, the remaining fall-backs were triggered by too tight monitoring limits and problems with one payload causing effects on the satellite bus, due to a shared fuse of the PCDU.

Table 2.2 FDIR triggered Safe Mode Fall-backs

Safe Mode Occurred	System back to Idle	Cause and Resolution
2017-08-21 19:20:27	2017-08-22 11:26:57	Rotation rate of the S/C was over its limit, FDIR triggered safe mode fall-back. Rotation monitoring limits were set too tight, loosening the limits to allow peaks (but not continuous high rotation) worked.
2017-10-03 08:02:31	2017-10-03 08:50:13	FOG3 hardware error and missed reply. Was marked as faulty by FDIR, as fault counter and recovery counter were not decremented due to a OBSW bug. Both counters reset and bug fixed with following OBSW update.
2019-02-21 15:28:56	2019-02-22 10:28:55	MICS NIR did not consume any power (sporadic internal error in the MICS) and was marked as faulty. STR on same fuse was also marked as faulty, triggered fall-back to safe mode.
2019-03-19 22:57:15	2019-03-20 09:46:58	Attitude determination output was set to invalid due to a too restrictive monitoring. Caused a RW control speed monitoring event to force a fall-back to safe.
2019-03-23 15:01:45	2019-03-25 09:01:36	Same MICS NIR power monitoring problem
2019-03-26 15:09:57	2019-03-27 09:21:40	Same MICS NIR power problem. Disabled temporally power monitoring for MICS, waiting for OBSW update. MICS NIR still functioning correct.

This leads to an overall availability of the satellite system of 98.04% for payload operations. Furthermore it should be noted, that the time required to recover the satellite is mainly driven by operational factors, including ground station passes and work shifts. On a positive note, the satellite was recovered in most cases within a single pass. On the one hand, this demonstrates the robustness and strengths of the chosen mode hierarchy concept in the OBSW, but also the ability of the operations team to react quickly and purposefully to anomalies. [1]

2.2 Performance - Satellite Platform Pointing Capabilities

The satellite bus features a three-axis stabilized attitude control system (ACS) with two star trackers (STR), four fibre optical gyros (FOGs) and as main actuators four reaction wheels (RWs). Four pointing modes are implemented, nadir, inertial, target and sun pointing. For basic attitude control and for the desaturation of the reaction wheels magnetorquer, magnetometers and sun sensors are used. Overall a pointing knowledge of 7 arcseconds and a pointing accuracy of below 150 arcseconds is achieved. Position data is collected using three GPS receivers. The three GPS receivers on board the Flying Laptop have already been used to perform attitude determination of the satellite. [2]

Figure 2.1 shows the combined pointing error during a target pointing over a ground station pass with an elevation between 10° and 48°, when settled a RMS error of 45.78 arcseconds was reached. The satellite switches 5 minutes before the pass from sun-pointing idle mode to ground station target pointing. Slew rates of up 1.5°/s for quick target acquisition or multiple passes are possible. With this achieved pointing accuracy, successful optical communication links could be established. [3]

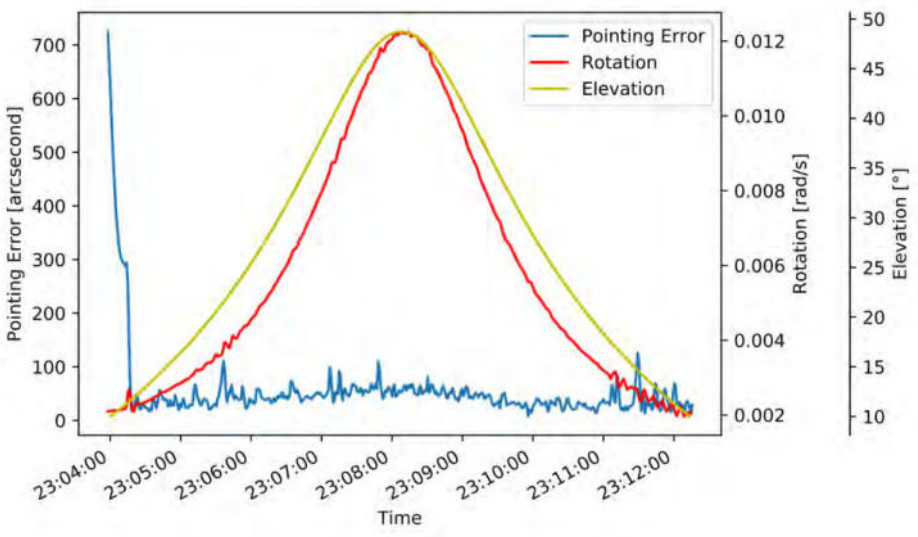

Figure 2.1 Target Pointing Error and Rotation on 2018-12-20

2.3 Performance - Satellite Platform Power Supply

The solar panels can provide a maximum of up to 270 W of electrical power, the satellite bus consumes in its Idle mode around 40 W of power, for continuous payload operations up to 100 W are available depending on the satellites orientation. Figure 2.2 shows the battery state of charge (SOC) in red and the bus power in blue for a 24 h period with continuous payload operations in nadir pointing mode. The grey shaded areas mark periods when the satellite is in eclipse. Despite being in nadir pointing mode and therefore in a suboptimal not continuous sun orientation the SOC never drops below 88%. During most orbits, the battery can be charged fully with the exception of three subsequent communication windows with active transmitters.

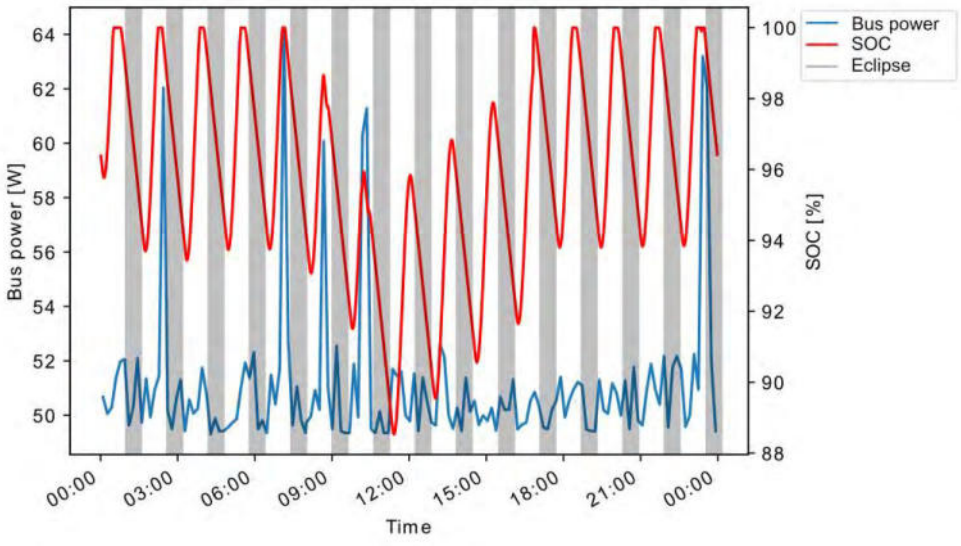

Figure 2.2 Battery SOC and Satellite Bus Power

3 SATELLITE OPERATIONS

The Launch and Early Operations Phase (LEOP) was finished within 4 days, the first image with the wide-angle camera was taken and downlinked on the 5th day after launch, demonstrating the high-performance and reliability of the satellite, but also the well planned operations and previous verification tests on ground. Since then, the satellite has been operated regularly and continuously. [4]

3.1 Ground Station Network

The commercial S-band frequency is used for communication with the satellite. This provides good compatibility with professional ground stations, even though the satellite is nominally operated via the institute's own ground station. The compatibility enables to build up a network of ground stations as being used during the LEOP, leading also to high reliability for the operation of the satellite and a high number of usable passes. All ground infrastructure is in secured network with a connection to DLR via Space Link Extension (SLE). In any case, the operation is fully conducted from the control centre at the University of Stuttgart and is highly automated.

3.2 Operations Execution

Operations for the Flying Laptop mission are organised as following: A Flight Director is responsible for one week of operations, his or her duty include coordination with external payload stakeholders, approving of recommendations and basic health monitoring. Typically, five to six passes are used each day, only one pass each working day is used to command the satellite, the remaining passes are all downlink-only passes with prescheduled downlinks of TM and payload data. Only one antenna controller needs to attend the pass in the control room, due to legal reasons when using the uplink, his or her responsibility is to monitor the antenna and to send a prepared command stack to the satellite.

In the considered period more than 4570 passes were executed, 1700 of them with uplink so far. During these uplink passes around 254 000 tele commands (TC) were sent to the satellite and more than 347 million telemetry (TM) parameters were received. A complete TM archive of the mission is available and is intensively analysed, providing a valuable data basis for further improvements and verification of design models.

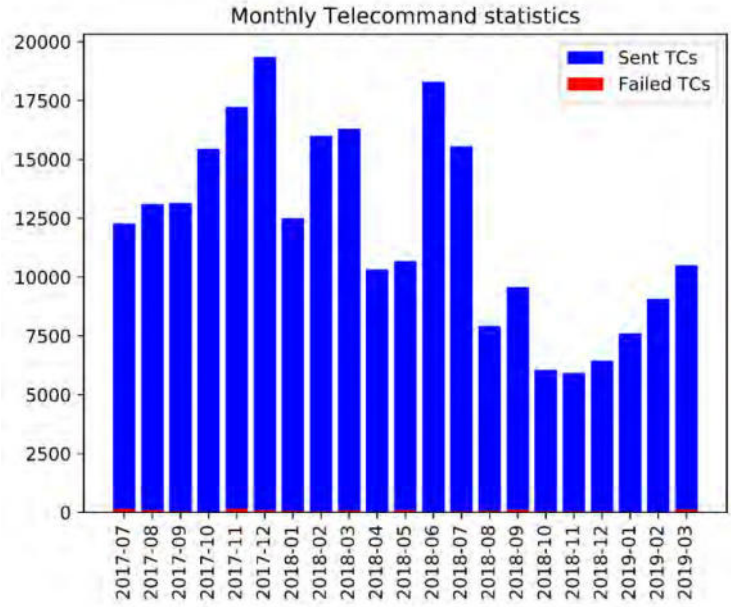

Figure 3.1 Monthly TC statistics

Figure 3.1 shows the number of TCs send each month to the satellite; only 1498 TCs failed or were declined so far, those failed mostly because of mission planning errors, like conflicts resulting in the wrong mode or parameter for a TC. The in-orbit OBSW Updates (in Dec. 17, Feb. 18, Jul. 18 and Sep. 18) are also clearly visible as a complete software image consisting of around 5000 TCs needs to be sent to the satellite. After the third OBSW update operations related simplifications were added, reducing the amount of TCs for mode changes significantly. In January 2019 an update to the mission planning system introduced a payload campaign ticket type, which allows for automated planning of repeated payload data takes and therefore drastically increases the number of payload data takes and sent TCs to the satellite. Around 450 TCs per daily uplink pass are nowadays sent to the satellite. [5]

Such a high amount of TCs cannot be created manually in the given time and additionally, such an immense amount of manual work would be error prone. Therefore, flight dynamics, mission planning and command stack creation is fully automated. Most of the commands are not executed live during a pass, but between the passes to a predefined time as so called time-tagged TCs. Highly automated operations are necessary to fulfil all requests for the different payloads. [6]

3.3 Orbit Data

Continuous on-board GPS measurements are used to generate an own set orbit data and TLEs, which are then used in the mission planning system and for antenna control. Figure 3.2 shows 14 TLEs from Norad in calendar week 14, year 2019 and their respective position error around epoch date compared to the on-board GPS measurements. As no orbit control system was implemented, the Flying Laptop is exposed to orbit drift. Figure 3.3 shows that the semi major axis is reduced by only 1 km and LTAN drifted from 11:30 to 10:30, showing direct effect on pass and observation times. To fulfil the European Code of Conduct for Space Debris Mitigation the satellite system includes a de-orbit mechanism to ensure that the satellite will be removed from orbit within 25 years.

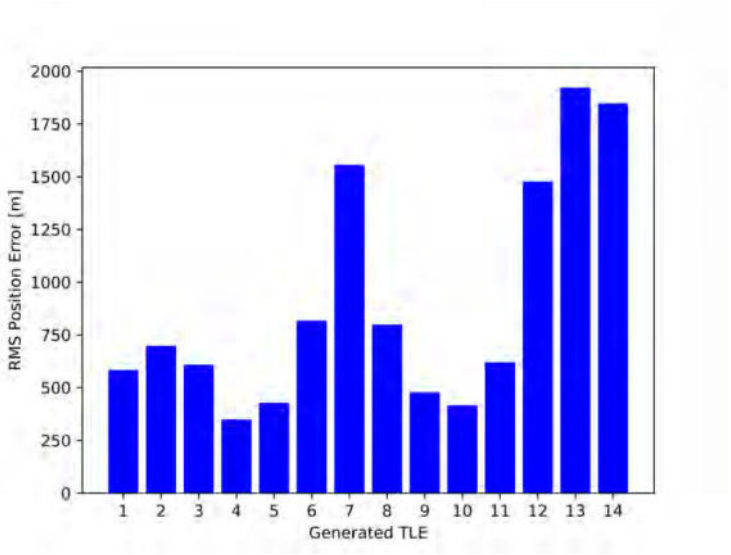

Figure 3.2 Comparison between NORAD TLE and GPS

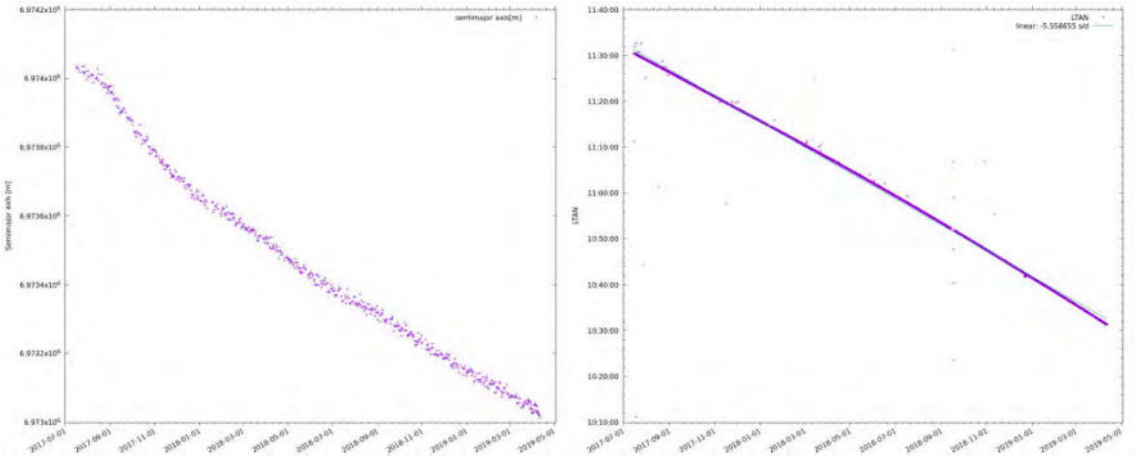

Figure 3.3 Orbit semi-major axis and LTAN drift

4 CONCLUSION

The detailed insights given above on the status of the in-orbit mission of the Flying Laptop satellite proof the robustness of the satellite platform and its readiness for a large number of state of the art payloads: The satellite platform provides a dependable, high pointing accuracy, which is often required by a variety of payloads or communication components. The power subsystem of the Flying Laptop allows for a continuous operation even of combined payloads, still minimising the wear on the power subsystems and thus allowing long-term missions. Furthermore, the overall availability of the satellite system is outstanding, on the one hand due to the high reliability and robustness of the satellite bus with its redundancy and FDIR scheme as well as its carefully developed and tested flight software, and on the other hand due to its operations approach.

It is a major advantage, that the satellite system knowledge and its operation is under one roof at the University of Stuttgart. The operational phase was extremely well prepared and throughout the mission, continuous work is invested to further automate and improve the operations, leading to an increased efficiency and to reduced error rates. A further

factor for the reliability of the satellite operation is the use of a ground station network. Early on it was taken care to set up a secure and stable interface to professionally managed ground stations, which is continuously maintained and further developed. Short communication paths, well prepared operation procedures and a well designed fall-back policy for operation provide a perfect set-up for an agile satellite operations team and thus for reliable satellite operations.

Building up on these factors the original mission goals of the Flying Laptop satellite have been significantly extended, with additional scientific tasks and further in orbit verification activities of the new technologies, and its operational lifetime has been doubled.

5 ACKNOWLEDGEMENTS

The launch and operations of the Flying Laptop satellite has been funded by the Federal Ministry for Economic Affairs and Energy of Germany (BMWi)

6 REFERENCES

[1] S. Gaisser, U. Mohr, B. Baetz, K. Klemich, J. Keim, J. Eickhoff and S. Klinkner, "In-Flight Experience with an Object-Oriented Flight Software," in *The 4S Symposium*, Sorrent, 2018.

[2] A. Hauschild, U. Mohr, M. Markgraf and O. Montenbruck, "Flight Results of GPS-Based Attitude Determination for the Microsatellite Flying-Laptop," in *ION ITM* , 2018.

[3] C. Fuchs, C. Schmidt, J. Keim, F. Moll, B. Rödiger, M. Lengowski, S. Gaißer and D. Giggenbach, "Update on DLR's OSIRIS Program and first results of OSIRISv1 on Flying Laptop," in *SPIE LASE*, San Francisco, 2019.

[4] K. Klemich, J. Keim, N. Bucher, J. Burgdorf, M. Böttcher, S. Wenzel, U. Mohr, B. Baetz, S. Gaißer, P. Hagel and S. Klinkner, "The Flying Laptop University Satellite Mission: Ground Infrastructure and Operations after one Year in Orbit," in *DLRK*, Friedrichshafen, 2018.

[5] S. Wenzel, J. Keim and S. Klinkner, "Payload Mission Planning and Data Handling for a University Small Satellite Ground Segment," in *to be published 12th IAA Symposium on Small Satellites for Earth Observation*, Berlin, 2019.

[6] J. Keim, K. Klemich, N. Bucher, J. Burgdorf, S. Klinkner and J. Eickhoff, "Operational Experience of the Transition from Initial to Nominal Operations of the University Small Satellite "Flying Laptop"," in *69th International Astronautical Congress*, Bremen, 2018.

The TUBIN mission within the context of present and future satellite-based fire detection systems

Julian Bartholomäus, Marc Lehmann, Merlin F. Barschke

Technische Universität Berlin, Institute of Aeronautics and Astronautics
Marchstr. 12, 10587 Berlin, Germany
Phone: +49 30 314-24182, Mail: julian.bartholomaeus@tu-berlin.de

Abstract: In recent years, the abundance of wildfires has been increasing for the majority of biomes and a trend towards a higher number of fires even affecting those areas that were formerly spared from extensive wildfires such as boreal forests and tundra has become apparent. These wildfires inject a significant amount of gases and aerosols into the atmosphere and thereby impact the global climate. To foster an effective wildfire management and to monitor the impact and abundance of such fires, data related to these events need to be collected and transferred to the user at a global scale. Important characteristics of these data are radiometric and geometric resolution, as well as the time coverage. Among other sources, satellites have been used for more than two decades to generate such data and continue to do so today. While dedicated fire detection products remain restricted to only a few satellite systems, there are several satellites with fire detection capabilities. This paper presents an overview on past, present and proposed satellite missions enabling satellite-based detection of active fires. Here, the different missions are compared against one another in terms of fire detection approaches and instrumentation.

1. INTRODUCTION

Wildfires have become more and more prevalent throughout the past decades and their numbers are projected to increase for the majority of biomes currently threatened by them. Moreover, those regions that were previously spared from wildfires are in danger of turning into wildfire territory in the medium to long-term [1]. Additionally, wildfires are a significant contributor to the global greenhouse gas emissions themselves totalling 6% of global 2014 fossil fuel CO2-emissions on average between the years 1997 to 2016 [2]. Furthermore, vegetation that is lost to wildfires can no longer serve as a carbon sink as sequestration of carbon dioxide is inhibited [3]. Apart from the ecological damage, economic losses have been increasing as well with more than eleven wildfire seasons within the last 20 years reaching a net economic damage of more than 1 billion US dollars [4]. With increasing greenhouse gas emissions and interconnected higher temperatures, wildfires are both symptom and cause of climate change.

To monitor the effects and the prevalence of wildfires and to aid effective wildfire management strategies, wildfire data needs to be collected and provided to the user at a global scale. Here, the merit of the collected data is decided by its geometric and radiometric resolution and temporal coverage. An effective approach to collecting global data sets have been satellite missions equipped with instrumentation usable for deducing information regarding past and present wildfire occurrences.

Examples of satellite missions or instruments providing fire products are MODIS, NOAA-AVHRR and SPOT [5,6,7]. Here, the provided data ranges from active fire detection to the detection of fire scars and the corresponding vegetation classification and mapping in various spectral bands at varying geometric and radiometric resolutions. Looking into small satellite missions, the most notable mission to date is the BIRD mis-

sion [8] and its successors TET-1 and BIROS [9] that are specifically aimed at active fire detection in the infrared regime.

Another small satellite mission aimed at the detection of active high-temperature events in the thermal infrared range of the electromagnetic spectrum is the TUBIN mission of Technische Universität Berlin. It employs microbolometer sensor arrays in conjunction with a VIS camera based on a CMOS array for wildfire detection.

This paper is aimed at presenting the TUBIN mission and to classify it within the context of past, present and future satellite-based fire detection missions. To this end, it introduces the different data products and the corresponding physical parameters derived within the data sets. Additionally, different approaches to fire detection are outlined. Lastly, the TUBIN mission for space-based detection of wildfires is introduced.

2. FIRE DATA PROVIDED FROM SPACE MISSIONS

In order to monitor forest fire and other high-temperature events from space, there are several different principles that can be used. Most commonly, the remote sensing system dedicated to the detection of high-temperature events aims at detecting the heat emitted by active fires. To this end, sensor suites sensitive within the infrared range of the electromagnetic spectrum are employed (i.e. MODIS, VIIRS, AATSR) [5]. Since the spectral radiance difference between background pixels and fire pixels is the highest for the MWIR range between 3 and 5 µm and decreases for higher and lower wavelengths [5], most sensor systems use an MWIR channel for their fire detection algorithm. Further channels in the SWIR or TIR range are used for false alarm rejection or cloud masking [10].

Another approach to fire detection is constituted by the detection of the smoke plume associated with a wildfire. In conjunction with the direction of the wind and the overall shape of the plume, the position of the fire can be derived with high accuracy. Examples of this approach can be found within studies for the AVHRR imagery [11]. Tracing aerosols within the atmosphere can also serve as an indicator for the presence of fires.

During night-time, it is possible to detect fires due to their irradiative properties within the VIS range, as well. Examples of this can be found for the DMSP-OLS instrument [12].

Next to satellite missions aimed at detecting active fires, there are several missions dedicated to detecting burn scars and comparing the vegetation status of areas affected by wildfires such as the SPOT VEGETATION instrument [7].

As is evident, most of the spacecraft with fire detection capabilities have been conventional spacecraft equipped with large and heavy instrumentation that almost exclusively require active cooling. Using channels sensitive within the medium-wavelength infrared region of the electromagnetic spectrum, most apply dual or multi-channel algorithms to distinguish fire from background pixels.

Looking into small satellite mission, the general approach to fire detection has been based on the use of infrared sensors. Here, examples can be found in BIRD and its suc-

cessors TET-1 and BIROS for the 100 kg class and in UNIFORM-1 for the 50 kg class [13, 14]. The bi-spectral approach developed within conventional satellite missions has been applied on the BIRD satellite family to detect high-temperature events. The BIRD mission denotes the first successful, dedicated fire detection satellite mission using a small satellite. Another notable example of a small satellite mission has been proposed by the Canadian Space Agency. The Canadian wildland fire monitoring system (CWFMS) employs several sets of MIR and TIR line arrays for wildfire detection to be verified on a small satellite platform [15]. The entities of the same sensor system are tilted with respect to one another to allow for a wide swath width and, consequently, improved revisit times for its region of interest. While these spacecraft employ a conventional fire detection algorithm, using cooled MWIR detectors and supplemental SWIR and TIR channels, ALOS-2 and UNIFORM-1 employ a single channel fire detection algorithm based on microbolometer technology sensitive in the TIR range of the electromagnetic spectrum [13,14,16]. In the same vein, the TUBIN mission is dedicated to investigating the capability of microbolometers for the detection of high-temperature events.

An overview over selected system's parameters of different present and future satellite-based fire detection systems is compiled within table 2.

3. THE TUBIN MISSION FOR WILDFIRE DETECTION

The TUBIN mission is a 20 kg-class mission aimed at the detection of high-temperature events. It is the second instalment of the TUBiX20 satellite platform developed at Technische Universität Berlin [17]. The TUBIN mission is scheduled to be launched at the end of 2019 with a mission duration of one year. The satellite is three-axis stabilised and equips a total of three camera payloads that are mounted onto a common optical deck [18]. The payload consists of two microbolometer focal plane arrays that are tilted with respect to the nadir direction to form a wider combined swath that coincides with the swath of the VIS camera. While the camera assembly is mounted onto a middle deck within the satellite, the corresponding baffles are situated on the outer cover of the satellite. The main parameters of the TUBIN payload are summarised in table 1.

Table 1: Properties of the TUBIN payloads at 550 km [18]

	TIR camera	**VIS camera**
Technology	Microbolometer	CMOS
Pixel pitch	17 µm	1.67 µm
Bandwidth	7.5 µm – 16.5 µm	400 nm – 800 nm
Resolution	640 x 512	3664 x 2748
GSD	155.83 m	40.11 m
Swath width (combined)	109 km (147 km)	147 km
Focal length	60 mm	22.9 mm
f-number	1.25	1.4
NETD @ 300 K (detector)	0.05	n/a

Table 2: Overview on remote sensing systems with active fire detection capabilities [6,8,9,13-16,18-29]

System	Spectral bands	Swath width	Spatial resolution	Revisit time	launch date	Satellite mass
ASTER	14 bands (VIS to TIR)	60 km	15/30/90 m	16 days	1999	4.9 tons
(A)ATSR	VIS,SWIR,MIR,TIR	500 km	1 km	3 to 4 days	1991/1995/2002	2.4/2.5/8.2 tons
AVHRR	6 bands VIS to TIR	2900 km	1100 m	daily	1978-2012	4.2 tons
BIRD/TET-1/BIROS	VNIR,MIR,TIR	~500 km	185 m	3 to 4 days	2001/2012/2016	94/115/130 kg
CIRC	TIR	128 km / 83 km	200 m/130 m	N/K	2014/2015	2.1 tons / ISS
CWFMS	VIS,SWIR,MIR,TIR	1200 km	400 m	N/K	N/K	140 kg
DIEGO	NIR, MIR, TIR	75 km / 350 km	< 30 m/< 60 m	N/K	N/K	mounted on ISS
DMSP-OLS	VIS,TIR	3000 km	560 m	daily	1976-2014	1.2 tons
ECOSTRESS	SWIR, TIR	384 km	38 x 69 m	~ 4 days	2018	mounted on ISS
LANDSAT (8)	11 (VIS to TIR)	185 km	30/100 m	16 days	1982-2013	2.6 tons
MODIS	36 bands (VIS to TIR)	2330 km	250/500/1000 m	daily	1999/2002	3.1 and 4.9 tons
NIRST	MIR, TIR	182 km	351 m	7 days	2011	1.3 tons
Sentinel-3	11 bands (VIS to TIR)	1407 km	500 m/1000 m	1.9 days	2016/2018	1.3 tons
SEVIRI	11 bands (VIS to TIR)	3 km	3 km	15 min	2002-2015	2 tons
TUBIN	TIR,VIS	150 km	157/40 m	N/K	2019 (tbc)	23 kg
UNIFORM-1	TIR,VIS	100 km	157/86 m	N/K	2014	50 kg
VIIRS	VIS to TIR	3000 km	375/750 m	12 h	2011	2.3 tons

By tilting the optical axes with respect to the spacecraft's nadir direction, the imaged swath in the TIR regime can be widened to match the swath width of the VIS imager, which will be used for georeferencing and cloud detection purposes. With this configuration, the overlapping area of the two TIR cameras can be used for noise reduction purposes while the widened swath increases the probabilities of imaging a fire in continuous imaging mode.

Figure 1: CAD rendering of the TUBIN spacecraft

The operation scenarios will be aimed at validating the capabilities to detect wildfires in the beginning of the mission by comparing fire positions with reference sensors. In later stages of the mission upon refining the algorithms for different areas of the globe, a more automatised approach to wildfire detection with continuous imaging of those areas prone to wildfires is planned. Here, an automated pre-selection of the gathered data is envisaged to make use of the data downlink capacities more efficiently. The TUBIN fire detection algorithm has been developed and validated using ASTER data containing wildfires or volcanoes located within the territory of the United States. The developed algorithm proved successful in detecting more than a third of those fire pixels filled with fire by more than two thirds [30].

4. THE TUBIN MISSION IN CONTEXT OF SPACE-BASED FIRE DETECTION

The derivation of satellite-based fire products has been driven by the requirements of the user community that extracts those parameters from the data, that are the most useful for their field of application. According to [15], these include the Fire Radiative Power (FRP), the location of the hotspot, the rate of spread as well as the mapping of the burnt area. Since the mapping of burnt area is not comparable to active fire detection, this parameter will not be discussed within this section.

The FRP of a detected fire pixel is a figure of merit that is connected to the fuel consumption of the wildfire, aerosol production and release of trace gases [31]. Generally, it is derived from the MIR channels or, within the bi-spectral approach, retrieved from a combination of MIR and TIR channels. FRP is determined within data products of several sensor systems listed in table 1, for instance, MODIS, BIRD family, Sentinel-3, SEVIRI and VIIRS.

For determining the location of hotspots and high-temperature events, the satellite system is required to detect a wildfire and identify its position on Earth. This figure of mer-

it is closely related to the rate of spread in the method of monitoring it since both are reliant on the (recurring) localization of high-temperature events. For the rate of spread, the time between two detections of the same wildfire determines the usability of the data for firefighting purposes [15].

Within the TUBIN mission, the UNIFORM-1 mission as well as the two missions employing the CIRC sensor, the detection of high-temperature events is based on the contrast of the scene within the TIR range. Using a single-channel approach, background pixels are screened for obvious and candidate fire pixels and evaluated using global and local threshold algorithms. Doing so, the retrieval of the FRP cannot be realised. Within the TIR range, the portion of the incident radiation originating from active fires with respect to the incident background radiation can be underestimated or overestimated depending on the constitution of the background pixels [32]. Instead of an FRP, the fire detection algorithm outputs a binary decision of whether each pixel contains an active fire or not. Fires localised by the TUBIN fire detection algorithm are referenced within their geographical frame. To this end, the TUBIN mission employs a camera sensitive within the VIS region of the electromagnetic spectrum. Here, the better detectability of landmarks can be used to support georeferencing of the wildfire data.

The detection of the rate of spread will be feasible using microbolometer technology if the wildfire is of detectable intensity. Using the orbit configuration of TUBIN, the period between two consecutive passes over the same area ranges from a few days to about a month depending on the location of the target. This duration will generally be too long for a usable estimate on the rate of spread of an occurring wildfire. Based on the results of the mission concept of a nanosatellite constellation for global wildfire monitoring [33], the temporal resolution can be drastically increased by employing a constellation of twelve spacecraft launched into three orbital planes and, thus, yielding daily global coverage and, consequently, more frequent recurring passes for areas of interest. Doing so, an improved potential for monitoring the rate of spread can be realised. To this end, the configuration of the spacecraft can be altered to include more TIR imagers to widen the swath or further reduce the SNR in accordance with the results of TUBIN.

5. CONCLUSION

Wildfires pose severe economic and environmental threats and, therefore, detailed data is needed to effectively manage wildfires and estimate their impact on affected ecosystems. Satellites have provided and keep providing both real-time data to manage firefighting efforts and statistical data such as the progression of burnt area locally and globally. While the detection of high-temperature events has been restricted to large and heavy satellites in the past, the BIRD mission has paved the way for small satellite mission in the field of fire detection. Further advancements in the miniaturization of satellite components have made it possible for even smaller satellites to pursue wildfire detection.

The TUBIN mission is a proof-of-concept mission for the design of a satellite within the 20 kg-class that is capable of detecting fires at medium spatial resolution. The resolution ranges in between the moderate resolution sensor systems that provide very high temporal coverage such as MODIS and VIIRS/AVHRRR (cf. table 2) and specialised high-resolution spectrometers with comparably low temporal resolution such as ASTER and

LANDSAT. While the FRP of high-temperature events may not be distinguishable within the TIR range on its own, the localization of high-temperature events can be realised with a cost-efficient payload and platform design.

ACKNOWLEDGEMENTS

The TUBIN mission is funded by the Federal Ministry for Economic Affairs and Energy (BMWi) through the German Aerospace Center (DLR) on the basis of a decision of the German Bundestag (Grant No. 50 RM 1102).

6. REFERENCES

[1] Moritz, M. A., Parisien, M. A., Batllori, E., Krawchuk, M. A., Van Dorn, J., Ganz, D. J. and Hayhoe, K. (2012). Climate change and disruptions to global fire activity. Ecosphere, 3(6), 1-22.

[2] Van Der Werf, G. (2017). Global fire emissions estimates during 1997-2016. Earth System Science Data., 9(2), 697.

[3] Pan, Yude, et al. (2011). A large and persistent carbon sink in the world's forests. Science, 1201609.

[4] Smith, A., Lott, N., Houston, T., Shein, K., Crouch, J. and Enloe, J., U.S. Billion-Dollar Weather & Climate Disasters 1980-2018, NOAA. Available online at: https://www.ncdc.noaa.gov/billions/events.pdf (accessed November 2018)

[5] Giglio, L., Csiszar, I., Restás, Á., Morisette, J.T., Schroeder, W., Morton, D., and Justice, C.O. (2008). Active fire detection and characterization with the advanced spaceborne thermal emission and reflection radiometer (ASTER). Remote Sensing of Environment, 112(6), 3055-3063

[6] AVHRR Fire Detects from the Fire Identification, Mapping and Monitoring Algorithm (FIMMA). Available online at: https://www.ssd.noaa.gov/PS/FIRE/Layers/FIMMA/fimma.html (accessed January 2019)

[7] Zhang, Y.H., Wooster, M.J., Tutubalina, O., and Perry, G.L.W. (2003). Monthly burned area and forest fire carbon emission estimates for the Russian Federation from SPOT VGT. Remote sensing of environment, 87(1), 1-15.

[8] Zhukov, B., Briess, K., Lorenz, E., Oertel, D., and Skrbek, W. (2005). Detection and analysis of high-temperature events in the BIRD mission. Acta Astronautica, 56(1-2), 65-71.

[9] Lorenz, E., Mitchell, S., Säuberlich, T., Paproth, C., Halle, W., and Frauenberger, O. (2015). Remote Sensing of High Temperature Events by the FIREBIRD Mission. International Archives of the Photogrammetry, Remote Sensing and Spatial Information Sciences

[10] Giglio, L., Schroeder, W., and Justice, C.O. (2016). The collection 6 MODIS active fire detection algorithm and fire products. Remote Sensing of Environment, 178, 31-41.

[11] Chrysoulakis, N., Herlin, I., Prastacos, P., Yahia, H., Grazzini, J., and Cartalis, C. (2007). An improved algorithm for the detection of plumes caused by natural or technological hazards using AVHRR imagery. Remote Sensing of Environment, 108(4), 393-406.

[12] Elvidge, C.D., Nelson, I., Hobson, V.R., Safran, J., and Baugh, K.E. (2001). Detection of fires at night using DMSP-OLS data. Global and Regional Vegetation Fire Monitoring from Space: Planning a Coordinated International Effort, 125-144.

[13] Hiramatsu, T., Yamaura, S., Akiyama, H., Sato, N., Morita, K., Otani, T. and Araki, Y. (2015). Early results of a wildfire monitoring microsatellite UNIFORM-1.

[14] Fukuhara, T., Kouyama, T., Kato, S., Nakamura, R., Takahashi, Y., and Akiyama, H. (2017). Detection of Small Wildfire by Thermal Infrared Camera With the Uncooled Microbolometer Array for 50-kg Class Satellite. IEEE Transactions on Geoscience and Remote Sensing, 55(8), 4314-4324.

[15] Hamel, J.-F. et al. (2015), The Innovative Microsatellite-Based Canadian Wildland Fire Monitoring System. 66th International Astronautical Congress (IAC), Jerusalem, Isreal.

[16] Kato, E., Katayama, H., Naitoh, M., Harada, M., Nakamura, R., Nakau, K., and Sato, R. (2013). Compact infrared camera (CIRC) for earth observation adapting athermal optics. In UV/Optical/IR Space Telescopes and Instruments: Innovative Technologies and Concepts VI (Vol. 8860, p. 88600C). SPIE.

[17] Barschke, M., and Gordon, K. (2014). TUBiX20–A Generic Systems Architecture for a Single Failure Tolerant Nanosatellite Platform. 65th International Astronautical Congress (IAC), Toronto, Canada.

[18] Barschke, M.F., Bartholomäus, J., Gordon, K., Lehmann, M., and Brieß, K. (2017). The TUBIN nanosatellite mission for wildfire detection in thermal infrared. CEAS Space Journal, 9(2), 183-194.

[19] Lasaponara, R., and Lanorte, A. (2007). Remotely sensed characterization of forest fuel types by using satellite ASTER data. International Journal of Applied Earth Observation and Geoinformation, 9(3), 225-234.

[20] Pedelty, J., Devadiga, S., Masuoka, E., Brown, M., Pinzon, J., Tucker, C., ... & Roy, D. (2007, July). Generating a long-term land data record from the AVHRR and MODIS instruments. In Geoscience and Remote Sensing Symposium, 2007. IGARSS 2007. IEEE International (pp. 1021-1025). IEEE.

[21] Schroeder, W., Oliva, P., Giglio, L., Quayle, B., Lorenz, E., and Morelli, F. (2016). Active fire detection using Landsat-8/OLI data. Remote sensing of environment, 185, 210-220.

[22] Elvidge, C.D., Baugh, K.E., Dietz, J.B., Bland, T., Sutton, P.C., and Kroehl, H.W. (1999). Radiance calibration of DMSP-OLS low-light imaging data of human settlements. Remote Sensing of Environment, 68(1), 77-88.

[23] Schroeder, W., Oliva, P., Giglio, L., and Csiszar, I.A. (2014). The New VIIRS 375 m active fire detection data product: Algorithm description and initial assessment. Remote Sensing of Environment, 143, 85-96.

[24] Marraco, H., and Phong, L.N. (2006, May). NIRST: a satellite-based IR instrument for fire and sea surface temperature measurement. Non-Intrusive Inspection Technologies (Vol. 6213, p. 62130J). SPIE.

[25] Rienow, A., Hartmann, M., Heinemann, S., Henkel, H., Jürgens, C., Oertel, D., Rücker, G. and Schultz, J. (2018), DIEGO – Dynamic Infrared Earth Observation on the ISS Orbit. 69th International Astronautical Congress (IAC), Bremen, Germany.

[26] ECOSTRESS Instrument. Available online at: https://ecostress.jpl.nasa.gov/instrument (accessed January 2019)

[27] Roberts, G.J., and Wooster, M.J. (2008). Fire detection and fire characterization over Africa using Meteosat SEVIRI. IEEE Transactions on Geoscience and Remote Sensing, 46(4), 1200-1218.

[28] Wooster, M.J., Xu, W., and Nightingale, T. (2012). Sentinel-3 SLSTR active fire detection and FRP product: Pre-launch algorithm development and performance evaluation using MODIS and ASTER datasets. Remote Sensing of Environment, 120, 236-254.

[29] Simon, M., Plummer, S., Fierens, F., Hoelzemann, J. J., & Arino, O. (2004). Burnt area detection at global scale using ATSR-2: The GLOBSCAR products and their qualification. Journal of Geophysical Research: Atmospheres, 109(D14).

[30] Bartholomäus, J., Barschke and M.F. and Lehmann, M. (2018), Development of a single-channel fire detection algorithm for the TUBIN mission. 69th International Astronautical Congress (IAC), Bremen, Germany.

[31] Freeborn, P. H., Wooster, M. J., Roy, D. P., & Cochrane, M. A. (2014). Quantification of MODIS fire radiative power (FRP) measurement uncertainty for use in satellite-based active fire characterization and biomass burning estimation. Geophysical Research Letters, 41(6), 1988-1994.

[32] Wooster, M. J., Roberts, G., Perry, G. L. W., & Kaufman, Y. J. (2005). Retrieval of biomass combustion rates and totals from fire radiative power observations: FRP derivation and calibration relationships between biomass consumption and fire radiative energy release. Journal of Geophysical Research: Atmospheres, 110(D24).

[33] Grosshans, J. and Barschke, M.F., Mission concept of a nanosatellite constellation for global wildfire monitoring, AIAA SPACE and Astronautics Forum and Exposition, AIAA SPACE Forum, AIAA 2017-5267.

Infrared Remote-Sensing and Results of the DLR FireBIRD Mission

Winfried Halle, Xavier Amigues,Wolfgang Bärwald, Ines Ernst, Christian Fischer, Susanne Koldewey, Andreas Kotz, Axel Lauterbach, Matthias Lieder, Thomas Säuberlich, Martin Schlicker, Christian Schultz, Friedrich Schrandt, Agnieszka Soszynska, Thomas Terzibaschian, Ingo Walter, Andreas Wojtkowiak

DLR, Institute of Optical Sensor Systems, Rutherfordstr. 2, 12489 Berlin, Winfried.Halle@dlr.de

Abstract: Forest- and vegetation fires have become more and more out of control worldwide resulting in a devastating impact on the world's environment. Beside the detection of the fire hotspot itself it is important to evaluate different parameters to support the work of the firefighters (e.g. mean fire temperature, length-of-fire front, cluster size and fire location). On the other hand fires around the world have a major impact on the atmosphere and influence the climate. This influence can be calculated by the fire-radiative -power (FRP) which measures the radiant energy released per time unit by the fires. The German Aerospace Center (DLR) is making a major contribution to fire detection with the FireBIRD constellation. This constellation consists of the two satellites TET-1 (Technology Experiment Carrier) built by industry, launched in 2012 and BIROS (Bi-spectral Infrared Optical System) built by DLR in Berlin and launched in 2016. A new compact bi-spectral infrared system was developed for both satellites capable to detect and evaluate smaller fires and hot spots compared to other infrared remote-sensing systems (e.g. Modis sensor, Sentinel-3). The BIROS satellite is also carrying different new technological experiments for the in-orbit demonstration of features for the next generation of remote sensing satellites.

1. INTRODUCTION

FireBird is defined as a constellation of two small satellites mainly dedicated to the investigation of high temperature events. The first satellite TET-1 was launched on 12. June 2012. The second satellite- BIROS- was launched on 22. June 2016. The outstanding feature of the infrared instruments is their higher ground sample resolution and dynamic range compared to systems such as MODIS as shown in Table 1 and Figure 1.

The comparison with infrared instruments on other satellites will be completed with details of the spectral band design as shown in Figure 2.

2. MISSION DESIGN

Both satellites are flying in a constellation to improve the coverage of the areas of interest. In Figure 3 is shown an example. On the left side is shown the MWIR Image and the planned data take swath for TET at 26. 01. 2017 06:37 UTC (night time), on the right side is shown the MWIR Image and the planned data take swath for BIROS at 28. 01. 2017 13:50 UTC (day time). The images are difficult to compare because of the different time of day and the different contrast due to the huge fire events at 26th January. But it demonstrates the opportunity of the constellation covering the same area within of two days because they have different orbital nodes.

2.1. OPERATION

In Figure 4 is shown the general FireBird Operation Schema. The satellites will be operated by the German Operation Center GSOC with support of the Institute of Optical Sensor Systems in Berlin where the satellites were designed.

	3 line-Camera (3 line FPA)	2 Infrared- Cameras
Wave length	460 - 560 nm 565 - 725 nm 790 - 930 nm	MWIR: 3,4 - 4,2 µm LWIR: 8,5-9,3 µm
Focal length	90,9 mm	46,39 mm
FOV	19,6°	19°
F-Number	3,8	2,0
Detector	CCD- Zeile	CdHgTe Arrays
Detector cooling	Passive, 20 ° C	Stirling, 80 - 100 K
Pixel size	7 µm x 7 µm	30 µm x 30 µm
Number of Pixel	3 x 5164	2 x 512 staggered
Quantization	14 bit	14 bit
Ground Resolution	42,4 m	356 m
GSD	42,4 m	178 m
Swath width	211 km km	178 km
Data rate	max 44 MBit/	0,35 MBit/s
Accuracy	100m on ground	100m on ground

Table 1 Main FireBird camera parameters

The commanding and the control of the satellites will be executed via the antennas in Weilheim. The receipt and the archiving of the scientific data will be realised in the German Data Center in Neustrelitz. Other DLR ground stations will be included on demand.

Nevertheless the DLR ground station net is not sufficient to compensate the disadvantage of the S Band downlink. Therefore additional receiving opportunities are desirable, so in South Africa and in Brasilia.

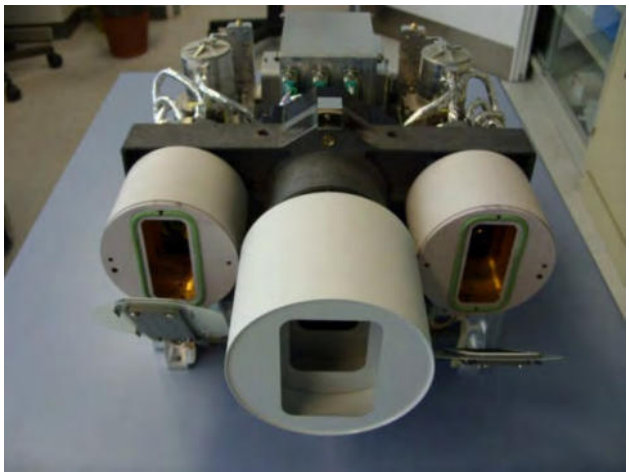

Figure 1 FireBird camera for TET and BIROS

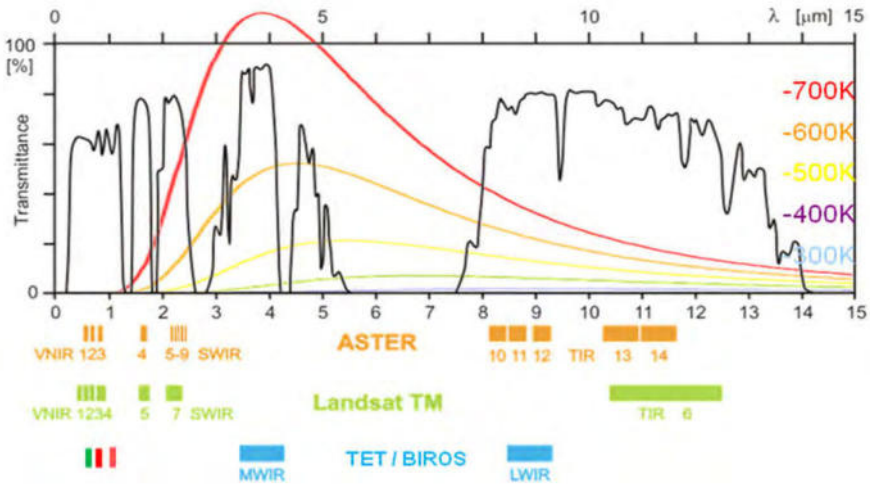

Figure 2 Spectral Design of the FireBird instruments

2.2 The BIROS Satellite

The main payload as described in the introduction is unitary for both satellites. Additional to this the BIROS satellite is equipped with various technological experiments which can contribute in case of a successfully testing to a remarkably improvement of the mission design.

2.2.1 Propulsion Technology: A new High Torque Wheel for a high agility was developed and accommodated in BIROS payload compartment together with a cold-gas propulsion system. The High Torque Wheel will allow very rapid pointing manoeuvres to expand the swath or to perform stereo recordings. The cold-gas propulsion system was mainly used to execute Formation flying manoeuvres with the Pico Sat.

2.2.2 The Pico Sat Launcher: A Pico Sat launching Unit was accommodated on BIROS for separation of BEESAT-4 of the Technical University Berlin. BEESAT-4 is equipped with a GPS receiver and a Satellite Interlink transmitting the GPS data to BIROS. With this combination could be collected a lot of data regarding a constellation fly with several satellites

2.2.3 The OSIRIS experiment: OSIRIS (OSIRIS (Optical Space Infrared Downlink System) is a new onboard optical communication terminal, developed at DLR. Three different laser systems for downlink communications will achieve data rates up to 1 Gbit/s. A beacon laser in uplink will support the BIROS attitude control. It may also be used for an optical uplink.

2.2.4 The OrbComm Modem: BIROS contains a technical experiment using a hardware VHF modem allowing the communication with an ORBCOMM satellite. Via this modem it will be possible to inform directly the ground users via email and SMS about an on-board detected hot-spot with the concerning geo-location.

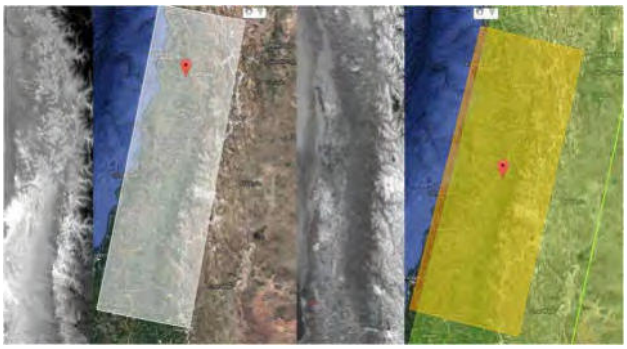

Figure 3 MWIR Image and planned Swath of TET-1(left) and BIROS (right)

2.3 Data acquisition

The data take planning process will be supported by the planning tool SPOT (Figure 4) developed by DLR GSOC (German Space Operation Center). Based on the actual TLE the SPOT tool gives an overview of the satellite orbits at any day.

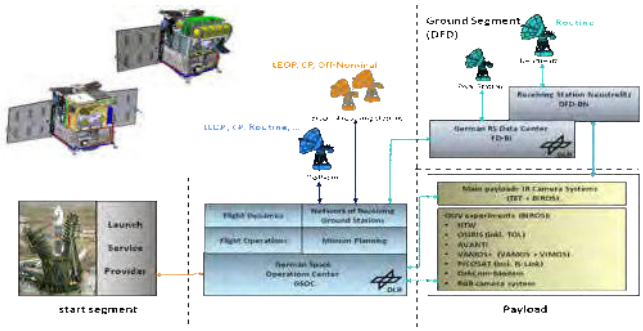

Figure 4 General FireBird Operation Schema

With this it is very easy to get an overview of the possible targets covered by the orbits. It is also possible to select certain targets and ask for all possible data takes within a selected period.

Collecting all incoming planning requests SPOT is managing the necessary recourses like the thermal and the power regime, the available mass memory on board (400 MB) and the available ground stations (currently Neustrelitz in Germany and a polar station). Based on this recourse management it is possible to acquire up to 10 data takes per day.

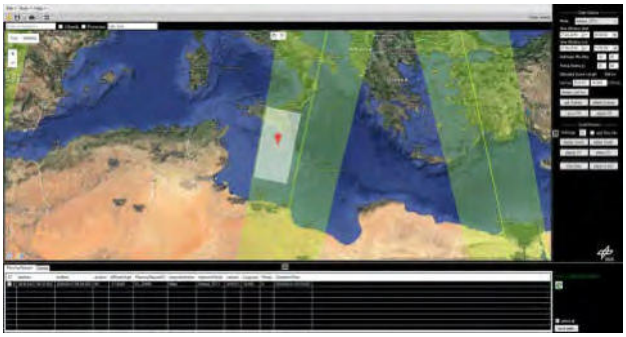

Figure 5: GUI of the data take planning tool SPOT

The user can choose one of four standard instrument configurations which were mainly establish to save on board memory capacity and to minimize the downlink data volume. During the night vision measurements (Fire Night) the visual bands will be switched off. At day the GSD of the visual bands can be switched between 40m and 160m and it can be selected which of the visual bands should be used and transmitted to Earth. In the consequence this is a decision between the GSD and the area to be monitored.

2.4 Data processing and Data Products

The down linked data sets will be collected, sorted and archived in the DLR DFD ground station in Neustrelitz. There is also implemented the Ground Processing Unit generating the FireBird data products.

The level 0 dataset includes -depending on the selected operation mode- up to five measurement files, two calibration files for the infrared cameras and an attitude file.

Based on these raw data files the L1b standard products will be generated. L1b products are radiometric calibrated radiances on top of atmosphere with geographic annotation and related Meta Data Information. This information can be delivered in an ENVI conform format with additional XML files or in a HDF-EOS-5 format.

The L1b standard products are the base for the higher L2 data products. Currently is implemented only the Bi Spectral method for the analysis of High Temperature Events (HTE) as a L2 data product. Other methods like Sea Surface Temperature (SST) are planned.

Valid products will be registered in the DLR EOWEB Catalogue (see Figure 5). Here registered user can search for products of interest and in case of success place orders for level 1b products. These products will be reprocessed from the archived L0 products.

3.) RECENT RESULTS

Since 2013, TET-1 acquired approximately 6000 data takes. With BIROS about 500 Data takes were already done. The most of applications are the detection of hot spots and high temperature events.

3.1 High Temperature Events

Several quite catastrophic fire events occurred in the last two years.

3.1.1 Kalimantan: On the ISRSE36 were shown the images of huge peat fires in October 2014 caused by the El Ninio phenomenon. One year later we had to record much stronger events as shown in Figure 6.

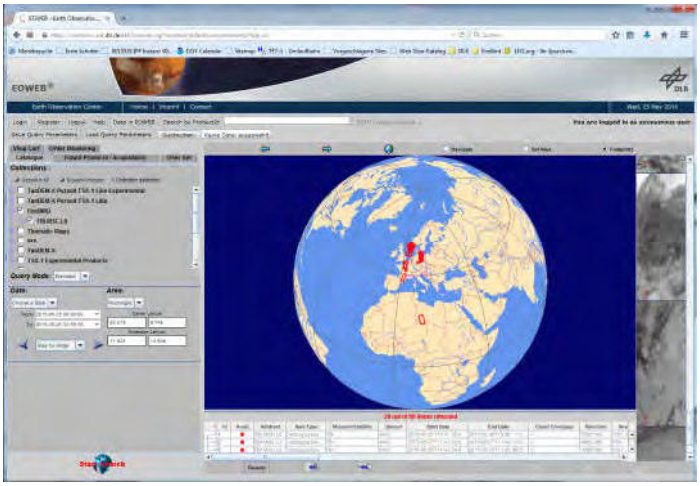

Figure 5: GUI of the DLR EOWEB Catalogue

In the comparison with MODIS is clearly seen the trade-off between ground resolution and swath width. Moreover the TET-1 spectral bands demonstrate a better penetration through the smoke layers. The reason has to be investigated in detail.

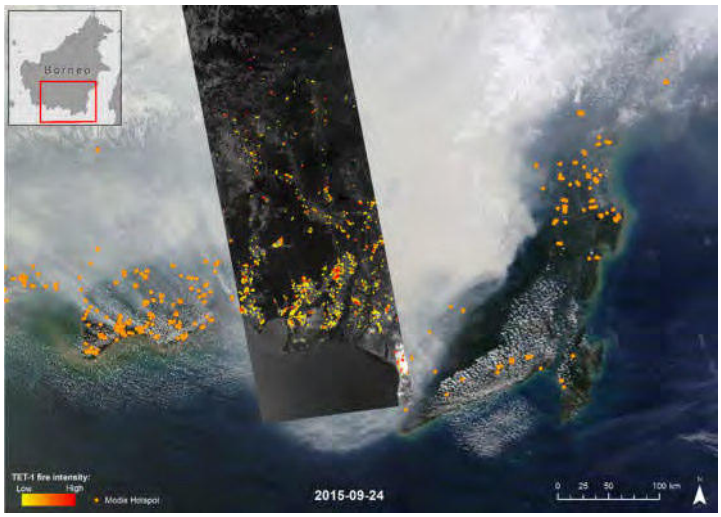

Figure 6 TET imagery with detected fires in Kalimantan superimposed on MODIS from 24 September 2015 (©RSS)

3.1.2 Portugal: Figure 7 shows the development of the fire events in Portugal in the period 11.-14. August 2016. MODIS data serve hereby as a map back up.

3.1.3 Israel: In November 2016 wildfires started in Israel and spread rapidly over the country on the following days. On November 25 at 11:25 UTC, DLR's TET-1 satellite captured major hot spots in the region (Figure 8).

Figure 7 Fires in Portugal 11.-14. August 2016 (© DLR ZKI)

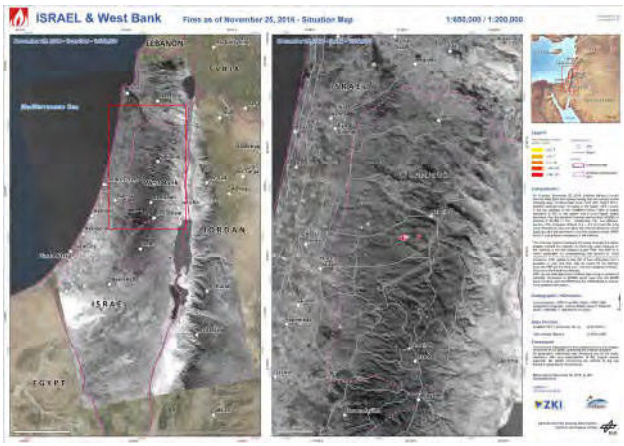

Figure 8 Fires in Israel 25. November 2016 (© DLR ZKI)

3.1.4 Chile: On January 24, 2017, the International Charter 'Space and Major Disasters' was activated for forest fires in Chile. The DLR/ZKI is responsible for the Project Management of this Charter Call and supports the 'Chilean National Office of Emergency of the Interior Ministry' (ONEMI) of Chile with the provision of satellite data and value added disaster information products. Figure 9 is based on a TET-1 data take at January 26, 2017.

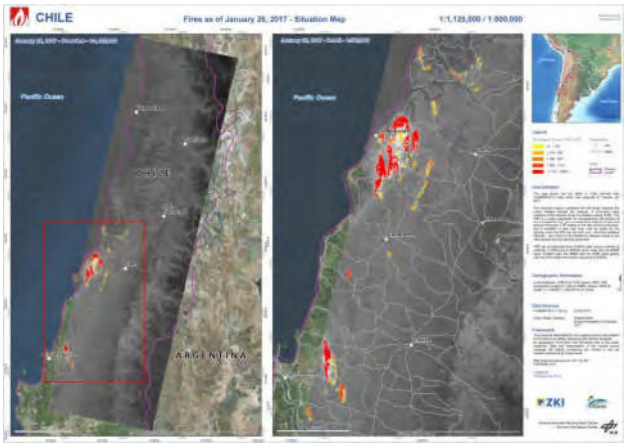

Figure 9 Fires in Chile 26. January 2017 (© DLR ZKI)

3.1.5 BIROS HTE Products: As shown in Figure 3 BIROS was also applied to the fire observation in Chile. But currently the BIROS instrumentation is up to now in the commissioning phase and is less operational. Further more for the day time images in January were not added the visible band and so it was not possible to generate a L2 product. Meanwhile these restrictions are overcome. In Figure 10 is shown the BIROS L2 product of a data take over Qatar at 20.April 2017 and the comparison with the related VIIRS product.

Figure 10 BIROS L2 Product of Gas flares in Qatar (left) and comparison with a related VIIRS product

5. Conclusions

The BIROS satellite is the second satellite in the FireBIRD Mission together with TET Satellite (launched in 2012) to observe fires and hot spots in a fire monitoring constellation. With the successive launch of BIROS in the mid of 2016 with an Indian launcher on PSLV-C34 Cartosat 2c mission and after the finalized commissioning phase of the IR-Camera BIROS could deliver as the TET-1 Satellite Level 1 and Level 2 Fire data products in high quality. FireBird supports Charta and other international acitivities in disaster management.

A number of technological experiments were carried out and show the promising potential for further development of small satellite technology. We demonstrated enhanced agility as well as a new propulsion approach. Autonomous proximity operation as a first step for rendezvous and docking has been successfully finished. Also a high agility experiments demonstrate the potentials for IR –Stereo applications.

6. References

[1] E. Lorenz, G. Rücker, T.Terzibaschian, D.Klein, J.Tiemann FireBird - A small satellite fire monitoring mission: Status and first results; Geophysical Research Abstracts Vol. 16, EGU2014-16546, 2014 EGU General Assembly 2014

[2] Zhukov, B. Lorenz, E., Oertel, D., Wooster, M., Roberts, G. 2006. Spaceborne Detection and Characterization of Fires during the Bi-spectral Infrared Detection (BIRD) Experimental Small Satellite Mission (2001-2004, Remote Sens. Environm. 100, 29-51

[3] Florian Siegert, - Detection and Characterization of Low Temperature Peat Fires during the 2015 Fire Catastrophe in Indonesia Using a New High-Sensitivity Fire Monitoring Satellite Sensor (FireBird) https://doi.org/10.1371/journal.pone.0159410 /2016

[4] Maibaum, Olaf und Montenegro, Sergio und Terzibaschian, Thomas (2008) Robustness as Key to Success for Space Missions. In: Robust Intelligent Systems Springer. Seiten 233-250. ISBN ISBN-10: 1848002602, ISBN-13: 978-1848002609

[5] Reile, Hubert und Lorenz, Eckehard und Terzibaschian, Thomas (2013) The FireBird Mission – A Scientific Mission for Earth Observation and Hot SpotDetection. Small Satellites for Earth Observation, Digest of the 9th International Symposium of the International Academy of Astronautics. Wissenschaft und Technik Verlag. ISBN 978-3-89685-574-9.

[6] Halle, W. und Venus, H. und Skrbek, W. (2000) Thematic data processing on board the satellite BIRD. In: Imaging Spectrometry VI, 4132, Seiten 118-125. SPIE. SPIE's 45th Annual Meeting , 30 July - 4 August 2000, San Diego, California, USA. ISBN 0-8194-3777-8

Nanosat-based detection and tracking of launch vehicles

Caroline Schweitzer[1], Clemens Horch[2], Max Gulde[2], Norbert Scherer-Negenborn[1], Norbert Wendelstein[1], Karin Stein[1]

[1]Fraunhofer IOSB
Gutleuthausstr. 1, 76275 Ettlingen, Germany
Phone: +49 7243 992361, Mail: caroline.schweitzer@iosb.fraunhofer.de

[2]Fraunhofer EMI
Ernst-Zermelo-Straße 4, 79104 Freiburg, Germany

Abstract:

Effective sensor technology for space based early warning and detection is a key component in the defense against immediate threats. These sensors have to be designed and optimized based on realistic infrared signatures of both, background (atmospheric, terrestrial) and rocket exhaust plume (or: ballistic missile exhaust plume). In both cases, the lack of observations causes the use of comprehensive simulation tools, either instead or in addition to ground measurement data. In the paper, we will present the preparatory investigations carried out for the conceptual design of an electro-optical (EO) payload based on a nanosatellite platform for the purpose of space-based early warning. Initially, this will comprise a description of the atmospheric simulation tool used at Fraunhofer IOSB, the application of those, and the assessment of detection and tracking algorithms. We will then give a short side note about ground measurement data. To conclude the paper, the experimental spacecraft based on nanosatellite technology (ERNST) will be introduced with a special focus on the EO payload designed by Fraunhofer EMI.

1. INTRODUCTION

In the fields of early warning, one is depending on reliable image exploitation: Only if the applied detection and tracking algorithms work efficiently, the threat approach alert can be given fast enough to ensure an automatic initiation of the countermeasure. In order to evaluate the performance of those algorithms for an electro-optical (EO) nanosatellite-based sensor system, test sequences need to be modelled as realistic and detailed as possible. Since the signature of background and target (missile) are both influenced by the atmospheric conditions that the future system will be exposed to, the application of comprehensive atmospheric modelling tools is essential.

In this paper we introduce the atmospheric modelling tool MATISSE (Moderation Aeration for Imaging and Simulation of the Scènes et de leur Environnement [1]). We then describe how it is applied for the image sequence generation of a hypothetic deployment scenario. We show, how detection and tracking algorithms are tested based on these resulting image streams and conclude our paper by presenting the experimental spacecraft based on nanosatellite technology designed by Fraunhofer EMI.

2. ATMOSPHERIC MODELLING

In order to test the performance of a particular sensor concept for its use in space, realistic image sequences are created and subsequently evaluated with image processing algorithms. In these sequences, not only the entire observation geometry is modelled (including detector and sensor), but also the influence of the atmosphere on the detection range of such an EO system. The presence of clouds, different earth backgrounds and the prevailing meteorological conditions contribute to the overall

signature of the observed background. At Fraunhofer IOSB, the radiative transfer code MATISSE is used for this step. It was developed by ONERA / France and is currently being extended by several functions in cooperation with Fraunhofer IOSB. MATISSE is suitable for modelling both, the lower and the upper atmosphere. The calculation of radiance and transmission along the line of sight from sensor to target is included in the software as well as a visualization of the results for the field of view (FOV) of a user-defined sensor (Figure 1). For this purpose, the sensor-side characteristics such as pixel resolution, detector size and filter transmission are considered.

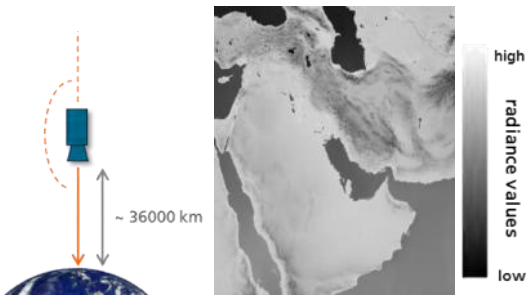

Figure 1: Example for the application of the image-mode in MATISSE: FOV of a satellite in geostationary orbit.

In order to check the suitability of the software MATISSE for this dedicated field of application, numerous validation steps have already been carried out. MATISSE was tested in the available wavelength bands for atmospheric and terrestrial background, and successfully validated [2][3][4][5].

3. DEPLOYMENT SCENARIO

The performance of an early-warning sensor can be evaluated and optimized on the basis of a realistic deployment scenario: Next to the observation geometry, the resulting spectral information of the observed background and the ballistic missile are included.

3.1 Selected spectral bands within the infrared (IR) range

The optical payload of the nanosatellite platform is a dual-channel infrared camera. The selected area in the mid-wave infrared (MWIR) is within the range of an atmospheric window and thus offers the opportunity to observe a ballistic missile already during launch. The second band lies within the short-wave IR (SWIR). Here, the background signal is strongly absorbed and the observation of the earth's surface is not possible. However, the missile signature is less absorbed as soon as it reaches a certain altitude – while having the background still at a low level. Thus, a favourable signal-to-background ratio is created and the missile can be detected and tracked reliably. The same applies, if the missile is in front of the space background (presupposed a slant range observation). For more information on spectral IR bands appropriate for space-based early warning refer to [6]. Figure 2 shows an example of the simulated FOV of a satellite-based sensor for the introduced narrow bands within the SWIR and MWIR.

Figure 2: Exemplary representation of the FOV of a satellite-based sensor in SWIR and MWIR. The spectral background image was calculated using the atmospheric model MATISSE. It can be seen that in the SWIR the earth's background signal is strongly absorbed by the atmosphere, while the surface structure in the MWIR is still recognizable. Both figures have the same scaling.

The combined use of the two spectral channels in the SWIR and MWIR allows the missile to be tracked from launch up to the point of burnout of the last stage. However, unlike radar apertures, a missile launch on the ground cannot be observed if clouds block the line-of-sight.

3.2 Observation geometry

In order to prepare the payload optimally for its mission in space, it is necessary to fit the dynamic range of the sensor to the expected signals from earth background, clouds and ballistic missile. This is the only way to ensure that there is a sufficiently high signal-to-background ratio and that the ballistic missile can be reliably detected. Hence, a representative overflight scenario was created and served as a basis for the follow-on investigations.

For future in-orbit validation, Cape Canaveral in Florida, USA, provides a realistic opportunity to observe rocket launches. Therefore, the overflight of the nanosatellite was simulated for an orbit of 700 km with an inclination of 98.2°. The path runs from south-southeast to north-northwest with the fixation point (image centre) Cape Canaveral. The sequence starts at an observation angle of + 120° zenith angle and ends at -120°. Figure 3 illustrates the overflight scenario.

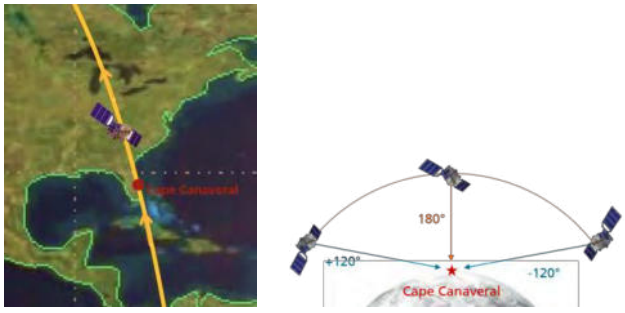

Figure 3: Illustration of the overflight scenario. The satellite is observing and tracking Cape Canaveral.

3.3 Ballistic missile

The one-stage long-range ballistic missile adopted for the scenario was modelled on the basis of calculations made by Industrieanlagen-Betriebsgesellschaft mbH (IABG, Germany). The rocket is launched off from the Cape Canaveral spaceport and heads east across the Atlantic. The total flight (consisting of boost and free-flight phase) lasts for

854 s. The rocket reaches an apogee of approx. 450km and a ground range of 2000 km. Figure 4 shows the missile altitude as a function of time.

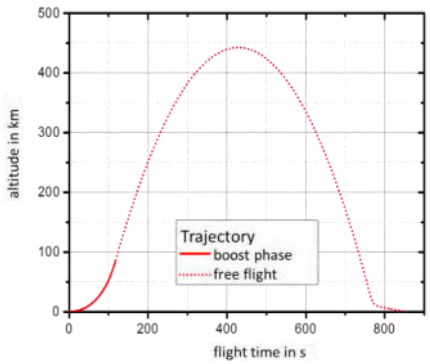

Figure 4: Trajectory of the ballistic missile.

For the simulation, only the boost phase of the rocket was considered, since within the given spectral ranges the plume supplies the predominant part of the IR radiation and the heating up of the rocket body itself is negligible.

4. SCENARIO SIMULATION

Having the scenario as described in Chapter 3 as a basis, we simulated the corresponding background images using MATISSE. Additionally, we took into account the predominant climatological and environmental conditions of the observed area. The resulting 459 frames were then assembled into a nearly 7.5 minute flyover sequence. In Figure 5, and by way of example, individual images of the overflight sequence are displayed. The images represent the ascending part of the trajectory and are provided with information on the corresponding zenith angle.

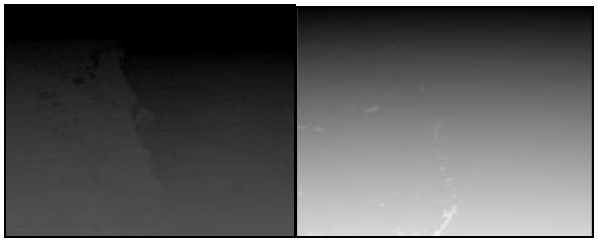

Figure 5: Individual images of the overflight sequences for a zenith angle of 123° in the two defined spectral bands. Left: SWIR, right: MWIR. For each band a different grey scaling has been applied (see Figure 1).

For our simulations we assumed the following characteristics of the detector: 1280 x 1024 pixels, 15 µm pixel pitch and 0.15 µrad instantaneous FOV (IFOV). Furthermore, the spectral responsivity of the chosen filters was also included.

In a post-processing step, we overlaid the entire sequence with a cumulus cloud layer. Therefore, we computed the corresponding spectral radiances using MATISSE, applied a cloud mask and assembled clear sky image and resulting cumulus mask. An exemplary image is shown in Figure 6.

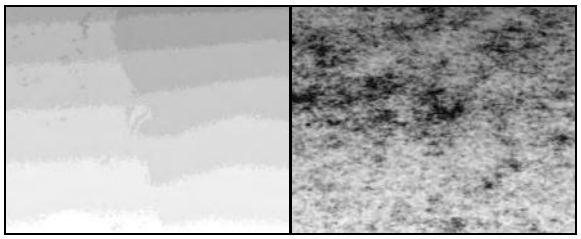

Figure 6: MWIR image with and without cumulus clouds at an observation angle of 127.9° (zenith). Left: clear sky image, right: overcast image (clear sky image + cumulus cloud cover mask). Scaling see Figure 1.

In a last step, the spectral data of the ballistic missile was integrated into the sequences for the given altitudes and aspect angles. Here, both the spectral sensitivity of the detector and the spectral transmission of the filters and optics used were taken into account.

Using MATISSE, the transmission between missile and satellite was then determined for each second of the boost phase and all overcast conditions, and subsequently applied to the missile signal. As an example, the irradiance in the SWIR band is displayed in Figure 7, left. For cloudy conditions, the missile signal is received after approx. 30 s of flight, as soon as cloud break is reached.

The "footprint" of the missile as it appears on the detector matrix is shown in Figure 7, right. Here, the movement of both, missile and satellite has been taken into account. Along this footprint, the corresponding time-, angle- and altitude-dependent irradiance was inserted into the matching image of the sequence, of course having accounted for atmospheric effects.

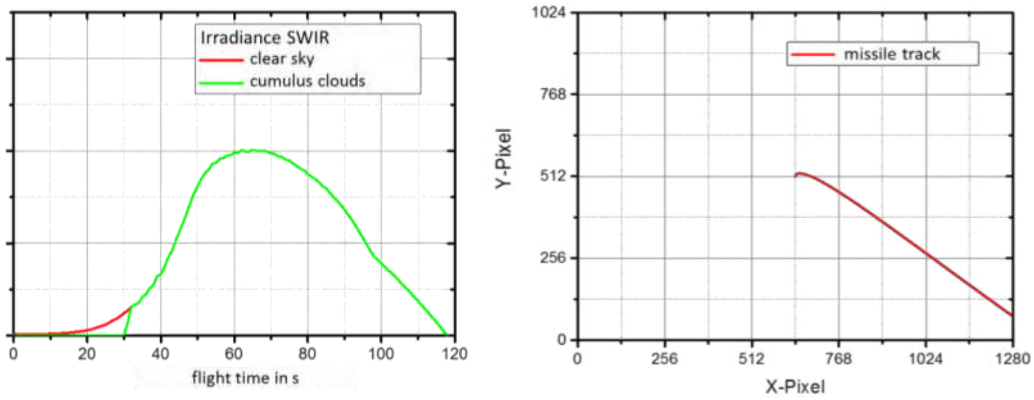

Figure 7: Left: Irradiance of the ballistic missile in the SWIR as a function of flight time. Right: Missile track on the detector matrix. The movement of both, missile and satellite, has been taken into account.

For an even more realistic representation, detector noise is synthetically added to the sequences.

5. ANALYSIS

To evaluate the effectiveness of the sensor design, detection and tracking algorithms are applied to each of the four sequences (clear sky and overcast for MWIR and SWIR). In the present case – and as a first part – the "hot-spot detector" developed by Fraunhofer IOSB was used to analyse the sequences. In short, this algorithm compares the

brightness of a certain pixel with the respective maximum brightness of the surrounding pixels. A detailed description of the hot-spot detector is given in [7].

For the second part, the tracking, the corresponding algorithm assembles suitable object references from the prior step (detection). For each reference in the current image, an object reference in the previous image is searched for. If the existing object reference from the previous image already belongs to an object track, the velocity estimated for this track is also included. The velocity estimation can be carried out with the help of a Kalman filter. In the present case, the simplest version of a Kalman filter, an α-β-filter, was adequate. In order to bridge gaps possibly occurring in the track, not only object references from the previous image, but also from "older" ones are used.

In Figure 8 the two-part analysis of the image stream is visualized, exemplary for the MWIR: The first row represents alarms observed by the detection algorithm, and the second row shows the result of the applied tracking-algorithm. Here, only one alarm, the ballistic missile signal, is left and tracked until burn-out of the rocket stage.

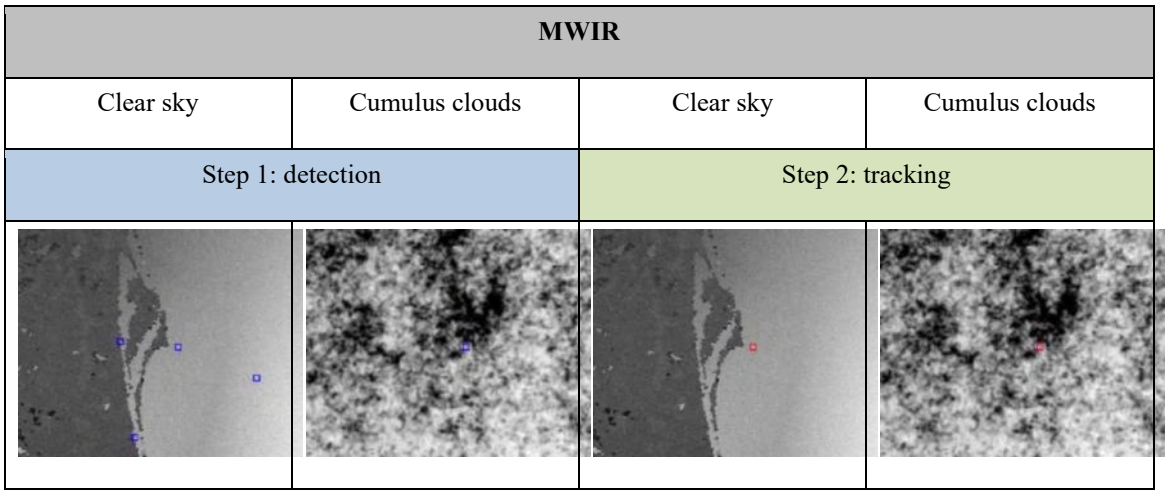

Figure 8: Results of detection and tracking.

As a conclusion, the applied combination of the introduced detection- and tracking algorithms results in a reliable observation of the ballistic missile. The missile is detected shortly after launch or cloud break, respectively, and tracked until its point of burn-out. At this point, the 3D-information of the velocity, direction and position is estimated and can be used to pre-instruct fire-control radars (and successively countermeasures) on ground. For a stereo-tracking scenario (at least two nanosatellites) the estimation of the 3D-information would be even more precise.

6. EXPERIMENTAL SPACECRAFT BASED ON NANOSATELLITE TECHNOLOGY

Fraunhofer EMI currently designs and builds a 12U nanosatellite to host the imaging payload. The mission is called ERNST (Experimental Spacecraft based on Nanosatellite Technology) and its main goal is to evaluate the utility of a nanosatellite mission for scientific and military purposes. Figure 9 shows a rendered image of the satellite. The satellite is currently being integrated at Fraunhofer EMI and will be available as an engineering model in 2018. Subsequently, thermal vacuum, vibration, and radiation testing will be performed, further pursuing space qualification.

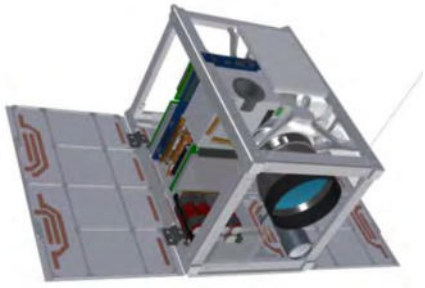

Figure 9: The ERNST nanosatellite

CubeSats are classified by their size, which is measured in Units, referring to the approximate 10×10×10 cm³ volume from the CubeSat standard [8]. Larger CubeSats fill multiples of this 1U cube. Common sizes are 1U, 2U, 3U and 6U. Most requirements of the MWIR payload (dimensions, mass, power budget) exceed the capabilities of 1-3U CubeSats. Therefore, we pursue the concept of building a 12U nanosatellite using components from the maturing CubeSat market. More details on the integration of a 12U CubeSat have been described in [9].

Parts of the satellite structure make use of additive design and manufacturing methods in order to optimize its behavior for both thermal and vibrational loads from the payload's cryocooler [10]. Gulde et al. [11] describe the adapted thermal design methodology for ERNST and especially the 3D-structured radiator design. For de-orbiting, a drag sail as presented by Sinn et al. [12] will be unfolded.

6.1 The EO payload

The MWIR payload consists of a commercially available infrared lens, a filter pendulum for switching between multiple spectral bands and the infrared detector unit, which is actively cooled by a Stirling cryocooler to 77K. The detector unit comprises a 1.3 Megapixel InSb sensor with a spectral range of 3-5 µm. The image data is passed to the so-called Data Processing Unit (DPU), which handles the processing and storage of the captured image data as well as the controlling of the payload's subsystems. Figure 10 shows a block diagram with all main components. This system can be seen as a successor to the DPU currently flying on the Kent Ridge 1 microsatellite [13]. More details on the data handling have been described by Horch et al. [14].

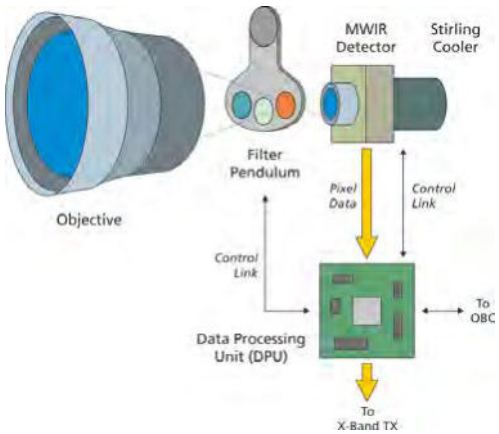

Figure 10: Block diagram of the main payload components

The payload is designed to accomplish two objectives: the search and tracking of ballistic missiles during their boost phase as well as the continuous IR measurement of the Earth's surface in two spectral bands.

For the continuous recording of the Earth's surface, the pointing of the satellite is 30° with respect to nadir in the direction of travel (Figure 11, A). At an altitude of 700 km, the detector has in a swath width of 164 km (Figure 11, B), resulting in a pixel footprint of maximally 112 x 145 m2. The payload is designed to accomplish two objectives: the search and tracking of ballistic missiles during their boost phase as well as the continuous IR measurement of the Earth's surface in two spectral bands. For the continuous recording of the Earth's surface, the pointing of the satellite is 30° with respect to nadir in the direction of travel (Figure 11, A). At an altitude of 700 km, the detector has in a swath width of 164 km (Figure 11, B), resulting in a pixel footprint of maximally 112 x 145 m^2. In this mode, the filters are iterated at a frequency of 0.1 Hz, which allows for the recording of continuous, connected stripes in each band with an image-to-image overlap of about 10 % (Figure 11,C).

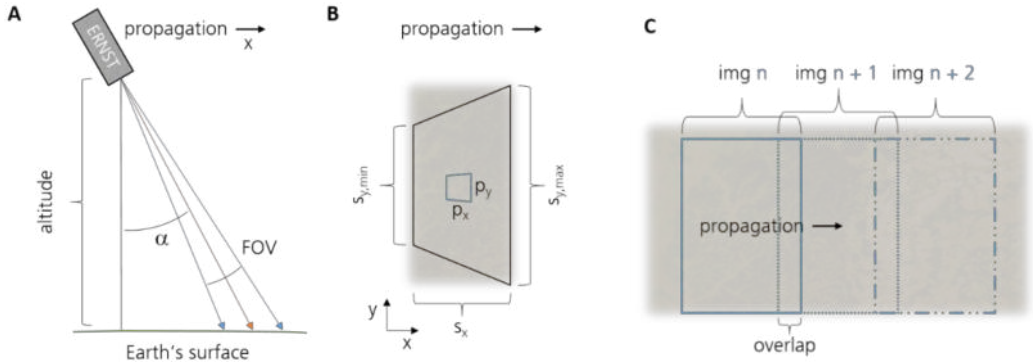

Figure 11: ERNST pointing and image recording. A: Satellite pointing forward by α with respect to nadir. B: Exaggerated perspective distortion of the recorded image with indicated swath width S_y. Pixel footprint $p_x \times p_y$. C: Contiguity of images per band ensured by overlap of sequentially recorded images.

As detailed above, we initiate the tracking of rocket plume signatures manually. The search subsequently takes places in a predefined region. In this scenario, the satellite slowly rotates such that the intersection of the detectors optical axis with Earth's surface remains fixed for as long as possible. The maximum angular speed hereby is 0.6°s-1. The minimal size of the monitored area is around 10.000 km2, represented by a rectangle with dimensions of 115 km x 92 km. To detect the plume with high probability, the pixel footprint must not exceed an area of about 500 x 500 m2, effectively limiting the minimum elevation of the satellite as seen from the Earth's surface to 35°. At an orbital altitude of 700 km, this allows for a continuous monitoring time of 8:30 min.

7. CONCLUSION

The paper introduced the possibility to carry out space based early warning from a nanosatellite-based platform. For the given mission, the possibility to detect and track a medium-range ballistic missile up until its point of burn-out was illustrated.

8. REFERENCES

[1] L. Labarre, K. Caillault, S. Fauqueux, C. Malherbe, A. Roblin, B. Rosier and P. Simoneau , "An Overview of MATISSE-v2.0" Proceedings of 7828, (2010).

[2] L. Labarre, K. Caillault, et al., "MATISSE-v2.0 : new functionalities and comparison with MODIS satellite images" Proc. SPIE 8014, (2011).

[3] C. Schweitzer, K. Stein, N. Wendelstein, L. Labarre, K. Caillault, S. Fauqueux, C. Malherbe, A. Roblin, B. Rosier, and P. Simoneau, "Validation of the background simulation model MATISSE : Comparing results with MODIS satellite images" Proc. SPIE 8178, (2011).

[4] C. Schweitzer, C. Malherbe, K. Stein.: "Validation of MATISSE background images and cloud simulations: comparing results with MODIS satellite images" Proc. SPIE 8890, (2013).

[5] C. Malherbe, C. Schweitzer: "Validation of clouds modeled by MATISSE code with MODIS satellite images" ITBMS, International IR Target and Background Modeling & Simulation Workshop, Proceedings, Toulouse, (2013).

[6] C. Schweitzer, K. Stein., N. Wendelstein: "Evaluation of appropriate sensor specifications for space based ballistic missile detection." Proc. SPIE 8541, (2012).

[7] A. Kohnle, R. Neuwirth, W. Schuberth, K. Stein, D.H. Höhn, R. Gabler, L. Hofmann, W. Euing, "Evaluation of Essential Design Criteria for IRST Systems" Proc. SPIE Vol. 2020, Infrared Technology XIX (1993).

[8] S. Lee et al., "CubeSat Design Specification," Rev. 13, The CubeSat Program, Cal Poly SLO, Feb. 2014. Accessed on: Aug. 15 2017.

[9] C. Horch, M. Schimmerohn, and F. Schäfer, "Integrating a large nanosatellite from CubeSat components – Challenges and solutions," in 68th International Astronautical Congress (IAC), Adelaide, Australia, 2017.

[10] M. Bierdel, A. Pfaff, M. Jäcklein, M. Schimmerohn, and M. Wickert, "Multidisciplinary Design Optimization of a Satellite Structure by Additive Manufacturing," in 68th International Astronautical Congress (IAC), Adelaide, Australia, 2017.

[11] M. Gulde et al., "Managing high thermal loads in small satellites - analysis, design, and verification of a 3D-printed radiator," in 68th International Astronautical Congress (IAC), Adelaide, Australia, 2017.

[12] T. Sinn, N. Reichenbach, and P. Seefeldt, "The development of a passive de-orbit subsystem for small and micro satellites," in 68th International Astronautical Congress (IAC), Adelaide, Australia, 2017.

[13] C. Horch, N. Domse, F. Schäfer, and M. Buhl, "High level software development for a stand-alone data processing and storage unit for a microsatellite hyperspectral payload," in Small satellites for earth observation. Digest of the 10th International Symposium of the International Academy of Astronautics (IAA) 2015, 2015, pp. 207–210.

[14] C. Horch et al., "An MWIR payload with FPGA-based data processing for a 12U nanosatellite," in Small Satellites for Earth Observation. 11 International Symposium of the International Academy of Astronautics 2017, 2017, pp. 339–342.

Teledyne's High Performance Infrared Detectors for Space Missions

Paul Jerram

Teledyne-e2v
Waterhouse Lane, Chelmsford UK, CM1 2QU
Phone: +44 1245 453495, Mail: paul.jeram@teledyne.com

Abstract: Teledyne is one of the world's leaders in the provision of infrared sensors for Earth science, planetary science, and astronomy. This paper presents Teledyne's focal plane array technologies that provide high performance for space missions, with sections on substrate-removed HgCdTe *(that provides simultaneous visible / IR detection)* and fully depleted HgCdTe *(that enables detectors to be operated at significantly increased temperatures)*. We give examples of the image sensors provided for a number of flight programs, including Euclid, WFIRST, AVIRIS-NG, ECOSTRESS, and NEOCam.

1. INTRODUCTION

Mercury Cadmium Telluride (HgCdTe or MCT) is used in applications where the highest performance IR detectors are required. HgCdTe achieves the highest quantum efficiency and lowest dark current of any IR detector material.

HgCdTe is a II-VI detector material with 50% of the atoms (Hg, Cd) from column II of the period table of elements and 50% of the atoms (Te) from column VI. The bandgap of HgCdTe is tuned by adjusting the ratio of mercury to cadmium. This allows detectors to be made with cut off wavelengths from NIR to LWIR.

The basic structure of a hybrid IR focal plane array is shown in Fig. 1. The HgCdTe material is grown at Teledyne using molecular beam epitaxy (MBE) with a double-layer planar hetero-junction (DLPH) detector architecture, which produces the highest performance HgCdTe material. It is then processed to form an array of photodiodes that are bump bonded to pixels in the Readout Integrated Circuit (ROIC). The HgCdTe photodiode array and the ROIC are separately optimized and a given ROIC can be hybridized to several types of detector materials (e.g. HgCdTe, Si, InGaAs).

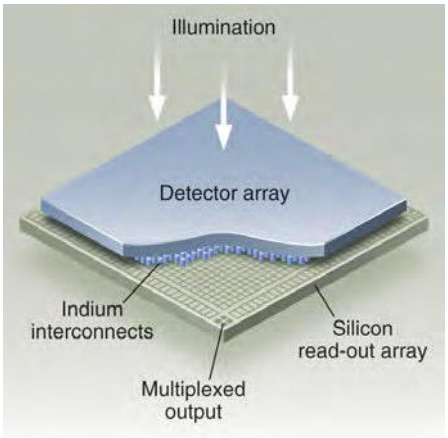

The composition of the HgCdTe detector array determines the operating wavelength range, the quantum efficiency, the dark signal and the radiation performance

The silicon read-out array defines the readout noise, peak signal, frame rate or cadence, operating modes including windowing, interfaces, radiation performance, linearity and anti-blooming performance

The interconnect process is critical in determining the operability or percentage of fully functioning pixels

Figure 1: Hybrid Infrared FPA architecture

2. TECHNOLOGY DEVELOPMENT

Substrate removed technology: Teledyne has developed a process for removal of the CdZnTe substrate material, which is now standard for all NIR, SWIR and MWIR focal plane arrays made by Teledyne. Substrate removal involves taking off all of the CdZnTe substrate after hybridization to leave a layer of HgCdTe that is only 7 to 10 µm thick. After substrate removal an anti-reflection (AR) is deposited on the HgCdTe. In addition to giving a large increase in quantum efficiency at wavelengths below 1.3 µm, substrate removal also eliminates fluorescence from cosmic rays absorbed in the CdZnTe substrate and removes Fabry-Perot fringes that can occur in the substrate with narrow band illumination, such as in spectrometers

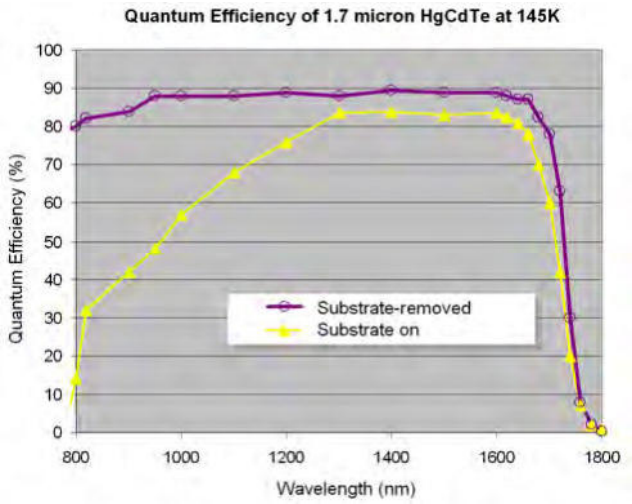

Figure 2: Quantum Efficiency of a substrate removed HgCdTe detector with 1.7µm cutoff compared to the same detector type without substrate removal

Fully depleted HgCdTe: Teledyne has developed a process to fabricate lightly doped HgCdTe detectors that can be fully depleted with minimal (1-2 volt) reverse bias. A fully depleted detector removes most of the free electrons which suppresses the Auger-1 dark current to the point where "dark current" is dominated by the radiative background seen by the detector. Depending on cutoff wavelength and operating temperature, the radiative background is a factor of 10 to 100 lower than Rule07 (Auger-1) dark current. This gives a major advantage for space applications, enabling operation at a much higher temperature with passive cooling or smaller cryo-coolers. Figure 3 shows the increase in operating temperature that can be obtained with the use of fully depleted HgCdTe detectors.

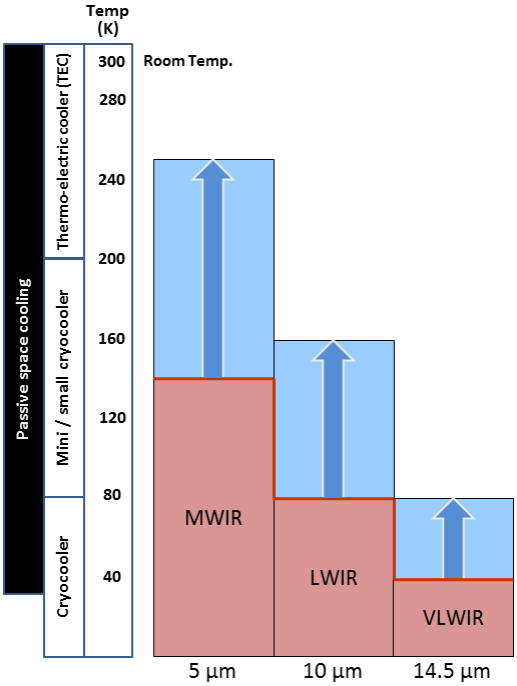

- For high flux (300K scenes), operating temperature can doubled for the same dark signal
  - Less expensive cooling options
  - Longer cooler operating lifetime
  - Able to operate LWIR with mini cryo-coolers
- For low flux applications
  - Lower dark current at standard operating temperature
  - Higher operating temperature
  - Longer cooler operating lifetime
- Status
  - Demonstrated 10× to 100× reduction in dark current
  - 128×128, 1280×480, and 640×512 arrays have been tested
  - MWIR operated up to 250K
  - LWIR operated up to 160K
- Strong funding for development
- Developing partnerships with aerospace primes for system insertion

Figure 3: Increase in operating temperature from the use of fully depleted HgCdTe

ROIC technology developments

New ROICs have been developed for Earth observation and planetary observation applications that have flexible formats. The CHROMA ROIC which is optimized for spectrometers (hyperspectral imaging) has 30 µm square pixels, a capacitive transimpedance amplifier (CTIA), and has been produced in four different formats: 320×480, 640×480, 1280×480, and 1600×480 pixels with a pixel full well capacity of 700 ke-, 1Me-, and 5 Me-. CHROMA has been used by the Jet Propulsion Laboratory (JPL) in a number of spectrometers including AVIRIS-NG, NEON, PRISM, and Europa MISE.

The most recent ROIC development at Teledyne has been the CHROMA-D / GeoSnap ROIC. This is a highly flexible stitched format that can be fabricated in a number of different formats. The ROIC stitch blocks are shown in the left side of Fig. 4. Stitching is a well-established fabrication process for making large imaging sensors.

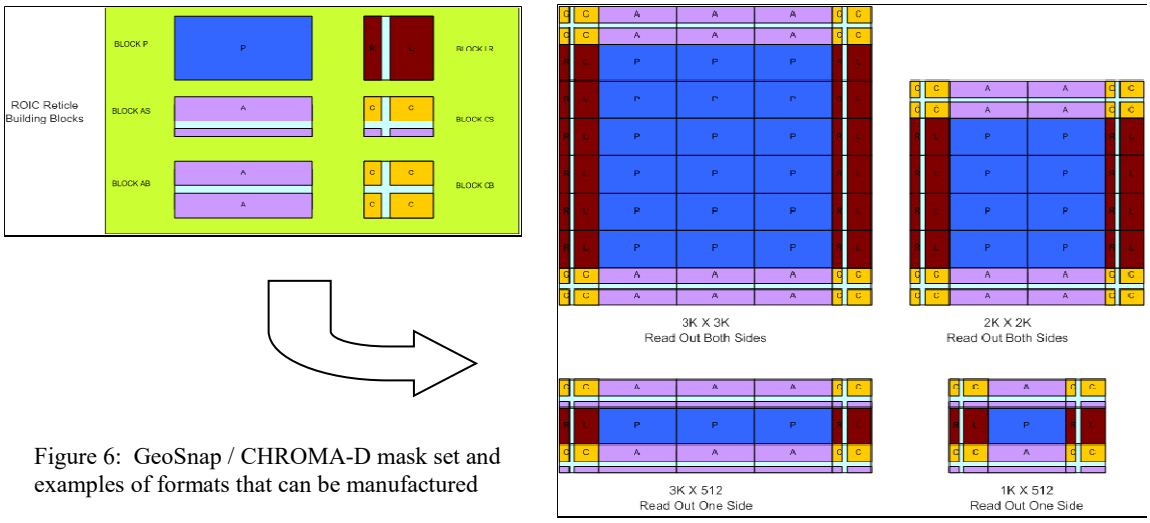

Figure 6: GeoSnap / CHROMA-D mask set and examples of formats that can be manufactured

The pixel stitch block (P, shown in blue) is 512 rows by 1024 columns of 18 µm square pixels. The CHROMA-D ROIC has digital input and digital output greatly easing the interface to external electronics. This ROIC has a CTIA pixel cell with two gains (row programmable) and 14 bit column parallel ADCs. To date, the GeoSnap / CHROMA-D array has been manufactured in 2K×2K, 2K×512, and 3K×512 formats.

3 EXAMPLES OF DEVICES APPLICATIONS

3.1 Astronomy

The HxRG family of detectors are the most widely used detector in ground-based and space astronomy instrumentation. Most space missions and ground-based observatories have used the 1K×1K format (H1RG) or 2K×2K format (H2RG) 18 µm pixel pitch arrays that have been available for over 15 years. The newest generation HxRG arrays are the 16 million pixel H4RG arrays, that are made in 10 µm (H4RG-10) and 15 µm (H4RG-15) pixel pitch. The H4RG-15, which at 6×6 cm size is the largest format high performance astronomy array available, is now a mature product.

3.2 Space

The HxRG family of detectors is also widely used in space applications, for example 16 H2RG detectors are used in the Euclid NISP focal plane and the H4RG-10 focal planes currently under manufacture for WFIRST will be the largest infrared detectors operating in space when it launches in the mid 2020s.

ECOSTRESS (ECOsystem Spaceborne Thermal Radiometer Experiment on Space Station) is a multispectral instrument operating with wavelengths from 4 to 12 µm. This JPL instrument, installed on the ISS in July 2018, operates in whiskbroom mode, rapidly scanning across the Earth in a direction orthogonal to the spacecraft orbit. To do this, the multi-spectral array must read out at 30,000 frames per second, reading 4 rows of pixels from 8 bands to achieve 100% pixel operability per band.

A number of new Earth Observation missions are in development using the new CHROMA-A and CHROMA-D ROICs. The first of these that is operational is an airborne instrument; The Airborne Visible Infra-Red Imaging Spectrometer – Next Generation (AVIRIS-NG) instrument, which was developed by the Jet Propulsion Laboratory (JPL) for airborne observations.

4 SUMMARY

HgCdTe technology remains the infrared detector of choice for space applications for which performance is critical. Teledyne has a proven track record for making high performance HgCdTe and a unique capability to produce the largest format arrays. Recent developments in HgCdTe technology continue to increase the sizes of the arrays and new ROICs provide increased capabilities with digital I/O that provides a much simpler user interface.

The capability of Teledyne to produce large infrared arrays has enabled a number of space astronomy missions that are currently under development including Euclid, WFIRST, and JWST.

Flight Results of MarconISSta: Monitoring and Analysis of Radio Frequency Use from Low Earth Orbit

Martin Buscher, Max Kramer, Robert Marx, Alex Sullivan, Brian Treacy, Klaus Brieß

Technische Universität Berlin, Department of Aeronautics & Astronautics, Chair of Space Technology
Marchstr. 12, 10587 Berlin, Germany
Phone: +49 30 314 75872, Mail: martin.buscher@tu-berlin.de

Abstract: MarconISSta is an on-orbit spectrum analysis payload that was launched to the International Space Station (ISS) in May 2018. It was part of the ESA Horizons mission, during which ESA astronaut Alexander Gerst was the first German commander of the space station and led more than 35 European experiments. MarconISSta was operated between August 2018 and February 2019. The experiment used a LimeSDR software defined radio to measure the signal strength of received RF signals in VHF, UHF, L and S band. The antennas for data reception were supplied by the Amateur Radio on the ISS (ARISS) group. In return, MarconISSta will provide an analysis of the radiation pattern of the ARISS antennas as well as performance analyses for the ARISS transceivers on board. A space-hardened Raspberry Pi computer (Astro Pi), which is operated on the ISS since 2015, was provided by ESA. This device was used for controlling the LimeSDR, as well as for processing and storing the data. More than 800 MB of data were recorded each week and forwarded to TU Berlin without crew interaction. This paper presents some of the flight results of MarconISSta. It gives insight on the current use of the above-mentioned frequency bands with a highlight on amateur radio use. The main tool for visualization are heatmaps for various RF channels during different daytimes which are presented and analyzed in this work. Additionally, it puts highlight on various preeminent users of the bands that highly influence the utilization of the band. The paper concludes with an outlook on the future use of MarconISSta components on the ISS as well as further plans for spectrum analysis from space.

1. INTRODUCTION

RF spectrum for satellite communication has been increasingly used over the past 15 years. Most of the available bands are shared between two or more services [1] and with the rise of Cubesats and related small satellites, the risk for interference grew significantly. Various research groups have found that interference can originate from terrestrial sources that have an impact on small satellite operators [2,3], however small satellites and their ground stations can disturb other systems as well [4,5].

Figure 1: MarconISSta logo

MarconISSta is a student-driven project [6] at Technische Universität Berlin that was installed on the International Space Station (ISS) in August 2018. Until February 2019, it investigated the use of various bands in the VHF, UHF, L band and S band ranges, identifying multiple users and “hot” regions around the globe. This paper shall summarize some of the results of the experiment. Chapter 2 briefly introduces the experiment setup, chapter 3 shows first flight results. Conclusions and further steps are presented in chapter 4.

2. EXPERIMENT SETUP

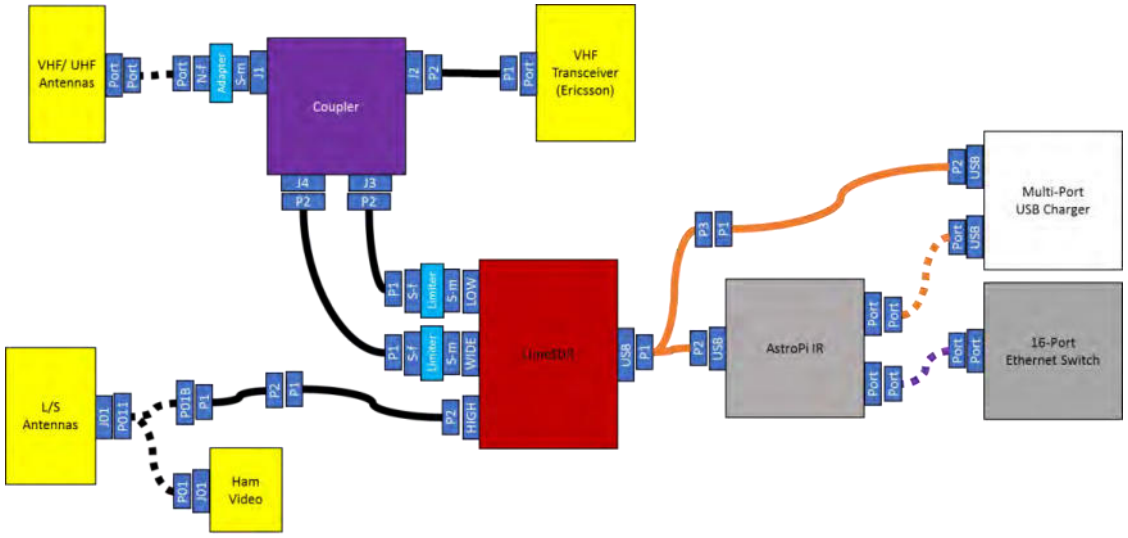

Figure 2: Experiment Setup. Yellow components are owned by ARISS, grey and white are owned by ESA. Cables highlighted by dashed lines were already on board. All other components were installed for MarconISSta

The experiment setup is shown in Figure 2. The core elements are the commercial off-the-shelf device LimeSDR which receives the spectrum data via three RF input ports. Two of these ports are connected to the VHF/UHF antennas of the Amateur Radio on the ISS (ARISS) group. Since the antennas are continuously used for APRS and voice transmissions, the LimeSDR had to be connected via an RF coupler, introducing losses of 20 to30 dB. To prevent high power damage from the on-board VHF transceiver, RF limiters are integrated in the signal line. The third LimeSDR RF input is connected to a currently unused L/S band patch antenna. The LimeSDR is controlled by an Astro Pi computer. This computer consists of a Raspberry Pi 1, housed in a space-qualified housing and supplemented by several buttons and sensors for crew interaction. Two Astro Pis were originally sent to the ISS for educational purposes, however one of them could be used for MarconISSta during 2018/19. The Open Source Software Soapy Power [7] runs on the Astro Pi to generate CSV formatted files containing signal strength values. These files are downloaded once per week. Astro Pi and LimeSDR are powered via USB. The ISS LAN network is used to forward and downlink the data.

3. FLIGHT RESULTS

Approximately 11 GB of data were recorded. The focus of the assessment was on radio amateur bands (144-146 MHz, 435-438 MHz, 1260-1270 MHz, 2400-2450 MHz). However, other bands of interest were investigated as well (137-138 MHz, 148-174 MHz, 2025-2290 MHz). The results would exceed the page limit of each paper. It can be summarized that all investigated bands are used more heavily than expected. The strongest peaks originate from radar systems, but also narrow-band stations can be frequently found in the data. Figure 3 exemplarily shows the capabilities of MarconISSta.

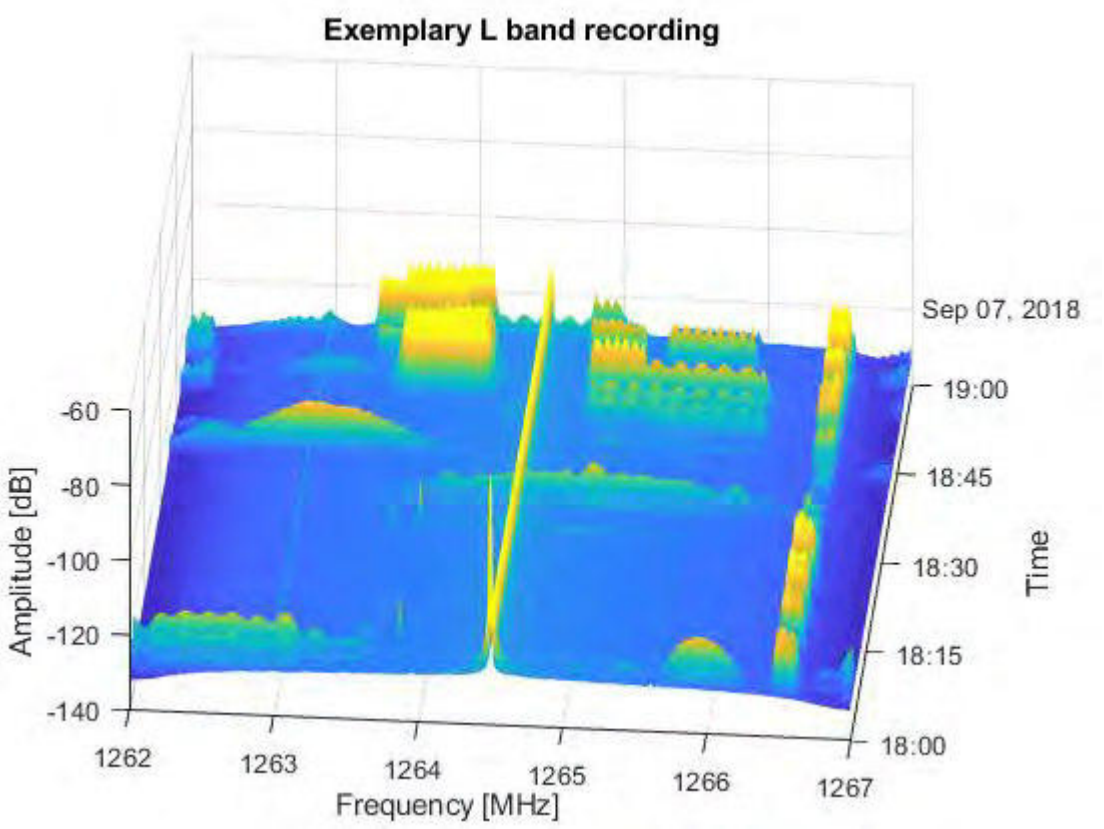

Figure 3: Sample recording of L band frequencies in the range 1262 MHz to 1267 MHz. Several peaks can be seen that originate from strong (terrestrial) signals.

The figure shows a common distribution of signals in the L band. The measurement was taken in the East-Asian region. The peak in the center (1264.5 MHz) is the DC offset of the LimeSDR, which is a constant internal "disturbance" of the frequency range. All other time-invariant signals, e.g. the weak constant signal around 1263 MHz, also derive from internal sources. The other high peaks in the band can be explained by (terrestrial) radar sources and other sources yet to be defined. Doppler shift can be recognized as well as modulation shapes.

Other measurements give insight to the various systems aboard the ISS, e.g. figure 4 and figure 5. Figure 4 shows that starting from around 18:50 UTC on August 24th 2018, a wide-band disturbance was received by MarconISSta. This signal is repeated every 2 minutes and led to some confusion. It was later found out, that the ISS APRS system that is one of the ARISS systems for amateur purposes was (re)activated during this time, which was not known to many people. Using MarconISSta, it could be acknowledged that the system is functional.

Figure 5 presents a noise yet to be identified. The noise around 2403 MHz varies over each orbit with repeating patterns. It is expected that the noise is connected to the ISS power system. Although it is unlikely that the source of the noise can be identified and interrupted, it is valuable to know that this time-varying noise exists.

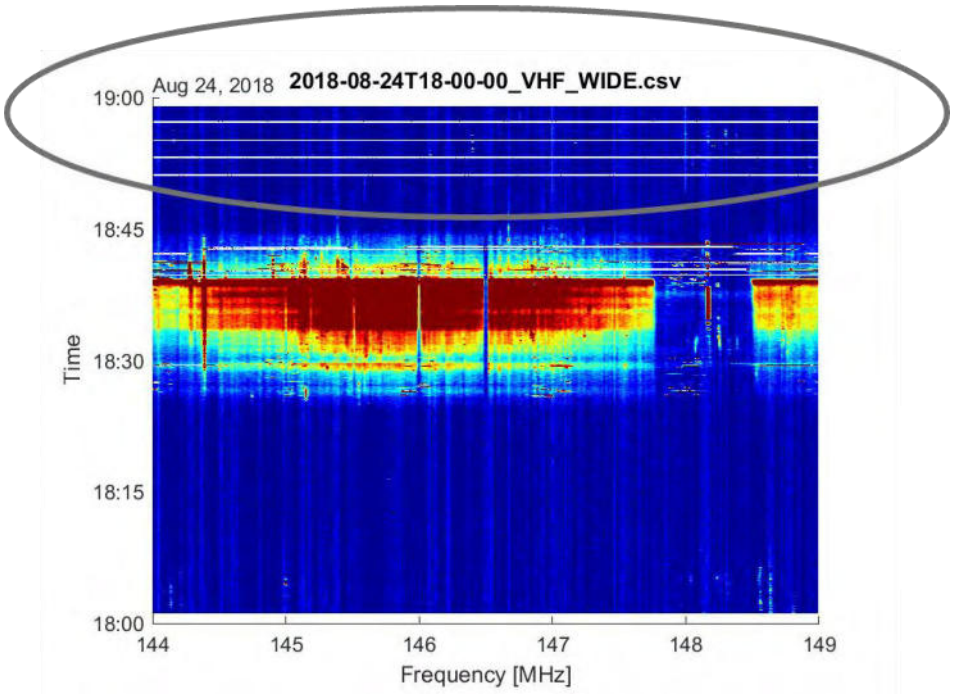

Figure 4: Waterfall plot of the VHF region 144 MHz to 149 MHz. At 18:50 UTC an APRS signal on the ISS was activated and from this time repeated every 2 minutes. MarconISSta clearly confirms the functionality of the system.

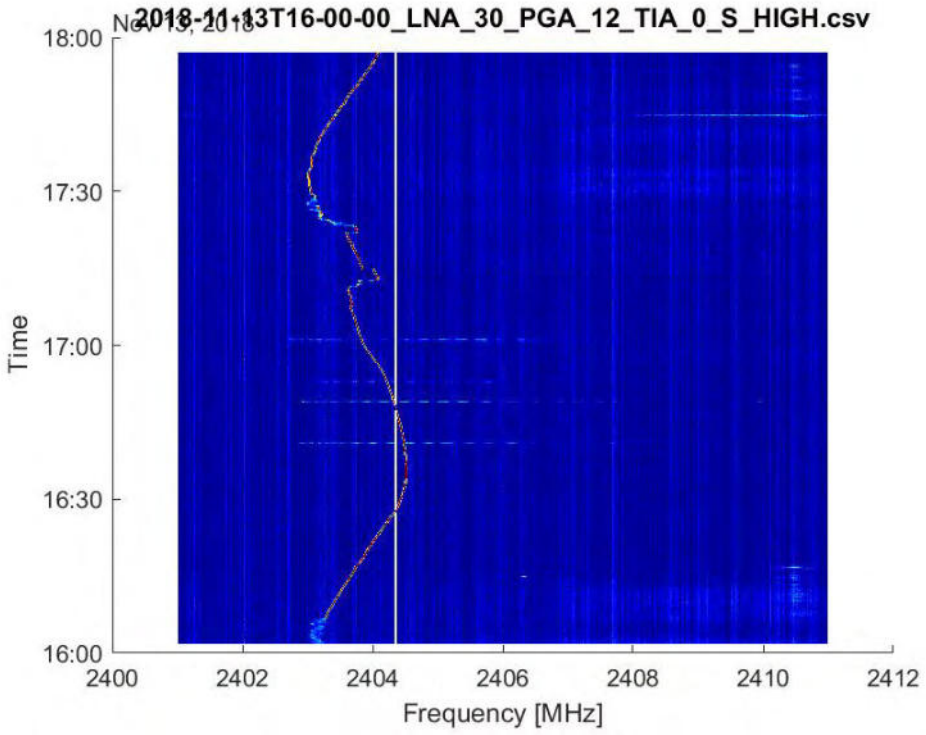

Figure 5: Time-varying noise around 2403 MHz. It is believed that this artefact originates from the ISS power system.

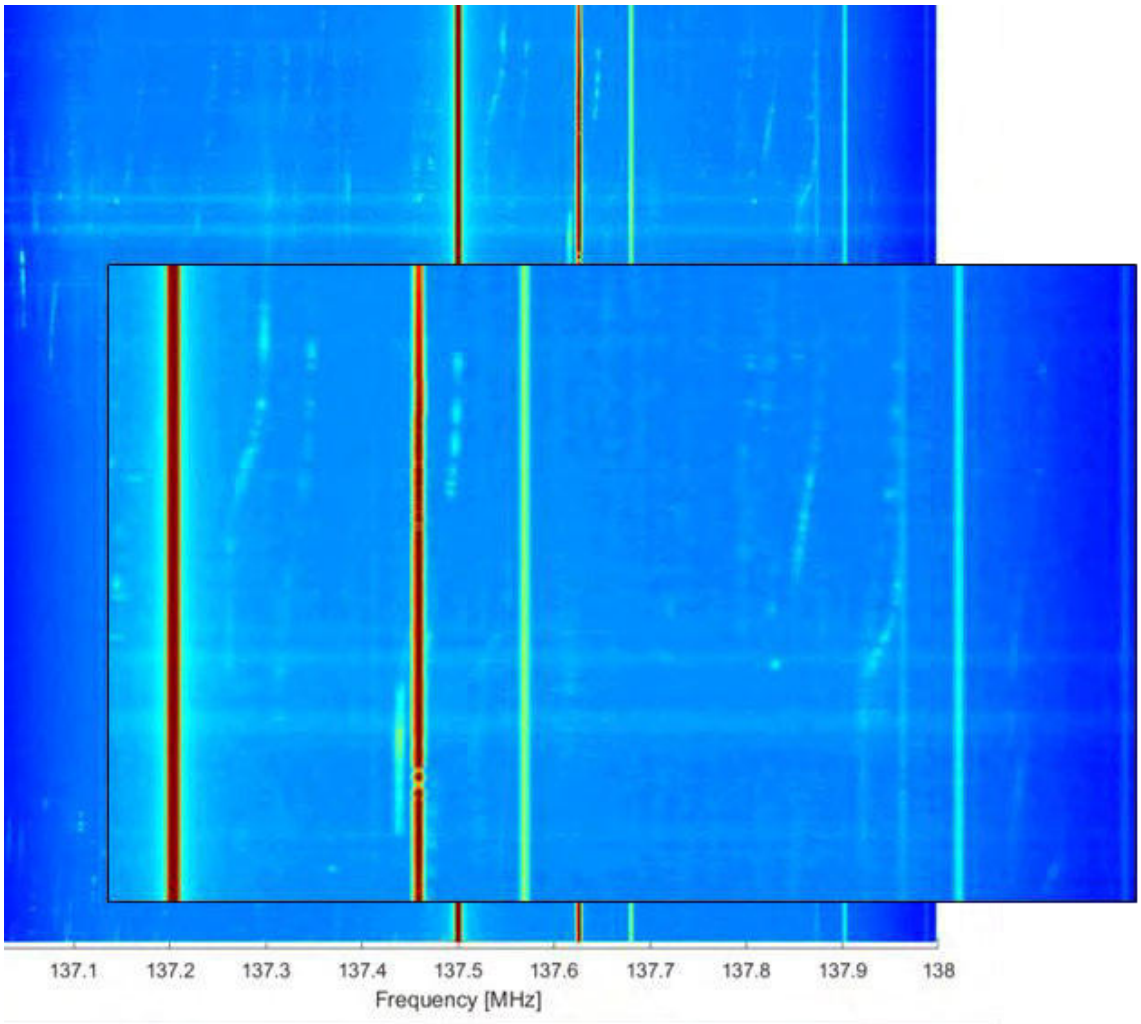

Figure 6: Inverted Doppler shift in the 137-138 MHz band

Figure 6 presents a paradox result of measurements in the 137-138 MHz range. The waterfall plot shows several Doppler shifted signals. The duration of the signals is around 5 to 15 minutes, accordingly it can be assumed that the signals have terrestrial source or target. The paradox element of this measurement is that the Doppler shift is inversed to the shift that would be expected. During approach and departure to a resting transmitter, a receiver goes from high frequencies to lower frequencies. However, the plot shows a variation from lower to higher frequencies. The source for this behaviour is yet to be found.

Figure 7 shows heatmaps of three different channels in the 1260 MHz to 1270 MHz range. Clearly, global use of the channels varies significantly. While the use of all channels in North America and Europe is high, for South America, Africa and the Asian and Pacific regions is highly variant.

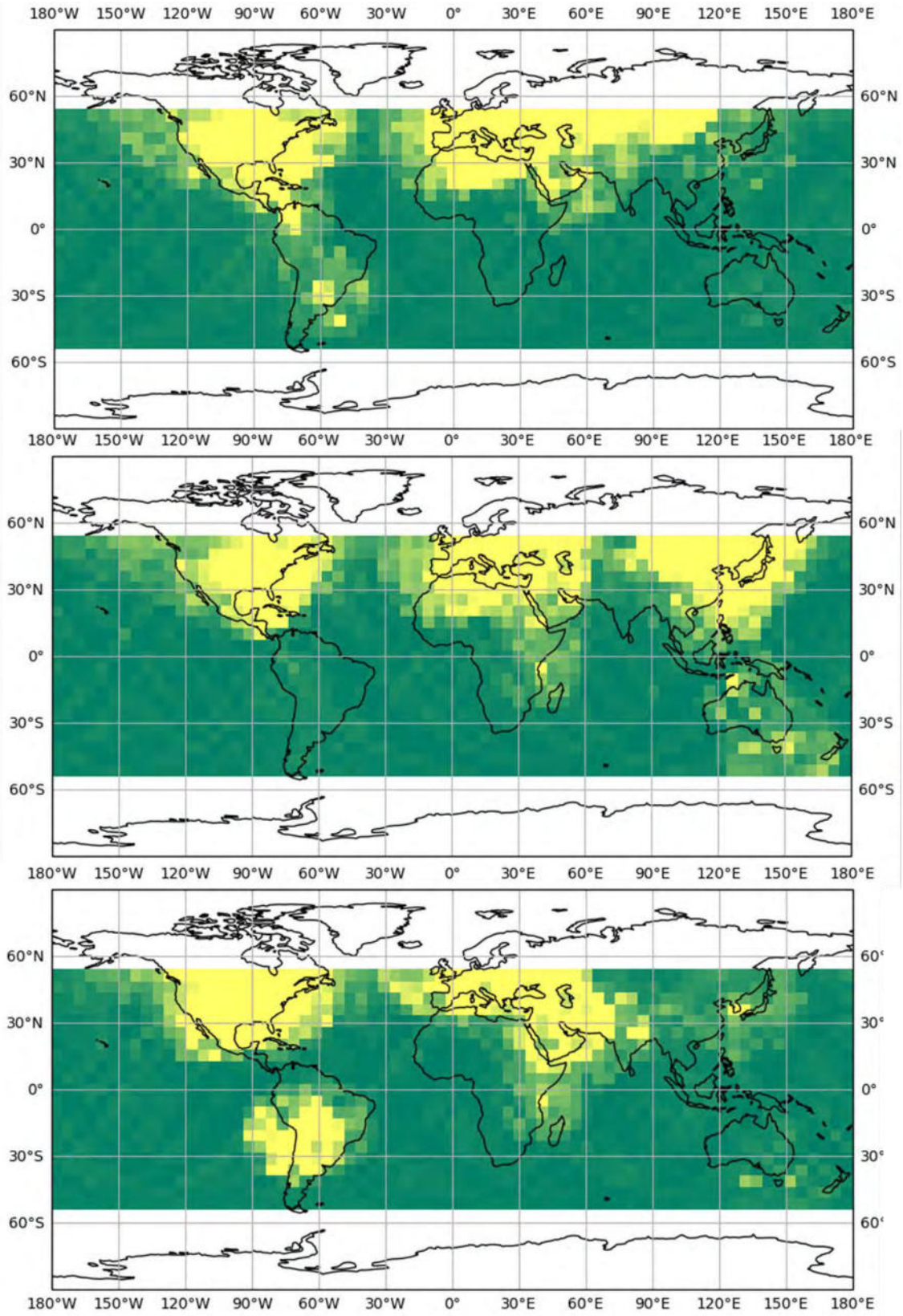

Figure 7: Heatmap of three different channels between 1260 MHz and 1270 MHz. It can be easily identified how local use of the channels varies.

5. CONCLUSIONS AND OUTLOOK

MarconISSta produced significantly more data than anticipated. While the experiment was originally planned to run for few days only, automatic operations allowed almost continuous operations from August 2018 until February 2019. The results identify several regions of interest, highly occupied bands and strong interferers. It is expected that the analysis of the flight results would need at least another year.

The experiment raised interest of several stakeholders. DLR and ESA currently investigate the possibilities of a second phase of MarconISSta, either repeating and extending spectrum analysis or using other capabilities of the LimeSDR, e.g. as testbed for software decoder systems. The data will be further examined and processed. A web interface [8] was implemented to give anybody the chance to create individual heatmaps. The MarconISSta blog [9] will continuously inform about latest developments.

5. ACKNOWLEDGEMENTS

The authors would like to express their gratitude to the various supporters of the project: ARISS for granting the use of their antennas, DLR for financial and programmatic support, ESA for integration support and BioTESC for operational support.

6. REFERENCES

[1] ITU Radiocommunication Sector, Radio Regulations, Geneva, Switzerland, 2016)

[2] F. Aguado Agelet et al., Preliminary noise measurements campaign carried out by HUMSAT-D during 2014, ITU Symposium and Workshop on small satellite regulations and communication systems, Prague, Czech Republic, March 2015

[3] S. Busch et al., In-Orbit Performance and Lessons Learned of a Modular and Flexible Satellite Bus for Future Picosatellite Formations, Acta Astronautica, Vol. 117 (2015), Elsevier 73–89.

[4] M. Buscher, Investigations on the Current and Future Use of Radio Frequency Allocations for Small Satellite Operations, Doctoral Thesis, Berlin 2019

[5] ITU-R, Report ITU-R SA.2348-0, Current practice and procedures for notifying space networks currently applicable to nanosatellites and picosatellites, Geneva, Switzerland, 2015

[6] I. Skrypnyk, J. Bhat-Hire, M. Buscher, Design and AIV of on-going ISS based student project for analysis of RF spectrum utilization, 32nd Annual AIAA/USU Conference on Small Satellites, Logan, Utah, USA, 2018, 4-9 August

[7] Michal Krenek, Soapy Power Git Webpage, https://github.com/xmikos/soapy_power, (accessed 06.09.18)

[8] A. Bauer, M. Buscher, F. Boyer, J. Diez, MarconISSta Database, http://www.data.marconissta.com, (accessed 05.05.19)

[9] M. Buscher, MarconISSta Blog, http://www.marconissta.com, (accessed 31.01.19)

Solving the chicken-and-egg problem for optical downlinks - a report on an End-2-End approach

[2]Philipp Biller, [1]Christopher Schmidt, [1]Christian Fuchs, [2]Herwig Zech, [2]Matthias Motzigemba

[1]German Aerospace Center (DLR), Institute of Communications and Navigation, Muenchner Straße 20, 82234 Wessling

[2]Tesat Spacecom, Gerberstrasse 49, 71522 Backnang

Abstract: With the increasing need for higher data rates on small LEO spacecraft, highly compact laser communication systems are required to overcome the limitations in the downlink channel. Tesat has a long heritage in 1064nm wavelength optical communications for data relay and long-range applications. With the cooperation of the German Aerospace Center (DLR) the portfolio is extended by 1550nm wavelength communication technology for direct-to-earth and short range applications on Small- and CubeSats.

CubeSat missions made its way from technology demonstration missions and university projects towards commercial applications with the increasing capability of small-scale sensors, like hyperspectral camera systems. Small low-earth-orbit spacecrafts with a weight of 100 to 500 kg can carry imaging sensors with very high resolutions on ground which are generating large amounts of data in the earth observation. Both mission scenarios demand high data rates in the downlink channel and these needs are addressed with a laser communication transmitter (CubeLCT, TOSIRIS). On the other hand, the availability of optical ground stations is required to be able to receive these large data rates on the ground and enable more missions to make use of the large downlink capabilities these optical downlink systems can offer.

This paper will give an overview over the end-2-end approach for optical direct-to-earth communication.

1. INTRODUCTION

Increasing sensor resolutions drive the need for higher data rate capabilities in the downlink channel for nanosatellites in the LEO orbit. Nanosatellites come with a total weight of 1-10 kg and play an increasing role in the overall small satellite market, which consists of satellites with a total weight of 1-50 kg. **Fehler! Verweisquelle konnte nicht gefunden werden.** shows the number of nano- and microsatellites in the time between 2013 and 2018 as well as the prediction for 2019. It shows that the number of satellites increased since 2016 and reached over 400 in 2018. The major driver of this number is the class of Nanosatellites with 1-10 kg. This trend is estimated to continue over the next years to a total number of launched satellites of 2600.

Drivers for these satellites are four major applications: space based internet constellations, internet of things from space, earth observation both for scientific and commercial applications.

The latter one demand for a high bandwidth in the downlink of the data generated or received in space to the ground.

This is driven by the user demand for high spatial and spectral resolution (earth observation) or a large number of users (IoT) and on the other hand by the availability of technologies that can generate, process or receive such data amounts.

The coincidence of these two trends, user demand and available technology for data generation or handling in-orbit shifted the bottleneck towards the downlink from space to ground. The limitations in the conventional downlink technologies are strong, such as limited available bandwidth in RF-transmitter technologies, regulatory issues in the x-band for non-earth observation missions and also in size, weight and power limitations of todays nano- and microsatellite requirements.

This bottleneck can be solved by the use of optical communication technologies.

2. OSIRIS TECHNOLOGY AND RELATED PRODUCTS

The Institute of Communications and Navigation (IKN) of the German Aerospace Center (DLR) is working on the development of highly compact optical communication payloads for small LEO satellites. Initially started as a project for a prototype development, it has evolved towards a space program in the meantime – Optical Space Infrared Downlink System (OSIRIS). OSIRIS started as a development of prototypes for scientific measurements on the Earth Observation satellites Flying Laptop of the University of Stuttgart and BiROS of DLR. **Fehler! Verweisquelle konnte nicht gefunden werden.** shows the flight hardware for both missions while Table 1 lists the physical parameters of the payloads.

	Flying Laptop	**BiROS**
OSIRIS weight:	1,3 kg	1,65 kg
OSIRIS power consumption:	26 W	37 W
OSIRIS data rate:	Up to 200 Mbit/s	Up to 1 Gbit/s
OSIRIS downlink wavelength:	1550 nm	1550 nm
OSIRIS beacon wavelength:	N/A	1560 nm
OSIRIS pointing:	Satellite Body Pointing	Satellite Body Pointing
Launch Date:	July 14th, 2017	June 22nd, 2016

Table 1: Payload parameters of OSIRIS

Based on the flight model development for Flying Laptop and BiROS, the OSIRIS technology has been analyzed for further miniaturization.

The next development steps which are performed in close cooperation with Tesat have the focus on commercialization of the OSIRIS technology in two product lines for small satellites and CubeSats. The 100Mbps CubeL Laser Communication Transmitteris especially designed for cubesat missions and the 10Gbps TOSIRIS laser communication terminal is optimized for applications on small satellite platforms or other LEO platforms (like ISS). Both are shown in Fig 1.

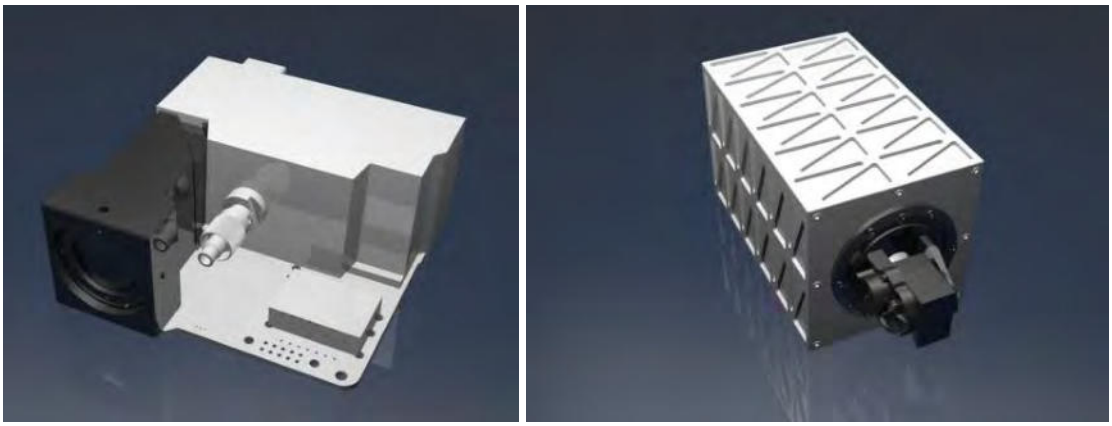

Figure 1: 100Mbps CubeLCT model (left) and 10Gbps TOSIRIS LCT model (right)

The technical parameters are quite different as the developments had different objectives (see Tab. 2).

	TOSIRIS	CubeLCT
Application	Smallsat LEO to ground laser communication solution based on Tesat's longterm industrial experience and DLR Institute of Communications and Navigation's research knowledge	Cubesat LEO to ground laser communication solution based on Tesat's longterm industrial experience and DLR Institute of Communications and Navigation's research knowledge
Range	LEO to ground	LEO to ground
Channel Data Rate	10 Gbit / sec LEO to Ground; 1 Mbit / sec TC Channel from Ground to LEO	100 Mbit / sec LEO to ground and 1 Mbit / sec TC Channel from ground to LEO
Weight	5 kg	360 gr
Size	28 cm x 20 cm x 15 cm	90 x 95 x 35 mm (~ 0,3 U)
Power	50 W	8 W
Pointing	full hemispherical, coarse beam pointing mechanism included	S/C body pointing +/- 1° + integrated Fine Steering Mirror
Lifetime	5 years in LEO orbit	5 years in LEO orbit
Data Interface	Ethernet or Spacefiber	LVDS
Available	FM available end of 2019, 1st mission on Airbus' Bartolomeo platform on the ISS	1st Mission PIxL in 2019, FM available
Technical features	Laser communication terminal optimized for 60 cm aperture optical ground station with uplink beacon, 1550 nm IM DD technology, 10 min. communication time / ground station pass. • integrated terminal controller for autonomous terminal operation • integrated mass memory • uplink TC channel from optical ground station Reference implementation for CCSDS standard	Expandable for Optical Intersatellite Links Laser communication terminal for lowest size, weight and power consumption; optimized for 60 cm aperture optical ground station with uplink beacon; 1550 nm IM DD technology; 10 minutes communication time per ground station pass; CCSDS compatible

Table 2: Technical parameters CubeL

3. COMMERCIAL OPTICAL GROUND STATION NETWORK

Introducing new technologies for the downlink from space to ground in the optical domain instead of the well-known RF frequency bands leads to a change in the ground

segment as well. The existing RF ground infrastructure can no longer be used. Furthermore optical downlinks are more sensitive to weather effects and thus need a higher site diversity. Therefore a global optical network on the best sites will be the game changer. DLR and partners assessed such a global optical network by taking into account a sophisticated global cloud atlas in the research program Onubla [2] with very promising results for the downlink rates.

To enable more programs and missions the use of optical ground links for the downlink of the data the optical ground station infrastructure must be easily accessible. Thus Tesat and the Institute of Communications and Navigation (IKN) of the German Aerospace Center (DLR) cooperate also in this field and will follow the upcoming CCSDS standard for down-to-earth links (O2K). In the future Tesat will take the responsibility from space to ground until the data is available for the end-user and introduce the first optical ground station (see Fig. 2) which is based on space debris and space situational awareness technology for excellent open loop tracking performance.

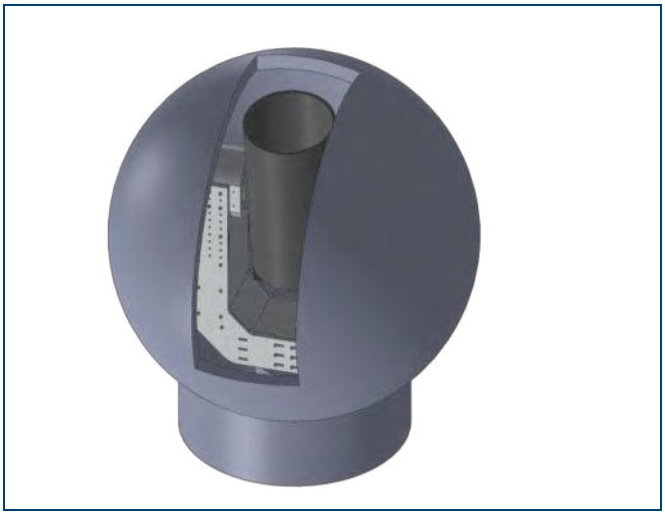

Figure 2: CAD model of Tesat's turn-key optical ground station

To enable a global and easy to accessible platform Tesat started a cooperation with KSAT of Norway (one of the largest satellite service operators) for the first global commercial optical ground network. The initiative foresees to introduce Tesat's optical ground stations into the existing RF-ground network infrastructure.

5. REFERENCES

[1] SpaceWorks Enterprises Inc., "2018 Nano/Microsatellite Market Forecast, 8th Edition",http://www.spaceworkscommercial.com/download-forecast/Nano-Microsatellite-Market-Forecast-8th-Edition_2018.pdf, checked January 5th, 2019

[2] Fuchs, Christian & Poulenard, Sylvain & Perlot, Nicolas & Riedi, J & Perdigues, Josep. (2017). Optimization and throughput estimation of optical ground Networks for LEO-downlinks, GEO-feeder links and GEO-relays. 1009612. 10.1117/12.2254795.

S-Net First Year in Orbit - Verification of a Nanosatellite Network in S Band

Walter Frese[1], Zizung Yoon[2], Klaus Brieß[3], Siegfried Voigt[4]

[1]Department of Aeronautics and Astronautics, Technische Universität Berlin
Marchstr. 12, 10587 Berlin, Germany
Phone: +49 30 314 25611, Mail: walter.frese@tu-berlin.de

[2]Department of Aeronautics and Astronautics, Technische Universität Berlin
Marchstr. 12, 10587 Berlin, Germany
Phone: +49 30 314 24438, Mail: zizung.yoon@tu-berlin.de

[3]Department of Aeronautics and Astronautics, Technische Universität Berlin
Marchstr. 12, 10587 Berlin, Germany
Phone: +49 30 314 21339, Mail: klaus.briess@tu-berlin.de

[4]German Space Administration (DLR Raumfahrtmanagement)
Koenigswinterer Str. 522-524, 53227 Bonn, Germany
Phone: +49 30 123 456, Mail: siegfried.voigt@dlr.de

Abstract: The S band Network for co-operating Satellites (S-Net) is a cluster of four nanosats developed by the Technische Universität Berlin (TUB) and successfully launched in February 2018. Since that time the S-Net satellites have performed a number of communication experiments using intersatellite links. Networked swarms of small satellites provide new opportunities for a large range of missions including data collection with distributed sensors (e.g. animal research), disaster monitoring or machine-to-machine communication. Especially the upcoming M2M serviced based on small communication terminals placed in areas with a weak infrastructure will require a cost-efficient space-born solution for low-latency data collection and delivery using narrowband multi-hop intersatellite links. This paper describes the on-orbit results and gives a short description of the communication network architecture of the mission S-Net. It is based on a software defined radio with an output power of 27 dBm and an RF bandwidth of 120 kHz in S band. A low power consumption of around 10 Watt and a weight of approximately 0.5 kg make this solution suitable for small satellites. The proprietary communication protocols have been developed to meet the requirements of a wide range of applications and orbital geometries. In fact, the use of low gain antennas in combination with an automatic antenna search algorithm allowed a significant weakening of the requirements on the attitude control. Furthermore, no fixed orbital geometry is required. All this make the developed technology suitable for satellite swarms, where the signals can come randomly in time and direction. The bandwidth efficiency has increased due to the use of an adaptive coding and modulation technique. A reliable intersatellite communication has been demonstrated over a wide range of distances from nearly zero up to 200 kilometers with low gain antennas with the maximum gain of approximately 6 dBi only. Furthermore, the routing problems arising in a non-centralized 3-D network are addressed and a solution, which was successfully verified on S-Net, is described. Finally, future work based on S-Net is discussed.

1. INTRODUCTION

The advantages of small satellite constellations with intersatellite link (ISL) capability have been thoroughly discussed and several missions proposed; for instance, in [1]. Only a handful of missions, however, have been successfully realized in the past, most of them with the purpose of technology demonstration. The majority of past missions used narrow band UHF links with P2P communication between only two nodes [2].

The FASTRAC mission demonstrated two-way communication between two nanosatellites for the first time [3]. This was done using a UHF crosslink operating at 9.6 kbit/s

over 10 km. CanX 4&5 is similar to FASTRAC. The ISL in this case is again a two-way crosslink using S band with an effective data rate of 10 kbit/s at distances up to 5 km [4]. Only recent concepts and missions such as EDSN [5], GAMASAT [6] and CPOD [7] are planning the implementation of more sophisticated ISL techniques such as the increase of bandwidth in S band, extension of communication range and multi-hop routing protocols. A notable mission is NASA's EDSN, which was unfortunately lost in a launch failure in Nov. 2015 [8] [9].

2. MISSION OVERVIEW

The primary mission goal of S-Net is to demonstrate an S band based multipoint ISL network within a nanosatellite constellation. The goal can be subdivided into following objectives: i) demonstration of multipoint ISL with S band transceiver, ii) verification of ISL communication protocols, iii) precise analysis of nanosatellite formation behavior considering orbital perturbations and, finally, iv) demonstration of the practical feasibility of nanosatellites for communication applications.

The four S-Net nanosatellites were successfully launched in 2018 into a Sun-synchronous low Earth orbit. The nano spacecrafts (satellite mass: 8.7 kg) were designed for a lifetime of one year, the satellite bus is fault-tolerant with only few single points of failure (SPOF). The network communication is maintained by a set of predefined rules operating independently of all four satellites. More details to the S-Net mission and to the S-Net nanosatellite bus architecture are given in [11].

3. S BAND TRANSCEIVER

The S band transceiver called “SLink” was verified within a real spaceborne network for the first time. SLink is a software-defined radio (SDR) designed to provide high-performance communications for small spacecraft in uplink, downlink and intersatellite link. Transceiver’s technology is based on commercial-of-the-shelf (COTS) parts. Table 1 shows some of parameters of the transceiver.

Table 1: Parameters of S band radio.

Parameter	Value
Frequency ISL, DL	2210.2 ... 2269.8 MHz
Frequency UL	2024.2 ... 2109.8 MHz
Range ISL	100 km nominal, up to 800 km (restricted by TDD slot lengths)
Bit rate DL/UL/ISL	0.674...3.394 Mbps / 30.8...252 kbps / 8.8...126.55 kbps
Symbol rate ISL	80 kHz (RF bandwidth: 120 kHz)
Symbol rate DL	1.4 MHz (RF bandwidth: 2 MHz)
Multiplexing	TDD, P2P
Modulation ISL	DBPSK, DQPSK, 8-ADPSK 16-ADPSK (option)
Coding	Convolutional r = 1/2, r = 3/4, r=1 for uplink and downlink only
Decoding	Viterbi, soft decision
RF output	27 dBm
Power	<12 W
Mass/Volume	<450 g with housing, 140×80×65 mm3

SLink provides three types of communication services: uplink (UL), downlink (DL) and intersatellite link (ISL). S-Net satellite implements seven S band low gain circularly polarized planar antennas: one UL antenna and six further DL/ISL antennas, each of with a half-power beam width of nearly 90°. Six planar ISL/DL antennas, one antenna for each of the side panels of the satellite, are used (see Fig. 1). The RF signal is distributed through a power switch. S-Net utilizes an ISL antenna configuration and communication techniques, which are especially suitable for communication within a satellite swarm and requires no specific antenna pointing or orbital geometry.

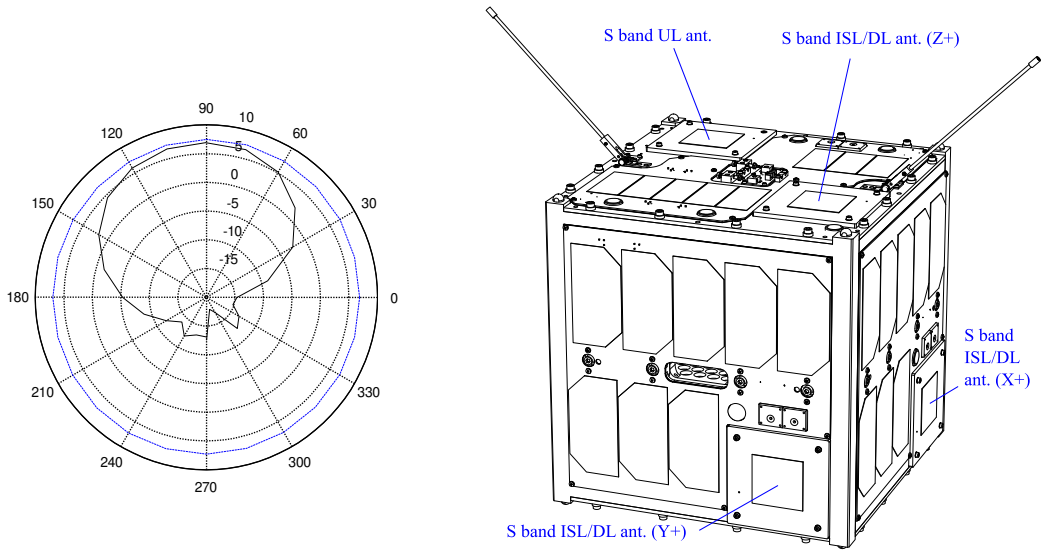

Figure 1: Antenna pattern (azimuth: dashed) and S-Net satellite and antenna configuration.

The configuration with six orthogonally arranged ISL antennas opens some interesting possibilities: truly distributed communication control algorithms with no central master can be used, as each terminal would be always ready to receive signals from others, despite of the direction these signals are coming from. The second advantage: no active antenna pointing required, helping to save power. On the other hand, some new requirements on communication terminal have emerged as a consequence of this antenna configuration. At the beginning of a communication session the receiver has to be able to find out on which of the six antennas a signal is available. The transmitter, for its part, if it doesn't have information about the orientation of the receiver has first to find out a suitable transmit antenna. This functionality is part of the automatic gain control and antenna search algorithm (AGC&ANS). All the six antennas will be selected in row at both sides in same order but for different time intervals. Once the receiver detects a signal it stops to switch the antennas and answers using currently selected antenna. The transmitting terminal stops, for its part, to switch its antennas if it detects the answers. For ISL a time-division duplexing (TDD) point-to-point (PTP) protocol on the same center frequency is used. The time slots for both terminals involved in a P2P session have different lengths resulting in two different achievable bitrates for each of the directions.

For the ISL differential phase modulation in combination with two convolutional forward error correction codes with constraint length k = 9 and the polynomials [561,753] is used. The code with r = 3/4 is built through perforation from the base code with r = 0.5. The decoder (non-coherent) uses a soft decision Viterbi algorithm. Three different

basic modulations in combination with three types of coding lead for the ISL to six possible combinations, resulting in bit rates up to 90.55 kbit/s for standard 8-ADPSK and r = 3/4 and up to 121 kbit/s for the optional 16-ADPSK modulation. Adaptive coding and modulation (ACM) helps to optimize the data throughput, as the link budget can change during a session as a result of the change of the antenna pointing. Two ends of a session are called caller and responder herein. A caller satellite is the initiator of a session establishment process. A responder satellite receives session establishment parameters from a caller. The modulation and coding of the P2P link is commanded by the caller sat and transferred to the responder sat in every frame. The signal-to-noise ratio (SNR) of the responder is transmitted back to the caller, so the caller can make decisions about the suitable modulation and coding for both sides. For the uplink and for the downlink different modulations (e.g. QAM) are used. The highest data rate on the downlink is 3.394 Mbit/s, using a symbol frequency of 1.4 MHz. For the downlink and for the ISL identical symbol rate of 80 kHz is used resulting in a RF bandwidth of approximately 120 kHz, whereby on the downlink it would be 2 MHz.

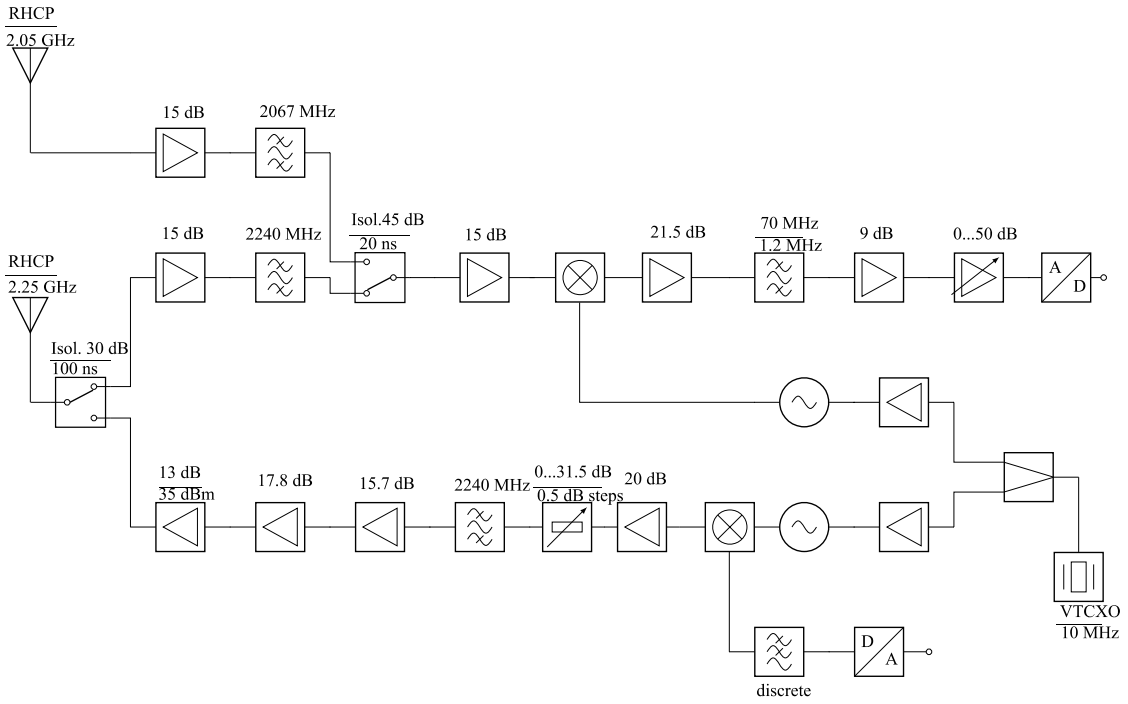

Figure 2: RF block diagram of S band transceiver.

Fig. 2 shows a block diagram of the RF components of the transceiver. The receiving path is shown on the top and the transmitting path on the bottom of the picture. Please note that the six ISL/DL antennas are approximated with one antenna and the dedicated antenna switch is not shown on the picture. One single receiving path is used for the uplink and the intersatellite link. Nevertheless, as the central frequencies for these both services are different, the received signals are fed into the receiver path using separate antennas, LNAs and filters. The transmitting path is the same for the downlink and the intersatellite link. The received signals are sampled directly on the intermediate frequency (IF) of 70 MHz and are filtered digitally afterwards. Before down-converting to the IF two image rejection filters are used for both ISL and UL frequencies (on the top left in Fig. 2). To maintain a suitable signal amplitude on the output of the receiver

branch (see on the top right of Fig. 2) a variable gain amplifier with a dynamic range of 50 dB is used. A closed-loop feedback control system implemented in software and used as a part of a combined automatic gain control and antenna search algorithm (AGC&ANS).

The design of the transmitting path is straight forward. The data, generated with the digital-to-analog converter (D/A) is directly up-converted and amplified by the two stages of the power amplifier. The output RF power with an acceptable level of nonlinear distortion can be maintained in the range up to 28.5 dBm for all modulations and even be slightly higher for lower order modulations like BPSK or QPSK. The output RF power of the transmitter and can be adopted in 0.5 dB steps with a digital step attenuator.

4 TOPOLOGY AND LINKS

The network topology is determined by i) orbital configuration, ii) operating mode and desired QoS (quality of service) and iii) possible resource differences between the satellites. The orbital configuration is the most heavily weighted factor affecting the basic network topologies. The four S-Net satellites were deployed simultaneously into the same orbit (580 km height SSO). To keep the space segment simple, a propulsion system was intentionally omitted, and therefore the relative formation was be mainly controlled by the separation parameters from the launcher's upper stage. The goal was to keep the satellites in a range to enable a stable ISL for at least four months. Finally, very low relative drifts could be achieved in orbit solely by the precise control of the deployment parameters of the S-Net satellites. It was even possible to reduce the distances between satellites using atmospheric drag present at a 580 km height (see Fig. 3).

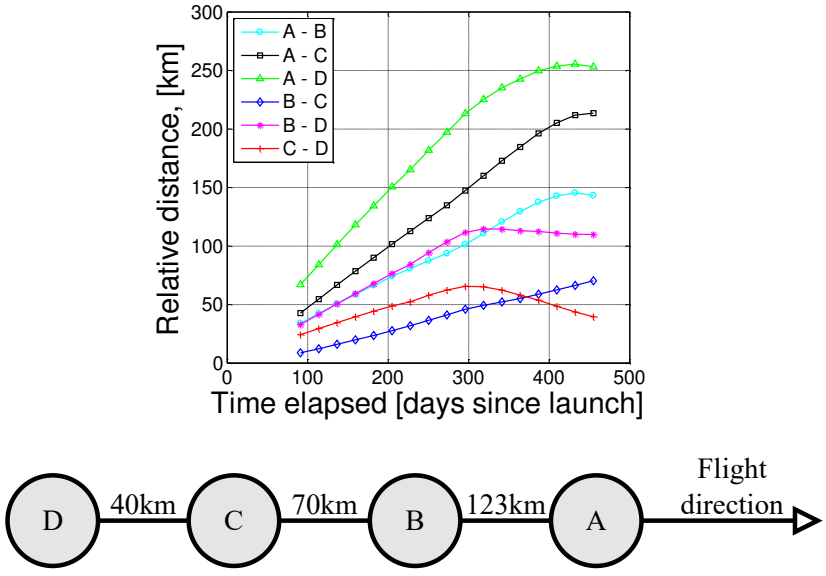

Figure 3: History of relative distances and current (more than one year after launch) orbital geometry (bottom).

For S-Net three channel access methods for nanosatellite networks are realized and verified: centralized star architecture with a communication master, token passing and random access (RA). RA and token passing in a small satellite network with four nanosat-

ellites are analyzed in this paper. A token passing scheme is collision-free, easy to implement and proposed to be a good choice for formations with a small number of nodes. More advanced concept is the random access. RA is preferred for meshed topologies where multi-hoping is unavoidable and there is a great number of nodes. The data flows are shown for both schemes in Fig. 4. The high-speed data flow on the groundlinks doesn't have a significant impact on the timing compared to the low-speed crosslinks and are not considered in this paper.

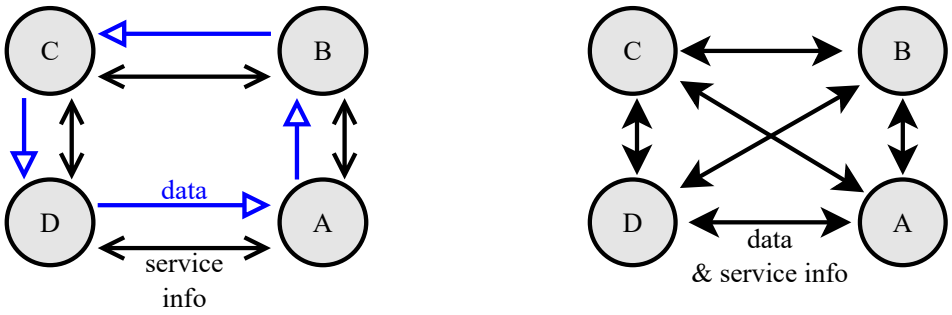

Figure 4: Data flow. Token passing (left) and random access (right).

The variable length data in case of token passing is transferred from one satellite to other in one direction, i.e. A-B-C-D-A-B… from the example from Fig. 4. Together with the data bi-directional service information is transferred like addressing, token flag, packet numbers required for ARQ acknowledging etc. In the data to be transmitted from A to C it needs to be stored in B first, even though it can be transmitted to C directly.

In case of RA the data can be exchanged between all four satellites directly. A fully connected communication graph is shown on Fig. 4 as a general example. In case a direct data transfer is not possible, one or more additional hops are involved, the data is stored and forwarded until in comes at a data sink. Because the satellite movements are highly predictable, the communication graph can be calculated independently in every satellite using Dijkstra's algorithm. The orbital elements can be updated on different ways including ground station as the simplest one. The 3D orbital geometry can be approximated with a 2D case if the satellites are distributed through orbits with similar heights. The routing aspects of S-Net are described in [11]. The paths for the data to go will be calculated in every node independently (distributed algorithm).

5 PERFORMANCE ANALYSIS

Fig. 5 (on the left side) shows the cumulative distribution function for establishing of a P2P session. In 90% of the cases a P2P connection can be established within a time of 1500 msec or faster using AGC only. From this moment on the messages can be transferred from responder to caller and vice versa with a small delay affected by the propagation time and by the automatic repeat request protocol (ARQ) in presence of packet errors. The AGC algorithm can be easily completed with an antenna search functional part (ANS) by adding an antenna switch after each gain sweep. ANS slightly decrease the performance: in 90% of the cases a P2P connection can be established within a time of 3500 msec or faster.

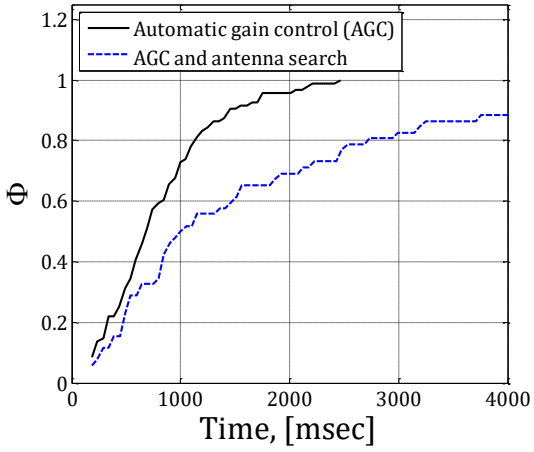

Figure 5: Cumulative distribution function of the session establishing time.

The signal-to-noise ratio (SNR) measurement data with and without antenna pointing could be gathered during very long P2P sessions (see Fig. 6). As already mentioned in previous sections, in general case there is no need for an active antenna pointing because every one of the six intersatellite link antennas services its direction and an automatic antenna search is implemented. The SNR performance was verified in two attitude control modes: free tumbling mode and target pointing mode. In free tumbling mode both satellites participating in a P2P session are oriented in fully random manner and can change their orientation during a session. The dashed line in the middle of Fig. 6 (lest side) shows this case. The transition levels of the ACM algorithm are shown. Fig. 6 (left) shows two more cases, both corresponding to a very disadvantageous antenna pointing. The communication over distances less than 100 km is possible independent of the orientation. Links over long distances of 200 km and more could be established as well using antenna pointing.

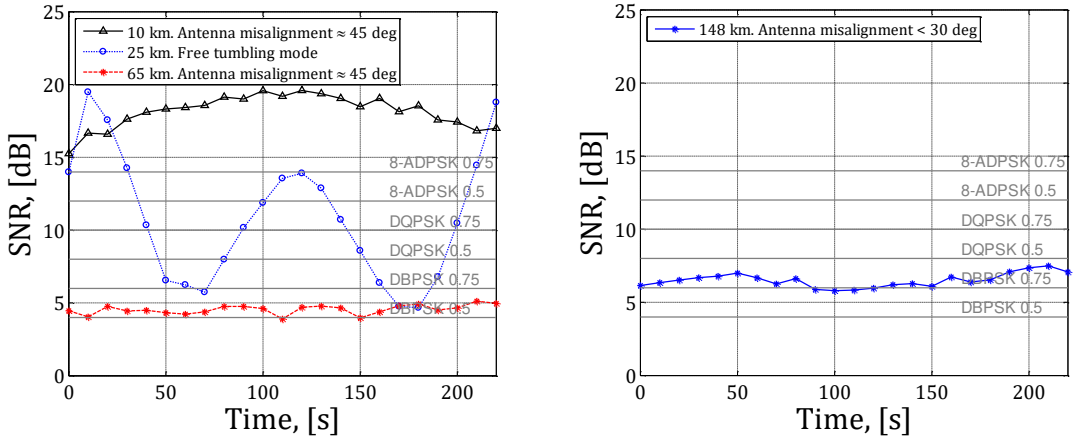

Figure 6: Signal-to-noise ratio during some very long P2P sessions.

Fig 7 shows a performance comparison between token passing and random access. The geometry and data generation rate in each satellite is the same: 30 byte/s. In case of a token passing each of the satellites receives not only packets addressed to it but also the data packets of the next two satellites on the line. On Fig. 7 the first satellite receiving

data is A, the token master is D at this time. Some service information (200 byte) is transferred from A to D, but the main data flow is from D to A (4000 byte of data and service information). After A/D session A will became the token master and starts to transmit data and service information to B and receive service information from B. In case of a random access much less amount of data, at least in a fully connected graph, needs to be transferred per session, hence the bandwidth utilization is better.

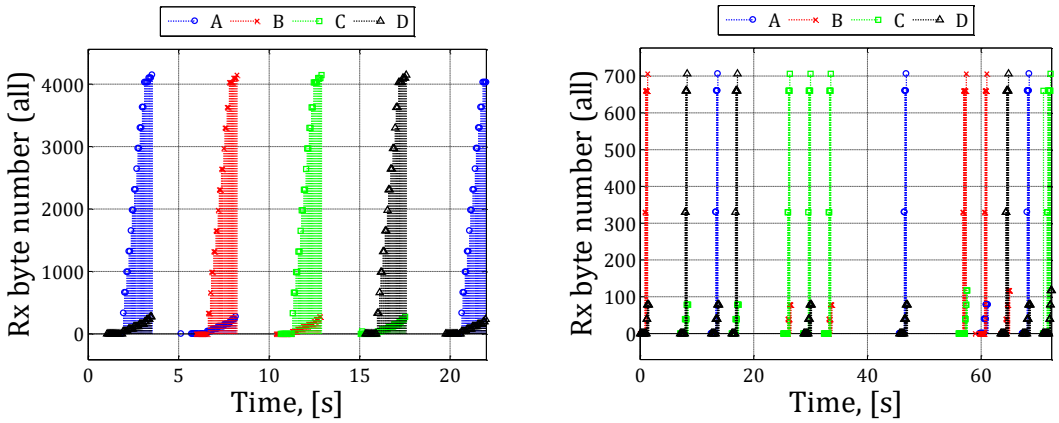

Figure 7: Data flow for token passing (left) and random access.

The payload has been developed using COTS technology, which, in general, can withstand a total radiation dose of approximately 10 krad. During environmental testing campaign on ground the hardware was charged with 20 krad without failure. On higher loads an increase in power consumption could be observed beginning with a total dose of few krad. However, one year (calculated total dose in LEO of 4.8 krad) after launch the payload doesn't show any significant changes in power consumption. No single event upsets (SEU) and no losses in functionality could be observed yet.

6 CONCLUSIONS, FURTHER WORK AND ACKNOWLEDGEMENTS

The S-Net mission provided a proof for an intersatellite networking by a cluster of four nanosatellites over distances of more than 200 km. The project demonstrated the practical feasibility of nanosatellites for communication applications with low data rates. Currently, the work on a next satellite mission of the TU Berlin called SALSAT is active. SALSAT bases on the S-Net satellite bus; S band transceiver is used for downlink and uplink only. Through an improved isolation between transmitting and receiving paths of the transceiver up- and downlink communication can be performed simultaneously in frequency division duplex mode making SLink suitable for TM&TC.

The R&D project SLink, on which this paper is partly based, is a co-operation between the Technische Universität Berlin and the company IQ wireless. We are grateful to all project participants for their contributions. The projects S-Net and SLink were implemented on behalf of the Federal Ministry of Education and Research (ger. Bundesministerium für Bildung und Forschung, BMBF) under grant numbers 50YB1225 and 50YB1009 respectively.

7. REFERENCES

[1] R. Radhakrishnan, W. W. Edmonson, F. Afghah, R. M. Rodriguez-Osorio, F. Pinto, and S. C. Burleigh. Survey of inter-satellite communication for small satellite systems: Physical layer to network layer view. In IEEE Communications Surveys Tutorials, volume 18, pages 2442–2473, Fourthquarter (2016).

[2] Craig Underwood, Mike Crawford, and Jeff Ward. A low-cost modular nanosatellite based on commercial technology. In AIAA/USU Small Satellite Conference, Utah (1998).

[3] Aaron Smith, Sebastian Munoz, Eric Hagen, Gregory Johnson, and Glenn Lightsey. The FASTRAC satellites: Software implementation and testing. In 22nd Annual USU/AIAA Small Satellite Conference, Logan, Utah, (2008).

[4] S Armitage, L Stras, G Bonin, and R Zee. The CANX-4/-5 nanosatellite mission and technologies enabling formation flight. In International Workshop on satellite constellation and formation flight, Lisbon (2013).

[5] J. Hanson, J. Chartres, H. Sanchez, and K. Oyadomari. The EDSN intersatellite communication architecture. In 28th Annual AIAA /USU Conference on Small Satellites (2014).

[6] Pedro Rodrigues, Ricardo Mendes, Pedro Sinogas, André Oliveira, and Karim Mellab. Enabling intersatellite link platform for multi-satellite missions. In Proceedings of the 66th International Astronautical Congress, number IAC-15-B2.5.7 (2015).

[7] Williams Austin. Cubesat proximity operations demonstration (CPOD) vehicle avionics and design. In CubeSat Workshop (August 2015).

[8] James Chartres, Hugo Sanchez, and John Hanson. EDSN development lessons learned. In 28th Annual AIAA /USU Conference on Small Satellites, Utah (2014).

[9] J. Hanson, J. Chartres, H. Sanchez, and K. Oyadomari. The EDSN intersatellite communication architecture. In 28th Annual AIAA /USU Conference on Small Satellites (2014).

[10] Walter Frese, Klaus Briess, and Zizung Yoon. A network architecture for inter-satellite communication of distributed nano spacecraft systems. In Proceedings of 60th Deutscher Luft- und Raumfahrtkongress, pages 1451–1461, Bonn, DGLR e.V. (2011).

[11] Walter Frese, Zizung Yoon, Klaus Briess, and Siegfried Voigt. Communication Network in LEO: In-Orbit Verification of Intersatellite Link by Nanosatellite Cluster S-Net. In Proceedings of 69th International Astronautical Congress (IAC), (2011).

Design and analysis of the offset Parabolic Antenna to be used in C band Communication Satellites

Abdelaziz HIMEUR, Ali Kara-Omar, Lahcène Hadj-Abderrahmane

Centre de Développement des Satellites
Pos 50 ilot T12 Bir El Djir, 31130 Oran, Algérie
Phone +213 555 208 799 Mail: ahimeur@cds.asal.dz
akaraomar@cds.asal.dz
lhadjabderrahmane@cds.asal.dz

Abstract: Many type of reflector antenna have been extensively employed in communication satellite as single reflector, dual reflector and offset reflector. The reflector type depends on satellite payload requirement; we focus on the case of an offset single parabolic antenna, which is one of the most antenna type used in geostationary satellite. The most important advantage of the offset reflector is the aperture blockage prevention from the feed. This paper presents a C-band parabolic antenna design methodology used on board communication satellite for both downlink and uplink and the relevant results. The parameters of the offset antenna are evaluated to achieve the optimal diameter for maximum edge-of-coverage (EOC) directivity. By setting the geometric parameters, the optimal antenna diameter is founded to achieve the maximum directivity at the edge of coverage. By introducing these results in grasp software, the antenna radiation pattern is given. The proposed antenna is planned to be used for future Algerian communications satellite.

Keywords—Geostationary, antenna, Algeria, edge of coverage, pattern

1. INTRODUCTION

Communication satellites have multiple reflector antennas that provide various services, witch is classified in accordance with ITU Radio Regulations. Typical satellite services that employ reflector antennas include the following:

• Fixed satellite services (FSS) is used in C-band, Ku-band or Ka-band providing both uplink and downlink beams from one antenna or using two antennas .The study is applicable for region 1 (see figure 1). C-band is used for many advantages as:

- Single beam for a large geographic coverage.
- Resilience to rain fade, especially in region which have high rainfall rate [1].

• Broadcast satellite services (BSS) is used to transmit or retransmit the signal by satellites to be received directly by the general public. It provides mostly downlink beams over a coverage region such North Africa. [2]

• Broadcast satellite services (BSS) that provide mostly downlink beams over a coverage region such North Africa. [1]

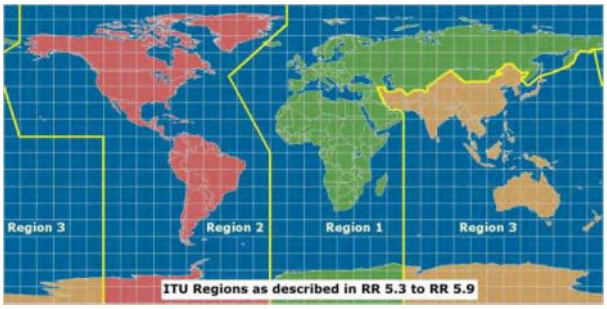

Fig. 1. ITU Regions [3]

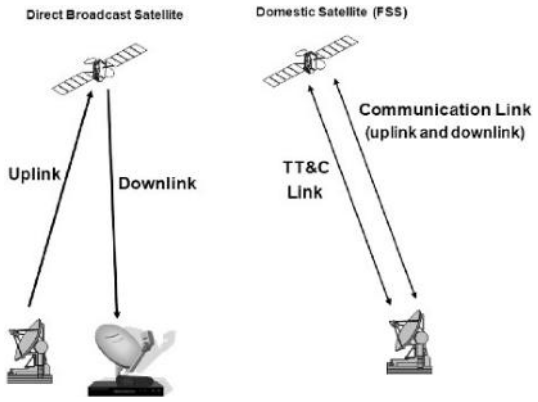

Fig. 2. Illustration of FSS and BSS services [4]

The offset reflector can be used to minimize aperture blockage effects and side lobe levels. Several work have already performed in this way [5]

The proposed antenna could be used for the future Algerian communication satellite by considering the FSS service with national beam in C-band. This paper is organized as follows. Section II describes the design topology of the single parabolic antenna. Section III introduces the geometric parameters. Finally, the simulation results are presented in section IV.

2. TYPOLOGIES OF SINGLE PARABOLIC REFLECTOR ANTENNAS

Considering a global pointing error (Beam pointing error) BPE = 0.12 °, and a circular beam of 3.52° (see figure 3), maximum EOC directivity must be achieved.

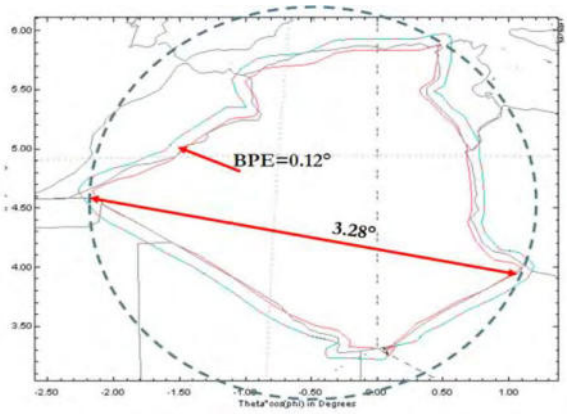

Fig. 3. Antenna coverage

Two configurations are possible, they are:
• Center reflector configuration [6]: the feed illuminates the antenna center of diameter D_p and create a shadow zone due to the feed position on the reflector axis. In this case, the antenna efficiency is reduced (see figure 4a).

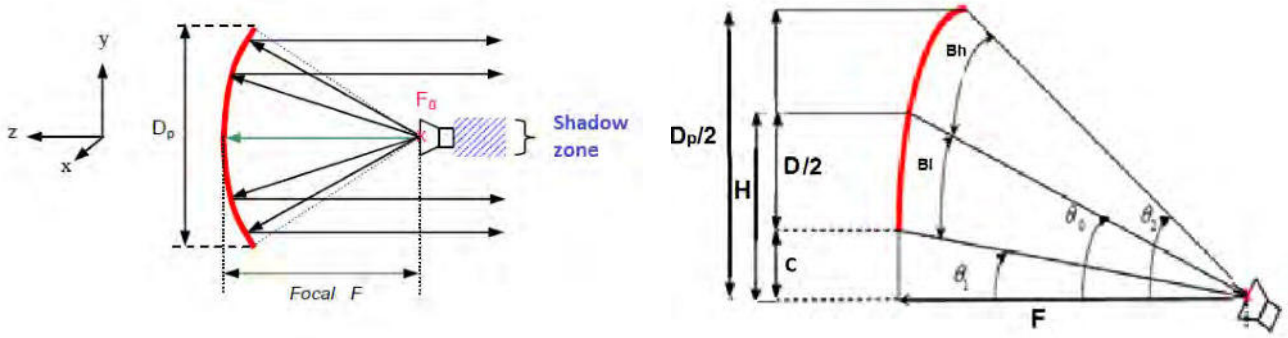

(a) (b)

Fig. 4. Parabolic reflector configuration centered (a) and offset (b)

• Offset reflector configuration [6]: this is currently the most commonly used. The mask effects are limited by shifting the feed. The diameter D/2 is identified by the pointing angle θ_0, as mentioned in Figure 3b.

$$\theta_1 = 2artg(\frac{H}{2F}) \text{ (1)} \qquad \theta_2 = 2artg(\frac{H+D}{2F}) \text{ (2)} \qquad \theta_0 = 2artg(\frac{H+\frac{D}{2}}{2F}) \text{ (3)}$$

- θ_0: is the source pointing angle or the parabolic interception angle.
- H: is the offset
- D: is the reflector diameter
- F: is the focal

Therefore, the center reflector will be used for earth stations where the masking effect is negligible compared to the large size of the reflector.
In the following sections, we focus the study on the offset reflector.

3. GEOMETRIC PARAMETERS

3.1 The reflector diameter D

The diameter D will be chosen according to the gain and the angle of the used beam.

3.2 The offset H

The offset H is set according to the size of the feed; it should not be too low to avoid a shadow zone and a large diffraction on the reflector lower edge. It should not be too large to avoid a high level of cross polarization for a symmetrical reflector [7]

- If the offset $H \leq D/2$: no clearance.
- If the offset $H > D/2$: clearance.

The clearance C is defined as the distance between the lower edge of the reflector and the focal axis in the offset geometry.

3.3 The focal F of the reflector or the ratio (F/D_p)

This parameters is limited by congestion and the deployment difficulty on board satellites.

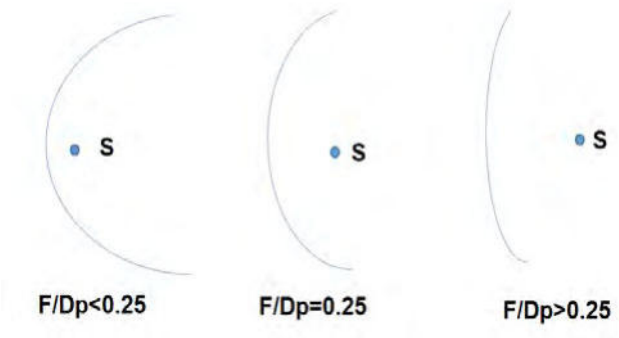

Fig. 5. The ratio (F/Dp)

Figure 5 illustrates the different case of configuration:

• For $F/D_p < 0.25$: the antenna is located in the space between the reflector and the aperture plane and the illumination tapers away towards the reflector edge.
• For $F/D_p > 0.25$: the feed is located outside the aperture plane which results in a uniform illumination, but the overflow effect increases in this case.
Overflow means the radiation from the feed that is directed toward the reflector. The focal length is expressed in terms of the reflector diameter and the antenna depth.

The telecommunications applications require an F/D_p often high. However, according to the space constraint, the antenna size should be limited.

3.4 Surfaces, Gain, Efficiency, Directivity D_0

- The physical area of the aperture plane is given by: $Aphy = \frac{\pi D^2}{4}$ **(4)**
- The effective area of the reflector is equal: $Aeff = Aphy * \eta = \eta * \frac{\pi D^2}{4}$ **(5)**
- The gain expression is given according to the surface of the aperture plane by:

$$G = Aphy * \eta * (\frac{4\pi}{\lambda^2}) = (\frac{\pi D}{\lambda})^2 * \eta \quad \textbf{(6)} \qquad D_0 = G_{\max} = 10 * \log\left[\left(\frac{\pi * D}{\lambda}\right)^2 * \eta\right] \quad \textbf{(7)}$$

With η is the antenna efficiency

$$\eta = K_1 * K_2 \quad \textbf{(8)}$$

The parameters K1 and K2 are the gain factors which are respectively dependent on [8]:

• Edge Taper Losses which correspond to an aperture whose the illumination is not uniform.

• Losses by Spillover which correspond to the energy radiated by the primary source which is not intercepted by the focusing element.

The edge taper (T) is a value which describes the feed radiation intensity at the edge of the reflector relative to the center. The edge taper is the value often used when referring to the feed pattern. The edge taper is related to the feed number n by the expression:

$$n = \frac{T_{dB}}{20\log(\cos(\mathrm{Bl})^2} \quad \textbf{(9)}$$

$$K_1 = \frac{\left(T + \frac{2}{\pi}\right)^2}{T^2 + \frac{4T}{\pi} + 0.5} \quad \textbf{(10)}$$

n : is the feed number
T: is the edge taper often expressed in dB
K1: is the factor related to the edge taper losses given by:
Where T is the linear taper parameter

Spillover losses are due to an aperture angle of the primary source main lobe. A fraction of the radiated power by the source do not intercept the reflector, so the antenna gain will be decreased.

K2 can be expressed as function of edge taper and n=1 by :

$$K_2 = \frac{\int_0^{Bh} \cos(x)\sin(x)\,dx}{\int_0^{\frac{\pi}{2}} \cos(x)\sin(x)\,dx} = 2\int_0^{Bh} \cos(x)\sin(x)\,dx \quad \textbf{(9)}$$

$$Bh = ar\cos(10^{\frac{T_{dB}}{20}}) \quad \textbf{(10)}$$

The gain factors K1 and K2 vary in opposite direction .

According to the edge taper given by figure 6, it is thus necessary to find a trade-off between the losses by overflow (important if the source is not very steering) and the losses by edge taper (important if the source is steering) to obtain the maximum output of the focusing element. It is thus necessary to seek the maximum of the total factor gain K1× K2 according to the edge taper. This maximum antenna efficiency is η=84.79 % and it is obtained for an edge taper T= -16 dB.

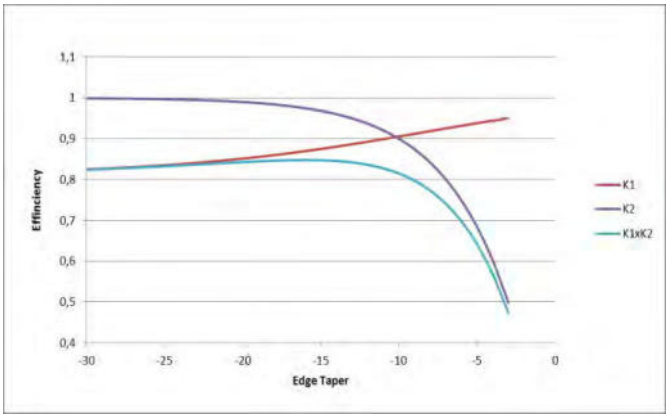

Fig. 6. Equation Gain factors and reflector efficiency

3.5 Radiation pattern, Roll-off, EOC Directivity

The radiation pattern of a reflector consists of a main lobe and side lobes. The half power beamwidth is defined as [9]:

$$\theta_3 = \frac{70\lambda}{D} \quad (13) \qquad \theta_n = \theta_3\sqrt{\frac{N}{3}} \quad (14)$$

Where

- θ_3 :is the radiation pattern
- θ_n : is the coverage angle

The roll-off N is the difference between the maximum axial directivity D_0 and the directivity at the edge of coverage Deoc (figure 7). In the Gaussian approximation, the roll-off N is given by:

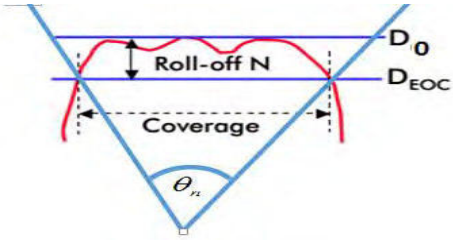

Fig. 7. The roll off related to D_0 and the Deoc

$$N = 3\left(\frac{\theta_n}{\theta_3}\right)^2 \quad (15) \qquad D\_EOC = D_0 - N \quad (16) \qquad N = 3\left(\frac{\theta_n}{\theta_3}\right)^2 = 3\left(\frac{3,52}{\theta_3}\right)^2 \quad (17)$$

4. SIMULATION RESULTS

The key parameters for this typical example using grasp software are then:

Freq = 5.4 GHz, F/D_p = 1, Feed tapper = -16 dB, Offset H = 5D/8, Efficiency = 0.84
Figure 8 shows the antenna diameter variation from 0.6 m to 1.8 m and take into account the roll off and D_EOC variation.

Table 1 EOC directivity & directivity D_0 versus the reflector size

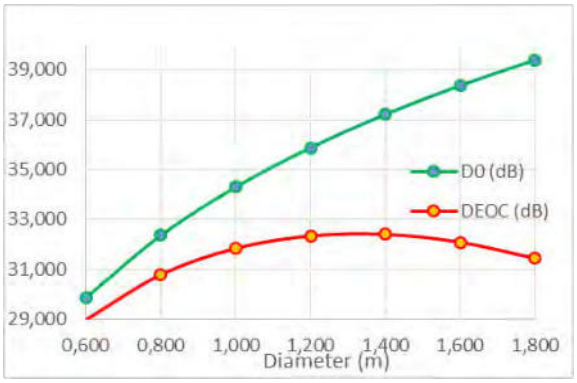

Diameter D (m)	D0(dB)	Theta(°)	Roll off(dB)	DEOC (dB)
0,6	29,854	6,481	0,885	28,969
0,8	32,353	4,861	1,573	30,780
1,0	34,291	3,889	2,458	31,833
1,2	35,875	3,241	3,539	32,336
1,4	37,214	2,778	4,817	32,396
1,6	38,374	2,431	6,292	32,082
1,8	39,397	2,160	7,963	31,433

Fig. 8. EOC Directivity & directivity D_0 variation with the reflector size for the national beam case.

Referring to the figure 8 and table 1, we notice that the maximum directivity increase between 0.6 m and 1.8 m. Also, the value of the directivity coverage is maximum between 1.2 m and 1.4 m. This should give an idea of the practical value of proposed antenna. We will therefore, focus on these results and spread this interval with a step of 0.04 m, as shown in figure 9 and table 2.

Table 21 D-EOC directivity versus reflector size with step of 0.04 m

Diameter D (m)	D_0(dB)	Theta(°)	Roll off(dB)	DEOC (dB)
1,2	35,875	3,241	3,539	32,336
1,24	36,160	3,136	3,779	32,380
1,28	36,435	3,038	4,027	32,408
1,32	36,703	2,946	4,283	32,420
1,36	36,962	2,859	4,546	32,416
1,4	37,214	2,778	4,817	32,396

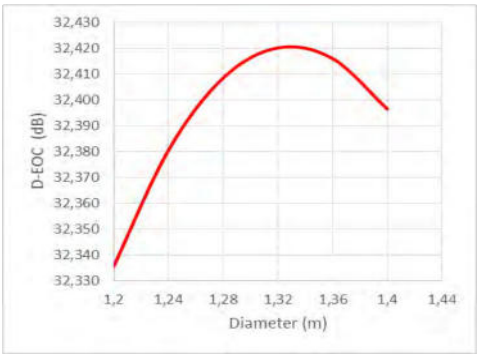

Fig. 9. Zoom of EOC directivity versus reflector size

The directivity D_EOC (θ_n=3.52°) has a maximum of 32.42 dB for D =1.32 m and a roll off N= - 4.28 dB

Figure 10 shows the antenna radiation pattern with diameter equal to 1.2 m, 1.32 m and 1.4 m.

Figure 11 shows the maximum gain (D_0=36.25 dB) for an antenna diameter of 1.32 m representing then the optimum configuration using GRASP [7].

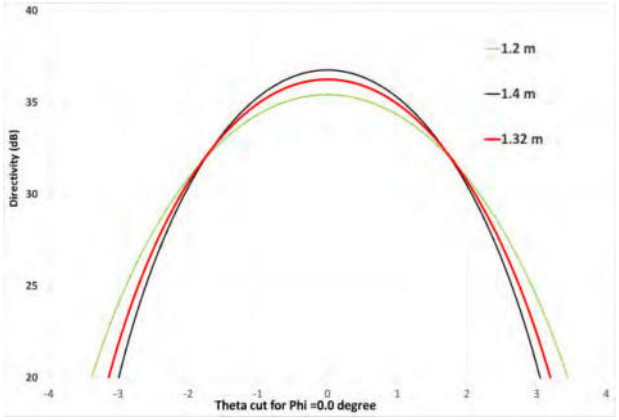

Fig. 10. Evolution of radiation pattern for different antenna size

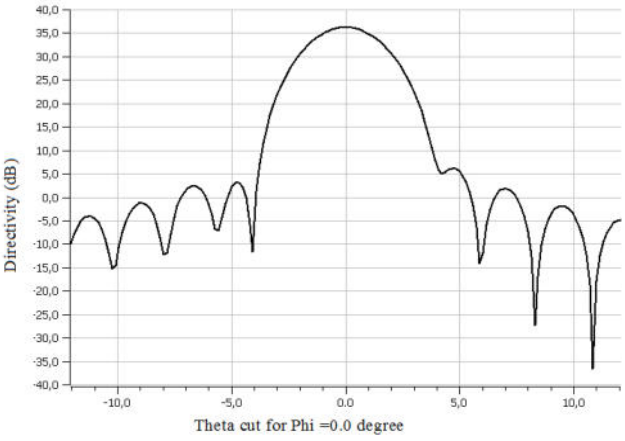

Fig. 11. Evolution of radiation pattern for D=1.32 m

5. CONCLUSION

The offset-parabolic reflector is used since many years for different applications. Recently, analytical and numerical models have been developed for this device which can show the advantages of its electrical properties.

The proposed design is focused on maximizing the D_EOC and minimizing the spill over losses among all the coverage region.

In conclusion, we have designed a C-band offset-reflector antenna which consists of an optimum configuration with the following parameters in the case of national coverage.

- Antenna diameter D=1.32 m
- Roll-off N = - 4.28 dB
- Directivity end of coverage D_EOC = 32.42 dB,
- Maximum gain D_0=36.25 dB

It is anticipated that the proposed design will provide an important impetus to the future use of the C-band antenna implemented on board the second Algerian Telecommunication Satellite.

6. REFERENCES

[1] https://asiavia.org/wp-content/uploads/2018/08/SAT-PRES-the-importance-of-c-band-and-the-threat-of-IMT-in-this-band-20140526.pdf

[2] Sudhakar Rao, Handbook of Reflector Antennas, Vol 3, Chapter 2,ARTECH HOUSE,2013

[3] https://www.itu.int/en/ITU-R/terrestrial/broadcast/Pages/Bands.aspx

[4] K. K. Chan and F. Hyjazie, "Design of overlapping gridded reflectors for frequency reuse,"IEEE APS/URSI Symposium Digest, pp. 149–152, 1985.

[5] .Hal Schrank, et al, Design of Offset-Parabolic-Reflector Antennas for Low Cross-Pol and Low Sidelobes, IEEE Antennas and Propagation Magazine, Vol. 35, No. 6, pp 46-49, December 1993,

[6] THESE_MENUDIER-CYRILLE Caractérisation des performances d'antennes à réflecteurs paraboliques illuminées par une source focale BIE Application à l'optimisation d'une couverture multimédia

[7] AlAN W RUDGE, et al, Offset-parabolic Antennas: A review, IEEE, vol 66, NO. 12, DECEMBER 1978

[8] L. Hadj Abderrahmane ; M. Benyettou, A Ka Band Offset Dish Antenna to be Used for the Future Algerian Telecommunication Satellite, Aerospace Conference, 2007 IEEE

[9] Yi Yi Aye, et al, Transmit and Receive Antenna Design for C-band Satellite Communication,International Journal of Science, Engineering and Technology Research (IJSETR),Volume 1, Issue 1, July 2012

[10] TICRA Eng., "GRASP10-Single and Dual Reflector Antenna Program Package," Copenhagen, Denmark

Wireless intra-spacecraft communication with inspaWSN protocol stack based on IR-UWB

Martin Drobczyk[1], André Lübken[2]

[1]German Aerospace Center
Institute of Space Systems, Avionics Department
Robert-Hooke-Str. 7, 28359 Bremen, Germany
Phone: +49 421 24420 1164, Mail: martin.drobczyk@dlr.de

[1]German Aerospace Center
Institute of Space Systems, Avionics Department
Robert-Hooke-Str. 7, 28359 Bremen, Germany
Phone: +49 421 24420 1164, Mail: andre.luebken@dlr.de

Abstract: In recent years, many attempts were made to replace wired connections with wireless communication networks in spacecraft and launchers. The benefits include a simplification of the harness design and routing as well as a reduction of harness cables and thus mass in space systems. However, commonly used wireless communication techniques are less reliable compared to their wired counterparts. Moreover, they are sensitive to RF interferences and multipath fading, which is an important design driver in a spacecraft environment with highly reflective enclosures. This paper presents a novel wireless protocol architecture for intra-spacecraft wireless sensor networks (inspaWSN), which makes use of the impulse-radio ultra wideband (IR-UWB) PHY according to IEEE 802.15.4-2011 and an optimized low latency and deterministic network protocol (LLDN) in order to achieve the strict requirements on existing spacecraft networks, e.g. low and deterministic latency behavior for the attitude and orbit control system (AOCS). The implementation and evaluation of the proposed protocol stack is performed on an STM32 microcontroller network consisting of 3 nodes. The results in this paper show that it is able to fulfill the strict timing requirements in order to accomplish deterministic communication with a latency of 10 ms and less in a typical AOCS configuration.

1. INTRODUCTION

Data exchange among spacecraft subsystems is usually achieved by employing field bus systems like SpaceWire. The necessary cable harness for these connections, however, is a significant cost driver in development and construction of these systems. In addition, the harness contributes up to 10% to the dry mass of a satellite and leads to additional launch costs.

Low power wireless sensor networks could be employed to reduce the design and integration cost of these wired systems and have proven their robustness on earth e.g. in industrial control applications. Benefits include: Mitigating risks of breaking cables or connector problems; easier accommodation and handling and faster setup of assembly, integration and test (AIT) tasks. Recent studies have already shown wireless sensor network operation in space is a viable approach ([1] and [2]).

The typical setup of such a wireless sensor network (WSN) aboard a spacecraft consists of a central coordinating unit that is directly connected to the on board computer and numerous sensor nodes distributed throughout the satellite structure providing the data connection for the different sensors and actuators of the subsystems. The most challenging one is the attitude and orbit control system (AOCS) comprised of e.g. sun sensors, magnetic field sensors, star trackers and reaction wheels or magnetic torquers as actua-

tors. In order to guarantee the correct operation of the AOCS control algorithms, its latency and reliability requirements must be strictly adhered to.

Hence, a wireless data link needs to provide a reliable, deterministic and low latency connection for these sensors and actuators. This is achieved by employing a modified alternative time division multiple access (TDMA) medium access control (MAC) layer from the 802.15.4-2015 standard originally designed for low latency industrial automation systems. Another problem arises from the highly reflective enclosure, in which the RF components will be operated. This results in interferences due to multipath fading effects when using traditional narrowband RF systems. The proposed protocol stack mitigates these issues by introducing impulse-radio ultra wideband (IR-UWB) in the physical layer of the stack.

2. SPACECRAFT SENSOR OVERVIEW

Satellite systems contain a considerable amount of sensors to monitor and control mission-critical functions. Various types of sensors track the in-orbit performance, but they are also used in AIT activities to support the qualification of the satellite in different test campaigns. The sensors are usually assigned to the related subsystems of a satellite. The *thermal subsystem* sensors monitor temperatures and have a typical sampling rate of 10s-30s with no specific latency requirements. The *mechanical subsystem* uses sensors to check mechanisms in orbit (e.g. for solar panel deployment). Sensors in the *electrical subsystem* track currents and voltages. They are highly integrated into the different components and are an example of sensors not suitable for a WSN deployment. The *AOCS subsystem* finally is comprised of several sensors and actuators controlling the spacecraft attitude. It needs a reliable connection with low and deterministic latency with high sampling rates of up to 100 Hz.

The requirements for the wireless network architecture presented in this paper are derived from the DLR satellite Eu:CROPIS, demanding a deterministic latency under 10 ms.

3. PROTOCOL ARCHITECTURE

This work considers the first two layers of a typical network stack, the physical and the MAC layer, that are needed to provide the functionality outlined above. The upper layers can either use a traditional internet protocol stack, e.g. utilizing 6LoWPAN as a base for typical IoT networks or make use of the CCSDS [6] protocols specified for space applications.

3.1 IR-UWB PHY

The base of the implemented network stack is built upon an IR-UWB PHY that conforms to the IEEE 802.15.4-2011 [4] extension of the standard. Ultra Wideband possesses a low power spectral density avoiding interference with other RF sensitive systems. The transmission is also resilient against multipath fading effects, which is common for the metal enclosures of spacecraft or launchers.

IR-UWB can be operated on several channels in the range of 3.5 GHz to 6.5 GHz. Common narrowband technologies like Wi-Fi, Bluetooth or ZigBee cause interference

with other systems operating in the same frequency spectrum. IR-UWB on the other hand generates short pulses (< 2 ns) to transmit the data. This short pulse duration thus spreads the spectrum to approx. 500 MHz using the same power output, which leads to a very low power spectral density. Due to the low signal level for any given frequency, UWB can easily coexist with other RF applications operated in the same frequency spectrum [5].

The pulse duration also allows UWB to be nearly immune against the multipath fading effects experienced within the highly reflective metal enclosures of a spacecraft structure [6]. Compared to other available PHYs for WSNs like ZigBee, WirelessHART or ISA100.11a, it provides a much higher data rate (up to 27.1 Mbps) and in turn allows to achieve the low latency required for the proposed application [1].

3.2 LLDN based MAC

The robust UWB physical transmission scheme is combined with a modified version of the low latency deterministic network (LLDN) MAC layer specification proposed in the IEEE 802.15.4e [7] extension, which ultimately was not included in the current 802.15.4 revision of the standard.

The additional MAC Layers of the 802.15.4 extension usually try to add robustness to the transmission over the traditional narrowband PHYs, e.g. by employing a channel hopping scheme. LLDN, however, is a simple TDMA approach with fixed timeslots and reduced header information. It only allows a star topology and thus deterministic and low latency for our desired application.

An LLDN network divides the time into superframes, which in turn are divided into equally-sized time-slots. A detailed chronogram of the operations that take place within one slot is shown in Fig. 1. A network coordinator takes care of assigning these slots to the nodes in a separate configuration phase and will send out beacon frames to synchronize the network. Since the slots for the nodes are configured beforehand, overhead for addressing is not needed as these can be inferred from the slot number. Another feature to shrink the header size are group acknowledgements (GACK), which allow the omission of separate ACK frames in most cases, as the coordinator will give out ACK information with the beacon transmission.

Although, from the same standard the LLDN scheme is not compatible with the UWB PHY layer, since some features like carrier sensing are not possible on a UWB Network and thus need to be implemented differently. A standard LLDN network uses longer slot times that include a contention based access time period for all nodes of the network and a time period for the coordinator in addition to the exclusive time period for the node the slot is assigned to. This mechanism prolongs the superframe and additional ACK frames and a CCA mechanism are needed. Using the bidirectional timeslots of the standard allows the same use cases with reduced need for a CCA scheme. However, during the non-time-critical management phases of the network this is not possible and a simple ALOHA scheme is used instead.

In addition management frames sent out by the coordinator allow to flexibly reconfigure the network to e.g. utilize a higher data rate compared to a typical WSN to transmit bigger blocks of data like firmware updates or payload data.

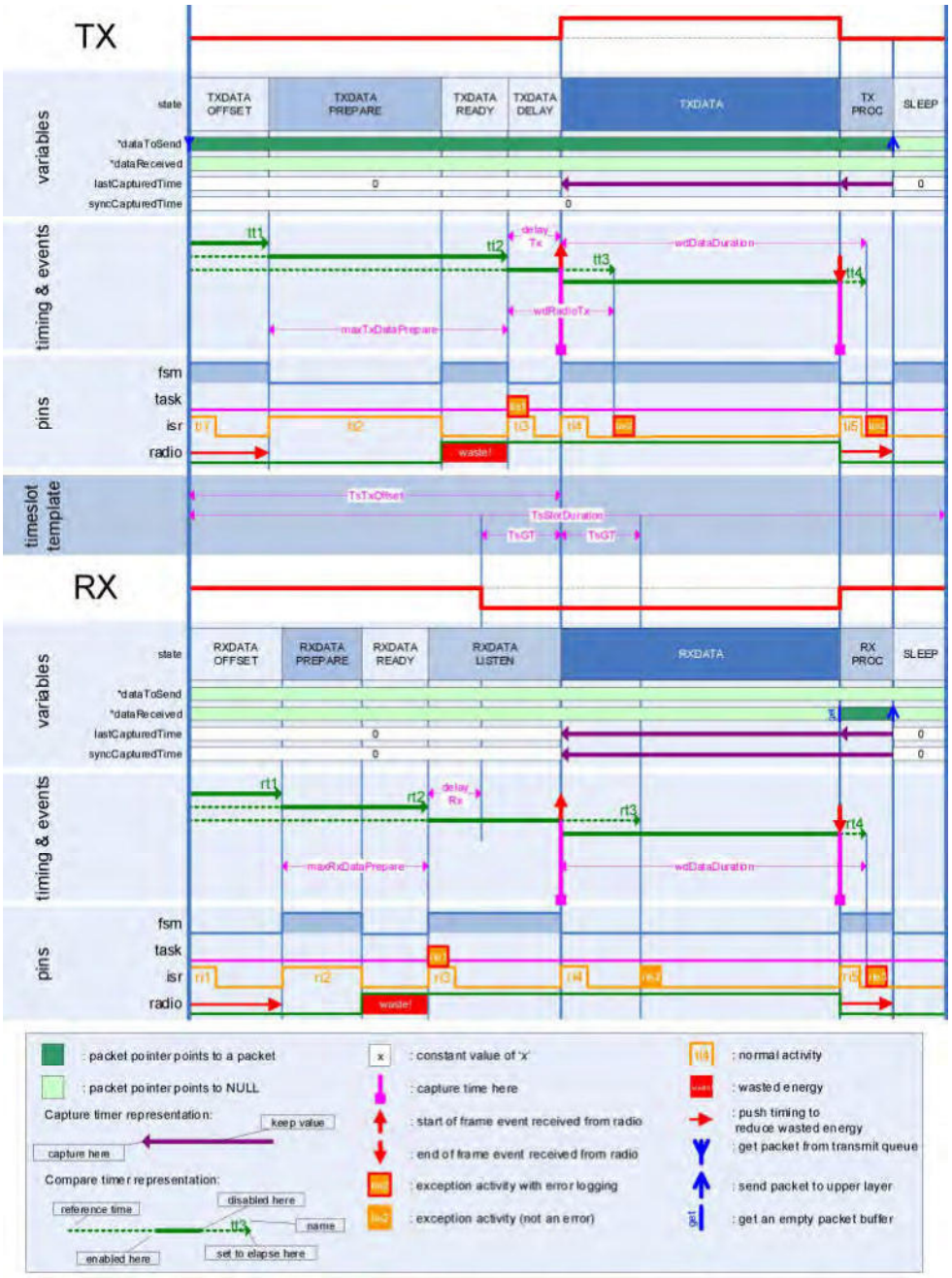

Figure 1: Chronogram of the LLDN MAC A single LLDN Slot is comprised of different phases the RX and TX node have to go through. In the first interrupts the node is prepared for the upcoming transmission in order to minimize the time needed during the actual event. This is done to reduce the time the receiving node stays in the RXDATA LISTEN phase, where the receiver draws a significant amount of power. Offsets from the precalculated reception time to the actual time are caused by clock drift and used to reconfigure the timers so the nodes stay synchronized.

4. EVALUATION

The proposed system architecture has been implemented on an STML151 Cortex M3 low power micro controller combined with a Decawave DW1000 UWB transceiver and integrated into an existing RTOS System. In a test network of three nodes an average minimum latency of 3.4 ms was achieved.

Two separate tests were conducted. In the first one the uplink processing was synchronized to the respective slot, which is possible because LLDN uses a fixed slot plan. This allows the minimum latency of 3.4 ms between generation of e.G. sensor data and its processing on the receiving node. Due to the fixed arrangement of the slots after they have been configured in the configuration phase of the LLDN protocol, this latency is also deterministic.

Results showed that a significant portion of this time, however, is consumed by the processing of the packets on the node and network coordinator. Latency proved to be deterministic due to the strict network topology and MAC scheme with jitter of about 100 µs.

In a second test the parameters regarding slot length and number of slots in the superframe were chosen in a way that allowed the modified LLDN MAC to be comparable to the popular TSCH MAC. Test data was queued for transmission at random intervals to spread communication attempts over the duration of the superframe of 60 ms. Results in Fig. 2 show that the TSCH MAC produces outliers where packets where received in the next superframe. This is caused by the rescheduling of slots that is usually used to switch channels on narroband PHYs used with TSCH. Deterministic latency is thus not achievable utilizing TSCH in this configuration.

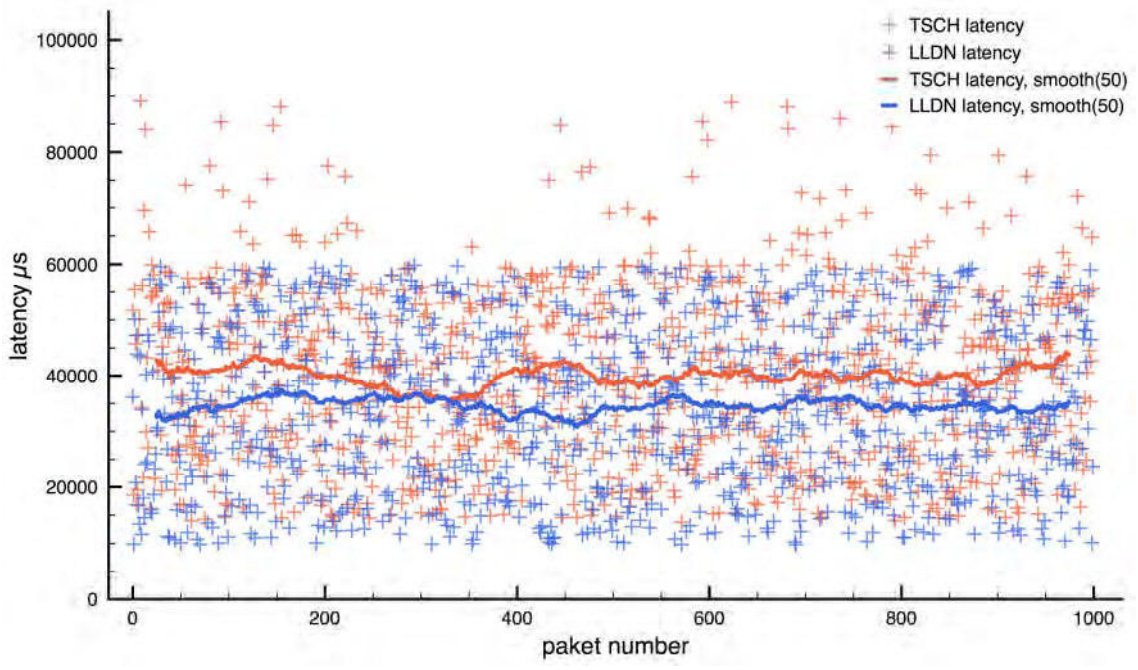

Figure 2: LLDN and TSCH mode latency comparison

Energy consumption is on par with other systems of this class with 3.63 mJ per packet for a standard wireless node. Deep sleep of a node is also possible and only requires a resynchronization to the network on wakeup, as LLDN does not keep track of the node state.

5. CONCLUSIONS

In this paper we presented inspaWSN, a novel wireless protocol architecture for intra-spacecraft wireless sensor networks. Key driver for its requirements were AOCS systems with their strict timing demands.

The required latency of 10 ms is easily met, but a usage of a more capable microcontroller with respect to computing power could further reduce the latency. The utilized IR-UWB PHY layer with the low overhead of the modified LLDN MAC proofs to be a robust combination. Future work will include further modification of the LLDN to optimize it for the specific requirements of intra-spacecraft communication. A second step will be the development of a low overhead transport layer to support applications developed for the platform.

It is planned to integrate inspaWSN into a future DLR satellite mission as a technology demonstrator payload in order to achieve a technology readiness level (TRL) of 8.

6. REFERENCES

[1] M. Drobczyk and H. Martens, “A study on low-latency wireless sensing in time-critical satellite applications”, presented at IEEE Sensors 2016, Orlando, USA, 30 Oct. -3 Nov., 2016.

[2] H.J. Beestermöller, H.-J. Borchers, H. Luttmann, J. Sebald, M.-C. Sinnreich, M. Schneider and V. Schmid, “Wireless-Sensor Networks in Space Technology Demonstration on ISS” presented at 12. Dresdner Sensor-Symposium 2015, Dresden, Germany, Dec 7-9 2015.

[3] CCSDS (Consultative Committee for Space Data Systems) Blue Book: 133.0-B-1: Space Packet Protocol, Consultative Committee for Space Data Systems, NASA, 2003.

[4] IEEE Std 802.15.4-2011: Part 15.4: Low-Rate Wireless Personal Area Networks (LR-WPANs), IEEE Computer Society: New York, NY, USA, 2011.

[5] M. Hirose, T. Kobayashi, A. Tomiki, T. Toda, "Effects of inner volume on UWB propagation channels within closed spaces," presented at IEEE International Conference on Ultra-WideBand (ICUWB), Paris, France, 1-3 Sept. 2014, pp.62-67.

[6] M. Drobczyk, M. Lehmann, C. Strowik, “EMC characterization of the UWB-based wireless positioning and communication experiment (wireless Compose) for the ISS”, presented at IEEE WISEE 2017, Montreal, Canada, Oct 10-12, 2017.

[7] IEEE Std 802.15.4e-2012: Part 15.4: Low-Rate Wireless Personal Area Networks (LR-WPANs) (Amendment to IEEE Std 802.15.4-2011), IEEE Computer Society: New York, NY, USA, 2012.

High-speed X-band Transmitter Development

Hyeun-pil Jin[1], Young-jin Joo[1], Jae-hoon Lee[1], Sung-min Park[1], Young-wook Sirl[1]
Jae Min Ahn[2]
[1]Satrec Initiative Co., Ltd.
[2]Chungnam National University
Daejeon, the Republic of Korea
Mail: hpjin@satreci.com

Abstract: Satrec Initiative has developed a 600Mbps-class X-band transmitter for small and mid-sized satellites in a national R&D program. Currently, the payload data rate is supported up to 550Mbps using the 4D-8PSK-TCM modulation method with 2.75 bit/symbol efficiency, and RF output power is tested up to 10W with SSPA. A high-speed communication signal processing technique that generates 12-bit wide-band DAC signal oversampled at 1600MHz with a single FPGA enables scalability for transmission of even wider band signal. The overall transmission speed is expected to be achievable up to 1.2Gbps when a higher order modulation scheme is adopted by simple reprogramming of FPGA without significant hardware modification. In this paper, the design, implementation and verification of the transmitter are presented.

1. INTRODUCTION

As technology evolves, the capability of a small satellite system is expanding rapidly especially in its resolution of earth observation. While many companies are competing to develop small satellite systems with higher resolution, Satrec Initiative has developed the SpaceEye-X satellite system with ground sample distance of 0.5 meters and continues research for higher resolution. [1] Accordingly, increased image data have necessitated higher image transmission to balance the mission performance of the satellite system. Satrec Initiative has developed a 600Mbps-class X-band transmitter for which the design and test results are presented in this paper. With 4D-8PSK-TCM 2.75 Mode modulation method [2], the payload transfer rate is 550Mbps, and RF Power Amplifier can be output up to 10W. Vibration tests, thermal vacuum tests, and TID tests were conducted to confirm that they met the target requirements for space environment. In addition, the baseband signal processing technology of the XTU600 operates on a single FPGA with a 12bit wideband DAC at a 1600Msps symbol rate. This broadband high-speed signal processing technology can be a basic technology that can make full use of the 375MHz band allocated to the X-band frequency for space. Therefore, if the CCSDS high-order modulation scheme (for example, SCCC 64APSK) is applied in the future, the transmission rate is expected to be 1.5Gbps or higher.

In this paper, the design and the test results of the XTU600 developed by Satrec Initiative. And then we will take look at what to consider for X-band 1.2Gbps transmission and suggest the solutions.

2. XTU600 OVERVIEW

The design specifications of the high-speed X band transmitter XTU600 developed by Satrec Initiative are presented in Table 1. XTU600 adopted CCSDS 4D-8PSK-TCM channel coding and has a transmission rate of 600Mbps at a modulation rate of

200Mbaud/s. The code rate can be selected within 2, 2.25, 2.5, 2.75, and the actual payload data rate with the 2.75 Mode would be 550Mbps. And the pre-equalizer function, which is processed in the baseband, can improve the signal quality of the transmitter RF output by pre-compensating the linear distortion over the transmission path. The power amplifier using high efficiency GaN SSPA has a gain above 40dB and the out-of-band signal of PA output is rejected by the RF channel filter. The final output power of XTU600 can be up to 10W.

Table 1. Design Specification

Item	Detail
Transmission Speed	600Mbps
Modulation	4D-8PSK-TCM(2, 2.25, 2.5, 2.75 Mode)
Baud rate	200Mbaud/sec
Oversampling	x8
Roll-off	0.35
DAC Clock	1600MHz
Occupied Bandwidth	< 300MHz
RF Frequency	8025 to 8400MHz
RF Output Power	> 10W
RF Output Es/N0	> 27dB (with Pre-Equalizer in TxModem)
VSWR	< 1.5 : 1
Mass	< 3kg
Volume	244 x 194 x 68 mm^3
Power Consumption	< 120W (Power supply :22 ~ 34 VDC)
Input Interface	LVDS SERDES Interface
TM/TC Interface	CAN Interface

Figure 1. High-speed X-band Transmitter XTU600

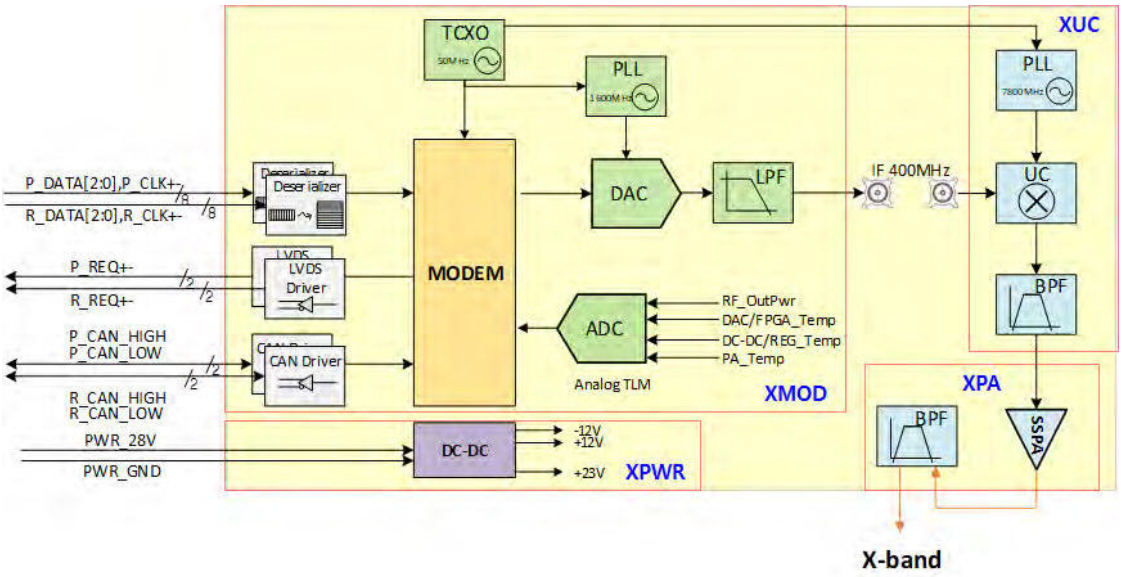

Figure 2. Block Diagram of XTU600

3. HARDWARE DESIGN

3.1 Interface

The data input section of XTU600 has a data rate of up to 800Mbps through the LVDS SERDES link and has a "Data-pull" [3] interface that receives one transmission frame when it sends a data request signal to the mess memory device. With via the CAN interface XTU600 can be controlled and transmit the status information itself. Therefor transmitter status such as current RF power intensity, temperature and voltage status of Power Amp can be monitored. It is supplied with unregulated 28V DC power and internally distributes various voltage power to individual units via DC-DC converter.

3.2 Digital Hardware

In the MODEM hardware, a FPGA is capable of high-speed signal processing to generate 1600Msymbol/s by the parallel processing implementation method. Currently, 8PSK symbols are generated at 200Mbaud/s and it has a data rate of 600Mbps. In the future, if a high-order modulation scheme such as 64APSK would be applied it could be transmitted over the bit rate of 1200Mbps. We believe that baseband high-speed signal processing technology can be also applied to Ka-band broadband transmission technology in the future. The high-speed DAC converts the 400MHz IF signal at a 1600MHz clock, and the image signal of DAC output is rejected by the band-pass filter.

3.3 RF Up-converter

The RF up-converter consists of mixer, local oscillator with PLL, and band-pass filter. The IF signal at the DAC output is converted to X-band frequency through the mixer and local oscillator.

3.4 SSPA

High efficiency GaN SSPA has a gain above 40dB and can output 8PSK signal up to 23.5W. The out-of-band signal of SSPA output is removed through the band-pass filter so that minimizing an interference in the deep space frequency area. The final output is 10W with band-pass filter and transmission line loss.

4. TEST RESULT

4.1 Environmental Test

To verify the operation of the space environment, XTU600 had qualification tests which are vibration test, thermal vacuum test, and TID test. The results are shown in Table 2.

Table 2. Environmental Test Results

Test item	Test Specification	Result
Vibration	Base on ECSS-E-10-03A	12.25 G rms(3-Axis)
Thermal Vacuum	Operating Temp : -20 ~ +50℃ Storage Temp : -35 ~ +60℃ 10-5 Torr 8 cycle, RFT : 2hr, FFT : 4hr	Pass
Radiation	Total Ionizing Dose Cobalt 60	Normal operation up to 12krad(Si)

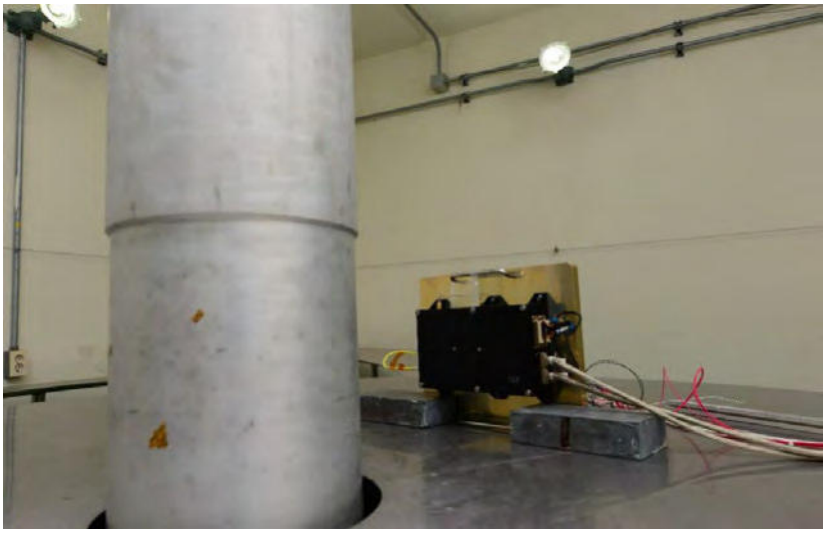

Figure 3. Irradiation Test

4.2 SNR Performance

When the output is 10W with 4D-8PSK-TCM, normally the output SNR was measured to be more than 29dB and the constellation is presented in Figure 4.

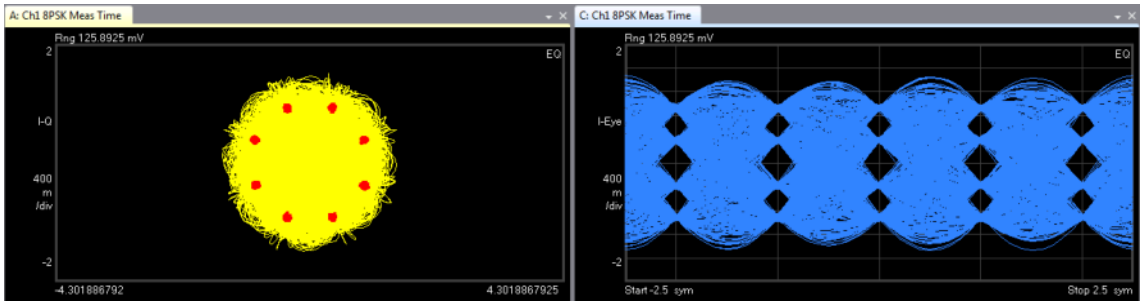

Figure 4. The output SNR on 10W SSPA

4.3 Additional Test

Experimentally we tried to test for higher modulation scheme up to 64APSK and measure the output constellation. The physical data rate of 64APSK can be seen 1.2Gbps due to operating with 200Msps. The outputs of modulator for 16APSK, 32APSK and 64APSK are showed in Figure 5. Because XTU600 is already equipped with high-speed flexible poly phase SRRC filter and 1.6Gsps DAC can output variable modulation scheme. In addition, we are going to employ VCM/ACM channel coding like SCCC or DVB-S2 in Q3/2019 and we expect to realize the full performance of giga-class X-band transmitter in Q4/2019.

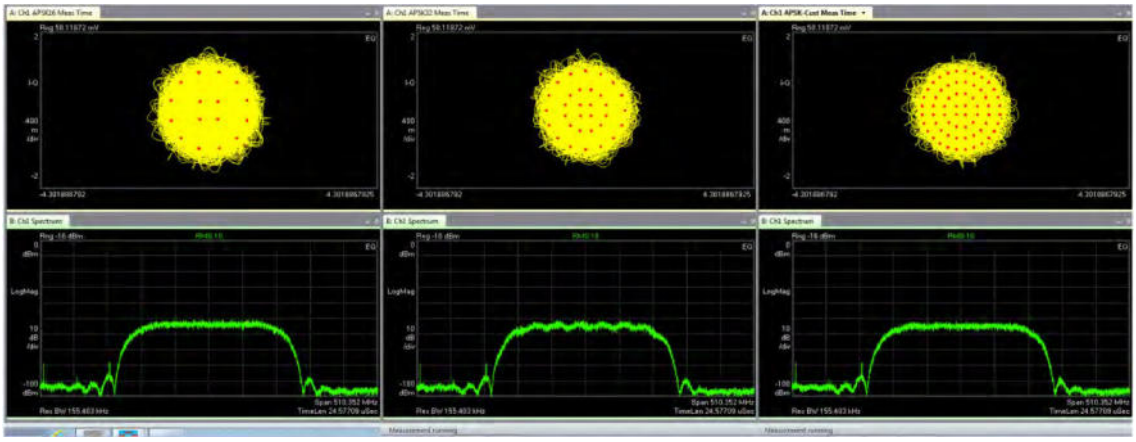

Figure 5. Constellations and Spectrum of 16APSK (Left), 32APSK (Center) and 64APSK (Right)

5. SUMMARY

Satrec Initiative has developed a 600Mbps X-band transmitter for small and mid-sized satellites. We verified its function through various space environmental tests. As the additional test, we expect that the basic technology of XTU600 could be applied to giga-class transmission through high-speed signal processing technology with higher modulation scheme. Therefore, we are planning to implement a Gbps transmitter with applying CCSDS SCCC [4] or DVB-S2 [5] coding as well as a cost effective optimization design in the future.

6. REFERENCES

[1] E. Kim, H. Lee and E. D. Kim, "Sub-half meter imaging satellite, SpaceEye-X," 2017 8th International Conference on Recent Advances in Space Technologies (RAST), Istanbul, 2017, pp. 125-127.
[2] CCSDS 401.0-B-28
[3] CCSDS 130.12-G-1
[3] CCSDS 131.2-B-1
[4] CCSDS 131.3-B-1

An Experience of Satellite UHF - Ground Stations as the Basis for Academic Cooperation

Livio Gratton[1], Martin Buscher[2], Sascha Kapitola[2], Claus Rosito[1], Apiwat Jirawattanaphol[3], Sebastián Marinsek[4], Pablo Bernadí[1], Camila Mucanna[1]

[1]Instituto Colomb
25 de Mayo y Francia, 1650. San Martín, Argentina
Phone: +54 11 4006 1500, Mail: lgratton@conae.gov.ar

[2]Technische Universität Berlin
Marchstraße 12, 10587 Berlin, Germany
Phone: +49 30 314 75872, Mail: martin.buscher@tu-berlin.de, sascha.kapitola@tu-berlin.de

[3]Kyushu Institute of Technology
1-1, Sensui, Tobata, Kitakyushu,804-8550 Fukuoka, Japan
Phone: +81 93 884 3229, Mail: p350945j@mail.kyutech.jp

[4]Instituto Antártico Argentino
25 de Mayo 1143, San Martín, Argentina
Phone: +54 11 2033 1420, Mail: smarinsek@dna.gov.ar

Abstract: In 2017, the Instituto Colomb (IC), created by agreement between the Argentine Space Agency (CONAE), and San Martín National University (UNSAM), organized the 1st IAA Latin American Symposium on Small Satellites in Buenos Aires, to promote collaboration of Latin American and worldwide organizations. The implementation of a university satellite´s Ground Station was identified as a suitable means to collaborate with more experienced partners. The Technische Universität Berlin (TU Berlin) offered to assist the IC, resulting in a plan for the IC to install two UHF antenna ground stations (GSs), in the UNSAM Miguelete Campus, and in an Argentine scientific station in Antarctica. Once the GSs were operational, they started downloading data and transmitting commands to the BEESAT TU Berlin missions. This opened the door for collaboration with the Kyushu Institute of Technology (Kyutech), and its BIRDS program. TU Berlin and Kyutech benefited from new GSs to download their missions´ data, and the capability to issue commands from the Southern Hemisphere, while the IC had the opportunity to benefit from the experience of institutions with expertise in university satellite missions. This paper describes the cooperation implementation and focuses on the technical challenges overcome to use the GSs to operate with different missions from different universities, in different environments.

1. INTRODUCTION

In March 2017, the Instituto Colomb (IC), created by agreement between the Argentine Space Agency (CONAE), and San Martín National University (UNSAM), organized the 1st IAA Latin American Symposium on Small Satellites in Buenos Aires, to promote collaboration of Latin American organizations, among themselves and with non-regional partners. In spite of the CONAE having a substantial heritage in space missions and UNSAM on the educational side, the IC was a newcomer in the 'Lean Satellites' field. In that sense, the implementation of a university satellites' Ground Station (GS) was identified as a suitable means to collaborate with more experienced partners. The Technische Universität Berlin (TU Berlin) offered to assist the IC in analyzing the possibilities of cooperation, and a willingness to cooperate emerged, resulting in a plan quickly established for the IC to install two UHF antenna ground stations, one in the UNSAM Miguelete Campus, and the second one in an Argentine scientific station in Antarctica, with the technical support of engineers from TU Berlin. This opened the door for collaboration

with other institutions, particularly the Kyushu Institute of Technology (Kyutech), and its BIRDS program. This paper briefly describes the way the cooperation was implemented, but focuses on the technical challenges that had to be overcome to use the GSs to operate with different missions from different universities, including the details of the issues found and mistakes made in the process and how they were solved, and the peculiarities of installing and operating a GS in Antarctica.

2. BACKGROUND

In this chapter a brief description of the different actors of this collaboration and their experience is included.

2.1 Instituto Colomb

The IC is located in the Miguelete Campus, in San Martín, Buenos Aires Province. It benefits from the contribution from CONAE, which has launched five scientific missions (from 68 to 3000 kilos). CONAE has as part of its facilities and sites, the Teófilo Tabanera Space Center, in Córdoba, where among many other activities, four Master programs on space topics function, in partnership with national universities.

It also benefits from the experience of and interaction with UNSAM´s 19 academic units and more than 17000 students. Giving its initial steps, it focuses on 'lean satellites', aiming at having as much national and international cooperation as possible. To continue in that direction, it will host the 2nd IAA Latin American Symposium on Small Satellites, in Buenos Aires and Bariloche, in November 2019.

2.2 Technische Universität Berlin

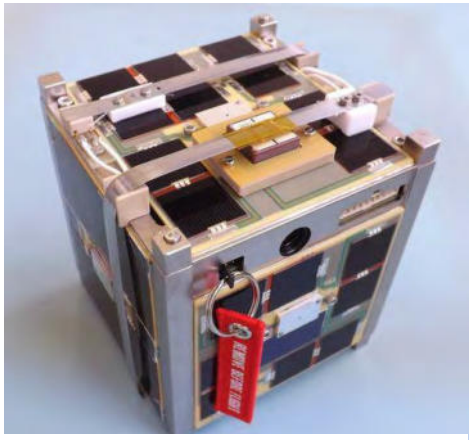

Figure 1: BEESAT-4

TU Berlin has to-date launched 16 satellites into Low-Earth orbit. Nine of these satellites are still operational which poses challenges in the planning of multi-mission operations. Additional ground stations at remote locations are desired to optimize these operations. In particular, the BEESAT CubeSat series can be used to train students and foster international collaboration. The latest of these satellites – BEESAT-4 – has been used to verify that the combined use of multiple ground stations (TU Berlin, Miguelete Station, Antarctica) is advantageous in various aspects. Researchers and students from Berlin and Buenos Aires, being spatially separated by almost 12000 km, coordinated the joint operations of BEESAT-4, planning image downloads, monitoring and, commanding activities.

Figure 2 shows an image of Antarctica taken by BEESAT-4. Although the ground resolution of low-cost cameras is comparatively low, the images are still valuable for researchers from Instituto Antártico Argentino, as discussions in August 2018 have shown. For example, these pictures can help the researchers to identify ice-free ship navigation routes, movement of barrier ice and even migration of animals.

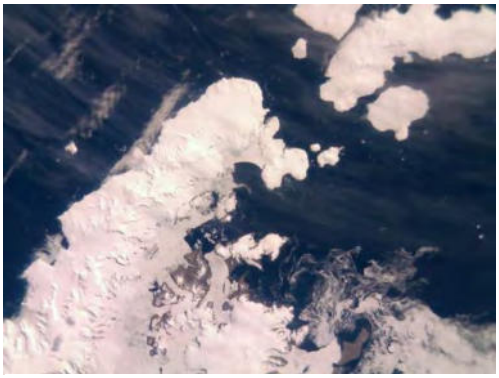

Figure 2: Picture of Antarctic Peninsula, taken by BEESAT-4

2.3 Kyushu Institute of Technology

Kyushu Institute of Technology initiated the BIRDS project in 2015 as an educational program to assist capacity building for emerging space programs in developing countries. The project purpose is to build constellations of 1U CubeSats. Currently, eight satellites of BIRDS-1 and BIRDS-2 are operating. The BIRDS constellation operates using a network of 15 ground stations called the BIRDS GS Network. Figure 3 shows the location of each ground station. In January 2018 and 2019, the BIRDS GS Operation Workshop was held at Kyutech. A representative from each country was invited to share their experience and recommendations for future operations in the workshop. The workshop also provided lectures on satellite communication and training of GS installation.

Figure 3: Members of BIRDS ground station network

2.4 Instituto Antártico Argentino

The Instituto Antártico Argentino is the Argentine state organization that defines, leads, controls, coordinates and, disseminates the Antarctic technological-scientific activity in Argentina.
It is, in many aspects, a pioneer in Antarctic research at the international level. Having a scientific crew from the Institute overwintering is an invaluable asset to periodically check, operate and maintain the GS in San Martín Station.

3. THE INSTITUTIONAL COLLABORATION

After the 10th IAA Small Satellites Symposium in Berlin in 2017, a visit was organized of personnel from the IC to TU Berlin. It included the ground station. From the IC it was suggested to add a GS of the IC in Antarctica to TU Berlin's UHF network. The complication of this particular collaboration is that it initially included four organizations: CONAE, UNSAM, The Argentine Antarctic authority (DNA) and TU Berlin. It was decided to do a scheme of two separate agreements, one between the DNA and CONAE, and one between both universities. To build the trust between all parties, the agreements mention a willingness to collaborate, but no commitment on funds or resources, but opening the

doors for joint work. This implementation, with the spirit of agreements being 'enablers' rather than 'enforcers' for all parties involved, allowed a fast building of trust and practical implementation at a fast pace.
During a visit to Argentina of faculty from Kyutech, the benefit for the IC and for the BIRDS program was established, including the IC's GSs in the BIRDS network.

4. THE MIGUELETE GROUND STATION

Figure 4: UHF Antenna being set up at Miguelete campus

The Miguelete Ground Station (ETM) was the spearhead of this collaboration. It had two parallel, concurrent tasks: 1) to build the ground station and 2) to develop the capabilities (team, infrastructure, resources) to actually operate and maintain it. This was considered a necessary step towards the installation of an Antarctic GS.
The setup and components bought are based on TU Berlin's existing ground stations. The operating band is 70 cm UHF. A 2-week visit of TU Berlin personnel was organized in UNSAM's Miguelete Campus. They led the set-up of the GS and the training of the operators, mostly UNSAM students. A meeting with scientists in a broad array of fields who could also benefit from small satellite technology was also organized, with many potential collaborations emerging.
The "operators" group is composed of students and faculty. The know-how acquired during this setup and early operations phase was condensed in manuals and standard operating procedures that serve both Miguelete and Antarctic GSs.

Figure 5: Operators training session at the Colomb Institute during TUB visit.

During the Miguelete GS setup, several issues arose involving mechanical a mismatch between parts and poor documentation of the building steps. For example, when trying to fit the crossboom trough the rotor, a small screw on the inside was blocking the way and it had to be adjusted. This implied taking the cross-boom aside, opening the rotor, adjusting the screw, closing the rotor and passing the boom. This step was not documented in the manual of the rotor and accordingly took some time to be identified. Had it arose in Antarctica, it would have jeopardized the whole mission. Similar minor mechanical indeterminate cases were identified and solved beforehand on the hardware destined to Antarctica. That includes long bolts that needed to be slightly bent to accommodate mast diameter, careful step by step procedure to assemble the radiating elements, identifying vertically polarized and horizontally polarized radiating elements inputs with phasing harness cable lengths, and relative position of the radiating elements to the cross-boom.
During the operation in the following months, it was found that vertical antenna pointing degraded slightly over time. It is believed that this is due to the fact that the bolts fastening the cross-boom halt it in place only by mechanical pressure but there is no pass-thru mating constraining the rotation of the rotor to the rotation of the cross-boom. This requires

periodical checkups and fixing. To avoid this problem, a pass-through mate was added to the fastening of the cross-boom, fixing vertical pointing to rotor pointing.
Horizontal antenna pointing was found to fail on hard power offs, resetting the azimuth value to a random number on those cases. As mitigation, a UPS system was added and a soft shutdown procedure was included. A horizontal pointing recalibration procedure was also developed and is performed after every hard power off event.
The most difficult problem to solve was an erratic spiking of standing wave ratio (SWR) during some transmissions. After carefully checking each part separately, the culprit was thought to be the power splitter. But after lab checking, it proved to be ok. After spending several turns trying to find the problem, it was noticed that under certain wind conditions a part of the RF wire would go into a position in which it would get pinched by the room's door when fully opened. Changing the way the RF cable is led into the room solved the problem and saved the replacement of a perfectly functional power splitter.
Currently, the Miguelete ground station is regularly used for operations of BEESAT-2 and BEESAT-4. For the TechnoSat mission it sometimes serves backup passes. During passes, housekeeping and image data is downloaded or time-tagged telecommand lists are uploaded to the small satellites.

Kyutech invited a student to the BIRDS GS Operation Workshop in Kyushu during January 2019, and as a result, the adjustment of the GSs to download data from the BIRDS satellites was done, taking place since March. The student who attended the BIRDS Ground Stations Workshop returned to Argentina with the necessary tools (software) and knowledge to expand the activities at the Miguelete GS to BIRDS satellites' operation. The biggest challenge faced regarding this task was that TU Berlin's software was designed for a Linux operation system, while BIRDS' was for Windows.
After trying various options, BIRDS' software could be run in Linux successfully with an emulator that makes programs designed for different operating systems to be compatible. And, what is more, the tracking software provided by TU Berlin could be used for tracking BIRDS's satellites without affecting the operation.
During late February, other minor adjustments were needed to fully adapt BIRDS' operating technology. And finally, in March, ETM was ready to start tracking and downlinking data from BIRDS' Buthan-1, Maya-1, and Uitmsat-1 satellites.
During April, documentation regarding Birds' CubeSats installation and tracking was developed by the operators at Miguelete Ground Station in a plan to implement the same solutions at the Antarctic Ground Station and for other satellites that have software not compatible with TUB's. A similar action was needed for Satellogic's TITA, which carries a testing platform on board t developed at LabOSat-UNSAM.

5. THE SAN MARTÍN GROUND STATION

A plan was established by Instituto Antártico Argentino to send a party of four members to the San Martín Antarctic Station to set up a GS of the IC. Two members of the IC, and two members of TU Berlin, on commission to the IC, participated in the expedition. Both in Argentina and Germany, a prime crew and backups were designated and went through all the medical checkups and other exams requested to participate in an Antarctic campaign. This proved essential in the success, as for different reasons two of the original people designated could not participate, and a diminished crew would most probably not have been able to complete the installation.

Figure 6: San Martin Station, Antarctica

The initial challenge was to set up the GS in Antarctica in the assigned time of only three days (the time required to do the complete San Martin Station change of personnel and download of supplies for the year-around stay of the station's crew). For this reason, procedures were written and practiced on land.

Given the weather conditions on the Drake Passage, the departure from Ushuaia was delayed. This time was used to refine the procedures and practice them inside the ARA Almirante Irizar icebreaker. Once the Station was reached on April 7th, the predicted weather conditions required further reducing the available time to just 20 hours.

Visual inspection of the San Martin Base Laboratory (LASAN) was necessary to determine the best location for the mast from the preselected options based on pictures. which needed to be fixed to the wall. Due to cable lengths and previously installed equipment, feasible locations to fix the mast to the wall were fairly limited. On the inside, a heating duct obstructed the higher end of the wall, so drilling from the inside out was not possible and care had to be taken so as to not damage the duct. Because of the length of the truss, and the fact that the roof stood out, it the initial plan to fit it evenly along the wall was confirmed not possible. As this was considered as a possibility, a couple of wooden pieces (taken for this purpose) were used to install it vertically but separated from the wall. Once the holes were drilled through the wall and the wooden pieces, some extra drilling was needed to correctly align the rods fixing the mast. This became a more challenging task than expected, and the expertise of the departing LASAM crew, of their whole year at the station, proved invaluable.

In the meantime, the antennas were assembled indoors by some of the members, together with the supporting cross-boom, and customized clamps to ensure that the construction would withstand the high wind loads. Additionally, all electronic components like the transceiver, computer and rotator controller were set up in the laboratory. All software components were prepared at UNSAM before shipping and were checked and updated on the ship prior to arriving at San Martin station. Once the mast was up, the rotator with the antennas was moved to the building's rooftop from where they were fixed to the mast. Fortunately, there already was a set of cables passing to the inside through a hole on the wall, such that no new hole was needed for the antenna and rotator cables. A thick hose

was used to guide the cables from the antenna, through the truss and into the box where the hole was, in order to protect them from the harsh weather conditions in winter. Every hole or union was sealed with silicone to keep them free from snow or water.

Figure 7: Antenna installation.

While the rotator and cables were being installed on the roof, three groups of two people each took care of the winds (steel guy cables), which were attached to existing hooking point near LASAN. This required some training on the Almirante Irizar, because of the special wiring pattern needed for the task. This could not have been made in the available time (less than 24 hours), if it was not for the spontaneous voluntary help of other participants in the Antarctic campaign, including members of the Dirección Nacional del Antártico, Instituto Antártico Argentino, students from ITBA and UTN, Ejército Argentino personnel; completely unrelated to the GS setup project; in a show of 'Antarctic camaraderie'. Once all outdoor equipment was set, a calibration phase was needed to make sure the antenna was correctly positioned, which led to some corrections in the outdoor setup. When this was done, the installation was tested during several satellite passes, during which telemetry data was received from the satellites BEESAT-2, BEESAT-4 and TechnoSat into the early hours of April 8th, for the joy of everyone involved in Antarctica and the ones holding their breath in Buenos Aires and Berlin (following on *WhatsApp*).

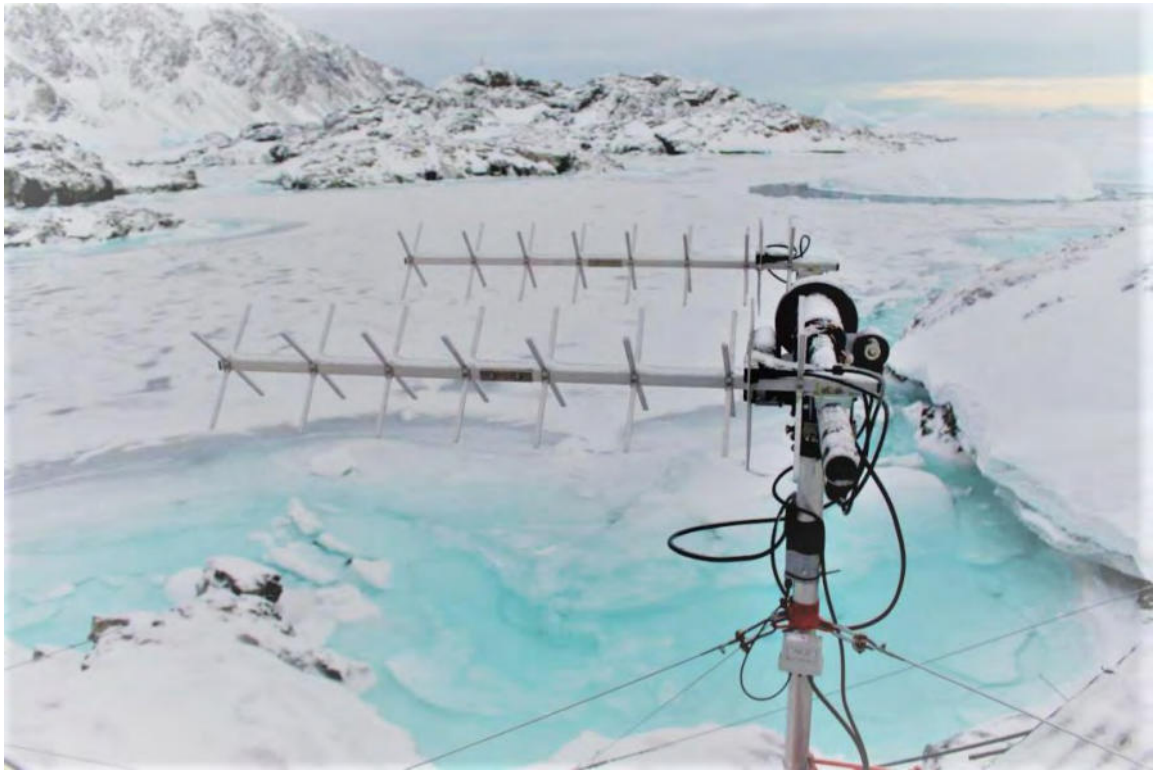

Figure 8: Fully installed antenna in the Antarctic Ground Station (as of June 2019)

6. DATA USE AND APPLICATIONS

During the Summer Antarctic Field Campaign, there were several activities that were aided by the images taken by TechnoSat and BEESAT-4 satellites, including scientific and logistic activities. From the point of view of logistics, as soon as cloud-free scenes from an area of interest were received, they were forwarded to the people involved in it. One of the users was the Almirante Irizar Icebreaker, which added them to their available data to deal with sea ice in its way to the destination.

Monitoring of the large iceberg A68 in the Antarctic Peninsula was also possible during the whole summer. The iceberg is located in the south of Marambio Station and confirming its position and orientation was possible by means of the access to the satellite data.

With all the data recorded and downloaded for the whole season, statistics of area coverage and cloud cover percentage are being carried out to be compared with other available sources of image (i.e. Landsat, Sentinel, MODIS, etc.). After filtering the images, some areas of interest will be chosen, as ice-shelves, icebergs and glaciers with an on-going monitoring program. The analysis of the images recorded during the beginning of March will be very useful because the date of the coverage is not the same as for the other mentioned satellites. This last summer was very cloudy and storms occurred well often, and these images were taken in coincidence with the only few days with a clear sky over the glaciers in the northern part of the Antarctic Peninsula.

7. CONCLUSIONS

Through the connections established by IAA events, setting up two UHF ground stations in Miguelete Campus and Antarctica was a project that allowed the collaboration of several organizations: UNSAM, The Instituto Colomb, TU Berlin, The Instituto Antártico Argentino, CONAE, Kyutech, DNA, and others. This required on one side a particular elaboration of the institutional relationships. On the other many technical and logistical problems that had to be solved. The peculiarities of an Antarctic activity and campaign added some specific challenges, and the exhaustive preparation allowed meeting the objective in spite of unpredicted difficulties. Some of the procedures that were developed in the weeks and months before the campaign had to be changed due to the adapted timetable and also to unforeseen logistical discrepancies to the initial plans. However, due to the thorough planning and the development of several alternative plans for the critical elements, the station could be set up in only 20 hours, marking a new record in installation time for the experienced staff. There are already concrete achievements through these activities, including two operational GSs and the use of data of university satellite missions. The main goal was also achieved, to open the doors for future collaboration, including setting up of other GSs, and joining the needs of scientists with the development of Ad-Hoc payloads, with future university missions already being developed.

Payload Mission Planning and Data Handling for a University Small Satellite Ground Segment

Sebastian Wenzel[1*] **Jonas Keim**[1] **Sabine Klinkner**[1]

[1]Institute of Space Systems (IRS), University of Stuttgart, Stuttgart, Germany

[*]To whom correspondence should be addressed; E-mail: swenzel@irs.uni-stuttgart.de.

Abstract: The small satellite *Flying Laptop*, launched in July 2017, was developed and built by graduate and undergraduate students at the Institute of Space Systems of the University of Stuttgart with support by space industry and research institutions.[*] The mission goals are technology demonstration, earth observation and serving as an educational satellite. At a mass of 110 kg, it features three-axis stabilized attitude control and several payloads, including an AIS receiver, a multi spectral camera system and a wide angle camera. The satellite is fully operated from the Control Center at the University of Stuttgart. To command the satellite's payloads a Python package was developed which is used for operations documentation and mission planning. When all constraints are met and no mission schedule conflict exists, observations are commanded for every opportunity. The payload data coming from the satellite is fragmented and unprocessed and therefore not in the condition to be used scientifically. This paper gives an overview of the data request system, the mission planning, the commanding and verification architecture as well as the handling and provision framework for the received payload data as general idea as well as the implementation for the *Flying Laptop* project.

1 INTRODUCTION

To serve as an educational satellite the *Flying Laptop* was designed to enable payload operations and data handling for Students. To fulfill this goal it is necessary to implement a mission planning system as well as a payload reception and provision chain. The payload mission planning system for an earth observation satellite should provide an easy to use interface to request payload data takes without a deep understanding of the satellite system and its underlying processes. It should result in a dynamic process to optimize satellite utilization and inform about all ongoing tasks related to the request. The historically grown mission planning system and data reception concept for the small satellite program of the University of Stuttgart led to the idea of a more general approach, suitable for different satellite missions, and therefore payloads to process, to ensure the reusability for future purposes.

2 PAYLOAD MISSION PLANNING SYSTEM

To perform payload data takes, several tasks need to be processed, some of these tasks are visible for the user and are related directly to the data take e.g. the calculation of observation times, monitoring tasks and payload data provision. Other underlying tasks may not be visible for the user, these tasks include a seamless integration into the mission planning process and on-board storage handling for the

[*]The launch and operations of the Flying Laptop satellite has been supported by the Federal Ministry for Economic Affairs and Energy of Germany (BMWi) and the Ministry of Science, Research and the Arts of the State of Baden-Württemberg

spacecraft and are mostly related to the commanding part for the satellite system. This separation allows to keep the actual process in handling the payload request streamlined.

2.1 Payload Request Handling

The goal for the payload mission planning system was to develop a system that fully automates the handling of payload request. Requesting data takes with the different payloads should be possible using a simple frontend defining only a bare minimum of necessary parameters. To organize and document the operations for the *Flying Laptop* mission the open-source browser-based ticket tracking system Redmine is used. This system is used as a front-end for the payload mission planning system. For payload data takes a specific ticket and workflow is defined, tracking the status of the data take and requiring the following parameters: the position (latitude, longitude and altitude), lighting condition, the minimum elevation and satellite orientation (nadir, off-nadir, target or inertial). Depending on the used payloads the number of images, integration times and the interval between images can also be defined. A observability calculation is then triggered, resulting in a report indicating all possible observation times and a ground track and field of view (FOV) visualization of the cameras as shown in figure 1.

Data takes can then be requested on a single or repetitive basis, leading to an automated process where a command stack for each possible observation is created and combined to a single stack for an uplink pass shortly before the data take. This process is controlled in the back-end of the mission planning system and performs all necessary steps i.e. on-board memory allocation, conflict check with other satellite activities and payload data dump allocation. After a successful uplink to the satellite the backend process checks the received telemetry after the payload data take for the correct execution e.g. payload telemetry and on-board storage write processes. The received images are checked using the *Front API* described in 3.3 after the planned downlink pass, in case of missing or invalid images a re-dump is scheduled. When all images are received the on-board memory is deallocated. Until now 1027 payload request were handled.

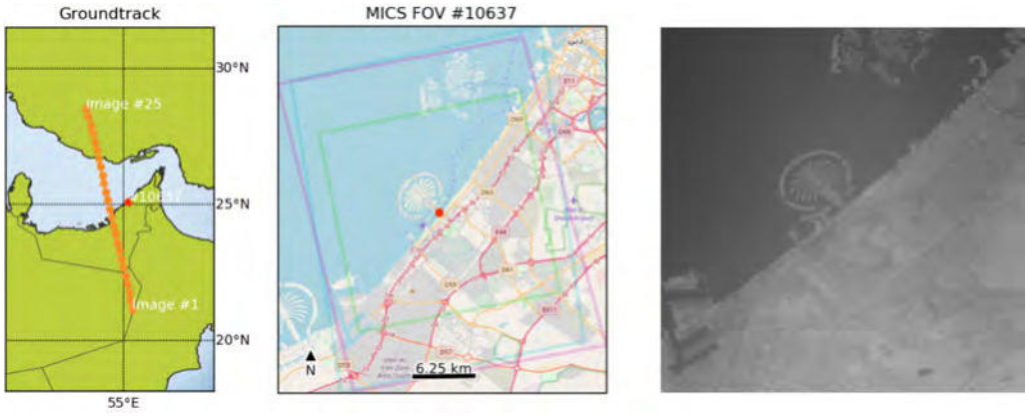

Figure 1: Mission Planning output and corresponding image

2.2 Realization

The back-end of the payload mission planning system is based on a self developed Python package to handle payload requests. The package interacts with Redmine via its REST API and several other Python modules. These modules are dealing with the necessary processes for each state of a payload request. For the observation time calculation and visualization latest available orbit information and a sgp4 propagator and the Matplotlib Basemap Toolkit is used. For the commanding part a self developed module interacting with the satellites Mission Information Base (MIB), for command and parameter definition, is used to create a command stack. For flight dynamics data, on-board payload data storage and the mission schedule, a mySQL database is used. Modules handling requests for uplink and payload data downlink passes, memory allocation and task scheduling were implemented. These modules are also providing a API to access information stored in the database. [5]

3 PAYLOAD DATA HANDLING CONCEPT

Satellite missions often include multiple payloads, creating a variety of data, used by different scientists. That raises the necessity for a versatile handling concept. The university background of the *Flying Laptop* mission resulting in limited resources as well as manpower compared to bigger missions led to the following requirements:

- Automatic

  To ensure a seamless process with a minimum of user interaction, the data handling should be automatic to the largest possible extend. This includes the data input from multiple ground stations.

- Reusable

  The Institute of Space Systems will be operating future satellite missions including different payload types and data formats. This raises the need for a payload handling concept which can be adapted, extended and used again for future missions.

- Multiple Payloads

  A variety of data from different payloads has to be processed and therefore has to be routed through the pipeline.

- Scalable

  To ensure a fast data processing, the handling concept should provide the possibility to grow. This includes a multi mission - multi playoad scalability as well as a concept to execute tasks in parallel.

- Easy deployment

  To simplify updates and a dynamic growth of a running payload handling pipeline, the deployment of the pipeline should be automatized as much as possible.

- ECSS / CCSDS conformity

  The *Flying Laptop* mission is compliant with ECSS (European Cooperation for Space Standardization) and CCSDS (Consultative Committee for Space Data Systems) standards for telemetry and telecommanding [6] as well as for the payload downlink. This should be reflected in the payload data handling.

- Open source

  To improve the code base and support students around the world, the pipeline concept and software implementation of the framework should be open to use. In addition, only free software and software tools should be utilized in the specific *Flying Laptop* mission pipeline.

- Multiple programming languages

  To utilize the great variety of existing libraries, the processing pipeline should not be limited to one programming language. This also enables students with different background to implement tasks.

- Easy monitoring

  The operation of the *Flying Laptop* satellite is done by a team of personnel with multiple areas of focus. With a growing payload handling approach, the amount of error causes is rising. For these reasons, the pipeline should be easy to monitor by people not involved in their implementation.

- Security

  For internal as well as interfaces exposed to the web, there should be security measures to prevent unwanted access. This allows only authorized users to access data or the pipeline itself.

The requirements above led to a handling concept using nodes, described in the following, fulfilling dedicated tasks. For the *Flying Laptop* Mission, the nodes currently implemented are shown in figure 2.

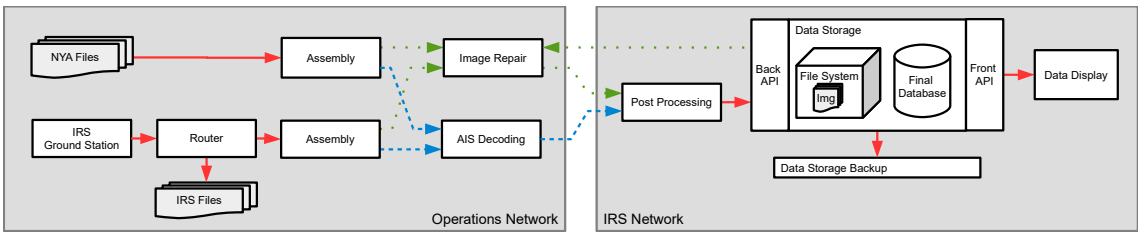

Figure 2: Payload Data Handling for the *Flying Laptop*. Red solid: all payload data flow, green dotted: image data flow, blue dashed: AIS data flow

The described handling pipeline is currently processing the data to a raw format without any calibration. This corresponds to a ESA level 1 product [4]. To simplify the deployment of the data handling chain, a continuous integration approach using the *jenkins* framework is used.

3.1 Nodes for the *Flying Laptop* data handling

Incoming data frames have to be merged into valid payload data. The following section describes the implementation of these steps for the *Flying Laptop* mission and refers to figure 2.

3.1.1 Payload Data Input

The *Flying Laptop* mission utilizes multiple ground stations for its payload data downlink as well as the commanding and telemetry link. To deal with the resulting challenges, the designed ground processing environment should be capable of processing different data input streams which can contain data in multiple processing states.

The handling of multiple input sources is enabled by the flexibility of using nodes as described earlier. The Flying Laptop currently receives its payload data from the Institute of Space Systems (IRS) ground station in Stuttgart, designed for the purpose of the mission, and a ground station located in Ny-Ålesund (NYA) which belongs to the German Research Centre for Geosciences in Potsdam. The data from Ny-Ålesund are received in files which are periodically inserted to the payload handling system in Stuttgart. Data received from the IRS ground station can be directly routed to the processing chain, but are also recorded in files for backup purposes. As displayed in figure 2, multiple payload streams are handled. The red, solid line stands for all payload data, the blue, dashed line is the AIS data flow and the dotted green line represents the image data flow. The separation of the data is done by applying different sink URLs depending on the payload, using the interface concept described in section 3.3.

3.1.2 Data Assembly and Identification

The *Assembly* node extracts payload data from the received frames before sending them to the *Repair* node for image restoration or the *AIS decoding*. It therefore represents the interface between frames according to the CCSDS standard and payload data packets e.g. images with their corresponding meta data. The implementation of this node is done in Java and utilizes mutliple threads to extract, assemble, identify and send the payload data.

3.1.3 Image Repair

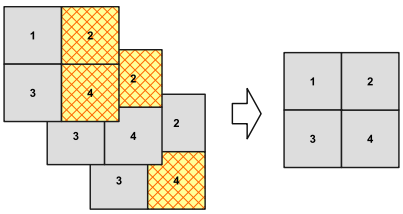

Figure 3: Images with invalid pixels (shaded) are combined to a valid one

Problems with the data reception at the ground station of the IRS as a result of WiFi interference are causing corrupted data frames. The frames can be found but not always reconstructed with the implemented coding [1]. This led to a data repair concept, implemented in Java code, for the images taken by the satellite. Missing frames are tagged and can be extracted in the image as invalid pixel, shown with the shaded squares in figure 3. By sending the data multiple times, the pixel can eventually be corrected.

3.1.4 Post-Processing

The post processing node for the Flying Laptop mission is currently only modifying meta data. This includes the latitude and longitude calculation of the intersection between the camera view axis and an earth ellipsoid as well as the sun- and elevation angle of the recorded data. It also uses the interface described in section 2.2 to get mission planning information to append to the data packet. With a python implementation a Flask app is spawned to process the data with the architecture described in section 3.2.

3.1.5 Payload Database

As database solution a MongoDB was chosen, providing a document based noSQL approach to store data. The document based approach has the advantage that different states of the payload objects can be stored in the same database if needed. It also provides a better horizontal scalability. Nevertheless handling a relatively small amount of data, as described in 3.5, these advantages might not have a great effect for the *Flying Laptop* mission.

3.2 Node Framework

To simplify the creation of new nodes, the implementation architecture for each one follows a similar concept. Behind the receiving interface part of the node, a first in first out (FIFO) buffer is implemented, taking the incoming data. The dedicated data handling for the node is done between this incoming buffer and an outgoing FIFO buffer. The latter takes the data that will then be pushed to the next node.

Since the incoming and outgoing buffers are working in separate threads, it is possible to process the data in between in parallel. With this concept, it is not possible that the actual data processing of a receiving node slows down a sending one until the receiving buffer is full.

3.3 Interface Concept

Several types of interfaces can be found for the payload handling concept of the *Flying Laptop*. In this context *internal* refers to communication inside the processing chain and *external* refers to interaction between a user or administrator and the handling pipeline or an input of files from an external source.

- CCSDS conform input (external),
- Node communication (internal),
- User interfaces for data access (external),
- Database interfaces (internal),
- Monitoring interfaces (internal and external),
- Mission Planning interfaces (internal)

The connection to the IRS ground station as well as the connection from the *Router* to the *Assembly* node, shown in figure 2, is transferring a stream of Telemetry Frames defined using the CCSDS standard. The interfaces of the Ground Station and Router were given as a client-server socket architecture [6].

For the communication between the nodes of the pipeline, an approach was needed capable of handling multiple data input from different sources in parallel. This type of data exchange is widely spread over the internet using a one to many type of architecture. It was therefore decided to implement a web service based architecture, posting data to HTTP server. This enables the possibility to run single nodes, waiting for data to handle, independent from each other.

By using similar interfaces it is possible to spawn and chain the nodes at will, to ensure a flexible payload handling distributed over multiple hardware or software instances. Ultimately this enables the possibility to create distributed computing networks of an arbitrary size.

With the decision of using a MongoDB to store the data, the JavaScript Object Notation JSON [3] and Binary JSON (BSON) [2] was the exchange format of choice for the HTTP posts at the beginning of the *Flying Laptop* mission. This was further maintained since JSON is a common exchange serialization format providing the capability to store all needed data types for the mission.

To push new data to the payload database, it was chosen to use an API based approach. This interface therefore represents another HTTP sink for data as the nodes, described before.

To access the data a browser based front end was designed [6]. It is using the *Front API*, shown in figure 2 to access the payload database.

3.4 Used Hardware

The payload handling pipeline, except the database, is currently running on commodity hardware. This also includes the front end applications. The operation system of choice was Linux to ensure a free of charge implementation. The database is storing the payload data on hard-drives and is running on a dedicated server providing the storage capacity and backup solution. As a test environment for the payload handling, an average commercial computer is used, proving that the current concept is well suited to be executed with a low processing power demand.

3.5 Performance

The DDS transmitter of the satellite sends the data with a speed of 10 Mbit/s [1]. The maximum download time for one pass over the IRS ground station is roughly 11 min. This results in 6600 Mbit or 825 Mbyte of payload data that have to be handled.

3.25 images can be extracted from the stream of payload data per second as a maximum. Compared to the 1.8 images per second transmitted from the satellite, the payload handling pipeline is well suited for the current task.

Until the submission time of this text there were 1854 passes scheduled with payload data downlink over the NYA and IRS ground stations. This results in 16712 unique MICS and 15336 unique PAMCAM images so far. The number of raw, not decoded AIS messages received through the satellites lifetime is 463247.

4 Summary and Outlook

A payload mission planning system was implemented providing an easy to use interface. The handling of payload request is entirely automated and thus means no extra work for the operations team, this allows to carry out a large variety of individual payload data takes.

Many of the requirements stated in section 3 are already met by the implemented handling pipeline. It could be shown that a simple processing network for a small satellite mission can be implemented using different, free of charge software tools, running on commodity hardware. The node concept with standard interfaces provides the needed flexibility and is implemented using multiple programming languages including Java, Python and JavaScript. Nevertheless there are multiple features to be implemented in the future. The security concept is still in an early state, using http with ssl encryption for some nodes by wrapping them into apache servers with a valid certificate. It is also foreseen to use API keys for the node to node communication as an authentication measure. The monitoring is still in an early state and will be expanded in the future to provide an easy overview of the running payload handling network for all users. To provide a higher speed and therefore a better usability of the database through the front end, the data storage concept will be improved. For the current production pipeline the images are saved as binary files along with the meta data. This will be improved after further testing and development of the separated image and meta storage concept shown in figure 2.

A mayor issue with the parallel processing approach is data consistency. It has to be ensured that data processed in one node is not modified in another at the same time. The current data handling pipeline is not implemented parallel for the consistency critical parts.

References

[1] M A Boettcher, B M Butt, and S Klinkner. Low-cost approach for a software-defined radio based ground station receiver for CCSDS standard compliant s-band satellite communications. *IOP Conference Series: Materials Science and Engineering*, 152:012033, oct 2016.

[2] BSON. BSON. `http://bsonspec.org/`, 2019. [Online; accessed 29-April-2019].

[3] ECMA. Standard ECMA-404: The JSON Data Interchange Syntax. `http://www.ecma-international.org/publications/files/ECMA-ST/ECMA-404.pdf`, 2017. [Online; accessed 29-April-2019].

[4] F.Delhaise, A.Ercolani, and J.Zender. Spacecraft and payload data handling. volume SP-1295, page 2, November 2007.

[5] Jonas Keim, Kai Klemich, Nico Bucher, Jonas Burgdorf, Sabine Klinkner, and Jens Eickhoff. *Operational Experience of the Transition from Initial to Nominal Operations of the University Small Satellite Flying Laptop.* 2018.

[6] Kai Klemich, Nico Bucher, Maximilian Böttcher, Johannes Braun, Sebastian Hilpert, Sabine Klinkner, and Jens Eickhoff. *A Ground Segment for Small Satellite Operations in a University Context Combining Professional and Custom Software Tools.*

Automatic Operation System and Design Method with Reliability and Accessibility Design for Precursory Electric Field Observation CubeSat Demonstrator Prelude

Ryo Futamata[1], Masahiko Yamazaki[1], Masashi Kamogawa[2], Fumika Seki[1], Nozomi Fukushima[1]

[1]Nihon University
7-24-1, Narashinodai, Funabashi, Chiba, Japan
Phone: +81 47 469 5430, Mail:
yamazaki.masahiko@g.nihon-u.ac.jp
csri15099@g.nihon-u.ac.jp

[2]Institute of Oceanic Research and Development, Tokai University
3-20-1, Orido, Shimizu, Shizuoka, Japan
Phone: +81 42 329 7484, Mail:
kamogawa@gakegei.ac.jp

We propose a data management method for automatic operation of Precursory Electric Field Observation CubeSat Demonstrator Prelude, and a design method for improving the mission success rate in this paper. In the design method for improving the mission success rate, the accessibility to the state of satellite system is improved and the design method using information obtained from that is performed in three aspects of design, development / verification, and operation as shown below. 1) Evaluation method and redesign method of design to improve the degree of mission achievement, 2) visualization of verification items without omission, 3) the framework for specifying abnormality dealing.

1. INTRODUCTION

1.1 Current Status of CubeSat

In recent years, the launch of CubeSat (1 to 50 kg) has been increasing[1]. One of the factors is the increase in constellation satellites that can be developed at low cost and in a short period of time. Securing of operator and increase in operation costs are inevitable problems with the increase in launch of CubeSat in the future. The mission success rate of CubeSat is low, the mission achievement status of university satellites launched from 2010 to 2017 has reached full success with 15.7% [2]. Practical use of CubeSat requires a framework for the design to efficiently and effectively obtain user-convincing levels of reliability while securing cost merits [3]. It is also important to visualize the condition of the satellite and comprehensively under-stand it by improving the accessibility to the condition inside the satellite in design, development / verification, and operation.

1.2 6U CubeSat Prelude

1.2.1 Prelude Mission Background

Recent studies have repeated pre-seismic ionospheric disturbances are significant. Regarding the decrease of night-time VLF (very low frequency) electromagnetic field's intensity, the result of elucidating earth's electromagnetic environment satellite "DEMETER" showed it is statistical superiority by the 289 cases of M4.8 earthquake of the whole earth as shown Fig.1 for 2.5 years [4]. However, DEMETER didn't specialize in the measurement of electric field intensity and quality and quantity of the data are insufficient, so it has not been possible to identify the mechanism of the generation. Therefore, in this

project, we develop 6U CubeSat like Fig.2 having the VLF sensor capable of acquiring continuous waveform data of electric field intensity in the VLF band before earthquake occurrence in sun synchronous orbit whose altitude about 600km and aim to operate and acquire more detailed pre-seismic ionospheric observation data.

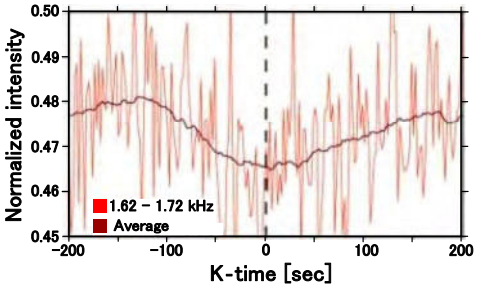

Fig. 1 Pre-Seismic Phenomenon Data of DEMETER

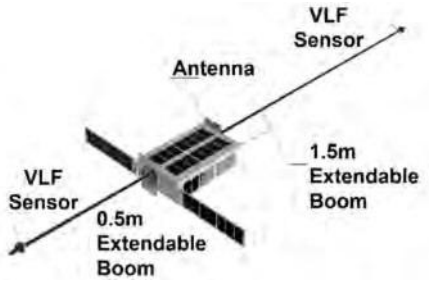

Fig. 2 6U CubeSat Prelude

1.2.2 Prelude Mission Overview

DEMETER observed the VLF electric field intensity with a resolution of 1024 [bit] and 0.5 [Hz] and succeeded in observing the decrease in the average value of the electric field intensity, which is considered to be an earthquake precursor. In order to observe this phenomenon with higher resolution and samples, PRELUDE adds to the continuous observation (Survey mode) with 256 [bit] and 0.5 [Hz], and at an orbit condition that passes near the epicenter, about 13 [kHz] raw waveform data of VLF band frequency (Burst mode). It is estimated that the probability that Prelude passes 500 km from the epicenter and is in the shade occurs once every 3 days when the earthquake of M4.8 or more [5]. We have designing for automatic operation to solve the increase of operation cost, which is the problem of CubeSat in this project. In order to realize the automatic operation and reduce the operation cost, the satellite must not only be designed for the automatic operation but also be reliable enough to fulfill the mission. Therefore, we improve the accessibility to the information of the satellite state and use it to improve the reliability in each of design, development / verification and operation. Especially in operation, we aim to monitor the health of systems suitable for automatic operation.

2. PURPOSE OF THIS STUDY

We propose following two points, to find out management method of science observation data and satellite design with high mission achievement for realization of Prelude's automatic operation. (1) Management method of scientific observation data for automatic operation. (2) System construction method with high reliability and accessibility.

3. DATA MANAGEMENT METHOD FOR AUTOMATIC OPERATION

3.1 Data Management by Drive-Recorder method

Scientific CubeSat such as Prelude need to manage the large data with limited resources. In this mission, it is necessary to keep more than 1.5 GB per day until earthquake occurrence information is uplinked from the ground station. Therefore, we adopted the same method as the drive recorder, which locks the recorded data when an impact of an accident and overwrites everything else. In order to perform this data management, this satellite has two SD cards, temporary storage SD and data management SD, for mission data management. A large amount of data acquired in Burst mode by the drive recorder method is

constantly overwritten on the temporary SD card. When the earthquake occurrence time is received from the ground station, the corresponding data is moved to Data management SD. Such data management makes it possible to minimize the data storage area and prevent data loss when an event occurs.

3.2 Automatic Retransmission of Mission Data

We have designed a management method of mission data based on automatic operation in Prelude. Downlink data of CubeSat occasionally be lost due to noise. Operators need to understand such missing data and send re-downlink commands to the satellite. In order to aim at automatic operation including the missing data, it is necessary to design so that the identification of the missing data can be easily done. Therefore, in order to make it easy to select data to be re-downlinked individually, it is managed using file names and addresses that indicate the location of the data. Such automatic retransmission of mission data is realized by managing the ground and satellites with the same database with file name and data address. The satellite receives the file name and address number of the missing mission data from the ground station as an uplink and re-downlinks only the designated missing data. After that, the satellite downlinks the file containing mission data to be transmitted. Thus, introducing method can easily manage data by file name and address number realize a data management method suitable for automatic operation.

4. SYSTEM CONSTRUCTION METHOD WITH GOOD RELIABILITY AND ACCESSIBILITY

The accessibility to the internal state of the satellite is improved and the information is used so that a system with low maintenance and reliability suitable for automatic operation can be obtained. In this section, we propose a method to improve reliability and accessibility from three viewpoints of design, development / verification and operation. The methods are the following three points. (1) Design evaluation method and design reconstruction method to improve mission achievement, (2) Visualization of verification items for verification without omission, (3) Framework to identify abnormal dealing. We explain about these in this section.

4.1 Design Evaluation and Reconstruction Methods to Improve Mission Achievement

This is to improve the reliability of satellites. The method has three steps. (1) design requirement for improving the mission achievement level is clearly defined, (2) the method which evaluate it quantitatively, (3) system reconfiguration method based on the evaluation results.

4.1.1 Define design requirements

Table1 shows six design requirements and corresponding implementation methods as design requirements for system architecture with high mission achievement rate. The design requirement is that the architecture is required to realize an ideal system at each stage of development, verification and operation.

Table 1 Requirement for design to improve the reliability of mission achievement

No	Requirement	Realization approach
1	Recovering from defects	Software and hardware reset of the system
2	Using another one in place of faulty function	Building a redundant system

3	Reducing the impact of defects	Organizing related functions in one module
4	Testability	Reducing the interface
	(Easily finding the cause of defects happened at the test)	Standardize the interface
		Organizing related functions in one module （Testing only with relevant parts）

4.1.2 Evaluation of Design Requirements

We quantitatively evaluate how well the system architecture meets the design requirements shown in Table1. In this research, we propose an evaluation and reconstruction method of satellite system using matrix in that functions between elements can be expressed more compactly than diagrams, and it is easy to understand the correction points of the architecture. DSM, Design Structure Matrix, is a typical example of the method of presenting the system architecture by a matrix. DSM is a network modeling tool that is used to present the elements that make up a system and their functions. The DSM maps functions between N system elements and is represented as a square N × N matrix. In the method we propose, elements of DSM are components. The rows of the matrix indicate the output destination, and the columns indicate the input source. The circle in the white area of Fig.4 is the input-output between subsystems, in the light blue area is that between subsystem A, and the green area is that between subsystem B. The weighting level of elements incorporating redundancy and reset is set to half, considering that the risk is dispersed and at least one return from failure.

Table 2 Example of Requirement level definition

Level	contents
4	Needed to function as a satellite
3	Needed to achieve minimum success
2	Needed to achieve full success
1	Needed to achieve extra success

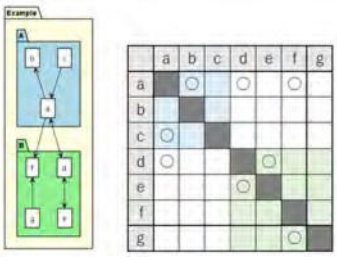

Fig. 3 Example of applying DSM to system architecture – 1

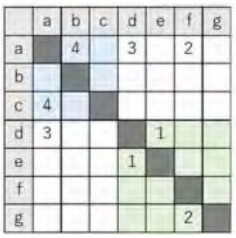

Fig. 4 Example of applying DSM to system architecture - 2

R_{in}, the sum of the requirement levels of elements that do not affect other subsystems, is 12 in the example of Fig.5. R_{de}, the sum of the required levels of the elements affecting the white area, that is, the outside of the subsystem is 8. Also, the index indicating how much each subsystem depends on each other is Dependency D. Dependency D is the number of numbers in the white area on the matrix, and D is 3 in this example. Risk for mission accomplishment is quantitatively evaluated using requirement level and dependency D. The evaluation equation is Eq. (1). Calculated using Eq. (1), the risk in Fig.5 is 36.

$$Risk = R_{in} + R_{de} \times D \quad (1)$$

4.1.3 System reconfiguration method

We consider the configuration to reduce the risk in the mission achievement based on the evaluation results of the system architecture. In order to ensure that changes in each subsystem do not greatly affect the entire system, reduce the inter-subsystem functions and reduce the dependency, and then perform functions with high risk within the subsystem reduce the risk of failing the mission by setting reset and redundancy. There are two ways to reduce the level of "how important is the function for achieving the mission" of each component, reset and redundancy. It is effective to provide redundancy for failures of components that are not space proven or environment-sensitive components, and that reset is effective for failures due to lack of ground design and manufacturing. After the system reconfiguration, the system architecture is evaluated again, and the reconstruction is evaluated by quantitatively judging whether Risk has been reduced.

4.2 Visualization of Verification Items for Verification without Omission

We propose the method in order to perform the verification of CubeSat without omission. It is the functions and systems are hierarchized respectively and extracted, and the relationship between the systems and functions is visualized using a matrix, and the verification items, locations, timing of performing verification.

4.2.1 System verification

According to the INCOSE definition, system verification is "verifying that all elements of the target system have the intended function and fulfill the assigned performance requirements" [6]. Therefore, based on the idea of this INCOSE, this study will clarify verification items and locations by detailed refinement of satellite systems and functions in stages.

4.2.2 Visualization process

It consists of the following four steps. This section shows the outline procedure and purpose, and the details in the next and subsequent sections. Step 1: Hierarchy of target system, Step2: Decomposing the operation mode and functions, Step 3: Visualization of relationships by matrix, Step 4: Creation of matrix in each hierarchy.

4.2.3 Step1 Hierarchy of target system

In order to verify the system in stages, the hierarchy of the system is defined and decomposed to decide the timing of the verification. If it is a simple product, there are few functions for that product, so it is relatively easy to understand the system or component that supports the function. However, CubeSat fulfill the functions required as satellites by interlinking elements such as multiple components. Therefore, by defining the hierarchy of the target system (system level) as shown in Table 3, the verification to be done at each development stage is clarified to prevent omission and leakage of the verification.

Table 3 Structure of Satellite Model

System Level	*Definition*	*Example of satellite*
Level 1	Target System	Satellite
Level 2	Main Component	Subsystem
Level 3	Component	MPU, Sensor

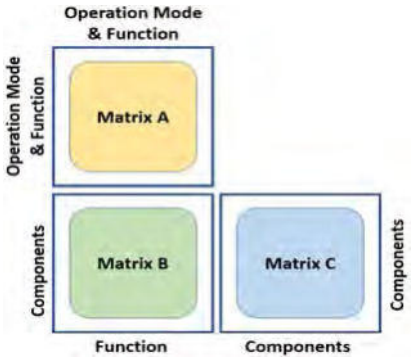

Fig. 5 Multidomain Matrix Model

4.2.4 Step2 Decomposing the operation mode and functions

The functions required for the system are identified based on the hierarchy of Step1. At the Level 1 system level, the operation mode is identified. In addition, the minimum functions required to operate satellites will be identified from system requirements and requirements of the rocket side. At Level 2, consider the sequence in the operation mode defined in Level 1 and find out the functions at the subsystem level. Furthermore, at level 3, we will find out more detailed component level functions. As functions are assumed to be used repeatedly in various modes, the function is developed while organizing using a matrix. In this way, we will clarify the relationship between functions with different verification timings.

4.2.5 Step 3: Visualization of relationships by matrix

The relationship between model and function is visualized by multi-domain matrix (MDM) as shown in Fig.6 [7]. MDM is a matrix of two or more elements. In this paper, we express relationships using three matrices of function-function, function-component and component-component. Since the elements of the system and their interactions can be expressed on a matrix, the order of verification can be clarified by rearranging elements such as functions and components, and the influence on other functions can also be seen. The detailed structure and view of each matrix are shown below.

Matrix A shows input-output relationship among functions. Focusing on the row of the matrix, you can see the output destination. Thus, if the function does not operate due to a failure, you can understand which functions may be affected. Focusing on the column of the matrix, you can see input source. Thus, if the function does not operate, it makes it easy to detect failure factors in the function level. In addition, you can clarify the optimal verification order by rearranging matrix A.

Matrix B shows relationship among functions and components. The row of matrix B shows functions related the component. Focusing on the row of the matrix, you can know verification items for each components and range of influence if the component does not operate. On the other hand, the columns of matrix B shows components in order to realize the function. Focusing on the column of the matrix, if the function does not operate, it makes it easy to detect failure factors in the component level.

Matrix C shows input-output relationship among components. Focusing on the row of the matrix, you can see the output destination. Thus, if the component does not operate due

to a failure, you can understand which components may be affected. Focusing on the column of the matrix, you can see input source. Thus, if the component does not operate, it makes it easy to detect failure factors in the component level.

4.2.6 Step 4: Creation of matrix in each hierarchy

Based on the systems and functions of each hierarchy identified in Step 1 and Step 2, a matrix of Step 3 is created in each hierarchy.

4.3 The Proposal of the Framework to Identify Abnormal dealing method

Health monitoring of CubeSat launched in the past was limit check function by simple modeling and health check by visual confirmation of data. However, classification of abnormal patterns, pursuit of causes, and construction of a standard mechanism for optimum handling corresponding to each pattern are not sufficient. In addition, it is very important to clarify how to decide dealing abnormality, reducing the burden on the operator in automatic operation. In this paper, we propose a framework to connect the method of dealing with the cause of the anomaly and the result of satellite dealing. Within that framework, we focus on determining the abnormal mode without omission and propose it as Mixed fault analysis. The complex failure analysis method is a combination of dynamic (targeted control that interacts between components) and static (targeted components) analysis. We also explain the method of deciding the top event of the fault without omission and aim to fully search fault modes.

4.3.1 The Framework to Identify Abnormal dealing method

We propose the framework shown in Fig.6 as a framework that enables anomaly detection and coping with anomalies. In this framework, there is a data-driven anomaly detection phase by machine learning for telemetry data groups, and a phase that identifies possible anomaly modes in satellites by using mixed fault analysis methods. Then, compare the feature (abnormal value, telemetry pattern) of the abnormal telemetry data group obtained as a result of these two phases with the feature (abnormal value, telemetry pattern) of the failure mode obtained by complex failure analysis. By finding something similar in their characteristics, we clarify to the operator the abnormal mode and the corrective measures that are occurring in the satellite. In addition, in this framework, complex fault analysis and telemetry design can be implemented during satellite development to provide feedback to hardware and software design, enabling design that is easy to detect and deal anomalies.

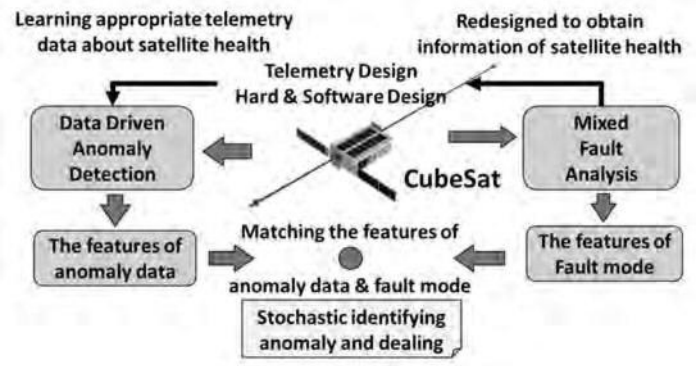

Fig. 6 Framework for dealing abnormality

4.3.2 Proposal of Mixed Fault Analysis

In the conventional failure analysis, the method was not clear about the top event to be analyzed. So, in this research, we propose comprehensive functional analysis and a method using the results as pretreatment for static and dynamic failure analysis FMEA and STPA. Fig.7 is the whole picture. The key to achieving fault analysis with coverage in this framework is the interaction control model as shown Fig.8 that is the target of failure analysis. This targets the Main-Main function consisting of several single functions, based on the result of functional analysis, and consists of components, interrelationship (data, operation, instruction, control), control relation, control action, range It reflects the input from the outside. According to this interaction control model diagram, failure analysis of STPA and FMEA is performed to comprehensively identify failure modes. dispersed and at least one return from failure.

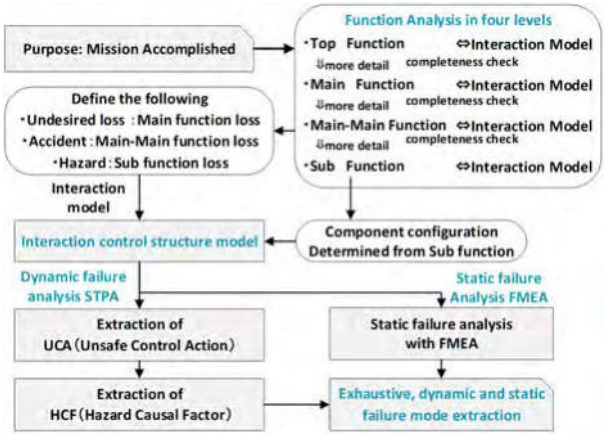

Fig. 7 The Framework of Mixed Fault Analysis

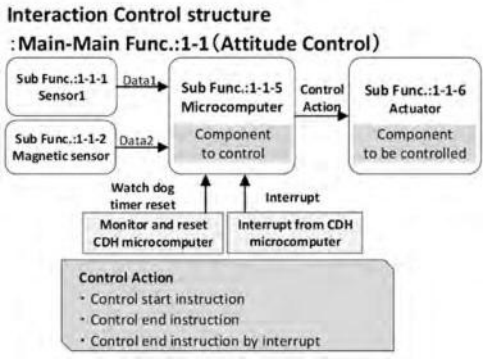

Fig. 8 Interaction Control structure

5. EXAMINATION AND CONCLUSION

The accessibility to the internal state of the system has been improved by expressing the satellite system with a matrix and using fault analysis. By utilizing the internal information obtained there, we have been able to propose a method for maintaining reliability from the design stage / verification to the automated operation, with a view to automatic operation. We also explained how to manage data for automatic operation. In the future, it is necessary to advance and evaluate the implementation of the method proposed.

6. REFERENCES

[1] Space Works: 2019 Nano/Micro Satellite Market Forecast 9th Edition, At. https://www.spaceworks.aero/nano-microsatellite-forecast-9th-edition-2019/, 2019
[2] Michael Swartwout, Reliving 24 Years in the Next 12 Minutes: A Statistical and Personal History of University-Class Satellites, 2018
[3] Hironori, S. and Yasuo, A.: A Quantitative Evaluation for a System with Design Complexity and Its Application to Microsatellites, JSASS No64 2016.6 p145
[4] M.Kamogawa : EOS Preseismic lithosphere-atmosphere-ionosphere coupling, 2006
[5] F.Nemec et al., Geophys. Res. Lett : Spacecraft observations of electromagnetic perturbations connected with seismic activity, 2008
[6] INCOSE : Systems Engineering Handbook , INCOSE-TP-2003-002-03.1 , August 2007
[7] S.D.E.a.T.R.Browning : Design Structure Matrix Methods and Applications, Massachusetts Institute of Technology, 2012, P234.

Automated Operations of BEESAT-9: A CubeSat with a Fluid-Dynamic Actuator and GPS receiver

Sascha Kapitola[1], Sebastian Grau[1], Sascha Weiß[1]

[1]Technische Universität Berlin
Marchstr. 12, 10587 Berlin, Germany
Phone: +49 30 314 79464, Mail: sascha.kapitola@tu-berlin.de

Abstract: BEESAT-9 is a single unit CubeSat currently built by Technische Universität Berlin (TUB) as a successor mission of BEESAT-4, to be launched in the second quarter of 2019. The CubeSat is equipped with a modern GNSS receiver suitable for very small satellite applications. A novel picosatellite fluid-dynamic actuator is mounted in parallel to the satellite's x axis for technology demonstration. This will be the first liquid metal attitude actuator on a CubeSat. A combination of an orthogonal set of reaction wheels with a liquid metal actuator enables operational scenarios for novel Earth observation applications, like e.g. highly agile stereo-imagery from a single spacecraft. Together with the camera system, BEESAT-9 offers all the capabilities to demonstrate those kind of operational scenarios. This work presents a concept of highly automated operations for the BEESAT-9 mission for which the overall objective is to increase utilization of the satellite and its scientific payloads while reducing the workload on ground station staff. To remain applicable for future and other small satellite missions, general components will be introduced, which allow specialization for specific missions.

1 INTRODUCTION

Berlin Experimental and Educational Satellite 9 (BEESAT-9) is a 1U Cubesat currently built by the Chair of Space Technology at TUB. The primary mission objective is to demonstrate precise in-orbit position determination and orbit propagation with a new global navigation satellite system (GNSS) receiver suitable for applications on very small satellites. As a secondary payload, a novel fluid dynamic actuator will be flown as a technology demonstration. Following the much larger fluid-dynamic actuator on TUB's TechnoSat mission [1] [2], this will be the first liquid metal attitude actuator on a single unit CubeSat. Dynamic characteristics of liquid metal actuators are fundamentally different from reaction wheels. Therefore, a combination of an orthogonal set of reaction wheels with a liquid metal actuator enables operational scenarios for novel Earth observation applications.
The satellite and its scientific payloads will be operated by TUB, like its predecessors. During former BEESAT missions, it was observed that regular operations, even of such small spacecrafts, require a lot of attention and manual intervention by the team. It is expected that the number of conducted experiments and therefore the scientific outcome of technology demonstration missions can be increased by reducing or even eliminating the bottleneck of manual intervention.
This paper describes a concept for automated operations, using the BEESAT-9 mission as an example. Therefore, mission specific modes of operations are presented and used to derive tasks which are suitable for automation. Finally, a concept is presented to integrate new building blocks for automated operations in the existing ground segment of TUB.

2 SYSTEM OVERVIEW

BEESAT-9 is a 1U CubeSat and is based on the highly redundant satellite bus already flown in the BEESAT-1, -2 and -4 missions. Being a direct descendant of the BEESAT-4 mis-

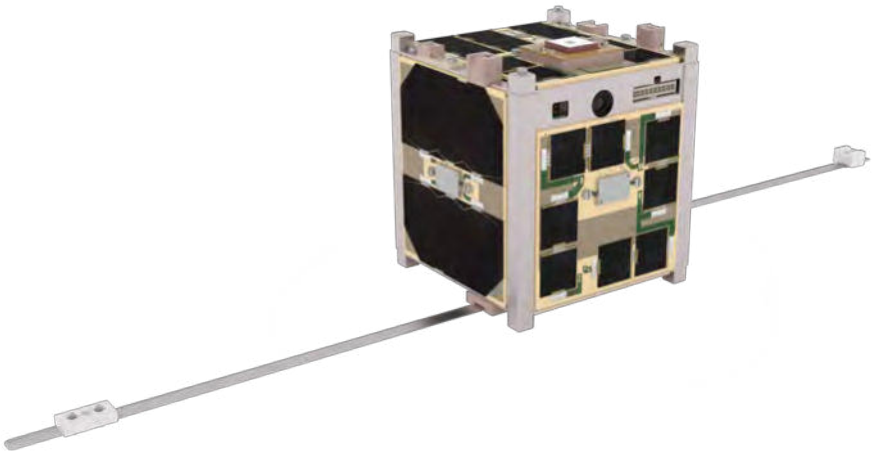

Figure 1: 3D rendering of BEESAT-9 by TUB/Marc Lehmann

sion, the spacecraft features identical subsystems [3]. In order to demonstrate precise in-orbit determination, the satellite is equipped with a different GNSS receiver that is accommodated on a revised payload data handling (PDH) board compared to its predecessor. The HT-GNSS200 from Hyperion Technologies offers faster position acquisition on a smaller footprint and power consumption than the Phoenix receiver on the BEESAT-4 mission [4], [5].

As a secondary payload, BEESAT-9 hosts a picosatellite fluid-dynamic actuator (pFDA) for in-orbit demonstration of this novel type of attitude control actuators on a CubeSat mission. The white pFDA channel can be seen on top of the stack in Figure 2. It is placed directly under the GNSS antenna which is located on top of the structure shown in Figure 1. The

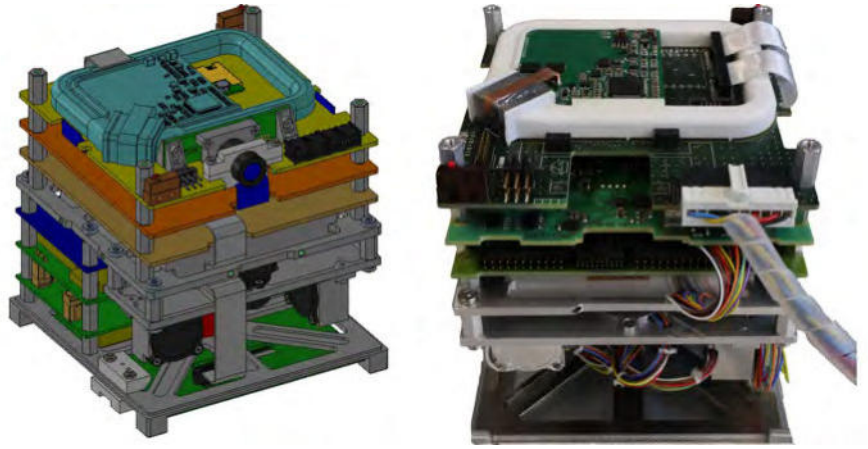

Figure 2: CAD drawing and qualification model of BEESAT-9

dynamic properties of the actuator are investigated in orbit, which is expected to create more than 1000 µN m of torque and has an expected angular momentum capacity of 100 µN m s, resulting in actuator saturation in under 4 s.

Together with the three orthogonal reaction wheels and the magnetic coils, the pFDA offers unique and novel modes of operation for image acquisition. Together with the operation

modes enabled by the GNSS receiver, these are presented in the following chapter.

3 MODES OF OPERATION

This sections gives a brief overview of different modes of operation during the BEESAT-9 mission. To plan and execute those modes, steps in the process of operations shall be identified which are suitable to automate. Those modes reflect the primary and secondary mission objectives.

3.1 GNSS Receiver

The implemented GNSS receiver supports fast position acquisition with a time to first fix (TTF) of less than 90 seconds [4]. Additionally, a power down mode is supported to save energy and enable fast re-acquisition of the position. The modes of operation for the GNSS receiver aim at determining the orbit of BEESAT-9, decreasing the level of manual intervention with each mode. Furthermore, acquired images or other events shall be tagged with position information. The following list enumerates the different modes of operation of the GNSS receiver:

1. Ground Based Orbit Determination: The process of determining orbit parameters is executed on ground, ideally as soon as packets with position data were received from the satellite. The steps of increasing the level of automation are:
    a) Manual execution of position acquisition and evaluation of recorded data with approaches like the one presented in [6].
    b) Automated planning of position acquisitions with manual data evaluation. The process of automated planning includes the generation of timelines and time tagged commands for all subsystems needed in the mission scenario e.g. Attitude Control System (ACS) and PDH.
    c) Automated planning of position acquisitions with automated data evaluation. The processing steps shall be executable in a framework that supports easy automation.
2. On-Board Orbit Determination
    a) Position data is processed on-board to generate orbital elements [7], acquisition and processing procedures are commanded from the ground
    b) Satellite is in a mode to automatically acquire position data and process it

3.2 Fluid-Dynamic Actuator

The unique combination of three orthogonal reaction wheels, a single pFDA, and six magnetic coils enables a great variety of actuator combinations. Therefore, it is the goal of testing different configurations of the available attitude control actuators:

1. Reaction Wheel Backup Configuration: The reaction wheel mounted in x direction is taken out off the control loop and replaced by the pFDA. Challenges here would be the fundamentally different dynamic characteristics of the two types of actuators, that need to be controlled by the same control law.

2. Over-Actuated Configuration: All three reaction wheels are combined with the pFDA in this configuration. Overactuation of the attitude actuators is then achieved along the body-fixed x axis. Challenges here would be the distribution of torque and angular momentum between the fluid-dynamic actuator and the reaction wheel on the x axis.
3. Full Actuator Configuration: Up to ten actuators (up to three reaction wheels, one pFDA, six magnetic coils) are combined in this configuration. Challenges are the parallel operation of the agile attitude control actuators together with the magnetic coils to perform e.g. permanent angular momentum desaturation.

The following list gives an overview of possible attitude control modes and operation scenarios that are enabled by the pFDA.

1. Fast Off-Nadir Image Acquisition: The pFDA is used to perform fast off-nadir reorientation of the spacecraft to point to different targets that are parallel to the ground track.
2. Synthetic increase of Swath-Width: Use the pFDA to synthetically increase the width of the camera swath by pointing the camera in a repeated pattern off-nadir.
3. Fast Stereo Imagery of Multiple Targets: The pFDA is used to perform fast along-track reorientation of the spacecraft to point to a sequence of targets, where each target is then observed twice from different view angles.

4 AUTOMATED OPERATIONS

4.1 Requirements

Requirements for operating BEESAT-9 were deduced from its intended modes of operation presented in section 3. The following list enumerates required top-level functions of the ground segment to enable automated operations:

1. Planning of mission scenarios to prepare GNSS data acquisitions and pFDA operations, which includes
   a) Submitting planning requests as input for a mission planning system
   b) Scheduling algorithms and resource modeling
   c) Generate timelines and sequences of telecommands to be uploaded
2. Automated operations of satellite passes which is to:
   a) Execute procedures, especially those for uploading commands, during a pass
   b) Download data from on-board memories
3. Execution of data processing steps for different mission scenarios / payloads
   a) Processing steps shall be implemented in a way that they can be initiated automatically on reception of specific data packets

4.2 Concept

The general concept for supporting automated operations in the future is based on a Service Oriented Architecture (SOA) as proposed in [8]. SOA has the advantage of loose coupling of

different building blocks in contrast to a monolithic architecture where the whole functionality is included in one application. SOA allows for easy integration of new features in an environment of multiple services. Each service in the system shall have reduced responsibility to support easy maintenance, make it easier to reuse and to support small clean interfaces. At the moment of writing, a microservice architecture as described in [9] is planned to be used as a specific variant of SOA. There are missions which are using that kind of approach successfully [10] [11].
An overview of general services is given in Figure 3 and presents a layered approach. The organization into layers is informal and is used to group services into logical domains for mission operations.

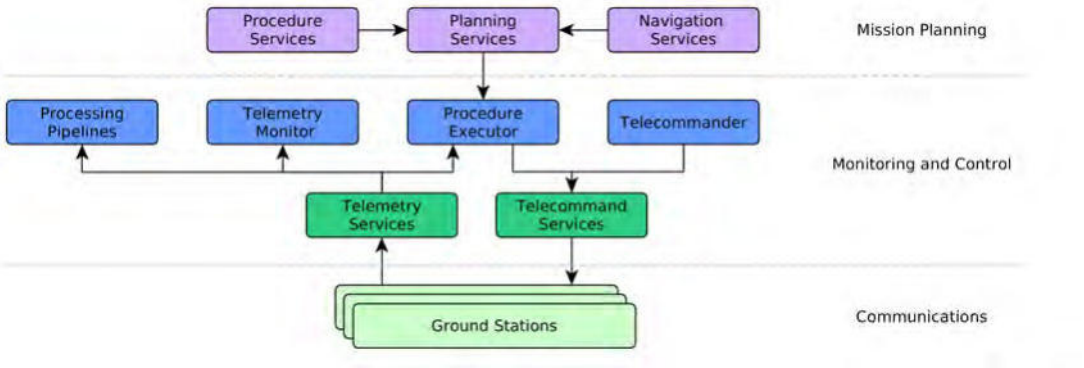

Figure 3: General services in the ground segment

The *Telemetry Service* provides information about packet structures as well as data packets to upper level services in the mission control center. Whereas the *Telecommand Service* provides the same for the uplink. Those services are the endpoints for upper level monitoring and control services to ground stations. *Telemetry Monitor* and *Telecommander* are existing building blocks for manual operations. Services for mission planning, navigation, orbit propagation etc. are found on the upper layer to prepare timelines and mission plans which are to be executed on the spacecraft. Planning services are fed with planning requests as the input and generate timelines as sequence of procedures as the output. The *Procedure Executor* is responsible for controlling the spacecraft in realtime during a pass. Although most mission scenarios are executed via time-tagged commands, a small portion of procedures e.g. upload of time-tagged command lists need to be executed during a pass over a ground station. Processing of payload or housekeeping data is accomplished in processing pipelines. Different pipelines shall be established in a unified framework to process different types of data. The execution of a processing pipeline shall be triggered on reception of data packets to automatically provide higher level data products.

5 CONCLUSION

The BEESAT-9 CubeSat is a technology demonstration mission which will carry a GNSS receiver and a novel picosatellite fluid dynamic actuator (pFDA) into orbit. Based on experiences from former missions at TUB, operations of the satellite shall be automated as much as possible. This is to increase utilization of the satellite while reducing manual workload for the operations engineers on the ground. The paper presented mission scenarios to be executed

as modes of operations for the payloads. Especially, the level of automation for operating the GNSS receiver shall be increased step by step while gaining experience of the device in orbit. A block scheme of the ground segment illustrated how new building blocks will be integrated into the mission control center. In general, a service oriented architecture (SOA) was proposed to isolate functionalities into single blocks with well defined interfaces. As a more precise variant of SOA, microservies are planned to be used for the implementation of such an architecture. It allows for decoupling of autonomous building blocks (services) with well defined interfaces and heterogeneous technologies to be used [9]. The chosen architecture does not only favor a flexible way of isolating responsibilities but also provides opportunities to integrate new functionalities at a later point in time without changing existing parts of the system. This is very important for the BEESAT-9 mission, since the operations phase is approaching soon and the methods and concepts presented in this paper will be introduced when the satellite is already in orbit.

6 ACKNOWLEDGMENTS

The BEESAT-9 satellite is funded by the German Aerospace Center (DLR) within the BEESAT-4 project under the identification number FKZ 50 RM 1229. Furthermore, we would like to thank EXOLAUNCH for providing the opportunity to launch BEESAT-9.

REFERENCES

[1] D. Noack et al. “FDA in space – First in-orbit results of a fluid dynamic attitude control system”. In: *Small Satellites Systems and Services Symposium*. 2018.

[2] M. F. Barschke et al. “Initial orbit results from the TUBiX20 platform”. In: *69th International Astronautical Congress*. 2018.

[3] S. Kapitola, S. Weiß, and K. Brieß. “Flight Experience and Operations with the CubeSat BEESAT-4”. In: *11th IAA Symposium on Small Satellites for Earth Observation*. Berlin, Apr. 2017.

[4] Hyperion Technologies. *GNSS200*. `https://hyperiontechnologies.nl/products/gnss200/`. 2019 (accessed May 2, 2019).

[5] Deutsches Zentrum für Luft- und Raumfahrt e.V. *Phoenix - Spaceborne GPS Receiver*. `https://www.dlr.de/rb/Portaldata/38/Resources/dokumente/GSOC_dokumente/RB-RFT/Phoenix_DataSheet_v11.pdf/`. 2019 (accessed May 2, 2019).

[6] M. Greene and R. Zee. “Increasing the Accuracy of Orbital Position Information from NORAD SGP4 Using Intermittent GPS Readings”. In: *23rd Conference on Small Satellites*. Jan. 2009.

[7] S. T. Goh and K. Low. “Real-time estimation of satellite’s two-line elements via positioning data”. In: *2018 IEEE Aerospace Conference*. Mar. 2018, pp. 1–7. DOI: `10.1109/AERO.2018.8396414`.

[8] T. Erl. *Service oriented architecture : concepts, technology, and design*. eng. 6. print. 2006. ISBN: 0131858580.

[9] S. Newman. *Building Microservices*. 1st. O'Reilly Media, Inc., 2015. ISBN: 1491950358, 9781491950357.

[10] A. Lill et al. "Agile Mission Operations in the CubeSat Project MOVE-II". In: *2018 SpaceOps Conference*. DOI: 10.2514/6.2018-2635. eprint: https://arc.aiaa.org/doi/pdf/10.2514/6.2018-2635.

[11] M. Sordi, D. Heulet, and F. Liège. "Experiment feedback on a microservices architecture". In: *2018 SpaceOps Conference*. DOI: 10.2514/6.2018-2335. eprint: https://arc.aiaa.org/doi/pdf/10.2514/6.2018-2335.

Urban greenspace, public health, and environment margin: Improved management of the greenness in making comfortable living environment in the context of climate change

Kim-Anh Nguyen[1,2] and Yuei-An Liou[1*]

[1]Center for Space and Remote Sensing Research, National Central University,

Address: No. 300, Jhongda Rd., Jhongli District, Taoyuan City 32001, Taiwan, R.O.C. Phone: + 886 3 4227151 #57631

[2]Institute of Geography, Vietnam Academy of Science and Technology,

Address: No. 18 Hoang Quoc Viet Rd., Cau Giay, Hanoi, Vietnam.

Abstract: We introduce a WebGIS platform that aims to improve urban greenspace management by using all documented activities and facilities connected to maintenance of trees and urban green areas. The WebGIS platform works for multimedia-devices to support local authorities to take appropriate and effective measures for greenspace management, and to promote active involvement of citizens. To demonstrate the benefits of the platform, Daan Park of Taipei is chosen as a testbed. Multi-sensor satellite images were utilized to derive urban greenspace characteristics and a field campaign by using a mobile Lidar was conducted to acquire the information about the park's greenspace and objects, such as stock of trees, street and playground furniture, lawn areas, pavements, hedges etc., which are subsequently documented into programs. Then, management, maintenance and care of all things of interest in the park, such as furniture, lawn mowing, pruning trees, fertilization, pest control, etc. can be programmed and implemented. Progress in implementing the WebGIS platform for the Daan Park is reported. A new component of assessing green space's ecosystem service function into the platform is also proposed.

Keywords: Urban Greenspace; multi-sensor satellite images; Lidar; citizen science; ecosystem service; WebGIS

1. INTRODUCTION

More than half of the world's population live in the urban areas. In Europe, approximately 75% of the people live in urban areas (World Bank, 2013). In Asia, urban population increases from 19.2% to 49.6% in the timeframe 1955-2018 and it is predicted that urban population will reach 63% in 2050 (Worldometers). **Figure 1** shows Taipei City and its population density, and weather extreme events. Urban greenspace (UGS) such as parks, forests, community gardens, and green roofs is a vital component of any urban area. It plays an important role in urban heat mitigation, reducing pollution, and providing critical ecosystem services (Nguyen *et al*. 2018). It also serves social events, physical activities, and psychological well-beings. In the meantime, it plays a major role in enhancing urban eco-environment and model life quality for urban citizens. Thus, urban planners, designers, and ecologists must improve UGS strategies not only to maintain its greenness, but also to enhance its multifunctional eco-services. Remote sensing and GIS are powerful tools in measuring multifunctional UGS. In particular, GIS spatially assists in UGS management for display, visualization and interaction with users. Satellite images are utilized to derive the area, density, height, structure, species, canopy cover and greenness of the UGS. At city scale, obtaining pure green space pixels from medium or coarse-resolution remote sensing images is challenging. In contrast, various satellites and small satellites data with higher spatial resolution promise a great potential in achieving precise information of the environmental information at urban scale (Nguyen *et al*. 2016, 2018; Liou *et al*. 2017, 2018).

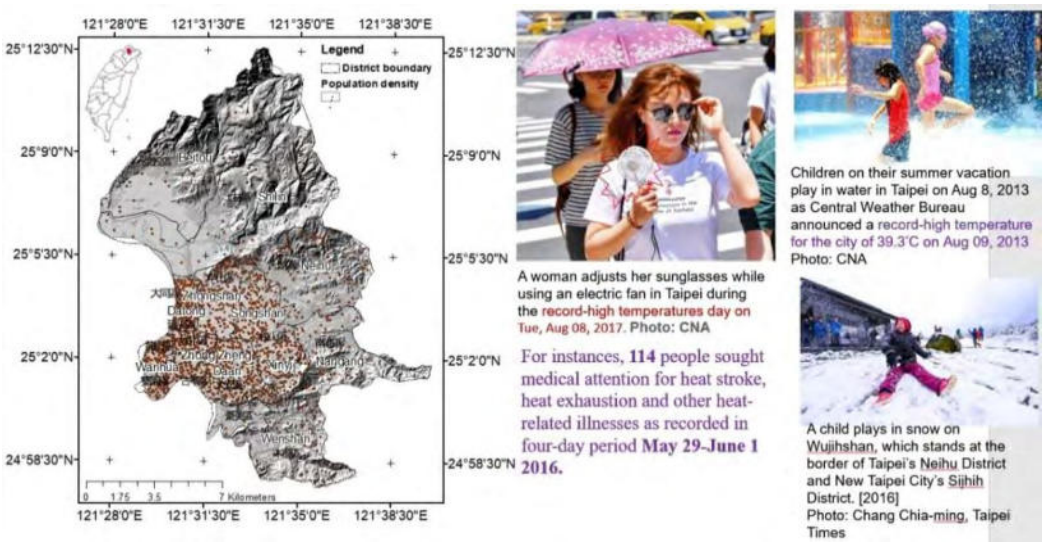

Fig. 1. Taipei City and its population density, and weather extreme events.

2. METHOD AND MATERIALS

Firstly, multi-sensor satellite images (Formosat-5, Spot 7, Landsat 8, and Sentinel 2A and 2B) are used to derive urban greenspaces characteristics at different scales (park, street, and urban areas) in Taipei City. Secondly, GIS techniques are used to analyze the urban greenspaces features and build the GIS database for urban greenspaces as described in **Figure 2**.

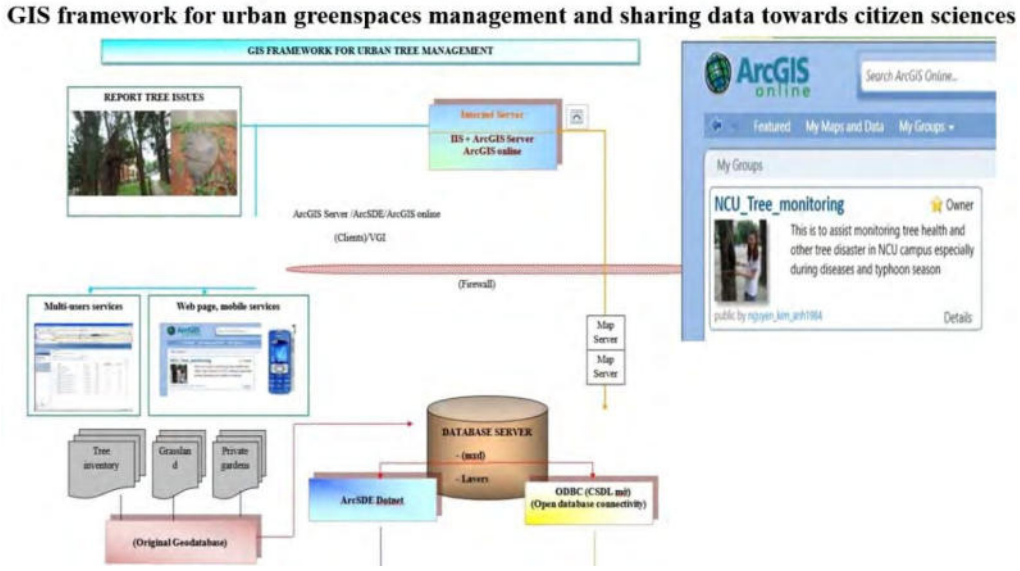

Fig.2. GIS framework for urban greenspaces management and data sharing towards citizen sciences.

3. RESULTS AND DISCUSSION

Urban greenspaces of urban Taipei City are extracted and the areas where equal 1ha or over are selected for further analysis. The cooling effects can be seen from **Figure 3** and **Table 1**. Statistical results show that an urban greenspace within 300 meters has a significant effect on cooling temperature with mean Land Surface Temperature (LST) as 23 ºC. However, there is no significant difference in the cooling effect for the ranges of 300–500 and 500-1000 meters, which exhibit mean

LSTs of 24.2 ºC and 24.4 ºC, respectively.

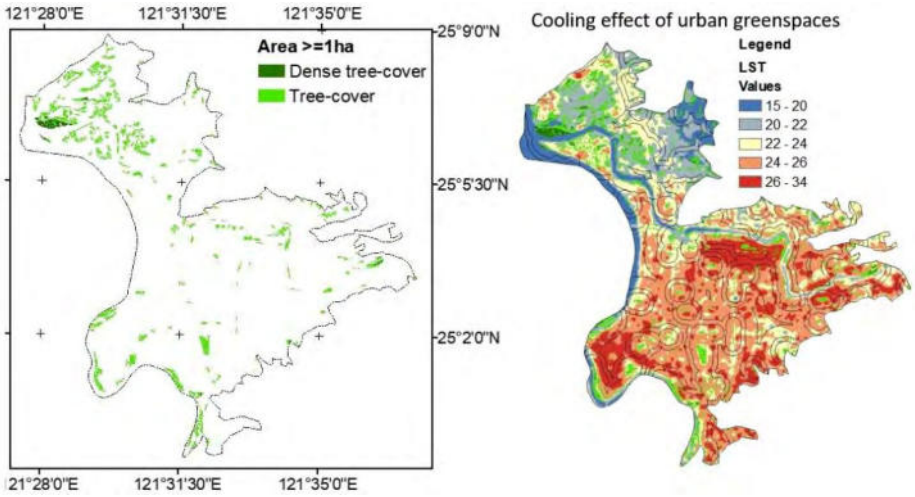

Fig. 3. Urban greenspaces derived from Sentinel 2 data and its cooling effect.

Table 1. Cooling effect of urban greenspaces.

Proximity to UGS (m)	Number of pixels	Area (sq. m)	Mean LST	STD
< 300	61792	55612800	23.0	2.4
300 - 500	26459	23813100	24.2	2.4
500 - 1000	31403	28262700	24.4	2.1

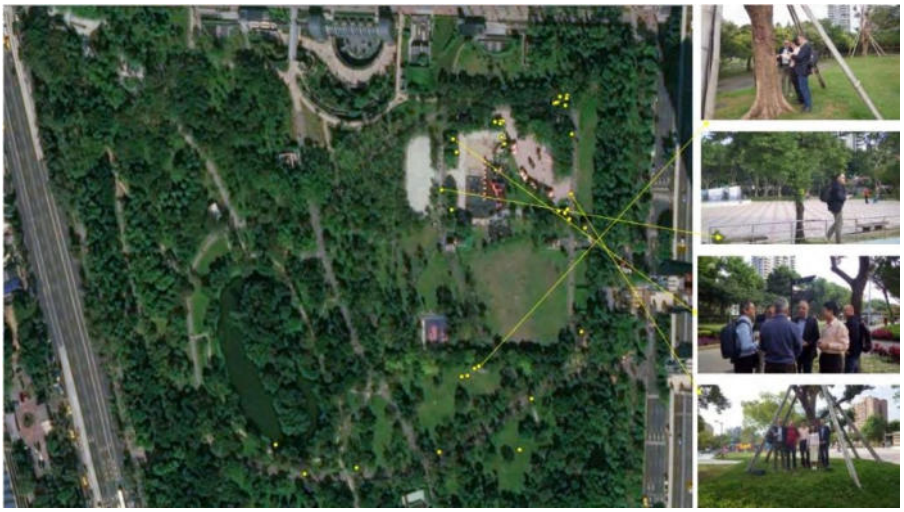

Fig. 4. Daan Forest Park and field survey photos.

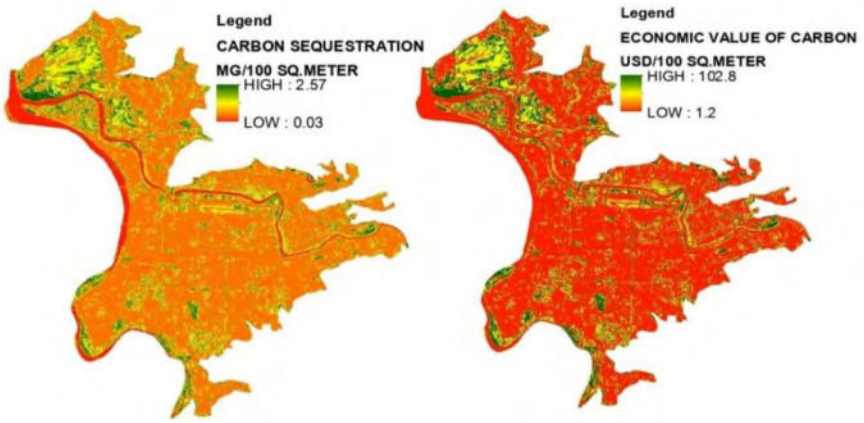

Fig. 5. Carbon storage and economic value of urban greenspaces.

Figure 4 shows Daan Forest Park and field survey photos. **Figure 5** gives preliminary estimates of carbon storage and economic value of urban greenspaces. It indicates that high values of carbon storage and economic highly correspond to greenspace as expected.

4. CONCLUSION

This study contributes to further applications of multi-sensor satellite images in urban greenspaces planning and management, and advancing urban greenspaces science to address environment and its association with public health concerns. It is clear that better management in urban greenspaces with well-developed tree-canopy plays a vital role in making city more livable and better adapted to the weather extremes. In addition, urban greenspaces and its proximity combined with other environmental indicators can be used to derive patterns of heat stress risk, which provide valuable inputs for designing climate change adaption strategies as well as emergency response for risk reduction especially during summer in specific regions of concern. Also, a newly developed remote sensing index, Normalized Difference Latent Heat Index (NDLI) (Liou el al., 2018), which has been demonstrated sensitive to surface water availability may be used to assess the value of greenspaces on reducing heat stress in the future studies.

5. REFERENCES

[1] World bank. 2013.

[2] Worldometers.

[3] Nguyen, T.H., Liou, Y.A., Nguyen, K.A., Sharma, R.C., Tran, D.P., Liou, C-L, Dao, D.C. Assessing the effects of land-use types on surface urban heat island for developing a comfortable living Hanoi City. *Remote Sensing*, 10(12), 1965; doi.org/10.3390/rs10121965.

[4] Liou, Y.A., Nguyen, K.A and Li., M.H., 2017. Assessing spatiotemporal eco-environmental vulnerability by Landsat data*, Ecological Indicators*. Volume 80, September 2017, Pages 52–65. doi.org/10.1016/j.ecolind.2017.04.055.

[5] Nguyen, K.A, Liou, Y.A., Li, M.H. and Tran, T.A. 2016. Zoning eco-environmental vulnerability for environmental management and protection*. Ecological Indicators*, Vol 69, Pages 100–117.

[6] Liou, Y.-A., Le, M.S. and Chien, H. 2018. Normalized difference latent heat index for remote sensing of land surface energy fluxes, *IEEE Transactions on Geoscience and Remote Sensing*, doi: 10.1109/TGRS.2018.2866555.

ACKNOWLEDGMENT

We appreciate the financial support of Taiwan's Ministry of Science and Technology under project codes 105-2221-E-008-056-MY3, 107-2111-M-008-036 and 107-2622-E-008-006-CC3.

OPS-SAT – opening a satellite to the internet

Dominik Marszk[1], José Luís Feiteirinha[2], Benjamin Fischer[3], Daniela Taubert[4], Thorsten Graber[5], André Lofaldli[3], Mehran Sarkarati[3], David Evans[3], Mario Merri[3]

[1] IMS Space Consultancy GmbH
Robert-Bosch-Str. 5, 64293 Darmstadt, Germany
Mail: dominik.marszk@esa.int

[2] Serco GmbH
Robert-Bosch-Str. 5, 64293 Darmstadt, Germany
Mail: jose.luis.feiteirinha@esa.int

[3] European Space Operations Centre
Robert-Bosch-Str. 5, 64293 Darmstadt, Germany
Mail: name.lastname@esa.int

[4] LSE Space GmbH
Robert-Bosch-Str. 5, 64293 Darmstadt, Germany
Mail: daniela.taubert@esa.int

[5] Solenix Deutschland GmbH
Robert-Bosch-Str. 5, 64293 Darmstadt, Germany
Mail: thorsten.graber@esa.int

Abstract: OPS-SAT is a flying hardware and software laboratory in a form of a triple unit CubeSat currently being built by the European Space Agency and scheduled to launch in Q4 2019.
To this date, over 100 entities from 18 countries have registered proposals to fly an experiment on OPS-SAT. To accommodate the needs of all these entities, ESOC offers the experimenters a multitude of access mechanisms to both the ground and space systems of the mission.
In this paper we discuss the safety and security challenges, trade-offs, and lessons learned involved in exposing the ESA ground and space systems over internet to a wider community in an unprecedented scope for the space agency. Finally, we present the OPS-SAT's space and ground segment, focusing on the uniqueness required to reach the presented challenges.

1. INTRODUCTION

1.1. Mission goal

OPS-SAT is a flying hardware and software laboratory in a form of a triple unit CubeSat currently being built by the European Space Agency and scheduled to launch in Q4 2019. The mission's primary goal is to break the "has never flown, therefore it will never fly" cycle. This prevents many ideas from ever reaching the real world environment, as they are deemed too risky, or too expensive to implement and test. In order to achieve this it was necessary to design secure space and ground segments immune to both purposeful and accidental damage. To minimize such risk, we have enclosed all mission subsystems in robust safety mechanisms, allowing the users from around the world to use the satellite for an in-orbit experimentation without risk for the satellite. [1]

1.2. Main mission features

To increase the spectrum of possible applications, the mission includes multiple subsystems representative of a typical spacecraft, plus some novel ones. These subsystems consist of a programmable Satellite Experimental Processing Platform (SEPP – based on a dual core ARM CPU + FPGA), Attitude Determination and Control System (ADCS), GNSS receiver, HD camera, UHF software-defined radio receiver, optical receiver, S-band radio transceiver, X-band transmitter. [1] [2]

To date, over 100 entities from 18 countries have registered experiment proposals to fly on OPS-SAT. These include space agencies, multi-national corporations, universities, and one-man shows. To accommodate such a group of people with very diverse backgrounds, resources, and domains of interest, ESOC offers the experimenters multiple access mechanisms, from remote experiment execution with basic real-time telemetry and telecommanding link forwarding, to higher-level application interfaces such as file uplink and downlink, space-to-ground data mirroring, lightweight web-based monitoring and control system and a user-friendly on-board API wrapping the lower level interfaces.

Furthermore, to ease the process of testing and validation required to qualify the experiment for uplink, we provide scheduled access slots to the satellite's engineering model. Experimenters can also use those access slots to test software, simulate their operations and get acquainted with the operational setting.

2. MISSION DATA SYSTEM INTERFACES

OPS-SAT's requirement from the mission data system is to facilitate a large variety of experiments, wanting to utilize and access the satellite through different links and different layers of the communication stack. In order to meet that requirement, we have developed a set of solutions meant to readily fit the majority of our users.

2.1. Space segment data system

Developing, testing, deploying, and operating the spacecraft On-Board Software (OBSW) is a difficult task due to the extra requirements derived from the uniqueness of the environment and the hardware design, as well as desired reliability. We aim to minimize any extra, repeatable effort spent by the OPS-SAT users in that area. We are going to achieve that through providing the experimenter community with a comprehensive, fully functional reference firmware and software stack running on the SEPP, consisting of:

- reference Altera Cyclone V SoC design,
- baseline configuration and FPGA IP cores handling all of the SEPP interfaces like CAN, I2C, SPI, SpaceWire, radio transceivers bypass,
- embedded Linux system image,
- protocol bridge applications allowing access the CCSDS-compliant data streams on CAN and SpaceWire buses through a TCP socket,
- set of userspace libraries, implementing drivers for all of the payloads connected to the SEPP,
- Nanosat MO Framework (NMF) – a set of Java libraries implementing CCSDS MO Services standards in a form of abstract software components, enabling the users to quickly build experiments as portable applications, already including a simple, service-oriented Monitoring & Control interface; the apps are also executable in a desktop simulation environment. [3][4]

2.2. Ground segment data system

The OPS-SAT ground segment was developed with two major drivers in mind. One was to reuse and innovate as much as possible of the ESA Mission Control System (MICO-

NYS [5]) baseline – a software suite shared not only by ESA missions but also by other major European space industry actors – making it not only the first real-life use of this software for a CubeSat mission, but also the first use of this software together with a space system using CCSDS MO Services instead of ECSS Packet Utilization Standard, also making OPS-SAT mission an early adopter of the latest MICONYS features like CCSDS File Delivery Protocol (CFDP) implementation. Another driver was to meet the already discussed unique requirements of the mission. Keeping that in mind allowed us to create a hybrid ground data system consisting of:

- a fully representative operational network, with the same MCS core (SCOS-2000) as every other ESA mission uses to the day, including bleeding edge features, like CCSDS File Delivery Protocol (CFDP) or support for CCSDS MO Services.
- a set of applications first time demonstrated in OPS-SAT, like Data Proxy, allowing to dynamically switch between different Ground-Space interfaces, NMF Ground MO Proxy, serving as a protocol-bridge and a ground data archive for NMF experiments, or Lightweight MCS, serving as a GUI for the experiment applications developed on top of the NMF.

A high level diagram of the ground and space systems with focus on the experimenter interfaces was demonstrated on the Figure 1. A diagram going into more details of the system was demonstrated on the Figure 2.

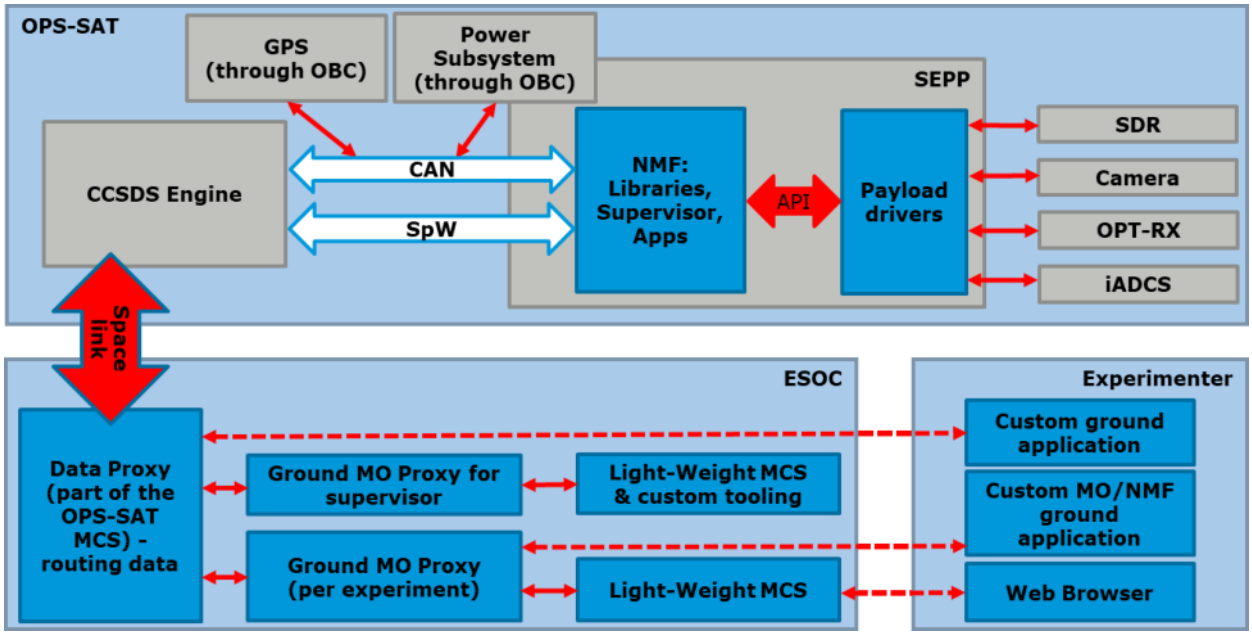

Figure 1 – High level OPS-SAT system diagram from the experimenter perspective

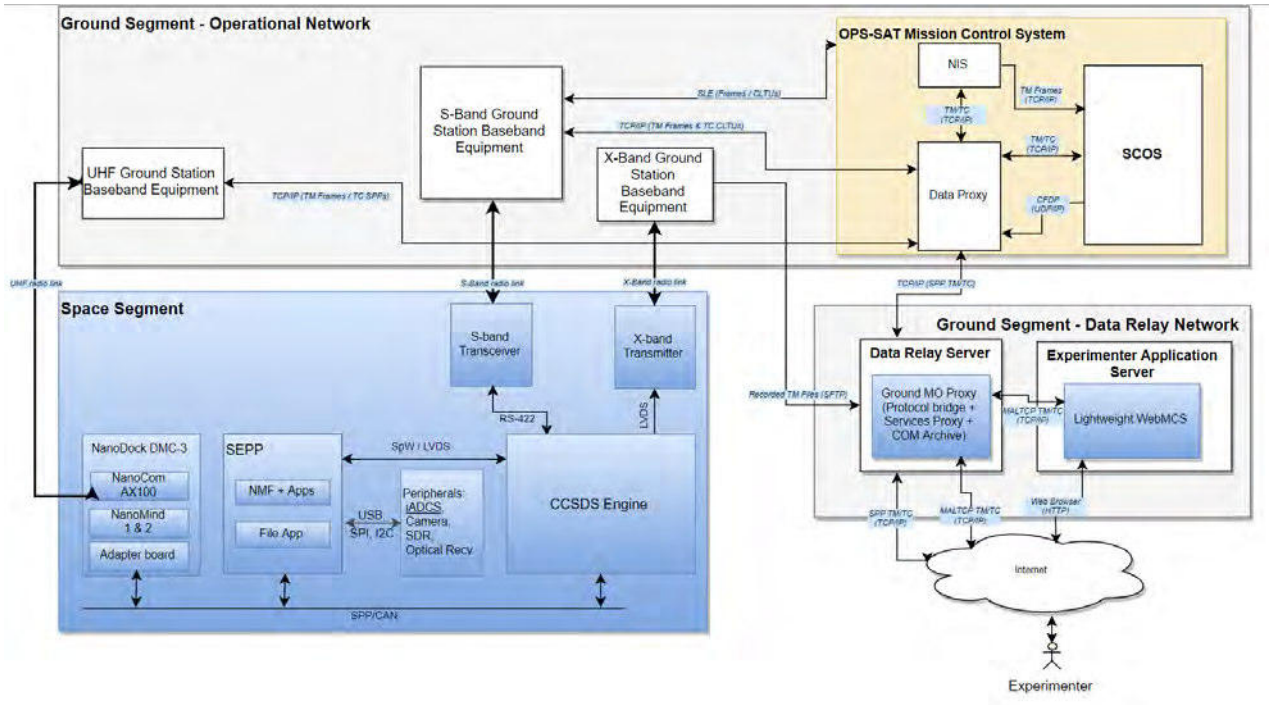

Figure 2 – OPS-SAT data system diagram with focus on the interfaces

3. SECURITY AND SAFETY ASPECTS OF THE MISSION DATA SYSTEMS

3.1. Domain separation and risk assessment

In order to compartmentalise the risk assessment and allow it to be addressed at different levels, the mission subsystems were grouped into a few domains: Data Relay network, Development and Validation Chain network, Operations network, Spacecraft Experimental Payload Platform, and Spacecraft bus, as displayed on the Figure 3.

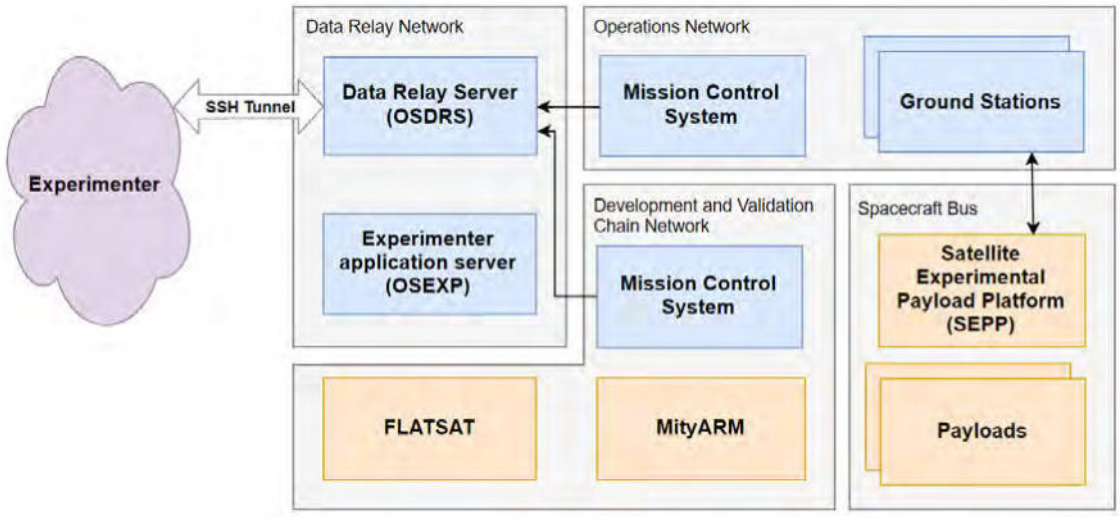

Figure 3 – OPS-SAT security domains separation

Threat and impact in each domain were rudimentarily assessed and given a numeric level, on a scale from 0 to 5 as two main risk factors. The definitions are assumed to be the following:

- **Threat level** is a potential estimated number of events involving external actors trying to access and use the system in a manner they should not. Whether it may be because of a malicious intent, or a lack of proper knowledge.
- **Impact level** is a potential level of damage that can be done from within a particular domain.
- **Risk level** is a measure of the extent to which an entity is threatened by a potential circumstance or an event, calculated as a sum of threat and impact level, resulting with a number on a scale from 0 to 10. [6]

Domain	Threat (T)	Impact (I)	Risk (T+I)
Data Relay network	5	2	7
Development & Validation Chain network	3	3	6
Operational network	0	5	5
SEPP	2	2	4
Spacecraft hardware bus	1	4	5

Table 1 – Risk assessment for different mission domains

3.2. Security and safety measures implemented in the given domains

This subsection outlines the general system design measures taken in order to minimize the security and safety risks for the mission.

All systems have detailed access logging enabled by default, both for user and administrator accounts. Furthermore, a daily backup is performed to data centres distributed over different parts of the agency. This is critical for live monitoring of the system and any eventual post-failure analysis and recovery.

3.2.1. Data Relay network

The data relay network has been assessed to be at the highest risk, as it is the part of the system accessible from the internet. Potential impact on the whole system is rather low, as the Data Relay Server (DRS) is still well separated from the rest of the mission network. Risk mitigation measures include:

- Firewalled access to the DRS with a whitelist of the IP addresses which can access the server.
- Externally audited network configuration.
- Regular reviews of the active accounts on the server.
- Enforcing strong passwords or public-key authentication accessing the server.
- chroot isolation of the users.
- Restriction of binaries executable by the experimenters.

3.2.2. Development and Validation Chain network

The network containing the OPS-SAT Development and Validation chain has been determined to be at a moderately high risk, as the current design will allow automatically scheduled and executed remote access time slots for the registered experimenters. Po-

tential impact is average, as the satellite's engineering model could be damaged by an improperly designed or malicious experiment. Risk mitigation measures include:

- Manual pre-screening of the experimenters and the experiment designs before granting them an access and execution rights on the validation chain.
- Distinguishing between different types of experiments, requiring different access levels to the system.
- Monitoring of the validation chain by an external hardware. The monitoring hardware could shut down the experiment in case of an abnormal behaviour, possibly restricting the execution rights to the user until a manual review by a mission engineer.

3.2.3. Operational network

The risk to the operational network is moderate. Although the threat has been determined to be very low (as the network is well isolated and invisible to the external actors), the potential impact to the mission could be very high as any external actor accessing the Mission Control System could control and damage the spacecraft using easily understandable interfaces. Risk mitigation measures include:

- Complete separation of the mission operational LAN from any other networks and missions operated by ESA.
- Password protected access to all operational machines and to the Mission Control System software.
- Disallowing any incoming connection to the operational network by design. Any kind of data transfer, including relaying of the experimenter data, has to be initiated from the inside.

3.2.4. Satellite Experimental Payload Platform (SEPP)

The risk to the SEPP is rather low, as the typical experiment will have restricted execution rights within the system. Safety measures include:

- Mandatory successful execution of the experiment in the development and validation chain prior to granting an authorization for executing the experiment in space.
- Isolation of the experiments through restricting access to the hardware interfaces of the SEPP by using mechanisms provided by the Linux Kernel and additional modules like *SELinux* or *iptables owner*. [7]
- Requirement to package the experiments on ESA side (by an automated system).
- Wrapping the payload devices drivers into an API enabling remote calls, allowing a complete separation of many experiments from the hardware interfaces.

3.2.5. Spacecraft hardware bus

The risk in the domain of the spacecraft bus is moderate. The potential threat has been determined to be low. The potential impact is high, as having a sufficient level of knowledge, a malicious user could control or damage the spacecraft hardware. Additionally, an improper software implementation could also cause a loss of the control over the satellite and a damage to the hardware. Risk mitigation measures include:

- Providing a well-tested set of drivers implementing the satellite payload interfaces.

- Granting a privileged user access to the SEPP (and therefore the satellite bus) on a basis of an exception requiring a proper justification.
- Reviewing the privileged experiments with an extra scrutiny.
- Requirement to perform project build and packaging on ESA side.
- Automatic cyclic resets of the satellite hardware.

4. CONCLUSION

The OPS-SAT project is a mission posing a multitude of unique challenges not yet tackled in such depth by any previous ESA project. One of the principles guiding the design decisions of various safety and security mechanisms of the innermost systems of the mission is Hanlon's Razor – a user having an access to a particular mission subsystem is much more likely to cause a damage without intending it, than to have evil intentions. The concrete experience derived from the ground and space system design, implementation, and operations is going to provide a foundations for any future project posed with a similar set of challenges. Such projects are expected to become more common now, as the space industry is experiencing the next stage of commercialization and integration with other industries, technologies, and on-line services.

5. REFERENCES

[1] D. Evans and A. Lange, OPS-SAT: Operational Concept for ESA'S First Mission Dedicated to Operational Technology, SpaceOps 2016 conference

[2] OPS-SAT – eoPortal Satellite Missions Directory: https://directory.eoportal.org/web/eoportal/satellite-missions/o/ops-sat (accessed January 2019)

[3] C. Coelho, O. Koudelka, M. Merri, NanoSat MO framework: When OBSW turns into apps, 2017 IEEE Aerospace Conference (2017)

[4] C. Coelho, A Software Framework for Nanosatellites based on CCSDS Mission Operations Services with Reference Implementation for ESA's OPS-SAT Mission (2017)

[5] ESA, MICONYS software suite: https://www.esa.int/Our_Activities/Operations/gse/MICONYS (accessed April 2019)

[6] National Institute of Standards and Technology, Guide for Conducting Risk Assessments, NIST Special Publication 800-30 Revision 1, 15-16 (2012)

[7] Stephen Smalley, Configuring the SELinux Policy, National Security Agency (2005)

The UN COPUOS space sustainability guidelines in the context of small satellites

Peter Martinez[1,2]

[1]Secure World Foundation
525 Zang St, Suite D, Broomfield, Colorado 80021, United States
Phone: +1 303 554 1560, Mail: pmartinez@swfound.org

[2]SpaceLab, University of Cape Town
Dept Elec Eng, Rondebosch 7700, South Africa

Abstract: Small satellites have revolutionized the space arena and lowered the barriers to entry for many aspiring space actors. This has led to a phenomenal growth in the number of small satellites in orbit. This trend, together with the growing space debris population has given rise to concerns about the long-term sustainability of outer space activities. In 2010, the United Nations Committee on the Peaceful Uses of Outer Space (UN COPUOS) established the Working Group on the Long-Term Sustainability (LTS) of Outer Space Activities. The Working Group was tasked with producing a set of voluntary, non-binding guidelines for all space actors to help ensure the long-term sustainable use of outer space. The Working Group's mandate ended in June 2018. During its mandate, the UN COPUOS member States agreed on twenty-one guidelines and a context-setting preambular text. These voluntary, non-binding guidelines are applicable to all space actors and all phases of the mission life cycle. This paper describes the LTS guidelines, with emphasis on their applicability to small-satellite developers and operators.

1. INTRODUCTION

Small satellites are becoming increasingly more capable and are finding application in areas that were previously the domain of much larger satellites. Their low costs and relatively short development times, largely fueled by the growing availability of commercial off-the-shelf components, are bringing space activities within reach of many academic institutions and small companies. This has led to a proliferation of small satellites and a growing number and diversity of space actors. By some estimates, the coming years will see thousands of new small satellites placed in orbit. This rapid and huge increase in the number of space objects poses a concern for the long-term sustainability of space activities, especially since many small satellites are short-lived and some may potentially even be too small to be trackable.

In an effort to promote international norms of behavior in outer space activities, the United Nations Committee on the Peaceful Uses of Outer Space (UN COPUOS) has been working on a series of guidelines for the long-term sustainability of outer space activities. In June 2018, the first phase of this process came to an end, with twenty-one guidelines, which were agreed by consensus of 87 COPUOS member States. The agreed guidelines comprise a collection of internationally recognized measures for ensuring the sustainability of space activities and enhancing the safety of space operations.

The guidelines address the policy, regulatory, safety, international cooperation and capacity-building aspects of space activities. These guidelines are voluntary and non-binding, although many States may choose to incorporate elements of the guidelines in their national regulatory frameworks for outer space activities, as has been the case with the COPUOS space debris mitigation guidelines. In this paper, we discuss the guidelines in the context of the small-satellite community. Apart from supporting the implementation of the guidelines through compliance, small satellites may also support research and development of ways to support the sustainable exploration and use of outer space, thereby contributing to enhancing the implementation practice of the guidelines.

Given that these are guidelines for the long-term sustainability of outer space activities, it is instructive to define what is meant by this term. Such a definition is contained on the COPUOS document containing these 21 consensus guidelines:

> *The long-term sustainability of outer space activities is defined as the ability to maintain the conduct of space activities indefinitely into the future in a manner that realizes the objectives of equitable access to the benefits of the exploration and use of outer space for peaceful purposes, in order to meet the needs of the present generations while preserving the outer space environment for future generations.*

2. THE GUIDELINES

The twenty-one agreed guidelines [1] comprise a collection of internationally recognized measures for ensuring the long-term sustainability of outer space activities and for enhancing the safety of space operations. They address the policy, regulatory, operational, safety, scientific, technical, international cooperation and capacity-building aspects of space activities. They are based on a substantial body of knowledge, as well as the experiences of States, international intergovernmental organizations and relevant national and international non-governmental entities. Therefore, the guidelines are relevant to both governmental and non-governmental entities. They are also relevant to all space activities, whether planned or ongoing, as practicable, and to all phases of a space mission, including launch, operation and end-of-life disposal.

The purpose of the guidelines is to assist States and international intergovernmental organizations, both individually and collectively, to mitigate the risks associated with the conduct of outer space activities so that present benefits can be sustained, and future opportunities realized. Consequently, the implementation of the guidelines should promote international cooperation in the peaceful use and exploration of outer space.

These twenty-one agreed guidelines represent the low-hanging fruit of the LTS discussions, but they also mark a significant step forward in that they represent the tangible progress that has been made in COPUOS in addressing space sustainability. The first set of agreed guidelines creates a foundation for further consensus building in COPUOS.

The guidelines are intended to support the development of national and international practices and safety frameworks for conducting outer space activities while allowing for flexibility in adapting such practices and frameworks to specific national circumstances. They are also intended to support States and international intergovernmental organiza-

tions in developing their space capabilities in a manner that avoids causing harm to the outer space environment and the safety of space operations.

The guidelines are voluntary and not legally binding under international law. The existing United Nations treaties and principles on outer space provide the fundamental legal framework for these guidelines. However, despite their non-binding status under international law, the guidelines can have a legal character in the sense that States may choose to incorporate elements of the guidelines in their national legislation, as has been the case with the UN COPUOS space debris mitigation guidelines.

3. RELEVANCE OF THE LTS GUIDELINES TO THE SMALL-SATELLITE COMMUNITY

International space law does not distinguish between large and small satellites. All satellites, regardless of their size or mass, are legally classified as *space objects*. This term also applies to the thousands of non-functional satellites that serve no useful purpose and could be considered as space debris.

Under international space law, States are responsible for providing authorization and ongoing supervision of the space activities of non-State entities under their jurisdiction and control. However, many of these small satellites are launched as university projects, and it is important to realise that, as students graduate and professors change their interests, lose funding, move to other positions or retire, some of these small satellites could be "orphaned".

Another important issue has to do with frequency usage of small satellites. This has become a serious enough issue that the ITU is developing regulations applicable to small satellites. In the meantime, small satellite operators should follow the guidelines for responsible use of spectrum and orbit.

Small satellites will usually be secondary payloads, which means that their orbit is usually dictated by the primary payload. Since primary payloads are often large, costly satellites, they will be placed in long-lived orbits. In contrast, small satellites often have short lifetimes, and this is perfectly adequate for missions where the main objective is a proof of concept of a technology on orbit, or perhaps the real purpose is to train people on the ground. Such missions realise their benefits within a short time of the spacecraft being placed in orbit, so long mission lifetime is not a requirement. Small satellite operators should be responsible in their selection of orbits to ensure that the orbital lifetime of the satellite does not exceed the nominal operational lifetime by many times. In this regard, there is a growing sense in the space community that, in an era of mega constellations of small satellites with orbital life of 3-5 years, the so-called "25-year rule" (actually still a recommendation not yet formally adopted by the IADC) needs to be revised downwards.

The LTS guidelines also have one guideline that is specifically aimed at the small satellite community. This guideline addresses the fact that many small satellites are at the limit of trackability. Satellite designers are encouraged to implement technical means to ensure that their satellites are trackable.

Lastly, in planning small satellite missions, consideration should be given at the outset to post-mission disposal. This is the topic of an IAA study, which is due to be published in 2019. There are several non-propulsive means of harnessing aerodynamic drag to shorten orbital lifetime.

4. CONCLUSION

The COPUOS LTS guidelines provide a set of internationally agreed best practices that should be implemented by all space actors to ensure the safe and sustainable use of outer space. Small satellite operators are encouraged to implement these guidelines to the extent that it is practicable to do so. The exponential growth in the number of satellites in orbit over the past few years is enabled by the development of small satellites. This is giving rise to mega-constellations that will pose huge challenges to the safety of space operations. This will give rise to pressure on small satellite operators to be responsible users of outer space and to implement post-mission disposal as part of a debris mitigation strategies to avoid leaving non-functional satellites in orbit for times that greatly exceed their mission lifetimes. This will create a market for COTS solutions geared for post-mission disposal of small satellites.

5. REFERENCES

[1] Guidelines for the long-term sustainability of outer space activities. UN document A/AC.105/C.1/L.366

The Sunsensor of the future.

Bragging spree or reality?

Johan Leijtens[1)], Dick Broekmans[1)], Frank Stelwagen[2)], Gert van der Horn[2)]

[1)]Lens R&D,'s-Gravendijckseweg 41b 2201 CZ (the Netherlands)

Email: jls@lens-rnd.com tel +31 (71) 20 20 123

[2)] SystematIC Design b.v., Elektronicaweg 20, 2628 XG Delft (the Netherlands)

1 Summary

In the period 2004 to 2010, the Dutch contract research organisation TNO developed a small digital Sunsensor called the mini-DSS. This sensor was based on a dedicated active pixel sensor called APS+ and the prototype build, showed very good performance (as reported during the ESA GNC conference in 2011). Despite this, the development was never taken to the next level and as far as known digital Sunsensor developments at TNO have stopped in 2010.

The TNO systems engineer at that time involved in the digital Sunsensor developments (Johan Leijtens) founded Lens R&D in 2012 and has been involved in the development of high reliability Sun sensing solutions ever since. Lack of funding however prevented the development of a compact and affordable high reliability digital Sunsensor even though this has been on the development roadmap from the beginning.

Recently, an ESA Artes contract has been signed between ESA and Lens R&D that is to lead to a small but highly reliable (and affordable) true digital Sunsensor dubbed the Intensity Based Image Sensor (IBIS). A dedicated imaging chip is under development in frame of this contact which is expected to lead to a solution that not only provides a small and highly reliable Sunsensor, but also exhibits a very low power dissipation while providing an accuracy that is sufficient for 99% of all space missions.

2 Specifications

It is expected that in the future large telecommunication satellites will use all electrical propulsion to raise the orbit from the initial GTO to Geostationary orbit. This all electric propulsion will have a very high specific impulse, but will provide only limited thrust capabilities. Consequently, manoeuvring is not easy and it is expected that each satellite will use several Sunsensors to provide a full spherical field of view. Given the low perigee of the GTO, these sensors should be albedo insensitive to avoid significant pointing errors at or near this perigee. As the satellites are expected to use normal solar cells without concentrators, the power output of the solar panels will be cosine dependent on the angle of incidence. This in turn means that a very high pointing accuracy is not required. Furthermore, there is a desire to have sensors with a digital interface only for future missions which can be cost effectively procured.

Discarding the albedo issues, an analogue Sunsensor with a digital interface could fulfil all the requirement and provide a very robust solution, but the desired albedo insensitivity will mandate the use of a true digital Sunsensor for which ESA has defined the system requirements in frame of the digital Sunsensor for telecom applications.

The defined specifications are given below.

Fields	Requirements	Specification
Functional	Output	Sun direction in SC frame
Performance (over full thermal & dynamics environment)	Angular accuracy (including tolerance to solar flares, SEU, albedo and stray light)	- Over full FOV: 5° (3 sigma) - Over accurate FOV: 1° (3 sigma) (target 0.5°)
	Field Of View full cone	- Full FOV: Hemisphere - Accurate FOV: +/-30°
Interfaces	Full system Mass	400 g
	Sensor Dimensions (without electronic)	120 x 120 x 60 mm
	Electronics Dimensions (if deported)	100 x 100 x 50 mm
	Average power consumption	2 W
	Average power dissipation	2 W
	Thermal accommodation	No radiator shall be used
	Supply voltage	5V regulated OR 12V OR 28V OR 50V unregulated
	Data interfaces	Digital: type TBD
Design and PA	Redundancy	Internal
	Lifetime	15 years in GEO
	Thermal cycles	7000
	Reliability	100 FIT @ 30°C
	Radiation	-Electronic components: 100Krad -Optics: 300 Krad -Detector if any: 1 Mrad -SEU tolerant
	No ITAR components	ITAR free
Environment	Dynamics	Angular rate: +/- 100°/s
	Temperature	-Storage and operational: -40 to +75°C -Extension for Solar Array accommodation: -80 to +100°C (TBC)
	Vibration and shocks	-Sine: 20 g peak -Random: 27 g rms -Shock: 3000g from 2 to 10kHz

As can be seen the desired sensor is not specifically small, low weight, low power or accurate, but rather the hemispherical field of view, the high rotation rate and the environmental requirements are most demanding. Furthermore, there is one driving requirement which is not mentioned in this table which is the target price of 35k€ for an internally redundant system.

3 Digital Sunsensor implementation

At this moment in time, it is strongly believed that a hemispherical field of view Sunsensor is not the optimum solution.

The only way known to produce a true digital Sunsensor is to use a 2D imaging array and a pinhole or multiple slit detector arrays. It is strongly believed that the most cost-effective way to produce a small digital Sunsensor is to use a CMOS sensor and a pinhole instead of a CCD or slit based designs because a lot if not all processing and interface electronics can be integrated on chip and a compact solution can be created. The disadvantage of using a slit or pinhole-based design is that it will be impossible to provide a full hemispherical view without using imaging optics which in turn will largely increase the complexity and consequently the price of the sensor.

Next to this, accommodation on a satellite without obstruction in at least some part of the field of view will be very difficult to achieve due to the large number of protruding parts on a satellite. (solar panels, antennae, electronics boxes, etc)

Consequently, the new focus is on a (single chip-based) small digital Sunsensor which uses a single pinhole aperture to image a Sun spot on a small 2D detector array which contains all the required active components needed for power regulation, clock generation, signal processing and interfacing. Although it will be impossible to use this circuit without some supporting electronic components, the development target is that no (expensive) active components will be required and the auxiliary components can be limited to capacitors (for decoupling and timing purposes) and resistors only. Once proven, this will limit the bill of materials and will strongly contribute to producing Sunsensors cost effectively in the future.

In order to make a high quality cost effective Sunsensor it is deemed necessary to design a detector that avoids the use of a (costly) intensity reducing filter but still prevents (pixel) saturation. Next to this a detection principle will be selected that uses as little power as possible. The latter is needed because a Sunsensor is looking directly at the Sun as a precursor to operation and consequently is prone to absorption of solar radiation. This means that a sensor with a small exposed surface will absorb less solar radiation and will be easier to manage from a thermal point of view. This also means that it will be necessary to limit the power consumption as much as possible, because (given the small size of the sensors) any substantial power dissipation can quickly lead to hotspot generation internal to the sensor. As the exterior of the sensor will have to be minimized as far as possible, the available radiator surface to reject heat is also very limited and any heat absorbed or dissipated will have to be transported out mainly through the mounting feet.

Another aspect that needs due consideration is the on-chip signal processing performed in order to increase the robustness of the Sunspot detection against bright, bad or dead pixels. Such signal processing helps to prevent (especially when the sensor reaches end of life due to radiation damage) false Sunspot detections or missing Sunspot detection, and so improves the robustness of the sensor.

In order to further improve upon the Sun detection reliability, it is currently foreseen to implement digital line filtering after pixel threshold detection as shown below.

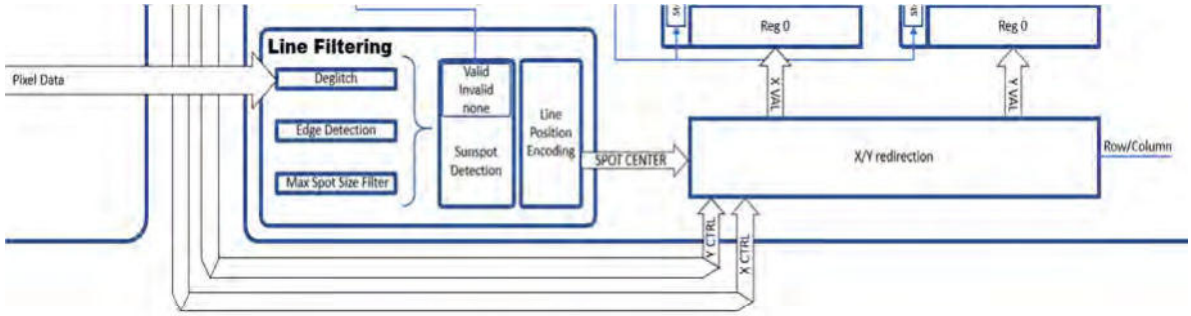

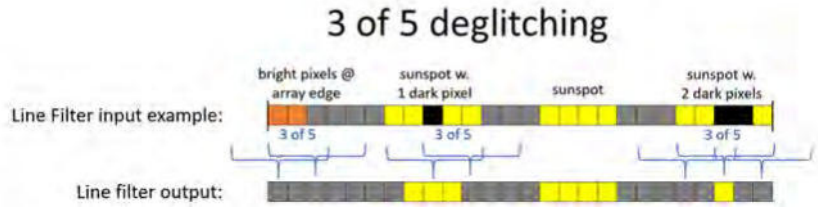

For every pixel independently it is determined if the Sun detection threshold is exceeded. As the Sun will be imaged on several consecutive pixels, at least three out of 5 pixels shall exceed this threshold before a sunspot detection is signalled. This avoids a false detection even if two bright pixels adjacent to each other exist, and still provides a positive Sun detection even if two bad or dead pixels fail to exceed the threshold signal. Theoretical analysis of two-dimensional filtering of the array data using this '3 out of 5 deglitching' algorithm in combination with a 10 pixel large Sunspot image have shown to give a very reliable and accurate Sun-angle detection even under circumstances where multiple deficiencies in the imaging array exist.

Although the data interface to be used is currently still under evaluation, it has become obvious that the overall power consumption of the sensor will - to a large extend - be driven by the power consumption of the data interface selected. This is due to the fact that a high-fidelity data communication generally requires significant currents on the data interface. Limiting the currents or lowering the voltages on the data interface increases the susceptibility to electromagnetic interference (EMI). Therefore, selection of the optimal hardware interface

and protocol to be used for the data communication is one of the critical trades in consideration for this Sunsensor development.

4 Bragging spree or reality

Lens R&D has engaged in this ESA design activity being convinced that the current team will come up with a working demonstrator that meets all posed requirements with exception of the hemispherical field of view. Lessons learned from past developments and new ideas developed in the cause of the last 7 years of Lens R&D's existence in combination with some critical requirements that have changed will be core to the solution. Probably the most critical design driver will be the desire to have a redundant system for a recurring cost of less than 35k€. As membrane based systems can only have fields of view in the order of ±60° without the use of imaging optics, which would drastically increasing system costs, it is proposed to limit the field of view and use more sensors to provide the spherical coverage provided. Spherical coverage will require two hemispherical field of view Sunsensors and in the ESA case this would mean a budget of 70k€ per satellite. Most often, only the prime sensor is redundant though which means that 6 sensors plus 1 redundant sensor should be able to cover the required functionality. This leads to a budget of only 10k€ for a non-redundant but fully ESA qualified sensor which will be a daunting task to achieve but doesn't seem impossible given the current state of developments.

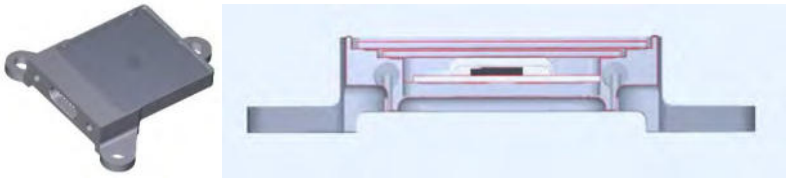

The current design (which resemble the BiSon Sunsensors quite closely) entails a design with two membranes (one with a small pinhole and the other with a secondary mirror reflector to keep the heat from the Sun out) and is based on a single chip 5*5mm^2 0.18µm CMOS chip produced in a European foundry. Using various Design Against Radiation Effects (DARE) measures to increase the resistance to cosmic radiation is expected to produce a very resilient sensor. Utilising the results obtained during several years of product and production optimisation for the BiSon Sunsensors (some of which are shown below) should allow to produce the sensors in a cost-effective way as long as there are enough units to be manufactured.

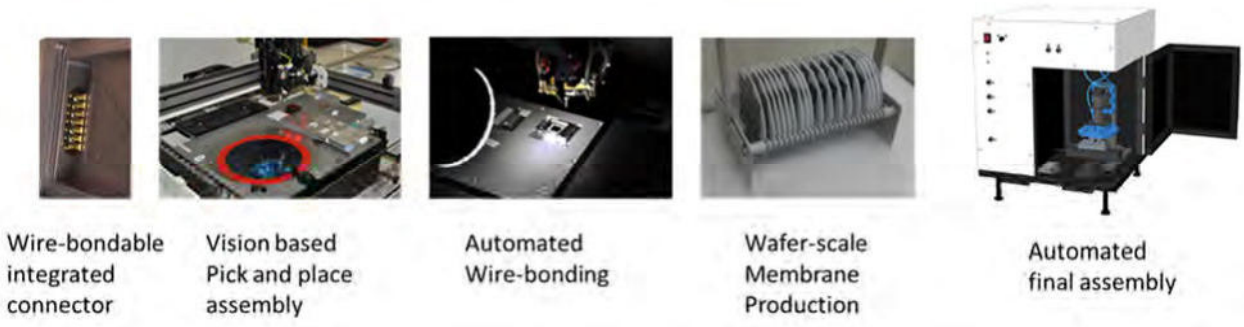

Despite the fact that a lot of the production flow foreseen is quite well understood, it is by no means ensured that the sensors can be very cost-effectively produced, as much will depend on how effectively known good die (KGD) can be selected. For analogue Sunsensors, it is known that dark-current measurements are a good way to select KGD, but for a CMOS sensor, there is much more functionality that needs to be verified. Consequently, it is expected that a substantial part of the final costs will be dependent on how effectively the required KGD can be selected and substantial design efforts are consequently devoted to design for test activities which should lead to a better testability for the final design.

Although the current project only entails the concoction of a functional demonstrator, the results will show that claiming to be able to develop a small and affordable high reliability Sunsensor is not just a bragging spree but a first step on a realistic path to produce the Sunsensor of the future.

Hybrid Propulsion for Low-cost Access to Space

Mario Kobald[1], Christian Schmierer[2]

[1]HyImpulse Technologies GmbH
Langer Grund c/o DLR, 74239 Hardthausen, Germany
Phone: +49 6298 28622, Mail: kobald@hyimpulse.de

[2]HyImpulse Technologies GmbH
Langer Grund c/o DLR, 74239 Hardthausen, Germany
Phone: +49 6298 28656, Mail: schmierer@hyimpulse.de

Abstract: Increased demand for small satellite launch capabilities drives on the search for low-cost launch vehicles. The development and production cost of hybrid rocket engines can be a small fraction of liquid propulsion systems thanks to their inherent safety and reliability. Paraffin/Liquid Oxygen (LOX) based hybrid rocket engines are developed from the German start-up company HyImpulse Technologies GmbH in cooperation with the DLR Institute of Space Propulsion. A concept for a mini-launcher called SL-1 has been designed by HyImpulse and the development of a 75 kN (sea level) hybrid rocket engine is on-going. In the first project phase, a 75 kN hybrid rocket engine using liquid oxygen and a paraffin-based fuel is being developed in an engineering model configuration. This engine will be the largest hybrid rocket engine tested in Europe up to date, and will be commercialized in a flight version by the new space start-up HyImpulse. With the hybrid rocket engine technology a low-cost approach but at the same time a high performance vehicle with a turbopump-fed hybrid rocket engine can be realized. Hybrid rockets are safe, as they have a zero TNT equivalent and their propellants are non-toxic or hazardous, reducing greatly the overall costs.

1. INTRODUCTION

SL-1 is a novel small launcher based on very innovative hybrid propulsion system which uses paraffin/ LOX and is based on DLR's successful STERN program with the University of Stuttgart HEROS sounding rocket. On November 8th, 2016 at 10:30 a.m. the hybrid sounding rocket HEROS 3 was launched from the ESRANGE Space Center to an apogee altitude of 32,300m (106,000 ft). This set a new altitude record for European student and amateur rocketry and a world altitude record for hybrid rockets built by students. The 7.5m long rocket was using N2O and a Paraffin-based fuel to produce 10,000N of thrust. The dry mass of the rocket was only 75 kg thanks to a CFRP structure for the most part. The rocket performed the record breaking flight at perfect weather and visibility conditions, see Figure 1, reaching a maximum airspeed of 720 m/s and Mach 2.3. The rocket performed a soft landing with two parachutes and can be reused. Flight data and engine performance data has been published and analyzed. The flight data shows excellent stability of the combustion, a well-known challenge of hybrid rockets. Engine performance data proves very high efficiency and stable combustion as

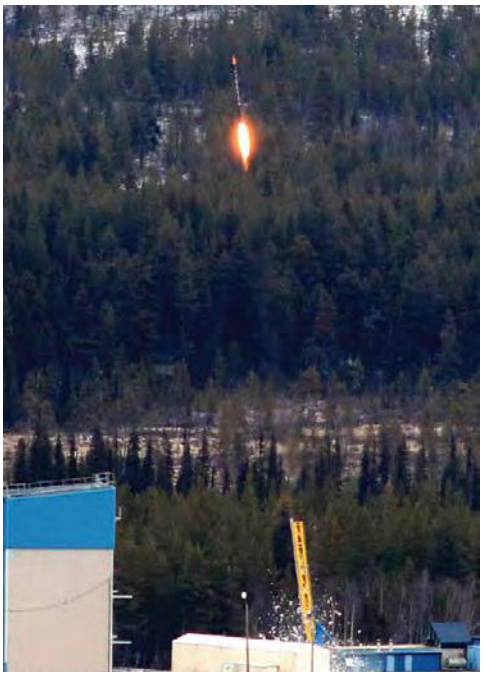

Figure 1 HEROS 3 Launch from Esrange

in the ground tests. Engine and flight trajectory simulations show very good agreements with the flight data.The HEROS family of rockets is developed around a hybrid rocket engine developed by HyEnD and tested at DLR and University of Stuttgart students from 2006 to 2016. HyEnD was led by the founders of HyImpulse and focused on developing its own hybrid rocket engines in different scales from 250N to 10000N thrust and has gained extensive experience and knowledge.

Hybrid rocket engines have distinct advantages compared to classical solid or liquid propellant rocket engines. In comparison to solid rocket engines, hybrid rocket engines offer huge safety advantages during storage and handling. These advantages lead to reduced total costs of such a hybrid rocket engine. Controllable thrust including shut off and restart capability are further advantages. Less piping and valves due to only one liquid component being used introduce less complexity and reduced costs compared to liquid rocket engines. A hybrid-propellant rocket is a rocket with a rocket motor which uses rocket propellants in two different phases: one solid and the other either gas or liquid. The hybrid rocket concept can be traced back at least 75 years. Hybrid rockets avoid some of the disadvantages of solid rockets like the dangers of propellant handling, while also avoiding some disadvantages of liquid rockets like their mechanical complexity. Because it is difficult for the fuel and oxidizer to be mixed (being different states of matter), hybrid rockets are much less dangerous and less prone to failures compared to liquids or solids. Like liquid rocket engines, hybrid rocket motors can be shut down easily and the thrust is throttleable. The theoretical specific impulse (Isp) performance of hybrids is generally higher than solid motors but lower than liquid engines. Isp as high as 400 s has been measured in a hybrid rocket using metalized fuels. Hybrid systems are more complex than solid ones, but they avoid significant hazards of manufacturing, shipping and handling solid rocket motors by storing the oxidizer and the fuel separately. Inherent safety in handling, storage and testing is one of the key advantages of hybrid propulsion and also greatly reduces the costs. Therefore, hybrid propulsion will also be used in manned space tourism applications like SpaceShipTwo.

2. SMALL LAUNCHER DESIGN

A feasibility study of HyImpulse for the SL-1 smallsat launcher based on LOX-paraffin hybrid rocket engines has successfully resulted in a concept for a launcher in the range of 500 kg payload to LEO, which is currently not being developed by any party in the EU. The foreseen concept is based mainly on the propulsion technology which has been developed by the HyImpulse founders at the DLR Institute of Space Propulsion and Stuttgart University for more than 7 years. The idea behind a hybrid rocket launcher is to keep the propulsion system as simple and safe as possible but in the same time boost the performance and keep the inherent safety, which is offered by propellants in different states of matter. The concept for the SL-1 launcher includes three stages. The concept is using the same engine design in the first and second stage resulting in a serial production of the main combustion chamber, turbopumps and feed system components, as 11 main engines are produced per rocket. This results in more than 130 engines per year for the targeted launch rate of 12 launches per year. This can massively reduce the cost per component and per launcher. The first stage will have 7 engines, each with 75 kN thrust at sea level, see also Figure 2. The second stage will have 4 engines with 100 kN thrust each in vacuum conditions. The main difference will be the nozzle expansion ratio between the first and the second stage. The turbopumps will be driven by a gas

generator. The gas generator will use a liquid propellant (combination of Ethanol/LOX). A pressurization gas for the LOX tank will be necessary. The first stage therefore is composed of the following subsystems & components:

- 7 x 75 kN hybrid rocket engines with a thrust frame, turbopump system & tubing and valves
- LOX tank (composite, acting also as the airframe)
- Propellant tank for gas generator fuel and pressurization gas
- Guidance system
- Measurement and motor control system, power supply
- Stage separation mechanism
- Optional recovery system
- Optional aerodynamic control surfaces
- Flight Termination System (FTS)

The second stage has a very similar layout as the first stage with the only difference being:

- 4 x 100 kN hybrid rocket engines with turbopump system
- No recovery system, no control surfaces

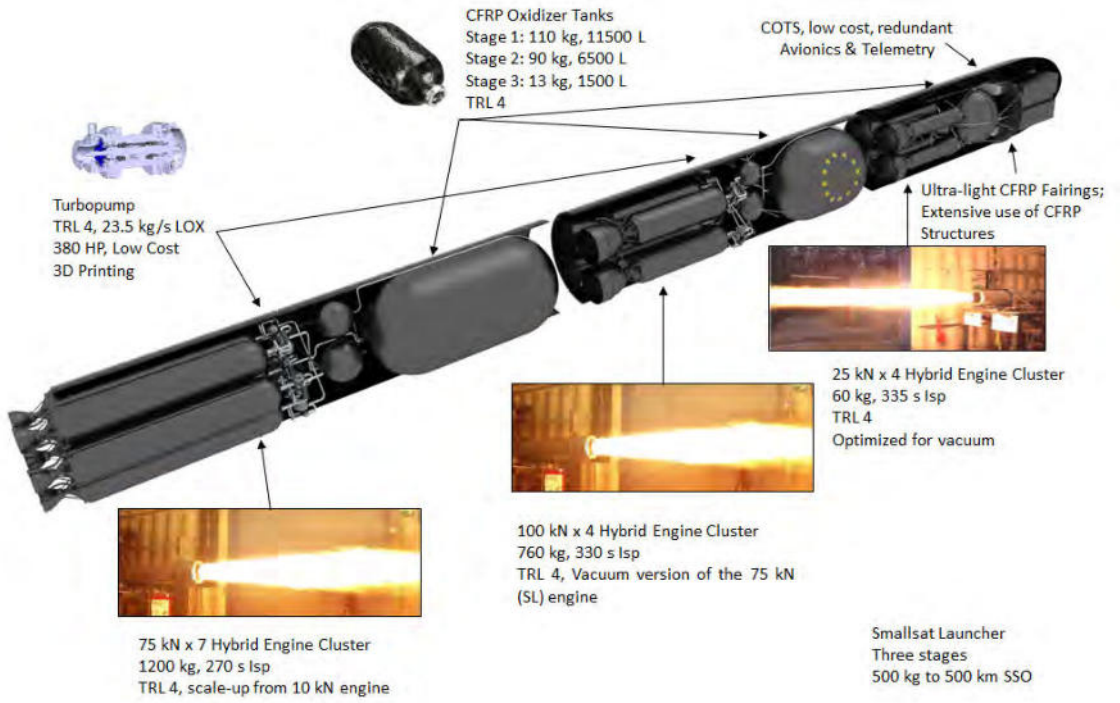

Figure 2 SL-1 Small Launcher SL-1 Specifications and current TRLs

The third stage will be propelled by a cluster of a smaller version of the same engine. They will be fired in pairs of 2 in order to reduce the maximum acceleration. For hybrid rocket engines, in order to reduce thrust, the length of the fuel grain and the oxidizer mass flow need to be adjusted, which makes an adaption in thrust very easy. The third

stage won't need a turbopump. A pressurization system is sufficient using a low combustion chamber pressure but a high nozzle expansion ratio. The third stage needs additionally an attitude control system, based on either cold gas or monopropellant thrusters. The third stage houses also the GNC, avionics and downlink systems. The third stage therefore has the following subsystems and components:

- 4x25 kN hybrid rocket engine, pressure-fed (sequential burns in pairs of 2)
- Thrust frame
- LOX tank
- Pressurization tank
- Tubing and valves
- Measurement and motor control system
- Payload adapter and separation system, dispenser for multiple satellites
- GNC, avionics, power supply, telemetry system, flight termination system
- RCS thruster system
- Payload fairing

3. Hybrid Propulsion and 75kN hybrid rocket engine

The proposed 75 kN hybrid engine uses a paraffin-based fuel and LOX as propellants, since paraffin offers a much higher regression rate. Today, green and non-toxic propellant combinations are desired. Therefore, only LOX, N2O and H2O2 are meaningful for such applications. Their vacuum ISP performance with our baseline paraffin-based fuel is shown in Figure 3, calculated with NASA CEA program. It is clearly seen that our combination LOX/Paraffin offers by far the highest theoretical vacuum specific impulse with more than 360 sec. Also, it offers by far the lowest price (LOX << 1€/kg and Paraffin < 3€/kg, in comparison Nammo as competitor uses H2O2 > 10€/kg and HTPB ~ 20€/kg), handling and storage is also simple. MON30 is the second best performance, but only useful for very limited applications due to its toxicity. H2O2 is used by Nammo and its hybrid sounding rocket. In its widely available form of 87.5% concentration has actually a lower performance than N2O. H2O2 above 95% has a slightly better performance, however it is not available in large quantities, the price is high, transportation and shipping is restricted. Evonic, for example, is selling 98% H2O2 in larger quantities only via a special production facility which needs to be installed on the launch site. Therefore, we exclude H2O2 as oxidizer from our candidates. The advantages and key characteristics of paraffin-based fuels are listed below. The hybrid rocket fuel used at HyImpulse is a proprietary advanced Paraffin-based fuel, specifically developed for the use in the SL-1 launcher. With its particularly tuned composition the fuel has a high regression rate, compared to classical hybrid rocket fuels like HTPB, a high mechanical strength, and a good elasticity. These factors make it perfectly fit for the application in a small launch vehicle. Liquefying fuels like Paraffin have a great advantage over classical fuels like HTPB. Hybrid rockets are characterized by the combustion in the boundary layer of the flow along the combustion chamber. While the flow in the center of the fuel port is oxidizer rich, the boundary flow close to the fuel surface is fuel rich. Naturally, fuel and oxidizer have to mix in order to form a combustible mixture. With classical fuels, the regression rate is thereby limited by the heat flux which can reach the fuel through this boundary layer flow field. This limitation causes a very slow regression rate for HTPB. Therefore, HTPB fuels usually have complex geometries like wagon wheel multiport fuel grains, in order to make up for the low regression rate by increas-

ing the fuel's surface massively. The problem with these geometries is that they cause high residual fuels at the end of the burn. Most wagon wheel shaped structures cannot burn until the fuel is depleted as otherwise large fragments of fuel could detach and damage the combustion chamber or nozzle. In addition, manufacturing a wagon wheel structure is more expensive than a single port circular paraffin fuel grain.

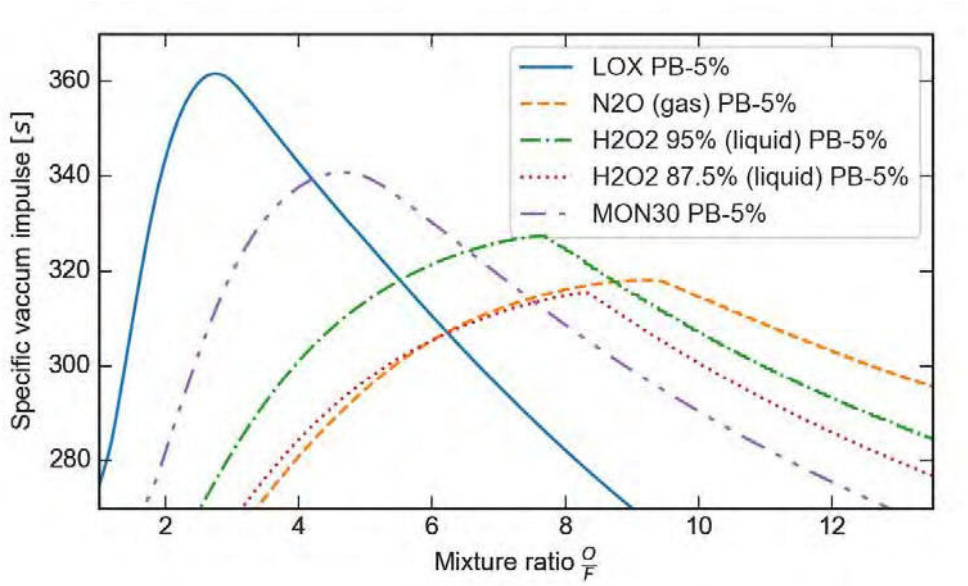

Figure 3 Performance comparison for different fuels

Liquefying fuels like Paraffin solve this problem by producing a melt layer, which forms waves on its surface and causes droplet entrainment into the combustion flow. By this, the fuel mass flow is not limited anymore, as the fuel droplets make their way into the oxidizer rich flow without vaporizing, thereby avoiding the limitation of the heat flux to the fuel grain. This enables 3-5 times higher regression rates for paraffin compared to HTPB based fuels at similar mass fluxes and makes single port fuel grains possible with high fuel utilization.

Pure paraffins can have low mechanical strength and the regression rate is sometimes even too fast, resulting in uncontrolled combustion behaviour. This problem is solved with the Paraffin blend used at HyImpulse. This technology advantage is unique in Europe. Figure 4 (right) shows regression rates for some hybrid rocket fuels over the oxidizer mass flux in the fuel grain's port. From literature there is a curve of HTPB and the paraffin-based fuel SP-1a. As it can be seen easily, the paraffin-based fuel SP-1a has a much higher regression rate than HTPB (factor of about 3).

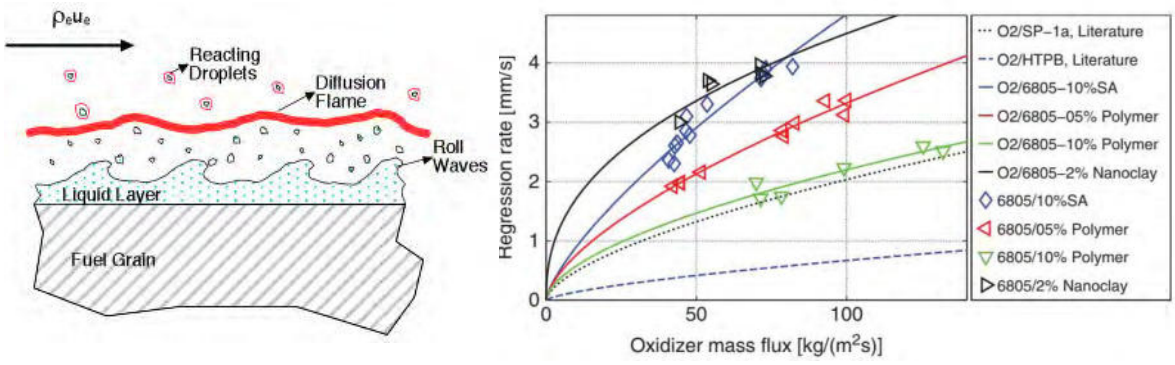

Figure 4 (left) Droplet Entrainment Process with Liquefying Solid Fuels (Right); Regression rates of different hybrid rocket fuels

The measurement points are different fuels which have been developed at the DLR Lampoldshausen in the past years and are now commercialized within HyImpulse. As can be seen, the purer paraffins with only 2% nanoclay as an additive have a much higher regression rate than HTPB (factor up to 8). By refining the mixtures with polymers it was achieved to reach a still high regression rate, smooth combustion and a mechanically stable fuel. The advantage of these fuels is, that by slightly varying the composition of the fuel, the regression rate and mechanical properties can be adjusted to the specific needs of a certain application. The founders of HyImpulse have been awarded with the AIAA Hybrid Rockets best paper award at the Joint Propulsion Conference 2014 for this research and results.

Since the paraffin fuel of HyImpulse has such good regression rates and mechanical properties, it is possible to design a 75 kN rocket combustion chamber with a single monolithic fuel grain of about 3 m length with a simple hollow cylindrical shape. The flight weight engine will be designed with composite materials which can be directly layered onto the fuel grain, forming a very cheap and easy combustion chamber. The fuel grain on the front side is connected to a pre-combustion chamber which is designed to optimally vaporize the LOX. This pre-combustion chamber is lined with insulation material. As a matter of fact, as the regression rate of HTPB is much lower than of the paraffin fuel blend, HTPB can be used as the insulation material. At the front of the pre-combustion chamber a metal injector dome is connected to the insulation material, where the LOX is injected into the combustion chamber. At the aft end of the paraffin fuel grain, a post-combustion chamber lined with insulation material is connected, which is passing into the nozzle. The whole component will be wrapped in composite material in order to reduce the dry mass to its minimum.

4. REFERENCES

Presented at 12th IAA Symposium on Small Satellites for Earth Observation
6 – 10 May 2019, Berlin, Germany
IAA-B12-1404

The SWF Handbook for New Actors in Space

Peter Martinez[1,2]

[1]Secure World Foundation
525 Zang St, Suite D, Broomfield, Colorado 80021, United States
Phone: +1 303 554 1560, Mail: pmartinez@swfound.org

[2]SpaceLab, University of Cape Town
Dept Elec Eng, Rondebosch 7700, South Africa

Abstract: Advances in space technology over the past 10-15 years have greatly lowered the barriers to entry for new space actors. This had led to a dramatic increase in the number and diversity of new space actors and also new kinds of space activities. New space actors show great resourcefulness and creativity in their use of these new technological possibilities. However, it is often the case that these new actors are less aware than established actors of the international policy, security and regulatory dimensions of their proposed space activities. This has raised concerns that the growing number of new actors in space may destabilize the space environment, creating tensions between nations. For this reason, the Secure World Foundation has developed a *Handbook for New Actors in Space* that provides a broad overview of the fundamental principles, laws, norms, and best practices for the peaceful, safe and responsible conduct of activities in outer space. The Handbook is intended for two categories of new actors: national governments beginning to develop their policies and regulations governing space activities, and universities, start-up companies and other non-governmental entities taking their first steps in space activities. The Handbook provides practical guidance for the developers of small satellite missions on a whole range of legal and regulatory issues. The Handbook also addresses responsible space operations and provides an overview of the various mission processes, from payload review, to launch service procurement, pre-launch coordination and post-mission disposal.

1. INTRODUCTION

Small satellites have lowered the entry barriers to space activities for many aspiring space actors, with the result that there is now a much greater number and diversity of space actors than there was ten years ago. At the same time, the capabilities of small satellites have grown tremendously. Small satellites are now being used to develop new kinds of space activities involving rendezvous and close proximity operations, such as on-orbit servicing and active debris removal. Such capabilities hold out huge hopes, but also pose huge concerns with regard to space security and space sustainability. Many of these developments are driven by possibilities presented by advances in technology and by the increasing availability of commercial off-the-shelf components and subsystems specifically designed for small satellites.

The small satellite community comprises a wide range of diverse actors, ranging from established space actors, to start-up companies, research organizations and academic institutions. Small satellites have also opened many new avenues for people to enter the space community. These new space actors show great resourcefulness and creativity in their use of the new technological possibilities presented by small satellites.

However, it is often the case that these new actors are less aware than the more established space actors of the international policy, security and regulatory dimensions of their proposed space activities. This has raised concerns that the growing number of new actors in space may destabilize the space environment, creating tensions between nations. For this reason, the Secure World Foundation has developed a *Handbook for New Actors in Space*[1] that provides a broad overview of the fundamental principles, laws, norms, and best practices for the peaceful, safe and responsible conduct of activities in outer space. The Handbook is intended for two categories of new actors: national governments beginning to develop their policies and regulations governing space activities, and universities, start-up companies and other non-governmental entities taking their first steps in space activities. The Handbook provides practical guidance for the developers of small satellite missions on a whole range of legal and regulatory issues. The Handbook also addresses responsible space operations and provides an overview of the various mission processes, from payload review, to launch service procurement, pre-launch coordination and post-mission disposal. This paper describes the main elements of the Handbook.

2. THE HANDBOOK

The Handbook aims to bring information that is available in many sources together into a single concise publication of practical value for those involved in planning, conducting, authorizing or supervising space activities. While entire textbooks running into hundreds of pages have been written on many of the topics discussed in this Handbook, it aims to distil the most salient facts in a compact and readable form. Rather than aiming to be a comprehensive compendium covering every fact and nuance of this incredibly rich field, the commentary in the Handbook is broad and comprehensive but contains only the most fundamental principles and topics, followed by a list of references for those wishing to delve more deeply into a specific topic.

The Handbook is structured in three chapters. Chapter One deals with the international framework for space activities. It discusses the fundamental legal principles of international space law and introduces the most important and relevant topics in international space law and how they apply to States. This Chapter covers, inter alia, the registration of space objects, frequency filing issues and export controls, and other topics that are often completely mysterious to the uninitiated. The emphasis is on providing practical guidance. For example, the Handbook contains the registration form for the UN Register of Objects Launched into Outer Space, to show that the registration information required is not overly detailed and could easily be provided by any State involved in space activities.

Chapter Two discusses how national space policy and national regulation apply to space, beginning with rationales for developing space policy and discussing in particular how to broadcast goals internationally and give guidance domestically. The chapter also includes a discussion of the common elements of national space legislation. Because national governments are directly responsible for their national space activities, including the activities of non-governmental entities such as corporations and universities, national space policy and regulation are very important for governments to understand.

Governments initiating their space capabilities or drafting their space policies would be well served with an understanding of Chapter Two.

Chapter Three addresses responsible space operations and covers aspects of every phase of a space activity, from pre-launch frequency selections and coordination, to payload review, launch services agreements between launch providers and operators, and mission and post-mission concerns. The Chapter ends with a section on End-of-Life considerations for a satellite and the various post-mission disposal options open to those who would like to be responsible users of outer space.

The following core principles are conveyed throughout the Handbook:

- Outer space is an area that is not subject to state sovereignty or national appropriation, and all humankind is free to explore and use outer space for peaceful purposes.

- National governments are ultimately responsible (and also potentially liable) for the space activities of non-governmental entities under their jurisdiction and/or control, including their citizens and entities incorporated within their territories, as well as non-national actors launching from within their jurisdiction.

- Harmful contamination of outer space and celestial bodies is prohibited.

- Actors need to be aware of the need to protect the Earth's environment and populations from the risks posed by space launch activities by observing national and international rules, including giving notices to aviators and mariners.

- States are encouraged to become party to the space treaties, and several of these treaties already constitute customary international law.

- Registration of space objects in a national registry allows states to assert jurisdiction over their space objects. International registration of space objects can be implemented under the Registration Convention (obligatory for States that have ratified this convention), or under UN General Assembly Resolution 1721 B (XVI).

- Radiofrequency coordination and allocation are required to prevent harmful interference – for every space and ground station around the world, and for every frequency used.

- Space debris is a growing problem. There are internationally agreed guidelines and standards designed to mitigate the creation of new debris and to limit the long-term presence of non-functional space objects in certain protected orbital regions. Adherence to these guidelines and standards is strongly recommended.

- Responsible operations of a satellite in orbit are essential to detecting and avoiding threats or dangerous situations that could result in damage to that satellite or the satellites of others.

- Satellite operators need to know about the space environment and other space objects in order to operate their satellites in a safe and responsible manner.

- Sharing of information on planned space activities (e.g. launches, manoeuvres and other space operations) can help to promote transparency and reduce the chance of misperceptions, miscalculations and mistrust, and are considered to be transparency and confidence-building measures in space activities. Responsible actors in space will observe these norms of behaviour, particularly given that consultations are required for any space activity that may potentially harmfully interfere with the space activities of another State.

- Space activities and their use of advanced technologies that can be used for dual civilian and military purposes raise concerns regarding technology transfer safeguards, export control laws, and intellectual property issues. To avoid conflict, States should have appropriate regulatory regimes in place to address these issues.

The Handbook was issued in 2017 and represents the state of the field as of late 2016. The rapid pace of technological and regulatory developments around the world means that the Handbook will have to be updated every few years. We are already starting to consider elements of the Handbook that may need to be updated in the coming years, as well as important new topics that have emerged since the first edition of the Handbook was conceived in 2014. In this regard, the author of this paper would welcome suggestions for additional topics or other improvements from the users of the current edition of the Handbook.

3. AVAILABILITY OF THE HANDBOOK

The first edition of the Handbook was issued in English only, which limits its use outside of the anglophone world. In order to increase the reach of the Handbook to the Spanish-speaking countries, we have started to translate it into Spanish, in partnership with the Mexican Space Agency. The Spanish edition of the Handbook is expected to be issued by the end of 2019.

The Handbook is available for free download from the Secure World Foundation's website at the link https://swfound.org/handbook. Printed softcover copies may be pur-

chased from Amazon for $25, and a Kindle edition is also available via Amazon for $10.

5. REFERENCES

[1] Handbook for New Actors in Space, Secure World Foundation, 144pp. ISBN 978-0-692-45413-8 (2017)

Effective thermal testing and design solutions for PocketQube subsystems

Timo Rühl[1a], Jasper Bouwmeester[1b]

[1]Faculty of Aerospace Engineering, Delft University of Technology
Kluyverweg 1, 2629HS Delft, Netherlands
Mail: (a) timo.ruehl@community.isunet.edu (b) jasper.bouwmeester@tudelft.nl

Abstract: The PocketQube promises to be the next step in the miniaturization of space technology. The ambitious goals of achieving rapid design-to-orbit cycles while lowering the cost of accessing space requires cost- and time-effective test strategies. This paper proposes a thermal screening method for PocketQube subsystems to identify temperature-critical hotspots and verify their compliance against operational hardware limits. Key elements of the test method are an infrared (IR) scan at ambient conditions. The IR scan is complemented by an estimation of the flight temperature using experimentally derived graphs that describe the vacuum heating of thermal hotspots. The combination of IR scan and temperature estimation enables a hotspot compliance check without thermal-vacuum testing. Moreover, the study indicates that pressure requirements for thermal-vacuum testing of PocketQubes can be moderated. Numerical analysis shows that, due to the small form factor of PocketQubes, pressure levels by three orders of magnitude larger than those used in environmental test standards for larger satellites suffice to maintain the resulting error below 5K. Both the screening method and moderation in vacuum requirements contribute to the development test methods requiring minimum effort concerning necessary equipment.

1. INTRODUCTION

The PocketQube is an emerging satellite class, which pushes the miniaturization of space technology beyond the well-established CubeSats [1]. A showstopper in the success story of nano- and picosatellites are their high mission failure rates [2]. Design flaws and workmanship errors are the primary reasons for the low mission success rates [2], [3]. Pre-flight testing and verification are typically effective means to reveal design deficiencies and incorrect assemblies. Stringent cost and schedule restrictions, together with inefficiencies throughout the design process, often motivate nano- and picosatellite developers to postpone environmental testing towards the end of the design lifecycle, where recovering for design flaws is considerably inefficient [3], [4]. The project circumstance of nano- and picosatellite missions require, therefore, test strategies that facilitate early design evaluation requiring minimum effort concerning cost and necessary equipment.

This paper proposes a thermal screening method to support verification programs in the thermal domain during early development phases. The methodology provides a quick means to check compliance with the hot-side temperature requirements. The necessary steps to implement the test method enable, moreover, to investigate the required pressure levels for thermal-vacuum testing of PocketQube subsystems, which directly relate to the cost of the laboratory equipment.

2. TEST METHODS FOR POCKETQUBE SUBSYSTEMS

2.1 Thermal screening method for thermal hotspots

The introduction of the PocketQube poses new challenges to thermal engineering. The low mass of PocketQubes implies larger temperature oscillations on orbit [1] and parallel research at the TU Delft indicates that PocketQubes reach steady-state conditions during the sunlit part of the orbit [5]. Moreover, the miniaturization from CubeSats to PocketQubes increases the system-level power density by a factor of two [1]. These circumstances motivate to develop a test methodology to verify compliance of PocketQube subsystems with the hot-side temperature requirements.

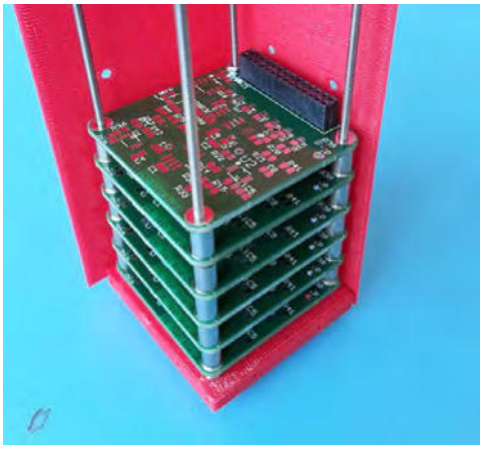

Figure 1 - Delfi-PQ subsyst

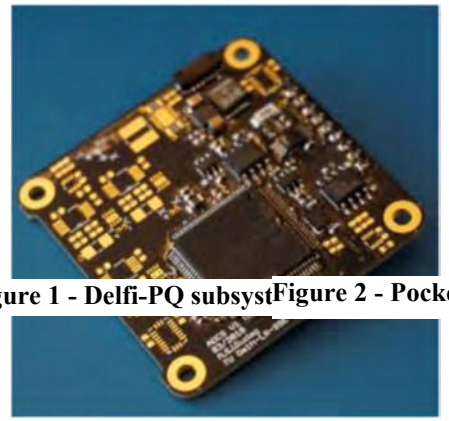

Figure 2 - PocketQube subsystem [10].

The proposed test method leverages the advantages of infrared imaging to identify thermal hotspots and measure their temperature increase relative to the board. Diagrams describing the vacuum heating of thermal hotspots complement the ambient IR temperature screen. The combination of IR screen and heating diagrams enables to perform a judgment whether critical temperatures occur without thermal-vacuum testing. Figure 3 outlines the thermal screening method, which includes the following steps:

1. A thermal simulation model of the entire satellite assembly estimates the maximum subsystem temperature during flight. The level of detail in early thermal simulation models is typically low. The subsystem boards are usually represented by a few thermal nodes averaging the power dissipation of all electronic components over the board area or volume.
2. Thermal simulation models rely on parameter and modelling assumptions, which result in differences between predicted and flight temperatures. This paper defines an uncertainty margin to account for the model uncertainties.
3. An IR scan of a subsystem board in a laboratory environment yields a temperature map, which contains information on thermal hotspots. The combination of a simulation model of the entire and a subsystem IR scan enables to capture the system-level thermal interaction of all subsystems during various operational scenarios and resolves the board-level thermal behavior concerning hotspots.
4. Experimentally derived graphs describe how much more hotspots heat up in vacuum due to the absence of natural convection cooling.

5. The summation of all previous contributions yields an estimate of the maximum hotspot temperature during flight. Comparing the estimated temperature with the operational hardware limit shows if a hotspot is critical concerning overheating.

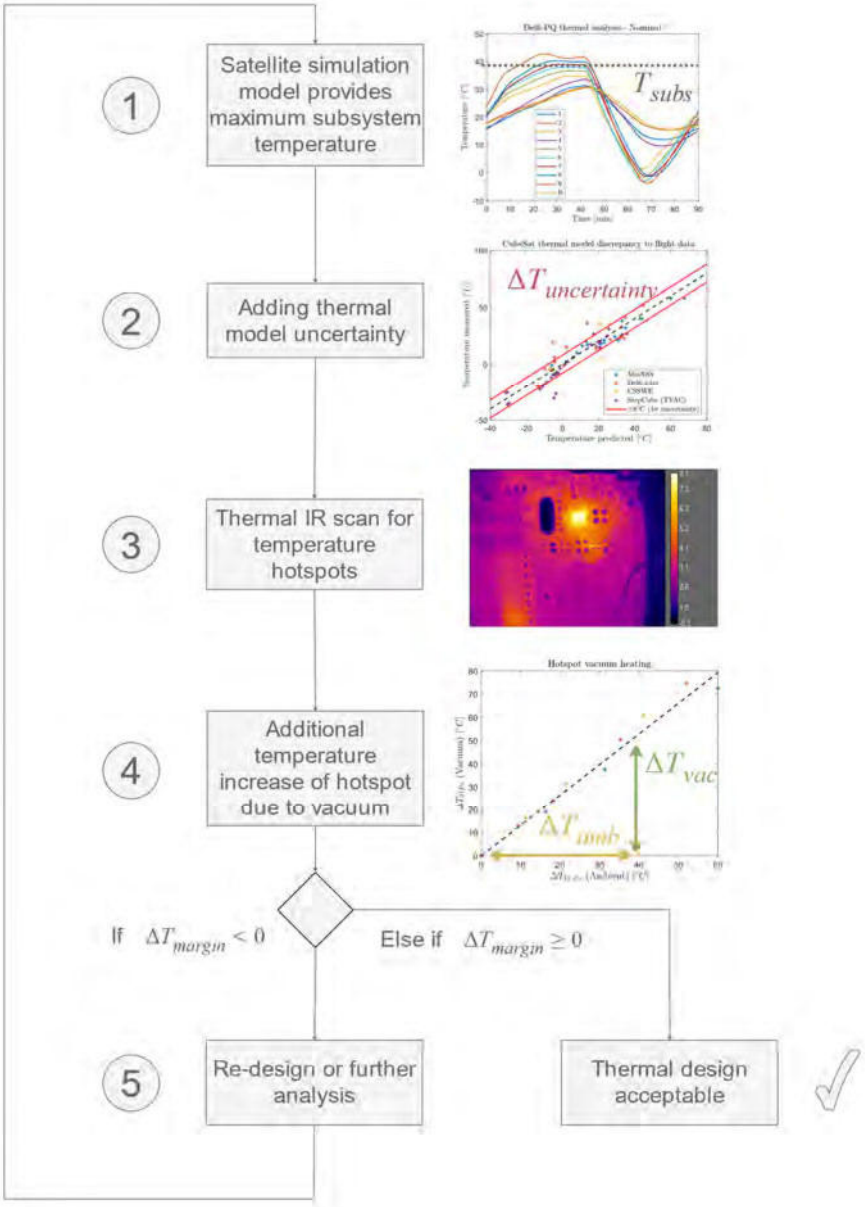

Figure 3 – Thermal screening methodology to assess thermal hotspots.

2.2 Pressure requirements for thermal-vacuum testing

The vacuum quality of a test facility determines its cost and the amount of residual gas in the test environment. Residual gases introduce inaccuracies concerning flight conditions. The residual gas creates additional heat paths through convection and gas conduction that introduce temperature errors compared to ideal vacuum conditions.

Quantification of the temperature error allows choosing the necessary pressure levels for thermal-vacuum testing. The acceptable temperature error due to inaccuracies in the vacuum representation must be lower than the uncertainty that the testing tries to im-

prove. The thermal model uncertainty margin (step 2 in the screening method) provides a potential reference value for the acceptable temperature error for system-level thermal balance testing.

3. TEST METHODOLOGY

3.1 Implementation of the thermal test methodology

The experimental part of this research focuses on characterizing the performance of a commercial-off-the-shelf thermal IR camera (step 3 – screening method) and describing the vacuum heating of thermal hotspots (step 4).

The performance characterization of the IR camera uses the electronic components of an Arduino as a case study. The electronic components resemble potential components on PocketQube subsystem boards concerning geometric size and circuitry layout. Thermocouple measurements provide a reference to compare the performance of both techniques in measuring temperatures.

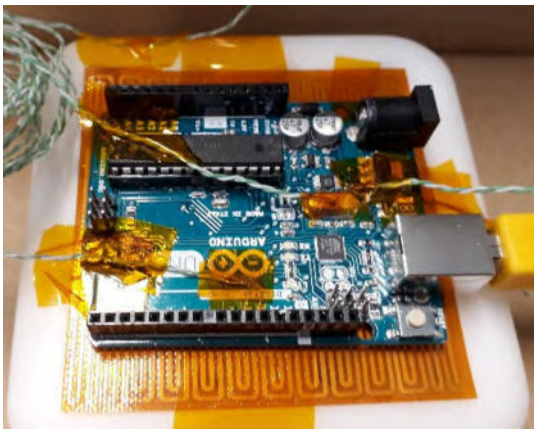

Figure 4 – Arduino board on heater foil including taped thermocouples. IR camera (FLIR A35) is in hovering above the Arduino board at appr. 10 cm distance.

The analysis for the hotspot vacuum heating uses test board with the PQ-9 subsystem footprint and surface mount resistors as the hotspot component. Resistors are flexible towards manipulating the power dissipation. Moreover, the resistors provide a worst-case scenario for the hotspot vacuum heating because of their small size and conduction to the board. Larger semiconductor components show better heat sinking capabilities due to their size and mounting to the board. Figure 5 shows three out of the eight test boards investigated in this study. The boards enable to study the hotspot behavior concerning geometric size (single and double resistor) and board layout (resistor mounted on FR4 or continuous copper plane).

Figure 5 – Electrical layout of the three test boards considered in this paper.

The experimental set-up for the vacuum tests, see Figure 6, consists of hanging the test items from the chamber ceiling using fluorocarbon mono-filament fibers and taped thermocouples for temperature measurements. The experiments in the vacuum chamber are repeated by using IR measurements at ambient conditions for comparison, see Figure 7.

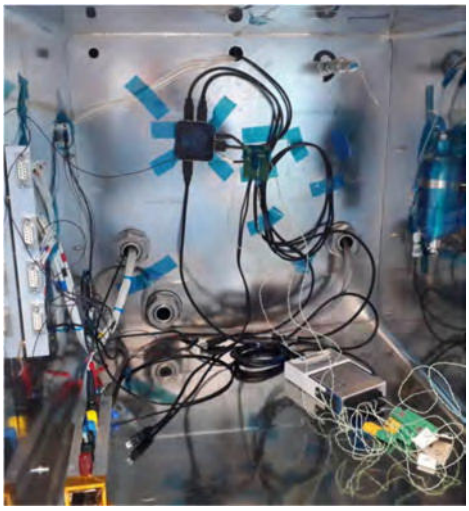

Figure 6 – Vacuum-chamber test set-up including thermocouple measurements.

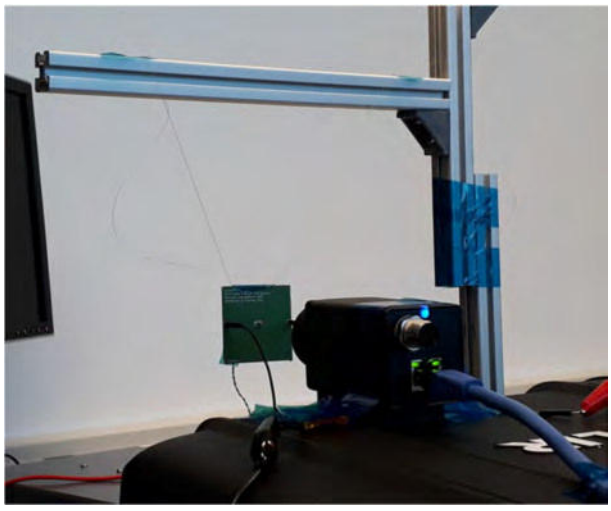

Figure 7 – IR camera set-up at ambient conditions.

3.2 Natural convection at subatmospheric pressure

The pump of the vacuum test chamber achieves an ultimate pressure of $21Pa$. A description of the heat transfer coefficient at this pressure enables to numerically determine the temperature error compared to testing under ideal vacuum conditions of $0Pa$.

The experimental test set-up consists of two rectangular copper plates with the footprint of a Delfi-PQ subsystem board. In between the copper plates an electronic heater foil is applied. The experimental set-up for the copper test item resembles the configuration shown in Figure 6.

The test sequence consists of, first, heating the copper plates to a steady-state temperature and, then, measuring the temperature response during the natural cooling process. The transient heat balance of the cooling process enables to determine the heat transfer

coefficient due to natural convection phenomena. The emissivity of the copper test item and conductive heat loss through the cabling are calibrated using the thermal IR camera.

4. RESULTS

4.1 Thermal screening method

The performance characterization shows thermal IR imaging achieves the same accuracy as thermocouples in measuring the relative temperature increase of the resistors and the Arduino, see the comparison in Figure 8. On the other hand, taped thermocouples prove unreliable in maintain sufficient contact pressure to measure hotspot temperatures.

The IR imaging requires calibration for the background radiation and emissivity of the body of interest. Digital image subtraction using a reference image of an inactive test board is a simple means to remove the background radiation. The dominant disturbance is the reflected IR radiation that the camera itself emits. Above $10K$ temperature increase, IR imaging of high-emissivity components requires for emissivity correction as described in [6], whereas low-emissivity components require first the application of a high-emissivity fluid.

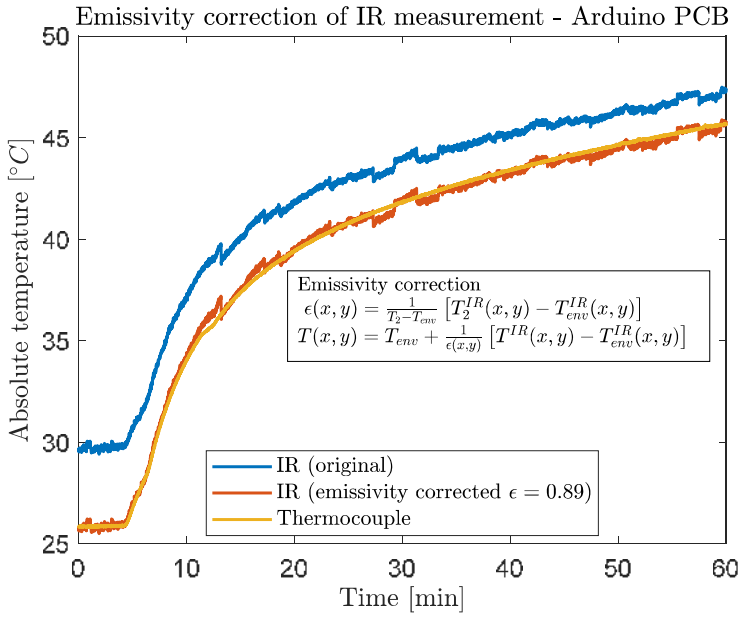

Figure 8 – Performance comparison IR and thermocouple measurement for heating the Arduino.

The analysis of the hotspot vacuum heating uses test boards with a PocketQube subsystem footprint and surface mount resistors as the hotspot component. The diagram in Figure 9 describes the hotspot vacuum heating concerning geometric size and board layout. The graph shows the resistor temperature increase at ambient pressure condition in comparison to the increase in a vacuum environment.

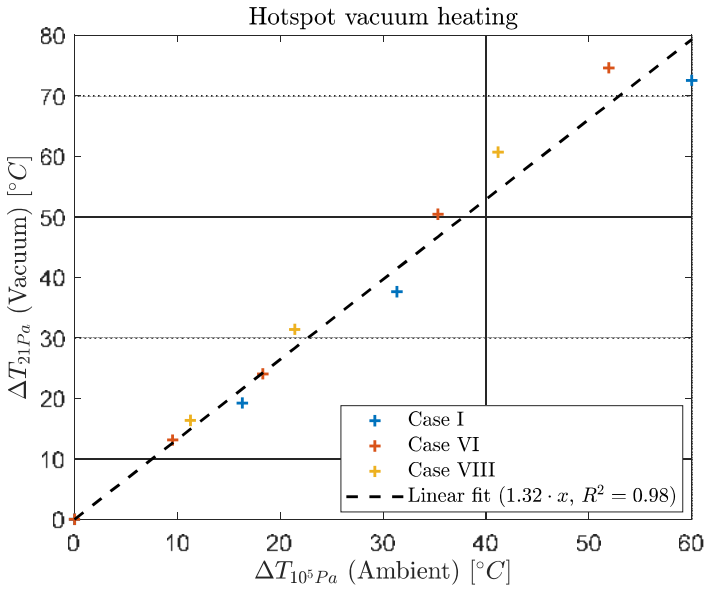

Figure 9 – Thermal hotspot heating for ambient and vacuum measurement.

Table 1 details the steps of the screening methodology to estimate the maximum hotspot temperature. The test board VIII serves as a showcase considering similarity in board layout and hotspot size to the Delfi-PQ communication subsystem.

Table 1 – Application of the thermal screening method to showcase testboard.

Step	Description	Temp. [°C]
(1)	Max. subsystem temperature with satellite simulation model.	42
(2)	Thermal model uncertainty margin (see section 4.2).	+8
(3)	Ambient temperature increase (0.5W - dissipation).	+21.4
(4)	Vacuum Temperature increase.	+11.0
(5)	Total temperature of the hotspot component.	∑ 81.4

4.2 Thermal model uncertainty margin

The derivation of a thermal model uncertainty margin uses flight and test data of four CubeSat missions: Delfi-n3xt, MinXSS, CSSWE, StepCubeLab. The distribution of the error between simulation and measurement yields a $\pm 8K$ standard deviation assuming a Gaussian distribution of the temperature error, see Figure 10. The standard deviation implies a 68% (1σ) confidence that the actual flight data remain within the predicted boundaries. The higher risk acceptance of nano- and picosatellite missions justifies the lower confidence level compared to the 2σ margin used in environmental standards for traditional satellites [7].

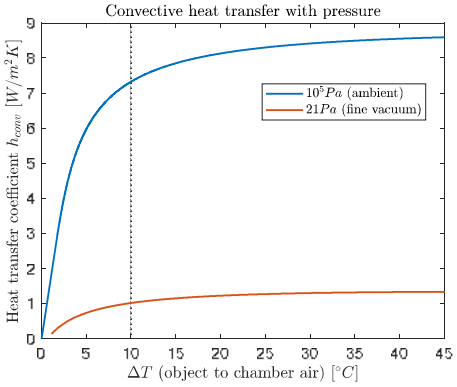

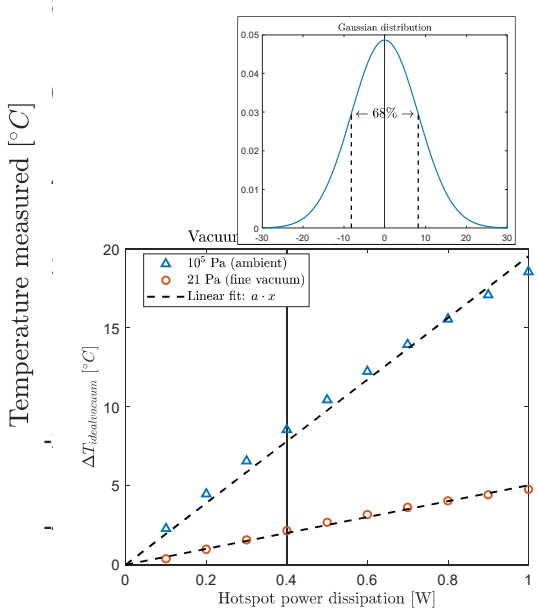

Figure 10 – Deviation between predicted and measured temperature for CubeSats.

4.3 Pressure requirements for thermal-vacuum testing of PocketQube subsystems

The graphs in Figure 11 describe the convection heat transfer coefficient at subatmospheric pressures. The data provide input to numerically determine the temperature error concerning ideal vacuum conditions of $0Pa$. Figure 12 shows that pressure levels by three orders of magnitude larger than those used in environmental test standards for larger satellites [8] suffice to maintain the error below $5K$.

Figure 11 - Convection heat transfer at atmospheric and subatmospheric pressure.

Figure 12 – Temperature error due to vacuum quality for testing of PocketQube subsystems.

5. CONCLUSIONS

This paper proposes a thermal screening method to check compliance of thermal hotspots with the hot-side temperature requirements. The methodology omits the necessity to conduct vacuum testing to perform an early estimation of the maximum flight temperatures. The available diagram describes the behavior of resistors providing a worst-case scenario of the thermal behavior of hotspot components. Moreover, the study illustrates that pressure requirements for thermal-vacuum testing of PocketQubes can be

moderated. Both the screening method and moderation in vacuum requirements contribute to the development of cost- and time-effective test strategies for PocketQubes.

6. REFERENCES

[1] S. Speretta *et al.*, "Cubesats to pocketqubes: Opportunities and challenges," in *Proceedings of the 67th International Astronautical Congress*, 2016.

[2] M. Swartwout, "Secondary spacecraft in 2016: Why some succeed (And too many do not)," in *IEEE Aerospace Conference Proceedings*, 2016.

[3] C. Venturini, B. Braun, D. Hinkley, and G. Berg, "Improving Mission Success of CubeSats," El Segundo, Calif., USA, 2018.

[4] M. Langer and J. Bouwmeester, "Reliability of CubeSats – Statistical Data, Developers' Beliefs and the Way Forward," in *30th Annual AIAA/USU Conference on Small Satellites*, 2016.

[5] R. Avila de Luis, "Standardized Thermal Control Solutions for PocketQubes," Delft University of Technology, 2019.

[6] O. Breitenstein, W. Warta, and M. Langenkamp, *Lock-in Thermography*, 2nd ed. Berlin, Germany: Springer-Verlag Berlin Heidelberg, 2010.

[7] D. G. Gilmore, *Spacecraft thermal control handbook: Volume I*, 2nd ed. El Segundo, Calif., USA: Aerospace Press, 2002.

[8] ECSS, "ECSS-E-ST-10-03C - Space Engineering, Testing," 2012.

[9] DelfiSpace, "DelfiSpace," *Twitter*, 2016. [Online]. Available: https://twitter.com/DelfiSpace.

[10] S. Radu, M. S. Uludag, S. Speretta, J. Bouwmeester, E. K. A. Gill, and N. Chronas Foteinakis, "Delfi-PQ: The first pocketqube of Delft University of Technology." International Astronautical Federation, IAF, 2018.

ELSA-CS, a High-Performance Solar Array for 6U CubeSats

J. Watzinger[1], S. Masante[1], S. Sagaria[1], A. Lourenço[1], G. van Ginkel[2]

[1]Space Structures GmbH
Fanny-Zobel-Str. 11, 12435 Berlin, Germany
Phone: +49 30 814 549 700, Mail: info@spacestructures.de

[2]German Orbital Systems GmbH
Reuchlinstr. 10-11, 10553 Berlin, Germany
Phone: +49 30 340 60 309, Mail: info@orbitalsystems.de

Abstract : ELSA-CS is a 6U form-factor modular solar array, which can be stacked in configurations up to 4 panels per wing. The peak nominal power at beginning of life of a CubeSat equipped with two ELSA-CS 4-panel wings is 150 watt. Versions with single wing and fewer panels are possible, due to the modular design of the solar array. The stowed solar array has a maximum total thickness of 6.5 mm and can be mounted on most of the commercially available CubeSat structures. ELSA-CS is designed for operations in orbits from LEO to GEO. The structure of the panels is made of carbon fiber reinforced polymer and the panels are articulated with planar hinges. The deployment is actuated via torsion springs located at the hinges and the single failure-tolerant release mechanism is testable on-ground. Power and signal routing are realized on polyimide-based circuit boards. Design and verification phases of the Solar Array are described.

Topic: Spacecraft concepts and sub-systems

1. INTRODUCTION

The on-board power generation for CubeSats is becoming more and more a limiting factor in mission design. The increasing average size of CubeSats allows for more complex and power-hungrier payloads and propulsion systems. This relatively new design requirement is very demanding: increasing the surface of the solar arrays has a great influence on other fundamental features and subsystems of the satellite, such as mass, ballistic coefficient, AOCS, thermal control, release and deployment mechanisms and compatibility with containerized launch.

ELSA-CS is a 6U form-factor modular solar array and it is available in stacked configurations up to 4 panels per wing. Its design is modular and allows for configurations with fewer panels without affecting the mechanical and electric interface to the CubeSat. ELSA-CS is compatible with deployers currently on the market for operations in orbits from LEO to GEO.

Figure 1: Double wing ELSA-CS Solar Array

Based on system requirements for CubeSats, the product development included:

- Definition of the requirements and performance
- Mechanical design of the structure, release mechanism and interfaces
- Electrical and electronic circuitry design
- Mechanical and thermal verification of the design
- Prototyping and testing

2. MECHANICAL DESIGN

Design is compliant with the CubeSat Design Specification [1] [2]. Carbon fiber reinforced polymer is used as main structural material and the panels are articulated with planar hinges. The deployment is actuated via torsion springs located at the hinges and the single failure-tolerant release mechanism is testable on-ground. After testing the solar array can be folded back with no need to replace parts.

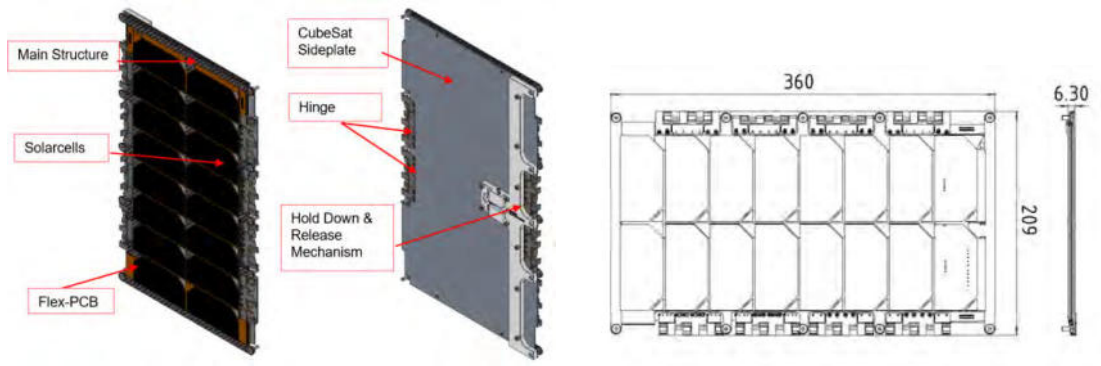

Figure 2: ELSA-CS – Folded configuration and general dimensions

3. MECHANICAL AND THERMAL VERIFICATION

3.1 Structural Analysis

The CAD model of the stowed solar array was converted into a FEM (Finite Element Model) with the applicable masses and material properties. Static and dynamic analyses were performed with Nastran [4] and margins of safety for the stress distribution were computed.

The first natural frequency of the stowed panel is 104Hz.

The equivalent static load of 15 gRMS [3], separately applied on the three main axes, generates stresses in the materials which yield positive margins of safety. The out-of-plane displacement of the panel was also evaluated, and it is low enough to avoid contact between the solar cells.

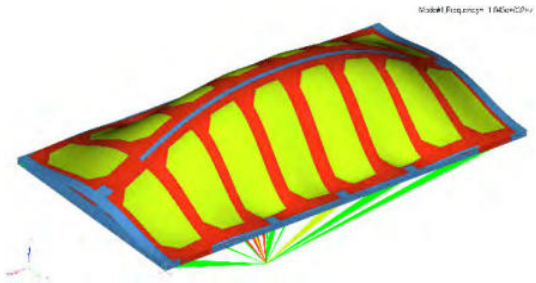

Figure 3: Modal analysis: first natural mode 104Hz

3.2 Thermal Analysis

The illumination conditions vary largely depending on orbital position and altitude. Worst cases, respectively for cold and hot operation were analyzed with Thermica software package [5]. Several load cases were defined for geostationary and sun synchronous orbits. Maximum and minimum temperatures are compatible with the chosen components operational range.

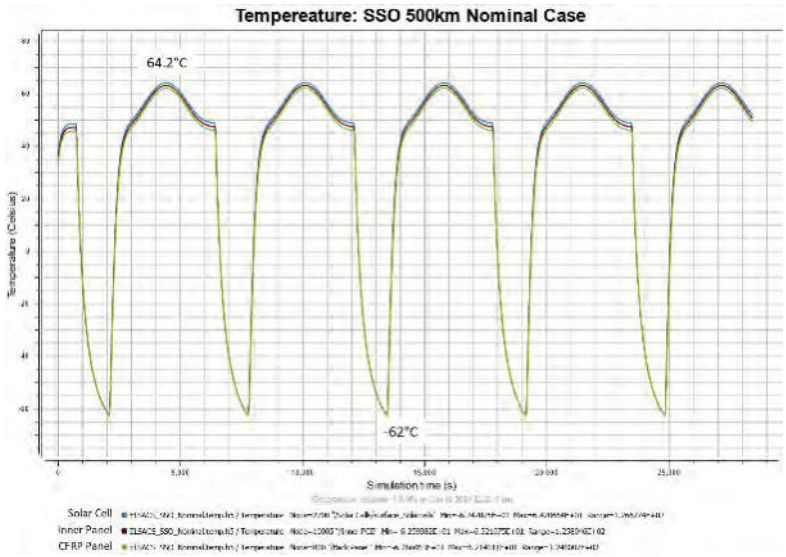

Figure 4: Thermal analysis: temperature excursion in SSO 500km

3.3 Deployment Analysis

A Multibody System (MBS) model was set up to predict the unfolding behavior of the Solar Array and the forces and torques arising during deployment and latch-up. Strength of the materials was verified accordingly. The Solar Array unfolds and latches-up in approximatively one second.

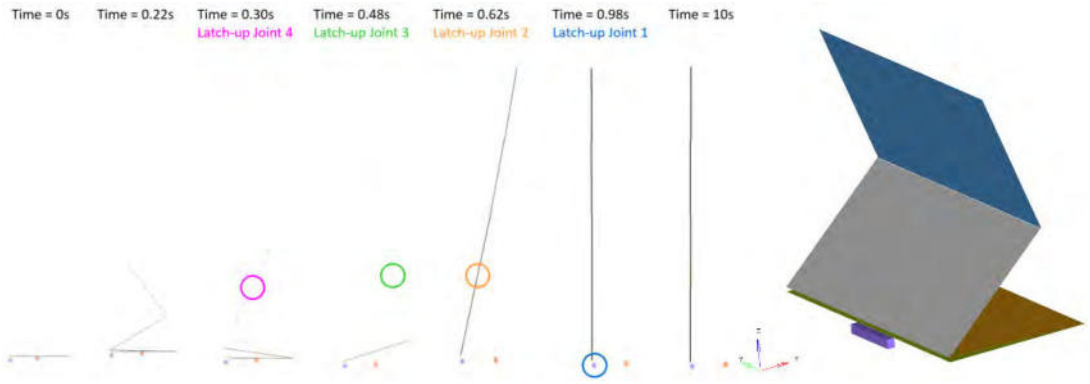

Figure 5: ELSA-CS – Unfolding sequence and 3D-Model at t=0.22s

4. ELECTRICAL AND ELECTRONIC DESIGN

The electronics of the array is based on a flexible PCB. The substrate material of the Flex-PCB is high temperature resistant polyimide. Each panel of the Solar Array delivers the

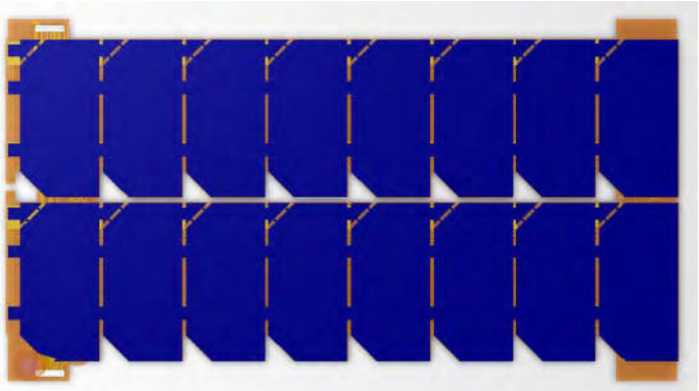

Figure 6: ELSA-CS PCB with Solar Cells

generated power on a dedicated channel, available for connection at the satellite bus. An individual panel hosts 16 solar cells and the total peak power is 19W. The Solar Array in one wing configuration (4 panels) can supply up to either 1A at 70V or 4A at 19V (@BOL and @PPP).

5. CONCLUSIONS

The development and the verification of the ELSA-CS Solar Array is presented in this paper. With a peak power of 150W, in the two-wing configuration, ELSA-CS Solar Array broadens the range of instruments and propulsion systems that a CubeSat nanosatellite can autonomously power. The modular design allows nonetheless for smaller versions and helps reducing unit manufacturing costs. The mechanical and electrical design was verified against operational and non-operational environments occurring during SSO and GEO missions.

The system level, electric and electronic design was carried out by German Orbital Systems GmbH, while Space Structures GmbH was responsible for the structural, thermal, and deployment mechanisms design and analysis. Prototyping, testing and manufacturing is being performed in-house. At the time of the submission, the project successfully passed the Critical Design Review and Manufacturing Readiness Review milestones.

German Orbital Systems GmbH and Space Structures GmbH acknowledge the financial support of EFRE EU Fund and of the Investitionsbank Berlin.

6. REFERENCES

[1] CubeSat Design Specification, Revision 13.0, The CubeSat Program, Cal Poly SLO (2015)

[2] 6U CubeSat Design Specification, Revision 1.0, The CubeSat Program, Cal Poly SLO (2018)

[3] General Environmental Verification Standard (GEVS), GFSC-STD-7000A, NASA Goddard Space Flight Center (2013)

[4] MSC Nastran 2018, MSC.Software GmbH (2018)

[5] Systema Thermica 4.8.1, Airbus Defence and Space SAS (2018)

Delivery of Multiple Small Satellites via Soyuz-2 and Fregat
Symposium Topic Addressed: Launch Systems

Mila Savelyeva, Valeriya Barashkova
Mail: savelyeva@gklaunch.ru, barashkova@gklaunch.ru
GK Launch Services
26/1 Prospekt Mira Ave., 129090 Moscow, Russia
Phone: +7 (495) 150-44-71, Mail: info@gklaunch.ru

ABSTRACT:

The GK Launch Services (GK) will participate in an International Academy of Astronautics 12th IAA Symposium on Small Satellites by offering launching of multiple payloads into almost any type of orbits via cluster or dedicated missions on Soyuz-2 with or without the use of Fregat Upper Stage. The problem to deliver numerous SmallSats to different orbits within one mission can be solved by the use of Fregat by having the multiple restart capability of its main thruster that allows up to 7 ignitions. The baseline price of an entire launch in Soyuz-2.1/Fregat configuration is $48,5m. The price for a dedicated launch without Fregat is $ 35m. Due to lighter weight of SmallSats the relevance to use provider that offers competitive price per kg of payload increases. Due to Soyuz-2 capability to uplift up to 4,8 tones to SSO, GK offers 20,000-30,000$ per kilo. To increase access to space for SmallSats and CubeSats of mass up to 120kg, we increased the transparency of launch pricing by introducing an online price calculator on our website: https://calc.gklaunch.ru/#/. It forms the price proposal within 1 business day based on expected launch date, whether the SC needs a deployer/ separation system or not, fueling, insurance and other specific requirements.

INTRODUCTION:

1.1 GK Launch Services

GK was founded by Glavkosmos and International Space Company Kosmotras on 25th April 2017, as an official operator of Roskosmos, providing commercial launches services via Soyuz-2 from the Russian spaceports Vostochny, Baikonur and Plesetsk. The name of the company is formed as follows: “G” stands for Glavkosmos and “K” for Kosmotras.

Image1: Formation of GK (GK, 2019).

1.2 Key partners

The key partners of GK for commercial missions are as follows:

- RKTs Progress (Progress Rocket and Space Center): manufacture of Soyuz-2 rockets;
- NPO Lavochkin (Lavochkin Research and Production Association): manufacture of Fregat Upper Stage.
- TsENKI (Center for Operation of Space Ground-Based Infrastructure): control and operation of Cosmodrome infrastructure, LV pre-launch processing and launch, general coordination of launch campaigns.

Image 2: Main subcontractors of GK (GK, 2019).

1.3 Soyuz-2 LV

There are currently 2 variations of Soyuz-2 LV utilized by GK. Soyuz-2.1a is a launch vehicle designed for orbital insertion of various purposes satellites and LV features high injection accuracy, as uplift capability is achieved by the advanced control system and enhanced engines of three stages. The upgraded Soyuz-2.1b version uses a new engine on the third stage, which has improved performance providing higher uplift capacity. Soyuz-2.1a and Soyuz-2.1b LVs are both under serial production in the 'Progress Rocket & Space Center'. An average LV production cycle is 22-24 months. Development of Soyuz-2 LV was based on maximum heritage with previously developed and proven systems and units, utilization of proven work technologies and standard flight trajectories and their associated drop zones.

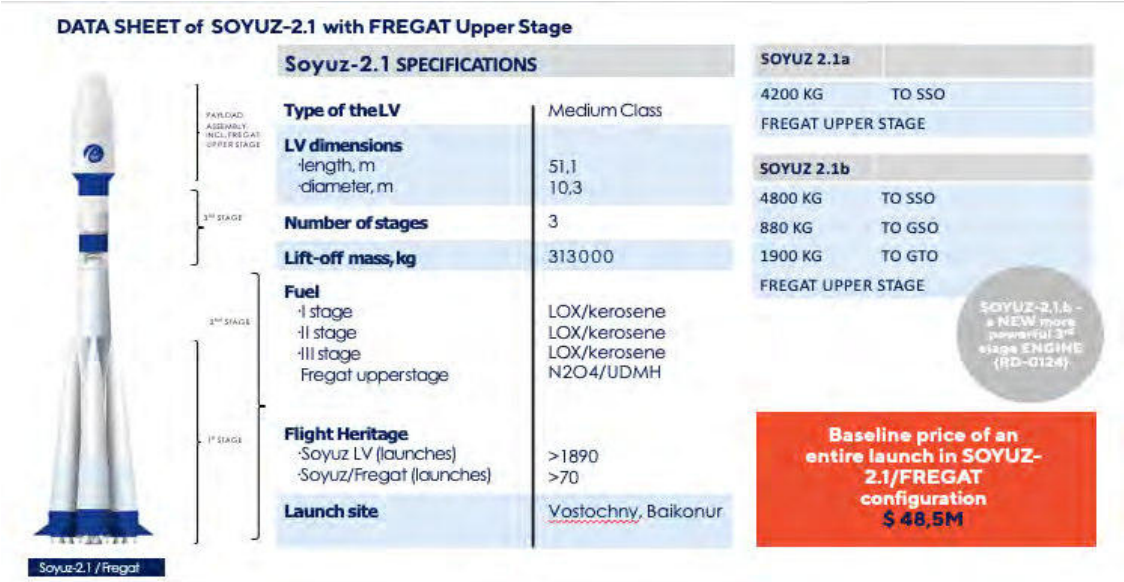

Image 3: Data Sheet of Soyuz-2.1 with Fregat Upper Stage (GK, 2019).

1.4 Launch options

Existing launch options are: dedicated mission, cluster mission and the tandem dual mission. We offer an optimized solution for dedicated missions: Soyuz-2.1b without Fregat upper stage. Cluster missions are offered with the Fregat Upper Stage.

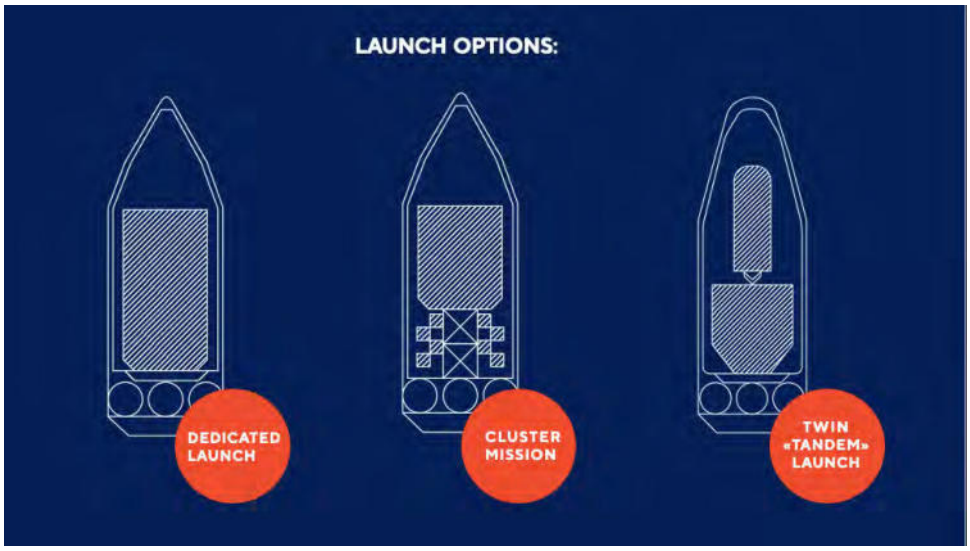

Image 4: Launch options (GK, 2019).

2 FREGAT UPPER STAGE

Fregat is known for its long successful flight heritage and orbit injection accuracy. Fregat upper stage is an autonomous and flexible stage that is designed to operate as an orbital vehicle. It extends the capability of the lower three stages of the Soyuz vehicle to provide access to a full range of orbits. The upper stage consists of six spherical tanks (four for propellant, two for avionics) arrayed in a circle, with trusses passing through the tanks providing structural support. Since 2000, the Fregat Upper Stage designed and produced by our partner Lavochkin Association has been successfully used in tandem with Soyuz-2 launch vehicle.

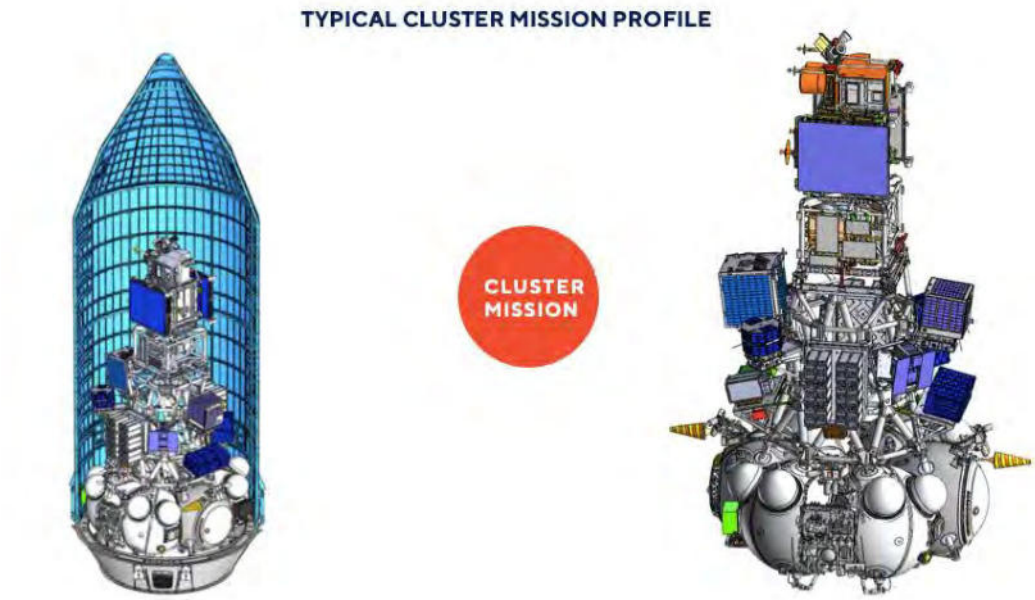

Image 5: Typical launch options from the inside of a cluster mission (GK, 2019).

2.1 Key features of Fregat

• Multi-purpose conception. It provides the delivery of satellites to different orbits within one mission.
• Accuracy. It provides the highest accuracy in delivering satellites to their target orbits.
• Reliability. Fregat upper stage has a flight proven record of high reliability, which along with the historically highest success rate of Soyuz-2 will ensure to accurately deliver several satellites to needed orbits.

2.2 Injection scenario of the typical cluster mission with Fregat Upper Stage.

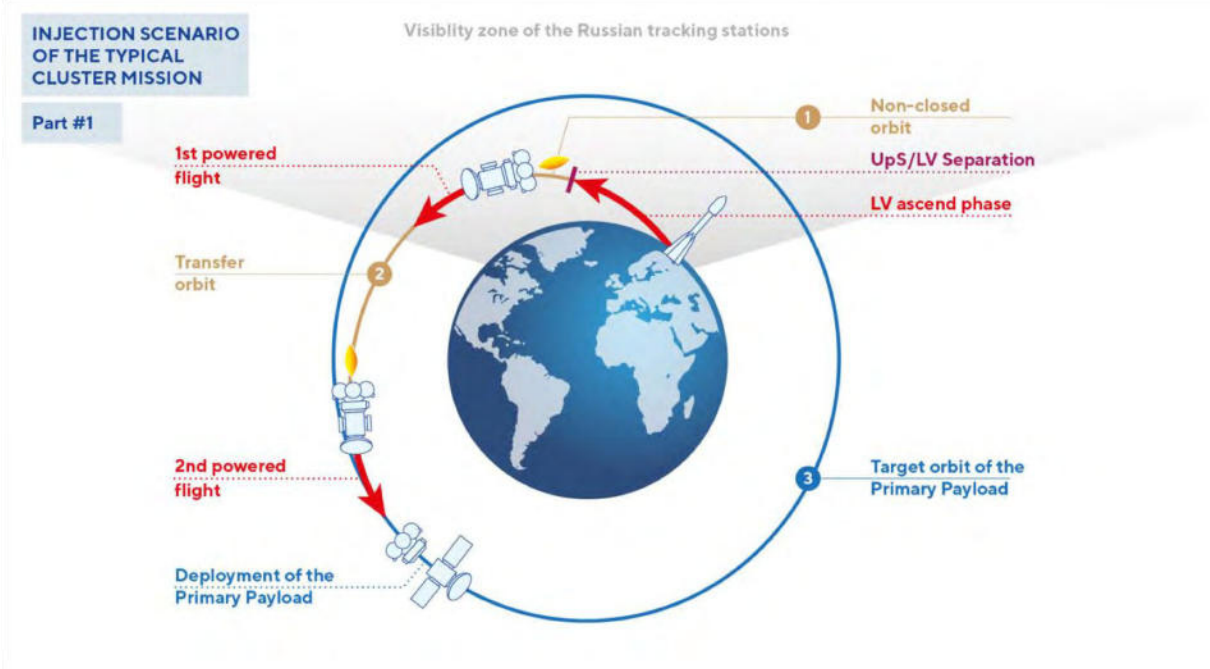

Image 6: Injection scenario part 1 (GK, 2018).

Image 7: Injection scenario part 2 (GK, 2018).

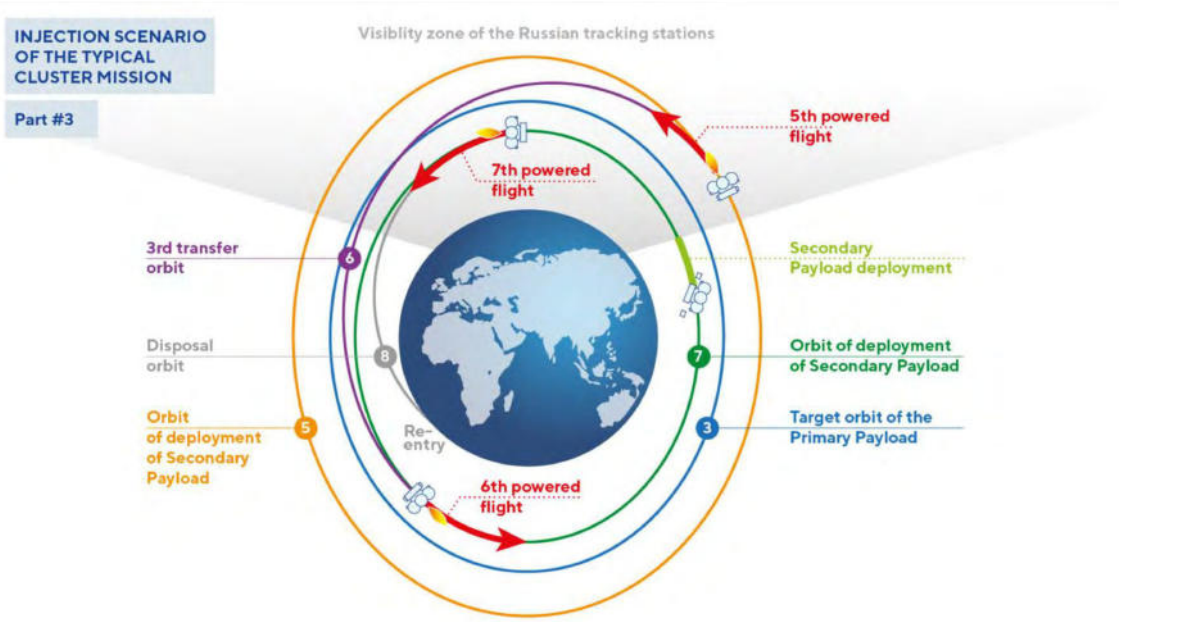

Image 8: Injection scenario part 3 (GK, 2018).

3. LAUNCH FREQUENCY:

Image 9: Soyuz-2 Launch Site Locations (GK, 2018).

3 cosmodromes for launching « Soyuz-2».

- Vostochny (Amur Region, Russia). It is a new Russian Cosmodrome in Far East region with the total area of about 700 sq.km and developed transport network. The rocket blasts off from a dedicated Soyuz-2 Launch Complex.
- Baikonur (Kyzylorda Region, Kazakhstan). It is the largest spaceport in the world that leads in the number of rocket launches ever carried out. Its total area amounts to 6,717 sq.km. The Cosmodrome territory is leased by Russia till 2050. Launches of Soyuz-FG, Soyuz-2.1a and Soyuz-2.1b are executed from Site 31.
- Plesetsk (Arkhangelsk Region, Russia). The total area of the range is 1,762 sq.km

3.1 Vostochny cosmodrome

Vostochny Spaceport provides Russia with an independent access to space for commercial launches. The spaceport brings new opportunities for youth, and over 80,000 jobs for the Far Eastern Region. Moreover, due to mostly unpopulated areas covered with water of the Far East, launches are becoming safer and easier to perform. The distance from Moscow to Blagoveshchensk Airport is 5,700 km and the flight time is 7.5 hours. The local area has a well-developed transport network. The International Airport is located 15km north-west of the city of Blagoveshchensk. Mission ground tracks go through sparsely populated areas and waters of the Far East thus making the flights safe and easy. Vostochny spaceport has all means to become the technological center of the future space cluster.

The existing infrastructure at Vostochny contains a Soyuz-2 launch pad, a universal technical complex, a telemetry complex, living quarters, as well as roads, railways and support systems and facilities.

The launch table with an exhaust-gas outlet is the main facility at the launch pad and is intended for accommodating aggregates and systems that serve to LV mounting onto the table, its servicing, pre-launch preparation, fueling and launching, as well as for accommodating LV ground support equipment, check-out and launch support equipment

of the carrier rocket, upper stage and spacecraft. It also holds various supply systems and work places of operators and service personnel.

The launch control station houses special Launch Vehicle, upper stage and spacecraft ground support equipment, automated control systems for the entire LV preparation and launch cycle, workplaces for operators, and supply systems which maintain required operational environment for equipment and personnel.

The Universal Technical Complex (UTC) is intended for the operations of after-shipment inspection and tests, assembly and integration, stand-alone and integrated tests of the rocket, upper stage, spacecraft and a fully assembled launch vehicle, as well as for the upper stage and spacecraft fueling. The Universal Technical Complex includes a storage facility for LV units, a transfer gallery, an assembly, integration and test building for Launch Vehicle, an AITB for spacecraft, upper stage and space head module, a fueling station. UTC comprises 121 buildings with total area of 170 thousand square meters, where 1,800 people per shift can work. Various facilities, utility systems and transportation lanes spread across 42 hectares of land.

3.2 LV AITB at Vostochny and Baikonur

The LV AITB is designed for accommodation of technological equipment and for LV assembly, initial check, stand-alone and integrated tests. On the left side of the Image 10, you can see LV Processing at Baikonur and on the right side at Vostochniy. The LV AITB accommodates two LV integration work stations, while the capacities of the SC AITB allow operations with any spacecraft and upper stages of the today's space industry. The LV unit storage facility has a heated air lock and serves for acceptance, storage and provision of "dry" (non-fueled) 1st, 2nd and 3rd LV stages, fairings and interstages delivered from manufacturers.

Image 10: Halls of test and assembly at Baikonur (left) and at Vostochny (right) (GK, 2018).

4. ONLINE LAUNCH PRICE CALCULATOR FOR CUBESATS AND SMALLSATS:

We are witnessing a growing demand for launches of small spacecraft into LEO. It is forecasted that the segment of SC of up to 50 kg will be rapidly increasing. To get a wider access to space for SmallSats and CubeSats, we introduced an online price calculator on our website: https://calc.gklaunch.ru/#/. Now, we are working closer with the customers who are willing to launch their SmallSats or CubeSats onboard Soyuz-2, while our pricing has become more transparent. It is noteworthy that the proposal can include insurance for SC transportation, processing, and launch.

Launch price calculator allows calculation of the price for the launch of SC of up to120kg. First, you will need to select your SC type and size. Second, if you already have a deployer/separation system, you will have to specify it, so that we could check its compatibility, otherwise, we'll recommend you a provider. For SmallSats launch price calculation, specify the required type of fueling. Third, indicate whether you require an insurance. Insurance will cover your expenses if something goes wrong at the stage of SC processing for launch or during SC launch. Also, choose the launch window that suits you. Then, select the required satellite orbit and specify inclination, altitude and LTAN for us to offer you the most suitable launch opportunity. Finally, leave your details and the price proposal containing the full and transparent information from the original source concerning the pricing of the launch service will be formed and sent to you within 1 business day.

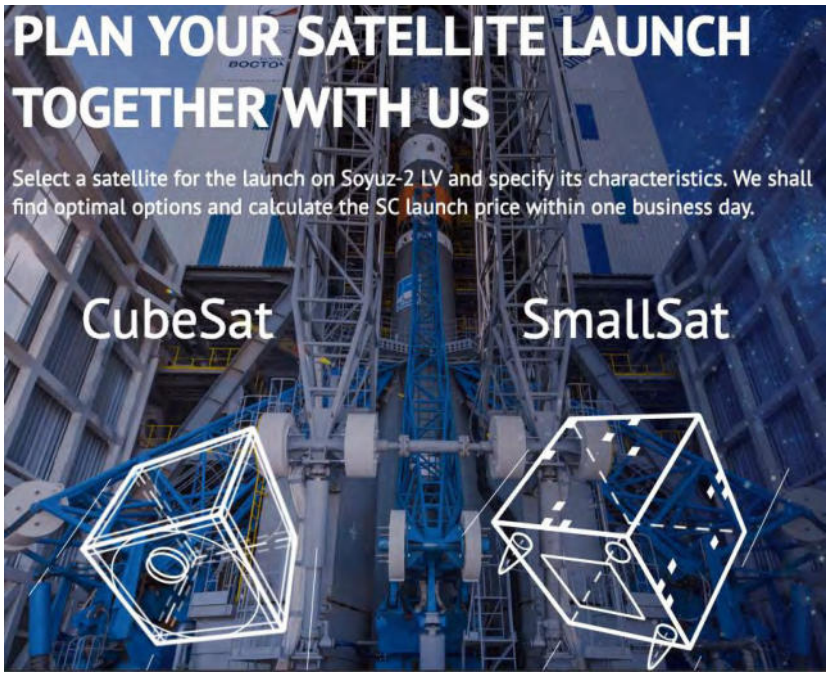

Image 11: GK's online calculator landing page (GK, 2019).

5. UPCOMING LAUNCHES BY GK:

Image 12: Upcoming launches (GK, 2019).

To join our launches, please email us on: sales@gklaunch.ru.

6. CONCLUSION:

We look forward to joining scientists, engineers and managers to exchange information and present new ideas, covering small satellite mission objectives that can increase their access to space!

With the best regards, team of GK Launch Services.

Stratospheric Balloons: low-cost platforms for science and technology development

F. Friedl-Vallon[1], K. Dannenberg[2], P. Raizonville[3], A.Vargas[3]

[1]Affiliation
Karlsruher Institut für Technologie, Kaiserstr. 12, 76131 Karlsruhe, Germany
Phone: +49 721 60824834, Mail: felix.friedl-vallon@kit.edu
[2]Affiliation
Rymdstyrelsen, Hemvärnsgatan 15,17154 Solna, Sweden
[3]Affiliation
CNES, 18 avenue Edouard Belin, 31401 Toulouse, France

Abstract: Stratospheric balloons are useful platforms for various research and technology needs. In particular, they can be used for proof of concept demonstrations in preparation of new space and Earth observation missions. A typical balloon flight duration varies from a few hours to several weeks, depending on the choice of season, launch site and flight trajectory. Payloads can be flown at altitudes of 15-40 km. Stratospheric balloons can be operated at relatively low cost and are characterized by short lead times from the experiment idea to the flight.
The balloon infrastructure project HEMERA is funded by the European Commission within its program Horizon 2020. The major objective of HEMERA is to enlarge the user community of stratospheric balloons within the field of research and technology. The project is coordinated by the French space agency CNES and involves 13 partners from various space agencies and scientific institutions in Europe and Canada. Six balloon campaigns with a target total payload mass of 150 kg are foreseen within HEMERA. These campaigns will offer free of charge balloon flights to users and scientists from various science fields and/or for technology tests. Individual payload masses can vary from less than one kg up to several tens of kg. In addition, several sounding balloon flights are foreseen for smaller payloads of up to 3 kg. The launch sites will be Esrange in Sweden, Timmins in Canada, and Aire sur L'Adour in France.

1. INTRODUCTION

Stratospheric balloons give access to near space between 15 km and 40 km and thus provide a complimentary vehicle to aircraft, unmanned aerial vehicles, rockets and satellites. Balloons offer a less expensive way of observing earth or the universe from above most of the atmosphere than satellites. They provide a slow and stable moving platform which is advantageous for Lagrangian type of atmospheric studies or medium to long term observations of astronomical objects. Balloon flights can be achieved within shorter time-frames than satellites and use the most recent technologies. In addition, most balloon systems and payloads are recovered and can be upgraded to fly again. For all this reasons balloons are an excellent test facility for new space technologies.

Up to beginning of this year, only a few national programs for balloon-borne activities and corresponding facilities existed in the European Union (CNES for France, SNSA for Sweden, ASI for Italy). They were funded by the national agencies and as such were open only to a limited number of scientists and countries (mainly France, Sweden, Italy and Canada). In the past, the scientific community occasionally led joint European scientific projects, as well as balloon activities with the support of ESA for satellite mission validation. However, due to the absence of a joint European balloon program, there was only limited cooperation among technical and research teams on joint development projects or common balloon-related activities.

The HEMERA project aims to improve from this situation (https://www.hemera-h2020.eu/). It intends to build up a European Infrastructure for scientific ballooning and will coordinate, support and enlarge the community in Europe, Canada and associated countries at flight operator, scientific and industrial levels. HEMERA is funded by the Horizon 2020 framework program of the European Union. Partners are space agencies and space access providers, scientific bodies (research centers and universities) and industry.

HEMERA has three major elements: provision of Trans-National Access (TNA) to balloon flights, networking to strengthen and enlarge the user community and joint research (JRA) to improve ballooning technology and scientific instrumentation.

Table 1. Participants in the HEMERA project

Participant	**Organization name**	**Country**
1	Centre National d'Etudes Spatiales (CNES, coordinator)	France
2	Swedish National Space Agency	Sweden
3	Agenzia Spaziale Italiana (ASI)	Italy
4	Deutsches Zentrum für Luft- und Raumfahrt e.V. (DLR)	Germany
5	Canadian Space Agency (CSA)	Canada
6	SSC	Sweden
7	Andoya Space Center	Norway
8	Airstar Aerospace	France
9	Centre National de la Recherche Scientifique (CNRS)	France
10	Karlsruher Institut für Technologie (KIT)	Germany
11	Cranfield University	United Kingdom
12	Istituto Nazionale di Astrofisica (INAF)	Italy
13	Heidelberg University	Germany

HEMERA will coordinate European activities in the field of ballooning in order to provide better and coordinated balloon access to the troposphere and stratosphere for scientific and technological research, attract new users to enlarge the community accessing the balloon infrastructure and foster scientific and technical collaboration and enlarge the fields of science and technology research conducted with balloons. It intends to improve the balloon service offered to scientific and technical users through innovative developments and it will promote standardization, synergy, complementarities and industrialization through joint developments.

2. TRANS NATIONAL ACCESS (TNA)

From the user perspective, HEMERA will essentially provide two services: it offers a possibility to fly small to medium payloads at no cost on CNES or SSC gondolas under Zero Pressure Balloons (ZPB) and sounding balloons (SB). In addition to the flight itself, travels and subsistence for experimenters are funded by HEMERA. The cost for the development and construction of the payload is not included, though. Instruments have to be provided by the scientific organization or the company that wants to use this service.

The second service will be virtual access: the data acquired during those flights will be collected and made publicly accessible on a dedicated web portal, as well as a set of past balloon flight data. This service will be provided by CNRS and INAF.

Access to the balloon flights will be organized through a proposal process with an independent review panel. The proposals shall allow the review panel to judge scientific or technological quality, feasibility, maturity and novelty in science or technology. The proposal process will be executed for the HEMERA consortium by the Swedish National Space Agency (Rymdstyrelsen). The first call is closed and the proposers have been informed, as second call will be issued in December 2019.

Table 2. Timeline of TNA possibilities during the HEMERA infrastructure project

Timeline	**Activity**
July 2018	1. Call for Proposals (closed)
January 2019	Selection of Payloads (1. Call)
Summer 2019	First Flights with SSC from Esrange and with CNES from Timmins
December 2019	2. Call for Proposals will be issued
February 2020	Submission of Proposals (2. Call)
May 2020	Selection of Payloads (2. Call)
Summer 2020	*2. Flight possibilities with CNES and SSC*
From Jan. 2021	*3. Flight possibility with SSC*
Summer 2021	*3. Flight possibility with CNES*

In total six flights with ZPBs for up to 150 kg payload will be performed within the HEMERA project: three flights will be performed by SSC from Esrange near Kiruna, Sweden and three flights will be performed by CNES from Esrange and Timmins in Canada. In addition, 20 flights with SBs for up to 3 kg payload will be performed by CNES from Aire sur l'Adour.

Gondolas will be provided by CNES/SSC. Several instruments will fly on one gondola. Light instruments are preferred to allow more users to fly. All instruments/gondolas will be recovered. Flight levels of up to 38 km and down to 15 km can in principle be accessed. The exact level will depend on total mass of payload and gondola and on meteorological conditions. CNES will fly from Esrange and Timmins in summer only, SSC will provide service from Esrange only but all year round. Service from Aire-sur-l'Adour in France will be offered by CNES all year round but only for SB.

Wind directions in Esrange and Timmins are in early summer to the west and in winter to the east. In the so-called turn around periods in spring and late summer/autumn wind speeds are very low and long flights can be accomplished. This is the favourite time for HEMERA flights. Esrange offers three large buildings for balloon and payload preparation, laboratories, and a clean room. The balloon pad has a size of 450x500m (see fig. 2). The impact area for free falling objects has a size of 5600 km². Timmins is equipped with a building for balloon preparation and a hangar for payload integration.

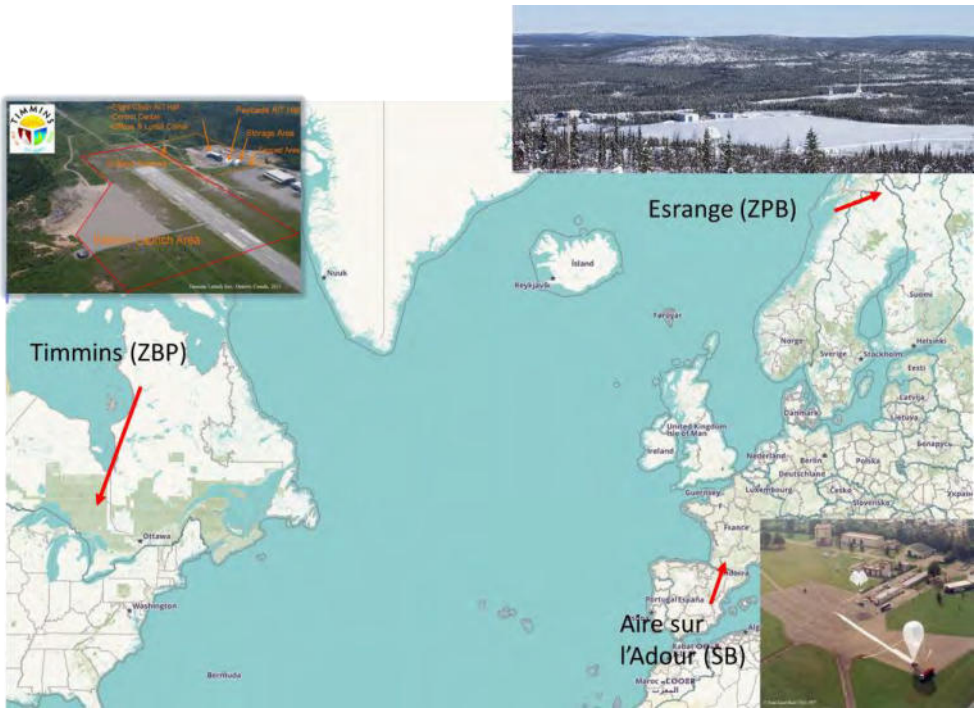

Figure 1. Launch sites for ZPB and SB flights

In the HEMERA "flight ticket", the following services are included: general management and planning of HEMERA flight, provision of launch vehicle and subsystems necessary for a flight mission with recovery, assembly of selected experiments into the payload gondola, pre-flight testing of the payload gondola (TM & TC), provision of laboratory facilities at the Esrange/Kiruna or Timmins launch site, daytime or night-time launch, operations, piloting and recovery of the gondola payload, data transmission with provisions of real time data from payload and disassembly of the experiments from the payload gondola. Optional services during campaign or flight are the provision of meteorological data, and in particular of meteorological soundings. The figures and tables on the next pages provide essential information about the technical boundary conditions of the HEMERA flights. Exhaustive information can be found in the User Manual for ZPB Infrastructure Access[1].

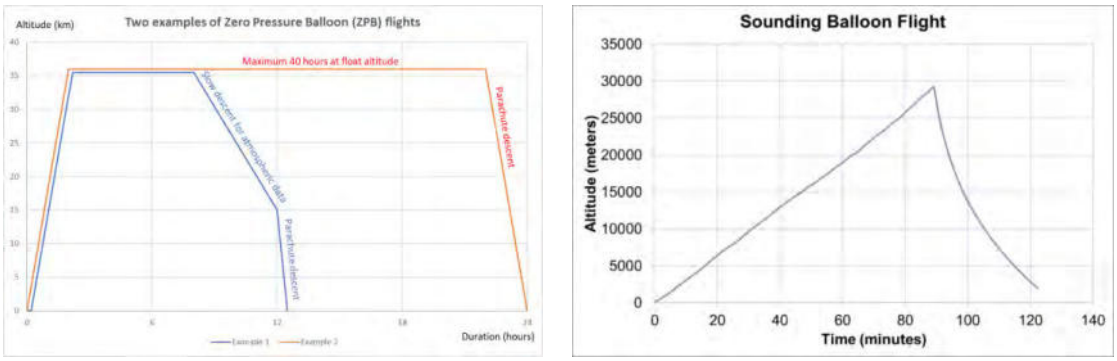

Figure 2: Examples for chronologies of typical stratospheric Zero Pressure Balloon flights and Sounding balloon flights

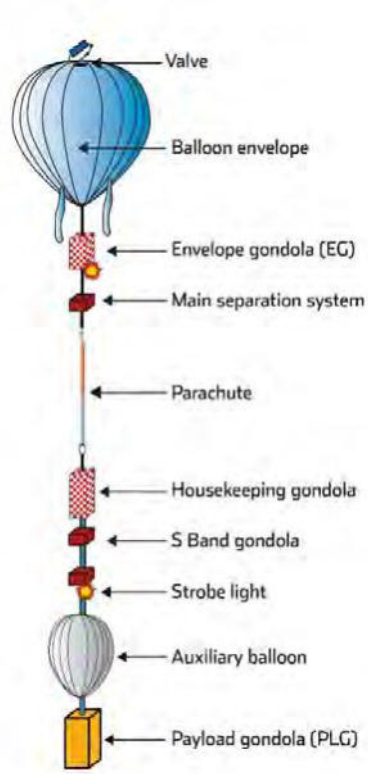

Figure 3. Typical flight configuration for a CNES Zero Pressure Balloon flight. The vertical extension of the whole flight train including balloon envelope is approximately 200 m. The SSC configuration is very similar, but needs no auxiliary balloon.

Figure 5. Launch methods - Left panel: Launch with auxiliary balloon (CNES) – Right panel: Launch with Hercules vehicle (SSC)

Table 3. Characteristics of HEMERA Zero Pressure Balloon flights

	CNES	**SSC**
Zero Pressure Balloons flight characteristics:	Balloon volumes: 150,000 m^3 Flight levels: ~15 km (120 hPa) up to ~33 km (7 hPa) Combined payload gondolas: 250 up to 450 kg Flight profiles: constant ceiling / slow descent Flight durations: up to 38 hours Ascent speed: 5 m/s Slow descent speed: 1 to 5 m/s Landing velocity: 5 to 7 m/s (shock absorbers)	Balloon volumes: 150,000 m^3 Flight levels: ~15 km (120 hPa) up to ~35 km (5,6 hPa) Payload gondola up to 250-450kg (150 kg of experiments included) Flight profiles: constant ceiling / slow descent Flight durations: up to 48 hours during turn around period (spring & autumn – otherwise 4-5 hours) Ascent speed: 4-5 m/s Slow descent speed: 1 to 5 m/s Landing velocity: 5 to 7 m/s (shock absorbers)
Payload requirements for ZPB:	Typically, 150 kg of payload mass per flight Nominally 5 experiments per flight Minimum of 5 kg per experiment Volume constraints in link with gondola sizes	Typically, 150 kg of payload mass per flight Nominally 5 experiments per flight Reserved volume for each Experiment: L x W x H: 500 x 500 x 800 mm^3-
Available gondola (L x l x h)	BANA: 2 m x 0.8 m x 1 m HELIOS: 2.06 m x 1.43 m x 1.44 m CARMENCITA: 2.45 m x 1.85 m x 2,20 m	New gondola under construction: Octagon 1800 x 1800 mm^2 x adjustable height
On-board communication device:	TC max rate: 70 kbit/s TM max rate: 1500 kbit/s 4 asynchronous links: RS232, RS422 or RS485 6 to 10 Ethernet links in UDP or TCP 12 STOR links	2 Mbps duplex nominal, decreasing with range. 10 Ethernet 10/100 Base 2 asynchronous duplex RS-232/422 channels.
On-board optional services	Secured Li-Ion power source: ~- 28 V (up to 1000 W) High performance pointing information (stellar sensor): < 1 arcsec, Pointing rotator: azimuth control < 1 arcmin, axis and elevation control, door opening, actuators, … Thermal monitoring, Date and GPS location, On-board cameras, On-board accelerometers	Relays for external use - on/off, upon request Accelerometer upon request

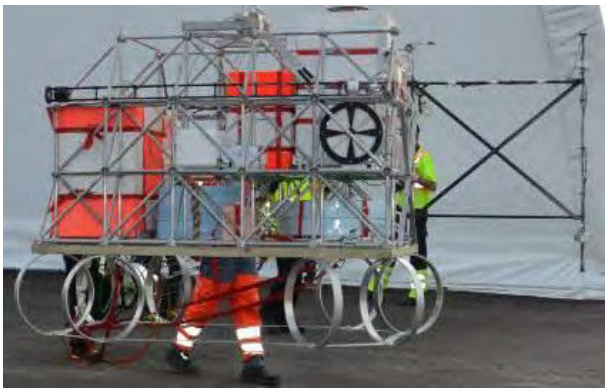

Figure 5: CNES HELIOS gondola.

3. JOINT RESEARCH (JRA)

In parallel to the TNA activities, JRA shall prepare improved services for the future. Activities encompass the development of a light weight flight train, of a telemetry system for the users based on satellite communication and of larger balloon envelopes. In addition the launch methodologies will be simplified.

The light weight flight train will offer simpler and cheaper flight opportunities for lighter payloads. It will be developed through adaptation of the existing flight train for superpressure balloons. It will be optimal for payload gondola masses between 20 kg and 150 kg and for balloon volumes of 5 000 m3, 12 000 m3 and 35 000 m3. It shall support flight duration from hours to one week. Control of balloon and payload will be primarily accomplished with satellite communication (Iridium).

On the scientific side the definition and development of a set of lightweight innovative instruments (SLII) to provide key atmospheric data for users of the Trans National Access is a key activity. SLII shall provide essential climate variables like pressure, temperature, wind, concentrations of ozone, water-vapor, methane, carbon dioxide, aerosols complemented by altitude and Gamma-ray atmospheric background information. Instruments will be calibrated/validated in atmospheric chambers so they can serve as reference instruments. Visualization and interpretation software will be provided for SLII instruments and for atmospheric data generated by balloons in general. A complementary scientific activity is the search for synergy options and common tools for the infrared hyperspectral imaging technique at European level as preparatory work for future balloon and satellite missions.

4. CONCLUSION

HEMERA is an effort to set up a European infrastructure for stratospheric balloons. It shall provide a long term perspective for science and technology development relying on this platform. In short term perspective, HEMERA will provide trans-national access to European users from science and industry and will thus extend the existing national user communities. In long term perspective, HEMERA will perform groundwork to extend the opportunities stratospheric ballooning can offer and to achieve better cost effectiveness.

5. REFERENCES

HEMERA User Manual for ZPB Infrastructure Access https://www.hemera-h2020.eu/opportunities/call-for-proposals

Global launch booking system: why it is time to go online

Ksenia Lisitsyna[1], Andrey Maksimov[2]

[1]Precious Payload Inc.
251 Little Falls Drive, Wilmington, New Castle County, Delaware 19808-1674
Phone: +79052117522, Mail: ksenia.lisitsyna@preciouspayload.com

[2]Precious Payload Inc.
251 Little Falls Drive, Wilmington, New Castle County, Delaware 19808-1674
Phone: +971 55 2262337, Mail: i@andrey-maximov.com

Abstract: Despite an image of a cutting-edge technology industry, space sector has felt the impact of IT boom to a lesser extent. Precious Payload is an initiative started in late 2016. Its goal is to design, build and promote an open standard for orbital launches booking. It is a system similar to Expedia but for smallsats less than 500 kg. The company supports the idea that space sector can follow the path of travel industry. In the core of the booking platform is a GDS – global distribution system – architecture. It is a computerized network system that enables transactions between various market players and provides pricing, availability and reservation functionality. At the moment, Precious Payload is offering several services for the companies on different launch campaign stages starting from preparing a feasibility study to making the first launch arrangements.

1. INTRODUCTION

For the past seven years, space market has been developing at a tremendous speed. New satellite operators and private launch providers have been joining governmental agencies on the way to making space commercially effective. Space business is growing, and the space industry must adapt using new tools and methods. Inability to exchange the information on the growing market using the traditional methods that had been effective twenty and even ten years ago brought up a number of problems including significant launch delays, lack of pricing transparency, rebooking options and information about rideshares availability. Industry 4.0 movement has already started influencing space sector and we are going to show why platform economy is a solution to the key problems that modern launch providers have when it comes to rideshare management and occupancy rate for their launch vehicles.

2. CHANGES PREMISES AND THE MARKET

We have missed our chance to create a space economy back in the Apollo days, but it seems that today we have been given a second opportunity. We have defined four major trends that make us believe in the sustainable future of business in space. These trends have formed the environment necessary for private industry to pick up what was in the last century considered to be the governmental work and bring it to the general public.

- The introduction of a standard CubeSat form factor and the development of venture class launch vehicles has lowered the entrance barrier to the industry
- This year a new standard called Launch Unit has been introduced by the Aerospace Corporation [2]. This standard will help midsized payloads to avoid the launch bottleneck and get affordable launch to space.
- Upcoming mega-constellations of the satellites will also increase the demand in timely rideshare and dedicated launches.
- The return of heavy-lift launch vehicles and the perspectives of the lower costs have given the second birth to the bigger payloads. Now, when the launch prices

tend to decrease, missions that are including bigger satellites have more chances to be pulled off by private companies.

Lower entrance barriers and sustainable approach open space industry and market for both technological downstream and using the experience of other industries.
Fig. 1 is showing the forecast for the number of smallsats ready for the launch for the next five years and the growing launch capacities. According to an expected trend, we can expect the prices for the launches going down which makes significant changes possible [1]. According to our analysis it will be up to eighty launch providers in full operational mode by 2021. Most of them will be managing venture class launch vehicles and will be based in the countries we tend to consider space faring nations. This kind of oversupply on the launch services market creates the need to aggregate clients without regional limitations. Some of the launch providers have already started investing in online booking systems (Fig. 2), several companies are working on the online marketplaces where launch providers can market their capacities.

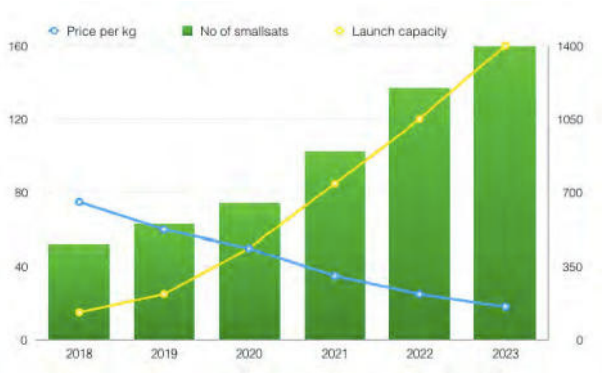

Figure 2. The balance between launch capacity, number of satellites and launch prices

Figure 1 Examples of online booking interfaces

3. TYPICAL LAUNCH BOOKING PROCESS

Typical workflow for launch booking process can be slightly different but usually it is consistent with the following steps:

Step 1: general request and preliminary research, gathering of all possible commercial offers, contacting all commercial players available: 45-100 days;

Step 2: confirmed commercial offer/binding quote based on technical information provided by SO: 30-60 days;

Step 3: time required for a broker to get the final offer with the consideration of primary payload contracted for the launch: 20-40 days.

All in all, it will be more than 200 days or 6 months without insurance procurement. That is the scenario when both launch provider and satellite operator fulfill their agreements according to the schedule and do not change the conditions or requirements.

4. WHAT IS WRONG ABOUT IT?

Traditional approach to the launch slots marketing has a number of pain points that are limiting mission planning and expansion of space related activities:

- No guarantees for launch in case the LP is not ready or has to postpone the launch;
- Launch campaign easily spans for 12-18 months;
- Pricing is not transparent;

• Rebooking to other launch providers is not possible;
• No information on possible rideshare opportunities;
• Business development is based on networking, conferences, public talks and is purely scalable for launch providers.

As the result rockets often fly half-empty and launch providers are losing their revenue; satellite companies go bankrupt because of delay; prices do not go down; new players have a high entry barrier. Satellite companies have already lost more than $140M because of the launch delays. Up to 38% of launch capacity on the modern launch vehicles is not utilized. Up to 30% of secondary payloads lose their slots because they are not ready for the launch. Those who missed the window of opportunity had to quit or play a difficult catch-up game.

The New Space economy means new ways of doing business. Opening the High Frontier requires us to rethink current models of what it takes to launch a satellite to space. We have seen not that long ago that whole new markets were born when businesses realized the potential of the Internet and online commerce.

5. PRECIOUS PAYLOAD SOLUTION

5.1 GDS is saving the travel industry in the 90s

A global distribution system is a computerized network system owned or operated by a company that enables transactions between travel industry service providers (mainly airlines, hotels, car rental companies, and travel agencies). The GDS usually uses real-time inventory (for e.g. number of hotel rooms available, number of flight seats available, or number of cars available) to service providers [4]. Travel Agencies traditionally relied on GDS for services, products and rates in order to provision travel-related services to the end consumers. Thus, a GDS can link services, rates and bookings consolidating products and services across all three travel sectors: i.e., airline reservations, hotel reservations, car rentals.

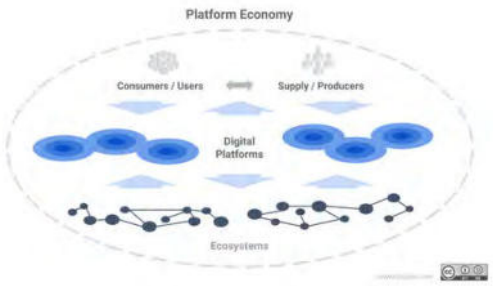

Figure 3 Platform economy ecosystem

5.2 How can we use it in space industry?

Lowering the cost of launching to space is crucial to lift the economy off-Earth. We rely on new private players to solve this problem, but if these pioneers do not get enough traction and disappoint their investors, the bubble will burst, and we will remain grounded.

Precious Payload is building a product that allows launch operators manage their manifest and rideshare slots via the system in real time. Clients with satellite missions are able to browse and reserve the slots, with special algorithms helping find the suitable launch opportunities by running the analysis over a number of technical and business constraints.

The business model suggests creating a portfolio of value-added products to be offered via the e-commerce platform together with launch services. The first such added value product is the procurement of insurance for smallsats. Partnership with AON enables

Precious Payload to develop a first of its kind platform that allows to see real-time insurance quotes for different launch options and procure the insurance without leaving the website.

All of the above, and much more, will eventually become a reality. It has happened in cargo shipment, airlines, car rentals, and the hotel booking industries. When the amount of inventory and volume of concurrent bookings becomes high, there is the need to create a separate, independent architecture that will manage availability. It may seem early with the current amount of rocket launches per year but shall become a reality when three to five companies, with 50–100 launches each carrying 3–12 small satellites, enter the market [3].

A global distribution system is a well-known concept of an industry standard that manages the inventory available on carriers. The space launch market is becoming mature enough to benefit from such a system. At Precious Payload, we believe that developing an industry-wide launch booking system is a key concept necessary for creating a sustainable private space launch economy for smallsats.

5.3 RFQ exchange system for early adopters.

As a first step towards the standardized exchange of information we have created a system where payload owners can send requests for quotations for their missions to all the launch providers, we have an agreement with, and get a proposal without any need to search for contacts, do networking, spend money for conferences. Even though the system looks very simple, it's a powerful tool for organizing a free flow of information at the market.

We are currently collecting requests from all types of satellite operators including commercial satellite operators, universities, research institutions.

5. CONCLUSION

Platform economy is a proven solution that has already being used in various sectors and it will enable fast feasibility analysis, efficient management of launch campaigns, rideshare management tools and transparent pricing for the whole market. We believe that changing the perspective of the launch booking process from networking to standardization will make the launch booking process better controlled and forecast. The ability to get in touch with the majority of launch providers in one ecosystem is already shifting the perspective and it is the first step to make future possible.

6. REFERENCES

[1] C. Niederstrasser, Small Launch Vehicles – A 2018 State of the Industry Survey. Published by the Utah State University Research Foundation.

[2] https://aerospace.org/launch-u, (accessed 15.09.2018)

[3]A.Maximov, Orbital bookings. Published by SpaceWatch.global, 2 September 2017.

[4] What is global distribution system (GDS)? Definition and meaning. Businessdictionary.com. Retrieved on 2013-08-20.

TriasRnD.com – Testing. Simplified.

Stefan Schmidt

TriasRnD.com
‘s-Gravendijckseweg 41b, 2201 CZ Noordwijk, The Netherlands
Mail: stefan@triasrnd.com

Abstract: With the growing number of industrial actors in the space and high-tech industry, the number of products and services required for creating a spacecraft is increasing. In addition to that, the mission, scientific and commercial objectives are becoming steadily more ambitious. Stronger competition, faster lifecycles and an increasing cost pressure are asking for higher reliability while system engineers are challenged as never before in the space industry. The result: a new quality of complexity, especially true for SME’s.
As a response to that, ***TriasRnD.com*** was founded to simplify as far as possible tasks in the space industry; to reduce complexity and to allow space companies and institutes to share their resources in a simple, faster and much more efficient and convenient way. TriasRnD.com is an online tool allowing to search, filter and directly contact external testing services in the space and high-tech industry. By accepting only active service providers, which offer a commercial service to external clients, high quality and short response times, which are core of the philosophy of the platform, are ensured. Or in short: Testing. Simplified.

1. INTRODUCTION

Without doubts our world has a lot of problems and of course *Trias* cannot solve all the problems. But it can start to try to make the world better, a little bit every day. One challenge we are facing is digitization combined with a steady growing complexity of our daily life. Don't you have the feeling too, that the engineering tasks are becoming more complicated and not simpler anymore?

Especially in high-tech sectors like the space industry, where design iterations are very costly and everything has to be optimized: time-to-market, costs, reliability, political aspects, resources, and many more, complexity becomes the highest risk for space projects. I believe that research and development can become simpler again. We have the tools available today. We just have to use them in such a way that we simplify processes and tasks, reducing complexity, increasing transparency and helping engineers to let them again do what they are best in: solving problems.

Figure 1 TriasRnD.com

TriasRnD.com was founded with the mission to simplify the "testing world" of the high-tech industry such as the space industry. Testing does not have to be complicated by definition, especially the organization and optimization of test campaigns. But people are overloaded with administration, in-transparency and the selection of the right facility, the right time as well as shifting schedules. Thus, for test facilities and for engineers, I believe that there is a simpler, a more convenient, more elegant and last but not least a more cost-efficient way.

2. MADE FOR SME'S

System and test engineers need a faster, more cost-efficient and flexible way to identify, filter and book the most suitable test facility for their development or operational project. Often the engineer does not have the right test facility in-house or the facility is not available in time, or the facility is large and too expensive for the verification budget. TriasRnD.com offers an easy way to search, filter and ask for a quote of alternatives.

On the other hand, *test facilities* are very expensive to operate and maintain (recurring costs for staff, equipment, calibration). If a facility is not used for 100%, then the specific cost per test increase. The facility manager often does not have the capacity for reaching out to additional external customers to fill the gaps in his test schedule. This is especially true for smaller test houses and laboratories. TriasRnD.com offers an easy way to present the facility to the space community and to simplify the booking process.

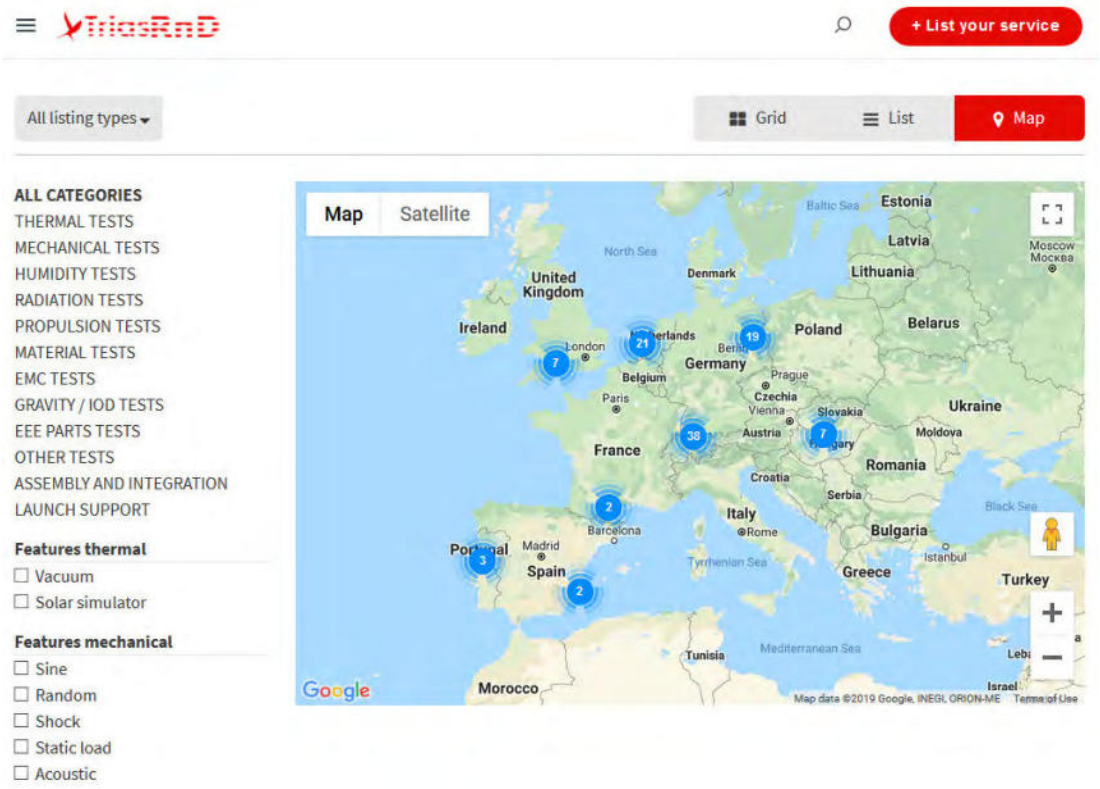

Figure 2 Companies and Institutes on TriasRnD.com (2019-01-30)

SME test houses and hardware manufacturer do not have the same resources as the large corporate companies in the space industry. By bringing test houses and manufacturers together on one platform, both parties gain a high visibility in the industry and more importantly get a tool to behave like a procurement section of a larger corporate company when it comes to trade-offs and test campaign organization.

Until today, more than 21+ companies with more than 100+ testing services are active on the TriasRnD.com platform, most of them from Europe, e.g. RUAG Space Switzerland, DLR, Tesat-Spacecom, Astro- und Feinwerktechnik, Sonaca Space, Fraunhofer INF, German Orbital Systems, PLD Space, Swedish Space Corporation (SSC), ZARM Test Center, and many more.

3. THE PLATFORM AS A DAILY TOOL

The platform is built for engineers to simplify their work. To keep the database up to date, the test service providers are self-responsible for their own content, which means, that they create their own account and maintain their listings. They can open, change, close and reopen listings, e.g. in case of a facility upgrade.

3.1 Categories

The different test services are listed in predefined categories, based on the ECSS-E-ST-10C, like:

- *Thermal Tests* incl. thermal cycling in ambient and vacuum with or without solar simulation
- *Mechanical Tests* incl. sine and random vibration testing, as well as shock and pyro shock testing, static load and acoustic testing
- *Humidity Tests* with different climate chambers also able to do thermal cycling, with preprogrammed humidity loads

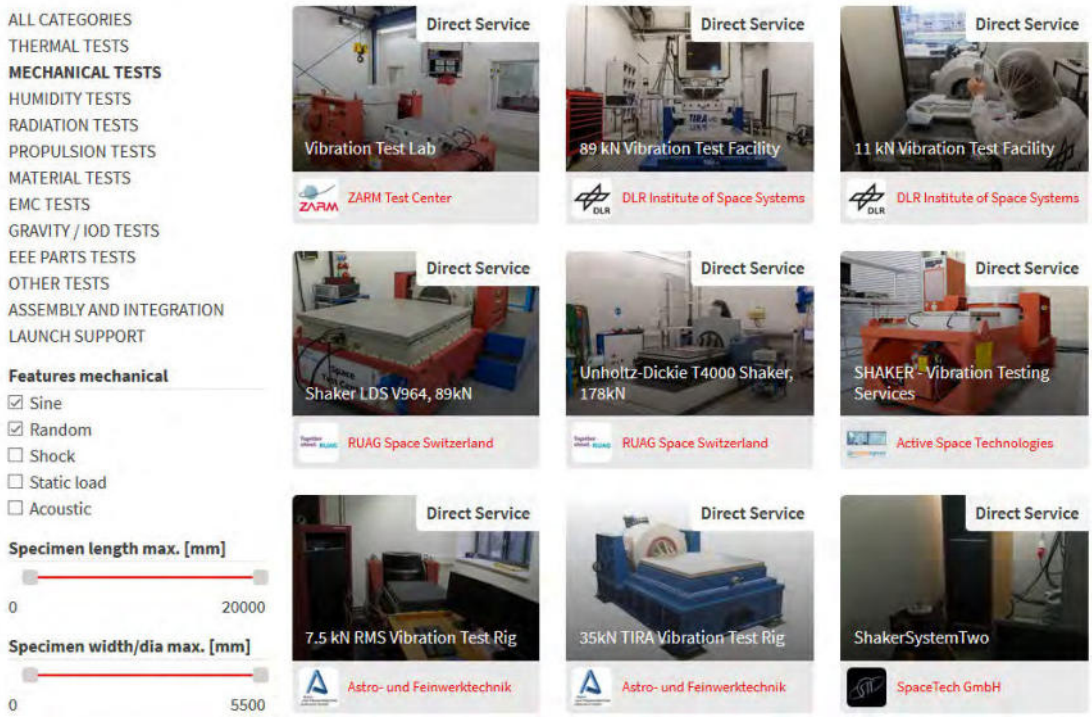

Figure 3 Selection of Mechanical Tests with filters applied on TriasRnD.com (2019-01-30)

Other categories have emerged from user feedback and requests, like e.g.:

- *Radiation Tests* incl. TID and VUV testing
- *Material Tests* incl. e.g. outgassings tests, spectrometer measurements, CTE tests, tensile and hardness measurements, X-ray and optical microscopy and also ultrasonic testing

- *Gravity / IOD* Tests incl. centrifuge testing, sounding rocket flights, on-orbit verification and microgravity testing

Not described in detail here are EEE Parts Tests, EMC Tests and other services.

3.2 Filter

Further, it is possible to filter the service listings by predefined key parameters, like the maximum specimen length, width, diameter and height, as well as for the maximum allowed mass for each test facility if applicable. Some filter parameters are only set up for dedicated categories. For example, lower and higher temperature ranges are filters for thermal tests and different accelerations can be filtered for mechanical (vibration) tests. For test services that are provided in a cleanroom environment, the required clean-room classes according to ISO 14644-1 can be selected, allowing the user to filter for them as well. Radiation services can be filtered by their source, e.g. electron, gamma, proton, UV.

3.3 Price and Availability

After the user has created a free account, it is possible to get directly in contact with the test service provider via the TriasRnD.com platform. Using the internal messaging system as a shortcut for requesting the price and the availability, an email is sent from the platform directly to the responsible of the test laboratory. If the test provider replies, then an email is sent back to inform the user.

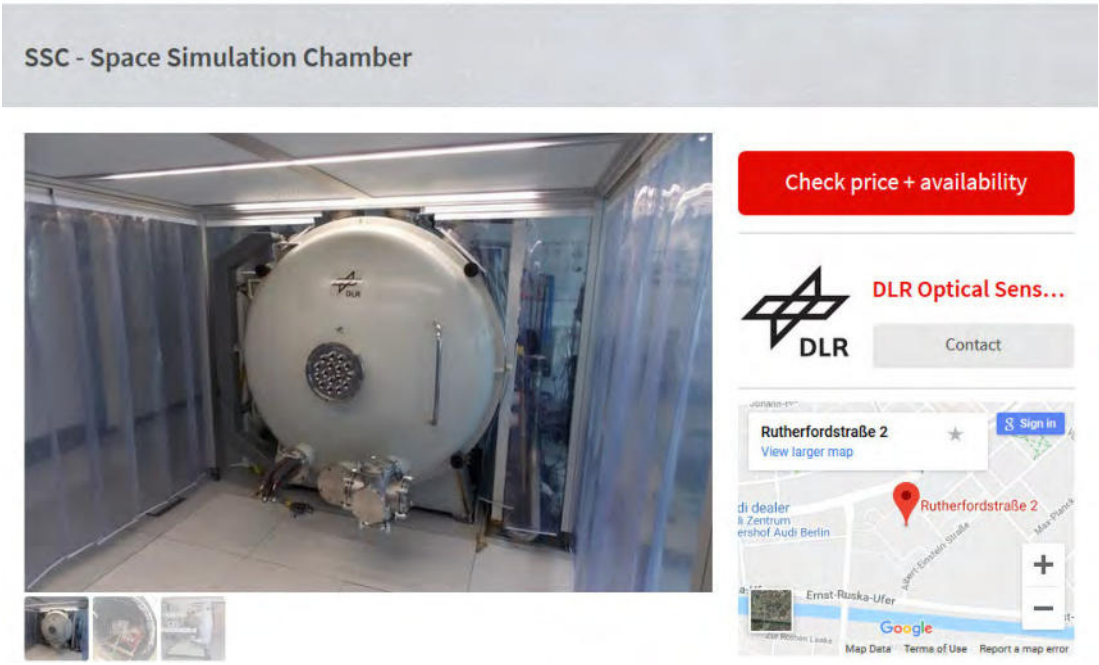

Figure 4 TVAC chamber from DLR (2019-01-30)

4. CONCLUSION

TriasRnD.com is an online tool for engineers that enables the space industry to collaborate in a smarter and more efficient way, while creating a common place to look for test

facilities and services with the goal to reduce complexity, to simplify our daily work and finally to make the world a little bit better.

PAPELL: Mechanic-free Actuators through Ferrofluids

Manfred Ehresmann[1,2], Franziska Hild[2], Kira Grunwald[2], Christopher Behrmann[2], Robin Schweigert[2], Martin Siedorf[2], Adrian Causevic[2], Saskia Sütterlin[2], Nicolas Heinz[2], Daniel Bölke[2], Georg Herdrich[1]

[1]Institute of Space Systems University of Stuttgart
Pfaffenwaldring 29, 70469 Stuttgart, Germany
Phone: +49 711 685-69599,
Mail: ehresmann@irs.uni-stuttgart.de, herdrich@irs.uni-stuttgart.de

[2]Small Satellite Student Society KSat e.V., University of Stuttgart
Pfaffenwaldring 29, 70469 Stuttgart, Germany
Mail: projektleitung@papell.ksat-stuttgart.de

Abstract: PAPELL is a technology demonstration experiment that has been conducted on the ISS. It utilizes magnetic fields and a magnetisable liquid - ferrofluid and is a non-mechanical actuator. This principle can be exploited to move individual ferrofluid droplets, air bubbles and solids within dedicated experiment areas to demonstrate the capabilities, potential and limitations of this non-mechanical pump. It is expected that highly-reliable, long lifetime, low wear and tear mechanisms can be developed through the exploitation of the principles behind the PAPELL experiment. Concepts for future non-mechanical actuation applications based on ferrofluid interaction are briefly discussed.

1. INTRODUCTION

The student experiment “Pump Application using Pulsed Electromagnets for Liquid re-Location" (PAPELL) on the International Space Station reiterates the initial idea of the ferrofluid inventor S. Papell [1, 2]. His aim was to develop a magnetisable rocket propellant, which can be drawn to a combustion chamber with a strong permanent magnet. This would make large, cumbersome and highly-mechanical turbopumps obsolete. Unfortunately, the addition of incombustible particles in the form of iron oxide particles to a propellant generates significant thermodynamic challenges. Nonetheless, ferrofluids can be utilised for creating non-mechanical actuators useful for many applications in space and on Earth.

A ferrofluid is a super paramagnetic liquid. Magnetisable nanoparticles of approximately 10 nm size coated with an anti-coagulant are suspended in a carrier fluid. Ferrofluids often consist of iron oxide particles, and hydrocarbon-based carrier fluids. Such ferrofluids are long term stable and do not suffer from evaporation, sedimentation or other degradation effects. By applying a sufficiently strong external magnetic field, the iron oxide particles align themselves according to the applied magnetic field lines. By this, the iron oxide particles become attracted to the strongest point of the magnetic field source, which moves the particles and surrounding carrier liquid.

A series of electromagnets can be utilised to produce local magnetic field sources, which allow to transport individual ferrofluid droplets without mechanical interaction. An example illustration of a transport process from one electromagnet to the next is given in Fig. 1. A notable bridges forms during the transport process, as the vector to the centre of the electromagnets is the line of highest magnetic field strength.

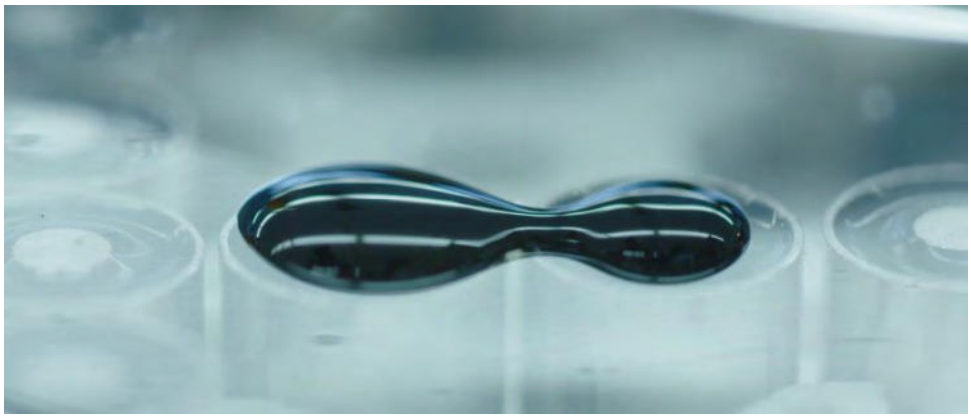

Figure 1 Laboratory model experiment: Non-mechanical ferrofluid droplet transport from one inactive electromagnet to another active electromagnet [3].

Removing mechanics from a system, especially for space systems, is overall desired for any engineering discipline. Mechanisms are a system liability with respect to fault probability and lifetime limitation. Thus, mechanisms shall be avoided generally. If mechanisms are a necessity their shortcomings need to be mitigated with significant development and qualification effort, which drives overall costs. By using mechanisms that function on magnetic interaction, rather than conventional solid body interactions, high-reliable low-cost solid-state devices can be developed. The technology demonstration experiment PAPELL proofed the capabilities of a solid-state pumping device [4].

For space flight in particular high-reliable, minimal maintenance and low cost technological solutions are in high demand. The cost of any mechanism to be operated on a spacecraft is significant, as functionality, reliability and durability have to be demonstrated by respective qualification procedures and materials of high quality have to be utilised. Nonetheless, the number of mission failures due to mechanical issues is not zero. Thus, the application of conventional mechanics is always a liability to any mission success. Removing the mechanical aspects and transitioning to solid-state devices allows for higher reliability, faster development und lower overall costs, as qualification and material tolerances can be realised simpler.

2. Experiment Setup

The PAPELL experiment on the ISS is housed within a DreamUp NanoLab [5] of 10 x 10 x 15 cm³ volume. As single external interface a USB-B is given, which serves as power and data link. The experiment operates autonomously, with the option for remote commanding, updating and upload of new experiment instructions. The final assembly of

Figure 2 PAPELL Flight model prior to final close-up and sealing for ISS operation[6, 7].

the experiment is given in Fig. 2, which illustrates the compactness of the design. The experiment consists of two dedicated experimental areas, with distinct experiments to be performed. Conducted experiments are observed visually and data on occurring magnetic fields, temperature, vibrations and noise levels are recorded.

Initially ferrofluid is stored in two separate bladder tanks, connected to a single fault tolerant feeding system. One of two membrane pumps is used to draw ferrofluid from one bladder tank and feed the designated experimental area. Controlling the valves of the systems allows each tank to fill each experiment area separately.

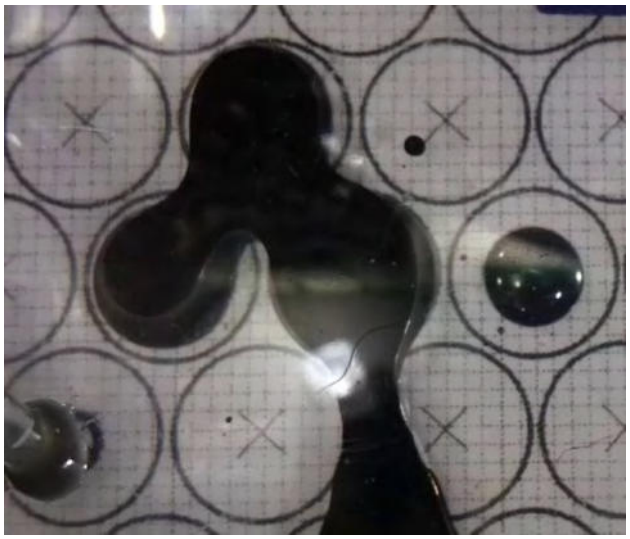

Figure 3 PAPELL Experiment area 1 in-orbit example footage: Transported ferrofluid on multiple active electromagnets and a single separated droplet. A circle has a diameter of 10 mm.

For experimenting on the ISS the utilised ferrofluid has been classified as hazard level 2 liquid, requiring multiple layers of containment. Three distinct layers of containment have been implemented within the experiment. The first layer of containment is the outermost NanoCube shell provided by DreamUp. The second layer of containment is 3d printed polyamide housing sealed with commercially available silicone. The third layer of containment is the feeding system and the connected experimental areas. To allow for pressure relief, of the experimental areas and to allow for relaxation of the bladder tanks membranes have been implemented in strategic positions. These allow relief between containment layer two and three. The membranes are only passable by air and have been tested to be sealing for ferrofluid.

2.1 Experimental Areas

PAPELL contains of two experimental areas. First, an area with a free movement grid containing 37 electromagnets in a hexagonal pattern has been implemented. Ferrofluid is permitted here to flow freely between activated electromagnets. This area is dedicated to basic experiments of ferrofluid manipulation and interaction. An example of an experiment conducted in this area is given in Fig. 3.

The second experimental area is a constrained system, where electromagnets are used to transport ferrofluid droplets within a rectangular pipe system. Within the limited operational time successful experiments where only conducted in the first area. Planned experiments of area two will be part of post-flight experiments.

As ferrofluid contains iron oxide nanoparticles, which are inherently black and can be captured by any minimal surface roughness it tends to strongly stain most surfaces. This effect would hinder optical observation severely. To mitigate this a super hydrophobic and oleophobic coating was applied to all surfaces in contact with ferrofluid. The coating is a nanostructured PTFE (Teflon) called “Flouropor” [4], which allows for fully repelling the utilised ferrofluid “APG13” commercially available from Ferrotec. In experimental

area 1 a marking grid for enhanced visual analysis is implemented above the electromagnet grid and below a Flouropor coated top foil.

2.2 Preliminary Results

The in-orbit experiments of PAPELL experiment area 1 have been a success. The conducted experiments allow to obtain a proof of concept. The following processes were repeated achieved in the microgravity environment of the ISS.

1. Ferrofluid droplet generation
2. Ferrofluid droplet transport
3. Ferrofluid droplet splitting
4. Ferrofluid droplet merging

These four processes are the basic conditions required for a digital microfluidic circuit [3] indicating versatile applications.

Furthermore, the transport processes required significantly less time in comparison to Earth based experiments [8] and the ferrofluid behaviour was well reproducible. No degradation effect was observed. Occurring magnetic fields are marginal and other disturbances (i.e. vibrations, noise), have been measured to be below detectable noise levels [8].

Further, the experiment showed that in a microgravity environment the consideration of adhesion to walls, as well as the cohesion and surface tension of ferrofluid are major factors that drive the dynamic behaviour.

Multiple modes of ferrofluid transportation between active electromagnets have been observed. The most simple transport mode is ferrofluid in the vicinity of an active electromagnet, which is drawn to the centre of said electromagnet. This transport mode was not as reliable as initially assumed. As ferrofluid would need to become very near to the outer boundaries of the utilised magnets as the outer iron shell does locally confine the magnetic fields very well.

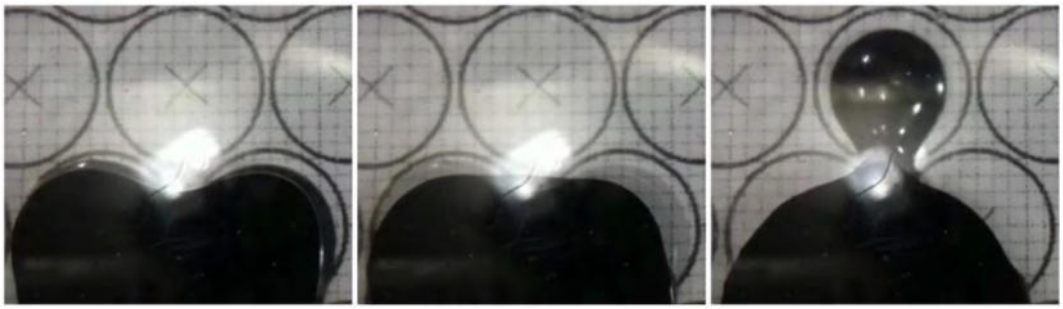

Figure 4 PAPELL Experiment area 1 in-orbit example footage: Overspill transfer example. Frame 1: two lower electromagnets are active, negative curvature bridge in between. Frame 2: Negative ferrofluid curvature relief, top electromagnet active Frame 3: Transfer of ferrofluid.

The second transfer mode observed on the ISS is driven by surface tension, which allows for a successful “overspill” transfer, once electromagnets are no longer operated. This is illustrated in Fig. 4. Here two active electromagnets concentrate ferrofluid onto each

other, and a bridge forms between the two centres resulting in a negative curvature of the ferrofluid surface. Once the attraction of the two initially active electromagnets is removed, the now classical fluid tries to minimize its surface energy by obtaining a minimal positive curvature. Thus, the negative curvature ferrofluid bridge bulges out and spills over the boundary to the active top electromagnet. This transport mode proved to be highly reliable and was frequently utilised to initialise the ferrofluid position for further experiments.

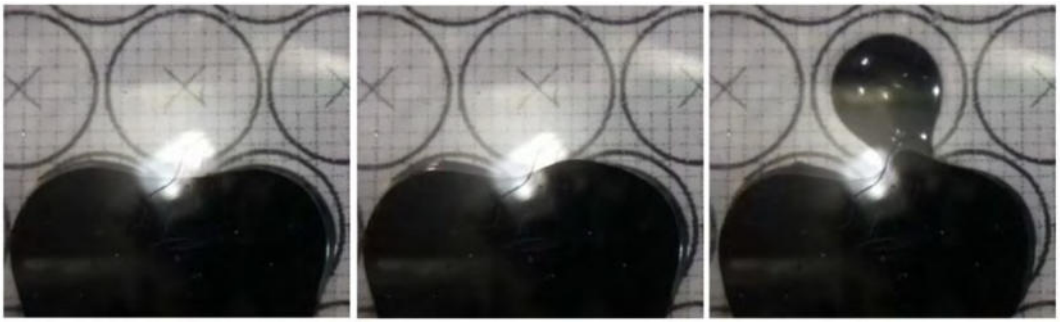

Figure 5 PAPELL Experiment area 1 in-orbit example footage: Polarity transfer example. Frame 1: two lower electromagnets are active, negative curvature bridge in between. Frame 2: Top centre electromagnet additionally active, forming of an S-bridge Frame 3: Transfer of ferrofluid between electromagnets of opposing polarity.

A third mode of ferrofluid transfer was observed on the ISS. This requires at least two active electromagnets of opposing respective polarity. Similar to permanent magnets, the magnetic fields lines of for example two opposing north poles do not connect and will diverge from each other forming a line of minimal magnetic field in the terminator between. Here the flow of ferrofluid would be hindered, as ferrofluid always tends to flow to a maximum of the magnetic field. While the field lines of a north and a south pole of a permanent magnet would connect and form a bridge of uniform magnetic field strength. Thus, magnetic field polarity can be exploited to generate barriers and flow paths for ferrofluid. In Fig. 5 this process is illustrated. Initially only the lower two electromagnets are active, which happen to have opposing polarity. When the third electromagnet in the top centre is activated as well, the assembly of magnetic fields form a barrier from left lower corner to the top and a bridge from the right lower corner to the top. The second frame shows the initial formation of an S-shaped bridge, which then allows the full transfer of ferrofluid. The polarity driven transfer has been observed to be the fastest of the three ferrofluid transport modes.

3. APPLICATIONS

The PAPELL experiment successfully demonstrated that reliable, repeatable manipulation of ferrofluid through magnetic fields is feasible in a microgravity environment. Future mechanic-free applications range from simple (e.g. valves or thermal and electrical switches) over advanced (e.g. generic pumps and attitude control systems) to complex systems (e.g. electric/magnetic propulsion systems).

Simple concepts require only a single droplet of ferrofluid that is transferred from an initial to an operating position. In the case of a mechanical switch or valve, a droplet can be utilised to block a path. For the cases of electric or thermal switch a single droplet can

be used to short circuit two electrical contacts or heat exchangers. Alternatively, secondary working fluids can be manipulated through ferrofluid interaction to achieve the desired physical effect.

A generic pump is a pump that is indifferent to the medium to be transported. By using a ferrofluid droplet as a “liquid piston” arbitrary (states of) matter can be transported, with the requirement that the transported medium does not negatively interfere with ferrofluid properties itself. For example, a simple piston pump similar to a membrane pump can be realised with ferrofluid, as two ferrofluidic valves are required and a single oscillating ferrofluid droplet can be used to generate a pressure gradient within the device.

A simple attitude control system can be produced by transporting ferrofluid in circular pipe systems. The amount of angular momentum stored by this way is small. Nonetheless, spacecraft attitude and to a limited degree rotation rates can be adjusted.

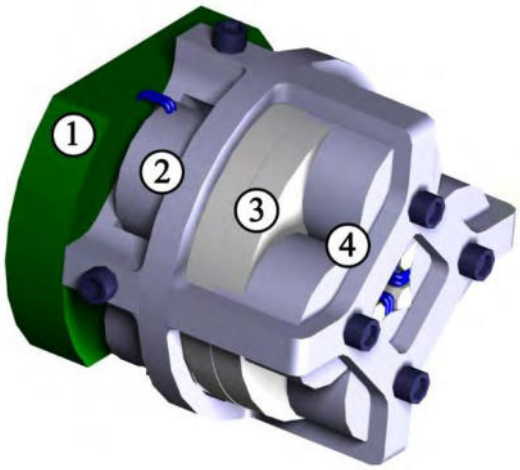

Figure 6 Preliminary Ferrofluid Attitude Control System CAD model. (1) Controlling PCB. (2) Group of four Electromagnets (3) Ferrofluid containing racetrack (4) Group of four electromagnets. The prototype has a length of 51 mm and a diameter of 55 mm.

A preliminary CAD model of a ferrofluid attitude control system is given in Fig. 6. The minimal size system requires at least four electromagnets with full polarity transfer capability. Thus, the polarity of each electromagnet has to be fully controlled through appropriate circuity. In the case of the preliminary CAD in Fig. 6, two groups of four electromagnets are implemented allowing for direct transfer and polarity transfer operation capabilities. Optimal operation will be part of future prototyping effort.

In the current setup, up to two separate droplets of ferrofluid can be actuated. The capability to store rotational momentum of this attitude control system can be enhanced by using a secondary high-density liquid that does not degrade or mix with ferrofluid and is non-magnetic.

It can be assumed that such a system is significantly cheaper to produce and qualify in comparison to reaction wheels, as the required components are commercially available. The system is independent from external magnetic field allowing application in orbits, where magnetorquers can no longer be utilised.

4. OUTLOOK

The obtained in-orbit experiment data of PAPELL is going to be analysed in greater detail. Especially ferrofluid behaviour in microgravity with relation to its viscosity, surface tension, magnetic saturation, magnetic field polarity interaction and direct interaction with the utilised electromagnets. Furthermore, experiments successfully conducted on the ISS are to be repeated with the flight hardware on Earth and follow-up experiments are to be performed. This data will be exploited to drive the follow-up prototype and hardware development with the aim of future space application.

5. ACKNOWLEDGEMENTS

The PAPELL project was made possible by the "Überflieger" competition of the German Aerospace Center (DLR) [5, 9] issued in early 2017. The submission of "PAPELL" was among the three selected German student experiments that have been granted a 30-day operation phase on the ISS. Experimenting, analysing, designing, procuring, manufacturing and assembling was achieved by a dedicated team of the Small Satellite Student Society of the University of Stuttgart (KSat e.V.), who were able to deliver the payload for final inspection and manifesting in less than one year after the competition selection.

The "Überflieger" competition was made possible through a partnership between DLR and DreamUp, working in conjunction with NanoRacks, LLC and its Space Act Agreement with NASA. It is funded by the Federal Ministry for Economic Affairs and Energy based on a resolution by the German Bundestag (grant number: 50JR1705).

6. REFERENCES

[1] S. S. Papell, Low viscosity magnetic fluid obtained by the colloidal suspension of magnetic particles, U.S. Grant US3215572A, (1963)

[2] S. S. Papell and C. O. Faber, On the Influence of nonuniform Magnetic Fields on Ferromagnetic Colloidal Sols, NASA Technical Note TN D-4676, Lewis Research Center Cleveland, Ohio (1968)

[3] M. Ehresmann, F. Hild, K. Grunwald, S. Sütterlin, N. Heinz, S. A. Aslan, F. Grabi, M. Sauer, R. Schweigert, P. Ziegler, M. Hell, S. Hofmann, M. Schneider, F. Frank, C. Korn, A. Causevic, K. Waizenegger, A. Behnke, V. Hertel, P. Sahli, D. Bölke, M. Siedorf, C. Behrmann, T. Ott, J.-E. Brune and G. Herdrich, PAPELL: Solid-state pumping mechanism, Human Space Flight Conference, Toulouse, France (2018)

[4] F. Hild, K. Grunwald, S. Sütterlin, N. Heinz, S. A. Aslan, F. Grabi, M. Sauer, R. Schweigert, P. Ziegler, M. Hell, S. Hofmann, M. Schneider, F. Frank, C. Korn, A. Causevic, K. Waizenegger, A. Behnke, V. Hertel, P. Sahli, D. Bölke, M. Siedorf, C. Behrmann, T. Ott, J.-E. Brune, M. Ehresmann and G. Herdrich, Final Student Experiment Design of a Non-mechanical Pumping System on the ISS, IAC-18,E2,3-GTS.4,1,x45087, 69th International Astronautical Congress, Bremen, Germany (2018)

[5] J. Weppler, C. Lemack, T. Steinpilz, G. Musiolik, M. Kruß, T. Demirci, F. Jungmann, A. Krämer, J. Tappe, M. Aderholz, J. Teiser, G. Wurm, T. E. Koch, Y. Schaper, R. Nowok, A. Beck, O. Christ, P. T. Genzel, M. Lindner, Y. Matschey, D. M. Leber, S. Rempt, F. Schmuck, D. Spahr, B. Winkler, F. E. Brenker, F. Hild, K. Grunwald, M. Ehresmann, S. Sütterlin, N. Heinz, S. A. Aslan, F. Grabi, M. Sauer, R. Schweigert and G. Herdrich, Überflieger - A Student Competition for ISS Experiments, IAC-17,E1,3,112,x37659, 68th International Astronautical Congress, Adelaide, Australia, (2017)

[6] S. Sütterlin, N. Heinz, F. Hild, K. Grunwald, M. Hell, S. Hofmann, P. Ziegler, C. Korn, M. Schneider, F. Frank, M. Ehresmann, G. Herdrich and D. Helmer: PAPELL: Experiments, Prototyping and Mechanical Engineering, 2nd Symposium on Space Educational Activities, Budapest, Hungary (2018)

[7] K. Grunwald, F. Hild, S. Sütterlin, N. Heinz, S. A. Aslan, F. Grabi, M. Sauer, R. Schweigert, M. Ehresmann and G. Herdrich: PAPELL: Student team lead tenets and challenges in an international project, 2nd Symposium on Space Educational Activities, Budapest, Hungary (2018)

[8] K. Grunwald, Operation and Analysis of the ISS Experiment PAPELL, Bachelor Thesis, IRS-18-S-128 Institute of Space Systems, University of Stuttgart (2018)

[9] J. Weppler and C. Lemack, Überflieger - Update and Lessons Learned, IAC-18,E1,4,1,x46692, 69th International Astronautical Congress, Bremen, Germany (2018)

GUSDON (Global University Space Debris Observation Network): improvements on space debris optical monitoring offered by a global University network

Fabio Santoni[1], Fabrizio Piergentili[2], Rei Kawashima[3], Paolo Marzioli[2], Marco Acernese[2]

[1]Department of Astronautics, Electric and Energy Engineering (DIAEE) – Sapienza University of Rome
Via Eudossiana 18, 00184 Rome (Italy)
Phone: +39 366 675 0167, Mail: fabio.santoni@uniroma1.it

[2]Department of Mechanical and Aerospace Engineering (DIMA) – Sapienza University of Rome
via Eudossiana 18, 00184 Rome (Italy)

[3]UNISEC-Global (University Space Engineering Consortium)
UNISEC-Global Office, Central Yayoi 2F, 2-3-2, Yayoi, Bunkyo, Tokyo 113-0032, Japan

Abstract: Space debris monitoring usually implements optical observation by means of ground-based telescopes, which can achieve great precision with standardized, low-cost hardware. When including multiple optical observatories in a network, it is easy to significantly improve the significance of the collected data, the frequency of the measurements and the precision of the determined space debris orbits. GUSDON (Global University Space Debris Observation Network) is a project proposed by UNISEC (University of Space Engineering Consortium) Global and the S5Lab (Sapienza Space Systems and Space Surveillance Laboratory) team at Sapienza University of Rome for the establishment of a distributed observatories network all over the world. The network will be based on the sharing of all the collected data, in order to achieve brilliant scientific results in the field of space debris tracking, as well as a great educational return for all the people that will be involved from Universities and other institutions. In this paper, the GUSDON project is described, along with the potential relevance of the collected data and observatory network joint operations.

1. INTRODUCTION

The increasing population of space debris is fueling the cooperation of many international institutions for the tracking and cataloguing of space objects. In fact space debris represent a severe threat for the exploitation of space, because of the risk of potential in-orbit collisions, capable of destroying operative satellites and, more generally, of severely damaging space-based infrastructure. Moreover, large objects that, uncontrolled, re-entry the atmosphere, may impact the ground and damage on-ground infrastructure, representing also a life threat for the world population. An average number of 40 objects belonging to such a category per year, completes a re-entry [1]. Publicly available catalogues of space objects orbital estimates provide just modest accuracy information [2]. Two line elements (TLE), that currently constitute the most common format through which such information is provided, are a set of orbital parameters, whose propagation is generally considered reliable for just few days, or even just few hours as in the case of re-entering objects. Moreover, classified objects are not included in catalogues, and, in general, large gaps in the update of orbital estimates may occur for all objects. These circumstances are leading to an ever-increasing international effort for the sharing of data and the establishment of international networks of sensors.

Optical observations, which are usually applied to space debris monitoring, are able to achieve significant precision with simple, low budget hardware, and with standardized software able to allow the autonomous operations of an observatory and their data anal-

ysis. By increasing the number of observing sensors located in different sites, it is possible to dramatically improve the accuracy of the orbit determination solutions. A distributed optical network, indeed, allows to observe multiple arcs of the same orbit. In addition, sensors distributed in different sites provide redundancy to the network, allowing to perform observations even when some telescopes cannot observe due to bad weather conditions. In general, a distributed optical network allows to track a greater number of objects with respect to a single sensor.

GUSDON (Global University Space Debris Observation Network) is a project aimed at establishing a University optical network with autonomously managed observatories all over the world. The GUSDON idea was proposed in the framework of the 5th UNISEC (University Space Engineering Consortium) Global Meeting in November 2018. GUSDON is targeted at improving the significance of the space debris optical data acquired by Universities and educational institutions by developing a joint data exchange platform that will support the data integration upon the establishment of the observation network.

The proposing team is both from UNISEC Global and Sapienza University of Rome. At Sapienza, the Sapienza Space Systems and Space Surveillance Laboratory (S5Lab) research team already controls a small observatories network ([3], [4]), composed of several observatories between central Italy and Kenya. The Sapienza S5Lab team is available and interested in establishing fruitful collaborations for supporting the installation of new telescope stations in all the newly involved institutions, for the achievement of the GUSDON objectives.

This paper will deal with the idea of a Global University observation network, the GUSDON project. After an introduction on the typical configuration of each observatory, the analyses on the potential impact of such a network will be presented.

2. GUSDON

As referred in Section 1, while radar systems are costly and require qualified operators even for basic monitoring operations, optical observation systems are easily applicable to Universities and related students for their low cost, easiness of use, low risks related to operations and maintenance. Both already installed and new telescope stations could be involved in GUSDON. While the already existing observatories may need basic updates for completing the observational tasks, a standard configuration has been evaluated for the institutions that want to develop their observatory from scratch. The standard configuration is composed by:

- A Newtonian optical tube with large Field of View (approximately 1.5 degrees);
- A high resolution visible band (VIS) Charge-Coupled Device (CCD);
- A PC-controllable motorized mount, able to perform fast re-aligning and tracking of targets in Low Earth Orbit (angular speed of up to 3.5 degrees/second).

Besides the standard hardware configuration, software tools that were already extensively tested by the Sapienza S5Lab observation network will be distributed for the management of the observations. In particular, an observations scheduler will permit to

autonomously define the telescope tasks of each night. This tool allows to switch among the visible targets of each observation night, by connecting to the most reliable astrometric measurements databases, and also to define a priority for each completed task.

The educational scope of the project is of paramount importance, since the project will be addressed to institutions that do not have expertise in the observatories installation, maintenance and operations and that want to be involved in this field of research by developing their observatory from scratch. Moreover, the involvement in the network will allow to gain great educational return at all stages of the observatories development and operations, for all the people (students at all levels, University researchers, staff and Professors) that will be part of the observatory teams.

As a final remark, the results achievable by the GUSDON project are depending on the efficient data sharing among the involved institutions. As preliminary data sharing concept, it would be needed for the observatory that all institutions share, access and process the acquired data by the network for a more efficient and effective scientific data obtainment. The importance of the data sharing among all the involved institutions will be described with more detail in the next paragraph.

3. DATA COLLECTION PROCESSES

The GUSDON data collection and processes will start from the raw optical data acquisition to orbit determination and photometric analyses. The data collection will consider several phases that are shown in Figure 1.

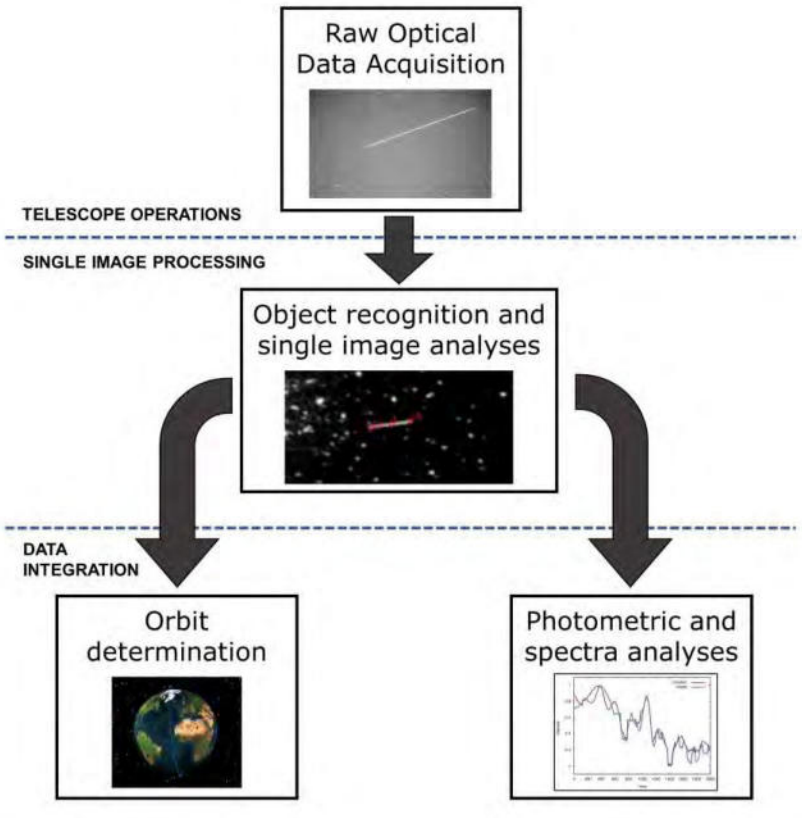

Figure 1: Data acquisition and processing processes in GUSDON.

The management of a telescope network includes the acquisition of telescope images from the telescope and of videos of the tracked objects. Then, images need to be processed singularly to obtain the tracklet celestial coordinates, object identifications, or tracklet luminous intensity. The data acquired from single images can be then integrated for estimating the object orbit or for more advanced analysis, such as on photometric data.

4. RELEVANCE

The main advantage that a distributed optical network such as the one proposed in this paper may provide is the possibility of observing target objects multiple times in a relatively short time interval. Moreover, taking measurements along different arcs of the orbit increase the accuracy of the obtainable orbital estimates and facilitates the orbit determination process. An evaluation of the impact of an increased number of observatories on the accuracy of the orbit determination exploiting the produced measurements has been performed by considering the non-functional satellite Envisat (SSN 27386) and 7 potential telescopes locations (see

Table 1, Figure 2). A TLE ("TLE 2") of epoch 2018/12/21 13:55:46.194 UTC has been back-propagated in order to generate pseudo-observations of topocentric right ascension and declination during the 2018/12/20, at a frequency of 1 per minute. A zero-mean, white Gaussian noise with a standard deviation of 5 arcsecs has been added to the measurements, in order to consider a realistic error characterizing a possible experimental setup. When multiple passes were visible from one site in the considered time interval, just the measurements taken in one of the passes were used. Then, different orbit determinations have been performed, by using as the initial guess a TLE ("TLE 1") of epoch 2018/12/19 23:00:21.364 UTC and as state vector the 6 orbital elements. Each orbit determination has been performed by cumulating the measurements taken by a different number of observatories. Then, the obtained orbital estimates have been propagated from the epoch of the truth TLE forward in time for the duration of one orbital period, and the mean position error has been computed (see Figure 3, Table 2).

Table 1 Locations of the considered observatories

Location	Number of measurements (RA, Dec)
Rome (41.957777° N, 12.505555° E)	5
Berlin (52.520008° N, 13.404954° E)	6
Malindi (-2.996373° N, 40.193791° E)	7
New Delhi (28.644800° N, 77.216721° E)	7
Sydney (-33.867487° N, 151.206990° E)	6
Tokyo (35.652831° N, 139.839478° E)	5
Washington (47.751076° N, -120.740135° E)	6

Figure 2 Locations of the considered observatories

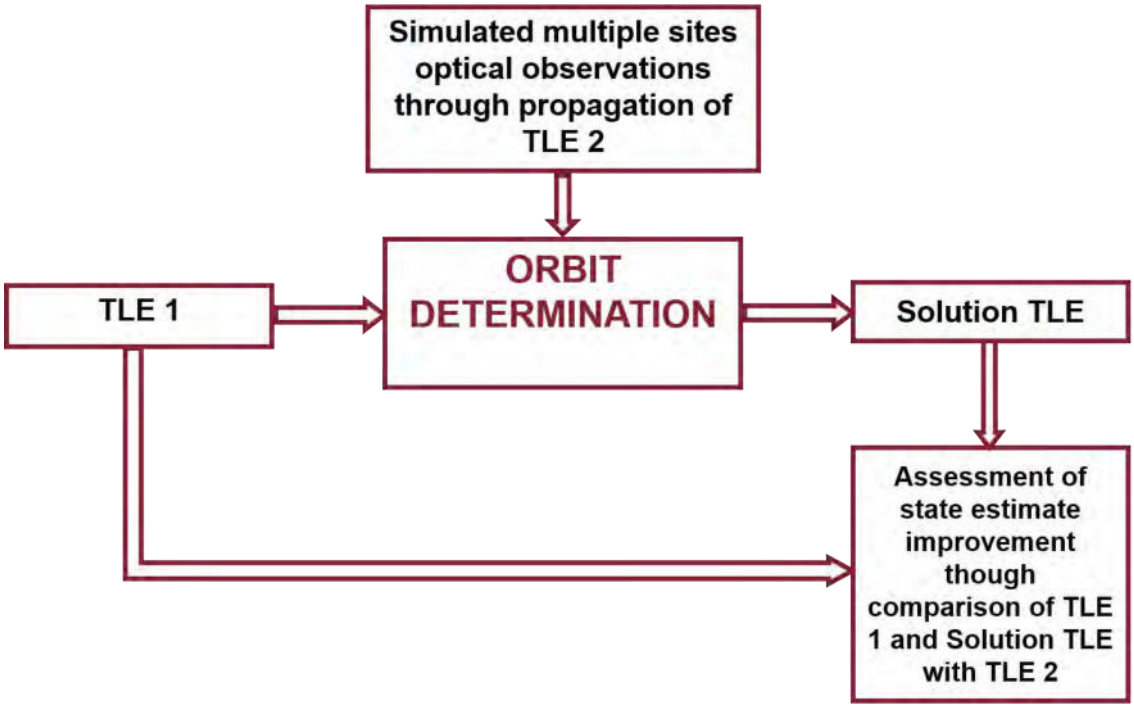

Figure 3 Basic scheme of the algorithm for the assessment of orbit determination solution accuracy

Table 2 Mean position errors of the orbit determination solutions during 1 period from the epoch of the truth TLE, for the different configurations of observatories

Observatories configuration	Mean solution position error from the epoch of the truth TLE during 1 orbital period (initial guess: 0.163 km)
R	170.948 km
R-B	0.937 km
R-B-M	1.102 km
R-B-M-N	0.087 km
R-B-M-N-S	0.048 km
R-B-M-N-S-T	0.047 km
R-B-M-N-S-T-W	0.031 km

R=Rome; B=Berlin; M=Malindi; N=New Delhi; S=Sydney; T=Tokyo; W=Washington

By using just one site the solution is largely inaccurate, while it becomes more and more accurate as the number of observatories increases.

The availability of a distributed network increases, moreover, the possibility of tracking objects in the very last phase of a re-entry. For this orbital regime, indeed, it is fundamental to track continuously the involved space object. The more the object is close to complete the re-entry, the more important is taking measurements for the estimation of the actual re-entry date and location. This capability of tracking such objects in the last few hours of their orbital life can be granted only by a distributed network of sensors.

By extrapolating the light-curves through photometric analysis it is possible to estimate the attitude and the angular velocity of the tracked object. This information can be used to improve the orbit prediction, since the atmospheric drag force is also influenced by the attitude. Also in this case, the availability of a large number of observatories permits to acquire measurements separated by smaller time gaps, thus improving the accuracy of the attitude reconstruction.

5. CONCLUSIONS

The increasing population of space objects poses a threat to in-orbit and on-ground infrastructure. Due to this ever-growing space objects population, a proper monitoring of space debris can accomplished only through the extensive employment of distributed networks of sensors. Optical sensors, in particular, are characterised by relatively low cost and, for most purposes, do not require to be operated by highly trained personnel. These circumstances make optical telescopes to be particularly adequate for the employment by university institutions. The S5Lab at Sapienza University of Rome already owns and operates a network of optical telescopes devoted to the research and monitoring of space debris. In this paper the constitution of GUSDON, an international observatory network involving multiple cooperating universities from all over the world, has been proposed. The network will benefit from the well-established expertise of Sapienza University in the building, maintenance and operation of networks of optical sensors. Joining the GUSDON project will grant the access to a dramatically increased quantity

of data, produced by all the cooperating institutions. Moreover, the proposed collaboration will offer the unique educational opportunity consisting in the training of student staff, that will acquire the necessary know-how for the use of the network. An analysis has been performed, aimed at assessing the orbit determination solution accuracy granted by measurements acquired by different configurations of distributed optical sensors. 7 possible observatories locations have been considered, distributed in all continents. The analysis has shown a dramatic increase of the quality of the orbit determination solution obtainable by increasing the number of involved telescopes.

REFERENCES

[1] W. Ailor, "Space Debris Reentry Hazards," presented at the Scientific &Technical Subcommittee of th e United Nations Committee on the Peaceful Uses of Outer Space, 2012.

[2] D. Vallado and P. Cefola, "Two-line element sets - Practice and use," *Proceedings of the International Astronautical Congress, IAC*, vol. 7, pp. 5812–5825, Jan. 2012.

[3] S. Hadji Hossein *et al.*, "Sapienza Space Systems and Space Surveillance Network (S5N): a high coverage infrastructure for space debris monitoring.," presented at the 69th International Astronautical Congress (IAC), Bremen, Germany, 2018.

[4] F. Piergentili *et al.*, "EQUO: An equatorial observatory to improve the Italian space surveillance capability," presented at the Proceedings of the International Astronautical Congress, IAC, 2015, vol. 4, pp. 2677–2683.

On-Orbit Verification of a Modular Propulsion System MICROJET 2000 in the framework of BIROS and BEESAT-4 Small Satellite Formation Flying Demonstration AVANTI

Dr. Harry Adirim[1], Dr. Winfried Halle[2], Matthias Kreil[1], Michael Kron[1], Matthias Lieder[2], Thomas Terzibaschian[2], Sascha Weiß[3]

[1]Aerospace Innovation GmbH
Winterfeldtstr. 97, 10777 Berlin-Schöneberg, Germany
Phone: +49 30 3101 7881, Mail: info@aerospace-innovation.com

[2]DLR, Institute of Optical Sensor Systems
Rutherfordstr. 2, 12489 Berlin, Germany
Phone: +49 30 6705 5559, Mail: Winfried.Halle@dlr.de

[2]Technical University of Berlin, Institute of Aeronautics and Astronautics
Marchstr. 12, 10587 Berlin, Germany
Phone: +49 30 3147 9464, Mail: sascha.weiss@tu-berlin.de

Abstract: The BIROS mini-satellite architecture is based on DLR's space proven technology, developed in the frame of the very successful BIRD and TET-1 missions. BIROS is equipped with a modular "green" MICROJET 2000 resistojet propulsion system developed by Aerospace Innovation GmbH in cooperation with DLR. The addition of BIROS completes the two-satellite-constellation with TET-1 as the space segment of the FireBIRD mission for earth observation purposes. The two-satellite-constellation is essential for active fire observation and related fire disturbance and climate variables investigations. As secondary mission objectives, BIROS embarked several hardware and software technology demonstrations, among which the BEESAT-4 single unit CubeSat built by the Technical University of Berlin and AVANTI (Autonomous Vision Approach Navigation and Target Identification), conceived, developed, and operated by the German Space Operations Center (GSOC). BEESAT-4 has been released in-orbit by means of a dispenser which provided an equivalent separation delta-v of ca. 1.5 m/s. After the implementation of the so called thruster firing mode of the propulsion system and the client observation mode the optical navigation experiment AVANTI was started to fly autonomously again in the direction of BEESAT-4 to the distance of ca. 50 m.

1. INTRODUCTION

DLR has developed a dedicated space instrumentation on the first satellite BIRD (Bispectral Infrared Detection) which is used to detect hot spot events such as forest and vegetation fires, volcanic activity, burning oil wells and coal seams. Launched in 2001 BIRD has successfully operated in polar orbit for many years. Due to recent technological evolvements, it was possible to remarkably improve the design of the infrared camera system for the following satellites TET-1 which was launched in 2012 and the BIROS launched in June 2016. The overall satellite design became more compact and lightweight.

The BIROS mini-satellite architecture is based on DLR's space proven technology, developed in the frame of the very successful BIRD and TET-1 missions. The addition of BIROS completes the two-satellite-constellation with TET-1 as the space segment of the FireBIRD mission for earth observation purposes. The two-satellite-constellation is especially essential for active fire observation and related fire disturbance and climate variables investigations.

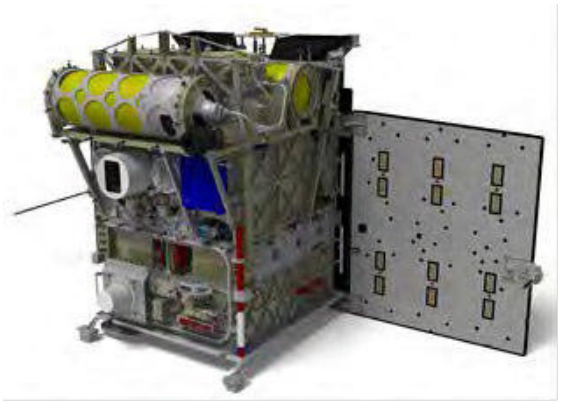

Fig.1: BIROS Satellite with the Propulsion System and Payload Segment

Fig.2: BIROS Flight Model

The main mission goals for the FireBIRD mission are:

- Test of a two-satellite-configuration for infrared remote sensing of high temperature events on earth's surface
- Active fire detection & monitoring and analysis of the results
- Supply of data products for fire induced carbon emissions, assessment and delivery of data products to the user
- On-board processing of active fire attributes for fire management support.

2 BIROS SPACECRAFT FEATURES

The BIROS Satellite is based on the TET Satellite bus design. The spacecraft was designed for an application in low earth orbit (main parameters s. table 1) with a minimum of 5 years lifetime in orbit. To operate a fire monitoring constellation with two satellites at least one satellite has to have an orbit control possibility in form of a propulsion system. This is an additional feature of BIROS compared to TET.

Missions Parameter	**Satellite: TET - BUS Evolution**		
Orbit	500 km sun synchronous	Satellite Mass	Approx. 135 kg
Inclination	97.6 °	Dimensions	580 x 880 x 680 mm^3
Mission Operation	DFD-BN, GSOC	Payload Mass	Approx. 60 kg
Mission Reparation	5 Years	Power Bus	Approx. 50 W
Mission Duration	≥ 2.5 Years	Communication	S-Band / UHF
Launcher	PSLV-34, 22th of June 2016		

Table 1: Overview of BIROS-Mission main parameters

The BIROS satellite bus consists of the following main functional systems:

- Attitude and Orbit Control Subsystem (AOCS),
- MICROJET 2000 Propulsion Subsystem (PS),
- Power Subsystem (PCS),

- Communication Subsystem (CS), including telemetry & telecommand Subsystem (TM/TC)
- Payload Data Handling (PPU) Subsystem,
- Spacecraft Bus Computer (SBC),
- Thermal Control Subsystem (TCS) and
- Platform Structure.

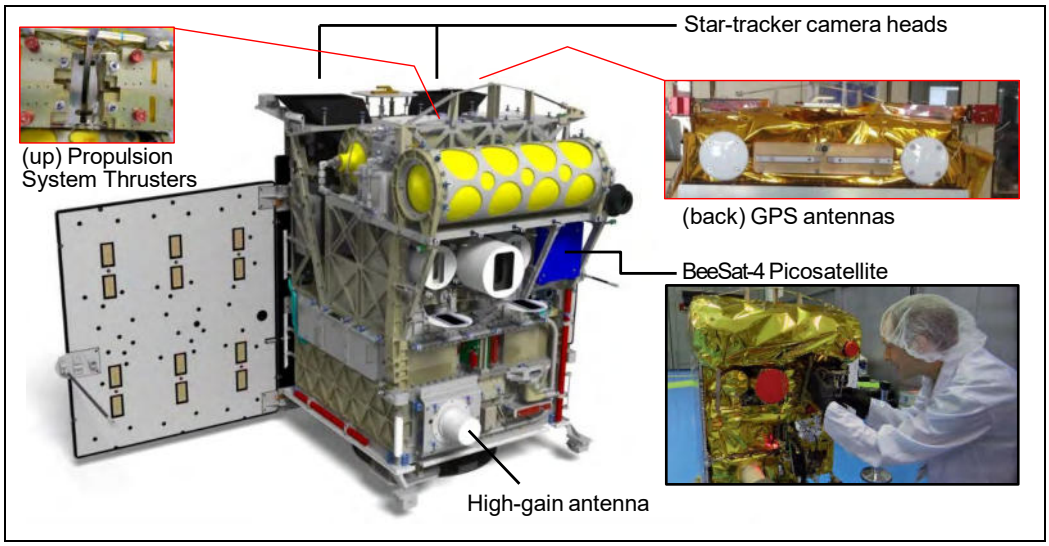

Fig.3: BIROS bus and payload assembly (left); in pre-launch configuration (bottom-right)

3 THE MAIN PAYLOAD SENSOR – SYSTEM OF THE DLR-FIREBIRD MISSION

Both satellites (TET and BIROS) are equipped with a three-line ccd-camera with a 40 m ground pixel size in the red, green and near infrared spectral range, and a 370 m ground pixel size camera in the mid and thermal infrared with a swath of 185 km in using MCT technology.

	VIS	2 Infrared-Camaras
Wavelength	0.5 µm, 0.6 µm, 0.8 µm Green, Red, NIR	MWIR: 3.4 – 4.2 µm; LWIR: 8.5-9.3 µm
Focal Length	90.9 mm	46.39 mm
FOV	19,6°	19°
Aperture	3.8	2.0
Detector	CCD- Zeile	CdHgTe Arrays
No of Pixel	3 x 5164	2 x 512 staggered
Quantisation	14 bit	14 bit

Table 2: Parameter of the FIREBIRD optical main payload

After the commissioning phase of BIROS the fire-products can also be generated as from the TET satellite. Fig 4 shows the Level-2 product of a data take.

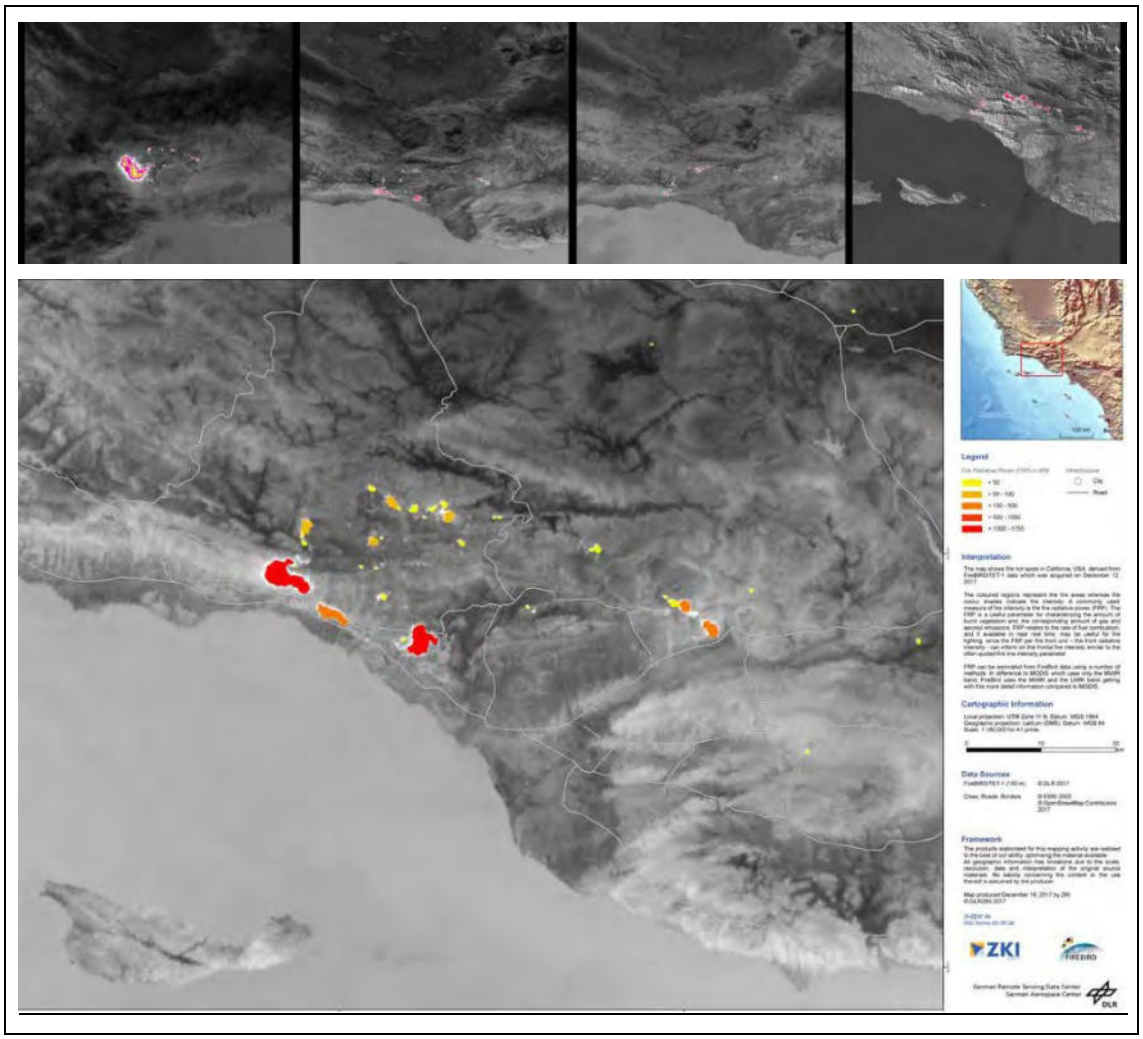

Fig.4: US-California December 12, 2017 (DLR/ZKI, DLR Center for Satellite-Based Crisis Information (Zentrum für Satellitengestützte Kriseninformation))

4 BIROS PROPULSION SYSTEM MICROJET 2000

BIROS is equipped with a MICROJET 2000 gas resistojet developed by Aerospace Innovation GmbH in cooperation with DLR, configured into two independent lines comprising all the functional elements. The MICROJET is a modularly designed propulsion system for nano-, micro- and mini-satellites based on the gas-resistojet concept. It consists of a “Pressure Tank Unit” (PST) with Nitrogen which is filled or drained, respectively, through a “Fill and Drain Unit” (FDU), a “Flow Control Unit” (FCU) which is responsible for the control of correct propellant mass flow, as well as one or more “Thruster Units” (THU). Each of these THUs contains a pulse valve and a nozzle for the actual thrust generation. The entire MICROJET 2000 system configured into two independent lines measures ca. 55 cm x 49 cm x 18 cm and has a total mass of ca. 2 x 10 kg, including propellant.

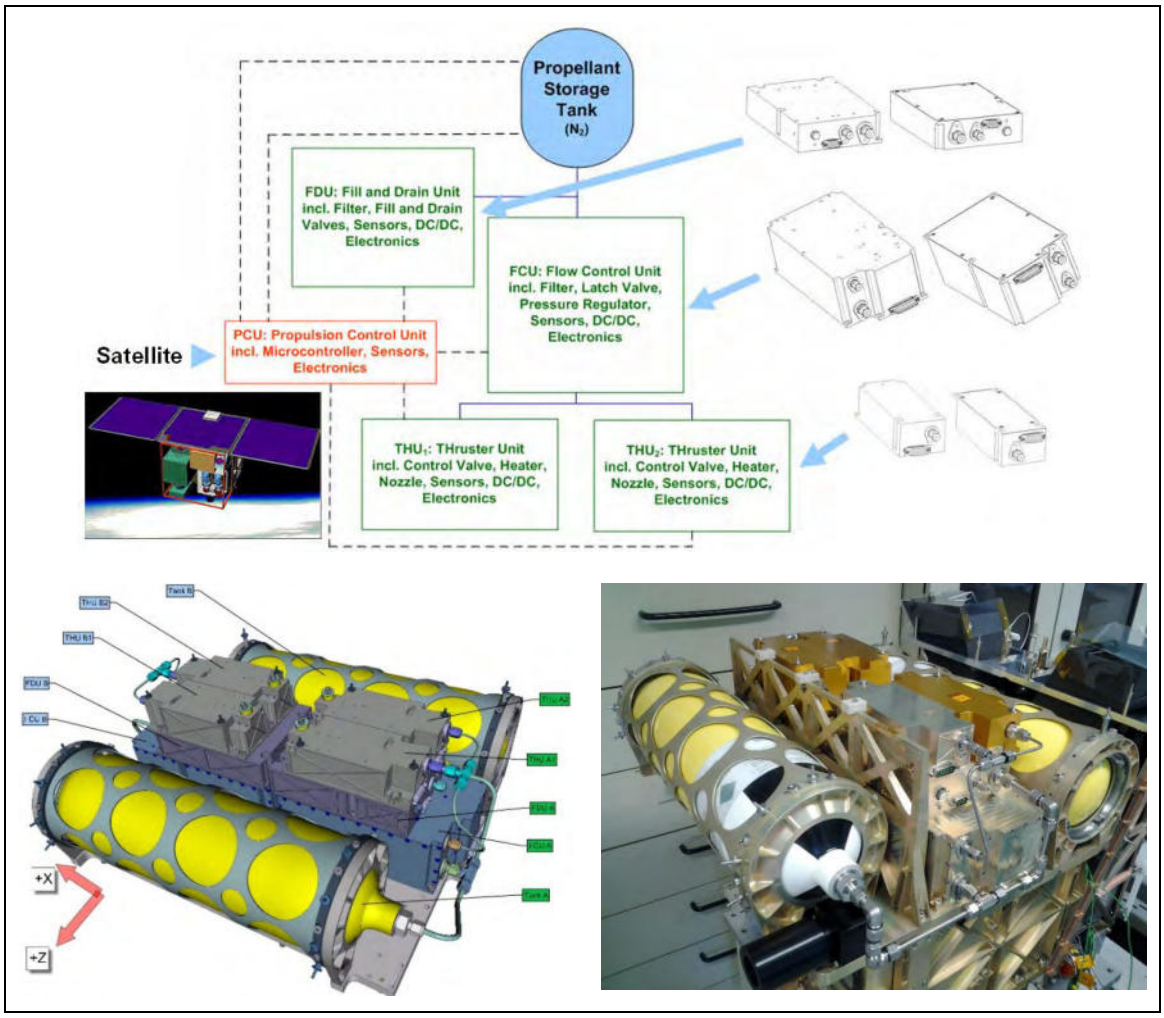

Fig.5: MICROJET 2000 propulsion system architecture and implementation on BIROS satellite

Throughout the selection process of the reference configuration, several different ways to accommodate the propulsion system on BIROS have been investigated. Finally, the cost- and time-saving approach was selected, in which the largest possible evolution of the TET-1 satellite bus has been implemented. Additionally, a modular propulsion system architecture was applied to be able to easily adapt any subsequent modifications.

Working Fluid	Nitrogen (N_2) at max. expected operating pressure of 310 bar (MEOP)
Pressure Vessels	310 bar composite over-wrapped pressure vessels, available from 1 to 9 litres
Electric Power and I_{sp}	35.9 W (Resistojet mode incl. 20 W for heating, ca. c_e=952 m/s) 11.6 W (Cold Gas mode, ca. c_e=718 m/s)
Thrust	Option A (Resistojet mode): ca. 67 mN per thruster Option B (Cold Gas mode): ca. 118 mN per thruster
Vcc (nominal)	18 V – 24 V
Status	EQM qualified in 2014, FM qualified in 2015, application in space since June 2016
Remarks	Incl. DC/DC converters, pressure transducers, temperature sensors, ECSS based development and testing, no pyrotechnic valves, no ITAR parts, COTS design

Table 3: Main characteristics of the MICROJET propulsion system

5 AUTONOMOUS NAVIGATION, TARGET IDENTIFICATION AND PROXIMITY OPERATIONS

As secondary mission objectives, BIROS embarked several hardware and software technology demonstrations, among which the BEESAT-4 single unit CubeSat built by the Technical University of Berlin and AVANTI (Autonomous Vision Approach Navigation and Target Identification), conceived, developed, and operated by the German Space Operations Center (GSOC). BEESAT-4 has been released in-orbit on the 9th of September 2016 by means of a single picosatellite launcher device which provided an equivalent separation delta-v of circa 1.5 m/s. While carrying out its independent experimental activities, BEESAT-4 has been used as noncooperative target for the sake of the AVANTI demonstration.

A technological demonstration conducted by GSOC proved the viability to perform far- to close range autonomous proximity operations with respect to a noncooperative flying object using only optical angle measurements. Within AVANTI, the Earth-observation BIROS satellite played the role of a chaser spacecraft with an agile propulsion system, which autonomously approached down to circa 50 m of inter-satellite distance the BEESAT-4 picosatellite, simply using a head of its star-tracker as monocular camera.

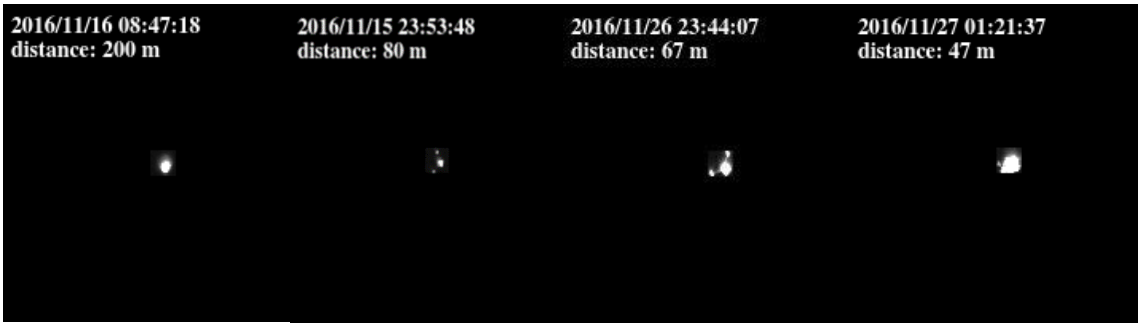

Fig.6: Mid-close range rendezvous with BEESAT-4

6 CONCLUSIONS

The BIROS satellite is the second satellite in the FireBIRD Mission together with TET Satellite (launched in 2012) to observe fires and hot spots in a fire monitoring constellation. With the successful launch of BIROS in the mid of 2016 with an Indian launcher (PSLV-C34) and the finalized commissioning phase of the IR-Camera, BIROS could deliver as the TET-1 satellite Level 1 and Level 2 data products for different applications. The sensor is also capable to evaluate the normal temperature phenomena. BIROS also carries different experiments form other DLR institutes in form of new space hardware and software.

The first in orbit experiment was the successful separation of the BEESAT-4 from the Technical University of Berlin on 6th of September 2016. After the implementation of the so called thruster firing mode of the propulsion system and the client observation mode the optical navigation experiment AVANTI was started to fly autonomously again in the direction of BEESAT-4 to the distance of ca. 50 m. This was possible with a propulsion system developed by the Aerospace Innovation GmbH together with DLR.

7 REFERENCES

[1] Adirim H.: Presentation in the frame of OOV program KoM, Bonn, 13.1.2005

[2] Adirim H., Lo R.E., Pilz N., Kreil M.: "Hot Water Propulsion Development Status for Earth and Space Applications", AIAA-2006-4566, Session 43 PC-4, 42nd AIAA Joint Propulsion Conference, Sacramento, CA, 9 - 12 July 2006

[3] Harry Adirim, Norbert Pilz, Matthias Kreil, Michael Kron, Andrei Mitrofanow: "On-Orbit-Verification of Small Satellite Propulsion System Aquajet on TET-1", 2nd TET Customer Day, Kayser-Threde, Munich, July 5.-6., 2010

[4] Dr. Harry Adirim, Norbert Pilz, Matthias Kreil, Michael Kron, Andrei Mitrofanow: „On-Orbit-Verifikation des Kleinsatellitenantriebssystems AQUAJET auf TET-1", TET-01 Endpräsentation Phase E, DLR, Bonn, 4.12.2013, AI: Aerospace Innovation GmbH

[5] Dr. Harry Adirim, Matthias Kreil, Michael Kron, Andrei Mitrofanow, Dr. Winfried Halle, Matthias Lieder, Wolfgang Bärwald, Steffen Babben, Thomas Terzibaschian: "Innovative Modular Propulsion Systems for Small Satellites", IAA-B10-1106P, Proceedings of the 10th IAA Symposium on Small Satellites for Earth Observation, April 20-24, 2015 Berlin, Germany

[6] H. Adirim, M. Kreil, M. Kron, A. Mitrofanow, W. Halle, M. Lieder, W. Bärwald, S. Babben, T. Terzibaschian: MODULAR PROPULSION SYSTEM FOR MINI-SATELLITE BIROS, The 4S Symposium, 30 May – 3 June 2016, Valletta, Malta

[7] K. Brieß, W. Bärwald, E. Gill, W. Halle, H. Kayal, O. Montenbruck, S. Montenegro, W. Halle, W. Skrbek, H. Studemund, T. Terzibaschian, H. Venus: "Technology Demonstration by the BIRD Mission", 4th IAA Symposium on Small Satellites for Earth Observation, Berlin, Germany, April 7-11, 2003; - also published in Acta Astronautica, Vol. 56, Issues 1-2, Jan. 2005

[8] G. Gaias, J.-S. Ardaens, C. Schultz: THE AVANTI EXPERIMENT: FLIGHT RESULTS, 10th International ESA Conference on Guidance, Navigation & Control Systems, 29 May - 2 June 2017, Salzburg, Austria

[9] Halle, W., Terzibaschian, T.: "The DLR-BIROS-Satellite for fire-detection and technological experiments", IAA-B10-0201, DLR, Proceedings of the 10th IAA Symposium on Small Satellites for Earth Observation, April 20-24, 2015 Berlin, Germany

[10] Halle, W., Amigues, X., Kotz, A., Schultz, C., Bärwald, W.: "Universal Small Satellite Platform BIROS suitable for different payload accommodations", IAA-B10-1011P, DLR, Proceedings of the 10th IAA Symposium on Small Satellites for Earth Observation, April 20-24, 2015 Berlin, Germany

[11] Halle, W., Adirim, H., Fischer, Ch., Bärwald, W., Terzibaschian, T, Säuberich, T.: "Recent Results of the DLR FireBIRD-Mission" Small Satellites, System & Services Symposium (4S), 28 May – 1 June 2018, Sorrento, Italy

[12] E. Lorenz, G. Rücker, T. Terzibaschian, D.Klein, J.Tiemann, FireBird - A small satellite fire monitoring mission: Status and first results; Geophysical Research Abstracts Vol. 16, EGU2014-16546, 2014 EGU General Assembly 2014

[13] Lemke, N. M. K., Föckersperger, S., Eckert, S., Turk, M.: "The success story of TET-1 for the first OOV mission and future opportunities", IAA-B9-0903, Proceedings of the 9th IAA Symposium on Small Satellites for Earth Observation, Berlin, Germany, April 8-12, 2013

[14] Raschke, C., Terzibaschian, T., Halle, W.: "A New Actuator System for High Agility Demonstration with the Small Satellite BIROS", IAA-B10-1413P, DLR, Proceedings of the 10th IAA Symposium on Small Satellites for Earth Observation, April 20-24, 2015 Berlin, Germany

[15] Hubert Reile, Eckehard Lorenz, Thomas Terzibaschian, "The FireBird mission - a scientific mission for Earth observation and hot spot detection", Proceedings of the 9th IAA Symposium on Small Satellites for Earth Observation, Berlin, Germany, April 8-12, 2013

[16] Stephan Roemer, Winfried Halle, "TET-1 and BIROS A semi-operational Fire Recognition Constellation", UN/Austria/ESA Symposium on Small Satellite Programs for Sustainable Development: Payloads for Small Satellite Programs, Sept. 21-24, 2010, Graz, Austria

[17] https://directory.eoportal.org/web/eoportal/satellite-missions

[18] http://www.aerospace-innovation.com

[19] https://www.dlr.de/eoc/en/desktopdefault.aspx/tabid-11932/20674_read-49933

Gefördert durch:

Bundesministerium für Wirtschaft und Energie

aufgrund eines Beschlusses des Deutschen Bundestages

PASSAT: Passive Bi-Static SAR Constellation – Progress and Trial Results

Craig Underwood[1], George Atkinson[2], Alp Sayin[2], Mike Cherniakov[2], Michail Antoniou[2], Alex Dyer[1]

[1]Surrey Space Centre, University of Surrey,
Guildford, Surrey, GU2 7XH, UK
Phone: +44 1483 689809, Mail: c.underwood@surrey.ac.uk, a.dyer@surrey.ac.uk

[2]Dept. of Electronic, Electrical and Systems Engineering, University of Birmingham,
Edgbaston, Birmingham, B15 2TT, UK
Mail: *GMA241@student.bham.ac.uk*, *a.sayin@bham.ac.uk*, *m.cherniakov@bham.ac.uk*, *m.antoniou@bham.ac.uk*

Abstract: Persistent monitoring of large areas using spaceborne Synthetic Aperture Radar (SAR) is a challenging problem for various defence and civil applications. The PASSAT project was proposed and undertaken by the University of Birmingham, under the sponsorship of the UK Defence Science and Technology Laboratory, to analyse the concept of a fully passive (receive only) spaceborne SAR system based on a constellation of CubeSats. By making use of terrestrial transmitters (e.g. Digital Video Broadcasting – Terrestrial (DVB-T) or similar transmitters of opportunity), the problem of having to carry a high power pulsed radar transmitter on the satellite is eliminated. Instead, the satellite only need carry a suitable receiver, antenna and signal storage facility. It is expected that such a system would provide imaging of populated areas with a potential resolution of ~2-3 m. In this paper, we describe progress towards the design of such a system, including the results of a series of ground-based and airborne trials which make use of DVB-T transmissions from the Sutton Coldfield transmitter. In the processed images, roads, wind turbines, electricity pylons, hedgerows and trees are all clearly identified.

Acronyms/Abbreviations:

AMSL	Above Mean Sea Level
DAB	Digital Audio Broadcasting
DEM	Digital Elevation Map
DLR	Deutsches Zentrum für Luft-und Raumfahrt (German Aerospace Centre)
DSTL	Defence Science and Technology Laboratory (UK)
DVB-T	Digital Video Broadcasting – Terrestrial
EIRP	Effective Isotropic Radiated Power
FM	Frequency Modulation
GEO	Geostationary Earth Orbit
GNSS	Global Navigation Satellite System
GPS	Global Positioning System
GPSDO	GPS Disciplined Oscillator
IMU	Inertial Measurement Unit
ISS	International Space Station
LEO	Low Earth Orbit
PASSAT	Passive Receiver SAR Satellite
RF	Radio Frequency
RTK	Real-Time Kinematic
SAR	Synthetic Aperture Radar
SDR	Software Defined Radio
SNR	Signal to Noise Ratio
SSD	Solid State Drive
TV	Television
UHF	Ultra-High Frequency
UK	United Kingdom
USRP	Universal Software Radio Peripheral
VHF	Very High Frequency

1. INTRODUCTION

Space-borne Synthetic Aperture Radar (SAR) has proven itself to be a highly capable remote sensing technique, with a plethora of applications. The great advantage of SAR is that it provides day or night imaging, independent of weather conditions. However, this comes at the cost of needing to provide the "illuminating" radiation, which hitherto has required SAR satellites to carry high power radar transmitters. As a result, existing space-borne SAR systems typically require large and/or complex spacecraft platforms, which come at substantial financial cost. This, in-turn, puts practical restrictions on the number of instruments that can be orbited, and this is problematic given the increasing demands for persistent or near-persistent monitoring applications, which would require a large number of SAR satellites to be effective.

One potential solution to this problem could be to make use of passive, rather than active, spaceborne SAR systems. These would utilise existing transmissions from other sources for imaging purposes, thus forming a bi-static or multi-static arrangement. Our proposal concerns such a system: the Passive SAR Satellite (PASSAT) constellation [1,2]. Due to the passive nature of the satellites, the receiver, storage, and data downlink components would require only a small volume, and the power requirements would be modest, thus the passive SAR payload could be accommodated on a nano-satellite (e.g. a CubeSat) in the 10-20kg class, enabling multiple satellites to be deployed from a single launch. The smaller size, as well as the smaller power requirements of a receive-only system means that the PASSAT system would be much cheaper and less complex than a constellation of active SAR satellites – even SAR micro-satellites (100-500kg) – in a similar low Earth orbit (LEO).

In PASSAT, the transmitters of opportunity are ground-based broadcasting stations, e.g. Digital Video Broadcasting – Terrestrial (DVB-T) transmitters. These were chosen as, globally, DVB-T coverage of populated areas is quite extensive (e.g. in the UK nearly 90% of the land is within DVB-T coverage, not to mention littoral waters). We also found DVB-T provides the best source signal properties, including a relatively high transmission power (10-250kW), thus reducing the required satellite receiver antenna gain, as well as providing a sufficient bandwidth (7.6MHz) to give a reasonable range resolution: approximately 20m for an ideal geometric scenario. A visualization of the concept is shown in Fig. 1. System link parameters are described in [3].

Fig. 1. The PASSAT System Concept

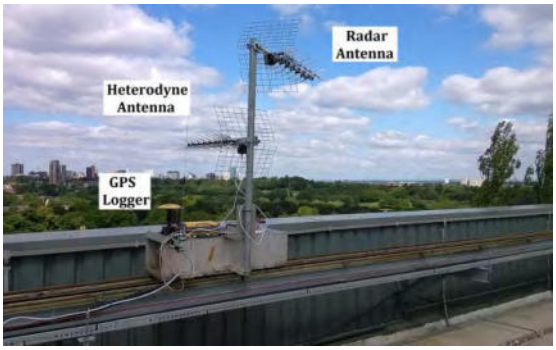

Fig. 2. Proof-of-Concept Trial

2. PASSAT DEMONSTRATOR GROUND TRIALS

To test and verify the concept, in 2015 a relatively crude "proof-of-concept" trial was carried out from the roof of the University of Birmingham using a 40m long "railway track" (Fig. 2). The receiving hardware was based on National Instrument's two-channel Universal Software Radio Peripheral (USRP) The first channel had a standard commercial Yagi digital TV antenna pointed towards the transmitter location (Sutton Coldfield), to record the direct "heterodyne" signal. The signal recorded in this channel was used as the reference for range compression in the image formation algorithm. The second channel, called the "radar" channel, had a similar Yagi antenna pointed towards the imaging scene for image formation. A professional GPS receiver was also used to record the receiver's position and speed with high accuracy (Real-Time Kinematic - RTK specifications) and update rate (20 Hz).

Sutton Coldfield DVB-T broadcasting station was selected as the transmitter, both because it is located towards the North (so the full aperture length could be used) and because of its high transmit power (~200 kW Effective Isotropic Radiated Power – EIRP), which would help in testing our image formation algorithms. The transmitter was located ~17.7km away from the receiver and the transmitter height was 433m above mean sea-level (AMSL). The signal captured for image formation was the 650 MHz DVB-T channel, which is UHF#43. Both the scattered and direct DVB-T transmissions were received and processed, and after signal processing, strong echoes were obtained, which could be associated with buildings in the neighbourhood of the University, showing that the basic concept was sound.

In January 2018, a series of road trials were conducted to obtain further DVB-T data sets for the production of passive SAR imagery. Bartley Reservoir, close to the University of Birmingham, was chosen as a location as it presented a near quasi-monostatic geometry, as well as a straight road to provide a linear aperture. Figure 3 shows an aerial view of Bartley Reservoir, with the vehicle path shown in yellow, the imaging direction indicated by the green arrow, and the Sutton Coldfield transmission station indicated by the red lines. The same 650 MHz DVB-T channel was used for the experiment, with the transmitter now located 21.63km from the centre of the aperture, at an angle of 73 degrees from the direction of motion of the receiver. The full length of the road was 500m, however, for a typical measurement a roughly 400m aperture was produced in which the vehicle was travelling at a relatively constant speed of 8.94 m/s (20 mph) for approximately 40 seconds per measurement. The receiver was mounted on the University of Birmingham's mobile laboratory, a Land Rover Discovery approximately 4m above the ground.

The receiver was based on the same USRP used in the proof-of-concept test, and similarly two antennas were used, however, this time they were patch antennas with a 50 degree beam-width, custom-made at the University of Birmingham. These were mounted on 1.5m long poles attached to the roof of the vehicle, placing them a total of 3m above ground level. The antennas had band-pass filters for interference rejection. The USRP streamed "I" and "Q" samples (10 MHz bandwidth) from both channels to a laptop computer.

Simultaneously to the radar measurement, a high precision SpatialFog Inertial Measurement Unit (IMU) and GPS receiver record the position of the vehicle with a high update rate [4]. The SpatialFog unit was connected to the same control laptop as the USRP and the position data was recorded to the same Solid State Drive (SSD).

Figure 4 shows the processed SAR image (colour scale = 0dB (red) to -45 dB (blue) relative to most intense return signal) overlaid on a topographic satellite map. Careful inspection of the image reveals that many of the strong returns are from trees, bushes and forested areas. However, along the motorway towards the bottom of the image, there can be seen a series of strong, almost point-like returns, which, after inspection of the ground-truth image, are found to be from a series of electricity pylons. The reservoir (dark blue) is also clearly outlined, by the paths and roadways around it, as is the general effect of the terrain. Note the pylons are behind the hill as seen by both the receiver and transmitter – which appears to indicate the radar can see objects "over the horizon" which a conventional microwave SAR would not.

Fig. 3. Image of the Bartley Reservoir Road

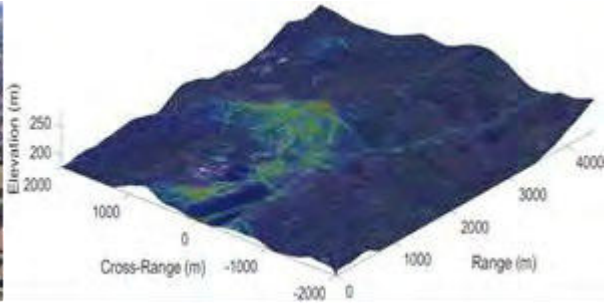

Fig. 4. Topographic Map of the Area and SAR Image

3. PASSAT DEMONSTRATOR AIRBORNE TRIALS

Following the success of the ground-based demonstrator, the hardware was re-packaged ready for flight in an airborne demonstration (Fig.5). The same USRP receiver and twin patch antennas were used, only this time the antennas were mounted behind the (RF transparent) windows of carrying aircraft (a 4 seat Cessna 172N Skyhawk) (Fig. 6).

Fig. 5. Flight-Ready PASSAT Radar System

Fig. 6. Cessna 172N Skyhawk Carrier

The equipment provided signal sample data and position/attitude data, synchronized post-flight using timestamps from the USRP and SpatialFog **G**PS-disciplined oscillators (GPSDOS)**.** As before, the DVB-T transmitter used was Sutton Coldfield. The primary target area (Bruntingthorpe) was located nearly 46 km away from the transmitter. Apart from the airfield itself, the area is rural and contains farmland surrounded by tree lines and hedge rows. The measurements were made at an aircraft altitude of 600m above

mean sea level (AMSL), i.e. ~167m above the top of Sutton Coldfield transmitter's aerials and ~500m above ground level. Experimental parameters are shown in Table 1.

Table 1: Experimental System Parameters

Property	**Value**	**Unit**
Carrier Frequency	650	MHz
Bandwidth	7.6	MHz
Transmit Power	200	kW
Transmitter Mast Height	264	m
Transmitter Distance	45.1	km
Transmitter Grazing Angle	0.5	degrees
Receive Antenna Beamwidth	50	degrees
Bistatic Angle	5	degrees
Dwell Time	8	s
Average Ground Speed	240	km/h
Aircraft Heading	12	degrees
Aircraft Altitude (AMSL)	600	m

The bistatic angle is defined as the angle between the transmitter and receiver lines-of-sight and the centre of the target area. The imaging geometry at Bruntingthorpe is shown in Figure 7.

Fig. 6. Satellite Image (Bing Maps) of the Bruntingthorpe Target Area with the Flight Path of the Aircraft (black line), Distance and Direction to the Transmitter (white line), and the Distance to the Airfield (yellow line) Shown

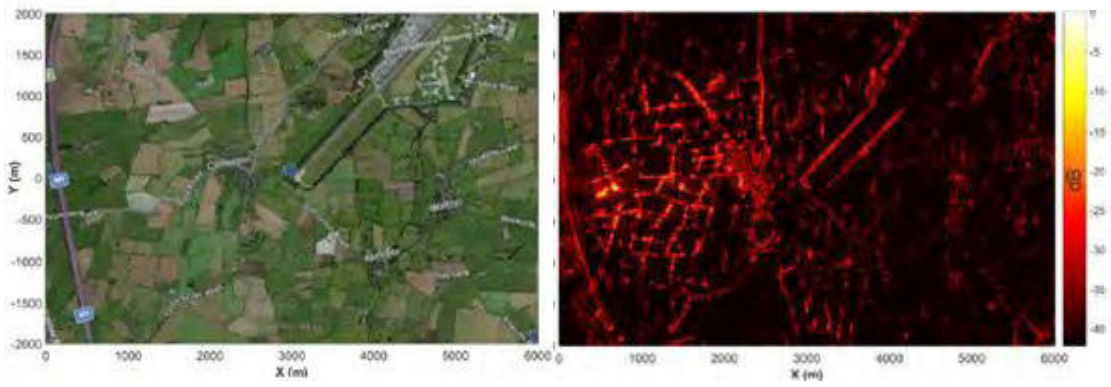

Fig. 7. (left) Satellite Image (Bing Maps) of Bruntingthorpe Area, (right) Passive SAR Image

A SAR image from the target area is shown in Figure 7 (right) next to a satellite photograph of the area (taken from Bing Maps) Figure 7 (left). The image was formed with a dwell time of 8s, corresponding to an overall aperture length of approximately 371 m.

A good correspondence between the SAR image and the photograph can be observed. In particular, locations of high echo intensity coincide with the locations and orientations of trees, hedgerows and buildings in the image. Hedgerows follow the outline of the airstrip, which are also visible in the SAR image. Additionally, there are points of high echo intensity in the SAR image which coincide with the locations of aircraft parking spots in the middle of the airfield. The path of the M1 motorway can be seen towards the left hand edge of the image.

Figure 8, which shows enlargements of the target area displays these features more clearly (e.g. as seen by comparing the PASSAT SAR images (Figs. 8(a) and (c)) with the Bing maps (Figs. 8(b) and (d)). Reflections from flat terrain are not visible, but at the low grazing angles of the transmitter and the receiver this is expected.

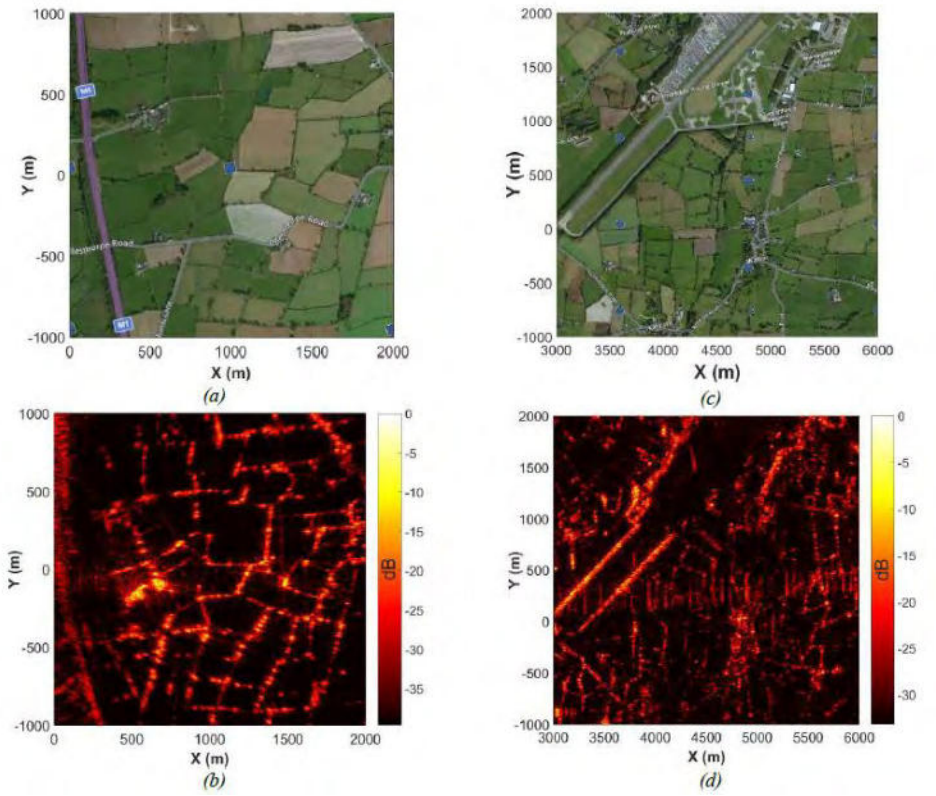

Fig. 8. Enlargements of Target Area: (a) Satellite Image and (b) SAR Image of the Same Rural Area Showing Headgerows, Trees and Buildings; (c) Satellite Image and (d) SAR Image of Airfield Area

4. PASSAT IN-ORBIT DEMONSTRATOR PLANNING

Before a constellation of PASSAT satellites is established, it will be important to gain confidence by means of a spaceborne demonstrator. This would be the next logical step following the current airborne trial work.

A basic requirements analysis has demonstrated that a 12U CubeSat would be a realistic basis for forming the platform for a fully operational PASSAT satellite [1], however, a basic "proof-of-concept" demonstrator could be accommodated in a 6U platform.

The satellite would carry a compact software define radio (SDR) receiver, tuned to the relevant UHF frequencies, which would capture and sample the direct DVB-T transmitted signal and the scattered signals from the terrain "visible" to the transmitter, and within the beam-width of the satellite's 12-15 dBi gain UHF receiving antenna. A dwell time on target of 80 seconds would give an azimuth resolution of a few meters. Assuming 8-bits per sample, and 16 MHz sampling rate, this requires approximately 1.2 Gbytes of on-board data storage, which could easily be accommodated using flash memory storage. From this perspective, it is envisaged that the radar payload (not including the antenna) could be accommodated in a "1U" CubeSat volume.

Surrey recently demonstrated the prototype of a suitable high-gain deployable UHF helical antenna for this mission. The 10 turn, 1.2m long spring-loaded antenna deploys from a ~4U volume (Figures 9 and 10). This gives ~8U for the bus subsystems and propulsion unit. If we can relax the gain requirements, then it should be possible to mount two patch antennas, similar to those used on the airborne demonstrator, as flat deployables on a 6U CubeSat. The gain would be ~6-8dBi given circular polarization.

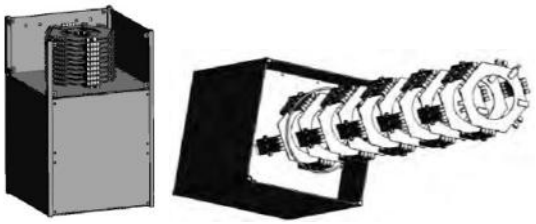

Fig. 9. CAD representation of the SSC Deployable Helical Antenna (12U CubeSat)

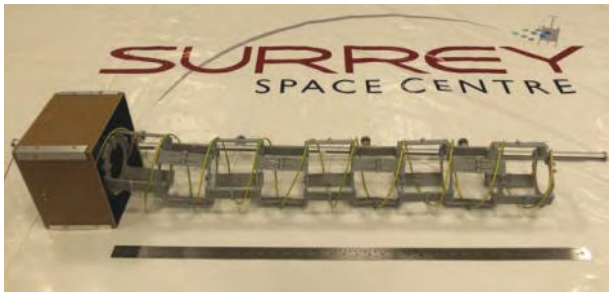

Fig. 10. Prototype SSC Deployable Helical Antenna

Assuming no on-board processing, to download the signal sample data in a single pass, a downlink data rate of approximately 18 Mbps would be required, given a 10% data packet overhead. Lossless data compression could reduce this by a factor of 3 (6 Mbps). This would require a bespoke S-band transmitter, however, for a simple demonstrator, more time could be allowed for downlinking the images, in which case a smaller 2Mbps commercial-off-the-shelf CubeSat S-band downlink transmitter (see [5] for example) would be feasible, allowing one image data set to be downloaded each day.

The peak power demand of the payload and downlink transmitter would be ~6-10W for no more than 10 minutes, which is well within the capability of a 6U or 12U CubeSat. Body mounted solar arrays should be sufficient, but deployed arrays could be used to increase the power available.

In order to operate and maintain a controlled constellation of spacecraft, a degree of orbit control is required to phase the spacecraft around their orbits and to maintain spacecraft separation. Orbit control may also be required at the end of mission in order to dispose of the LEO spacecraft into the atmosphere within the 25 year period, post end-of-life, currently specified for UK missions. To this end, Surrey has developed a butane-based propellant system for CubeSats, designed to give 5–10 mN thrust range at ~ 80s Isp, A 1.5U volume would provide enough propellant to meet the orbit control and disposal requirements .

We conclude that a full PASSAT demonstrator should be feasible with a 12U CubeSat platform (approximately 2U for avionics, 1.5U for propulsion, 1U for the receiver payload, 3U for the S-Band downlink and 4U for the stowed deployable antenna), and that a simple proof-of-concept demonstrator, using deployable patch antennas, could be achieved with a 6U CubeSat. Launching two 6U CubeSats together would allow multi-static SAR imaging and formation flying experiments to be carried out.

5. CONCLUSIONS

This paper has summarised progress into the investigation of the PASSAT concept. Following a ground-based trial, an airborne technology demonstrator was built and a PASSAT airborne campaign was flown. Images were acquired and the validity of the demonstrator and the image formation algorithms was confirmed. Design work on a spaceborne demonstrator is in progress. A suitable basis for the receiver/on-board data storage elements of the payload has been identified and a prototype of a suitable deployable high gain UHF helical antenna has been designed, built and tested. A 6U CubeSat could be used for an initial in-orbit demonstrator mission, and a fully operational constellation would be feasible based on 12U CubeSats.

Acknowledgements

Work reported in this paper was supported by the Centre for Defence Enterprise (CDE) of the UK MoD, project no. CDE 38496. The authors thank Almat Aviation Ltd. for their support in organising and conducting the airborne trials.

6. REFERENCES

[1] C. Underwood et al., “PASSAT: Passive Imaging Radar Constellation for Near-Persistent Earth Observation”, Paper presented at the 68th International Astronautical Congress (IAC), Adelaide, Australia, 25-29 September 2017. IAC-17-B1.3.3

[2] M. Antoniou, A.G. Stove, H. Ma, H. Kuschel, D. Cristallini, P. Wojaczek, C. I. Underwood, A. Moccia, A. Renga, G. Fasano, M. Cherniakov, “Passive SAR Constellation for Near-Persistent Earth Observation: Prospective and Issues”, *IEEE Aerospace and Electronic Systems Magazine*, 33(12):4-15, DOI: 10.1109/MAES.2018.170178.

[3] H. Ma, A.G. Stove, G. Atkinson, C.I. Underwood, M. Cherniakov, M. Antoniou, “Passive SAR Using Small Satellite Receivers for Persistent Earth Observation”, Paper presented at the International Conference on Radar Systems 2017, Belfast, UK, October 2017.

[4] “Spatial FOG | Advanced Navigation”, [Online]. Available: http://www.advancednavigation.com.au/product/spatial-fog, [Accessed 10-Sep- 2018]

[5] ClydeSpace S-band Transmitter Specifications, [Online], Available: https://www.clyde.space/products/35-cput-sband-cubesat-transmitter, [Accessed: 5-Sep-2017]

CloudCT – Computed Tomography of Clouds by a Small Satellite Formation

Klaus Schilling[1], Yoav Y. Schechner[2], Ilan Koren[3]

[1] Zentrum für Telematik, Magdalene-Schoch-Str. 5, 97074 Würzburg, Germany,
Phone: +49 931 615633 10, Mail: klaus.schilling@telematik-zentrum.de
[2] Technion - Israel Institute of Technology, Haifa, Israel,
Phone: +972 4829 3236, Mail: yoav@ee.technion.ac.il
[3] Weizmann Institute of Science, Rehovot, Israel,
Phone: +972-8-934-2522, Mail: ilan.koren@weizmann.ac.il

Abstract: Clouds are recognized to be the main source of uncertainty in global climate models. Part of this problem is driven by lack of proper observations of shallow convective clouds. In context a distributed networked system of small satellites is used to use multipoint observations to characterize such clouds. A formation of 10 pico-satellites with high accuracy attitude determination and pointing capacity is used to retrieve 3D properties of clouds by a computed tomography approach, in high spatial and temporal resolutions. Data obtained by these measurements will be used to improve and train high resolution, cloud resolving models with the objective to improve longer term climate predictions.

1. INTRODUCTION

Clouds play a lead role in Earth's energy budget and water cycle, and contribute the largest uncertainty to our climate understanding [17]. Out of all cloud types, warm shallow clouds that are abundant and often below the instruments resolution, contribute greatly to this uncertainty [4], [2]. Current atmospheric retrievals use a plane-parallel assumption, which is incompatible with the 3D heterogeneous nature of warm convective clouds [13]. There is an acute need for improvement of cloud-resolving models that will capture correctly properties and feedbacks of such clouds. Outputs of such models would yield better parametrization scheme that describe the physics of warm convective and stratiform clouds, and the clouds' sensitivity to environmental changes in global climate models.
To address this challenge, CloudCT bridges an observational gap. The sensing approach uses cloud scattering-tomography, relying on a formation of small satellites. They will simultaneously image cloud fields from multiple directions. Scattering tomography is developed to derive the 3D volumetric structure of cloud fields, base-to-top profiles of droplets' size and their variance, volumetric distribution of optical extinction and rain indicators.

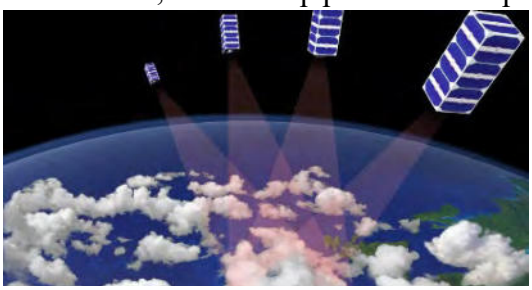

Fig.1: Multi-perspective cloud measurements by the satellite formation

Satellites at a mass of a few kilograms, so-called pico- and nano-satellites, were initially mainly used as motivating tool in system engineering education [14], but dramatic technology development lead to a majority of commercial satellites since 2014. Such pico-

and nano-satellites exhibit increasing performance capabilities, making them attractive for science applications [20], [12]. As launcher costs scale with mass, nowadays in particular multi-satellite missions, using sensor network technologies on-board of small satellites can be applied in-orbit to enable innovative observation methods [1], [6], [15], [16]. In CloudCT a formation of satellites will be realized, enabling self-organization in orbit. This is based on an electric propulsion system for orbit control to correct drift by orbit perturbations and relative navigation methods, to yield a formation topology offering optimal observation conditions.
In CloudCT, interdisciplinary synergies from pico-satellite system engineering, cloud modelling, and tomographic imaging are expected to enable new sensor network approaches for innovative Earth observation. This is expected to improve the input for climate models and therefore narrow their uncertainties. It will yield a database of 3D macro and micro structure of warm cloud fields, while setting the stage for next-generation global observations by distributed networked spacecraft.

2. CLOUD MODELLING

Unlike weather models, whose forecast time spans days, global climate models (GCM) predict climate trends in a scale of dozens of years. The typical resolution of GCM is 100 km and therefore, most warm clouds are in a sub-grid scale and have to be parametrized [11]. To reduce GCM errors, better understanding of cloud processes and sensitivities is needed. This is done using high resolution, cloud resolving models, which describe interactions dynamical, microphysical and radiative processes, as known in the state of the art. However, current cloud resolving models lack resolution and capacity to properly represent the nonlinear behavior of cloud systems, including aspects of cloud aerosol interactions, cloud feedbacks, mixing, turbulence, rain-processes and cloud-radiation interaction [8]. To study feedbacks, tune processes and validate models, shallow convective clouds are particularly important, but they are largely overlooked by current measurement methods.
In CloudCT, cloud resolving models will be used in two phases. At the early stage (modeling phase I) the cloud models will be used to train and validate the retrieval algorithms. The models will be used to simulate high resolution scenes. For each scene, the radiation signature will be calculated in accord to the sun and satellites geometries. This will serve as input for the algorithms that in return will be trained to retrieve cloud properties. The algorithms, the spectral regimes as well as the best satellite formations, will be optimized by interactively link the cloud resolving model results to the algorithm via radiative calculations. Once in orbit (modeling phase II) the flow of information between models and observations will be reversed. CloudCT will provide spaceborne data and products on macro and microphysical properties of warm clouds. These will serve to improve the capacities of cloud resolving simulations, in sub-cloud to cloud field scales. Measured macro-scale properties such as size distributions of clouds, spatial organization of clouds in the field and cloud evolution in time [5], as well as microphysical properties (e.g., liquid water content, droplets effective radius and variance), as well as their dependence on environmental thermodynamic properties, will test models for improving dynamical and microphysical schemes. Cloud trends observed as a function of thermodynamic and aerosol properties will help to pinpoint which part of a model should be improved. Moreover, differences between observations and simulations of transitions between cloud to a (so-called) cloud-free atmosphere will guide us on how to improve mixing and entrainment schemes. Better understanding of the main physical processes that control shallow

warm clouds and their interactions will yield better and more realistic parametrizations of such clouds in GCMs, hence improved climate predictions.

3. COMPUTED TOMOGRAPHY APPROACH

To reduce uncertainties in cloud models we need to (a) image warm clouds, particularly small ones, in high resolution, and (b) analyze the properties of the clouds, based on the images. There is a challenge to focus on internal properties of clouds. External properties, such as cloud 3D shape can be derived by adapting rather standard multi-view stereo, based on images taken simultaneously from the satellite formation [19]. It is far more challenging to remotely sense, in 3D, internal characteristics such as cloud droplet concentration and size. Current methods for probing cloud characteristic assume a layered (one-dimensional) structure, in which radiation diffuses mainly vertically. In contrast, when dealing with small clouds, the cloud's periphery is not far from points inside. We thus derive retrieval based on 3D radiative transfer in a 3D heterogeneous medium.
The solution is motivated by medical computed tomography (CT). In typical medical CT, however, there is control over an active radiation source, and the imaging model assumes a linear relation to the internal content. In multi-scattering radiative transfer, the relation is non-linear, requiring analysis based on 3D radiative transfer. Reference [7] recently showed that such analysis improves Xray-CT. Nevertheless, in large scale remote sensing of atmospheric scattering, imaging is passive, relying on solar radiation. Recent progress addresses models and algorithms for scattering-based passive CT, including tests by using airborne data from JPL's AirMSPI instrument [9], [10]. To enable 3D sensing from the ground, a ground-based wide area dense network of untethered sky cameras was used [18]. These developments set the stage for spaceborne observations in CloudCT.
Spaceborne CT requires a large number of simultaneous viewpoints: this will be realized by a large formation of small satellites. Each satellite will carry radiometrically-calibrated optical cameras. Scattering by cloud droplets and other aerosols is pronounced in and around visible wavelengths. The ground resolution is expected to be about 50 meters. This resolution, obtained from low earth orbit, means pointing accuracy which challenges design and control of small satellites. While engineering the system, optimization of its parameters (wavelengths, formation topology, orbit, solar angles etc.) will be done using simulations of cloud fields by cloud resolving models, 3D radiative transfer, platform jitter and camera noise.

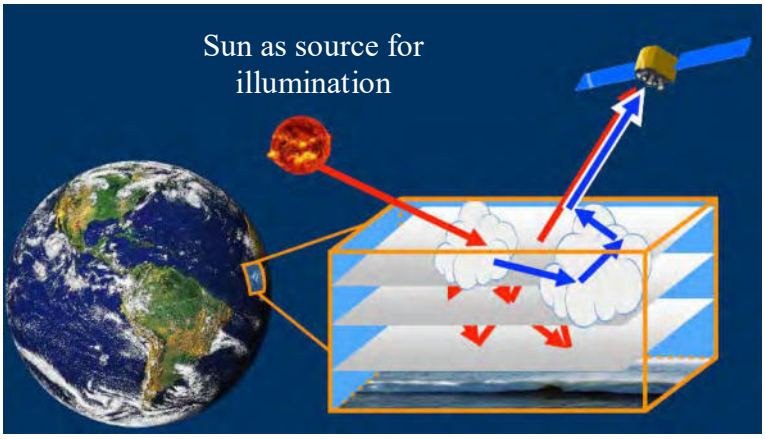

Fig.2: Illuminated by the Sun, the backscattered light from different cloud layers is detected by the satellites from different directions. Sensor data fusion algorithms generate 3D-images by postprocessing of data from the satellite formation.

4. SMALL SATELLITE FORMATIONS

The performance and lifetime capabilities of the class of pico- and nano-satellites (in the 1kg to 10 kg range) dramatically improved in the recent years. In particular, high precision attitude control by miniature reaction wheels as well as orbit control by electric propulsion systems provide all essential functions for joint measurements by satellites cooperating in a formation. This offers innovative application potential for distributed sensor networks in Earth observation, such as CloudCT.

4.1 Satellite Design

Terrestrial requirements for miniature and power-efficient electronics, in particular in the automotive sector and for cellular phones, lead to significant technology progress. The "new space" approach takes advantage of these impressive commercial developments. Nevertheless, the deficits of miniaturization are higher noise levels and, in particular in the context of space applications, higher susceptibility for radiation effects. Here software for filtering and for FDIR (fault detection, identification and recovery) receives a significant role as technology enabler for usage in space [[3], [15]. Such concepts have already been applied on the satellite UWE-3 (launched 2013), which exhibited this way seamless operations since launch, today already for 5.5 years, despite encountered frequent SEUs (single event upsets) and latch-ups caused by radiation in a polar orbit in 600 km altitude. Thus at a mass of just 3 kg in CloudCT a related satellite capable of formation flying is designed (cf. Fig. 3).

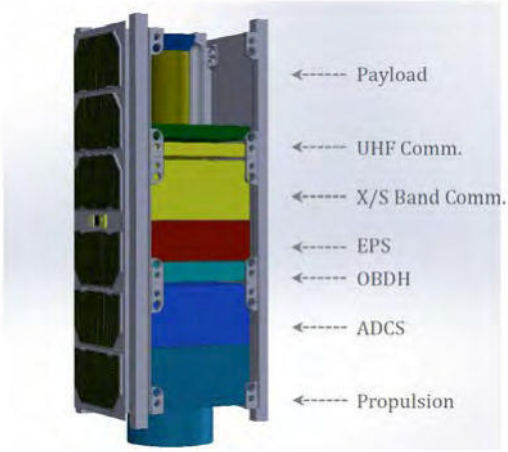

Fig. 3: CAD model of the ClouCT spacecraft

For coordinated joint observations of clouds, precision attitude control to observe same target areas from different perspectives. Due to recent miniature reaction wheels (cf. Fig.4), appropriate 3-axes attitude control systems can be composed in order to achieve the necessary pointing accuracies at the level of pico-satellites.

Fig.4: The miniature reaction wheel (from S^4/Wittenstein) with low nominal power consumption.

4.2 Orbit Design

The orbits in this multi-satellite system are designed in such a way that the average disturbance per revolution is similar for all spacecraft. In case of two satellites, this is realized by a helix orbit, where an identical semi-mayor axis in combination with a small eccentricity and a difference in the argument of perigee $\Delta\omega$ of 180° leads to one rotation of the two satellites around each other during one orbit revolution (see Fig. 5). This principle used earlier in the Tandem-X or CAN-X4/5 missions can be extended to multi-satellite missions to so-called cartwheel configurations. Here the satellites are subsequently placed on the reference orbit or rotate around a virtual center on the reference orbit.

Fig.5: Helix orbit

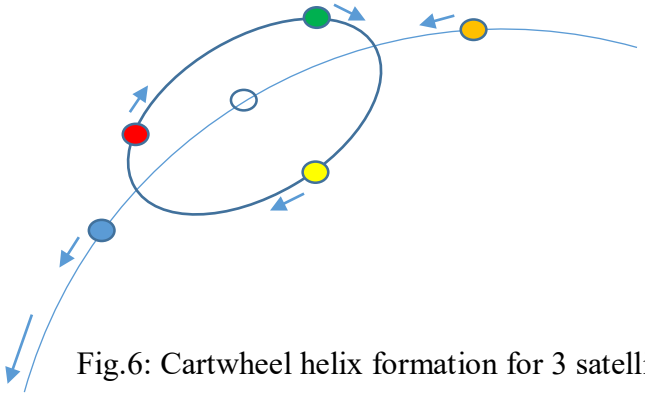

Fig.6: Cartwheel helix formation for 3 satellites

4.3 Satellite Formations

To realize the novel tomography approach, distributed control algorithms coordinate the multi-satellite system in a formation on basis on relative navigation sensor measurements. While in a classical constellation each satellite is individually controlled from ground control, in a formation the satellites self-organize via inter-satellite links. In addition, advanced in-orbit autonomy, distributed computing, and networked control contribute to efficient self-organization. The formation initialization after deployment from the launcher adaptor in the delivery rockets upper stage, as well as the drift compensation by orbit perturbations of the different satellites are realized by an electric propulsion system. New challenges refer also to ground testing of formation characteristics: The crucial inter-satellite links and coordinated attitude control for observations in the formation are tested by high precision turntables.

Fig.7: The high precision, high dynamics turntables to characterize in hardware-in-the-loop-tests intersatellite links and coordinated pointing control in observations.

5. CONCLUSIONS

Clouds have a key role in Earth's energy balance and its water cycle, as even small errors in assessing clouds' properties can lead to major inaccuracies in climate predictions. By combining interdisciplinary synergies from spacecraft engineering, imaging and cloud physics, innovative Earth observation methods are developed to characterize the clouds' external and internal properties in 3 dimensions. The computed tomography approach in CloudCT takes images simultaneously from many directions around the clouds to generate by sensor data fusion methods related 3D-images. This new data will serve to train cloud resolving models to better capture warm cloud properties and climate sensitivities. The appropriate satellite technology base is provided by a networked self-organizing formation of small and agile satellites, employing an electric propulsion system and a precision 3-axes attitudes control system composed of miniature reaction wheels to coordinate the proper observation geometry. This interdisciplinary approach in the CloudCT mission aims to investigate approaches for improvements in longer term climate predictions.

ACKNOWLEDGEMENTS

The authors acknowledge the financial contributions and the inspiring framework of the ERC Synergy Grant "CloudCT". Precursor works of Prof. Koren on climate models were supported by an ERC Consolidator Grant and for Prof. Schilling on satellite formations by an ERC Advanced Grant. Prof. Schechner's research is partly done in the Ollendorff Minerva Center, funded through the BMBF. In addition, he is a Landau Fellow – supported by the Taub Foundation.

6. REFERENCES

[1] Alfriend, K. T., S. R. Vadali, P. Gurfil, J. P. How, L. S. Breger, 2010. *Spacecraft Formation Flying. Dynamics, Control and Navigation,* Elsevier Astrodynamics

[2] Bony S., J.L. Dufresne, *Marine boundary layer clouds at the heart of tropical cloud feedback uncertainties in climate models,* Geophys. Res. Lett., 32 (2005)

[3] Busch, S., P. Bangert, S. Dombrovski, K. Schilling; UWE-3, In-Orbit Performance and Lessons Learned of a Modular and Flexible Satellite Bus for Future Pico-Satellite Formations, Acta Astronautica *Vol. 117*. 2015, pp.73-89)

[4] Dagan, G., I., Koren, O. Altaratz, Lehahn, *Shallow Convective Cloud Field Lifetime as a Key Factor for Evaluating Aerosol Effects*, iScience, 10 (2018)

[5] Dagan G, Koren I, Kostinski A, Altaratz O: *Organization and oscillations in simulated shallow convective clouds,* Journal of Advances in Modeling Earth Systems 10 (2018), pp. 2287-2299,

[6] D'Errico (ed.), M. *Distributed Space Missions for Earth System Monitoring*. Springer Verlag 2012

[7] Geva, A., Y. Y. Schechner, J. Chernyak, R. Gupta, *X-ray computed tomography through scatter*, Proc. ECCV (2018).

[8] Guichard F., Couvreux F., *A short review of numerical cloud-resolving models*, Tellus A: Dynamic Meteorology and Oceanography, 69 (2017)

[9] Levis, A., Y. Y. Schechner, A. Aides, A. B. Davis, "*Airborne three-dimensional cloud tomography*," Proc. IEEE ICCV (2015).

[10] Levis, A. Y. Y. Schechner, A. B. Davis, *Multiple-scattering microphysics tomography*, Proc. IEEE CVPR (2017).

[11] Lopez, P., *Cloud and Precipitation Parameterizations in Modeling and Variational Data Assimilation*: A Review. J. Atmos. Sci. 64 (2007) pp. 3766–3784

[12] NAS report "Achieving Science with CubeSats", 2016, www.nap.edu/cubesats

[13] Platnick, S., King, M. D., Ackerman, S. A., Menzel, W. P., Baum, B. A., Riedi, J. C., Frey, R. A. *The MODIS cloud products: Algorithms and examples from Terra.* IEEE Transactions on Geoscience and Remote Sensing, 41 (2003), 459–473.

[14] Schilling, K., *Design of Pico-Satellites for Education in System Engineering*, IEEE Aerospace and Electronic Systems Magazine 21 (2006), pp. 9-14.

[15] Schilling, K.; "Perspectives for Miniaturized, Distributed, Networked Systems for Space Exploration*"*, *Robotics and Autonomous Systems* Vol. 90 (2017), p. 118–124

[16] Schilling, K.; Tzschichholz, T.; Motroniuk, I.; Aumann, A.; Mammadov, I.; Ruf, O.; Schmidt, C.; Appel, N.; Kleinschrodt, A.; Montenegro, S.; Nuechter, A.; TOM: A Formation for Photogrammetric Earth Observation by Three CubeSats; *4th IAA Conference on University Satellite Missions, Roma,*. 2017, IAA-AAS-CU-17-08-02

[17] Trenberth, K. E., Fasullo, J. T., Kiehl, J., *Earth's global energy budget,* B. Am. Meteor. Soc, 90 (2009) 311–323.

[18] Veikherman, D. A. Aides, Y. Y. Schechner, A. Levis, "*Clouds in The Cloud*," Proc. ACCV (2014), pp. 659-674.

[19] Zakšek, K.; James, M.R.; Hort, M.; Nogueira, T.; Schilling, K.; *Using picosatellites for 4-D imaging of volcanic clouds: Proof of concept using ISS photography of the 2009 Sarychev Peak eruption*, Journal Remote Sensing of Environment. Vol. 210, 2018, pp: 519-530

[20] Zurbuchen, T. H., R. von Steiger, S. Bartalev, X. Dong, M. Falanga, R. Fléron, A. Gregorio, T. S. Horbury, D. Klumpar, M. Küppers, M. Macdonald, R. Millan, A. Petrukovich, K. Schilling, J. Wu, and J. Yan ; "*Performing High-Quality Science on CubeSats*", Space Research Today, Vol. 196 (August 2016), pp. 10-30.

Global Digital Elevation Model from a Formation of Small Synthetic Aperture Radar Satellites -Requirements and Opportunities of MirrorSAR-

Josef Mittermayer[1], Gerhard Krieger[1]

[1]German Aerospace Center (DLR), Microwaves and Radar Institute,
Oberpfaffenhofen, 82234 Wessling, Germany
Phone: +49 8153 28 2373, Mail: josef.mittermayer@dlr.de

Abstract: The paper discusses the feasibility of small satellite SAR missions. Two example systems are analyzed in terms of components, systems and performance parameters. The dispersed SAR for ship monitoring consists of 13 small satellites. MirrorSAR for a global DEM mission is built from 1 large transmit and 3 small receive satellites. The requirements on hardware and system key components are discussed.

1 INTRODUCTION

The Synthetic Aperture Radar (SAR) satellites currently in orbit consist of large single satellites typically larger than 10 m^3 and heavier than 1 ton. These satellites are inflexible and fixed to certain applications during their entire life time that lasts typically from 5 to 15 years. The TerraSAR-X (TSX) satellites [2] launched in 2007 and 2010 are such classic large SAR satellites. However, their flexibility to update many instrument settings during the mission has set a new standard, e.g. two new operating modes were put into operation after launch [8]. Both TSX satellites are still in operation. Together they form the TanDEM-X (TDX) mission, too, which created a Digital Elevation Model (DEM) of the Earth by surface measurement from two different viewing angles. This technique is known as SAR interferometry [1]. A decisive factor is the distance between the two satellites, the so-called baseline (BL). However, the two TSX satellites have the disadvantage of their large physically rigid radar antennas, which cannot be altered in shape and arranged in more than two positions. Stimulated by new developments in small, cheap and serially produced satellites - often entitled by the term NewSpace - novel concepts for SAR Earth observation missions are emerging, which are replacing large singular SAR satellites with formations of small satellites.

This paper discusses whether SAR missions with small satellites are feasible, whether there are advantages over missions with large satellites, and which technologies need to be newly or further developed for realization of small SAR satellites systems.

Two SAR NewSpace concepts are discussed, i.e. the Small Satellite Dispersed SAR (SSDS) [3], in a formation for ship detection and identification in section 2, and more detailed the MirrorSAR [4] in a formation for global DEM generation in section 3.

2 SMALL SATELLITE DISPERSED SAR FOR SHIP OBSERVATION

Figure 1 shows the SSDS acquisition geometry for ship detection and identification. It consists of 13 small X-band SAR satellites in a 1500 km orbit. Each satellite has Tx/Rx-capability, is able to point to 13 elevation swaths and to switch between fore and aft illumination. For ship detection, all satellites point forward and map adjacent swathes that combine to a total swath of 1300 km at a resolution of 10 meter. Once a ship has been detected, all satellites point towards aft using the elevation swath that covers the ship. The combination of all satellites provides a resolution of 1 m. The time available for onboard ship detection and commanding for identification acquisition is 48 s in the worst case, which is the near range swath at 17° incidence angle.

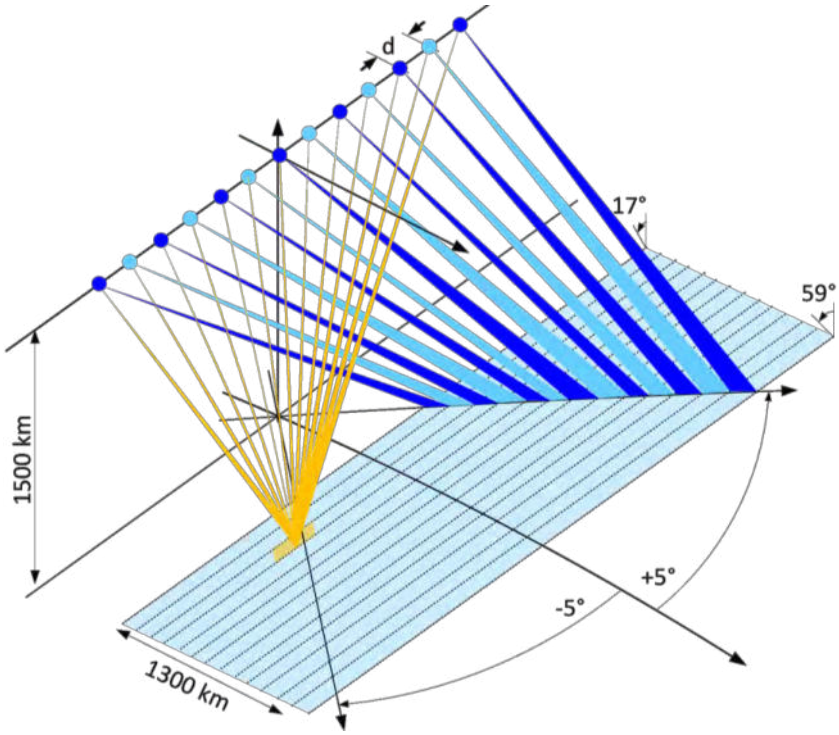

Figure 1: Distributed SAR configuration in close formation providing capabilities for wide area ship detection (blue) and high resolution ship identification (yellow).

The satellites fly in a SAR-train orbit configuration [5], i.e. on the same orbit with along-track separations. The difficulty is to obtain a gap free synthetic aperture with a sub-meter sampling in along-track, typically between 0.5 m and 1 m. In [3], the Dispersion Method is defined, which separates the satellites by more than 100 m and nevertheless achieves a gapless synthetic aperture with sub-meter sampling. The relative satellite along track positioning accuracy is required to be significantly smaller than Nyquist [3]. The distribution of the echo reception to several satellites allows for a reduction of the system PRF as virtual phase center positions are substituting physical ones. The reduced PRF allows for an increased swath width compared to single satellite SAR systems.

Figure 2 shows in blue more details about the acquisition in detection mode. The gap free synthetic aperture is switched between the 13 swaths in a ScanSAR acquisition scheme, e.g. [6], as follows. All satellites point to a strip for a short time, which is derived from the desired azimuth resolution, and acquire a burst of raw data. This is symbolized in the figure by the dark blue squares. Then the next swathes are acquired one after the other. The small acquired burst of raw data is sufficient to calculate a larger piece of the swath. This is shown in light blue in the figure. A complete coverage of all swathes is achieved when the return time to a certain swath is short enough so that the calculated pieces are overlapping.

In identification mode, the swath width can be reduced to for example 10 km in the cross-swath direction in order to decrease the amount of raw data. This is shown in Figure 2 by the smaller width of the yellow swath. The full synthetic aperture is acquired for one swath. Its extent is shown in orange. The limited extent of the swath is shown in yellow.

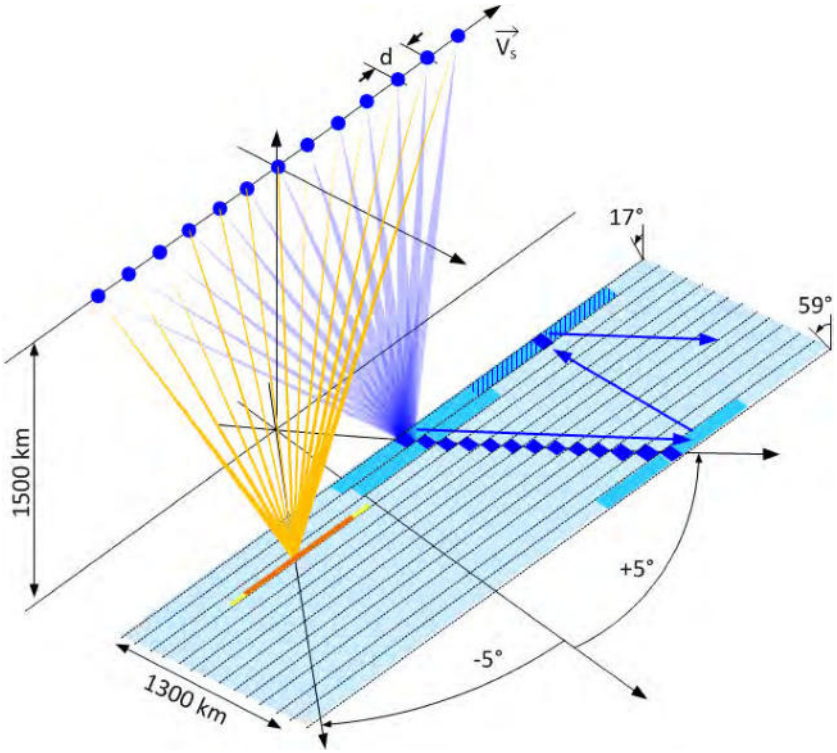

Figure 2: Distributed SAR with detection mode in ScanSAR acquisition (blue) and identification mode in stripmap acquisition (yellow). Note, the smaller scaling in azimuth, which is the flight direction, and ground range, which is the cross-flight direction on ground.

In terms of flexibility, redundancy and individual power reduction it is advantageous that all satellites are equipped with Tx/Rx functionality. Thus, the individual satellite average transmit power is small, i.e. in the range of a few Watts.

One possible concept for the image processing is to perform on-board processing for the detection mode and on-ground for the identification mode. In detection mode, a data rate from each individual satellite to one processing satellite is required in-between 15 to 30 MBit/s, depending on the incidence angle. In identification mode, assuming a scene size of 10 km x 10 km and 1 m resolution, each satellite acquires raw data with a data rate of about 65 Mbit/s. All satellites together need to downlink about 3.5 Gbit of raw data for one scene.

3 MIRRORSAR FOR GLOBAL DEM GENERATION

Up to now TDX [1] provides the best global Digital Elevation Model (DEM). As shown in Table 2, it took 3.5 years to complete the DEM in a resolution of 12 m x 12 m horizontally with a relative height error of 2 m defined as 90% linear point-to-point error $\Delta h_{90\%}$ [1]. This error corresponds to about 2.33 times the standard deviation. TDX is composed of two large TSX satellites [2], each of them about 5 m in length and with a diameter of 2.4 m. Table 1 provides satellite parameters while Figure 3 shows on the left the two TSX satellites that form the overall TDX space segment.

The essential core of MirrorSAR [4] is the distribution of the Tx and Rx antennas on separate platforms, the reduction of the Rx satellites functionality down to a transponder that only forwards the ground radar echoes back to the Tx satellite, and a dual baseline (BL) acquisition. As can be seen in Figure 3 on the right, the larger Tx satellite illuminates the ground and the three smaller Rx satellites receive the backscattered radar signals. The Rx satellites only mirror the radar signals via an inter-satellite link back to the Tx satellite.

The down conversion of all received radar signals is performed on-board the Tx satellite based on the same oscillator that had already been used for the Tx pulse generation. Therefore, the phase synchronization of the bi-static radar signals is not more complex than with a monostatic radar. The hardware requirements for the Rx satellites are extremely reduced. They do not perform radar signal down conversion, do not have a mass memory or a downlink functionality. They are therefore lightweight and have low power demands. A MirrorSAR system is defined in Table 3. It provides the DEM performance of Table 2 on the right.

sun-synchronous orbit	514 km
size	5 m along track x 2.4 m diameter
wet mass	~1200 kg
x-band radar antenna dimension	4.8 m along track x 0.8 m elevation
x-band downlink rate	300 MBit/s
average transmit power	450 W
incidence angle	20° - 45°

Table 1: TerraSAR-X satellite parameters

	TanDEM-X	MirrorSAR
global acquisition duration	~3.5 years	~5 months
DEM horizontal resolution	12 m x 12 m	6 m x 6 m
relative height error (90% p-t-p error)	2 m	1 m

Table 2: Estimated MirrorSAR and verified operational TanDEM-X DEM performance

Tx & Rx antennas (azimuth x elevation)	3 m x 0.9 m
Tx average power	600 W
Tx bandwidth / PRF	150 MHz / 6.2 kHz
satellite dimensions	>1 m^3 (Tx) <<1 m^3 (Rx,unflatable antenna)
swath width / incidence angle	20 km / 40°
optical mirror link bandwidth	3 x 150 MHz
small / large cross-track baselines	around 200 m / around 1200 m
acquisition data rate	~3 x 1 Gbit/s
D/L data rate (one station north and south)	~3000 Mbit/s

Table 3: MirrorSAR parameters

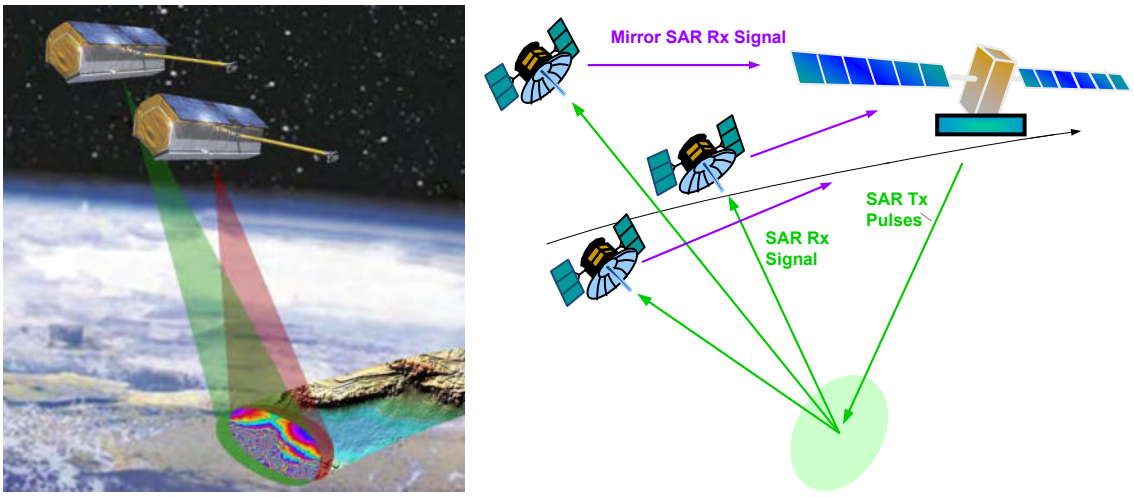

Figure 3: (left) TanDEM-X space segment consisting of two large TerraSAR-X satellites. (right) MirrorSAR system with its large transmit satellite and 3 small receive satellites that mirror back the ground received radar signals to the Tx satellite.

Dual BL acquisition means to acquire at least two interferometric BLs at the same time. In interferometry, a large BL provides good height accuracy while a small BL means accurate phase unwrapping [4]. One close formation orbit concept that provides the required BLs in a save way is to fly the Rx satellites in helix orbits [1] around a virtual position on the orbit of the Tx satellite. Figure 4 on the left shows for an example orbit formation the relative BLs of three Rx satellites Rx1, Rx2, and Rx3 to that virtual position Rx0. The interferometric BLs result from the differences in the relative BLs. Figure 4 on the right provides the height error estimated from the MirrorSAR example parameters and BLs. It is around 1m up to latitudes of 60° above/below equator. For TDX, it took about 3.5 years to obtain two global acquisitions for two different BLs, which suffer from surface changes in-between the two acquisitions. One main advantage of MirrorSAR is the dual BL acquisition that provides a better DEM in shorter time. Only 5 months are required in case that a very high downlink capacity is available.

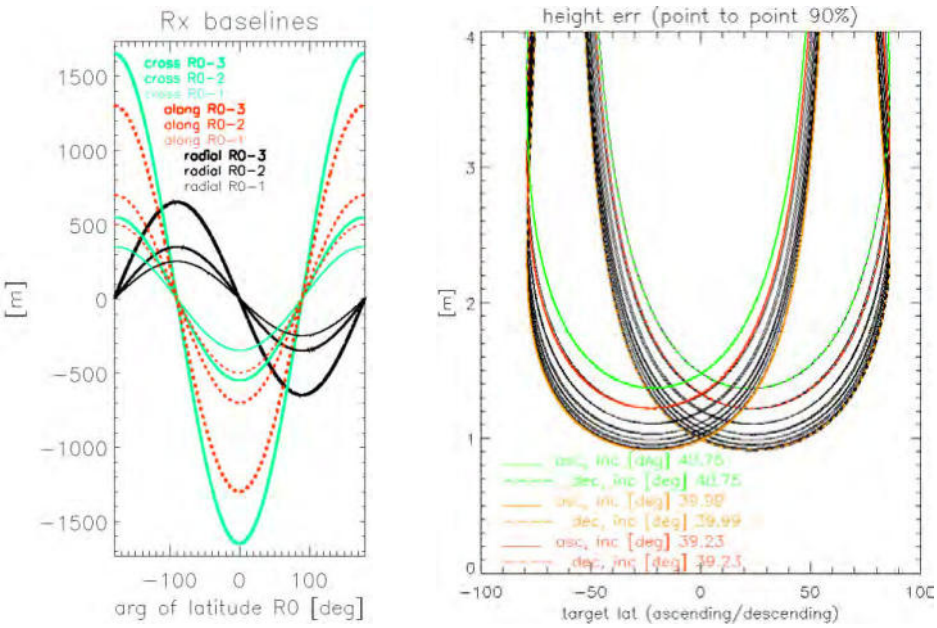

Figure 4: (left) Relative baselines between the Rx satellites 1,2 and 3 and the virtual orbit position Rx0. (right) Estimated height error of the example MirrorSAR system.

4 DISCUSSION ON TECHNIQUES AND COMPONENTS

The system analysis and performance estimates for the Small Satellite Dispersed SAR (SSDS) and MirrorSAR examples show that a distributed SAR with small satellites is feasible, has potential to improve the performance and at the same time can reduce costs. However, some hardware or system components still need to be improved or made available for space.

A key element for MirrorSAR is the inter-satellite link (ISL) from the Rx satellites back to the Tx satellite. An ideal solution would be an optical link or a RF-link with a frequency high enough to allow for amplitude modulation by the radar signal. The amplitude modulation overcomes synchronization problems. However, the availability of affordable optical links is still open. There are alternatives [4], which transmit the Tx radar signal also to the Rx satellites as a reference signal, and use the lower frequencies for the inter-satellite link.

In the SSDS detection mode example, there is the need to exchange 13 times 15-30 Mbit/s between the small satellites via a inter-satellite links. It would rather be an inter-satellite network.

Another challenge in MirrorSAR is the high D/L rate of ~3Gbit/s and the high orbit duty cycle of ~10 min required to complete the global acquisition within 5 months. A relaxation of the global acquisition duration allows for both, a reduced D/L rate and a lower orbit duty time, e.g. a 16 months global acquisition demands 800 Mbit/s and 3 minutes orbit duty time. Nevertheless, solutions for D/L are still investigated. Relay satellites could help to reduce the D/L rate by increasing the D/L contact times. However, this is costly. Optical downlink systems allow for much higher data rates. The phase preserving optical laser terminal OSIRISV3 is scheduled for test on-board the ISS for mid 2019 with downlink data rates of 10 - 100 GBit/s [7]. In the SSDS detection mode, a downlink volume of 3.5 Gbit is required for one scene of 10 km x 10 km.

There is also potential for on-board data compression due to the availability of parallel SAR channels with similar raw data. For example in MirrorSAR there are three channels on-board the Tx sat.

In a SAR train formation, it is considered possible to achieve a relative along-track accuracy in the order of decimeters, which is sufficient for the SSDS synthetic aperture generation. The deterministic formulation of the dispersed SAR allows an inter-satellite separation of 156 m with an oversampling factor of 1.2. Other approaches that base on random positioning of the satellites require a higher oversampling.

The Helix concept is well proven by the TanDEM-X mission. Interleaved Helix-orbits allow to realize the required MirrorSAR constellation. The Helix concept is not expected to be feasible for dispersed SAR but could be combined with the SAR train. For example, several SAR trains fly interleaved Helixes and provide several baselines.

In MirrorSAR, the radar transmit power of 600 W average can be provided by the larger Tx satellite. In the SSDS example, the average power is reduced to a few Watts due to the alternating transmission of all small satellites. However, in the current design, it re-

quires a peak power of 1.8 kW, which is too high. There are solutions in development, for example a simultaneous transmit all satellites with divided radar bandwidth.

The size of the MirrorSAR Rx satellites is reduced compared to monostatic missions. The size of the Tx satellite is reduced as well. It shows a volume of about 4 m^3 compared to 23 m^3 for a TerraSAR satellite. However, more detailed design work is required.

The antenna size required in the provided X-band examples is about 3 m x 0.9 m for MirrorSAR Tx and Rx, and 1.5 m x 0.7 m for the Dispersed SAR example SSDS. The antenna dimensions are expected to remain in further developments. Unfolding mechanisms seem to provide good solutions in case of further reduced bus dimensions.

5 REFERENCES

[1] G. Krieger, A. Moreira, H. Fiedler, I. Hajnsek, M. Werner, M. Younis, and M. Zink, "TanDEM-X: A Satellite Formation for High-Resolution SAR Interferometry", IEEE Transactions on Geoscience and Remote Sensing, vol. 45, no. 11, pp. 3317–3341, 2007.

[2] W. Pitz and D. Miller, "The TerraSAR-X Satellite", IEEE Transactions on Geoscience and Remote Sensing, vol. 48, no. 2, pp. 615–622, 2010.

[3] J. Mittermayer, P. López-Dekker, T. Kraus, G. Krieger, "Small Satellite Dispersed Synthetic Aperture Radar", Proc. Small Satellites Systems and Services, Valletta, Malta, 2016.

[4] G. Krieger, M. Zonno, J. Mittermayer, A. Moreira, S. Huber, M. Rodriguez-Cassola, "MirrorSAR: A Fractionated Space Transponder Concept for the Implementation of Low-Cost Multistatic SAR Missions", Proc. of EUSAR 2018, Aachen, 2018.

[5] J. P. Aguttes, "The SAR train concept: Required antenna area distributed over N smaller satellites, increase of performance by N", in Proc. IGARSS, 2003.

[6] A. Moreira, J. Mittermayer, R. Scheiber, "Extended Chirp Scaling Algorithm for Air- and Spaceborne SAR Data Processing in StripMap and ScanSAR Imaging Modes", IEEE Trans. Geoscience and Remote Sensing, vol. 34, no. 5, pp. 1123–1136, Sep. 1996.

[7] https://artes.esa.int/sites/default/files/13%20-%20Schmidt%20DLR.pdf

[8] S. Buckreuss et al.,"Ten Years of TerraSAR-X Operations", Remote Sensing, 2018, DOI: 10.3390/rs10060873, ISSN 2072-4292.

A CUBESAT BASED GNSS CONSTELLATION FOR PLANETARY & EARTH SYSTEM EXPLORATION

Norbert Frischauf, Manfred Wittig
SpaceTec Capital Partners, 80331 Munich, Germany
email: frischauf@spacetecpartners.eu

Otto Koudelka
Graz University of Technology, 4400 Graz, Austria

The global space economy reached USD 329 bn in 2016, having grown on average by 5.1% p.a. in between 2005 and 2016. During this period, the global space economy saw periods of stagnation and of strong growth, at times even outgrowing the overall global economy. While the governments were the driving forces in the 20th century (e.g. Apollo-programme, International Space Station (ISS), as well as GPS), today it is the commercial activities that are setting the pace, accounting for USD 253 bn or 76% of the global space economy in 2016. Albeit rather recent, the commercialisation of space is to intensify in the coming years, as the space sector experiences rapid growth in new approaches to space development. The so-called "NewSpace" trend, thrives upon technology and business model innovations that allow for a significant reduction of costs, the provision of new products and services as well as for a broadening of the customer base. As this comes along with increased returns for companies and investors, the onset of a whole new wave of commercial activities within the space sector is the result.

A clear indication that this NewSpace movement is picking up speed is the fact that space ventures have attracted over USD 18.4 bn of investment, including USD 4.5 bn in debt financing, since 2000. This rise of new entrants has brought with it new opportunities for innovations in products, services and processes which, in turn, have created spill-over effects to various industries in- and outside of the space sector. Miniaturisation, agile development, faster generation change and an increase utilisation of industrial standards are trends that go along with NewSpace, possibly best showcased by the advent of Cubesat based constellations, serving Earth Observation (such as utilised by Planet), communication (Spire, Orbcomm) and other purposes. Satellite communication and Earth Observation, together with Satellite Navigation make up for the most profitable commercial space activities, but while the first two have seen successful commercial endeavours, Satellite Navigation – as far as the space segment is concerned – is still a pure institutional activity.

Today's Global Navigation Satellite Systems utilise Hydrogen MASER, Rubidium and Caesium based Atomic Clocks to achieve highest accuracy and availability for positioning and timing purposes. Of all these Atomic Frequency Standards (AFS), the Rubidium based Atomic Clocks are by far the smallest, lightest and cheapest ones, which would make them the natural candidate for a GNSS constellation made up of CubeSats. However, this small form factor comes with a drawback - limited accuracy and stability. As such, a pure Rb-based GNSS may experience frequency jumps that ultimately limit the system to 10-20 m accuracy**,** a level that does not satisfy today's GNSS requirements. But what resembles a mediocre accuracy level for terrestrial applications will still be of high value when it comes to in-space-navigation and planetary exploration. Space projects in the applications, science and exploration domain intending to conduct formation flying and/or docking procedures or aiming to pursue the build-up of an infrastructure on the Moon, Mars or the asteroids are concerned with positioning/navigation accuracy requirements calling exactly for these levels. A particular challenge is the topic of achieving high landing accuracies on another celestial body, a key issue triggered by the fact that the set-up of a base will call for the consecutive landing of several elements – all in close vicinity to each other. Although landing error ellipses have shrunk over time (from 280x100 km for Viking in 1976 to 150x20 km for Spirit and opportunity in 2004 and 20x6.5 km for Curiosity in 2012) they are still too big for a staggered build-up of an outpost.

So while a CubeSat based GNSS Constellation may not (yet) satisfy the stringent requirements of terrestrial applications and services, it may still provide for an invaluable infrastructure when it comes to planetary exploration, especially when it is possible to use the very same GNSS constellation for communication and remote sensing purposes. Bearing this in mind, this paper will discuss the key requirements, constraints and considerations, which drive the design and set-up of such a CubeSat based GNSS Constellation, which will likely become an indispensable infrastructure for any planetary exploration activity that goes beyond the one-off-visit type.

I. INTRODUCTION

GPS, the Global Positioning System, traces its origins back to the year 1973. In this year the cornerstone of this successful GNSS was laid over the Labour weekend at the Pentagon in a meeting, which was later called the infamous "Lonely Halls Meeting"[1]. Left abandoned in a place that usually busts with activity, 12 military officers discussed over a period of three days the creation of the Defense Navigation Satellite System (DNSS) thereby conceiving a system that was later known as Navstar or Global Positioning System – GPS.

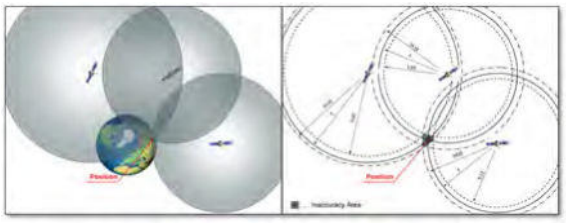

Figure 1: The working principle of systems like GPS and Galileo builds upon measuring the time difference between emission and reception of a signal sent by a satellite (left image). Dependent on the error of this time measurement, the final position is to a certain degree inaccurate (right image).

GPS' working principle is fairly easy as it makes use of only two physical factors: the constant speed of light and the fact that we can measure time differences relatively precisely. The combination of these two things leads to a satellite-based system, where a satellite emits a time-stamped signal; the personal receiver combines it with its own time reference, and measures its distance to the satellite by calculating the time difference with the signal's speed (the speed of light). If one combines the signals of four satellites, the receiver can calculate latitude, longitude, and elevation as well.

Of course things are not that easy, when it comes to details. In aiming to achieve a performance with accuracies in the meter scale and a high service robustness, it became clear that GPS would have to rely on a big space segment with many satellites and certain revolutionary technologies, such as space qualified atomic clocks, but most of all GPS would had to call for significant amounts of money, not millions but billions of US Dollars. Back then, such amounts of money could only be spent by governmental budgets and the request to spend billions of Dollars to allow for the necessary research, development, deployment and operation of a complex constellation of navigation satellites could be only justified if there was the need to mitigate a risk of such gravity that it would endanger the very existence of the USA - such as the Cold War arms race.

In the end it was the nuclear threat to the USA that convinced the US Congress to invest into GPS. In the period of 1973 to 2002, 6.3 billion US Dollars - excluding military equipment and launch cost - were spent on Navstar-GPS. The operational costs amount to approximately 750 million US Dollars per year[2]. For this amount of money, the USA obtained a system that acted as force multiplier to its nuclear deterrent - and the world got its first and so far only truly operational Global Navigation Satellite System (GNSS). Although military doctrine demanded that the former Soviet Union was to launch its own 'counter'-system to GPS – GLONASS, was started in 1976 - it is only recently that the first truly civilian GNSS is to be started – Galileo.

II. THE TRANSFORMATION OF GNSS FROM A PURE MILITARY INTO A DUAL-USE SYSTEM

Retrospectively looking, it does not come as a surprise that it took 40 years until the first non-military GNSS was to be rolled out. Galileo intends to serve civilian and commercial applications and hence it requires a thriving GNSS market to afford the costs of building and maintaining it. Today, this market is there as the worldwide Global GNSS downstream market is surpassing the €100 bn threshold (Figure 2).

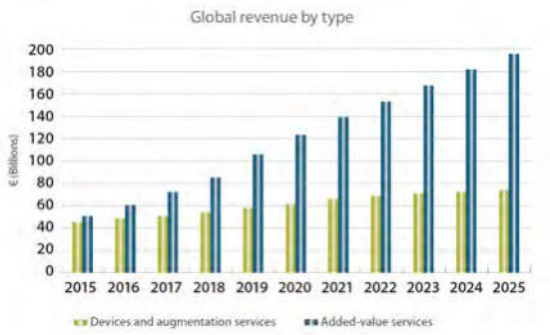

Figure 2: Global GNSS Downstream Market Evolution 2015-2025 (Source: GNSS Market Report Issue 5, 05/2017)

According to a market report by the GSA[3], today's GNSS market is mostly fuelled by Road (50.0%) and LBS (43.4%) applications. Next in line are surveying (2.6%), agriculture (1.3%), maritime and aviation (both 0.7%), timing & synchronisation (0.7%), drones (0.5%) and rail with 0.1% (refer to Figure 3).

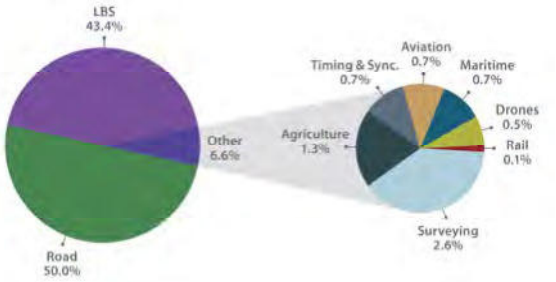

Figure 3: Cumulative Core Revenue 2015-2025 (Source: GNSS Market Report Issue 5, 05/2017)

While these number are indeed impressive, they fail entirely to demonstrate the strength of the GNSS uptake within the civilian markets, which manifests itself best when the number of GNSS receivers produced per year for the civilian and the military market segment. The following graphic (Figure 4), extracted from the article "Assured PNT for Our Future: PTA" by Bradford Parkinson[4], puts the respective market numbers in perspective.

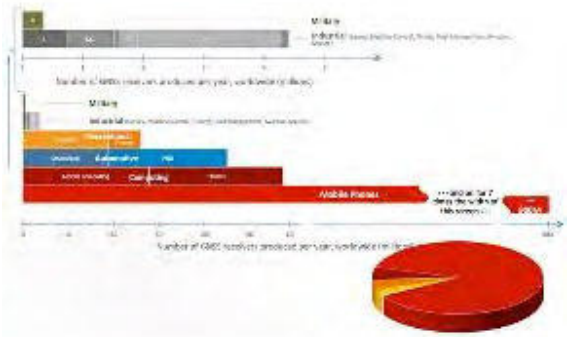

Figure 4: GNSS Market Size in 2012 (Source: Frank van Diggelen, GPS World)

The one thing which is immediately visible is the huge discrepancy in produced receiver (RX) numbers; while there are less than half a million military RX produced, RX for industrial uses such as survey and machine control, amount to about 4.5 million, still highly superseded by recreation, automotive, and computing with 26, 45 and 58 million RX respectively. But this is next to nothing when comparing it to the mobile phone market, where one company alone produces more than 900 million GPS-equipped smartphones per year.

Obviously the civilian markets have adopted GNSS for their uses. And consequently it is them that start to be an important player when it comes to setting up the requirements that drive the design of GPS, GLONASS, Galileo and especially Galileo as it is the only truly civilian system.

III. GNSS USERS AND THEIR SPECIFIC NEEDS

III.1. LBS

For the mass market a set of strong, interference resistant signals coming from a well filled constellation is all that is required. Many of the current mass market receivers (such as the ones built into mobile phones) are able to track three of four different satnav-systems, thereby benefitting from a bigger number of visible satellites. In the future the higher-end mass market receivers will add a second frequency (L1/L5 or E1/E5) to minimize the effect of the ionosphere and thereby improving the positioning accuracy.

III.2. Road

For vehicles such as cars and trucks, currently we see mass-market chips being used in their navigation devices. With the move to driverless road vehicles, these units will have to be replaced by receivers that can provide a certain measure of integrity and come with anti-spoofing features. Even then, driverless road vehicle will continue to rely on sensor fusion with radars, cameras and accelerometers.

Fleet management relies on a quasi-continuous flow of information (including position and velocity) from the vehicle to the control centre. Given the high socio-economic and commercial values, which are at stake (passengers, transported freight, etc.), security-related features such as anti-spoofing and resistance to jamming will be considered essential - not least because the same devices might be used for establishing the input to next generation road tolling systems.

III.3. Surveying

For the professional market in surveying, geodesy etc., the existing networks of reference stations providing differential corrections will be expanded (to shorten the virtual baselines) and will be upgraded to make use of all available signals on all visible GNSS constellations. Signal structures offering good resistance against multipath as well as a short time to first fix are desirable.

While surveying requires the highest level of position accuracy, there are generally no integrity requirements attached to this type of service and it is expected that Real Time Kinematic (RTK) solutions will continue to be used.

III.4. Agriculture

In precision farming applications wide area differential GNSS[5] solutions are commonly used as the position accuracies required are in the decimetre range for most farming processes, such as tillage, seeding and spraying. For some operations such as planting row crops and strip tillage higher accuracies achieved by RTK with real or virtual reference stations are needed.

III.5. Aviation

2011 saw 15,000 commercial aircraft operating, a number that is supposed to increase to 31,000 in 2030. This increase of aircraft operating in the years to come is fuelled by surging passenger numbers. From 80 million airline passengers per year in 2009, analysts predict that the airlines will have to serve a market of 220 million passengers in the year 2029[6]. At the same time 250,000 General Aviation (GA) aircraft will stay ahead by one order of magnitude; the FAA forecasts an increase of the active general aviation fleet[a] at an average annual rate of 0.5 percent over the 21-year forecast period, growing from an estimated 220,670 in 2012 to 246,375 aircraft by 2033[7].

Non-respective if a passenger flies in an airliner or a small two-seater aircraft, all will have to land at an international, regional or private airport – the natural congestion point. Latest by then aviation navigation becomes critical as velocities are high, airspace is limited and reaction times are short. Already in flight, aviation demands the highest possible robustness and integrity of navigation systems - be they land- or space-based. But when it comes to approach and landing the room for navigational errors becomes very small; at that point airplane movements need to be controlled and coordinated tightly to ensure safety and to avoid congestions (refer to Figure 5).

Figure 5: The Runway System of Amsterdam Airport Schiphol (EHAM) (Source: Wikipedia)

Naturally airports like Schiphol, where airplanes land and take-off in carefully orchestrated 'slots', place the highest constraints on the related air navigation systems. The requirements are such that even the least stringent precision approach of type Instrument Landing System Category I – often abbreviated as ILS CAT I - requires an approach accuracy of 16 metres laterally and 4 metres vertically. Obviously a 'normal' GNSS service with an accuracy in the order of 7-15 m is not sufficient anymore under such circumstances. And even if GNSS had the accuracy, how would a pilot and the air traffic controller know that the GNSS data is trustworthy, when ionospheric disturbances, clock drift, and satellite orbit errors can compromise a single satellite or the entire service?

The answer to these questions is the creation of an additional system, which is implemented on top of GNSS to *augment* its navigational service – consequently this system is called Space Based Augmentation System (SBAS). Conceived and first developed in the 1990s in the United States, an SBAS provides an integrity function; hence a constant feedback loop to the pilot telling him whether the navigation signal is reliable to enable safe flight navigation and landings. Although today's global navigation satellite systems have a better accuracy than their predecessors and the availability of GNSS services has increased due to the fact that there are several GNSS constellation in operation, the integrity requirement cannot be satisfied by GNSS alone - an SBAS is therefore an integral part of a complete GNSS based air navigation solution.

[a] An active aircraft is one that flies at least one hour during the year.

For commercial and recreational aviation, integrity will continue to be the key requirement. A good part of the northern hemisphere is covered by Satellite-based augmentation systems (SBAS) such as WAAS, EGNOS, GAGAN and MSAS and in principle, by extending the infrastructure, the remaining landmasses could equally well be covered. The evolution of SBAS is underway - the next generation will be a dual frequency (L1/L5) system and some of the SBAS will incorporate more than one constellation (currently only GPS is implemented).

It goes without saying that spoofing and jamming are big threats to aviation users, be it for the risk of experiencing a Controlled Flight Into Terrain (CFIT) accident or facing the risk of losing the Airborne Collision Avoidance System (ACAS) functionality due to false PNT data. Spoofing is especially dangerous as these attacks exploit the lack of encryption and authentication of civilian GPS signals by imitating the legitimate signals with the purpose of modifying the localisation or time result of a victim. As a thorough discussion of the threat and the potential countermeasures would go far beyond the scope of this paper, we recommend the interested reader to take a look at papers such as "*Crowd-GPS-Sec: Leveraging Crowdsourcing to Detect and Localize GPS Spoofing Attacks*"[8].

III.6. Maritime

The maritime segment employs GNSS to satisfy the demand for navigation (in open sea or in specific situations, such as harbour entrances and approaches) and positioning (e.g. vessel monitoring, traffic management, locator beacons for distress situations, etc.) of vessels and crews.

Over the years, the use of positioning in the maritime sector has become more and more widespread with different categories of vessels, beacons and ports using GNSS for different purposes.

Table 1: Global number of vessels, beacons and ports (Source: GNSS Market Report Issue 4, 03/2015)

Vessels	[illegible]	[illegible]	[illegible]	[illegible]
Beacons	[illegible]			
Ports	[illegible]	[illegible]		

Owing to the nature of the sea, which exposes vessels from vast and open to narrow and highly congested areas (e.g. the English Channel), as well as to restricted waters (e.g. port approach, inland waterways), accuracy and integrity are a key element of the navigation and the positioning (e.g. manoeuvring, traffic management, Search and Rescue operations, marine engineering) solution.

As stated within the aviation chapter above, SBAS can satisfy the integrity requirement to some extent, however with specific limitations (e.g. coverage on the open sea and/or at coastal regions). Taking into consideration that the amount of maritime users is limited (though much larger than the aviation community, with approx. 250,000 GA aircraft), similar approaches to the aviation sector may be used and non-surprisingly the maritime sector has developed an equivalent to the aviation sector's ADS-B – AIS, a maritime tracking system, installed on-board of large vessels.

The Automatic Identification System (AIS) is an automatic tracking system used on ships and by vessel traffic services (VTS) for identifying and locating vessels by electronically exchanging data with other nearby ships, AIS base stations, and satellites. When satellites are used to detect AIS signatures then the term Satellite-AIS (S-AIS) is used. AIS information supplements marine radar, which continues to be the primary method of collision avoidance for water transport.

Figure 6: AIS Map showing global Shipping Tracking by Satellite (Source: Marinetraffic[9])

Information provided by AIS equipment, such as unique identification, position, course, and speed, can be displayed on a screen or an ECDIS. AIS is intended to assist a vessel's watch standing officers and allow maritime authorities to track and monitor vessel movements. AIS integrates a standardized VHF transceiver with a positioning system such as a GPS or LORAN-C receiver, with other electronic navigation sensors, such as a gyrocompass or rate of turn indicator. Vessels fitted with AIS transceivers can be tracked by AIS base stations located along coast lines or, when out of range of terrestrial networks, through a growing number of satellites that are fitted with special AIS receivers which are capable of de-conflicting a large number of signatures.

The International Maritime Organization's International Convention for the Safety of Life at Sea requires AIS to be fitted aboard international voyaging

ships with gross tonnage (GT) of 300 or more, and all passenger ships regardless of size.

III.7. Space

Spacecraft in Low Earth Orbit (LEO) orbit, well below the GNSS MEO constellations can make use of this well proven and highly accurate navigation infrastructure. However, due to the high velocity of the LEO spacecraft (approx. 8 km/s or 28,800 km/h), a standard GNSS receiver for terrestrial applications would not work, because the tracking loop in the receiver hardware, respectively the firmware, are set for moderate Doppler shifts. If one wants to utilise GNSS-based navigation in LEO, specific receivers have to be employed featuring tracking loops, which are adapted to accommodate high Doppler shifts. It is only for a few years that these type of specifically in-space-navigation receivers have become commercially available at low cost. In the following chapter we take a closer look at the key requirements, constraints and considerations that govern the use of GNSS for in-space-navigation.

IV. GNSS-BASED IN-SPACE-NAVIGATION…

IV.1. …At the Earth

Although GNSS builds upon space assets to deliver its services, it is rather recently that GPS and Co. have found their way into the navigation systems of spacecraft. One of the earliest and possibly still one of the most stringent space missions relying on GNSS for navigation purposes was the Automated Transfer Vehicle (ATV).

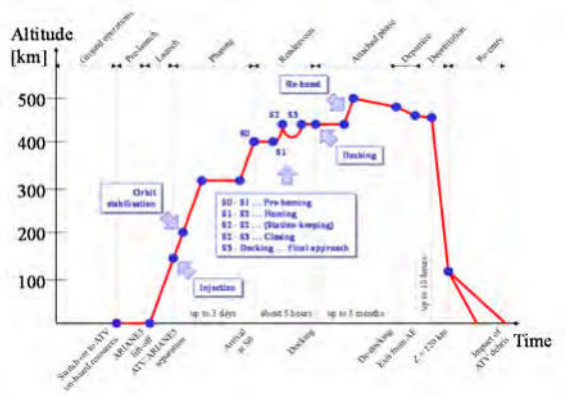

Figure 7: The Phasing of Operations of the ATV when flying, docking and leaving the ISS (Source: IEEE VTC99, 1999[10])

IV.1.1. *The ATV: A Master Example for autonomous and accurate In-Space-Navigation*

Realised as a 20.7 unmanned spacecraft launched by an ARIANE 5 into Low Earth Orbit (LEO), the ATV's mission was to re-supply and re-boost the International Space Station (ISS).

Figure 8: ESA's Automated Transfer Vehicle-2 (ATV-2) "Johannes Kepler" approaching the ISS (Source: ESA/NASA[11])

Since its first voyage in April 2008 until its last one in 2015, the Automated Transfer Vehicles were part of the supply ships to the Space Station. Approximately every 17 months, the ATVs carried 6.6 tonnes of cargo to the Station 400 km above the Earth[12].

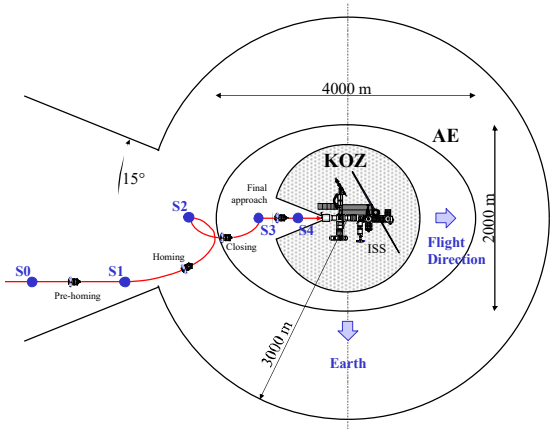

Figure 9: The Flight Path of the ATV when performing its autonomous Docking Sequence (Source: IEEE VTC99, 1999[13])

What makes this project so special is that the ATV was the first spacecraft to initiate and commence a docking manoeuvre in fully autonomous mode, only relying upon on-board calculations, derived from Absolute/Relative GPS data and information from an optical rendezvous system for the final docking sequence. As ISS crew safety had to be ensured at all

times, exceptional requirements, constraints and design drivers were governing the development of the navigation and the communication subsystem of the ATV, calling for example for the utilisation of absolute and relative GPS navigation when approaching the ISS.

The ATV's Absolute GPS Navigation (AGPS)

The ATV's AGPS navigation filter determines the orbital position of the ATV during the rendezvous phase. This information is used as the primary means of navigation at the beginning of the rendezvous when the proximity link between ATV and ISS is not yet established or when this link cannot be maintained like it is possibly in case of an ATV wave-off command.

The AGPS filter structure is based on an extended Kalman filter, which uses the raw measurements of a GPS receiver in order to update a propagated orbital state vector. The navigation vector also includes the GPS receiver clock drifts. The processed measurements are the GPS pseudo-range (accuracy: 5 m, 1σ) and the Doppler which is used to estimate the pseudo range rate (accuracy: 5 cm/s, 1σ). Full observability of the AGPS state vector is ensured only with at least 4 GPS satellites visible. An all-in-view processing is applied for AGPS.

The major drivers for the achievable AGPS performance are the Selective Availability and the ionospheric effects. The typical order of magnitude of AGPS 1σ-accuracy is better than 60 meters in position and 0.1 m/s in velocity.

The ATV's Relative GPS Navigation (RGPS)

Relative GPS navigation (RGPS) is the primary navigation means for the long-range leg of the rendezvous operations, e.g. from acquisition of the proximity link between ATV and ISS at 30 km down to 500 m (because of the concern about the GPS Multipath effects). The basic principle is to use the single differences of the GPS raw data, obtained quasi-simultaneously by the ATV and the ISS GPS receivers. This allows a direct cancellation of common error sources in the GPS signal as seen by both vehicles like selective availability, ionospheric effects.

A linearized Kalman filter scheme is used in order to perform optimal hybridisation of the GPS differential observables with a relative dynamics model (first order Clohessy-Whiltshire model).

The processed measurements are the GPS pseudo-range and the carrier cycle count (accuracy: 6 mm, 1σ) which is back differentiated in order to estimate the average range rate over the last measurement interval.

The RGPS State vector is of dimension 8 as it includes not only the relative state vector but also the relative clock bias and drift. Full observability of the RGPS state vector is obtained only with at least 4 common visible GPS satellites. This drives the antenna concept on ATV and ISS (structural blockages and Multipath effects), the attitude profile of each spacecraft and the number of channels for each receiver (more than 6). The selection of satellites is based on the best configuration of 4 (simplified volume criteria).

The relative dynamics prediction model uses the commanded thrust accelerations. The absolute S/C-attitude is needed as input for the filter in order to compensate for the lever arm between GPS antenna and center of mass. The state update algorithm contains also a rejection filter like AGPS based on innovation estimations.

The RGPS filter is run at 1-Hz frequency. The de-synchronization between the two receivers must be limited to 100 milliseconds. The RGPS filter is also capable to cope with an acquisition delay of the ISS GPS data through the proximity link of up to 2s.

With good visibility conditions and synchronization of both receivers, the typical performance of RGPS 3σ-accuracy is 5 m in position and 5 cm/s in velocity when accounting for the rendezvous manoeuvres. RGPS convergence time is typically a few minutes[14].

IV.1.2. In-Space-Navigation for smaller Spacecraft like OPS-SAT

As stated above, specifically designed in-space-navigation receivers have only recently become commercially available, opening the door for new applications in space. Today, many CubeSat missions include GPS receivers to improve the position determination (e.g. the GomSpace GOM-X series). Most of the time, the Kepler elements provided by NORAD are not accurate enough for many applications. The ESA nanosatellite mission OPS-SAT shall be presented here as an example (Figure 10).

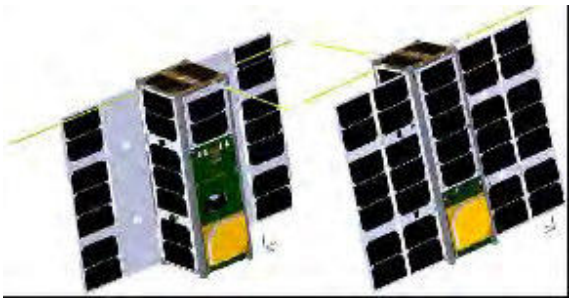

Figure 10: Illustration of the OPS-SAT Nanosatellite Configuration with Solar Arrays deployed; Left: Front View; Right: Rear View (Source: ESA[15])

OPS-SAT is a 3U CubeSat[21] with the purpose to demonstrate and validate in Space new operational concepts. Furthermore, it provides to experimenters a versatile platform to carry out hard- and software experiments.

Figure 11: Photo of the Lustbühel Observatory serving as the Laser Station (Source: TU Graz[16])

A particular interesting one is an optical receiver experiment. In Graz a Laser ranging station for satellite geodesy and space debris monitoring exists. Its powerful pulsed Laser allows to transmit pulse-position modulated signals (Figure 11). A small receiver with a single-photon counting module, developed by MEW Aerospace in cooperation with TU Graz is integrated in OPS-SAT. It receives data from the Laser station (Figure 12).

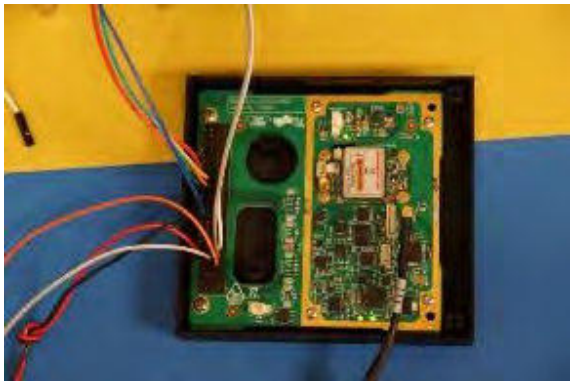

Figure 12: Optical Receiver inside OPS-SAT

A pre-requisite for this experiment is a very good position knowledge of the satellite. For this purpose the avionics include a Novatel GNSS receiver which delivers position data via telemetry to ESOC. The orbital parameters are refined there and will be delivered to the Laser station which subsequently tries to find the spacecraft. Retroreflectors on the Nadir face of OPS-SAT facilitate first the acquisition and then the tracking of the satellite.

IV.1. …Outside the Earth's Sphere

Navigating on the Moon, on Mars and the Asteroids

Future Moon bases, as well as mobile exploration platforms such as Moon and Mars rovers will require navigation facilities. Several projects suggested to use optical navigation with terrain mapping and gyros. Clearly, a Moon- or Mars-based satellite navigation system would be advantageous, but an expensive endeavour.

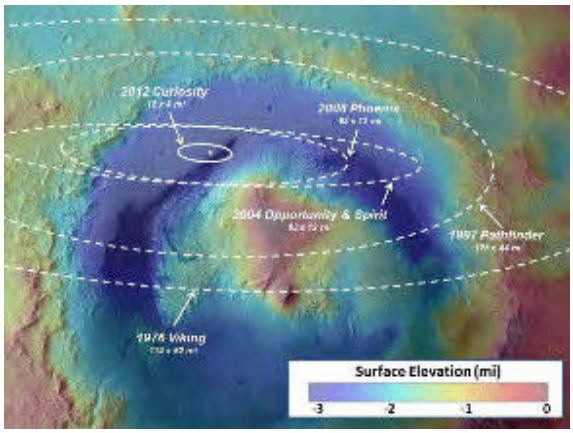

Figure 13: Landing Accuracy on Mars: A Historical Perspective (Source: NASA[17])

A particular challenge is the topic of achieving high landing accuracies on another celestial body, a key issue triggered by the fact that the set-up of a base will call for the consecutive landing of several elements – all in close vicinity to each other. Although landing error ellipses have shrunk over time (from 280x100 km for Viking in 1976 to 150x20 km for Spirit and opportunity in 2004 and 20x6.5 km for Curiosity in 2012, refer to Figure 13) they are still too big for a staggered build-up of an outpost.

A low-cost solution may be an implementation that was used in the US TRANSIT system, the forerunner of GPS. TRANSIT used by the US Navy operated at frequencies of 150 and 400 MHz. The accuracy was between 15 and 500 m. For some applications on the Moon, Mars or other celestial bodies this may be fully sufficient.

The satellites send their ephemerides and a timing signal continuously. The relative movement between spacecraft and ground receiver produces a Doppler shift of the carrier frequency. Using the position of the satellite, the timing reference and the Doppler shift the position of the receiver can be calculated. In principle, a two-dimensional fix can be determined with a single satellite, however, with some time delay. In case of the original TRANSIT system this was in the order of 30 minutes. Three ground stations at minimum are needed on ground to triangulate the navigation satellite and to provide exact ephemerides.

V. GNSS IN THE ERA OF NEWSPACE

The global space economy reached USD 329 bn in 2016[b], having grown on average by 5.1% p.a. in between 2005 and 2016. During this period, the global space economy saw periods of stagnation and of strong growth, at times even outgrowing the overall global economy. While the governments were the driving forces in the 20th century (e.g. Apollo-programme, International Space Station (ISS), as well as GPS), today it is the commercial activities that are setting the pace, accounting for USD 253 bn or 76% of the global space economy in 2016. Albeit rather recent, the commercialisation of space is to intensify in the coming years, as the space sector experiences rapid growth in new approaches to space development. The so-called "NewSpace" trend, thrives upon technology and business model innovations that allow for a significant reduction of costs, the provision of new products and services as well as for a broadening of the customer base. As this comes along with increased returns for companies and investors, the onset of a whole new wave of commercial activities within the space sector is the result.

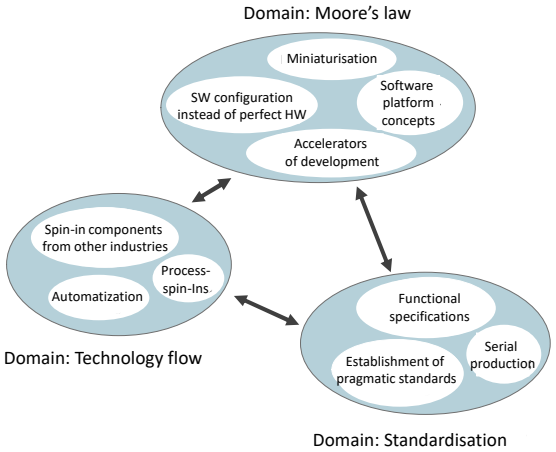

Figure 14: The three Main Drivers of NewSpace (Source:NewSpace, 2017[18])

A clear indication that this NewSpace movement is picking up speed is the fact that space ventures have attracted over USD 18.4 bn of investment, including USD 4.5 bn in debt financing, since 2000[c]. This rise of new entrants has brought with it new opportunities for innovations in products, services and processes which, in turn, have created spill-over effects to various industries in- and outside of the space sector. Miniaturisation, agile development, faster generation change and an increase utilisation of industrial standards are trends that go along with NewSpace, possibly best showcased by the advent of Cubesat based constellations, serving Earth Observation (such as utilised by Planet), communication (Spire, Orbcomm) and other purposes. Satellite communication and Earth Observation, together with Satellite Navigation make up for the most profitable commercial space activities, but while the first two have seen successful commercial endeavours, Satellite Navigation – as far as the space segment is concerned – is still a pure institutional activity.

A major reason for the institutional dominance is the high cost in setting up and operating a GNSS like GPS or Galileo. As stated in the introduction, the US invested 6.3 billion US Dollars on Navstar-GPS in the period of 1973 to 2002 - excluding military equipment and launch cost. To add to that, the operational costs amount to approximately 750 million US Dollars per year. Such amounts of money are way too high for any commercial venture, hence even the civilian Galileo

[b] *The Space Report 2017*, Space Foundation

[c] *Start-up Space*, Bryce, January 2018

system builds entirely upon institutional funding – at least for the roll-out and the early operations.

This observation is likely to remain valid for some years – even with the advent of NewSpace. Space tourism, Lunar and asteroid mining, they all - as well as other NewSpace projects in the applications, science and exploration domain intending to conduct formation flying and/or docking procedures or aiming to pursue the build-up of an infrastructure on the Moon, Mars or the asteroids – might act as drivers for GNSS systems around the Moon, Mars or an asteroid. However, all these (NewSpace) markets are still too infant to justify commercial investments into any non-terrestrial GNSS. If such investments are to be made commercially feasible, such GNSS need to be made drastically "lighter and cheaper" while still satisfying the needs of NewSpace. Is this possible? To answer this question we will have to look into the technological constraints.

VI. KEY CHALLENGES AND CONSTRAINTS FOR A CUBESAT BASED GNSS CONSTELLATION FOR PLANETARY EXPLORATION

VI.1. Atomic clocks – the key technologies of every GNSS

Today's Global Navigation Satellite Systems utilise Hydrogen MASER, Rubidium and Caesium based Atomic Clocks to achieve highest accuracy and availability for positioning and timing purposes. Of all these Atomic Frequency Standards (AFS), the Rubidium-based Atomic Clocks are by far the smallest, lightest and cheapest ones, which would make them the natural candidate for a GNSS constellation made up of CubeSats. However, this small form factor comes with a drawback - limited accuracy and stability. As such, a pure Rb-based GNSS may experience frequency jumps that ultimately limit the system to 10-20 m accuracy**,** a level that does not satisfy today's GNSS requirements. But what resembles a mediocre accuracy level for terrestrial applications will still be of high value when it comes to planetary exploration. Any exploration strategy concerned with the build-up of an infrastructure on the Moon, Mars or the asteroids is concerned with landing accuracy requirements calling exactly for these levels. This is due to the fact that the set-up of a base will call for the landing of several elements – all in close vicinity to each other.

Figure 15: A small-scale Rubidium Atomic Clock with an Allan Deviation ≤ $8*10^{-12}$ (Source: sparkfun[19])

Rubidium clocks have the size of a small matchbox (Figure 15). Commercial-Off-The-Shelf (COTS) items (non-space-qualified) only cost a few hundred Euros.

Recently, chip-scale atomic clocks have also become commercially available. They have a mass of 35 g, the volume is smaller than 17 cm³ and the power consumption surmounts to 120 mW only. The short-term stability is $1*10^{-11}$. This is two orders of magnitude less than a good Caesium frequency standard, so not satisfactory for the stringent requirements of a GNSS for terrestrial applications. But as stated before, the accuracy may suffice for many exploration applications

VI.2. CubeSat Capabilities

CubeSats and small satellites have matured significantly over the last years. Commercial constellations for remote sensing, AIS and ADS-B, meteorology and telecommunications have been realised offering a variety of new services.

CubeSat buses up to 12U can be procured from several vendors with flight-proven avionics. Even a 3U Cubesat with deployable solar arrays can generate around 30 W. Powerful processors with FPGAs and a software-defined radio front-end can be used as a signal generator. The necessary timing reference could be a miniaturised atomic clock as discussed before. Such small spacecraft operated within a constellation could provide a relative low-cost navigation infrastructure for exploration missions, certainly on the Moon.

The experience with the BRITE asteroseismology mission[20], consisting of five nanosatellites shows that demanding requirements can be met with small, inexpensive spacecraft. BRITE is successfully in orbit for 5.5 years and two more years of operational life-time can be expected[20].

VI.1. Operational Aspects

Both the small form factor and the low power consumption of the Rubidium and/or the Chip-Scale Atomic Clocks (CSAC) allow for a readily integration of these Atomic Frequency Standards into a CubeSat of standard size 3U to 12U. GNSS constellations however do not only feature satellites that circle the Earth, transmitting a beacon with their accurate in-space-position at a specific time stamp, but do also include a mission control center that permanently tracks the GNSS satellites to obtain their exact position and the current velocities, such that a 6-dimensional phase vector can be calculated. This phase vector is calculated for and uploaded onto each satellite of the GNSS constellation, so that the ephemeris data is always accurate.

Due to orbital dynamics (Sun's and Moon's gravity, relativistic effects, etc.) numerous disturbances act on the satellites and hence the ephemeris data has only a limited operational validity.

The permanent updating of this ephemeris data is key to ensure usability of the GNSS and while it seems feasible that one can track the satellites of a Lunar-based CubeSat based GNSS constellation from the Earth, the same effort looks rather impossible for any system of that sort, which circles Mars or any asteroid.

In the long run it may be possible that such a CubeSat-based GNSS constellation may exert a self-control mechanism by utilising advanced sensor fusion algorithms including occultation observations, star tracker data and pattern recognition methods of specific ground features on the concerning celestial body. In aiming to achieve accuracy levels in the order of 10-100s of meters such a sensor fusion algorithm is likely to require advanced calculatory capabilities, which are attributed to (weak) Artificial Intelligence (AI) systems. It goes without say that such AI systems do not exist yet, but may become available in 10-20 years.

VII. CONCLUSIONS

Based on the results of the infamous "Lonely Halls Meeting", GPS became a reality in 1995 offering cost-effective Position, Navigation and Timing (PNT) services, 24 hours a day, seven days a week and in all types of weather.

Starting from a pure military application, GPS evolved both in scope and range; today GPS is only but one of four GNSS and serves – together with GLONASS, Galileo and Beidou - many more markets than only the military one. As of 2015, the worldwide GNSS core market surpasses the €70 bn threshold, achieving a Compound Annual Growth Rate (CAGR) of 8.3%. Obviously the civilian markets have adopted GNSS for their uses such that today's GNSS market is mostly fuelled by Road (50.0%) and LBS (43.4%) applications. Next in line are surveying (2.6%), agriculture (1.3%), maritime and aviation (both 0.7%), timing & synchronisation (0.7%), drones (0.5%) and rail with 0.1%

Although GNSS builds upon space assets to deliver its services, it is rather recently that GPS and Co. have found their way into the navigation systems of spacecraft. One of the earliest and possibly still one of the most stringent space missions relying on GNSS for navigation purposes was the Automated Transfer Vehicle (ATV), a 20.7 unmanned spacecraft launched by an ARIANE 5 into LEO to re-supply and re-boost the International Space Station – all in fully autonomous mode, only relying upon on-board calculations, derived from Absolute/Relative GPS data and information from an optical rendezvous system for the final docking sequence. Flown in between 2008 and 2015 the ATV's navigation system was capable to process the GPS pseudo-range (accuracy: 5 m, 1σ) and the Doppler to estimate the pseudo range rate (accuracy: 5 cm/s, 1σ) to very high accuracy levels.

The advent of specifically designed in-space-navigation receivers opened the door for new applications in space. Today, many CubeSat missions include GPS receiver to improve the position determination. The ESA nanosatellite mission OPS-SAT was analysed as an example for an innovative optical receiver experiment, which builds upon accurate initial GPS-derived positioning data.

In recognising the particular challenge of achieving high landing accuracies on another celestial body a TRANSIT like positioning system may prove to provide for accuracies between 15 and 500 m, which may suffice for exploration applications on the Moon, on Mars or other celestial bodies.

Albeit NewSpace applications may be a big driver for a Moon/Mars/Asteroid-centric GNSS, the CAPEX and OPEX related costs of any terrestrial-like GNS are way too high. In aiming to reduce this cost, the concept of a CubeSat based GNSS constellation for planetary exploration was deeper analysed.

By relying on Rubidium and/or the Chip-Scale Atomic Clocks, which feature both a small form factor and low power consumption, an integration of these Atomic Frequency Standards into a CubeSat of standard size 3U to 12U seems technically feasible.

Operational aspects however are still an issue that will have to be overcome; in particular the limited validity of ephemeris data and the difficulties in tracking the GNSS satellites once they are stationed on another celestial body. Implementing a self-control mechanism, which utilises advanced sensor fusion algorithms to ultimately achieve accuracy levels in the order of 10-100s of meters may provide a solution to these challenges. Such a sensor fusion algorithm however is likely to require advanced calculatory capabilities, which are attributed to (weak) Artificial Intelligence (AI) systems. It goes without say that such AI systems do not exist yet, but may become available in 10-20 years.

VIII. GLOSSARY

- ACAS - Airborne Collision Avoidance System
- ADS-B - Automatic Dependent Surveillance – Broadcast
- AIS - Automatic Identification System
- ANS - Air Navigation Systems
- ANSP - Air Navigation Service Provider
- APV - Approach Procedure with Vertical Guidance
- CAGR - Compound Annual Growth Rate
- CFIT - Controlled Flight Into Terrain
- DME - Distance Measuring Equipment
- EGNOS - European Geostationary Navigation Overlay Service
- FAA - Federal Aviation Administration
- GA - General Aviation
- GAGAN - GPS Aided GEO Augmented Navigation
- GBAS - Ground Based Augmentation System
- GNSS - Global Navigation Satellite System
- GPS - Global Positioning System
- GT – Gross Tonnage
- IAP - Instrument Approach Procedure
- ICAO - International Civil Aviation Organisation
- ILS - Instrument Landing System
- LBS - Location Based Service
- MAC - Mid-Air Collision
- MSAS - MTSAT Satellite Augmentation System,
- MTOM - Maximum Take-Off Mass
- NDB - Non-Directional Beacon
- NPA - Non-Precision Approach
- PBN - Performance-Based Navigation
- PNT - Position, Navigation and Timing
- RA - Resolution Advisory
- RNP - Required Navigation Performance
- SDCM - System for Differential Corrections and Monitoring
- SBAS - Space Based Augmentation System
- SSR - Secondary Surveillance Radar
- TA - Traffic Advisory
- TACAN - Tactical Air Navigation
- VOR - VHF Omnidirectional Radio Range
- VTS – Vessel Traffic Service
- WAAS - Wide Area Augmentation System

IX. ACKNOWLEDGEMENTS

OPS-SAT is carried out under ESA Contract 4000117431/16/D/SR. The authors are grateful to Mr.David Evans, the Technical Officer at ESOC and all his colleagues at ESOC for the continuing support.

The authors also wish to acknowledge the support by the Austrian aeronautics and Space Agency, in particular Dr. Stephan Mayer, as well as the insights provided by Colonel Christian Markus, Institute for Military Geoinformation of the Austrian Armed Forces.

The BRITE-Austria Mission is made possible by the Austrian Aeronautics and Space Applications Program ASAP.

X. REFERENCES

[1] Prof. Bradford Parkinson, Highlight Lecture: Origins, Surprises and Future of GPS, IAC 2010, 28/09/2010

[2] http://www2.ocgi.okstate.edu/gpstools/overview1.htm. accessed in August 2013

[3] GSA, GNSS Market Report Issue 5, May 2015, page 10; available via www.gsa.europa.eu

[4] GPS World, "Assured PNT for Our Future: PTA", Parkinson B., 01/09/2014, http://gpsworld.com/assured-pnt-for-our-future-pta/, accessed in September 2015

[5] C. Kee, B.W. Parkinson, and P. Axelrad, "Wide Area Differential GPS," Navigation, Journal of the U.S. Institute of Navigation, vol. 38, no. 2, Summer 1991

[6] Frischauf N., Koudelka O., Wittig M., Global In-Flight Internet Service – A Proposal for a Satellite Mission, IAC-11-B.2.3.6, IAC-12, Naples, Italy, October 2012

[7] FAA Aerospace Forecast, Fiscal Years 2013-2033, page 58

[8] Jansen K., Schäfer M., Moser D., Lenders V., Pööper C., Schmitt J., Crowd-GPS-Sec: Leveraging Crowdsourcing to Detect and Localize GPS Spoofing Attacks, http://www.lenders.ch/publications/conferences/sp18_2.pdf, accessed in March 2019

[9] http://www.marinetraffic.com/en/p/satellite-ais, accessed in November 2014

[10] Aguilar-Sanchez, I., Paris, D., Allard, F., & Frischauf, N., "The navigation and communication systems for the Automated Transfer Vehicle", Vehicular Technology Conference, 1999 IEEE 49th (pp. 1187-1192). Houston, TX, USA), 07/1999, DOI: 10.1109/VETEC.1999.780535

[11] https://spaceflight.nasa.gov/gallery/images/station/crew-26/html/iss026e037172.html, accessed in September 2018

[12] http://www.esa.int/Our_Activities/Human_Spaceflight/ATV, accessed in September 2018

[13] Aguilar-Sanchez, I., Paris, D., Allard, F., & Frischauf, N., "The navigation and communication systems for the Automated Transfer Vehicle", Vehicular Technology Conference, 1999 IEEE 49th (pp. 1187-1192). Houston, TX, USA), 07/1999, DOI: 10.1109/VETEC.1999.780535

[14] Aguilar-Sanchez, I., Paris, D., Allard, F., & Frischauf, N., "The navigation and communication systems for the Automated Transfer Vehicle", Vehicular Technology Conference, 1999 IEEE 49th (pp. 1187-1192). Houston, TX, USA), 07/1999, DOI: 10.1109/VETEC.1999.780535

[15] https://directory.eoportal.org/web/eoportal/satellite-missions/o/ops-sat, accessed in September 2018

[16] https://directory.eoportal.org/web/eoportal/satellite-missions/o/ops-sat, accessed in September 2018

[17] https://www.nasa.gov/mission_pages/msl/multimedia/pia16039.html, accessed in September 2018

[18] Frischauf N., Horn R., Kauerhoff T., Wittig M., Baumann I., Pellander E., and Koudelka O., "NewSpace: New Business Models at the Interface of Space and Digital Economy: Chances in an Interconnected World", New Space, 04/08/2017, Mary Ann Liebert Inc., https://doi.org/10.1089/space.2017.0028

[19] https://www.sparkfun.com/products/14830, accessed in September 2018

[20] http://www.tugsat.tugraz.at/, accessed in September 2018

[20] Koudelka, O., R.Kuschnig, M.Wenger, Operational Experience with a Nanosatellite Science Mission, 69th IAC, B4.3.6, Bremen, 2018

[21] Koudelka, O., C.Coelho, D.Evans, The OPS-SAT Nanosatellite Mission – A Flexible Platform for On-Board Experiments, 11th IAA Small Satellite Symposium, Berlin, 2017